EXPERIMENTAL AND PETROLOGICAL STUDIES OF PHENOCRYST ASSEMBLAGES IN SCOTTISH PERMO-CARBONIFEROUS BASALTIC ROCKS.

Douglas G. Russell

Ph. D. Thesis
University of Edinburgh
1984

EX BIBL. UNIV. EDINBURGEN.

Declaration

This thesis has been composed by me and is my own work, except where duly acknowledged.

Douglas G. Russell

TO DORIS

ABSTRACT OF THESIS

Porphyritic basalts and hawaiites from the Scottish Permo-Carboniferous petrographic province have been the subject of experimental and petrological studies to determine the conditions of crystallisation of the observed phenocrysts.

Isothermal atmospheric pressure melting experiments have produced glasses coexisting with olivine, clinopyroxene, plagioclase and oxide minerals. An expression is presented which relates the Fe^{3+}/Fe^{2+} ratio of glass to temperature, fO_2 and glass composition. Using this, the olivine-liquid Fe^{2+}-Mg KD is 0.30 $\pm$ 0.03 in basic melts, increasing to 0.35 in lower temperature, more evolved melts.

Mineral temperature equations predict liquidus phases and temperatures at atmospheric pressure in natural basic and ultrabasic compositions. At the 95% confidence level, the most reliable equations are precise to better than $\pm$ 19° C for olivine, $\pm$ 14° C for plagioclase and $\pm$ 16° C for clinopyroxene. Rudimentary mineral composition equations have been combined with the mineral temperature equations in a crystallisation model developed with Dr. C. E. Ford. This model predicts details of the equilibrium crystallisation of basic magmas. Empirical correction factors have extended the model to high pressures. Applied to the Scottish lavas the model predicts low pressure crystallisation of pl $\pm$ ol phenocryst assemblages, moderate pressure crystallisation of ol + cpx + pl assemblages, and moderate to high pressure crystallisation of cpx $\pm$ ol assemblages.

Whole rock compositional trends can be modelled by dominant clinopyroxene + olivine + aluminous spinel fractionation. Phenocryst textures include those characteristic of rapid growth and partial resorption. Glomeroporphyritic textures often indicate cotectic assemblages. Clinopyroxene phenocrysts are augites and salites. Large, partially resorbed clinopyroxenes have near-homogeneous cores with high Al^{VI}/Al^{IV} ratios (up to 0.8) interpreted as indicating high pressure crystallisation. Small, zoned clinopyroxenes typically have low Al^{VI}/Al^{IV} ratios and may have grown during ascent of the magmas. Less magnesian clinopyroxenes with moderate Al^{VI}/Al^{IV} ratios could have crystallised from hawaiitic magmas at crustal pressures.

Olivine phenocrysts have a range of compositions up to Fo_{87}. Low Ca contents of the more forsteritic phenocrysts may indicate high pressures of crystallisation. Plagioclase phenocrysts have a range of compositions up to An_{83}. Complex zoning is mainly attributed to kinetic effects of crystal growth, but in some cases may indicate significant volatile pressures in the magmas. Highly aluminous spinels, low in Cr, are interpreted to have crystallised at high pressures. More common, lower Al/Cr spinels are interpreted to have crystallised at lower pressures and have a compositional range extending to titanomagnetites. From the experiments and natural Fe-Ti oxides, the magmas are believed to have had oxygen fugacities near the Ni - NiO buffer.

Polybaric phenocryst crystallisation has been recognised in the samples. Observed phenocrysts are predicted to have crystallised in the range 0 Kb, 1150° C to 11½ Kb, 1235° C. Some bulk compositions are predicted to have equilibrated with clinopyroxene-bearing assemblages at upper mantle pressures up to 19½ Kb, 1370° C. Samples from composite intrusions are predicted to have equilibrated with preserved phenocrysts at mid to high crustal pressures.

Four major stages of phenocryst growth are proposed. 1) Large, high Al^{VI}/Al^{IV} clinopyroxenes ± olivines ± aluminous spinels crystallised at upper mantle pressures (<15 Kb). 2) Large olivines + clinopyroxenes + plagioclases ± oxide phases crystallised at mid to high crustal pressures. 3) Plagioclases and/or olivines ± oxide phases crystallised at low to mid crustal pressures. 4) Small, rapidly grown olivines + clinopyroxenes + spinels crystallised from basic magmas during ascent from upper mantle pressures. Stages 1 - 3 characterise phenocrysts from the Dinantian volcanism. Stage 4 appears to be characteristic of the later Silesian-Permian volcanism. On the basis of the preserved phenocrysts many magmas are inferred to have been erupted from high pressures within several tens of hours.

LASCIATE OGNI SPERANZA VOI CH'ENTRATE!

Dante.

CONTENTS

'WHERE SHALL I BEGIN, PLEASE YOUR MAJESTY?' HE ASKED.
'BEGIN AT THE BEGINNING,' THE KING SAID, GRAVELY, 'AND GO ON TILL YOU COME TO THE END: THEN STOP.'

Lewis Carroll.

CHAPTER 1

INTRODUCTION

1.1 Statement of the Problem

The Scottish Permo-Carboniferous petrographic province is dominated by porphyritic basaltic and hawaiitic lavas and intrusions. Olivine, clinopyroxene, plagioclase and oxide minerals are the main phenocryst phases present. A classification scheme based on the phenocryst assemblages has been widely used as an aid to field mapping of the basic rocks (MacGregor, 1928). Despite the importance of the phenocrysts in understanding the field relationships of the lavas, there has been little effort directed towards interpreting the origin of the phenocrysts themselves. Indeed, there are few available analyses of the phenocryst minerals other than optical determinations. The problem approached in this study is the understanding of the conditions of crystallisation of the phenocryst minerals and assemblages. Experimental and petrological investigations of basic rocks from the province have been carried out to this end.

1.2 The Scottish Permo-Carboniferous Volcanism

The samples belong to a petrographic province stretching from the Scottish Highlands to the English Midlands and Southwest. In the west, the province extends to south-west Ireland. Volcanic activity occurred in this province from early Carboniferous to early Permian times, with the greatest volume having been erupted in the Dinantian (estimated as 6000 km^3 by Tomkeieff, 1937). Most research has been concentrated on the lavas and hypabyssal intrusions of the Midland Valley and Northumberland Basin, from which areas all the investigated specimens were collected. Figures 1-1 and 1-2 illustrate the geographical and temporal distributions of the main Scottish outcrops.

In the Scottish area, several workers have identified three main episodes of activity (e.g. Upton, 1982; Macdonald et al., 1977; Francis, 1983). A Dinantian episode, characterised by large volumes

of mildly alkaline basalt to hawaiite magmas, produced the main lava successions. Macdonald (1975) recognised the tholeiitic associations of some of this magmatism, especially in the Scottish Borders. However, his major review of the petrochemistry emphasised the slightly nepheline- or hypersthene-normative (transitional) nature of the basic lavas of this stage.

A post-Dinantian episode produced some hypersthene-normative compositions but was interpreted by Macdonald et al. (1977) as being characterised by quite undersaturated magmas, trending towards nephelinites. Taken with the Dinantian episode, these stages were considered by Macdonald et al. (1977) to represent two thermal cycles, each becoming more undersaturated with time. De Souza (1979), with the aid of isotopic dating, recognised a single thermal event, peaking early in the Dinantian and declining progressively to the Permian with increasingly undersaturated magmas. Francis (1978, 1983), however, cautioned against a literal interpretation of the data of Macdonald et al. (1977). He suggested that the lack of suitable compositions of early Silesian age in the set of data produced an artificial division. Tuffs, a major component of the erupted assemblages in the Silesian, are frequently not analysable for initial magma composition. Thus, the variation in generated magmas through Namurian and Westphalian times is not well established.

The late Carboniferous - early Permian magmas were often very undersaturated. Francis (1983) suggested they may be distinct from the early Carboniferous magmas, and pointed to the intervening episode of intrusion of quartz dolerites. This latter stage represented a completely distinct event of sill and dyke emplacement, with no recognised extruded lavas. It is generally accepted that these quartz tholeiites were not associated with the earlier and later alkalic episodes and appear to indicate a brief event at approximately 295 m.y. (Fitch et al., 1970). No samples from this episode have been investigated in the study. Many of the tholeiites contain no fresh olivine or low-Ca pyroxene and are difficult to interpret petrographically, (Walker, 1935, 1965; Macdonald et al., 1981). Macdonald et al. (1981) have characterised the suite as high Fe-Ti type typical of tensional environments and associated large-scale magma generation.

The Midland Valley and Northumberland Basin represent graben and half-graben structures, respectively. Both are defined by features of pre-Carboniferous origin. Holmes (1965), discussing the association of rift valleys and alkaline magmatism, noted the tendency for volcanic activity to be developed at fractures within a graben, rather than at the bounding fractures. Francis (1978, 1983) confirmed this for the Scottish Permo-Carboniferous province, emphasising the role of pre-existing faults and folds, perhaps controlled by deep-crustal fractures (Upton, 1982). The Dinantian to early Silesian volcanism appears to have been partly controlled by earlier NE-SW Caledonoid fractures. In the Clyde Pateau, lines of volcanic necks with this orientation have been described by Whyte and MacDonald (1974) and Craig and Hall (1975). Activity was concentrated in the Midland Valley and northern margin of the Northumberland Basin in Scotland. In contrast, the late Carboniferous quartz dolerite intrusions were associated with dominantly E-W fracturing. This has been interpreted variously as being associated with the Hercynian orogeny to the south (Francis, 1978) or with the earliest stages of opening of the northern North Atlantic Rift (Russell and Smythe, 1978). The later Carboniferous and early Permian magmatism was associated with rifting along NNW to ENE trends (Francis, 1983). Notably, this late episode of activity extended well beyond the graben structures, forming the very undersaturated dykes of the Scottish Highlands (e.g. camptonites and monchiquites in Argyll, described by Gallagher, 1963). In this way the late alkalic magmatism was distinct from the earlier Carboniferous episode.

The underlying cause of the event(s) producing the Carboniferous-Permian volcanism is not yet established. Accepting that the magmas were ultimately derived by partial melting of a peridotitic mantle, several possible mechanisms for this have been proposed. The mantle itself is believed to have been similar to that producing present-day oceanic alkali basalts, and was perhaps phlogopite-bearing (Macdonald, 1980). Studies of xenolith suites from undersaturated rocks have indicated the mantle was locally very heterogeneous under Britain (Upton et al., 1983), though larger scale variations in trace element concentrations were recognised by

Macdonald (1980). Geophysical studies (Bamford et al., 1978) and inclusion studies (Upton et al., 1976, 1983; Graham and Upton, 1978) have established that the mantle occurs at depths of 30 - 40 km, underlying a high-grade, feldspathic metamorphic basement (granulite-facies), in the Midland Valley and Northumberland Basin areas. MacDonald and Whyte (1981) have suggested this situation has not been substantially modified since Carboniferous times. Several authors (e.g. Upton, 1982; Francis, 1983; Macdonald et al., 1984) have emphasised the intra-plate continental character of the northern British Permo-Carboniferous volcanism, not directly influenced by possible subduction processes to the south of Britain.

With the above comments in mind, only those models explaining within-plate volcanism appear to be applicable to the Permo-Carboniferous province. De Souza (1979) has suggested a tectonic setting far to the rear of a Hercynian subduction zone, with subduction-related mantle upwelling producing alkaline magmatism. The absence of evidence for any subduction component in the volcanism makes this model difficult to assess. However, the role of Hercynian plate motions involving subduction to the south of Britain may be critical. Upton (1982) has suggested that tensional stresses, produced by these plate motions, reactivated earlier fracture systems and helped to generate the magmas, or allowed their passage through the crust. Leeder (1982) has developed a model from the same driving force, where the process of lithospheric stretching, proposed by McKenzie (1978) for the formation of sedimentary basins, can account for the structural and magmatic features of the province. The geophysical evidence of crustal structure is consistent with some degree of crustal thinning. Dixon et al. (1981) have further shown that alkaline magmas can be generated as a direct result of lithospheric stretching, prompting Leeder (1982) to suggest this origin for the Dinantian volcanism of northern Britain. Macdonald et al. (1984), in a study of Dinantian tholeiites in Derbyshire, also envisaged magmas rising from depth along fractures in thinned crust. These authors suggested the large volume of magmas associated with the Midland Valley and Northumberland Basin, compared to other areas such as Derbyshire, may reflect the easy passage of liquids along Caledonian fracture zones reactivated by stretching.

It is anticipated that the ultimate origin of the magmas will not be revealed by investigation of the phenocryst assemblages. The phenocrysts have recorded the subsequent evolution of the magmas on their way to eruption or emplacement. Most recent published studies (e.g. Macdonald, 1975; MacDonald and Whyte, 1981) have invoked polybaric crystal fractionation mechanisms to explain the compositional variations from magnesian basalts to hawaiites. High pressure (>10 Kb) fractionation of clinopyroxene-dominated assemblages and near-surface fractionation of olivine + plagioclase + magnetite assemblages have been suggested. The present study has identified pressure-temperature conditions where different phenocryst assemblages crystallised. Assuming the fractionated assemblages have been represented by phenocrysts in the sample collection, the results of this study may help to understand the evolution of the Permo-Carboniferous basic rocks.

1.3 Aims of Study

There were three major aims of this study. The first was the prediction of the phase relations of basaltic compositions over a range of temperatures and pressures. Equations predicting liquidus temperatures, phases and compositions presented in this study have been combined with an experimental crystallisation model, developed in collaboration with Dr. C. E. Ford. This computer-based model has predicted the phase relations, compositions and proportions of phases for the bulk compositions under investigation.

The second aim was the characterisation of the main textural and chemical features of the phenocrysts in the sample collection. This has included the recognition of cotectic equilibria as well as disequilibrium features in the phenocryst assemblages.

Thirdly, combining evidence from the experimental model and the study of the natural assemblages, the temperatures and pressures of crystallisation of the phenocrysts have been estimated. This has led to a simplified model of the main stages of phenocryst growth in magmas from the province.

1.4 The Samples

The choice of a suitable range of rocks for study depended on three factors. Firstly, a broad range of compositions was required. Because of the empirical nature of the equations in the experimental crystallisation model, only samples within the compositional range of the data sets can be modelled with confidence. For this reason, the sample collection was designed to encompass the range of basic compositions present in the Scottish Permo-Carboniferous suites, thus allowing the model to be applicable to the great majority of basic lavas and intrusions (when fresh) in the province. By studying only basic rocks (less than approximately 52 wt % SiO_2 and composed largely of calcic plagioclases and magnesian pyroxenes $\pm$ olivines, Williams et al., 1982) the aim was to restrict the investigations to essentially anhydrous equilibria.

Secondly, a broad range of phenocryst compositions and assemblages was required. The samples contained various combinations of olivine, clinopyroxene, plagioclase and oxide mineral phenocrysts. By examining such a range, the aim was to identify relative differences in the conditions of crystallisation of the different phenocryst assemblages.

Thirdly, it was important to include samples which represented possible liquid compositions. Very altered samples, or those significantly modified by phenocryst accumulation, have bulk compositions which can be extremely difficult to interpret. The project has been based on the belief that it is possible to relate phenocrysts to the host rock. Although many of the rocks are highly porphyritic, there are compositionally equivalent aphyric or sparsely porphyritic examples for most of them (Macdonald, 1975). Only the most plagioclase-phyric rock types appear to have few aphyric equivalents and may frequently represent plagioclase accumulation. Macdonald (1975) also described samples of similar bulk composition which show a range of phenocryst assemblages. These he interpreted as evidence for progressive phenocryst crystallisation from similar liquids. On the basis of these observations, none of the samples in the present study have been assumed to have undergone phenocryst

accumulation, although the investigation has identified several samples subsequently.

The investigated samples were supplied by Dr. R. Macdonald (Lancaster University), supplemented by six collected by the author. All originated from central and southern Scotland. Powders supplied by Dr. Macdonald were used in the experiments. Thin sections cut from associated hand specimens were used for petrographic study and electron microprobe analysis. Whole rock analyses have been obtained by microprobe analysis of glass beads fused from the powders, and by reference to published descriptions of the samples (Macdonald, 1975; Macdonald et al., 1977; Clark, 1956). Brief details of the samples are presented in Appendix 1, including sample identifier, source area, phenocryst assemblage and phenocryst modal proportions. Except for those samples collected for the present study, the rock identifiers have been taken directly from Dr. Macdonald's catalogue. Parts of this catalogue have been tabulated in Macdonald (1975) and Macdonald et al. (1977). The initial selection of the samples was made by Dr. Macdonald and covers a broad range of basic compositions, phenocryst contents, source areas and ages. Such a collection is suited to establishing a petrochemical grid, as individual samples are not directly related to one another. However, while the aim of interpreting the phenocrysts was not affected, the poor coverage of individual lava successions has restricted the discussion of local magmatic evolution.

Classification of the rocks as basalts, basaltic hawaiites and hawaiites has followed Macdonald (1975). Distinctions were made on the basis of normative anorthite content (An) of the bulk compositions. Basalts have $An>50$. Basaltic hawaiites have $45<An<50$. Hawaiites have $30<An<45$. Some of the hypabyssal intrusions have been referred to using the terminology of the original published descriptions. Little emphasis has been placed on detailed classification of these rocks in the present study, because there is no simple correlation between the phenocryst assemblages of interest and the host rock types. To have rigidly separated the samples on the basis of rock type would have artificially separated similar

phenocryst assemblages. In all, 42 porphyritic rocks and 4 ultramafic inclusions have been investigated.

1.5 The Approach Adopted in this Study

Isothermal atmospheric pressure melting experiments, carried out under controlled oxygen fugacities, have provided a large set of glasses (interpreted as quenched liquids) coexisting with combinations of olivine, high-Ca clinopyroxene, plagioclase, spinel, magnetite, ilmenite and apatite. Microprobe analysis of the phases in the experimental charges has resulted in sets of mineral-glass compositional pairs, and sets of glass compositions coexisting with individual phases, at known temperatures.

For the sets of glass compositions, it has been assumed that the temperature at which a mineral crystallises is a function of the melt composition (French, 1971; Roeder, 1975; Nathan and Van Kirk, 1978). Therefore, equations have been derived using least-squares multiple linear regression, relating melt composition to temperature for olivine, clinopyroxene, plagioclase and spinel (including magnetite). These mineral temperature equations, taken together, predict the liquidus phase or phases of basaltic liquids at atmospheric pressure.

For the sets of mineral-glass pairs, it has been assumed that the concentration of an element in the mineral is a function of the concentration of that element in the melt, at a given temperature. Rudimentary mineral composition equations describing this have been derived by least-squares regression for the same minerals as for the mineral temperature equations.

To extrapolate these equations beyond the range encompassed by the experiments, comparable data from published studies have been incorporated. In the case of the mineral composition equations, this has allowed some estimate of the effects of pressure.

The equations have been combined with expressions describing equilibrium and fractional crystallisation, developed by Dr. C. E. Ford. A computer program developed in association with Dr. Ford allows the

experimental modelling of the crystallisation of basic liquids. With the incorporation of simple pressure correction factors into the mineral temperature equations, it has been possible to predict the equilibrium phase relations of the samples in this study at a range of pressures, up to 20 Kb or more.

The natural rocks have been studied to find evidence bearing on the origin of the included phenocrysts. Variations in bulk composition have been considered, although these were not examined rigorously since direct links between samples have not been established. The main emphasis has been placed on the petrography and mineral chemistry of the phenocrysts themselves. Textural evidence of rapid crystal growth and partial resorption indicates disequilibrium processes, which can not be adequately dealt with in the crystallisation model. Other evidence indicating cotectic behaviour has helped to define the conditions in which phenocrysts crystallised. Systematic variations in phenocryst compositions, together with individual crystal zoning trends, have provided qualitative estimates of the conditions of origin of the phenocrysts.

Combining the evidence from the natural rocks with the predicted phase relations of the experimental crystallisation model, interpretation of the origin of some phenocrysts has been attempted. The ability of this approach to identify possible common stages of evolution between samples has been discussed together with limitations of the model. Because of mineral equilibration problems in the experiments, limited knowledge of the effects of pressure on mineral compositions crystallising, and the complexity of the natural phenocrysts themselves, the comparison of predicted mineral compositions and observed phenocryst compositions has been restricted to simple element ratios, such as $Mg/(Mg + Fe^{2+})$ and $Ca/(Ca + Na + K)$. Some discussion of the origin of the phenocrysts has been made in the light of evidence from published studies.

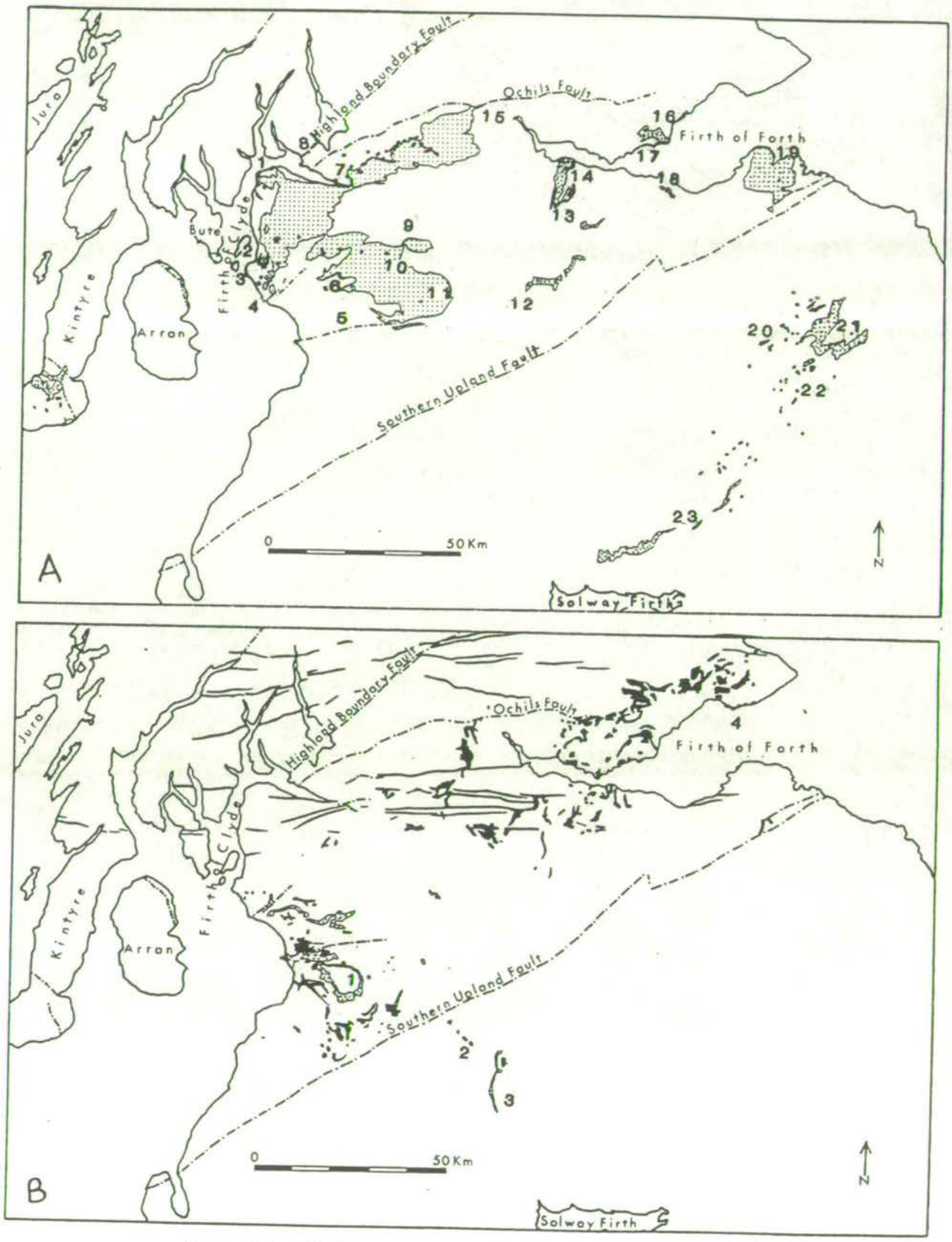

Figure 1-1. Principal outcrop areas of Dinantian (A) and Silesian & early Permian (B) extrusives (stippled) and intrusions (solid) in central and southern Scotland, from Upton (1982).

A) 1,Greenock; 2,Great Cumbrae; 3,Little Cumbrae; 4,Ardrossan; 5,Kilmarnock; 6,Dunlop; 7,Dumbarton; 8,Ben Bowie; 9,Glasgow; 10,Eaglesham; 11,Strathaven; 12,Lanark; 13,Bathgate; 14,Linlithgow; 15,Stirling; 16,Kirkcaldy; 17,Burntisland; 18,Edinburgh; 19,North Berwick; 20,Melrose; 21,Kelso; 22,Jedburgh; 23,Langholm.

B) 1,Mauchline; 2,Sanquhar; 3,Thornhill; 4,Elie.

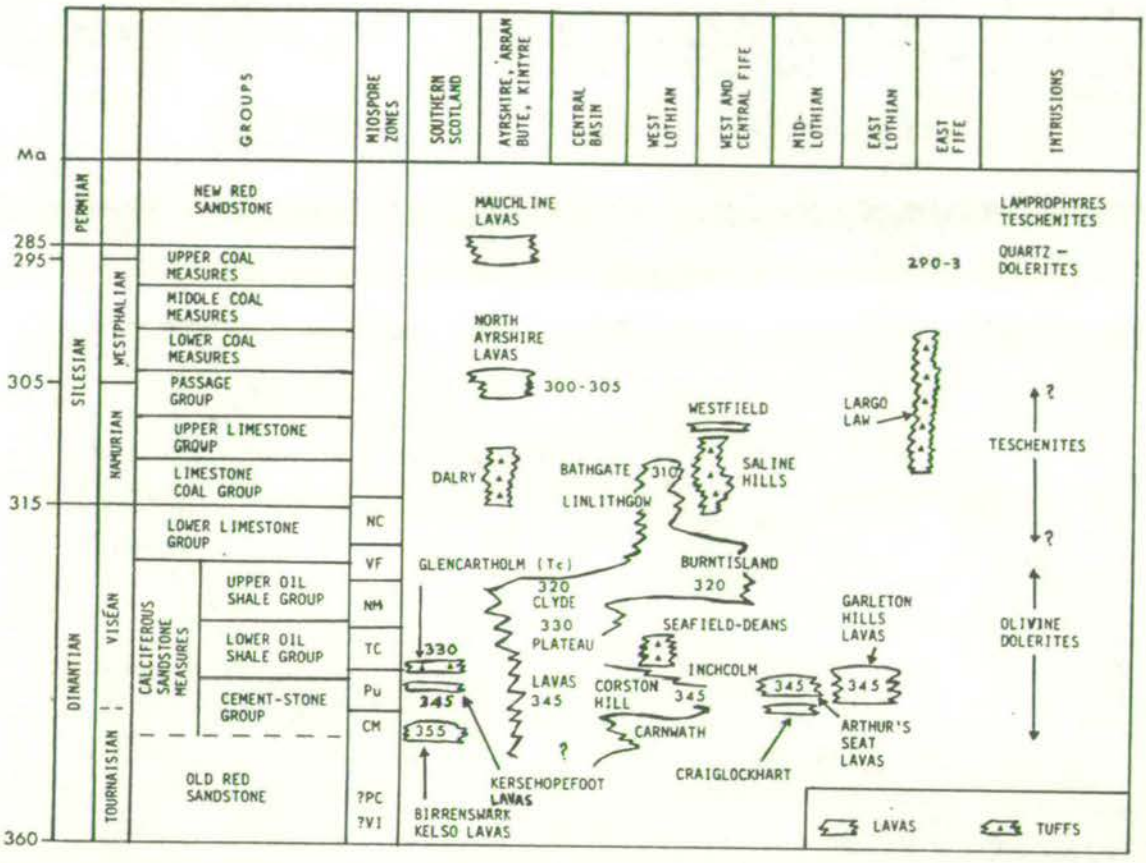

Figure 1-2. Range and distribution of Carboniferous and early Permian volcanism in central and southern Scotland, from Francis (1983). Dates (radiometric) are mainly from De Souza (1974,1979).

CHAPTER 2

EXPERIMENTAL TECHNIQUES

2.1 Introduction

The main aims of the experimental programme were twofold. Firstly, by melting a range of natural basic rocks at atmospheric pressure over a range of temperatures and oxygen fugacities, a series of experimental charges composed of crystals plus glass (quenched liquid) were obtained. The compositions of the coexisting crystals and glass, as determined by electron microprobe, have provided the basis for the predictions of crystal-liquid equilibria made in later chapters. Secondly, the experiments have provided some evidence on the origin of the phenocryst assemblages frequently used to classify these rocks.

2.2 Starting Materials

Samples provided by Dr. R. Macdonald had been ground in colmonoy (a nickel-chrome alloy) and particle sizes were <100μ. Early experiments carried out on these rock powders frequently contained large zoned crystals, interpreted as relics from the starting material. As a result the powders were re-ground in an agate micronizer in acetone until particle sizes were <15μ.

2.3 Furnace Operation

The atmospheric pressure experiments were carried out in a vertical quench furnace, consisting basically of an alumina tube surrounded by a Pt 10% Rh heating element, and made air-tight by O-rings. A control thermocouple embedded in the furnace was linked to a West Instruments Ltd. Viscount controller. The controller was capable of maintaining the thermocouple to within 0.15° C of a set point for the duration of a run. A further thermocouple sat about 1 cm above the samples inside an inner alumina tube in the axial probe assembly. With a calibration correction, this axial thermocouple allowed the operator to monitor the sample temperature at all stages of the experiment. By measuring the temperature of the axial thermocouple at various depths in the furnace, two thermal

profiles were obtained (see Figure 2-1). An appropriate gas mixture was passed through the furnace, and a dummy assemblage of samples was attached to the probe assembly during the determination of the profile, to closely duplicate the normal operation of the furnace. Temperatures were measured at 1 cm intervals after allowing 45 minutes for the thermocouple to stabilise. By calibrating the furnace, and running samples at the position of the thermal maximum, the possibility of superheating was greatly reduced. Due allowance was made for the variation with temperature of the position of the thermal maximum. Previous studies (Humphries, 1975) have indicated the horizontal temperature gradient to be less than ½° C in these furnaces. Further details of the experimental set-up used in this study are contained in Biggar and O'Hara (1969).

2.4 Temperature Measurement

During a run, the temperature was monitored by measuring the E.M.F. of the axial thermocouple, using a galvanometer and precision potentiometer with ice/water junction. The E.M.F. was converted to a temperature using conversion tables for Pt : Pt 13% Rh thermocouples. A calibration correction value was added to this obtained temperature to give the run temperature of the samples. The calibration correction value was found from melting experiments on lithium metasilicate. This compound has a known melting point of 1208° C (see Biggar, 1972), and so the apparent temperature of the axial thermocouple can be calibrated against the melting point of the lithium metasilicate. Small amounts of the calibrant were placed in a crimped Pt capsule and run with a typical sample assembly to mimic normal run conditions. Run times were kept to less than 3 hours to avoid possible volatilisation of Li. The run product was often difficult to interpret as some glass occurs in runs at temperatures well below 1208° C. In this study, samples composed entirely of 1) glass or 2) glass + elongate acicular quench crystals or 3) glass + spherulite-like clusters of quench crystals, were interpreted as having been run at 1208° C or higher. Samples composed largely of original lithium metasilicate with more than 20% glass or quench crystals were interpreted as having been run within 5° C of the melting point. Samples with only a few percent glass or

quench crystals probably represented runs at temperatures well below 1208° C. In this way the melting point of lithium metasilicate was bracketed to within 2 - 3° C normally. Experiments were run at temperatures between 1074° C and 1334° C. In this range the melting point of lithium metasilicate is central. However, at the more extreme ends of the range the calibration correction value may change by a further 1 - 2° C. Bearing in mind additional factors possibly affecting the absolute run temperature (i.e. variation of the controller temperature, drift in the output E.M.F. of the thermocouple between calibrations, slight differences in the position of the run assembly relative to the furnace thermal maximum) the overall precision of the quoted run temperature is estimated as being ± 3° C on average.

2.5 Oxygen Fugacity Control

The oxygen fugacity of the furnace atmosphere was controlled by a $CO_2 - H_2$ gas mixture with an approximate flow rate of 1 cm/sec down through the furnace (see Biggar, 1974a; and Humphries, 1975, for details). A katharometer measured the proportions of each gas in the mixture. The relative amounts of H_2 and CO_2 were chosen from Deines et al. (1974) to give oxygen fugacities corresponding to the position of the Ni - NiO buffer in most cases, and less commonly to the Fe - FeO buffer. The original choice of the Ni - NiO buffer was made on the basis of numerous estimated oxygen fugacities and temperatures from iron-titanium oxides in basalt lavas (cf. Haggerty, 1976, for compilation). This choice was supported by studies of the natural assemblages, described in Chapter 6. In order to extrapolate mineral temperature equations over a range of oxygen fugacities, a number of experiments were run at the Fe - FeO buffer. Calibration samples of NiO powder on Ni wire, or Fe_2O_3 powder on Pt wire, were added to many of the runs to check the proximity to the appropriate buffer. These runs are shown in Figure 2-2 with oxygen fugacities from Deines et al. (1974) and the positions of the buffer curves from Ulmer (1971). There appears to be good agreement between the predicted oxygen fugacities of Deines et al. (1974) and the buffer samples, relative to the buffer curves. Thus the quoted oxygen fugacity for each run is that predicted by Deines et al. (1974). The precision in these quoted figures is approximately ± 0.2 log

units fO_2. The use of $H_2 - CO_2$ mixtures means H_2O is formed in the reaction. As a result, about 0.25 bars H_2O pressure occurs in the furnace and this may have had a small effect on the determined phase relations. Biggar (1981) compared two compositions at atmospheric pressure using $CO - CO_2$ and $H_2 - CO_2$ mixtures at low oxygen pressures. One composition run in a $CO - CO_2$ atmosphere produced plagioclase + olivine, when only a few plagioclase crystals were present in comparable conditions in an $H_2 - CO_2$ atmosphere. The bulk Na content of these two charges is not known, so variable Na volatilisation must be considered as a cause of the difference. However, it is possible that the low water pressure in the $H_2 - CO_2$ run depressed the liquidus by a few degrees, relative to the "dry" $CO - CO_2$ run. Further research is required to assess the differences in determined phase relations using $CO - CO_2$ and $H_2 - CO_2$ gas mixtures.

2.6 Sample Holder Materials

The problems of finding a holder material that will not react with natural silicate compositions are well known (e.g. O'Hara and Humphries, 1977; Grove, 1981). For high temperature melting studies on basalts, capsules of Pt and its alloys have been widely used despite the recognised large losses of Fe from the samples. In an attempt to reduce these losses, Presnall and Brenner (1974) introduced wire loops in place of capsules. By greatly lowering the area of contact between sample and holder, the samples retained nearly all their Fe. The advantages and disadvantages of wire loops have been further assessed by Donaldson (1979), and Corrigan and Gibb (1979). Donaldson (1979) showed that Fe losses for Pt_{80} Rh_{20} wire increased as run time increased and as oxygen fugacities decreased. Significant losses of Na and K occurred at the Ni - NiO buffer and became severe at the Fe - FeO buffer, particularly for Na. However, for experimental runs of up to 1 day at the Ni - NiO buffer, experimental losses were small and Fe, Na and K recoveries were all >90%. Corrigan and Gibb (1979), using Pt and Ag_{40} Pd_{60} wires, found similar losses to Donaldson of Fe and Na at the Ni - NiO buffer, and emphasised the importance of a high ratio of sample to metal in reducing Fe loss. Again, to keep Na losses down, they suggested run

times of "less than a few days". Biggar (1978) and Benhamou (1978) employed the wire hook technique in the Edinburgh laboratories, and found improved iron recoveries for Pt wire compared to Pt capsules, although some samples still lost up to 32% of their iron to hooks. In this study, a few early experiments were made with Pt wire hooks but all later runs employed Fe-doped Pt hooks (0.2 mm diameter). The Fe-doped wire hooks were made either by the process of Ford (1978), or by re-using Pt wire hooks for all experiments on individual compositions, as suggested by Walker et al. (1979). Re-using Pt-Fe alloys for experiments on individual compositions is believed to minimise Fe exchange in runs at only slightly differing conditions. As the saturation technique of Walker et al. (1979) requires initial runs with Pt, which may involve significant Fe exchange, it was thought preferable to start with presaturated wire. The main problem with the alloy is its brittle nature. The wire is liable to break when being wound on to the supporting frame and so its re-use is virtually impossible. To overcome this difficulty, small hooks of Pt-Fe wire were welded onto lengths of malleable Pt wire. Thus, the wire could be attached to the frame repeatedly yet the sample was only in contact with the Fe-doped hook. With careful handling, examples of this arrangement lasted for up to nine consecutive runs.

To compare the Fe recovery from Pt hooks with that from Pt-Fe hooks, a near-aphyric hawaiite was melted about 10° C above its liquidus at Ni-NiO, using both wire types, for 5 hours and 24 hours. Wavelength dispersive microprobe analyses of the resulting glasses were made. Two samples on each wire type were run and analysed. In all cases most of the Fe loss occurred in the first 5 hours. The samples on Pt lost 8.5 - 10% of their Fe in 5 hours, and 13 - 15% in 24 hours. The samples of Pt - Fe wire lost 1 - 2.5% of the Fe in 5 hours, and 2 - 4% in 24 hours. Potassium recovery was about 95% for all samples, with fractionally more being lost in the 24 hour run. Sodium recovery was also about 95% for all samples, with the initial assumption of no loss during microprobe analysis. All the figures have been based on the analysis given for MV39B by Macdonald (1975). Clearly, for this sample, Pt-Fe wire hooks gave very good results for the problematic major elements. All the samples lost consider-

able amounts of Ni to their wire holders, even in the shorter run time. The microprobe analyses also showed that the charges were all essentially homogeneous, although there appeared to be slightly enhanced Fe loss within a few microns of the Pt wire hooks.

An isolated, very small amount of sample in contact with Pt wire lost 98% of its Fe, illustrating that the use of wire hooks does not guarantee good Fe recovery. In general, as large a bead as possible should be placed on the wire hooks, as emphasised by Corrigan and Gibb (1979).

During the experimental programme, 5 compositions were melted at the Fe-FeO as well as at the Ni-NiO buffers. Pt-Fe wire hooks were used also at the lower oxygen fugacities. Relative to the results at Ni-NiO, the runs at Fe-FeO generally gave slightly poorer recoveries for Fe. Three compositions gave Fe values within a few percent of the Ni-NiO values (MV160, MV402, MV40B). Two compositions lost significant Fe, (MV166, MV106); the poorest recovery being 85% of the equivalent Ni-NiO value (MV166 at near liquidus temperatures). However, the vast majority of the runs on these two compositions gave very similar recoveries to the Ni-NiO values, with the problem declining markedly with falling temperature. The problem of sodium and potassium loss was more severe at Fe-FeO but was very strongly dependent on the starting composition and temperature. Only one composition showed K loss (MV166). At near-liquidus temperatures, up to 40% of the Ni-NiO K value was lost, although K recovery increased dramatically at lower temperatures. MV166 also showed the most severe sodium loss. Up to 50% of the Ni-NiO value was lost at the highest temperatures but, like K, Na recoveries increased greatly at lower temperatures. MV160 and MV106 lost some Na at near-liquidus temperatures; perhaps up to 15% of the Ni-NiO value at worst, but generally very little. MV402 and MV40B gave similar recoveries for Na at Fe-FeO as at Ni-NiO.

In summary, Pt-Fe wire hooks appear to give good recoveries of Fe, and possibly Na and K, at Ni-NiO. At Fe-FeO, Fe recoveries are still acceptable but Na and K losses may be considerable, depending on composition. Losses of Fe, Na and K increase with

increasing temperature and run time, and with decreasing oxygen fugacity, but are also strongly dependent on starting composition. In the above discussion, Fe losses were greatest for the most mafic compositions (and hence highest temperatures liquidi). Volatile losses were also significant for the most mafic compositions, but were most severe in the nepheline-normative, mafic, high temperature charges. In this study, recoveries of all the major elements appear good, with the possible exceptions of the specific cases cited above. Molybdenum capsules may be more suitable for experiments at the Fe - FeO buffer (Biggar, 1970).

2.7 Run Procedure

Experiment temperatures were preset a number of hours before the samples were placed in the furnace. This avoided possible temperature fluctuations affecting the samples. Up to six samples could be attached to a supporting Pt frame, although five was a usual maximum to avoid any contact between neighbouring beads. This included temperature and buffer calibrants if any. Biggar (1978) suggested polyvinyl alcohol to moisten powdered samples into beads for placing on the wire hooks, but in this study distilled water was found to be more convenient. Once the wire hooks with drying sample had been wound onto the frame, together with calibrants, the frame was carefully attached to the furnace probe with thin Pt fuse wire. The whole assembly was placed in the top of the furnace and carbon dioxide was passed through the system to flush out air. Hydrogen was then mixed with the carbon dioxide to the required proportions. This gas mixture was always obtained before the samples reached run depth. Meanwhile the probe assembly was lowered 3 cm every 15 minutes until the samples were 2.5 cm above run depth. The assembly was left at this position for a full hour. Then the samples were lowered 1 cm per 10 minutes until 0.5 cm above run depth. After a further 10 minutes the assembly was lowered to the run depth. In this way, any superheating of the samples was avoided. Run time commenced from this point and was normally 5 - 24 hours. Temperature calibration runs were usually 2 - 2½ hours, which was probably long enough to establish equilibrium ferric-ferrous ratios in the samples (Thornber et al., 1980), but not long enough for Li

volatilisation to affect the calibrant. The upper limit of 24 hours was chosen to avoid possible Na and K volatilisation problems (see previous section). At the end of the run, the thermocouples were read and the support frame was dropped into a beaker of shallow water, by blowing the fuse wire. On average, fewer beads shattered on quenching in shallow water than in a near-full beaker. Quenching is very rapid by this technique and no typical quench crystallisation features were found in the charges.

2.8 Sample Identification

The sample beads were crushed with an agate mortar and pestle and the wire hook stored for re-use after each run. As microprobe analysis was one of the main aims of the project, most samples were mounted on a glass slide in araldite and then polished. Sample identification was usually based on optical examination of these slides, frequently confirmed by microprobe analysis. A useful additional step in preparation of the samples prior to identification was to polish the slides on a cloth lap with very fine alumina powder. This etched strong relief into the phases in the charges and proved invaluable in distinguishing minerals. Samples were re-polished before analysis to remove the strong relief. In addition to glass, six crystal phases were identified:

a) OLIVINE was colourless in transmitted light with high positive R.I. relative to glass. At near-liquidus temperatures it was frequently euhedral, but at lower temperatures usually formed rounded crystals. In reflected light, olivine appeared pinkish-white with a pronounced etched relief above the surrounding glass, which appeared grey.

b) PLAGIOCLASE was colourless in transmitted light with low negative R.I. relative to glass. At near-liquidus temperatures it formed euhedral, slightly elongate, plate -like crystal laths. At lower temperatures the habit was similar although more rounded. In reflected light, plagioclase was a darker grey than the host glass and usually had a slight negative relief relative to the glass.

c) CLINOPYROXENE was colourless in transmitted light with high positive R.I. relative to glass. In habit it was similar to rounded olivine crystals, although it could occasionally be distinguished by the occurrence of slightly elongate grains. In reflected light, it appeared greyish-white and had no etched relief relative to the glass. These characteristics of clinopyroxene in reflected light allowed it to be easily distinguished from olivine.

d) 'SPINEL' was translucent brown at high temperatures and opaque at lower temperatures in transmitted light. At near-liquidus temperatures large euhedral crystals occasionally occurred, but generally the 'spinel' formed very small rounded grains. In reflected light, 'spinel' was very bright pinkish-white and had a very pronounced etched relief above surrounding glass. In general, the low temperature crystallisation of magnetite was marked by a significant increase in grain size, relative to the higher temperature Cr-spinels.

e) ILMENITE was opaque in transmitted light, forming small rounded grains. In reflected light, ilmenite was distinguished from coexisting magnetite by having a higher reflectivity.

f) APATITE was identified in only one sample. It was colourless in transmitted light with a slightly higher R.I. than the glass. Only rounded anhedral grains were observed. In reflected light it had similar reflectivity to plagioclase.

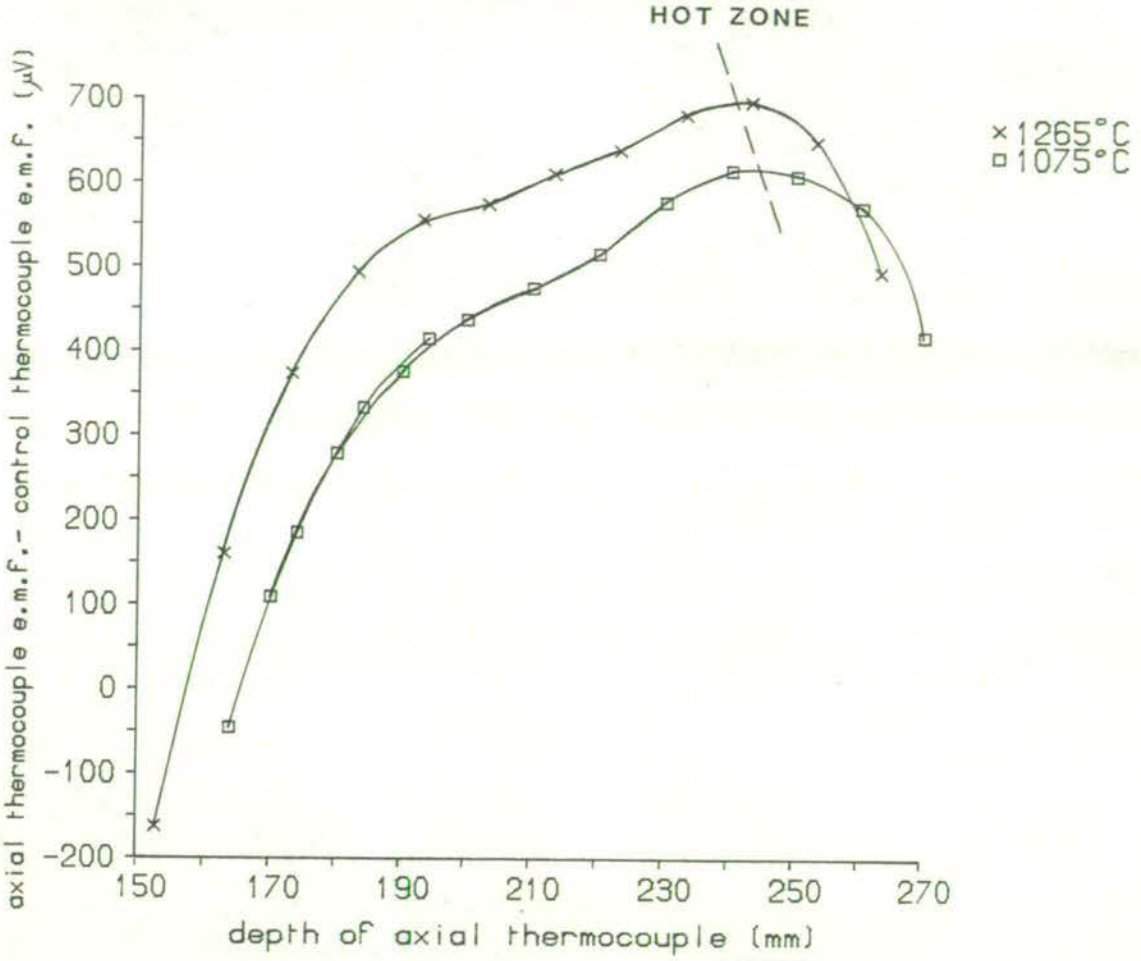

Figure 2-1. Thermal profile of Furnace 7, showing the variation in depth of the hot zone with temperature.

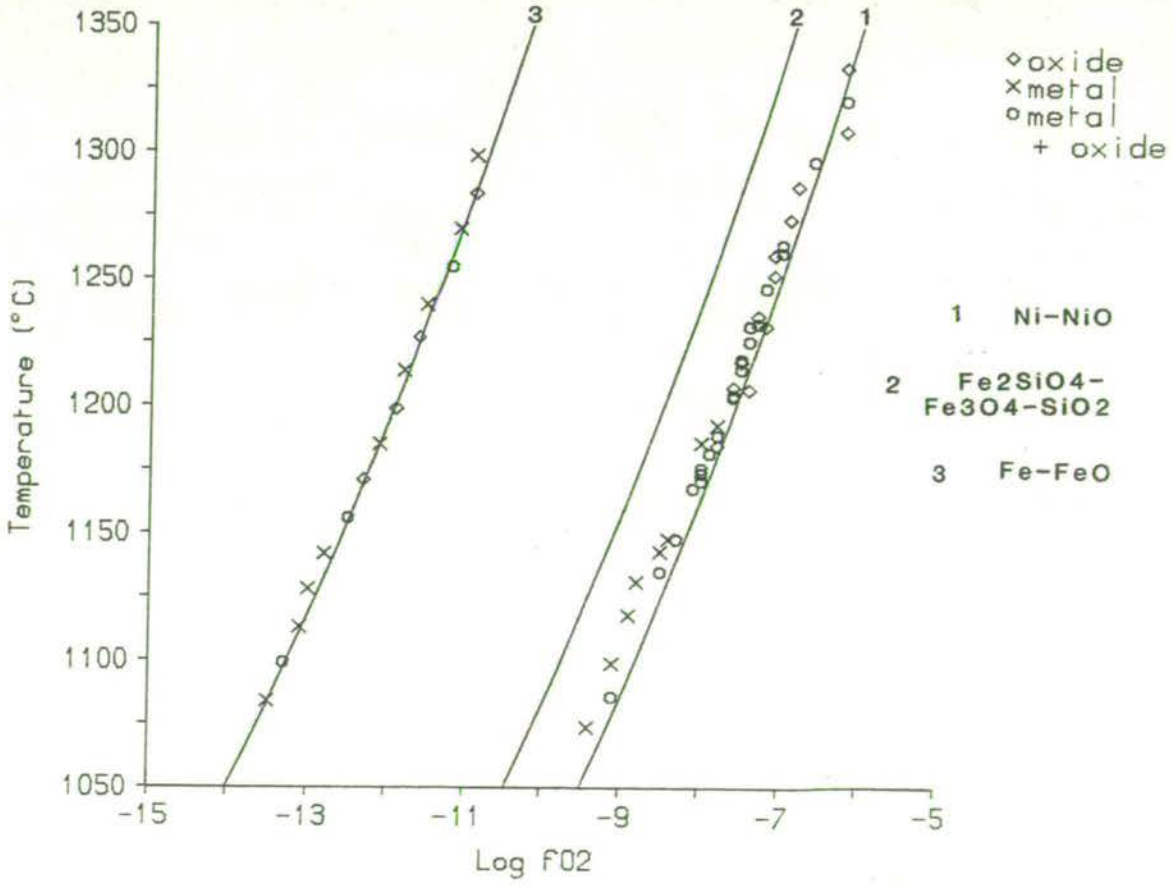

Figure 2-2. Resulting buffer assemblages in the experiments, relative to the Ni-NiO and Fe-FeO buffer curves of Ulmer (1971).

IT IS ALWAYS GOOD
WHEN A MAN HAS TWO IRONS IN THE FIRE.

Francis Beaumont.

CHAPTER 3

ESTIMATION OF THE FERRIC-FERROUS RATIO IN EXPERIMENTAL GLASSES

3.1 Introduction

Experiments on basaltic compositions at oxygen fugacities corresponding to the Ni - NiO buffer produce glasses with significant Fe_2O_3 contents. Electron microprobe analysis of these glasses can only determine the total Fe content, usually expressed as FeO. In crystalline phases, such as spinels, magnetites and ilmenites, it is possible to estimate the Fe_2O_3 content on the basis of assumed stoichiometry. However, for glasses, the usual course taken is to assume all Fe as FeO or to use a constant ferric-ferrous ratio (e.g. Fe^{3+}/Fe^{2+} in oceanic basalt glasses is often assumed to be 0.15).

For the purpose of determining mineral-liquid equilibria involving distinct Fe^{2+} and Fe^{3+} components, it is desirable to have some means of estimating the ferric-ferrous ratio in glasses over a range of temperatures, oxygen fugacities and liquid compositions.

A number of different ways of estimating FeO and Fe_2O_3 can be considered. Wet chemical analysis would probably be most reliable, but when crystalline phases are present it is often very difficult to accurately correct the glass composition. Where partition coefficients are well known it may be possible to calculate the FeO and Fe_2O_3 contents of glass from the coexisting mineral compositions. Unfortunately, few partition coefficients are sufficiently well known to precisely predict glass compositions. At best, distribution coefficients, such as the Fe^{2+}-Mg exchange coefficient between olivine and liquid, can be used to check the plausibility of a predicted FeO/Fe_2O_3 ratio (Cawthorn et al., 1973).

Empirical oxidation ratios are often applied to natural and experimental data. These ratios may have been deduced from numerous wet chemical analyses of supposed liquid compositions. Their limitations are probably only apparent when they are applied to suites of rocks which are of significantly different compositions to the reference suite, or when different oxidation ratios have occurred in similar melt compositions.

3.2 Empirical Expressions Excluding Melt Composition

An approach adopted for experimental glasses is to derive an expression relating the oxidation ratio to determinable parameters such as temperature and oxygen fugacity. This is most useful for modelling experimental results where the effects of adjusting the variables can be compared with observed variation. Roeder and Emslie (1970) presented an equation (1) relating the oxidation ratio in glasses to the oxygen fugacities of experiments on an olivine basalt at atmospheric pressure at 1200° C

$$\mathrm{Log}_{10} \frac{X_{FeO}}{X_{FeO_{1.5}}} = -0.20\ (\mathrm{Log}_{10} fO_2) - 1.04 \qquad \ldots (1)$$

Compositional terms are mole fractions. This equation fits their data well, illustrating the dependence of the oxidation ratio on the oxygen fugacity when temperature and composition are essentially constant. However, some consideration of the effect of at least temperature is desirable. Kennedy (1948) showed that increasing temperature at constant oxygen fugacity decreases the ferric-ferrous ratio of basaltic melts. Nathan and Van Kirk (1978) derived an equation (2) from published experimental data in the system Fe-Si-O.

$$\mathrm{Log}_{10} \frac{Fe^{3+}}{Fe^{2+}} = 2.852 + 0.188\ (\mathrm{Log}_{10} fO_2) - 0.00128\ T°K \ldots (2)$$

Compositional terms are in cation fractions. This equation fits the data closely and can be applied over a wide range of temperatures and oxygen fugacities. Its main limitation is its insensitivity to the effects of elements other than Fe and Si.

3.3 Empirical Expressions Including Melt Composition

Paul and Douglas (1965) studied the ferric-ferrous equilibrium in alkali silicate glasses. They found that, at constant temperature and oxygen fugacity, the ferric-ferrous ratio of the melts increased with increasing concentrations of K, Li and Na. K had the greatest effect. A positive correlation between ferric-ferrous ratio and total alkali (or normative feldspar) content of natural liquids has been shown by Carmichael et al. (1974). Further studies of the effect

of composition on the ferric-ferrous ratio in basaltic liquids have been described by Thornber et al. (1980). They confirmed the effect of K and Na in increasing the Fe^{3+}/Fe^{2+} ratio and have indicated similar effects (to a lesser degree) from the addition of Si, Al and Ca. Thornber et al. also showed that the effect on the ferric-ferrous ratio of adding these components decreased at higher temperatures.

In the approach adopted throughout this study, an empirical relation between ferric-ferrous ratio and oxygen fugacity, temperature and liquid composition has been derived. Initially, 103 experiments containing FeO and Fe_2O_3 determinations in glasses were obtained from Thornber et al. (1980), Hill and Roeder (1974) and Fudali (1965). Of these, 19 were discarded due to evidence of Fe loss, inconsistency with similar experimental data, or the possibility of the presence of crystalline phases which had not been corrected for. The remaining experiments have known temperature, oxygen fugacity and major element bulk composition. The composition can be thought of as a set of distinct element terms. Expanding the approach of Nathan and Van Kirk (1978), the ferric-ferrous ratio of the melt may be considered to be a function of the temperature, oxygen fugacity and major element composition of the melt. A number of empirical formulations relating these terms have been derived by regression analysis. The regression coefficients were calculated by least-squares multiple linear regression using a computer program provided by Dr. R. F. Cheeney. The best fit to the data was obtained by an expression derived for Ln fO_2 which is presented below as equation (3), rearranged in terms of the ferric-ferrous ratio. The coefficient of least squares fit for the equation is 0.983 ($\sigma = 0.3\ \mathrm{Log}_{10} fO_2$).

$$\mathrm{Ln}\left(\frac{Fe^{3+}}{Fe^{2+}}\right) = -6.74193 + \frac{13446.6}{T^{\circ}K} + 0.21815\ (\mathrm{Ln}\ fO_2) - 1.63329(Al) + 8.35929(Ti) - 1.2928(\Sigma Fe) - 1.15052(Mg) + 2.01686(Ca) + 2.65990(Na) + 5.54450(K) \quad \ldots (3)$$

Compositional terms are in cation fractions with $\Sigma Fe = Fe^{2+} + Fe^{3+}$. Rearranging such equations can lead to significant errors (Williams, 1983), but predicted results are similar to those predicted for

basalts by the equation of Sack et al. (1980) which was derived from a larger data set. Sack et al. (1980) added 57 determinations of glass ferric-ferrous ratios to the published data, and from a data set of 143 experiments, generated an equation (4), by a least-squares method in similar fashion to that adopted in this study. Compositional terms in their equation are in mole fractions. FeO* refers to all Fe expressed as FeO.

$$\text{Ln}\left(\frac{X^{\text{LIQUID}}_{Fe_2O_3}}{X^{\text{LIQUID}}_{FeO}}\right) = -4.49933 + \frac{13184.7}{T^\circ K} + 0.21813\,(\text{Ln}\ fO_2)$$
$$- 2.15036\,(X_{SiO_2}) - 8.35163(X_{Al_2O_3})$$
$$- 4.49508(X_{FeO^*}) - 5.43639(X_{MgO})$$
$$+ 0.07311(X_{CaO}) + 3.54148(X_{Na_2O})$$
$$+ 4.18688(X_{K_2O}) \qquad \ldots\ (4)$$

3.4 Discussion

The main differences between equations (3) and (4) are in the choice of compositional terms incorporated. Sack et al.(1980), apart from having the broader compositional range in the initial data set, include a term for SiO_2 but ignore TiO_2. Equation (3) is only designed for basaltic compositions and has no Si term, but does include Ti as this can be significant in the compositions in the present study. The effect of Si is compensated for in the equation; as Si increases so the sum of the remaining cations must decrease. In practice, both equations respond in the same way to variations in Si and Ti. Neither equation considers the effects of P, Cr or Mn. Both equations show an increase in the ferric-ferrous ratio as K, Na, Ca, Ti or the fO_2 increase. Decrease of the ferric-ferrous ratio can be produced by increasing Si, Al, total Fe, Mg or temperature.

Eighteen analysed compositions from Sack et al. (1980) are considered approximately similar to glasses produced in this study. When equation (3) is applied to those compositions the results are slightly higher predicted ferric iron contents than the wet chemistry indicates (on average 0.2 wt % Fe_2O_3 higher). Sack et al.'s own equation (4), also predicts a slightly high ferric-ferrous ratio for these eighteen compositions in general, so the differences in calculated values are less. Bearing in mind that these data were

used in the derivation of equation (4), this latter equation would be expected to predict the results better than equation (3). However, when the associated experimental problems and precision levels are considered it is likely that the differences in predictions are not significant. Of more importance is the extrapolation of the equations to regions outside the ranges of the input data sets, particularly to lower temperatures and higher oxygen fugacities. Neither equation can be guaranteed under these circumstances, although equation (4) can probably be applied to a broader compositional range of igneous melts. Extrapolating to low temperatures may lead to significant errors. Sack et al. have shown that equation (4) produces an acceptable fit of natural data down to approximately 1100° C at least. Although equation (3) has not been tested in this way, it is considered significant that equation (3) predicts the ferric-ferrous ratios of the lowest temperature basic glasses in the data set of Sack et al. better on average than equation (4). In the absence of a better means of predicting ferric-ferrous ratios, and since equation (4) is not considered to be significantly better for the basaltic compositions discussed here than equation (3), the analyses recalculated by equation (3) in the remainder of the thesis have not been reprocessed. For much of the argument, the absolute values of FeO and Fe_2O_3 are less important than the relative values between glasses.

Future development of these empirical equations could begin to consider the role of melt structure in determining ferric-ferrous ratios. Dickenson and Hess (1981) have indicated the different roles of elements as charge-balancing cations and network modifiers, showing that the generalised picture of a single effect for an element, presented above, is over-simplified. More judicious choice of starting compositions could be used to extend the temperature and oxygen fugacity range adequately. Kilinc et al. (1983) carried out ferric-ferrous determinations of natural liquid compositions equilibrated in air. They combined their results with the data of Sack et al. (1980) and have produced an equation which predicts the ferric-ferrous ratios of a range of natural silicate melts at high oxygen fugacities. Although high oxygen fugacities are of lesser interest in the present study, the data emphasise that equilibration

of lavas in air does not result in the conversion of all Fe to Fe^{3+}.

The ferric-ferrous ratio in a natural silicate liquid is a function of (at least) temperature, oxygen fugacity and melt composition. Using equation (3), the ferric-ferrous ratio in an alkali-rich basalt can be higher than that in a similar, but alkali-poor basalt at the same temperature and oxygen fugacity.

Examples of the Results for Equations 1 - 4

Three examples of using the equations are presented in Table 3-1. Electron microprobe analyses of olivine-glass pairs from the atmospheric pressure experiments have been tabulated. The olivine-liquid Fe^{2+}-Mg exchange coefficient (KD) has been calculated for each pair. If the range of KD from 0.28 - 0.36 is taken to represent the values found in terrestrial basalts (Langmuir and Hanson, 1980) then all the equations produce plausible results. In detail, the higher values of the range of Langmuir and Hanson were produced in high pressure melting experiments (Bickle et al., 1977).

For the tabulated results for GL3, equations (1) and (2) predict values of KD which may be anomalously high. For equation (1) (Roeder and Emslie, 1970), the high KD probably results from extrapolating the equation to high temperatures away from 1200° C, where the equation was based. For equation (2) (Nathan and Van Kirk, 1978), the value of KD = 0.33 is only high compared to the results for equations (3) and (4). Equation (3), used throughout the present study, produces values of KD which lie comfortably within accepted ranges of the coefficient. Equation (4) (Sack et al., 1980) also produces results close to the commonly used value of KD = 0.30, and consistently predicts KD values which are 0.01 less than those of equation (3). This reflects the lower predicted Fe_2O_3 contents of glasses using equation (4), compared to equation (3). However, bearing in mind this systematic difference, both equations produce quite acceptable results and there seems to be no reason to doubt values calculated using either equation.

Table 3-1

Typical olivine-glass pairs from the experiments, with predicted FeO and Fe_2O_3 values, and resulting values of the olivine-liquid Fe^{2+}-Mg KD.

Temp.	1140° C		1200° C		1256° C	
$Log_{10} fO_2$	-8.5		-7.6		-7.0	
Phase	OL1	GL1	OL2	GL2	OL3	GL3
SiO_2	38.24	47.34	37.72	45.58	40.27	45.70
Al_2O_3	-	14.50	-	14.98	-	14.12
ΣFeO	22.94	12.32	15.77	11.03	13.23	11.57
MgO	36.97	4.86	43.13	7.22	45.89	9.61
CaO	0.48	8.99	0.62	11.69	0.37	11.29
Na_2O	-	3.18	-	2.64	-	2.57
K_2O	-	1.93	-	1.18	-	0.96
TiO_2	-	3.99	0.16	2.98	0.12	2.97
MnO	0.27	-	0.20	0.19	0.21	-
Cr_2O_3	-	-	-	-	-	0.22
NiO	0.36	-	0.23	-	0.37	-
TOTAL	99.26	97.11	99.83	97.49	100.46	99.01

EQUATION	GL1			GL2			GL3		
	FeO	Fe_2O_3	KD	FeO	Fe_2O_3	KD	FeO	Fe_2O_3	KD
1. Roeder & Emslie (1970)	10.11	2.46	0.298	8.33	3.00	0.317	8.05	3.91	0.344
2. Nathan & Van Kirk (1978)	9.63	2.99	0.313	8.25	3.09	0.320	8.39	3.54	0.330
3. This Study	9.58	3.04	0.315	8.69	2.60	0.304	9.28	2.54	0.299
4. Sack et al. (1980)	9.93	2.66	0.304	8.96	2.30	0.295	9.62	2.17	0.288

Note: In the recalculation of the glasses Cr_2O_3 is considered with Al_2O_3, and MnO is considered with FeO.

BASIC RESEARCH IS WHEN I'M DOING WHAT I DON'T KNOW I'M DOING.

Wernher Von Braun.

CHAPTER 4

EXPERIMENTAL RESULTS

4.1 Introduction

Samples from the Scottish Permo-Carboniferous province were among the first to be examined in experimental melting and crystallisation studies (Hall, 1805). Since those early pioneering experiments, the experimental petrology of compositions from the province has been largely neglected. Recent high pressure experiments by Chapman (1975, 1976), and Ford and Macdonald (1978), have been aimed at specific problems, rather than the characterisation of the lavas. The experimental results presented in this chapter represent the first major attempt to characterise the melting relations of basic lavas from the province at atmospheric pressure.

A total of 40 different compositions were investigated in 183 melting experiments, producing approximately 700 charges. Five compositions were only melted above their liquidus temperature to provide glasses for bulk analysis by electron microprobe. The remaining 35 compositions were melted at 10 - 15° C intervals from above their liquidus temperature, to temperatures where olivine + clinopyroxene + plagioclase + Fe-Ti oxide minerals coexisted with melt. Most experiments were carried out at oxygen fugacities corresponding to the Ni - NiO equilibrium. Five of the samples were also investigated at oxygen fugacities corresponding to the Fe - FeO equilibrium. After the discovery that the supplied powders had been crushed in colmonoy, resulting in Ni and Cr contamination, five samples were re-crushed in agate and investigated to determine their spinel liquidus temperatures.

The main aim of the experiments was to provide data for the development of the experimental crystallisation model, described in Chapter 5. The present chapter indicates the strengths and weaknesses of the experimental data for this purpose. Further, the results illustrate the overall similar phase relations for most samples, representing a large number of lava successions over a long period of time. Several aspects of the crystal-liquid and crystal-

crystal equilibria have been examined. However, in view of the main aim of the experiments, the exhaustive study of equilibria possible with such a large database has been deferred.

Appendix 2 contains the details of each experiment on the individual samples. Details include the experiment number, temperature, run duration, oxygen fugacity, wire hook material, and the observed resulting phase assemblage.

Representative analyses of the phases from the experimental charges are listed in Appendix 4. Glass analyses have been recast with respect to ferric iron using equation (3) in Chapter 3. Spinel phases and ilmenites have been recast assuming stoichiometry.

4.2 The Assessment of Equilibrium in the Experiments

In the use of coexisting mineral and glass analyses to derive expressions which predict mineral crystallisation temperatures and compositions, the fundamental assumption is that the experimental phases are at equilibrium. It is extremely difficult to prove that equilibrium has been achieved in experiments on basaltic compositions, particularly where plagioclase and clinopyroxene are involved. Ideally, equilibrium may be confirmed when the same phase assemblage, compositions and proportions result from numerous different pathways to given experimental conditions of temperature, pressure and oxygen fugacity, from several different starting materials, such as glass, gel or rock powder. Extended experimental times should have no effect on the experimental result, although it is not often possible to conduct experiments on a time scale comparable to that operating on the natural assemblages.

In order to obtain sufficient data to derive a comprehensive set of temperature and composition equations, it is clearly not practicable to establish thoroughly that each experiment has reached complete equilibrium. However, it is desirable to look for evidence for and against equilibrium in the experiments. Three factors are considered to be important. Firstly, was the bulk composition of the starting material modified during the experiment? Secondly, were the equilibrium phase assemblage and phase compositions produced during

the experiment? Thirdly, distinct from the experiment itself, do the microprobe analyses accurately reflect the compositions of the individual phases?

1. The problems of experimental control of the bulk compositions were discussed in the previous chapter. For the great majority of the experiments, run on Pt-Fe wire hooks at oxygen fugacities near the Ni - NiO buffer, for times up to 24 hours, there is no evidence for significant Fe loss or alkali volatilisation. Ni can be assumed to be lost rapidly to the wire hook, even in short duration experiments. Some early experiments using Pt wire suffered from noticeable Fe loss. Some of the high temperature experiments at the Fe - FeO buffer lost significant amounts of Fe, and, in fewer cases, also lost Na and K. For the Ni - NiO buffer experiments, the choice of wire hooks and the relatively short run times are believed to have resulted in essentially unmodified major element compositions.

2. It can be very difficult to assess whether the equilibrium phase assemblage and phase compositions were obtained in an experiment. It is easier to identify disequilibrium than to identify equilibrium. Homogeneous phases, with identical compositions throughout an experimental charge, are evidence for equilibrium. In the experiments described here, glasses were found to homogeneous, even in short experiment times. For the equilibrium ferric-ferrous ratio to be established in a basaltic liquid, Thornber et al. (1980) have indicated that run times of over 2 hours are required. Mineral phases produced in the experiments were usually too small for zoning to be identified by microprobe analysis. The earliest experiments, which were for calibration purposes, used the supplied rock powders without further crushing and produced large olivine crystals which were very zoned. The main series of experiments on the finely crushed powders produced small olivine crystals in which no zoning was identified. The similarity of olivine compositions throughout individual charges is taken to indicate that olivine-liquid equilibrium was achieved in the runs of 5 - 24 hours duration. In the lowest temperature experiments on individual starting compositions, the microprobe analyses indicated a small range of olivine compositions were occasionally present (e.g. Appendix 4,

analyses 135 - 137 from sample MV521). Using these olivine compositions to derive olivine-liquid Fe^{2+}-Mg distribution coefficients produces a small range of KD (0.306 - 0.326 for analyses 135 - 137 with glass analysis 134). The olivines in the low temperature runs are also usually smaller and more rounded than those of the near-liquidus runs. The evidence indicates it is not safe to assume that olivine equilibration rates are constant over the melting interval of basaltic compositions.

Other minerals show more evidence of disequilibrium. Spinel phases produced in the experiments were usually too small for analysis, but where several analyses were made on an individual charge a range of compositions was often found (e.g. Appendix 4, analyses 389 - 392). For individual starting compositions, experiments at different temperatures produced systematic changes in spinel composition, suggesting an approach to equilibrium. However, because of the possibly variable effects of Cr contamination, it is not clear how much of the Cr-Al-Fe^{3+} variation is applicable to the original samples. Rates of spinel equilibration are clearly slower than for olivine, but the spinel $Mg/(Mg + Fe^{2+})$ ratio varies with temperature in an analogous fashion to olivine, and is interpreted as indicating some equilibration during the experiments. Magnetites and ilmenites appear to have equilibrated during the experiments, on the basis of similar compositions throughout individual charges. It is notable, however, that analysis totals remain low even after recasting for ferric iron (e.g. Appendix 4, analyses 940 - 941 for magnetite, 930 - 932 for ilmenite).

Plagioclase compositions from individual charges can show a broad range, indicating equilibrium was not achieved (e.g. Appendix 4, analyses 1338 - 1346 representing $An_{55.4}$ - $An_{64.2}$). This is to be expected, as Drake (1976) has suggested experiment times of several hundred hours for plagioclase-liquid equilibration. Walker et al. (1979) noted detectable ranges of plagioclase composition from charges run for 1 - 3 days. This was attributed to the preservation of relics from the original rock powder. A similar interpretation is proposed for the range of compositions preserved in the present study. The data in this study suggest that plagioclase approached the

equilibrium composition in experiments near the plagioclase liquidus temperature (e.g. Appendix 4, analyses 211 - 214 representing $An_{65.7}$ - $An_{67.7}$). At progressively lower temperatures an increasing range of plagioclase compositions was preserved. However, euhedral crystals were developed in some charges where a range of plagioclase compositions was identified. This is interpreted as evidence for plagioclase being a stable phase with the coexisting liquid. The implied equilibrium is local. The concept of surface equilibrium allows the liquid to be taken as in equilibrium with plagioclase, although not necessarily of the plagioclase core compositions.

The preservation of relics must change the course of the melting relations away from that of the equilibrium situation. In the study there is no evidence that this process had a significant effect on the melt compositions, although it is expected to have occurred at the lowest temperatures. The sequence of crystallisation in the samples has not been affected.

Clinopyroxene is affected by the same equilibration problems as for plagioclase. Relics from the original rock powder have probably been preserved in these relatively short run times, similar to the situation described by Walker et al. (1979). Whereas plagioclase often crystallises in these compositions at high temperatures favouring rapid equilibration, clinopyroxene is usually the last silicate phase to appear in the studied melting intervals. As a result, there is less evidence for the clinopyroxene compositions approaching equilibrium in the experiments. Surface equilibrium is indicated by the occurrence of euhedral crystals in some charges, although there is usually a range of compositions preserved (e.g. Appendix 4, analyses 8 - 12).

3. The final assessment of whether equilibrium has been achieved is based on the microprobe analyses of the coexisting phases. A small apparent range of compositions can be attributed to microprobe precision. This is described in Appendix 3. A larger range of compositions can be produced by problems associated with the collection of the analyses. Two problems are identified. Firstly, Na (and to a lesser extent K) migration during analysis is a recognised problem (e.g. Autefage, 1980; Autefage and Couderc, 1980).

In the present study this is likely to have been confined to glass analyses. The extent to which this has affected the analyses is uncertain, although many of the lower temperature glasses are alkali-rich and may have suffered some losses. Since the majority of the glass analyses were collected using the EDS technique, there is no easy way of identifying Na loss. Comparisons of analyses collected using the EDS and WDS techniques probably reveal more about the relative calibrations of the systems than about the effects of alkali losses. However, the WDS analyses indicate that Na and K losses were not significant in those glasses studied. It is believed that the EDS analyses will not have been affected to any greater extent than for the WDS analyses. Only the most Na- and K-rich glasses should be viewed with caution.

Secondly, there is the problem of contamination of the analysed point by neighbouring phases. Because many of the minerals formed very small crystals there is commonly a component in the analyses from the enclosing glass. Thus, significant Al in olivine, Mg in plagioclase, and Si in oxide phases are attributed to glass contamination. The reader is advised to remember this when examining analyses in Appendix 4. Although most poor analyses were discarded when compiling this appendix, a number were left to illustrate approximate compositions in charges where better analyses were not available. Low glass analysis totals may be an artefact of the microprobe ZAF correction procedure, although there may be an undetermined volatile component due to the glasses having been produced in a $CO_2 - H_2$ atmosphere.

A further problem has been the detection of Na in clino-pyroxenes. Due to the low sensitivity of the EDS detector during the period when the bulk of the analyses were collected, the 0.5 wt % or so Na_2O in the pyroxenes was below the detection limit. This makes estimation of the ferric iron content in these pyroxenes very uncertain.

Bracketed Phase Equilibria

Nearly all of the experiments presented in this study were of the melting type, i.e. the temperature of a rock powder was raised

directly to that of the experiment. Other workers have adopted crystallisation experiments, i.e. the sample temperature is raised to above its liquidus, to melt pre-existing crystals, and then lowered to the experiment temperature. Fisk et al. (1980) used this techinique in a study of tholeiitic basalts. A major difference between the two types of experiments is in the meaning of the determined phase boundaries. The melting experiments determine the maximum temperature to which a phase will persist. Crystallisation experiments determine the temperature at which a phase will nucleate, usually a minimum estimate of the equilibrium crystallisation temperature for the phase. Also, melting experiments based on finely crushed powders tend to produce numerous, small crystals; crystallisation experiments tend to produce relatively few, large crystals. There is no guarantee that either type of experiment will lead to bulk equilibrium in short experiment times. However, the occurrence of euhedral crystals in the near-liquidus runs of these melting experiments is interpreted as evidence for growth during the experiments, and hence evidence against the metastable persistence of crystals to above liquidus temperatures.

One series of experiments was carried out to compare the temperature of disappearance of plagioclase in melting experiments, with the temperature of its appearance in crystallisation experiments. Five samples were investigated. In the crystallisation experiments, the samples were raised to 10 - 15° C above their plagioclase liquidus temperature (as determined in the melting experiments). After 5 hours, the samples were cooled to 10 - 15° C below their plagioclase liquidus temperature and left for 16 hours to equilibrate. Samples MV521, MV703 and MV514 produced plagioclase in the crystallisation experiments, occurring as relatively few, large crystals up to 200 μm in length. Phase compositions from the crystallisation experiments were similar to those in the melting experiments for MV521 and MV703. MV514 contained slightly more Mg-rich olivine and glass in the crystallisation experiments than expected from the melting experiments. Samples MV74 and MV72 failed to produce plagioclase in the crystallisation experiments. These two samples have the lowest whole rock Mg# [defined as the cation ratio $100^* \ Mg/(Mg + Fe^{2+})$] of the five studied specimens.

Samples MV514 and MV72 were also heated above their olivine liquidus temperature in the crystallisation experiments. In both cases, large euhedral olivines were present in the resulting charges. Samples MV521 and MV703 contained numerous small olivines, consistent with the interpretation that they were present at the initial heating stage of the experiments. The large crystals developed in the crystallisation experiments are interpreted to have crystallised after the heating stage. The crystallisation experiments and phases are labelled 'reversal' in appendices 2 and 4.

The absence of plagioclase from the crystallisation experiments on MV74 and MV72 is attributed to the problem of nucleating phases from initially superheated melts (e.g. Gibb, 1974). Since one of the primary aims of the experiments was to define the liquidus surface of plagioclase in basaltic compositions, by means of coexisting glass analyses, the nucleation problems of the crystallisation experiments would have been a serious drawback. The melting experiments are believed to be more useful in defining plagioclase liquidus temperatures.

In summary, the melting experiments described in this study are believed to have produced homogeneous olivines and glasses in most cases. Spinels, plagioclases and clinopyroxenes show some evidence of not having fully equilibrated. However, the concept of surface equilibrium allows the glass compositions to be taken as representing equilibrium with these phases. The generally good control of the starting compositions, together with the lack of quench phases or overgrowths, suggests the experimental results represent the equilibrium phase assemblages. At low temperatures there may have been some deviation from the equilibrium phase proportions and glass compositions, due to the preservation of relics.

4.3 Phase Relations

Table 4-1 lists the starting compositions of the investigated samples. These are averaged electron microprobe analyses of all-glass charges. The Fe_2O_3 content of each sample was calculated using equation (3) of Chapter 3, assuming the sample was above its liquidus temperature at the Ni - NiO buffer. The table lists the samples in

order of decreasing Mg#. Sample MV403F was not melted above its liquidus temperature but from the experimental evidence is similar to sample MV403.

4.3.1 Experiments at the Ni - NiO buffer

Figure 4-1 shows the melting temperature of each phase plotted against the whole rock Mg#. Several points can be noted.

1. The trend is for sample liquidus temperatures to fall as Mg# decreases. If the silicate minerals only are considered, then liquidus temperatures decrease from 1328° C when Mg# is 70, to 1130° C when Mg# is 37. The slope of decreasing sample liquidus temperature with Mg# becomes less steep towards low Mg# values.

This trend is not as well defined as those obtained for other groups of basic rocks. Data for five suites reported by Thompson (1972a) produce smooth trends in comparison to the present study. This may reflect the wide range of lava successions represented by the sample collection. Other effects, such as sample alteration or phenocryst accumulation, may also account for some scatter.

2. For the 21 samples with Mg# greater than 57 the silicate liquidus phase is olivine. Although the Mg# value may vary, this result is similar to published studies of other suites (e.g. Thompson, 1972a; Fisk et al., 1980).

3. Also for samples with Mg# greater than 57, the higher the Mg# value, in general, the larger the temperature interval between olivine and the next silicate mineral.

4. For the same group of samples, with only rare exceptions, the sequence of appearance of the silicate minerals with decreasing temperature is olivine followed by plagioclase followed by high-Ca pyroxene.

5. For the samples with Mg# less than 57, 8 have plagioclase as their silicate liquidus phase, 3 have olivine + plagioclase, and 3 have olivine.

6. For the same low Mg# group, clinopyroxene never appears at higher temperatures than olivine and plagioclase.

7. Clinopyroxene is never the sample liquidus phase in these experiments. This contrasts with the natural rock phenocryst assemblages where augite is often present. At high Mg# values in the experiments, clinopyroxene usually appears within 35° C of plagioclase. At low Mg# values this gap may be over 100° C. The near-absence of assemblages of olivine and clinopyroxene without plagioclase, in the experiments, contrasts with the common phenocryst assemblage of olivine + augite + spinel.

8. As sample Mg# decreases, the temperature of appearance of plagioclase shows no marked trend. In comparison, the temperatures of appearance of clinopyroxene and olivine show a clear decrease. As a result, plagioclase becomes the silicate liquidus phase at intermediate values of Mg#, whereas clinopyroxene does not approach the liquidus in the studied compositional range.

9. In one sample (MV93), clinopyroxene crystallises at higher temperatures than plagioclase. Sample MV93 is quite distinct from the other samples, having high CaO and low Al_2O_3 contents.

10. In many samples, the actual liquidus phase is a translucent brown or opaque spinel phase. This has been found to range from Cr-Al spinel at high temperatures to titanomagnetite at low temperatures. In some high Mg# samples, the temperature of appearance of spinel is similar to that of olivine. In many lower Mg# samples, the spinel phase is the liquidus phase by several tens of degrees.

11. Ilmenite was recognised in experiments on 11 of the samples, usually near the lowest studied temperatures. In these samples, ilmenite often crystallised at similar temperatures to clinopyroxene. The absence of ilmenite, from the melting intervals of the more Mg-rich samples, may simply indicate ilmenite crystallises at significantly lower temperatures than clinopyroxene in these samples.

12. Apatite was recorded from experiments on one composition (MV51). This sample has the lowest Mg# and highest P_2O_5 content of the investigated range. Apatite was only found at the lowest

temperature (1074° C).

13. Low-Ca pyroxene was not identified in any of the experimental charges.

14. The most common silicate phase assemblages found in the experiments are olivine + glass, olivine + plagioclase + glass, plagioclase + glass, and olivine + clinopyroxene + plagioclase + glass. Using these experimental data in the crystallisation model means these assemblages are best constrained.

Spinel Crystallisation at the Ni - NiO Buffer

Spinel was found to be the most common liquidus phase in the investigated samples. This is not surprising for the high Mg# samples, as small amounts of spinel accompany olivine phenocrysts in the natural rocks. However, this result was not expected for the lower Mg# samples, where spinel is often the liquidus phase by a large temperature interval. Associated with this observation it was discovered that some experimental olivines contain high levels of Ni (up to approximately 1 wt % NiO). These two anomalies are attributed to the samples having been crushed in colmonoy, resulting most notably in Cr and Ni contamination (see comments by Leake, 1979, and reply by Fettes and Macdonald, 1979). This has been confirmed by Dr. R. Macdonald (pers. comm.).

Hill and Roeder (1974) and Onuma and Tohara (1983) have shown that the addition of Cr to a melt can dramatically increase the temperature of appearance of spinel. In a basaltic melt investigated by Hill and Roeder (1974), the effect of 150 ppm Cr was to raise the spinel crystallisation temperature by 50° C. Unfortunately, it is not possible to predict how much Cr has been added to samples in this study from the crushing. To investigate the problem, 5 samples were re-crushed in agate in Edinburgh, and together with their contaminated equivalents, were melted at the Ni - NiO buffer to determine the liquidus temperature of spinel in each. Figure 4-2 shows the results plotted against whole rock Mg#. Re-crushed samples have suffix 'F'. Differences in Mg# between pairs of samples are due to slight variations in bulk composition rather

than experimental or analytical error. For the lower Mg# samples, the revised spinel liquidus temperatures of the uncontaminated samples are now at or below the silicate mineral liquidus temperatures. For the higher Mg# samples, spinel is much less affected, but now crystallises within a few degrees of olivine.

To support the suggestion that Cr contamination from colmonoy is the cause of the spinel anomaly, microprobe analyses were made of charges from temperatures above the spinel liquidus. Cr and Ni concentrations in the glasses are shown in Table 4-2. Very long analysis times produced adequate precision to compare pairs of samples. Despite the fact that Ni is rapidly lost to the Pt alloy hook, all the suspect samples had much higher concentrations of Ni than the re-crushed samples. Cr levels were generally much lower in the re-crushed lower Mg# samples, as expected. Less marked changes in higher Mg# samples reflect the much smaller changes in spinel liquidus temperatures, between re-crushed and suspect sample pairs.

Hill and Roeder (1974) presented results suggesting that the effect of Cr addition diminished as the initial Cr content of the melt increased. Thus, 100 ppm Cr added to an initial concentration of 100 ppm Cr can increase the spinel liquidus temperature by 50° C, whereas the same amount added to an initial 400 ppm Cr might only increase the spinel liquidus temperature by 10° C. The limited data presented in this study appear to be in agreement with Hill and Roeder's data.

Although it is impossible to predict quantitatively the effect of Cr contamination, it seems likely that the five re-crushed samples illustrate the general trend. Most spinel liquidus temperatures would be revised downwards, with greater changes at lower values of Mg#. At the higher Mg# end of the range, spinel may still appear a few degrees above olivine in some cases, but it is expected that olivine will be the more common liquidus phase.

For lower Mg# samples, a spinel phase would be expected to crystallise near the silicate mineral liquidus temperatures.

As will be seen later, the early crystallisation of a trace

amount of Cr-Al spinel has no noticeable effect on the major element melt composition. The silicate phase relations are believed to be unaffected.

Hill and Roeder (1974) also noted the disappearance of early Cr-spinel down temperature after the appearance of clinopyroxene. Ti-magnetite crystallised as the spinel phase after a further drop in temperature. In this study, only the distinctive sample MV93 shows this behaviour at the Ni - NiO buffer. An early Cr-spinel disappears within 15° C below the clinopyroxene liquidus temperature. Only after plagioclase has joined the crystallising assemblage does an opaque phase reappear. This is titanomagnetite, similar to the situation noted by Hill and Roeder. All the remaining samples at the Ni - NiO buffer show a continuous series of spinels from early Cr-Al spinels through to titaniferous magnetites at lower temperatures. This may reflect the late appearance of clinopyroxene in these samples.

The concentration of Cr in the melt is clearly one of the major factors in determining the temperature of appearance of spinel. Unfortunately, the Cr concentration in the glasses is rarely known, as it falls below levels routinely determined by electron microprobe analysis.

4.3.2 Experiments at the Fe - FeO buffer

In order to examine the effect of lower oxygen fugacities on the phase relations, 5 samples were melted at oxygen fugacities corresponding to the Fe - FeO equilibrium. Despite increased experimental problems, discussed in Chapter 2, the results illustrate the changes at the more reducing conditions. Figures 4-3 to 4-7 show the combined results from the Fe - FeO and Ni - NiO buffers for each sample.

The most pronounced change shown by the plots is the rapid decrease in spinel crystallisation temperature as the oxygen fugacity decreases. This is due partly to the corresponding decrease in the ferric-ferrous ratio of the melt. Only sample MV160 crystallised a spinel phase in the investigated melting interval. This was a Cr-rich ulvospinel which disappeared at low temperatures after the

appearance of clinopyroxene (in similar fashion to MV93 at the Ni - NiO buffer). Note that sample MV160 does not show this behaviour at the Ni - NiO buffer (Figure 4-5).

The olivine crystallisation temperature shows little variation between the two buffers for each sample. For sample MV40B, there is a clear increase in the temperature of appearance of olivine at the Fe - FeO buffer. It is probable there is a similar increase for olivine in samples MV166, MV106 and MV402 at the Fe - FeO buffer. Since the experiments were conducted at 10 - 15° C intervals, the increase for these samples is difficult to prove, but is in agreement with modal analysis of the charges. Sample MV160 has very similar olivine crystallisation temperatures at the Ni - NiO and Fe - FeO buffers. The proposed slight increase in olivine crystallisation temperatures, at more reducing conditions, could be due to the rise in ferrous iron in the melt, stabilising olivine to higher temperatures. A slight increase in olivine crystallisation temperature, at more reducing conditions, is in agreement with the generalised phase diagram for basalts of Biggar (1974b).

The effect of lower oxygen fugacity on the plagioclase crystallisation temperatures in these samples is very slight for MV166, MV106, MV160 and MV40B. For sample MV402, there may be a decrease in plagioclase crystallisation temperature at the Fe - FeO buffer, although the difference is well within the temperature interval between experiments.

Clinopyroxene crystallised as the third silicate mineral in each sample. There is little change in its crystallisation temperature at the more reducing conditions. The increase in the ferrous iron content of the melt (and the corresponding decrease in the ferric iron content) has had no discernible effect on clinopyroxene crystallisation temperatures.

Sample MV160 produced ilmenite at both oxygen buffers. The limited data suggest that ilmenite crystallisation temperatures increase slightly at lower oxygen fugacities.

For the samples in this study, it is likely that reducing the oxygen fugacity from that of the Ni - NiO buffer produces a rapid decrease in spinel crystallisation temperatures. The silicate minerals do not appear to be greatly affected, although the olivine crystallisation temperature may increase towards lower oxygen fugacities. Ilmenite may show a similar slight increase in crystallisation temperature.

4.4 Phase Chemistry

4.4.1 Variation in glass composition

Figures 4-8 to 4-26 illustrate the changes in glass composition with temperature, and with coexisting phase assemblage, for a selection of the starting compositions. The samples are listed in terms of decreasing whole rock Mg#. 15 of the plots relate to experiments at the Ni - NiO buffer, with the remaining 4 plots showing equivalent experiments for samples MV166, MV106, MV40B and MV402 at the Fe - FeO buffer. All Fe has been expressed as FeO to allow a rapid assessment of Fe recovery in the individual charges.

In many compositions, olivine is present throughout the melting interval (e.g. Figures 4-8 and 4-10). The decrease in glass MgO content in these samples is quite regular, and could be used as a substitute for temperature on the X - axis of the plots. A similar regular decrease of glass Al_2O_3 content with temperature in samples with plagioclase-dominated melting intervals (e.g. Figure 4-21) could allow a similar substitution.

There are consistent trends of glass composition associated with the crystallisation of different phase assemblages. These are taken as evidence for the internal consistency of the data. As noted, olivine crystallisation is accompanied by a marked decrease in glass wt % MgO. The frequent association of high temperature spinel with the olivine is not believed to have had a discernible effect on the glass major element composition. Figure 4-24, for MV13, shows a spinel + glass stage from approximately 1220° C to 1160° C where spinel crystallisation has not significantly modified the coexisting glass major element composition. The glass composition variations,

when coexisting with olivine and spinel, are therefore attributed to the effect of olivine. As olivine crystallises, there are increases in wt % CaO and Al_2O_3 in the coexisting glasses (e.g. Figures 4-13, 4-16 and 4-17). Other elements show little variation, although extensive olivine crystallisation is marked by slight increases in the Na, K, Ti and P contents of the glasses.

In addition to the rapid decrease in wt % Al_2O_3, plagioclase crystallisation is marked by increases in glass wt % MgO and ΣFeO, and decrease in glass wt % Cao (e.g. Figures 4-21, 4-22 and 4-25).

None of the samples shows the effects of clinopyroxene crystallisation alone. However, sample MV93 (Figure 4-9) shows a stage of olivine + clinopyroxene crystallisation. This is marked by pronounced decreases in glass wt % MgO and CaO, and increases in glass wt % Al_2O_3 and Na_2O.

Olivine + plagioclase crystallisation in this study is marked by decreasing glass wt % MgO and Al_2O_3 (e.g. Figures 4-11, 4-20, 4-21, 4-24 and 4-25). There is usually an associated increase in ΣFeO. Wt % CaO stays nearly constant (e.g. Figure 4-21) or may show a slight increase (e.g. Figure 4-11).

Olivine + clinopyroxene + plagioclase crystallisation in these samples is marked by decreasing glass wt % MgO and CaO, with wt % Al_2O_3 staying nearly constant (e.g. Figure 4-16) or decreasing (e.g. Figures 4-13 and 4-18). Some samples indicate a slight increase of Al_2O_3 with cooling (e.g. Figures 4-8 and 4-20), but this has not been well established, and may reflect the problems of obtaining unmodified glass compositions from highly crystalline charges (Biggar, 1983). ΣFeO often shows a marked increase during this stage of cotectic crystallisation, until opaque oxide minerals become significant.

The crystallisation of ilmenite ± titanomagnetite assemblages is marked by decreases in glass wt % TiO_2 and ΣFeO (e.g. Figures 4-12 and 4-21). In Figure 4-24, for MV13, the decrease in ΣFeO and levelling off of TiO_2, from 1135° C, is interpreted to mark the crystallisation of significant amounts of titanomagnetite. The decrease in TiO_2, from approximately 1110° C, marks the crystallisation

of ilmenite.

Apatite crystallisation was recognised in sample MV51 (Figure 4-26). The effect on glass compositions is to decrease the wt % P_2O_5. The glass wt % CaO may also decrease more rapidly than would be ascribed to clinopyroxene crystallisation. The apatite crystallised when the glass wt % P_2O_5 was approximately 2-5%, with over 50 wt % SiO_2. Crystallisation of apatite from a melt of this composition at 1080° C agrees well with experimental studies of apatite solubility, reported by Green and Watson (1982).

SiO_2 was not included in the plots of melt composition because the relatively poor precision of its determination concealed many of the expected trends. In general, hypersthene- and quartz-normative initial compositions showed a gradual increase of glass wt % SiO_2 with increasing crystallisation. Nepheline-normative initial compositions showed little variation in the glass wt % SiO_2 with crystallisation.

Visual estimates of the degree of crystallinity of charges can be very misleading because of uneven distribution of phases. Qualitative guides to crystallinity are the more incompatible elements, such as K and P, and to a lesser extent Ti and Na. Using the rates of increase in concentration of these elements as indicators, the degree of crystallinity of the charges increased more rapidly with decreasing temperature for olivine + clinopyroxene + plagioclase assemblages, than for olivine-only assemblages (e.g. Figure 4-16). This is consistent with visual estimates. Use of these elements quantitatively is unwise. Although TiO_2 has been used successfully in published studies of tholeiites (e.g. Biggar and Kadik, 1981), in the present study it is strongly affected by crystallisation of opaque oxide phases. Na_2O may be affected by plagioclase crystallisation, and both Na and P may be affected by volatilisation during the experiments. P concentrations in these samples are often low and were not always determined in the glass analyses. K may be the most useful indicator, although it is incorporated in small amounts in plagioclase. K volatilisation is not believed to have been a major problem in the experiments at the Ni - NiO buffer.

Treating all Fe as FeO conceals the relative Fe^{2+} and Fe^{3+} variations. The recast glass compositions show increasing Fe^{3+}/Fe^{2+} ratios towards low temperatures. If ΣFeO has increased at low temperatures then both Fe_2O_3 and FeO may have increased, although usually FeO has decreased slightly. With the crystallisation of the opaque oxide phases, both FeO and Fe_2O_3 decrease. In the Fe - FeO buffer experiments, because of the low Fe_2O_3 contents, the decrease in ΣFeO with crystallisation of opaque oxide phases is largely marked by decreasing FeO.

Glasses Coexisting with Olivine + Clinopyroxene + Plagioclase

Figures 4-27 and 4-28 show the projections from olivine onto CS-MS-A and diopside onto CA-M-S, respectively, (O'Hara, 1968), for glasses coexisting with olivine, clinopyroxene and plagioclase produced in the experiments. The glasses have been distinguished on the basis of their normative character. In Figure 4-27 there is clear separation of nepheline-normative glasses from quartz-normative glasses, with the hypersthene-normative glasses overlapping both groups. The position of the olivine + clinopyroxene + plagioclase cotectic at 1 atm. (from O'Hara, 1968) has been marked. The cotectic glasses in the present study form a similar trend but are displaced to higher values of coordinate A. Also, the cotectic is shown to extend into very nepheline-normative compositions at one side, and at the other, extends into O'Hara's field of low-Ca pyroxene. Although it is not easy to prove that low-Ca pyroxene was indeed absent from these charges, the data indicate that the cotectic assemblage of olivine + clinopyroxene + plagioclase was present.

The olivine- diopside-plagioclase plane is also indicated in the figures. This plane has been shown to represent a thermal divide at low pressures (Yoder and Tilley, 1962), separating nepheline-normative from hypersthene- and quartz-normative basic compositions. Clearly, in Figure 4-27, the projected position of the plane suggests that hypersthene- and some quartz-normative glasses lie on the nepheline-normative side of the divide. However, the path of evolution of individual glass compositions follows the normative classification. Thus, nepheline-normative glasses move to lower values of MS and higher values of A as temperature decreases (e.g. for

sample MV521, the glass composition from 1158° C projects to CS35-MS40-A25, the glass composition from 1129° C projects to CS39-MS32-A29). Hypersthene + olivine-normative glasses and hypersthene + quartz-normative glasses move to lower values of CS and higher values of MS as temperature decreases (e.g. for samples MV167, the glass composition from 1131° C projects to CS30-MS46-A24, the glass composition from 1118° C projects to CS27-MS49-A24). The data from MV167 also show a transition from higher temperature olivine-normative compositions to lower temperature quartz-normative compositions, crossing the position of the diopside-plagioclase-low-Ca pyroxene plane (shown in Figure 4-28). This plane does not represent a thermal divide in the atmospheric pressure experiments of the present study. The one-atmosphere cotectic marked on Figure 4-28 (from Jamieson, 1970) is seen to have a different orientation to the experimental data presented here.

Discrepancies between the experimental data and the published cotectics may be partly due to the complicating presence of Fe-Ti oxide phases in these experiments. Further, the cotectic glasses in this study are relatively low in Mg (<7 wt % MgO) and rich in alkalis, and are distinct from the compositions used to derive the published cotectics.

Despite the discrepancies, the experimental data presented here illustrate the operation of the olivine-clinopyroxene-plagioclase thermal divide at atmospheric pressure on nepheline-normative and hypersthene-normative basaltic compositions.

4.4.2 Olivine-glass relations

This section describes coexisting olivine and glass in charges which may also contain plagioclase and/or clinopyroxene and/or oxide phases. Slight Ni contamination of the samples appears in the resulting charges as relatively high Ni concentrations in olivine. Up to approximately 1 wt % NiO occurs, but on average, values around 0.5% are found. As the average increase in NiO is small, no compensating factor has been applied.

A number of authors have noted a simple correlation between glass MgO concentration and experimental temperature in olivine-

bearing charges (e.g. French and Cameron, 1981, for a compilation of basic compositions). Figure 4-29 shows a plot of MgO wt % versus temperature, for all the experimental glasses coexisting with olivine in the present study, irrespective of oxygen fugacity or other coexisting phases. Least squares linear regression analysis produces the relation,

$$\text{Temperature } (^\circ C) = 26.097\ (\text{wt \% MgO glass}) + 1008$$
$$\text{correlation coefficient } (r) = 0.981 \qquad \ldots (1)$$

Temperatures predicted by this empirical thermometer have an approximate precision of $\pm$ 15° C. Figure 4-29 should not be applied to a broad range of olivine-bearing magmas, as the relation can only be regarded as linear over a limited temperature range. Also, the location of the trend is affected by the major-element compositions of the melts used. However, the trend is a useful guide for the Scottish Permo-Carboniferous basic magmas.

When glass wt % FeO is plotted against wt % MgO, as in Figure 4-30, there is a large spread of data. A set of olivine composition contours has been added, illustrating that a range of olivine compositions can coexist with a glass of constant MgO content. Satisfactory temperature contours can not be added to this diagram, but as expected they are approximately normal to the MgO axis. When olivine compositions are plotted against experimental temperature (Figure 4-31) the trend is quite clear, although there is a large spread of compositions at most temperatures. Offset to the right of the main group is a narrow trend of points which imply a more forsteritic olivine for any given temperature, relative to the main group. This small group is entirely from experiments on the compositionally distinct MV93. The scatter in the main group is largely due to compositional differences between individual samples, rather than analytical precision.

Empirical distribution coefficients have been examined which relate the concentration of an element in a mineral and in a liquid to the experimental temperature, using equations of the form

$$\text{Ln } K = \text{Ln}\left(\frac{X^i_{\text{mineral}}}{X^i_{\text{melt}}}\right) = A + \frac{B}{T}$$

EX BIBL. UNIV. EDINBURGEN.

where K is the distribution coefficient, X^i is the cation fraction of component i in the phase of interest, T is absolute temperature, and A and B are constants derived by regression analysis.

Ln K versus 10000/T plots for olivine-glass equilibria are shown in Figures 4-32 to 4-35 where i is Mg, Fe^{2+}, Ca and Mn. In general, the distribution coefficients increase as temperature decreases, forming the basis of a geothermometer. The importance of bulk composition on these trends is difficult to assess, so the thermometers may only be applied confidently to compositions within the range studied. Figure 4-32 for Mg indicates that K(Mg) is always greater than unity (i.e. Ln K>0) in natural compositions. The scatter of data increases towards lower temperatures, partly due to experimental and analytical errors, but variations due to bulk compositional effects probably also contribute. A least squares regression line through the data in Figure 4-32 has the equation

$$\text{Ln } K(Mg) = \frac{8180}{T^\circ K} - 3.881 \qquad r = 0.956 \qquad \ldots (2)$$

A similar trend for Ln $K(Fe^{2+})$ is shown in Figure 4-33. In the studied range $K(Fe^{2+})$ is always greater than unity, but if the trend is extrapolated to higher temperatures (than about 1325° C) then $K(Fe^{2+})$ falls below unity. It should be noted that some of the scatter may be due to errors in estimating melt Fe^{2+}. A regression line through the data has equation

$$\text{Ln } K(Fe^{2+}) = \frac{9150}{T^\circ K} - 5.737 \qquad r = 0.955 \qquad \ldots (3)$$

The trend for Ca shown in Figure 4-34 shows more scatter than for the previous two plots. This is mainly due to low precision in determining Ca in olivine. K(Ca) is usually less than 0.1, but if extrapolated to lower temperatures, higher values may occur. Published data from natural rocks imply that K(Ca) can often be much smaller than suggested here, perhaps reflecting the importance of other compositional and pressure controls. For the illustrated data set, a regression line has the equation

$$\text{Ln } K(Ca) = \frac{8060}{T^\circ K} - 8.608 \qquad r = 0.670 \qquad \ldots (4)$$

Watson (1979) has shown that Ca determinations in olivine may be affected by secondary fluorescence of Ca in surrounding glass. In view of the small size of many of the olivine crystals in the present study it is likely that this has occurred here, resulting in over-estimates of the Ca content of some olivines. It is difficult to assess how much of a problem this has been.

The data for Mn in Figure 4-35 show great scatter, due mainly to poor precision in determining low levels of Mn in olivine and glass. However, a poor trend of increasing Ln K(Mn) with decreasing temperature can be seen. This is consistent with the observation of some Mn enrichment in olivines at low temperatures and in low Mg# glasses. The data suggest that K(Mn) rises above unity as temperature falls below 1250 - 1300° C. A regression line through the data has low precision,

$$\text{Ln } K(Mn) = \frac{8410}{T°\,K} - 5.412 \qquad r = 0.493 \qquad \ldots (5)$$

K(Ni) appears to be always much greater than unity, with values mainly in the range 7 to 25. Ni loss to the wire hook may result in over estimates of K(Ni).

Roeder and Emslie (1970) related the FeO/MgO ratio of olivine and coexisting basaltic liquids in an exchange distribution coefficient (KD). The Fe^{2+}-Mg KD is defined as follows

$$KD = \frac{(Fe^{2+})_{OL} \cdot (Mg)_{LIQ}}{(Mg)_{OL} \cdot (Fe^{2+})_{LIQ}}$$

Composition terms are in cations. OL is olivine and LIQ is liquid (glass). Roeder and Emslie found that KD was approximately constant at 0.30 $\pm$ 0.03 for tholeiitic compositions, with observed fluctuations within experimental precision. Longhi et al. (1978) noted compositional effects in lunar basalts which influenced KD. They found distinct averages of 0.28 for high-Ti basalts and 0.33 for low-Ti basalts. Langmuir and Hanson (1980) suggested the maximum range of KD for terrestrial basalts is 0.28 - 0.36, taking into account compositional and pressure effects. In the present study for the bulk of olivine-glass pairs, KD appears to lie between 0.28 and

0.35. It should be remembered that the Fe^{2+} content of the melt is set by recalculation rather than by measurement. Different recalculation equations appear to change the KD limits slightly, but not to change the overall pattern. For example, using the equation of Sack et al. (1980) to recast the ferric-ferrous ratio, KD ranges from 0.27 to 0.34. The values of KD discussed below have been calculated from glasses which were recast using equation (3) of Chapter 3.

Figure 4-36 shows the variation in coexisting glass and olivine compositions from the experiments. Curves of KD = 0.30 and 0.35 have been marked. The high Mg# pairs cluster round the line of KD = 0.30 but at low Mg# values the trend is towards KD = 0.35. Figure 4-37 shows the variation of KD with temperature. KD is nearly constant above 1150° C but increases as temperature falls towards 1074° C. The scatter of values at any given temperature is more than can be attributed to experimental and analytical errors. It is likely to be due to bulk compositional difference between samples (Ford et al., 1983). Significantly, the degree of crystallinity begins to increase rapidly from approximately 1150 - 1160° C as olivine + clinopyroxene + plagioclase crystallise together. Coexisting melt compositions change rapidly from these temperatures downwards, suggesting that the increase in KD may be more related to composition than to temperature. Figure 4-38 shows the variation of KD with glass wt % SiO_2, suggesting an overall slight increase in KD as SiO_2 increases. Although this is an over-simplification, supporting evidence for an increase in KD with increasing residual nature of the coexisting melt has been published by Hoover and Irvine (1978). Working in a synthetic system, these authors found that KD rose from 0.31 - 0.33 in moderate to high Mg# melts, to 0.45 in low Mg# melts near a liquid immiscibility field. While temperature can not be ruled out as a factor in the variation of KD it seems that composition may be more important in these instances.

Figures 4-36 to 4-38 include the data from the Fe - FeO buffer together with the more voluminous data from the Ni - NiO buffer. No significant difference has been found between the two groups, suggesting that KD is independent of oxygen fugacity. Further

development of the olivine-liquid data in this study, together with published data, has allowed Ford et al. (1983) to relate variations in KD to changes in temperature, pressure and melt composition. KD has been shown to increase as pressure increases, in agreement with earlier studies (Bender et al., 1978; Longhi et al., 1978; Chapman and Freestone, 1978).

4.4.3 Spinel-glass relations

Relatively few pairs of spinel-glass analyses were obtained due to the small crystal size of spinel in the experimental charges. Compositionally, the spinel phases range from Cr-Al spinels in the highest temperature charges to titanomagnetites in the lowest temperature charges.

Figure 4-39 shows the variation in spinel Mg# [100* Mg/(Mg + Fe^{2+})] with experimental temperature. The apparent step at approximately 1130° C largely separates higher temperature spinels from lower temperature magnetites. The step is interpreted to result partly from a change in spinel composition, with the increasing incorporation of an ulvospinel component at low temperatures. The simple substitution of Fe^{2+} for Mg in the spinel is complicated by the paired substitution of Ti and a divalent cation for two trivalent cations. The overall trend is still clear, however. Like olivine, as the temperature decreases so the spinel phase Mg# also decreases. This is largely due to changes in the coexisting melt composition caused by the crystallisation of the silicate ferromagnesian phases, particularly olivine. The variation in spinel composition is evidence for an approach to equilibrium by the spinels during the experiments.

Some systematic trends in spinel composition are apparent from the data. At the Ni - NiO buffer, as temperature decreases so MgO, Al_2O_3 and usually Cr_2O_3 decrease. This is balanced by an increase in the concentrations of TiO_2, FeO, Fe_2O_3 (calculated assuming stoichiometry) and total Fe in the spinels. These variations are consistent with the published experimental data of Hill and Roeder (1974) and Fisk and Bence (1980).

Dickey and Yoder (1972) noted an increase in the Cr/Al ratio of spinels with increasing temperature above the solidus, in experimental studies of the system $CaO-MgO-Al_2O_3-Cr_2O_3-SiO_2$. In the present study, Cr/Al and $Cr/(Cr + Al + Fe^{3+})$ variations are more complex. In some cases the Cr_2O_3 content of spinels increases towards lower temperatures as the Al_2O_3 content drops. For example, spinel from MV403 has 22 wt % Cr_2O_3 and 36 wt % Al_2O_3 at 1208° C, and 31 wt % Cr_2O_3 and 16 wt% Al_2O_3 at 1151° C. Spinel from MV106 has 19 wt % Cr_2O_3 and 30 wt % Al_2O_3 at 1191° C, and 27 wt % Cr_2O_3 and 23 wt % Al_2O_3 at 1177° C. Other samples show increases in the Cr/Al ratio towards lower temperatures although the Cr_2O_3 contents of the spinels have decreased (e.g. MV406, MV521 and MV164). Figure 4-40 illustrates the range of 100* Cr/(Cr + Al) with temperature for experimental spinels in this study.

The pattern of initially increasing Cr/Al ratio followed by rapid decrease of the ratio, as temperature decreases, has been described in experimental studies (Fisk and Bence, 1980). Similar variation has been described from natural rocks, where decreasing temperature is replaced by decreasing Mg/Fe^{2+} ratio (Ridley, 1977). Both Ridley, and Fisk and Bence, have attributed the increasing Cr/Al ratio stage to the associated crystallisation of plagioclase, rapidly depleting the Al_2O_3 content of the coexisting melt. However, the magnitude of the changes in spinel composition seems far larger than the associated changes of Al content of the melt. While the data in this study also suggest that plagioclase crystallisation is a factor in the variation of spinel composition, an alternative explanation is proposed. Osborn (1979) has described a peritectic reaction involving olivine + plagioclase + spinel in a synthetic basalt-like system. Initial olivine + spinel crystallisation, as seen in the present study, when joined by plagioclase results in spinel reacting with the melt. In equilibrium crystallisation the spinel will gradually change composition and dissolve. The same process operating in natural melts could show increasing Cr contents of the spinel to stabilise the phase at lower temperatures (Jackson, 1979), with the available Cr distributed through a smaller amount of spinel than at higher temperatures. The variation in Figure 4-40 is therefore interpreted as indicating the olivine + plagioclase+spinel

reaction at moderately high temperatures, producing increases in Cr/Al ratio. At low temperatures, a rapid increase in the volume of crystallising spinel (as titanomagnetite) results in rapid depletion of available Cr.

The variation in the proportions of the trivalent cations, Cr, Al and Fe^{3+}, is shown in Figure 4-41. Temperature essentially decreases in the direction of increasing Fe^{3+}. Hence the effect of lowering temperature is reflected initially by increasing Fe^{3+}/Al ratios and later by increasing Fe^{3+}/Cr ratios in the spinel phases.

At the Fe-FeO buffer, spinel was only observed in sample MV160 and was only analysed from one experiment. Compared to spinels in experiments on MV160 at comparable temperatures at the Ni-NiO buffer, the lower fO_2 spinel phases are poorer in Fe_2O_3 and total Fe. They are markedly higher in Cr and Cr/Al ratio. The more reduced spinels have slightly higher contents of MgO, TiO_2, FeO and Al_2O_3 compared to the spinels from the Ni-NiO buffer. These trends of spinel composition with oxygen fugacity are similar to those described by Hill and Roeder (1974), although in the published data FeO showed little variation.

The element distribution between spinel and glass has been examined using Ln K - inverse temperature variations. Figure 4-42 for Fe^{2+} indicates that $K(Fe^{2+})$ is greater than unity in these experiments (i.e. Ln K>0), and increases as temperature decreases. A regression line through this data has the equation

$$\text{Ln } K(Fe^{2+}) = \frac{13710}{T} - 8.327 \qquad r = 0.897 \qquad \ldots (6)$$

$K(Fe^{3+})$ has higher values than $K(Fe^{2+})$ at any given temperature (excluding the experiments at the Fe-FeO buffer where estimates of the spinel and glass Fe_2O_3 contents are very imprecise). The data are quite scattered but by regression analysis

$$\text{Ln } K(Fe^{3+}) = \frac{8370}{T} - 3.927 \qquad r = 0.474 \qquad \ldots (7)$$

The distribution data for Ti are also very scattered for the analysis pairs from experiments above 1130° C. In this region K(Ti) falls below unity as temperature increases. The lower temperature experiments show a regular variation from K(Ti) = 5 at 1130° C, to

K(Ti) = 10 at 1074° C.

K(Mg) does not vary in a simple way with temperature for the data set taken as a whole. Individual samples have K(Mg) increasing as temperature decreases. K(Mg) varies from 1.2 to 2.3 in the experiments. However, the broad range of K(Mg) at any given temperature suggests that the distribution coefficient can not be considered as a function of temperature alone, and is probably affected by melt composition.

Figure 4-43 shows the variation of Ln K(Al) over the studied temperature range. K(Al) has a broad range of values from 2.6 to 0.3. At temperatures above approximately 1160° C, K(Al) is quite variable but greater than unity. At lower temperatures K(Al) decreases rapidly, perhaps due to the peritectic reaction involving olivine + plagioclase + spinel described above.

The distribution data for Cr, Mn and Ni are greatly affected by the poor precision of the analyses of these elements in the spinel and/or the glass. K(Cr) is probably very high, as expected, perhaps >1000 in some cases. K(Ni) is also high, as 1 wt % NiO has been found in some magnetites. However, maximum values of K(Ni) = 30 may be overestimates, due to Ni loss to the wire hook. K(Mn) is generally greater than unity in these experiments, with most values in the range 1 - 3.

A spinel-glass Fe^{2+}-Mg exchange distribution coefficient (KD) can be calculated in similar fashion to that for olivine, where spinel replaces olivine in the expression. Unlike the KD for olivine, KD for spinel is quite variable (Figure 4-44). Values of KD increase with decreasing temperature, from approximately 1 near 1300° C to approximately 4 at 1074° C. The pattern of variation is similar to that shown for spinel Mg# in Figure 4-39, with an apparent step near 1130° C.

4.4.4 Spinel-olivine relations

For many of the charges with analysed spinel there are corresponding analysed olivines. Figure 4-45 shows the variation in spinel $Mg/(Mg + Fe^{2+})$ plotted against the forsterite content of the

coexisting olivine. Data from a charge at the Fe-FeO buffer plot near the main trend suggesting the effect of oxygen fugacity is small.

Figure 4-45 can be used to predict approximately the $Mg/(Mg + Fe^{2+})$ ratio of spinels coexisting with olivine when the spinels are too small for analysis. Pairs of analyses which plot on the trend may be in equilibrium. Roeder et al. (1979), in a discussion of olivine-spinel geothermometry, took a number of coexisting natural olivine and spinel pairs and heated them at magmatic temperatures for several days. They noted large changes in the Mg/Fe^{2+} ratios of the minerals which they interpreted as approaches to equilibrium. It is interesting to note that their original mineral pairs would plot well off the trend in Figure 4-45, whereas the heated minerals would plot on the trend or its extrapolation. This is taken as evidence of an approach to equilibrium of the olivine-spinel pairs in the present study.

Figure 4-46 illustrates the variation of the spinel-olivine Fe^{2+}-Mg distribution coefficient (KD) with temperature, where KD is defined as

$$KD = \frac{(Fe^{2+})_{SP} \cdot (Mg)_{OL}}{(Mg)_{SP} \cdot (Fe^{2+})_{OL}}$$

Composition terms are in cations. SP is spinel. OL is olivine. The overall pattern reflects the 'step' at 1130° C seen in the spinel-glass data. KD is obviously quite variable rising from approximately 3 at 1260° C to approximately 11 at 1074° C.

No satisfactory olivine-spinel thermometer calibration has been found using the spinel $Cr/(Cr + Al + Fe^{3+})$ ratio. This is attributed to the complicating effect of the proposed spinel reaction in the presence of olivine and plagioclase.

4.4.5 Plagioclase-glass relations

A few hundred pairs of plagioclase-glass analyses were obtained from the experimental charges. As has been described, many of the charges indicate a range of plagioclase compositions, interpreted as due to preserved relics. Individual samples may show consistent

changes in plagioclase composition with temperature. However, frequently at low temperatures, there is little evidence for an approach to equilibrium of the plagioclases. Figure 4-47 shows the variation in plagioclase composition with temperature for sample MV702. The trend is for the anorthite content of the plagioclases to decrease with decreasing temperature. Complete equilibration has not occurred. For comparison, the natural rock was found to contain plagioclase compositions up to An_{76}. The highest temperature experimental plagioclases may therefore have grown during the experiments.

To aid discussion of the data, plagioclase-glass pairs have been discarded from the lowest temperature experiments on each sample where plagioclase equilibration has not occurred. At higher temperatures, where disequilibrium was still apparent, no analyses were discarded so as to avoid any interpretive bias. The remaining data show a poor correlation between anorthite content of the plagioclase and experimental temperature (Figure 4-48).

Correlations between plagioclase compositions and simple element ratios in the coexisting glasses are usually very poor. There is, however, a distinct correlation between the orthoclase content of the plagioclases and the 100* K/(Ca + Na + K) ratio of the coexisting glasses (Figure 4-49). This may be supporting evidence for some equilibration of the plagioclase compositions in these relatively short duration experiments.

Figure 4-50 shows a plot of experiment temperatures versus the normative anorthite content of glasses coexisting with plagioclase. The trend has a spread of approximately 20° C and contains data from the experiments at the Fe-FeO buffer, suggesting the relation is not influenced by oxygen fugacity. All the available glasses have been plotted, regardless of whether the coexisting plagioclases were considered to be equilibrium products or relics. At the highest temperatures, only plagioclase ± spinel coexist with the glasses. The main group of glasses at slightly lower temperatures also coexist with olivine. The lowest temperature glasses contain clinopyroxene in addition to the earlier phases. Clearly, the trend is unaffected

by coexisting phases. When the normative wt % An/(An + Ab + Or) ratio is considered against temperature the same general relation is apparent, but with more scatter. The inclusion of the Na and K components appears to weaken the correlation, perhaps because of problems in analysing these elements precisely in glasses.

The element partitioning between plagioclase and glass has been examined on the basis of Ln K versus inverse temperature variations, and is compared with the data of Drake (1976) whose experiments of several hundred hours duration approached equilibrium. As for the pyroxenes in the next section, single element distribution coefficients can only be regarded as approximately describing the partitioning. Complex coupled substitutions occur in both plagioclase and clinopyroxene.

K(Ca) in this study is always greater than unity, which is consistent with the data of Drake (1976). Drake suggested that K(Ca) falls below unity at temperatures above 1430° C. Although there is no pattern discernible in the present data set taken as a whole, K(Ca) appears to range from 1.05 to 1.7 in the temperature range from 1074 to 1252° C. Some more reliable points from high temperature experiments on MV702 indicate a decrease in K(Ca) towards higher temperatures. These few points considered reliable agree well with the regression equation for K(Ca) published by Drake.

K(Na) also shows a spread of values with no consistent pattern for the data set as a whole. Taking points considered reliable (from sample MV702), K(Na) increases as temperature decreases, rising above unity in the approximate temperature region from 1150 to 1200° C. Over the studied temperature range for the whole data set, K(Na) varies from 0.7 - 1.8. The more reliable data are in general agreement with the data of Drake.

K(K) shows the same scatter of values as the previous coefficients but always remains below unity in the compositions studied. Values of K(K) mainly lie in the range 0.1 - 0.3.

K(Al) appears to show a slight increase as temperature decreases which is consistent with Drake's data. However, a similar trend

might be expected even if the plagioclases had not equilibrated since the Al_2O_3 content of the melt decreases rapidly as temperature decreases. The range of values of K(Al) is 1.6 - 2.3, although the high temperature MV702 data suggest values in the lower part of this range.

Values of K(Si) show less scatter than the other plagioclase coefficients and appear to increase slightly as temperature decreases. This conflicts with the data of Drake (1976) where K(Si) is nearly constant at 0.9. In this study K(Si) mainly ranges from 0.95 to 1.1 with the MV702 data producing values of 0.97 to 1.02. The discrepancy with the published data may indicate disequilibrium, but alternatively, the different values of K(Si) may be related to the compositions of the studied basalts. Villemant et al. (1981), in a study of phenocryst-matrix distribution coefficients for an alkali basalt series, found that the average plagioclase K(Si) was 1.02. Their range of values shows a decrease from 1.08 to 0.96 as the degree of crystallisation increases.

The partitioning of Fe and Mg between plagioclase and liquid may prove to be a useful petrogenetic indicator. Grove and Bence (1979) noted the increase in the Fe and Mg contents of plagioclases produced in progressively faster cooling-rate experiments. In the present study, relatively high levels of Fe and Mg in plagioclase probably reflect slight glass contamination of the analyses. Fe as FeO contents of plagioclase may reach 1wt % in these experiments, but the analytical problems prevent detailed discussion. Mg contents of the plagioclases are probably below the detection limit of the EDS.

4.4.6 Clinopyroxene-glass relations

All of the pyroxenes found in the charges are high-Ca clinopyroxenes, broadly described as augites. Fewer mineral-liquid pairs are available, from a narrower temperature range, than for plagioclase and olivine. This reflects the late appearance of augite in the crystallisation sequence of the studied samples. Whereas several samples show a wide temperature range of plagioclase stability, only the anomalous MV93 shows a comparable range of augite crystallisation.

With individual starting compositions it is often difficult to see significant changes in the coexisting augite compositions as melt composition and temperature change. This is probably because the experiment times were not long enough for equilibration, hence numerous relic compositions were preserved. However, augites from near clinopyroxene liquidus temperatures are often euhedral and have compositions which are distinct from lower temperature augites from the same starting composition. Figure 4-51 shows the variation of augite 100* Mg/(Mg + Fe) cation ratio with temperature. Except where stated, all Fe is expressed as FeO. Few of the augites have significant Fe_2O_3 content on the basis of stoichiometry calculations. This is due to analytical problems rather than genuinely ferric iron-free augites. Despite the problems there is a trend of increasing Mg/(Mg + Fe) with increasing temperature. While some of the compositions forming this trend may reflect equilibrium values, others are likely to be relics from the starting powders.

It was noted earlier that the crystallisation of pyroxene is always accompanied by olivine and usually by plagioclase. The coexisting glasses reflect the crystallisation of pyroxene-bearing assemblages with marked changes in their CaO and MgO contents (Figure 4-52). The overall consistency of the data is clear. With the exception of glasses from MV93 which form the slightly offset minor trend at high CaO values, the remainder of the glasses form a smooth trend of compositions which coexist with olivine + clinopyroxene + plagioclase $\pm$ Fe-Ti oxides. Data from the experiments at the Fe-FeO buffer are included in the trend. When this trend is compared with similar liquid compositions coexisting with olivine, clinopyroxene and plagioclase from tholeiitic provinces, compiled by Biggar (1983), the present data lie within the main cluster of trends and extend to much lower MgO and CaO contents. Either the glass CaO or MgO content could be used as an experimental temperature indicator when considering the clinopyroxene-bearing charges.

The element partitioning between augite and glass has been examined as in previous sections. Where possible, the Fe_2O_3 content of the pyroxenes has been calculated assuming stoichiometry. For these pyroxenes, Fe_2O_3 values are probably underestimated. In

consequence, FeO values will be overestimated and Mg# values are probably low. For many elements the variation of the distribution coefficients may be reflecting changes in melt composition more than in pyroxene compositions.

K(Mg) is always greater than unity in this study, increasing as temperature falls. By regression analysis

$$\text{Ln } K(Mg) = \frac{18350}{T^\circ K} - 12.061 \qquad r = 0.844 \qquad \ldots (8)$$

This equation suggests that K(Mg) falls below unity at temperatures above 1250° C, which is in good agreement with the equation of Grove and Bence (1979), and in acceptable agreement with the equation of Gamble and Taylor (1980) which predicts 1225° C. Both of these published studies were based on experiments on lunar basaltic compositions at low oxygen fugacities. Each equation has a significantly different rate of change of K(Mg) with temperature, perhaps due to the different starting compositions.

$K(Fe^{2+})$ also increases as temperature falls. There is considerable scatter of the Ln $K(Fe^{2+})$ data shown in Figure 4-54. For comparison with published data

$$\text{Ln } K(Fe^{2+}) = \frac{13130}{T^\circ K} - 9.595 \qquad r = 0.591 \qquad \ldots (9)$$

The equation predicts that $K(Fe^{2+})$ falls below unity at temperatures above 1100° C. This is approximately 100° C above the equivalent temperature predicted by Grove and Bence (1979) and Gamble and Taylor (1980). Much of the scatter in Figure 4-54 may be due to errors in estimating the pyroxene Fe^{2+} content.

K(Ca) is always greater than unity in this study and apparently increases as temperature falls. A regression line through the data has the equation

$$\text{Ln } K(Ca) = \frac{9810}{T^\circ K} - 6.248 \qquad r = 0.775 \qquad \ldots (10)$$

Compared to the two lunar composition studies, K(Ca) here is significantly higher and increases more rapidly over the studied range. In

the two published studies K(Ca) rises only very slightly as temperature falls. The phenocryst-matrix studies of Villemant et al. (1981) on alkali basalts found that augite K(Ca) rises from 2 to 3 in the earlier stages of crystallisation, comparable to the values for K(Ca) presented here.

K(Si) appears to rise above unity at temperatures above approximately 1130° C in the present study. K(Si) varies from 1.05 to 0.9. These values are consistent with those estimated from natural compositions by Villemant et al. (1981).

The distribution of Ti and Al between the clinopyroxenes and glasses is complex because of the importance of the Ti-Al substitutional couple in the pyroxenes. Ti and Al substitute for Si and divalent cations. No simple relation has been found between the Ti and Al contents of the pyroxenes and those of the coexisting glasses. K(Al) is usually less than 0.5. K(Ti) varies from 0.2 to 1.2.

K(Cr) is always greater than unity, but because of the poor data on Cr concentrations in the melt there are no reliable estimates of the coefficient. It is difficult to show that Cr values in the augites have changed in any way from the natural starting compositions.

Based on few analyses K(Na) is less than 0.3. For comparison, the study of Villemant et al. (1981) found values of K(Na) from 0.1 to 0.3 for alkali basalts.

Data for K(Mn) are poor because of the low precision of the Mn analyses in both pyroxenes and melt. A weak trend suggests an increase of K(Mn) from 0.4 to 3 as temperature decreases. Grove and Bence (1979) reported similar values.

Although the analysis of FeO in the pyroxenes is probably an overestimate, it is possible to examine in general terms the augite-liquid Fe^{2+}-Mg distribution coefficient (KD). This is calculated in the same way as the olivine-liquid KD, where augite replaces olivine in the expression.

Thompson (1974b) reported a constant value of 0.29 for KD, for 3 samples over a range of pressures and temperatures. Some higher values were ascribed to errors in estimating the melt compositions. In the present study, KD shows a range of values at any given temperature. Figure 4-55 illustrates the range of KD which is mainly from 0.22 to 0.38 over the studied temperature range. Grove and Bence (1979) and Gamble and Taylor (1980) suggested that KD decreases with decreasing temperature, from 0.26 - 0.28 at 1160° C, to 0.20 at 1090° C.

4.4.7 Clinopyroxene-olivine relations

The Fe-Mg distribution between the minerals is briefly considered in this section. In the augite analyses all Fe is expressed as FeO. Fe_2O_3 is recognised to be a likely component in the pyroxenes but, as described above, is difficult to estimate.

Figure 4-56 shows the Mg# of olivines (as % forsterite) versus the Mg/(Mg + Fe) ratio of coexisting augites. There is a discernible positive correlation, with many of the pyroxenes having higher Mg/(Mg + Fe) values than the coexisting olivines. Taking the likely ferric iron content of the pyroxenes into account, most of the augites would have higher Mg# values than the coexisting olivines. Natural examples of coexisting olivine and augite, crystallised from basic or ultrabasic magmas, show that the pyroxene Mg# is greater than the Mg# of coexisting olivine (e.g. Wilson, 1982). This relation extends to high pressures (Elthon et al., 1982).

4.4.8 Relations involving ilmenite

Ilmenite-glass relations

Ilmenite and coexisting glass were analysed in 14 charges although ilmenite was recognised in several more. The samples range over 35° C from 1092 to 1127° C.

The temperature of appearance of ilmenite is related to the Ti content of the melt. In the compositions studied here, ilmenite first crystallises from melts of 5 $\pm$ 1 wt % TiO_2. Unlike the other Fe-Ti oxide phase, magnetite, the temperature of crystallisation of

ilmenite does not appear to be greatly affected by changes in the ferric-ferrous ratio of the melt.

The $Mg/(Mg + Fe^{2+})$ ratio of the ilmenites shows a positive correlation with temperature, as shown in Figure 4-57. The data set includes ilmenite from the Fe-FeO buffer experiments. FeO and Fe_2O_3 contents of the ilmenites were calculated assuming stoichiometry. The ilmenites appear to have equilibrated, at least with respect to Mg and Fe^{2+}, within the duration of the experiments.

The only element to show a simple correlation of distribution coefficient with temperature is Ti. By least squares regression analysis

$$\text{Ln } K(Ti) = \frac{18760}{T°K} - 10.985 \qquad r = 0.855 \qquad \ldots (11)$$

Over the 35° C temperature range K(Ti) increases from 12 to 17.

Other elements show no simple correlations. $K(Fe^{2+})$ ranges from 3.5 to 4.5. $K(Fe^{3+})$ ranges from 3 to 4.5. Since the concentration of these components in the ilmenites was calculated on the basis of stoichiometry there may be significant errors in the values used. There is some uncertainty about the analyses as after recalculation the totals were still low. K(Mg) shows a narrow range from 1.8 to 2.2. Al is always low in these ilmenites and may be affected by slight contamination from the surrounding glass. K(Al) apparently ranges from 0.1 to 0.04. Mn analyses in ilmenite and glass are of low precision but K(Mn) appears to be usually greater than unity, ranging from 0.9 to 5. Cr data for these samples have very poor precision but K(Cr) is clearly much greater than unity.

The ilmenite-liquid Fe^{2+}-Mg distribution coefficient (KD) can be calculated as for the olivine-liquid KD, with ilmenite substituting for olivine. The range of values of KD is shown in Figure 4-58 plotted against melt wt % MgO. Most of the values are approximately 2.0 ± 0.1. There appears to be little variation within the narrow temperature and composition range studied. The two points plotting distinctly below the main trend with KD = 1.7 are

from an experiment at the Fe-FeO buffer. All the other points are from the Ni-NiO buffer experiments. KD may be sensitive to oxygen fugacity.

Magnetite-Ilmenite Relations

Twelve magnetite-ilmenite pairs were collected from the experiments. After recalculating into the appropriate end-members, the pairs were processed through the equations of Spencer and Lindsley (1981) which predict the temperature and oxygen fugacity of equilibration. This recent study is intended to replace the classic study of Buddington and Lindsley (1964) in the temperature range of interest here. The predicted temperatures range from 950 to 1250° C depending on how the minor elements (Cr, Al, Mn and Mg) are accounted for. The experiment temperatures range from 1092 to 1124° C. Errors in predicted oxygen fugacity, in terms of $\log_{10} fO_2$, range from + 1 to - 3 units.

Regardless of the quality of the experimental data in the present study, the geothermometer and oxygen barometer can not be exploited to the full unless a reliable way is found of estimating the effect of the minor elements. The procedure which has been adopted incorporates parts of the method of Anderson (1968) and Lindsley (unpublished). Initially the analyses are recast assuming a stoichiometric formula by recalculating for Fe^{3+}.

For ilmenite; subtract Mg and Mn as $MgTiO_3$ and $MnTiO_3$ and discard. Discard Al and Cr. The remaining Ti is calculated as ilmenite. Remaining Fe is calculated as haematite. The ilmenite and haematite values are then recast to unity.

For magnetite there are two possible procedures. If there is excess Mg over ½(Cr + Al) then the ulvospinel is calculated from (Ti - ½Mn - ½ excess Mg), and the remaining Fe is calculated as magnetite. Alternatively, if there is excess ½(Cr + Al) over Mg then the ulvospinel is calculated from (Ti - ½Mn), and the remaining (Fe - excess ½(Cr + Al)) is calculated as magnetite. The obtained ulvospinel and magnetite values are then recast to unity.

Using the above method of recalculation, and Spencer and Lindsley's equations, the predicted temperatures and oxygen fugacities were compared with the experimental values. The predictions are low by 2 to 58° C and differ by +0.3 to -0.7 $\log_{10}$ units of oxygen fugacity. Using the published diagram of Buddington and Lindsley, the predictions are low by 2 to 49° C and differ by 0 to -0.9 $\log_{10}$ units of oxygen fugacity. In both cases the effect of lower temperatures and oxygen fugacities is to move the determined points approximately down the Ni - NiO buffer, where the experiments were based. Thus the correct oxygen buffer may still be identified though the temperature on it is perhaps suspect.

Ilmenite-olivine relations

A positive correlation can be found between the ilmenite $Mg/(Mg + Fe^{2+})$ ratio and the forsterite content of coexisting olivine, as shown in Figure 4-59. A correlation with temperature can also be seen, as would be expected. Andersen and Lindsley (1979) have calibrated an olivine-ilmenite thermometer based on experimental studies in a synthetic system. The data from the Fe - FeO buffer are in agreement with this thermometer to within 15° C. At the Ni - NiO buffer the predicted temperatures are much lower than the experimental temperatures. This is perhaps due to the effect of the minor elements on the recalculation of the ilmenite and olivine end-members used in the thermometer, but may be due to the variation of the ilmenite-liquid KD with oxygen fugacity, unlike the olivine-liquid KD.

4.5 Summary

The experiments were carried out primarily to provide data for the development of mineral temperature equations and mineral composition equations. The results discussed in this chapter illustrate that complete equilibrium was not always achieved in experiments involving spinel, plagioclase or high-Ca pyroxene. Homogeneous glass and olivine compositions were produced. The assumption of surface equilibrium allows the glass compositions to be taken as representing equilibria with the crystal phases.

The results indicate that olivine is the silicate liquidus

phase for the most magnesian basalts, joined or replaced by plagioclase in the less magnesian samples (Mg# <57). Clinopyroxene does not approach the liquidus of any of the studied compositions, and usually crystallises at lower temperatures than both olivine and plagioclase. Spinel liquidus temperatures have been increased by Cr contamination of the supplied powders. Experiments on uncontaminated material at the Ni - NiO buffer suggest that Cr-Al spinel is a near-liquidus phase in the more magnesian compositions, with titanomagnetite a near-liquidus phase in the less magnesian compositions.

The sequence of phases in the experiments on the Mg-rich samples, olivine followed by plagioclase followed by clinopyroxene, contrasts with the observed phenocryst phases in these samples, typically olivine + clinopyroxene. The absence of clinopyroxene from the liquidus in a broad range of rocks, which show evidence of evolution involving clinopyroxene, has been interpreted by Thompson (1972a) as evidence for higher pressure crystallisation of the clinopyroxene. This explanation for the origin of at least the clinopyroxene phenocrysts in the present study will be examined in later chapters, with additional evidence from the natural rocks and the experimental crystallisation model.

Glass and olivine compositions show regular variations with temperature suggesting good internal consistency of the data set. Spinel phases, plagioclases, clinopyroxenes and ilmenites also show compositional variations with temperature, suggesting some approach to equilibrium. The sensitivity of glass compositions to the nature of the coexisting mineral assemblage indicates the analyses may be used with some confidence to derive mineral temperature equations. The glass compositions range from nepheline-normative to quartz-normative and illustrate the operation of the olivine-clinopyroxene-plagioclase thermal divide at low pressures.

For glasses coexisting with olivine, there is a good positive correlation between experimental temperature and the MgO content of the glass. Simple geothermometers have been presented which relate distribution coefficients, for elements between olivine and glass, to experimental temperature. The Fe^{2+}-Mg exchange distribution

coefficient (KD) for olivine and liquid is nearly constant at 0.30 ± 0.03 for the higher temperature, magnesian compositions and is independent of oxygen fugacity. At lower temperatures, KD increases to 0.35. This is attributed to compositional effects, with a positive correlation noted between KD and glass SiO_2 content.

Spinel compositions produced in the experiments show a positive correlation between Mg# and experimental temperature. Cr-Al-Fe^{3+} variations are complex, partly due to the effect of associated olivine + plagioclase crystallisation and to incomplete equilibration. Comparisons of coexisting olivine and spinel Mg# values with published data indicate good agreement, suggesting some equilibration of the spinel compositions. The spinel-liquid KD (analogous to that of olivine-liquid) is quite variable, ranging from approximately 1 at high temperatures to near 4 at low temperatures. The Cr contamination of the rock powders makes it difficult to relate directly the experimental spinel compositions to those in the natural rocks.

There is a good positive correlation between experimental temperature and the normative anorthite content of experimental glasses coexisting with plagioclase. Although affected by equilibration problems many samples show a progressive decrease in the anorthite content of experimental plagioclase with decreasing temperature. Most, if not all, of the anomalous plagioclase compositions are relics from the starting rock powder.

The experimental clinopyroxene data have been affected by incomplete equilibration and by analytical problems. The ranges of compositions found are attributed to the preservation of relics. The absence of Na in the pyroxene analyses makes the estimation of ferric iron very uncertain. Some equilibration of the pyroxenes may have occurred in the experiments as there are positive correlations of the clinopyroxene Mg/(Mg + Fe) values with experimental temperature and with coexisting glass and olivine Mg#. It is unlikely that the experiment times in this study have allowed any significant equilibration of the minor elements in the pyroxenes.

Limited ilmenite data indicate that crystallisation of the phase is partly governed by the Ti content of the melt, and is largely independent of the ferric-ferrous ratio of the melt. There is a positive correlation of ilmenite Mg# with experimental temperature and with coexisting glass and olivine Mg#. The ilmenite-liquid Fe^{2+}-Mg KD at the Ni - NiO buffer is 2.0 $\pm$ 0.1. A single experiment from the Fe-FeO buffer has a KD of 1.7, suggesting a possible effect of changing oxygen fugacity. Coexisting magnetite-ilmenite pairs from the experiments produce slightly low predicted temperatures from the thermometers of Buddington and Lindsley (1964) and Spencer and Lindsley (1981), but correctly identify the experimental oxygen buffer.

The main use of the experimental data is presented in the next chapter with the derivation of the temperature and composition equations for the experimental crystallisation model. Comparison of the natural phenocryst assemblages with the experimental data is made using the extended version of this model in Chapter 7.

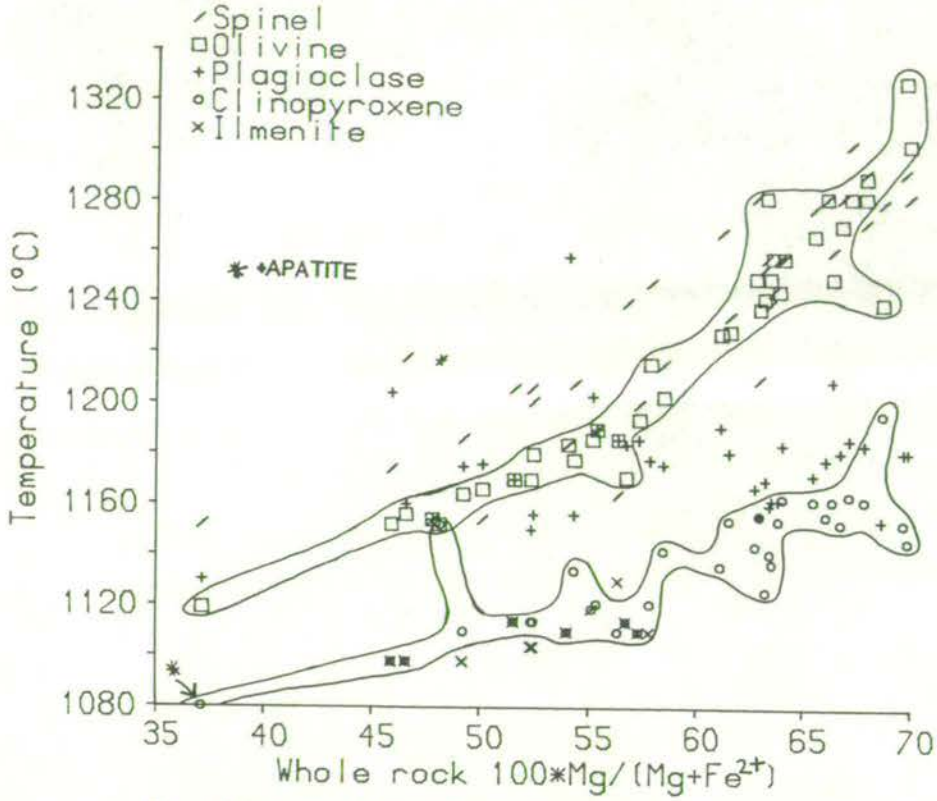

Figure 4-1. Liquidus temperatures of phases in experiments at the Ni-NiO buffer, plotted against whole rock 100*Mg/(Mg+Fe^{2+}). The circled fields enclose the olivine and clinopyroxene data.

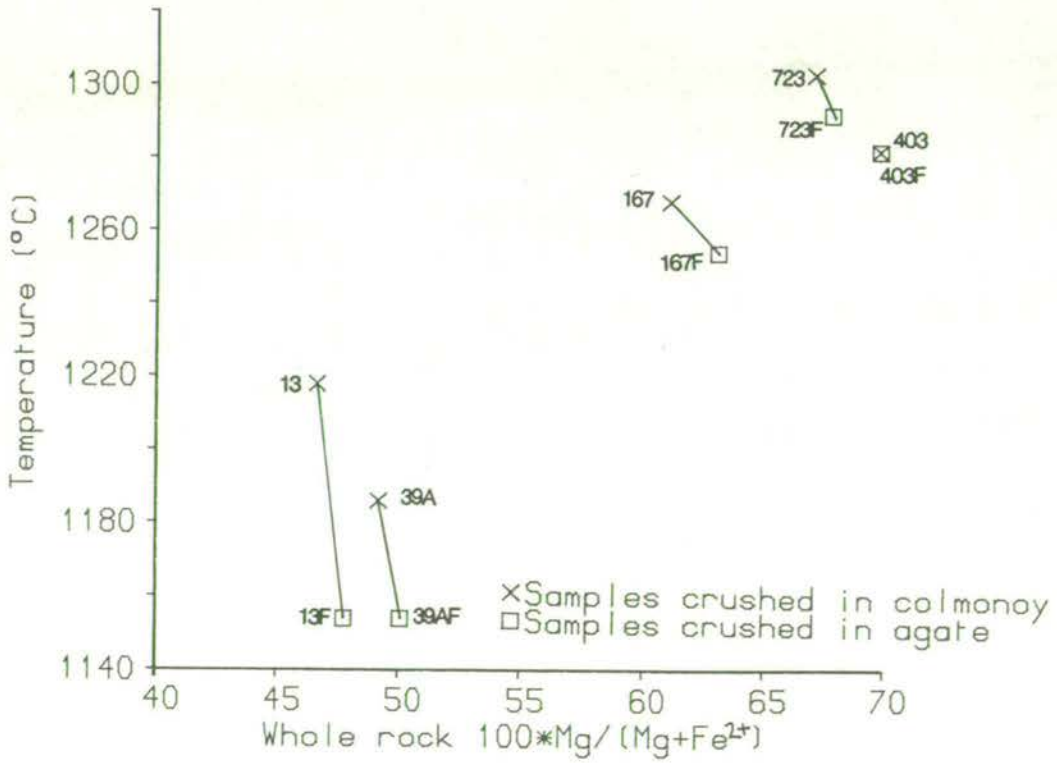

Figure 4-2. Spinel liquidus temperatures plotted against whole rock 100*Mg/(Mg+Fe^{2+}), for sample pairs crushed in colmonoy or in agate.

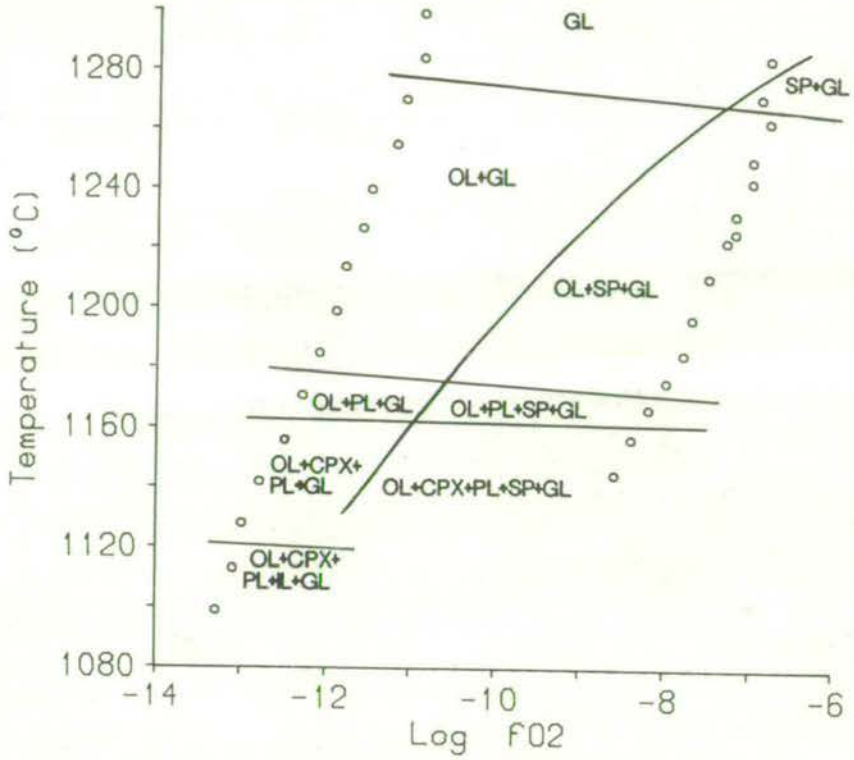

Figure 4-3. T - fO2 phase relations for sample MV166.

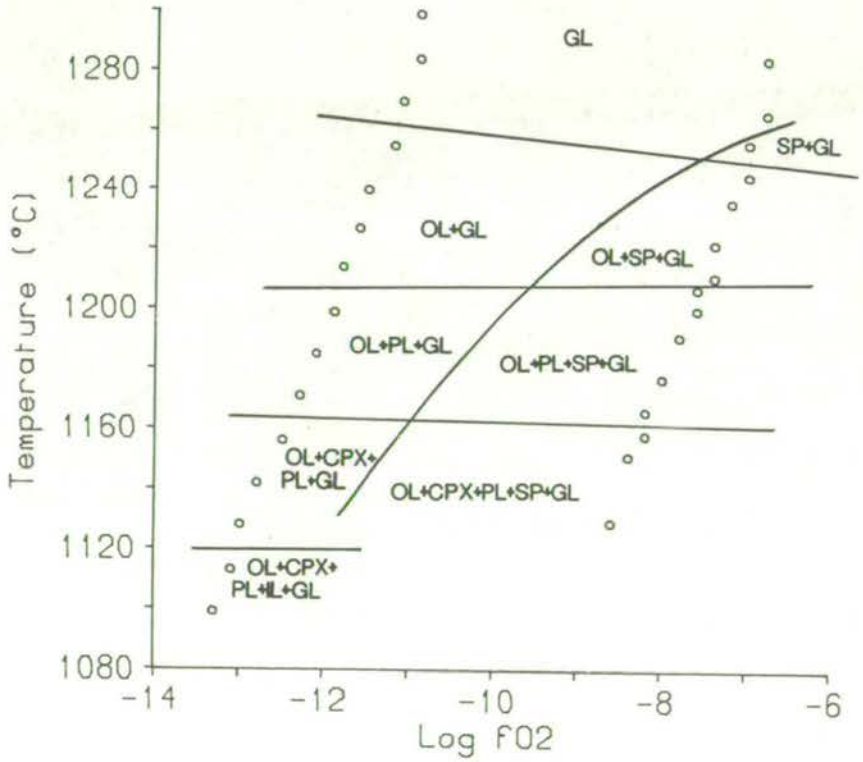

Figure 4-4. T - fO2 phase relations for sample MV106.

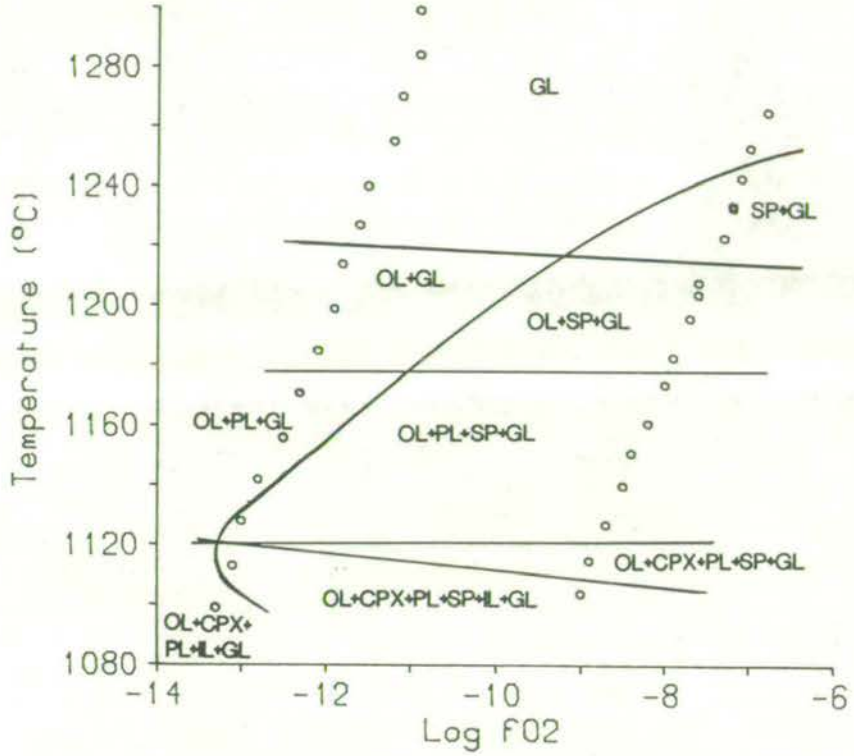

Figure 4-5. T - fO2 phase relations for sample MV160.

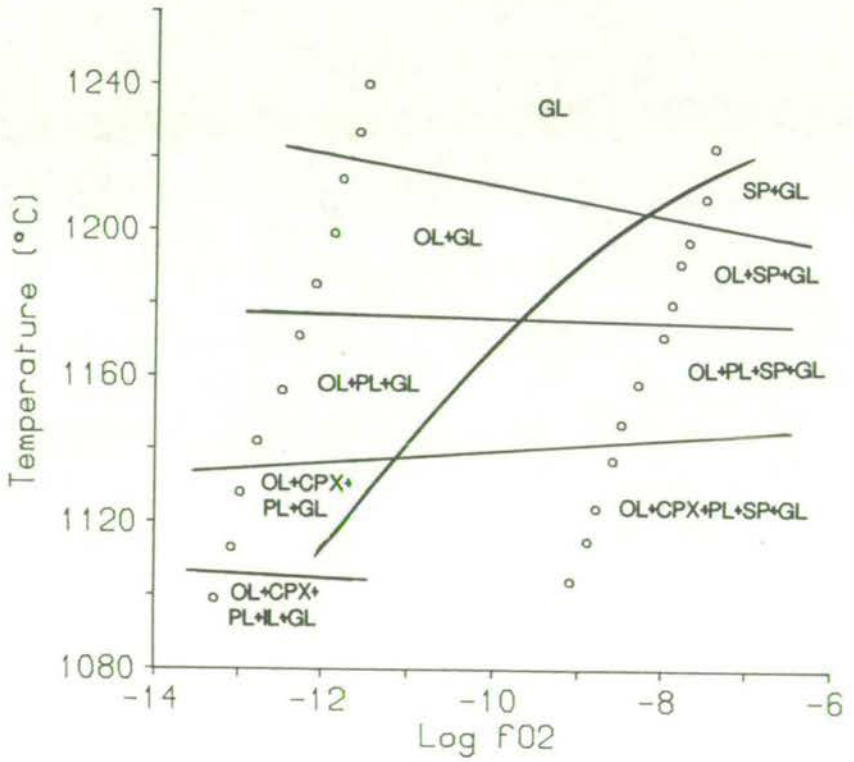

Figure 4-6. T - fO2 phase relations for sample MV40B.

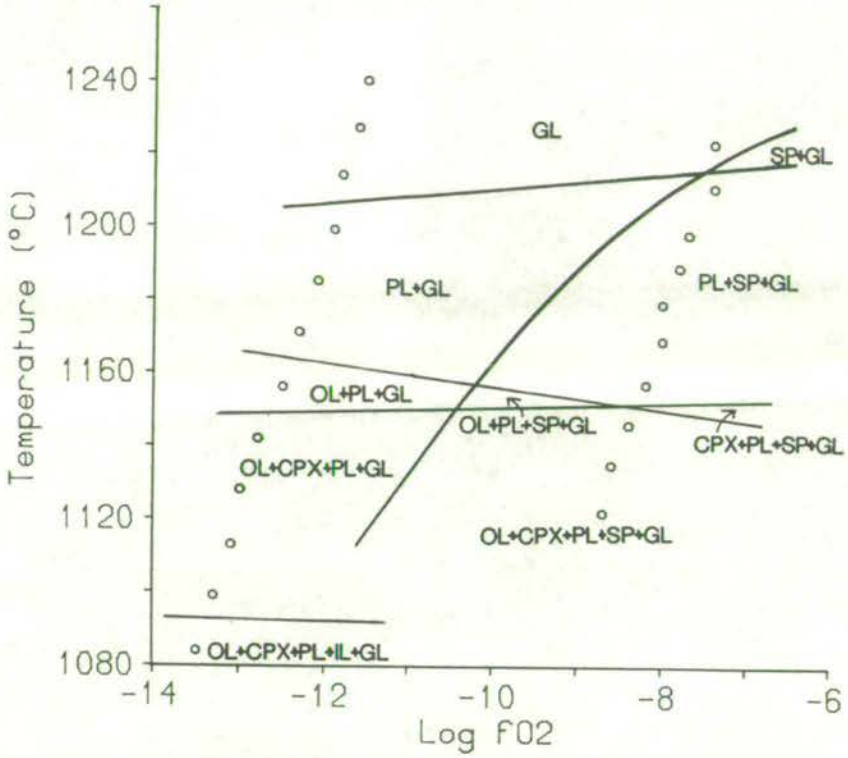

Figure 4-7. T - f02 phase relations for sample MV402.

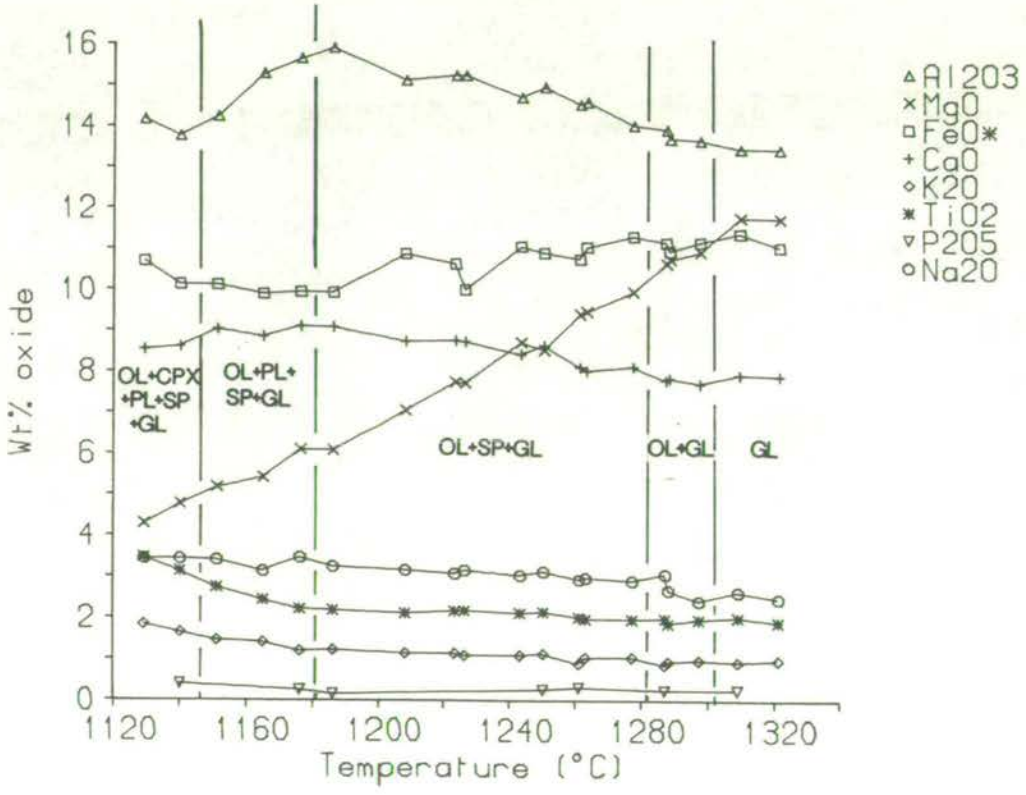

Figure 4-8. Variations in glass composition and coexisting phase assemblage with temperature, for sample MV403 at the Ni-NiO buffer.

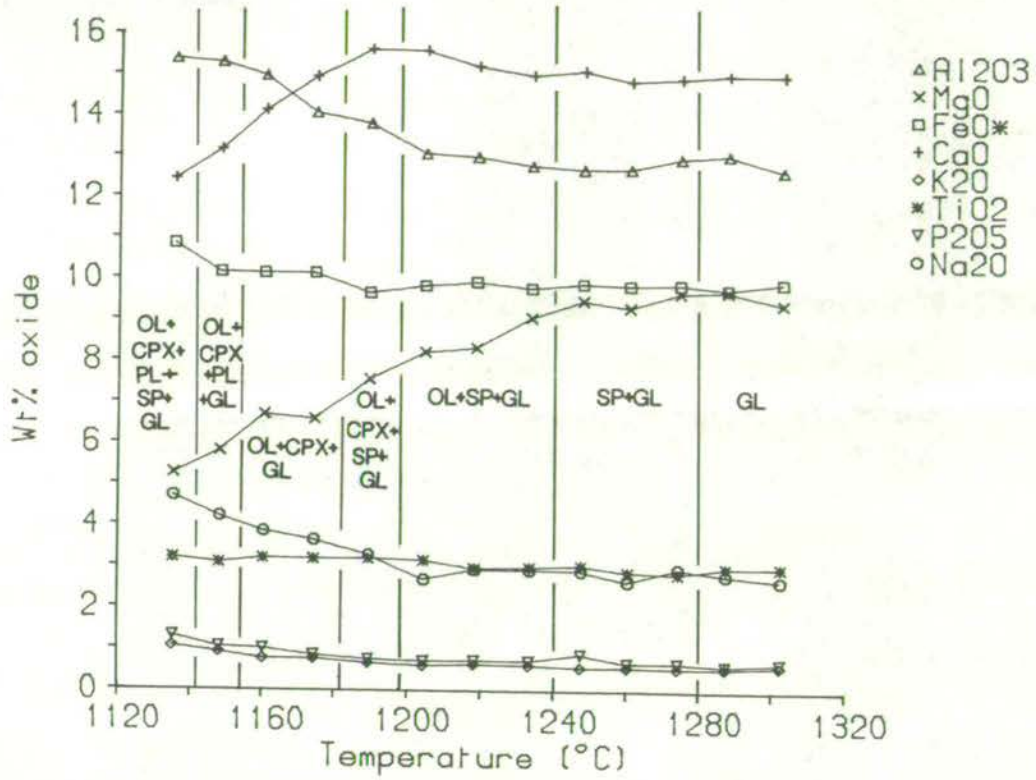

Figure 4-9. Variations in glass composition and coexisting phase assemblage with temperature, for sample MV93 at the Ni-NiO buffer.

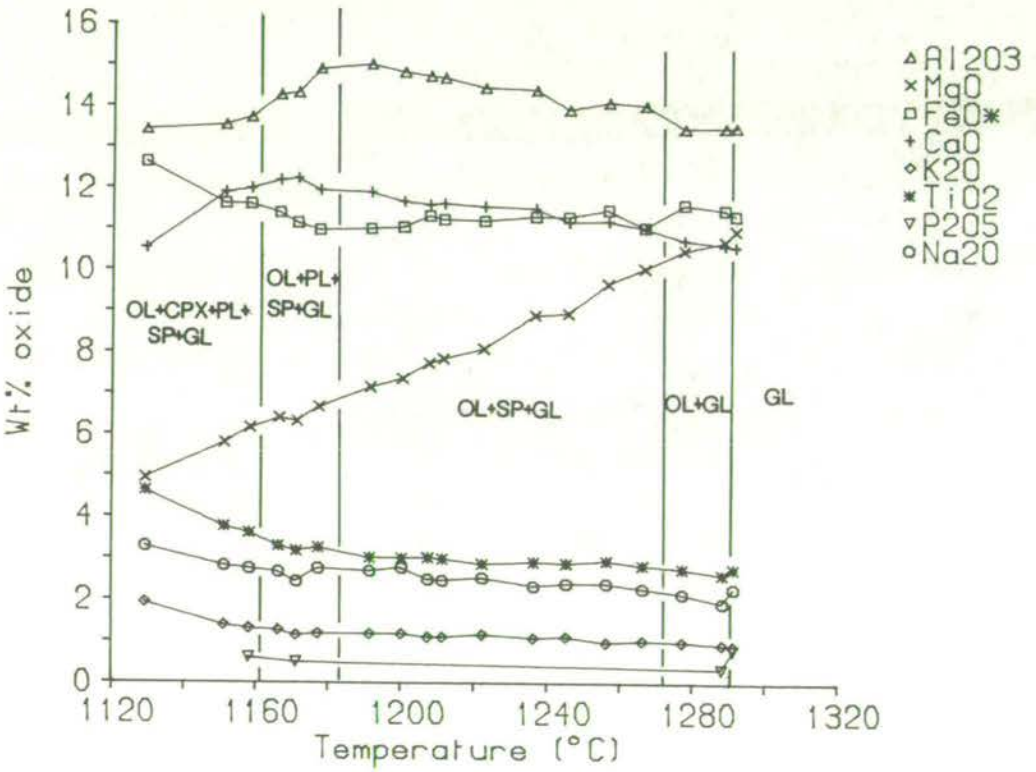

Figure 4-10. Variations in glass composition and coexisting phase assemblage with temperature, for sample MV521 at the Ni-NiO buffer.

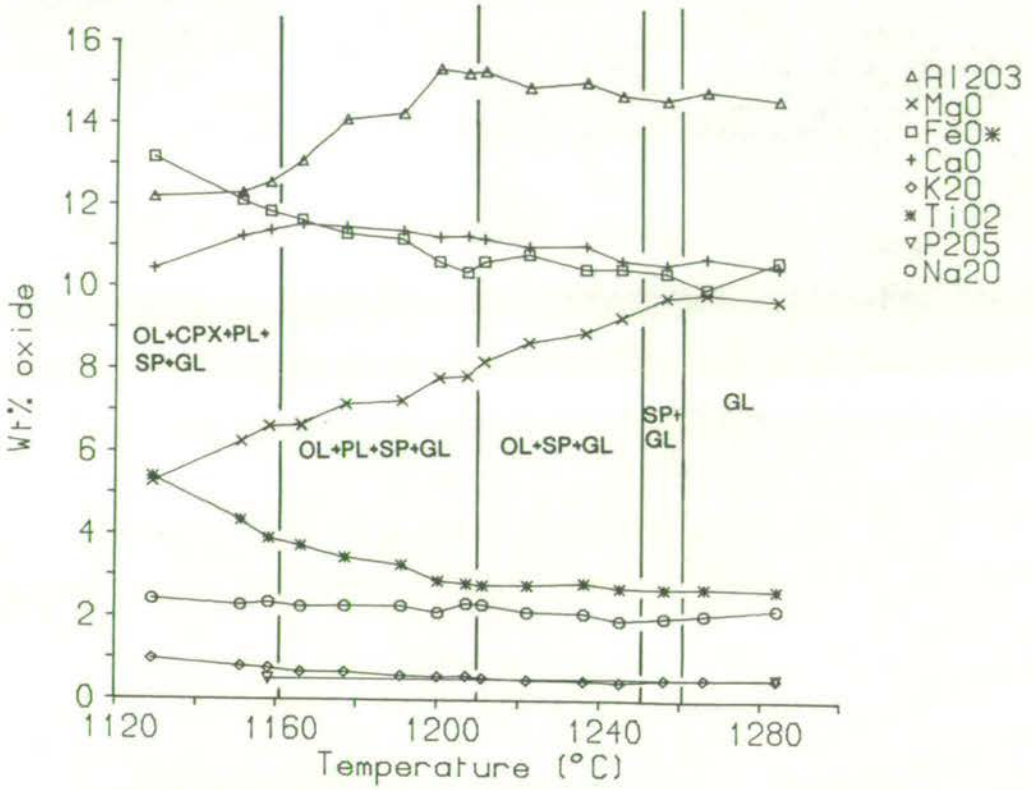

Figure 4-11. Variations in glass composition and coexisting phase assemblage with temperature, for sample MV106 at the Ni-NiO buffer.

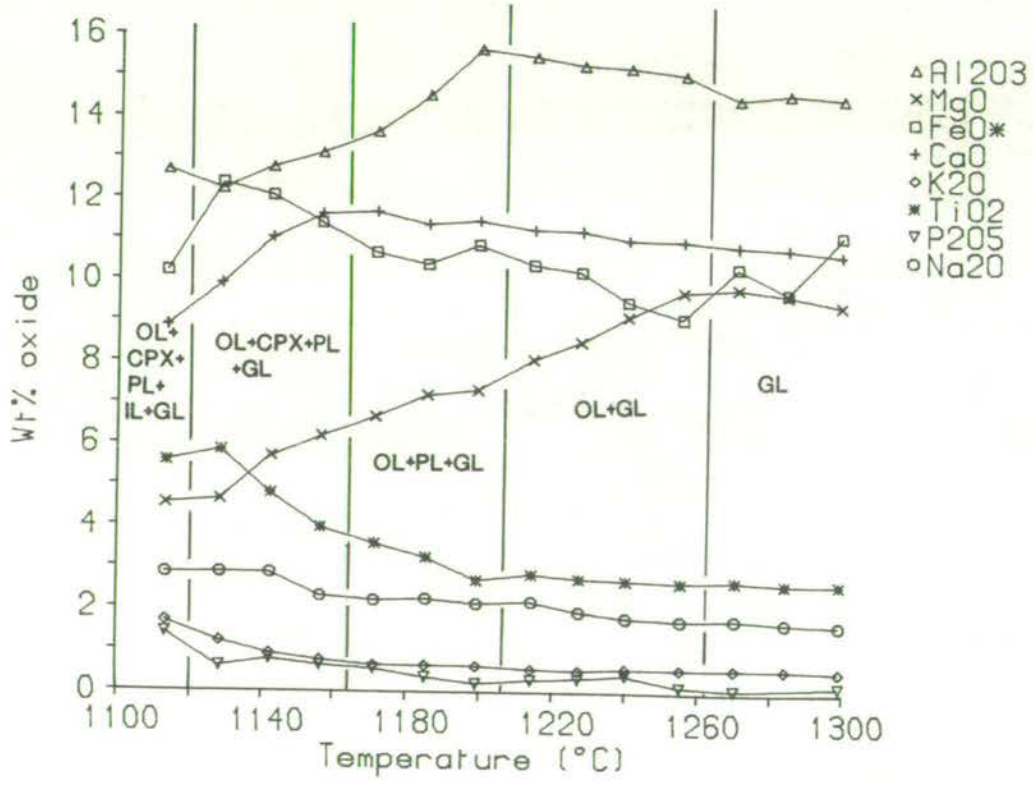

Figure 4-12. Variations in glass composition and coexisting phase assemblage with temperature, for sample MV106 at the Fe-FeO buffer.

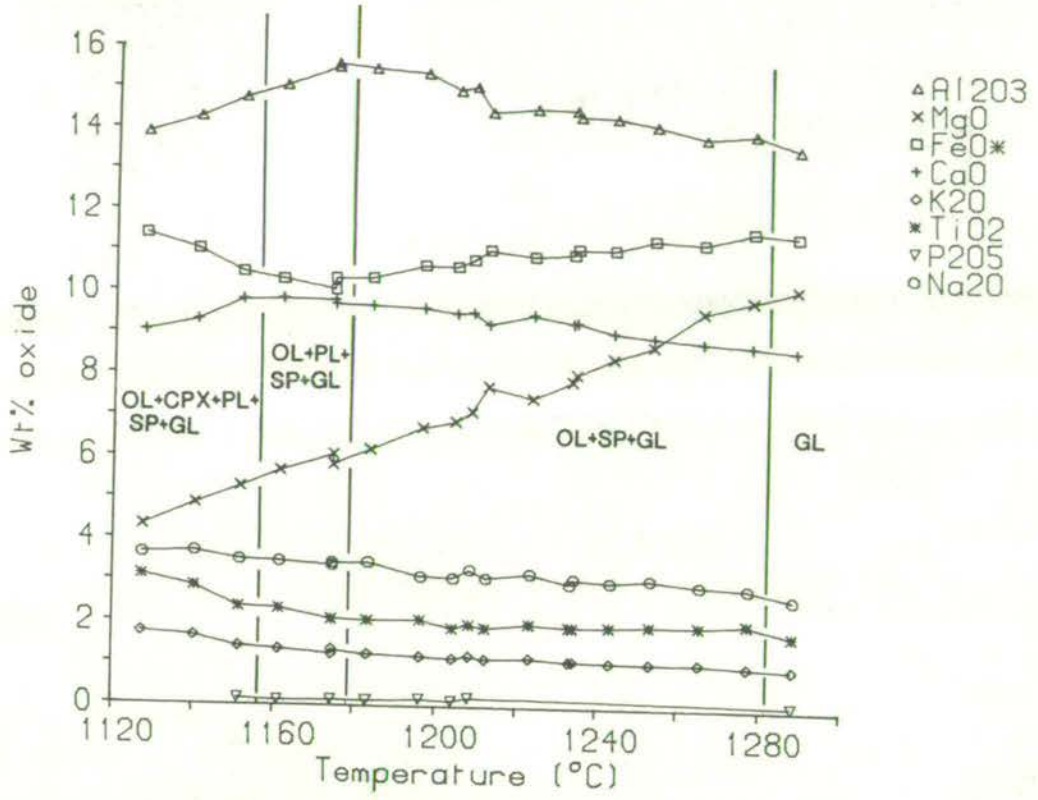

Figure 4-13. Variations in glass composition and coexisting phase assemblage with temperature, for sample MV164 at the Ni-NiO buffer.

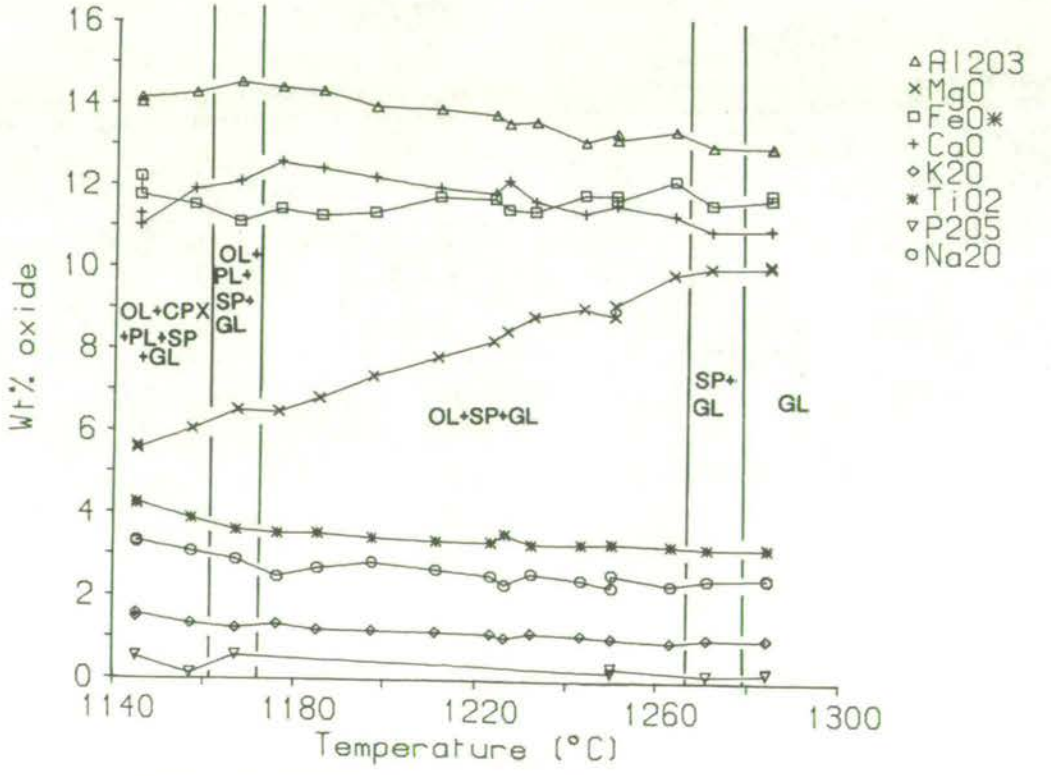

Figure 4-14. Variations in glass composition and coexisting phase assemblage with temperature, for sample MV166 at the Ni-NiO buffer.

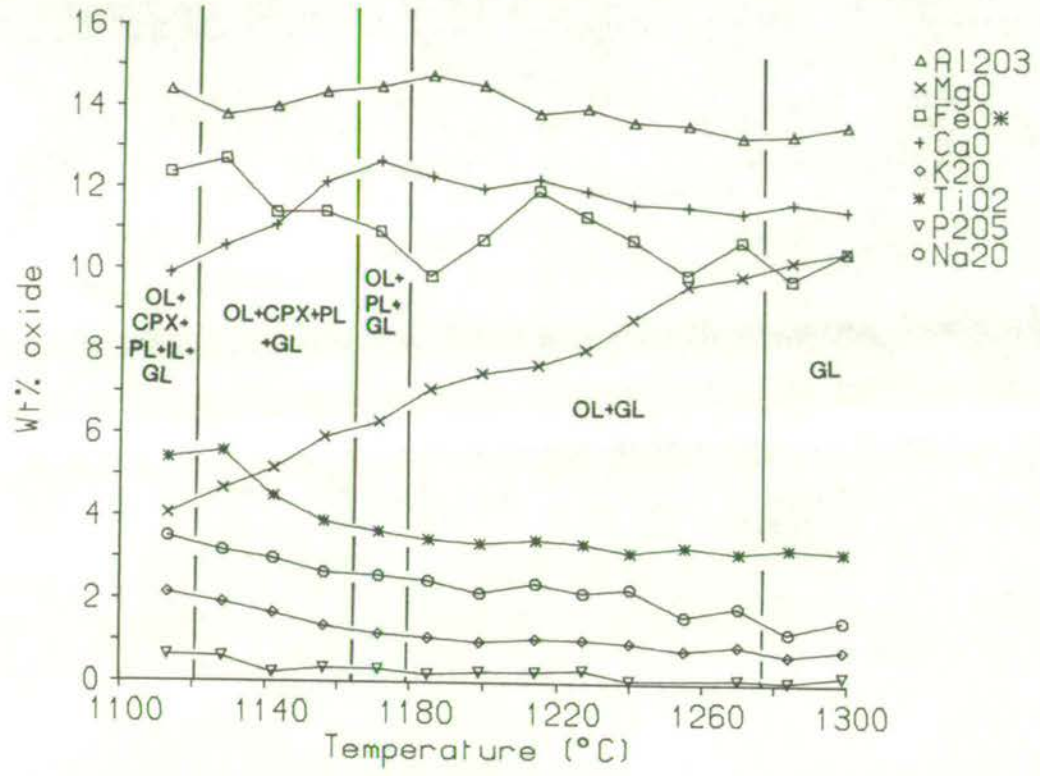

Figure 4-15. Variations in glass composition and coexisting phase assemblage with temperature, for sample MV166 at the Fe-FeO buffer.

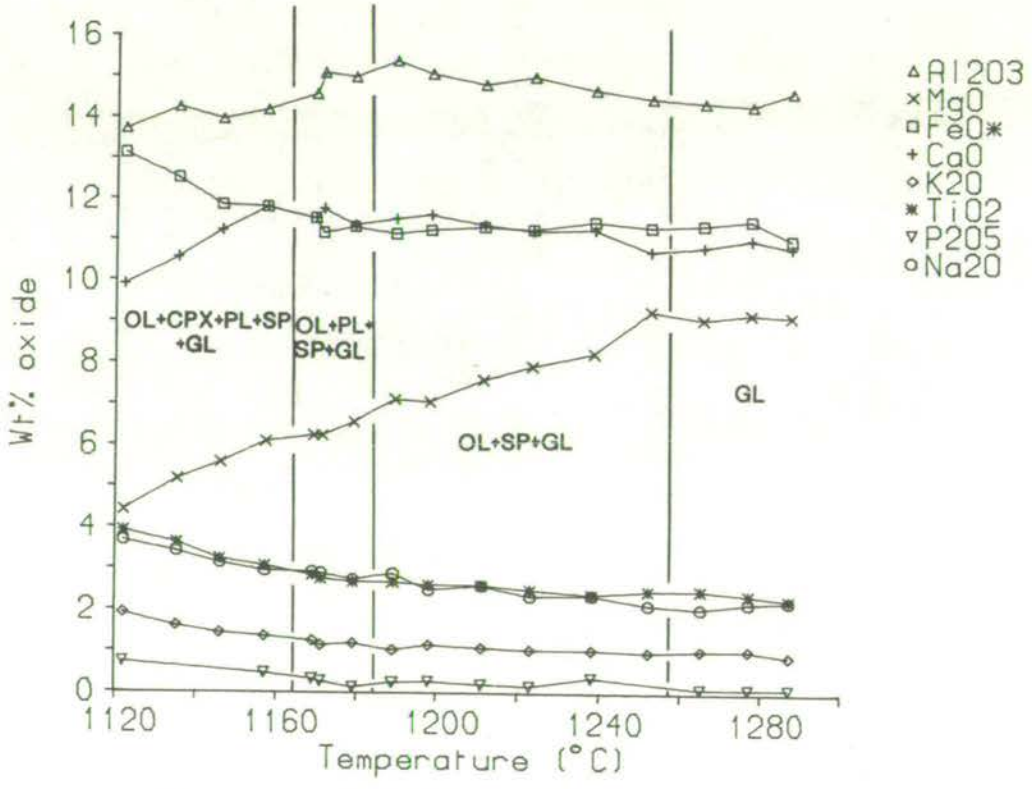

Figure 4-16. Variations in glass composition and coexisting phase assemblage with temperature, for sample MV703 at the Ni-NiO buffer.

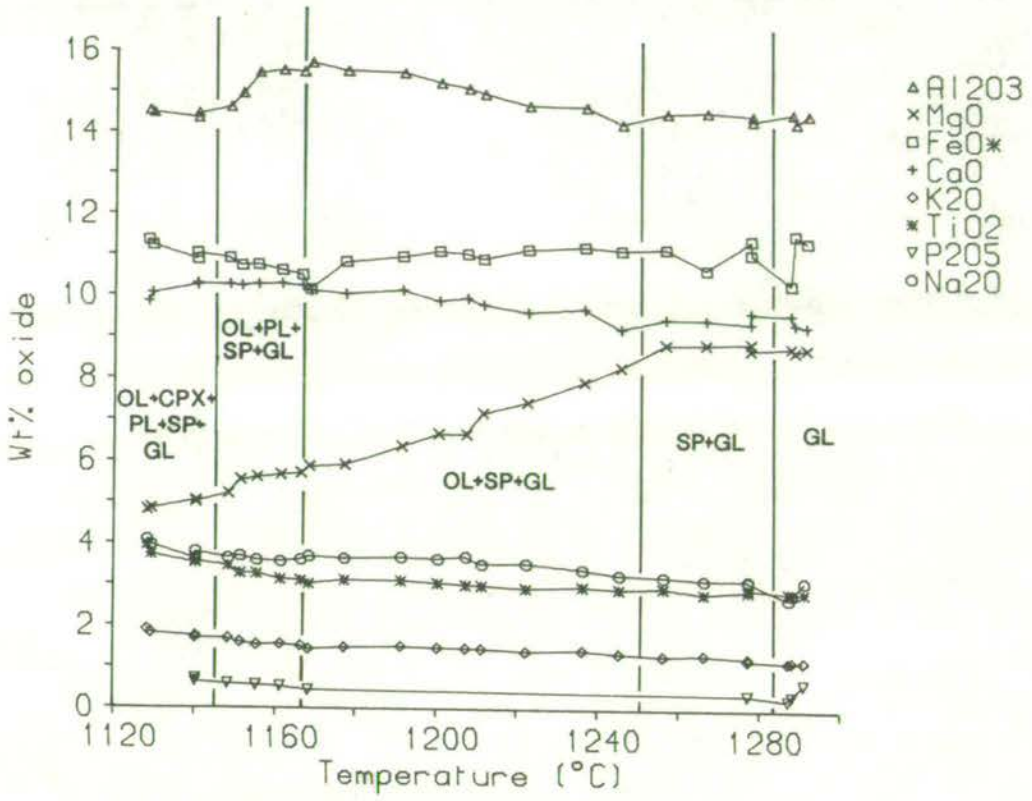

Figure 4-17. Variations in glass composition and coexisting phase assemblage with temperature, for sample MV406 at the Ni-NiO buffer.

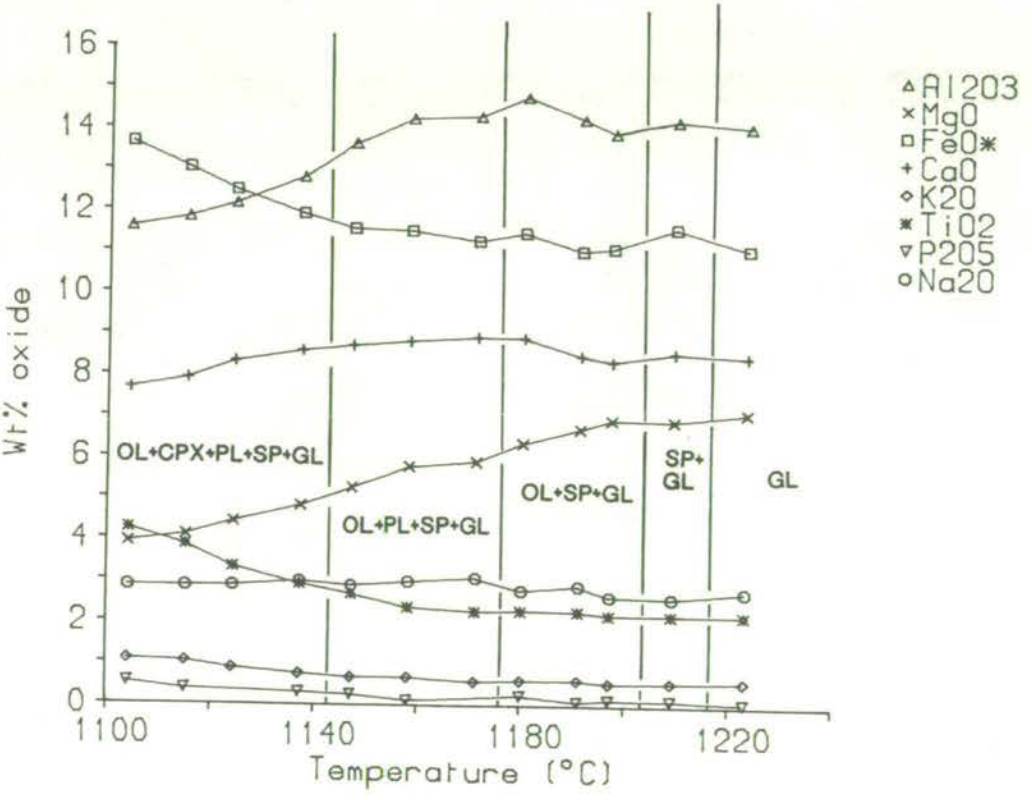

Figure 4-18. Variations in glass composition and coexisting phase assemblage with temperature, for sample MV408 at the Ni-NiO buffer.

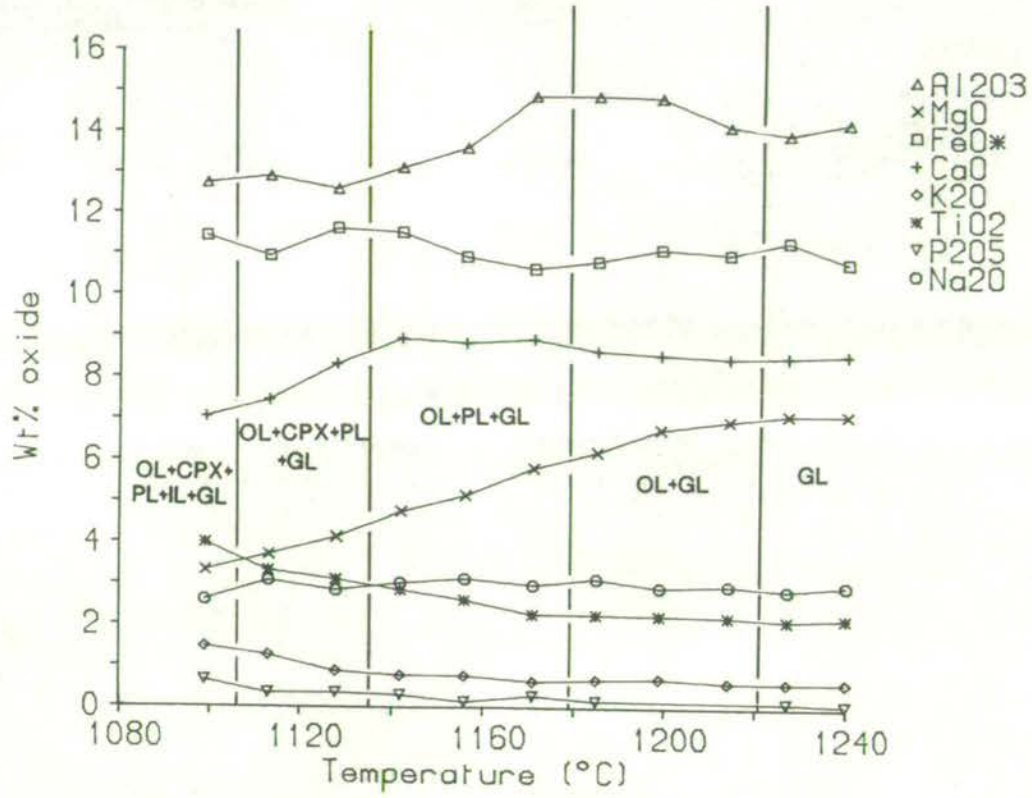

Figure 4-19. Variations in glass composition and coexisting phase assemblage with temperature, for sample MV408 at the Fe-FeO buffer.

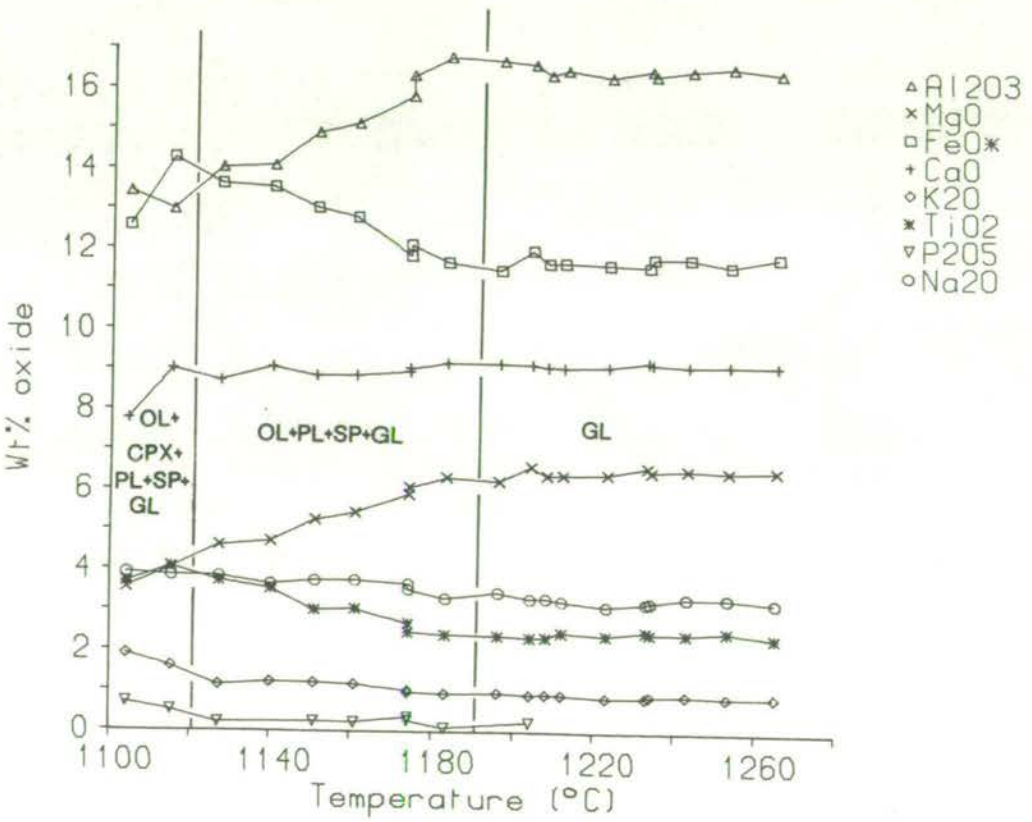

Figure 4-20. Variations in glass composition and coexisting phase assemblage with temperature, for sample MV704 at the Ni-NiO buffer.

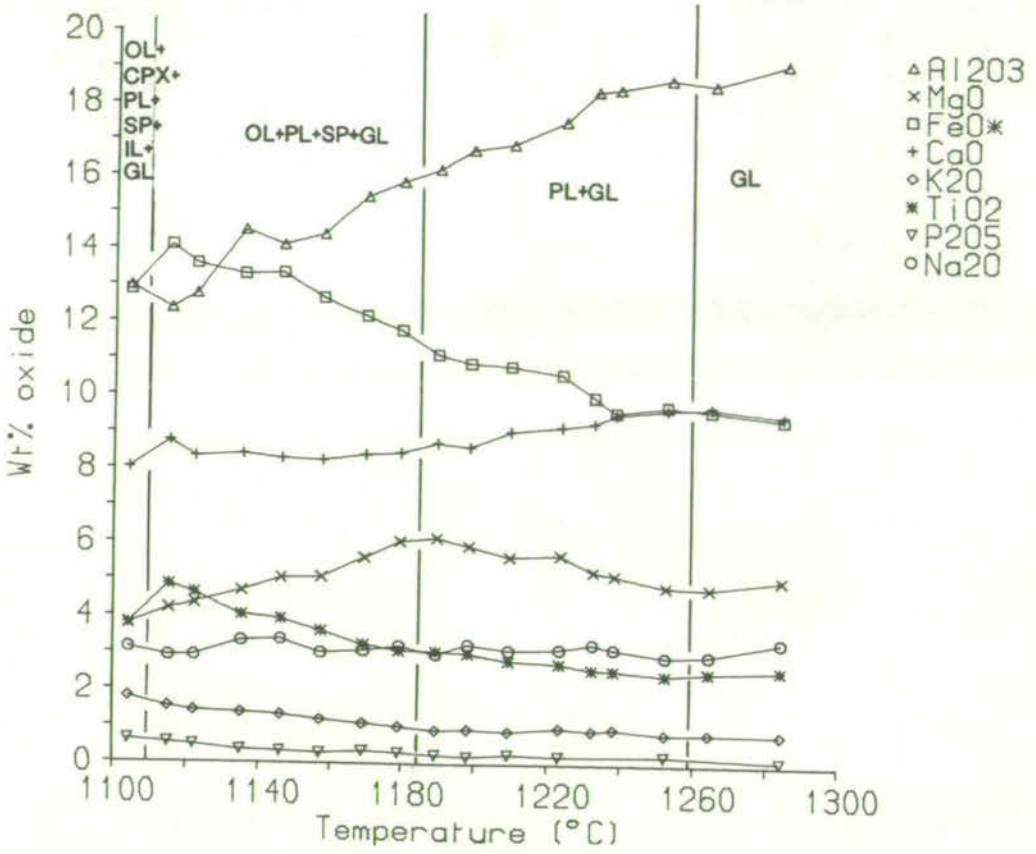

Figure 4-21. Variations in glass composition and coexisting phase assemblage with temperature, for sample MV702 at the Ni-NiO buffer.

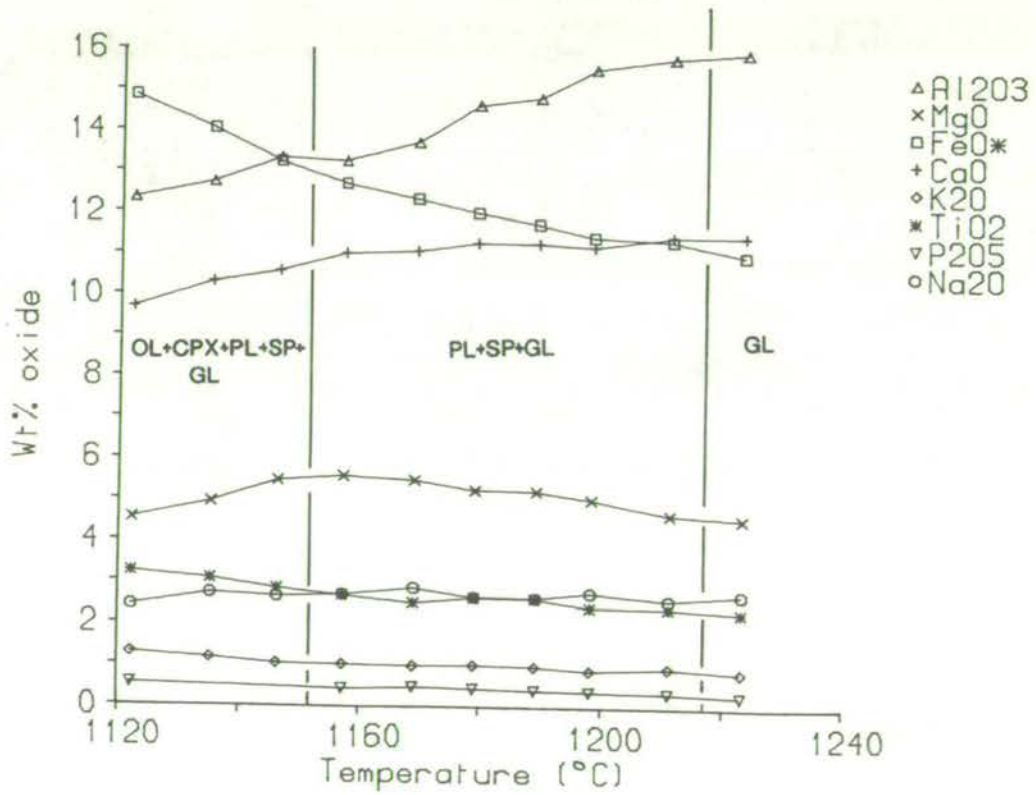

Figure 4-22. Variations in glass composition and coexisting phase assemblage with temperature, for sample MV402 at the Ni-NiO buffer.

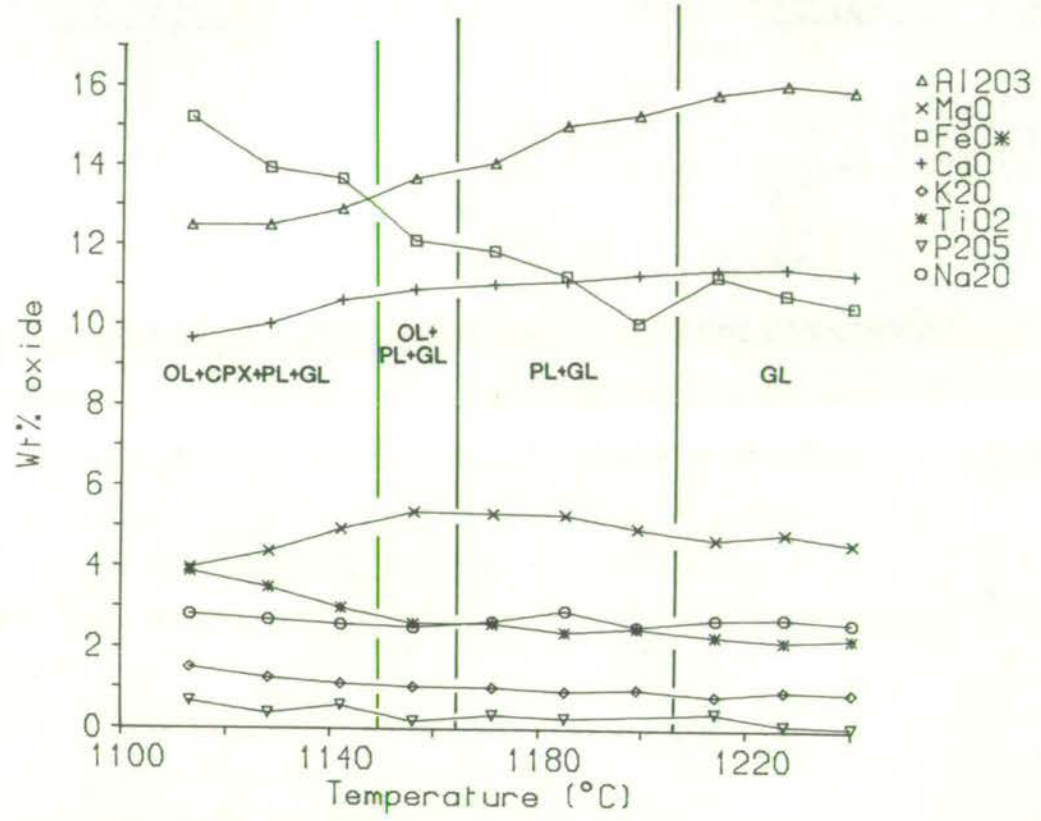

Figure 4-23. Variations in glass composition and coexisting phase assemblage with temperature, for sample MV402 at the Fe-FeO buffer.

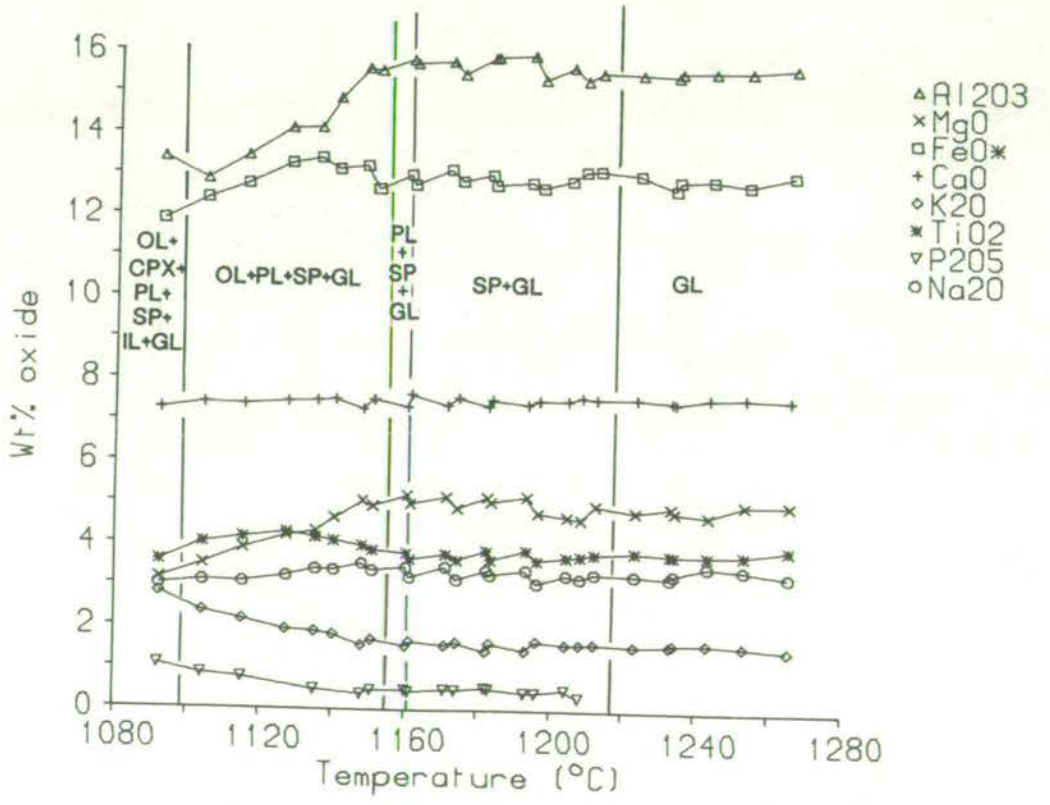

Figure 4-24. Variations in glass composition and coexisting phase assemblage with temperature, for sample MV13 at the Ni-NiO buffer.

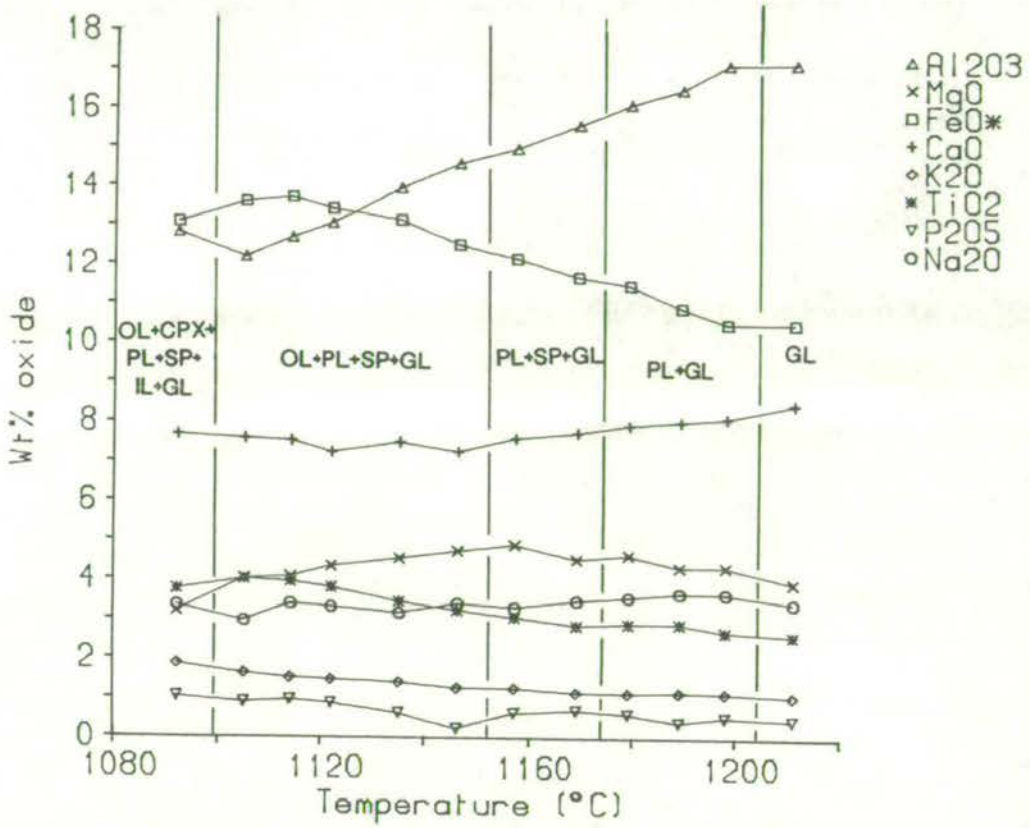

Figure 4-25. Variations in glass composition and coexisting phase assemblage with temperature, for sample MV40A at the Ni-NiO buffer.

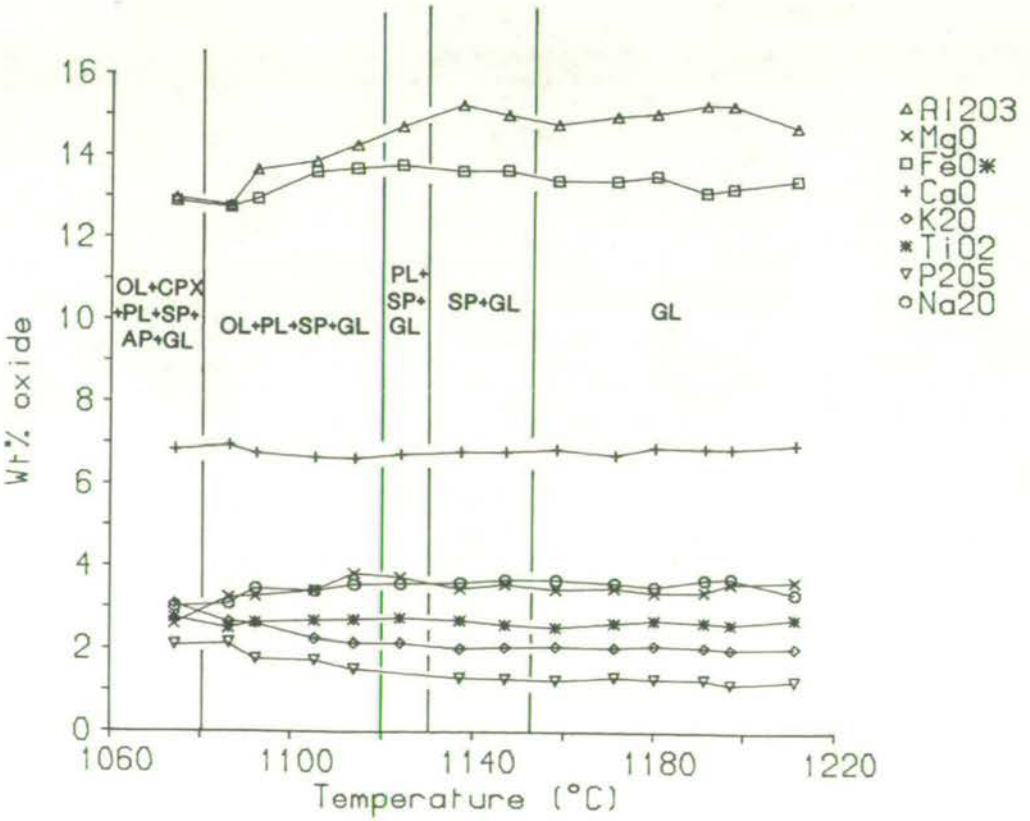

Figure 4-26. Variations in glass composition and coexisting phase assemblage with temperature, for sample MV51 at the Ni-NiO buffer.

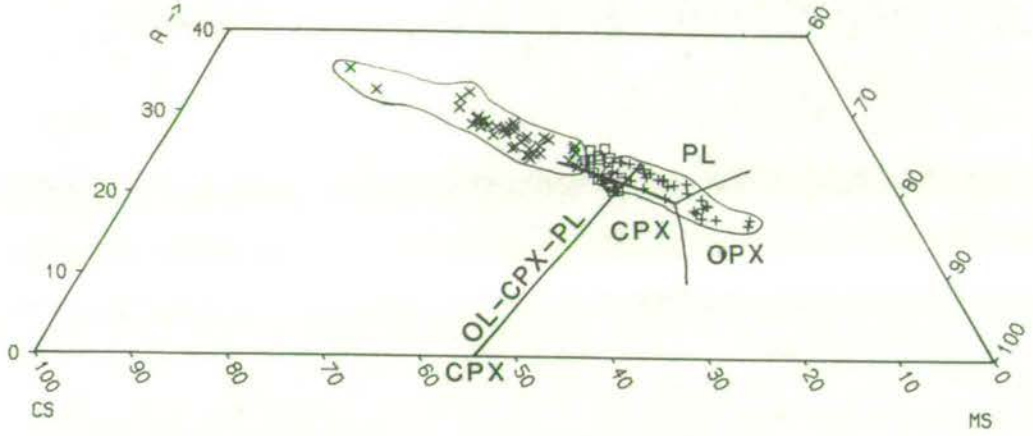

Figure 4-27. Experimental glasses coexisting with olivine + clinopyroxene + plagioclase, projected from OL onto CS-MS-A. Phase boundaries from O'Hara (1968).
X Ne-normative, □ Hy-ol-normative, + Hy-qz-normative

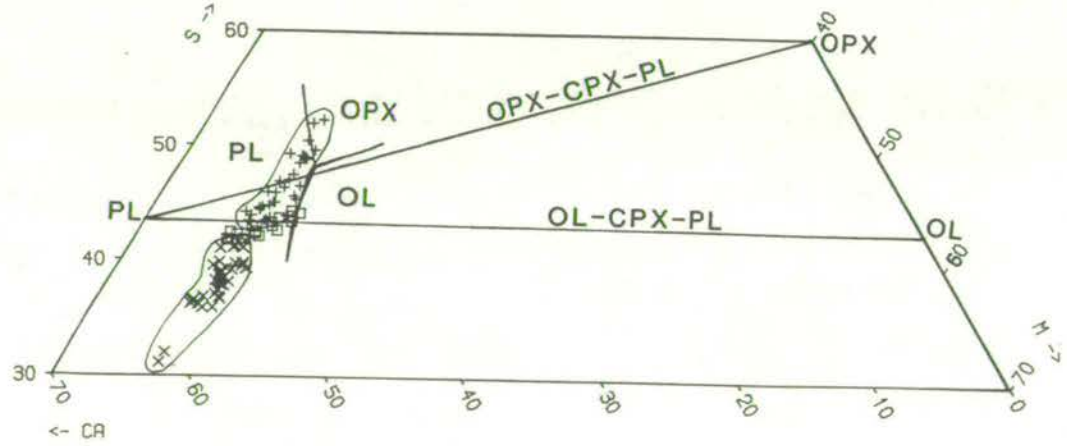

Figure 4-28. Experimental glasses coexisting with olivine + clinopyroxene + plagioclase, projected from DI onto CA-M-S. Phase boundaries from Jamieson (1970).
X Ne-normative, □ Hy-ol-normative, + Hy-qz-normative

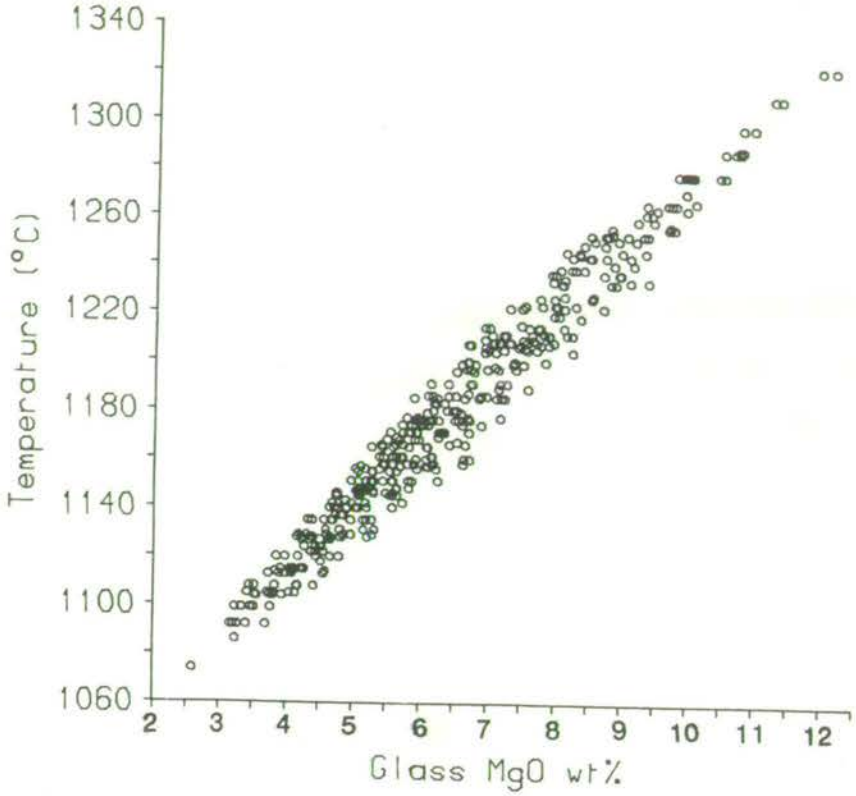

Figure 4-29. Experimental glasses coexisting with olivine.

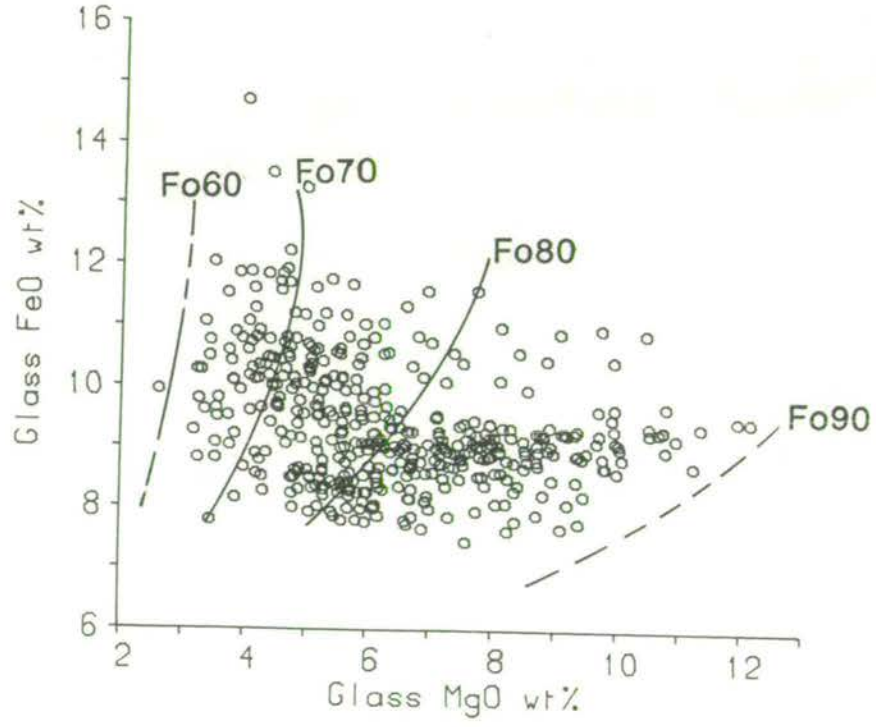

Figure 4-30. Experimental glasses coexisting with olivine, contoured for olivine composition.

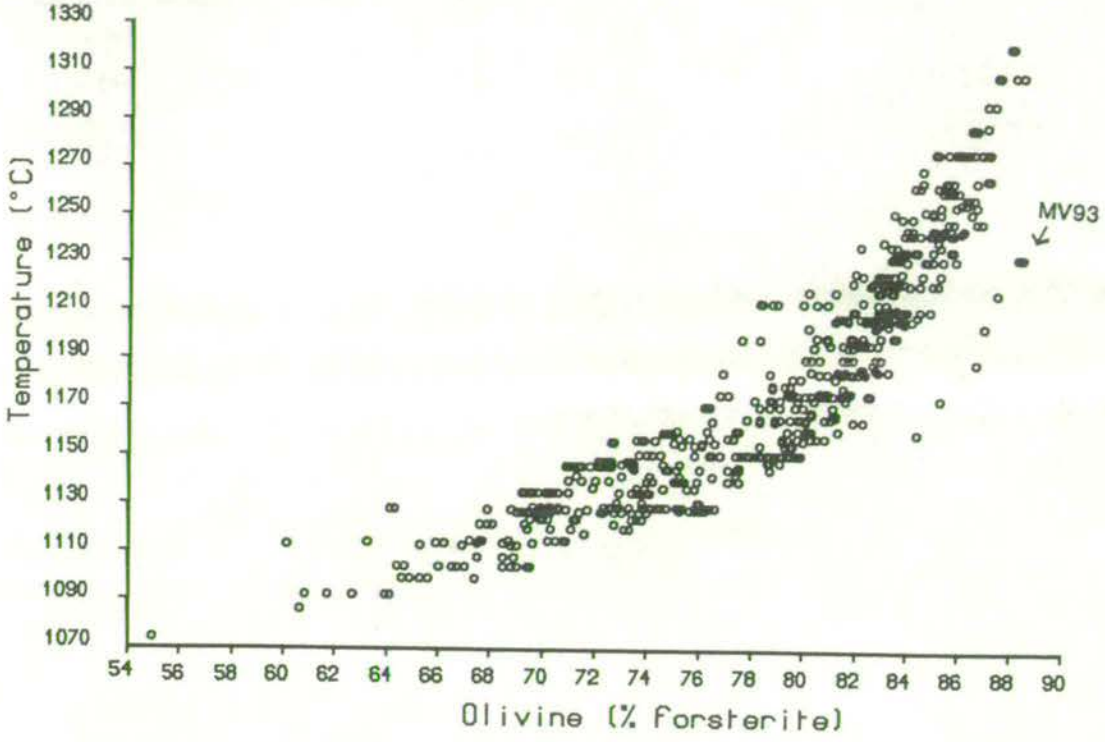

Figure 4-31. The variation of experimental olivine composition with temperature.

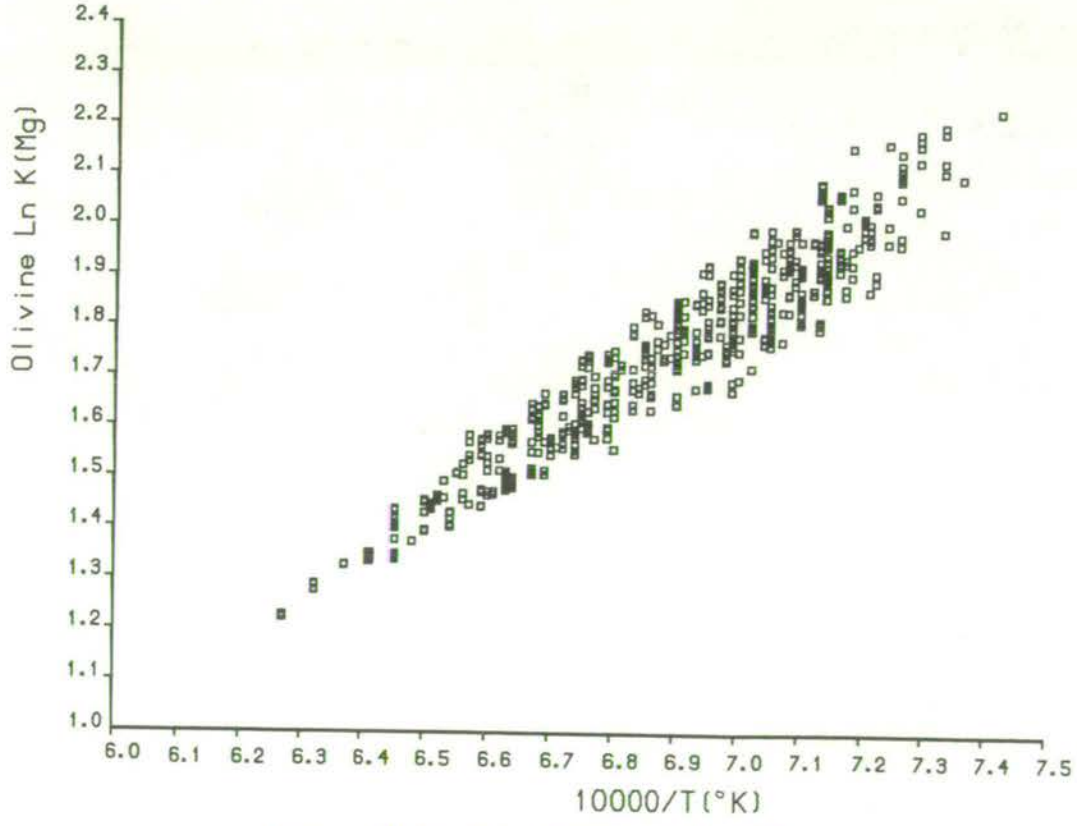

Figure 4-32. Olivine-glass, variation of Ln K(Mg) with reciprocal temperature.

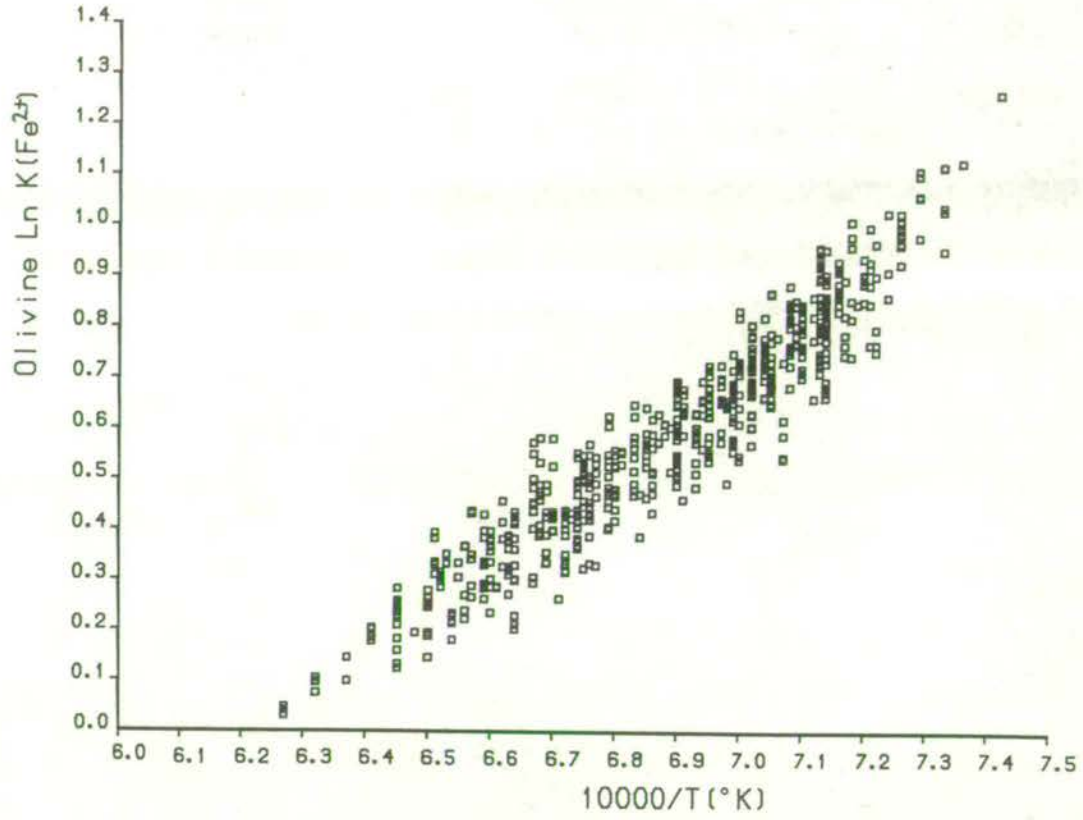

Figure 4-33. Olivine-glass, variation of Ln $K(Fe^{2+})$ with reciprocal temperature.

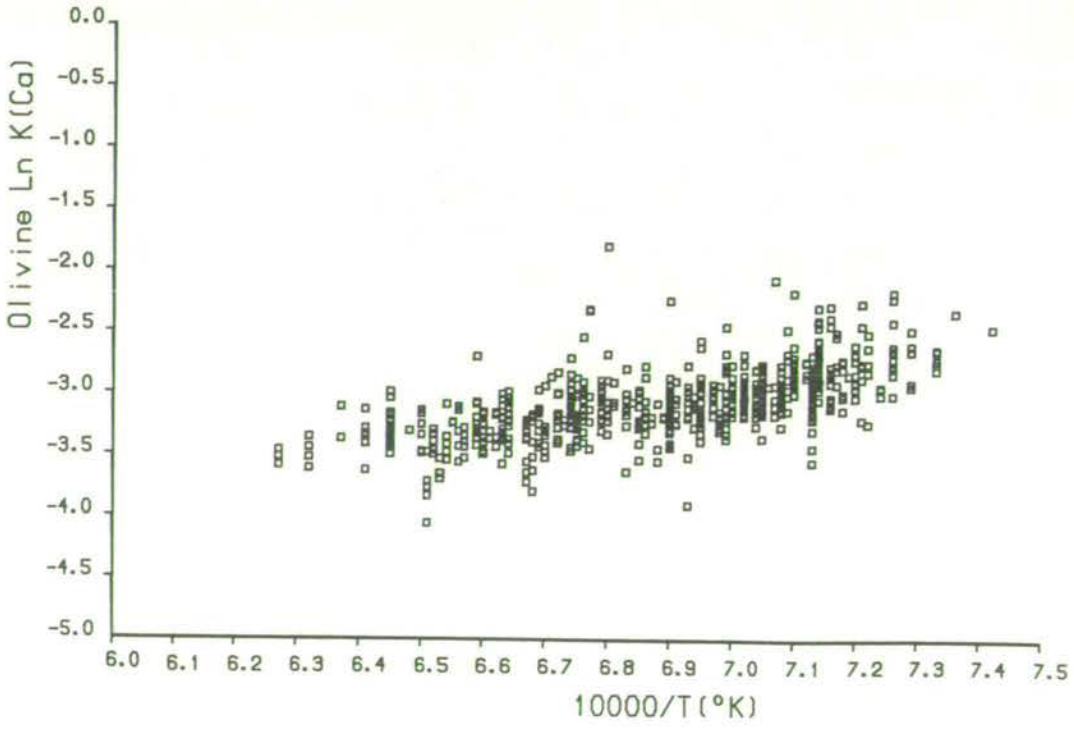

Figure 4-34. Olivine-glass, variation of Ln K(Ca) with reciprocal temperature.

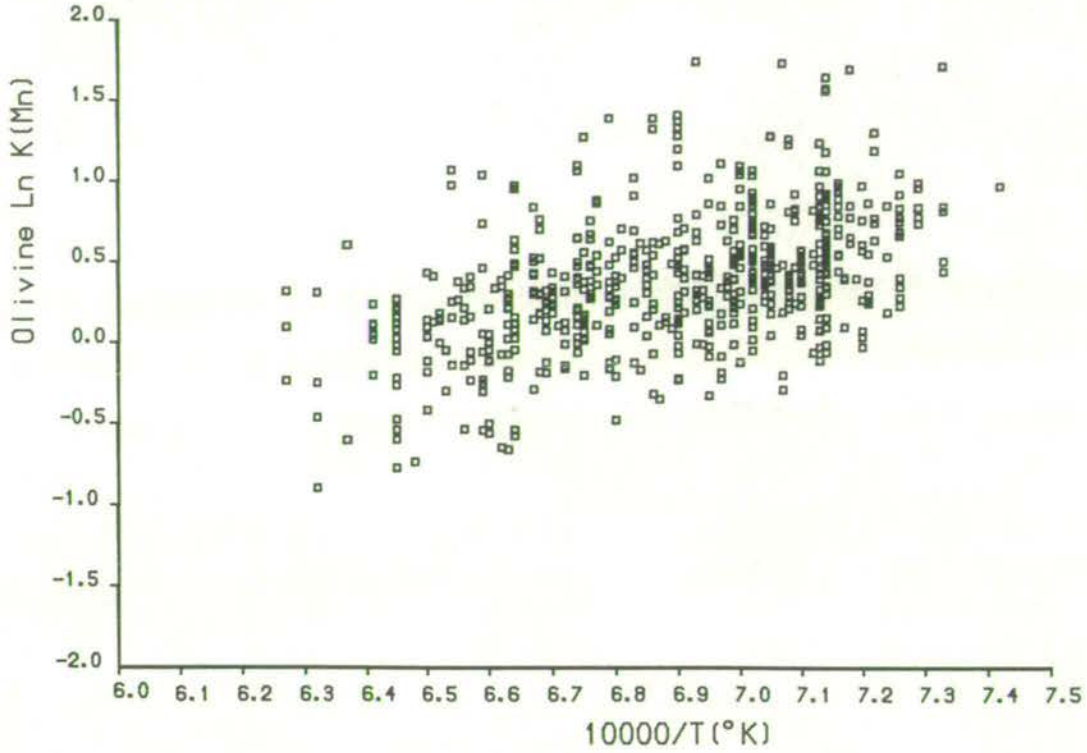

Figure 4-35. Olivine-glass, variation of Ln K(Mn) with reciprocal temperature.

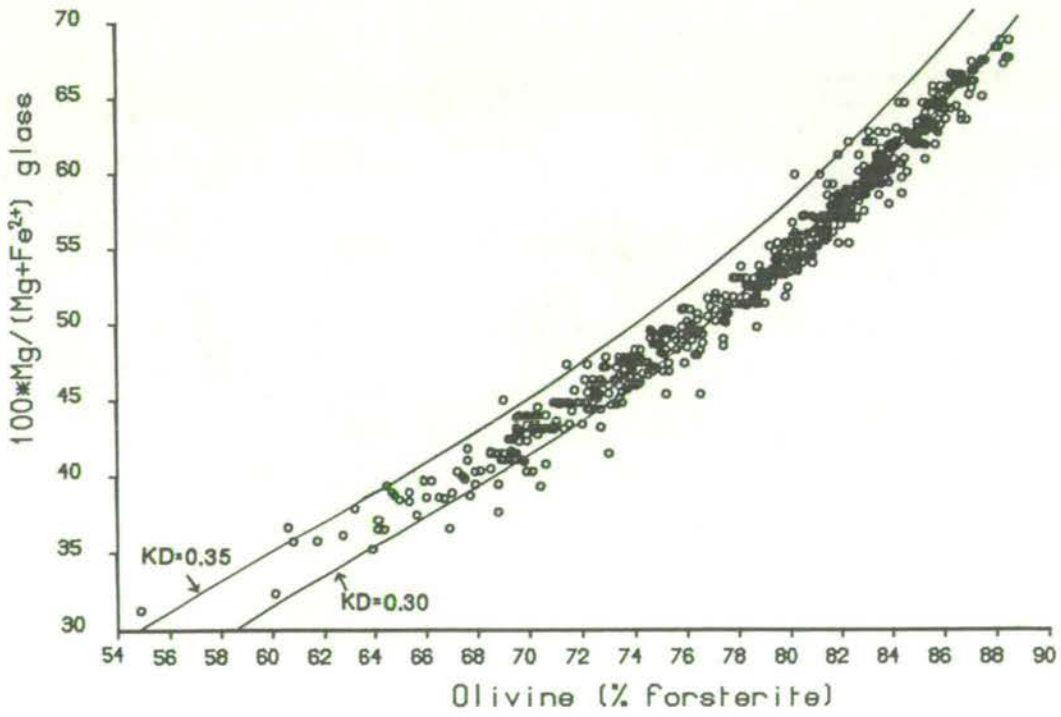

Figure 4-36. Coexisting olivine and glass compositions, with curves for the Fe^{2+}-Mg exchange distribution coefficient (KD) at values of 0.30 and 0.35.

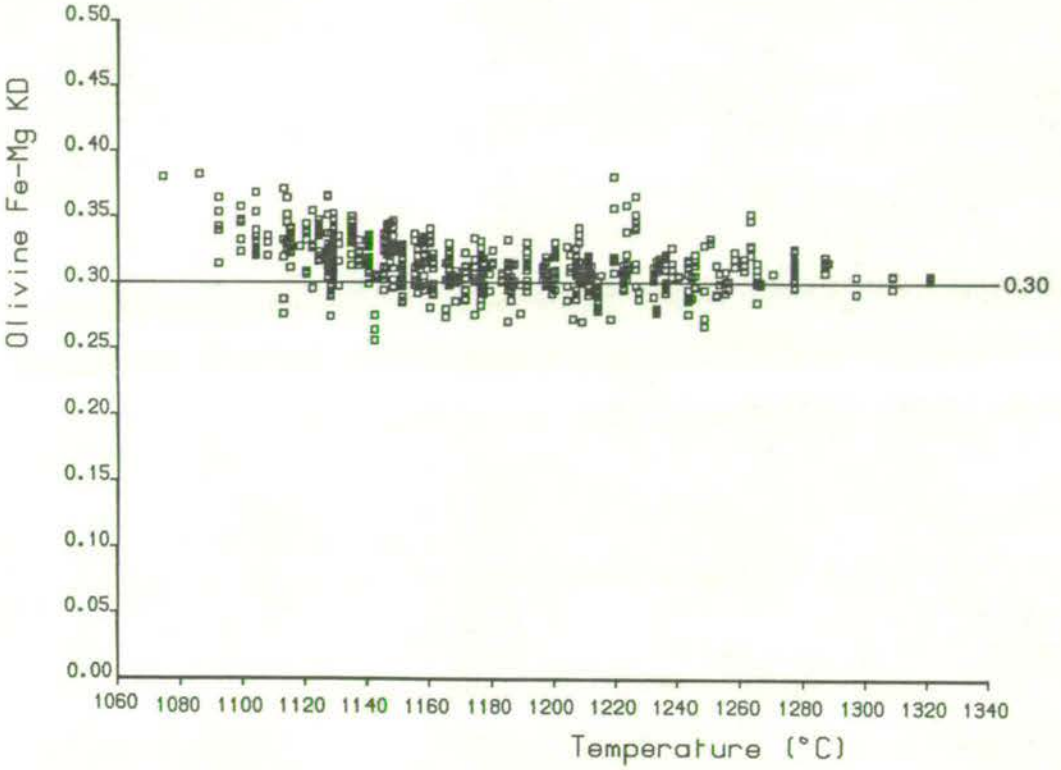

Figure 4-37. Variation of the olivine-glass Fe^{2+}-Mg KD with experimental temperature.

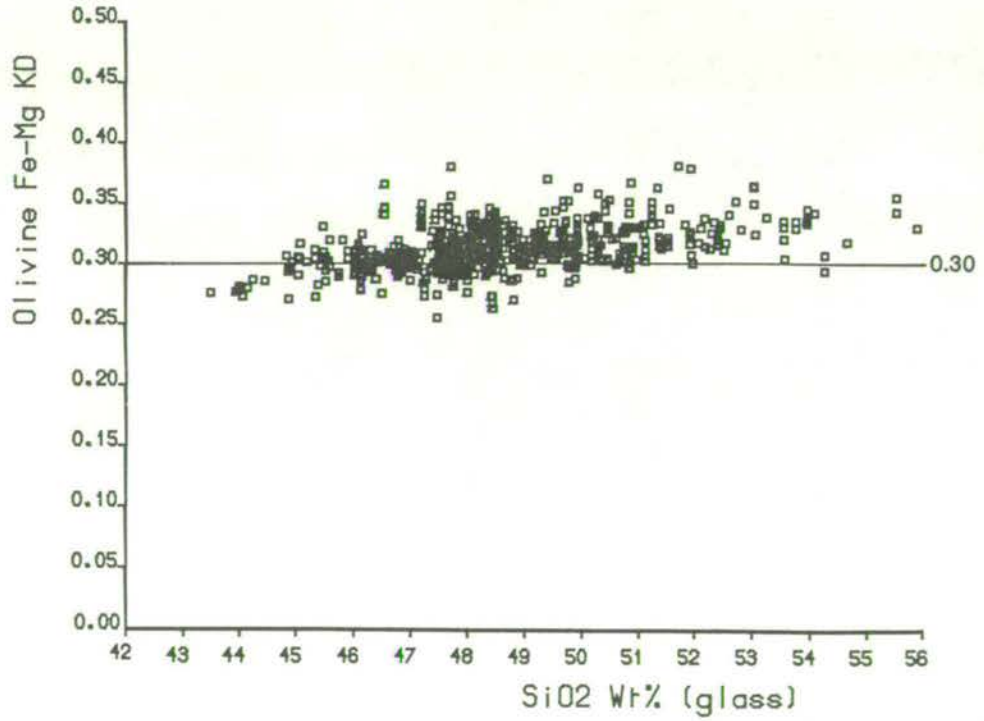

Figure 4-38. Variation of the olivine-glass Fe^{2+}-Mg KD with glass wt% SiO_2.

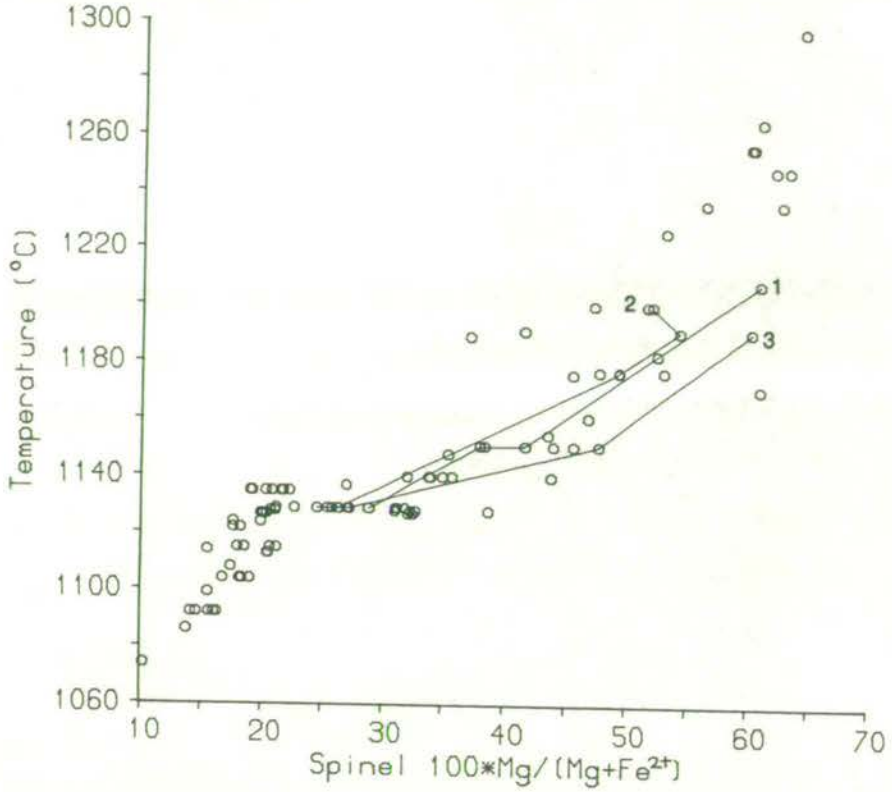

Figure 4-39. Variation of spinel 100*Mg/(Mg+Fe^{2+}) ratio with experimental temperature.
Tie lines join spinels from the same sample, at different temperatures. 1 MV403, 2 MV106, 3 MV521.

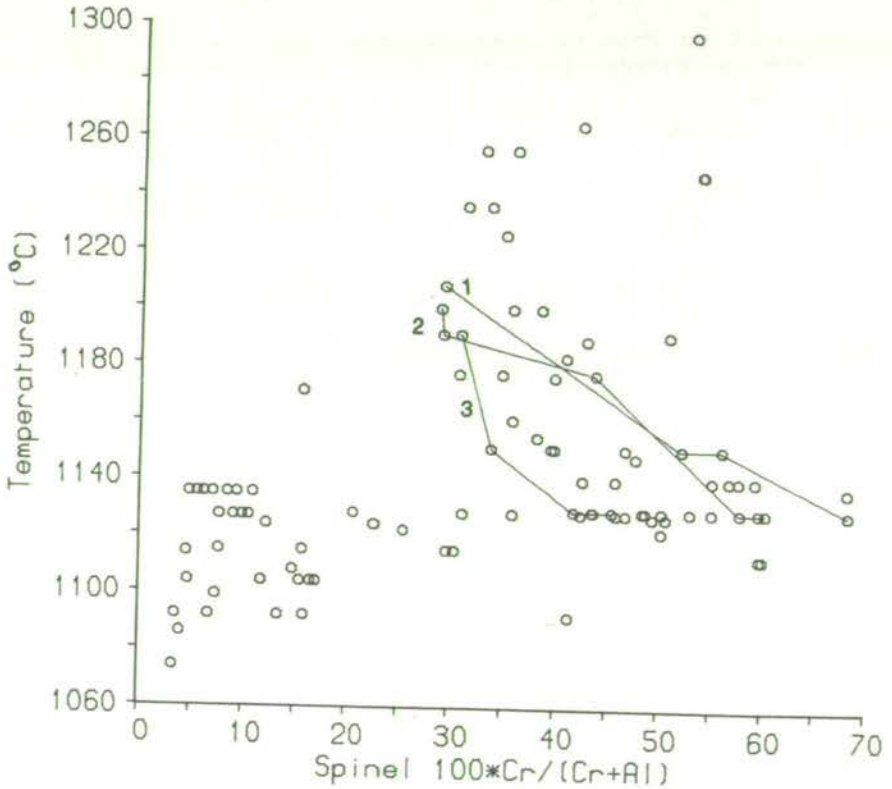

Figure 4-40. Variation of spinel 100*Cr/(Cr+Al) ratio with experimental temperature.
Tie lines join spinels from the same sample, at different temperatures. 1 MV403, 2 MV106, 3 MV521.

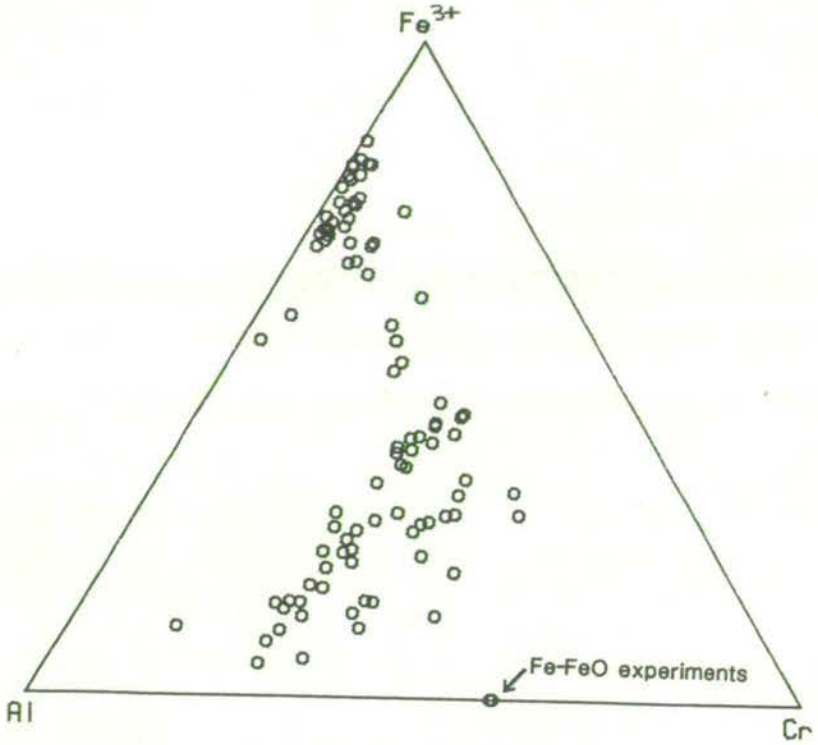

Figure 4-41. Cr - Al - Fe^{3+} relations of the experimental spinel phases.

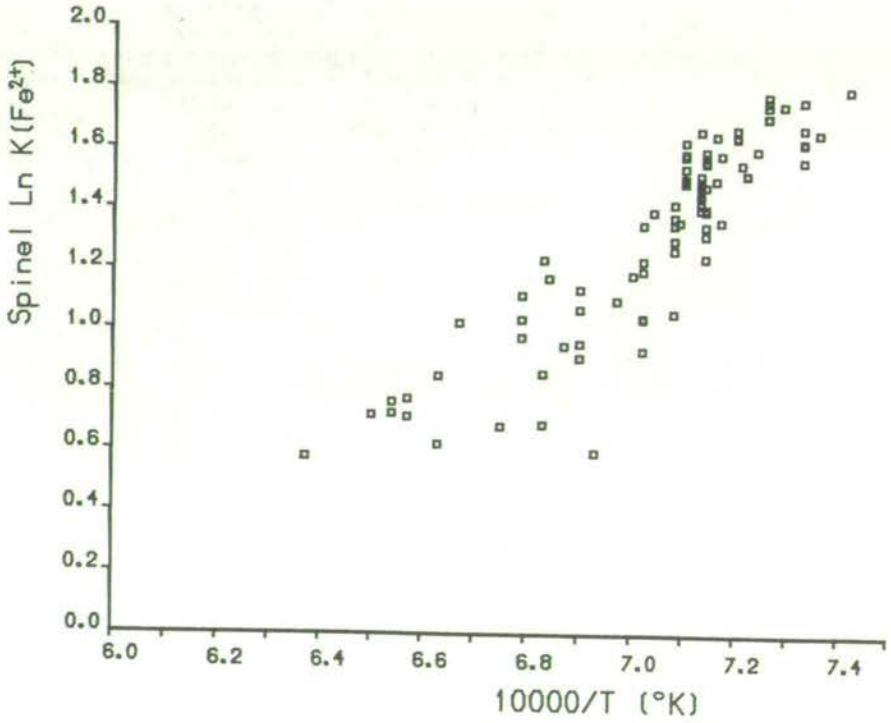

Figure 4-42. Spinel-glass, variation of Ln $K(Fe^{2+})$ with reciprocal temperature.

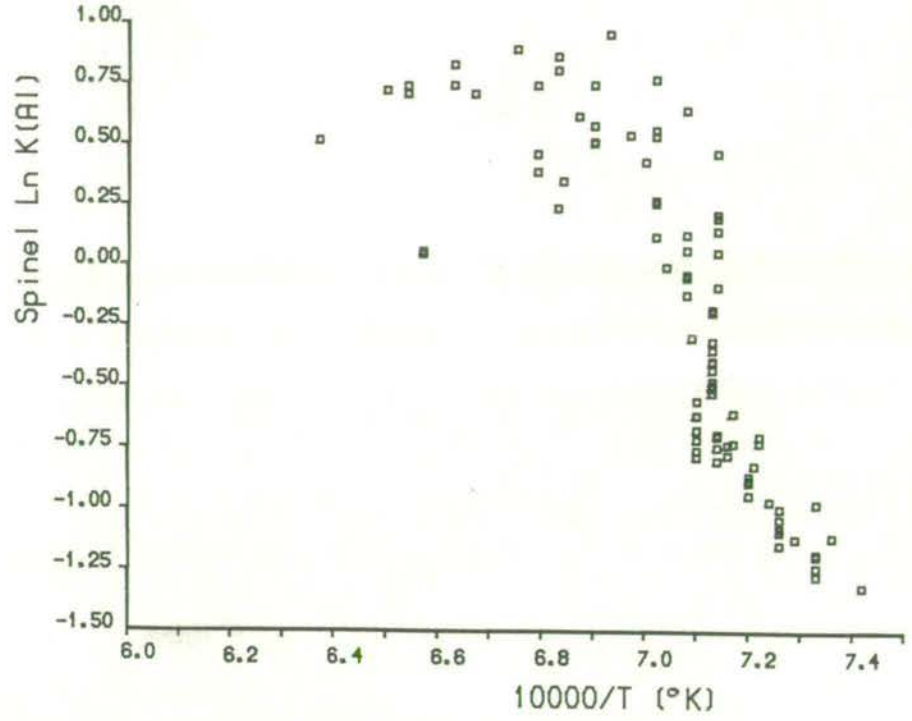

Figure 4-43. Spinel-glass, variation of Ln K(Al) with reciprocal temperature.

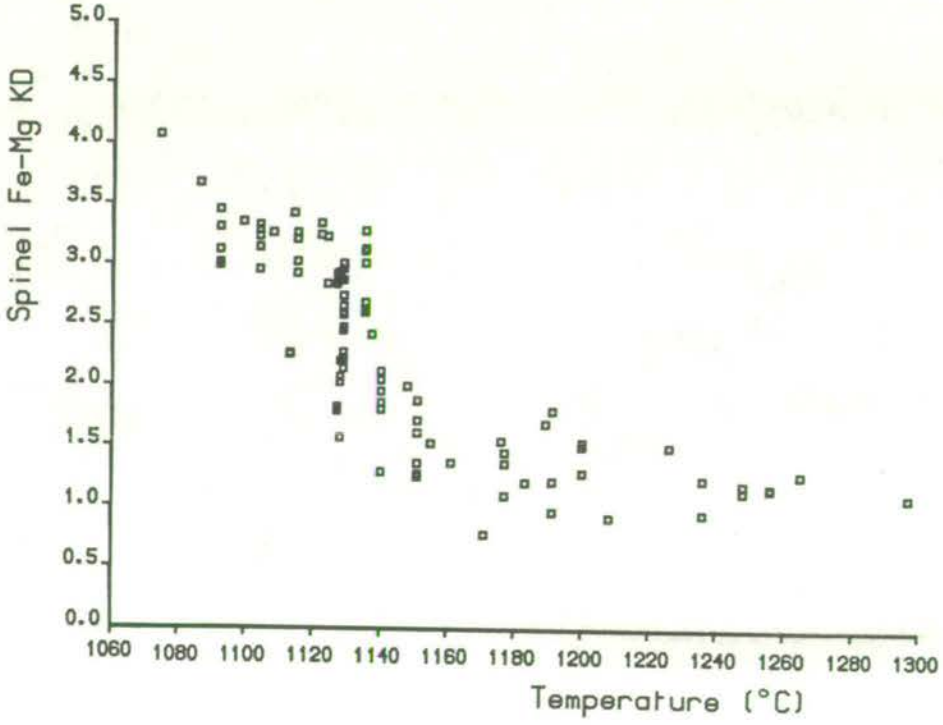

Figure 4-44. Variation of the spinel-glass Fe^{2+}-Mg exchange distribution coefficient (KD) with experimental temperature.

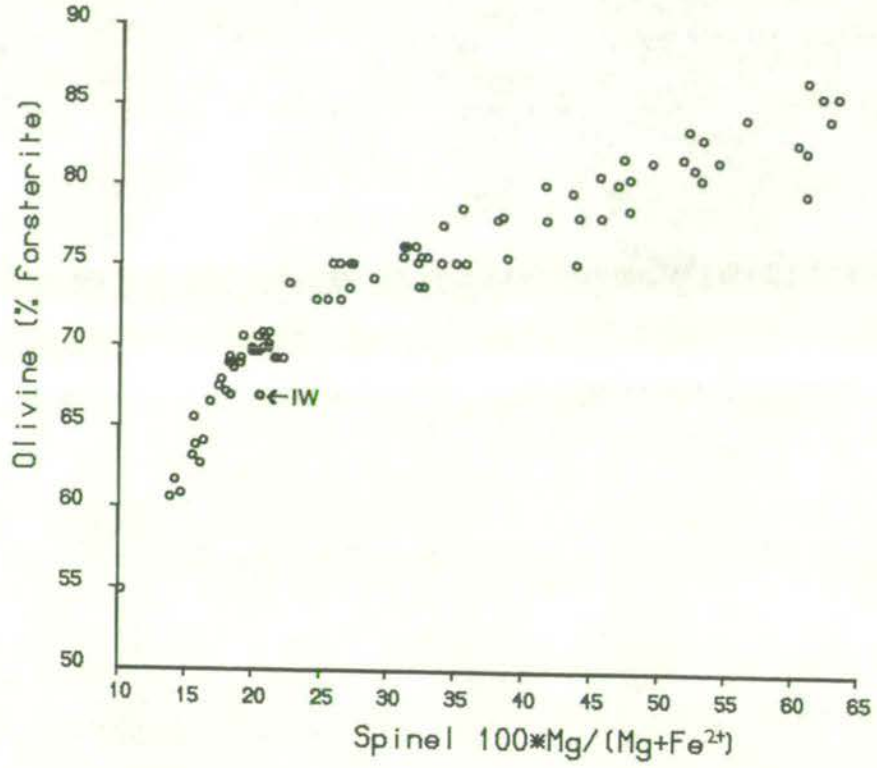

Figure 4-45. Compositions of coexisting olivine and spinel. Pairs from experiments at the Fe-FeO buffer are marked (IW).

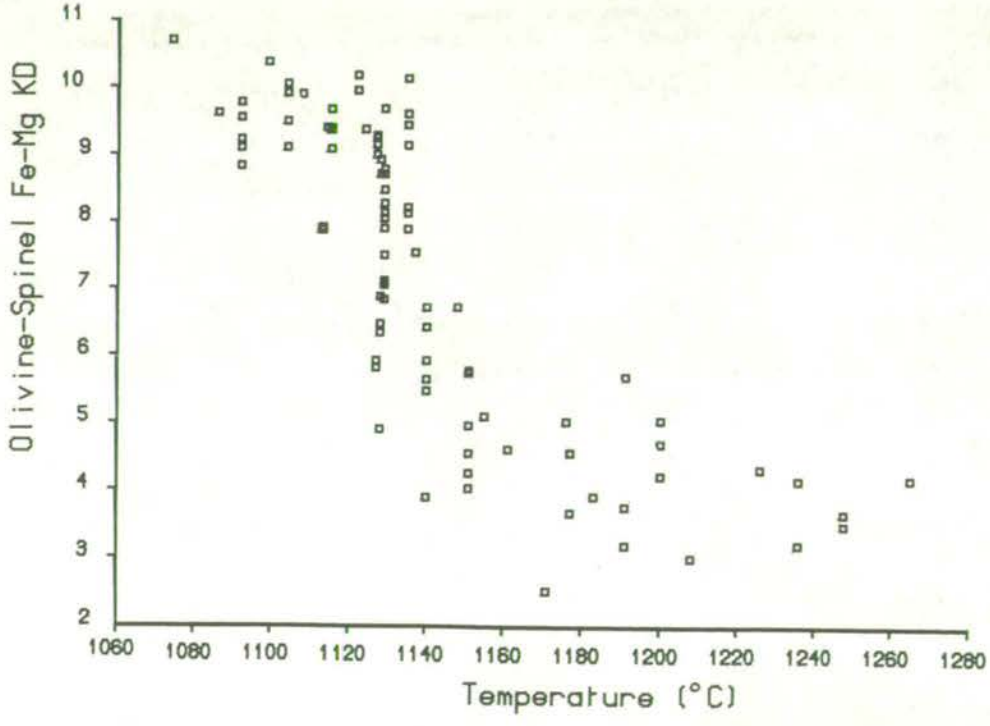

Figure 4-46. Variation of the olivine-spinel Fe^{2+}-Mg exchange distribution coefficient (KD) with experimental temperature.

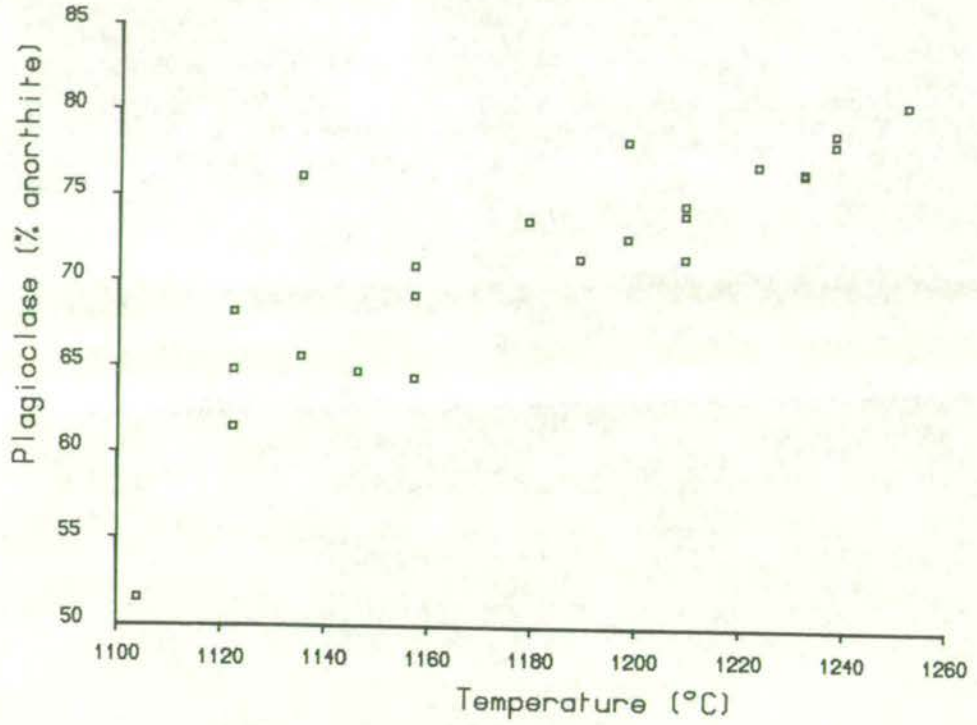

Figure 4-47. Variation of plagioclase composition with experimental temperature, for sample MV702.

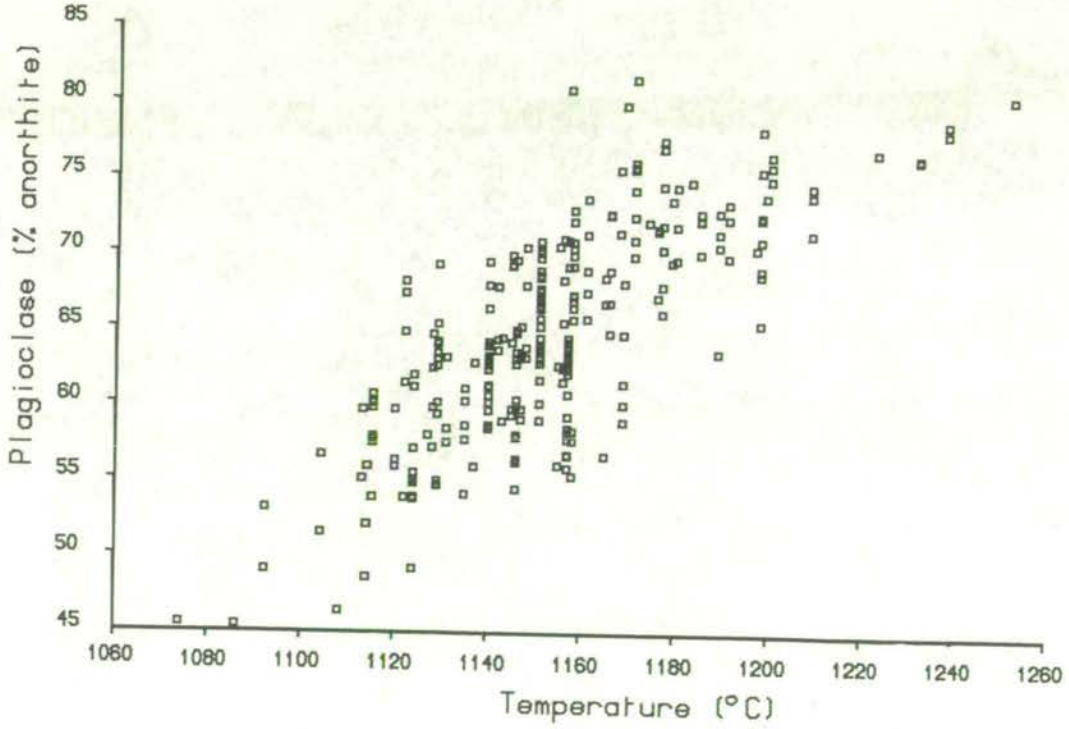

Figure 4-48. Variation of plagioclase composition with experimental temperature, for the reduced data set of all samples.

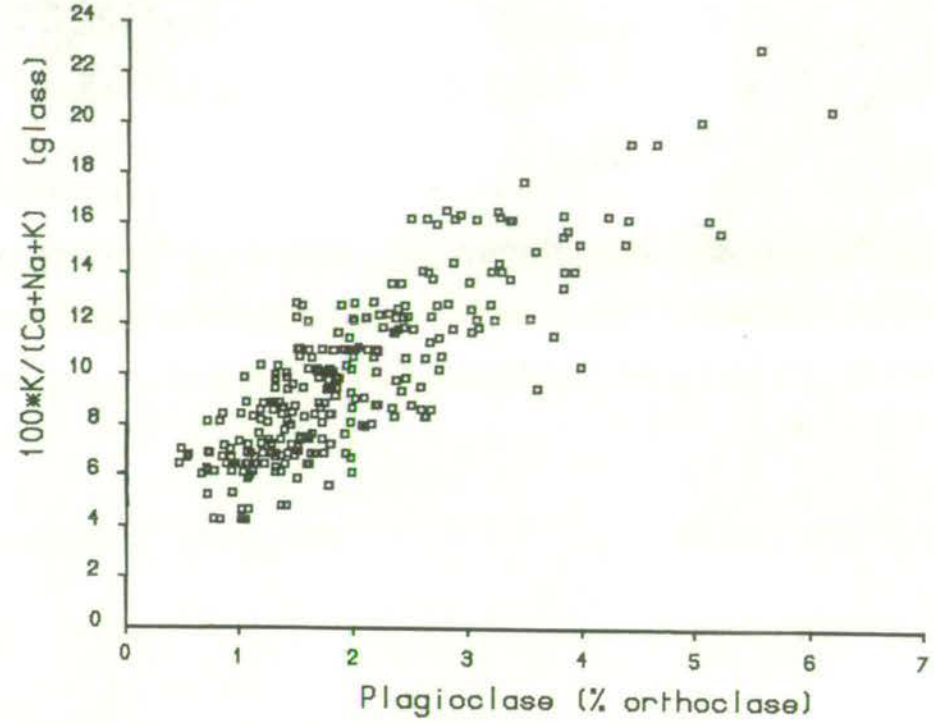

Figure 4-49. Plagioclase %orthoclase content versus coexisting glass composition.

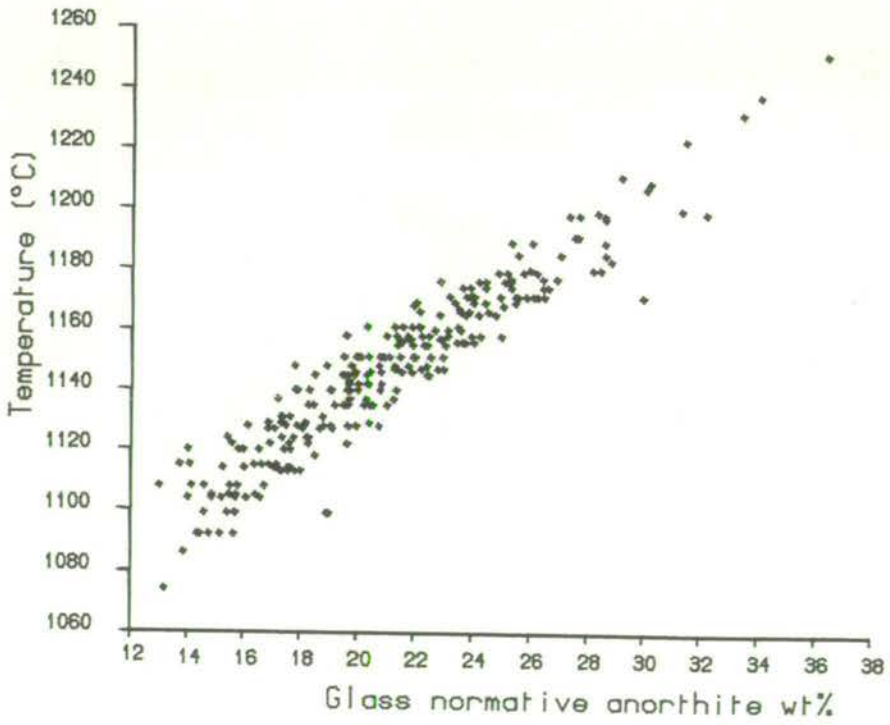

Figure 4-50. Experimental temperature versus the wt% normative anorthite content of glasses coexisting with plagioclase.

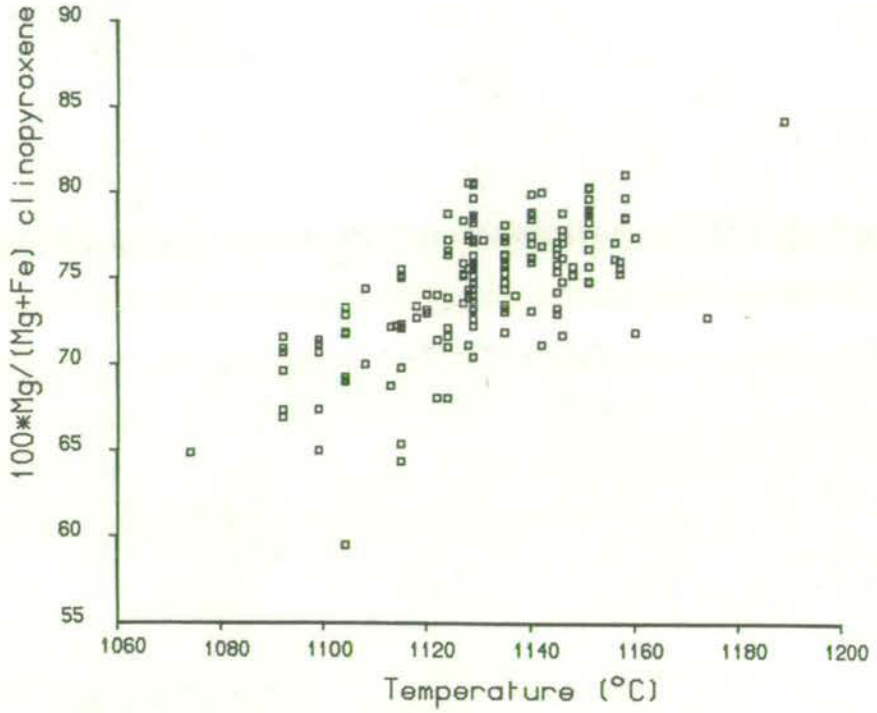

Figure 4-51. Variation of augite 100*Mg/(Mg+Fe) ratio with experimental temperature.

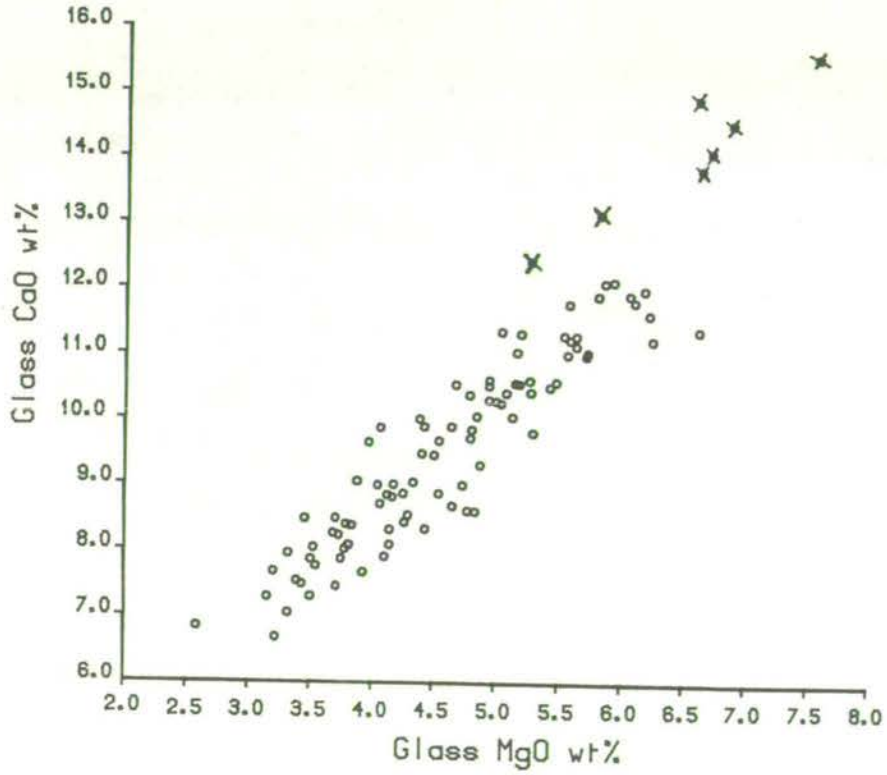

Figure 4-52. Variation of the wt% MgO and CaO contents of glasses coexisting with clinopyroxene.
Glasses from sample MV93 are distinguished (X).

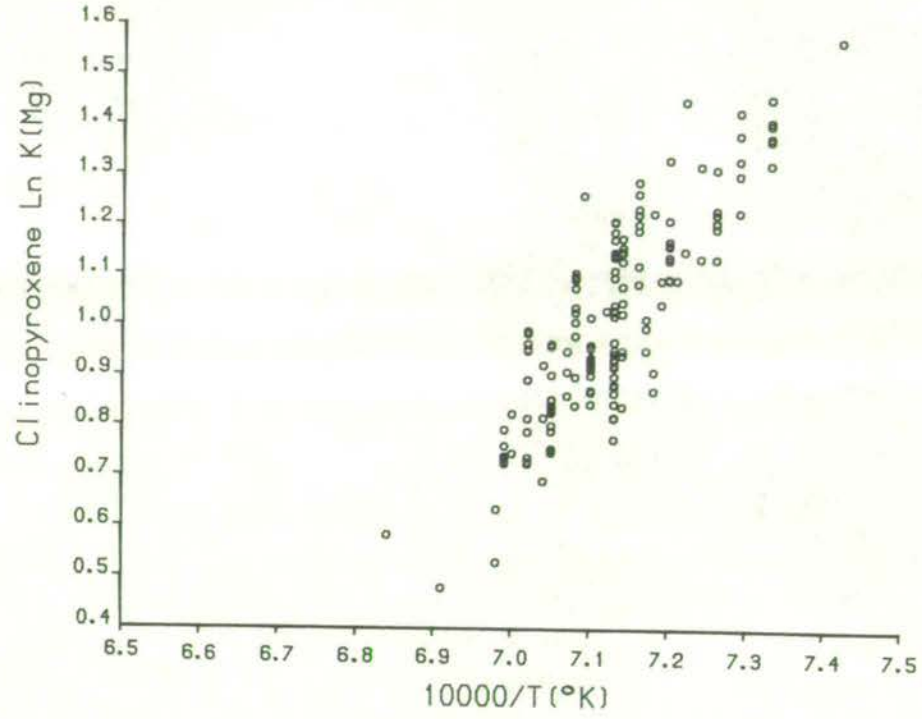

Figure 4-53. Clinopyroxene-glass, variation of Ln K(Mg) with reciprocal temperature.

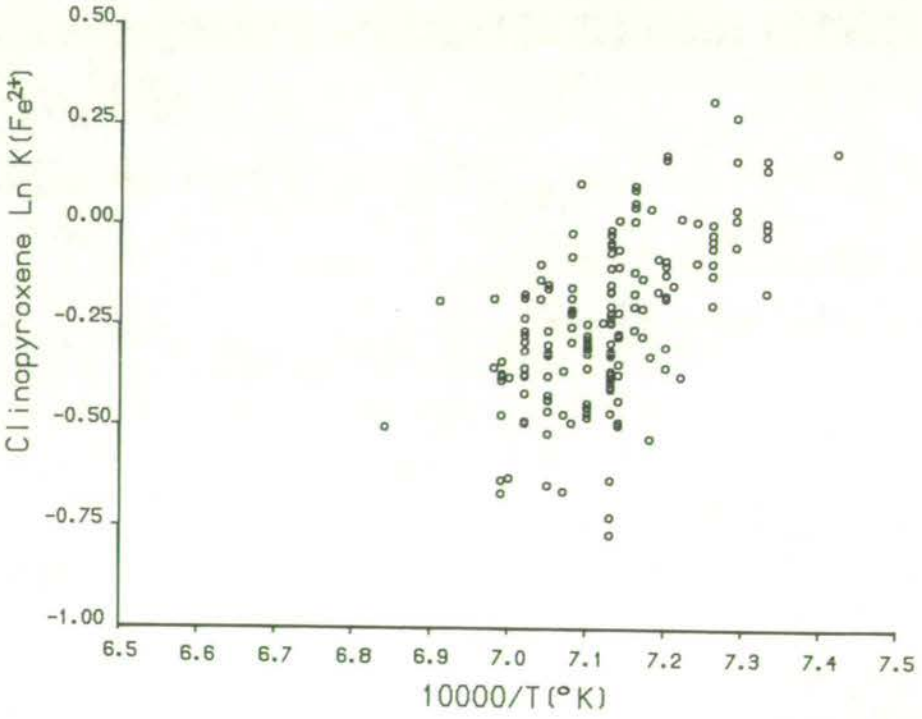

Figure 4-54. Clinopyroxene-glass, variation of Ln $K(Fe^{2+})$ with reciprocal temperature.

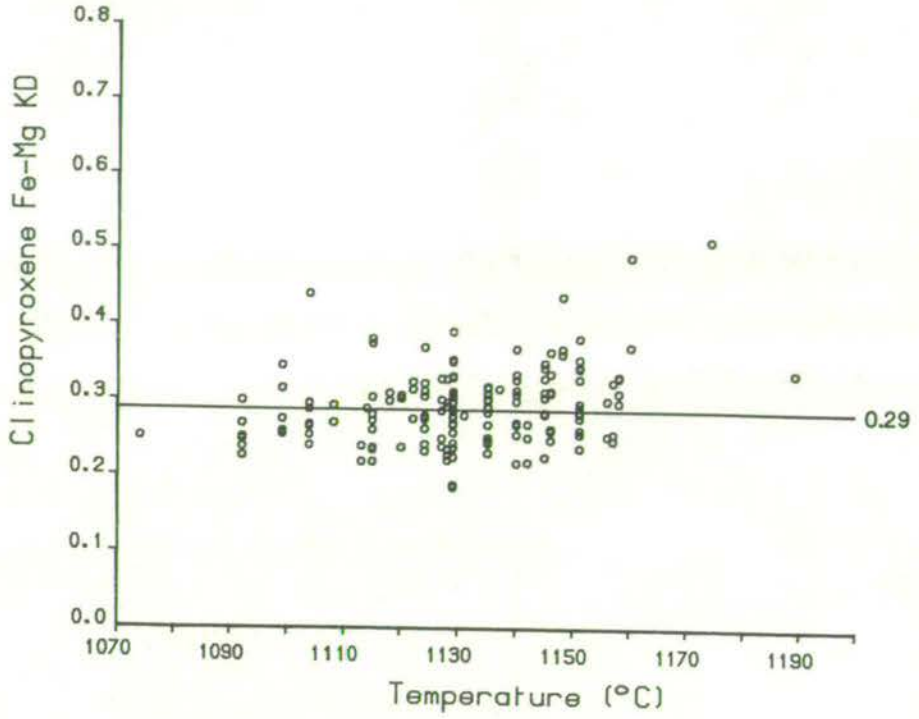

Figure 4-55. Variation of the clinopyroxene-glass Fe^{2+}-Mg exchange distribution coefficient (KD) with experimental temperature.

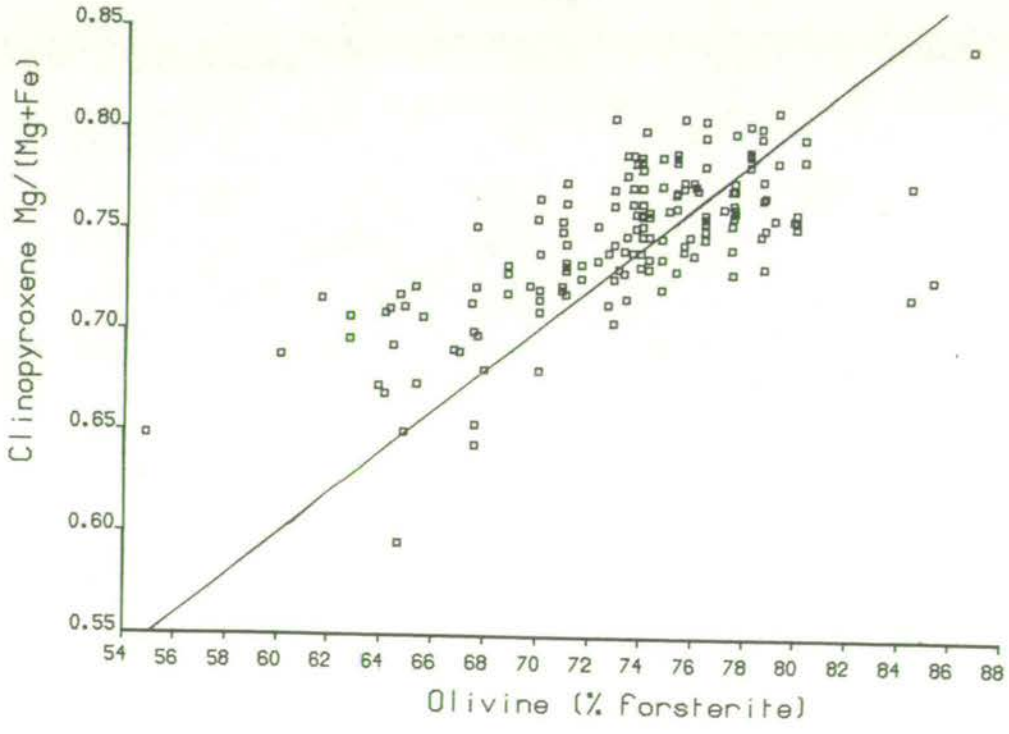

Figure 4-56. Compositions of coexisting olivine and clinopyroxene.
All Fe as FeO.

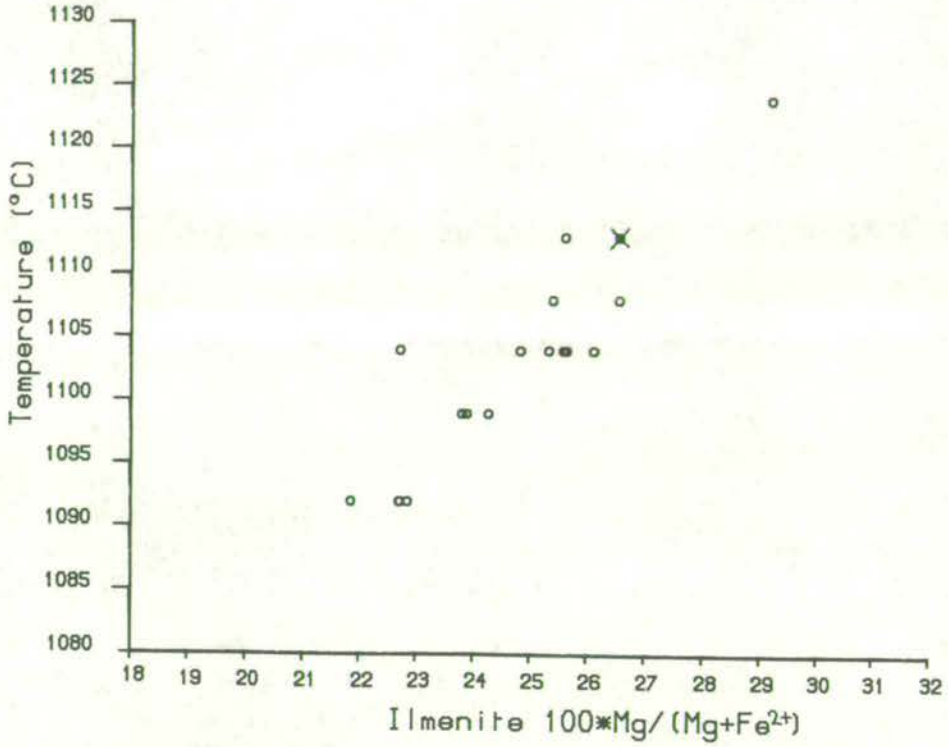

Figure 4-57. Variation of the ilmenite 100*Mg/(Mg+Fe^{2+}) ratio with experimental temperature.
The ilmenite from the experiments at the Fe-FeO buffer is marked ✱.

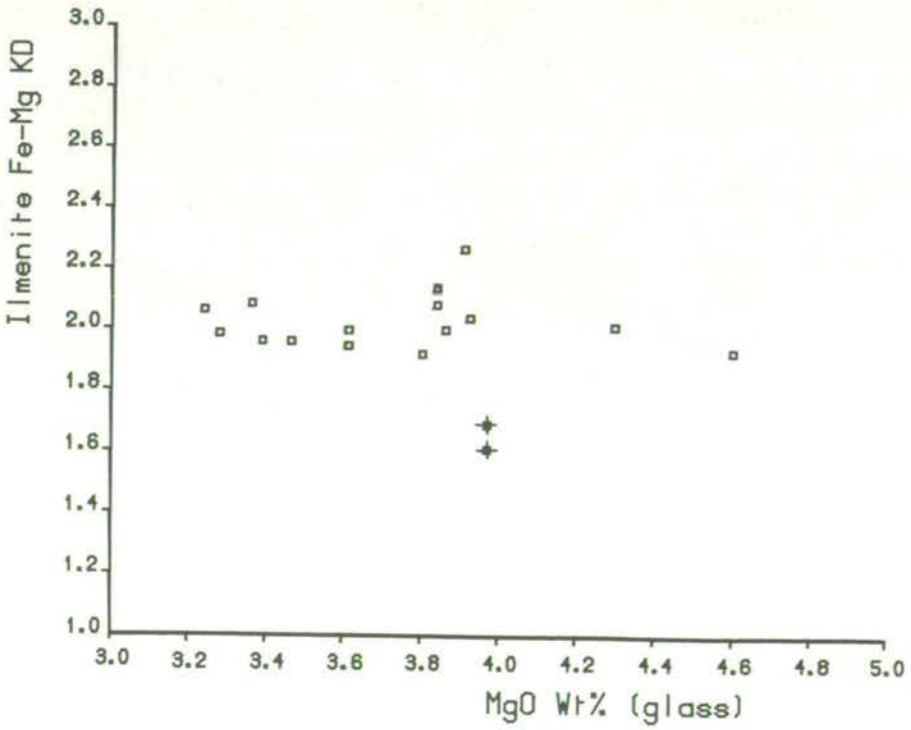

Figure 4-58. Variation of the ilmenite-glass Fe^{2+}-Mg exchange distribution coefficient (KD) with glass wt% MgO.
The data from experiments at the Fe-FeO buffer are marked ✦.

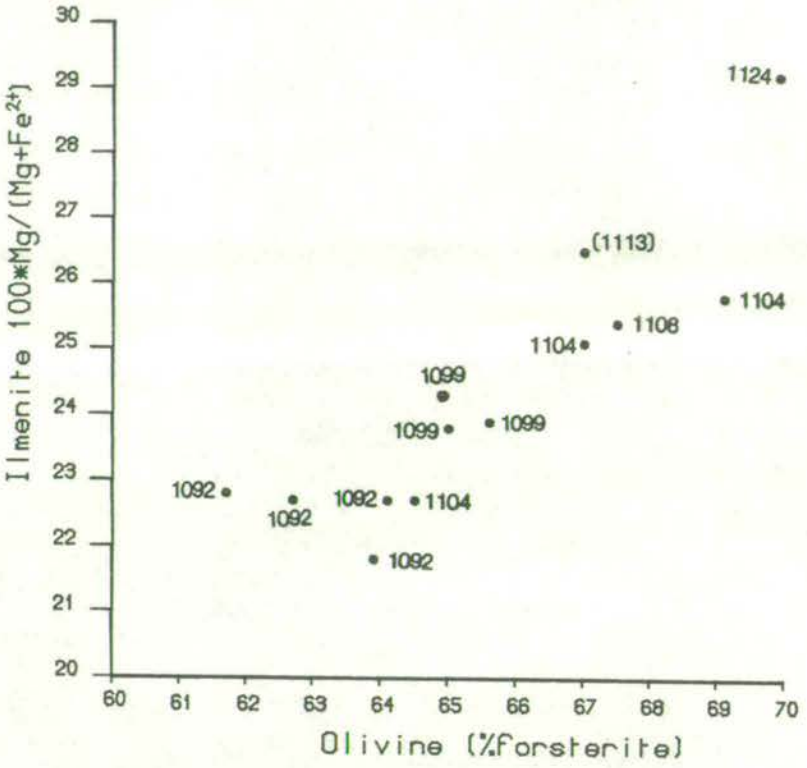

Figure 4-59. Compositions of coexisting olivine and ilmenite, with experimental temperatures marked for each pair. The temperature in brackets marks a pair from the experiments at the Fe-FeO buffer.

Table 4-1.Compositions and Mg# of samples investigated experimentally.
Fe2O3 estimated as described in the text.
No composition is available for MV403F.

	MV403.	ES2058.	MV93.	MV521.	MV723F.	MV723.	MV109.	MV106.
SiO2	48.99	45.78	43.12	44.79	47.48	47.78	45.51	45.57
TiO2	1.95	1.92	2.99	2.76	1.53	1.57	2.74	2.67
Al2O3	13.45	13.01	12.93	13.51	14.65	14.72	13.98	14.62
Cr2O3	0.00	0.13	0.09	0.00	0.06	0.04	0.10	0.00
Fe2O3	2.39	2.25	2.23	2.30	2.06	2.22	2.24	2.10
FeO	9.06	9.73	7.85	9.28	8.48	8.68	8.91	8.79
MnO	0.20	0.17	0.11	0.18	0.17	0.18	0.19	0.16
MgO	11.75	12.49	9.64	10.98	10.00	9.94	10.01	9.72
NiO	0.00	0.07	0.02	0.00	0.06	0.04	0.00	0.00
CaO	7.90	9.11	14.82	10.59	9.79	9.93	10.51	10.51
Na2O	2.55	2.26	3.16	2.28	3.19	2.84	2.71	2.21
K2O	0.95	1.02	0.51	0.90	0.91	0.79	0.65	0.51
P2O5	0.25	0.23	0.70	0.79	0.07	0.19	0.42	0.53
TOTAL	99.44	98.17	98.17	98.36	98.46	98.91	97.97	97.39
Mg#	69.8	69.6	68.6	67.8	67.8	67.1	66.7	66.3

	MV164.	MV166.	MV718.	MV703.	MV520.	MV178.	MV114.	MV716.
SiO2	48.03	44.29	43.94	45.39	46.07	47.25	49.07	44.16
TiO2	1.82	3.22	3.29	2.39	2.28	2.92	2.64	3.56
Al2O3	13.64	13.04	12.69	14.47	14.85	13.68	13.88	13.53
Cr2O3	0.00	0.00	0.09	0.00	0.09	0.00	0.08	0.00
Fe2O3	2.37	2.53	2.70	2.38	2.36	2.51	2.41	2.92
FeO	9.38	9.56	11.09	9.18	8.38	9.17	8.68	10.91
MnO	0.18	0.16	0.15	0.20	0.15	0.17	0.15	0.10
MgO	10.22	10.15	11.29	9.16	8.29	8.94	8.45	10.50
CaO	8.71	11.03	9.88	10.92	10.88	9.07	8.13	9.21
Na2O	2.84	2.49	2.60	2.16	2.58	2.42	3.20	2.70
K2O	1.00	1.04	0.44	0.99	1.80	1.69	1.47	0.56
P2O5	0.11	0.22	0.23	0.11	0.21	0.33	0.10	0.17
TOTAL	98.30	97.73	98.39	97.35	97.95	98.15	98.26	98.32
Mg#	66.0	65.4	64.5	64.0	63.8	63.5	63.4	63.2

	MV167F.	MV78.	MV406.	MV400.	MV501.	MV167.	MV408.	MV160.
SiO2	46.50	43.93	46.22	45.05	47.73	46.74	51.57	46.78
TiO2	2.63	2.93	2.87	2.54	2.31	2.72	2.19	3.25
Al2O3	14.84	13.88	14.41	14.91	14.11	15.10	14.11	15.38
Cr2O3	0.05	0.00	0.00	0.09	0.03	0.03	0.00	0.06
Fe2O3	2.28	2.56	2.45	2.27	2.45	2.35	2.29	2.69
FeO	9.29	9.56	9.28	9.25	9.28	9.27	9.06	9.50
MnO	0.18	0.26	0.23	0.33	0.31	0.15	0.00	0.18
MgO	8.93	9.09	8.77	8.73	8.31	8.16	7.13	7.30
NiO	0.00	0.00	0.00	0.00	0.00	0.02	0.00	0.00
CaO	9.22	11.00	9.37	11.16	10.08	9.27	8.50	8.68
Na2O	2.67	3.14	3.15	1.27	2.58	2.86	2.76	2.83
K2O	0.89	0.98	1.20	1.44	1.02	1.07	0.59	1.33
P2O5	0.53	1.03	0.50	0.41	0.25	0.56	0.07	0.25
TOTAL	98.01	98.36	98.46	97.45	98.47	98.31	98.28	98.23
Mg#	63.1	62.9	62.7	62.7	61.5	61.1	58.4	57.8

Table 4-1 continued.

	MV514.	MV74.	MV72.	MV516.	MV704.	MV506.	MV122.	MV702.
SiO2	47.40	48.25	46.22	47.68	46.74	48.22	50.82	47.96
TiO2	2.77	3.07	3.58	2.54	2.42	2.44	2.78	2.61
Al2O3	16.74	16.13	15.80	15.80	16.49	16.87	13.66	19.17
Cr2O3	0.02	0.00	0.00	0.00	0.04	0.00	0.02	0.00
Fe2O3	2.54	2.52	2.59	2.39	2.62	2.21	2.70	1.95
FeO	9.30	8.28	9.40	9.08	9.35	8.22	8.99	7.69
MnO	0.14	0.08	0.19	0.18	0.15	0.14	0.06	0.12
MgO	7.00	6.09	6.79	6.31	6.48	5.66	6.00	5.07
CaO	8.76	8.79	8.58	8.62	9.14	9.10	8.51	9.53
Na2O	2.67	3.12	2.46	3.21	3.33	3.31	2.91	3.38
K2O	1.47	1.35	1.34	1.51	0.90	1.36	1.11	0.84
P2O5	0.36	0.20	0.40	0.30	0.23	0.51	0.20	0.12
TOTAL	99.17	97.88	97.35	97.62	97.89	98.04	97.76	98.44
Mg#	57.3	56.7	56.3	55.3	55.3	55.1	54.3	54.0

	MV39B.	MV121A.	MV71A.	MV52.	MV39AF.	MV39A.	MV402.	MV13F.
SiO2	49.14	51.95	47.44	46.75	47.53	47.61	48.74	47.38
TiO2	3.17	2.72	3.51	3.67	3.52	3.51	2.31	3.82
Al2O3	14.29	14.34	15.72	15.64	15.26	15.12	15.97	15.73
Cr2O3	0.01	0.04	0.04	0.02	0.02	0.01	0.06	0.02
Fe2O3	2.88	2.58	2.54	2.77	2.83	2.92	2.45	3.06
FeO	10.00	8.75	9.09	9.84	10.22	10.31	8.81	10.26
MnO	0.18	0.12	0.19	0.17	0.21	0.17	0.07	0.20
MgO	6.18	5.38	5.49	5.87	5.76	5.60	4.58	5.26
NiO	0.01	0.00	0.00	0.00	0.02	0.01	0.00	0.02
CaO	8.01	7.43	9.14	8.91	8.42	8.54	11.49	7.42
Na2O	3.33	3.43	2.67	3.23	3.22	3.30	2.73	3.46
K2O	0.88	1.34	1.51	1.08	0.60	0.79	0.86	1.52
P2O5	0.47	0.38	0.36	0.32	0.40	0.56	0.29	0.42
TOTAL	98.55	98.46	97.69	98.27	98.00	98.45	98.37	98.57
Mg#	52.4	52.3	51.9	51.5	50.1	49.2	48.1	47.8

	MV13.	MV40A.	MV165.	MV51.
SiO2	47.39	49.63	49.29	49.09
TiO2	3.83	2.62	3.14	2.63
Al2O3	15.64	17.16	16.55	15.02
Cr2O3	0.01	0.17	0.07	0.00
Fe2O3	3.13	2.48	2.67	3.12
FeO	10.11	8.29	8.89	10.55
MnO	0.17	0.19	0.13	0.22
MgO	4.94	3.95	3.76	3.49
NiO	0.01	0.00	0.00	0.00
CaO	7.57	8.48	5.83	6.88
Na2O	3.49	3.44	3.69	3.70
K2O	1.55	1.07	2.94	2.05
P2O5	0.29	0.46	0.40	1.25
TOTAL	98.13	97.94	97.36	98.00
Mg#	46.6	45.9	43.0	37.1

Table 4-2

SAMPLE	Cr ppm	Ni ppm	SPINEL LIQUIDUS TEMPERATURE AT Ni - NiO	SAMPLE Mg#
MV13	170	200	1218 ± 5° C	46.6
MV13F	10	70	1154 ± 6° C	47.8
MV39A	200	330	1186 ± 3° C	49.2
MV39AF	80	100	1154 ± 6° C	50.1
MV167	370	310	1268 ± 6° C	61.1
MV167F	380	140	1254 ± 6° C	63.1
MV723	560	630	1303 ± 6° C	67.1
MV723F	460	150	1292 ± 5° C	67.8
MV403	460	340	1282 ± 5° C	69.8
MV403F	460	260	1282 ± 5° C	(69.8)*

Cr and Ni concentrations in glasses above the spinel liquidus temperature. Samples with the suffix 'F' have been crushed in agate. Others were initially crushed in colmonoy.

* MV403F not analysed above its liquidus, but is very similar to MV403.

IF THE CREATOR HAD A PURPOSE IN EQUIPPING US WITH A NECK, HE SURELY MEANT US TO STICK IT OUT.

Arthur Koestler.

CHAPTER 5

MINERAL TEMPERATURE EQUATIONS, MINERAL COMPOSITION EQUATIONS, AND AN EQUILIBRIUM CRYSTALLISATION MODEL

5.1 Previous Work

Although a great deal of research has been carried out in experimental igneous petrology, many of the studies have been directed towards specific problems and have produced results which can only be applied qualitatively to other situations. In particular, the major-element chemistry of liquids (glasses) and coexisting crystals has been examined in numerous experimental studies, yet it remains difficult to predict liquidus temperatures, and the nature and composition of liquidus phases, in suites not directly investigated.

In the absence of unifying models, simple coefficients have been used to calculate the compositions of coexisting phases. In a study of olivine tholeiites, Roeder and Emslie (1970) found the olivine-liquid Fe^{2+}-Mg distribution coefficient (KD) was equal to 0.30. This value has been used frequently in modelling olivine crystallisation from melts. However, the range of values of KD in terrestrial basalts suggested by Langmuir and Hanson (1980) is 0.28 - 0.36. Ford et al. (1983) in a study of olivine-liquid equilibria, including the data presented in this thesis, have shown that KD may range from 0.25 - 0.40 in some circumstances. Clearly, assuming a constant value of KD may lead to significant errors in quantitative modelling.

Attempts have been made to derive predictive models of magmatic crystallisation applicable to a wide range of compositions. French (1971) derived equations predicting the temperature of crystallisation of olivine, plagioclase and clinopyroxene from the composition of the starting materials. Multiple linear regression analysis related the major element composition of basic and intermediate samples to the experimentally determined temperature of appearance of each phase. Although the number of available analyses was very restricted and experimental errors were probably significant,

the success of this approach illustrated it is possible to relate liquidus temperatures and phases to bulk composition. French and Cameron (1981) extended the initial model by deriving an equation for each phase within a restricted compositional range. They divided basalts into groups according to the sequence of crystallisation of olivine, plagioclase and clinopyroxene (Cameron and French, 1977). Whereas a single equation for each phase over the entire range of basalts produced a poor fit of the data, by subdividing compositions the same form of equation produced a much improved fit within each group. The need to reduce the range over which an equation is applied reflects the problems in predicting phase relations from the simple component oxides alone. A further problem with this type of approach is the use of starting compositions which may have been substantially modified during experiments. This particularly applies to the data used by French and Cameron, most of which predate modern techniques of experimental control and may have been affected by Fe exchange. In addition, the model of French and Cameron (1981) provided no means of calculating coexisting mineral compositions.

With the rapid increase in the use of electron microprobes throughout the 1970's, analyses of the coexisting glasses and crystalline phases in experimental charges became available. In a study of olivine $\pm$ plagioclase fractionation, Roeder (1975) derived liquidus equations for olivine and plagioclase by multiple linear regression analysis, assuming experimental temperature as a function of coexisting melt composition. Each equation calculates the liquidus temperature of a phase from a liquid composition, independent of the other phase. The phase with the higher predicted temperature is the liquidus phase for that liquid composition. Apart from the absence of a clinopyroxene equation, Roeder's model suffers from using equations unable to follow any curvature of the liquidus surfaces. Mineral compositions were calculated from equations relating distribution coefficients to temperature.

Nathan and Van Kirk (1978) presented an ambitious computer model of fractional crystallisation which considered nine different minerals. Mineral temperature equations were derived in similar fashion to Roeder (1975), using the compositions of supposed

coexisting liquidus. The phase with the highest predicted temperature was taken as the liquidus phase. The coexisting mineral composition was assumed to be a simple function of the liquid composition. Nathan and Van Kirk also presented their own equation to recast Fe^{2+} and Fe^{3+} in the liquid composition. Although the mineral temperature equations essentially consist of terms representing each of the major elements in the liquid (excluding Si), there are two further melt terms included. Firstly, a log function of the essential elements in the phase under consideration, and secondly, a square root term of the Al, Na and K contents of the liquid. These terms effectively allow curvature of the planar surface predicted by the other compositional terms, and so can approximate the natural situation more closely. Perhaps the main disadvantage of the mineral temperature equations generated by Nathan and Van Kirk, lies in the data chosen for the regression analysis. The data consist largely of analyses of starting compositions and synthetic compositions, rather than analyses of glasses produced in experiments coexisting with crystalline phases. Since the model depends on the ability to correctly identify the liquidus phase and temperature, errors in the mineral temperature equations are critical.

Hostetler and Drake (1980) used a powerful statistical technique on a set of 230 glasses to derive equations which allowed the correct prediction of the liquidus phases. They noted that, for the same data set, the mineral temperature equations of Nathan and Van Kirk (1978) frequently misidentified the liquidus phase. However, as presented, their approach does not account for magmas containing ferric iron and more importantly does not calculate temperatures. The technique can indicate multiple saturation of a liquid with some confidence, within the compositional range of the data set, but it is not clear how such equilibria would be dealt with in a crystallisation model.

An alternative approach has been adopted by Langmuir and Hanson (1981) who derived single-component distribution coefficients as a function of pressure, temperature and composition. When these coefficients are combined with mass balance calculations and the assumption of stoichiometry in the crystallising phase it is possible to calculate

phase equilibria in the system under consideration. The coefficients are calculated from crystal-liquid analyses in the system of interest. As a result, this technique can be equally applied to simple binary systems through to natural basalts. Its application is restricted when the coefficients can not be expressed as a function of pressure, temperature and composition, i.e. when there are inadequate crystal-liquid analyses in the system of interest.

In a further development of the Langmuir and Hanson (1981) approach, Nielsen and Dungan (1983) have used a two-lattice melt model to calculate distribution coefficients. By considering the melt as composed of two quasi-lattices, the network formers and the network modifiers, there is a significant reduction of the effect of composition on the distribution coefficients. This allows the model to be applied to a wider range of magmas than the original Langmuir and Hanson (1981) formulation.

The thermodynamic approach to predicting liquidus phases, temperatures and compositions has been mainly restricted to relatively simple synthetic systems (e.g. Weill et al., 1980). Extrapolation to natural melts has been hampered by a lack of quantitative information on the thermodynamic properties of complex, multicomponent, silicate melts. However, the ultimate aim of a phase equilibria model applicable to all magmas is likely to be achieved only when the thermodynamic data become available. This is particularly true of the effects of volatiles and pressure. Mixing models, such as that proposed by Ghiorso et al. (1983), show the ability of thermodynamically based models to extrapolate beyond their database.

5.2 Derivation of Mineral Temperature Equations

The approach adopted here is essentially an extension of the equations presented by Roeder (1975) and Nathan and Van Kirk (1978). Empirical equations calculating the liquidus temperature for each major crystalline phase are developed for anhydrous basic rocks at atmospheric pressure from the major element analyses of experimental glasses. Equations are given for olivine, high-Ca pyroxene, low-Ca pyroxene, plagioclase and spinel from the data presented here

and from other sources. This work was carried out in collaboration with Dr. C. E. Ford, who wrote the main computer program combining mineral temperature equations, mineral composition equations, and crystallisation routines. Dr. R. F. Cheeney provided the computer program to calculate the regression coefficients.

It was recognised from published experimental glass analyses that the equations presented by Nathan and Van Kirk (1978) frequently predicted temperatures several tens of degrees different to the experimental temperatures. Clearly, for a model of magmatic crystallisation to be successful, it is essential to be able to predict the liquidus phase (or phases) and temperature accurately. This is particularly important when modelling cotectic crystallisation. As a result, the set of data used by Nathan and Van Kirk was discarded and replaced by experimental glasses coexisting with crystalline phases from the present study. For the equations to be applicable to a wide range of magmas, an extensive search of the literature was undertaken to provide experimental liquid compositions in equilibrium with the crystalline phases of interest. Since the present study produced no glasses recognised to be in equilibrium with low-Ca pyroxene, the equation presented here has been derived entirely from other studies (both published and unpublished).

The database contains 815 glasses coexisting with olivine (455 from this study); 393 glasses coexisting with plagioclase (281 from this study); 217 glasses coexisting with high-Ca pyroxene (99 from this study); 585 glasses coexisting with spinel (474 from this study); and 177 glasses coexisting with low-Ca pyroxene. The total number of experiments represented by this set is significantly less than the sum of the glasses as many compositions coexist with two or more crystalline phases. A small number of glasses coexist with other phases, such as ilmenite and apatite, but it was felt they were insufficient to generate suitable mineral temperature equations.

The ferric-ferrous contents of the glasses were set using equation (3) in Chapter 3 in this study. The equation of Sack et al. (1980) does not result in a significantly improved or worsened fit of the data to the equations described below. Experiments run in

molybdenum, iron or graphite capsules were assumed to have oxygen fugacities corresponding to one $\log_{10}$ unit below the Fe-FeO buffer (O'Hara and Humphries, 1977).

New coefficients for the Mineral Temperature Equations of Nathan and Van Kirk (1978)

Assuming the experimental crystallisation temperature of each phase to be a function of the glass composition, new coefficients were generated for the Nathan and Van Kirk equations by least-squares multiple linear regression analysis. As the data set used here is significantly different to that used by Nathan and Van Kirk, one can not directly compare correlation coefficients, standard deviations, etc. However, the use of actual experimental glass compositions, from a wide range of experimental studies, is considered to be a major improvement on the often indirectly-derived data available to Nathan and Van Kirk. The coefficients are presented in Table 5-1 along with the coefficient of correlation (r), and standard deviation (σ) of the predicted temperatures from the experimental temperatures. The number of analyses quoted for each equation is generally less than in the original database. This is because the coefficients for each equation were calculated up to three times, with analyses being discarded if the predicted temperature was more than 3σ° C from the experimental temperature. For most of the rejected analyses the composition in question was clearly not consistent with neighbouring experiments. However, for some of the glasses coexisting with spinel there were no obvious discrepancies, and the large errors may be related to the Cr contamination referred to previously. The other factor likely to cause large errors in acceptable compositions is the inability of the equations to model the complete range of glasses. As will be shown below, a modified form of the mineral temperature equations results in fewer discarded analyses and improved fit, and of those rejected, a higher percentage are clearly discrepant compositions.

New Mineral Temperature Equations

There are three main developments presented in this study. Firstly, the range of each equation is reduced by splitting the data

at thermal divides. Secondly, each mineral temperature equation is considered partly as a function of two simple mineral end-members. Thirdly, new terms are presented to model the curvature of each liquidus surface.

It is difficult to model accurately the curvature of a liquidus surface over a wide compositional range. This factor contributes to the relatively large standard deviations presented in Table 5-1, particularly for olivine which represents the broadest data set in terms of composition and temperature. However, splitting the data about thermal divides simplifies the situation by reducing the degree of curvature to be accommodated by individual equations. A more accurate fit of the data can be produced. As a result, each of the glass sets has been divided into two subsets about planes representing thermal divides within the $XO-YO-R_2O_3-ZO_2$ projection system (O'Hara, 1976). Glasses coexisting with olivine or high-Ca pyroxene or plagioclase have been divided by the plane olivine-clinopyroxene-plagioclase. This approximately separates the glasses into nepheline- and hypersthene-normative compositions, considered schematically here as low-Si and high-Si respectively. Glasses coexisting with spinel have been split by the plane spinel-olivine-plagioclase. In practice this is not entirely satisfactory since high temperature spinel crystallisation has a negligible effect on major-element glass composition. Glasses coexisting with low-Ca pyroxene have been divided about the plane low-Ca pyroxene-plagioclase-clinopyroxene. This is stable at high pressures in natural compositions, and at atmospheric pressure in iron-rich compositions in the system $MgO-FeO-SiO_2$. Unfortunately, only 20 glass compositions fall on the low-Si side of this plane, too few to produce a reliable equation for low-Ca pyroxene. The low-Si side of the plane corresponds approximately to olivine-normative compositions, and so it has not been possible to apply a low-Ca pyroxene mineral temperature equation to most of the basalts in this study. Leaving the low-Ca pyroxene data as one equation does not help this problem, as extrapolating to the compositions of interest frequently predicts unrealistic temperatures.

Dividing each set of glasses into two, the form of the mineral temperature equation is the same for both subsets. Temperature is

related to glass composition. Thus the basic form is established:

$$T°C = C_0 + C_1.Si + C_2.Ti + C_3.Al + \quad .....$$

The 'C' terms are coefficients. The elemental terms are cation fractions. Since the sum of the nine component fractions (Si, Ti, Al, Fe^{3+}, Fe^{2+}, Mg, Ca, Na, K) is unity, only eight of these can be regarded as independent variables. As will be described below, Fe^{2+} is not included as a term for olivine, pyroxenes and spinel, and Na is excluded from the plagioclase equation.

Each mineral in the scheme is regarded as a product of two major end-members, to a first approximation. Thus olivine is considered as being composed of a forsteritic and a fayalitic component. As the basic equation is written, the effect of changing a component, say Na, would be the same for forsterite as for fayalite. Therefore, a further term has been added to modify each component according to the proportions of the end-members. For olivine, $Mg/(Mg + Fe^{2+})$ ($\equiv$ M) serves this function, modifying calculated temperatures for a forsteritic component. All the compositional terms other than Mg have this modifying extra term. Pyroxenes and spinel have been treated in identical fashion. Plagioclase is regarded as composed of anorthitic and albitic components. Thus, for plagioclase, M = Ca/(Ca + Na). These modifying terms allow the slope of the liquidus surface to vary according to the proportions of end-member components in the glass. This nearly doubles the number of terms in each equation:

$$T°C = C_0 + C_1.Si + C_2.Si.M + C_3.Ti + C_4.Ti.M + \quad .....$$

In order to accurately model a liquidus surface, the equations must also be able to accommodate curvature. Terms a_9 and a_{10} in the equations of Nathan and Van Kirk (1978), see Table 5-1, serve this role to some degree. These terms and numerous others have been examined to see which produces the greatest improvement in fit. One term was devised from a consideration of the curvature of the forsterite-fayalite join:

$(Mg + Fe^{2+}).M^R.(1-M)$ Curvature term 1 (CT1)

$R = M/(1-M)$ where M has a value corresponding to the maximum liquidus surface deviation from a straight line between forsterite and fayalite. From the phase data of Bowen and Schairer (1935), R has a value of 1.5. The $M^R.(1-M)$ portion of the term therefore reaches a maximum value at the position of maximum deviation from a straight line, and produces a zero value for the whole term at forsterite and fayalite. The $(Mg + Fe^{2+})$ portion of the term scales down the effect away from the join. A similar term can be generated for plagioclase from the albite-anorthite join, where R = 0.43:

$$(Ca + Na).M^{0.43}.(1-M) \qquad \text{plagioclase CT1}$$

For the pyroxenes and spinel, other values of R are probably appropriate. However, from the available data the value of R = 1.5 appears to give a satisfactory result.

Additional terms attempt to model the curvature of the liquidus surfaces in natural systems. Several variations were tried, none of which was entirely satisfactory. The following two terms were found to improve the fit of the olivine equation.

$$[0.66 - (Mg + Fe^{2+})].[\ X - (Mg + Fe^{2+})] \qquad \text{.... CT2 (olivine)}$$

$$M.[0.66 - (Mg + Fe^{2+})].[\ X - (Mg + Fe^{2+})] \qquad \text{.... CT3 (olivine)}$$

X is the average value of $(Mg + Fe^{2+})$ in the glasses coexisting with olivine. Thus X = 0.20 in the high Si group, and X = 0.18 in the low-Si group. Note that as these terms are designed to produce curvature in the natural compositions away from the mean composition, the terms are zero for forsterite, fayalite and the average values. Similar terms are used for glasses coexisting with spinel, where the average $(Mg + Fe^{2+})$ value has been set at X = 0.15 for both glass subsets:

$$[0.33 - (Mg + Fe^{2+} - Ti)].[0.15 - (Mg + Fe^{2+} - Ti)] \quad \text{CT2 (spinel)}$$

$$M.[0.33 - (Mg + Fe^{2+} - Ti)].[\ 0.15 - (Mg + Fe^{2+} - Ti)] \quad \text{CT3 (spinel)}$$

Ti is introduced to simplistically model the effect of an ulvospinel component in the spinel phase.

No suitable additional curvature terms have been found which significantly improve the fit of the equations for plagioclase and the pyroxenes.

Two additional terms are included in the spinel temperature equations. It has been noted that Cr is an important component in determining spinel crystallisation temperatures. Therefore, a Cr^{3+} term and $M.Cr^{3+}$ term are present. At very reducing experimental conditions Cr^{2+} may be significant and so an empirical relation giving the Cr^{3+} portion of ΣCr has been used (Ford et al., 1983), from the data of Schreiber and Haskin (1976). However, the very poor precision with which Cr is usually determined in natural glasses means that the effect of Cr is only poorly modelled by the equations.

The concentrations of the minor elements, Mn, Ni and Co, have been incorporated into Mg and Fe^{2+}. The proportions were determined according to the relative liquidus temperatures of all the end-member compositions of olivine. 0.46(MnO) + 0.3(CoO + NiO) is added to FeO. 0.54(MnO) + 0.7 (CoO + NiO) is added to MgO. For natural basaltic compositions the effects of these additions are trivial. However, for compositions rich in any of these elements significant errors may be produced. P_2O_5 has not been incorporated in these equations although it can reach over 4 wt %. Unfortunately, for a large portion of the database P was not determined and for many other compositions the low concentration is of poor precision. If an apatite mineral temperature equation was developed from this database then P would have to be included.

The final form of the mineral temperature equations is thus established, using the olivine equations as an example.

$$T^{\circ}C = C_0 + C_1.Si + C_2.Si.M + C_3.Ti + C_4.Ti.M + C_5.Al + C_6.Al.M + C_7.Fe^{3+} + C_8.Fe^{3+}.M + C_{11}.Mg + C_{13}.Ca + C_{14}.Ca.M + C_{15}.Na + C_{16}.Na.M + C_{17}.K + C_{18}.K.M + C_{21}.CT1 + C_{22}.CT2 + C_{23}.CT3$$

The pyroxene equations are similar but do not contain the curvature terms $C_{22}.CT2$ and $C_{23}.CT3$. The spinel equations are similar to olivine, although the curvature terms CT2 and CT3 have a different

form and terms $C_{19}.Cr^{3+}$ and $C_{20}.Cr^{3+}.M$ are added . The plagioclase equations have terms $C_9.Fe^{2+}$, $C_{10}.Fe^{2+}.M$ and $C_{12}.Mg.M$ but lose terms C_{14}, C_{15} and C_{16}. These equations also have a different form of $C_{21}.CT1$ and have no $C_{22}.CT2$ and $C_{23}.CT3$ terms.

Coefficients for these equations, derived by least-squares multiple linear regression analysis, are given in Table 5-2. Apart from data collected in this study, the references of sources providing analyses used in the derivation of the equations are listed in Table 5-3.

The standard deviations of the errors in the predicted temperatures are all less than 10° C at the 1σ level. Compared to the fit of the same database to the equations of Nathan and Van Kirk (1978) the new equations are a clear improvement. The correlation coefficients are all better and fewer analyses were discarded, from having predicted temperatures greatly different to the experimental temperatures. To some extent the standard deviations reflect the number and range of compositions within each subset. Thus, the wide range of available studies of olivine-bearing hypersthene-normative glasses is reflected by a relatively large standard deviation. The very good fit and small standard deviation of the low-Si group of clinopyroxene-bearing glasses are partly due to the very limited range of data available. For each pair of mineral equations, the correlation coefficient and standard deviation of the low-Si region are better than those of the high-Si region. This study provides most of the data for the low-Si equations, indicating where the emphasis has been in most published studies.

There are a number of factors affecting the accuracy of mineral temperature equations. At the most basic level, three pieces of information are required to provide data for the equations from an experiment. First is the experimental temperature, which is usually known to within ± 3° C. Second is the nature of the coexisting crystalline phases, which need to be in local equilibrium with the liquid. Nucleation problems or failure to melt xenocrysts can give misleading assemblages. Third is the composition of the liquid. Microprobe (EDS) analyses of the glasses presented in this

study have a precision amounting approximately to a 5°C range in the predicted temperature. This range may be less in practice as nearly all the glasses used are averages of several analyses. However, particularly as the degree of crystallisation increases, the effects of glass analysis contamination and volatilisation can produce large errors in glass composition. In this situation the equations themselves help. If, in a series of experiments on a single composition, the equations fit most of the data closely, then an occasional glass with a large error (i.e. large values of experimental temperature - predicted temperature) may be regarded as suspect. This approach was used successfully on the present data set at an earlier stage. Some suspect analyses were discarded. New microprobe analyses were obtained which were consistent with those of neighbouring experiments, suggesting analytical error was indeed the problem. In summary, from the experimental and analytical viewpoint, it is probably not reasonable to expect equations to be more accurate than $\pm$ 5° C. Inter-lab differences in experimental and analytical procedures will also have an effect.

Less easy to assess are errors due to the inability of the equations to precisely follow a liquidus surface. Systematic errors in individual data sets might reveal this. In the database used here for example, some very Fe-rich compositions (>20% FeO) have slightly high predicted temperatures for the olivine liquidus.

When glasses from high pressure experiments are applied to the equations, systematic positive errors are produced. These errors increase with increasing pressure, reflecting increasing liquidus temperatures with pressure for the main minerals.

The equations occasionally predict the presence of phases not observed from an experiment. For most compositions the errors are only a few degrees and could indicate a nucleation problem or phase identification problem. The few crystallisation-type experiments in the data set have observed assemblages which fit the equations, and point to non-nucleation of phases observed in corresponding melting experiments.

A further problem, unique to the spinel equations, is due to the difficulty of obtaining glass analyses with accurate FeO, Fe_2O_3 and Cr_2O_3 concentrations. The present database is not satisfactory in that respect and some reservations must be expressed about the spinel equations, especially regarding the Cr-contaminated samples used here.

Range of Compositions Over Which the Equations are Applicable

A thorny problem lies in adequately defining the compositional range over which these mineral temperature equations may be satisfactorily applied. For example, extrapolating the low-Ca pyroxene temperature equation to some olivine-normative compositions results in errors of several hundred degrees. It is because of this difficulty that so much effort was put into developing the compositional range of the database.

The high-Si olivine equation probably encompasses the greatest temperature and compositional range of all the equations. The main concentration of analyses (and hence where the equations are most sensitive) lies in the compositional range of basalts. Picrites, alkali olivine basalts, transitional and tholeiitic basalts are all well represented. Basanites, hawaiites and andesites also feature prominently, although it should be noted that the equations have no provision for volatile elements at this stage. Many of the glasses in the database coexist with more than one crystalline silicate phase and so one-atmosphere-pressure cotectics are quite well defined. There is no convenient way of illustrating the absolute range of compositions represented in the database, but for anhydrous basic magmas, the equations for olivine, high-Ca pyroxene and plagioclase should give acceptable results. However, care should be exercised when applying these equations, as extrapolation may not be easily recognised and can lead to large errors. Conveniently for this study, the experimental data presented here are approximately split between the high- and low-Si regions for the mineral temperature equations. Within each region these data form a very large group and are fitted very closely by the equations (because coefficients derived by regression analysis are influenced by the quantity of data).

One area where the equations are known to be suspect is with the spinel equations at reduced oxygen fugacities. The experimental evidence clearly shows the marked decrease in spinel crystallisation temperature between the Ni - NiO and Fe - FeO buffers but this is not reflected in the predicted spinel temperatures.

The analyses given in Table 4-1, of the starting compositions used in the study, were not incorporated into the database. If the spinel equation is ignored, because of the lack of precise Cr determinations, then the silicate mineral temperature equations can be used to predict the liquidus phase, and temperature, of those compositions for which there is experimental confirmation. The results are shown in Figure 5-1. The correct silicate liquidus phase is always predicted, usually within 10° C of the experimental determination. Because the experiments were carried out at 10 - 15° C intervals, uncertainties in the experimental determinations of the liquidus temperatures are comparable to the apparent discrepancies in the predictions. Therefore, the agreement between experimental and predicted temperatures is almost within error limits. Admittedly, this is a gentle test of the equations, but it is very important that with the much expanded database the equations can be successfully applied to compositions of interest in this study.

5.3 Mineral Composition Equations

At equilibrium, with standard states of pure phases at the pressure and temperature of interest,

$$\Delta G^\circ = \Delta H^\circ - T\Delta S^\circ + (P - 1)\Delta V^\circ = -RT \text{ Ln } K$$

where ΔG°, ΔH°, ΔS° and ΔV° represent the changes in Gibbs free energy, enthalpy, entropy and volume respectively, involved in the equilibrium reaction. T is absolute temperature. P is pressure. R is the gas constant. K is the equilibrium constant, relating the activities of the reaction components in the crystal and liquid phases.

Rearranging the above equation

$$\text{Ln } K = \frac{\Delta S^\circ}{R} - \frac{\Delta H^\circ}{RT} - \frac{(P - 1)\Delta V^\circ}{RT}$$

If it is assumed that ΔH°, ΔS° and ΔV° are constant over a limited range of compositions and pressures then a simplified version of the equations can be produced

$$\text{Ln } K = A + \frac{B}{T} + D\left(\frac{P}{T}\right)$$

where A, B and D are constants. In the absence of known activity-composition relationships, K is simplified to the distribution coefficient ($X^i_{mineral}/X^i_{melt}$) where X^i is the concentration of element i in the phase of interest. This basic form of describing element partitioning between minerals and melts is a gross oversimplification of the real situation as it assumes the partitioning is a function only of temperature and pressure. For the compositional range described in Chapter 4, this approach produced a good fit of the data for Fe^{2+} and Mg in olivine and liquid. Poorer fits for elements in other phases may reflect greater sensitivity of distribution coefficients to composition, incomplete equilibrium, and the inappropriate assumption of single-element distribution coefficients rather than the activity-composition relationships of equilibrium constants (Nielsen and Dungan, 1983). As the purpose of the mineral composition equations is to calculate the composition of minerals crystallising from a given melt composition, the final equations used to calculate these compositions have the form

$$\text{Ln}(X^i_{mineral}) = A + \frac{B}{T} + C\ \text{Ln}(X^i_{melt}) + D\left(\frac{P}{T}\right)$$

P is pressure in bars. The compositional components (X^i) are concentrations of element i in cation fractions, with Fe^{2+} and Fe^{3+} distinguished.

The constants A, B, C and D have been derived from an analytical database, by regression analysis using least-squares methods.

The database contains analyses of coexisting mineral-glass pairs. Glass analyses are usually averages of several microprobe analyses of an individual experimental charge. The mineral analyses from an individual charge sometimes show significant variation and

so were not averaged. This is particularly applicable to plagioclase and high-Ca pyroxene. As a result, there are considerably more mineral-glass pairs in the database than there are separate experiments. As would be expected, the largest subset of the database is that containing olivine-glass pairs. Of the 1008 pairs present, 697 come from this study. The next largest group is that for plagioclase, containing 453 pairs of which 419 come from this study. The high-Ca pyroxene group contains 207 pairs, 169 from this study. The spinel group contains 122 pairs, 96 from this study. The low-Ca pyroxene group contains 50 pairs, all from other sources. For each group the bulk of the data is from atmospheric pressure experiments, with no data at all for high pressure spinel-glass pairs.

All the data consist of microprobe analyses. Glasses were recast using equation (3) in Chapter 3. Fe_2O_3 in the spinel and pyroxenes has been estimated on the basis of mineral stoichiometry. For the spinel from this study, recasting the analyses to calculate Fe_2O_3 still resulted in lowish totals ($\sim$98%). For the pyroxenes from this study, recasting the analyses usually produced no Fe_2O_3. It is likely that these two effects are partly due to experimental and analytical problems.

The equation coefficients and associated correlation coefficients are presented in Table 5-4. Satisfactory fits of the data are produced by a number of the equations. Fe^{2+} and Mg in olivine have correlation coefficients greater than 0.7. Of the major elements in high-Ca clinopyroxene, Si and Fe^{2+} have correlation coefficients greater than 0.7. Many of the mineral composition equations for low-Ca pyroxene have high correlation coefficients, reflecting the limited number and range of compositions represented in the database. For plagioclase, Ca, Na and K have correlation coefficients greater than 0.75. The spinel composition equations have high correlation coefficients for Fe^{2+}, Mg and Ti in particular, although Al and Mn also have correlation coefficients at or above 0.7. These high correlation coefficients also reflect the limited number and range of compositions in the database for spinel.

The relatively poor fit for other elements, such as Mg in high-Ca pyroxene where $r = 0.58$, partly reflects the broad range of

compositions which are being modelled by these rudimentary equations. In addition, mineral-liquid pairs which do not represent equilibrium reduce the fit of the equations to the data. For the minor elements, such as Mn in high-Ca pyroxene where r = 0.43, poor fits can be partly attributed to the low precision of the microprobe determination of the elements in the minerals and/or the melts. The quoted partitioning equations for some elements have no practical significance as they reflect contamination of the mineral analyses, e.g. Al and Ti in olivine are due to a small glass component in some analyses. In calculating the composition of the minerals from these equations, the elements attributed to contamination of the analyses have been disregarded. Thus, Al and Ti have been ignored in predicted olivine compositions, K in high-Ca pyroxenes, and Si and Ca in spinels. Because of severely limited data Cr has been disregarded in high-Ca pyroxenes, and Na in low-Ca pyroxenes.

When the equations are fitted only to the experimental data of the present study there are marked improvements in some correlation coefficients. For olivine, both Fe^{2+} and Mg have correlation coefficients greater than 0.9. This indicates the ability of the equations to model variations over a restricted compositional range. For olivine, high-Ca pyroxene, plagioclase and spinel, the experimental data from this study form by far the largest contributions to the individual sets of mineral equations. As a result, the equations fit these data best. The other data, provided from sources in Table 5-3, essentially allow the equations to be extrapolated away from the compositional range of the present study.

Mineral compositions produced from these equations have not been constrained by stoichiometry. In general this has little effect on the predicted compositions used in the present study. However, in detail the equations occasionally predict excess Si in olivine for example. Deviations from stoichiometry are usually within the range covered by microprobe precision. The major element ratios used to calculate mineral end-member proportions are not affected.

Effects of Pressure on the Mineral Compositions

In addition to references in Table 5-3, high pressure mineral-glass data have been incorporated in the database from Thompson (1972b), Mysen and Kushiro (1977), Jaques and Green (1979, 1980), Takahashi (1980) and Stolper (1980). The accuracy of the pressure effects in Table 5-4 is likely to be low because of severely limited data and increased experimental problems. Some predictions of the equations may be considered.

For olivine, the effect of increasing pressure is to produce more Fe-rich compositions for a given melt composition and temperature. If the rate of increase of the olivine liquidus temperature with pressure is low (<5° C/Kb) then liquidus olivines will become more Fe-rich with pressure. This implies a slight increase in the Fe^{2+}-Mg KD with pressure as proposed by several authors (e.g. Bender et al., 1978; Ford et al., 1983).

A similar situation is identified for high-Ca pyroxenes. For a given temperature and melt composition the pyroxene becomes more Fe-rich with pressure. If the pyroxene liquidus temperature increases quite rapidly with pressure (say 12° C/Kb) then liquidus pyroxenes will have very similar values of Mg# at low and at high pressures. Low-Ca pyroxenes are predicted to become more Fe-rich at higher pressures for a given melt composition and temperature.

Plagioclase compositions are predicted to become more sodic and potassic at higher pressures for a given melt composition and temperature. Assuming that the plagioclase liquidus temperature increases with pressure at approximately 1 - 10° C/Kb, then liquidus plagioclase compositions are predicted to become significantly more sodic and potassic at higher pressures.

The range over which the mineral composition equations may be applied is difficult to establish. However, because of the rudimentary form of the equations, it is suggested they are best applied to mildly alkalic basalts, similar to those in the present study. As will be shown in the next section, these simple equations can satisfactorily predict the main end-member proportions of the

major phases in the atmospheric pressure experiments of this study.

5.4 Application of the Equations in an Equilibrium Crystallisation Model

Equations describing equilibrium crystallisation have been developed by Dr. C. E. Ford. When these equations are combined with the glass Fe^{3+}/Fe^{2+} recast equation, mineral temperature equations, and mineral composition equations described here, the product is a complete equilibrium crystallisation model. The large number of repetitive calculations to be executed makes this ideally suited to a computer application.

A convenient way of illustrating the model is to show, for representative basalts, the predicted crystallisation temperatures of each phase together with the predicted liquid compositions, and to compare these with the observed experimental results. Two compositions are examined, one hypersthene-normative basalt and one nepheline-normative basalt, to test both sets of mineral temperature equations. The starting compositions are from Table 4-1. The actual analyses are not in the database. The model was found not to deal satisfactorily with spinel crystallisation and so only the initial crystallisation temperature of the spinel has been calculated. The absence of spinel from the crystallisation sequence has a negligible effect at high temperatures. At lower temperatures, where titanomagnetite can be important, there may be a significant effect on the Fe and Ti contents of the coexisting liquid. Figures 5-2a and 5-2b show the observed and predicted glass compositions and phase crystallisation temperatures. The predicted glass compositions have been normalised to 100%, unlike the experimental analyses which usually total 97 - 99%. This explains why the predicted glass compositions for the more abundant oxides, particularly SiO_2, plot above the experimental determinations.

Overall, the level of agreement between observed and predicted phases and liquid compositions is very high. Thus, the initial crystallisation temperature of each silicate mineral is predicted to within 10° C of its experimentally determined temperature. For

spinel, the errors are 9° C and 28° C. When the coexisting liquids are considered, the pattern of oxide variation with temperature is similar between experimental and predicted compositions. Bearing in mind the normalisation effect, many of the differences between predicted and observed paths are within analytical precision. At lower temperatures, the predicted Fe_2O_3 contents of the liquids are higher than those calculated from the experimental compositions for both samples. In the nepheline-normative basalt, the predicted TiO_2 content also outstrips the experimental value significantly at lower temperatures. Three factors may account for these discrepancies. Firstly, the presence of the titanomagnetite in the experimental charges is not accounted for in the predicted compositions. Secondly, errors in the glass Fe^{3+}/Fe^{2+} recast equation may generate differences. Thirdly, the crystallisation model deviates significantly from the Ni - NiO buffer at low temperatures. The predicted oxygen fugacities are over half a $\log_{10}$ unit more oxidising than the experimental values, which results in over-estimated Fe_2O_3 values. However, these reservations apart, the crystallisation of the two basalts has been closely followed in the model.

The mineral compositions predicted by the model agree well with the analysed experimental phases. For sample MV521; at 1280° C, Fo_{87} is the predicted and the analysed olivine composition; at 1177° C, Fo_{82} and An_{74} to An_{78} were analysed, compared with Fo_{81} and An_{74} predicted; at 1159° C, Fo_{80} and An_{71} (interpolated) occur experimentally, compared with Fo_{79} and An_{71} predicted. Clinopyroxene Mg# values between experiments and predictions are difficult to compare, because of uncertainties about the Fe^{3+}/Fe^{2+} ratio of the experimental pyroxenes. However, compositions are similar. Spinel analyses from the experiments are relatively few. At approximately 1150° C, analysed spinel has Mg# value = 48, compared with predicted Mg# = 39. At approximately 1130° C, the observed spinel Mg# is 25 - 27 compared with predicted Mg# = 30. Predicted phase proportions appear to be consistent with the observed proportions. Plagioclase is predicted to appear after 12% olivine has crystallised. Clinopyroxene is

predicted to appear after 30% olivine + plagioclase has crystallised (in the proportions 3 : 2, olivine : plagioclase). At lower temperatures, the model predicts the plagioclase and clinopyroxene proportions increase rapidly, relative to the olivine.

For sample MV106; at 1245° C, Fo_{86} is the predicted and the analysed olivine composition; at 1200° C, Fo_{84} and An_{76} were analysed, compared with Fo_{83} and An_{77} predicted; at 1156° C, Fo_{79} and An_{70} were analysed, compared with Fo_{78} and An_{72} predicted. Again, clinopyroxene Mg# values are difficult to compare but appear to have been similar in the model and in the experiments. Spinel analysed in a charge from 1191° C had Mg# = 54, compared with predicted spinel Mg# = 55 at 1200° C. Plagioclase is predicted to appear after 6% olivine has crystallised. Clinopyroxene is predicted to appear after 38% olivine + plagioclase has crystallised (in the proportions 2 : 3, olivine : plagioclase). At lower temperatures, the proportions of plagioclase and clinopyroxene are predicted to increase rapidly, relative to olivine. Again, the phase proportions appear to be similar to those observed in the experiments. The rate of increase of crystallinity with decreasing temperature is predicted to be lowest at the olivine stage, higher at the olivine + plagioclase stage, and highest at the olivine + clinopyroxene + plagioclase stage. After their initial crystallisation, both clinopyroxene and plagioclase rapidly equal and then exceed the proportion of olivine in the crystallising assemblages, with decreasing temperatures.

A further general check of the model is to use it to predict the initial crystallisation temperatures of each major phase in the experimentally studied basalts. With the reservations about the spinel temperature equations at low oxygen fugacities, expressed above, only the experiments at the Ni - NiO buffer have been tested in this way for spinel. Figures 5-3 a - d show the predicted and observed temperatures for olivine, high-Ca pyroxene, plagioclase and spinel, respectively. Initial compositions are from Table 4-1. For olivine, with the exception of the most evolved composition (MV51), the model predicts the crystallisation temperatures very well. Most of the errors lie within the expected precision of the experiments and

analyses. For high-Ca pyroxene, the situation is slightly poorer, with lower temperature compositions showing a larger scatter about the experimental temperatures. The problem appears to be that a satisfactory treatment of titanomagnetite is lacking. Crystallising the oxide mineral appears to have an unduly large effect on the predicted temperature of appearance of pyroxene in the model. Taken as a whole, however, the high-Ca pyroxene data are satisfactory. For plagioclase, the model predicts temperatures similar to those determined in the experiments. The two rocks with the highest experimental crystallisation temperatures of plagioclase (MV702 and MV402) have low predicted temperatures. It is not clear whether this reflects a problem of the plagioclase temperature equations or of the starting compositions used. For spinel, the overall trend in crystallisation temperatures is predicted, but the discrepancies are very large. The form of the spinel temperature equations may be inadequate, or more likely, the Cr contamination and the poorly determined Cr contents of the samples produce the large errors. Revision of the database with precise Cr analyses in glasses coexisting with spinel is desirable. The uncontaminated samples shown in Figure 5-3d, have relatively small predicted errors. Low predictions relative to experimental temperatures may indicate high Cr contamination.

In summary, the equilibrium crystallisation model can reproduce major features of the experiments on basic compositions of interest in this study, satisfactorily predicting crystallisation sequences, liquidus temperatures, phase compositions and phase proportions.

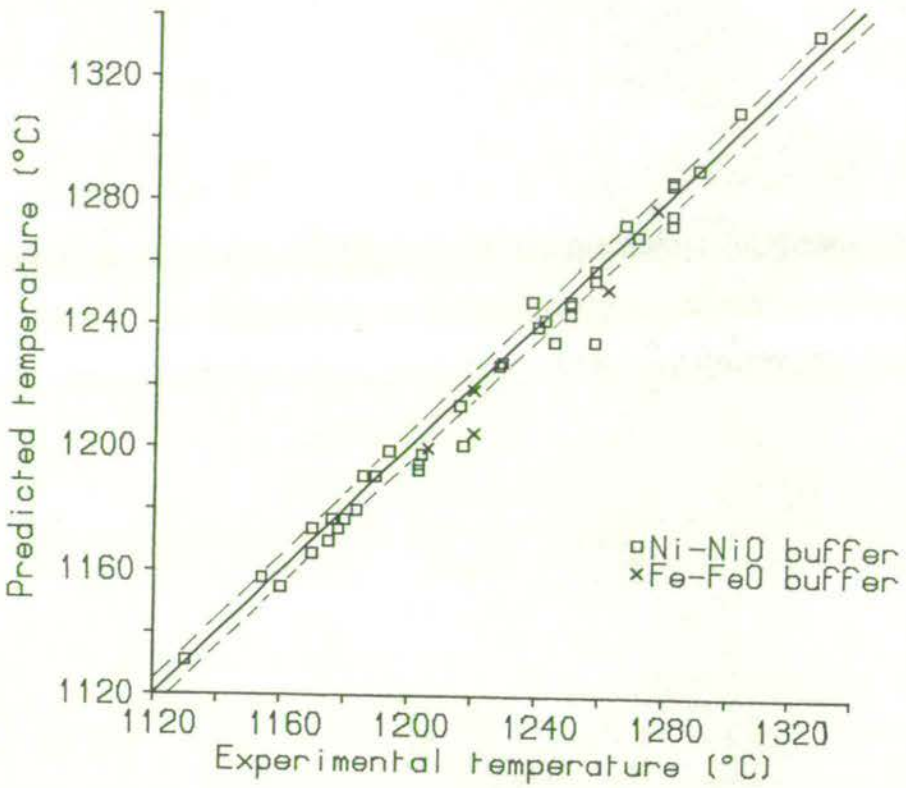

Figure 5-1. Predicted and experimental sample liquidus temperatures (ignoring spinel) for the starting compositions.
Solid line is the 1:1 relation, dashed lines represent ± 5° C.

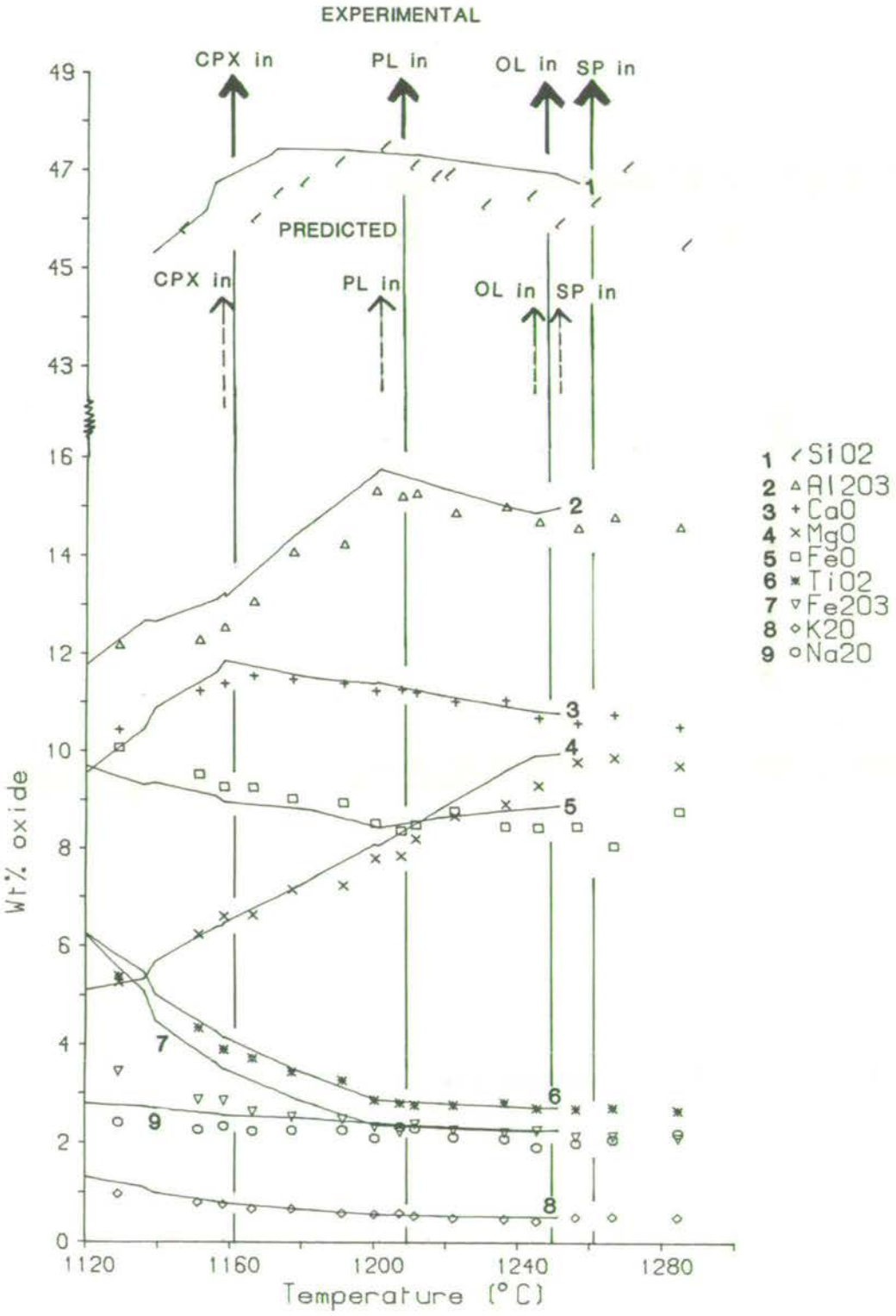

Figure 5-2a. Predicted (line) and experimental (point) variations in melt composition and coexisting phase assemblage with temperature, for MV106 (Hy-normative basalt). Experiments from the Ni-NiO buffer, predictions based on constant oxygen content from the Ni-NiO buffer at 1285°C.

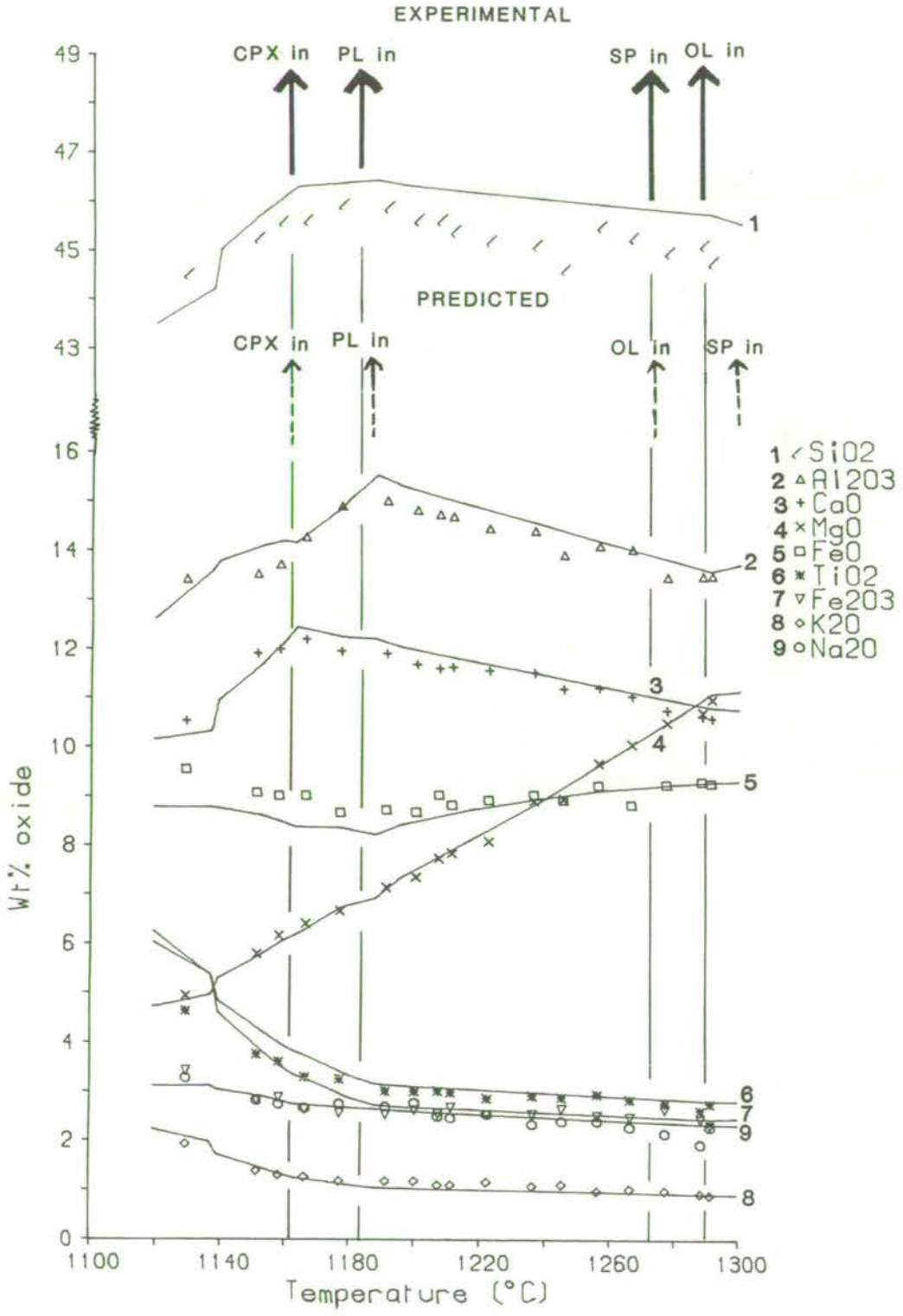

Figure 5-2b. Predicted (line) and experimental (point) variations in melt composition and coexisting phase assemblage with temperature, for MV521 (Ne-normative basalt). Experiments from the Ni-NiO buffer, predictions based on constant oxygen content from the Ni-NiO buffer at 1295°C.

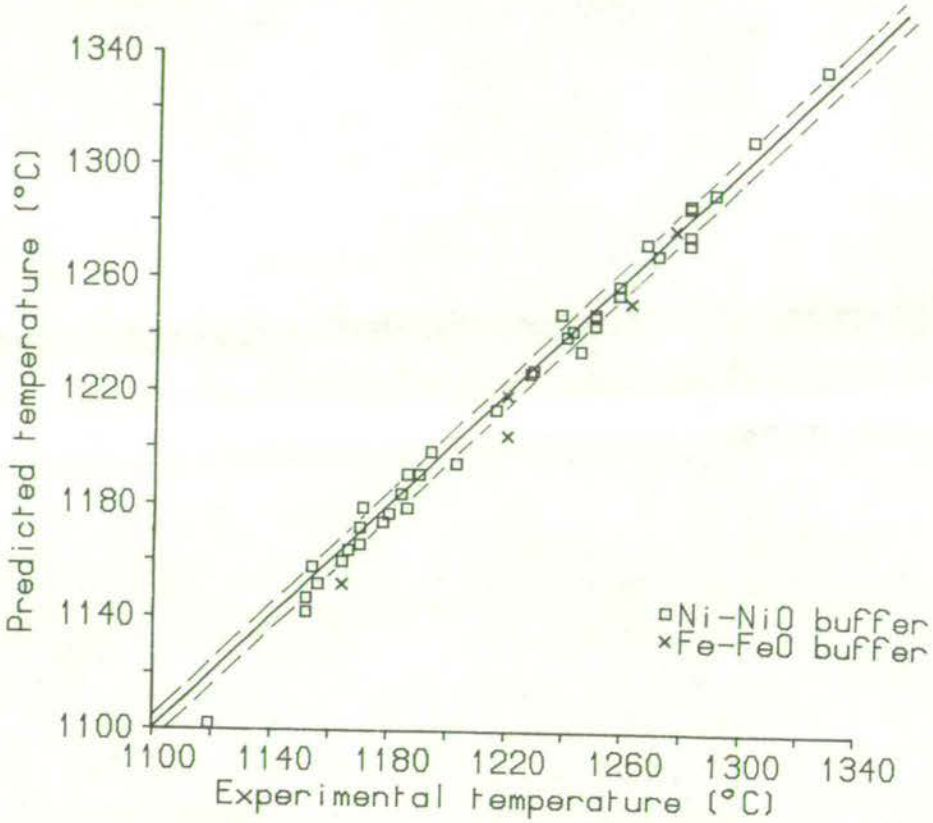

Figure 5-3a. Predicted and experimental olivine liquidus temperatures. Solid line represents the 1:1 relation, dashed lines represent ± 5°C.

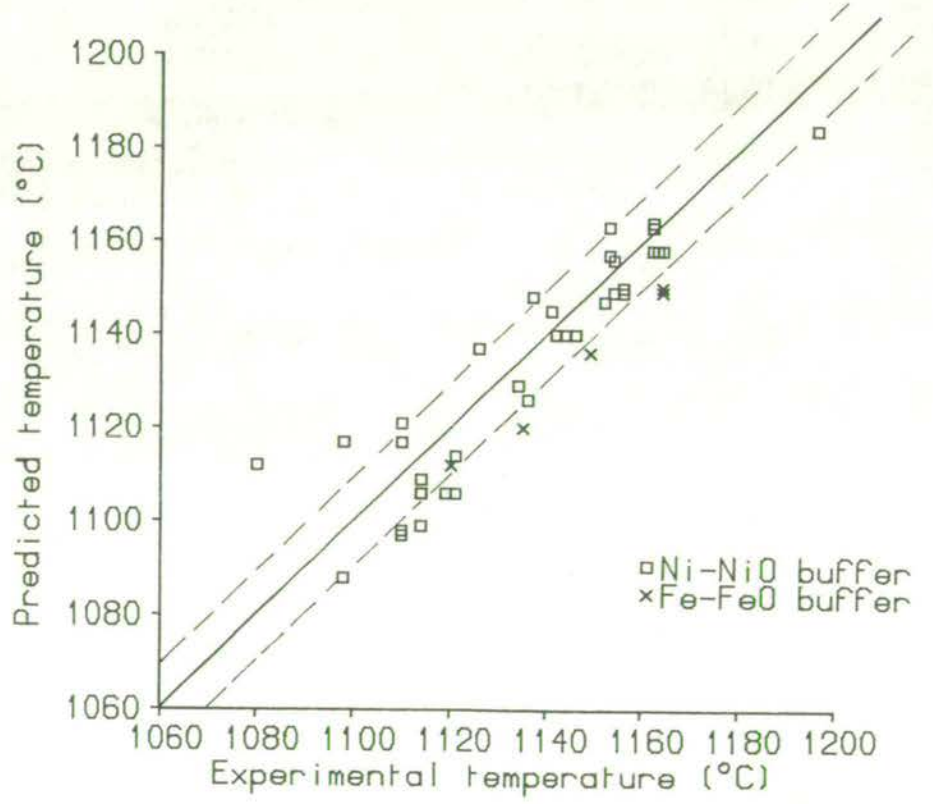

Figure 5-3b. Predicted and experimental high-Ca pyroxene liquidus temperatures. Solid line represents the 1:1 relation, dashed lines represent ±10°C.

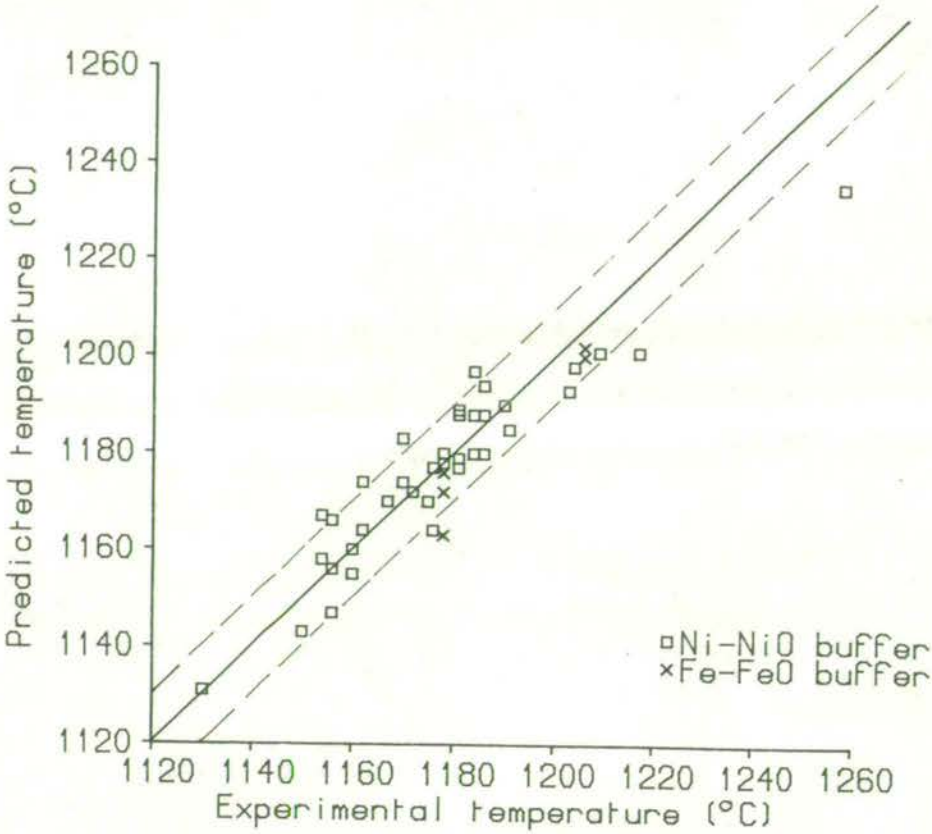

Figure 5-3c. Predicted and experimental plagioclase liquidus temperatures. Solid line represents the 1:1 relation, dashed lines represent ±10°C.

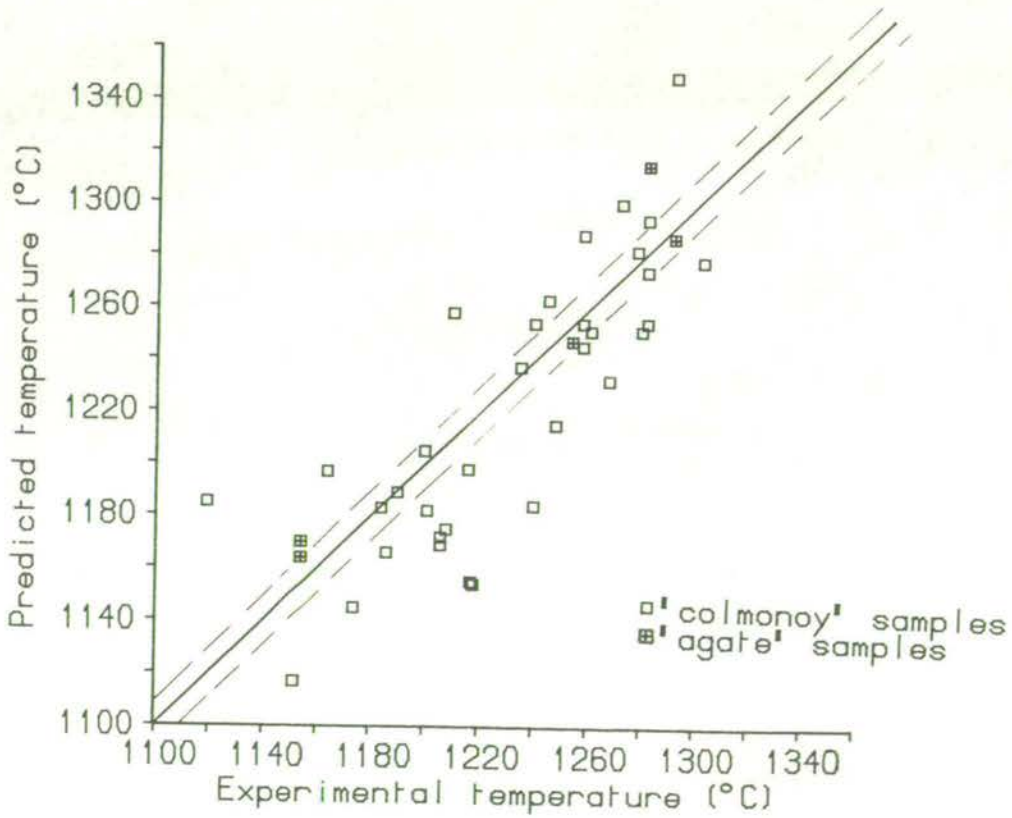

Figure 5-3d. Predicted and experimental spinel-phase liquidus temperatures. Solid line represents the 1:1 relation, dashed lines represent ±10°C.
Samples are distinguished on the basis of whether they were crushed in colmonoy or in agate containers.

TABLE 5-1

New coefficients for the mineral temperature equations of Nathan and Van Kirk (1978).

MINERAL		OLIVINE	HIGH-CA PYROXENE	PLAGIOCLASE	SPINEL/ MAGNETITE	LOW-CA PYROXENE
Constant	a_0	1114.5	890.39	1134.6	876.27	1655.8
Al	a_1	356.74	-173.72	1500.3	-122.52	-58.044
Ti	a_2	-522.43	-700.24	373.88	-415.50	-391.35
Fe^{3+}	a_3	29.855	-678.68	337.80	-126.47	1937.8
Fe^{2+}	a_4	259.55	-285.90	97.726	403.60	-604.28
Mg	a_5	1404.9	636.18	381.94	2117.1	360.79
Ca	a_6	-142.15	717.57	319.73	-312.99	-385.63
Na	a_7	345.27	164.49	-776.39	-552.91	1274.5
K	a_8	178.06	-77.738	-1572.5	-428.02	-1893.8
Log Term*	a_9	124.12	-170.00	224.26	-10.451	342.81
$\sqrt[2]{Al(Na+K)}$	a_{10}	402.36	-437.82	232.84	1342.8	-800.95
Cor. coeff (r)		0.979	0.991	0.976	0.978	0.994
Std. devn. (1σ)°C		16.2	9.8	7.6	10.6	12.1
No. of anal. (n)		781	209	369	560	168

* This term is dependent on the mineral of interest

olivine = $\text{Ln } \sqrt[3]{(Mg + Fe^{2+})^2 (Si)}$

high-Ca pyroxene = $\text{Ln } \sqrt[4]{(Ca)(Mg + Fe^{2+})(Si)^2}$

plagioclase = $\text{Ln } \sqrt[5]{(Na + Ca)(Al)(Si)^3}$

spinel/magnetite = $\text{Ln } \sqrt[3]{(Fe^{2+})(Fe^{3+})^2}$

low-Ca pyroxene = $\text{Ln } \sqrt[2]{(Mg + Fe^{2+})(Si)}$

Note: Glass element concentrations are in cation fractions.

The number of figures quoted is not significant: they are given to reduce rounding errors.

TABLE 5-2

Coefficients for the mineral temperature equations used in this study.

Mineral / Si Zone		OLIVINE High	OLIVINE Low	HIGH-CA PYROXENE High	HIGH-CA PYROXENE Low	PLAGIOCLASE High	PLAGIOCLASE Low	SPINEL High	SPINEL Low	LOW-CA PYROXENE High
(constant)	C_0	633.16	971.17	1194.5	931.23	331.93	949.34	934.39	1244.1	1213.6
Si	C_1	648.35	207.13	-259.04	249.98	740.20	-120.55	366.98	-63.133	-201.12
Si.M	C_2	-298.35	-182.20	477.42	48.046	-320.25	482.06	-526.08	-142.96	381.72
Ti	C_3	205.96	-204.86	-305.57	218.49	-823.37	-1400.5	449.32	-1886.1	-310.84
Ti.M	C_4	-358.54	-516.75	-1119.9	-1586.5	1756.6	2321.2	-901.58	2820.5	-1033.9
Al	C_5	216.76	169.33	-326.54	-448.32	1578.1	999.33	426.18	1138.4	-408.18
Al.M	C_6	261.92	-13.973	-250.54	377.99	835.95	598.30	-394.40	-1847.0	-62.920
Fe^{3+}	C_7	-18.762	-1535.0	-1227.4	-983.54	3553.3	1573.6	-607.09	89.544	5036.7
Fe^{3+}.M	C_8	-77.094	2545.9	1727.6	905.84	-4312.8	-2378.5	168.61	877.64	-8917.6
Fe^{2+}	C_9					13.314	-376.13			
Fe^{2+}.M	C_{10}					614.05	9.6243			
Mg	C_{11}	1777.0	1535.9	230.90	606.12	374.63	1142.1	1681.2	657.86	572.66
Mg.M	C_{12}					337.10	-1761.6			
Ca	C_{13}	975.01	695.20	1081.7	934.10	968.22	-102.22	511.20	-598.03	1055.7
Ca.M	C_{14}	23.422	-550.78	183.79	490.84			-1491.6	-1847.7	-283.37
Na	C_{15}	127.72	402.49	-163.85	96.450			2030.4	2162.4	-296.31
Na.M	C_{16}	335.06	-186.92	-361.20	546.87			-377.96	-2476.6	-1564.5
K	C_{17}	1094.3	791.84	381.13	-696.74	1016.5	-786.64	2119.9	4488.1	2526.5
K.M	C_{18}	204.53	61.717	-282.54	-1697.0	-2990.3	-389.25	-1786.7	-4202.4	-4989.7
Cr^{3+}	C_{19}							5116.4	8431.1	
Cr^{3+}.M	C_{20}							15770.0	15067.0	
CT1	C_{21}	3170.8	1353.3	1565.2	4559.6	3636.3	-2375.9	-30096.0	-22652.0	11476.0
CT2	C_{22}	-2133.1	-1891.8					-3181.3	9252.2	
CT3	C_{23}	2378.9	2249.3					3998.3	-23010.0	
Cor. coeff. (r)		0.995	0.996	0.995	0.998	0.985	0.986	0.986	0.989	0.998
Std. devn. (1σ) °C		9.2	5.8	7.9	3.0	6.6	5.0	9.4	7.0	7.2
No. of analyses (n)		480	316	156	61	260	126	277	291	152

Note: Compositional terms, given in cation fractions, are explained in the text. The number of figures given is not significant: they are quoted to reduce rounding errors. The terms 'HIGH' and 'LOW' refer to Si-rich and Si-poor sides respectively of the relevant thermal divides.

TABLE 5-3

List of sources of analyses used in the derivation of the mineral temperature equations.

SOURCE	MINERAL COEXISTING WITH GLASS				
	OL	CPX	PL	SP	Low-Ca PX
AKELLA et al. (1976)	X			X	
ARNDT (1976)	X				
ARNDT (1977)	X			X	
BENDER et al. (1978)	X		X		
BICKLE (1978)	X			X	
BIGGAR (1981, pers. comm.)	X	X			X
BIGGAR et al. (1971)	X	X	X	X	X
BOIVIN (1980)	X	X	X	X	
J. A. CRAVEN (pers. comm.)	X	X		X	
DELANO (1977)	X		X	X	
DELANO (1980)	X			X	X
DUKE (1976)	X	X			
FISK & BENCE (1980)	X		X	X	
FORD et al. (1972)	X		X	X	X
GROVE (1981)	X		X		
GROVE & BEATY (1980)	X	X	X		X
GROVE & BENCE (1977)	X		X	X	X
GROVE et al. (1982)	X	X	X	X	X
GROVE & RAUDSEPP (1978)			X		X
GROVE & VANIMAN (1978)	X	X	X		X
HART & DAVIS (1978)	X				
HUEBNER (1975)	X	X			X
HUEBNER et al. (1976)	X	X	X	X	X
HUMPHRIES (1975)	X	X	X		X
IRVING et al. (1978)	X			X	
KUSHIRO (1972a)	X	X			X
KUSHIRO (1972b)		X	X		
LEEMAN et al. (1976)	X		X		
LONGHI & BOUDREAU (1980)	X	X			X

SOURCE	MINERAL COEXISTING WITH GLASS				
	OL	CPX	PL	SP	Low-Ca PX
LONGHI et al. (1976)			X		X
LONGHI et al. (1978)	X				
MERRILL & WILLIAMS (1975)	X		X		X
NABELEK (1980)	X				
NIELSEN & DRAKE (1979)		X			X
O'HARA et al. (1974)	X	X	X	X	X
RHODES et al. (1979)	X	X	X	X	X
ROEDER (1974)	X	X	X	X	
ROEDER & EMSLIE (1970)	X	X	X	X	
STOLPER (1976, 1977)	X		X	X	X
THORNBER et al. (1980)	X				
WALKER et al. (1976)	X		X	X	X
WALKER et al. (1972)	X		X	X	X
WALKER et al. (1979)	X	X	X	X	X
WATSON (1977)	X		X	X	

(Table 5-3 continued)

TABLE 5-4

Coefficients for mineral composition equations.

OLIVINE	$\ln X^i_{mineral} = A + \frac{B}{T°K} + C \ln X^i_{melt} + \frac{D(P_{bars})}{T°K}$				Correlation coefficient (r)
ELEMENT (i)	A	B	C	D	n = 1008
Si	-1.1258	59.824	0.011324	-0.00098794	0.69
Al	-12.899	10911	0.35883	-0.0058065	0.39
Fe^{2+}	-7.1727	9958.8	0.65922	0.026491	0.93
Mg	0.21692	-675.77	0.18143	-0.0030156	0.74
Ca	-6.9313	6117.8	1.1501	-0.015364	0.73
Ti	-8.1225	6068.6	0.82080	0.015693	0.68
Mn	-9.9031	8843.8	0.36436	0.014586	0.73
HIGH-CA PYROXENE					r
ELEMENT (i)	A	B	C	D	n = 207
Si	-0.61280	233.41	0.41884	0.0025491	0.75
Al	8.4483	-11327	1.8592	-0.067192	0.73
Fe^{3+}	0.68163	-9628.1	-0.24613	0	0.18
Fe^{2+}	-10.611	13019	0.57587	0.099356	0.73
Mg	-3.6049	4194.4	0.38891	0.033341	0.58
Ca	-0.12705	-1846.8	0.057401	-0.049827	0.65
Na	-0.71978	-2758.2	0.86624	0.031490	0.86
K	39.738	-51227	2.3578	-0.77615	0.85
Ti	7.3240	-11439	0.97999	-0.086118	0.75
Mn	-9.6547	6970.0	0.28431	0.051647	0.43
Cr	6.2039	-14236	0.24056	-0.20091	0.49

LOW-CA PYROXENE	$\ln X^i_{mineral} = A + \frac{B}{T°K} + C \ln X^i_{melt} + \frac{D(P_{bars})}{T°K}$				Correlation coefficient (r)
ELEMENT (i)	A	B	C	D	n = 50
Si	-0.59450	-205.90	-0.017463	-0.0041652	0.67
Al	-5.2735	5240.7	1.2550	0.12756	0.89
Fe^{3+}	-15.583	10034	-0.62190	0	0.58
Fe^{2+}	-4.8718	6163.0	0.76069	0.017176	0.95
Mg	-0.42071	543.67	0.48282	-0.0022596	0.86
Ca	-8.3127	13063	1.9207	0.092386	0.71
Na	-6.3301	2303.9	0.54975	0.058282	0.90
Ti	-9.9961	10734	0.82958	0.087375	0.94
Mn	-4.9079	5152.2	0.76031	0.022213	0.93
Cr	-6.3241	5219.6	0.43346	0.0096389	0.70
PLAGIOCLASE					r
ELEMENT (i)	A	B	C	D	n = 453
Si	-1.3348	1182.5	0.31850	0.0073031	0.72
Al	0.53570	-2798.8	-0.15078	-0.0083721	0.62
Fe^{2+}	-8.7606	4187.4	-0.43160	-0.15529	0.31
Mg	1.7583	-8830.5	0.35919	-0.18521	0.32
Ca	1.3504	-3441.8	0.41848	-0.034074	0.80
Na	-6.4389	7806.6	0.63849	0.092112	0.78
K	-4.2650	4061.1	1.0316	0.079441	0.86
Ti	-2.1192	-723.49	0.97897	-0.26140	0.50

(Table 5-4 continued)

SPINEL	$\ln X^{i}_{mineral} + A + \frac{B}{T°K} + C \ln X^{i}_{melt} + \frac{D(P_{bars})}{T°K}$				Correlation coefficient
ELEMENT (i)	A	B	C	D	n = 122
Si	-20.121	17686	-3.4385	-	0.36
Al	18.240	-20683	3.0915	-	0.85
Fe^{3+}	-5.7836	11783	1.1656	-	0.67
Fe^{2+}	-6.5432	13119	1.5468	-	0.95
Mg	2.1181	-3071.3	0.76258	-	0.94
Ca	-8.4663	6668.7	0.61791	-	0.45
Ti	-16.226	26683	1.4261	-	0.94
Mn	-9.8267	8214.6	0.28831	-	0.70
Cr	19.041	-28514	0.20443	-	0.66

Compositional terms are in cation fractions. n is the number of mineral-liquid pairs in each group. The number of figures given is not significant. They are quoted to avoid rounding error.

(Table 5-4 continued)

THE GREAT TRAGEDY OF SCIENCE - THE SLAYING OF A BEAUTIFUL HYPOTHESIS BY AN UGLY FACT.

T. H. Huxley.

CHAPTER 6

THE NATURAL ROCKS

6.1 Introduction

This chapter deals with the petrography and major element composition of the rocks, and the chemistry of the phenocrysts. The range of compositions considered is from basalt to hawaiite. More evolved types are present in the province, including mugearites, trachytes and rhyolites. These latter rocks contain phenocryst assemblages with hornblende, and more rarely biotite, developed. It would be inappropriate to include such samples, with evidence of significant volatile pressures, in this study which is based on anhydrous mineral assemblages.

It has been pointed out that the rocks forming the basis of this study were erupted or emplaced over a very large period of time (about 90 m.y.), and in a large number of geographically distinct settings. While providing a wide spread of compositions within the basalt spectrum, this choice of samples presents some problems in considering how to discuss their chemistry and mineralogy. One approach would be to describe the basalts in relation to their geographical setting. This would perhaps be the most desirable as closely related compositions could be taken together. Macdonald (1975) has indicated how distinct magmatic lineages can be recognised on a geographical basis. However, the coverage of most districts is so poor as to make detailed discussion impracticable. The approach adopted here, therefore, considers the collection of samples as a whole. This undoubtedly conceals many fine details but allows general aspects of the province to be identified, when combined with previous research.

6.2 Previous Work

The Permo-Carboniferous igneous rocks of Scotland have been studied in considerable detail since the days of James Hutton. Much of the work has concentrated on the field relations and petrographic aspects of the lavas, minor intrusions and tuffs. In addition to

mapping by the Geological Survey, the occurrence of major coalfields of Carboniferous age has led to a great body of published information on the stratigraphic relationships of the lavas and tuffs, particularly. The presence of several local universities and geological societies has resulted in numerous specific studies of lava successions. Unfortunately, there has not been an accompanying effort to clarify the variations in rock and mineral chemistry in the province. This has restricted detailed petrogenetic discussion. With the notable exceptions of papers by Tomkeieff (1937) and MacGregor (1948), there was little detailed discussion of the origin and evolution of the igneous rocks from the petrochemical viewpoint until Macdonald (1975). More recently, interest in the province appears to have been rekindled, particularly with respect to trace element, isotope and inclusion studies (e.g. De Souza, 1979; Upton et al., 1983). Although there has been a fairly rapid increase in available whole rock data, the corresponding mineral chemistry has only rarely been reported. Without phenocryst analyses, much of the discussion of the igneous rocks has been speculative.

While the stratigraphic relationships of the lavas are not of prime concern in this study, the earlier research provides many pointers to the origin of the phenocryst assemblages. Several eruption mechanisms have been proposed for the province. Upton (1982) and Francis (1983) reviewing these mechanisms have indicated the large number of vents and necks identified. For the main episode of volcanism, in the Dinantian, Upton (1982) stated that most of the volcanoes were small and quite short-lived. Some fissure eruptions may have occurred (Francis et al., 1970) although these are less well established. At least one strato-volcano is believed to have existed, in the Campsie Hills (Craig, 1980). Francis (1983) has suggested that there may have been others, associated with many of the more salic compositions. For the Silesian to Lower Permian magmatism, evidence indicates that small vents and necks were very numerous, with explosive eruptions frequent. Sill complexes were also abundant. An episode of intrusion of quartz dolerite sills occurred in the Upper Carboniferous, but a consensus of opinion on these rocks suggests they represent a distinct event unrelated to

the compositions in this study (Macdonald et al., 1981).

A further feature of the main Permo-Carboniferous volcanism was its concentration along structural planes of weakness such as faults, fold axes and hinges (Francis, 1978). Francis (1983) has recognised a controlling Caledonoid NE-SW trend for the Dinantian volcanism, partly based on field evidence of lines of vents with that orientation (Whyte and MacDonald, 1974). The later volcanism was also interpreted by Francis (1983) as having exploited planes of weakness, although the dominant trend was considered to approximate to NW-SE. Upton (1982) has presented similar views, although his interpretation of the evidence for the later volcanism was that a wider range of trends can be identified. MacGregor (1948) first suggested that the magmas exploited fissures in ascending from depth, with the hawaiites and more salic differentiates having been generated in near-surface magma chambers. Small sub-volcanic magma chambers are likely to have been present for the Dinantian lavas (Upton, 1982). More rare, larger magma chambers under strato-volcanoes could have been important in the origin of the more salic lavas. The later Silesian to Lower Permian magmas do not appear to have been associated with near-surface magma chambers on the basis of field evidence. Many of the more undersaturated compositions of this later volcanism also carry inclusions of presumed deep crustal or upper mantle origin. A wide range of inclusions has now been described (Upton et al., 1983), some of which retain an igneous texture and represent high pressure crystallisation of basaltic compositions. Although there is some debate on the significance of these inclusions to the host magma (Sparks et al., 1977), it is clear from many occurrences that rapid transport of the inclusions from the upper mantle is required to explain the lack of re-equilibration (Wass, 1980). For these rocks at least, there would appear to be little possibility of evolution in low pressure magma chambers.

Geochemical evidence on the origin of the phenocryst assemblages has been largely restricted to discussions based on whole rock compositions. Tomkeieff (1937) established the continuous range of rock types from very undersaturated basanitic compositions through to rhyolites. About 80% of the rocks are hawaiitic or more basic.

The most abundant types are feldspathic basalts, basaltic hawaiites and hawaiites. In more detailed surveys, Macdonald (1975) and Macdonald et al. (1977) have indicated the dominant role of slightly nepheline-normative and slightly hypersthene-normative (transitional) basalts in the main Dinantian episode, and more nepheline-normative basalts in the later volcanism. Although they emphasised the mildly alkaline nature of the volcanism, these authors also identified regions where quite hypersthene-normative basalts are dominant (e.g. Ayrshire Passage Group lavas). Some examples in the Scottish Borders are also quartz-normative in basic lavas, suggesting tholeiitic affinities. Macdonald (1975) proposed from limited evidence that there was a discernible increase in the degree of undersaturation of the lavas throughout the Carboniferous. This theme was elaborated upon by Macdonald et al. (1977) who suggested there were two cycles of increasing undersaturation. Based on K - Ar dating of the Permo-Carboniferous basic rocks, De Souza (1979) distinguished an overall, imperfect single trend of increasing undersaturation. His data suggest the earliest volcanism in the province, the Birrenswark and Kelso lavas in the Scottish Borders, was silica-saturated and ranged to the latest episode, the very undersaturated Highland lamprophyre dykes. Regardless of the origin of this variation, which may owe a great deal to the prevailing stress regime (Dixon et al., 1981; Leeder, 1982), a wide range of parental magmas were available over the time-span of the province.

Compared to the time encompassed by the province as a whole, individual lava successions were of quite limited duration (De Souza, 1979). Macdonald (1975) was able to distinguish individual magmatic lineages on the basis of degree of silica saturation, Na_2O/K_2O and FeO/MgO ratios. In addition, he proposed three volcanic associations, into which the geographically distinct successions could be placed. Firstly, there is an association with rocks ranging from ankaramites through to rhyolites or trachytes. Possible areas of this association are Kintyre, East Lothian, Edinburgh and Kelso. Secondly, there is an association dominated by feldsparphyric hawaiites with less common basalts and salic differentiates. Examples of this association include the Campsie Fells and Carnwath areas. Thirdly, there is an association

dominated by olivine ± clinopyroxene microphyric basalts with some ankaramites, but with few, if any, more differentiated compositions. Examples of this association include Burntisland, West Lothian and the Ayrshire Passage Group. Macdonald et al. (1977) were unable to distinguish individual magmatic lineages for this third group of areas, and suggested the individual lavas were the products of single melting events.

Macdonald (1975) examined individual areas from associations 1 (Kintyre) and 2 (Early Campsie Fells). Having noted that the mildly alkalic basalts were associated with the widest range of erupted lavas, Macdonald considered both successions in terms of fractionation processes. Evidence quoted for fractionation processes from basaltic parental magmas included the lack of compositional gaps in the lavas, the dominance of basalt and the progressively smaller bulk of more evolved compositions, high-pressure cumulate inclusions, and a correlation between the bulk chemistry and phenocryst assemblage of the lavas. For the Kintyre succession, a generalised progression of phenocryst assemblages was discerned. The most primitive lavas carry olivine + clinopyroxene phenocrysts. More evolved lavas have olivine + clinopyroxene + plagioclase phenocrysts, then olivine + clinopyroxene + plagioclase + magnetite, then olivine + plagioclase + magnetite. Clinopyroxene has been lost as a phenocryst phase in the more evolved lavas (hawaiites). If the Kintyre lavas are to be explained in terms of fractionation processes, then the disappearance of a major phenocryst phase needs to be accounted for. Macdonald (1975) presented similar bulk composition data for the Early Campsie lavas. In this suite clinopyroxene is absent from the phenocryst assemblages, but simple extract calculations relating basalts to basaltic hawaiites require a large clinopyroxene component. For both successions Macdonald argued that low-pressure fractionation mechanisms would not have produced the observed variation, as clinopyroxene would not have been lost from the phenocryst assemblages. Thus he inferred a higher pressure stage of evolution involving clinopyroxene. Supporting experimental evidence for high pressure clinopyroxene fractionation in basalts has been presented by Thompson (1974a) in a study of Scottish Tertiary basalts.

Petrographic evidence has been available from the Permo-Carboniferous province for some time. MacGregor (1932) and Hamilton (1956) have recognised the highly resorbed nature of some clinopyroxene phenocrysts in basalts, and have interpreted the texture as indicating the clinopyroxene was out of equilibrium with the melt. For the Early Campsie basaltic hawaiite to hawaiite trend, Macdonald showed that extract calculations involving olivine + plagioclase + magnetite could explain the variation, consistent with low pressure fractionation processes. For the Early Campsie lavas, Macdonald presented a strong case for higher pressure evolution involving clinopyroxene-bearing assemblages. Two such assemblages are consistent with the bulk compositional trend. First is an olivine + clinopyroxene + plagioclase assemblage, crystallised at pressures of 9 Kb or greater. Second is an aluminous clinopyroxene-only assemblage which may have crystallised at 13 Kb or greater. The more evolved rocks were explained by Macdonald in terms of fractionation of the observed olivine + plagioclase + magnetite phenocryst assemblages. The Kintyre lavas show a trend in the most basic compositions consistent with olivine + clinopyroxene fractionation, interpreted by Macdonald as a high-pressure stage. Again, the olivine + plagioclase-phyric (and olivine-phyric) more evolved lavas were suggested to represent lower pressure evolution.

A further indicator of high-pressure fractionation is the frequent occurrence of slightly nepheline-normative basalts associated with hypersthene-normative differentiates. These compositions cross the low-pressure olivine-clinopyroxene-plagioclase thermal divide in a normative classification (Yoder and Tilley, 1962). It is worth noting that none of the compositions studied experimentally at atmospheric pressure show a similar trend. Minimum pressures of 4 Kb (Presnall et al., 1978) to 8 Kb (O'Hara, 1968) have been advanced, above which the plane of the divide may be crossed to produce the hypersthene-normative compositions.

In a major- and trace-element study of the Campsie Fells lavas, MacDonald and Whyte (1981) interpreted the evolution of the series in terms of a polybaric fractional crystallisation model. Following Macdonald (1975), and from similar lines of evidence, these authors

recognised an upper mantle stage of aluminous clinopyroxene fractionation. At intermediate pressures (less than 8 Kb) within the crust, fractionation of the observed olivine + plagioclase + magnetite phenocrysts was believed to have been important. Fractionation within a few kilometres of the surface, perhaps with significant partial pressures of water, was considered to be the source of the more salic lavas. The main difference between the interpretation of Macdonald (1975) and MacDonald and Whyte (1981) appears to be in the placing of the olivine + plagioclase + magnetite phenocryst assemblage. The latter authors placed this stage at deeper levels within the crust, partly on the basis of petrographic evidence of phenocryst disequilibrium, the lack of evidence of suitable high level magma chambers, and partly on preliminary experimental studies of a Clyde Plateau alkali basalt (Ford and Macdonald, 1978). The experimental evidence, from a basalt containing phenocrysts of olivine, clinopyroxene and plagioclase, indicated olivine + plagioclase at the liquidus from atmospheric pressure up to approximately 8 Kb. At this pressure there is a possible three-phase cotectic situation with clinopyroxene joining the other phases. At high pressures clinopyroxene is the liquidus phase. The addition of magnetite to the phenocryst assemblage in the Campsie Fells lavas was attributed by MacDonald and Whyte (1981) to high oxygen fugacities in the magmas at crustal levels.

There are few published analyses of the phenocryst phases in the Permo-Carboniferous igneous rocks. In a study primarily concerned with inclusions in undersaturated rocks from Fife, Chapman (1976) presented analyses of clinopyroxene phenocrysts. These are moderately aluminous and titaniferous augites (more specifically salites) with titanaugite (titansalite) rims. On the basis of the mineral chemistry and associated inclusions, Chapman placed the origin of these phenocrysts at "relatively shallow crustal levels". From his discussion a pressure of several kilobars is implied. It is worth noting that in all his basalts the augite phenocrysts are accompanied by olivine. Unfortunately, due to alteration no analyses are available of these olivines. The inclusion association of these basalts was interpreted as cognate by Chapman. The mineral

assemblages of these inclusions imply significant volatile pressures, which may be atypical of the samples under consideration in the present study.

6.3 Terminology

It is worth clarifying two aspects of the rocks before discussing the samples examined in this study. First is the classification scheme for the basalts, used throughout the older literature, which is based on type localities of particular phenocryst assemblages (Markle, Dunsapie, Craiglockhart, Jedburgh, Dalmeny and Hillhouse). Secondly, it is necessary to consider the criteria for recognising crystals as phenocrysts.

The classification scheme presented by MacGregor (1928) was based on the size and nature of the phenocrysts, and standardised earlier similar schemes (e.g. Allan, 1924). The main aims were to aid the petrographer dealing with large numbers of thin sections, and the field geologist mapping the lava successions. The success of the scheme is indicated by its continued use up to the present time. Table 6-1 is based on Table 1 of Macdonald (1975) and gives the modern petrologic equivalent of the MacGregor categories. The main difference between the two versions is the recognition that in modern terms, basaltic hawaiite and hawaiite were major components of the volcanism. The division between micro- and macro-porphyritic assemblages, set at 2 mm by MacGregor, was arbitrary with no obvious petrogenetic significance at the time. Despite this, only the Jedburgh and Markle categories appear to be direct equivalents. Macdonald (1975) distinguished two groups of Dunsapie basalts. Assemblages of olivine + plagioclase + clinopyroxene usually occur in basaltic rocks, whereas the additional presence of magnetite phenocrysts characterises basaltic hawaiites. This last observation emphasises perhaps the main reason for the longevity of the MacGregor classification. The phenocryst assemblage present in the basalts is often a useful indicator of the rock composition. Thus the Jedburgh and Markle categories are usually hawaiitic compositions, whereas the Hillhouse category is largely made up of the most primitive basalts in the province. That is not to suggest the

different types simply reflect varying proportions of the main phenocryst minerals. Although most of the basalts are markedly porphyritic, Macdonald (1975) stated there are aphyric or sparsely porphyritic equivalents over the whole basaltic compositional range. The only exception to this is the group consisting of highly plagioclase-phyric rocks where plagioclase accumulation is likely. Macdonald also described three lavas from Kintyre with identical bulk compositions but quite distinct phenocryst assemblages of olivine (trace), olivine + clinopyroxene (30%) and olivine + clinopyroxene + plagioclase (35%). He interpreted these lavas as representing different degrees of crystallisation of an initially ankaramitic magma, and warned against too rigorous a use of the MacGregor classification.

In this study of the origins of phenocrysts it is appropriate to consider the rocks in terms of their phenocryst assemblages. Variations in bulk composition could be examined in terms of the modern classification, but since that imposes artificial divisions on an essentially continuous data set the emphasis here will be more mineralogical. Therefore, bearing in mind the warning of Macdonald (1975), the correlation between rock composition and phenocryst assemblage is used in the discussion below. No distinction is made between the micro- and macro-porphyritic groups which most previous workers consider to be a purely textural division (MacGregor, 1928; Tomkeieff, 1937; Macdonald, 1975). In the first instance the aim is to group like phenocryst assemblages with like, rather than imply a petrogenetic significance.

The above discussion of classification of phenocryst assemblages essentially revolves around only four minerals, namely olivine, clinopyroxene, plagioclase and magnetite. Ideally these are recognised as phenocrysts by their occurrence as larger grains set in a finer or glassy groundmass. No petrogenetic implications are made in that definition. Unfortunately, it is common for phenocrysts to be taken as minerals crystallised at an earlier stage from the host melt. This is clear from the association with the term xenocryst, where similar sized minerals are interpreted not to have crystallised from the host. The further descriptive term

megacryst also appears to suffer from petrogenetic associations. From a purely descriptive viewpoint it is desirable to avoid any petrogenetic implications in listing phenocryst assemblages. Thus, within this study a phenocryst is defined as any mineral which is petrographically distinct from the groundmass. In this way, very small crystals such as Cr-Al-spinel inclusions in olivine can be regarded as phenocrysts, although they may be smaller than the matrix magnetites. Similarly, crystals exhibiting resorption textures or reaction rims are described as phenocrysts rather than xenocrysts. Experimental studies have clearly indicated how different minerals can be in equilibrium with a given liquid composition under different conditions of pressure and temperature. The identification of a phase as a true xenocryst can be very difficult (Cox et al., 1979, pp. 187 - 188). Also, crystallisation studies have shown that a porphyritic texture can be developed during the quenching episode of a magma (e.g. Lofgren et al., 1974). Petrogenetically, some phenocrysts may be more closely associated with the groundmass than with other phenocrysts. There is therefore, no intrinsic assumption that a phenocryst phase was present in a magma before eruption or intrusion. By extension of this argument the term 'phenocryst assemblage' is simply taken as the list of phenocrysts present. No assumption is made of equilibrium between phases.

A final point concerning the recognition of phenocrysts is related to their abundance. Should the presence of a single large grain of a mineral be enough evidence to classify it as a phenocryst phase? From the definition given above the answer is yes! A single thin section is a very poor level of sampling a lava flow, and ideally, numerous sections would give a better idea of phenocryst phases. Experimentally, the recognition of another phase in a crystallising assemblage can be of great importance in defining the pressure and temperature conditions of origin.

For the reasons outlined above, the given phenocryst assemblage is often at variance with the assemblage quoted by the other workers on these rocks (**cf.** Macdonald, 1975; Macdonald et al., 1977; Clark, 1956). The main differences are the recognition of spinels as phenocryst phases and the inclusion of trace amounts of other phases.

The distinction between spinel and magnetite phenocrysts is necessary. The presence of magnetite in phenocryst assemblages has been noted by Macdonald (1975) as indicating hawaiitic compositions. In the present study, large opaque phases have been found to be aluminous spinels in some cases, with quite different implications for the host rock. If the presence of magnetite is to be used as an indicator, then it is essential that the samples are studied in reflected light or by electron microprobe, rather than the standard thin section, in order to avoid misidentification of the oxide phases.

6.4 The Petrography and Composition of the Samples

6.4.1 The range of compositions and their degree of alteration

A wide range of compositions is discussed in this section from very undersaturated monchiquite through basanite, alkali olivine basalt, hypersthene-(± quartz-) normative basalt and basaltic hawaiite to hawaiite. The collection consists of lavas and near-surface intrusions, and may be considered as a volcanic association (Upton, 1982). Mildly alkaline and transitional basalts (hypersthene -normative) are best represented. All the rocks show some degree of alteration. This ranges from only slight alteration of the olivine (e.g. MV109), to quite reddened samples with no fresh olivine preserved (e.g. MV71A). For the 46 samples examined only 10 contain no fresh olivine at all. Other minerals appear to be less affected although MV520 contains no fresh plagioclase despite having quite fresh olivine. As Macdonald (1975) pointed out, relatively fresh olivine can be found in many of the basaltic rocks with careful searching. The limited amount of sample available in this study for thin section analysis may not be representative of the source lava as a whole. The effect of the alteration on the composition of the rocks is difficult to assess in detail without much more extensive sampling. For most it is assumed the main result is a readjustment of the original iron oxidation state (Macdonald, 1975). In consequence, the iron content of each bulk composition has been recast using the method described in Chapter 3. Each composition has been recast assuming it was liquid at the Ni - NiO buffer. The Ni - NiO buffer was chosen as a suitable guide to the oxidation state of the magmas on the basis of coexisting iron-titanium oxides (discussed below). The bulk compositions used have been taken from Table 4-1 and from the original published descriptions of the samples. All the rocks studied experimentally have been examined using the electron microprobe, with the exception of MV167 for which no hand specimen could be obtained. In addition, two spinel lherzolite nodules (F2 and F3) and two wehrlite nodules (F1 and F4) were examined from the Fidra basanite (East Lothian). Samples of the Lion's Haunch intrusion (AS1 and 36017) and the Whinny Hill intrusion (AS2) were also studied from Arthur's Seat, Edinburgh.

6.4.2 Phenocryst assemblages

The phenocrysts identified in these samples are olivine, clinopyroxene, plagioclase, spinel, titanomagnetite, ilmenite and (from one sample, MV121A) orthopyroxene. The distinction between spinel and titanomagnetite is somewhat arbitrary, as there is a complete compositional and textural range from translucent brown spinel to opaque titanomagnetite. In general, titanomagnetites occur as large discrete grains set in the groundmass or as small inclusions near the edges of other phenocrysts. Spinels tend to occur as small inclusions in the cores or interiors of other phenocrysts, notably olivine and to a lesser extent clinopyroxene. The exception to this is a group of highly aluminous, chrome-poor spinels which can occur as large grains set in the groundmass. Numerous combinations of these phenocrysts occur. For convenience in the discussion only the main silicate phases are listed in the following phenocryst assemblages. These are olivine + clinopyroxene (16 samples), olivine + clinopyroxene + plagioclase (17 samples including the orthopyroxene-bearing MV121A), olivine (3 samples), olivine + plagioclase (2 samples) and plagioclase (4 samples). Spinel occurs in all the olivine + clinopyroxene and olivine assemblages, in 5 of the olivine + clinopyroxene + plagioclase assemblages, but not in the olivine + plagioclase or plagioclase assemblages. Titanomagnetite occurs in 4 of the olivine + clinopyroxene assemblages, 9 of the olivine + clinopyroxene + plagioclase assemblages, both of the olivine + plagioclase assemblages, 2 of the plagioclase assemblages, but not in the olivine assemblages. Ilmenite only occurs as discrete phenocrysts in the plagioclase-bearing assemblages (in 6 of the 23 samples).

Upton (1982) noted a correlation between the size of the phenocrysts and their abundance. This appears to be reflected in the present collection, where the more porphyritic rocks frequently contain the largest phenocrysts. There are several exceptions to this general rule, but it should be investigated in more detailed petrographical studies. Other observations can be made from the phenocryst modes, although usually being based on a single thin section they should be treated cautiously. Appendix 1 contains

estimates of the modal abundances of the phenocrysts in the sample collection. Taking the bulk composition Mg# (from the recast analysis) as an indicator of the degree of fractionation, the proportion of opaque oxides in the phenocryst assemblage is often higher in the lower Mg# samples. The proportion of clinopyroxene in the phenocryst assemblages is usually higher in the higher Mg# samples. The proportion of olivine tends to be higher in the olivine + clinopyroxene assemblages than in the plagioclase-bearing assemblages. Modally therefore, clinopyroxene is often a major component in the less fractionated samples. The proportion of olivine in the assemblages decreases with Mg# and with the appearance of plagioclase. Magnetite and ilmenite form larger proportions of the assemblages at lower Mg#'s. Plagioclase is often the dominant phenocryst in the lower Mg# samples. There is no apparent correlation between Mg# and the volume of phenocrysts present. Similarly there is no correlation of Mg# with phenocryst size. The persistence of individual phenocryst phases with whole rock Mg# is shown in Figure 6-1. Some of the gaps are due to imperfect sampling but a few points can be noted. The highest Mg# samples usually have a phenocryst assemblage of olivine + clinopyroxene + spinel. Spinel is not a common phenocryst in samples with Mg# <60. Plagioclase and magnetite become common phenocrysts in samples with Mg# <65 approximately. Ilmenite is restricted to samples with Mg# <60. It is likely that the details of phenocryst occurences are different for the individual lava successions. Macdonald (1975) distinguished the ranges of phenocrysts in Kintyre and the Early Campsies on the basis of normative An/(An + Ab). He showed that clinopyroxene was present in the Kintyre lavas at normative values where it was absent from the Early Campsies.

Taking the illustrated ranges together with the modal data, a simplified interpretation can be made. The most basic rocks carry olivine + clinopyroxene + spinel phenocrysts. At lower Mg#'s plagioclase and magnetite join the phenocryst assemblage. Spinel is lost soon after this and at low Mg#'s ilmenite can join the assemblage. Clinopyroxene is gradually lost as a phenocryst phase towards lower Mg#'s. The proportion of olivine may also fall as the proportion of plagioclase increases.

6.4.3 Petrographic notes

The sequence of assemblages listed in the previous section is not a result of simple low-pressure crystallisation. Clinopyroxene would not have been lost from the assemblage in that case. Indeed, the petrographic evidence indicates clinopyroxene was out of equilibrium with the melt in many samples (e.g. AS2, MV166, MV160, MV52). Texturally, the phenocrysts are highly resorbed with irregular outlines and groundmass-filled embayments (MacGregor, 1932). These textures are often so extreme as to suggest that in other samples the clinopyroxene could have been lost completely.

Many of the phenocrysts present in these rocks are not euhedral and complete. This observation, taken together with complex zoning, indicates these crystals represent disequilibrium assemblages either through rapid growth from a melt or through reaction with the melt. Any explanation of the origin of the phenocrysts should take account of this petrographic evidence. Unfortunately, the interpretation of the textures is often difficult as growth and resorption processes can produce similar results (Drever and Johnston, 1957; MacKenzie et al., 1982).

Dynamic crystallisation studies have duplicated many of the textures found in these rocks. Donaldson (1976) has described a range of olivine habits produced at varying cooling rates from basic melts. While his later studies have shown a complex interplay of factors controlling such textures, it is likely that most if not all of the hopper olivines found in this study result from rapid crystallisation of an undercooled melt (e.g. MV109, MV178, MV516, MV71A, MV400). Plate 1 illustrates skeletal olivine from sample MV109. This habit appears to be a feature of those microporphyritic rocks where only small (<2 mm) olivine and augite (+ spinel) phenocrysts occur. Of the examples noted, only MV71A has associated plagioclase phenocrysts. Partial alteration of olivine, particularly at the margins, makes it difficult to recognise all skeletal phenocrysts, but the larger (up to 1 cm) olivines tend to be complete and range from euhedral to rounded. In the isothermal experiments of this study, near-liquidus crystals were frequently euhedral, but at lower temperatures anhedral grains were the norm

despite no obvious reaction relationships. Therefore, a rounded habit can not be taken as conclusive evidence of resorption. The olivines in samples AS2, MV166, MV160, MV716 and MV718 are very rounded and embayed in some cases. The lack of any apparent crystallographic control on their habit suggests these may be resorbed phenocrysts. Plate 2 illustrates rounded and embayed olivine phenocrysts from MV718. However, the possibility of these forms having been produced by slight undercooling should not be discounted (Drever and Johnston, 1957). Clustering of olivine phenocrysts was only observed in the microporphyritic rocks (e.g. MV521, MV516, MV402). Very rare devitrified quenched glass inclusions occur in some of the large olivines of AS1/36017, perhaps indicating quite rapid growth.

The problems of identifying resorption and growth textures in plagioclase phenocrysts have been discussed by Dungan and Rhodes (1978), Gutmann (1977) and Kuo and Kirkpatrick (1982). In addition, dynamic crystallisation (Lofgren, 1974) and partial melting (Tsuchiyama and Takahashi, 1983) experiments have produced laboratory duplication of many of the common feldspar habits. In the sample collection under study there are examples of both resorption and rapid growth textures, frequently within the same thin section. Growth textures are taken to include incomplete plagioclases with a box-work internal structure (Lofgren, 1974), e.g. MV702, AS1. Plate 3 illustrates skeletal plagioclase from MV702. Such crystals may enclose devitrified quenched glass or groundmass, like the matrix. A second growth texture recognised has small glass/matrix inclusions orientated in a regular way, usually through the core of the crystal e.g. AS1. The large elongate crystal in the upper portion of plate 4 illustrates this. This appears to be an extension of the box-work habit where smaller, numerous, often elongate inclusions have been trapped. A further growth texture is characterised by a euhedral core surrounded by a further euhedral zone rich in very small inclusions. An outer euhedral clear zone completes the phenocryst e.g. MV160. In contrast, the clearest examples of resorption have anhedral rounded clear cores surrounded by a very dense zone of small inclusions. The step from core to resorbed zone is marked by a large increase in the anorthite component of the plagioclase

e.g. AS1, MV122. Plate 5 illustrates this resorption texture for a feldspar in MV122. Note also phenocrysts in the lower part of plate 4. These crystals are typical of those produced in the partial melting experiments of Tsuchiyama and Takahashi (1983). A second resorption texture is essentially an extension of the first where the core is very densely sieved, often with a central irregular quench portion. Plate 6 illustrates an example of this texture from MV39A. In this case, there may be no recognisable relict material. A third resorption texture is not marked by inclusions. In crossed polarised light a rounded original core can be seen, overgrown by euhedral zones of a more calcic plagioclase e.g. AS1. In all of these proposed growth and resorption textures, there is usually an outer clear portion which picks out the habit of the overgrown plagioclase e.g. plates 4, 5 and 6.

In some of the examples considered to be highly resorbed, the outer rim indicates the supposedly resorbed crystal is euhedral, e.g. plates 4 and 6. There is little doubt that resorption has occurred. The problem is whether the densely sieved area can be attributed to resorption or to growth. Tsuchiyama and Takahashi (1983) have shown that such sieved zones can be produced in partial melting experiments. The texture has not yet been synthesised in crystallisation studies. The authors also noted that in melting studies the residual crystal becomes compositionally zoned, and ultimately reaches equilibrium with the melt. Therefore, by extension to the natural environment, it is suggested here that the euhedral sieved zones are the re-equilibrated products of the resorption process, i.e. the sieve textures are resorptional and the relict plagioclases have re-equilibrated at their margins, and so may be near euhedral.

Clusters of plagioclase phenocrysts occur in several samples, e.g. MV72, MV74, AS1/36017, MV402. In the case of MV402, the plagioclase is often in laths around clusters of clinopyroxene, which points to the later crystallisation of the feldspar.

Normal, reverse and oscillatory zoning have also been observed in phenocryst plagioclases in these rocks, e.g. MV160, AS1.

Loomis (1982) produced numerical simulations of plagioclase growth, and has predicted normal zoning as a consequence of constant cooling rates, with reverse zoning as a product of isothermal or decreasing cooling rates (perhaps associated with increasing concentrations of volatiles). Experimental studies are in general agreement with this model (Lofgren, 1980; Smith and Lofgren, 1983). The origin of oscillatory zoning is less clear, but experimental duplication of this texture strongly suggests a mechanism controlled by crystal growth kinetics (Smith and Lofgren, 1983).

The resorbed clinopyroxenes have been referred to earlier. Cores of these crystals generally show only limited zoning. In contrast, many of the unresorbed, euhedral clinopyroxene phenocrysts in these rocks have pronounced concentric, oscillatory and sector (hourglass) zoning, e.g. the well-known example of the Crawfordjohn essexite (MV520). Plate 7 illustrates a sector-zoned augite phenocryst from MV520. The significance of sector zoning has been discussed in numerous papers (e.g. Strong, 1969; Wass, 1973; Nakamura, 1973; Dowty, 1976; Shimizu, 1981). The features common to these interpretations are disequilibrium crystallisation and relatively rapid growth. Strong (1969) suggested an initial swallow-tail augite, with later infilling to produce the two distinct compositions. However, the evidence of continuous oscillatory zoning through the sectors (MV520) argues for a single growth phase. Trace element studies (Shimizu, 1981) support a model of rapid crystal growth and associated slow diffusion rates near the crystal surface, related to the pyroxene chain structure. The composition and melt properties are likely to be important, as Wass (1973) has noted the frequent occurrence of this texture in titanaugites. Although rapid crystallisation is believed to be one of the required factors in producing sector zoning, it should not be assumed this is necessarily a low-pressure phenomenon only. Wass (1979) has described sector-zoned clinopyroxene megacrysts from eastern Australia which, on the basis of several lines of evidence, are probably of high-pressure origin.

Few other clinopyroxene textures can be confidently ascribed to rapid disequilibrium growth. Some small phenocrysts have fairly

numerous inclusions in their cores, apparently similar to groundmass mineralogy. However, these cores are often distinct from the rims and groundmass pyroxenes in terms of colour or composition, and so may be exhibiting less pronounced resorption textures, e.g. MV403, MV521, MV93. Like the plagioclase phenocrysts, resorbed and rapidly grown clinopyroxenes may be present in the same sample. Some clinopyroxene phenocrysts illustrate a sieved texture, either throughout or restricted to outer areas of the crystal, in which the sieved portion is extremely rich in grains of Fe - Ti oxides. This texture is interpreted as resulting from reaction between the pyroxene and host melt, and is associated with other clearly resorbed pyroxenes, e.g. AS2, or with a pronounced rounding of the pyroxene, e.g. MV39A. Plate 8 illustrates a partially resorbed augite from AS2 with the sieved areas rich in opaque phases. This texture is distinct from the commonly observed inclusion-rich rims around pyroxene phenocrysts. In these latter cases the included minerals are very similar to the groundmass, and the enclosing pyroxene is very similar to the groundmass pyroxene. This is interpreted as an overgrowth produced essentially at the time of quenching of the magma, e.g. MV166, MV52. Clusters of pyroxene phenocrysts occur in some of the samples, e.g. MV402, MV78, MV406. In MV106 the clinopyroxenes occur in radially arranged aggregates and often show sector zoning, suggesting a rapid growth origin. In MV521, there are small clusters of pyroxenes around olivine phenocrysts, suggesting a later origin for the augites.

Spinel phenocrysts are dominantly found as euhedral to rounded inclusions in olivines and, to a lesser extent, clinopyroxenes. They are noticeably uncommon in plagioclases. Some of the rounded spinels may have been reacting with the melt at the time of their inclusion (e.g. MV178 on compositional evidence discussed below), but there is no strong evidence for this. The group of highly aluminous spinels found as discrete phenocrysts, appear to have been out of equilibrium with the melt at the time of quenching, as they are rounded and have a sharply bounded rim against an outer layer of magnetite and ilmenite, e.g. MV166, MV514. Plate 9 illustrates the association of partially resorbed aluminous spinel and partially resorbed clinopyroxene phenocrysts in sample MV166.

Magnetite phenocrysts are often irregular in habit. This is interpreted as a growth feature as they are usually very similar in composition to the groundmass. The same situation seems to apply to ilmenite phenocrysts, with the exception of sample MV121A. In this rock the ilmenites are rounded with a rim of magnetite, perhaps indicating disequilibrium.

The orthopyroxene phenocrysts in MV121A are rounded, but lack any pronounced reaction rim, although there is a slight increase in clinopyroxene and plagioclase at the orthopyroxene margins. Notably, the clinopyroxene phenocrysts in this sample are also rounded. There is no well-developed armouring of the orthopyroxenes as developed at Nuanetsi (Cox and Jamieson, 1974).

Other petrographic features indicating disequilibrium in the preserved phenocryst assemblages, include the occurrence of two distinct species of individual phenocryst phases. Thus in MV40A, there are examples of both pale green and pale brown clinopyroxene phenocrysts. The more resorbed species in this case is the more Fe-rich pale green variety. MV121A also contains two clinopyroxene phenocryst types. In this sample, the much less abundant green ferroaugite variety is very resorbed compared to the rounded pale brown augite species. MV52 contains two distinct generations of olivine on the basis of phenocryst size. This is reflected in their compositions, with the larger type more forsteritic. Samples AS1/36017 contain two distinct generations of plagioclase phenocrysts. The more sodic variety is associated with marked resorption, absent from the calcic phenocrysts (plate 4). Other samples may contain distinct groups of plagioclase phenocrysts, although these are not as well defined as the previous examples (e.g. MV39A, MV40A, MV13). MV122 also contains two distinct plagioclase phenocryst compositions. Both types are shown in plate 5. Resorption is associated with the more sodic variety. Although plagioclase compositions can be greatly affected by small changes in the conditions of crystallisation, detailed study of several sections of each sample may reveal others containing distinct phenocryst varieties. Several possibilities should be borne in mind concerning the origin of these distinct groups of phenocrysts. Firstly, a mixing of two

porphyritic magmas could preserve two distinct assemblages. Secondly, the incorporation of blocks of porphyritic rock can introduce xenocrysts to the host melt. Thirdly, an episode of higher pressure or otherwise distinct crystallisation can be preserved, and then superceded by a low pressure assemblage. These options will be considered with the aid of the mineral compositions.

Groundmass textures of the lavas indicate rapid crystallisation. In some, a trachytic texture is developed by the groundmass plagioclases, e.g. MV514, MV121A. Flow alignment of the plagioclase phenocrysts occurs in a few samples, e.g. MV52, MV702. In the intrusive rocks, coarser groundmass textures are often developed, suggesting longer periods of time for re-equilibration, e.g. ES2058. The larger grain size makes identification of phenocryst phases difficult in some cases, e.g. MV165, MV723, MV164, MV520.

6.4.4 Major element chemistry of the rocks

Detailed discussion of the chemistry of the individual lava successions is beyond the scope of this study. The reader is referred to Macdonald (1975), and Macdonald et al. (1977) for the relevant information. In this section the sample collection will be discussed as a whole, with distinctions being made using the phenocryst assemblages. Undoubtedly, this treatment will be more generalised than is desirable, but some important features of the suite can be identified. Using the Mg# as an index of differentiation, it is possible to examine the variation in degree of silica saturation of the samples. Figure 6-2 illustrates the normative (mole %) nepheline and "quartz" (quartz + quartz in hypersthene) of the rocks. The more magnesian rocks are either mildly nepheline- or hypersthene-normative. There are no low Mg# samples which are nepheline-normative. Genuinely quartz-normative samples only appear at lower Mg#'s. The trend from high Mg# to low Mg# is from initially transitional compositions to more hypersthene-normative and quartz-normative compositions. Macdonald (1975) noted a small proportion of evolved nepheline-normative rocks, but recognised that the intermediate rocks are dominantly less undersaturated than their associated basalts. In terms of the AFM plot of Macdonald

(1975), the current samples occupy the Fe -enrichment segment of the trend. More evolved compositions would show the later Fe depletion characteristic of the suite.

The phenocryst assemblages are identified on an alkali-silica plot (Figure 6-3), and illustrate that the plagioclase-phyric groups generally have higher SiO_2 and $Na_2O + K_2O$ contents than the olivine + clinopyroxene-phyric group. The dividing line between alkaline and tholeiitic compositions can be taken as confirmation of the transitional alkaline nature of the province. Simple oxide variation diagrams have been used to show systematic variations in the sample compositions (Figure 6-4, a - f). The wide distribution of olivine as a phenocryst phase throughout the collection supports the use of MgO plots. Inasmuch as the collection can be taken as a whole, the trends are consistent with fractionation from basaltic parental magmas (Macdonald, 1975). It is probable that olivine or other Fe - Mg phases were involved in such processes (O'Hara, 1965, 1968), so that the direction of decrease of MgO was the direction in which fractionation proceeded. The plots of Figure 6-4 indicate relatively simple trends, suggesting one fractionation scheme could qualitatively link the samples. SiO_2, Na_2O and Al_2O_3 show clear trends of increasing as MgO decreases. K_2O and TiO_2 show very poor trends in similar fashion. Only CaO shows a marked decrease with decreasing MgO. In terms of fractionation involving the minerals present in the samples as phenocrysts, only olivine, clinopyroxene, spinel, plagioclase and perhaps magnetite, are volumetrically significant enough to be considered.

From the experimental sections, the effects of crystallising combinations of these phases at low pressures can be assessed. If plagioclase was a major component of a fractionated assemblage, then the Al_2O_3 content of the rocks could, depending on proportion, stay nearly constant or decrease, contrary to the observed variation (Figure 6-4b). Plagioclase-only crystallisation does produce the pattern of lower Al_2O_3 with higher MgO in the coexisting liquid, but once olivine begins to crystallise, the more normal decrease in the liquid MgO occurs. There is no evidence for an initial plagioclase-only fractionating assemblage. Clinopyroxene as a major component

of the fractionating assemblage would result in a marked decrease in CaO as MgO fell. This is in fact the case (Figure 6-4c). Other element variations are consistent with this, although the increase in SiO_2 with differentiation is unlikely if a clinopyroxene-only assemblage was involved. This problem is resolved if olivine and spinel (aluminous) are added to the scheme. The simple variation diagrams suggest the fractionating assemblage consisted of a large proportion of clinopyroxene, with much lesser amounts of olivine and spinel. The spinel is needed to explain the increase in SiO_2 in particular, but the assemblage common to all the variation diagrams includes olivine. None of these diagrams conclusively show plagioclase can not have been a member of a fractionating assemblage. However, for the more basic samples at least, any plagioclase fractionating must have been a very small proportion of the assemblage. Certainly, the most satisfactory single explanation of the trends in these two-element variation diagrams is a fractionation assemblage of clinopyroxene + lesser spinel and olivine. Extract calculations (Wright and Doherty, 1970) indicate the variation in major element composition can be produced by fractionation of clinopyroxene, olivine and spinel in the proportions 6 : 1 : 1. Mineral compositions used were phenocrysts from MV514 and MV403. The petrographic evidence of olivine + clinopyroxene + spinel phenocrysts in the most basic samples agrees with this interpretation, and also argues for the lack of plagioclase in the assemblage. Only sample AS2 has plagioclase phenocrysts in the high Mg# group; in this rock there is a small proportion of feldspars, but as will be described in the mineral chemistry section, there is evidence for possible phenocryst accumulation, modifying the major element composition to appear more magnesian. The poor trends of K_2O and TiO_2 variation reflect the inter-district differences noted by Macdonald (1975). Macdonald (1980), with additional trace element data, suggested these differences are due to chemically distinct areas of source mantle.

Further support to the proposed importance of clinopyroxene in the fractionation assemblages is given in Figure 6-5. CaO/Al_2O_3 variations with whole rock Mg# have been used successfully in other studies to identify phases involved in differentiation processes

(e.g. Fisk et al., 1982). Olivine fractionation decreases the Mg# without significantly altering the CaO/Al_2O_3 ; plagioclase fractionation from basic magmas such as these, increases the CaO/Al_2O_3 with little effect on the Mg#; clinopyroxene decreases both the Mg# and CaO/Al_2O_3, with the slope of the trend depending largely on the alumina content of the pyroxene; spinel decreases the Mg# and increases the CaO/Al_2O_3 (rapidly if it is very aluminous). The variation in Figure 6-5 is consistent with clinopyroxene fractionation, and while not excluding plagioclase, it is also consistent with additional olivine + spinel fractionation.

It is difficult to assess the role of magnetite fractionation, but from the discussed AFM diagram variation, and the relatively late appearance of the phase as a phenocryst, it is not believed to be major within the range of this sample collection. More evolved compositions may have evolved partly by significant magnetite fractionation (Macdonald, 1975).

The preceding discussion shows that taking the samples as a group, allows a simple fractionation scheme involving phases present as phenocrysts to explain the major-element variation. However, it must be emphasised that this interpretation is of a general nature, and may not be appropriate to all the samples (e.g. those arrowed in Figures 6-4, 6-5). The variation diagrams do not exclude the possibility of olivine-only fractionation at the highest Mg#'s, and fractionation of plagioclase-bearing assemblages at low Mg#'s.

As a first approximation, the phenocryst assemblages are taken to be in equilibrium with each other and with the matrix. Some estimate of the pressure range of their formation is possible from a consideration of projections in CMAS (O'Hara, 1968), ($XO-YO-R_2O_3-ZO_2$ of Jamieson, 1970). Figure 6-6 shows the studied bulk compositions projected from the olivine composition point, onto the plane CS-MS-A. The phase boundaries for one-atmosphere and 10 kilobars are taken from O'Hara (1968). The projected plane OL-DI-PL represents the low pressure thermal divide between essentially nepheline-normative and hypersthene-normative compositions, as represented in this scheme. Because of limited data for the spinel phases, this brief discussion

will be restricted to the silicate phenocrysts. The circled field encloses experimental glasses coexisting with olivine + clinopyroxene + plagioclase determined in this study, and partly coincides with the one-atmosphere phase relations of O'Hara (1968). All the compositions from this study have been recast with respect to ferric and ferrous iron content, using the equation presented in Chapter 3.

If the two main phenocryst assemblages (olivine + clinopyroxene and olivine + clinopyroxene + plagioclase) are considered in terms of the shown phase boundaries, then some discrepancy with the one-atmosphere data of O'Hara is apparent. The olivine + clinopyroxene assemblage, if taken as representing an equilibrium, would be cotectic with plagioclase at low pressures. In order to bring all these samples within the olivine + clinopyroxene field, an increase in pressure is required up to approximately 10 Kb. The evidence for the olivine + clinopyroxene + plagioclase phenocryst assemblage is more uncertain. Taking the O'Hara phase boundaries, these samples could have equilibrated at a range of pressures from one-atmosphere up to several kilobars. However, from the field of experimental glasses determined in this study, the samples could represent low-pressure evolution. Using a second projection, from diopside onto CA-M-S, some of the olivine + clinopyroxene + plagioclase phenocryst-bearing samples plot apart from the one-atmosphere experimental data (Figure 6-7). In this projection the effect of pressure on the olivine-clinopyroxene-plagioclase cotectic is to shift it towards olivine. This reflects the decreasing primary phase volume of olivine with increasing pressure (O'Hara, 1968). An increase of only a few kilobars would be adequate to account for the separate olivine + clinopyroxene + plagioclase phenocryst assemblages. Thus, qualitatively, the phenocryst assemblages could represent higher pressure olivine + clinopyroxene crystallisation with lower pressure olivine + clinopyroxene + plagioclase crystallisation. This scheme is largely dependent on taking the samples as representing equilibrium assemblages, and accepting the O'Hara phase boundaries.

6.5 Mineral Chemistry

Representative analyses of the phenocryst and groundmass mineral compositions, discussed in the following sections, have been tabulated in Appendix 5.

6.5.1 Olivine

Olivine is present as a phenocryst phase in nearly all of the samples under discussion, and is preserved fresh or only partially altered in the majority. Alteration products appear to be of the iddingsite and bowlingite types, probably indicating relatively low temperatures of formation, at least partly due to weathering. Olivine is frequently recognisable as a groundmass phase.

The range of olivine phenocryst compositions analysed in these samples is Fo_{87-52}. Taking the variation as a whole, rocks with low Mg#'s tend to have a range of olivines with lower forsterite contents than high Mg# samples. Figure 6-8 illustrates this for the analysed phenocryst cores. The wide range of olivine compositions in any given sample represents two effects. Firstly, a genuine range of different core compositions, and secondly, an apparent range produced by analysing sections through zoned crystals which do not include the core. The curves on Figure 6-8 mark values of the olivine-liquid Fe^{2+} - Mg exchange coefficient (KD). The Fe_2O_3 content of the rocks has been calculated, assuming the compositions were liquid at oxygen fugacities near the Ni - NiO buffer, using the equation in Chapter 3. Despite an uncertainty in the whole rock ferrous iron content, many of the samples have their most forsteritic olivine close to or between the curves. The importance of this observation is that many of the rocks contain olivines which could have been in equilibrium with the bulk composition at their liquidus. This supports Macdonald (1975), who suggested many of the highly porphyritic rocks of the suites represented liquid compositions (on the basis of a complete range of near-aphyric chemically equivalent samples). Many of the porphyritic rocks in the present study are interpreted to have suffered no phenocryst enrichment.

Those rocks whose analysed olivine phenocrysts are too fayalitic to be in equilibrium with the bulk composition, may be interpreted in a number of ways. Firstly, if the rock has accumulated Fe-Mg mineral phenocrysts, then there is a likelihood of the predicted liquidus olivine composition being too Mg-rich. This is a possible explanation for some highly porphyritic samples, e.g. MV520 (Mg# = 64, predicted olivine Fo $\sim_{85}$, most forsteritic analysed olivine Fo_{75}), AS2 (Mg# = 70, predicted olivine Fo $\sim_{89}$, most forsteritic analysed olivine Fo_{82}). Secondly, if the magma has crystallised slowly, allowing the olivine composition to maintain equilibrium, then Fe-rich olivines will be present relative to the predicted liquidus olivine compositions. This effect (equilibrium crystallisation) is probably a factor in most of the samples, and could account for some samples which have no suitably Mg-rich compositions preserved, e.g. MV723 (Mg# = 67, predicted olivine Fo $\sim_{87}$, most forsteritic analysed olivine Fo_{73}), MV114 (Mg# = 63, predicted olivine Fo $\sim_{85}$, most forsteritic analysed olivine Fo_{78}). Thirdly, significant discrepancies can arise from incorrect assumptions. Thus, if the magma was very reduced, then the predicted liquidus olivine in Figure 6-8 would be too Mg-rich. This results from increased ferrous iron content in a reduced melt. Similarly, if the olivine crystallised at high pressures, then the predicted liquidus olivine in Figure 6-8 would be too Mg-rich because of the increase of KD with pressure (Ford et al., 1983). Samples MV718 and MV716 contain only a few percent of quite rounded, small olivine phenocrysts in a fine-grained matrix, and may reflect these origins. (MV718, Mg# = 64, predicted liquidus olivine composition at atmospheric pressure Fo $\sim_{86}$, most forsteritic analysed olivine Fo_{76}; MV716, Mg# = 63, predicted liquidus olivine composition at atmospheric pressure Fo $\sim_{85}$, most forsteritic analysed olivine Fo_{72}). Fourthly, of course, the olivine phenocrysts may appear too fayalitic simply because more Mg-rich crystals were not found. Notably, only one sample (MV165) has a predicted liquidus olivine composition (Fo $\sim_{71}$) which is much less forsteritic than the most forsteritic analysed olivine (Fo_{79}). The simplest explanation of this is that the phenocryst is a xenocryst. This gains support from the other olivine phenocryst compositions in this sample, which are more Fe-

rich than predicted. A magma mixing mechanism might produce a similar result, but there is no evidence for that in the sample.

The minor components of olivine point to differences between the main phenocryst assemblages. Figure 6-9 illustrates the correlation between the nickel content of an olivine and its fosterite value. There is a clear positive correlation between the two quantities, consistent with the more forsteritic olivines crystallising from more Ni-rich magmas. The data for the two main phenocryst assemblages (olivine + clinopyroxene and olivine + clinopyroxene + plagioclase) show considerable overlap. The plagioclase-bearing group extends to lower Ni and forsterite values, but does not reach as high values as the plagioclase-free group. The two samples with olivine + plagioclase phenocryst assemblages have low Ni and forsterite contents, consistent with derivation by fractionation of the more primitive olivine + clinopyroxene + spinel assemblage. The three olivine + spinel-phyric samples show a wide range of Ni and forsterite contents. The apparent displacement to higher Ni values for a given forsterite value relative to the olivine + clinopyroxene + spinel group, may be simply an effect of the limited range of samples available. However, in agreement with the major-element variation, the Ni-forsterite relations indicate that MV723 and MV165 of the olivine + spinel-phyric group, are less primitive than many of the olivine + clinopyroxene + spinel-phyric group. The olivine + clinopyroxene + plagioclase-phyric group could have evolved by fractionation or continued crystallisation of the olivine + clinopyroxene + spinel-phyric group. The apparent agreement between the Ni content of the olivine phenocrysts, and the major element variations, is confirmed by Figure 6-10. Taken overall, there is a positive correlation between the Ni content of the olivine, and the host whole rock Mg#. In detail there are numerous exceptions. Samples MV723 and AS2 have much lower olivine Ni contents for their Mg# than average. This is consistent with the discrepancies in the forsterite values discussed above. Samples MV39A and MV52 have higher olivine Ni contents than average, consistent with their containing two distinct groups of olivine phenocrysts. The general decrease in olivine Ni content with whole rock Mg#, is consistent with fractionation of a Ni-bearing assemblage

to produce the lower Mg# samples, reflected to some degree by the changing phenocryst assemblages.

The Ca content of the olivine phenocryst cores shows an analogous variation to that of the Ni content. Using the phenocryst assemblages as guides, Figure 6-11 distinguishes the various groups with respect to the olivine forsterite content. In a study of Ca in forsterite, from one-atmosphere experiments, Watson (1979) found a simple positive linear correlation between the Ca in olivine, and Ca in the coexisting melt independent of temperature. As described in the experimental results chapter, the olivines crystallised in the present study show a similar variation, although secondary fluorescence effects during analysis are likely to have distorted the data by increasing the apparent Ca content of the olivines. However, from a consideration of Figures 6-11, 6-4c and 6-8, the higher Ca olivines come from some of the lowest whole rock Ca samples. Even allowing for the effects of variable amounts of clinopyroxene phenocrysts in these rocks, the coexisting liquid compositions probably reflected the trend. Watson's experiments were carried out on Fe -free synthetic compositions; the poor correlation in Figure 6-11 between increasing olivine Ca and fayalite content may reflect some stabilising effect of Fe on Ca in olivine, although this is not apparent from the data of Ferguson (1978). A second possibility is that the lower Ca olivines reflect crystallisation at elevated pressures. This has been suggested in several studies (e.g. Stormer, 1973), although the origin of the lower Ca content has not been established. The idea of polybaric crystallistion of the olivine in the phenocryst assemblages of the province, would be consistent with other lines of evidence in this study and other published studies (e.g. Macdonald, 1975) based on whole rock chemistry. A further possibility was suggested by Donaldson et al. (1975), where the Ca content may be increased by increasingly rapid growth of the olivine. In this study there is no clear correlation between olivine habit and core Ca content. Regardless of the reason, the Ca content of the olivine phenocrysts is generally lower in the more Mg -rich samples carrying forsteritic olivines, than in the more evolved samples carrying more fayalitic olivines.

The concentration of Mn in olivine shows a positive correlation with increasing fayalite content (Figure 6-12). This variation has been identified in many suites, and is ascribed to major element fractionation independent of environment of crystallisation (Simkin and Smith, 1970).

The variations discussed above for phenocryst cores over the studied range of samples, are also frequently preserved on a lesser scale in zoning in individual phenocrysts. Figure 6-13 shows typical phenocryst zoning from core to rim for three crystals. The forsterite content decreases from core to rim as expected. For the relatively slowly cooled olivine from MV520, the decrease in forsterite content is gradual, whereas in the rapidly quenched 36017 samples, only the rim shows a markedly lower forsterite content. No marked reverse zoning was found in the olivine phenocrysts, perhaps reflecting a simple crystallisation history or the rapid re-equilibration suggested by the experimental results. Ca and Mn concentrations show an increase towards the rims. The Mn follows the increasing fayalite component, whereas the Ca increase is usually restricted to close to the rim. As the plot shows, the degree of enrichment of Ca and Mn in olivines in the same sample, can vary. In the figured crystals, Ni shows little variation towards the rim, with only the third sample showing a decrease. This is less typical of the suite as a whole, where decreasing Ni towards the edge is the norm. No marked decrease of Ca and Mn, or increase of Ni towards the rim of olivine phenocrysts was found, although some samples showed little variation. The increase in Ca at the rims may reflect the decrease in pressure of the magma between growth of the phenocrysts and eruption at the surface, or simply the kinetic effect of rapid quenching.

6.5.2 Plagioclase

Plagioclase phenocrysts are only abundant in the lower Mg# samples, where they may dominate the phenocryst assemblage. In general, the phase is preserved apparently unaltered, although no plagioclase is preserved in the studied sample of MV520, and slight alteration could explain some of the relatively low analysis totals

in Appendix 5. Plagioclase laths are always present as groundmass phases.

The range of plagioclase phenocryst core compositions is from An_{83} to An_{30}. Most fall into the calcic andesine to calcic bytownite categories. With the gradual decrease in the anorthite component of the plagioclases, there is a corresponding increase in the orthoclase component, although this remains low (Figure 6-14). Groundmass plagioclase compositions also cover a very broad range of calcic feldspars similar to the phenocrysts, but they extend to much more sodic and potassic varieties (e.g. ES2058). In addition to the complex zoning preserved in some samples, the range of phenocryst core compositions within a rock is commonly up to 15 An%. Phenocryst habits and sizes also show a large variation, from narrow laths a few hundred microns long to irregular crystals two centimetres in greatest dimension.

There is little correlation between the plagioclase compositions and the whole rock Mg#. The more calcic feldspars tend to occur in the more basic rocks, but this is not always the case (e.g. MV702, Mg# = 54, phenocryst range An_{77-65}). In chapter 4, a relation was noted between the normative anorthite content of glasses coexisting with plagioclase, and experimental temperature. Although there is no simple correlation between temperature and plagioclase composition, the normative feldspar content of the bulk composition may be a better indicator of plagioclase phenocryst composition than the whole rock Mg#. Figure 6-15 shows the normative anorthite wt % of the whole rock versus the range of plagioclase phenocryst core compositions present. If it is not interpreted too rigorously this plot can reveal useful information. There is a trend of increasing normative anorthite content with increasing anorthite content of the most calcic plagioclases. MV702 has a far higher normative anorthite content than the other samples. Samples AS1/36017 and AS2 contain anomalously calcic plagioclases for their bulk composition. Some samples have rather low anorthite content plagioclases for their bulk composition, e.g. MV39B, MV74, MV72. This discrepancy might be resolved with further analyses. Perhaps the greatest apparent use for the diagram is in distinguishing the "equilibrium" plagioclases

in samples where two distinct groups of compositions are present. Four samples fit into this category - AS1/36017, MV122, MV40B, MV40A. In each case the plot suggests that the higher-anorthite-content plagioclases are more consistent with plagioclases from neighbouring samples. This agrees with the petrographic and compositional evidence of resorption of the low anorthite content plagioclases. It is not suggested that the deviations from the trend in the examples discussed above necessarily indicate disequilibrium, merely that they are not consistent with the majority of the plotted samples. The high modal plagioclase phenocryst content of AS1/36017 and MV702 may explain their discrepancies as due to phenocryst accumulation. Sample AS2 has already been questioned as a possible liquid composition on the basis of olivine composition, and Figure 6-15 may be confirming these doubts. However, there is also the possibility that the samples studied here are not representative of those analysed by Clark (1956), whose compositions are being used for AS2 and AS1/36017.

A further difficult problem is in assessing whether the plagioclase phenocrysts could have been in equilibrium with other phenocryst phases. No correlation is apparent from the clinopyroxene data, but a possible relation with the olivine compositions has been found. Figure 6-16 shows the range of olivine phenocryst end-member compositions plotted against the most calcic plagioclase phenocryst for each sample. Where two groups of each phenocryst are preserved, each has been plotted in the hope of recognising related phases. A tentative "equilibrium" curve has been marked on the basis that it relates most of the individual samples. Although this is highly speculative, the curve does approximate closely the relation found by Tiezzi and Scott (1980) for coexisting olivine and plagioclase in a cumulate gabbro from the Mid-Atlantic Ridge. Longhi (1982), in a discussion of fractional crystallisation trends, has suggested that the olivine-plagioclase curve proposed here is not consistent with a simple fractionation process. Regardless of its origin, taking the curve as a guideline, it is possible to indicate some preferences for olivine-plagioclase pairs where two distinct groups are present. As suggested from other evidence, the low anorthite content plagioclases in AS1 are not related to the coexisting olivines, whereas the high

anorthite content plagioclases are. In sample MV40A the less anorthitic group appears to match the coexisting olivines better than the more anorthitic group. This contrasts with the whole rock normative anorthite data shown in Figure 6-15, but is consistent with the olivine compositions themselves, which appear to be out of equilibrium with the whole rock Mg#. Thus, for this sample, the olivine phenocrysts and less anorthitic plagioclase phenocrysts appear to be related to each other, but not to the bulk composition, whereas the higher anorthite content plagioclase phenocrysts may be related to the whole rock composition. For sample MV52 the plagioclase phenocrysts are associated with the more forsteritic olivine phenocrysts, which themselves could have crystallised from the bulk composition. The more fayalitic olivines in this sample appear anomalous with respect to the plagioclase phenocrysts and whole rock composition. Sample MV704 lies off the main trend with low forsterite olivines and/or too calcic plagioclases. Notably, on the basis of whole rock Mg#, the olivine phenocrysts were too fayalitic by about 10 mole %, predicted from the model. With that increase in the olivine forsterite content, the data from MV704 would lie on the main trend.

Many of the plagioclase phenocrysts preserved in these rocks display complex zoning patterns. Loomis (1982) has suggested that such zoning is often the result of disequilibrium growth processes, so that the preserved plagioclase compositions can not be assumed to be in equilibrium with the melt. Some of the difficulty in interpreting the plagioclase compositions may be due to these processes. In fact, where complex feldspars are preserved, studies have tended to consider their origin largely in isolation from the host melt (e.g. Kuo and Kirkpatrick, 1982; Pringle et al., 1974; Smith and Lofgren, 1983). Zoning is quite variable in different crystals within the same sample in this study. However, some general observations can be made. Although normal zoning is present to some degree in all the samples studied, reverse zoning is also quite common e.g. MV52, MV39A, MV160, AS1/36017. An example from sample AS1 illustrates most of the common zoning features (Figure 6-17). This euhedral complete crystal has three distinct zones designated core, mantle and rim. The core is oscillatory zoned with quite marked

variations in the anorthite content. The overall variation is towards more sodic compositions. The minor components show smaller but systematic variations. Fe has a slight decrease as Mg increases outwards. The orthoclase component mirrors the anorthite component as might be expected. Stepping over to the mantle, there is a large decrease in the anorthite component followed by continued normal zoning outwards. Fe is slightly lower than in the core, Mg is similar, and the orthoclase component increases gradually. The step into the rim zone is accompanied by a marked increase in anorthite content, although this reverse zoning is soon replaced by normal zoning to the crystal edge. The minor components Fe and Mg both show very marked increases at the inner edge of the rim zone, and then decrease slightly at the outer edge. The orthoclase component again mirrors the anorthite component, and is not markedly enriched at the outer edge as is found in less rapidly quenched compositions in the present study. This basic profile could be refined by a step-scanning analysis, but it is believed all the main features have been collected. Using the experimental and modelling studies referred to earlier, it is possible to interpret some of the history of this phenocryst. The oscillatory zoned core is likely to be a product of crystallisation of an undercooled melt. Loomis (1982) suggested oscillations are produced by local convection within the magma. However, strong evidence has been presented by Smith and Lofgren (1983), supporting the view that the zoning is related to the kinetics of crystal growth. Within the framework, the overall normal zoning of the core would reflect progressive undercooling. The discontinuous zoning from the core to the mantle is probably the result of a rapid change in temperature or pressure (perhaps volatile pressure). A simple reduction of pressure in a dry magma, say during ascent, would favour a more calcic mantle. A reduction in pH_2O might be associated with a more albitic zone (e.g. Pringle et al., 1974). This can not be discounted in the case of AS1/36017, although there is little evidence for significant volatile pressure. Injection of the magma into a much cooler environment without significant change in pressure might cause the step. The continued normal zoning of the mantle is consistent with further progressive undercooling (e.g. Loomis, 1982; Smith and Lofgren, 1983). The next discontinuous

step from mantle to rim is towards a more calcic composition. Perhaps the easiest explanation of this step is a reduction in pressure caused by the rapid uprise of the magma to near surface conditions. A sudden increase in temperature or volatile pressure is more difficult to envisage. The slight reverse zoning at the inner edge of the rim is a common feature after zoning discontinuities (Smith and Lofgren, 1983), and reflects a stage of isothermal or decreasing undercooling crystallisation, perhaps with increasing volatile pressure (Loomis, 1982; Smith and Lofgren, 1983). The final emplacement and quenching of the magma may be marked by the normal zoning to the edge. The rapid increase in Fe and Mg in the rim zone may be due to the rapid growth proposed for this stage.

The petrographic and mineral compositional evidence points to two distinct groups of plagioclase phenocrysts in AS1/36017. Limited profiles of crystals of each are shown in Figure 6-18. Profiles 3 and 4 are of high anorthite content phenocrysts. Profile 2 is of a low anorthite content phenocryst and profile 1 is of a less common intermediate variety ($\sim An_{58}$). Numbers 1 and 2 represent euhedral and subhedral plagioclases respectively, both with zones of resorption near their core, particularly number 1. Number 3 represents a skeletal plagioclase with some orientated interior inclusions interpreted as a rapid growth texture. Number 4 represents a near-euhedral, complete crystal with a visibly zoned rim. Only limited discussion is possible because of the few analyses per profile. However, the two profiles of lower anorthite content phenocrysts show a marked increase in the anorthite component from the resorption zone outwards (the first analysis of each is from an unaltered core, subsequent analyses cross the resorbed area). This is consistent with the other evidence of the lower anorthite content phenocrysts being out of equilibrium with the host. The rapid increase in Fe in profiles 1 and 2 as the anorthite component increases, suggests this period of growth may be comparable to the growth of the rim zone in the phenocryst described in Figure 6-17. It is tempting to suggest that the growth of the mantle zone illustrated in Figure 6-17 may be associated with the inclusion and partial resorption of the less anorthitic phenocrysts into the magma (perhaps as wall rock included during violent outgassing or as a

small amount of cooler porphyritic hawaiitic magma). Profiles 3 and 4 show similarities in anorthite contents. The higher Fe and Mg of the third grain is consistent with an origin by rapid growth. However, both crystals probably indicate the phenocryst composition crystallising from the host magma. In this sample, at least, it seems possible to distinguish inclusions in plagioclase related to rapid growth and to resorption. Clark (1956) emphasised the abundance of glomerocrysts of gabbroic assemblages in this basaltic hawaiite. It is suggested that the inclusion and disruption of cumulates is recorded by mantle zoning of Figure 6-17 and the low anorthite content plagioclases. Analyses of plagioclase in a feldspar glomerocryst in 36017 show compositions similar to the less anorthitic types.

It is not possible in this study to treat all the samples with complex plagioclase in such detail. However, it is likely that much of the above discussion applies to other rocks (e.g. MV122 has low anorthite content resorbed phenocrysts and higher anorthite content complete phenocrysts). Some of the reverse zoning noted probably reflects initial crystallisation at elevated pressures followed by rapid uprise of the magma. In other cases increasing volatile pressure could be the cause. The widespread normal zoning may simply reflect crystallisation under conditions of fairly rapid cooling. Some of the resorption textures probably reflect disequilibrium conditions in cognate phenocrysts rather than the suggested xeno-crystal origin proposed for sample AS1/36017. Slight resorption of relatively sodic higher pressure plagioclase phenocrysts at lower pressures is an expected feature (Pringle et al., 1974). The origin of the plagioclase phenocrysts in the samples, is discussed in the next chapter in conjunction with the experimental crystallisation model.

Preliminary cathodeluminescence studies of some plagioclase-phyric samples have been carried out. The low Fe and Mn concentrations in plagioclases favour luminescence. In sample AS1/36017 the two generations of plagioclase phenocrysts are clearly distinguished from each other and from the groundmass feldspars. Sample MV40A was also observed to contain distinct groups of

plagioclase phenocrysts. While the precise concentrations of minor elements producing the different colours of luminescence have not been determined, the qualitative distinction between plagioclases is a very promising result. This technique may allow a rapid assessment of the range of plagioclase compositions present in a sample, saving many hours of optical and microprobe study.

6.5.3 Clinopyroxene

High-Ca clinopyroxene phenocrysts are common throughout the more basic samples of this study and may be the dominant phenocryst in some compositions (e.g. MV520). Although there is rarely any visible indication of alteration of the phase, a sizeable proportion of the microprobe analyses have lowish totals, even after allowing for a ferric iron content. It is possible there is a degree of alteration to hydrous pyriboles at the scale of the crystal lattice (Veblen and Buseck, 1981). This could be confirmed by a transmission electron microscope study. However, the likely amount of alteration is not believed to have a significant effect on the mineralogical variation discussed below.

Considered in terms of the calcium, magnesium and iron end-members, there is a fairly restricted range of clinopyroxene compositions present in these samples (Figure 6-19). Most fall into the salite and augite categories of Deer et al. (1978), although there are some endiopside and diopside compositions. More Fe-rich varieties are virtually absent, with only a single phenocryst of ferroaugite analysed (MV121A). Phenocryst rim and groundmass, and phenocryst core compositions extend a short distance above the 50% wollastonite line. Because of the sometimes large percentage of other elements present in these pyroxenes (mainly Ti and Al), the simple end-member categories are not wholly appropriate. With Al_2O_3 up to 12 wt % (0.45 cations per 6 oxygens) and TiO_2 up to 5 wt % (0.15 cations per 6 oxygens), some pyroxenes would undoubtedly be classed as aluminous augite and titanaugite. The latter is confirmed by pronounced pleochroism. The compositional variation is continuous across the range and so, for convenience, the general term augite will be used in the discussion. All the compositions described have been recast with respect to their ferric and ferrous

iron content on the basis of stoichiometry (4 cations to 6 oxygens). The accuracy of the ferric iron estimates produced in this way is very dependent on the quality of the starting analyses. For this reason the details of the augite compositional variations are based on analyses using the wavelength dispersive spectrometry technique. The original analyses usually show a slight excess in number of cations per formula unit, characteristic of some ferric iron present assumed to be ferrous. Fe_2O_3 contents calculated in this way are usually low (around 1 to 3 wt %). Significantly higher values may be due to analytical error.

The augites show a wide range of colour in thin section from near colourless through pale pink, brown and rarely green to purplish brown, rich brown and very rarely, rich green. Although not studied in detail, compositional differences between these shades are apparent. Low Ti and Al augites have the least intense colour; increasing Ti plus Al produces the richer browns, particularly the purplish tints; and the more Fe-rich compositions are often shades of green. Phenocryst crystal habits can also be related to composition. There are perhaps three poorly defined groups. Firstly, a set characterised by large size, pronounced resorption textures, irregular habit and relatively unzoned cores. These have high Mg#, are mildly nepheline-normative, can be quite aluminous, and typically have high Al^{VI}/Al^{IV} values (up to 0.8). Al^{IV} is defined as tetrahedral Al and is expressed as cations per 6 oxygens where $Al^{IV} = 2-Si$. Al^{VI} is defined as octahedral Al where $Al^{VI} = \Sigma Al - Al^{IV}$. Like the ferric iron estimation, this subdivision of the Al content is susceptible to analytical error. However, the quite consistent variations found for most samples in accord with other evidence, suggest the Al^{VI}/Al^{IV} ratio can be used with some confidence to characterise pyroxenes. Augites in samples MV166, MV514, MV52, AS2, MV160 and ES2058 have the typical petrographic characteristics and relatively high Al^{VI}/Al^{IV} values of the first group. The second group have typically small size, oscillatory zoning sometimes with associated sector zoning, euhedral to subhedral habit with little or no suggestion of resorption and are often more purplish than the first group. These augites also have high Mg# and mildly nepheline-normative character, but may be very aluminous with high associated

Ti and relatively low Al^{VI}/Al^{IV} values. Typical examples of rocks containing these pyroxenes are MV406, MV106, MV78, MV109 and MV178, where $Al^{VI}/Al^{IV} \leqslant 0.3$. The third group of augites is perhaps the least well characterised. Typically the phenocrysts are of small to medium size, without pronounced zoning, with rounded or slightly resorbed appearance and often greenish brown in colour. Compositionally they have lower Mg# relative to the other two groups, and may have hypersthene-normative character, quite low Ti and Al contents and lowish Al^{VI}/Al^{IV} values. Possible rocks with these augites are MV121A, MV40A and MV39A where $Al^{VI}/Al^{IV} \leqslant 0.4$. Not all rocks have augite phenocrysts which can be easily slotted into any particular group. Some have pyroxenes with mixed characteristics and some may show a range of types. For example, rocks MV520, MV521 and MV403 contain augites which share features with those of the second group. In MV520 the crystals are unusually large; in MV403 and MV521 there is often a slightly sieved core to the phenocryst, perhaps due to resorption; and in all three some of the augites have higher Al^{VI}/Al^{IV} values than would be typical. Other grains in MV403 and MV521 are typical of the second group. If the different groups reflect real differences in origin, then samples showing characteristics of more than one group may indicate a complex crystallisation history.

Taking the range of clinopyroxene phenocrysts as a whole, there is limited variation of the augite Mg# with the host rock Mg#. Most of the phenocryst cores have Mg# = 75 - 90, with a tendency for lower whole rock Mg# samples to contain lower Mg# augites. The third group of augites described above, occur in lower Mg# rocks. Excluding the small lower Mg# augite group, the range of augite Mg# for the remaining samples is much less than the range of forsterite values for olivine phenocrysts. This partly reflects the more limited occurrence of the pyroxene phenocrysts. Cr_2O_3 concentrations in the phenocrysts are usually low (<0.5 wt %) although up to 1 wt % occurs. There is a trend of decreasing Cr concentration with decreasing augite Mg# (Figure 6-20) consistent with lower Mg# augites crystallising from melts already depleted in Cr, perhaps by fractionation of spinel or Cr-rich augite.

One of the criteria for distinguishing the different groups of augite is their normative character. Figure 6-21 illustrates the normative ranges of augite phenocryst cores plotted according to their host rock Mg#. The significance of this variation can be seen by comparison with Figure 6-2. Nepheline-normative augites occur in many of the hypersthene-normative rocks. At least some of the augites in the higher Mg# samples which appear hypersthene-normative, probably only do so because of analytical error. Overall, the trend shows an apparent decrease in nepheline-normative content of the pyroxenes, and appearance of hypersthene-normative types, as host rock Mg# decreases. In a fractionation scheme dominated by clinopyroxene, fractional crystallisation of the more nepheline-normative augites could produce the whole rock trend noted by Macdonald (1975), of mildly nepheline-normative basalts being associated with hypersthene-normative intermediate compositions. The augite compositional trend is consistent with this, as nepheline-normative augite phenocrysts are to be expected to occur in some of the hypersthene-normative rocks. The nepheline-normative, aluminous character of many of the more Mg-rich augites also supports Macdonald's hypothesis of a clinopyroxenite stage in the evolution of some lava successions.

Cameron and Papike (1981) have shown that individual suites of clinopyroxenes can be characterised on the basis of the relative importance of different substitutional couples. The minor elements (Ti, Al as Al^{IV} and Al^{VI}, Fe^{3+} and Na) appear most useful in this respect. Although the range of samples in this study is very broad in terms of age and type of basalt, the pyroxenes often show similar systematic variations. The most important minor element substitutional couples identified in these augite phenocrysts are $Ti - Al^{IV}$, $Fe^{3+} - Al^{IV}$, $Al^{VI} - Al^{IV}$ and $Na - Al^{VI}$. The Cr concentration is considered too low in general, to be of use in characterising the pyroxenes. The strong correlation between Ti and Al^{IV} is shown in Figure 6-22. Both phenocryst cores and rims show similar variation along a trend of $Ti : Al^{IV}$ ratio of approximately 1 : 3. In the more alkalic rocks, phenocryst rims and groundmass pyroxenes have consistently higher $Ti + Al^{IV}$ contents than the phenocryst cores.

The correlation between Fe^{3+} and Al^{IV} is shown in Figure 6-23. Like the previous couple, the phenocryst cores/rims and groundmass pyroxenes show similar variation along a trend of Fe^{3+} : Al^{IV} ratio of 1 : 3 approximately. It should be remembered that the Al^{IV} is calculated from the Si content of the pyroxene, and although the Fe^{3+} is based on stoichiometry, the main influence on the ferric iron estimation is the accuracy of the Si determination. Therefore, there is an element of circularity possible in considering Fe^{3+} - Al^{IV} variations. However, in the absence of evidence to the contrary, most of the analyses are believed to be of acceptable accuracy and so the trend in Figure 6-23 may be real. In that case the pyroxenes do not appear to have crystallised in a very reducing environment.

Al^{VI} - Al^{IV} relations are shown in Figure 6-24. At first sight there is only a barely detectable positive trend visible. However, a number of differences between pyroxene analyses can be found on inspection using the Al^{VI}/Al^{VI} ratio. Pyroxenes from nodules believed to have crystallised at mantle depths (Chapman, 1976) have the highest values of the ratio, in some cases exceeding 1 : 1. Phenocryst cores have a very broad range, but can reach comparable values to the lower end of the nodule group. Phenocryst rims and groundmass pyroxenes tend to have lower values still; the majority fall below the 1 : 4 line. Notably, a considerable number of the phenocryst cores also have very low ratio values.

Numerous authors have used the pyroxene Al^{VI}/Al^{IV} value as a qualitative pressure indicator, and have successfully distinguished relative pressures of origin using this in conjunction with other lines of evidence (e.g. Chapman, 1976; Wass, 1979; Larsen, 1981). Experimental data presented by Thompson (1974b) for a range of magma types, confirm the overall trend of increasing Al^{VI}/Al^{IV} with increasing pressure, but do not allow a precise calibration. Apart from the effects of bulk composition, the ratio is obviously very sensitive to analytical error and does not lend itself to precise determination from microprobe analyses. Experimental studies also indicate that the ratio can be affected by significant water pressures. Dolfi and Trigila (1983) found the Al^{VI}/Al^{IV} ratio decreased at constant temperature and pressure as the percentage of

water in the melt increased. Rapid growth of pyroxenes also decreases the Al^{VI}/Al^{IV} ratio, particularly noticeable in groundmass pyroxenes (Wass, 1979). Despite these possible problems, the trend shown in Figure 6-24 is in agreement with likely relative pressure relations. The high pressure nodules define a likely upper mantle pressure. Some of the phenocrysts suggest similar or slightly lower pressures, and a range of other phenocryst cores, as well as rim and groundmass compositions, point to low pressure origins. Taking Thompson's (1974b) experimental data on an alkali olivine basalt as a guide, augites with $Al^{VI}/Al^{IV} \simeq 0.6-0.7$ could have crystallised at approximately 10 Kb. This would be consistent with the nodule assemblages having formed at slightly higher pressures in the uppermost mantle under the Midland Valley. Phenocrysts could have crystallised at a range of depths from uppermost mantle to near surface pressures. This interpretation is consistent with the three groups of augite phenocrysts proposed earlier. The first group, which has the highest ratios, also shows spectacular resorption textures, suggesting the augites crystallised under significantly different conditions to the host matrix. The second group has the lowest ratios and few resorption textures. Their oscillatory and sector zoning suggest fairly rapid growth, which may have occurred at relatively low pressures during the ascent of the magma. However, the rapid growth might also have favoured incorporation of Al^{IV} into the pyroxene, lowering the Al^{VI}/Al^{IV} ratio. The third group have a wide range of Al^{VI}/Al^{IV} but do not reach the levels of the first group. Those showing resorption textures have the highest values and may have crystallised in the crust at several kilobars pressure.

The Al^{VI}-Al^{IV} relations for augites of a single sample are shown in Figure 6-25. This sample (MV166) contains pyroxenes of the first group, and the figure clearly separates the phenocryst cores from the rims and groundmass pyroxenes. The few exceptions can be shown to belong to the group with which they plot. Thus the anomalous "cores" are resorbed areas where the late quench pyroxene has filled the embayments. The anomalous "rims" are petrographically the outer edges of cores without significant quench overgrowth. Notably, the rims and groundmass pyroxenes have Al^{VI}/Al^{IV} values

≤ 0.25. This plot also shows that the total Al content is not a useful discriminant, as noted by Thompson (1974b), and if used would produce considerable overlap of the supposed high- and low-pressure groups.

Al^{VI} shows a slight positive correlation with Na, confirming the $Na - Al^{VI}$ substitutional couple (Figure 6-26a). The lack of a positive correlation between Na and Fe^{3+} (Figure 6-26b) suggests that in the analysed phenocrysts, Na is present mainly as a notional jadeite component rather than an acmite component. From a comparison with experimental studies (Thompson, 1974b) the relatively low Na content of the pyroxenes restricts the upper pressure limit of their crystallisation to approximately 15 Kb.

The petrographic aspects of the zoning have been discussed previously. Compositional variations associated with the augite profiles can be very pronounced. Three examples are illustrated which show the main features of pyroxenes in the sample collection. The main effect on the pyroxene end-member compositions in zoning from core to rim, is an increase in the wollastonite and ferrosilite components. Figure 6-27 shows the rim to rim variation for a pyroxene phenocryst from MV52 for selected elements. This is a typical member of the first augite group. Petrographically, this phenocryst has a highly resorbed anhedral core with a concentration of Fe - Ti oxides in the most sieved areas, plus an outer zone which is also anhedral and includes some magnetite grains. The transition between pale brown core and more strongly coloured, pinkish brown rim is quite sharp. Compositionally the core and rim are quite distinct. Compared to the rim, the core has lower Ca, Fe, Si and Ti, and higher Mg, Al, Na and Al^{VI}/Al^{IV}. The atypical core analysis (arrowed) occurs in a highly resorbed zone which is optically similar to the rim zone, and has a composition near to that of the rim. It indicates that in the case of the resorbed augites, some core analyses can give misleading results as they represent rim growth. By comparison with the published studies of $Al^{IV} - Al^{VI}$ variation, the core has quite high Al^{VI}/Al^{IV} values consistent with crystallisation at elevated pressures. In contrast, the extremely low values of the rim zone suggest growth at very low pressures. The rim compositions are

similar to the groundmass compositions and may have grown at the same time. The implication from this is that the augite crystallised at high pressures. It was carried into conditions with which it was out of equilibrium, where it was resorbed partially, but was preserved by the quenching episode of the magma. Although the phenocryst assemblage is olivine + clinopyroxene + plagioclase + magnetite, texturally the phases which may have been in equilibrium with the melt at the time of eruption are olivine + plagioclase + magnetite. In this sample there are two generations of olivine phenocrysts, of which the more forsteritic group could have been in equilibrium with the other phenocryst phases. In a broader context, many of the high Al^{VI}/Al^{IV}, resorbed augites have outer zones very similar to the groundmass pyroxenes. It seems that the host magmas were erupted or emplaced out of equilibrium with their pyroxene phenocrysts, e.g. MV166, MV514, AS2.

Figure 6-28 shows two augite phenocryst profiles from sample MV521. Both are small, euhedral, oscillatory zoned crystals with some inclusions at their core, perhaps due to resorption. Compared to the phenocryst in Figure 6-27 these augites show a more continuous variation from pale pinkish brown cores to purplish rims. In contrast to Figure 6-27, the phenocrysts in this plot show increased Ti and Al away from the core with less pronounced variation in the Ca and Na. The Al^{VI}/Al^{IV} variation is complex although the overall trend is towards low values at the rims. The reverse zoning with respect to Al^{VI}/Al^{IV} is difficult to explain in terms of pressure variations. Also, since it occurs in both profiles, it is not believed to be an artifact of the analyses. The textural evidence of oscillatory zoning may, by analogy with the plagioclase case, indicate fairly rapid growth. This may increase the Al^{IV} content of the pyroxene and so reduce the Al^{VI}/Al^{IV} ratio. It is tentatively suggested that the reverse Al^{VI}/Al^{IV} zoning indicates a period of rapid growth of the phenocrysts followed by a period of stabilisation. The possible history of these phenocrysts is initial growth at moderate pressures, less than those of the phenocryst in Figure 6-27, uprise with slight resorption, a period of rapid growth producing the oscillatory zoning and ultimately a quench rim associated with emplacement of the magma. The occurrence of some sector zoned

microphenocrysts supports the episode of rapid growth.

Apart from the described overall differences between the two types of augite phenocrysts in Figures 6-27 and 6-28, there is also a fundamental contrast in the growth of the rims of each. In the phenocryst illustrated in Figure 6-27, the Ti + Al^{IV} content of the crystal decreases towards the edge; in the augites shown in Figure 6-28, Ti + Al^{IV} increase towards the edges. Le Bas (1962) proposed that augites from tholeiitic magma would show a decrease in Al^{IV} with differentiation, whereas the augites from alkaline magmas would show a corresponding increase. This fits the described augites as sample MV52 is hypersthene-normative whereas MV521 is nepheline-normative.

Many of the smaller augite phenocrysts show sector zoning. However, in this sample collection the best development of the feature is in sample MV520 where hourglass augites can be over 1 cm in greatest dimension. Figure 6-29 shows a partial profile for selected elements from core to rim along neighbouring sectors of an oscillatory zoned phenocryst. The partly stepwise variation seen in the plot reflects this oscillatory zoning. The main differences between the sectors are in the concentrations of Mg, Al, Si and Ti. Ti and Al (as Al^{IV} and total Al) are concentrated in the dark sectors, while Mg and Si are enriched in the light sectors. Other components show only slight preferences. Ca, Fe^{3+} and Al^{VI} are slightly higher in the dark sectors whereas Fe^{2+} is slightly lower. Na and Mn show no consistent preference for either sector. The pale green clinopyroxene overgrowth to the sectors is quite distinct in character. In terms of the simple Ca - Mg - Fe end-members the dark sectors have distinctly higher wollastonite and lower enstatite values than neighbouring light sectors. These variations are in agreement with those found by other workers studying hourglass titanaugites, e.g. Wass (1973). The models proposed for the origin of the sector zoning probably also apply to the examples from this province. As described in the petrographic section, those models which combine rapid growth rates relative to diffusion rates, partly controlled by the pyroxene chain structure, appear to explain the observed features (Dowty, 1976). The additional role of melt

structure has been suggested by Duncan and Preston (1980) and might explain the frequent occurrence of sector zoned pyroxenes in alkalic compositions.

It is difficult to assess whether the clinopyroxene phenocrysts crystallised in association with other phenocryst phases. Petrographically, plagioclase phenocrysts often surround augite phenocrysts (e.g. MV402, MV74) or include partially resorbed augites (e.g. MV39A). These cases suggest the plagioclase phenocrysts started crystallising after clinopyroxene had ceased, although this is not a universal situation (e.g. MV520 where the sector zoned augite phenocrysts include some plagioclase laths). In terms of Mg#, olivine phenocrysts usually have a maximum value slightly lower than that of the clinopyroxene phenocrysts in any sample. This is the normal situation recorded by workers on assemblages with co-crystallising olivine and clinopyroxene (e.g. Wilson, 1982). Thus in many samples olivine and clinopyroxene may have crystallised together. There is often a similarity in size and growth or resorption texture of olivine and clinopyroxene phenocrysts in a sample, and it is tentatively suggested that this is a feature of magmas where both phases crystallised together. Thus, small size and rapid growth textures characterise both olivine and augite phenocrysts in some samples, e.g. MV109, MV521, MV106, MV406. In other samples, large rounded olivines and resorbed augites occur together, e.g. MV166, AS2, MV160, AS1/36017. A notable exception to this scheme is sample MV403 where large olivines are preserved with rare, small augites. In this rock the olivines tend to have higher Mg# values than the augites and may well have begun to crystallise significantly before the pyroxenes. This rock is also anomalous in that it is rich in normative hypersthene although it is very magnesian.

6.5.4 Spinel and Magnetite

Since the petrographic distinction between spinel and magnetite phenocrysts is rather arbitrary, and there is complete compositional variation between both extremes, it is appropriate to consider the two phenocryst types together. Spinel is most commonly a phenocryst phase in higher Mg# samples, where it occurs typically as inclusions in olivine phenocrysts and, to a lesser extent, in augite phenocrysts.

Discrete crystals of spinel set in the groundmass occur in a few samples, e.g. MV166, MV514, AS1/36017. Habits range from subhedral to rounded and ragged anhedral. Magnetite phenocrysts are most common in the lower Mg# samples where they occur as inclusions in the outer zones of silicate phenocrysts, particularly olivine, or as discrete grains in the matrix. Compositionally, some of the magnetite phenocrysts reported in the more magnesian rocks might be considered as spinels, but have been labelled as magnetite phenocrysts in Appendix 5, to emphasise the distinction from Mg-, Cr-rich inclusions in the olivines and/or pyroxenes. Habits range from euhedral to ragged anhedral. Much of the ragged appearance can be attributed to over-growth of groundmass Fe-Ti oxides, supported by the observation that the habit only occurs in discrete phenocrysts. Alteration of spinel phenocrysts does not appear to be a problem, probably due to their inclusion in other minerals. The magnetite phenocrysts are often fresh, but may show complex lamellae indicative of low temperature oxidation. In addition, analysis totals after recalculation for ferric iron can be low, possibly reflecting some degree of maghemitisation, e.g. MV78. This is quite common in groundmass magnetites. For all spinels and magnetites, the ferric iron content has been calculated on the basis of stoichiometry of 24 cations to 32 oxygens.

In terms of a Cr/Al & Mg/Fe^{2+} classification scheme, the spinels are dominantly magnesian pleonaste (ceylonite), picotite and chrome-pleonaste. Essentially this is a continuous series of Al-rich spinels, with very Cr-rich spinels absent. Figure 6-30 illustrates the spinel Mg# variation with 100* Cr/(Cr + Al). Taken overall, there is a range of spinels with Mg# $>$ 50 which can tentatively be subdivided into two groups on the basis of Cr/(Cr + Al). Firstly, a group with Cr/(Cr + Al) less than approximately 0.2 which has few associated lower Mg# spinels. Secondly, a group with initially higher Cr/(Cr + Al) values which extends to lower Mg# with increasing Cr/(Cr + Al). Where a range of spinel compositions is present in a sample, the variation is towards higher Cr/(Cr + Al) with falling Mg#, e.g. MV406, MV403, MV521, MV106, MV164, ES2058.

Sample MV178 spinel is distinguished in Figure 6-30. The analyses indicate a higher Mg# than any other sample, together with

low Cr/(Cr + Al). The spinel is anhedral, translucent brown and is enclosed in olivine. Both optically and compositionally this spinel is very similar to spinel analysed in the spinel lherzolites (F2 and F3). The spinel may be a xenocryst included in the growing olivine phenocryst from a disaggregated spinel lherzolite nodule.

Figure 6-30 also gives the silicate phenocryst assemblages associated with the spinels. Assemblages containing clinopyroxene $\pm$ plagioclase occur throughout the range. The olivine-only assemblage is restricted to the relatively high Cr/(Cr + Al) group.

The magnetites are effectively a continuation of the spinel compositions towards lower Mg#, and higher Fe^{3+} and Ti. The large amounts of Ti present indicate these are titaniferous magnetites.

There is a poor positive correlation between the highest Mg# spinel of a sample and the host rock Mg#. There is a much greater range of Mg# in the spinels compared to coexisting olivine phenocrysts. The spinels may be subject to Fe-Mg exchange with the host olivine/clinopyroxene after inclusion. However, the broad range of compositions in individual samples suggests spinel is a very sensitive indicator of the conditions in which it crystallises.

The complete range of spinels and magnetites shows several consistent compositional variations. Figure 6-31 shows the regular increase in $Fe^{3+}/(Cr + Al + Fe^{3+})$ as spinel Mg# decreases. A similar increase occurs for Ti/(Ti + Cr + Al) versus Mg#, although the Ti component increases only gradually from Mg# = 80 down to Mg# = 30, then increases rapidly at lower Mg#. Data are more scattered at these lower Mg# values. For these trends it is not possible to distinguish the individual groups of spinel.

When the $Cr/(Cr + Al + Fe^{3+})$ & Mg# variation is considered as in Figure 6-32, the trends are more complex. There are three main clusters of points; high Mg#, low $Cr/(Cr + Al + Fe^{3+})$ spinels; high $Cr/(Cr + Al + Fe^{3+})$, high to low Mg# spinels; and low $Cr/(Cr + Al + Fe^{3+})$, low Mg# magnetites. The high Mg# low Cr ratio spinels form the first group suggested above. The high Mg# high Cr ratio spinels form the second group. The magnetites can be seen to be a

continuation of the second spinel group. Taking only a few compositions as guides, some details of the variation can be discerned. Figure 6-33 shows spinels from samples in the Edinburgh area (Arthur's Seat and the Castle Rock). Each sample produces a trend at high Mg#, where the Cr ratio increases as the Mg# decreases. Fisk and Bence (1980) found this same variation within spinel from single experiments, which they attributed to $Cr-Fe^{2+}$ and $Mg-Al$ associations related to plagioclase crystallisation. There is no evidence in samples MV516 and AS2 for significant plagioclase crystallisation associated with the spinels. Sample AS1/36107 also shows a trend of decreasing Mg# with limited Cr ratio variation, and finally decreasing Cr ratio values to near zero at low Mg# values. The variation in Figure 6-32 is made up of similar trends with slight increases in the Cr ratio as Mg# falls, and low Cr ratio values at low Mg# values.

The variation can be viewed in terms of the Fe^{3+}-Cr-Al contents of the spinels. In Figure 6-34 there are clusters of spinel compositions at low Cr and moderate Cr contents corresponding to the first and second spinel group respectively. By comparison with Figure 6-30 the two groups can be seen to have comparable Mg# and Fe^{3+} contents, but have distinct Cr/(Cr + Al) values.

At least some of the low Cr/(Cr + Al) spinels are associated with the augite phenocrysts believed to have formed at high pressures, e.g. MV166, AS2, MV514. Several studies have described similar aluminous spinels in megacryst assemblages and nodule assemblages, consistently ascribing to them a high pressure origin, e.g. Binns et al. (1970); Evans and Nash (1979); Chapman (1975, 1976). Chapman (1975) described aluminous pyroxenes from the Scottish Permo-Carboniferous province which contained exsolved aluminous spinels. His experimental work pointed to high pressure (18 Kb) conditions where discrete spinels could crystallise. Chapman (1976) has described discrete aluminous spinels in a wehrlite from Fidra interpreted to have crystallised at high pressures from basic magmas. The two wehrlites described in the present study (F1 and F4) contain similar aluminous spinels and, by analogy with Chapman's (1976) interpretation of other Fidra wehrlites, have an igneous crystallis-

ation origin at 10-20 Kb. Such aluminous spinels have not been recognised as phenocrysts in this province previously. The examples analysed in this study are comparable with the nodule evidence and, at least in some samples, probably represent a high pressure origin. Haggerty (1979), in a comparative study of spinels from high pressures, concluded that in the upper mantle there is a positive correlation between increasing pressure and spinel Al/Cr ratio. This was based on nodules in volcanic suites. In contrast, Eales and Marsh (1983) presented evidence suggesting there is no significant pressure or temperature control on spinel Al/Cr ratios. The environment in which the mineral forms, was interpreted as the main factor, e.g. the nature of the coexisting silicate phases. Eales and Marsh (1983) proposed that high-Al, low-Cr spinels could have crystallised from aluminous melts together with clinopyroxene, but without plagioclase. However, within the data set used by Eales and Marsh to support their arguments, the only occurrences of spinels similar to the high Al/Cr varieties described in this study, come from high pressure origins. The interpretation of Haggerty (1979) is preferred as crystallisation at progressively lower pressures could produce the increase in Cr/Al ratio observed. The model of Eales and Marsh (1983) does not easily explain the increase in Cr content of the spinels with decreasing Mg#, assuming Mg# as a fractionation index.

It is suggested that the two groups of spinels proposed in this text represent two distinct origins; the low-Cr/(Cr + Al) group forming at high pressures, perhaps > 10 Kb; the higher Cr/(Cr + Al) group forming at lower pressures. This distinction is probably qualitative as melt composition is certain to be an important factor.

The magnetite phenocrysts have been shown to be a continuation of the spinel compositions towards lower Mg#, and high Fe^{3+} and Ti concentrations. However, in any one sample there is usually a restricted range of core compositions of spinels and magnetites forming two discrete groups. In some cases the compositional gap may be due to spinel reaction at high temperatures, with magnetite crystallising at markedly lower temperatures (Hill and Roeder, 1974; this study, melting relations of MV93). Sample MV406 shows a large compositional gap with respect to Mg# which may have been produced

in this way. Another possibility is that spinel crystallised throughout the cooling interval, with the included spinels recording higher temperatures, and the groundmass magnetites simply reacting with the melt to lower temperatures. This is a possibility for sample AS1/36017. Figures 6-32,33 show a rapid decrease in Cr content with decreasing Mg#. The simplest explanation of this, is that it results from crystallisation of large modal amounts of magnetite in which the limited Cr is very diluted. Although a high pressure origin for the magnetite phenocrysts can not be ruled out, the occurrence and composition of the phenocrysts are often similar to the groundmass magnetites.

The $Fe^{2+}/(Fe^{2+}+ Fe^{3+})$ ratio in spinel phases can be used to indicate relative crystallisation temperatures and oxygen fugacities (Dick and Bryan, 1978). The limited variation found for spinels in many samples in this study, suggests crystallisation took place at lower oxygen fugacities as temperature dropped. For example, seven spinels in sample MV400 range from Mg# = 30 to Mg# = 69, yet the $Fe^{2+}/(Fe^{2+}+ Fe^{3+})$ ratio only ranges from 0.64 - 0.67. Spinels in sample MV403 have a Mg# range of 43 to 70 in seventeen grains, and an $Fe^{2+}/(Fe^{2+}+ Fe^{3+})$ range of 0.69 - 0.88 with most values 0.75 - 0.80. Although there is more scatter in this group (probably due in part to analytical error), the Fe^{2+}/Fe^{3+} is consistently higher than for MV400 and may reflect a more reduced state at a given temperature. Taking the suite as a whole the spinels have a range of $Fe^{2+}/(Fe^{2+}+ Fe^{3+})$ of 0.6 - 0.8. With further study it may be possible to characterise individual lava successions on this basis. As an example, Arculus (1974) described a set of spinels from a Grenada basanitoid and presented five analyses. The range of $Fe^{2+}/(Fe^{2+}+ Fe^{3+})$ for these is 0.38 - 0.57, which is consistently lower at any Mg# than for this study, and suggests a more oxidising environment of crystallisation. Arculus and Wills (1980) using coexisting magnetite-ilmenite pairs from other samples from Grenada, found oxygen fugacities higher than the Ni - NiO buffer for the suite. Their results are consistent with coexisting pairs from the present study having crystallised under more reducing conditions. This is indeed the case as is described in the next section. It is not possible to distinguish between the two spinel groups on the basis of $Fe^{2+}/(Fe^{2+}+ Fe^{3+})$ ratio. This may

indicate that the magmas were not more reduced at high pressures than at low pressures, from coexisting magnetite and ilmenite pairs in the groundmass. This contrasts with the very low oxygen fugacities proposed for high pressure, aluminous spinel megacrysts by Arculus and Delano (1981).

Where spinels are included in more than one silicate phenocryst phase, compositional differences are quite common between the inclusions. In samples MV521 and MV403, the clinopyroxenes include spinels with lower Mg# values than spinel inclusions in the olivines. This may indicate the clinopyroxenes began crystallising after the olivines, although different closure temperatures or degrees of reaction with the host might also explain the result.

In samples MV166 and MV514 the outer zones of olivine phenocrysts contain higher Cr, much lower Mg# spinels than occur as discrete phenocrysts. This suggests to the author that the olivines could have grown and included Cr-bearing spinels after the discrete Cr-poor phenocrysts had ceased crystallising. There is clear evidence of reaction and resorption of the discrete spinels. This is clearly an unusual situation. The low Cr spinels are envisaged as having grown at high pressures. As the magma ascended, these early spinels began to be resorbed. At lower pressures, when a spinel phase again reached the liquidus, these lower Mg#, higher Cr spinels did not nucleate on the early spinels. Some of the late spinels may even have nucleated on the growing olivine phenocrysts while the early spinels continued to be resorbed. The increased Cr/Al ratio of the later spinels is interpreted as indicating lower pressure crystallisation (Haggerty, 1979).

Zoning in individual spinels usually follows the overall trends of the suite. Figure 6-35 shows some features of the zoning of a large spinel phenocryst in AS1/36017. From core to rim the Al ratio and Mg# decrease, and Fe^{3+} and Ti increase. The Cr ratio increases initially then decreases rapidly. The Cr/(Cr + Al) ratio (not shown) increases from the core until close to the rim, when crystallisation of large modal amounts of magnetite from the melt depleted the available Cr rapidly.

6.5.5 Ilmenite and coexisting Magnetite-Ilmenite pairs

Discrete primary ilmenite phenocrysts have only been identified in six samples, MV121A, MV13, MV39A, MV39B, MV40A and MV74. These are all plagioclase-phyric, low Mg# samples. Indeed ilmenite is the last phenocryst to occur in terms of decreasing Mg# (Figure 6-1). Several other samples contain ilmenite 'phenocrysts' which are texturally secondary. Ilmenite zones in magnetite phenocrysts in MV716 and MV718 are interpreted as high temperature oxidation products from titanomagnetite (Thy, 1982). Sample AS1 contains an Fe-Ti oxide-rich xenolith with rare ilmenite. The origin of this aggregate is uncertain. In the discussion below, both primary and secondary ilmenite 'phenocrysts' will be considered. In addition, ilmenite from wehrlite F4 is included. Wehrlite F4 otherwise contains a similar assemblage to F1, and on the basis of spinel and augite compositions represents a high pressure occurrence of ilmenite. The coexisting spinel has higher Al, and lower Cr and Ti than the spinel in the ilmenite-free F1 wehrlite. The ilmenite collection is completed by groundmass ilmenites consisting of discrete grains and exsolved lamellae.

The main compositional variations in the ilmenites are in the proportions of the dominant ilmenite, plus haematite and geikielite end-members. Haggerty (1976) showed that the Mg content of an ilmenite is strongly dependent on the host melt composition. Assuming Mg# as a fractionation index, the Mg content of the ilmenite should reflect the degree of evolution of the sample. Figure 6-36 shows the ilmenite Mn & Mg# contents. On the basis of their Mg# values, the three groups (groundmass, phenocryst and high-pressure inclusion) are quite well defined. The high pressure ilmenites have high Mg# values (up to 8.6 wt % MgO) consistent with crystallisation from a Mg-rich liquid. The effect of pressure on this compositional dependence may be to reduce the ilmenite Mg content with increasing pressure (Haggerty, 1976). The 'phenocryst' group has markedly lower Mg contents. In fact, the Mg# value of the primary ilmenites is less than 15 and it is the ilmenites of AS1, MV716 and MV718 which have values up to 25. The ilmenites of the latter samples appear to have equilibrated with more Mg-rich melts

than the ilmenites of the primary phenocryst samples. Groundmass ilmenites have values mainly similar to or less than the primary ilmenites. Mn concentrations show a progressive increase towards lower Mg# values. Haggerty (1976) has interpreted Mn concentrations in ilmenite as dependent on both composition and temperature. The variation seen here is consistent with crystallisation of ilmenite from increasingly Mn-rich melts at progressively low temperatures.

The overall variation in Figure 6-36 suggests high temperature crystallisation of ilmenites from a Mg-rich melt in the high pressure wehrlite; lower temperature crystallisation of the anomalous phenocryst ilmenites from less Mg-rich melts; crystallisation of the primary phenocrysts from less Mg-rich liquids again, and crystallisation of the groundmass ilmenites at still lower temperatures, from liquids of comparable or lower Mg content. The primary ilmenite phenocrysts appear to have crystallised just ahead of the groundmass ilmenites and show no clear evidence of having formed at an early high temperature or high pressure stage of evolution. Other elements do not discriminate the individual groups as efficiently. Al concentrations are overall lower in the groundmass ilmenites than in the phenocrysts or nodule ilmenites. Cr concentrations are highest in the wehrlite ilmenites and decrease rapidly with decreasing Mg content, consistent with progressive depletion of Cr from a melt. Ti contents of the primary ilmenite phenocrysts are lower than in the associated groundmass ilmenites. This is to be expected, as ilmenites crystallising along an oxygen buffer become richer in the ilmenite component at lower temperatures (Hammond and Taylor, 1982).

Coexisting magnetite-ilmenite pairs occur in many samples. These have been recast into magnetite-ulvospinel and ilmenite-haematite components, using the method described in Chapter 4. Using the model of Spencer and Lindsley (1981), Figure 6-37 shows the predicted temperature and oxygen fugacity of equilibration of the oxide phases. Many of the predicted temperatures are clearly too low to represent magmatic crystallisation, and indicate re-equilibration of the oxides during relatively slow cooling. In addition, some of the oxide pairs include a magnetite member which has exsolved ilmenite lamellae and may have altered partially to maghemite. However,

suspect pairs plot within the main trend, and so have been left in the set. The overall trend of pairs crosses the FMQ buffer at high temperatures and nears the Fe - FeO buffer at low temperatures. This variation is similar to, but slightly more oxidising than, the trend of the $FeO-Fe_3O_4$ buffer. The higher temperature pairs record possible magmatic temperatures, and suggest that the magmatic crystallisation of at least some of the oxide pairs took place at oxygen fugacities between the Ni - NiO and FMQ buffers, typical of many basic extrusive suites (Haggerty, 1976). The apparently reduced nature of some of the subsolidus pairs, if taken in isolation, would predict a very reduced environment of crystallisation for this suite, not consistent with the rest of the data. For interpretation of the oxygen fugacities of crystallisation of a suite of lavas, it is essential to find coexisting oxide pairs which still record magmatic temperatures and have not been modified at lower temperatures. The evidence for the samples in this study suggests that at eruption the oxygen fugacity corresponded to near the Ni - NiO buffer. The lack of any marked change in the $Fe^{2+}/(Fe^{2+} + Fe^{3+})$ ratio of associated spinels, suggests the earlier evolution of the magmas could have taken place under similar conditions.

6.5.6 Orthopyroxene

Orthopyroxenes occur as phenocrysts in sample MV121A alone. In this study low Ca-pyroxenes were noted in only three other samples, as an Fe-rich groundmass phase in MV40A, and as an enstatite in spinel lherzolites F2 and F3.

Macdonald (1975) described the orthopyroxenes in MV121A as xenocrysts. However, in the thin section examined, there is less clear evidence for a reaction relationship than is present for some aluminous clinopyroxene phenocrysts in other rocks. The orthopyroxenes are rounded, with a slight increase in clinopyroxene around the edges of some crystals, and have clearly been partially resorbed. Both groups of clinopyroxene phenocrysts present in this sample also show evidence of partial resorption. Compositions of the pyroxenes, together with coexisting pyroxenes from F2 and F3, are given in Figure 6-38. In terms of the Ca-Mg-(Fe + Mn) relations illustrated,

the bronzites from MV121A are markedly more Fe-rich and slightly more calcic than the enstatites of F2 and F3. Upton et al. (1983) presented orthopyroxene data from a wide range of nodules from the Permo-Carboniferous volcanic rocks. From Ca-Mg-Fe relations, the most similar pyroxenes to the phenocrysts of MV121A come from olivine-free pyroxenites, commonly websterites. In sample MV121A both groups of clinopyroxene phenocrysts (as well as coexisting olivine phenocrysts) are too Fe-rich to have been in equilibrium with the orthopyroxenes. The simplest explanation may be the orthopyroxenes represent an early stage of evolution at moderate pressures, replaced at lower pressures by an olivine + augite-bearing phenocryst assemblage. The sequence is based on the various degrees to which the phenocrysts show reaction or resorption. The mineral compositions are in broad agreement with this. Ferroaugite in MV121A appears to be quite anomalous, and is best interpreted as a xenocryst. The orthopyroxene phenocrysts are relatively aluminous (2 - 3 wt % Al_2O_3) and contain up to 0.4 wt % Cr_2O_3, and 0.5 wt % TiO_2. It is not possible to disprove the hypothesis that the bronzites are xenocrysts, but they do have compositions which could have crystallised from basaltic magma at several kilobars pressure (perhaps with significant pH_2O).

6.6 Concluding Remarks

The main conclusion of this chapter is that the samples contain phenocryst assemblages representing a broad range of environments of crystallisation, from probable upper mantle to near surface. Individual samples contain phenocrysts which crystallised at high pressures, alongside phenocrysts which may have grown near the final quenching stage of the magma. In this respect, using the terms phenocryst, and phenocryst assemblage in a purely descriptive, non-genetic sense, does cloud the recognition of simple crystallisation sequences. However, if the ideal use of the terms is to describe only phases in equilibrium with the host melt, then some of the classical petrographic divisions of this province would need revision or even disappear. In particular, the Dunsapie and Craiglockhart basalt types contain augites which, texturally at least, were not in equilibrium at the time of eruption. In other cases, skeletal

textures indicate another form of disequilibrium, and raise the possibility of the equilibrium phases not having nucleated, e.g. plagioclase. For this province at least, there seems to be no alternative to using the purely descriptive connotations, bearing in mind that the phenocryst assemblage may be suggesting a cotectic situation which simply never happened.

Combining the evidence from previous studies, petrography, major-element variation and mineral chemistry, it is possible to recognise a number of characteristic phenocryst trends. The overall variation in basalt composition can be explained by fractionation of an assemblage dominated by clinopyroxene with lesser amounts of olivine + spinel. That assemblage is identified in the basalts as phenocrysts of forsteritic olivine, aluminous (high Al^{VI}/Al^{IV}) augite and high Al, low Cr spinel. These phenocrysts are usually large, rounded and frequently, partially resorbed. The nepheline-normative character of the augite allowed mildly nepheline-normative basaltic melts to produce hypersthene-normative differentiates. The instability of the augite and spinel at low pressures can account for the resorption textures. Wehrlite and clinopyroxenite nodules described by Chapman (1976) and Upton et al. (1983) may represent the predicted high pressure fractionates, although they need not be cognate with the host rock.

With suitable cooling or temporary arresting of the magmas, perhaps in a magma chamber, plagioclase may have joined the phenocryst assemblages. There is no clear evidence for plagioclase in the highest pressure assemblages, and so plagioclase-phyric samples containing high-pressure clinopyroxenes are believed to have become cotectic with respect to plagioclase at lower pressures, perhaps in the lower crust. Indeed, on the basis of petrographic evidence, the clinopyroxene was probably unstable by this stage in a number of samples, so that some of the macroporphyritic OL + CPX + PL-phyric basalts were not cotectic with respect to clinopyroxene and plagioclase together. Where the high pressure assemblages were efficiently fractionated, the low-pressure phenocryst assemblages of olivine and/or plagioclase $\pm$ opaque oxides have become established. The possible addition of water to the melt at high crustal levels

could have been a major influence here, e.g. outgassing of a magma may have been the cause of large, abundant, skeletal plagioclases in some samples.

For many of the microphyric olivine + augite basalts a slightly different origin is envisaged. The habit of these microphenocrysts frequently indicates rapid growth. It is suggested that liquids in equilibrium with olivine + clinopyroxene + spinel at high pressures, were efficiently separated from the crystalline assemblages, and rising and cooling through the crust crystallised the same phenocryst assemblage, but with rapid-growth forms. These lavas were then erupted or emplaced without further evolution. Whether the high pressure macroporphyritic assemblage or simply a fractionated liquid rose through the crust may have depended on the local stress regime, combined with the effective magma density and viscosity. The abundance of the microphyric olivine + augite basalts in the later stages of the activity in the province, may reflect different pathways for uprise of the magma, effectively fractionating the high pressure assemblages. That the phenocryst range in the most primitive basalts encompasses three phases (olivine + augite + spinel), suggests the initial magmas were close to saturation for all three phases at their liquidus at high pressures.

Magnetite and ilmenite are believed to have joined the phenocryst assemblages at about the same stage as plagioclase or later. There is no evidence for an increase in the oxygen fugacities of the magmas associated with this.

To summarise, the evidence from the natural rocks is interpreted as showing polybaric phenocryst crystallisation from the upper mantle to near the surface. High pressure phenocryst phases were olivine (low Ca), clinopyroxene (high Al^{VI}/Al^{IV}) and spinel (high Al/Cr). At lower pressures, within the crust, olivine + plagioclase $\pm$ augite assemblages may have been produced. Associated spinels have lower Al/Cr values. Augites have lower Al^{VI}/Al^{IV} values. Olivine (high Ca) and/or plagioclase $\pm$ Fe-Ti oxide phases were the phenocryst phases most commonly crystallised at upper crustal levels. Some of the most magnesian magmas rapidly crystallised olivine + augite + spinel phenocrysts on their way to the surface over a broad

range of pressures. This generalised model will be discussed in the next chapter with the aforementioned data supplemented by the experimental data and crystallisation model.

PLATE I.
Skeletal olivine microphenocrysts in sample MV109. Note the alignment of phenocrysts and groundmass plagioclase laths.
Base length of the photograph represents 0.35 cm.
Taken under crossed polars.

PLATE II.
Rounded, partially resorbed olivine microphenocrysts in sample MV718.
Base length of the photograph represents 0.5 cm.
Taken in plane polarised light.

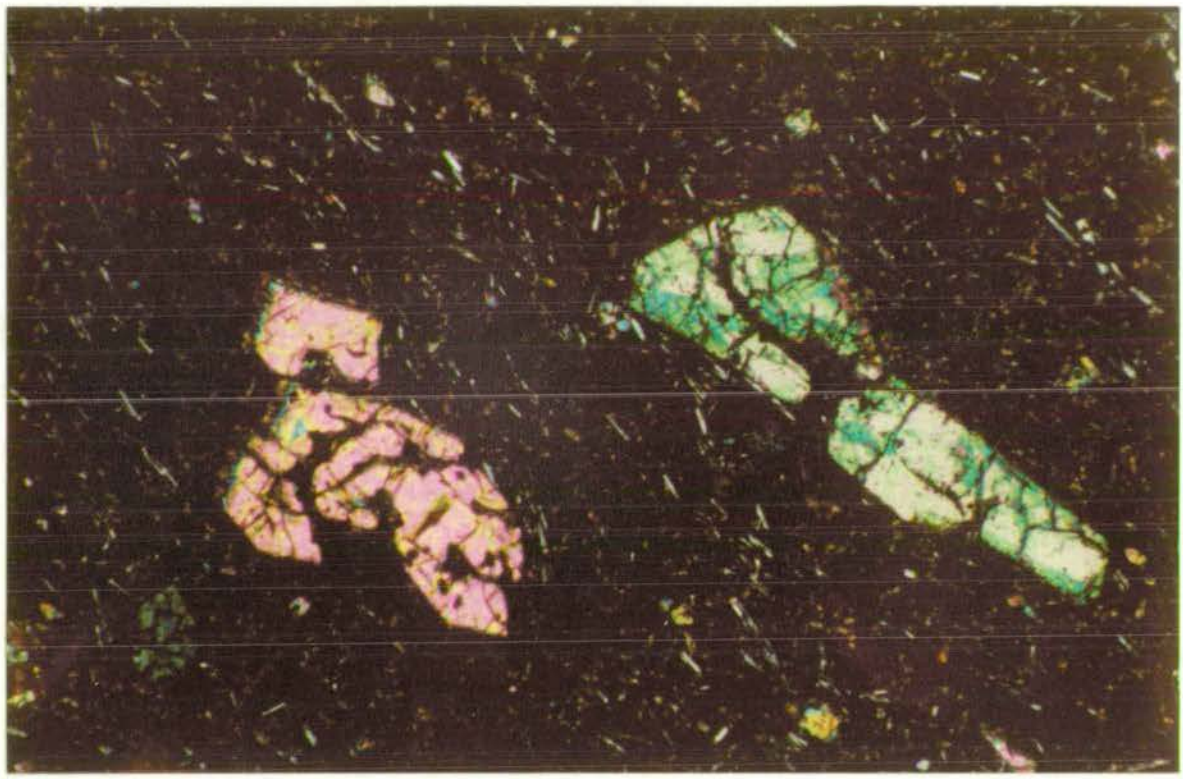

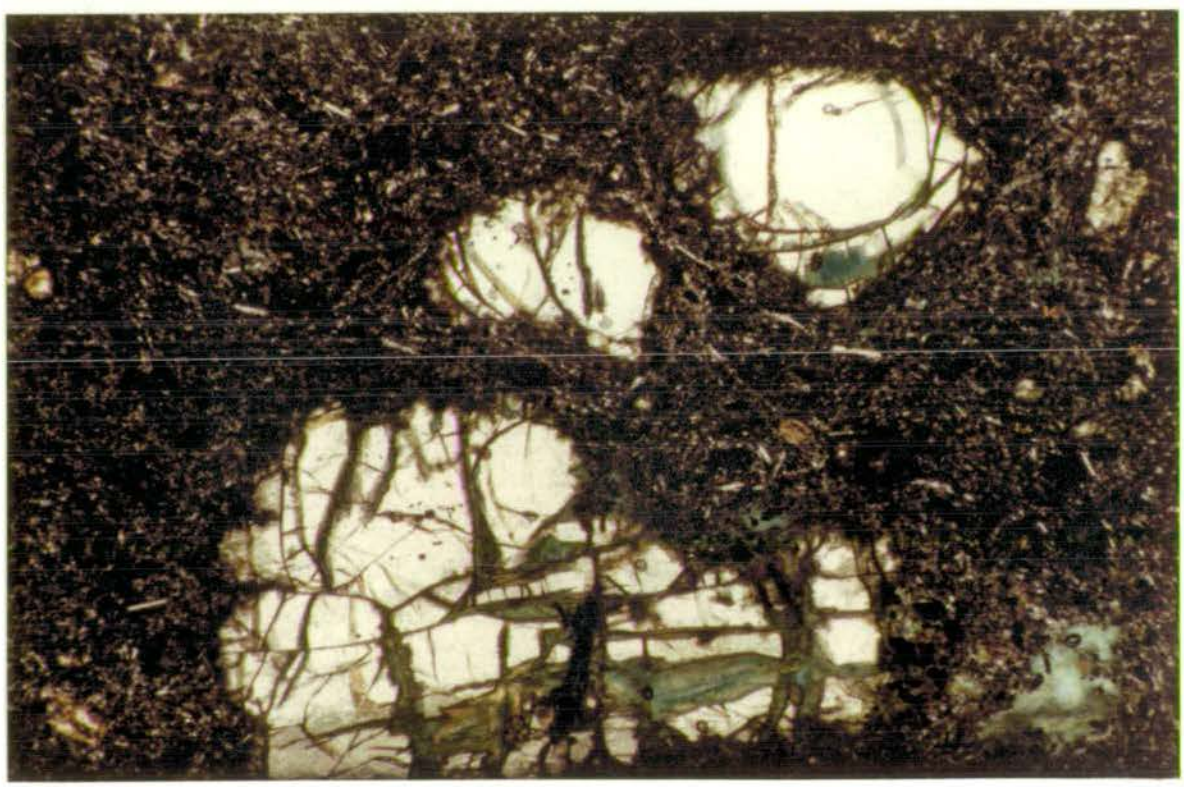

PLATE III.
Skeletal plagioclase macrophenocryst in sample MV702.
Note the small oscillatory zoned plagioclase at the top left of the plate.
Base length of the photograph represents 0.6 cm.
Taken under crossed polars.

PLATE IV.
The Lion's Haunch Basalt, sample AS1.
Phenocrysts include :- (1) plagioclase, slightly sieved throughout, interpreted as a growth texture; (2) plagioclase, highly sieved, interpreted as a resorption texture; (3) olivine; (4) augite, slightly resorbed; and (5) titanomagnetite.
Note that the highly sieved plagioclases (2) have rounded clear areas in their core, and have clear rims.
Base length of the photograph represents 1.2 cm.
Taken in plane polarised light.

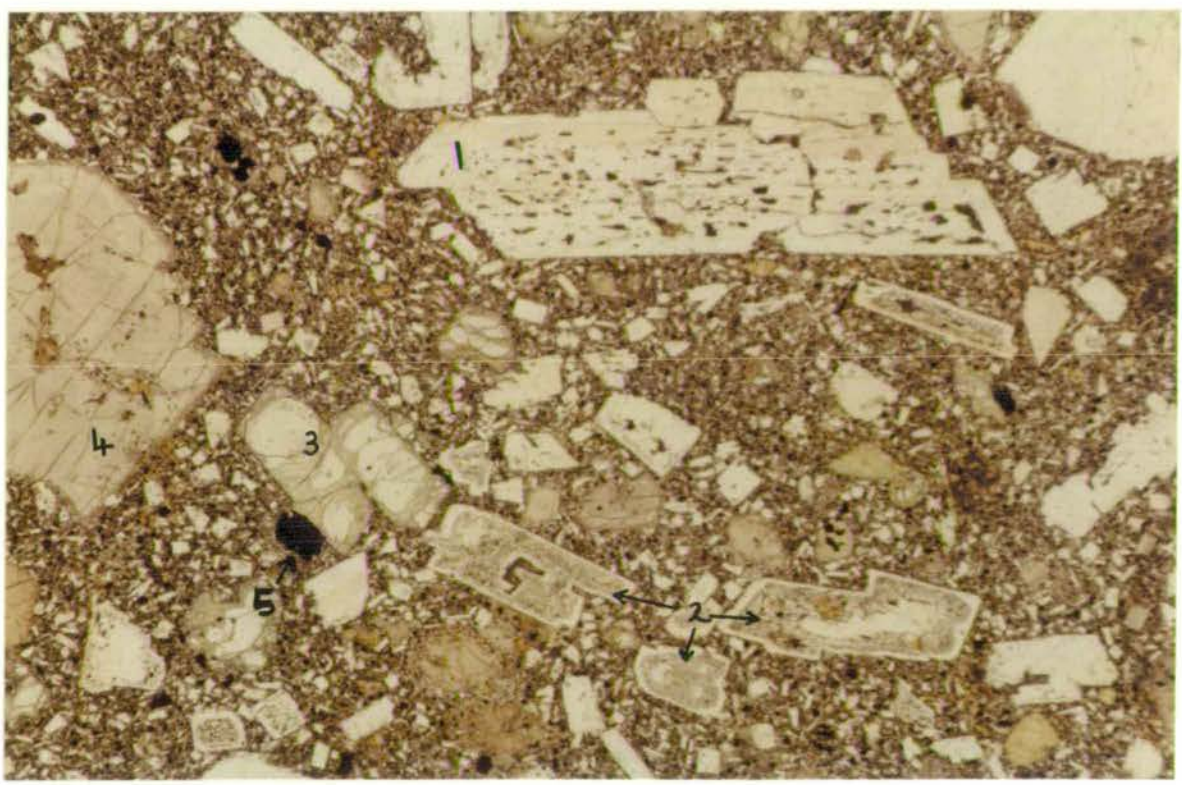
1
2
3
4
5
5

PLATE V.
Highly resorbed (left) and complete (right) plagioclase phenocrysts in sample MV122.
Note the irregular clear core and the clear rim of the resorbed plagioclase.
Base length of the photograph represents 0.4 cm.
Taken in plane polarised light.

PLATE VI.
Plagioclase macrophenocryst, highly resorbed throughout but with a clear rim, from sample MV39A.
Base length of the photograph represents 0.7 cm.
Taken under crossed polars (anomalous colour due to a slightly thick section).

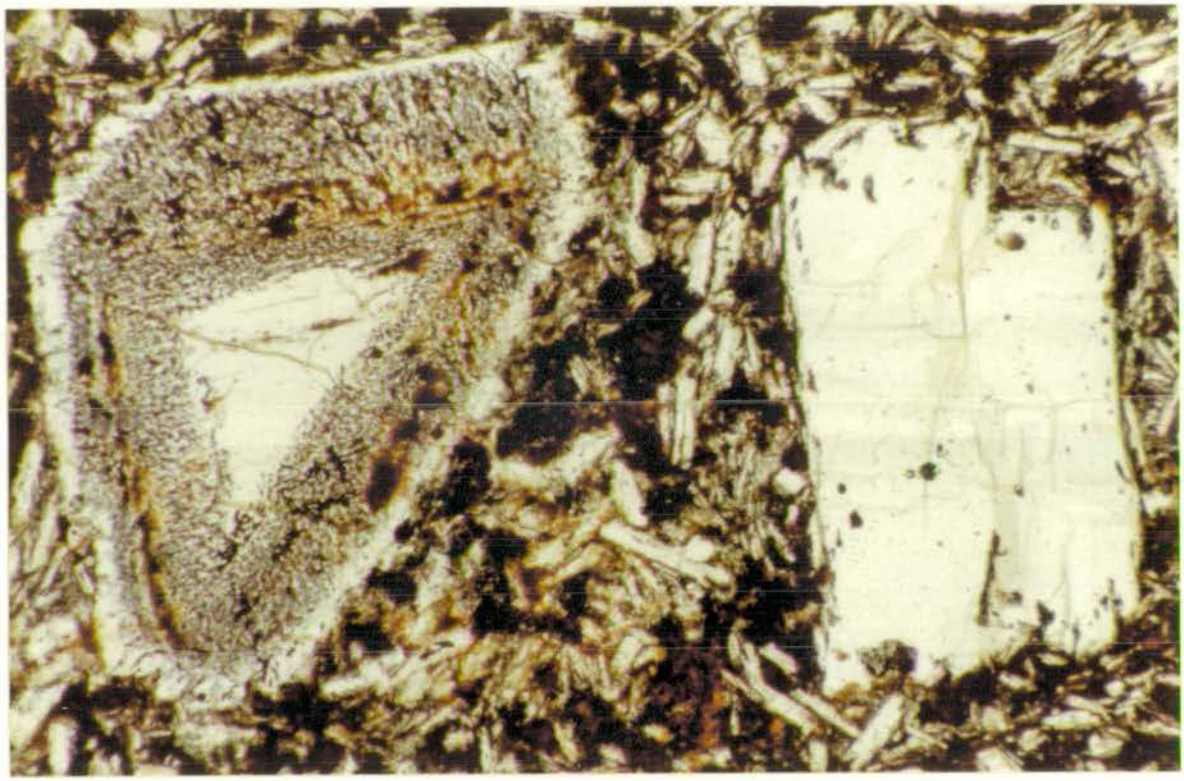

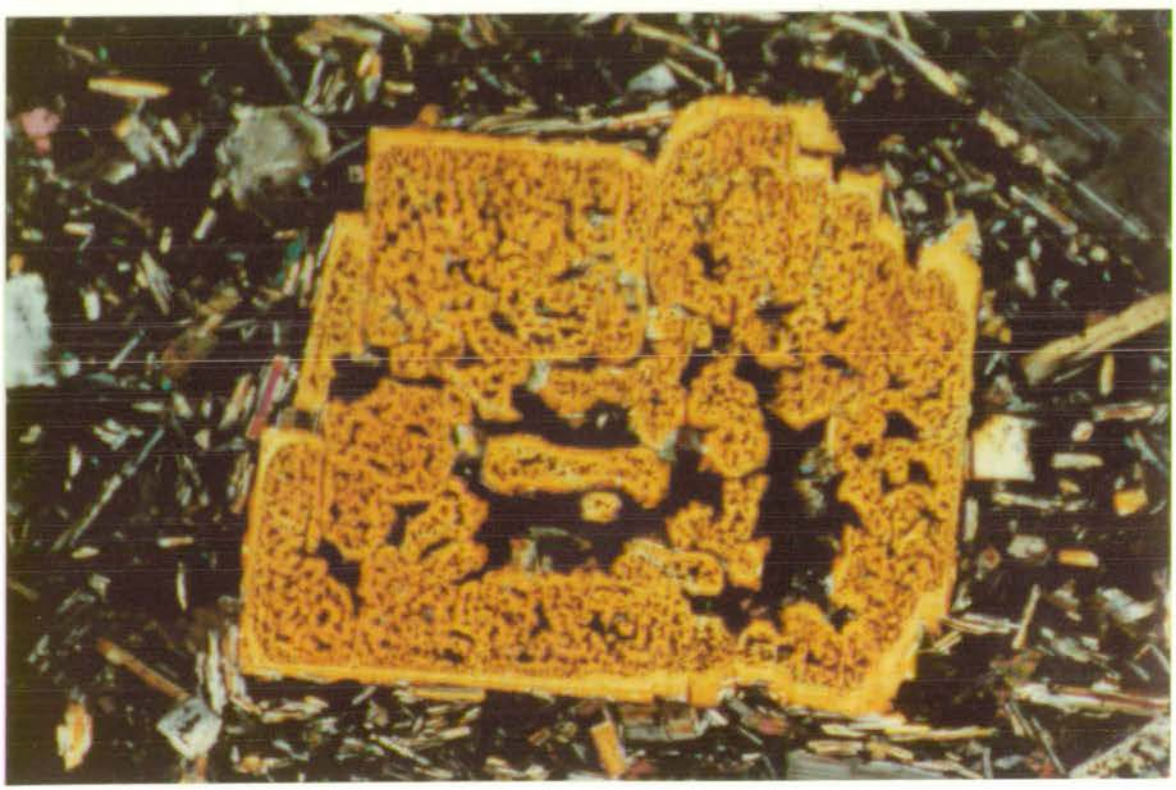

PLATE VII.
Sector-zoned augite macrophenocryst in sample MV520, the Crawfordjohn essexite.
Note the inclusion of two small olivine phenocrysts in the core of the augite, and also the concentrically arranged inclusions of plagioclase (altered). There is a small euhedral olivine phenocryst (ol) to the left.
Base length of the photograph represents 1.5 cm.
Taken under crossed polars.

PLATE VIII.
Highly resorbed augite macrophenocryst in sample AS2.
The dark appearance of the outer part of the augite is due to the inclusion of numerous small titanomagnetites.
Larger euhedral inclusions of aluminous spinel are also present (sp).
Base length of the photograph represents 0.9 cm.
Taken in plane polarised light.

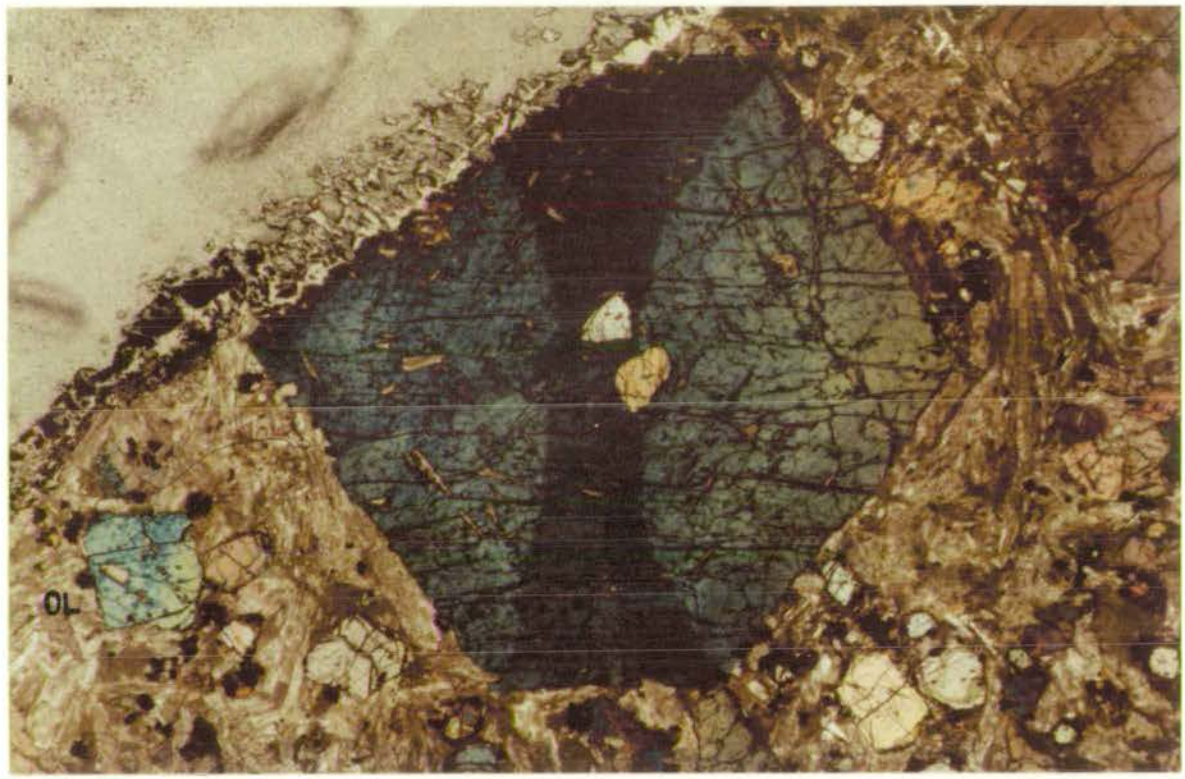
OL


SP
SP

PLATE IX.
Partially resorbed augite and aluminous spinel phenocrysts in sample MV166.
Note the stronger colour of the outer portion of the pyroxene relative to the core. Note also the slight increase in the concentration of plagioclase round the spinel.
Base length of the photograph represents 0.45 cm.
Taken in plane polarised light.

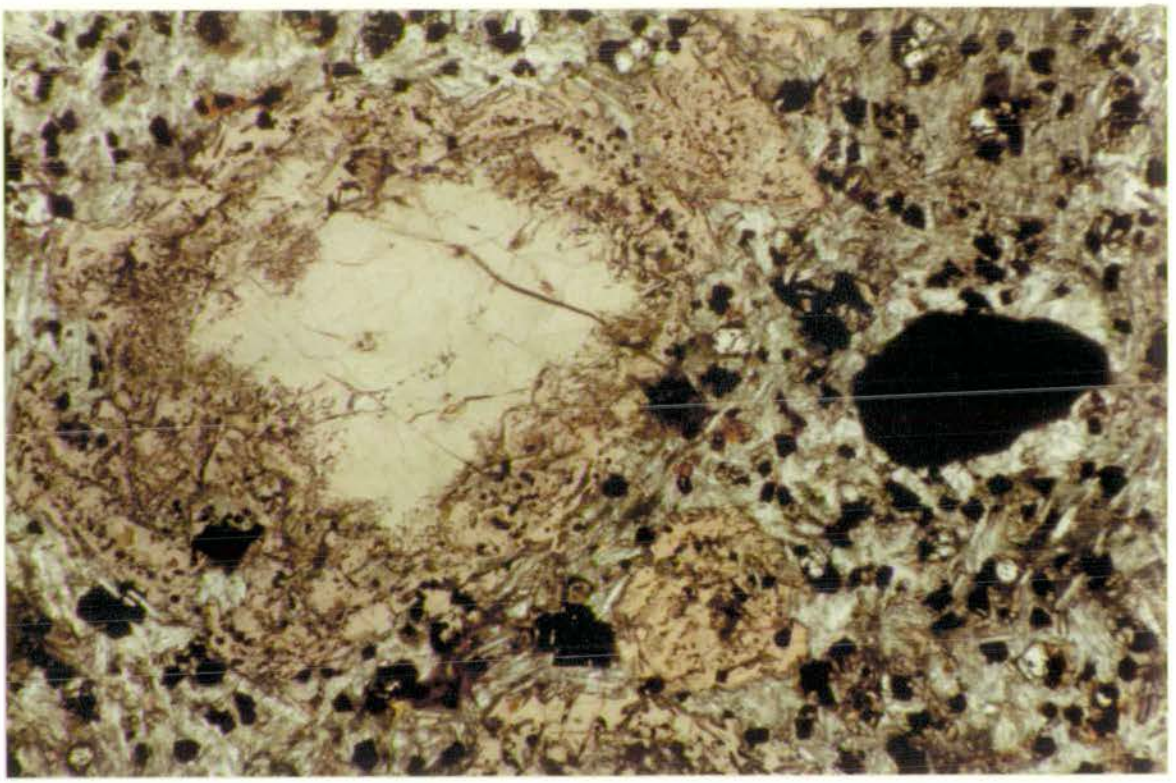

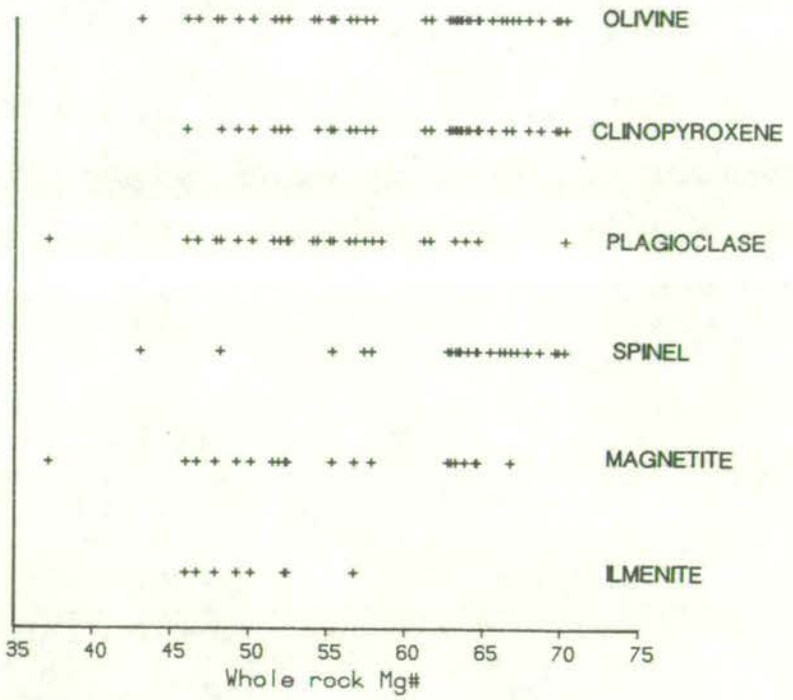

Figure 6-1. Phenocryst occurrence versus whole rock Mg# for the major phenocryst phases. Orthopyroxene occurs in sample MV121A where Mg# is 52.

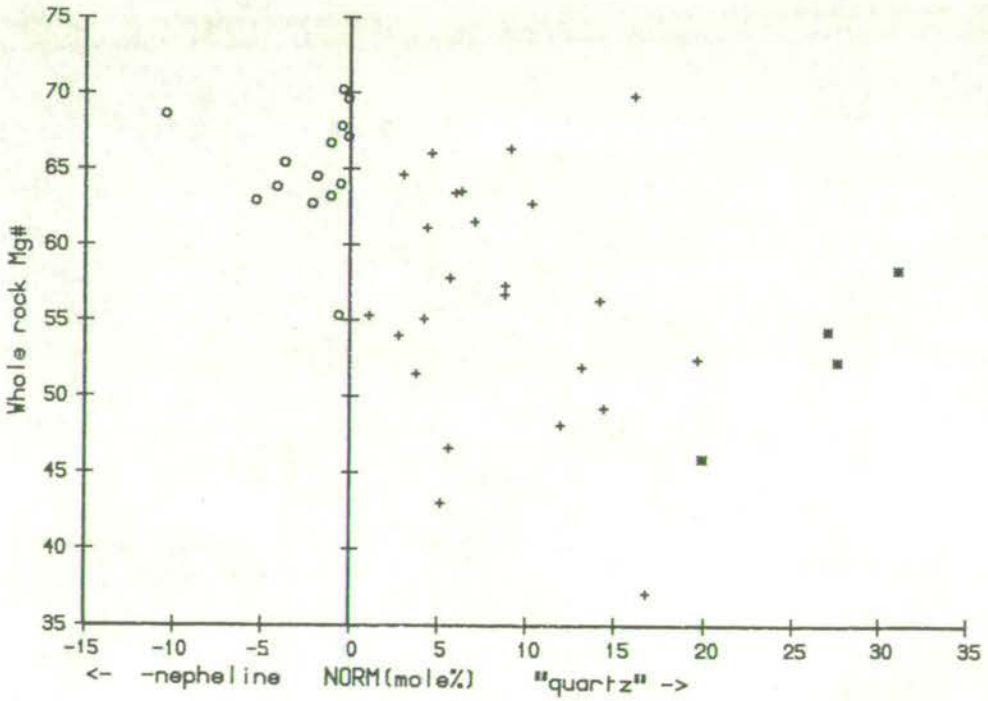

Figure 6-2. Degree of silica saturation versus whole rock Mg#. Normative 'quartz' = normative quartz + quartz in normative hypersthene .
O - Ne-normative, + - Hy-ol-normative, ✱ - Hy-qz-normative.

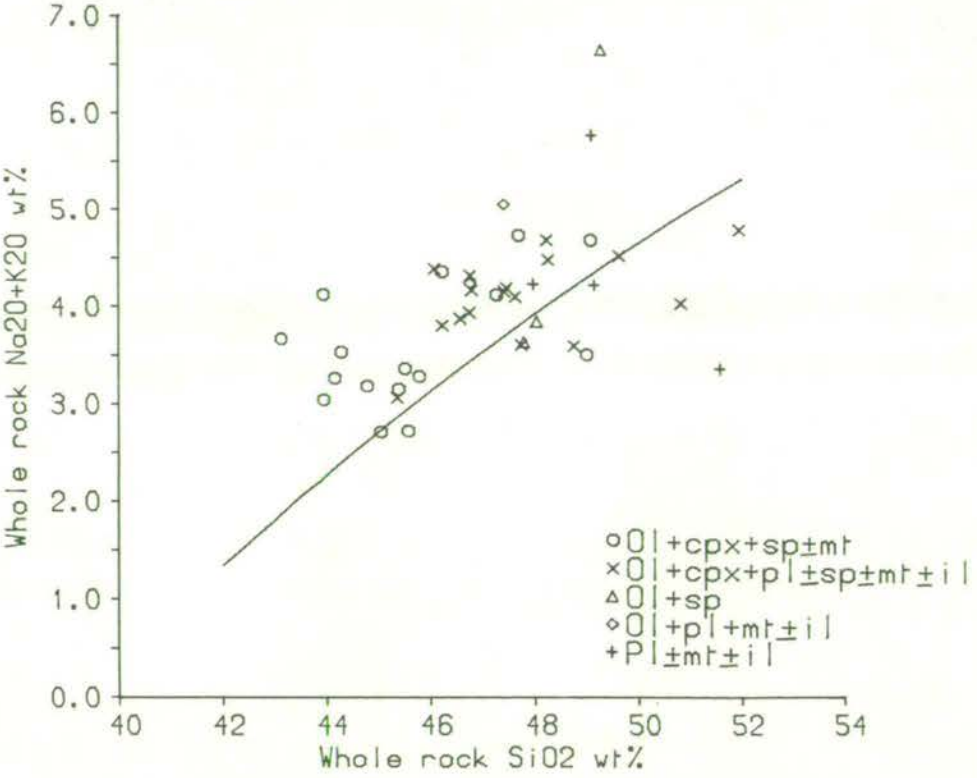

Figure 6-3. Whole rock alkali-silica plot. Individual phenocryst assemblages are distinguished. Dividing line between upper alkaline and lower tholeiitic compositions is from Irvine & Baragar (1971).

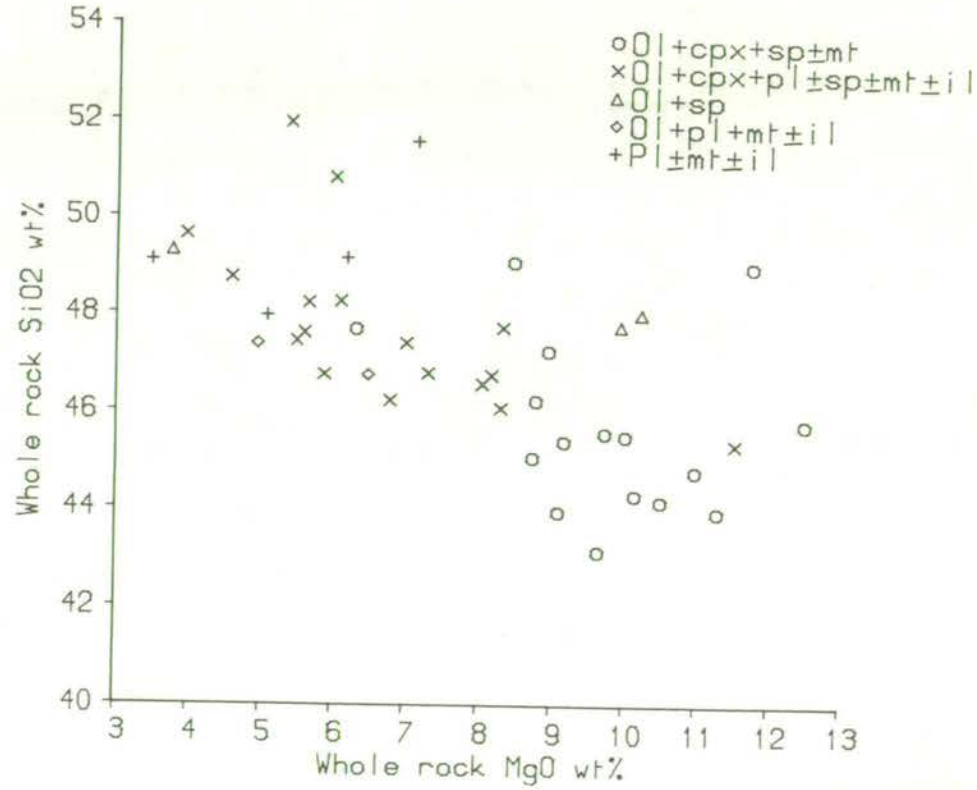

Figure 6-4a. Whole rock MgO wt% versus SiO2 wt%, with individual phenocryst assemblages distinguished.

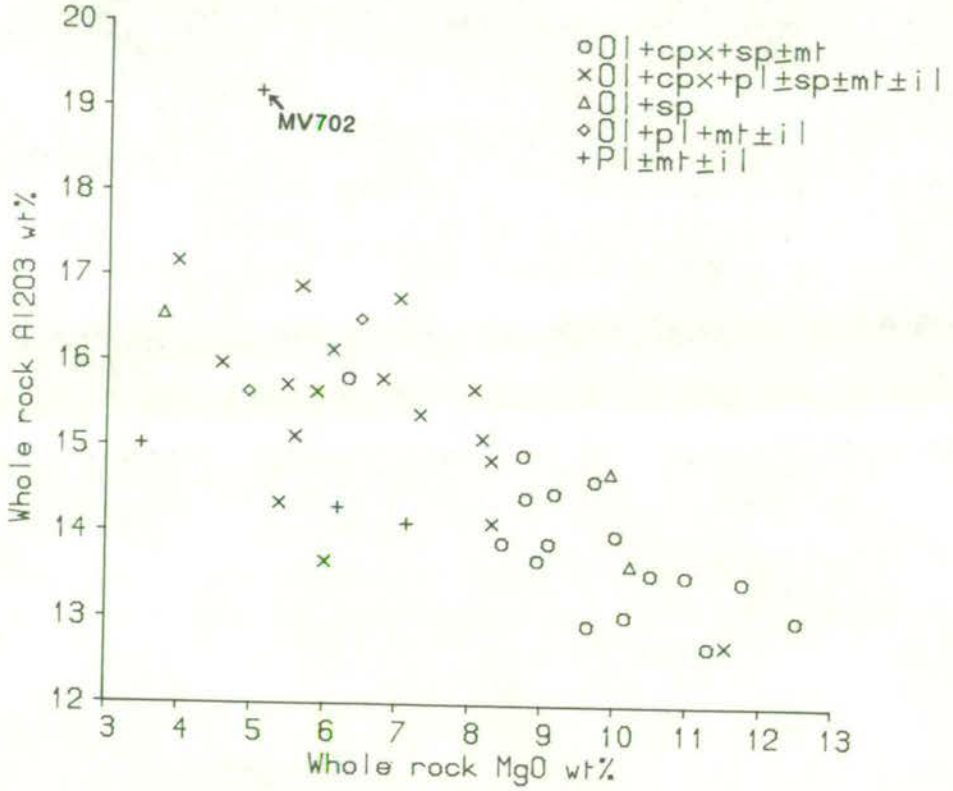

Figure 6-4b. Whole rock MgO wt% versus Al203 wt%, with individual phenocryst assemblages distinguished.

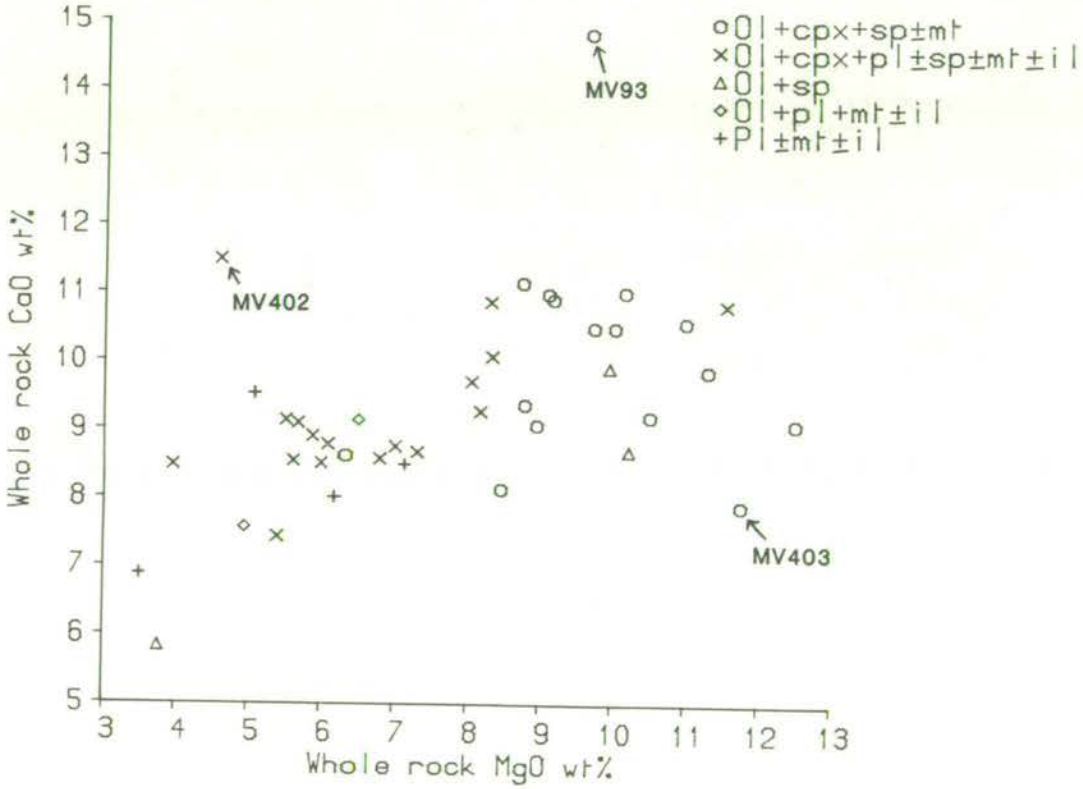

Figure 6-4c. Whole rock MgO wt% versus CaO wt%, with individual phenocryst assemblages distinguished.

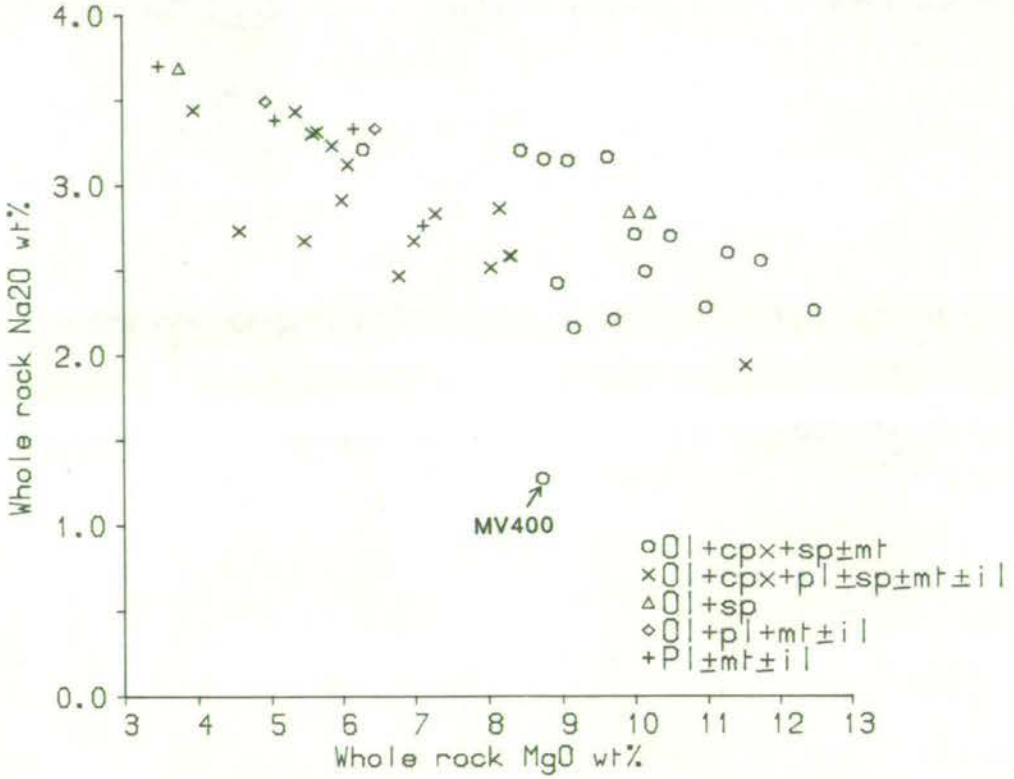

Figure 6-4d. Whole rock MgO wt% versus Na20 wt%, with individual phenocryst assemblages distinguished.

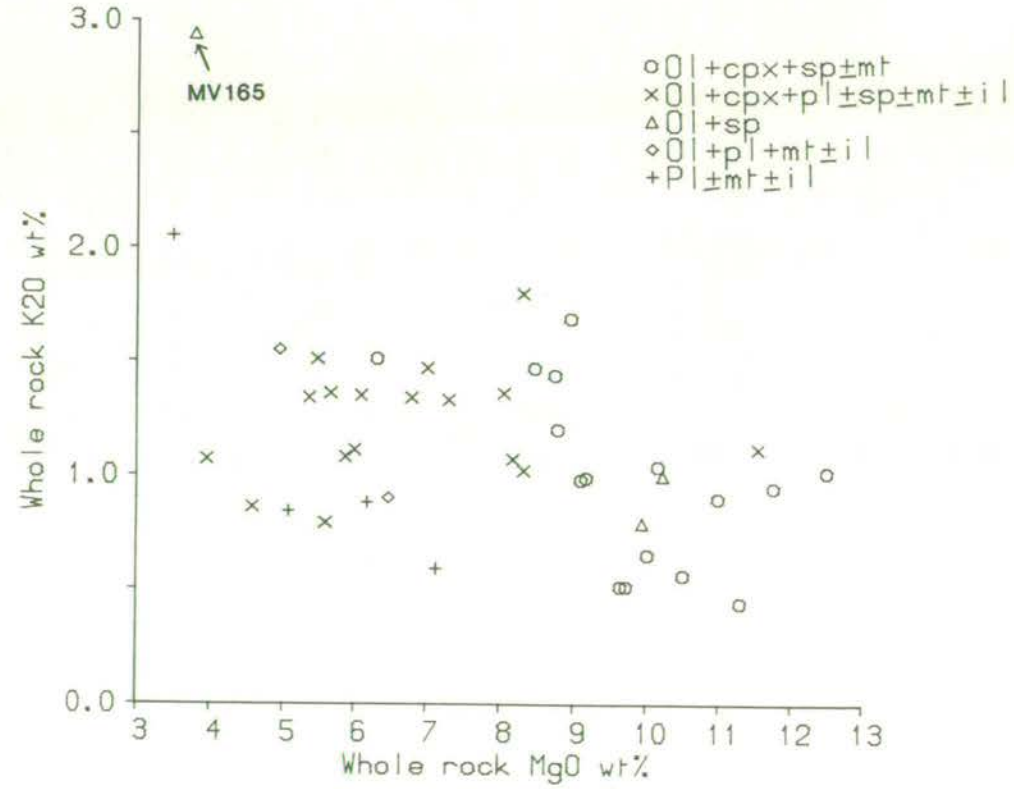

Figure 6-4e. Whole rock MgO wt% versus K20 wt%, with individual phenocryst assemblages distinguished.

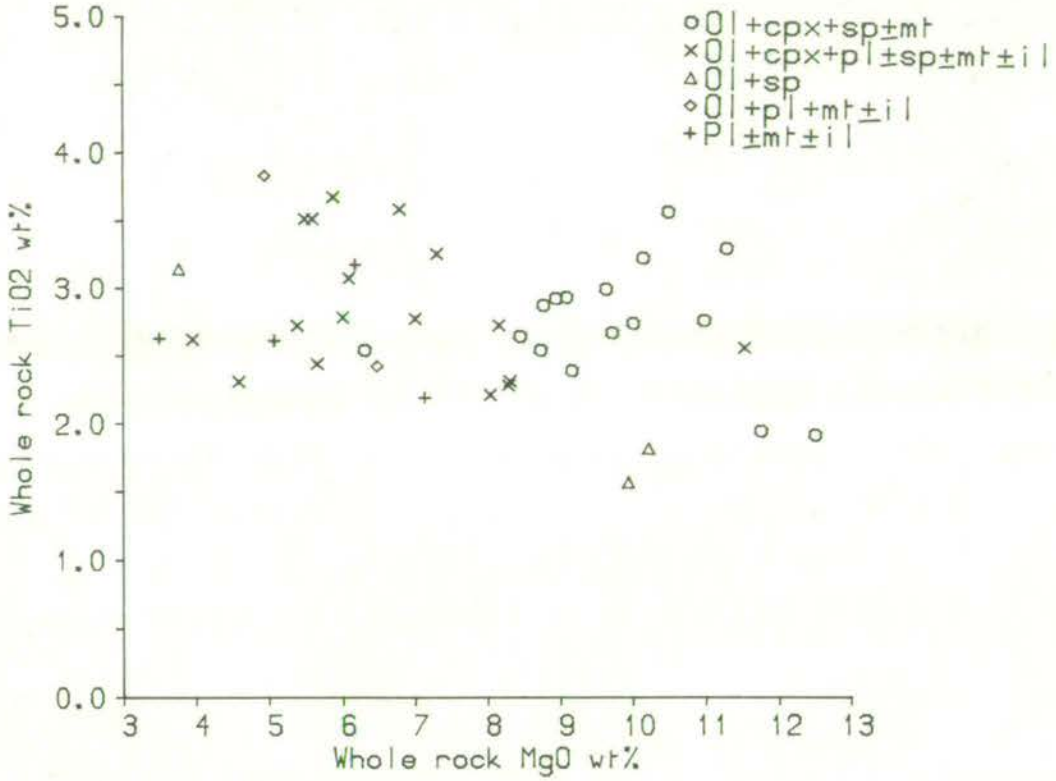

Figure 6-4f. Whole rock MgO wt% versus TiO2 wt%, with individual phenocryst assemblages distinguished.

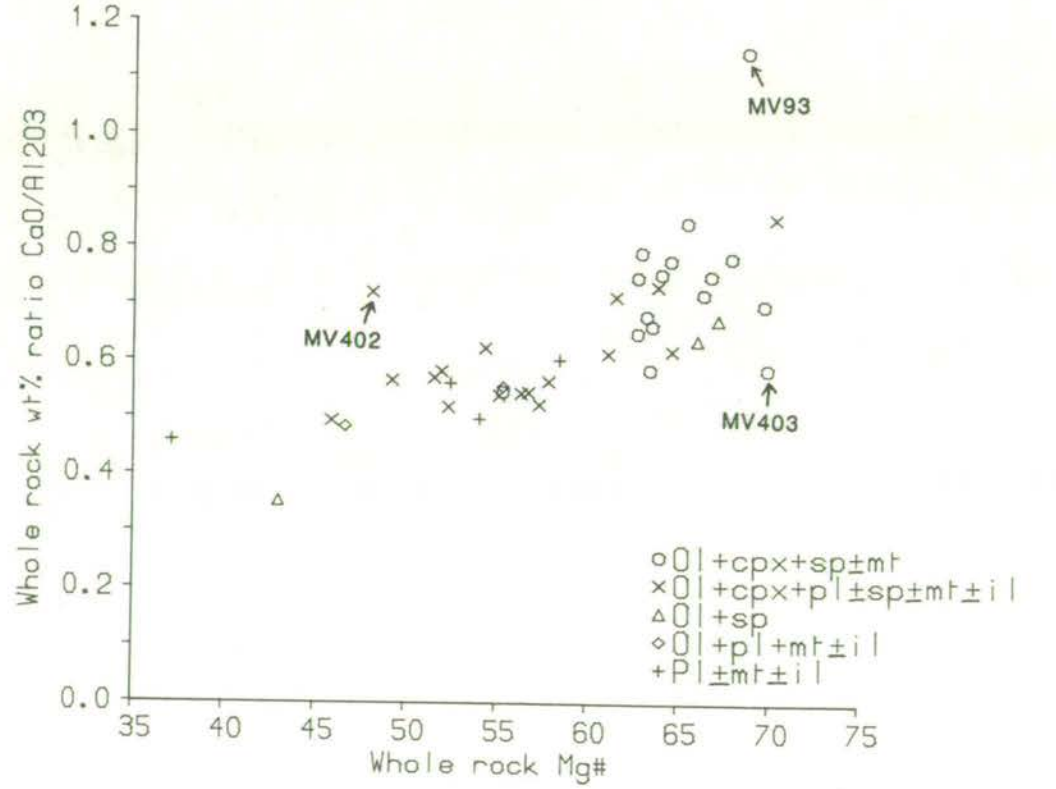

Figure 6-5. CaO/Al2O3 wt% ratio versus whole rock Mg#, with individual phenocryst assemblages distinguished.

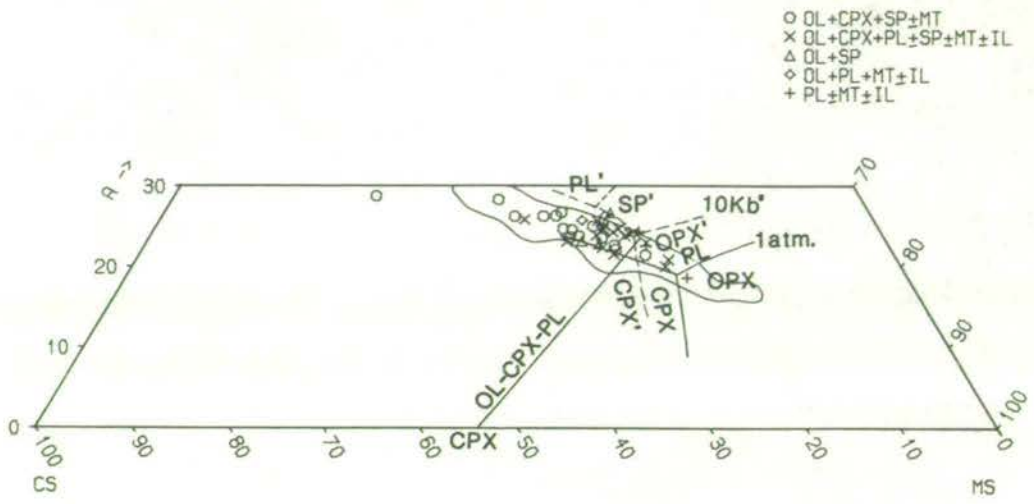

Figure 6-6. Projection from olivine onto CS-MS-A, with individual phenocryst assemblages distinguished. Phase boundaries from O'Hara (1968). Circled field marks the position of the glasses coexisting with olivine + clinopyroxene + plagioclase from the 1 atm. experiments in the present study.

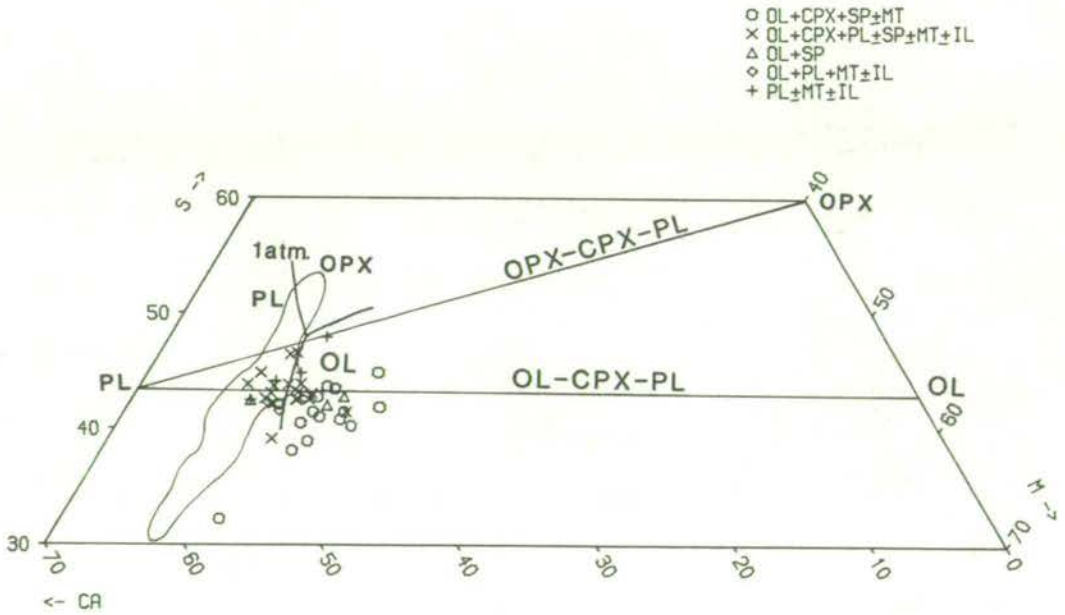

Figure 6-7. Projection from diopside onto CA-M-S, with individual phenocryst assemblages distinguished. Phase boundaries from Jamieson (1970). Circled field marks the position of the glasses coexisting with olivine + clinopyroxene + plagioclase from the 1 atm. experiments in the present study.

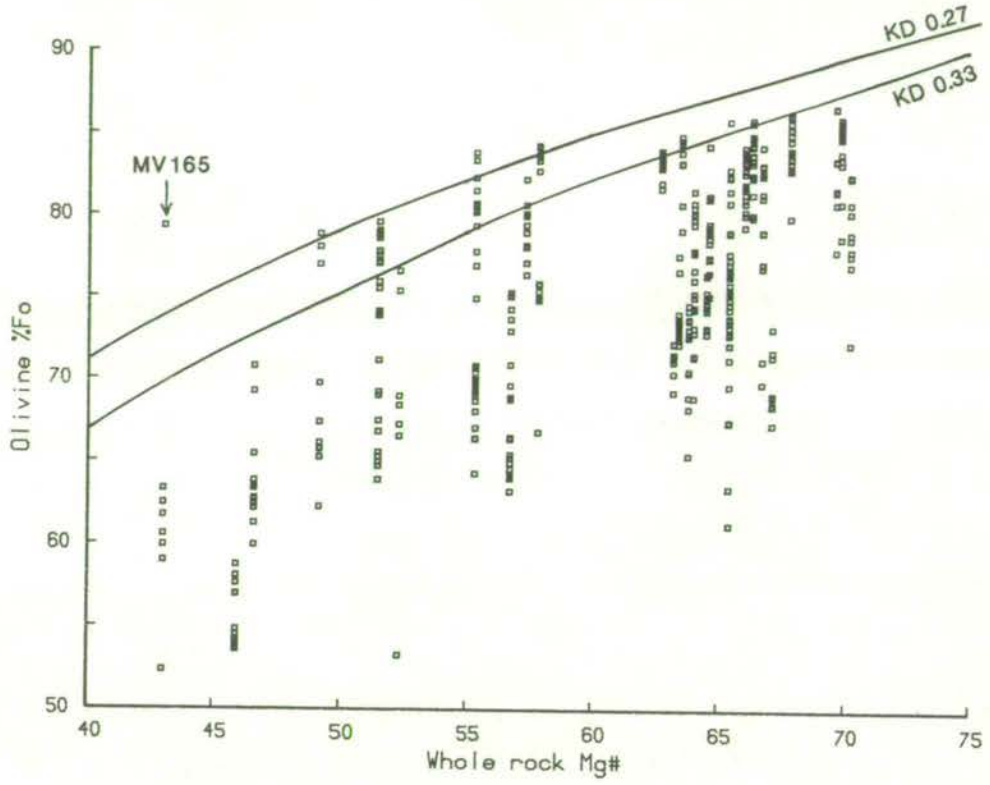

Figure 6-8. Forsterite content of olivine phenocryst 'cores' versus whole rock Mg#. Labelled curves mark values of the olivine-liquid Fe^{2+}-Mg KD.

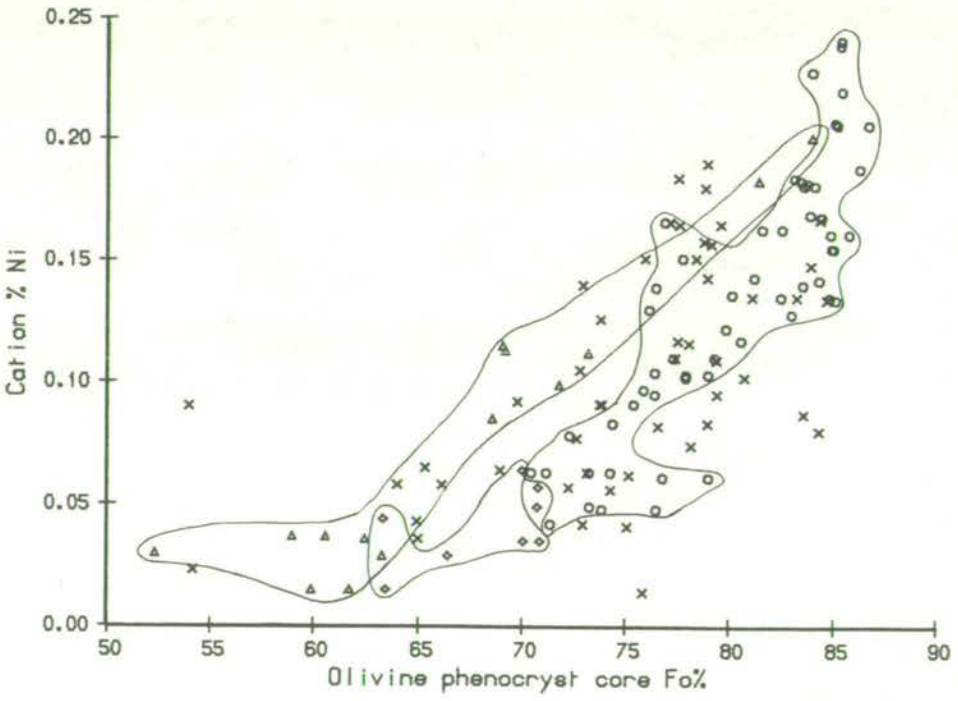

Figure 6-9. Olivine phenocryst 'cores' ; Ni variation with forsterite content. Individual phenocryst assemblages are distinguished.

- O OL+CPX+SP±MT (circled)
- X OL+CPX+PL±SP±MT±IL
- △ OL+SP (circled)
- ◇ OL+PL+MT±IL (circled)

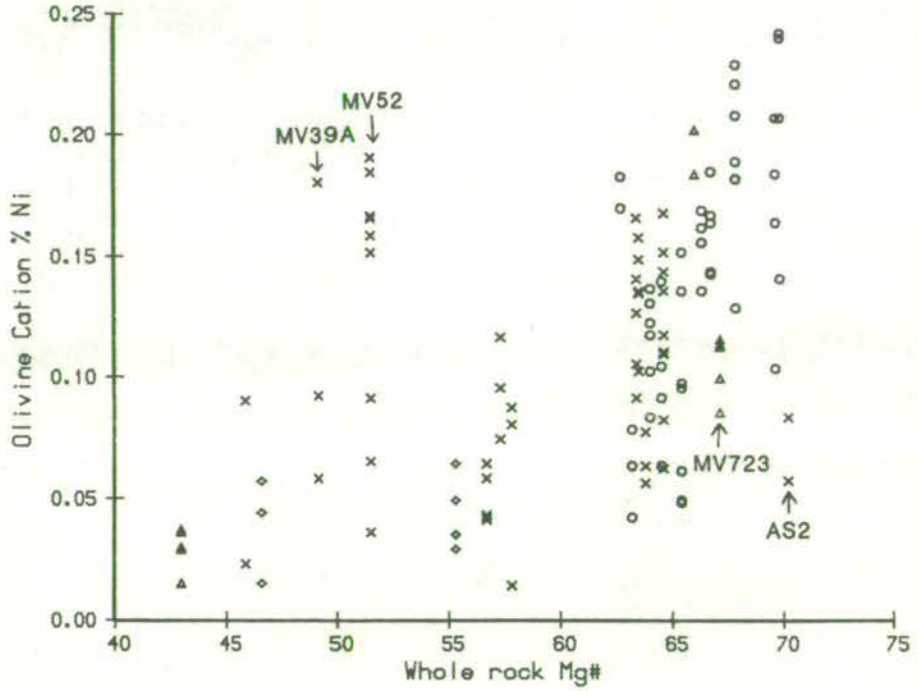

Figure 6-10. Ni content of olivine phenocryst 'cores' versus whole rock Mg#, with individual phenocryst assemblages distinguished.

○ OL+CPX+SP±MT
× OL+CPX+PL±SP±MT±IL
△ OL+SP
◇ OL+PL+MT±IL

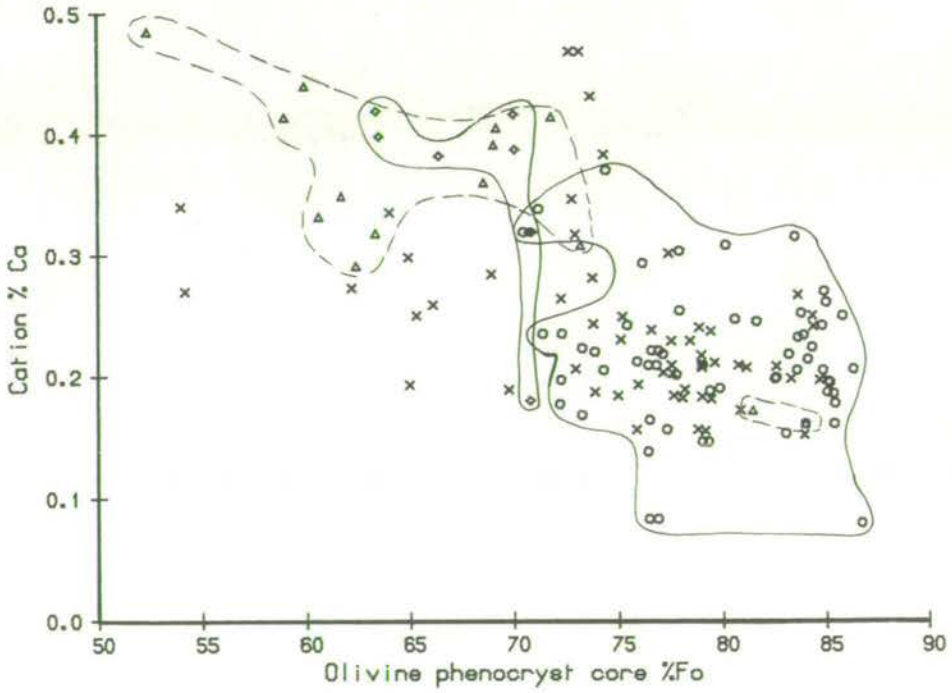

Figure 6-11. The Ca content of olivine phenocryst 'cores' versus the olivine forsterite content. Individual phenocryst assemblages are distinguished.

○ OL+CPX+SP±MT (circled)
× OL+CPX+PL±SP±MT±IL
△ OL+SP (circled by dashed lines)
◇ OL+PL+MT±IL (circled)

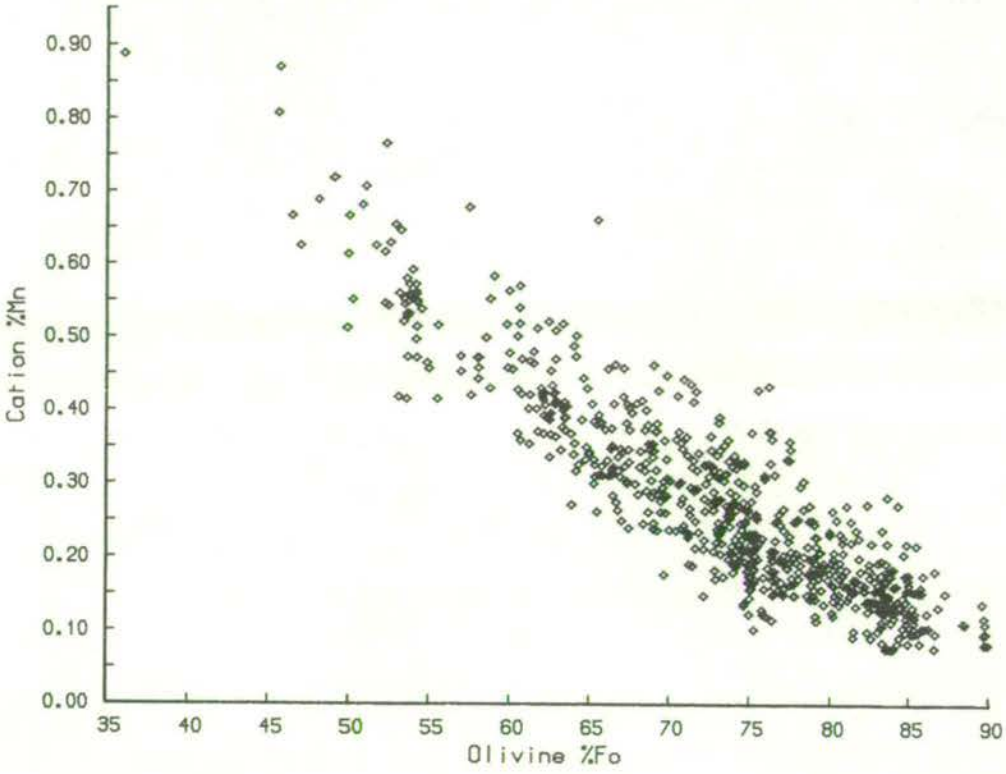

Figure 6-12. Variation in Mn content of olivines with forsterite content.

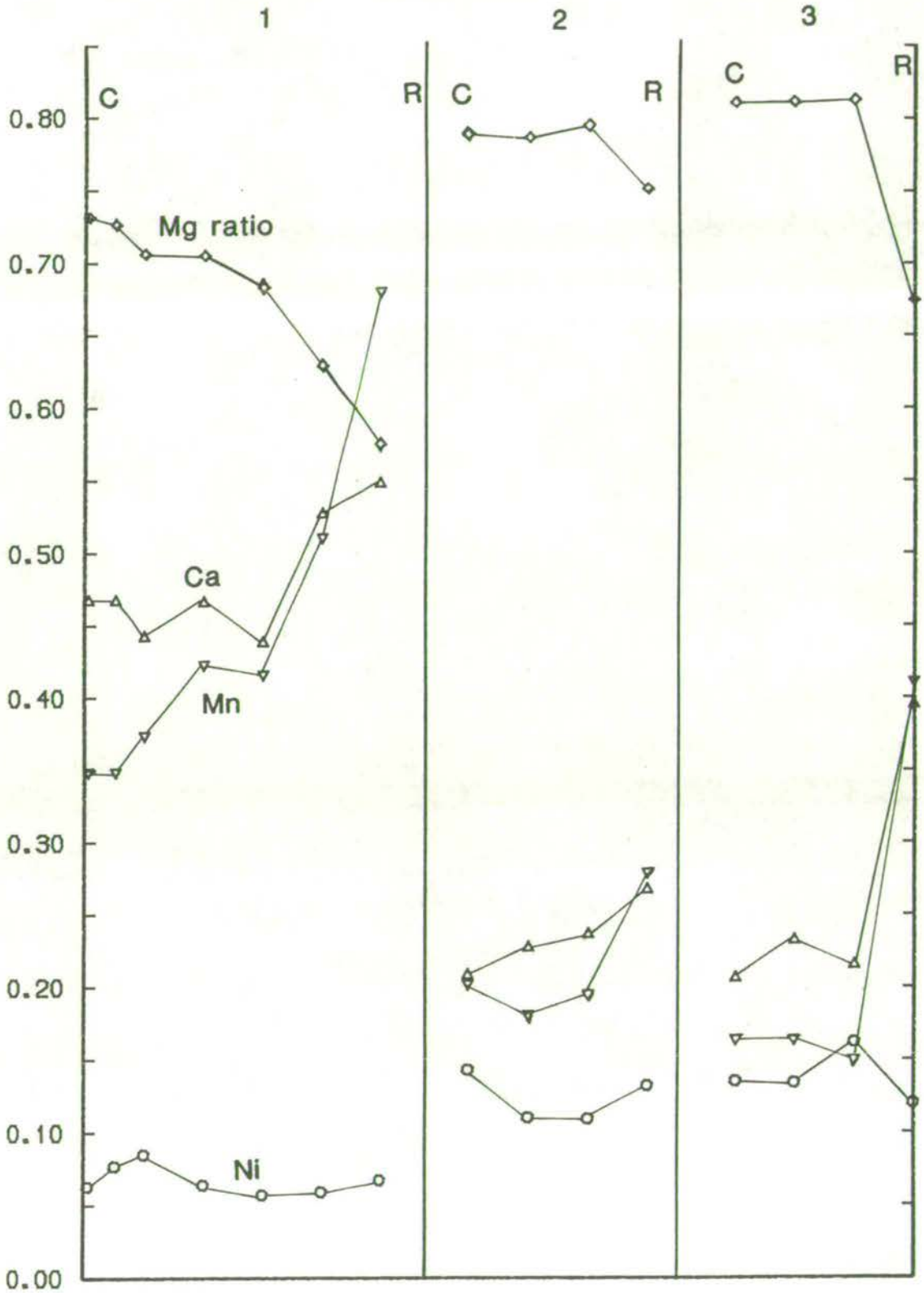

Figure 6-13. Partial composition profiles across three olivine phenocrysts, from core (left) to rim (right). Not to scale.

1. MV520 2. 36017 3. 36017

◇ $Mg/(Mg+Fe^{2+})$ cation ratio

▽ Mn
△ Ca
○ Ni
} cation %

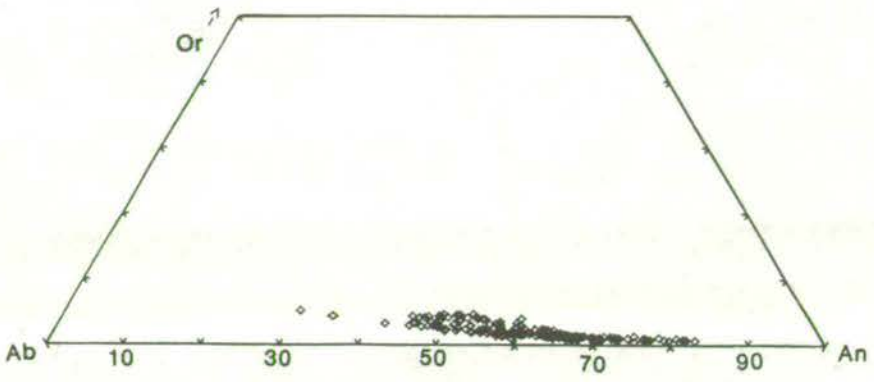

Figure 6-14. Range of plagioclase phenocryst core compositions.

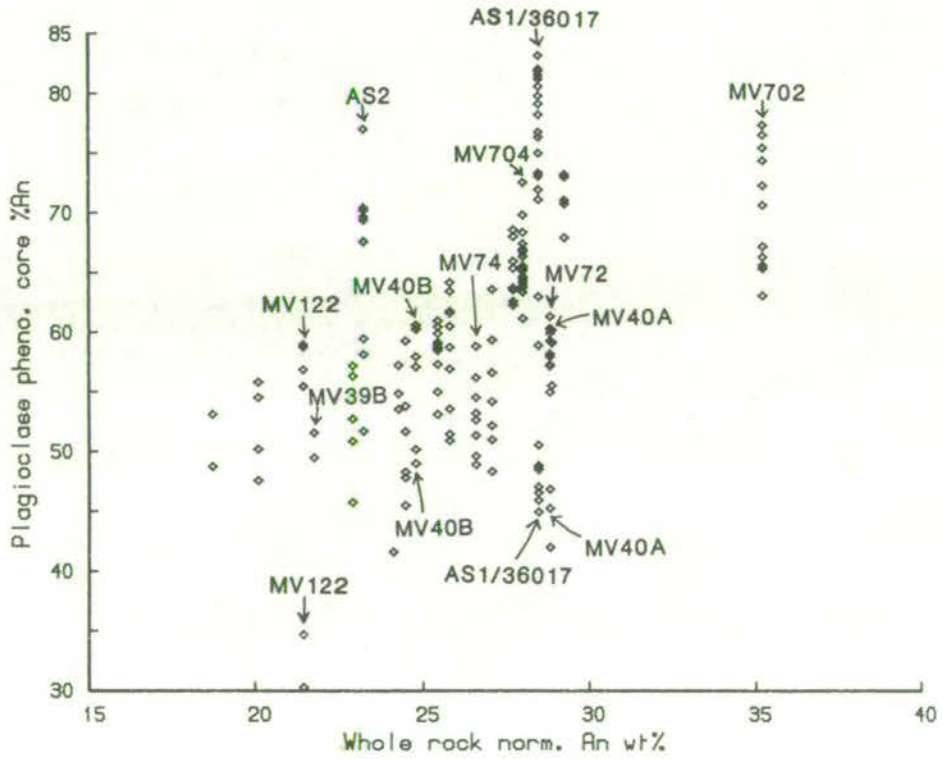

Figure 6-15. Whole rock normative anorthite wt% versus plagioclase phenocryst core compositions .

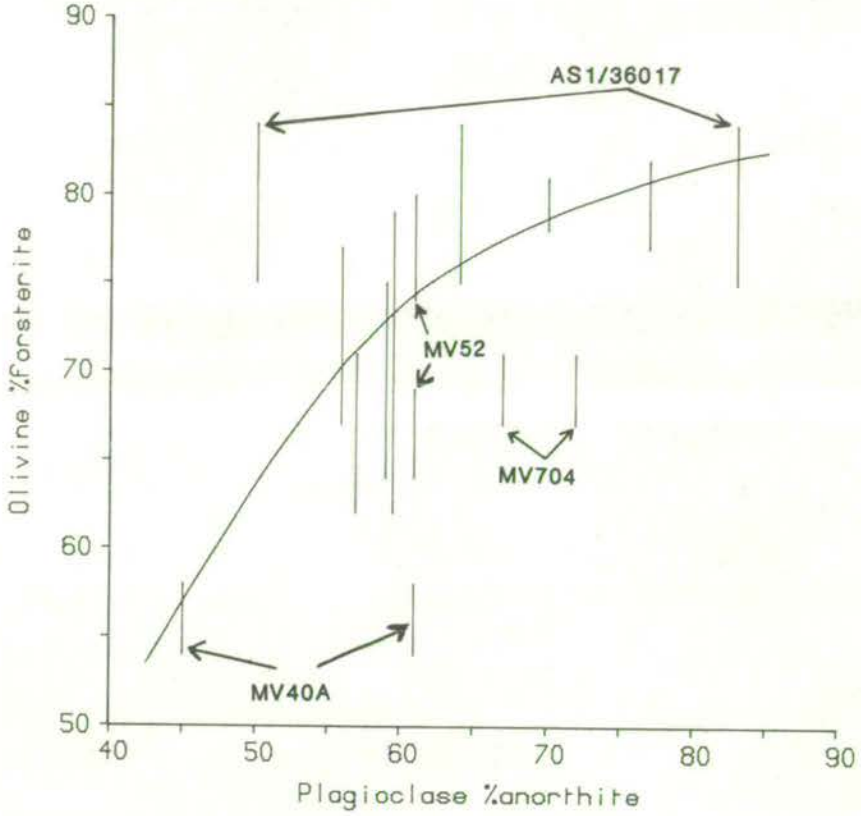

Figure 6-16. Ranges of olivine phenocryst core compositions versus the most calcic plagioclase phenocryst core compositions. The curve represents a tentative equilibrium relation.

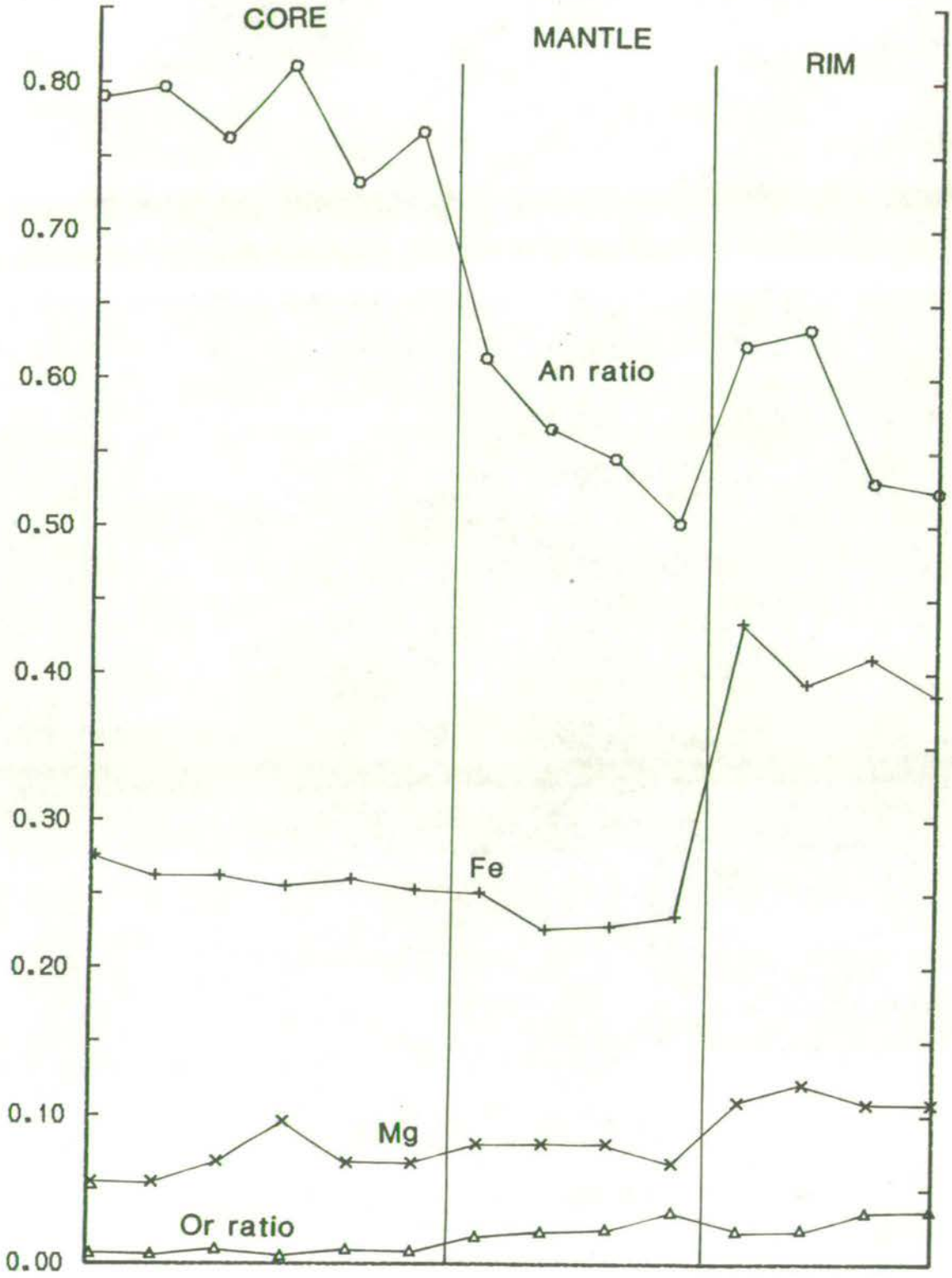

Figure 6-17. Partial profile across an euhedral complete plagioclase from core (left) to rim (right), from sample AS1/36017. Not to scale.

O An ratio, Ca/(Ca+Na+K) cation ratio

+ Fe
× Mg
} cation %

△ Or ratio, K/(Ca+Na+K) cation ratio

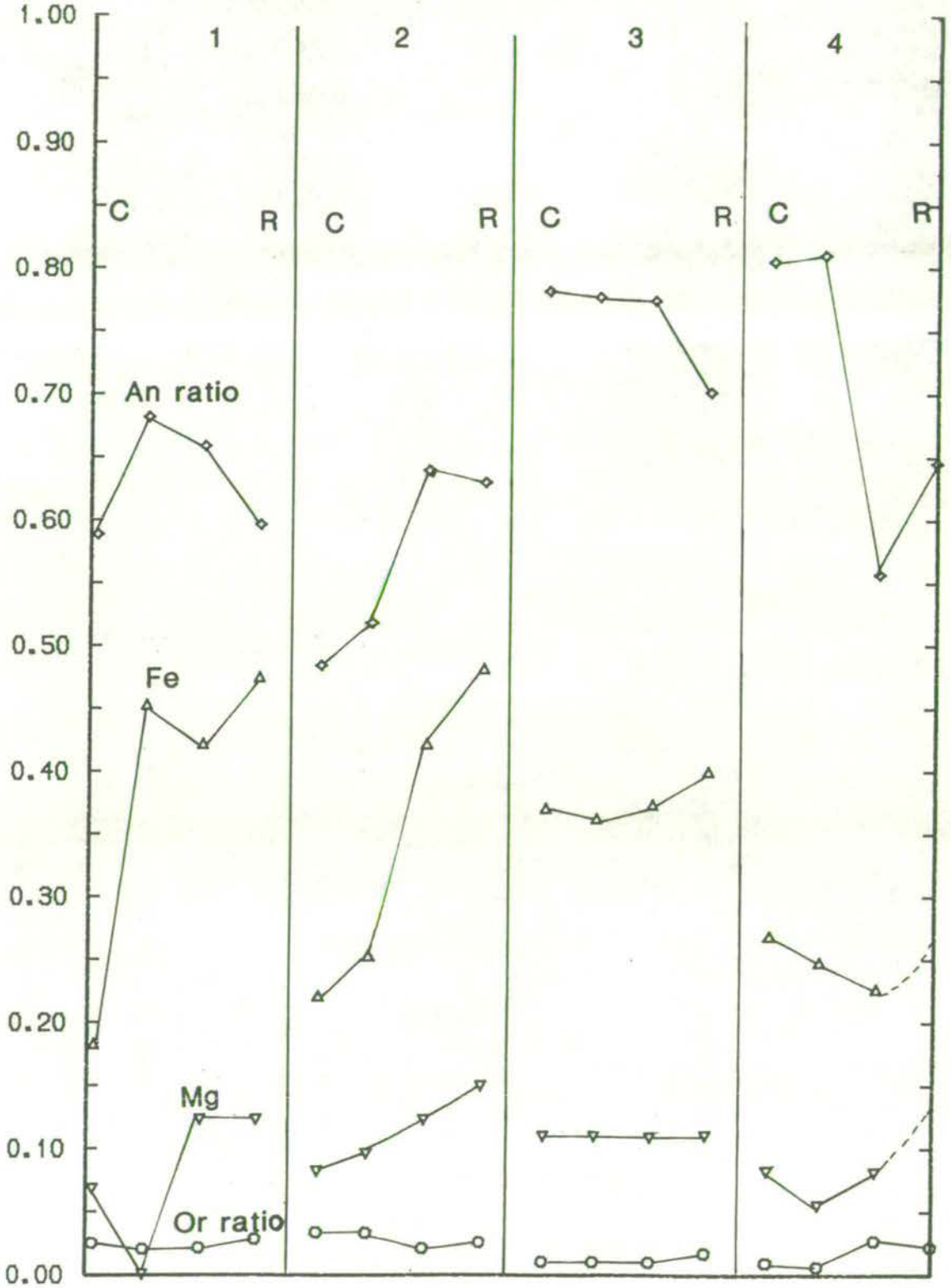

Figure 6-18. Partial profiles across four plagioclase phenocrysts from core (left) to rim (right). All are from sample AS1/36017. Not to scale.

◇ An ratio, Ca/(Ca+Na+K) cation ratio

△ Fe

▽ Mg

} cation %

○ Or ratio, K/(Ca+Na+K) cation ratio

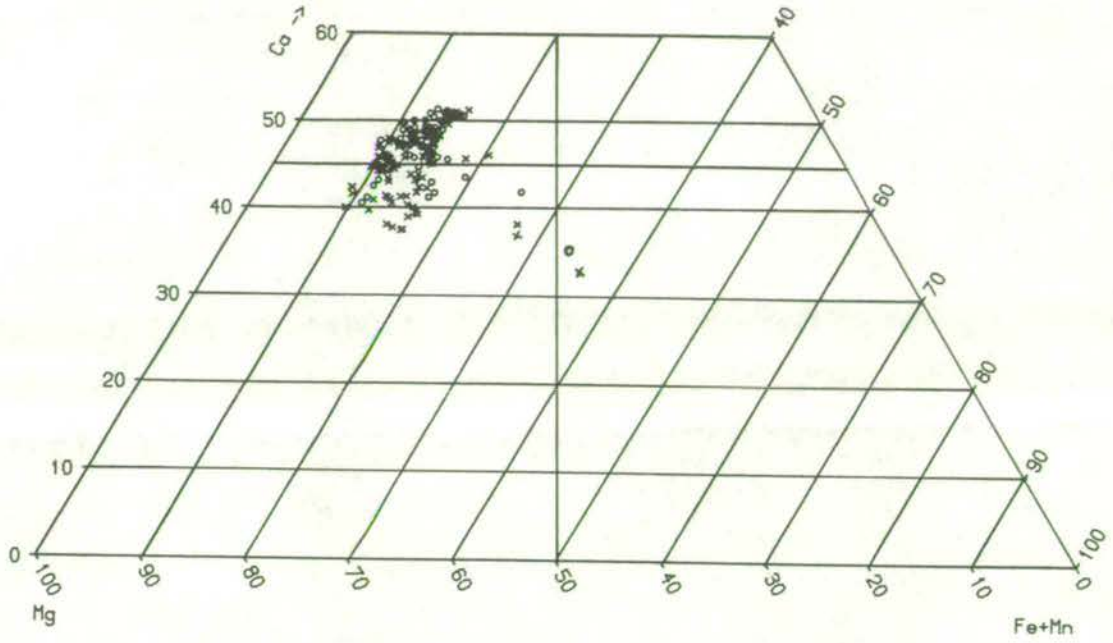

Figure 6-19. Compositional range of clinopyroxenes.
O phenocryst cores, X phenocryst rims and groundmass pyroxenes.

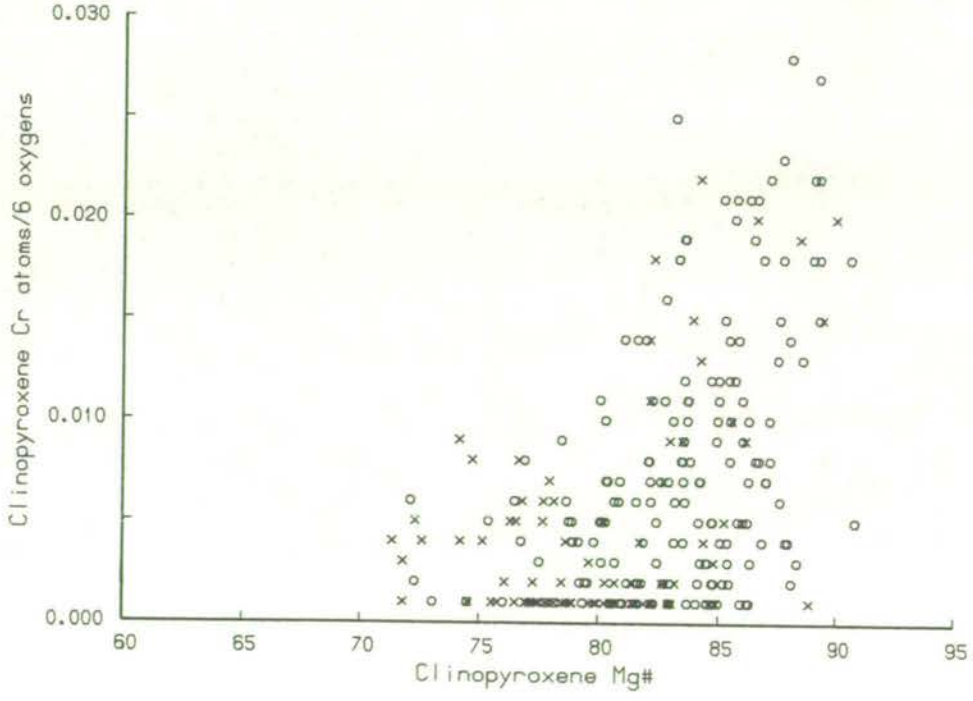

Figure 6-20. Clinopyroxene Mg#,[100*Mg/(Mg+Fe^{2+})], versus Cr content.
O phenocryst cores, X phenocryst rims and groundmass pyroxenes.

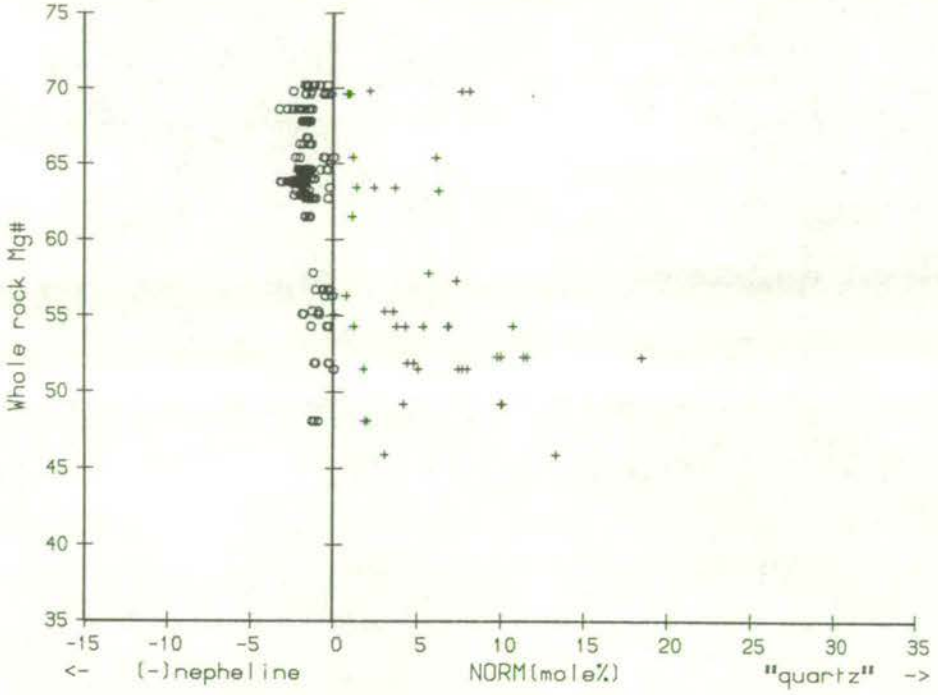

Figure 6-21. Normative character of augite phenocryst cores plotted against their host rock Mg#.
o Ne-normative augite
+ Hy-normative augite (calculated as equivalent quartz + olivine).

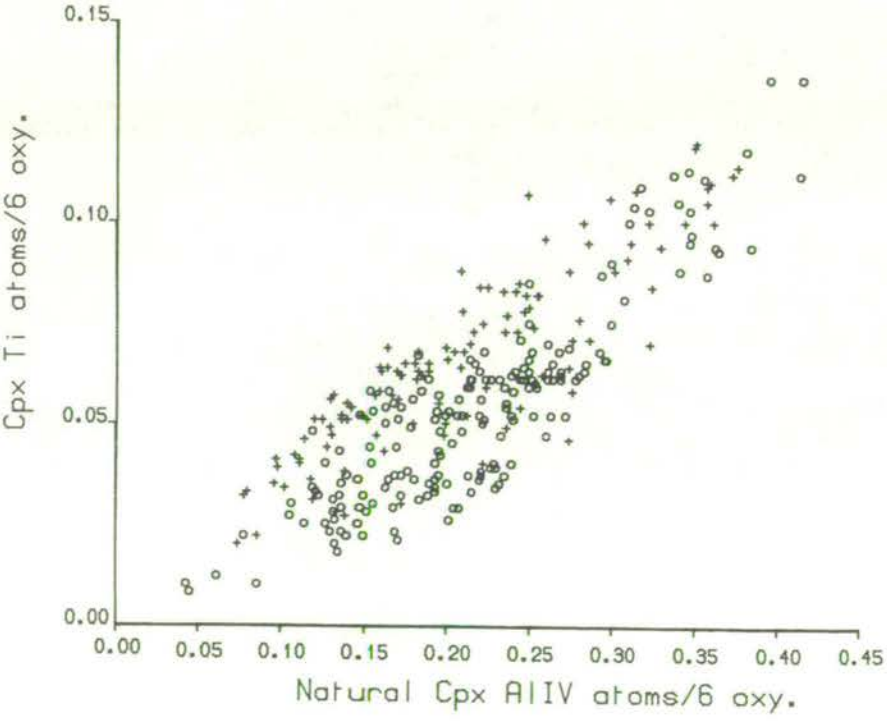

Figure 6-22. Ti versus AlIV in clinopyroxenes.
O phenocryst cores, + phenocryst rims and groundmass pyroxenes.

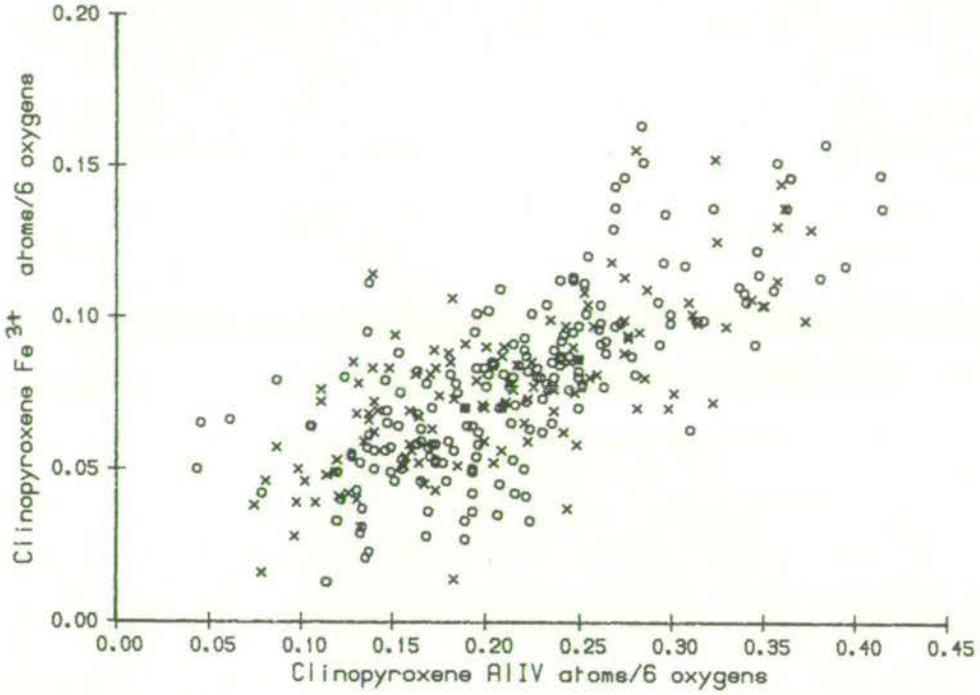

Figure 6-23. Fe^{3+} versus AlIV in clinopyroxenes.
O phenocryst cores, X phenocryst rims and groundmass pyroxenes.

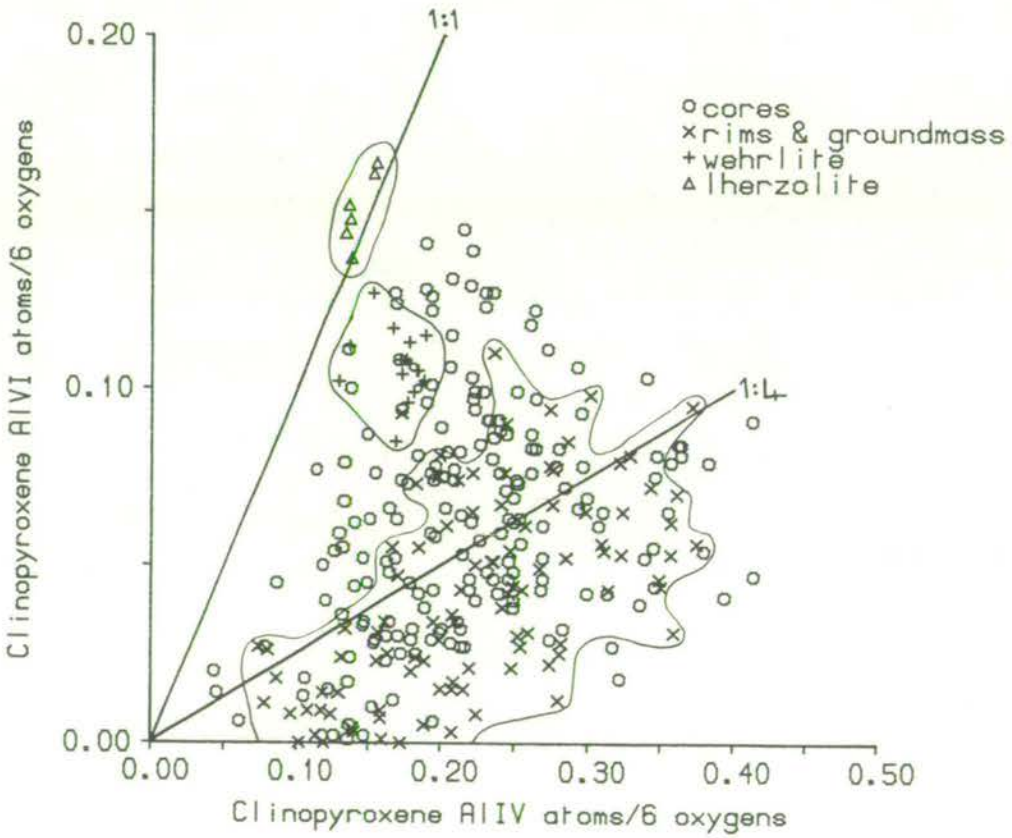

Figure 6-24. AlVI versus AlIV in clinopyroxenes.
Circled fields are for the pyroxenes in the wehrlite, lherzolite, and rims & groundmass groups.

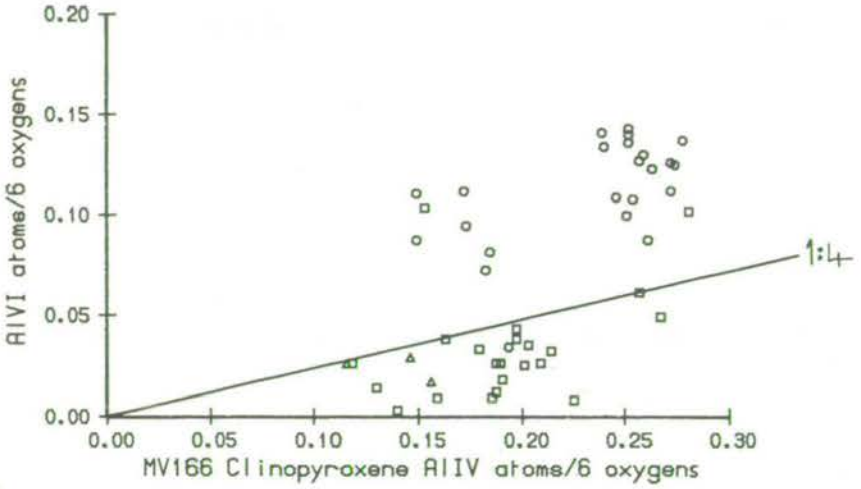

Figure 6-25. AlVI versus AlIV in clinopyroxenes from sample MV166.
○ phenocryst cores, □ phenocryst rims,
△ groundmass pyroxenes.

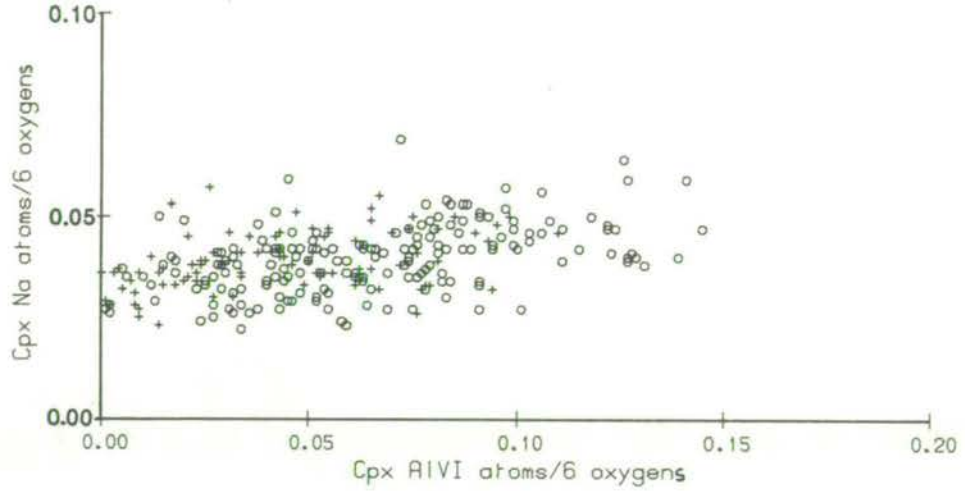

Figure 6-26a. Na versus AlVI in clinopyroxenes.
○ phenocryst cores, + phenocryst rims and groundmass pyroxenes.

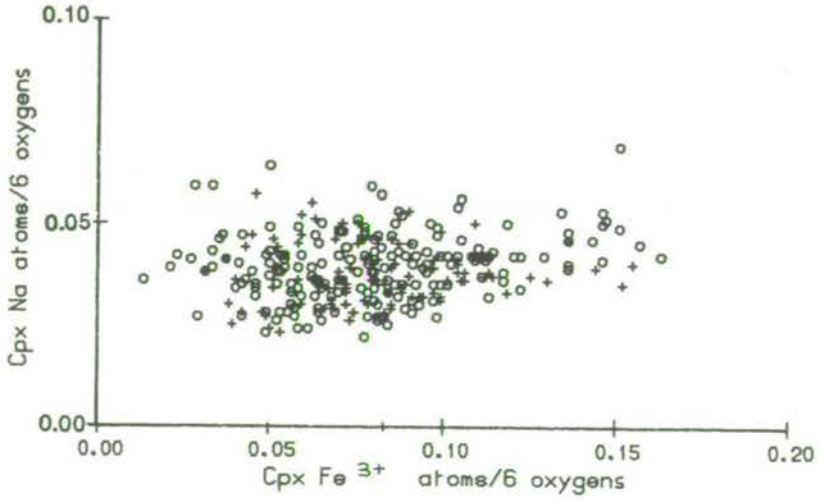

Figure 6-26b. Na versus Fe^{3+} in clinopyroxenes.
○ phenocryst cores, + phenocryst rims and groundmass pyroxenes.

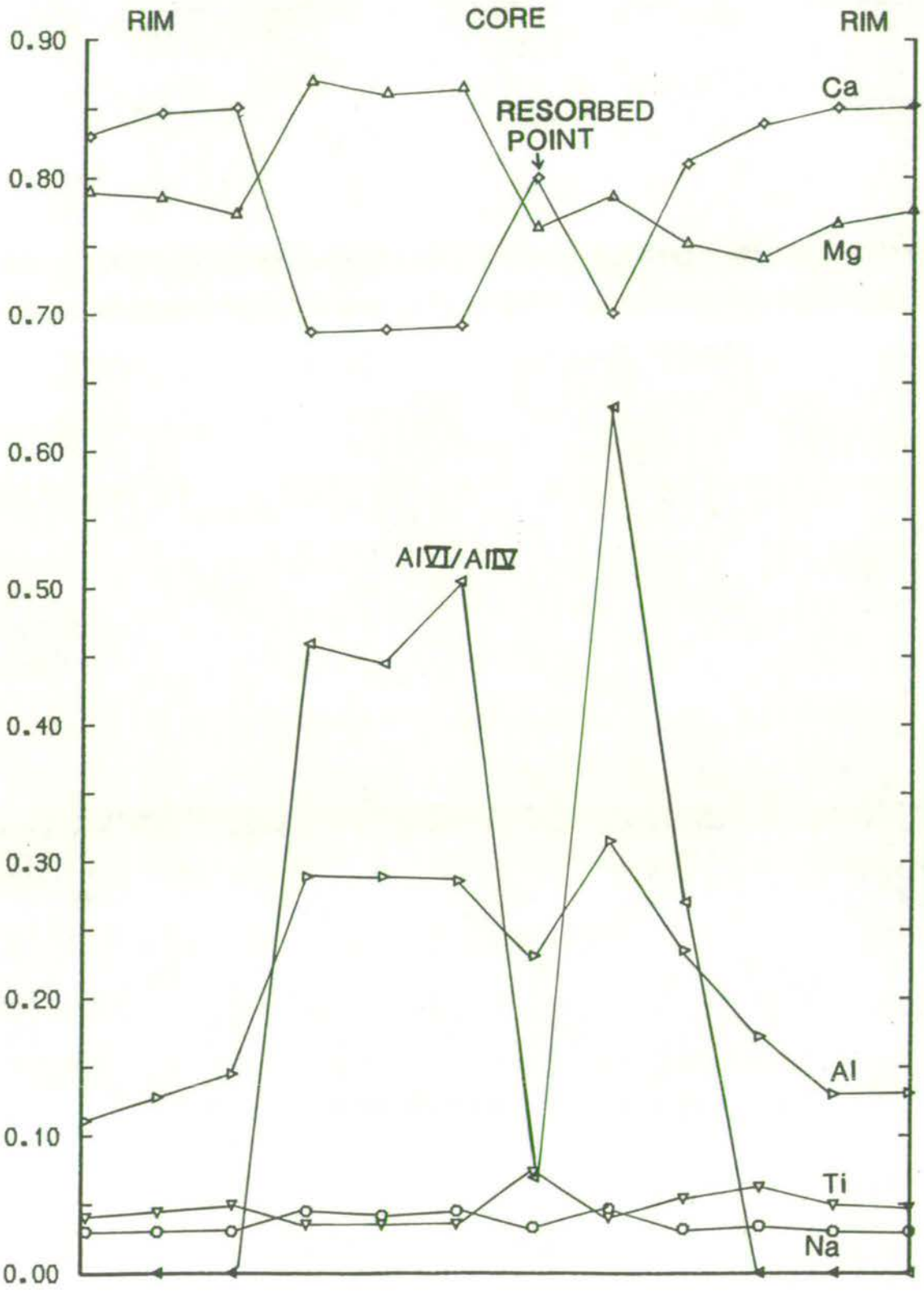

Figure 6-27. Rim to rim profile of a clinopyroxene phenocryst in sample MV52. Not to scale.

◇ Ca
△ Mg
▷ Al
▽ Ti
○ Na
} cations/6 oxygens

◁ AlVI/AlIV cation ratio

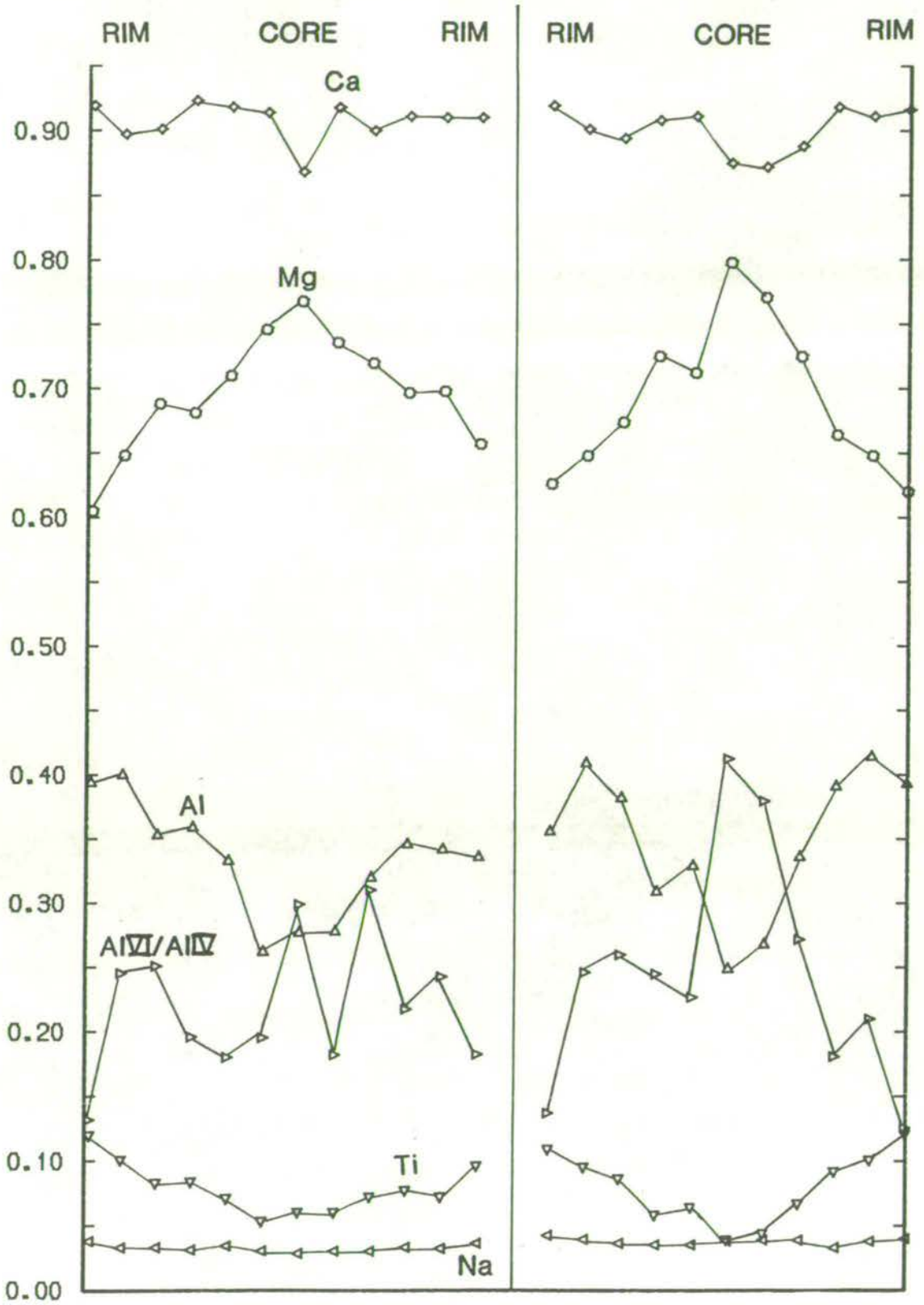

Figure 6-28. Two rim to rim profiles across clinopyroxene phenocrysts in sample MV521. Not to scale.

◇ Ca
○ Mg
△ Al
▽ Ti
◁ Na
} cations/6 oxygens

▷ AlVI/AlIV cation ratio

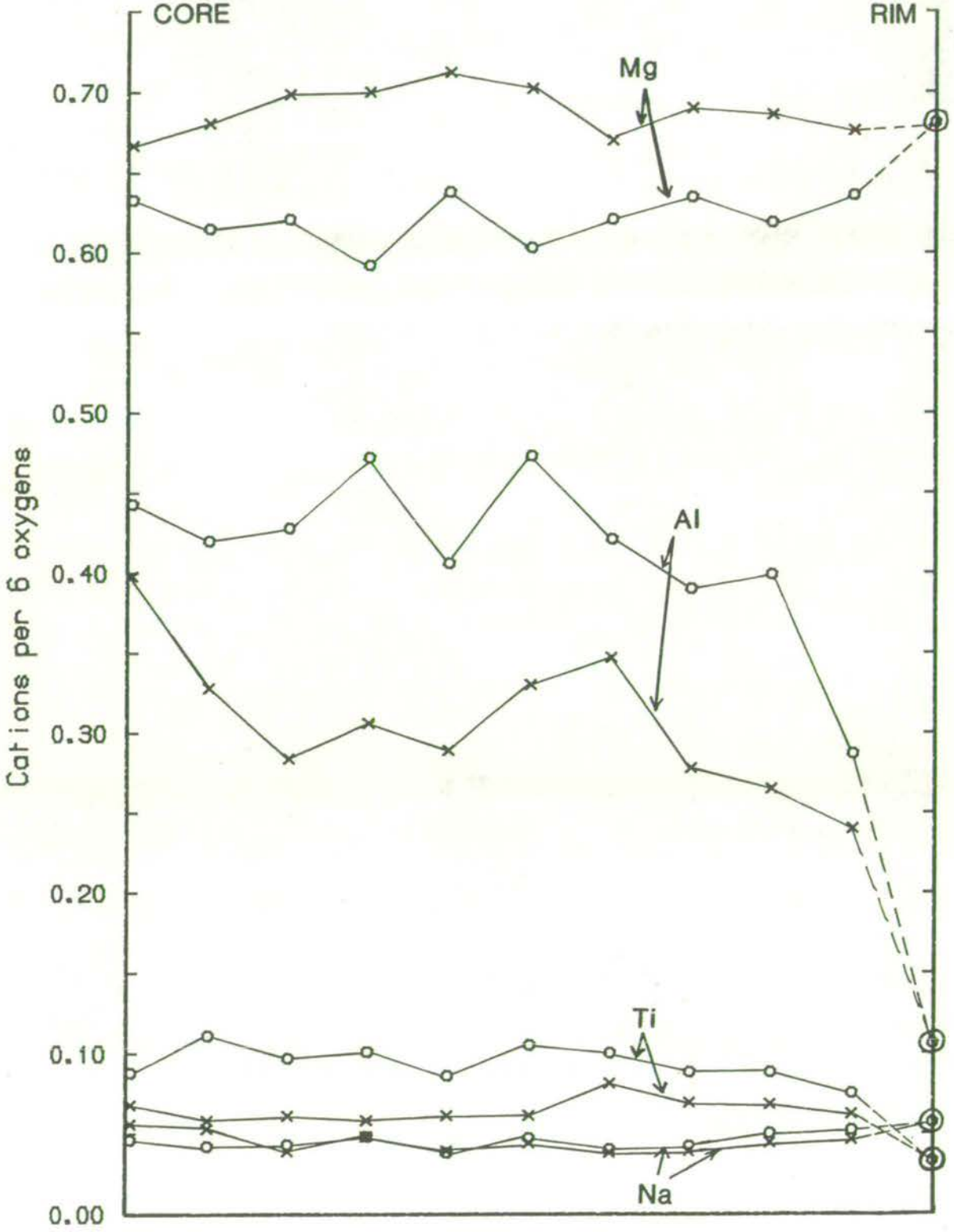

Figure 6-29. Partial profile across an hourglass clinopyroxene phenocryst in sample MV520, from core (left) to rim (right). Not to scale.
Points have been analysed in neighbouring sectors.
X light sector
O dark sector
◎ pale green overgrowth to both sectors.
Concentrations are in cations/6 oxygens.

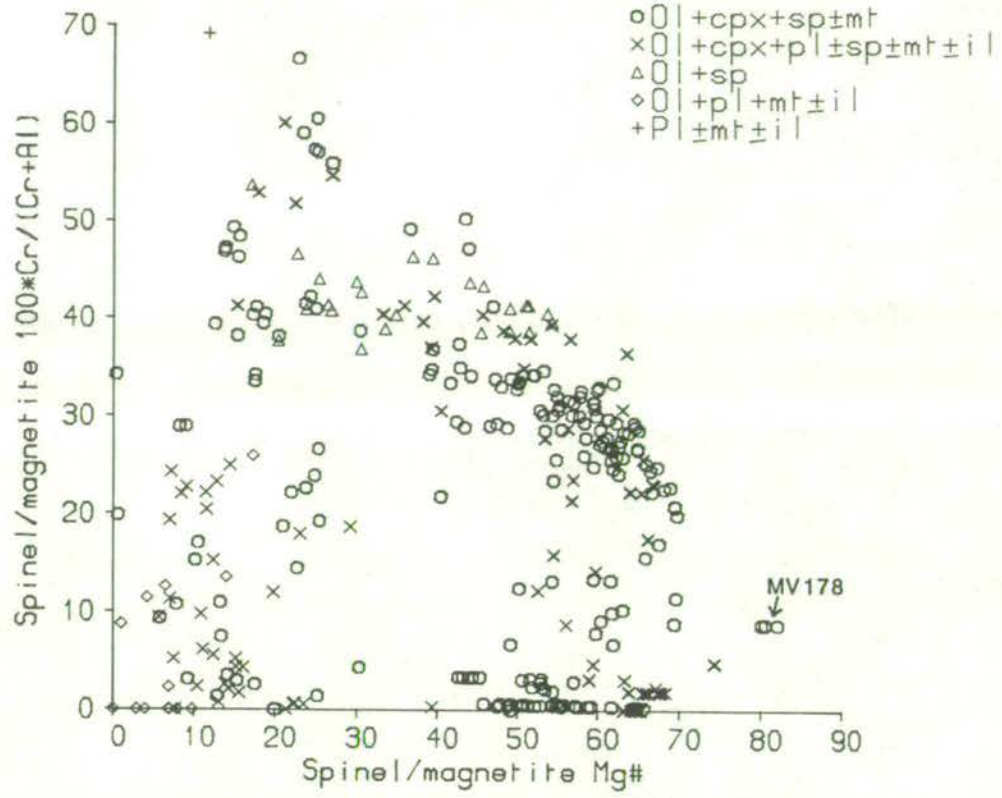

Figure 6-30. Spinel phase Mg#,[100*Mg/(Mg+Fe^{2+}) ratio], versus 100*Cr/(Cr+Al) ratio.
Individual phenocryst assemblages are distinguished.

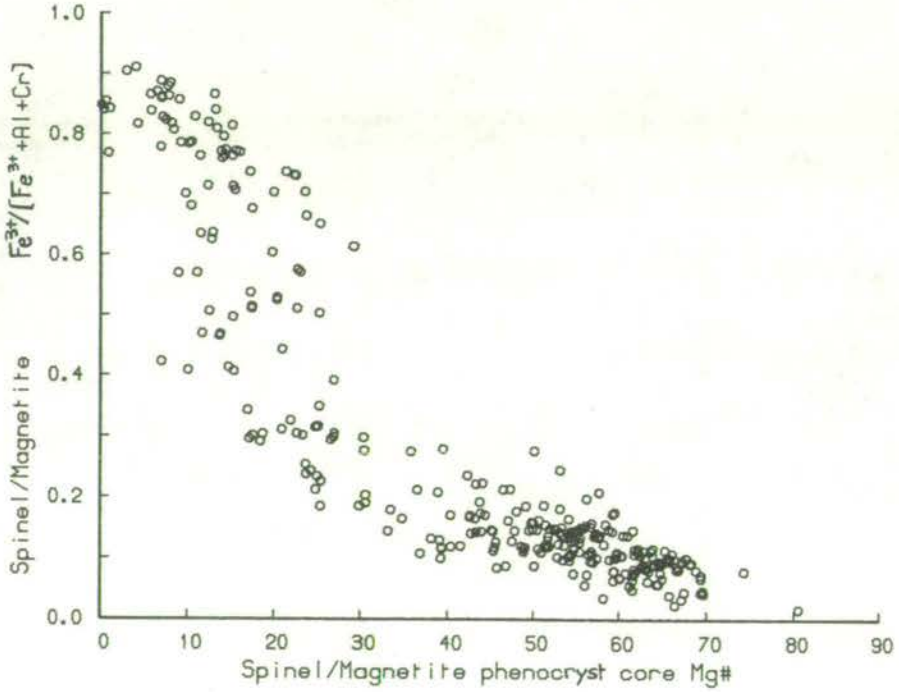

Figure 6-31. Spinel phase phenocryst cores, Mg# versus $Fe^{3+}/(Cr+Al+Fe^{3+})$.

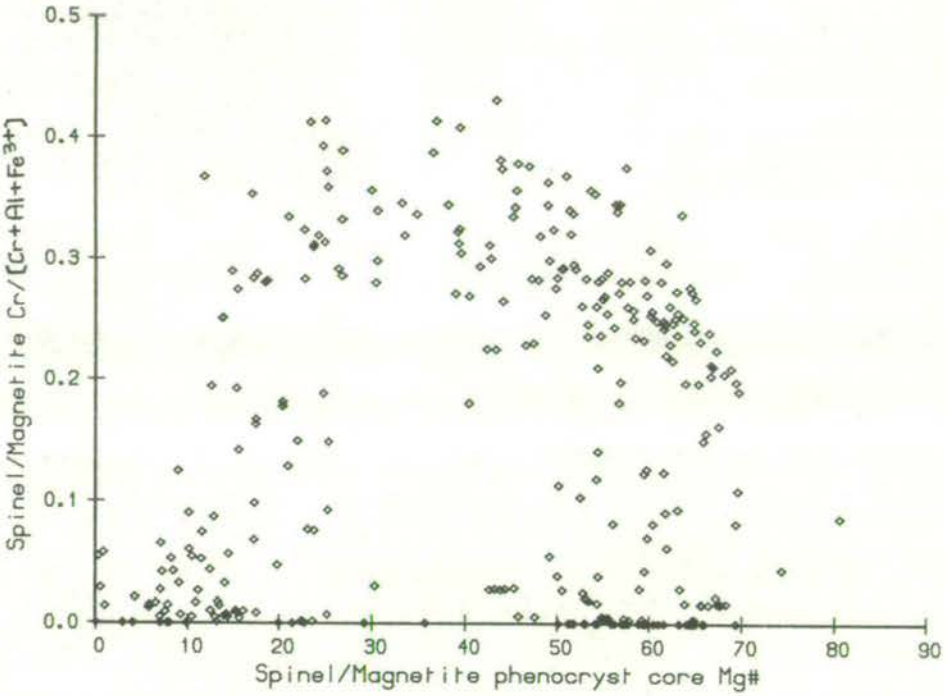

Figure 6-32. Spinel phase phenocryst cores, Mg# versus $Cr/(Cr+Al+Fe^{3+})$.

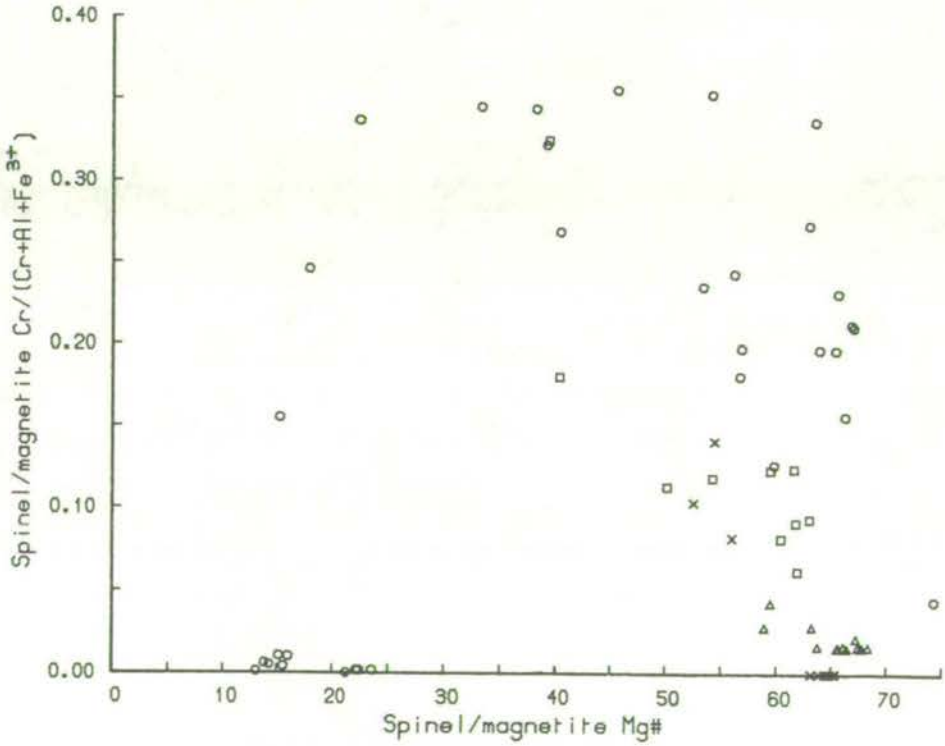

Figure 6-33. Spinel phases from samples in the Edinburgh area, Mg# versus $Cr/(Cr+Al+Fe^{3+})$.

× MV514, lava IV of Arthur's Seat
○ AS1/36017, Lion's Haunch Basalt of Arthur's Seat
△ AS2, Whinny Hill intrusion of Arthur's Seat
□ MV516, Castle Rock,Edinburgh

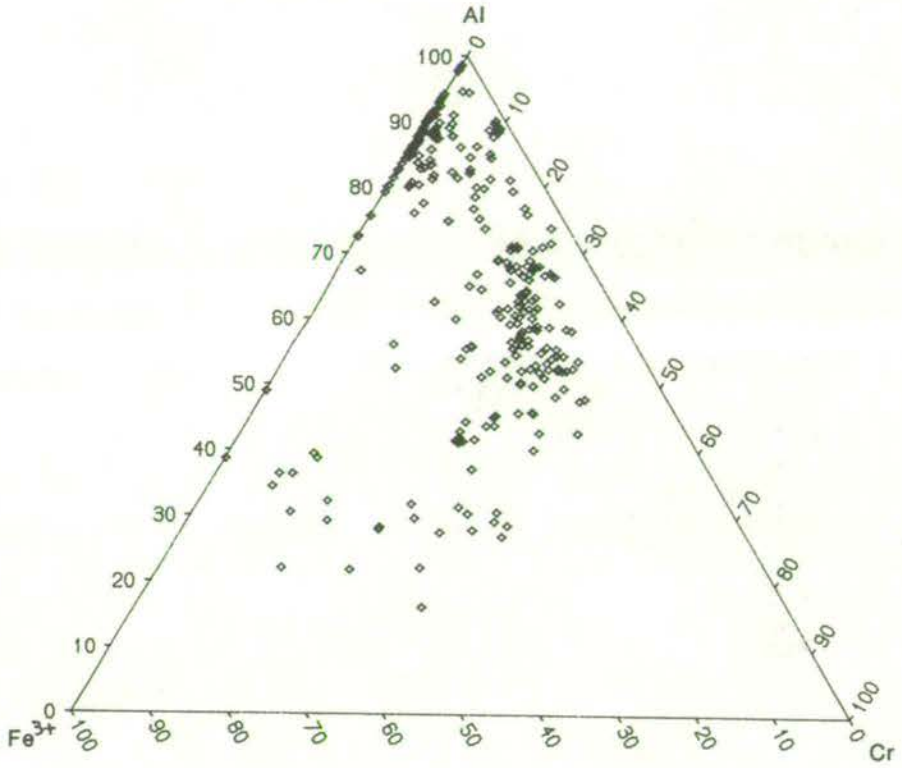

Figure 6-34. Spinel phenocrysts, Cr-Al-Fe^{3+} variations. cation %

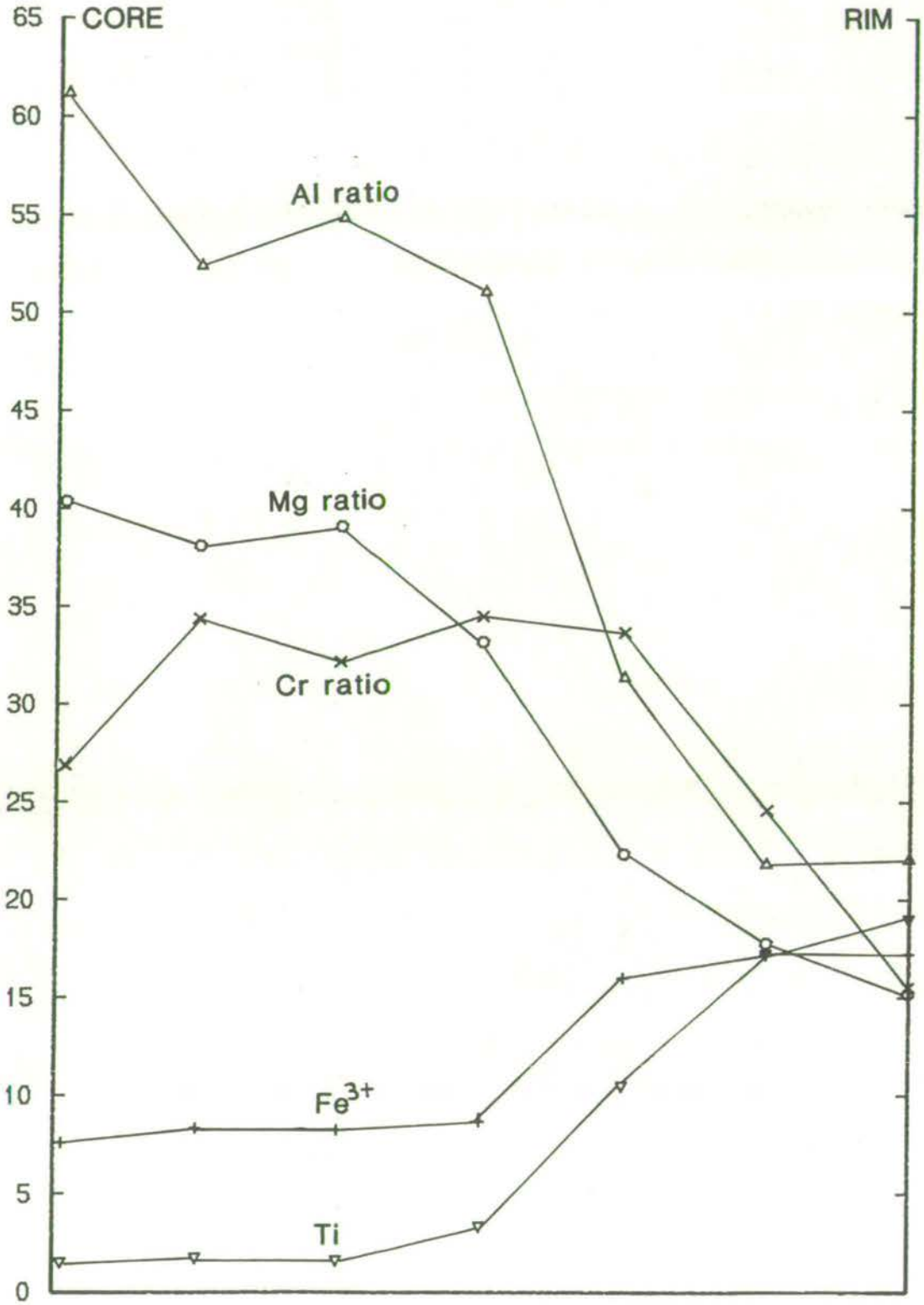

Figure 6-35. Partial profile across a spinel phenocryst from core (left) to rim (right), in sample AS1/36017. Not to scale.

- ○ $Mg/(Mg+Fe^{2+})$
- △ $Al/(Cr+Al+Fe^{3+})$
- × $Cr/(Cr+Al+Fe^{3+})$

} cation ratios

- \+ Fe^{3+}
- ▽ Ti

} cation %

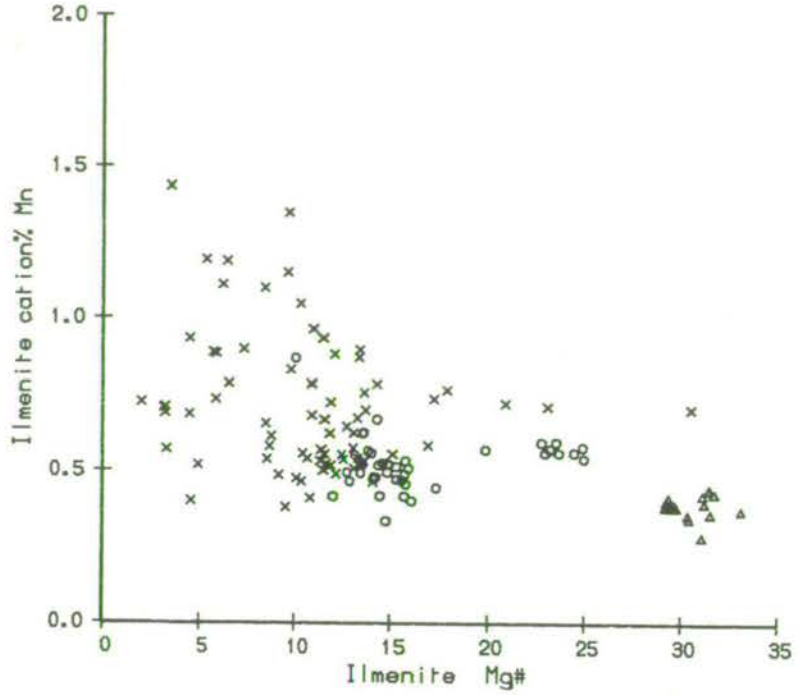

Figure 6-36. Ilmenite; cation % Mn versus Mg#.
△ wehrlite, F4
○ "phenocrysts"
× groundmass

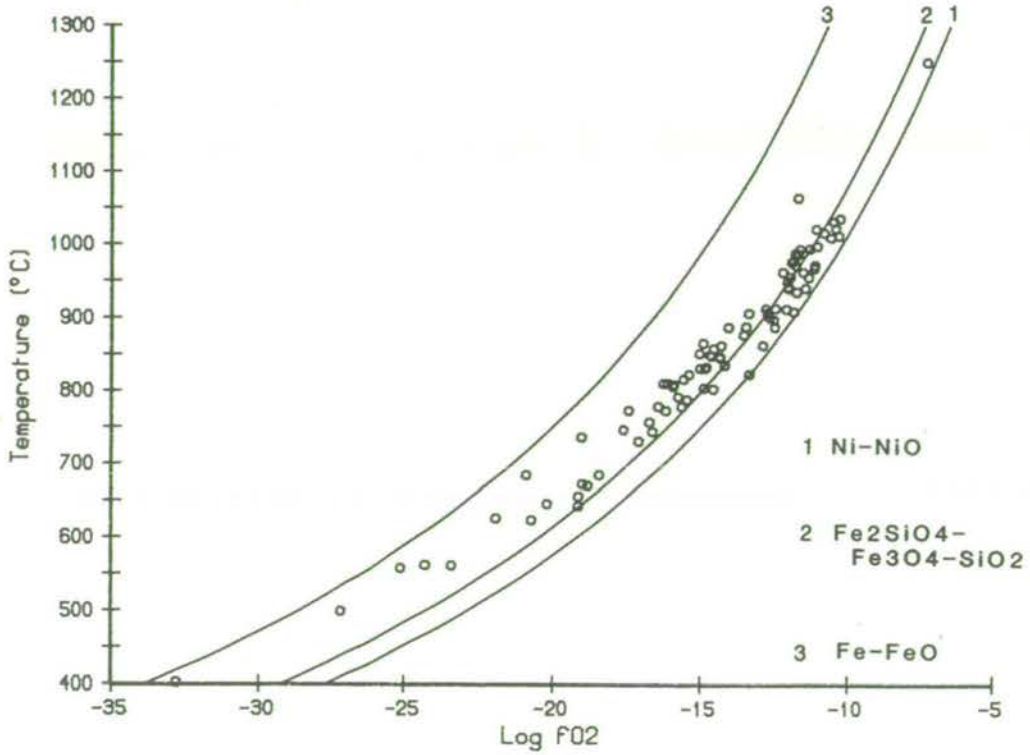

Figure 6-37. Temperatures and oxygen fugacities of coexisting magnetite - ilmenite pairs, calculated from the model of Spencer & Lindsley (1981).
Oxygen buffers are from Ulmer (1971).

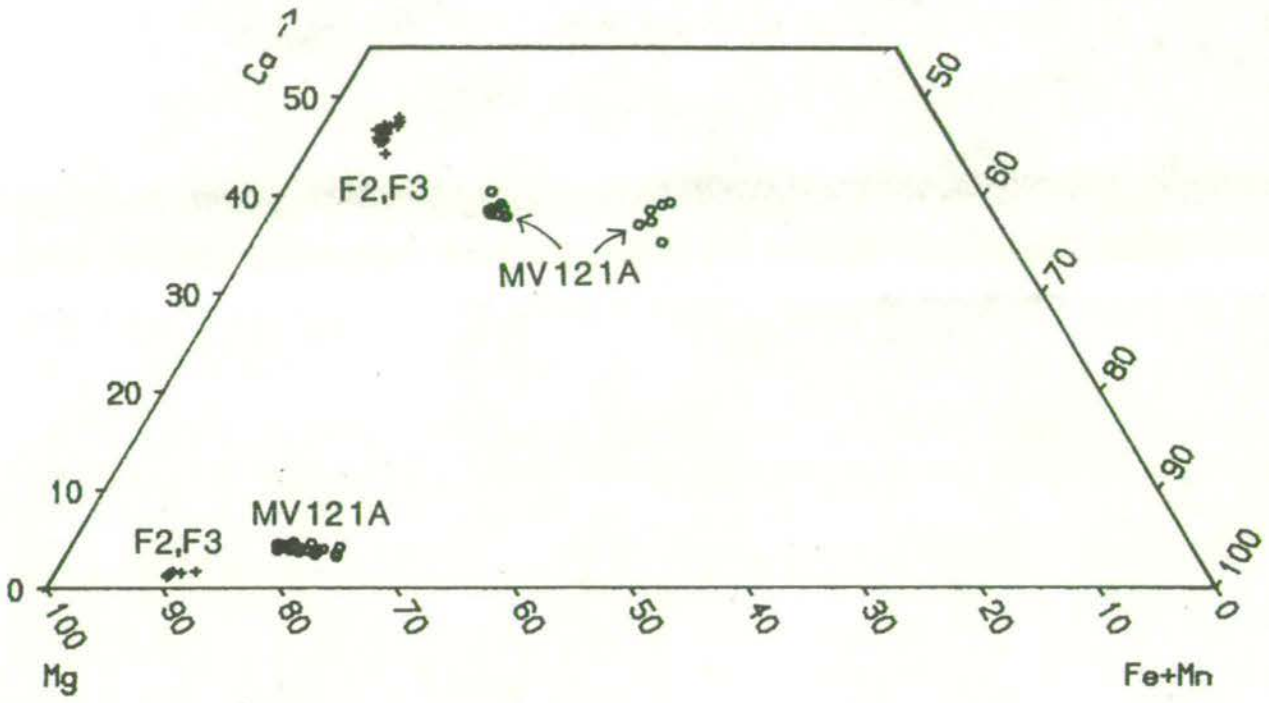

Figure 6-38. Coexisting clinopyroxenes and orthopyroxenes.
+ F2,F3 (spinel lherzolite nodules)
o MV121A (phenocrysts)

	MACGREGOR CATEGORY	PHENOCRYSTS ESSENTIAL	PHENOCRYSTS SOMETIMES PRESENT	MODERN TERMINOLOGY
MICROPHYRIC (<2 mm size)	Jedburgh	pl, ol		Microphyric ol-pl ± Fe-oxides-phyric (basaltic) hawaiites (occasionally basalt).
	Dalmeny	ol	cpx, pl	Microphyric ol- or ol+cpx-phyric basalt.
	Hillhouse	ol	cpx	Microphyric ol ± cpx-phyric basalt.
MACROPORPHYRITIC (>2 mm size)	Markle	pl, ol		Macroporphyritic ol-pl ± Fe-oxides-phyric basalts, basaltic hawaiites or hawaiites.
	Dunsapie	pl, ol cpx		Macroporphyritic ol-cpx-pl-Fe-oxides-phyric basaltic hawaiites, or ol-cpx-pl-phyric basalts.
	Craiglockhart	ol, cpx		Ankaramite.

TABLE 6-1

Comparison of the basalt nomenclature scheme of MacGregor (1928) with the modern chemical classification scheme (after Macdonald, 1975).

pl - plagioclase
ol - olivine
cpx - clinopyroxene.

WHEN YOU ARE A BEAR OF VERY LITTLE BRAIN, AND YOU THINK OF THINGS, YOU FIND SOMETIMES THAT A THING WHICH SEEMED VERY THINGISH INSIDE YOU IS QUITE DIFFERENT WHEN IT GETS OUT INTO THE OPEN AND HAS OTHER PEOPLE LOOKING AT IT.

A. A. Milne.

CHAPTER 7

APPLICATION OF THE EXPERIMENTAL MODEL TO THE NATURAL ROCKS AND THE INTERPRETATION OF THEIR PHENOCRYST ASSEMBLAGES

7.1 Extension of the Crystallisation Model to Higher Pressures

Much of the discussion in the last chapter hinges about the idea of phenocryst growth at elevated pressures. Since the crystallisation model described in Chapter 5 is based on one-atmosphere mineral temperature equations, clearly some means of accounting for the effect of increasing pressure is required. The mineral composition equations already include a term estimating the role of pressure. However, in the mineral temperature equations, because of the limited amount of published data, any pressure term would be very uncertain and could reduce the accuracy of the equations where they are best established, i.e. at low pressures. As a result, a separate means of correcting for pressure has been sought.

In general, the effect of pressure on the melting point of a mineral can be described by the Clausius-Clapeyron equation;

$$\frac{dT}{dP} = \frac{\Delta V}{\Delta S}$$

ΔV and ΔS are the volume and entropy of fusion respectively. As the volume and entropy of a liquid are usually greater than for the equivalent solid, the terms ΔV and ΔS are generally positive. Thus as pressure increases, the melting point also increases. In natural rocks it is not yet possible to precisely calculate the changes in mineral liquidus temperatures with pressure. However, numerous experimental studies under anhydrous conditions confirm the overall trend of increasing liquidus temperatures with increasing pressure, e.g. Thompson (1974a), Bender et al. (1978), Fujii and Bougault (1983).

As a first step towards quantifying the effect of pressure, an empirical temperature correction factor has been estimated from the many published studies of basic compositions. This approach, in an even more empirical form, was adopted by Fisk et al. (1980) with some success for estimating the depth of origin of phenocryst

assemblages in Icelandic and Reykjanes Ridge tholeiites. The factors used by these authors were 2° C/Kb for olivine, 6° C/Kb for plagioclase, and 10° C/Kb for clinopyroxene. For the factors used here, 32 published experimental studies have been considered. In each case, much of the variation of melting point with pressure for each mineral can be modelled by a constant factor. Ideally, the factors should be taken from segments of the phase diagrams where the mineral of interest is the sample liquidus phase. The change in temperature with pressure is not then influenced by the degree of crystallisation of earlier, higher temperature phases. However, for clinopyroxene this condition usually occurs at high pressures where there can be large errors in temperature and pressure measurement, and quite limited data. In order to have a large enough data set to consider any systematic variations, the changes in melting point with pressure have been taken from the phase diagrams, irrespective of whether the mineral is the rock liquidus phase. Although this results in average slopes for each mineral, the deviations from the experimental values throughout the determined range are usually well within experimental errors. For the studies examined, the ranges of values of increase in melting point with pressure are 1 - 8° C/Kb for olivine, 1 - 7° C/Kb for plagioclase, 8 - 13° C/Kb for clinopyroxene, 10 - 20° C/Kb for low-Ca pyroxene and 4 - 10° C/Kb for spinel. Clearly, such a wide spread of values for each phase would allow almost any desired phase diagram and inspire little confidence. However, if the starting compositions are grouped together into alkalic, tholeiitic, picritic and lunar categories, much more restricted ranges are found for each phase. Synthetic basic compositions have been excluded. The alkalic group has values of 4 $\pm$ 2° C/Kb for olivine, 3½ $\pm$ 1½° C/Kb for plagioclase, and 10 $\pm$ 2° C/Kb for clinopyroxene. The tholeiitic group has values of 2½ $\pm$ 1½° C/Kb for most olivine, 5 $\pm$ 1½° C/Kb for plagioclase and 10½ $\pm$ 2° C/Kb for clinopyroxene. The other groups are of less interest in this study, although notably, clinopyroxene has an average value of 11° C/Kb, and low-Ca pyroxene has an average value of 12° C/Kb, in both. Olivine averages at 6° C/Kb in the lunar group and 5° C/Kb in the picritic group. Plagioclase averages at 2° C/Kb in the lunar group and 5° C/Kb in the picritic group.

For the purposes of this study, due to the uncertainties in the spinel and low-Ca pyroxene equations in Chapter 5, these phases have not been included in the applied crystallisation model. The significance of these phases will be discussed below. For the remaining major minerals (olivine, clinopyroxene and plagioclase), pressure correction factors have been introduced to the crystallisation model to produce the following results. For undersaturated compositions the increase in melting point with pressure is 4° C/Kb for olivine, 3½° C/Kb for plagioclase, and 10° C/Kb for clinopyroxene. For saturated and oversaturated compositions the increase is 2½° C/Kb for olivine, 5° C/Kb for plagioclase, and 10° C/Kb for clinopyroxene. Phase diagrams produced using the crystallisation model do not usually have exactly these slopes, due to the effect of earlier crystallising phases. However, for the basaltic compositions at least, the resulting phase diagrams are very similar to comparable experimentally-determined phase diagrams. There is no reason to suspect that the samples in this study should be markedly different to many of the samples studied at high pressures. Indeed, even if there are small errors in the change of melting point with pressure, the resulting discrepancies are probably within experimental error up to at least 15 Kb. The main reservation in this approach is in the division of the samples into two groups. Although unavoidable on the basis of the published studies, this may give rise to errors if the starting compositions are incorrectly categorised. The main difference between the groups is in the relative values for olivine and plagioclase. For an undersaturated sample, with olivine at atmospheric pressure alone on the liquidus, plagioclase will not be on the sample liquidus at higher pressures. For saturated and oversaturated compositions, with olivine alone on the liquidus at atmospheric pressure, plagioclase can become the liquidus phase at higher pressures. For both groups, clinopyroxene has by far the greatest increase in melting point with pressure, and inevitably becomes the liquidus phase at high pressures. Also, for saturated and oversaturated samples with plagioclase on the liquidus at atmospheric pressure, the factors indicate that olivine does not reach the liquidus at higher pressures. The successful application of the model to the natural rocks described in later sections, is

believed to justify this empirical approach.

7.2 Application of the Crystallisation Model to the Natural Rocks

Individual pressure-temperature diagrams have been generated for the melting relations of each natural sample, using the model described in the previous section and Chapter 5. The model essentially predicts the equilibrium melting relations with additional information on mineral compositions and proportions. Several qualifications should be mentioned. The starting compositions used are those of all-glass experimental charges analysed by electron microprobe. As they contain no crystalline phases, the charges were not used in the derivation of the model. The assumed initial oxygen fugacity corresponds to the nickel-nickel oxide buffer. This corresponds to the main bulk of the input experimental data, and appears to be a reasonable estimate of the oxygen fugacities of the natural magmas at atmospheric pressure, estimated from the compositions of coexisting natural iron-titanium oxides. The model maintains constant total oxygen content of the sample throughout the crystallisation range, so that the buffer is not followed to low temperatures. This was noted in Chapter 5 and is not believed to have a major effect on the predicted results until high percentages of crystallisation are reached, by which time other factors make the model less reliable. The possible crystallisation of ilmenite has been ignored due to the very limited experimental data. The predicted relationships for spinel and low-Ca pyroxene have also been excluded from the modelling for the reasons discussed earlier. At low pressures, these minerals do not form a significant proportion of the assemblages at low to moderate percentages of crystallisation. In the later stages of crystallisation and at higher pressures, however, the absence of these phases could produce a significant deviation from the equilibrium relations. For example, in Chapter 6, it was indicated that aluminous spinel contributes to assemblages fractionating from the parental magmas. Also, possible equilibration of the sample compositions with an orthopyroxene-bearing mantle can not be recognised as in the examples of Thompson (1974a). Finally, the weight % modal proportions produced in the model are not directly comparable to the volume % proportions noted

in Appendix 1. However, bearing in mind these points, the model can provide strong evidence for the origin of the phenocryst assemblages.

7.2.1 Atmospheric Pressure

From a consideration of the experimental results and the predicted phase relations, several points can be made concerning the natural phenocryst assemblages. At atmospheric pressure the liquidus phases are olivine or plagioclase or both (ignoring spinel). With the notable exception of MV93, clinopyroxene does not appear in the crystallisation sequence before plagioclase. This contrasts sharply with the observed phenocrysts. In many samples, olivine + clinopyroxene phenocrysts occur together without plagioclase, e.g. MV521, MV166, MV403, ES2058, MV109. Clearly, the one-atmosphere crystallisation relations do not apply to these compositions. Similarly, for samples containing phenocrysts of olivine + clinopyroxene + plagioclase, the experimental evidence requires far higher percentages of crystallisation of plagioclase or total crystals to generate the assemblage than are observed in the natural assemblages, e.g. MV514, AS2, MV74, MV72. For these cases therefore, the one-atmosphere relations can not explain the assemblages found. Some natural rocks also contain more than one generation of a particular phenocryst phase, e.g. AS1/36017, MV122, MV40A, MV52. These can not be explained in terms of one-atmosphere equilibrium crystallisation of a single starting composition.

Where clinopyroxene is not a member of the phenocryst assemblage, it is often possible to relate the one-atmosphere experiments to the natural situation. The samples MV723 and MV164 are interpreted as having only olivine as a silicate phenocryst, which matches the experimental data of olivine as the liquidus phase. In the case of MV164, the most magnesian olivine phenocryst core composition (Fo_{84}) can be generated at atmospheric pressure at 1230° C in the assemblage olivine + liquid (+ spinel). The phenocryst assemblage of this sample can therefore be produced at atmospheric pressure, although the model suggests that a similar result can be generated at much higher pressures. Slight olivine accumulation is also a possibility in this sample. For MV723, the

evidence is less clear. The most forsteritic olivine phenocryst composition found (Fo_{73}) is too Fe-rich to have been preserved from the olivine + liquid stage of the experimental assemblage, and would not be the initial olivine to crystallise from the bulk composition (Fo_{87}). Significant olivine accumulation or lower temperature re-equilibration appears to be required to explain this anomaly.

Seven samples are experimentally cotectic with respect to olivine + plagioclase at their liquidus at atmospheric pressure. MV165 does not appear to contain any plagioclase phenocrysts, although this may indicate the rock represents a low-pressure liquid which had evolved to the olivine + plagioclase cotectic. The observed forsteritic olivine would then be interpreted as xenocrystal (suggested from compositional evidence in the previous chapter). Samples MV514, MV52, MV74, MV72 contain clinopyroxene phenocrysts in addition to olivine + plagioclase. In MV514, MV52 and MV74 the clinopyroxene forms a small proportion of the phenocryst assemblage, and has a composition strongly suggesting crystallisation at elevated pressures. If the clinopyroxene in MV514 is ignored, then the assemblage of olivine + plagioclase phenocrysts could be produced at atmospheric pressure, at 1190° C. Again, the model does not exclude generation of the same assemblage at higher pressures. Ignoring the clinopyroxene in the other samples does not lead to an atmospheric pressure fit for the olivine + plagioclase compositions. Samples MV13 and MV704 only contain olivine + plagioclase (+ magnetite) phenocrysts. Although this phase assemblage fits the one-atmosphere experimental data, the phenocryst compositions and modal proportions do not.

Seven samples have plagioclase as their one-atmosphere liquidus phase. For MV506, MV71A, MV39A and MV40A, the experimental crystallisation model at one-atmosphere does not reproduce the natural phenocryst modal proportions, predicting excess plagioclase with the correct phenocryst assemblage. Samples MV702 and MV51 contain plagioclase phenocrysts without coexisting olivine or clinopyroxene, and can be explained in terms of the experimental model at atmospheric pressure. In the case of MV702, the large percentage of phenocrysts (25% by volume) raises the possibility of phenocryst

accumulation. With the broad range of compositions preserved, together with the effects of total pressure, and pH_2O, and kinetic effects on plagioclase crystallisation, an apparent fit in the experimental model should not be taken as conclusive proof of an atmospheric pressure origin of the phenocrysts from an initially liquid composition. Disequilibrium processes, together with plagioclase accumulation, may be important factors in the origin of the very plagioclase-phyric rocks in this study. Plagioclase accumulation could account for the occurrence of plagioclase as the experimental liquidus phase in some samples. However, an alternative means of producing plagioclase at the atmospheric pressure liquidus is fractionation of an olivine + clinopyroxene assemblage at higher pressures.

MV402 contains clinopyroxene and olivine in addition to abundant plagioclase phenocrysts. Although the modal proportions can not be matched very well, the best fit at atmospheric pressure is at 1140° C, after a prolonged period of plagioclase crystallisation. This is at odds with the petrography of the natural rock, where plagioclase phenocrysts are often clustered round clinopyroxene phenocryst clots, implying the early growth of the clinopyroxene. Compositionally, these clinopyroxene phenocrysts have moderately high Al^{VI}/Al^{IV} values consistent with having crystallised at elevated pressures.

To summarise, taking the observed natural phenocrysts as single assemblages, very few can be explained by dry equilibrium crystallisation of an initially liquid composition. Of the many rocks containing olivine + clinopyroxene phenocryst assemblages, only MV93 actually shows an experimental assemblage at atmospheric pressure of olivine and clinopyroxene without plagioclase. Of the many rocks containing olivine + clinopyroxene + plagioclase phenocrysts, all show a comparable assemblage in the experiments but none fit the modal, compositional and petrographic data. The only natural assemblages closely matched by the experimental data are those involving olivine and/or plagioclase. In fact, only MV164 (olivine), MV702 and MV51 (plagioclase) provide close fits with the experiments, and even these could be explained by alternative models.

7.2.2 Higher pressures

Extension of the crystallisation model to higher pressures undoubtedly introduces more uncertainties into the interpretation of the results. The major factors are the effects of pressure on the mineral temperature equations (discussed above), and on the mineral composition equations. The quite limited experimental data on coexisting mineral and melt compositions at elevated pressures, probably lead to significant errors in the prediction of crystallising mineral compositions particularly. For example, the predicted Mg# of clinopyroxene is usually lower than that of coexisting olivine. This contrasts with studies of natural assemblages where the reverse is usually found (e.g. Wilson, 1982; Elthon et al., 1982). Similarly, the complex but important effect of pressure on the Al content of a clinopyroxene is very poorly defined in the model. Despite these reservations the crystallisation model gives results consistent with published experimental studies. In applying the model to the natural phenocryst assemblages, emphasis is placed on the phase relations and phase proportions calculated, and to a lesser extent on the mineral compositions predicted.

The large group of samples containing clinopyroxene phenocrysts can be most easily explained by crystallisation at elevated pressures. With increasing pressure, the near-surface equilibrium crystallisation sequence for the basic rocks (olivine followed by plagioclase followed by clinopyroxene) is replaced by olivine followed by clinopyroxene followed by plagioclase at intermediate pressures, and ultimately by clinopyroxene at the liquidus at the highest pressures. Figure 7-1 illustrates such a progression for MV406. This sample contains phenocrysts of olivine, clinopyroxene and spinel (+ magnetite). Clearly, in a simple equilibrium crystallisation interpretation of that assemblage, the minimum pressure is approximately 3 Kb, below which plagioclase would be a phenocryst rather than clinopyroxene. The apparent maximum pressure is approximately 15 Kb, above which clinopyroxene is not accompanied by olivine. As can be seen, the model predicts that equilibrium crystallisation of the bulk composition at 11 - 15 Kb will result in the loss of olivine from the crystallising assemblage at low temperatures, although olivine is the

liquidus phase. This feature has been produced in several experimental studies (e.g. Upton, 1971; Thompson, 1974a; Takahashi, 1980), and hence is not dismissed as a quirk of the model. However, it should be noted that in the latter two studies, low-Ca pyroxene was observed near the liquidus in the pressure-temperature region under discussion.

The predicted phase relations of other samples in this study indicate a slightly different result for olivine when clinopyroxene reaches the liquidus. Figure 7-2 shows the predicted relations for MV106. In this case, although the crystallisation temperature of olivine decreases rapidly at pressures greater than 12 Kb, early crystallised olivine is not lost at lower temperatures. Published experimental studies of basic rocks also show this relation (e.g. Thompson, 1974a; Arculus, 1975; Fujii and Bougault, 1983). For the samples in this study, the more basic compositions are usually nepheline-normative, have large high-pressure fields of olivine + clinopyroxene + liquid, and show olivine reaction at lower temperatures, as in Figure 7-1. The less magnesian samples are usually hypersthene- or quartz-normative, have plagioclase near the liquidus when clinopyroxene becomes the liquidus phase in place of olivine, and show a decrease in olivine crystallisation temperature with increasing pressure, as in Figure 7-2. The main distinction between these trends is apparent. For the first group, a composition initially in equilibrium with olivine can crystallise to an olivine-free, clinopyroxene + liquid assemblage. For the second group, a composition initially in equilibrium at high pressures with olivine, will remain so to much lower temperatures. In other respects the phase relations for MV106 have much in common with those of MV406. The naturally occurring phenocryst assemblage is olivine + clinopyroxene + spinel, yet the model predicts that anhydrous equilibrium crystallisation of the bulk composition will only produce this at pressures greater than 8 Kb, and less than 12 Kb. In Figures 7-1 and 7-2, the shaded regions indicate the pressure-temperature ranges which give the best experimental fits of the natural phenocryst assemblages, in terms of silicate phases, modal proportions and mineral compositions. In Figure 7-1, the range is based on the phase proportions and the most Fe-rich olivine phenocryst core

composition (Fo_{82}). There is no experimental fit of the clinopyroxene phenocryst Mg#. Changes in the oxidation state chosen, or in the slope of the mineral crystallisation curves with pressure, or uncertainty in the olivine phenocryst compositions used, can all significantly move the shaded region. In Figure 7-2, the shaded area has the same assemblage, proportions and mineral compositions as the natural rock. If the shaded areas are interpreted as showing the pressure and temperature conditions of formation of the phenocrysts, then the underlying assumption is that the assemblage can be considered as the product of a single equilibrium crystallisation stage of the bulk composition. This will be questioned in the next section.

Where plagioclase is present in the phenocryst assemblage with clinopyroxene, it is usually possible to find a region in the phase diagram which fits the natural data, with respect to assemblage and phenocryst proportions at least. Figure 7-3 illustrates the predicted phase relations of MV160, which contains phenocrysts of olivine, clinopyroxene, plagioclase and spinel (+ magnetite). The shaded area indicates the pressure-temperature range with the correct silicate assemblage, in approximately the same proportions as the natural rock. In this case, the predicted clinopyroxene Mg# is too low, but the olivine and plagioclase compositions fall in the range of phenocryst core compositions. However, since the phenocrysts show quite a broad spread of values, olivine Fo_{75-84} and plagioclase An_{51-64}, the predicted experimental results based on olivine and plagioclase composition, would fit over a large pressure-temperature region.

A different relation can be seen for MV72 in Figure 7-4. This sample contains olivine, clinopyroxene and plagioclase phenocrysts although no fresh olivine is preserved. On the basis of the phenocryst modal proportions, clinopyroxene Mg# and plagioclase anorthite content, the experimental best fit is shown shaded in the phase diagram. This region is close to a predicted point where olivine, plagioclase and clinopyroxene crystallise near to the liquidus. The possible significance of this cotectic situation at the liquidus will be discussed in the next section. However, it is apparent that a sample with olivine and plagioclase at the liquidus

at atmospheric pressure, will show olivine + plagioclase + clinopyroxene within a few degrees of a higher pressure liquidus, because of the relative slopes of the mineral crystallisation curves with pressure. A further example of this can be seen in Figure 7-5 for sample MV514. At atmospheric pressure, olivine and plagioclase crystallise together within about 10° C of the liquidus. At 11½ Kb, olivine, plagioclase and clinopyroxene crystallise within about 5° C of the liquidus. In this rock there are phenocrysts of olivine, plagioclase and very rarely, clinopyroxene and aluminous spinel. Modally, the high pressure near-liquidus occurrence of the three silicate phases provides the best fit of the natural assemblage. However, in order to fit the plagioclase predicted composition to that of the phenocrysts, a low pressure origin is required. If the clinopyroxene and aluminous spinel are not assumed to be part of the equilibrium phenocryst assemblage with olivine and plagioclase, then a good fit of the natural assemblage can be made. The shaded area at less than 4 Kb contains olivine + plagioclase in the same proportions and with the same compositions as the natural sample. Petrographic evidence suggests the observed phenocryst assemblage can not be treated as representing a single equilibrium crystallisation stage.

When clinopyroxene is not present in the phenocryst assemblage, the model usually indicates a possible low-pressure origin for the phenocrysts, as suggested by the atmospheric pressure experimental data. Figure 7-6 and 7-7 show the predicted phase relations for MV13 and MV704 respectively. Both samples contain phenocrysts of olivine, plagioclase and magnetite, and are cotectic with respect to these phases at their atmospheric pressure liquidus. The phase relations show a three-phase cotectic involving clinopyroxene at the liquidus at higher pressures, effectively setting a maximum temperature and pressure of origin for the phenocrysts in each rock. As indicated in the previous subsection, neither rock can be ideally explained in terms of atmospheric pressure equilibrium crystallisation. For MV13, the predicted olivine is marginally more forsteritic than the observed phenocrysts (Fo_{72} predicted relative to a natural observed maximum of Fo_{71}). However, allowing for this slight discrepancy, the best fit of the natural assemblage, in terms of modal proportions and mineral compositions, is at 3 - 5 Kb and 1160 - 1170° C (shaded area

in Figure 7-6). For MV704, the predicted olivine is significantly more forsteritic than the observed phenocrysts (Fo_{79} predicted relative to the natural observed maximum of Fo_{71}), although the rock only contains a few % of phenocrysts. The best fit of the modal proportions and plagioclase phenocryst compositions in the equilibrium crystallisation model, is at 2 - 4 Kb and 1190 - 1210° C (shaded area in Figure 7-7). The origin of the olivine composition discrepancy is not clear.

Sample MV164 serves as an example with olivine and spinel as phenocrysts. The shaded area in Figure 7-8 indicates the pressure-temperature region where the natural assemblage, modal proportions and mineral Mg# values are predicted to be reproduced by the equilibrium crystallisation model. Although the spinel composition which would crystallise has been calculated in the model, the effect of spinel crystallisation on the major elements is very small and has been ignored. With the spinel composition, the natural assemblage could have formed in the region 1180 - 1220° C, 0 - 4 Kb. If only the olivine composition is considered, then the possible pressure range is increased up to perhaps 9 Kb.

The second sample with olivine and spinel phenocrysts, MV723, discussed in the previous subsection, is predicted to have olivine at the liquidus up to 16 Kb, but no match of the natural compositions is found, with the observed phenocrysts more Fe-rich than those predicted by the model.

As an example of a rock containing only plagioclase phenocrysts, Figure 7-9 illustrates the predicted phase relations of MV702. The shaded area indicates where the approximate phenocryst modes and compositions are satisfied by the model. As stated above, there is an atmospheric pressure solution for this sample, which can be seen to extend up to 4 Kb in a temperature range of 1180 - 1220° C. Sample MV51 also has a possible atmospheric pressure origin for its plagioclase phenocrysts. With the extension of the model to higher pressures this produces a fit of 0 - 4 Kb at 1120 - 1150° C, where suitable plagioclase phenocrysts could have crystallised.

Similar matches of the predicted phase relations to the natural phenocryst assemblages can be made for most other samples. No

solution has been found for samples MV40B, MV39B and MV165, if their observed phenocrysts are interpreted as equilibrium crystallisation products of the bulk composition. Samples MV723, MV704, MV716, MV718, AS2 and MV40A appear to contain too Fe-rich olivine phenocrysts to fit plausible modal phase proportions in the model. Sample MV506 does not have a solution which reproduces the phenocryst proportions observed in the natural rock. Sample MV402 only produces a unique atmospheric pressure solution for the natural assemblage, inconsistent with petrographic evidence.

To summarise, the predictions of the experimental model for the basaltic compositions are as follows. At low pressures olivine is the dominant liquidus phase, and/or plagioclase in the less magnesian samples. Clinopyroxene becomes the liquidus phase at higher pressures, commonly over 5 Kb. The rapid increase in clinopyroxene crystallisation temperatures with pressure, relative to olivine and plagioclase, results in an olivine + clinopyroxene + liquid field in the predicted pressure-temperature phase diagrams. This matches the phenocryst assemblages found in many rocks which were not explained by the atmospheric pressure results. Similarly, for the numerous samples containing olivine, clinopyroxene and plagioclase phenocrysts, the assemblage and modal proportions of the phases can usually be reproduced at pressures of several kilobars. When clinopyroxene is absent from the phenocryst assemblage, the olivine and/or plagioclase phenocrysts can be modelled as low-pressure phases. The overall change in assemblage at the liquidus with increasing pressure, can be described as from olivine and/or plagioclase to olivine and/or clinopyroxene. Several samples have an intermediate assemblage and show olivine + plagioclase + clinopyroxene near the liquidus at pressures ranging from approximately 3 - 11 Kb. Most of these samples have olivine and plagioclase near the liquidus at one-atmosphere. No bulk compositions have clinopyroxene near the liquidus at atmospheric pressure. At high pressures, the more magnesian compositions, which have olivine at their liquidus followed by clinopyroxene, commonly show olivine reacting out at lower temperatures leaving clinopyroxene + liquid. In the less magnesian compositions, the olivine crystallisation temperature is depressed after clinopyroxene reaches the liquidus, but no olivine reaction is produced.

7.3 Interpretation of the Phenocryst Assemblages

Up to this stage the emphasis has been on interpreting the phenocrysts as simple assemblages produced by equilibrium crystallisation of the preserved bulk composition. This is a rather simplistic view of the problem, however, and ignores petrographic and compositional evidence from the natural rocks themselves, as well as from published studies of lavas and nodules. Regardless of the mechanisms controlling the compositions of erupted magmas in the province, the phenocrysts in any single sample need show no relation to those in any other sample. Each sample is therefore, viewed as representing a unique event, perhaps preserving phenocrysts from different stages in the magmatic history. Some phenocrysts may have crystallised from a composition quite unlike the preserved bulk composition, and others probably reflect fractional crystallisation rather than equilibrium crystallisation. Disequilibrium growth and resorption processes were also important in some rocks. In this section the samples have been placed in categories, on the basis of the evidence presented in preceding sections and in the last chapter. The categories are based on the phenocryst content of the rocks, and are designed to aid the explanation of the origin of the phenocrysts by identifying common types and groups. That this may artificially separate related compositions, is of secondary interest in this regard, as the purpose of the thesis is to explain the phenocrysts.

Seven categories are proposed. These identify the earliest preserved phenocrysts in each rock on the basis of petrographic evidence, phenocryst habit and composition, and the predicted pressure-temperature phase diagrams. The first group contains typically large, high Al^{VI}/Al^{IV} (up to 0.8) augite $\pm$ olivine. Later phenocrysts may also be present. Aluminous spinels are believed to be important early phenocrysts. The second group contains samples interpreted to have evolved to an olivine + clinopyroxene + plagioclase stage. Later phenocryst growth may also have occurred, but earlier stages are not clearly defined. The third group contains samples showing only olivine (+ spinel) as early phenocrysts. The fourth group contains samples containing small olivine + clinopyroxene + spinel phenocrysts. Key features of this group are that the

olivines are often skeletal and the pyroxenes show oscillatory and hourglass zoning. Some samples also contain distinct Cr-Al titanomagnetites. The fifth group contains samples which have evolved to an olivine + plagioclase + magnetite stage. The sixth group contains samples with only plagioclase ± magnetite phenocrysts. The seventh group contains the remaining samples which for various reasons do not fit into the other groups. It must be emphasised that this scheme is interpretive and some samples, discussed below, could be placed in other categories. This applies mainly to group 2 compositions, which could belong more to group 1. With further study some of the group 7 compositions could be assigned to other groups. More detailed discussion of the individual groups, together with the interpretation of the specific phenocryst assemblages, is given below.

Group 1

Ten samples are assigned to this group. Each has augite phenocrysts with high Al^{VI}/Al^{IV} values, high Mg# and pronounced resorption textures. Usually the augites appear to have been initially homogeneous, although MV122 contains quite large, oscillatory and sector-zoned phenocrysts. Although five of the samples also contain plagioclase phenocrysts, a key feature of this group is the interpretation that the augites started to crystallise before the feldspar. Three samples, with possibly two others, also indicate a later episode of augite phenocryst growth after a period of resorption. Olivine is always a phenocryst phase in these rocks, but may sometimes have crystallised later than the pyroxenes. High-Al, low-Cr spinels have been recognised in five of the samples in this group, and are occasionally preserved as inclusions in the pyroxenes, suggesting they crystallised at about the same time or earlier.

Sample MV166 contains the simplest assemblage, olivine + clinopyroxene + spinel phenocrysts. The clinopyroxene and most spinels have the characteristics described above, with no evidence for growth under changing conditions. The markedly darker pink rims of the pyroxenes are interpreted as late overgrowths on partially resorbed homogeneous cores, and probably grew at the time of emplacement of the magma. The spinels are usually rounded, with sharp reaction rims of titanomagnetite when they occur as distinct

phases in the groundmass. The olivine phenocrysts, like the augites, are large (macroporphyritic in the classification schemes) and show strong zoning towards Fe-rich margins. Some include small, low Mg# spinels with distinctly lower Al/Cr ratios compared to the larger dominant spinel group. Haggerty (1979) related increasing spinel Al/Cr ratios to increasing pressure in volcanic suites. While other factors such as melt composition and the nature of coexisting phases are bound to be important, this qualitative trend suggests the higher Mg# spinels grew at higher pressures than the lower Mg# spinels. From the petrography and phenocryst chemistry, the assemblage is interpreted as an early, high pressure clinopyroxene + aluminous spinel + olivine assemblage, with a later, lower pressure olivine + less aluminous spinel assemblage. It has been suggested that the whole-rock composition trends can be explained by olivine + clinopyroxene + spinel fractionation. However, the proportions indicated by extract calculations are very approximately 6 : 1 : 1 clinopyroxene : olivine : spinel, whereas the phenocryst proportions in the natural rocks never have these values. In MV166 there is considerably more olivine and less spinel than the extract proportions, although clinopyroxene is the most abundant phenocryst phase. If the phenocryst assemblage is investigated using the experimental crystallisation model, a broad pressure-temperature range is found where the observed assemblage is predicted (Figure 7-10). Much of the range is due to the broad set of phenocryst core compositions used. In the case of clinopyroxene, some of the supposed cores may have been modified by resorption. For olivine there may be a genuinely broad range of values representing prolonged crystallisation. Several other problems are apparent. Is the bulk composition relevant to the interpretation of the preserved phenocrysts? Did some of the phenocrysts crystallise from a quite different melt, or has the bulk composition been modified by phenocryst accumulation? No confident answer can be given to these questions other than to reiterate the findings of Macdonald (1975) and earlier workers, who noted that chemically equivalent aphyric or sparsely porphyritic rocks exist for almost the whole range of porphyritic lavas. Olivine phenocryst compositions and predicted equilibrium compositions are commonly used to suggest phenocryst accumulation or crystallisation from initially liquid, bulk compositions. In the case of MV166 the

close similarity of predicted liquidus olivine from the bulk composition (Fo_{87}), and the most forsteritic phenocryst core (Fo_{86}) suggests modifying processes were absent, although they can not be excluded on this basis. The very forsteritic phenocryst core composition does indicate that ideal equilibrium crystallisation has not occurred, as a more Fe-rich olivine would coexist with the abundant clinopyroxene for this bulk composition. A further problem is assessing the amount of clinopyroxene and aluminous spinel lost by resorption. The degree of corrosion of some phenocrysts is so great as to suggest that in favourable conditions, phenocrysts may be entirely resorbed.

Clearly, a precise interpretation of the predicted phase relations of Figure 7-10 would be meaningless. If the diagram is assumed to be relevant to the origin of the observed phenocrysts, then some interpretation can be made. From the compositions of the clinopyroxenes and aluminous spinels, a high pressure origin is indicated. Similar phases have been noted in nodules associated with lower crustal and upper mantle xenoliths (e.g. Chapman, 1976; Upton et al., 1983; this study, F1 and F4). The maximum pressure at which olivine could also be present is 17 Kb (less if the composition cooled significantly below its liquidus). A possible history can be outlined. The bulk composition may have undergone a period of equilibrium crystallisation at high pressures, less than approximately 15 Kb, during which the homogeneous aluminous spinel, augite cores and olivine were produced. Uprise into a cooler crust would take the magma into the olivine + liquid phase field, where partial resorption of the augite and probably the aluminous spinel occurred. Continued re-equilibration and growth of the olivine phenocrysts probably produced much of the range now preserved. At lower pressures still, a lower Mg#, less aluminous spinel joined the crystallising olivine. The magma was emplaced at this stage before plagioclase or augite appeared at the liquidus. Quench cooling produced the additional olivine, plagioclase, augite and magnetite seen as overgrowths or groundmass phases. If this process was relatively slow, then further re-equilibration of the olivine phenocrysts could have occurred. It is likely the magma travelled from lower crustal/upper mantle depths quite rapidly without any major pauses, as slow transport or residence

in an upper crustal, magma chamber would be expected to fractionate or completely resorb the high-pressure clinopyroxenes and spinels (Biggar and Clarke, 1976; Scarfe et al., 1980). From a comparison of the observed augite compositions with the experimental augites of Thompson (1974b), the pressure of origin of the phenocrysts is placed tentatively at 10 Kb, implying a temperature of approximately 1250° C from Figure 7-10.

The other samples in Group 1 can be interpreted in a similar fashion to MV166. ES2058 contains high Al^{VI}/Al^{IV} augites which probably crystallised at high pressures (perhaps 10 Kb from comparison with Thompson, 1974b). In this case there appears to have been further augite phenocryst growth after some resorption and before the groundmass composition crystallised. This is supported by petrographic descriptions of other samples from this intrusion presented by Henderson and Gibb (1983).

The experimental model predicts plagioclase will crystallise at low pressures before clinopyroxene, but no plagioclase phenocrysts have been observed. However, there are hydrous phases such as biotite in the groundmass, suggesting pH_2O may have been important at low pressures and could have suppressed the appearance of plagioclase. It is difficult to assess the stage at which the olivine phenocrysts crystallised, but since olivine is predicted to be the liquidus phase until very high pressures it is likely olivine crystallised initially with the augite. Relatively Cr-rich spinels included in the olivine are interpreted as indicating low-pressure olivine + spinel crystallisation. No highly aluminous spinels have been found. Although phenocryst accumulation is possible, the liquidus olivine composition predicted from the bulk composition, is similar to the most forsteritic phenocryst core. This sample is difficult to interpret, but early high-pressure olivine + clinopyroxene crystallisation is predicted to have occurred at 10 Kb, 1250° C or higher. Olivine (+ spinel) crystallisation with augite resorption could have taken place during ascent of the magma, with further growth of augite perhaps at shallow pressures at the time of emplacement of the intrusion.

MV703 contains clusters of very resorbed augites as well as small, euhedral olivines and small, zoned augites. The initial character of the resorbed augites is unclear, but they could have crystallised at high pressures by comparison with MV166 and ES2058. Small olivines associated with the clusters are comparable with the phenocrysts in the rest of the rock. The predicted phase relations suggest plagioclase would crystallise before clinopyroxene up to 4 Kb. The best fit of the observed olivine composition and phenocryst modes is 5 - 6 Kb at 1220° C. However, in line with the petrographic evidence, the majority of the augite phenocrysts probably did not grow in an episode of equilibrium crystallisation. The proposed interpretation is that early, high pressure crystallisation of augite $\pm$ olivine was followed by rapid uprise of the magma. Partial resorption of the early augite occurred, but during cooling augite rejoined the sequence, producing the small, zoned phenocrysts as the magma rose towards the surface. Olivine + Cr-Al-spinel also crystallised at this stage, presumably over 4 Kb to avoid plagioclase crystallisation. The predicted phase relations are shown in Figure 7-11 and suggest that at pressures over 11 Kb, initially crystallised olivine could have reacted out leaving augite + liquid.

MV93 may have had a similar history to MV703. Resorption of early clinopyroxene appears to have been followed by further growth of zoned augite. Since augite is the second phase to crystallise after olivine in this sample there is no minimum pressure estimate. Olivine is the predicted liquidus phase to 9 Kb where it is replaced by augite. This rock has been shown throughout the study to be quite distinct from the other samples and may have evolved in a different way, perhaps due to high volatile pressures. The high Ca content of this sample (nearly 15 wt % CaO) suggests clinopyroxene fractionation has not been an important process in its evolution. Several workers have argued that strongly undersaturated magmas are generated from source mantle by small degrees of partial melting, and are very sensitive to the amounts of CO_2 and H_2O present (e.g. Frey et al., 1978). If volatiles have been important in the later evolution of this magma, then the predicted phase relations will be inappropriate. The dry phase relations suggest the observed phenocrysts could have crystallised in the region 3 - 6 Kb, 1210 - 1230° C based on the

phenocryst modes. If much of the olivine crystallised on the way to the surface, then the pressure-temperature estimates would be revised upwards for the earliest phenocryst crystallisation.

MV514 and MV516 both contain very rare high Al^{VI}/Al^{IV} augite and aluminous spinel phenocrysts. In the case of MV514, the phase relations indicate that augite only nears the liquidus at 11½ Kb, although the associated olivine, plagioclase and less aluminous spinel phenocrysts could be explained at low pressures (Figure 7-5). Petrographically, the augite and aluminous spinel are large and slightly resorbed, whereas the olivine, plagioclase and less aluminous spinel are very small, with the plagioclase laths only slightly larger than similar laths in the matrix. The olivine is relatively Fe-rich compared to the augite, and the included Cr-Al-spinels have lower Mg# than the distinct, aluminous spinel. The predicted phase relations indicate a three-phase cotectic at the liquidus at 11½ Kb, 1235° C. However, it is considered unlikely for the large spinel to have crystallised with over 50% Al_2O_3 if there was another aluminous phase present, namely plagioclase. Inclusion studies have indicated aluminous spinels, similar to the observed phenocrysts, in clinopyroxene-bearing, plagioclase-free nodules (e.g. Irving, 1980; Upton et al., 1983). It is therefore suggested that at this pressure, plagioclase had been replaced by aluminous spinel in similar fashion to the transition, plagioclase lherzolite to spinel lherzolite. The phenocryst assemblage is interpreted as showing augite + aluminous spinel (± olivine, not observed) from at least 11½ Kb, 1235° C. This is consistent with a comparison of the pyroxene Al^{VI}/Al^{IV} values with those of Thompson (1974b). At lower pressures (less than 5 Kb), olivine + Cr-Al-spinel crystallised as the early phenocrysts were partially resorbed. At similar or lower pressures, plagioclase joined the assemblage, with the eruption temperature approximately 1180° C. This suggests the magma cooled by 55° C from the upper mantle to final eruption.

MV516 may have had a similar history to MV514, although plagioclase phenocrysts were not developed. The predicted phase relations suggest that aluminous spinel and augite could have been produced at 8 Kb, 1220° C. The dominant phenocryst, olivine, displays a skeletal habit and is interpreted as having grown at lower pressures

as the magma cooled and rose through the crust. Petrographically, the magma appears to have been emplaced near the plagioclase crystallisation temperature. Together with the composition and amount of olivine present, this suggests the magma was intruded, as Edinburgh Castle Rock, at 1170 - 1180° C.

AS2 is a highly porphyritic rock, and the sample investigated may not be representative of the bulk composition presented by Clark (1956). Certainly, the olivine phenocrysts are more Fe-rich than predicted by the crystallisation model. The rock also contains high Al^{VI}/Al^{IV} resorbed augite, aluminous spinel included in the pyroxenes, and slightly resorbed plagioclase phenocrysts. The association of the augite and spinel is taken to indicate high pressure crystallisation without plagioclase. By comparison with Thompson's (1974b) experimental pyroxenes, this could have occurred at approximately 10 Kb. The plagioclase is quite calcic (up to An_{77}) and is interpreted as a low pressure phase, although a xenocryst origin can not be ruled out, perhaps accounting for the resorption. Qualitatively, this sample is interpreted as containing olivine + clinopyroxene + spinel from lower crustal/upper mantle levels from an equilibrium crystallisation stage, with additional olivine ($\pm$ plagioclase and magnetite) at shallower depths.

MV402 contains plagioclase, augite, altered olivine and included spinel phenocrysts. The experimental model offers no plausible explanation for this sample apart from indicating plagioclase as the clear liquidus phase at low pressures. It is not apparent whether this is due to alteration, plagioclase accumulation or some evolution at significant water pressure. Qualitatively, the petrography and mineral chemistry indicate crystallisation of augite $\pm$ olivine at several kilobars with plagioclase crystallising distinctly later, often as laths round clusters of augite. The olivine displays a slightly skeletal habit and may have formed, with the included spinels, during uprise of the magma.

Sample AS1/36017, the Lion's Haunch Basalt, is highly porphyritic and may have been modified by crystal accumulation. The presence of high-Al, low-Cr spinels with high Al^{VI}/Al^{IV}, resorbed augites is taken to indicate some early high-pressure phenocryst

growth. However, zoning near the margins of some pyroxenes indicates continued or later crystallisation prior to resorption. Whether this could have been together with plagioclase is not clear, but as discussed in the last chapter, the plagioclase has recorded a complex history and may indicate significant water pressures. Olivine appears to have crystallised throughout, accompanied by spinel which initially was Al-rich and Cr-poor and shows, as Mg# falls, an increase in Cr, and a decrease in Al, and ultimately a rapid drop in both Cr and Al to titanomagnetite compositions. The interpretation of the phenocrysts is complicated by the inclusion and disaggregation of glomerocrysts of gabbroic mineralogy. These are believed to be xenoliths as their textures suggest prolonged annealing. A tentative history of this sample is outlined below. Initial olivine + clinopyroxene + aluminous spinel crystallisation, perhaps under equilibrium crystallisation conditions at high pressures, was followed by uprise with some continued growth of augite in addition to olivine and spinel. The magma may then have risen to a shallow level, accompanied by slight resorption of augite and an increase in water content. Plagioclase joined the assemblage and may indicate an outgassing event which also caused the disruption and inclusion of annealed cumulates. Uprise and intrusion of the magma into a cool near-surface environment completes the story. At emplacement, olivine + calcic plagioclase + magnetite is believed to have been the stable phenocryst assemblage. The earliest phenocrysts could have crystallised at lower crustal or upper mantle levels on the basis of the pyroxene compositions.

MV122 is the "odd-man-out" of this group. Although the augite phenocrysts have high Al^{VI}/Al^{IV} and high Mg# values, and are partially resorbed, they also display oscillatory and sector-zoning. Unfortunately, all the olivine is altered, but it appears to have been rounded or embayed. The feldspars show two distinct compositions. The lower anorthite content group are extremely resorbed. Anhydrous equilibrium phase relations are inappropriate for this sample. The augite is thought to have crystallised rapidly at several kilobars, and then been partially resorbed until eruption, when the groundmass augite provided a quench rim for the phenocrysts. The high anorthite content plagioclases (An_{55-59}) were, on the basis of the petrography,

stable at eruption. Inasmuch as the dry phase relations can be used, olivine may also have been stable at that stage. The origin of the low anorthite content plagioclases ($\sim An_{30}$) is not clear. The combination of high pressure, rapid crystallisation and resorption textures might best be explained by a magma mixing origin at elevated pressures. The low anorthite content plagioclases could have been phenocrysts in a hawaiitic magma which mixed with a more magnesian basaltic composition. Cooling of this magnesian magma may have generated the sector-zoned augites.

Group 2

There are nine samples in this group. The key feature is the interpretation that the earliest preserved phenocryst assemblage included plagioclase, in addition to olivine and augite. The evidence for this comes from the petrography of the samples and the predicted crystallisation relations. Six of the samples show olivine + clinopyroxene + plagioclase within approximately 15° C of their liquidus at high pressures. The range encompassed by these cotectics is 5½ - 10½ Kb, 1180 - 1220° C. Unlike MV514, there is no observed aluminous spinel in the samples, and no apparent reason to suspect plagioclase is unstable at the proposed cotectics.

MV74 and MV71A have quite similar predicted phase relations to those illustrated for MV72 in Figure 7-4. Each has plagioclase at the liquidus near the high pressure cotectic, 18° C above olivine and clinopyroxene in the case of MV71A, 13° C for MV74, 5° C for MV72. All contain sparse glomerocrysts of plagioclase and clinopyroxene, which do not have the annealed texture of the inclusions in AS1/36017 and may be cognate. Although olivine has not been identified in these glomerocrysts, the experimental model predicts olivine as a small proportion of the high pressure, cotectic assemblage. Notably, the best fit of the phenocryst assemblage in Figure 7-4 (for MV72) is displaced to lower temperatures and pressures from the liquidus 3-phase cotectic. This is to account for "extra" olivine and plagioclase in the phenocryst modes. Identical results are predicted for MV74 and MV71A. A possible interpretation for these samples is that initial phenocryst crystallisation, or equilibration with the glomerocryst assemblages, occurred at the liquidus 3-phase cotectic.

With uprise of the magma, further cooling produced the "extra" olivine and plagioclase phenocrysts. Such a history could account for partial resorption of the glomerocrysts with less evidence for resorption of discrete phenocrysts. Clinopyroxene compositions in MV74 and MV71A are consistent with a high-pressure origin, although those of MV72 are less characteristic. The proposed liquidus 3-phase cotectics are at 10½ Kb, 1220° C for MV72; 8½ Kb, 1210° C for MV74; and 7 Kb, 1190° C for MV71A. Each sample is predicted to have undergone further crystallisation of olivine + plagioclase (± magnetite) at near-surface pressures.

MV52 has similar predicted phase relations to the previous samples (Figure 7-12). Again, this sample has olivine + clinopyroxene + plagioclase at the liquidus at elevated pressures, 1190° C at 6 Kb, but the best fit of the phenocryst assemblage is predicted to be at lower temperatures and pressures. Initial crystallisation of the bulk composition at 6 Kb could have produced the clinopyroxene, plagioclase and more forsteritic, olivine phenocrysts. Uprise and cooling of the magma may have been associated with resorption of the early phenocrysts, particularly augite, and with further crystallisation of plagioclase and olivine (+ magnetite) at shallow levels. The distinctly more Fe-rich olivines are a possible result of this. However, this sample is part of a composite intrusion with MV51. The more Fe-rich olivines could have crystallised from a melt with composition similar to MV51, and could then have been separated into MV52 prior to emplacement of the intrusion. The later olivine and plagioclase crystallisation has the effect of moving the best predicted fit of the phenocrysts to lower temperatures and pressures.

MV39A and MV39B are the highly porphyritic and essentially aphyric components, respectively, of a composite intrusion. MV39B contains only sparse plagioclase and magnetite + ilmenite phenocrysts, which on their own can not be explained by the phase relations at any pressure and temperature. The phase relations for both rocks are shown in Figure 7-13a and b. The liquidus phase for MV39B is olivine up to 8 Kb where olivine, clinopyroxene and plagioclase all appear within 5° C of the liquidus at 1190° C. The mineral compositions predicted here, occur in the range of the phenocrysts of MV39A and include the rare plagioclases of MV39B itself. Thus MV39B could represent a

liquid composition which was in equilibrium with the olivine, clinopyroxene and plagioclase phenocrysts of MV39A at 8 Kb, 1190° C, and was separated from these phases (with the exception of a few plagioclases). If the phase relations of MV39A are considered, the bulk composition has plagioclase on the liquidus until high pressures. Notably, the highest temperature at which olivine, clinopyroxene and plagioclase could have coexisted is 1180 - 1190° C at 7½ - 8 Kb, similar to MV39B, although the predicted compositions fit less well. Using the groundmass composition separated by Macdonald (1975) from MV39A, the experimental model indicates olivine, clinopyroxene and plagioclase occur together within 6° C of the liquidus at 7 - 7½ Kb, 1180° C. Some plagioclase accumulation may account for plagioclase on the liquidus of MV39A bulk composition, and for the low pressure-temperature fit of the whole phenocryst assemblage shown in Figure 7-13b. The evidence is therefore interpreted as indicating olivine, clinopyroxene and plagioclase phenocrysts in equilibrium with bulk composition MV39B and separated MV39A groundmass at 7 - 8 Kb, 1180 - 1190° C. There is some indication of later plagioclase crystallisation, as rounded augite phenocrysts, with Fe-Ti oxides at their margins, are included in a clear plagioclase in MV39A. This does not appear to have been extensive enough to modify the phase relations significantly, but it suggests magnetite and ilmenite crystallised at an early stage also. The augite composition is consistent with crystallisation at lower crustal levels. The resorption of the more sodic plagioclases in these samples, is interpreted to have resulted from reaction of the high pressure phenocrysts with the melt at shallow levels. From the bulk composition MV39B, and separated groundmass MV39A, it appears olivine was the only possible equilibrium phase at intrusion. From these "quenched liquid" compositions it is suggested emplacement temperatures were 1165° C (MV39A) and 1180° C (MV39B) at least, implying little cooling from deep crustal levels.

The evidence for olivine + clinopyroxene + plagioclase crystallisation in MV520, the Crawfordjohn essexite, is mainly petrographic. Large oscillatory- and sector-zoned augites often include small olivines and plagioclase laths. Pyroxene accumulation may have occurred in this very porphyritic sample. The predicted olivine composition is more forsteritic than the observed phenocrysts,

consistent with ferromagnesian phenocryst enrichment. The zoning in the augites indicates that equilibrium crystallisation is an inappropriate model, and precludes any quantitative estimate of the phenocryst origins. The petrography suggests olivine may have been the phenocryst phase in the magma at intrusion. The augites and plagioclases are interpreted as having grown rapidly at the time of emplacement of the intrusion. There is no evidence in the investigated sample for an earlier, higher pressure origin for these spectacular pyroxenes. Other samples may contain a record of earlier phenocryst compositions.

Samples MV501 and MV160 have been included in this group on the basis of the experimental crystallisation model, although there is little other compelling evidence for olivine, clinopyroxene and plagioclase crystallising together. In MV501, there are very few plagioclase and augite phenocrysts relative to olivine. If these are interpreted as a single assemblage produced by equilibrium crystallisation, then the model indicates an origin at approximately 5 Kb, 1200° C. However, if the sample was originally liquid having reached the olivine-clinopyroxene cotectic, predicted at 10 Kb, 1250° C, then cooling during uprise through the crust could generate a similar assemblage. Olivine would crystallise throughout, initially accompanied by some augite and later by plagioclase. The petrographic evidence of slightly skeletal olivine and small zoned augite might indicate a rapid growth origin expected in this scheme. MV160 contains abundant olivine, clinopyroxene and plagioclase phenocrysts, which, as discussed for Figure 7-3, can be explained as a single phenocryst assemblage produced at 5 - 6 Kb, 1180 - 1200° C. However, the petrography and mineral chemistry suggest the most Mg-rich olivine and augite may have crystallised from a more primitive liquid than is now represented by the bulk composition. While the plagioclase zoning indicates a complex history, it can not be shown to have crystallised at the same time as the augite. From the Al^{VI}/Al^{IV} value of the augite, a deep crustal crystallisation is possible. The suggested pressure-temperature region of origin of the assemblage is probably a minimum estimate, for the augites at least. Some near-surface crystallisation of olivine and plagioclase is consistent with the petrography, which shows a broad range of textures.

The augite shows a single episode of growth, before a rim attributed to the quenching stage.

Group 3

Only three samples have been placed in this group, whose key feature is the presence of dominant, early olivine phenocrysts. The implication of early growth is to recognise complete olivine phenocrysts which may have formed by equilibrium crystallisation. This contrasts with the usually small, variably skeletal olivines of group 4, which represent disequilibrium processes.

MV723 and MV164 have already been discussed. The additional evidence casts no new light on the origin of olivine phenocrysts in MV723. However, from the olivine composition, and that of the enclosed Cr-Al-spinels, a low-pressure origin seems likely. Either phenocryst accumulation and/or prolonged re-equilibration to lower temperatures, may account for the Fe-rich phenocryst compositions relative to the olivine predicted from the bulk composition. Similarly, for MV164, from the Cr-Al-spinel compositions a low-pressure origin for the olivine phenocrysts is proposed, 0 - 4 Kb at 1180 - 1220° C from Figure 7-8.

MV403 contains abundant, large, complete olivine phenocrysts with spinel inclusions, and has additional rare, small augite phenocrysts. Figure 7-14 shows the predicted phase relations for this sample. The shaded area is the best experimental fit of the complete phenocryst assemblage. Like MV164, the spinel composition has been calculated but its effect on the crystallisation relations has been ignored. The predicted equilibration region is uncertain for several reasons. Firstly, it is very sensitive to fO_2, being based on Mg# for olivine and spinel. Secondly, the effect of pressure on spinel composition is not known, and so the upper temperature limit for the spinel phenocrysts must be regarded as speculative. Thirdly, there is the possibility of olivine accumulation in this sample, as the predicted olivine from the bulk composition is significantly more forsteritic than the observed phenocrysts. However, this may simply indicate the equilibrium crystallisation of the olivine. Fourthly, while the olivine may have

been produced by equilibrium crystallisation, it is difficult to envisage such an origin for the small, sometimes sector-zoned augites. The pyroxenes have lower Mg# than the olivines and include more Fe-rich spinels. The favoured interpretation is that the pyroxenes crystallised during ascent of the magma. If plagioclase crystallisation was not affected by volatiles or nucleation problems, and the bulk composition is appropriate, then Figure 7-14 indicates the augites crystallised at higher pressures than 6½ Kb. Rare augite phenocrysts may show resorption, and even more rarely have suitably high Al^{VI}/Al^{IV} values (~ 0.5) This implies the olivines crystallised at least at these depths and probably deeper. Included spinels can have over 50 wt % Al_2O_3, which may support a high pressure origin. Spinel composition trends show decreasing Al/Cr as Mg decreases perhaps indicating continued crystallisation to shallower levels. This is consistent with the petrography. From the absence of presumed equilibrium augite, the olivines are interpreted as having crystallised initially in the 7 - 11 Kb pressure range at temperatures greater than 1250° C. The higher pressure end of this range might be more plausible, as it does not demand a dramatic drop in temperature to crystallise the augite during ascent of the magma.

Group 4

Eight samples are assigned to this group. The key features are quite small, variably skeletal olivines and small, zoned (often oscillatory- and sector-zoned) augites. Each rock contains microphenocrysts of olivine, augite and spinel, with no observed plagioclase. The predicted phase relations all indicate a low-pressure field where plagioclase crystallises before clinopyroxene. Two examples have already been illustrated, MV406 (Figure 7-1) and MV106 (Figure 7-2). Although the assemblages can be interpreted in terms of equilibrium crystallisation, the evidence of phenocryst habits and zoning suggests that fractional crystallisation is more appropriate.

The crystallisation process is envisaged as having occurred during ascent of the magmas through a cool crust. The relative rates of undercooling of the magmas and their rates of ascent are probably unique for each sample. Similarly, it is impossible at this stage to

estimate the extent of nucleation problems, particularly with respect to plagioclase, caused by this process. The phenocrysts are assumed to have crystallised from a bulk composition which was initially liquid. However, this assumption does not exclude the possibility of phenocryst accumulation modifying the compositions used in this study. This is quite possible for MV521, which has variable modal abundances of phenocrysts throughout a small quarry (MacGregor, 1928). Comparing the liquidus olivine predicted from the bulk compositions with the most forsteritic phenocrysts analysed, samples MV406, MV106 and MV178 produce a good match. MV521 and MV109 contain slightly more Fe-rich olivine than predicted (2 and 3 mole % respectively). The discrepancies may be due to phenocryst accumulation, but if the fO_2 was lower than used in the calculation (Ni - NiO buffer), or if some re-equilibration has occurred, or if the more forsteritic cores were not analysed, then the rocks may still represent liquid compositions. MV114 has much less forsteritic olivine relative to the prediction (by 8 mole %) and may indicate some accumulation, although it only contains 10% phenocrysts. This sample is relatively coarse grained and may have cooled sufficiently slowly to re-equilibrate the olivine. MV400 and MV78 have no fresh olivine preserved in the investigated samples; the prediction is they should contain Fo_{84} and Fo_{85} respectively, at the Ni - NiO buffer. For the sake of discussion, all the samples are assumed to represent liquid compositions, bearing in mind the above comparisons.

If these phenocrysts grew under disequilibrium conditions, and show no evidence of equilibrium crystallisation, then any estimate of the pressure-temperature conditions of origin of the minerals must be speculative. The Al^{VI}/Al^{IV} of augite phenocrysts has been used as a pressure indicator, with values of 0.8 interpreted as reflecting upper mantle or lowermost crustal crystallisation. Groundmass augites in this study often show a wide spread of values in the region 0 - 0.3 consistent with other studies (e.g. Wass, 1979). Rapid crystallisation of these augites appears to have the effect of lowering Al^{VI}/Al^{IV} by increasing the Al^{IV} content. If this is applicable to the phenocrysts in group 4, then the Al^{VI}/Al^{IV} values of the augites may give a misleading impression of low-pressure crystallisation. Certainly, with the exception of MV521, whose augites occasionally

have Al^{VI}/Al^{IV} up to 0.4, the sample augites have values of 0.3 or less. In the low pressure regions implied by this, plagioclase should have crystallised before augite. The absence of plagioclase phenocrysts could indicate the magma did not reach the low-pressure olivine + plagioclase + melt field, but might be due to suppressed plagioclase crystallisation caused by rapid cooling, or a small volatile content of the melts. It may also be significant that all these group 4 samples contain olivine, augite and spinel phenocrysts. From a consideration of Figures 7-1 and 7-2, all-liquid magmas cooling during rapid ascent would probably crystallise olivine, but not augite. It is therefore tentatively suggested, that these liquids were initially in equilibrium with olivine, augite and spinel at high pressures. Early cooling could have produced augite phenocrysts, whereas later cooling would be expected to produce only olivine, perhaps with plagioclase. If this is the case, then the initial magmas came from 10 Kb, 1260° C (MV400), to 19½ Kb, 1340° C (MV521). These pressures would have corresponded to the upper mantle beneath Scotland in Permo-Carboniferous times. The olivine phenocrysts may have grown throughout ascent, whereas the augites may have been restricted to the early stages. Spinels ± magnetites may also have grown at a wide range of pressures. MV109 contains very aluminous, spinel inclusions in olivine (over 50 wt % Al_2O_3) which may have crystallised at lower crustal or upper mantle pressures. Other samples contain Cr-Al spinels interpreted as lower pressure phases. To summarise, samples MV521, MV109, MV178, MV406, MV78, MV114, MV106 and MV400 are interpreted as having been liquid at upper mantle depths, perhaps in equilibrium with olivine, augite and spinel. Undercooling associated with ascent through the crust, produced the observed phenocrysts. Using the equilibrium phase relations as a guide, the augite phenocrysts may have crystallised at mid- to lower crustal depths, although their compositions are more typical of low pressures. Olivine + spinel phenocrysts are predicted to have crystallised throughout ascent of the magmas. Magnetite phenocrysts in MV109 and MV406 are interpreted as late, near-surface compositions. If the augite compositions truly reflect a low-pressure origin, this implies plagioclase crystallisation was suppressed. If the predicted equilibrium phase relations can be applied to these samples, the best

fits of the phenocryst assemblages lie in the pressure range 4 - 14 Kb. Minimum eruption temperatures would have been 1160 - 1210° C to avoid the development of plagioclase phenocrysts.

Group 5

Three samples are assigned to this group, characterised by olivine and plagioclase on the liquidus at atmospheric pressure, and by the absence of augite phenocrysts. The phase relations for MV13 (Figure 7-6) and MV704 (Figure 7-7) have already been discussed. In both cases the olivine phenocrysts are more Fe-rich than predicted, but in other respects the assemblages can be modelled satisfactorily. The phenocrysts in MV13 could have crystallised at 3 - 5 Kb, 1160 - 1170° C, with a predicted point at 5½ Kb, 1170° C, where augite joins the other phases on the liquidus. The phenocrysts in MV704 can best be predicted at 2 - 4 Kb, 1190 - 1210° C, with augite joining these phases on the liquidus at 7½ Kb, 1220° C. These augite-bearing cotectic solutions for MV13 and MV704 lie in the pressure range for the 3-phase cotectics proposed for the Group 2 samples. A possible interpretation for these two samples is that they represent liquids separated from an olivine + clinopyroxene + plagioclase equilibrium, with the observed olivine + plagioclase + magnetite phenocrysts having grown at shallower levels. Although magnetite has not been included in the experimental model, the atmospheric pressure experiments on uncontaminated sample MV13F, showed olivine + plagioclase + Cr-Al-titanomagnetite together on the liquidus. The atmospheric pressure experiments on MV704 also showed a spinel phase at the liquidus with olivine + plagioclase.

MV165 was originally described as bearing forsteritic olivine + spinel phenocrysts. However, the mineral and bulk composition evidence indicates this olivine is xenocrystal and the sample contains a few Fe-rich olivine phenocrysts (up to Fo_{63}). The predicted phase relations suggest the bulk composition has olivine and plagioclase at the liquidus until 3 Kb where augite joins these phases. Study of other samples from the sill may reveal olivine and plagioclase $\pm$ augite phenocrysts. From the predicted phase relations this bulk composition would be liquid at 1130° C. The absence of

recognised plagioclase phenocrysts suggests plagioclase crystallisation has been suppressed by a small volatile pressure.

Group 6

Two samples make up this group which is characterised by low pressure plagioclase (+ magnetite) phenocrysts. The phenocrysts in MV702 can be explained by low pressure crystallisation at 0 - 4 Kb, 1180 - 1220° C, (Figure 7-9). The plagioclases are characteristically skeletal and very similar, suggesting a single rapid phase of growth. Since olivine is a phenocryst phase in most of the samples in this study, its absence is notable for the two Group 6 rocks. A possible explanation for MV702, consistent with the petrography, is that the sample was essentially aphyric, perhaps just saturated with plagioclase + olivine ± augite, at elevated pH_2O. The observed phenocrysts could have grown after the magma degassed. With a small water content, the predicted phase relations might resemble those of Group 2 and Group 5, with low-pressure olivine + plagioclase on the liquidus and augite joining the assemblage at mid- to lower crustal levels.

MV51 may be similar in origin to MV702, although the petrography does not indicate rapid phenocryst growth. The assemblage for this sample can be explained by crystallisation at 0 - 4 Kb, 1120 - 1150° C. Olivine is near the liquidus at low pressures, suggesting any water content of the magma was small. As has been suggested, the Fe-rich olivine phenocrysts in MV52 could have crystallised originally in MV51. The sample may therefore have been cotectic with respect to olivine and plagioclase before the separation of the olivine.

Group 7

Seven samples are placed in this group of problem rocks. MV167 was investigated experimentally, but no hand specimen was available for petrographical or mineralogical study. Without this, the interpretation of the predicted phase relations is speculative. At atmospheric pressure olivine is the liquidus phase (ignoring spinel) at 1230° C, followed by plagioclase then clinopyroxene. From the phenocryst modes of Macdonald (1975), the assemblage of olivine +

clinopyroxene + plagioclase can be reproduced by the model at 7-9 Kb, 1200 - 1220° C. Accordingly, the sample may belong to Group 2 above, with the same reservations as expressed for MV160.

MV716 and MV718 are very similar experimentally, petrographically, and mineralogically. Both contain subhedral to anhedral olivine phenocrysts which are far more Fe-rich than predicted from the bulk composition (Fo_{70-76} in the rocks relative to Fo_{86-87} predicted). Both contain rare clusters of partially resorbed clinopyroxenes with low Al^{VI}/Al^{IV} ($\leqslant 0.3$). Both also contain very aluminous spinels with over 50 wt % Al_2O_3, and 3 wt % Cr_2O_3 or less. No simple, low pressure origin has been recognised for these assemblages. Experimentally, olivine is the predicted liquidus phase to over 20 Kb, where it is replaced by clinopyroxene. However, the olivine phenocryst compositions are not predicted at any realistic fO_2, and there is no evidence of lower temperature re-equilibration. Both rocks are similar to basanites which carry high pressure inclusions. On this petrographic basis, together with the spinel compositions, a high pressure origin is suggested for the phenocrysts. The anomalous olivine and clinopyroxene compositions may have been generated under high volatile pressures, perhaps CO_2.

MV40B and MV40A are the essentially aphyric and highly porphyritic components, respectively, of a composite intrusion. MV40B contains only sparse plagioclase phenocrysts which are not predicted to be the liquidus phase at any pressure. As discussed in the last chapter, MV40A contains two distinct groups of augite and plagioclase phenocrysts, in addition to anomalously Fe-rich olivine phenocrysts, magnetite and ilmenite. Petrographically, only the more anorthite-rich plagioclase phenocrysts (An_{55-61}) do not have an embayed or resorbed appearance. The crystallisation model predicts that plagioclase is the liquidus phase up to high pressure for the MV40A bulk composition. Although the modal amounts of phenocrysts can be matched at 4 - 5 Kb, 1150 - 1160° C, the mineral compositions only agree with the anorthite-rich plagioclases. Macdonald (1975) separated the groundmass from MV40A. Using this groundmass composition, the experimental model predicts plagioclase is the liquidus phase at crustal pressures and has the same composition as

the anorthite-rich plagioclases at near-surface pressures. Olivine is predicted to be a near-liquidus phase at atmospheric pressure, although no phenocrysts of suitably forsteritic olivine have been found. If this separated groundmass is taken to represent quenched melt, then the implication is that MV40A was emplaced at approximately 1150° C, in equilibrium with the anorthitic plagioclase, but none of the other silicate phenocrysts. MV40B, if taken as aphyric, could have been emplaced near 1200° C. No simple relation between MV40A and MV40B has been found. The anomalous phenocryst assemblages may reflect a magma mixing origin. The two clinopyroxenes, while having very different bulk compositions, have very similar Al^{VI}/Al^{IV} values of 0.4, suggesting an origin at similar pressures of a few kilobars. The Fe-rich olivines may be associated with the more Fe-rich clinopyroxenes. The more Mg-rich clinopyroxene has no obvious associated minerals. It is tentatively proposed that the phenocrysts have been derived from two magmas. Clinopyroxene (Mg-rich variety) may have been the sole silicate phenocryst phase of a basic liquid mixed with a more evolved melt, bearing olivine, Fe-rich clinopyroxene and sodic plagioclase. The calcic plagioclase appears to be a near-surface phenocryst phase grown from the MV40A coexisting melt. The magnetite and ilmenite may be products of either the more evolved parent or the near-surface crystallisation. The mixing episode could have occurred at deep crustal levels.

MV121A is anomalous because of its orthopyroxene phenocrysts. Ignoring these, the remaining assemblage of olivine, clinopyroxene and plagioclase phenocrysts can be satisfactorily modelled using the bulk composition. The phenocryst modes and mineral compositions are all predicted to agree at 3½ - 4½ Kb, 1150 - 1160° C (see Figure 7-15). A magma rising and cooling towards the surface from this equilibrium would show olivine and plagioclase as stable phenocrysts with evidence of partial resorption of clinopyroxene. This is in fact the situation shown by the petrography. The single ferroaugite phenocryst present, can be interpreted as a xenocryst, consistent with its very resorbed appearance. Unfortunately, no estimate can be made of the conditions of origin of the orthopyroxenes. Their compositions are compatible with an earlier, higher pressure crystallisation from the magma, but it is not possible to demonstrate whether they are cognate or

disaggregated from inclusions. Either origin is consistent with the slight resorption developed at the orthopyroxene rims. The ilmenite phenocrysts in the sample are usually rimmed by titanomagnetite. They are interpreted as belonging to the olivine + clinopyroxene + plagioclase equilibrium, with the rarer titanomagnetite phenocrysts having crystallised later, perhaps during the final ascent of the magma.

MV506 is considered to be anomalous because of the predicted role of plagioclase in the crystallisation model. The sample contains approximately equal proportions of olivine, augite and plagioclase phenocrysts,yet the model indicates plagioclase is the liquidus phase to high pressures, and would crystallise in much greater proportions than the other phases. The sample is altered and contains no fresh olivine, but the degree of alteration does not appear excessive compared to other samples in this study. At 8 Kb, 1210° C, olivine, clinopyroxene and plagioclase crystallise together (25° C below the liquidus). Glomerocrysts of the three minerals occur in the sample, suggesting this equilibrium was attained. The augite phenocrysts have $Al^{VI}/Al^{IV} \sim 0.5$ which is compatible with crystallisation in the lower crust. In contrast, the predicted plagioclase compositions are more sodic than are observed as phenocrysts. As a possible solution to this,it is proposed that the magma had a significant volatile content. The effects of this would have been to suppress plagioclase more than olivine and augite and allowed the three phases to occur at the liquidus, with a better match of plagioclase phenocryst compositions. This implies that the sample was derived from a lower crustal equilibrium with olivine, clinopyroxene and plagioclase at approximately 8 Kb. This would fit into the range of pressures for Group 2 samples. The distinction from the Group 2 samples is made because of the proposed significant pH_2O for MV506.

7.4 Discussion of the Origin of the Phenocrysts

Much of the previous section was taken up with the interpretation of individual samples. There are a number of features common to several samples. As an aid to the discussion of these features, Figure 7-16 summarises the predicted pressures and temperatures of origin of the main assemblages. In addition, the diagram also shows

the predicted points where bulk compositions (labelled as liquid) would be in equilibrium with olivine and clinopyroxene. For the phenocryst assemblages, the mid-point of predicted ranges of pressure and temperature has been plotted. Where no estimate was considered possible the sample has not been included in the figure. Most points have been derived from the experimental crystallisation model, although for samples MV166, ES2058 and AS2 the pressures have been interpreted from pyroxene compositions, with the corresponding temperatures predicted from the model. The phenocryst assemblages are predicted to have formed in the range 0 - 12 Kb. Samples from Group 1 have phenocrysts crystallised at approximately 8 - 12 Kb, with MV93 the exception at 4½ Kb. Group 2 samples may also contain phenocrysts from this pressure range (olivine and/or clinopyroxene), but they are predicted to contain olivine + clinopyroxene + plagioclase assemblages from 4 - 11 Kb, at lower temperatures than for Group 1. Groups 3, 5 and 6 are interpreted, with the exception of MV403, to contain low-pressure phenocrysts from 0 - 4 Kb. MV403 is anomalous in that it appears to contain high-pressure olivine phenocrysts without accompanying clinopyroxene. Group 4 samples are predicted to contain phenocrysts which crystallised during ascent of the magma through the crust. The complex interplay of factors affecting crystallisation in this situation precludes any meaningful estimate of the pressures and temperatures of formation of their phenocrysts. If the samples represent high-pressure liquids, last in equilibrium with olivine + clinopyroxene-bearing assemblages, then their predicted origin lies in the range 10 Kb, 1255° C, to 19½ Kb, 1370° C.

High Pressure Phenocryst Crystallisation

MacDonald and Whyte (1981) have estimated the base of the crust beneath part of the Midland Valley at 9.4 Kb (the seismic MOHO). Upton et al. (1983) have suggested the MOHO beneath Scotland represents a chemical change from crustal feldspathic to mantle ultramafic composition. As the crystallisation model is largely based on temperature variation with composition, rather than pressure variation, the confidence which can be applied to pressures predicted in the model, is rather limited. For the sake of this discussion, the

base of the crust is taken to be at 10 Kb. Quoted pressures for individual samples may have a precision of $\pm$2 Kb which, in some cases, will straddle the MOHO. The mineralogical difference of aluminous spinel in the upper mantle and plagioclase in the lower crust, noted by Upton et al. (1983), is assumed to be reflected in the crystallising phenocryst assemblages. If this is the case, then samples which contain aluminous spinel phenocrysts might be interpreted as having undergone phenocryst crystallisation in the upper mantle, whereas assemblages containing plagioclase reflect a crustal equilibration. With the pressure of 10 Kb as a divider, only two samples do not appear to fit this simple model. MV516 has an anomalously low equilibration pressure (8 Kb). However, this pressure is $\pm$ 2 Kb and so could indicate uppermost mantle equilibration. MV72 has a predicted olivine+clinopyroxene+plagioclase stage at 10½ Kb. Within the precision limits this could indicate a lower crustal equilibration. There is a reasonable doubt for the high pressure crystallisation of this sample, as the observed augite compositions do not have the expected, high Al^{VI}/Al^{IV} characteristics.

Group 1 compositions containing aluminous spinel are believed to include phenocrysts from the uppermost mantle, while the Group 2 compositions are believed to show evidence for crystallisation at the olivine-clinopyroxene-plagioclase cotectic, mainly within the lower crust. Supporting evidence for plagioclase-free phenocryst assemblages in the upper mantle comes from inclusion studies. Upton et al. (1983) have indicated the abundance of olivine + clinopyroxene + aluminous spinel nodules in association with upper mantle lherzolites and lowermost crustal granulites. Many of the dunite, wehrlite and pyroxenite inclusions have preserved, igneous textures (e.g. F1 and F4 in this study), and are interpreted to be cumulates.

One of the predictions of the experimental crystallisation model was the disappearance of olivine from the crystallising assemblage of some compositions at high pressures. Upton et al. (1983) describe wehrlites and clinopyroxenites from Fidra where the spinels and pyroxenes from the wehrlites have higher Cr/Al ratios than those from the pyroxenites. If these assemblages represent

progressive crystallisation at constant pressure, the decrease in Cr/Al ratio from the wehrlites to the pyroxenites could indicate the lower temperature origin of the olivine-free inclusions. This is consistent with the predicted relation.

Extrapolating further, the loss of olivine from the crystallising assemblage may provide evidence for the origin of the compositional trends of the Early Campsie lavas and the Kintyre lavas described by Macdonald (1975). He indicated that olivine + clinopyroxene fractionation could explain the more basic members of the Kintyre succession, whereas clinopyroxene-only fractionation appeared to control the more basic lavas from the Early Campsie succession. MacDonald and Whyte (1981) later supported the concept of a clinopyroxene-only stage of evolution for the Campsie Fells lavas. In the light of the results presented here, it is suggested that the Kintyre lavas reflect the phase relations of a suitable parental magma composition at high pressures, where olivine + clinopyroxene were crystallised. The Campsie lavas were derived from magmas which had evolved to the clinopyroxene + liquid stage. It is notable that more primitive compositions are preserved in the Kintyre suite. This may indicate less fractionation at high pressures, rather than a more basic, parental magma than for the Campsie lavas. A basic magma rising through the mantle isothermally, to a point where it begins to crystallise isobarically, would be expected to crystallise olivine first (O'Hara, 1968). If, however, the magma maintains an equilibrium with olivine + clinopyroxene as it rises, then when it undergoes crystallisation isobarically, the clinopyroxene-only stage could be reached within a few degrees of the liquidus. Note that isobaric crystallisation is implied to be essential for this clinopyroxene-only stage, as reducing pressure would carry the magma into the olivine primary phase volume. Although differences in the phase relations of the parental magmas are possible for the two suites, it may be that the Kintyre parental magma rose to an uppermost mantle level without maintaining equilibrium with olivine + clinopyroxene, so that isobaric crystallisation involved an extensive olivine + clinopyroxene + liquid stage. The Campsie parental magma could have maintained the equilibrium as it rose to a level where isobaric crystallisation

ensued and olivine was rapidly lost. Magmas tapped from these two situations might then show the required controls.

No samples from these two suites have been included in this study, but one, ZP422, from the Campsie series has been investigated experimentally at high pressures by Ford and Macdonald (1978). On the basis of limited experimental evidence they recognised olivine + clinopyroxene + plagioclase on the anhydrous liquidus at 8 Kb, 1200° C. From other experiments with retained volatiles they have suggested lower pressure, clinopyroxene fractionation to produce the observed lava compositions from this initial cotectic. The bulk composition has been investigated using the experimental crystallisation model. While producing good agreement with most of the dry experimental runs of Ford and Macdonald, there is one critical difference. Ford and Macdonald identified only one charge above the liquidus in their anhydrous experiments, at 1 Kb, 1200° C. On the basis of this, they were able to identify the 3-phase cotectic at 8 Kb and olivine + plagioclase on the liquidus at atmospheric pressure. The model, however, indicates that at 1 Kb (anhydrous at the Ni - NiO buffer) olivine is the clear liquidus phase at 1220° C, 40° C above plagioclase. This is an area where the crystallisation model is well established and the predicted result is very likely. Extending the model to higher pressures thus produces a quite different relation to that published. There is no predicted 3-phase cotectic at the liquidus, as olivine is the liquidus phase to 9 Kb where it is replaced by clinopyroxene. A thin section of ZP422 shows quite abundant, altered olivine, plagioclase and augite phenocrysts. The augites have pronounced partial resorption textures, as do rare plagioclases, although most plagioclase phenocrysts occur as laths showing no sign of disequilibrium.

On the basis of the petrography and revised phase relations, it is suggested that the sample crystallised clinopyroxene at 9 Kb, 1240° C. This agrees well with MacDonald and Whyte's (1981) estimate of the base of the crust. If the magma then rose through the crust, cooling as it moved, then olivine and plagioclase would have crystallised. The plagioclase is predicted to have crystallised at near-surface pressures. The augite would be expected to be partially

resorbed during this stage. The eruption temperature is predicted to have been approximately 1160° C. This interpretation could be refined by mineral analysis. However, it appears to be a more plausible scenario than that presented by Ford and Macdonald (1978), as it does not require evolution to a 3-phase cotectic at the base of the crust, and does not require an influx of water at that same level. From a comparison with the compositions in this study, more evolved lavas than ZP422 are expected to show 3-phase cotectic relationships at elevated pressures involving olivine + clinopyroxene + plagioclase.

Preservation of Polybaric Phenocryst Crystallisation

Returning to Figure 7-16, it is evident that most of the interpreted samples show a lower crust to upper mantle stage of phenocryst growth or liquid evolution. If shallow (<10 km) magma chambers were widespread this would not be observed, as fractionation to low pressure 3-phase cotectics (olivine-clinopyroxene-plagioclase) would be expected to eradicate evidence of the earlier evolution. This is supported by the lack of identified near-surface magma chambers or cumulates, other than those associated with intermediate and salic derivatives. The preservation of probable high pressure augites and aluminous spinels also suggests the host magmas did not undergo a significant pause during ascent. Similarly, the preservation of glomerocrysts interpreted as from lower crustal levels, suggests no low pressure fractionation.

Macdonald (1975) showed for two representative lava successions that the bulk compositions reflect fractionation of clinopyroxene-bearing assemblages in the basic rocks, replaced by fractionation of plagioclase-bearing, clinopyroxene-free assemblages in the intermediate and more evolved rocks. The experimental model presented here, confirms the former assemblage has an elevated pressure origin, whereas the latter assemblage has a near-surface origin. This indicates for the basic rocks their compositions have not been greatly modified by evolution at near-surface pressures. For the more evolved rocks, shallow magma chambers controlling bulk composition trends are likely. From structural evidence, Francis (1983) and Upton (1982) interpreted much of the Dinantian volcanism as having been controlled by deep-seated fractures of the crust.

Ascent of the magmas along such planes of weakness could explain why high pressure stages of evolution are preserved. The abundance of small, short-lived volcanoes, pointed out by Upton (1982), is also taken to indicate the absence of large, shallow magma chambers where extensive fractionation could have occurred. The major-element composition variations discussed by Macdonald (1975) show individual fractionation trends towards increasing degrees of silica saturation from alkalic magnesian basalts. Macdonald suggested that the clinopyroxene necessary to any fractionation scheme explaining this variation, would need to be nepheline-normative. This is confirmed by the phenocryst analyses presented here. The aluminous, high Al^{VI}/Al^{IV} character of the augites further supports an early, high-pressure origin of these phenocrysts. In this study the association of high-Al, low-Cr spinels with the high-pressure augites has been emphasised. Fractionation involving spinel provides a better explanation of the observed compositional trends than schemes using only silicate phases. The occurrence of these aluminous spinels in rocks also containing plagioclase phenocrysts (e.g. AS1/36017, MV514, AS2), is interpreted as indicating polybaric evolution. It is suggested that the spinels crystallised with augite before any other aluminous phase (plagioclase). Further, the spinels may have formed as the stable, high-pressure aluminous mineral, analogous to the low to high pressure transition from plagioclase lherzolite to spinel lherzolite.

The low-pressure assemblages (< 3 Kb) shown in Figure 7-16 indicate that lavas were erupted in equilibrium with olivine and/or plagioclase. None of the plotted samples appear to have been in equilibrium with clinopyroxene at eruption, on the basis of anydrous equilibrium crystallisation. Several samples are interpreted to have preserved more than one phase of augite phenocryst growth, e.g. MV703, ES2058 and AS1/36017. ES2058, together with MV520, contains augite phenocrysts interpreted as having grown rapidly. In these two samples the oscillatory- and sector-zoned phenocrysts may have formed at the time of emplacement of the magmas, i.e. at depths of only a few kilometres. For the other samples, providing volatile pressures were low and plagioclase was not suppressed by rapid cooling of the magma, the later augite growth is believed to have occurred at mid-crustal levels or deeper.

Although few samples contain low-pressure assemblages which can be interpreted quantitatively, many of the others contain discrete phenocrysts or overgrowths which are best explained by crystallisation during ascent, perhaps at low pressures. The group 2 samples, showing a liquidus 3-phase cotectic at moderate pressures, commonly contain more plagioclase than predicted, if all the phenocrysts had grown at the cotectic. The crystallisation model predicts that a magma rising from the cotectic and cooling would crystallise further plagioclase and a modally small percentage of olivine.

The predicted phase relations may allow some estimation of the rate of cooling of the magmas during ascent. There is no indisputable evidence for superheating of any magma, which suggests minimum cooling rates of 2 - 4° C/Kb to stay below the sample liquidus temperature. MV514 contains two assemblages; the early assemblage is interpreted as having crystallised at 11½ Kb, 1235° C, with the finally erupted assemblage predicted at approximately 1180° C. The host magma has cooled at an average of 5° C/Kb from upper mantle depths to eruption. Group 1 sample MV166 contains two distinct generations of spinel. The more magnesian spinels occur as partially resorbed phenocrysts set in the groundmass. They are homogeneous and are interpreted as having grown at the same stage as augite phenocrysts, now also partially resorbed. Olivine also crystallised with these phases, in an assemblage interpreted as reflecting equilibrium crystallisation at approximately 10 Kb. Uprise and cooling of the magma at 5° C/Kb could have carried the phenocrysts into conditions where the augite and spinel were unstable. Olivine, however, continued to crystallise and, from inclusions preserved near the olivine margins, a less magnesian spinel appeared. Thus, olivine and spinel are interpreted to have crystallised at crustal pressures, although the pressure range in which this occurred is not clear. Similar cooling rates would satisfactorily explain many of the other phenocryst assemblages.

Similar examples of lower pressure crystallisation in addition to an earlier phenocryst assemblage, are common in the studied samples. MV516 contains olivine phenocrysts interpreted to have grown during magma ascent from an earlier clinopyroxene equilibrium. MV402

contains numerous plagioclase phenocrysts clustered around augite glomerocrysts. Early, augite phenocryst growth has been preserved, with later plagioclase phenocrysts indicating the low-pressure equilibrium. MV403 contains large olivine and small augite phenocrysts. From the petrography and mineral chemistry, the augite appears to have crystallised at a later stage than the most forsteritic olivine, perhaps during ascent of the magma. Samples MV501, MV160, MV167 and MV121A have all been interpreted as having passed through an olivine + clinopyroxene + plagioclase stage, yet they could contain early olivine and clinopyroxene phenocrysts, with plagioclase joining the assemblage after clinopyroxene had become unstable. Those samples interpreted as containing only near-surface phenocrysts, may be atypical of the suite since the investigated sections show no sign of earlier, higher pressure phenocrysts.

Origin of the Olivine + Clinopyroxene + Spinel Microphyric Basalts

The Group 4 samples have been interpreted as containing only phenocrysts grown during magma ascent. If this is true, and there has been no significant accumulation of phenocrysts, then the bulk compositions may show the P - T conditions of the last assemblage with which they equilibrated. The predicted phase relations for all of these rocks, show olivine as the liquidus phase until at least 10 Kb, where it is replaced by clinopyroxene. Clearly, if the liquids were only in equilibrium with one phase, there is a broad range of conditions applicable. However, it has been noted by other workers (e.g. Macdonald, 1975; Upton, 1982) that the most primitive bulk compositions contain olivine + clinopyroxene phenocryst assemblages. This has been found to be the case for the samples investigated in this study, with the additional note that spinel is also present. The bulk compositional variation has also been interpreted as explicable by olivine + clinopyroxene + spinel fractionation. Macdonald (1975) identified olivine + clinopyroxene fractionation as a mechanism for producing the Kintyre lavas. For the Early Campsie lavas, however, he considered clinopyroxene-only fractionation as responsible for the compositional trends. The samples in this study (in Group 4) show no evidence of clinopyroxene phenocryst growth before olivine. On the contrary, olivine may have appeared first in

some rocks, e.g. MV521. However, bearing in mind the rapid decrease of the clinopyroxene crystallisation temperature with decreasing pressure, it is suggested that any sample containing augite phenocrysts (crystallised during ascent) was probably saturated, or nearly so, with respect to clinopyroxene at its liquidus. The assumption is, therefore, the bulk compositions represent liquids which were in equilibrium with clinopyroxene, and probably olivine, at high pressures. Figure 7-16 shows the predicted pressure and temperature at which each group 4 sample (MV400, MV106, MV114, MV78, MV178, MV406, MV109 and MV521) has olivine and clinopyroxene on its liquidus. For these samples, a stage of rapid cooling is implied to have occurred at high pressures to produce the augite phenocrysts. This is not anticipated to have continued to low pressures, as plagioclase phenocrysts might have crystallised.

All other samples showing olivine + clinopyroxene at the liquidus at some stage, and considered to represent possible liquid compositions, have been marked on Figure 7-16 for comparison with the group 4 samples. The points have been labelled "LIQUID" in the key. Note that most of the predicted points lie on a trend of increasing pressure with temperature. MV93 lies off this trend towards higher temperatures, again showing its uniqueness in the studied rocks. For the remainder, all show olivine + clinopyroxene at their liquidus in the range 9½ - 22½ Kb. Essentially, the pressure range is confined to the upper mantle. The Group 4 samples lie within the range of the complete sample set. The slope of the trend with pressure is approximately 12° C/Kb, partly governed by the slope chosen for the change of clinopyroxene crystallisation temperature with pressure. Similar trends would result from different values of the pressure effects on mineral crystallisation temperatures.

If the trend is taken as real, and applicable to these samples, then it may be of petrogenetic significance. Two explanations are proposed. Firstly, the plotted pressure-temperature points may indicate where each composition was efficiently extracted from the main fractionation process, where crystallisation of high pressure olivine, clinopyroxene and spinel produced the liquid compositional trends forming the lava suites. The cluster of points in the region

9½ - 12 Kb, including rocks interpreted as containing high-pressure phenocrysts, could perhaps be envisaged as an uppermost mantle ponding of the magma in intrusions. Underplating mechanisms involving magma evolution at the region of the crust-mantle interface, have been proposed for Tertiary lavas in Queensland, Australia, (Ewart et al., 1980), and for flood basalts (Cox, 1980). Intrusion of parental magnesian basaltic magmas into this region, crystallisation of olivine + clinopyroxene + aluminous spinel assemblages, and then fractionation of the liquids, sometimes including the crystallising assemblage, appears to fit the evidence. For the higher pressure predictions, perhaps 30 km below the crust-mantle boundary, flow crystallisation in conduits might be more plausible. Irving (1980) described this mechanism for basanitic magmas in the pressure range 15 - 25 Kb. From a study of composite inclusions, he deduced that crystal-liquid separation in these conduits would be very efficient. In the Scottish Permo-Carboniferous province,the abundant wehrlite and pyroxenite inclusions could represent crystal segregates. The rarity of composite inclusions from the Scottish province may indicate that the nodule incorporation events were confined to the crust-mantle boundary, supported by the association of upper mantle peridotites and lower crustal granulites. Granulite-free inclusion assemblages may be more likely to provide the proposed composite inclusions. Irving also described aluminous spinels and augites comparable with those in the inclusions and with phenocrysts in the basalts of this study. If the crystallising assemblages in these conduits excluded olivine, then the predicted P - T points would be moved up-pressure along the trend into clinopyroxene + liquid equilibria. No phases have been identified in the basalts as having an origin in the pressure range above approximately 14 Kb. This could be interpreted as indicating both of the above mechanisms operated, with the segregation model of Irving (1980) providing the more efficient crystal fractionation process.

Secondly, the P - T points could represent the last equilibration of the compositions with mantle lherzolite. In the absence of a satisfactory low-Ca pyroxene mineral temperature equation this suggestion must be considered speculative. However, the points lie

slightly above or close to the experimentally-determined solidus of a relatively Fe-rich spinel lherzolite (Takahashi and Kushiro, 1983), plotted as a solid line in Figure 7-16, in the pressure range 11 - 24 Kb. The crystallisation model predicts the olivine in equilibrium with the bulk compositions to be Fo_{85-89}. The more magnesian end of this range is similar to olivine found in spinel lherzolite nodules. In addition, experimental studies of alkali olivine basalts have found olivine + clinopyroxene + low-Ca pyroxene at the liquidus at pressures and temperatures included in the trend of Figure 7-16, (e.g. Thompson, 1974a; Tatsumi et al., 1983).

Because of the abundance of suitable phenocryst or nodule mineral compositions for the 9 - 12 Kb end of the range, together with the evidence for fractionation of clinopyroxene-bearing assemblages, a crystal fractionation model is favoured for the lower pressure equilibrated rocks. At pressures greater than 12 Kb, the flow segregation model of Irving (1980) is favoured. This model can explain the features of the basalts without needing to interpret them as equilibrium primary melts from Fe-rich spinel lherzolite.

Orthopyroxene

Orthopyroxene-bearing nodules with igneous textures have been noted by Upton et al. (1983) from Bute. The compositions are similar to the phenocrysts described in MV121A, supporting a magmatic origin for the latter phenocrysts. Overall, however, orthopyroxene phenocrysts and orthopyroxene-bearing inclusions are rare in the province, and there is no evidence for a major role for the phase in the evolution of the basalts. Extract calculations across the range of compositions in this study do not indicate low-Ca pyroxene as a participating phase. However, the occurrence of low-Ca pyroxene in the groundmass of MV40A suggests the phase could occur as low-pressure phenocrysts in suitable, intermediate compositions.

Effects of Volatiles

Throughout this interpretation the emphasis has been on anhydrous phase relations. Within the compositional range investigated, there is little evidence for significant volatile

pressures at the time of phenocryst growth. MV702 may have recorded an episode of near-surface, rapid, plagioclase growth associated with degassing of a magma. The skeletal habit of the phenocrysts is compatible with this origin. This sample may have evolved to the olivine-plagioclase cotectic at low pH_2O, before the preserved phenocrysts crystallised. MV506 contains less modal plagioclase phenocrysts than expected from the crystallisation model, and may have evolved under significant pH_2O. However, in this sample the effects of alteration might also account for the discrepancy.

The abundance of plagioclase phenocrysts in many samples could be related to the water content of the magmas. Many of the plagioclase-phyric samples show plagioclase as the liquidus phase to high pressures. Evolution of the bulk compositions in water-undersaturated conditions, followed by uprise and associated loss of volatiles, could produce some of the observed skeletal plagioclase. Zoning in plagioclase in AS1/36017 could be explained in this way. However, plagioclase accumulation could also produce the experimental relations, with growth during ascent of the magma accounting for the rapid growth textures. At shallow levels, both possibilities are expected to occur. That volatiles are present in the magmas at these levels can not be disputed, e.g. hydrous silicates in the groundmass of ES2058.

At higher pressures, volatiles may have been important in the generation and early evolution of some rocks, e.g. MV716 and MV718. No satisfactory, anhydrous explanation of their phenocryst assemblages was found. MV93 is also a sample which might be better explained by invoking significant pH_2O and/or pCO_2.

Magnetite and Ilmenite

The role of magnetite crystallisation in preventing Fe-enrichment has been indicated by Macdonald (1975), and Upton (1982). It has not been possible to establish a satisfactory mineral temperature equation for this phase, and so quantitative estimates of the conditions of growth of the phenocrysts are limited. From the silicate phase relations and petrography, magnetite (and ilmenite) are interpreted to have crystallised at 7 - 8 Kb in MV39A/MV39B.

Confirmation of magnetite as a possible atmospheric pressure phenocryst phase was found in the experiments. For example MV13F, which contains olivine, plagioclase and titaniferous magnetite phenocrysts, is cotectic with respect to the three phases at its liquidus temperature, 1154° C. Magnetite is believed to be a possible phenocryst phase, therefore, from lower crustal levels up to the surface. Its occurrence as a phenocryst is restricted to less magnesian compositions, usually with associated plagioclase phenocrysts.

Ilmenite is even less well defined than magnetite, although it may occur up to high pressures, e.g. F4. As a phenocryst, ilmenite in this study is interpreted to have crystallised up to similar pressures to magnetite. Notably, none of the compositions studied in the melting experiments produced ilmenite at their liquidus. This may indicate that all the observed ilmenite phenocrysts were produced at a few kilobars pressure, or under significantly different conditions to the experiments.

7.5 Conclusions

Extrapolation of the crystallisation model to high pressures using empirical correction factors, allows the prediction of anhydrous equilibrium phase relations up to upper mantle pressures. Applying the model to the natural rocks, most of the observed phenocryst assemblages can not be explained at near-surface pressures. Higher pressure crystallisation could produce the assemblages, in some cases, but rarely explains all the features of the natural phenocrysts.

Utilising all the available information for each sample, seven groups of rocks have been set up. Each category contains samples showing a similar evolutionary stage, not implied to have occurred at the same pressure and temperature. Group 1 samples contain early crystallised, high Al^{VI}/Al^{IV} augite $\pm$ aluminous spinel $\pm$ olivine, but excluding plagioclase. Group 2 samples preserve a stage of olivine + clinopyroxene + plagioclase crystallisation. Group 3 samples contain early crystallised olivine phenocrysts. Group 4 samples contain microphenocrysts of variably skeletal olivine + oscillatory- and sector-zoned augite + spinel. Group 5 samples have evolved to a

stage with olivine + plagioclase ± magnetite at their liquidus. Group 6 samples contain only plagioclase ± magnetite phenocrysts. Group 7 contains samples which do not fit into other categories.

Combining the evidence from all the samples a simplified model can be produced. At pressures corresponding to the lowermost crust and the upper mantle, crystallisation of high Al^{VI}/Al^{IV} (up to 0.8) augite ± olivine ± aluminous spinel occurs. Isobaric crystallisation of magnesian basalts at these pressures may give rise to a clinopyroxenite stage of liquid evolution. Magmas extracted from this zone can be related by olivine + clinopyroxene + spinel fractionation, or clinopyroxene + spinel fractionation. Inclusions containing these mineral assemblages, showing igneous textures, are widespread throughout the province, and from associated inclusions, appear to have formed in the high-pressure range proposed for the phenocrysts.

At pressures corresponding to middle and lower crustal levels many samples appear to have evolved to an olivine + clinopyroxene + plagioclase (± magnetite and ilmenite) cotectic. Compositionally, these rocks are less magnesian than those showing the higher pressure evolution. Samples with over 6 - 7 wt % MgO are typical of the higher pressure stage, while samples with less than this characterise the crustal stage. It is likely these latter samples evolved to the olivine + clinopyroxene + plagioclase cotectic from the earlier clinopyroxene ± olivine ± spinel stage.

The implied concentration of lower crustal and upper mantle equilibration stages may provide support for the occurrence of magma intrusion at the region of the crust-mantle interface, suggested in underplating mechanisms by Ewart et al. (1980), and Cox (1980). In this study, the evidence is interpreted as showing early evolution, at the uppermost mantle levels, has not involved plagioclase. Magmas rising into the crust from this stage may be arrested and there evolve to the olivine + clinopyroxene + plagioclase cotectic. Magmas rising from this stage would then show olivine and/or plagioclase phenocrysts ± magnetite and ilmenite.

Relatively few samples contain only the low pressure olivine, plagioclase and magnetite phenocryst assemblages. Their bulk compositions are consistent with derivation from the higher pressure stages of evolution. Fractionation during ascent is possible and may explain some of the occurrences of composite lavas, and variations in composition during eruption (MacDonald, 1967). The usual inclusion of a hawaiitic component in these cases, is consistent with an origin during ascent from the less magnesian lower crustal 3-phase cotectic situation. Although entirely low-pressure phenocryst assemblages are rare in the investigated samples, most of the rocks are interpreted to have undergone further olivine and/or plagioclase $\pm$ magnetite phenocryst growth at low pressures.

The group 4 samples contain phenocrysts interpreted as having crystallised during ascent of the magmas. Assuming these compositions represent liquids, initially in equilibrium with olivine + clinopyroxene, the samples have an upper mantle origin. The favoured interpretation is that these melts were efficiently extracted from a flow crystallisation process in the upper mantle (Irving, 1980), and crystallised their observed phenocryst assemblages at a range of pressures during ascent.

Volatile pressures are not believed to have been important in the origin of the phenocryst assemblages in most of the samples. The possibility remains, however, that high volatile pressures may have played a role in the generation of some of the magmas, particularly the more undersaturated varieties. In the phenocryst assemblages, some plagioclase zoning and crystal habits can be interpreted as due to variations in the water content of the magmas. There is no clear evidence that this took place at anything other than low pressures. Published studies of more evolved rocks have explained much of the variation in compositions and phenocryst phases, as due to near-surface fractionation of magmas with significant water contents, perhaps originating from the surrounding sediments.

Comparing the above interpretation with the magmatic associations of Macdonald (1975), some comments can be made. Association 1 contains a range of compositions from ankaramites to trachytes and rhyolites. The ankaramites are believed to contain

high pressure, augite phenocrysts, and it is anticipated that careful study will reveal the common association of highly aluminous, low-Cr spinels. Crystallisation in the uppermost mantle could produce much of the compositional variation from basalt to hawaiite. Ascent into the lower crust could bring plagioclase into the crystallising assemblage, and further fractionation may occur. Crystallisation during uprise of olivine and/or plagioclase ± Fe-Ti oxides is expected to have occurred. Some near-surface magma chambers are probably present, and may account for the variation from hawaiite to mugearite and beyond. This suggests, for example, the volcano of Arthur's Seat had a small near-surface magma chamber where the evolved magmas were produced, perhaps with significant volatile contents.

Association 2, dominated by feldspar-phyric hawaiites, is also anticipated to have undergone the upper mantle, clinopyroxene-dominated fractionation stage. However, unlike association 1, the early stage compositions do not appear to have been erupted frequently, and the bulk of the magmas may only contain phenocrysts grown during ascent from a lower crustal olivine + clinopyroxene + plagioclase cotectic, or from an uppermost mantle clinopyroxene-bearing equilibrium.

Association 3 is dominated by olivine ± clinopyroxene microphyric lavas and intrusions. These are believed to be analogous to the Group 4 compositions in this study, and are interpreted accordingly. Liquids, perhaps having undergone flow crystallisation in the upper mantle, have risen from mantle depths to the surface without significant pauses in the crust. Phenocrysts are interpreted to have been produced by dynamic crystallisation during this ascent. The associated rare ankaramites may indicate magmas which were arrested at the crust-mantle boundary before ascent.

Accordingly, association 1 may contain phenocrysts produced at a range of pressures from uppermost mantle to near-surface. Association 2 may contain phenocryst assemblages dominated by crystallisation at middle to upper crustal levels, although it is anticipated that earlier stages will have been important in producing the hawaiitic bulk compositions, similar perhaps to association 1.

Association 3 may contain phenocrysts grown during ascent from upper mantle pressures to near-surface. The bulk compositions of this association are interpreted to show upper mantle stages of equilibration, consistent with their identification as the most primitive basalts (Macdonald, 1975). The abundance of association 3 lavas in Silesian times may indicate more direct ascent of the later magmas from the upper mantle to eruption. The implication of lower pressure stages in associations 1 and 2 may indicate that the uppermost mantle, and lower crustal, equilibration stages were largely confined to these associations and to the Dinantian volcanism.

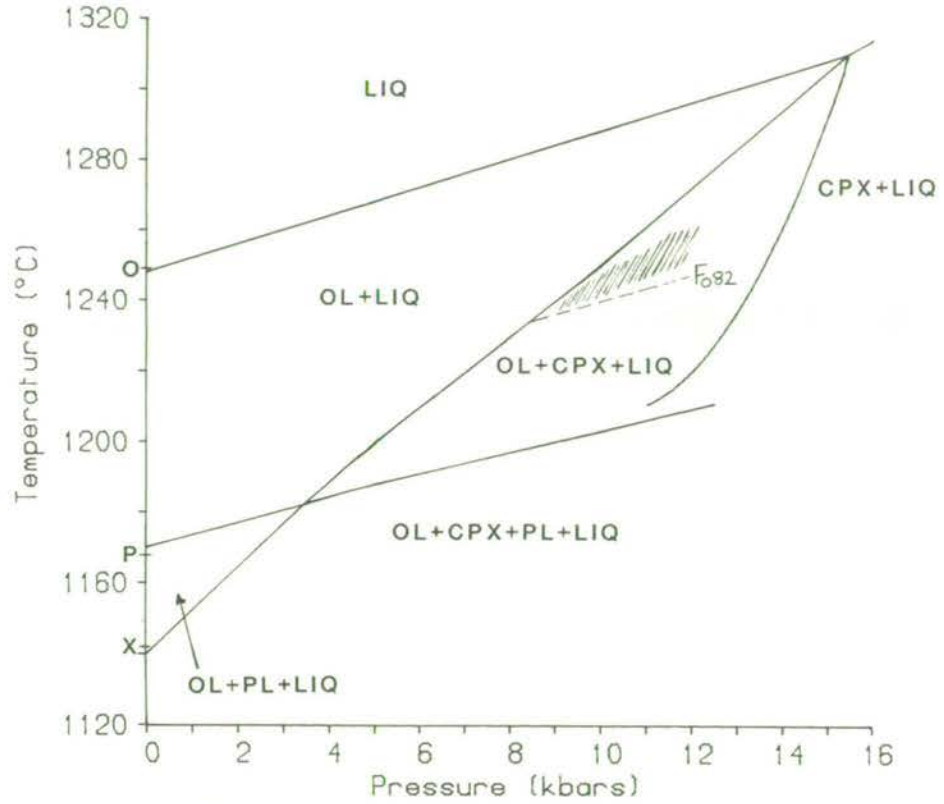

Figure 7-1. Predicted phase relations for sample MV406, with experimentally determined liquidus temperatures for olivine (O), plagioclase (P) and clinopyroxene (X) at 1 atm. Shaded area is the P-T range in which the model best predicts the observed phenocrysts. See the text for discussion.

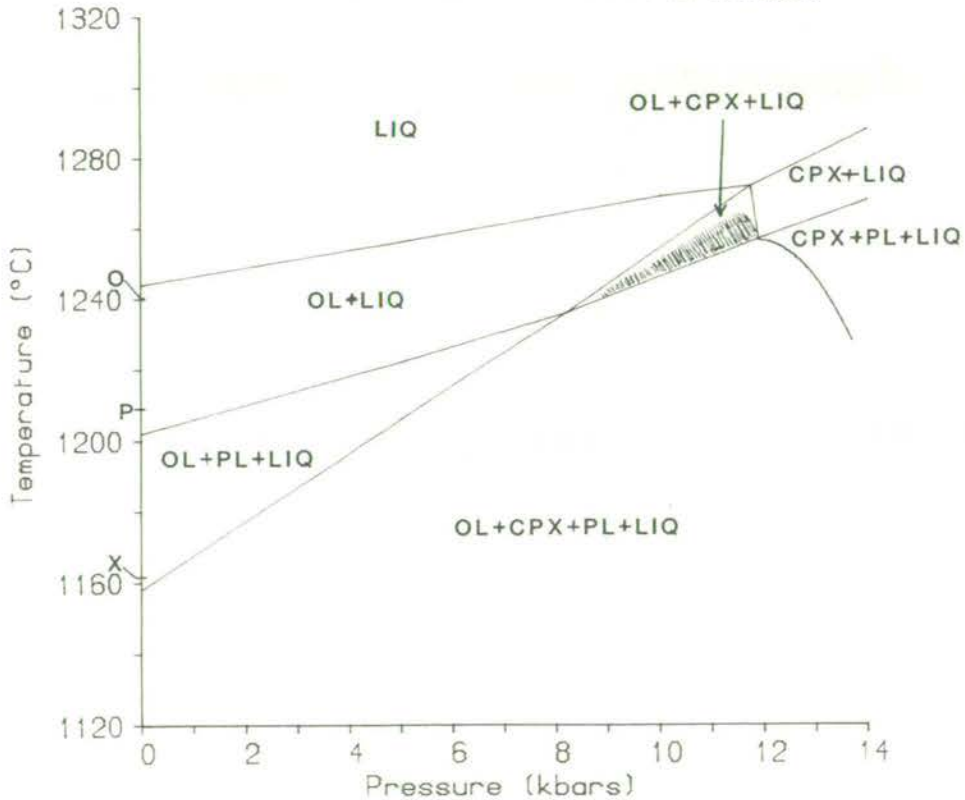

Figure 7-2. Predicted phase relations for sample MV106, with experimentally determined liquidus temperatures for olivine (O), plagioclase (P) and clinopyroxene (X) at 1 atm. Shaded area is the P-T range in which the model best predicts the observed phenocrysts. See the text for discussion.

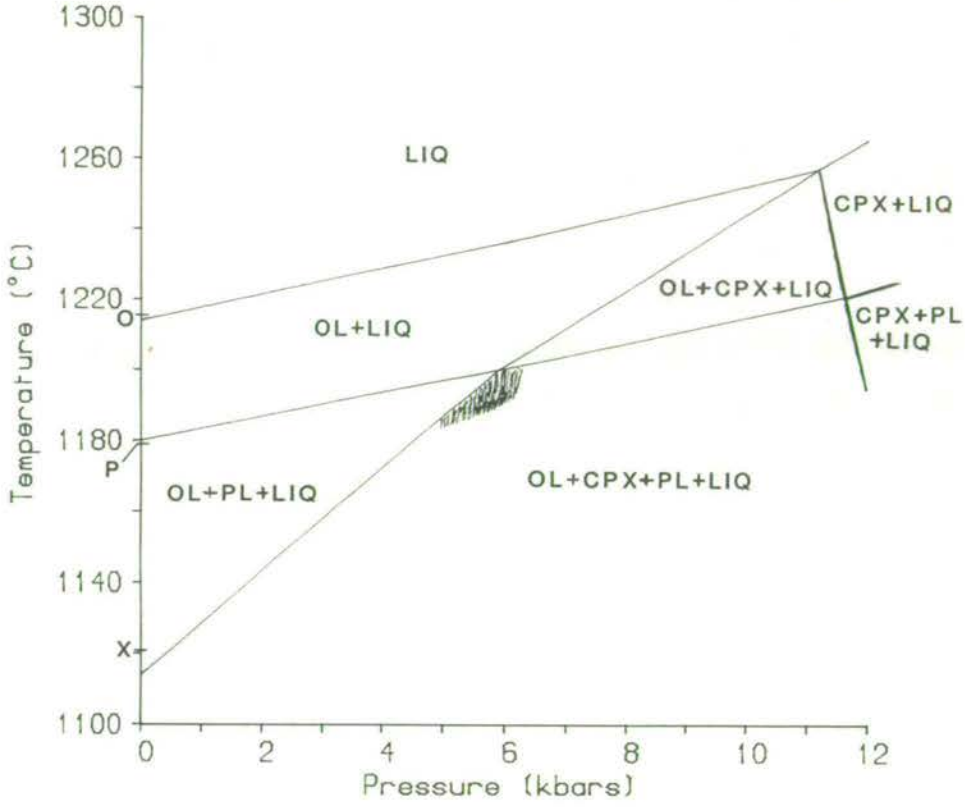

Figure 7-3. Predicted phase relations for sample MV160, with experimentally determined liquidus temperatures for olivine (O), plagioclase (P) and clinopyroxene (X) at 1 atm. Shaded area is the P-T range in which the model best predicts the observed phenocrysts. See the text for discussion.

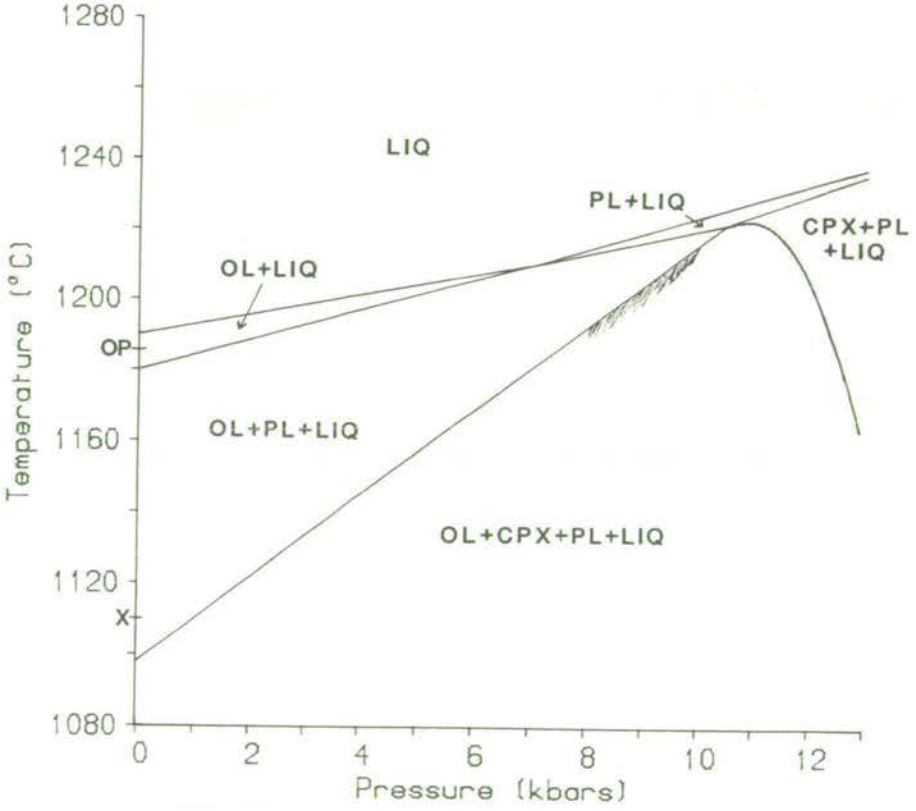

Figure 7-4. Predicted phase relations for sample MV72, with experimentally determined liquidus temperatures for olivine (O), plagioclase (P) and clinopyroxene (X) at 1 atm. Shaded area is the P-T range in which the model best predicts the observed phenocrysts. See the text for discussion.

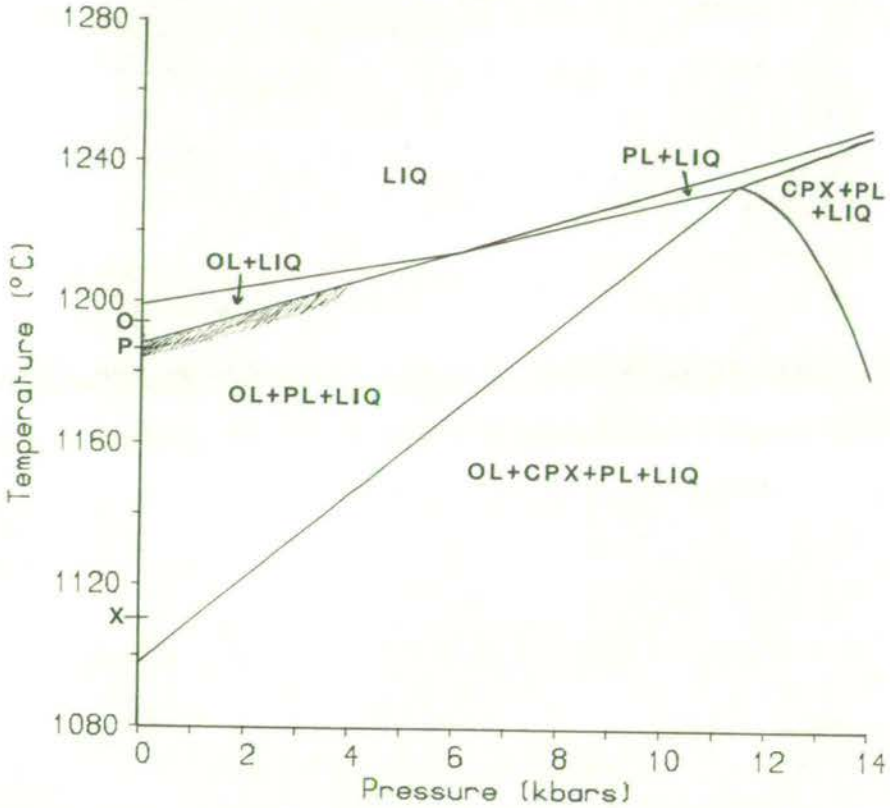

Figure 7-5. Predicted phase relations for sample MV514, with experimentally determined liquidus temperatures for olivine (O), plagioclase (P) and clinopyroxene (X) at 1 atm. Shaded area is the P-T range in which the model best predicts the observed phenocrysts. See the text for discussion.

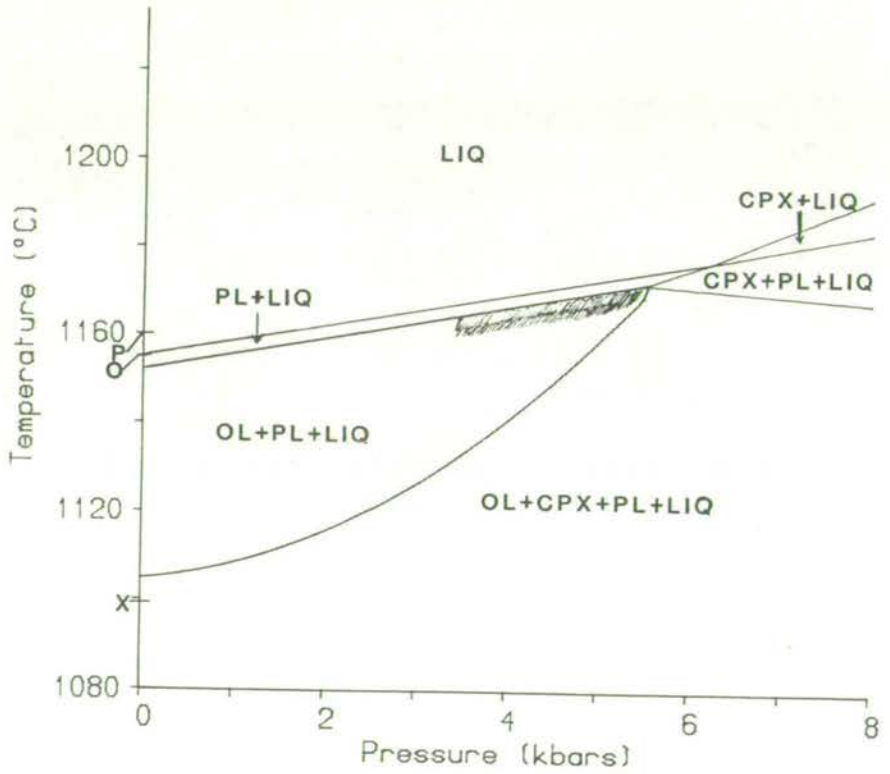

Figure 7-6. Predicted phase relations for sample MV13, with experimentally determined liquidus temperatures for olivine (O), plagioclase (P) and clinopyroxene (X) at 1 atm. Shaded area is the P-T range in which the model best predicts the observed phenocrysts. See the text for discussion.

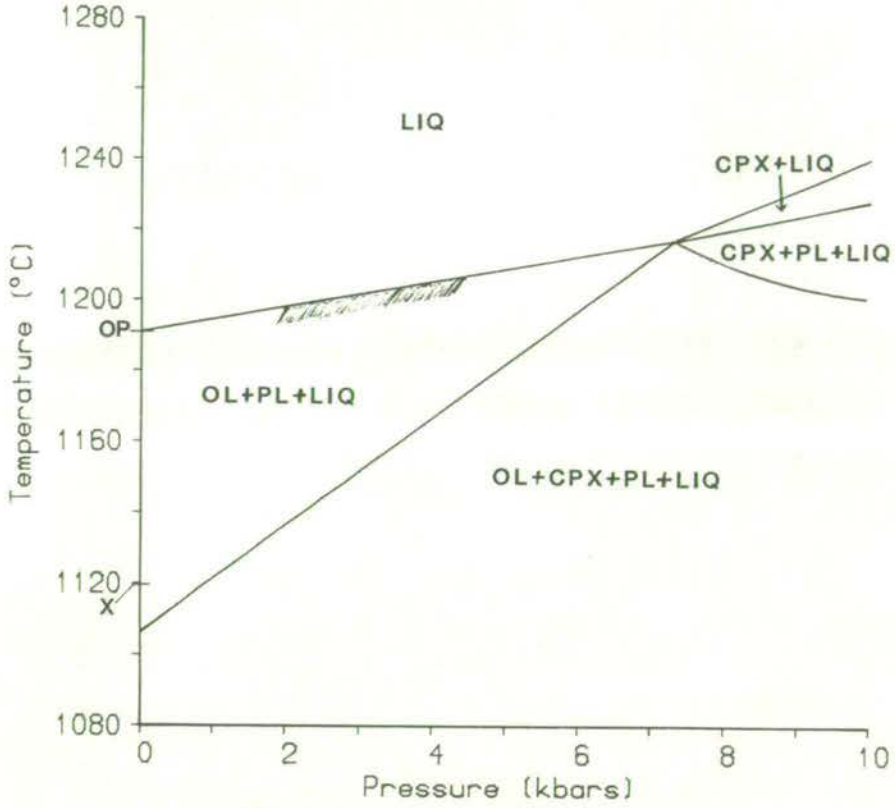

Figure 7-7. Predicted phase relations for sample MV704, with experimentally determined liquidus temperatures for olivine (O), plagioclase (P) and clinopyroxene (X) at 1 atm. Shaded area is the P-T range in which the model best predicts the observed phenocrysts. See the text for discussion.

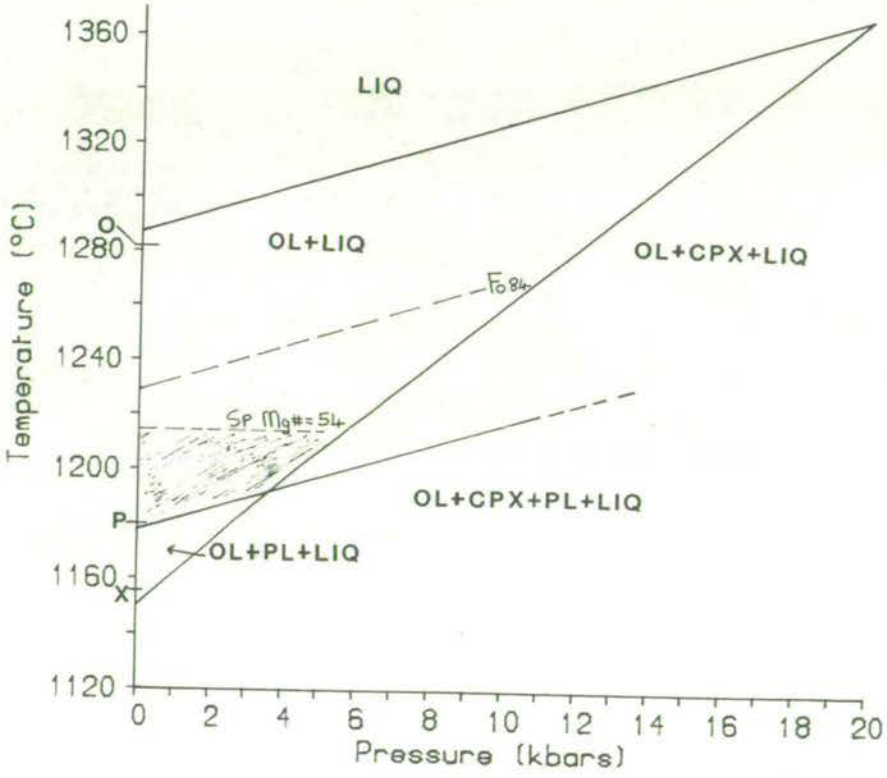

Figure 7-8. Predicted phase relations for sample MV164, with experimentally determined liquidus temperatures for olivine (O), plagioclase (P) and clinopyroxene (X) at 1 atm. Shaded area is the P-T range in which the model best predicts the observed phenocrysts. See the text for discussion.

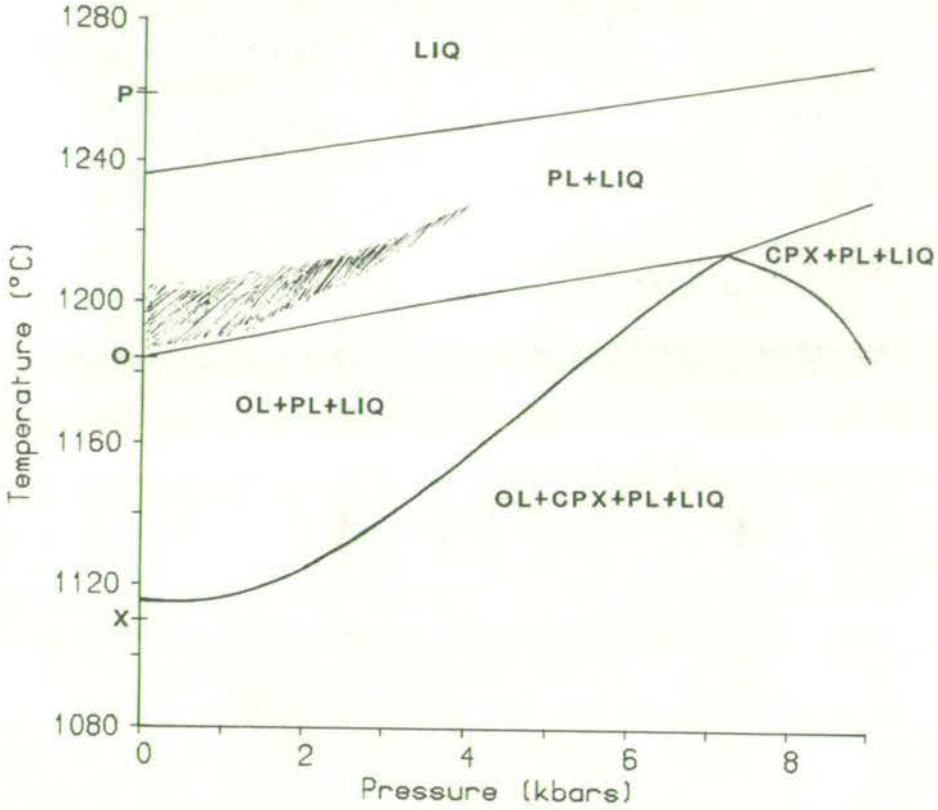

Figure 7-9. Predicted phase relations for sample MV702, with experimentally determined liquidus temperatures for olivine (O), plagioclase (P) and clinopyroxene (X) at 1 atm. Shaded area is the P-T range in which the model best predicts the observed phenocrysts. See the text for discussion.

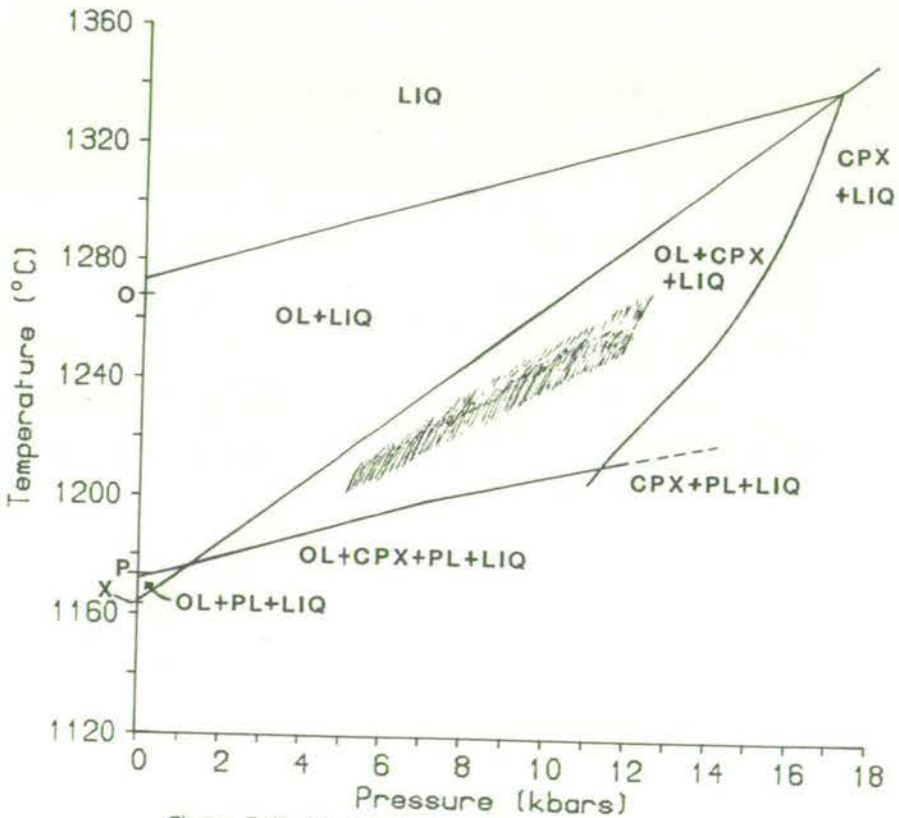

Figure 7-10. Predicted phase relations for sample MV166, with experimentally determined liquidus temperatures for olivine (O), plagioclase (P) and clinopyroxene (X) at 1 atm. Shaded area is the P-T range in which the model best predicts the observed phenocrysts. See the text for discussion.

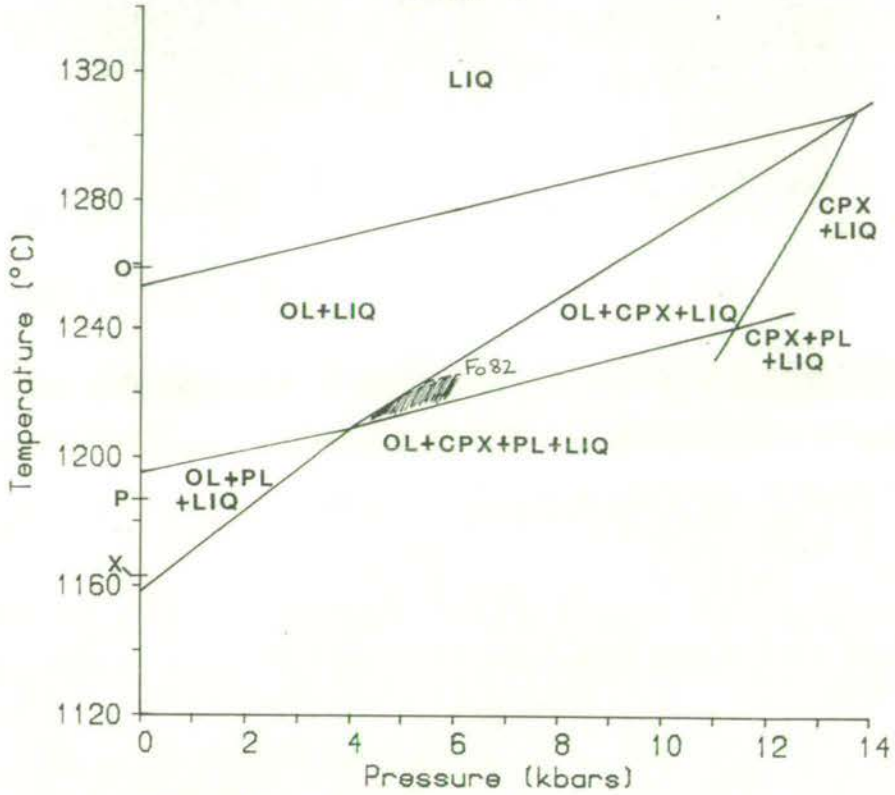

Figure 7-11. Predicted phase relations for sample MV703, with experimentally determined liquidus temperatures for olivine (O), plagioclase (P) and clinopyroxene (X) at 1 atm. Shaded area is the P-T range in which the model best predicts the observed phenocrysts. See the text for discussion.

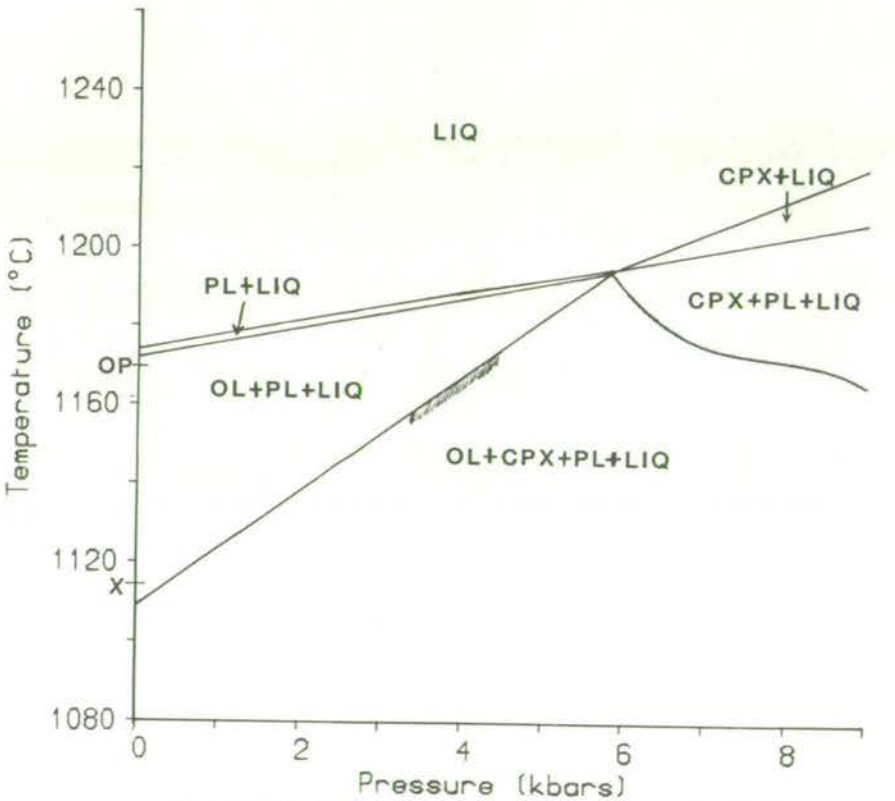

Figure 7-12. Predicted phase relations for sample MV52, with experimentally determined liquidus temperatures for olivine (O), plagioclase (P) and clinopyroxene (X) at 1 atm. Shaded area is the P-T range in which the model best predicts the observed phenocrysts. See the text for discussion.

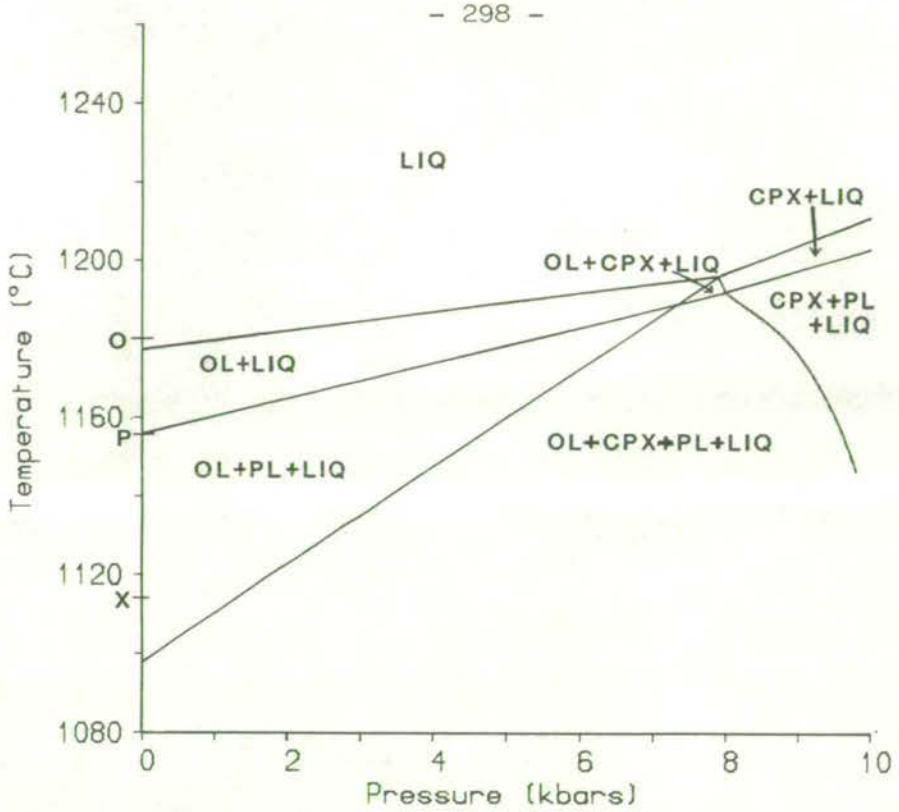

Figure 7-13a. Predicted phase relations for sample MV39B, with experimentally determined liquidus temperatures for olivine (O), plagioclase (P) and clinopyroxene (X) at 1 atm.

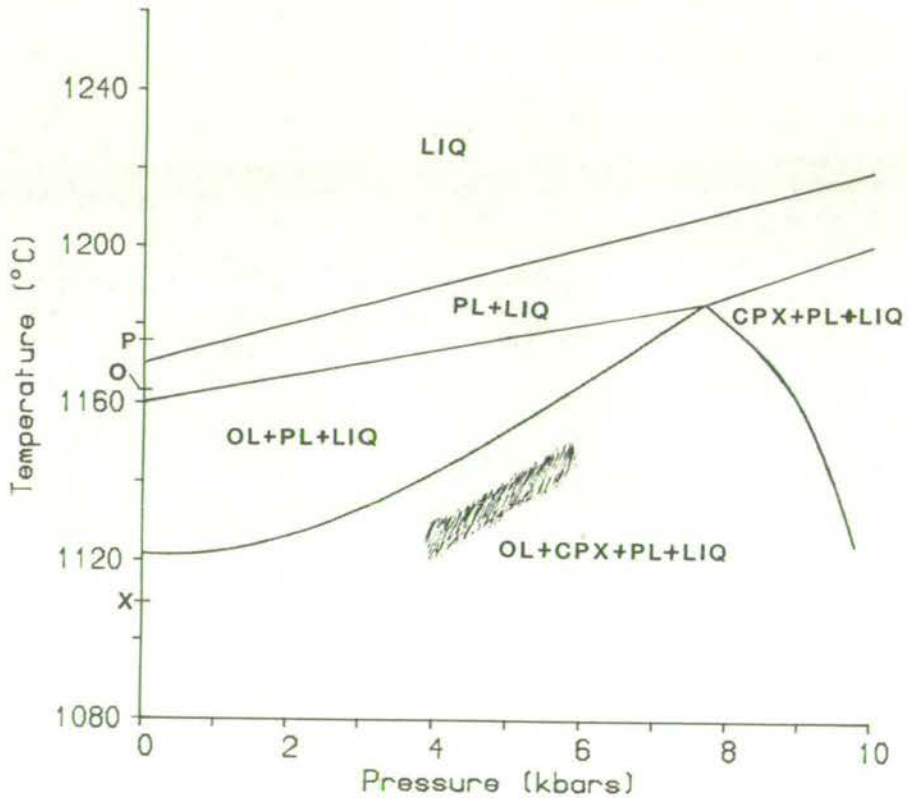

Figure 7-13b. Predicted phase relations for sample MV39A, with experimentally determined liquidus temperatures for olivine (O), plagioclase (P) and clinopyroxene (X) at 1 atm. Shaded area is the P-T range in which the model best predicts the observed phenocrysts. See the text for discussion.

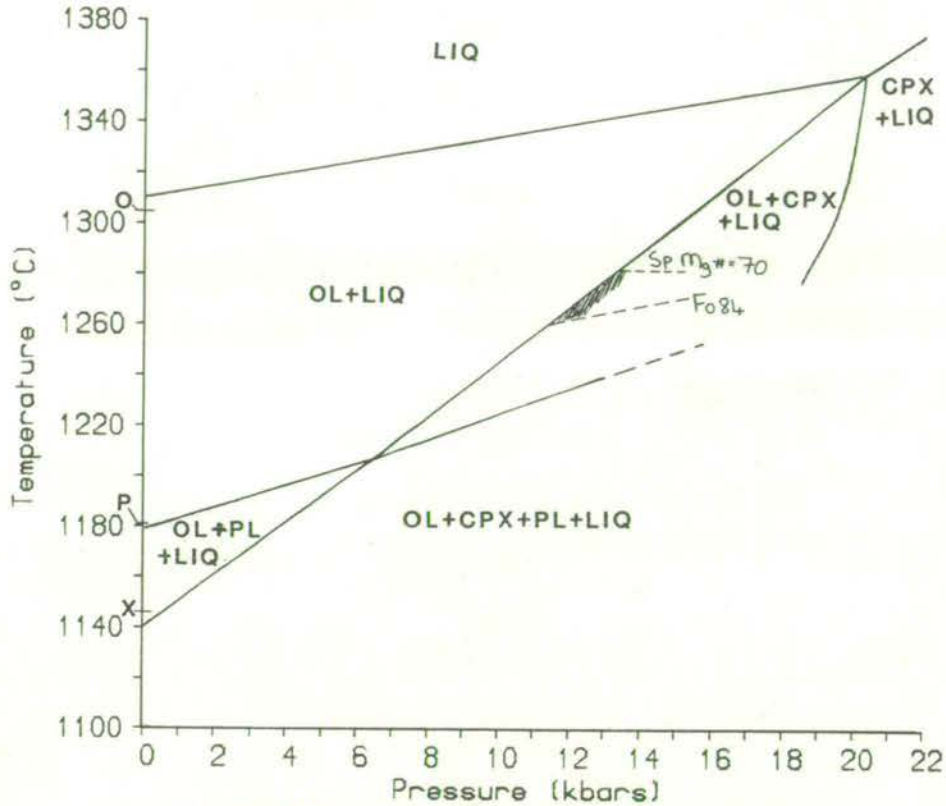

Figure 7-14. Predicted phase relations for sample MV403, with experimentally determined liquidus temperatures for olivine (O), plagioclase (P) and clinopyroxene (X) at 1 atm. Shaded area is the P-T range in which the model best predicts the observed phenocrysts. See the text for discussion.

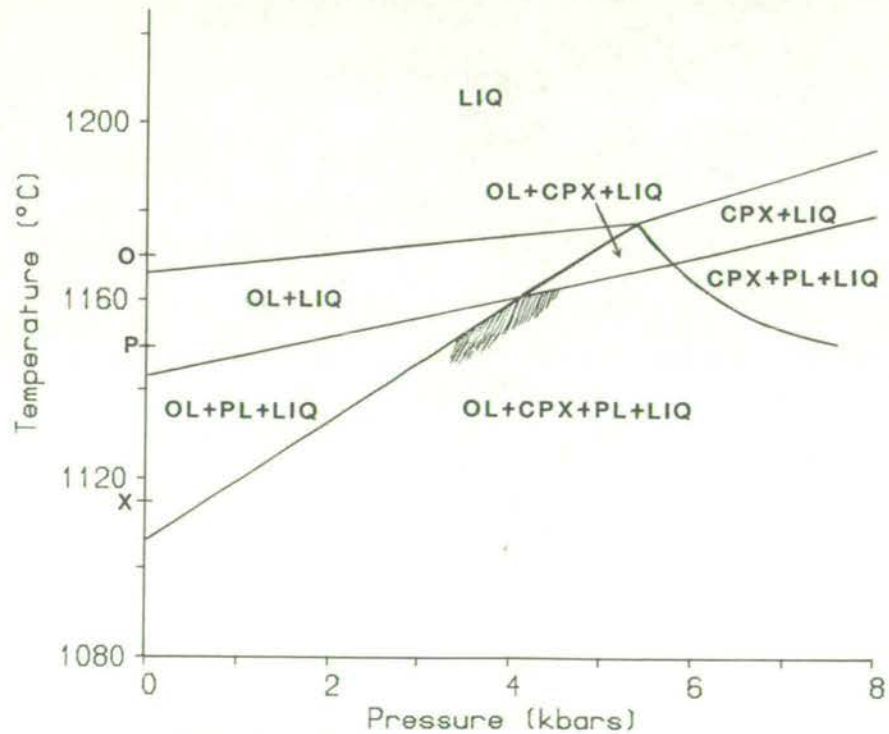

Figure 7-15. Predicted phase relations for sample MV121A, with experimentally determined liquidus temperatures for olivine (O), plagioclase (P) and clinopyroxene (X) at 1 atm. Shaded area is the P-T range in which the model best predicts the observed phenocrysts. See the text for discussion.

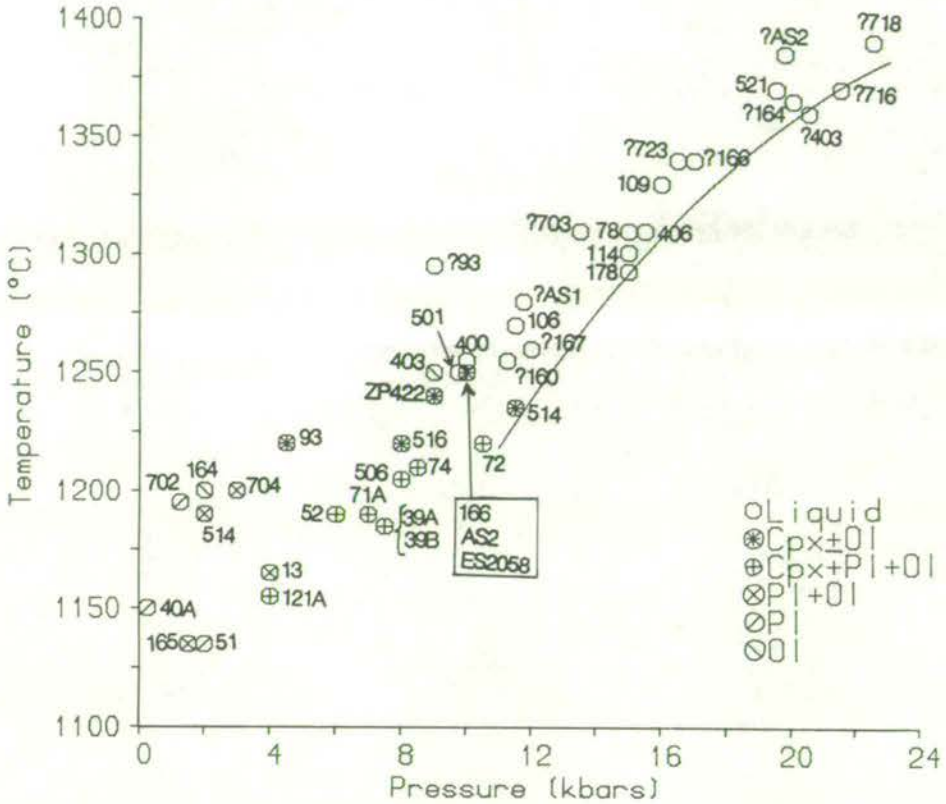

Figure 7-16. Estimated pressures and temperatures of origin of phenocryst assemblages and bulk compositions ('liquids'). The curve represents the experimental solidus of an Fe-rich spinel lherzolite, determined by Takahashi & Kushiro (1983). See text for discussion.

NO MAN ..... WHO HAS WRESTLED WITH A SELF-ADJUSTING CARD TABLE CAN EVER QUITE BE THE MAN HE ONCE WAS.

James Thurber.

CHAPTER 8

GENERAL SUMMARY AND CONCLUSIONS

8.1 Atmospheric Pressure Experiments

Isothermal melting experiments at atmospheric pressure on the range of bulk compositions from basalts to hawaiites, have indicated olivine is the liquidus phase (excluding spinel) for the high Mg# samples (Mg# $\geq$ 57 approximately), with plagioclase and/or olivine at the liquidus of lower Mg# samples. As sample Mg# decreases, initial olivine and clinopyroxene crystallisation temperatures decrease, with clinopyroxene never approaching the liquidus in the investigated range; plagioclase crystallisation temperatures show less clear variation although the highest plagioclase temperatures occur in the lower Mg# samples. With the exception of a single anomalous sample, clinopyroxene does not crystallise at higher temperatures than plagioclase, and never crystallises before olivine. The natural rocks commonly have phenocrysts of clinopyroxene without plagioclase, contrasting with the atmospheric pressure experiments. Similarly, the more magnesian samples show an extended range of temperatures where olivine is the only silicate mineral although the natural rocks dominantly contain two or more silicate phenocrysts, even when the percentage of phenocrysts is small.

Spinel was found to be the actual liquidus phase in most samples. This is ascribed to Cr contamination of the supplied powders. Duplicate experiments on re-crushed uncontaminated material indicated the effect of Cr is to raise spinel crystallisation temperatures. Experiments at low oxygen fugacities produced little change in the silicate mineral crystallisation temperatures but did show that spinel crystallisation is suppressed to near-solidus temperatures. Although spinel crystallisation is clearly sensitive to Cr content and oxygen fugacity, the experiments on uncontaminated samples indicated a spinel phase is a near-liquidus phase over a broad range of starting compositions at the Ni-NiO buffer. Microprobe analysis showed the oxide phase is typically Cr-Al spinel in high Mg# samples and titanomagnetite in low Mg# samples.

Microprobe analysis of the coexisting phases in the experimental charges indicated that homogeneous glass and olivine compositions were produced. Spinel phases were too small for detailed study, but showed consistent Fe^{2+}-Mg variations with temperature. A wide range of plagioclase compositions in individual charges indicated the preservation of relics from the starting material. Near-liquidus plagioclases showed a positive correlation between anorthite content and experimental temperature. Clinopyroxene compositions also indicated preservation of relics.

Systematic variations in glass compositions can be linked to the crystallisation of olivine (decrease of Mg), plagioclase (decrease of Al), clinopyroxene (decrease of Ca), opaque oxides (decrease of Fe $\pm$ Ti) and apatite (decrease of P). The percentage crystallinity of the charges increased slowly with decreasing temperature for olivine crystallisation, more rapidly for plagioclase or plagioclase + olivine, and very rapidly for clinopyroxene + plagioclase + olivine. The trend at low temperatures was towards a small proportion of olivine in the crystallising assemblages relative to plagioclase and clinopyroxene.

For the investigated samples there is a good positive correlation between the experimental temperatures and the wt % MgO contents of glasses coexisting with olivine. There is also a progressive decrease in the forsterite content of the olivines with decreasing glass Mg#. A simple positive correlation between experimental temperature and normative anorthite content of glasses coexisting with plagioclase has been found.

The ferric iron contents of the experimental glasses were calculated using an equation relating major-element compositions, temperatures, and oxygen fugacities, of published experimental glasses with known ferric-ferrous iron contents. The olivine-liquid Fe^{2+}-Mg KD has been calculated with glass iron content recast in this way. At higher temperatures (more basic compositions) KD is found to be approximately 0.30. At low temperatures (more evolved compositions) KD apparently increases to >0.35. Individual element mineral-liquid partition coefficients show a simple relation with temperature

for the range of compositions studied. Preliminary investigations of mineral-mineral equilibria indicate variations consistent with published studies for olivine-spinel (Fe^{2+}-Mg) and ilmenite-magnetite (T - fO_2).

8.2 Experimental Crystallisation Model

Detailed study of individual aspects of the experimental data has been restricted in favour of the development of a general model predicting the course of crystallisation of basaltic magma. Mineral temperature equations have been derived which relate experimental temperatures to compositional terms for glasses coexisting with individual minerals. With the addition of a large proportion of the available published experimental data, equations have been produced for olivine, plagioclase, clinopyroxene, spinel and low-Ca pyroxene. Because of a lack of Cr data for the spinel equation, and severely limited data for the low-Ca pyroxene equation, only the olivine, plagioclase and clinopyroxene equations are reliable. These latter equations can be used to predict the liquidus phase or phases of a basic natural composition, and are sufficiently sensitive to detect anomalies in sets of experimental data. At the 2σ (95%) confidence level the equations are precise to better than $\pm$ 19° C for olivine, $\pm$ 14° C for plagioclase, and $\pm$ 16° C for clinopyroxene. However, because of the nature of the equations and the method of their derivation it is difficult to assess the compositional range over which they may be applied with confidence. It is believed that a range of natural compositions from picrite to andesite will be satisfactorily modelled.

Mineral composition equations have been derived relating element concentrations in minerals to concentrations in coexisting glasses and experimental temperatures, for the same phases as the mineral temperature equations. The composition equations must be regarded as only a first approximation of the equilibria, and include a large number of mineral-glass pairs which can not be in equilibrium. Again, analyses from the literature have been added to the data sets. Some estimate of the effects of pressure on crystallising mineral compositions has been possible for the major

silicate phases. In particular, plagioclase is predicted to become more sodic at high pressures, consistent with published experimental studies.

The mineral composition equations are intended for use in combination with the mineral temperature equations in a crystallisation model, developed in conjunction with Dr. C. E. Ford. The predicted equilibrium crystallisation paths of compositions in this study match the experimentally determined data quite satisfactorily, with good agreement on liquid compositions and temperatures of appearance of the main silicate minerals. The predicted mineral compositions have not been discussed in detail but are clearly not sufficiently inaccurate to affect the other areas of agreement.

Empirical correction factors for the effect of pressure on the mineral temperature equations have been derived from a consideration of numerous published phase diagrams. Some compositional effect on the factors is apparent from synthetic system studies, but it is not yet possible to quantify this. From the published natural rock phase relations, clinopyroxene is expected to show an increase in crystallisation temperature of approximately 10° C/Kb, olivine an increase of 2 - 4° C/Kb, and plagioclase an increase of 3 - 5° C/Kb, in basic magmas.

Incorporating these factors into the model has allowed the prediction of the equilibrium phase relations of the compositions in this study up to perhaps 25Kb. Beyond this, garnet is a likely major phase. The replacement of plagioclase by spinel as a stable aluminous phase at high pressures, together with a role for high pressure low-Ca pyroxene, are possible sources of error not modelled at elevated pressures. Applying the model to the natural rocks, for anhydrous equilibrium processes, it is possible to predict the observed phenocryst assemblage and approximate phase proportions for most samples. Simple end-member compositions predicted in the model, particularly for olivine and plagioclase, may be used to further refine the estimates of the conditions of phenocryst growth.

Four main predictions emerge from the model. Assemblages including plagioclase but without clinopyroxene can be produced at low pressures. These are characterised by plagioclase and/or olivine (± magnetite and ilmenite) phenocrysts. Assemblages of olivine + plagioclase + clinopyroxene can be produced at moderate pressures (corresponding to middle to lower crustal levels). Assemblages of olivine + clinopyroxene can be produced at moderate to high pressures (corresponding to mid-crustal to upper mantle levels). Clinopyroxene-only assemblages are predicted to result from isobaric equilibrium crystallisation of the more basic compositions at high pressures, after a higher temperature stage of olivine crystallisation. The implication from this is that a clinopyroxene stage of magmatic evolution can be produced from compositions initially in equilibrium with olivine. These predictions apply to the investigated basalt to hawaiite range of samples.

8.3 The Natural Assemblages

Interpretation of the natural rocks and their phenocrysts is broadly in agreement with the experimental model but differs in the details. Although the collection comes from a large number of distinct suites, of widely differing ages, the bulk compositional variation from magnesian basalt to hawaiite can be qualitatively described by clinopyroxene-dominated fractionation. Plagioclase is not required in this assemblage but may play a role for the less magnesian samples. Published studies of individual lava successions have emphasised clinopyroxene ± olivine fractionation over similar compositional ranges to those studied here. It is suggested that spinel is also required for these schemes. This study indicates the importance of clinopyroxene in any fractionation model. Fractionation of clinopyroxene + olivine + aluminous spinel in the proportions 6 : 1 : 1 qualitatively describes the major element variations from magnesian basalt to hawaiite.

A comparison has been made with phase relations in the simplified system $XO-YO-R_2O_3-ZO_2$. If the samples are considered as unmodified products of equilibrium crystallisation, then the olivine

+ clinopyroxene phenocryst assemblages could have crystallised at elevated pressures, up to upper mantle pressures. The olivine + clinopyroxene + plagioclase phenocryst assemblages could have crystallised at relatively lower pressures within the crust.

The evidence from the petrography is believed to be critical to the understanding of individual phenocryst assemblages. The experimental model is based on equilibrium phase relations but the petrography indicates these are not always appropriate. Skeletal habit in olivines, skeletal habit and oscillatory-zoning in plagioclases, and sector- and oscillatory-zoning in clinopyroxenes, all indicate dynamic crystallisation interpreted as rapid growth from undercooled melts. Complex zoning in plagioclases in particular, also shows equilibrium crystallisation was not the only process operating on these lavas. Many phenocrysts were clearly out of equilibrium with the host liquid at some stage in their history. This is commonly inferred to have been the case at the time of eruption of many of the macroporphyritic clinopyroxene-phyric magmas. Partial resorption is indicated by rounding, embayment and development of sieve-textures. Large clinopyroxene phenocrysts with near-homogeneous cores show these resorption textures developed to varying degrees. Plagioclase phenocrysts may also be partially resorbed in this way, but in many cases the distinction between growth- and resorption-textures is difficult to make. Some samples are interpreted as containing both rapidly grown and partially resorbed plagioclase phenocrysts. Olivine phenocryst disequilibrium is less clear in these samples. Extreme rounding and some embayment, perhaps with concentrations of opaque minerals round the margins, probably indicates some partial resorption. Aluminous spinels are usually quite ragged in habit, except when enclosed in large clinopyroxenes, and these spinels were clearly not in equilibrium with the host liquid at the time of eruption. In general, the skeletal olivines and sector- and oscillatory-zoned augites, tend to be small, forming the microphyric rocks. Crystallisation from the magma during ascent may explain these phenocrysts. The commonly large, partially resorbed clinopyroxenes with homogeneous cores are often associated with large olivine phenocrysts and relatively large,

aluminous spinels. These phenocrysts could have formed by equilibrium crystallisation at depth, followed by uprise of the magma during which some resorption of the augites and spinels at least, took place. Such a generalisation based on size is not applicable to the plagioclase phenocrysts. While the very small complete phenocrysts are envisaged as having grown by near-equilibrium crystallisation at low pressures, the larger plagioclases probably represent crystallisation in a wide range of pressures and under quite variable conditions. The textural distinction of rapid-growth and resorption may indicate crystallisation during ascent, and early near-equilibrium crystallisation followed by ascent, respectively.

Glomeroporphyritic texture is developed in a few rocks. Clots of plagioclase and/or augite are most common, with olivine and magnetite occasionally present. The occurrence of cotectic points in the predicted phase relations, where olivine + clinopyroxene + plagioclase crystallise within a few degrees of the liquidus, is interpreted as evidence for a cognate origin for many of these clots. Partial resorption of the component phases is interpreted as a result of carrying high pressure compositions to lower pressures, rather than evidence for a xenolith origin. However, some probably represent xenoliths, perhaps stripped from wall-rock during ascent. The relative rarity of olivine in the postulated cognate clots may indicate olivine formed a minor proportion of the crystallising assemblage, as predicted by the experimental model. Where relative sequences of crystallisation are inferred by enclosing or surrounding relationships, the most common situation is plagioclase crystallising after clinopyroxene. Clinopyroxene may have begun to crystallise after olivine in some microphyric rocks.

Microprobe analysis has characterised the phenocryst compositions in the investigated samples. Three broad groups of clinopyroxenes have been proposed. Firstly, large phenocrysts with near-homogeneous cores have high Mg# and high Al^{VI}/Al^{IV} ratios (up to 0.8). These augites and salites are typically slightly nepheline-normative. The Al^{VI}/Al^{IV} ratios suggest crystallisation at elevated pressures up to approximately 15Kb. The partial resorption shown by most clinopyroxene phenocrysts in this group can

be interpreted as resulting from ascent of the host melt out of clinopyroxene-stable conditions. The second group of augites and salites are usually small in size, euhedral to subhedral, with high Mg#, and display sector- and/or oscillatory-zoning. Al^{VI}/Al^{IV} ratios are usually low (0.1 to rarely 0.4) which may indicate low-pressure crystallisation. However, the zoning is interpreted as indicating relatively rapid growth rates, perhaps from a cooling magma during ascent; this may decrease the Al^{VI}/Al^{IV} ratios and suggest an artificially low pressure of crystallisation. The third group of augites have lower Mg# than the previous groups, and are hypersthene-normative in character. These clinopyroxenes are not strongly zoned and may show slight partial resorption. Al^{VI}/Al^{IV} ratios range up to 0.4, interpreted as indicating crystallisation at lower pressures than the first group of pyroxenes. The first two groups may have crystallised from similar melt compositions. The third group is believed to have crystallised from more fractionated compositions.

Olivine phenocryst compositions range from Fo_{87} to Fo_{52}. Mn shows a negative correlation with forsterite contents, while Ni shows a positive correlation. The most forsteritic olivines with highest Ni contents are from olivine + clinopyroxene + spinel phenocryst assemblages. This is in agreement with the whole-rock evidence that the most primitive compositions contain olivine, clinopyroxene and spinel phenocrysts. From the experimental crystallisation model it is predicted that olivine is the most common liquidus phase at low pressures for these basalts. Crystallisation of melts of these compositions would be expected to generate olivine phenocrysts over a broad pressure range extending to the surface. Clear evidence for olivine crystallisation at high pressures is lacking. However, there is a broad increase in the Ca content of olivines as their forsterite content decreases, and as the bulk rock Ca also decreases. This is inconsistent with atmospheric pressure experimental studies of Ca in olivine and is interpreted as indicating a pressure effect. If this is the case, then the more forsteritic olivine phenocrysts crystallised at distinctly higher pressures than the least forsteritic olivines. Phenocryst rim and groundmass olivine

compositions are usually more calcic than core compositions.

Plagioclase phenocryst core compositions range from An_{83} to An_{30} with most falling in the labradorite and bytownite categories. Individual rocks can contain a wide range of plagioclase compositions, sometimes distinguished as two generations on the basis of phenocryst textures and anorthite contents. In these cases the more sodic varieties show variably developed partial resorption. From published experimental studies, widely developed normal zoning is attributed to crystallisation from a melt undergoing fairly rapid cooling; less widely developed reverse zoning may indicate near-isothermal crystallisation after some major change in conditions (often marked by discontinuous zoning), or, crystallisation under increasing volatile pressures, or, crystallisation at progressively lower pressures; oscillatory zoning is as yet poorly understood but appears to be produced by crystallisation from effectively under-cooled melts. The compositional zoning of phenocrysts in some samples is very complex and probably records the later stages of evolution of the host melt. For the Lion's Haunch basalt of Arthur's Seat, it is suggested that zoning records a stage of outgassing of the magma, tentatively associated with the incorporation of sodic plagioclase xenocrysts. Glomeroporphyritic clots of gabbroic mineralogy in this basalt contain similar plagioclases to the proposed xenocrysts. It is suggested the clots and xenocrysts represent disrupted shallow-level cumulates from a magma chamber, where the more evolved compositions of the Arthur's Seat volcano were derived.

In the investigated collection, partially resorbed plagioclases may indicate crystallisation at depth, followed by ascent to levels where these relatively sodic plagioclase compositions were unstable. Less commonly, the resorption may result from incorporation of plagioclase xenocrysts (e.g. perhaps AS1), or may be a result of magma mixing (e.g. perhaps MV40A). Skeletal textures may in some cases indicate rapid plagioclase growth after outgassing of magmas at shallow depths.

Spinels and/or magnetites are almost ubiquitously developed as phenocrysts in the studied samples. The largest spinel phenocrysts are highly aluminous (over 50 wt % Al_2O_3) and usually have little or no Cr. They are commonly associated with high Al^{VI}/Al^{IV} clinopyroxene phenocrysts. By this association, and from published studies, it is suggested these high Al/Cr spinels crystallised at high pressures. Although the Cr content of a melt will have some control on spinel composition, many samples also contain spinel with higher Cr in lower Mg# crystals. The interpretation suggested for this is that increasing pressure increases spinel Al/Cr ratios. Early high pressure spinels have high Mg# and high Al/Cr. Later lower pressure spinels have lower Mg# and lower Al/Cr. It is proposed that the highly aluminous, high Al/Cr spinels are considered as a first group, with a second group composed of lower Al/Cr spinels. This latter group represents the majority of spinels in the samples. Apart from having lower Al/Cr ratios (at a given Mg#) than first group spinels, the second group spinels tend to be smaller and show an overall variation to titanomagnetite compositions, similar to those developed as groundmass phases. Towards very low Mg#, there is a rapid decrease in spinel Cr and Al contents, and a rapid increase in Ti and Fe^{3+} contents. In agreement with published studies, the titanomagnetite phenocryst compositions are interpreted as having crystallised from the less primitive bulk compositions.

Ilmenite phenocrysts are only present in a few samples in the basalt to hawaiite range. Mg, Al, and Cr contents are low, and are interpreted as indicating low pressures of crystallisation, compared to ilmenites in an igneous spinel wehrlite nodule of presumed lowermost crust or upper mantle derivation. In the investigated collection, ilmenite phenocrysts are believed to have crystallised from the less basic compositions.

Orthopyroxene phenocrysts present in one sample are clearly not in equilibrium with the host rock. The phenocrysts are significantly less magnesian than enstatites in spinel lherzolites believed to be residual mantle compositions. The orthopyroxene phenocrysts may have crystallised at elevated pressures but it is not possible to discount a xenocrystal origin.

Coexisting magnetite-ilmenite pairs suggest that some lavas evolved at oxygen fugacities close to the Ni - NiO buffer at magmatic temperatures. This is consistent with the experimental results where uncontaminated samples have a spinel phase near the liquidus at similar oxygen fugacities.

8.4 Conclusions

Combining the evidence from the experimental and natural approaches, four distinct stages of phenocryst growth are envisaged:

1. Large, high Al^{VI}/Al^{IV} (up to 0.8) augites ± olivines ± aluminous spinels crystallised in the lowermost crust or upper mantle at pressures less than 15 Kb.

2. Large, moderate Al^{VI}/Al^{IV} (0.4 to 0.6) augites + olivines + plagioclases ± Fe-Ti oxides crystallised at mid to lower crustal levels.

3. Plagioclases and/or olivines ± Fe-Ti oxides crystallised at mid to upper crustal levels, perhaps during ascent of the magmas.

4. Small, rapid-growth olivines + clinopyroxenes + spinels crystallised during ascent from upper mantle levels, possibly at a broad range of pressures.

Stages 1 - 3 may occur in a single magma, whereas stage 4 is probably not associated with the others. This leads to a general model. Lower Carboniferous basic magmas, which show a broad range of phenocryst assemblages, are characterised by stages 1 - 3. The late Carboniferous basic magmas, characterised by microphyric olivine-clinopyroxene-spinel assemblages and limited compositional range, can be attributed to stage 4.

Wehrlite and clinopyroxenite inclusions, recorded from many areas of the province in association with lower crustal granulites and mantle lherzolites, are interpreted as evidence for the high pressure origin of the stage 1 of phenocryst crystallisation. Fractionation of the relatively aluminous, nepheline-normative clinopyroxene phenocrysts of this stage could also explain the observed

compositional trends, from mildly nepheline-normative magnesian basalts to hypersthene-normative hawaiites, noted by Macdonald (1975). Whether these trends are related to wehrlite or clinopyroxenite assemblage fractionation may depend on the degree of isobaric crystallisation of the parental magmas at the base of the crust. High degrees of crystallisation are expected to favour extracted magmas related by clinopyroxenite fractionation, although other factors, such as earlier melt evolution and initial melt compositions, are probably also important.

The second stage of phenocryst crystallisation, involving an olivine-gabbro assemblage, appears to be quite well defined from the samples in this study. However, in the study of compositional trends by Macdonald (1975), the main fractionating assemblages were identified as clinopyroxene ± olivine at high pressures, and olivine + plagioclase at low pressures. Macdonald suggested that fractionation of the early assemblage took the magmas by coincidence to near the olivine-plagioclase low-pressure cotectic. Invoking an intermediate stage where less magnesian basalts (< 6 - 7% MgO) reached the olivine-plagioclase-clinopyroxene cotectic may remove any need for coincidences. The similarity of changes in olivine and plagioclase crystallisation temperatures with pressure, implies that magmas at the olivine-plagioclase-clinopyroxene cotectic, at lower crustal levels, could have olivine-plagioclase cotectic behaviour at eruption.

The third stage, characterised by olivine and/or plagioclase ± Fe-Ti oxides, has been identified by Macdonald (1975) on the basis of whole rock trends. It is suggested that many of the basic samples in the present study show this phenocryst assemblage superimposed on earlier stages. Fractionation in the proposed low-pressure range after the second stage, during ascent or in near-surface magma chambers, may produce the observed compositional trends. The occurrence of composite intrusions and flows may be supporting evidence for the operation of fractionation processes at this stage. Textural and compositional evidence from plagioclases suggests there may be a significant role for water in the magmas at high levels, possible added from the surrounding crustal rocks. A

further stage not represented in the investigated collection is the development of near-surface magma chambers where significantly more evolved compositions may have been derived involving other phenocryst phases.

The fourth stage of the present study is considered to be separate from the gradual progression of the three previous stages. The observation has been made here, and in previous published studies, that the most primitive rocks contain olivine + clinopyroxene (+ spinel) phenocrysts. This is interpreted as indicating that the erupted magmas last equilibrated with clinopyroxene-bearing assemblages. The experimental model suggests this was at upper mantle pressures, yet the preserved phenocrysts are best explained by rapid crystallisation during ascent of the magmas. It is proposed that the absence of suitably high-pressure phenocrysts in these lavas reflects a different mode of fractionation to the other stages. The first and second stages may involve fractionation in sill-like intrusions near the base of the crust (Cox, 1980; Ewart et al., 1980). In contrast, the fourth stage may involve flow differentiation in dykes and veins in the upper mantle (Irving, 1980). Phenocrysts may grow on the margins of the channels rather than within the melt. In addition, there may be a role for significant volatile pressures. These may not favour suspension of high-pressure phenocrysts, and may provide a mechanism for rapid ascent from upper mantle levels.

The proposed four stages are intended as a simplification of the natural situation. In detail, all the individual samples do not fit easily into this model. However, it is believed that the preserved evidence of polybaric phenocryst growth would make any single classification scheme inadequate. The phenocryst assemblages in these rocks are partly a function of rate of ascent and rate of cooling of the magmas. Samples of similar composition can contain quite different phenocryst assemblages. The preservation of phenocrysts from high pressures is interpreted as indicating very limited fractionation at lower pressures. Many of these phenocrysts display partial resorption textures. From the rapid rate at which disequilibrium phases can be completely melted in experiments, it

is suggested that the host magmas rose from lower crustal or upper mantle levels in a matter of hours, rather than days. From the absence of overall evidence of superheating, the magmas are implied to have cooled by a few °C/Kb during ascent. It is emphasised that the magmas in this province probably had unique histories to generate their preserved phenocrysts. The present study has attempted to identify stages from combined experimental and natural mineral evidence.

ACKNOWLEDGEMENTS

My thanks to the staff and research students at the Grant Institute for their help and advice. Dr. K. R. Gill encouraged me to undertake a research project. Dr. C. Ford suggested the project, provided invaluable aid with the crystallisation model, and read the draft thesis. Dr. G. Biggar provided instruction and advice on the use of the atmospheric pressure experimental facilities.
Dr. P. Hill and Mr. C. Begg provided instruction in the use of the electron microprobe, and gave ready assistance at all hours, except Thursday evenings. Considerable thanks are due to Mr. A. Walker for his graphics and tabulation programs, and for his ready assistance with all computing problems. In addition to the above, the study has benefited from discussions with Prof. B. Upton, Drs. M. Fisk , J. Harris and R. Hunter, Mr P. Aspen, and fellow research students, particularly Mr. J. Craven and Ms. C. Hirst.

My thanks to Dr. R. Macdonald, Lancaster University, for providing most of the studied samples.

I am also grateful to my colleagues in the Edinburgh Microprobe Unit, Dr. P. Hill and Mrs. E. Cairns, for their tolerance, particularly during the latter stages of this project.

My thanks to Ms. Carol Jamieson for typing the thesis, and for her valiant attempts, with Mrs. J. Jamieson, to interpret and improve the manuscript.

Last, but by no means least, thanks are due to my family for their continual encouragement, and particularly to my wife Doris for her monumental patience and help.

This research was supported by a NERC studentship.

BIBLIOGRAPHY

Akella, J. R., Williams, R. J. & Mullins, O., 1976. Solubility of Cr, Ti and Al in coexisting olivine, spinel and liquid at 1 atm. Proc. Lunar Sci. Conf. 7th., 1179 - 1194.

Allan, D. A., 1924. The igneous geology of the Burntisland district. Trans. R. Soc. Edinburgh, 53, 479 - 502.

Andersen, D. J. & Lindsley, D. H., 1979. The olivine-ilmenite thermometer. Proc. Lunar Planet. Sci. Conf. 10, 493 - 507.

Anderson, A. T. Jr., 1968. Oxidation of the La Blache Lake titaniferous magnetite deposit, Quebec. J. Geol. 76, 528 - 547.

Arculus, R. J., 1974. Solid solution characteristics of spinels: pleonaste-chromite-magnetite compositions in some island-arc basalts. Yb. Carnegie Inst. Wash. 73, 322 - 327.

Arculus, R. J., 1975. Melting behaviour of two basanites in the range 10 - 35 kbar and the effect of TiO_2 on the olivine-diopside reactions at high pressures. Yb. Carnegie Inst. Wash. 74, 512 - 515.

Arculus, R.J. & Delano, J. W., 1981. Intrinsic oxygen fugacity measurements: techniques and results for spinels from upper mantle peridotites and megacryst assemblages. Geochim. cosmochim. Acta, 45, 899 - 913.

Arculus, R. J. & Wills, K. J. A., 1980. The petrology of plutonic blocks and inclusions from the Lesser Antilles island arc. J. Petrol. 21, 743 - 799.

Arndt, N. T., 1976. Melting relations of ultramafic lavas (komatiites) at 1 atm. and high pressure. Yb. Carnegie Inst. Wash. 75, 555 - 562.

Arndt, N. T., 1977. Partitioning of nickel between olivine and ultrabasic and basic komatiite liquids. Yb. Carnegie Inst. Wash. 76, 553 - 557.

Autefage, F., 1980. Variations de la teneur en sodium et en potassium dans des minéraux au cours de leur analyse à la microsonde électronique. Bull. Minéral. 103, 48 - 53.

Autefage, F. & Couderc, J.- J., 1980. Étude du mécanisme de la migration du sodium et du potassium au cours de leur analyse à la microsonde électronique. Bull. Minéral. 103, 623 - 629.

Bamford, D., Nunn, K., Prodehl, C. & Jacob, B., 1978. LISPB-IV. Crustal structure of northern Britain. Geophys. J. R. astr. Soc. 54, 43 - 60.

Benhamou, G., 1978. Comparisons of capsules and wire hooks for the experimental fusion of basalts. Progress in Experimental Petrology, NERC publication, 4, 120 - 121.

Bender, J. F., Hodges, F. N. & Bence, A. E., 1978. Petrogenesis of basalts from the project FAMOUS area: experimental study from 0 to 15 kbars. Earth planet. Sci. Lett. 41, 277 - 302.

Bickle, M. J., 1978. Melting experiments on peridotitic komatiites. Progress in Experimental Petrology, NERC publication, 4, 187 - 195.

Bickle, M. J., Ford, C. E. & Nisbet, E. G., 1977. The petrogenesis of peridotitic komatiites: evidence from high-pressure melting experiments. Earth planet. Sci. Lett. 37, 97 - 106.

Biggar, G. M., 1970. Molybdenum as a container for melts containing iron-oxide. Bull. Am. Ceram. Soc. 49, 286 - 288.

Biggar, G. M., 1972. Revised temperature calibration and scale. Progress in Experimental Petrology, NERC publication, 2, 86.

Biggar, G. M., 1974(a). Oxygen partial pressures: control, variation and measurement in quench furnaces at one atmosphere total pressure. Mineral. Mag. 39, 580 - 586.

Biggar, G. M., 1974(b). Phase equilibrium studies of the chilled margins of some layered intrusions. Contr. miner. Petrol. 46, 159 - 167.

Biggar, G. M., 1978. Wire hook supports for samples in atmospheric pressure quench furnaces. Progress in Experimental Petrology, NERC publication, 4, 118 - 120.

Biggar, G. M., 1981. Comparison of $CO:CO_2$ with $H_2:CO_2$ gas mixtures for controlling gas fugacities in furnaces at one atmosphere. Progress in Experimental Petrology, NERC publication, 5, 88 - 89.

Biggar, G. M., 1983. Crystallization of plagioclase, augite, and olivine in synthetic systems and in tholeiites. Mineral. Mag. 47, 161 - 176.

Biggar, G. M. & Clarke, D. B., 1976. Reaction rate of xenocrysts in synthetic basalt melts. Progress in Experimental Petrology, NERC publication, 3, 227 - 230.

Biggar, G. M. & Kadik, A., 1981. Phase relations of two ocean basalts at atmospheric pressure. Progress in Experimental Petrology, NERC publication, 5, 122 - 126.

Biggar, G. M. & O'Hara, M. J., 1969. Temperature control and calibration in quench furnaces and some new temperature measurements in the system $CaO-MgO-Al_2O_3-SiO_2$. Mineral. Mag. 37, 1 - 15.

Biggar, G. M., O'Hara, M. J., Peckett, A. & Humphries, D. J., 1971. Lunar lavas and the achondrites: petrogenesis of protohypersthene basalts in the maria lava lakes. Proc. Second Lunar Sci. Conf. 1, 617 - 643.

Binns, R. A., Duggan, M. B. & Wilkinson, J. F. G., 1970. High pressure megacrysts in alkaline lavas from northeastern New South Wales. Am. J. Sci. 269, 132 - 168.

Black, G. P., 1966. Arthur's Seat. Edinburgh: Oliver & Boyd.

Boivin, P., 1980. Données expérimentales préliminaires sur la stabilité de la rhönite à 1 atmosphere. Application aux gisements naturels. Bull. Minéral. 103, 491 - 502.

Bow, C., Biggar, G. M. & Krishnamurthy, P., 1976. Loss of iron and alkalis from samples at various fO_2 at atmospheric pressure. Progress in Experimental Petrology, NERC publication, 3, 141 - 143.

Bowen, N. L. & Schairer, J. F., 1935. The system, $MgO-FeO-SiO_2$. Am. J. Sci. 29, 151 - 217.

Buddington, A. F. & Lindsley, D. H., 1964. Iron-titanium oxide minerals and synthetic equivalents. J. Petrol. 5, 310 - 357.

Cameron, E. P. & French, W. J., 1977. The relationship of the order of crystallization of basalt melts to their classification and to the definition of rock series. Mineral. Mag. 41, 239 - 251.

Cameron, M. & Papike, J. J., 1981. Structural and chemical variations in pyroxenes. Am. Miner. 66, 1 - 50.

Carmichael, I. S. E., Turner, F. J. & Verhoogen, J., 1974. Igneous Petrology. New York: McGraw-Hill.

Cawthorn, R. G., Ford, C. E., Biggar, G. M., Bravo, M. S. & Clarke, D. B., 1973. Determination of the liquid composition in experimental samples: discrepancies between microprobe analysis and other methods. Earth planet. Sci. Lett. 21, 1 - 5.

Chapman, N. A., 1975. An experimental study of spinel clinopyroxenite xenoliths from the Duncansby Ness vent, Caithness, Scotland. Contr. miner. Petrol. 51, 223 - 230.

Chapman, N. A., 1976. Inclusions and megacrysts from undersaturated tuffs and basanites, East Fife, Scotland. J. Petrol. 17, 472 - 498.

Chapman, N. A. & Freestone, I. C., 1978. Phase relations and partitioning of Fe, Mg and Ca between olivine-liquid in picrite from 1 bar to 10 kbar. Progress in Experimental Petrology, NERC publication, 4, 255 - 257.

Clark, R. H., 1956. A petrological study of the Arthur's Seat volcano. Trans. R. Soc. Edinburgh, 63, 37 - 70.

Clough, C. T., Barrow, G., Crampton, C. B., Maufe, H. B., Bailey, E. B. & Anderson, E. M., 1910. The geology of East Lothian. Mem. geol. Surv. Scotland.

Clough, C. T., Hinxman, L. W., Wilson, J. S. G., Crampton, C. B., Wright, W. B., Bailey, E. B., Anderson, E. M. & Carruthers, R. G., 1925. The geology of the Glasgow district. Mem. geol. Surv. Scotland.

Corrigan, G. & Gibb, F. G. F., 1979. The loss of Fe and Na from a basaltic melt during experiments using the wire loop method. Mineral. Mag. 43, 121 - 126.

Cox, K. G., 1980. A model for flood basalt vulcanism. J. Petrol. 21, 629 - 650.

Cox, K. G., Bell, J. D. & Pankhurst, R. J., 1979. The interpretation of igneous rocks. London: Allen & Unwin.

Cox, K. G. & Jamieson, B. G., 1974. The olivine-rich lavas of Nuanetsi: a study of polybaric magmatic evolution. J. Petrol. 15, 269 - 301.

Craig, P. M., 1980. Volcanic geology of the Campsie Fells area, Stirlingshire. University of Lancaster. PhD thesis (unpubl.).

Craig, P. M. & Hall, I. H. S., 1975. The lower Carboniferous rocks of the Campsie-Kilpatrick area. Scott. J. Geol. 11, 171 - 174.

Day, T. C., 1930(a). Volcanic vents on the coast, from Tantallon Castle eastwards to Peffer Sands, and at Whitberry Point. Trans. Edinb. geol. Soc. 12, 213 - 233.

Day, T. C., 1930(b). The intrusive rock of Frances Craig, and the teschenite of Ravensheugh. Trans. Edinb. geol. Soc. 12, 260 - 262.

Day, T. C., 1930(c). Chemical analyses of thirteen igneous rocks of East Lothian. Trans. Edinb. geol. Soc. 12, 263 - 266.

Deer, W. A., Howie, R. A. & Zussman, J., 1978. Rock-forming minerals, Vol. 2A, Single-chain silicates. London: Wiley.

Deines, P., Nafziger, R. H., Ulmer, G. C. & Woermann, E., 1974. Temperature-oxygen fugacity tables for selected gas mixtures in the system C-H-O at one atmosphere total pressure. Bull. Earth and Mineral Sci. Expt. Station. 88, Pennsylvania State University, 1 - 129.

Delano, J. W., 1977. Experimental melting relations of 63545, 76015 and 76055. Proc. Lunar Sci. Conf. 8, 2097 - 2123.

Delano, J. W., 1980. Chemistry and liquidus phase relations of Apollo 15 red glass: implications for the deep lunar interior. Proc. Lunar Planet. Sci. Conf. 11, 251 - 288.

De Souza, H. A. F., 1974. Potassium-Argon ages of Carboniferous igneous rocks from East Lothian and the south of Scotland. University of Leeds. MSc thesis (unpubl.).

De Souza, H. A. F., 1979. The geochronology of Scottish Carboniferous volcanism. University of Edinburgh. PhD thesis (unpubl.).

Dick, H. J. B. & Bryan, W. B., 1978. Variation of basalt phenocryst mineralogy and rock compositions in DSDP hole 396B. Initial Rep. D.S.D.P. 46, 215 - 225.

Dickenson, M. P. & Hess, P. C., 1981. Redox equilibria and the structural role of iron in aluminosilicate melts. Contr. Miner. Petrol. 78, 352 - 357.

Dickey, J. S., Jr. & Yoder, H. S., Jr., 1972. Partitioning of chromium and aluminium between clinopyroxene and spinel. Yb. Carnegie Inst. Wash. 71, 384 - 392.

Dixon, J. E., Fitton, J. G. & Frost, R. T. C., 1981. The tectonic significance of post-Carboniferous igneous activity in the North Sea Basin. In: Illing, L. V. & Hobson, G. D. (eds.) Petroleum geology of the Continental Shelf of NW Europe. London: Institute of Petroleum, 121 - 137.

Dolfi, D. & Trigila, R., 1983. Clinopyroxene solid solutions and water in magmas: results in the system phonolitic tephrite-H_2O. Mineral. Mag. 47, 347 - 351.

Donaldson, C. H., 1976. An experimental investigation of olivine morphology. Contr. miner. Petrol. 57, 187 - 213.

Donaldson, C. H., 1979. Composition changes in a basalt melt contained in a wire loop of $Pt_{80}Rh_{20}$: effects of temperature, time, and oxygen fugacity. Mineral. Mag. 43, 115 - 119.

Donaldson, C. H., Usselman, T. M., Williams, R. J. & Lofgren, G. E., 1975. Experimental modeling of the cooling history of Apollo 12 olivine basalts. Proc. Lunar. Sci. Conf. 6, 843 - 869.

Dowty, E., 1976. Crystal structure and crystal growth: II. Sector zoning in minerals. Am. Miner. 61, 460 - 469.

Drake, M. J., 1976. Plagioclase-melt equilibria. Geochim. cosmochim. Acta, 40, 457 - 466.

Drever, H. I. & Johnston, R., 1957. Crystal growth of forsteritic olivine in magmas and melts. Trans. R. Soc. Edinburgh, 63, 289 - 317.

Drever, H. I. & MacDonald, J. G., 1967. Some new data on 'Kylitic' sills and associated picrites in Ayrshire, Scotland. Proc. roy. Soc. Edinb. 70, 31 - 48.

Duke, M. J., 1976. Distribution of the period-four transition elements among olivine, calcic clinopyroxene and mafic silicate liquids: experimental results. J. Petrol. 17, 499 - 521.

Duncan, A. M. & Preston, R. M. F., 1980. Chemical variation of clinopyroxene phenocrysts from the trachybasaltic lavas of Mount Etna, Sicily. Mineral. Mag. 43, 765 - 770.

Dungan, M. A. & Rhodes, J. M., 1978. Residual glasses and melt inclusions in basalts from DSDP Legs 45 and 46: evidence for magma mixing. Contr. miner. Petrol. 67, 417 - 431.

Eales, H. V. & Marsh, J. S., 1983. Al/Cr ratios of coexisting pyroxenes and spinellids in some ultramafic rocks. Chem. geol. 38, 57 - 74.

Eales, H. V., Reynolds, I. M. & Gouws, D. A., 1980. The spinel-group minerals of the central Karoo tholeiitic province. Trans. geol. Soc. S. Afr. 83, 243 - 253.

Elthon, D., Casey, J. F. & Komor, S., 1982. Mineral chemistry of ultramafic cumulates from the North Arm Mountain massif of the Bay of Islands ophiolite; evidence for high-pressure crystal fractionation of oceanic basalts. J. geophys. Res. 87, 8717 - 8734.

Evans, S. H., Jr. & Nash, W. P., 1979. Petrogenesis of xenolith-bearing basalts from southeastern Arizona. Am. Miner. 64, 249 - 267.

Ewart, A., Baxter, K. & Ross, J. A., 1980. The petrology and petrogenesis of the Tertiary anorogenic mafic lavas of southern and central Queensland, Australia - Possible implications for crustal thickening. Contr. miner. Petrol. 75, 129 - 152.

Ferguson, A. K., 1978. Ca-enrichment in olivines from volcanic rocks. Lithos, 11, 189 - 194.

Fettes, D. & Macdonald, R., 1979. Chemical composition of the Glen Garry vein complex: reply. Scott. J. Geol. 15, 256.

Fisk, M. R. & Bence, A. E., 1980. Experimental crystallization of chrome spinel in FAMOUS basalt 527-1-1. Earth planet. Sci. Lett. 48, 111 - 123.

Fisk, M. R., Bence, A. E. & Schilling, J.-G., 1982. Major element chemistry of Galapagos Rift zone magmas and their phenocrysts. Earth planet. Sci. Lett. 61, 171 - 189.

Fisk, M. R., Schilling, J.-G. & Sigurdsson, H., 1980. An experimental investigation of Iceland and Reykjanes Ridge tholeiites: I. Phase relations. Contr. miner. Petrol. 74, 361 - 374.

Fitch, F. J., Miller, J. A. & Williams, S. C., 1970. Isotopic ages of British Carboniferous rocks. C. R. 6me Congr. Int. Stratigr. géol. Carbonif., Sheffield 1967, 2, 771 - 789.

Ford, C. E., 1978. Platinum-iron alloy sample containers for melting experiments on iron-bearing rocks, minerals, and related systems. Mineral. Mag. 42, 271 - 275.

Ford. C. E., 1981. Parental liquids of the Skaergaard intrusion cumulates. Nature, 291, 25 - 29.

Ford, C. E., Biggar, G. M., Humphries, D. J., Wilson, G., Dixon, D. & O'Hara, M. J., 1972. Role of water in the evolution of the lunar crust; an experimental study of sample 14310; an indication of lunar calc-alkaline volcanism. Proc. Lunar Sci. Conf. 3rd , 207 - 229.

Ford, C. E. & Macdonald, R., 1978. Melting relations of a Midland Valley alkali basalt. Progress in Experimental Petrology, NERC publication, 4, 196 - 197.

Ford, C. E., Russell, D. G., Craven, J. A. & Fisk, M. R., 1983. Olivine-liquid equilibria: temperature, pressure and composition dependence of the crystal/liquid cation partition coefficients for Mg, Fe^{2+}, Ca and Mn. J. Petrol. 24, 256 - 265.

Francis, E. H., 1978. Igneous activity in a fractured craton: Carboniferous volcanism in northern Britain. In: Bowes, D. R. & Leake, B. E. (eds.) Crustal evolution in northwestern Britain and adjacent regions. Geol. J. Spec. Issue, No. 10, 279 - 296.

Francis, E. H., 1983. Carboniferous-Permian igneous rocks. In: Craig, G. Y. (ed.) Geology of Scotland. Edinburgh: Scottish Academic Press, 297 - 324.

Francis, E. H., Forsyth, I. H., Read, W. A. & Armstrong, M., 1970. The geology of the Stirling district. Mem. geol. Surv. Scotland.

French, W. J., 1971. The correlation between "anhydrous" crystallization temperatures and rock composition. Contr. miner. Petrol. 31, 154 - 158.

French, W. J. & Cameron, E. P., 1981. Calculation of the temperature of crystallization of silicates from basaltic melts. Mineral. Mag. 44, 19 - 26.

Frey, F. A., Green, D. H. & Roy, S. D., 1978. Integrated models of basalt petrogenesis: a study of quartz tholeiites to olivine melilitites from south eastern Australia utilizing geochemical and experimental petrological data. J. Petrol. 19, 463 - 513.

Frey, F. A. & Prinz, M., 1978. Ultramafic inclusions from San Carlos, Arizona: petrologic and geochemical data bearing on their petrogenesis. Earth planet. Sci. Lett. 38, 129 - 176.

Fudali, R. F., 1965. Oxygen fugacities of basaltic and andesitic magmas. Geochim. cosmochim. Acta, 29, 1063 - 1075.

Fujii, T. & Bougault, H., 1983. Melting relations of a magnesian abyssal tholeiite and the origin of MORBs. Earth planet. Sci. Lett. 62, 283 - 295.

Gallagher, M. J., 1963. Lamprophyre dykes from Argyll. Mineral. Mag. 33, 415 - 430.

Gamble, R. P. & Taylor, L. A., 1980. Crystal/liquid partitioning in augite: effects of cooling rate. Earth planet. Sci. Lett. 47, 21 - 33.

Ghiorso, M. S., Carmichael, I. S. E., Rivers, M. L. & Sack, R. O., 1983. The Gibbs Free Energy of mixing of natural silicate liquids; an expanded regular solution approximation for the calculation of magmatic intensive variables. Contr. miner. Petrol. 84, 107 - 145.

Gibb, F. G. F., 1974. Supercooling and the crystallisation of plagioclase from a basaltic magma. Mineral. Mag. 39, 641 - 653.

Graham, A.M. & Upton, B. G. J., 1978. Gneisses in diatremes, Scottish Midland Valley: petrology and tectonic implications. J. geol. Soc. Lond. 135, 219 - 228.

Green, T. H. & Watson, E. B., 1982. Crystallization of apatite in natural magmas under high pressure, hydrous conditions, with particular reference to 'orogenic' rock series. Contr. miner. Petrol. 79, 96 - 105.

Grove, T. L., 1981. Use of Fe Pt alloys to eliminate the iron loss problem in 1 atmosphere gas mixing experiments: theoretical and practical considerations. Contr. miner. Petrol. 78, 298 - 304.

Grove, T. L. & Beaty, D. W., 1980. Classification, experimental petrology and possible volcanic histories of the Apollo 11 high-K basalts. Proc. Lunar Planet. Sci. Conf. 11, 149 - 177.

Grove, T. L. & Bence, A. E., 1977. Experimental study of pyroxene-liquid interactions in quartz-normative basalt 15597. Proc. Lunar Sci. Conf. 8, 1549 - 1579.

Grove, T. L. & Bence, A. E., 1979. Crystallization kinetics in a multiply saturated basalt magma: an experimental study of Luna 24 ferrobasalt. Proc. Lunar Planet Sci. Conf. 10, 439 - 478.

Grove, T. L., Gerlach, D. C. & Sando, T. W., 1982. Origin of calc-alkaline series lavas at Medicine Lake volcano by fractionation, assimilation and mixing. Contr. miner. Petrol. 80, 160 - 182.

Grove, T. L. & Raudsepp, M., 1978. Effects of kinetics on the crystallization of quartz normative basalt 15597: an experimental study. Proc. Lunar Planet. Sci. Conf. 9, 585 - 599.

Grove, T. L. & Vaniman, D., 1978. Experimental petrology of very low Ti (VLT) basalts. In: Merrill, R. B. & Papike, J. J. (eds.) The view from Luna 24. New York: Pergamon, 445 - 471.

Guppy, E. M. & Thomas, H. H., 1931. Chemical analyses of igneous rocks, metamorphic rocks and minerals. Mem. geol. Surv. Gt. Br.

Gutmann, J. T., 1977. Textures and genesis of phenocrysts and mega-crysts in basaltic lavas from the Pinacate volcanic field. Am. J. Sci. 277, 833 - 861.

Haggerty, S. E., 1976. Opaque mineral oxides in terrestrial rocks. In: Rumble, D., III, (ed.) Oxide minerals (short course notes). Min. Soc. Amer. 3, 101 - 300.

Haggerty, S. E., 1979. Spinels in high pressure regimes. In: Boyd, F. R. & Meyer, H. O. A. (eds.) The mantle sample: inclusions in kimberlites and other volcanics. Washington: American Geophysical Union, 183 - 196.

Hall, J., 1805. Experiments on whinstone and lava. Trans. R. Soc. Edinb. 5, 43 - 75.

Hamilton, J., 1956. Mineralogy of basalts from the western Kilpatrick Hills and its bearing on the Scottish Carboniferous olivine basalts. Trans. Edinb. geol. Soc. 16, 280 - 298.

Hammond, P. A. & Taylor, L. A., 1982. The ilmenite/titanomagnetite assemblage: kinetics of re-equilibration. Earth planet. Sci. Lett. 61, 143 - 150.

Hart, S. R. & Davis, K. E., 1978. Nickel partitioning between olivine and silicate melt. Earth planet. Sci. Lett. 40, 203 - 219.

Heinrich, K.F.J., 1966. X-ray absorption uncertainty. In: McKinley, T. D., Heinrich, K. F. J. & Wittry, D. B. (eds.) The electron microprobe. London: Wiley, 296 - 377.

Henderson, C. M. B. & Gibb, F. G. F., 1983. Felsic mineral crystallisation trends in differentiating alkaline basic magmas. Contr. miner. Petrol. 84, 355 - 364.

Hill, R. & Roeder, P., 1974. The crystallization of spinel from a basaltic liquid as a function of oxygen fugacity. J. Geol. 82, 709 - 729.

Holmes, A., 1965. Principles of physical geology. London: Nelson.

Hoover, J. S. & Irvine, T. N., 1978. Liquidus relations and Mg-Fe partitioning on part of the system Mg_2SiO_4-Fe_2SiO_4-$CaMgSi_2O_6$-$CaFeSi_2O_6$-$KAlSi_3O_8$-SiO_2. Yb. Carnegie Inst. Wash. 77, 774 - 784.

Hostetler, C. J. & Drake, M. J., 1980. Predicting major element mineral/melt equilibria: a statistical approach. J. geophys. Res. 85, 3789 - 3796.

Huebner, J. S., 1975. Origin of the SiO_2 variation of mare basalt melts. Lunar Science VI (extended abstracts), 411 - 413.

Huebner, J. S., Lipin, B. R. & Wiggins, L. B., 1976. Partitioning of chromium between silicate crystals and melts. Proc. Lunar Sci. Conf. 7, 1195 - 1220.

Humphries, D. J., 1975. Phase equilibrium studies of some basalt-like compositions in the system $CaO-MgO-Al_2O_3-SiO_2-Na_2O-Fe-O_2$. University of Edinburgh. PhD thesis (unpubl.).

Irvine, T. N. & Baragar, W. R. A., 1971. A guide to the chemical classification of the common volcanic rocks. Can. J. Earth Sci. 8, 523 - 548.

Irving, A. J., 1980. Petrology and geochemistry of composite ultramafic xenoliths in alkalic basalts and implications for magmatic processes within the mantle. Am. J. Sci. 280A, 389 - 426.

Irving, A. J., Merrill, R. B. & Singleton, D. E., 1978. Experimental partitioning of rare earth elements and scandium among armalcolite, ilmenite, olivine, and mare basalt liquid. Proc. Lunar Planet. Sci. Conf. 9, 601 - 612.

Jackson, E. D., 1979. Further effects of fractional resorption. In: Yoder, H. S., Jr. (ed.) The evolution of the igneous rocks: Fiftieth anniversary perspectives. Princeton: Princeton University, 423 - 438.

Jamieson, B. G., 1970. Phase relations in some tholeiitic lavas illustrated by the system $R_2O_3-XO-YO-ZO_2$. Mineral. Mag. 37, 537 - 554.

Jaques, A. L. & Green, D. H., 1979. Determination of liquid compositions in high-pressure melting of peridotite. Am. Miner. 64, 1312 - 1321.

Jaques, A. L. & Green, D. H., 1980. Anhydrous melting of peridotite at 0 - 15 Kb pressure and the genesis of tholeiitic basalts. Contr. miner. Petrol. 73, 287 - 310.

Kennedy, G. C., 1948. Equilibrium between volatiles and iron oxides in igneous rocks. Am. J. Sci. 246, 529 - 549.

Kilinc, A., Carmichael, I. S. E., Rivers, M. L. & Sack, R. O., 1983. The ferric-ferrous ratio of natural silicate liquids equilibrated in air. Contr. miner. Petrol. 83, 136 - 140.

Kuo, L.-C. & Kirkpatrick, R. J., 1982. Pre-eruption history of phyric basalts from DSDP legs 45 and 46: Evidence from morphology and zoning patterns in plagioclase. Contr. miner. Petrol. 79, 13 - 27.

Kushiro, I., 1972(a). Determination of liquidus relations in synthetic silicate systems with electron probe analysis: the system forsterite-diopside-silica at 1 atmosphere. Am. Miner. 57, 1260 - 1271.

Kushiro, I., 1972(b). The system diopside-anorthite-albite: determination of compositions of coexisting phases. Yb. Carnegie Inst. Wash. 72, 502 - 507.

Langmuir, C. H. & Hanson, G. N., 1980. An evaluation of major element heterogeneity in the mantle sources of basalts. Phil. Trans. R. Soc. Lond. A297, 383 - 407.

Langmuir, C. H. & Hanson, G. N., 1981. Calculating mineral-melt equilibria with stoichiometry, mass balance and single-component distribution coefficients. In: Newton, R. C., Navrotsky, A. & Wood, B. J. (eds.) Thermodynamics of minerals and melts. New York: Springer-Verlag, 247 - 271.

Larsen, J. G., 1981. Medium pressure crystallization of a monchiquitic magma-evidence from megacrysts of Drever's block, Ubekendt Ejland, West Greenland. Lithos, 14, 241 - 262.

Leake, B. E., 1979. Chemical composition of the Glen Garry vein complex. Scott. J. Geol. 15, 255.

LeBas, M. J., 1962. The role of aluminium in igneous clinopyroxenes with relation to their parentage. Am. J. Sci. 260, 267 - 288.

Leeder, M. R., 1982. Upper Palaeozoic basins of the British Isles-Caledonide inheritance versus Hercynian plate margin processes. J. geol. Soc. Lond. 139, 479 - 491.

Leeman, W. P., Vitaliano, C. J. & Prinz, M., 1976. Evolved lavas from the Snake River Plain: Craters of the Moon national monument, Idaho. Contr. miner. Petrol. 53, 35 - 60.

Lofgren, G., 1974. An experimental study of plagioclase crystal morphology: isothermal crystallization. Am. J. Sci. 274, 243 - 273.

Lofgren, G., 1980. Experimental studies on the dynamic crystallisation of silicate melts. In: Hargraves, R. B. (ed.) Physics of magmatic processes. Princeton: Princeton University, 487 - 551.

Lofgren, G., Donaldson, C. H., Williams, R. J., Mullins, O., Jr. & Usselman, T. M., 1974. Experimentally reproduced textures and mineral chemistry of Apollo 15 quartz normative basalts. Proc. 5th Lunar Conf. 549 - 567.

Longhi, J., 1982. Effects of fractional crystallization and cumulus processes on mineral composition trends of some lunar and terrestrial rock series. Proc. 13th Lunar Planet Sci. Conf., J. geophys. Res. 87, A54 - 64.

Longhi, J. & Boudreau, A. E., 1980. The ortho-enstatite liquidus field in the system forsterite-diopside-silica at one atmosphere. Am. Miner. 65, 563 - 573.

Longhi, J., Walker, D. & Hays, J. F., 1976. Fe and Mg in plagioclase. Proc. Lunar Sci. Conf. 7, 1281 - 1300.

Longhi, J., Walker, D. & Hays, J. F., 1978. The distribution of Fe and Mg between olivine and lunar basaltic liquid. Geochim. cosmochim. Acta, 42, 1545 - 1558.

Loomis, T. P., 1982. Numerical simulations of crystallization processes of plagioclase in complex melts: the origin of major and oscillatory zoning in plagioclase. Contr. miner. Petrol. 81, 219 - 229.

MacDonald, J. G., 1967. Variations within a Scottish Lower Carboniferous lava flow. Scott. J. Geol. 3, 34 - 45.

MacDonald, J. G. & Whyte. F., 1981. Petrochemical evidence for the genesis of a Lower Carboniferous transitional basaltic suite in the Midland Valley of Scotland. Trans. R. Soc. Edinb. 72, 75 - 88.

Macdonald, R., 1975. Petrochemistry of the early Carboniferous (Dinantian) lavas of Scotland. Scott. J. Geol. 11, 269 - 314.

Macdonald, R., 1980. Trace element evidence for mantle heterogeneity beneath the Scottish Midland Valley in the Carboniferous and Permian. Phil. Trans. R. Soc. Lond. A280, 111 - 123.

Macdonald, R., Gass, K. N., Thorpe, R. S. & Gass, I. G., 1984. Geochemistry and petrogenesis of the Derbyshire Carboniferous basalts. J. geol. Soc. Lond. 141, 147 - 159.

Macdonald, R., Gottfried, D., Farrington, M. J., Brown, F. W. & Skinner, N. G., 1981. Geochemistry of a continental tholeiite suite: late Palaeozoic quartz dolerite dykes of Scotland. Trans. R. Soc. Edinb. 72, 57 - 74.

Macdonald, R., Thomas, J. E. & Rizzello, S. A., 1977. Variations in basalt chemistry with time in the Midland Valley province during the Carboniferous and Permian. Scott. J. Geol. 13, 11 -22.

MacGregor, A. G., 1928. The classification of the Scottish Carboniferous olivine-basalts and mugearites. Trans. geol. Soc. Glasg. 18, 324 - 360.

MacGregor, A. G., 1932. Note on corroded ferromagnesian phenocrysts in a Scottish basalt. Trans. Edinb. geol. Soc. 12, 329 - 333.

MacGregor, A. G., 1948. Problems of Carboniferous-Permian volcanicity in Scotland. Q. J. geol. Soc. Lond. 104, 133 - 153.

MacKenzie, W. S., Donaldson, C. H. & Guilford, C., 1982. Atlas of igneous rocks and their textures. London: Longman.

McKenzie, D., 1978. Some remarks on the development of sedimentary basins. Earth planet. Sci. Lett. 40, 25 - 32.

Merrill, R. B. & Williams, R. J., 1975. The system anorthite-forsterite-fayalite-silica to 2 kbar with lunar petrologic applications. Proc. Lunar Sci. Conf. 6, 959 - 971.

Mitchell, G. H. & Mykura, W., 1962. The geology of the neighbourhood of Edinburgh. Mem. geol. Surv. Scotland.

Mysen, B. O. & Kushiro, I., 1977. Compositional variations of coexisting phases with degree of melting of peridotite in the upper mantle. Am. Miner. 62, 843 - 865.

Nabalek, P. I., 1980. Nickel partitioning between olivine and liquid in natural basalts: Henry's law behaviour. Earth planet. Sci. Lett. 48, 293 - 302.

Nakamura, Y., 1973. Origin of sector-zoning in igneous clinopyroxenes. Am. Miner. 58, 986 - 990.

Nathan, H. D. & Van Kirk, C. K., 1978. A model of magmatic crystallization. J. Petrol. 19, 66 - 94.

Nielsen, R. L. & Drake, M. J., 1979. Pyroxene-melt equilibria. Geochim. cosmochim. Acta, 43, 1259 - 1272.

Nielsen, R. L. & Dungan, M. A., 1983. Low pressure mineral-melt equilibria in natural anhydrous mafic systems. Contr. miner. Petrol. 84, 310 - 326.

O'Hara, M. J., 1965. Primary magmas and the origin of basalts. Scott. J. Geol. 1, 19 - 40.

O'Hara, M. J., 1968. The bearing of phase equilibrium studies in synthetic and natural systems on the origin and evolution of basic and ultrabasic rocks. Earth Sci. Rev. 4, 69 - 133.

O'Hara, M. J., 1976. Data reduction and projection schemes for complex compositions. Progress in Experimental Petrology, NERC publication, 3, 103 - 126.

O'Hara, M. J. & Biggar, G. M., 1976. Inter-laboratory comparisons of the temperature of plagioclase entry in natural basic magmas. Progress in Experimental Petrology, NERC publication, 3, 131 - 134.

O'Hara, M. J., Biggar, G. M., Hill, P. G., Jefferies, B. & Humphries, D. J., 1974. Plagioclase saturation in lunar high-titanium basalt. Earth planet. Sci. Lett. 21, 253 - 268.

O'Hara, M. J. & Humphries, D. J., 1977. Problems of iron gain and loss during experimentation on natural rocks: the experimental crystallisation of five lunar basalts at low pressures. Phil. Trans. R. Soc. Lond. A286, 313 - 330.

Onuma, K. & Tohara, T., 1983. Effect of chromium on phase relations in the join forsterite-anorthite-diopside in air at 1 Atm. Contr. miner. Petrol. 84, 174 - 181.

Osborn, E. F., 1979. The reaction principle. In: Yoder, H. S., Jr. (ed.) The evolution of the igneous rocks: Fiftieth anniversary perspectives. Princeton: Princeton University, 133 - 169.

Paul, A. & Douglas, R. W., 1965. Ferrous-ferric equilibrium in binary alkali silicate glasses. Phys. chem. glasses, 6, 207 - 211.

Pearce, T. H., 1978. Olivine fractionation equations for basaltic and ultrabasic liquids. Nature, 276, 771 - 774.

Presnall, D. C. & Brenner, N. L., 1974. A method for studying iron silicate liquids under reducing conditions with negligible iron loss. Geochim. cosmochim. Acta, 38, 1785 - 1788.

Presnall, D. C., Dixon, S. A., Dixon, J. R., O'Donnell, T. H., Brenner, N. L., Schrock, R. L. & Dycus, D. W., 1978. Liquidus phase relations on the join diopside-forsterite-anorthite from 1 atm to 20 kbar: their bearing on the generation and crystallization of basaltic magma. Contr. miner. Petrol. 66, 203 - 220.

Pringle, G. J., Tremlath, L. T. & Pajari, G. J., Jr., 1974. Crystallization history of a zoned plagioclase (microprobe analysis of zoned plagioclase from Grand Manan tholeiite sheet). Mineral. Mag. 39, 867 - 877.

Rhodes, J. M., Lofgren, G. E. & Smith, B. P., 1979. One atmosphere melting experiments on ilmenite basalt 12008. Proc. Lunar Planet. Sci. Conf. 10, 407 - 422.

Richey, J. E., Anderson, E. M. & MacGregor, A. G., 1930. The geology of North Ayrshire. Mem. geol. Surv. Scotland.

Ridley, W. I., 1977. The crystallisation trends of spinels in Tertiary basalts from Rhum and Muck and their petrogenetic significance. Contr. miner. Petrol. 64, 243 - 255.

Roeder, P. L., 1974. Activity of iron and olivine solubility in basaltic liquids. Earth planet. Sci. Lett. 23, 397 - 410.

Roeder, P. L., 1975. Thermodynamics of element distribution in experimental mafic silicate liquid systems. Fortschrit. Mineral. 52, 61 - 73.

Roeder, P. L., Campbell, I. H. & Jamieson, H. E., 1979. A re-evaluation of the olivine-spinel geothermometer. Contr. miner. Petrol. 68, 325 - 334.

Roeder, P. L. & Emslie, R. F., 1970. Olivine-liquid equilibrium. Contr. miner. Petrol. 29, 275 - 289.

Russell, M. J. & Smythe, D. K., 1978. Evidence for an early Permian oceanic rift in the northern North Atlantic. In: Neumann, E.-R. & Ramberg, I. B. (eds.) Petrology and geochemistry of continental rifts. Dordrecht: Reidel, 173 - 179.

Sack, R. O. Carmichael, I. S. E., Rivers, M. and Ghiorso, M. S, 1980. Ferric-ferrous equilibria in natural silicate liquids at 1 bar. Contr. miner. Petrol. 75, 369 - 376.

Scarfe, C. M., Takahashi, E. & Yoder, H. S.,Jr., 1980. Rates of dissolution of upper mantle minerals in an alkali-olivine basalt melt at high pressures. Yb. Carnegie Inst. Wash. 79, 290 - 296.

Schreiber, H. D. & Haskin, L. A. (1976). Chromium in basalts: experimental determinations of redox states and partitioning among synthetic silicate phases. Proc. Lunar Sci. Conf. 7, 1221 - 1259.

Scott, A., 1915. The Crawfordjohn essexite and associated rocks. Geol. Mag. dec. 6, vol. 2, 455 - 461.

Shimizu, N., 1981. Trace element incorporation into growing augite phenocryst. Nature, 289, 575 - 577.

Simkin, T. & Smith, J. V., 1970. Minor element distribution in olivine. J. Geol. 78, 304 - 325.

Smith, R. K. & Lofgren, G. E., 1983. An analytical and experimental study of zoning in plagioclase. Lithos, 16, 153 - 168.

Sparks, R. S. J., Pinkerton, H. & Macdonald, R., 1977. The transport of xenoliths in magmas. Earth planet. Sci. Lett. 35, 234 - 238.

Spencer, K. J. & Lindsley, D. H., 1981. A solution model for coexisting iron-titanium oxides. Am. Miner. 66, 1189 - 1201.

Stolper, E. M., 1976. Experimental petrology of eucrite meteorites. University of Edinburgh. MPhil. thesis (unpubl.).

Stolper, E. M., 1977. Experimental petrology of eucrite meteorites. Geochim. cosmochim. Acta, 41, 587 - 611.

Stolper, E. M., 1980. A phase diagram for mid-ocean ridge basalts: Preliminary results and implications for petrogenesis. Contr. miner. Petrol. 74, 13 - 27.

Stormer, J. C., Jr., 1973. Calcium zoning in olivine and its relationship to silica activity and pressure. Geochim. cosmochim. Acta, 37, 1815 - 1821.

Strong, D. F., 1969. Formation of the hourglass structure in augite. Mineral. Mag. 37, 472 - 479.

Sweatman, T. R. & Long, J. V. P., 1969. Quantitative electron probe micro-analysis of rock-forming minerals. J. Petrol. 10, 332 - 379.

Takahashi, E., 1980. Melting relations of an alkali-olivine basalt to 30 kbars, and their bearing on the origin of alkali basalt magmas. Yb. Carnegie Inst. Wash. 79, 271 - 276.

Takahashi, E. & Kushiro, I., 1983. Melting of a dry peridotite at high pressures and basalt magma genesis. Am. Miner. 68, 859 - 879.

Tatsumi, Y., Sakuyama, M., Fukuyama, H. & Kushiro, I., 1983. Generation of arc basalt magmas and thermal structure of the mantle wedge in subduction zones. J. geophys. Res. 88, 5815 - 5825.

Thompson, R. N., 1972(a). The 1-atmosphere melting patterns of some basaltic volcanic series. Am. J. Sci. 272, 901 - 932.

Thompson, R. N., 1972(b). Melting behaviour of two Snake River lavas at pressures up to 35 Kb. Yb. Carnegie Inst. Wash. 71, 406 - 410.

Thompson, R. N., 1974(a). Primary basalts and magma genesis. I, Skye, North-West Scotland. Contr. miner. Petrol. 45, 317 - 341.

Thompson, R. N., 1974(b). Some high-pressure pyroxenes. Mineral. Mag. 39, 768 - 787.

Thornber, C. R., Roeder, P. L. & Foster, J. R., 1980. The effect of composition on the ferric-ferrous ratio in basaltic liquids at atmospheric pressure. Geochim. cosmochim. Acta, 44, 525 - 532.

Thy, P., 1982. Titanomagnetite and ilmenite in the Fongen-Hyllingen basic complex, Norway. Lithos, 15, 1 - 16.

Tiezzi, L. J. & Scott, R. B., 1980. Crystal fractionation in a cumulate gabbro, mid-Atlantic ridge, 26° N. J. geophys. Res. 85, 5438 - 5454.

Tomkeieff, S. I., 1937. Petrochemistry of the Scottish Carboniferous-Permian igneous rocks. Bull. Volcanol. 1, 59 - 87.

Tomkeieff, S. I., 1945. Petrology of the Carboniferous igneous rocks of the Tweed Basin. Trans. Edinb. geol. Soc. 14, 53 - 75.

Tomkeieff, S. I., 1952. Nepheline-basanite of Southdean, Roxburghshire. Trans. Edinb. geol. Soc. 14, 349 - 359.

Tsuchiyama, A. & Takahashi, E., 1983. Melting kinetics of a plagioclase feldspar. Contr. miner. Petrol. 84, 345 - 354.

Ulmer, G. C. (ed.), 1971. Research techniques for high pressure and high temperature. New York: Springer-Verlag.

Upton, B. G. J., 1971. Melting experiments on chilled gabbros and syenogabbros. Yb. Carnegie Inst. Wash. 70, 112 - 118.

Upton, B. G. J., 1982. Carboniferous to Permian volcanism in the stable foreland. In: Sutherland, D. S. (ed.) Igneous Rocks of the British Isles. London: Wiley, 255 - 275.

Upton, B. G. J., Aspen, P. & Chapman, N. A., 1983. The upper mantle and deep crust beneath the British Isles: evidence from inclusions in volcanic rocks. J. geol. Soc. Lond. 140, 105 - 122.

Upton, B. G. J., Aspen, P., Graham, A. M. & Chapman, N. A., 1976. Pre-Palaeozoic basement of the Scottish Midland Valley. Nature, 260, 517 - 518.

Upton, B. G. J. & Thomas, J. E., 1980. The Tugtutôq Younger Giant Dyke complex, South Greenland: fractional crystallization of transitional olivine basalt magma. J. Petrol. 21, 167 - 198.

Veblen, D. R. & Buseck, P. R., 1981. Hydrous pyriboles and sheet silicates in pyroxenes and uralites: intergrowth microstructures and reaction mechanisms. Am. Miner. 66, 1107 - 1134.

Villemant, B., Jaffrezic, H., Joron, J.-L. & Treuil, M., 1981. Distribution coefficients of major and trace elements; fractional crystallization in the alkali basalt series of Chaîne des Puys (Massif Central, France). Geochim. cosmochim. Acta, 45, 1997 - 2016.

Walker, D., Kirkpatrick, R. J., Longhi, J. & Hays, J. F., 1976. Crystallization history of lunar picritic basalt sample 12002: phase-equilibria and cooling-rate studies. Bull. geol. Soc. Am. 87, 646 - 656.

Walker, D., Longhi, J. & Hays, J. F., 1972. Experimental petrology and origin of Fra Mauro rocks and soils. Proc. Lunar Sci. Conf. 3rd, 797 - 817.

Walker, D., Shibata, T. & Delong, S. E., 1979. Abyssal tholeiites from the Oceanographer Fracture zone: II. Phase equilibria and mixing. Contr. miner. Petrol. 70, 111 - 125.

Walker, F., 1935. The late Palaeozoic quartz-dolerites and tholeiites of Scotland. Mineral. Mag. 24, 131 - 159.

Walker, F., 1965. The part played by tholeiitic magma in the Carbo-Permian vulcanicity of central Scotland. Mineral. Mag. 34, 498 - 516.

Wass, S. Y., 1973. The origin and petrogenetic significance of hour-glass zoning in titaniferous clinopyroxenes. Mineral. Mag. 39, 133 - 144.

Wass, S. Y., 1979. Multiple origins of clinopyroxenes in alkali basaltic rocks. Lithos, 12, 115 - 132.

Wass, S. Y., 1980. Geochemistry and origin of xenolith-bearing and related alkali basaltic rocks from the Southern Highlands, New South Wales, Australia. Am. J. Sci. 280A, 639 - 666.

Watson, E. B., 1977. Partitioning of manganese between forsterite and silicate liquid. Geochim. cosmochim. Acta, 41, 1363 - 1374.

Watson, E. B., 1979. Calcium content of forsterite coexisting with silicate liquid in the system $Na_2O - CaO - MgO - Al_2O_3 - SiO_2$. Am. Miner. 64, 824 - 829.

Weill, D. F., Hon, R. & Navrotsky, A., 1980. The igneous system $CaMgSi_2O_6 - CaAl_2Si_2O_8 - NaAlSi_3O_8$: variations on a classic theme by Bowen. In: Hargraves, R. B. (ed.) Physics of magmatic processes. Princeton: Princeton University, 49 - 92.

Whyte, F. & MacDonald, J. G., 1974. Lower Carboniferous vulcanicity in the northern part of the Clyde Plateau. Scott. J. Geol. 10, 187 - 198.

Williams, G. P., 1983. Improper use of regression equations in earth sciences. Geology, 11, 195 - 197.

Williams, H., Turner, F. J. & Gilbert, C. M., 1982. Petrography. An introduction to the study of rocks in thin sections. San Francisco: Freeman.

Wilson, A. H., 1982. The geology of the Great 'Dyke', Zimbabwe: the ultramafic rocks. J. Petrol. 23, 240 - 292.

Wright, T. L. & Doherty, P. C., 1970. A linear programming and least squares computer method for solving petrologic mixing problems. Bull. geol. Soc. Am. 81, 1995 - 2008.

Yoder, H. S., Jr. & Tilley, C. E., 1962. Origin of basalt magmas: an experimental study of natural and synthetic rock systems. J. Petrol. 3, 342 - 532.

APPENDIX 1

Sample Details

Investigated specimens are listed below in terms of decreasing Mg#, [100* Mg/(Mg + Fe^{2+})]. With the exception of F- and AS- samples collected by the author, the specimens were provided by Dr. R. Macdonald, Lancaster University. The information given for each is; sample identifier, rock type, source area and phenocryst assemblage (with the approximate modal percentage of each phenocryst). Other information sometimes present is a note on alteration, and any publications where the occurrence is described. Abbreviations used are ol (olivine), cpx (clinopyroxene), opx (low-Ca pyroxene), pl (plagioclase), sp (spinel), mt (titanomagnetite) and il (ilmenite). Spinels are distinguished optically from titanomagnetites on the basis of the formers' lower reflectivity. Spinels also commonly occur as inclusions in the interior zones of other phenocrysts.

AS2 ankaramite, Whinny Hill intrusion, Arthur's Seat, Edinburgh. ol (10%) + cpx (13%) + pl (<1%) + sp (<1%). Clark (1956) analysis recast from Table 5 (I).

MV403 macroporphyritic hypersthene-normative basalt lava, Burntisland. ol (10%) + cpx (1%) + sp (<1%). Macdonald et al. (1977).

ES2058 macroporphyritic essexite intrusion, Lennoxtown, near Glasgow. ol (10%) + cpx (10%) + sp (<1%). Clough et al. (1925); Guppy and Thomas (1931); Henderson and Gibb (1983).

MV93 microphyric 'monchiquite', Stenton, East Lothian. ol (15%) + cpx (12%) + sp (1%), no fresh olivine, feldspar-free. Clough et al. (1910).

MV521 microphyric alkali basalt sill, type Hillhouse basalt, near Linlithgow. ol (15%) + cpx (15%) + sp (1%). MacGregor (1928); Guppy and Thomas (1931).

MV723 microphyric alkali dolerite sill, Troon, Ayrshire. ol (5%) + sp (<1%). Drever and MacDonald (1967).

MV109 microphyric alkali basalt, Orrock Quarry, Fife. ol (10%) + cpx (1%) + sp (<1%) + mt (<1%).

MV106 microphyric hypersthene-normative basalt lava, Burntisland. ol (10%) + cpx (2%) + sp (<1%). Macdonald et al. (1977).

MV164 microphyric alkali dolerite sill, Gosford Bay, East Lothian. ol (12%) + sp (<1%). Macdonald (1975).

MV166 ankaramite intrusion, St Baldred's Cradle, East Lothian. ol (10%) + cpx (15%) + sp (1%). Day (1930a).

AS1/36017 macroporphyritic basalt, Lion's Haunch Basalt, Arthur's Seat, Edinburgh. ol (8%) + cpx (10%) + pl (18%) + sp (<1%) + mt (1%). Clark (1956) analysis recast from Table 5 (B).

MV718 microphyric alkali basalt, Lochgoin reservoir, North Ayrshire. ol (10%) + cpx (<1%) + sp (<1%) + mt (<1%). Richey et al. (1930).

MV703 microphyric basanite intrusion, Kersewell Quarry, Carnwath. ol (5%) + cpx (2%) + sp (<1%). Guppy and Thomas (1931).

MV520 macroporphyritic essexite intrusion, Crawfordjohn. ol (5%) + cpx (25%) + pl (?2%) + mt (<1%), no fresh plagioclase. Scott (1915); Clough et al. (1925).

MV178 microphyric transitional basalt, Hexpathdean Quarry, Tweed Basin, near Kelso. ol (7%) + cpx (<1%) + sp (<1%). Tomkeieff (1945).

MV114 microphyric transitional basalt, Borthwick Quarry, Duns, Tweed Basin, near Kelso. ol (8%) + cpx (5%) + sp (<1%). Tomkeieff (1945).

MV716 microphyric alkali basalt, Dunwan Hill, near Eaglesham. ol (7%) + cpx (<1%) + sp (<1%) + mt (1%). Richey et al. (1930).

MV78 microphyric basanite intrusion, Southdean, near Roxburgh. ol (8%) + cpx (7%) + sp (1%), no fresh olivine. Tomkeieff (1952).

MV406 microphyric alkali basalt lava, Burntisland. ol (13%) + cpx (5%) + sp (<1%) + mt (<1%). Macdonald et al. (1977).

MV400 microphyric hypersthene-normative basalt lava, Burntisland. ol (10%) + cpx (1%) + sp (<1%), no fresh olivine. Macdonald et al. (1977).

MV501 microphyric hypersthene-normative basalt lava, Barassie, Passage Group Lavas, Ayrshire. ol (8%) + cpx (<1%) + pl (trace), no fresh olivine. Macdonald et al. (1977).

MV167 macroporphyritic alkali basalt intrusion, Cairndinnis, East Lothian. ol (4%) + cpx (6%) + pl (11%), no hand specimen, data from Macdonald (1975).

MV40B sparsely porphyritic quartz-normative basalt, near-aphyric component of composite intrusion with MV40A, Lurgie Craigs, near Kelso. pl (1%). Macdonald (1975).

MV160 microphyric transitional basalt intrusion, Yellow Craig intrusion, East Lothian. ol (4%) + cpx (4%) + pl (8%) + sp (<1%) + mt (<1%). Day (1930c).

MV514 microphyric transitional basalt lava, Whinny Hill, Arthur's Seat, Edinburgh. ol (2%) + cpx (trace) + pl (1%) + sp (<1%). Clark (1956) lava III; Black (1966) lava IV.

MV74 macroporphyritic hypersthene-normative basalt intrusion, Burning Mount, East Lothian. ol (6%) + cpx (3%) + pl (18%) + mt (<1%) + il (<1%). Macdonald (1975).

MV72 macroporphyritic hypersthene-normative basalt flow, Kippielaw Quarry, East Lothian. ol (4%) + cpx (1%) + pl (8%), no fresh olivine. Macdonald (1975).

MV516 microphyric transitional basalt intrusion, Castle Rock, Edinburgh. ol (3%) + cpx (trace) + sp (trace). Mitchell and Mykura (1962).

MV704 microphyric nepheline-normative basalt, Harecairns, Lanarkshire. ol (2%) + pl (2%) + mt (trace). Guppy and Thomas (1931).

MV506 microphyric hypersthene-normative basalt lava, Symington, Passage Group Lavas, Ayrshire. ol (3%) + cpx (3%) + pl (3%), no fresh olivine. Macdonald et al. (1977).

MV122 macroporphyritic hypersthene-normative basalt lava, Watch Hill, Birrenswark lavas near Langholm. ol (7%) + cpx (8%) + pl (10%), no fresh olivine. Macdonald (1975).

MV702 macroporphyritic transitional basalt lava, Greenshield House, Carnwath. pl (25%), no fresh groundmass olivine. Guppy and Thomas (1931).

MV39B sparsely porphyritic hawaiite intrusion, near-aphyric component of composite intrusion with MV39A, Hareheugh Craigs, Kelso. pl (1%) + mt (trace) + il (trace). Macdonald (1975).

MV121A microphyric quartz-normative basalt, Howgill Sike vent intrusion, Langholm. ol (1%) + cpx (1%) + opx (1%) + pl (2%) + mt (trace) + il (<1%). Macdonald (1975).

MV71A macroporphyritic hypersthene-normative basalt lava, Kippielaw scarp, East Lothian. ol (1%) + cpx (1%) + pl (5%) + mt (1%), no fresh olivine. Macdonald (1975).

MV52 macroporphyritic basaltic hawaiite, central part of quarry in composite intrusion, Mellerstain Hill, Kelso. ol (5%) + cpx (<1%) + pl (10%) + mt (1%). Macdonald (1975). **cf** MV51.

MV39A macroporphyritic hawaiite intrusion, highly-porphyritic component of composite intrusion with MV39B, Hareheugh Craigs, Kelso. ol (3%) + cpx (5%) + pl (20%) + mt (2%) + il (1%). Macdonald (1975).

MV402 microphyric hypersthene-normative basalt lava, Burntisland. ol (5%) + cpx (3%) + pl (?15%) + sp (<1%), no fresh olivine. Macdonald et al. (1977).

MV13 microphyric hawaiite intrusion, Dunion Hill, Jedburgh. ol (1%) + pl (4%) + mt (<1%) + il (<1%). Macdonald (1975).

MV40A macroporphyritic hawaiite, highly-porphyritic component of composite intrusion with MV40B, Lurgie Craigs, near Kelso. ol (3%) + cpx (3%) + pl (22%) + mt (1%) + il (<1%). Macdonald (1975).

MV165 sparsely microphyric teschenite intrusion, Ravensheugh, East Lothian. ol (?1%) + sp (<1%). Day (1930b).

MV51 sparsely microphyric hawaiite, west end of quarry in composite intrusion, Mellerstain Hill, Kelso. pl (<1%) + mt (<1%). Macdonald (1975). **cf** MV52.

The four samples below are inclusions in basanite, from the Fidra drift, East Lothian. Their mineral assemblages are listed. Chapman (1976) described samples from this locality, see also Upton et al. (1983).

F1 spinel wehrlite, olivine + augite + spinel.

F2 spinel lherzolite, olivine + diopside + enstatite + spinel.

F3 spinel lherzolite, olivine + diopside + enstatite + spinel.

F4 spinel wehrlite, olivine + augite + spinel + ilmenite.

APPENDIX 2

Details of the experiments

The samples are listed mainly in order of decreasing Mg#.
Some paired samples are grouped together.
Abbreviations used:

Pt - Platinum wire hook
sPt - re-used Pt wire hook, Fe-saturated by basaltic melt
Pt-Fe - Pt wire hook, Fe-doped initially by the technique of Ford(1978), and then re-used for individual basalts

Gl - Glass
Ol - Olivine
Pl - Plagioclase
Cpx - Clinopyroxene
Spmt - Spinel/titanomagnetite
Il - Ilmenite
Ap - Apatite
Ml - Iron metal

Composition: MV403

Expt	Temp(^{0}C)	Time(hrs)	Log fO2	Holder	Assemblage
527	1321	16.5	-6.2	Pt-Fe	Gl
526	1309	19	-6.2	sPt	Gl
525	1297	22	-6.5	Pt-Fe	Ol+Gl
497	1288	18	-6.6	Pt-Fe	Ol+Gl
572	1287	4.5	-6.8	Pt-Fe	Ol+Gl
547	1277	14	-6.8	Pt-Fe	Ol+Spmt+Gl
451	1277	6.5	-6.6	Pt-Fe	Ol+Spmt+Gl
425	1263	7.5	-6.8	Pt	Ol+Spmt+Gl
555	1261	20	-7.0	Pt-Fe	Ol+Spmt+Gl
426	1250	5	-7.0	Pt	Ol+Spmt+Gl
427	1243	5	-7.1	Pt	Ol+Spmt+Gl
428	1226	8	-7.2	Pt-Fe	Ol+Spmt+Gl
429	1223	6	-7.3	Pt-Fe	Ol+Spmt+Gl
448	1208	3	-7.6	Pt-Fe	Ol+Spmt+Gl
516	1186	12.5	-7.9	Pt-Fe	Ol+Spmt+Gl
515	1176	16.5	-8.1	Pt-Fe	Ol+Pl+Spmt+Gl
514	1165	16	-8.2	Pt-Fe	Ol+Pl+Spmt+Gl
470	1151	17	-8.4	Pt-Fe	Ol+Pl+Spmt+Gl
509	1140	13	-8.6	Pt-Fe	Ol+Cpx+Pl+Spmt+Gl
471	1129	21	-8.6	Pt-Fe	Ol+Cpx+Pl+Spmt+Gl

Composition: MV403F

Expt	Temp(^{0}C)	Time(hrs)	Log fO2	Holder	Assemblage
572	1287	4.5	-6.8	Pt-Fe	Ol+Gl
547	1277	14	-6.8	Pt-Fe	Ol+Spmt+Gl
555	1261	20	-7.0	Pt-Fe	Ol+Spmt+Gl
543	1252	12.5	-7.1	Pt-Fe	Ol+Spmt+Gl

Composition: ES2058

Expt	Temp(^{0}C)	Time(hrs)	Log fO2	Holder	Assemblage
545	1334	12	-6.2	Pt-Fe	Gl
527	1321	16.5	-6.2	sPt	Ol+Gl
526	1309	19	-6.2	sPt	Ol+Gl
526	1309	19	-6.2	Pt	Ol+Gl
525	1297	22	-6.5	sPt	Ol+Gl
521	1287	16	-6.7	sPt	Ol+Spmt+Gl
522	1277	18	-6.8	sPt	Ol+Spmt+Gl
523	1265	17	-6.9	sPt	Ol+Spmt+Gl
516	1186	12.5	-7.9	sPt	Ol+Spmt+Gl
515	1176	16.5	-8.1	sPt	Ol+Pl+Spmt+Gl
533	1168	20	-8.1	Pt-Fe	Ol+Pl+Spmt+Gl
513	1161	14	-8.3	sPt	Ol+Pl+Spmt+Gl
587	1158	19	-8.2	Pt-Fe	Ol+Pl+Spmt+Gl
552	1148	22	-8.4	Pt-Fe	Ol+Cpx+Pl+Spmt+Gl
510	1145	18	-8.5	sPt	Ol+Cpx+Pl+Spmt+Gl

Composition: MV93

Expt	Temp(^{0}C)	Time(hrs)	Log fO2	Holder	Assemblage
580	1302	2	-6.6	Pt-Fe	Gl
572	1287	4.5	-6.8	Pt-Fe	Gl
570	1274	3.5	-6.9	Pt-Fe	Spmt+Gl
576	1260	4	-7.1	Pt-Fe	Spmt+Gl
578	1247	4	-7.2	Pt-Fe	Spmt+Gl
582	1233	4	-7.3	Pt-Fe	Ol+Spmt+Gl
584	1218	4	-7.5	Pt-Fe	Ol+Spmt+Gl
585	1204	18	-7.6	Pt-Fe	Ol+Spmt+Gl
579	1189	13.5	-7.8	Pt-Fe	Ol+Cpx+Spmt+Gl
581	1174	14	-8.0	Pt-Fe	Ol+Cpx+Gl
571	1160	12.5	-8.2	Pt-Fe	Ol+Cpx+Gl
577	1148	13	-8.3	Pt-Fe	Ol+Cpx+Pl+Gl
583	1135	13	-8.5	Pt-Fe	Ol+Cpx+Pl+Spmt+Gl

Composition: MV521

Expt	Temp(^{0}C)	Time(hrs)	Log fO2	Holder	Assemblage
4-253	1291	2	-6.7	Pt-Fe	Gl
497	1288	18	-6.6	Pt-Fe	Ol+Gl
451	1277	6.5	-6.6	Pt-Fe	Ol+Gl
439	1266	7.5	-6.8	Pt	Ol+Spmt+Gl
440	1256	6.5	-7.0	sPt	Ol+Spmt+Gl
441	1245	6	-7.0	sPt	Ol+Spmt+Gl
442	1236	6	-7.2	sPt	Ol+Spmt+Gl
443	1222	7	-7.4	sPt	Ol+Spmt+Gl
444	1211	6	-7.4	Pt-Fe	Ol+Spmt+Gl
445	1207	3	-7.6	Pt-Fe	Ol+Spmt+Gl
446	1200	6.5	-7.6	Pt-Fe	Ol+Spmt+Gl
447	1191	5	-7.8	Pt-Fe	Ol+Spmt+Gl
449	1177	14.5	-8.0	Pt-Fe	Ol+Pl+Spmt+Gl
528	1171	16	-8.2	Pt-Fe	Ol+Pl+Spmt+Gl (Reversal)*
450	1166	6.5	-8.2	Pt-Fe	Ol+Pl+Spmt+Gl
587	1158	19	-8.2	Pt-Fe	Ol+Cpx+Pl+Spmt+Gl
470	1151	17	-8.4	Pt-Fe	Ol+Cpx+Pl+Spmt+Gl
471	1129	21	-8.6	Pt-Fe	Ol+Cpx+Pl+Spmt+Gl

* Experiment held at 1197^{0}C for 5hrs then cooled to 1171^{0}C

Composition: MV723

Expt	Temp(^{0}C)	Time(hrs)	Log fO2	Holder	Assemblage
527	1321	16.5	-6.2	sPt	Gl
526	1309	19	-6.2	sPt	Gl
546	1297	3	-6.6	Pt-Fe	Spmt+Gl
525	1297	22	-6.5	sPt	Spmt+Gl
497	1288	18	-6.6	sPt	Spmt+Gl
549	1287	14	-6.6	Pt-Fe	Spmt+Gl
451	1277	6.5	-6.6	sPt	Ol+Spmt+Gl
413	1258	5.5	-6.8	Pt	Ol+Spmt+Gl
416	1255	1.5	-6.9	Pt	Ol+Spmt+Gl
417	1248	3	-7.0	Pt	Ol+Spmt+Gl
415	1244	2	-7.0	Pt	Ol+Spmt+Gl
414	1243	2	-7.0	Pt	Ol+Spmt+Gl
437	1211	6	-7.5	sPt	Ol+Spmt+Gl
418	1209	3	-7.5	Pt	Ol+Spmt+Gl
424	1208	2	-7.5	Pt	Ol+Spmt+Gl
421	1206	2	-7.6	Pt	Ol+Spmt+Gl
422	1205	2	-7.6	Pt	Ol+Spmt+Gl
436	1197	8	-7.7	sPt	Ol+Spmt+Gl
5-730	1187	14	-8.0	sPt	Ol+Spmt+Gl
438	1176	7	-8.0	sPt	Ol+Pl+Spmt+Gl
533	1168	20	-8.1	Pt-Fe	Ol+Pl+Spmt+Gl
513	1161	14	-8.3	sPt	Ol+Cpx+Pl+Spmt+Gl
470	1151	17	-8.4	sPt	Ol+Cpx+Pl+Spmt+Gl
471	1129	21	-8.6	sPt	Ol+Cpx+Pl+Spmt+Gl

Composition: MV723F

Expt	Temp(^{0}C)	Time(hrs)	Log fO2	Holder	Assemblage
546	1297	3	-6.6	Pt-Fe	Gl
549	1287	14	-6.6	Pt-Fe	Spmt+Gl
547	1277	14	-6.8	Pt-Fe	Ol+Spmt+Gl

Composition: MV109

Expt	Temp(^{0}C)	Time(hrs)	Log fO2	Holder	Assemblage
4-253	1291	2	-6.7	Pt-Fe	Gl
521	1287	16	-6.7	Pt-Fe	Gl
522	1277	18	-6.8	Pt-Fe	Spmt+Gl
523	1265	17	-6.9	Pt-Fe	Ol+Spmt+Gl
524	1252	20	-7.1	Pt-Fe	Ol+Spmt+Gl
516	1186	12.5	-7.9	Pt-Fe	Ol+Spmt+Gl
515	1176	16.5	-8.1	Pt-Fe	Ol+Pl+Spmt+Gl
513	1161	14	-8.3	Pt-Fe	Ol+Pl+Spmt+Gl
587	1158	19	-8.2	Pt-Fe	Ol+Pl+Spmt+Gl
552	1148	22	-8.4	Pt-Fe	Ol+Cpx+Pl+Spmt+Gl
510	1145	18	-8.5	Pt-Fe	Ol+Cpx+Pl+Spmt+Gl

Composition: MV106

a) Nickel-Nickel Oxide buffer

Expt	Temp(^{0}C)	Time(hrs)	Log fO2	Holder	Assemblage
5-729	1284	5	-6.8	sPt	Gl
439	1266	7.5	-6.8	Pt	Gl
440	1256	6.5	-7.0	sPt	Spmt+Gl
441	1245	6	-7.0	sPt	Ol+Spmt+Gl
442	1236	6	-7.2	sPt	Ol+Spmt+Gl
443	1222	7	-7.4	Pt-Fe	Ol+Spmt+Gl
444	1211	6	-7.4	Pt-Fe	Ol+Spmt+Gl
445	1207	3	-7.6	Pt-Fe	Ol+Pl+Spmt+Gl
446	1200	6.5	-7.6	Pt-Fe	Ol+Pl+Spmt+Gl
447	1191	5	-7.8	Pt-Fe	Ol+Pl+Spmt+Gl
449	1177	14.5	-8.0	Pt-Fe	Ol+Pl+Spmt+Gl
450	1166	6.5	-8.2	Pt-Fe	Ol+Pl+Spmt+Gl
587	1158	19	-8.2	Pt-Fe	Ol+Cpx+Pl+Spmt+Gl
470	1151	17	-8.4	Pt-Fe	Ol+Cpx+Pl+Spmt+Gl
471	1129	21	-8.6	Pt-Fe	Ol+Cpx+Pl+Spmt+Gl

Composition: MV106

b) Iron-Wustite buffer

Expt	Temp(^{0}C)	Time(hrs)	Log fO2	Holder	Assemblage
557	1300	13	-12.5	Pt-Fe	Ml+Gl
558	1299	3	-10.9	Pt-Fe	Gl
559	1284	13	-10.9	Pt-Fe	Gl
560	1270	5	-11.1	Pt-Fe	Gl
561	1255	15.5	-11.2	Pt-Fe	Ol+Gl
564	1240	4.5	-11.5	Pt-Fe	Ol+Gl
566	1227	5	-11.6	Pt-Fe	Ol+Gl
568	1214	5	-11.8	Pt-Fe	Ol+Gl
562	1199	20	-11.9	Pt-Fe	Ol+Pl+Gl
563	1185	15	-12.1	Pt-Fe	Ol+Pl+Gl
565	1171	11.5	-12.3	Pt-Fe	Ol+Pl+Gl
567	1156	12	-12.5	Pt-Fe	Ol+Cpx+Pl+Gl
569	1142	12	-12.8	Pt-Fe	Ol+Cpx+Pl+Gl
573	1128	16	-13.0	Pt-Fe	Ol+Cpx+Pl+Gl
574	1113	19	-13.1	Pt-Fe	Ol+Cpx+Pl+Il+Gl
575	1099	17	-13.3	Pt-Fe	Ol+Cpx+Pl+Il+Gl

Composition: MV164

Expt	Temp(^{0}C)	Time(hrs)	Log fO2	Holder	Assemblage
497	1288	18	-6.6	Pt-Fe	Gl
451	1277	6.5	-6.6	Pt-Fe	Ol+Spmt+Gl
452	1265	16	-6.8	Pt-Fe	Ol+Spmt+Gl
453	1253	8.5	-7.0	Pt-Fe	Ol+Spmt+Gl
454	1243	16.5	-7.1	Pt-Fe	Ol+Spmt+Gl
456	1234	17	-7.2	Pt-Fe	Ol+Spmt+Gl
455	1233	24	-7.2	Pt-Fe	Ol+Spmt+Gl
457	1223	19	-7.3	Pt-Fe	Ol+Spmt+Gl
458	1212	17	-7.4	Pt-Fe	Ol+Spmt+Gl
461	1208	3	-7.6	Pt-Fe	Ol+Spmt+Gl
460	1204	3	-7.6	Pt-Fe	Ol+Spmt+Gl
462	1196	5	-7.7	Pt-Fe	Ol+Spmt+Gl
463	1183	5.5	-7.9	Pt-Fe	Ol+Spmt+Gl
465	1174	16	-8.0	Pt-Fe	Ol+Pl+Spmt+Gl
464	1174	19	<-8	Pt-Fe	Ol+Pl+Spmt+Gl
466	1161	16	-8.2	Pt-Fe	Ol+Pl+Spmt+Gl
467	1151	16	-8.4	Pt-Fe	Ol+Cpx+Pl+Spmt+Gl
468	1140	19	-8.5	Pt-Fe	Ol+Cpx+Pl+Spmt+Gl
469	1127	5	-8.7	Pt-Fe	Ol+Cpx+Pl+Spmt+Gl

Composition: MV166

a) Nickel-Nickel Oxide buffer

Expt	Temp(^{0}C)	Time(hrs)	Log fO2	Holder	Assemblage
5-729	1284	5	-6.8	sPt	Gl
5-727	1271	6.5	-6.9	sPt	Spmt+Gl
425	1263	7.5	-6.8	Pt	Ol+Spmt+Gl
426	1250	5	-7.0	Pt	Ol+Spmt+Gl
427	1243	5	-7.0	Pt	Ol+Spmt+Gl
433	1232	6.5	-7.2	Pt	Ol+Spmt+Gl
428	1226	8	-7.2	Pt-Fe	Ol+Spmt+Gl
429	1223	6	-7.3	Pt-Fe	Ol+Spmt+Gl
437	1211	6	-7.5	sPt	Ol+Spmt+Gl
436	1197	8	-7.7	sPt	Ol+Spmt+Gl
434	1185	12	-7.8	sPt	Ol+Spmt+Gl
438	1176	7	-8.0	sPt	Ol+Spmt+Gl
5-728	1167	12	-8.2	sPt	Ol+Pl+Spmt+Gl
5-726	1157	12.5	-8.4	Pt-Fe	Ol+Cpx+Pl+Spmt+Gl
5-725	1145	15	-8.6	Pt-Fe	Ol+Cpx+Pl+Spmt+Gl
5-725	1145	15	-8.6	Pt	Ol+Cpx+Pl+Spmt+Gl

Composition: MV166

b) Iron-Wustite buffer

Expt	Temp(^{0}C)	Time(hrs)	Log fO2	Holder	Assemblage
557	1300	13	-12.5	Pt-Fe	Ml+Gl
558	1299	3	-10.9	Pt-Fe	Gl
559	1284	13	-10.9	Pt-Fe	Gl
560	1270	5	-11.1	Pt-Fe	Ol+Gl
561	1255	15.5	-11.2	Pt-Fe	Ol+Gl
564	1240	4.5	-11.5	Pt-Fe	Ol+Gl
566	1227	5	-11.6	Pt-Fe	Ol+Gl
568	1214	5	-11.8	Pt-Fe	Ol+Gl
562	1199	20	-11.9	Pt-Fe	Ol+Gl
563	1185	15	-12.1	Pt-Fe	Ol+Gl
565	1171	11.5	-12.3	Pt-Fe	Ol+Pl+Gl
567	1156	12	-12.5	Pt-Fe	Ol+Cpx+Pl+Gl
569	1142	12	-12.8	Pt-Fe	Ol+Cpx+Pl+Gl
573	1128	16	-13.0	Pt-Fe	Ol+Cpx+Pl+Gl
574	1113	19	-13.1	Pt-Fe	Ol+Cpx+Pl+Il+Gl
575	1099	17	-13.3	Pt-Fe	Ol+Cpx+Pl+Il+Gl

Composition: MV718

Expt	Temp(^{0}C)	Time(hrs)	Log fO2	Holder	Assemblage
580	1302	2	-6.6	Pt-Fe	Gl

Composition: MV703

Expt	Temp(^{0}C)	Time(hrs)	Log fO2	Holder	Assemblage
521	1287	16	-6.7	Pt-Fe	Gl
522	1277	18	-6.8	Pt-Fe	Gl
523	1265	17	-6.9	Pt-Fe	Gl
524	1252	20	-7.1	Pt-Fe	Ol+Spmt+Gl
529	1238	18.5	-7.3	Pt-Fe	Ol+Spmt+Gl
496	1223	19	-7.4	Pt-Fe	Ol+Spmt+Gl
473	1211	2.5	-7.4	Pt-Fe	Ol+Spmt+Gl
476	1198	19	-7.7	Pt-Fe	Ol+Spmt+Gl
477	1189	18.5	-7.8	Pt-Fe	Ol+Spmt+Gl
478	1179	9	-8.0	Pt-Fe	Ol+Pl+Spmt+Gl
528	1171	16	-8.2	Pt-Fe	Ol+Pl+Spmt+Gl (Reversal)*
479	1169	14	-8.0	Pt-Fe	Ol+Pl+Spmt+Gl
480	1157	19	-8.2	Pt-Fe	Ol+Cpx+Pl+Spmt+Gl
481	1146	20	-8.4	Pt-Fe	Ol+Cpx+Pl+Spmt+Gl
482	1135	6.5	-8.6	Pt-Fe	Ol+Cpx+Pl+Spmt+Gl
483	1122	19.5	-8.7	Pt-Fe	Ol+Cpx+Pl+Spmt+Gl

* Experiment held at 1197^{0}C for 5hrs then cooled to 1171^{0}C

Composition: MV520

Expt	Temp(^{0}C)	Time(hrs)	Log fO2	Holder	Assemblage
521	1287	16	-6.7	sPt	Gl
522	1277	18	-6.8	sPt	Gl
523	1265	17	-6.9	sPt	Gl
524	1252	20	-7.1	sPt	Spmt+Gl
543	1252	12.5	-7.1	Pt-Fe	Spmt+Gl
529	1238	18.5	-7.3	Pt-Fe	Ol+Spmt+Gl
530	1232	16	-7.4	Pt-Fe	Ol+Spmt+Gl
516	1186	12.5	-7.9	sPt	Ol+Spmt+Gl
515	1176	16.5	-8.1	sPt	Ol+Spmt+Gl
514	1165	16	-8.2	sPt	Ol+Spmt+Gl
587	1158	19	-8.2	Pt-Fe	Ol+Pl+Spmt+Gl
511	1151	18.5	-8.4	sPt	Ol+Cpx+Pl+Spmt+Gl

Composition: MV178

Expt	Temp(^{0}C)	Time(hrs)	Log fO2	Holder	Assemblage
525	1297	22	-6.5	Pt-Fe	Gl
547	1277	14	-6.8	Pt-Fe	Gl
540	1264	19	-7.0	Pt-Fe	Gl
524	1252	20	-7.1	Pt-Fe	Ol+Gl
543	1252	12.5	-7.1	Pt-Fe	Ol+Gl
529	1238	18.5	-7.3	Pt-Fe	Ol+Spmt+Gl
530	1232	16	-7.4	Pt-Fe	Ol+Spmt+Gl
531	1186	20	-8.0	Pt-Fe	Ol+Spmt+Gl
532	1176	20.5	-8.0	Pt-Fe	Ol+Spmt+Gl
533	1168	20	-8.1	Pt-Fe	Ol+Spmt+Gl
512	1155	24	-8.4	Pt-Fe	Ol+Pl+Spmt+Gl
534	1143	12.5	-8.5	Pt-Fe	Ol+Pl+Spmt+Gl
517	1131	12	-8.8	Pt-Fe	Ol+Cpx+Pl+Spmt+Gl
518	1120	20	-8.9	Pt-Fe	Ol+Cpx+Pl+Spmt+Gl
519	1108	21	-9.1	Pt-Fe	Ol+Cpx+Pl+Spmt+Gl

Composition: MV114

Expt	Temp(^{0}C)	Time(hrs)	Log fO2	Holder	Assemblage
439	1266	7.5	-6.8	Pt	Gl
440	1256	6.5	-7.0	sPt	Gl
441	1245	6	-7.0	sPt	Ol+Gl
442	1236	6	-7.2	sPt	Ol+Spmt+Gl
443	1222	7	-7.4	sPt	Ol+Spmt+Gl
444	1211	6	-7.4	sPt	Ol+Spmt+Gl
445	1207	3	-7.6	sPt	Ol+Spmt+Gl
446	1200	6.5	-7.6	sPt	Ol+Spmt+Gl
447	1191	5	-7.8	sPt	Ol+Spmt+Gl
449	1177	14.5	-8.0	sPt	Ol+Spmt+Gl
450	1166	6.5	-8.2	sPt	Ol+Spmt+Gl
512	1155	24	-8.4	Pt-Fe	Ol+Pl+Spmt+Gl
510	1145	18	-8.5	Pt-Fe	Ol+Pl+Spmt+Gl
490	1137	19	-8.6	sPt	Ol+Cpx+Pl+Spmt+Gl
491	1124	19	-8.8	sPt	Ol+Cpx+Pl+Spmt+Gl

Composition: MV716

Expt	Temp(^{0}C)	Time(hrs)	Log fO2	Holder	Assemblage
525	1297	22	-6.5	Pt-Fe	Gl
549	1287	14	-6.6	Pt-Fe	Gl
547	1277	14	-6.8	Pt-Fe	Ol+Gl
523	1265	17	-6.9	Pt-Fe	Ol+Gl
524	1252	20	-7.1	Pt-Fe	Ol+Spmt+Gl
529	1238	18.5	-7.3	Pt-Fe	Ol+Spmt+Gl
531	1186	20	-8.0	Pt-Fe	Ol+Spmt+Gl
532	1176	20.5	-8.0	Pt-Fe	Ol+Spmt+Gl
514	1165	16	-8.2	Pt-Fe	Ol+Pl+Spmt+Gl
511	1151	18.5	-8.4	Pt-Fe	Ol+Pl+Spmt+Gl
517	1131	12	-8.8	Pt-Fe	Ol+Pl+Spmt+Gl
518	1120	20	-8.9	Pt-Fe	Ol+Cpx+Pl+Spmt+Gl
519	1108	21	-9.1	Pt-Fe	Ol+Cpx+Pl+Spmt+Gl

Composition: MV78

Expt	Temp(^{0}C)	Time(hrs)	Log fO2	Holder	Assemblage
5-729	1284	5	-6.8	sPt	Gl
412	1260	1	-6.8	Pt	Gl
413	1258	5.5	-6.8	Pt	Gl
416	1255	1.5	-6.9	Pt	Gl
417	1248	3	-7.0	Pt	Gl
415	1244	2	-7.0	Pt	Gl
414	1243	2	-7.0	Pt	Gl
433	1232	6.5	-7.2	sPt	Ol+Gl
419	1214	2	-7.5	Pt	Ol+Gl
437	1211	6	-7.5	sPt	Ol+Gl
418	1209	3	-7.5	Pt	Ol+Spmt+Gl
424	1208	2	-7.5	Pt	Ol+Spmt+Gl
432	1207	2	-7.4	Pt	Ol+Spmt+Gl
421	1206	2	-7.6	Pt	Ol+Spmt+Gl
422	1205	2	-7.6	Pt	Ol+Spmt+Gl
436	1197	8	-7.7	sPt	Ol+Spmt+Gl
434	1185	12	-7.8	sPt	Ol+Spmt+Gl
438	1176	7	-8.0	sPt	Ol+Spmt+Gl
513	1161	14	-8.3	Pt-Fe	Ol+Spmt+Gl
511	1151	18.5	-8.4	Pt-Fe	Ol+Cpx+Pl+Spmt+Gl
509	1140	13	-8.6	sPt	Ol+Cpx+Pl+Spmt+Gl
472	1128	5.5	-8.7	Pt-Fe	Ol+Cpx+Pl+Spmt+Gl

Composition: MV406

Expt	Temp(^{0}C)	Time(hrs)	Log fO2	Holder	Assemblage
4-253	1291	2	-6.7	Pt-Fe	Gl
497	1288	18	-6.6	sPt	Gl
521	1287	16	-6.7	sPt	Gl
522	1277	18	-6.8	sPt	Spmt+Gl
451	1277	6.5	-6.6	Pt-Fe	Spmt+Gl
439	1266	7.5	-6.8	Pt	Spmt+Gl
440	1256	6.5	-7.0	sPt	Spmt+Gl
441	1245	6	-7.0	sPt	Ol+Spmt+Gl
442	1236	6	-7.2	sPt	Ol+Spmt+Gl
443	1222	7	-7.4	Pt-Fe	Ol+Spmt+Gl
444	1211	6	-7.4	Pt-Fe	Ol+Spmt+Gl
445	1207	3	-7.6	Pt-Fe	Ol+Spmt+Gl
446	1200	6.5	-7.6	Pt-Fe	Ol+Spmt+Gl
447	1191	5	-7.8	Pt-Fe	Ol+Spmt+Gl
449	1177	14.5	-8.0	Pt-Fe	Ol+Spmt+Gl
533	1168	20	-8.1	Pt-Fe	Ol+Spmt+Gl
450	1166	6.5	-8.2	Pt-Fe	Ol+Pl+Spmt+Gl
513	1161	14	-8.3	sPt	Ol+Pl+Spmt+Gl
512	1155	24	-8.4	Pt-Fe	Ol+Pl+Spmt+Gl
470	1151	17	-8.4	sPt	Ol+Pl+Spmt+Gl
552	1148	22	-8.4	Pt-Fe	Ol+Pl+Spmt+Gl
509	1140	13	-8.6	sPt	Ol+Cpx+Pl+Spmt+Gl
509	1140	13	-8.6	Pt-Fe	Ol+Cpx+Pl+Spmt+Gl
471	1129	21	-8.6	sPt	Ol+Cpx+Pl+Spmt+Gl
472	1128	5.5	-8.6	Pt-Fe	Ol+Cpx+Pl+Spmt+Gl

Composition: MV400

Expt	Temp(^{0}C)	Time(hrs)	Log fO2	Holder	Assemblage
580	1302	2	-6.6	Pt-Fe	Gl

Composition: MV501

Expt	Temp(^{0}C)	Time(hrs)	Log fO2	Holder	Assemblage
521	1287	16	-6.7	sPt	Gl
522	1277	18	-6.8	sPt	Gl
523	1265	17	-6.9	sPt	Gl
524	1252	20	-7.1	sPt	Gl
529	1238	18.5	-7.3	Pt-Fe	Gl
530	1232	16	-7.4	Pt-Fe	Spmt+Gl
539	1226	21	-7.4	Pt-Fe	Ol+Spmt+Gl
538	1215	16.5	-7.5	Pt-Fe	Ol+Spmt+Gl
531	1186	20	-8.0	Pt-Fe	Ol+Spmt+Gl
532	1176	20.5	-8.0	Pt-Fe	Ol+Pl+Spmt+Gl
514	1165	16	-8.2	sPt	Ol+Pl+Spmt+Gl
587	1158	19	-8.2	Pt-Fe	Ol+Pl+Spmt+Gl
511	1151	18.5	-8.4	sPt	Ol+Cpx+Pl+Spmt+Gl

Composition: MV167

Expt	Temp(^{0}C)	Time(hrs)	Log fO2	Holder	Assemblage
570	1274	3.5	-6.9	Pt-Fe	Gl
555	1261	20	-7.0	Pt-Fe	Spmt+Gl
412	1260	1	-6.8	Pt	Spmt+Gl
413	1258	5.5	-6.8	Pt	Spmt+Gl
416	1255	1.5	-6.9	Pt	Spmt+Gl
551	1248	16	-7.2	Pt-Fe	Spmt+Gl
417	1248	3	-7.0	Pt	Spmt+Gl
415	1244	2	-7.0	Pt	Spmt+Gl
414	1243	2	-7.0	Pt	Spmt+Gl
550	1236	3	-7.3	Pt-Fe	Spmt+Gl
433	1232	6.5	-7.2	sPt	Spmt+Gl
496	1223	19	-7.4	sPt	Ol+Spmt+Gl
548	1219	3.5	-7.5	Pt-Fe	Ol+Spmt+Gl
419	1214	2	-7.5	Pt	Ol+Spmt+Gl
437	1211	6	-7.5	sPt	Ol+Spmt+Gl
418	1209	3	-7.5	Pt	Ol+Spmt+Gl
424	1208	2	-7.5	Pt	Ol+Spmt+Gl
432	1207	2	-7.4	Pt	Ol+Spmt+Gl
421	1206	2	-7.6	Pt	Ol+Spmt+Gl
422	1205	2	-7.6	Pt	Ol+Spmt+Gl
436	1197	8	-7.7	sPt	Ol+Spmt+Gl
434	1185	12	-7.8	sPt	Ol+Pl+Spmt+Gl
438	1176	7	-8.0	sPt	Ol+Pl+Spmt+Gl
511	1151	18.5	-8.4	sPt	Ol+Pl+Spmt+Gl
509	1140	13	-8.6	sPt	Ol+Pl+Spmt+Gl
517	1131	12	-8.8	sPt	Ol+Cpx+Pl+Spmt+Gl
535	1118	20	-8.9	Pt-Fe	Ol+Cpx+Pl+Spmt+Gl

Composition: MV167F

Expt	Temp(^{0}C)	Time(hrs)	Log fO2	Holder	Assemblage
570	1274	3.5	-6.9	Pt-Fe	Gl
555	1261	20	-7.0	Pt-Fe	Gl
551	1248	16	-7.2	Pt-Fe	Spmt+Gl
550	1236	3	-7.3	Pt-Fe	Ol+Spmt+Gl
548	1219	3.5	-7.5	Pt-Fe	Ol+Spmt+Gl
542	1208	2.5	-7.6	Pt-Fe	Ol+Spmt+Gl
544	1205	2	-7.6	Pt-Fe	Ol+Spmt+Gl

Composition: MV40B

a) Nickel-Nickel Oxide buffer

Expt	Temp(^{0}C)	Time(hrs)	Log fO2	Holder	Assemblage
496	1223	19	-7.4	Pt-Fe	Gl
474	1209	3	-7.5	Pt-Fe	Spmt+Gl
484	1197	19.5	-7.7	Pt-Fe	Ol+Spmt+Gl
485	1191	18.5	-7.8	Pt-Fe	Ol+Spmt+Gl
486	1180	17.5	-7.9	Pt-Fe	Ol+Spmt+Gl
487	1171	17.5	-8.0	Pt-Fe	Ol+Pl+Spmt+Gl
488	1158	19	-8.3	Pt-Fe	Ol+Pl+Spmt+Gl
489	1147	18	-8.5	Pt-Fe	Ol+Pl+Spmt+Gl
490	1137	19	-8.6	Pt-Fe	Ol+Cpx+Pl+Spmt+Gl
491	1124	19	-8.8	Pt-Fe	Ol+Cpx+Pl+Spmt+Gl
493	1115	17.5	-8.9	Pt-Fe	Ol+Cpx+Pl+Spmt+Gl
494	1104	19	-9.1	Pt-Fe	Ol+Cpx+Pl+Spmt+Gl

Composition: MV40B

b) Iron-Wustite buffer

Expt	Temp(^{0}C)	Time(hrs)	Log fO2	Holder	Assemblage
557	1300	13	-12.5	Pt-Fe	Ml+Gl
564	1240	4.5	-11.5	Pt-Fe	Gl
566	1227	5	-11.6	Pt-Fe	Gl
568	1214	5	-11.8	Pt-Fe	Ol+Gl
562	1199	20	-11.9	Pt-Fe	Ol+Gl
563	1185	15	-12.1	Pt-Fe	Ol+Gl
565	1171	11.5	-12.3	Pt-Fe	Ol+Pl+Gl
567	1156	12	-12.5	Pt-Fe	Ol+Pl+Gl
569	1142	12	-12.8	Pt-Fe	Ol+Pl+Gl
573	1128	16	-13.0	Pt-Fe	Ol+Cpx+Pl+Gl
574	1113	19	-13.1	Pt-Fe	Ol+Cpx+Pl+Gl
575	1099	17	-13.3	Pt-Fe	Ol+Cpx+Pl+Il+Gl

Composition: MV160

a) Nickel-Nickel Oxide buffer

Expt	Temp(^{0}C)	Time(hrs)	Log fO2	Holder	Assemblage
452	1265	16	-6.8	Pt-Fe	Gl
453	1253	8.5	-7.0	Pt-Fe	Gl
454	1243	16.5	-7.1	Pt-Fe	Spmt+Gl
456	1234	17	-7.2	Pt-Fe	Spmt+Gl
455	1233	24	-7.2	Pt-Fe	Spmt+Gl
457	1223	19	-7.3	Pt-Fe	Spmt+Gl
461	1208	3	-7.6	Pt-Fe	Ol+Spmt+Gl
460	1204	3	-7.6	Pt-Fe	Ol+Spmt+Gl
462	1196	5	-7.7	Pt-Fe	Ol+Spmt+Gl
463	1183	5.5	-7.9	Pt-Fe	Ol+Spmt+Gl
465	1174	16	-8.0	Pt-Fe	Ol+Pl+Spmt+Gl
464	1174	19	<-8	Pt-Fe	Ol+Pl+Spmt+Gl
466	1161	16	-8.2	Pt-Fe	Ol+Pl+Spmt+Gl
467	1151	16	-8.4	Pt-Fe	Ol+Pl+Spmt+Gl
468	1140	19	-8.5	Pt-Fe	Ol+Pl+Spmt+Gl
469	1127	5	-8.7	Pt-Fe	Ol+Pl+Spmt+Gl
493	1115	17.5	-8.9	Pt-Fe	Ol+Cpx+Pl+Spmt+Gl
494	1104	19	-9.0	Pt-Fe	Ol+Cpx+Pl+Spmt+Il+Gl

Composition: MV160

b) Iron-Wustite buffer

Expt	Temp(^{0}C)	Time(hrs)	Log fO2	Holder	Assemblage
557	1300	13	-12.5	Pt-Fe	Ml+Gl
558	1299	3	-10.9	Pt-Fe	Gl
559	1284	13	-10.9	Pt-Fe	Gl
560	1270	5	-11.1	Pt-Fe	Gl
561	1255	15.5	-11.2	Pt-Fe	Gl
564	1240	4.5	-11.5	Pt-Fe	Gl
566	1227	5	-11.6	Pt-Fe	Gl
568	1214	5	-11.8	Pt-Fe	Ol+Gl
562	1199	20	-11.9	Pt-Fe	Ol+Gl
563	1185	15	-12.1	Pt-Fe	Ol+Gl
565	1171	11.5	-12.3	Pt-Fe	Ol+Pl+Gl
567	1156	12	-12.5	Pt-Fe	Ol+Pl+Gl
569	1142	12	-12.8	Pt-Fe	Ol+Pl+Gl
573	1128	16	-13.0	Pt-Fe	Ol+Pl+Spmt?+Gl
574	1113	19	-13.1	Pt-Fe	Ol+Cpx+Pl+Spmt+Il+Gl
575	1099	17	-13.3	Pt-Fe	Ol+Cpx+Pl+Il+Gl

Composition: MV514

Expt	Temp(^{0}C)	Time(hrs)	Log fO2	Holder	Assemblage
425	1263	7.5	-6.8	Pt	Gl
426	1250	5	-7.0	Pt	Gl
427	1243	5	-7.1	Pt	Gl
428	1226	8	-7.2	Pt-Fe	Gl
429	1223	6	-7.3	Pt-Fe	Gl
448	1208	3	-7.6	Pt-Fe	Gl
475	1203	2.5	-7.6	Pt-Fe	Gl
484	1197	19.5	-7.7	Pt-Fe	Spmt+Gl
485	1191	18.5	-7.8	Pt-Fe	Ol+Spmt+Gl
486	1180	17.5	-7.9	Pt-Fe	Ol+Pl+Spmt+Gl
528	1171	16	-8.2	Pt-Fe	Ol+Pl+Spmt+Gl (Reversal)*
487	1171	17.5	-8.0	Pt-Fe	Ol+Pl+Spmt+Gl
488	1158	19	-8.3	Pt-Fe	Ol+Pl+Spmt+Gl
489	1147	18	-8.5	Pt-Fe	Ol+Pl+Spmt+Gl
472	1128	5.5	-8.7	Pt-Fe	Ol+Pl+Spmt+Gl
493	1115	17.5	-8.9	Pt-Fe	Ol+Pl+Spmt+Gl
494	1104	19	-9.1	Pt-Fe	Ol+Cpx+Pl+Spmt+Il+Gl

* Experiment held at 1197^{0}C for 5hrs then cooled to 1171^{0}C

Composition: MV74

Expt	Temp(^{0}C)	Time(hrs)	Log fO2	Holder	Assemblage
439	1266	7.5	-6.8	Pt	Gl
440	1256	6.5	-7.0	sPt	Gl
441	1245	6	-7.0	sPt	Gl
442	1236	6	-7.2	sPt	Spmt+Gl
443	1222	7	-7.4	sPt	Spmt+Gl
444	1211	6	-7.4	sPt	Spmt+Gl
445	1207	3	-7.6	sPt	Spmt+Gl
446	1200	6.5	-7.6	sPt	Spmt+Gl
447	1191	5	-7.8	sPt	Spmt+Gl
449	1177	14.5	-8.0	sPt	Pl+Spmt+Gl
528	1171	16	-8.2	Pt-Fe	Spmt+Gl (Reversal)*
450	1166	6.5	-8.2	sPt	Ol+Pl+Spmt+Gl
512	1155	24	-8.4	Pt-Fe	Ol+Pl+Spmt+Gl
510	1145	18	-8.5	sPt	Ol+Pl+Spmt+Gl
517	1131	12	-8.8	Pt-Fe	Ol+Pl+Spmt+Gl
518	1120	20	-8.9	Pt-Fe	Ol+Pl+Spmt+Gl
519	1108	21	-9.1	Pt-Fe	Ol+Cpx+Pl+Spmt+Il+Gl
520	1099	15	-9.1	Pt-Fe	Ol+Cpx+Pl+Spmt+Il+Gl

* Experiment held at 1197^{0}C for 5hrs then cooled to 1171^{0}C

Composition: MV72

Expt	Temp(^{0}C)	Time(hrs)	Log fO2	Holder	Assemblage
474	1209	3	-7.5	Pt-Fe	Gl
484	1197	19.5	-7.7	Pt-Fe	Gl
485	1191	18.5	-7.8	Pt-Fe	Gl
486	1180	17.5	-7.9	Pt-Fe	Ol+Pl+Gl
528	1171	16	-8.2	Pt-Fe	Ol+Gl (Reversal)*
487	1171	17.5	-8.1	Pt-Fe	Ol+Pl+Gl
488	1158	19	-8.3	Pt-Fe	Ol+Pl+Spmt+Gl
489	1147	18	-8.5	Pt-Fe	Ol+Pl+Spmt+Gl
490	1137	19	-8.6	Pt-Fe	Ol+Pl+Spmt+Gl
491	1124	19	-8.8	Pt-Fe	Ol+Pl+Spmt+Il+Gl
492	1114	19.5	-8.9	Pt-Fe	Ol+Pl+Spmt+Il+Gl
495	1105	19	-9.0	Pt-Fe	Ol+Cpx+Pl+Spmt+Il+Gl

* Experiment held at 1197^{0}C for 5hrs then cooled to 1171^{0}C

Composition: MV516

Expt	Temp(^{0}C)	Time(hrs)	Log fO2	Holder	Assemblage
580	1302	2	-6.6	Pt-Fe	Gl

Composition: MV704

Expt	Temp(^{0}C)	Time(hrs)	Log fO2	Holder	Assemblage
452	1265	16	-6.8	Pt-Fe	Gl
453	1253	8.5	-7.0	Pt-Fe	Gl
454	1243	16.5	-7.1	Pt-Fe	Gl
456	1234	17	-7.2	Pt-Fe	Gl
455	1233	24	-7.2	Pt-Fe	Gl
457	1223	19	-7.3	Pt-Fe	Gl
458	1212	17	-7.4	Pt-Fe	Gl
461	1208	3	-7.6	Pt-Fe	Gl
460	1204	3	-7.6	Pt-Fe	Gl
462	1196	5	-7.7	Pt-Fe	Gl
463	1183	5.5	-7.9	Pt-Fe	Ol+Pl+Spmt+Gl
465	1174	16	-8.0	Pt-Fe	Ol+Pl+Spmt+Gl
464	1174	19	<-8	Pt-Fe	Ol+Pl+Gl
466	1161	16	-8.2	Pt-Fe	Ol+Pl+Spmt+Gl
467	1151	16	-8.4	Pt-Fe	Ol+Pl+Spmt+Gl
468	1140	19	-8.5	Pt-Fe	Ol+Pl+Spmt+Gl
469	1127	5	-8.7	Pt-Fe	Ol+Pl+Spmt+Gl
493	1115	17.5	-8.9	Pt-Fe	Ol+Cpx+Pl+Spmt+Gl
494	1104	19	-9.1	Pt-Fe	Ol+Cpx+Pl+Spmt+Gl

Composition: MV506

Expt	Temp(^{0}C)	Time(hrs)	Log fO2	Holder	Assemblage
5-727	1271	6.5	-6.9	Pt-Fe	Gl
474	1209	3	-7.5	Pt-Fe	Gl
484	1197	19.5	-7.7	Pt-Fe	Pl+Gl
485	1191	18.5	-7.8	Pt-Fe	Pl+Gl
486	1180	17.5	-7.9	Pt-Fe	Ol+Pl+Gl
487	1171	17.5	-8.0	Pt-Fe	Ol+Pl+Gl
488	1158	19	-8.3	Pt-Fe	Ol+Pl+Gl
489	1147	18	-8.5	Pt-Fe	Ol+Pl+Gl
490	1137	19	-8.6	Pt-Fe	Ol+Pl+Gl
491	1124	19	-8.8	Pt-Fe	Ol+Pl+Gl
492	1114	19.5	-8.9	Pt-Fe	Ol+Cpx+Pl+Spmt+Gl
495	1105	19	-9.0	Pt-Fe	Ol+Cpx+Pl+Spmt+Gl

Composition: MV122

Expt	Temp(^{0}C)	Time(hrs)	Log fO2	Holder	Assemblage
452	1265	16	-6.8	Pt-Fe	Gl
453	1253	8.5	-7.0	Pt-Fe	Gl
454	1243	16.5	-7.1	Pt-Fe	Gl
456	1234	17	-7.2	Pt-Fe	Gl
455	1233	24	-7.2	Pt-Fe	Gl
457	1223	19	-7.3	Pt-Fe	Gl
458	1212	17	-7.4	Pt-Fe	Gl
475	1203	2.5	-7.6	Pt-Fe	Spmt+Gl
462	1196	5	-7.7	Pt-Fe	Spmt+Gl
463	1183	5.5	-7.9	Pt-Fe	Spmt+Gl
465	1174	16	-8.0	Pt-Fe	Ol+Spmt+Gl
464	1174	19	<-8	Pt-Fe	Ol+Spmt+Gl
466	1161	16	-8.2	Pt-Fe	Ol+Spmt+Gl
467	1151	16	-8.4	Pt-Fe	Ol+Pl+Spmt+Gl
468	1140	19	-8.5	Pt-Fe	Ol+Pl+Spmt+Gl
469	1127	5	-8.6	Pt-Fe	Ol+Cpx+Pl+Spmt+Gl

Composition: MV702

Expt	Temp(^{0}C)	Time(hrs)	Log fO2	Holder	Assemblage
5-729	1284	5	-6.8	sPt	Gl
540	1264	19	-7.0	Pt-Fe	Gl
543	1252	12.5	-7.1	Pt-Fe	Pl+Gl
529	1238	18.5	-7.3	Pt-Fe	Pl+Gl
530	1232	16	-7.4	Pt-Fe	Pl+Gl
496	1223	19	-7.4	Pt-Fe	Pl+Gl
474	1209	3	-7.5	Pt-Fe	Pl+Gl
476	1198	19	-7.7	Pt-Fe	Pl+Gl
477	1189	18.5	-7.8	Pt-Fe	Pl+Gl
478	1179	9	-8.0	Pt-Fe	Ol+Pl+Spmt+Gl
479	1169	14	-8.0	Pt-Fe	Ol+Pl+Spmt+Gl
480	1157	19	-8.2	Pt-Fe	Ol+Pl+Spmt+Gl
481	1146	20	-8.4	Pt-Fe	Ol+Pl+Spmt+Gl
482	1135	6.5	-8.6	Pt-Fe	Ol+Pl+Spmt+Gl
483	1122	19.5	-8.7	Pt-Fe	Ol+Pl+Spmt+Gl
493	1115	17.5	-8.9	Pt-Fe	Ol+Pl+Spmt+Gl
494	1104	19	-9.1	Pt-Fe	Ol+Cpx+Pl+Spmt+Il+Gl

Composition: MV39B

Expt	Temp(^{0}C)	Time(hrs)	Log fO2	Holder	Assemblage
412	1260	1	-6.8	Pt	Gl
416	1255	1.5	-6.9	Pt	Gl
417	1248	3	-7.0	Pt	Gl
415	1244	2	-7.0	Pt	Gl
414	1243	2	-7.0	Pt	Gl
433	1232	6.5	-7.2	sPt	Gl
419	1214	2	-7.5	Pt	Gl
437	1211	6	-7.5	sPt	Gl
418	1209	3	-7.5	Pt	Gl
431	1209	24	-7.5	Pt-Fe	Gl
431	1209	24	-7.5	Pt	Gl
424	1208	2	-7.5	Pt	Gl
432	1207	2	-7.4	Pt	Gl
421	1206	2	-7.6	Pt	Gl
430	1206	5	-7.5	Pt-Fe	Gl
430	1206	5	-7.5	Pt	Gl
422	1205	2	-7.6	Pt	Gl
436	1197	8	-7.7	sPt	Spmt+Gl
434	1185	12	-7.8	sPt	Spmt+Gl
438	1176	7	-8.0	sPt	Ol+Spmt+Gl
513	1161	14	-8.3	sPt	Ol+Spmt+Gl
511	1151	18.5	-8.4	sPt	Ol+Pl+Spmt+Gl
509	1140	13	-8.6	sPt	Ol+Pl+Spmt+Gl
471	1129	21	-8.6	sPt	Ol+Pl+Spmt+Gl
518	1120	20	-8.9	sPt	Ol+Pl+Spmt+Gl
519	1108	21	-9.1	sPt	Ol+Cpx+Pl+Spmt+Gl
520	1099	15	-9.1	Pt-Fe	Ol+Cpx+Pl+Spmt+Il+Gl
501	1092	19.5	-9.3	sPt	Ol+Cpx+Pl+Spmt+Il+Gl

Composition: MV121A

Expt	Temp(^{0}C)	Time(hrs)	Log fO2	Holder	Assemblage
425	1263	7.5	-6.8	Pt	Gl
426	1250	5	-7.0	Pt	Gl
427	1243	5	-7.1	Pt	Gl
428	1226	8	-7.2	Pt-Fe	Gl
429	1223	6	-7.3	Pt-Fe	Gl
448	1208	3	-7.6	Pt-Fe	Gl
475	1203	2.5	-7.6	Pt-Fe	Spmt+Gl
516	1186	12.5	-7.9	Pt-Fe	Spmt+Gl
515	1176	16.5	-8.1	Pt-Fe	Spmt+Gl
514	1165	16	-8.2	Pt-Fe	Ol+Spmt+Gl
512	1155	24	-8.4	Pt-Fe	Ol+Spmt+Gl
510	1145	18	-8.5	Pt-Fe	Ol+Pl+Spmt+Gl
472	1128	5.5	-8.7	Pt-Fe	Ol+Pl+Spmt+Gl
518	1120	20	-8.9	Pt-Fe	Ol+Pl+Spmt+Gl
519	1108	21	-9.1	Pt-Fe	Ol+Cpx+Pl+Spmt+Gl
520	1099	15	-9.1	Pt-Fe	Ol+Cpx+Pl+Spmt+Il+Gl

Composition: MV71A

Expt	Temp(^{0}C)	Time(hrs)	Log fO2	Holder	Assemblage
580	1302	2	-6.6	Pt-Fe	Gl

Composition: MV52

Expt	Temp(^{0}C)	Time(hrs)	Log fO2	Holder	Assemblage
5-727	1271	6.5	-6.9	Pt-Fe	Gl
426	1250	5	-7.0	Pt	Gl
427	1243	5	-7.0	Pt	Gl
428	1226	8	-7.2	Pt	Gl
429	1223	6	-7.3	Pt	Gl
448	1208	3	-7.6	Pt-Fe	Gl
475	1203	2.5	-7.6	Pt-Fe	Spmt+Gl
516	1186	12.5	-7.9	Pt-Fe	Spmt+Gl
515	1176	16.5	-8.1	Pt-Fe	Spmt+Gl
514	1165	16	-8.2	Pt-Fe	Ol+Pl+Spmt+Gl
512	1155	24	-8.4	Pt-Fe	Ol+Pl+Spmt+Gl
510	1145	18	-8.5	Pt-Fe	Ol+Pl+Spmt+Gl
472	1128	5.5	-8.7	Pt-Fe	Ol+Pl+Spmt+Gl
518	1120	20	-8.9	Pt-Fe	Ol+Pl+Spmt+Gl
519	1108	21	-9.1	Pt-Fe	Ol+Cpx+Pl+Spmt+Il+Gl
520	1099	15	-9.1	Pt-Fe	Ol+Cpx+Pl+Spmt+Il+Gl

Composition: MV39A

Expt	Temp(^{0}C)	Time(hrs)	Log fO2	Holder	Assemblage
474	1209	3	-7.5	Pt-Fe	Gl
476	1198	19	-7.7	Pt-Fe	Gl
477	1189	18.5	-7.8	Pt-Fe	Gl
554	1182	18.5	-7.9	Pt-Fe	Spmt+Gl
478	1179	9	-8.0	Pt-Fe	Spmt+Gl
556	1171	3	-8.0	Pt-Fe	Pl+Spmt+Gl
479	1169	14	-8.0	Pt-Fe	Pl+Spmt+Gl
571	1160	12.5	-8.2	Pt-Fe	Ol+Pl+Spmt+Gl
480	1157	19	-8.2	Pt-Fe	Ol+Pl+Spmt+Gl
481	1146	20	-8.4	Pt-Fe	Ol+Pl+Spmt+Gl
482	1135	6.5	-8.6	Pt-Fe	Ol+Pl+Spmt+Gl
483	1122	19.5	-8.7	Pt-Fe	Ol+Pl+Spmt+Gl
492	1114	19.5	-8.9	Pt-Fe	Ol+Pl+Spmt+Gl
495	1105	19	-9.0	Pt-Fe	Ol+Cpx+Pl+Spmt+Gl
501	1092	19.5	-9.3	Pt-Fe	Ol+Cpx+Pl+Spmt+Il+Gl

Composition: MV39AF

Expt	Temp(^{0}C)	Time(hrs)	Log fO2	Holder	Assemblage
553	1193	17	-7.8	Pt-Fe	Gl
554	1182	18.5	-7.9	Pt-Fe	Gl
556	1171	3	-8.0	Pt-Fe	Pl+Gl
571	1160	12.5	-8.2	Pt-Fe	Ol+Pl+Gl
577	1148	13	-8.3	Pt-Fe	Ol+Pl+Spmt+Gl

Composition: MV402

a) Nickel-Nickel Oxide buffer

Expt	Temp(^{0}C)	Time(hrs)	Log fO2	Holder	Assemblage
496	1223	19	-7.4	Pt-Fe	Gl
473	1211	2.5	-7.4	Pt-Fe	Pl+Spmt+Gl
476	1198	19	-7.7	Pt-Fe	Pl+Spmt+Gl
477	1189	18.5	-7.8	Pt-Fe	Pl+Spmt+Gl
478	1179	9	-8.0	Pt-Fe	Pl+Spmt+Gl
479	1169	14	-8.0	Pt-Fe	Pl+Spmt+Gl
480	1157	19	-8.2	Pt-Fe	Pl+Spmt+Gl
481	1146	20	-8.4	Pt-Fe	Ol+Cpx+Pl+Spmt+Gl
482	1135	6.5	-8.6	Pt-Fe	Ol+Cpx+Pl+Spmt+Gl
483	1122	19.5	-8.7	Pt-Fe	Ol+Cpx+Pl+Spmt+Gl

Composition: MV402

b) Iron-Wustite buffer

Expt	Temp(^{0}C)	Time(hrs)	Log fO2	Holder	Assemblage
557	1300	13	-12.5	Pt-Fe	Ml+Gl
564	1240	4.5	-11.5	Pt-Fe	Gl
566	1227	5	-11.6	Pt-Fe	Gl
568	1214	5	-11.8	Pt-Fe	Gl
562	1199	20	-11.9	Pt-Fe	Pl+Gl
563	1185	15	-12.1	Pt-Fe	Pl+Gl
565	1171	11.5	-12.3	Pt-Fe	Pl+Gl
567	1156	12	-12.5	Pt-Fe	Ol+Pl+Gl
569	1142	12	-12.8	Pt-Fe	Ol+Cpx+Pl+Gl
573	1128	16	-13.0	Pt-Fe	Ol+Cpx+Pl+Gl
574	1113	19	-13.1	Pt-Fe	Ol+Cpx+Pl+Gl
575	1099	17	-13.3	Pt-Fe	Ol+Cpx+Pl+Gl
586	1084	21	-13.5	Pt-Fe	Ol+Cpx+Pl+Il+Gl

Composition: MV13

Expt	Temp(^{0}C)	Time(hrs)	Log fO2	Holder	Assemblage
452	1265	16	-6.8	Pt-Fe	Gl
453	1253	8.5	-7.0	Pt-Fe	Gl
454	1243	16.5	-7.1	Pt-Fe	Gl
456	1234	17	-7.2	Pt-Fe	Gl
455	1233	24	-7.2	Pt-Fe	Gl
457	1223	19	-7.3	Pt-Fe	Gl
458	1212	17	-7.4	Pt-Fe	Spmt+Gl
461	1208	3	-7.6	Pt-Fe	Spmt+Gl
460	1204	3	-7.6	Pt-Fe	Spmt+Gl
462	1196	5	-7.7	Pt-Fe	Spmt+Gl
553	1193	17	-7.8	Pt-Fe	Spmt+Gl
463	1183	5.5	-7.9	Pt-Fe	Spmt+Gl
554	1182	18.5	-7.9	Pt-Fe	Spmt+Gl
465	1174	16	-8.0	Pt-Fe	Spmt+Gl
464	1174	19	<-8	Pt-Fe	Spmt+Gl
556	1171	3	-8.0	Pt-Fe	Spmt+Gl
466	1161	16	-8.2	Pt-Fe	Spmt+Gl
571	1160	12.5	-8.2	Pt-Fe	Pl+Spmt+Gl
467	1151	16	-8.4	Pt-Fe	Ol+Pl+Spmt+Gl
577	1148	13	-8.3	Pt-Fe	Ol+Pl+Spmt+Gl
468	1140	19	-8.5	Pt-Fe	Ol+Pl+Spmt+Gl
583	1135	13	-8.5	Pt-Fe	Ol+Pl+Spmt+Gl
469	1127	5	-8.7	Pt-Fe	Ol+Pl+Spmt+Gl
493	1115	17.5	-8.9	Pt-Fe	Ol+Pl+Spmt+Gl
494	1104	19	-9.1	Pt-Fe	Ol+Pl+Spmt+Gl
501	1092	19.5	-9.3	Pt-Fe	Ol+Cpx+Pl+Spmt+Il+Gl

Composition: MV13F

Expt	Temp(^{0}C)	Time(hrs)	Log fO2	Holder	Assemblage
542	1208	2.5	-7.6	Pt-Fe	Gl
544	1205	2	-7.6	Pt-Fe	Gl
553	1193	17	-7.8	Pt-Fe	Gl
554	1182	18.5	-7.9	Pt-Fe	Gl
556	1171	3	-8.0	Pt-Fe	Gl
571	1160	12.5	-8.2	Pt-Fe	Gl
577	1148	13	-8.3	Pt-Fe	Ol+Pl+Spmt+Gl
583	1135	13	-8.5	Pt-Fe	Ol+Pl+Spmt+Gl

Composition: MV40A

Expt	Temp(^{0}C)	Time(hrs)	Log fO2	Holder	Assemblage
473	1211	2.5	-7.4	Pt-Fe	Gl
476	1198	19	-7.7	Pt-Fe	Pl+Gl
477	1189	18.5	-7.8	Pt-Fe	Pl+Gl
478	1179	9	-8.0	Pt-Fe	Pl+Gl
479	1169	14	-8.0	Pt-Fe	Pl+Spmt+Gl
480	1157	19	-8.2	Pt-Fe	Pl+Spmt+Gl
481	1146	20	-8.4	Pt-Fe	Ol+Pl+Spmt+Gl
482	1135	6.5	-8.6	Pt-Fe	Ol+Pl+Spmt+Gl
483	1122	19.5	-8.7	Pt-Fe	Ol+Pl+Spmt+Gl
492	1114	19.5	-8.9	Pt-Fe	Ol+Pl+Spmt+Gl
495	1105	19	-9.0	Pt-Fe	Ol+Pl+Spmt+Gl
501	1092	19.5	-9.3	Pt-Fe	Ol+Cpx+Pl+Spmt+Il+Gl

Composition: MV165

Expt	Temp(^{0}C)	Time(hrs)	Log fO2	Holder	Assemblage
580	1302	2	-6.6	Pt-Fe	Gl

Composition: MV51

Expt	Temp(^{0}C)	Time(hrs)	Log fO2	Holder	Assemblage
473	1211	2.5	-7.4	Pt-Fe	Gl
484	1197	19.5	-7.7	Pt-Fe	Gl
485	1191	18.5	-7.8	Pt-Fe	Gl
486	1180	17.5	-7.9	Pt-Fe	Gl
487	1171	17.5	-8.1	Pt-Fe	Gl
488	1158	19	-8.3	Pt-Fe	Gl
489	1147	18	-8.5	Pt-Fe	Spmt+Gl
490	1137	19	-8.6	Pt-Fe	Spmt+Gl
491	1124	19	-8.8	Pt-Fe	Pl+Spmt+Gl
492	1114	19.5	-8.9	Pt-Fe	Ol+Pl+Spmt+Gl
495	1105	19	-9.0	Pt-Fe	Ol+Pl+Spmt+Gl
501	1092	19.5	-9.3	Pt-Fe	Ol+Pl+Spmt+Gl
541	1086	16	-9.1	Pt-Fe	Ol+Pl+Spmt+Gl
537	1074	16	-9.4	Pt-Fe	Ol+Cpx+Pl+Spmt+Ap+Gl

APPENDIX 3

Details of Microprobe Analysis and Precision

Microprobe analyses were carried out using a Cambridge Instruments Microscan 5 with two crystal spectrometers and a Link Systems energy-dispersive system (EDS). Take-off angle was 75°. Operating conditions were as follows: Accelerating potential for all analyses was 20 kV. Probe current (measured at a Faraday cage) was 30nA for wavelength-dispersive spectrometry analysis (WDS) and 6nA for EDS analysis. Most analyses were performed with a focussed electron beam of approximately 1 - 2μ diameter, penetrating to a depth of approximately 3μ. A relatively small number of experimental glasses were analysed using the EDS with a de-focussed beam of up to 50μ diameter.

Standard materials were as follows, with the elements concerned given in brackets:

Magnesium fluoride (F)
Jadeite (Na)
Olivine (Mg in olivines)
Periclase (Mg in all other phases)
Corundum (Al)
Wollastonite (Ca, Si)
Apatite (P)
Pyrite (S)
Halite (Cl)
Orthoclase (K)
Rutile (Ti)
Baryte (Ba)
and pure metals (V, Cr, Mn, Fe, Co, Ni, Cu, Zn)

Initially, for WDS analysis, the basic X-ray counts were collected and processed through a separate computer program to calculate apparent concentrations. The apparent concentrations were then processed through a second program for full ZAF corrections, after Sweatman and Long (1969), using the absorption co-efficients of Heinrich (1966) to produce the final analyses. However, in 1981 automation of the spectrometers, together with on-line computer processing of the counts, allowed rapid WDS analysis of superior

precision to the EDS with comparable speed.

Before automation most analyses were produced using the EDS. This included a very high percentage of the analyses of experimental charges. EDS analysis involved the collection of an X-ray spectrum in 100 livetime seconds, followed by on-line computer processing involving the same ZAF correction procedure used in WDS analysis.

In WDS mode, the number of X-rays for an element in an unknown is related to the number of X-rays in that element's standard, read in the same session.

In EDS mode, the abundance of each element is related to an overall element calibration by a secondary cobalt standard. The cobalt standard is read throughout the session to account for system fluctuations. The overall calibration is updated regularly to account for long term drift over a period of years.

Precision determinations are presented in Table A3.1. Two methods are used. Firstly, for WDS analysis where the numbers of X-rays are known, precision calculations are applied. These are as follows:-

DETECTION LIMIT (3σ Level) $= \frac{3}{m}\sqrt{\frac{Rb}{Tb}}$ — Result as wt % oxide

PRECISION (1σ Level) $= \sigma = \frac{100}{\sqrt{Tp}} \cdot \frac{1}{\sqrt{Rp - \sqrt{Rb}}}$ % — Result as % of wt % oxide

m = counts above background per second per percent oxide
Rb = background count rate per second
Rp = peak count rate per second
Tb = time (seconds) on background
Tp = time (seconds) on peak

Secondly, for EDS and WDS analyses, repeated analysis of approximately the same point gives some idea of the precision for each element when other operational factors besides counting statistics are considered.

To some extent the presented precision determinations are 'best possible' figures. It is difficult to assess quantitatively the longer term effects of fluctuations in standard counts and calibrations, microprobe stability and operator behaviour. Many apparent discrepancies in the data could probably be explained by one or more of these indeterminate variables.

Table A3.1 Precision and Detection Limits for Typical Phases

a) GLASS

WDS 30nA 20KV

Glass unknown.
Precision based on one analysis.

	Wt % oxide	± 2 σ (Wt % oxide)	3σ (Wt % oxide) detection limit
SiO_2	46.80	0.335	0.046
TiO_2	1.51	0.096	0.031
Al_2O_3	15.31	0.160	0.024
Cr_2O_3	0.05	0.041	0.028
ΣFeO	10.81	0.174	0.031
MnO	0.18	0.045	0.028
MgO	9.84	0.137	0.021
CaO	9.94	0.184	0.023
Na_2O	3.15	0.111	0.023
K_2O	0.73	0.329	0.228
NiO	0.05	0.055	0.039
P_2O_5	0.18	0.293	0.243

WDS 30nA 20KV

Glass unknown.
Precision based on repeated analyses;
7 points.

	Mean	± 2σ (Wt % oxide)	% of Mean
SiO_2	46.40	0.697	1.50
TiO_2	1.55	0.070	4.54
Al_2O_3	15.21	0.162	1.07
Cr_2O_3	0.06	0.016	27.90
ΣFeO	10.72	0.138	1.29
MnO	0.16	0.024	14.50
MgO	9.90	0.120	1.21
CaO	9.89	0.114	1.15
Na_2O	3.15	0.079	2.52
K_2O	0.77	0.153	19.80
NiO	0.07	0.033	48.60
P_2O_5	0.16	0.131	80.70

EDS 6nA 20KV

Glass unknown.
Precision based on repeated analyses;
7 points.

	Mean	± 2σ (Wt % oxide)	% of Mean
SiO_2	48.10	0.606	1.26
TiO_2	1.46	0.068	4.66
Al_2O_3	14.51	0.514	3.54
Cr_2O_3	0.03	0.116	387.00
ΣFeO	10.75	0.188	1.75
MnO	0.16	0.168	105.00
MgO	9.77	0.176	1.80
CaO	10.11	0.124	1.23
Na_2O	2.55	0.418	16.40
K_2O	0.98	0.122	12.40
NiO	not detected		
P_2O_5	not detected		

(Large Na_2O range may be partly due to Na migration during analysis.)

Table A3.1 continued

b) OLIVINE

WDS 30nA 20KV

Olivine unknown.
Precision based on one analysis.

	Wt % oxide	± 2σ (Wt % oxide)	3σ (Wt % oxide) detection limit
SiO_2	37.70	0.218	0.028
Al_2O_3	0.03	0.037	0.027
ΣFeO	22.96	0.241	0.031
MnO	0.32	0.048	0.025
MgO	39.49	0.268	0.024
CaO	0.15	0.040	0.022
NiO	0.15	0.058	0.038

WDS 30nA 20KV

Olivine unknown.
Precision based on repeated analyses;
7 points.

	Mean	± 2σ (Wt % oxide)	% of Mean
SiO_2	37.60	0.020	0.57
Al_2O_3	0.02	0.020	98.00
ΣFeO	22.96	0.117	0.51
MnO	0.31	0.023	7.56
MgO	39.24	0.401	1.02
CaO	0.15	0.041	27.50
NiO	0.15	0.033	21.80

EDS 6nA 20KV

Olivine unknown.
Precision based on repeated analyses;
7 points.

	Mean	± 2σ (Wt % oxide)	% of Mean
SiO_2	38.84	0.966	2.49
Al_2O_3	not detected		
ΣFeO	23.08	0.498	2.16
MnO	0.25	0.078	31.20
MgO	38.85	0.456	1.17
CaO	0.16	0.086	53.80
NiO	0.16	0.224	140.00

Table A3.1 continued

c) PLAGIOCLASE

WDS 30nA 20KV

Plagioclase unknown.
Precision based on one analysis.

	Wt % oxide	± 2σ (Wt % oxide)	3σ (Wt % oxide) detection limit
SiO_2	51.26	0.345	0.040
TiO_2	0.07	0.036	0.025
Al_2O_3	31.09	0.208	0.022
ΣFeO	0.37	0.054	0.030
MgO	0.15	0.032	0.019
CaO	13.21	0.168	0.023
Na_2O	3.84	0.112	0.020
K_2O	0.24	0.037	0.018

WDS 30nA 20KV

Plagioclase unknown.
Precision based on repeated analyses;
6 points.

	Mean	± 2σ (Wt % oxide)	% of Mean
SiO_2	51.14	0.423	0.83
TiO_2	0.08	0.0212	26.50
Al_2O_3	30.87	0.228	0.74
ΣFeO	0.39	0.0413	10.60
MgO	0.13	0.0338	26.00
CaO	13.17	0.169	1.28
Na_2O	3.92	0.122	3.12
K_2O	0.23	0.0271	11.80

EDS 6nA 20KV

Plagioclase unknown.
Precision based on repeated analyses;
8 points.

	Mean	± 2σ (Wt % oxide)	% of Mean
SiO_2	52.17	0.972	1.86
TiO_2	0.04	0.126	427.00
Al_2O_3	29.96	0.674	2.25
ΣFeO	0.48	0.292	60.80
MgO	not detected		
CaO	13.37	0.244	1.82
Na_2O	3.76	0.370	9.84
K_2O	0.21	0.086	41.00

Table A3.1 continued

d) CLINOPYROXENE

WDS 30nA 20KV

Clinopyroxene unknown.
Precision based on one analysis.

	Wt % oxide	± 2σ (Wt % oxide)	3σ (Wt % oxide) detection limit
SiO_2	49.32	0.332	0.038
TiO_2	1.04	0.065	0.026
Al_2O_3	6.62	0.111	0.023
Cr_2O_3	0.50	0.050	0.026
ΣFeO	5.11	0.123	0.032
MnO	0.10	0.050	0.035
MgO	15.46	0.165	0.021
CaO	20.27	0.203	0.022
Na_2O	0.74	0.043	0.015

WDS 30nA 20KV

Clinopyroxene unknown.
Precision based on repeated analyses;
7 points.

	Mean	± 2σ (Wt % oxide)	% of Mean
SiO_2	49.47	0.265	0.54
TiO_2	1.03	0.049	4.77
Al_2O_3	6.56	0.217	3.30
Cr_2O_3	0.48	0.052	10.80
ΣFeO	5.18	0.234	4.53
MnO	0.12	0.032	26.80
MgO	15.34	0.436	2.84
CaO	20.19	0.532	2.64
Na_2O	0.74	0.023	3.12

EDS 6nA 20KV

Clinopyroxene unknown.
Precision based on repeated analyses;
7 points.

	Mean	± 2σ (Wt % oxide)	% of Mean
SiO_2	49.86	0.694	1.39
TiO_2	1.13	0.132	11.70
Al_2O_3	6.93	0.516	7.45
Cr_2O_3	0.47	0.172	36.60
ΣFeO	5.51	0.182	3.30
MnO	0.06	0.150	250.00
MgO	14.99	0.518	3.46
CaO	20.43	0.498	2.44
Na_2O	0.08	0.400	500.00

Table A3.1 continued

e) JADEITE

EDS 6nA 20KV

Jadeite standard.
Precision based on repeated analyses;
7 points.

	Mean	± 2 σ (Wt % oxide)	% of Mean
SiO_2	59.93	0.522	0.87
Al_2O_3	25.29	0.210	0.83
ΣFeO	0.11	0.224	204.00
CaO	0.04	0.104	260.00
Na_2O	15.21	0.346	2.27

EDS 6nA 20KV

Jadeite standard.
Precision based on 41 points collected
over approximately 2 years.

	Mean	± 2σ (Wt % oxide)	% of Mean
SiO_2	59.68	0.743	1.24
Al_2O_3	25.16	0.621	2.47
Na_2O	15.15	0.539	3.56

Jadeite standard.
(Wet chemical analysis).
Analyst - M J Saunders.

	Wt % oxide
SiO_2	59.43
Al_2O_3	25.00
Na_2O	15.28

APPENDIX 4

Representative analyses of phases in the experimental charges

Electron microprobe analyses of the experimental phases are tabulated below. Samples are listed mainly in order of decreasing whole-rock Mg#. Some paired samples have been grouped together.

Analysis titles are formatted to present the experimental conditions in a condensed form. The following phase abbreviations have been used :

GL - glass
OL - olivine
CPX - high-Ca clinopyroxene
PL - plagioclase
SPMT - spinel (Cr-Al spinel to titanomagnetite)
IL - ilmenite

The titles have been constructed using the sequence :

phase
rock identifier
experimental run number(R)
experimental temperature(C)
duration of the experiment in hours(HR)
log fO2(F)
phase assemblage in the charge(listed with the glass phase only)
wire hook material
probe analysis by EDS(E) or WDS(W) techniques.

Wire hook abbreviations are:

PT - platinum wire
SPT - platinum wire Fe-saturated by re-use
PTFE - platinum wire pre-saturated with Fe

The cation ratios given beneath the analyses are:

Mg# - $100*Mg/(Mg+Fe^{2+})$ for olivines, spinels and glasses
An - $100*Ca/(Ca+Na+K)$ for plagioclases

Fe2O3 contents of spinels and ilmenites have been calculated on the basis of stoichiometry. Fe2O3 contents of glasses have been calculated using the expression presented in Chapter 3.

	1	2	3	4	5	6	7	8	9	10	11
SiO2	51.48	39.20	38.86	38.53	52.31	54.18	52.86	50.51	49.31	51.18	50.30
TiO2	3.46	nd	nd	0.16	0.25	0.37	0.16	1.59	1.91	1.49	1.57
Al2O3	14.17	nd	nd	nd	28.65	27.36	28.14	4.39	5.27	3.37	3.71
Fe2O3	2.68	nd	nd	nd	nd	nd	nd	nd	nd	nd	nd
Cr2O3	0.05	nd	nd	nd	nd	nd	nd	0.49	0.38	0.56	0.54
FeO	8.28	23.09	23.19	22.96	1.23	1.35	1.06	8.31	8.41	8.35	8.08
MnO	0.11	0.32	0.35	0.30	nd	nd	nd	0.19	0.19	0.19	0.15
NiO	nd	0.25	0.35	nd	nd	nd	nd	nd	0.14	nd	0.17
MgO	4.29	37.27	36.81	37.58	nd	0.25	0.26	13.85	13.19	14.64	14.33
CaO	8.54	0.45	0.51	0.48	12.94	11.50	12.31	19.81	20.53	20.70	21.30
Na2O	3.43	nd	nd	nd	3.72	4.60	4.17	0.36	0.45	0.36	0.22
K2O	1.83	nd	nd	nd	0.29	0.40	0.33	nd	nd	nd	nd
total=	98.32	100.58	100.07	100.01	99.39	100.01	99.29	99.50	99.78	100.84	100.37
Mg#	48.0	74.2	73.9	74.5	-	-	-	-	-	-	-
An	-	-	-	-	64.6	56.6	60.8	-	-	-	-

1 GL35,MV403,R471,1129C,21HR,F-8.6,+OL+CPX+PL+SPMT+GL,PTFE,E
2 OL28,MV403,R471,1129C,21HR,F-8.6,PTFE,E
3 OL32,MV403,R471,1129C,21HR,F-8.6,PTFE,E
4 OL33,MV403,R471,1129C,21HR,F-8.6,PTFE,E
5 PL34,MV403,R471,1129C,21HR,F-8.6,PTFE,E
6 PL35,MV403,R471,1129C,21HR,F-8.6,PTFE,E
7 PL36,MV403,R471,1129C,21HR,F-8.6,PTFE,E
8 CPX30,MV403,R471,1129C,21HR,F-8.6,PTFE,E
9 CPX31,MV403,R471,1129C,21HR,F-8.6,PTFE,E
10 CPX32,MV403,R471,1129C,21HR,F-8.6,PTFE,E
11 CPX33,MV403,R471,1129C,21HR,F-8.6,PTFE,E

	12	13	14	15	16	17	18	19	20	21	22
SiO2	50.23	0.36	50.70	38.67	52.19	51.50	50.21	38.63	53.22	52.61	52.03
TiO2	1.97	9.29	3.13	nd	0.24	1.18	2.74	nd	0.27	0.17	0.22
Al2O3	3.21	8.30	13.77	0.18	28.47	2.81	14.24	nd	27.51	27.81	28.25
Fe2O3	nd	15.96	2.35	nd	nd	nd	2.31	nd	nd	nd	nd
Cr2O3	0.32	26.53	nd	nd	nd	0.47	0.03	nd	nd	nd	nd
FeO	9.05	30.17	8.01	21.57	1.01	7.69	8.03	20.29	1.35	1.07	1.07
MnO	0.16	0.20	0.14	0.35	nd	0.17	0.12	0.33	nd	nd	nd
NiO	nd	nd	nd	0.24	nd	nd	nd	0.31	nd	nd	nd
MgO	13.85	6.86	4.77	38.19	nd	14.85	5.18	40.18	0.23	nd	0.15
CaO	20.90	0.42	8.61	0.45	12.52	20.77	9.03	0.48	11.79	12.07	12.57
Na2O	0.44	nd	3.43	nd	3.89	nd	3.40	nd	4.53	4.25	3.92
K2O	nd	nd	1.64	nd	0.31	nd	1.45	nd	0.38	0.27	0.30
P2O5	nd	nd	0.39	nd	nd	nd	nd	nd	nd	nd	nd
total=	100.13	98.09	96.94	99.65	98.63	99.44	96.74	100.22	99.28	98.25	98.51
Mg#	-	28.8	51.5	75.9	-	-	53.5	77.9	-	-	-
An	-	-	-	-	62.8	-	-	-	57.7	60.1	62.8

12 CPX34,MV403,R471,1129C,21HR,F-8.6,PTFE,E
13 SPMT12,MV403,R471,1129C,21HR,F-8.6,PTFE,E
14 GL430,MV403,R509,1140C,13HR,F-8.6,+OL+CPX+PL+SPMT+GL,PTFE,E
15 OL144,MV403,R509,1140C,13HR,F-8.6,PTFE,E
16 PL179,MV403,R509,1140C,13HR,F-8.6,PTFE,E
17 CPX52,MV403,R509,1140C,13HR,F-8.6,PTFE,E
18 GL104,MV403,R470,1151C,17HR,F-8.4,+OL+PL+SPMT+GL,PTFE,E
19 OL71,MV403,R470,1151C,17HR,F-8.4,PTFE,E
20 PL92,MV403,R470,1151C,17HR,F-8.4,PTFE,E
21 PL94,MV403,R470,1151C,17HR,F-8.4,PTFE,E
22 PL95,MV403,R470,1151C,17HR,F-8.4,PTFE,E

	23	24	25	26	27	28	29	30	31	32	33
SiO2	0.57	50.58	38.98	49.73	39.12	50.01	39.86	49.89	39.66	39.59	39.99
TiO2	3.38	2.43	0.12	2.21	nd	2.18	nd	2.11	nd	0.12	nd
Al2O3	16.18	15.29	nd	15.66	nd	15.92	nd	15.13	nd	nd	nd
Fe2O3	13.44	2.17	nd	2.10	nd	2.13	nd	2.30	nd	nd	nd
Cr2O3	30.69	0.05	nd	nd	nd	nd	nd	nd	nd	nd	nd
FeO	23.31	7.94	18.61	8.05	17.14	8.00	17.16	8.81	16.63	16.42	16.39
MnO	nd	0.12	0.32	0.13	0.31	0.17	0.26	0.16	0.26	0.26	0.25
NiO	nd	nd	0.15	nd	0.32	nd	0.42	nd	0.21	0.29	0.43
MgO	9.21	5.41	41.94	6.10	41.97	6.08	42.76	7.06	43.00	43.05	43.41
CaO	nd	8.85	0.41	9.10	0.40	9.08	0.30	8.74	0.38	0.38	0.37
Na2O	nd	3.13	nd	3.46	nd	3.24	nd	3.16	nd	nd	nd
K2O	nd	1.40	nd	1.19	nd	1.22	nd	1.14	nd	nd	nd
P2O5	nd	nd	nd	0.25	nd	0.15	nd	nd	nd	nd	nd
V2O3	0.61	nd	nd	nd	nd	nd	nd	nd	nd	nd	nd
total=	97.39	97.37	100.53	97.98	99.26	98.18	100.76	98.50	100.14	100.11	100.84
Mg#	41.3	54.8	80.1	57.5	81.4	57.5	81.6	58.8	82.2	82.4	82.5

23 SPMT7,MV403,R470,1151C,17HR,F-8.4,PTFE,E
24 GL789,MV403,R514,1165C,16HR,F-8.2,+OL+PL+SPMT+GL,PTFE,E
25 OL268,MV403,R514,1165C,16HR,F-8.2,PTFE,E
26 GL730,MV403,R515,1176C,16.5HR,F-8.1,+OL+PL+SPMT+GL,PTFE,E
27 OL243,MV403,R515,1176C,16.5HR,F-8.1,PTFE,E
28 GL753,MV403,R516,1186C,12.5HR,F-7.9,+OL+SPMT+GL,PTFE,E
29 OL251,MV403,R516,1186C,12.5HR,F-7.9,PTFE,E
30 GL43,MV403,R448,1208C,3HR,F-7.6,+OL+SPMT+GL,PTFE,E
31 OL18,MV403,R448,1208C,3HR,F-7.6,PTFE,E
32 OL19,MV403,R448,1208C,3HR,F-7.6,PTFE,E
33 OL20,MV403,R448,1208C,3HR,F-7.6,PTFE,E

	34	35	36	37	38	39	40	41	42	43	44
SiO2	0.97	49.65	39.89	39.66	39.62	39.94	50.13	40.29	40.35	40.59	40.71
TiO2	1.08	2.17	nd	0.15	0.15	nd	2.18	nd	nd	nd	nd
Al2O3	35.79	15.25	nd	nd	nd	nd	15.25	nd	nd	nd	nd
Fe2O3	7.06	2.34	nd	nd	nd	nd	2.27	nd	nd	nd	nd
Cr2O3	22.03	nd	nd	nd	nd	nd	0.04	nd	nd	nd	nd
FeO	16.94	8.52	16.18	17.01	15.54	15.09	7.95	15.77	15.45	13.97	14.59
MnO	nd	0.08	0.19	0.15	0.15	0.18	0.13	0.22	0.24	0.17	0.11
NiO	nd	nd	nd	0.21	0.39	0.47	nd	0.26	0.28	0.41	0.21
MgO	14.73	7.75	43.36	43.04	43.86	44.06	7.72	43.45	43.74	45.51	44.93
CaO	nd	8.76	0.26	0.22	0.39	0.33	8.73	0.34	0.28	0.26	0.24
Na2O	nd	3.08	nd	nd	nd	nd	3.16	nd	nd	nd	nd
K2O	nd	1.14	nd	nd	nd	nd	1.09	nd	nd	nd	nd
V2O3	0.23	nd	nd	nd	nd	nd	nd	nd	nd	nd	nd
total=	98.83	98.74	99.88	100.44	100.10	100.07	98.65	100.33	100.34	100.91	100.79
Mg#	60.8	61.9	82.7	81.8	83.4	83.9	63.4	83.1	83.5	85.3	84.6

34 SPMT7,MV403,R448,1208C,3HR,F-7.6,PTFE,E
35 GL6,MV403,R429,1223C,6HR,F-7.3,+OL+SPMT+GL,PTFE,E
36 OL5,MV403,R429,1223C,6HR,F-7.3,PTFE,E
37 OL6,MV403,R429,1223C,6HR,F-7.3,PTFE,E
38 OL7,MV403,R429,1223C,6HR,F-7.3,PTFE,E
39 OL8,MV403,R429,1223C,6HR,F-7.3,PTFE,E
40 GL9,MV403,R428,1226C,8HR,F-7.2,+OL+SPMT+GL,PTFE,E
41 OLX3,MV403,R428,1226C,8HR,F-7.2,PTFE,E
42 OLX4,MV403,R428,1226C,8HR,F-7.2,PTFE,E
43 OLX5,MV403,R428,1226C,8HR,F-7.2,PTFE,E
44 OLX6,MV403,R428,1226C,8HR,F-7.2,PTFE,E

	45	46	47	48	49	50	51	52	53	54	55
SiO2	48.50	39.88	48.61	39.61	48.74	40.36	48.78	40.40	39.92	39.91	48.99
TiO2	2.11	0.17	2.14	nd	2.01	nd	1.97	nd	nd	nd	1.96
Al2O3	14.71	nd	14.96	nd	14.54	nd	14.60	nd	nd	nd	14.03
Fe2O3	2.35	nd	2.36	nd	2.12	nd	2.35	nd	nd	nd	2.45
Cr2O3	0.07	nd	nd	nd	0.04	nd	nd	nd	nd	nd	0.05
FeO	8.95	14.54	8.78	15.13	8.84	13.34	8.93	13.71	14.01	14.89	9.11
MnO	0.17	0.17	0.15	0.25	0.17	0.22	0.11	nd	nd	0.14	0.21
NiO	nd	0.49	nd	0.23	0.01	0.26	nd	0.47	0.17	0.21	nd
MgO	8.71	44.59	8.53	44.06	9.40	45.82	9.47	45.15	45.17	44.75	9.95
CaO	8.42	0.29	8.63	0.34	8.11	0.29	8.02	0.21	0.22	0.28	8.12
Na2O	3.03	nd	3.12	nd	2.93	nd	2.97	nd	nd	nd	2.90
K2O	1.09	nd	1.13	nd	0.89	nd	1.04	nd	nd	nd	1.04
P2O5	nd	nd	0.26	nd	0.31	nd	nd	nd	nd	nd	nd
total=	98.11	100.13	98.67	99.62	98.11	100.29	98.24	99.94	99.49	100.18	98.81
Mg#	63.4	84.5	63.4	83.8	65.5	86.0	65.4	85.4	85.2	84.3	66.1

45 GL697,MV403,R427,1243C,5HR,F-7.1,+OL+SPMT+GL,PT,E
46 OL226,MV403,R427,1243C,5HR,F-7.1,PT,E
47 GL692,MV403,R426,1250C,5HR,F-7.0,+OL+SPMT+GL,PT,E
48 OL225,MV403,R426,1250C,5HR,F-7.0,PT,E
49 GL1112,MV403,R555,1261C,20HR,F-7.0,+OL+SPMT+GL,PTFE,W
50 OL127,MV403,R555,1261C,20HR,F-7.0,PTFE,W
51 GL20,MV403,R425,1263C,7.5HR,F-6.8,+OL+SPMT+GL,PT,E
52 OL11,MV403,R425,1263C,7.5HR,F-6.8,PT,E
53 OL8,MV403,R425,1263C,7.5HR,F-6.8,PT,E
54 OL9,MV403,R425,1263C,7.5HR,F-6.8,PT,E
55 GL24,MV403,R451,1277C,6.5HR,F-6.6,+OL+SPMT+GL,PTFE,E

	56	57	58	59	60	61	62	63	64	65	66
SiO2	40.34	40.57	48.53	40.22	40.46	48.44	40.28	40.07	48.61	40.67	49.31
TiO2	nd	nd	2.02	nd	nd	1.98	nd	nd	1.86	nd	1.95
Al2O3	nd	nd	14.11	0.11	nd	13.93	nd	0.11	13.71	nd	13.67
Fe2O3	nd	nd	2.18	nd	nd	2.09	nd	nd	2.19	nd	2.22
Cr2O3	nd	nd	0.04	nd	nd	0.04	nd	nd	0.13	nd	nd
FeO	13.58	13.34	9.01	12.93	12.92	9.28	12.52	12.68	8.98	12.36	9.17
MnO	0.13	0.11	0.16	0.22	0.22	0.17	0.21	0.24	0.15	0.14	0.21
NiO	0.44	0.37	0.02	0.36	0.36	0.02	0.39	0.37	nd	0.55	nd
MgO	45.41	46.02	10.02	45.90	45.88	10.65	45.61	45.84	10.76	46.77	10.93
CaO	0.38	0.33	7.98	0.30	0.32	7.79	0.29	0.29	7.84	0.24	7.71
Na2O	nd	nd	3.00	nd	nd	3.06	nd	nd	2.67	nd	2.41
K2O	nd	nd	0.91	nd	nd	0.86	nd	nd	0.94	nd	0.97
P2O5	nd	nd	0.42	nd	nd	0.24	nd	nd	nd	nd	nd
total=	100.28	100.74	98.40	100.04	100.16	98.55	99.30	99.60	97.84	100.73	98.55
Mg#	85.6	86.0	66.5	86.4	86.4	67.2	86.7	86.6	68.1	87.1	68.0

56 OL19,MV403,R451,1277C,6.5HR,F-6.6,PTFE,E
57 OL20,MV403,R451,1277C,6.5HR,F-6.6,PTFE,E
58 GL1132,MV403,R547,1277C,14HR,F-6.8,+OL+SPMT+GL,PTFE,W
59 OL101,MV403,R547,1277C,14HR,F-6.8,PTFE,W
60 OL102,MV403,R547,1277C,14HR,F-6.8,PTFE,W
61 GL1102,MV403,R572,1287C,4.5HR,F-6.8,+OL+GL,PTFE,W
62 OL132,MV403,R572,1287C,4.5HR,F-6.8,PTFE,W
63 OL133,MV403,R572,1287C,4.5HR,F-6.8,PTFE,W
64 GL371,MV403,R497,1288C,18HR,F-6.6,+OL+GL,PTFE,E
65 OL121,MV403,R497,1288C,18HR,F-6.6,PTFE,E
66 GL384,MV403,R525,1297C,22HR,F-6.5,+OL+GL,PTFE,E

	67	68	69	70	71	72	73	74	75	76	77
SiO2	40.59	49.09	48.90	49.22	40.23	48.58	39.69	48.46	40.10	48.28	40.53
TiO2	nd	2.01	1.90	2.07	nd	2.04	nd	2.00	nd	1.97	nd
Al2O3	nd	13.46	13.44	14.90	nd	14.39	nd	14.11	0.09	13.88	0.11
Fe2O3	nd	2.43	2.23	2.17	nd	2.17	nd	2.20	nd	2.11	nd
Cr2O3	nd	nd	nd	0.02	nd	0.03	nd	0.04	nd	0.03	nd
FeO	11.96	9.19	9.04	8.71	14.07	8.88	13.58	9.08	13.08	9.31	12.86
MnO	0.13	0.21	0.20	0.16	0.25	0.17	0.19	0.15	0.22	0.17	0.20
NiO	nd	nd	nd	0.07	0.26	0.01	0.29	0.02	0.29	0.03	0.25
MgO	46.53	11.77	11.74	8.70	44.80	9.31	45.18	10.00	45.70	10.72	46.12
CaO	0.39	7.92	7.89	8.27	0.34	8.17	0.28	7.99	0.34	7.82	0.31
Na2O	nd	2.63	2.47	3.16	nd	2.98	nd	3.04	nd	3.07	nd
K2O	nd	0.93	0.98	1.07	nd	1.01	nd	0.91	nd	0.93	nd
P2O5	nd	0.25	nd	0.20	nd	0.17	nd	0.36	nd	0.30	nd
total=	99.60	99.89	98.79	98.72	99.95	97.91	99.21	98.36	99.82	98.62	100.38
Mg#	87.4	69.5	69.8	64.0	85.0	65.1	85.6	66.3	86.2	67.2	86.5

67 OL125,MV403,R525,1297C,22HR,F-6.5,PTFE,E
68 GL132,MV403,R526,1309C,19HR,F-6.2,-GL,SPT,E
69 GL128,MV403,R527,1321C,16.5HR,F-6.2,-GL,PTFE,E
70 GL1236,MV403F,R543,1252C,12.5HR,F-7.1,+OL+SPMT+GL,PTFE,W
71 OL141,MV403F,R543,1252C,12.5HR,F-7.1,PTFE,W
72 GL1114,MV403F,R555,1261C,20HR,F-7.0,+OL+SPMT+GL,PTFE,W
73 OL130,MV403F,R555,1261C,20HR,F-7.0,PTFE,W
74 GL1135,MV403F,R547,1277C,14HR,F-6.8,+OL+SPMT+GL,PTFE,W
75 OL104,MV403F,R547,1277C,14HR,F-6.8,PTFE,W
76 GL1105,MV403F,R572,1287C,4.5HR,F-6.8,+OL+GL,PTFE,W
77 OL134,MV403F,R572,1287C,4.5HR,F-6.8,PTFE,W

	78	79	80	81	82	83	84	85	86	87	88
SiO2	47.55	39.68	49.58	49.00	47.63	39.42	50.75	48.87	46.82	39.05	46.72
TiO2	2.84	nd	0.26	1.78	2.63	nd	0.20	1.98	2.52	nd	2.41
Al2O3	15.35	nd	30.56	5.19	15.10	nd	29.59	4.48	14.66	nd	14.94
Fe2O3	2.51	nd	nd	nd	2.56	nd	nd	nd	2.61	nd	2.41
Cr2O3	nd	nd	nd	0.21	nd	nd	nd	0.23	nd	nd	nd
FeO	8.33	19.26	1.13	7.23	8.37	19.57	0.81	7.62	8.42	18.92	8.32
MnO	0.13	0.34	nd	0.14	0.17	0.39	nd	0.17	nd	0.26	nd
NiO	nd	0.60	nd	0.15	nd	0.56	nd	nd	nd	0.49	nd
MgO	5.08	40.01	nd	13.40	5.15	40.64	nd	12.99	5.55	40.81	5.57
CaO	10.42	0.62	14.40	21.56	10.57	0.55	13.69	22.28	11.08	0.52	10.93
Na2O	3.53	nd	3.12	nd	3.63	nd	3.36	nd	3.22	nd	3.56
K2O	2.06	nd	0.47	nd	1.86	nd	0.33	nd	1.74	nd	1.72
P2O5	0.59	nd	nd	nd	0.55	nd	nd	nd	0.43	nd	0.57
total=	98.39	100.51	99.52	98.66	98.22	101.13	98.73	98.62	97.05	100.05	97.15
Mg#	52.1	78.7	-	-	52.3	78.7	-	-	54.0	79.4	54.4
An	-	-	69.9	-	-	-	67.9	-	-	-	-

78 GL1003,ES2058,R510,1145C,18HR,F-8.5,+OL+CPX+PL+SPMT+GL,SPT,E
79 OL329,ES2058,R510,1145C,18HR,F-8.5,SPT,E
80 PL310,ES2058,R510,1145C,18HR,F-8.5,SPT,E
81 CPX95,ES2058,R510,1145C,18HR,F-8.5,SPT,E
82 GL1085,ES2058,R552,1148C,22HR,F-8.4,+OL+CPX+PL+SPMT+GL,PTFE,E
83 OL348,ES2058,R552,1148C,22HR,F-8.4,PTFE,E
84 PL321,ES2058,R552,1148C,22HR,F-8.4,PTFE,E
85 CPX100,ES2058,R552,1148C,22HR,F-8.4,PTFE,E
86 GL412,ES2058,R587,1158C,19HR,F-8.2,+OL+PL+SPMT+GL,PTFE,E
87 OL134,ES2058,R587,1158C,19HR,F-8.2,PTFE,E
88 GL785,ES2058,R513,1161C,14HR,F-8.3,+OL+PL+SPMT+GL,SPT,E

	89	90	91	92	93	94	95	96	97	98	99
SiO2	39.31	46.80	39.42	48.90	46.51	39.06	46.39	39.49	46.13	40.38	46.37
TiO2	nd	2.19	nd	0.26	2.28	nd	2.06	0.11	1.94	nd	2.10
Al2O3	nd	15.57	nd	31.02	15.77	nd	15.56	0.16	14.32	nd	14.02
Fe2O3	nd	2.36	nd	nd	2.26	nd	2.32	nd	2.42	nd	2.41
Cr2O3	nd	nd	nd	nd	nd	nd	nd	nd	0.05	nd	nd
FeO	18.16	8.26	17.59	1.15	8.35	17.14	8.36	16.44	9.29	13.53	9.50
MnO	0.35	0.24	0.27	nd	0.07	0.26	0.12	0.22	0.18	nd	0.28
NiO	0.57	nd	0.47	nd	nd	0.63	nd	0.60	nd	0.72	nd
MgO	41.63	5.95	42.30	0.20	6.15	42.31	6.49	42.81	9.32	44.92	9.89
CaO	0.56	11.07	0.58	15.37	10.89	0.57	10.91	0.63	10.13	0.50	9.98
Na2O	nd	3.06	nd	2.58	3.11	nd	3.12	nd	2.67	nd	2.72
K2O	nd	1.48	nd	0.25	1.51	nd	1.55	nd	1.33	nd	1.20
P2O5	nd	0.45	nd	nd	0.45	nd	0.39	nd	0.32	nd	0.28
total=	100.58	97.43	100.63	99.73	97.35	99.97	97.27	100.46	98.10	100.05	98.75
Mg#	80.3	56.2	81.1	-	56.8	81.5	58.0	82.3	64.1	85.5	65.0
An	-	-	-	75.6	-	-	-	-	-	-	-

89 OL267,ES2058,R513,1161C,14HR,F-8.3,SPT,E
90 GL935,ES2058,R533,1168C,20HR,F-8.1,+OL+PL+SPMT+GL,PTFE,E
91 OL310,ES2058,R533,1168C,20HR,F-8.1,PTFE,E
92 PL299,ES2058,R533,1168C,20HR,F-8.1,PTFE,E
93 GL739,ES2058,R515,1176C,16.5HR,F-8.1,+OL+PL+SPMT+GL,SPT,E
94 OL246,ES2058,R515,1176C,16.5HR,F-8.1,SPT,E
95 GL749,ES2058,R516,1186C,12.5HR,F-7.9,+OL+SPMT+GL,SPT,E
96 OL249,ES2058,R516,1186C,12.5HR,F-7.9,SPT,E
97 GL1014,ES2058,R523,1265C,17HR,F-6.9,+OL+SPMT+GL,SPT,E
98 OL337,ES2058,R523,1265C,17HR,F-6.9,SPT,E
99 GL278,ES2058,R522,1277C,18HR,F-6.8,+OL+SPMT+GL,SPT,E

	100	101	102	103	104	105	106	107	108	109	110
SiO2	40.20	46.34	40.27	45.86	40.89	45.94	40.83	45.96	40.24	46.34	40.31
TiO2	nd	1.98	nd	1.91	nd	1.98	nd	1.92	nd	1.92	nd
Al2O3	nd	13.80	nd	13.67	nd	13.25	nd	13.23	nd	13.31	nd
Fe2O3	nd	2.27	nd	2.45	nd	2.39	nd	2.55	nd	2.38	nd
Cr2O3	nd	nd	nd	0.16	nd	nd	nd	nd	nd	nd	nd
FeO	13.07	9.37	12.95	9.69	12.22	8.72	10.79	9.36	11.60	9.46	11.25
MnO	0.24	0.17	0.20	0.12	0.25	0.18	0.28	0.24	0.17	0.21	0.18
NiO	0.59	nd	0.60	nd	0.70	nd	0.44	nd	0.79	nd	0.96
MgO	44.95	10.49	46.90	10.76	46.35	11.22	46.81	11.33	45.81	12.13	46.46
CaO	0.34	9.84	0.50	9.62	0.38	9.70	0.33	9.67	0.35	9.34	0.34
Na2O	nd	2.15	nd	2.45	nd	2.11	nd	2.30	nd	2.50	nd
K2O	nd	1.19	nd	1.16	nd	1.08	nd	1.05	nd	0.99	nd
P2O5	nd	nd	nd	0.17	nd	0.21	nd	0.12	nd	0.06	nd
total=	99.39	97.60	101.42	98.02	100.79	96.78	99.48	97.73	98.96	98.64	99.50
Mg#	86.0	66.6	86.6	66.4	87.1	69.6	88.5	68.3	87.6	69.6	88.0

100 OL101,ES2058,R522,1277C,18HR,F-6.8,SPT,E
101 GL661,ES2058,R521,1287C,16HR,F-6.7,+OL+SPMT+GL,SPT,E
102 OL219,ES2058,R521,1287C,16HR,F-6.7,SPT,E
103 GL387,ES2058,R525,1297C,22HR,F-6.5,+OL+GL,SPT,E
104 OL126,ES2058,R525,1297C,22HR,F-6.5,SPT,E
105 GL124,ES2058,R526,1309C,19HR,F-6.2,+OL+GL,PT,E
106 OL81,ES2058,R526,1309C,19HR,F-6.2,PT,E
107 GL126,ES2058,R526,1309C,19HR,F-6.2,+OL+GL,SPT,E
108 OL83,ES2058,R526,1309C,19HR,F-6.2,SPT,E
109 GL1988,ES2058,R527,1321C,16.5HR,F-6.2,+OL+GL,SPT,W
110 OL80,ES2058,R527,1321C,16.5HR,F-6.2,SPT,E

	111	112	113	114	115	116	117	118	119	120	121
SiO2	45.85	42.43	42.82	42.81	40.38	45.65	42.46	39.62	43.89	43.14	40.12
TiO2	1.95	3.19	3.08	3.26	0.15	2.53	3.24	nd	3.82	3.19	0.17
Al2O3	13.17	15.37	15.28	15.01	nd	7.67	14.65	0.11	8.78	13.79	nd
Fe2O3	2.26	2.81	2.61	2.51	nd	nd	2.51	nd	nd	2.44	nd
Cr2O3	0.07	nd	nd	nd	nd	0.61	nd	nd	0.15	0.12	nd
FeO	9.78	8.31	7.80	7.74	14.68	6.47	7.66	13.80	7.34	7.45	12.47
MnO	0.20	0.18	0.20	0.17	0.32	nd	0.18	0.28	0.12	0.25	0.24
NiO	0.14	nd	nd	nd	0.47	nd	nd	0.36	nd	nd	0.49
MgO	12.50	5.26	5.81	6.62	44.58	12.44	6.87	44.86	11.02	7.56	45.65
CaO	8.96	12.43	13.15	13.84	0.87	22.86	14.55	0.80	23.30	15.60	0.83
Na2O	2.38	4.70	4.21	4.10	nd	nd	3.76	nd	nd	3.28	nd
K2O	0.96	1.05	0.91	0.78	nd	nd	0.72	nd	nd	0.66	nd
P2O5	0.28	1.30	1.04	1.11	nd	nd	1.04	nd	nd	0.75	nd
total=	98.50	97.03	96.91	97.95	101.45	98.23	97.64	99.83	98.42	98.23	99.97
Mg#	69.5	53.0	57.0	60.4	84.4	-	61.5	85.3	-	64.4	86.7

111 GL1247,ES2058,R545,1334C,12HR,F-6.2,-GL,PTFE,W
112 GL308AA,MV93,R583,1135C,13HR,F-8.5,+OL+CPX+PL+SPMT+GL,PTFE,E
113 GL1114,MV93,R577,1148C,13HR,F-8.3,+OL+CPX+PL+GL,PTFE,E
114 GL1982,MV93,R571,1160C,12.5HR,F-8.2,+OL+CPX+GL,PTFE,W
115 OL347,MV93,R571,1160C,12.5HR,F-8.2,PTFE,E
116 CPX99,MV93,R571,1160C,12.5HR,F-8.2,PTFE,E
117 GL2003,MV93,R581,1174C,14HR,F-8.0,+OL+CPX+GL,PTFE,W
118 OL2000,MV93,R581,1174C,14HR,F-8.0,PTFE,W
119 CPX41A,MV93,R581,1174C,14HR,F-8.0,PTFE,E
120 GL263,MV93,R579,1189C,13.5HR,F-7.8,+OL+CPX+SPMT+GL,PTFE,E
121 OL100,MV93,R579,1189C,13.5HR,F-7.8,PTFE,E

	122	123	124	125	126	127	128	129	130	131	132
SiO2	47.64	42.99	40.16	42.59	40.00	43.06	40.24	40.73	43.01	43.06	43.19
TiO2	2.18	3.15	nd	2.96	nd	2.96	nd	nd	2.87	2.97	3.04
Al2O3	6.44	13.06	nd	13.00	nd	13.13	0.14	0.09	13.15	13.07	13.09
Fe2O3	nd	2.44	nd	2.39	nd	2.33	nd	nd	2.24	2.21	2.29
Cr2O3	1.45	nd	nd	nd	nd	0.06	nd	nd	0.05	0.08	nd
FeO	4.58	7.63	12.19	7.79	11.57	7.77	10.92	10.92	7.81	7.79	7.85
MnO	nd	0.18	0.23	0.15	0.19	0.18	0.23	0.23	0.16	0.19	0.18
NiO	nd	nd	0.58	nd	0.59	0.05	0.46	0.45	0.04	0.05	nd
MgO	13.72	8.22	45.75	8.34	45.39	9.36	46.76	46.81	9.82	9.77	9.70
CaO	23.35	15.57	0.79	15.21	1.00	14.60	0.77	0.67	14.53	14.58	14.76
Na2O	nd	2.69	nd	2.93	nd	3.36	nd	nd	3.18	3.27	3.16
K2O	nd	0.60	nd	0.63	nd	0.38	nd	nd	0.53	0.49	0.60
P2O5	nd	0.71	nd	0.72	nd	0.68	nd	nd	0.70	0.71	0.94
total=	99.36	97.24	99.70	96.71	98.74	97.92	99.52	99.90	98.09	98.24	98.80
Mg#	-	65.8	87.0	65.6	87.5	68.2	88.4	88.4	69.1	69.1	68.8

122 CPX40,MV93,R579,1189C,13.5HR,F-7.8,PTFE,E
123 GL318,MV93,R585,1204C,18HR,F-7.6,+OL+SPMT+GL,PTFE,E
124 OL110,MV93,R585,1204C,18HR,F-7.6,PTFE,E
125 GL316,MV93,R584,1218C,4HR,F-7.5,+OL+SPMT+GL,PTFE,E
126 OL109,MV93,R584,1218C,4HR,F-7.5,PTFE,E
127 GL1189,MV93,R582,1233C,4HR,F-7.3,+OL+SPMT+GL,PTFE,W
128 OL154,MV93,R582,1233C,4HR,F-7.3,PTFE,W
129 OL155,MV93,R582,1233C,4HR,F-7.3,PTFE,W
130 GL1249,MV93,R578,1247C,4HR,F-7.2,+SPMT+GL,PTFE,W
131 GL1178,MV93,R576,1260C,4HR,F-7.1,+SPMT+GL,PTFE,W
132 GL1985,MV93,R570,1274C,3.5HR,F-6.9,+SPMT+GL,PTFE,W

	133	134	135	136	137	138	139	140	141	142	143
SiO2	43.17	44.55	38.59	38.75	38.08	51.35	50.55	47.06	46.71	47.51	0.42
TiO2	2.98	4.63	nd	nd	nd	0.44	0.16	3.00	2.14	2.14	15.22
Al2O3	13.04	13.43	nd	nd	nd	28.41	30.13	6.91	6.81	5.62	7.66
Fe2O3	2.20	3.42	nd	nd	nd	nd	nd	nd	nd	nd	22.97
Cr2O3	0.08	0.03	nd	nd	nd	nd	nd	0.22	0.95	0.30	9.49
FeO	7.88	9.55	22.56	22.32	23.25	1.49	1.09	7.64	6.23	6.94	34.66
MnO	0.19	0.24	0.40	0.34	0.34	nd	nd	nd	nd	0.11	0.45
NiO	0.05	nd	0.27	0.36	0.36	nd	nd	nd	nd	nd	nd
MgO	9.75	4.94	37.38	37.82	36.94	0.28	0.21	12.04	12.90	13.28	7.29
CaO	14.45	10.53	0.73	0.62	0.50	12.63	14.17	22.44	22.58	22.76	0.38
Na2O	3.16	3.28	nd	nd	nd	3.73	3.25	0.39	0.27	0.21	nd
K2O	0.36	1.92	nd	nd	nd	0.54	0.34	nd	nd	nd	nd
P2O5	0.79	nd	nd	nd	nd	nd	nd	nd	nd	nd	nd
total=	98.10	96.52	99.93	100.21	99.47	98.87	99.90	99.70	98.59	98.87	98.54
Mg#	68.8	48.0	74.7	75.1	73.9	-	-	-	-	-	27.3
An	-	-	-	-	-	63.1	69.3	-	-	-	-

133 GL1138,MV93,R572,1287C,4.5HR,F-6.8,-GL,PTFE,W
134 GL11,MV521,R471,1129C,21HR,F-8.6,+OL+CPX+PL+SPMT+GL,PTFE,E
135 OL6,MV521,R471,1129C,21HR,F-8.6,PTFE,E
136 OL7,MV521,R471,1129C,21HR,F-8.6,PTFE,E
137 OL9,MV521,R471,1129C,21HR,F-8.6,PTFE,E
138 PL7,MV521,R471,1129C,21HR,F-8.6,PTFE,E
139 PL9,MV521,R471,1129C,21HR,F-8.6,PTFE,E
140 CPX10,MV521,R471,1129C,21HR,F-8.6,PTFE,E
141 CPX6,MV521,R471,1129C,21HR,F-8.6,PTFE,E
142 CPX8,MV521,R471,1129C,21HR,F-8.6,PTFE,E
143 SPMT2,MV521,R471,1129C,21HR,F-8.6,PTFE,E

	144	145	146	147	148	149	150	151	152	153	154
SiO2	0.21	0.37	45.28	39.78	51.09	50.17	49.09	48.85	48.35	0.30	45.61
TiO2	16.35	16.07	3.76	nd	0.28	0.21	1.77	2.30	1.97	3.27	3.61
Al2O3	6.81	7.00	13.54	nd	29.20	29.66	5.57	5.08	6.24	27.37	13.73
Fe2O3	23.99	23.09	2.82	nd	nd	nd	nd	nd	nd	13.16	2.88
Cr2O3	7.27	8.02	nd	nd	nd	nd	0.71	nd	0.40	20.80	nd
FeO	35.05	35.64	9.08	18.98	1.03	0.97	6.26	7.44	5.87	21.79	9.02
MnO	0.39	0.31	0.22	0.31	nd	nd	nd	0.25	nd	0.27	0.18
NiO	nd	nd	nd	0.36	nd	nd	nd	nd	nd	nd	nd
MgO	7.30	6.93	5.80	40.19	0.35	nd	13.75	12.43	13.38	11.06	6.17
CaO	0.37	0.46	11.90	0.57	13.56	14.34	22.61	22.69	23.36	nd	11.99
Na2O	nd	nd	2.82	nd	3.36	3.13	nd	nd	nd	nd	2.75
K2O	nd	nd	1.38	nd	0.37	0.38	nd	nd	nd	nd	1.30
P2O5	nd	nd	nd	nd	nd	nd	nd	nd	nd	nd	0.60
V2O3	nd	nd	nd	nd	nd	nd	nd	nd	nd	0.25	nd
total=	97.74	97.89	96.60	100.19	99.24	98.86	99.76	99.04	99.57	98.27	97.84
Mg#	27.1	25.7	53.2	79.1	-	-	-	-	-	47.5	54.9
An	-	-	-	-	67.5	70.1	-	-	-	-	-

144 SPMT3,MV521,R471,1129C,21HR,F-8.6,PTFE,E
145 SPMT4,MV521,R471,1129C,21HR,F-8.6,PTFE,E
146 GL94,MV521,R470,1151C,17HR,F-8.4,+OL+CPX+PL+SPMT+GL,PTFE,E
147 OL63,MV521,R470,1151C,17HR,F-8.4,PTFE,E
148 PL84,MV521,R470,1151C,17HR,F-8.4,PTFE,E
149 PL85,MV521,R470,1151C,17HR,F-8.4,PTFE,E
150 CPX42,MV521,R470,1151C,17HR,F-8.4,PTFE,E
151 CPX43,MV521,R470,1151C,17HR,F-8.4,PTFE,E
152 CPX44,MV521,R470,1151C,17HR,F-8.4,PTFE,E
153 SPMT6,MV521,R470,1151C,17HR,F-8.4,PTFE,E
154 GL410,MV521,R587,1158C,19HR,F-8.2,+OL+CPX+PL+SPMT+GL,PTFE,E

	155	156	157	158	159	160	161	162	163	164	165
SiO2	38.88	50.03	47.91	45.64	39.21	49.64	45.32	39.15	49.01	45.96	39.46
TiO2	0.11	1.58	2.02	3.30	0.12	0.16	3.18	0.21	nd	3.26	nd
Al2O3	nd	4.67	5.62	14.28	nd	30.62	14.33	nd	30.72	14.91	nd
Fe2O3	nd	nd	nd	2.64	nd	nd	2.48	nd	nd	2.56	nd
Cr2O3	nd	0.59	0.45	nd	nd	nd	0.04	nd	nd	0.04	nd
FeO	18.17	6.34	6.54	9.02	17.39	0.89	8.92	17.42	0.72	8.68	16.89
MnO	0.33	0.12	0.18	0.15	0.26	nd	0.12	0.27	nd	0.22	0.33
NiO	0.43	nd	nd	nd	0.35	nd	nd	0.44	nd	nd	0.39
MgO	41.46	13.97	13.46	6.41	41.50	nd	6.33	41.90	nd	6.67	42.16
CaO	0.69	20.83	22.12	12.19	0.59	14.61	12.24	0.69	15.18	11.95	0.58
Na2O	nd	0.30	nd	2.67	nd	2.91	2.44	nd	2.50	2.76	nd
K2O	nd	nd	nd	1.26	nd	0.21	1.14	nd	0.27	1.18	nd
P2O5	nd	nd	nd	nd	nd	nd	0.49	nd	nd	nd	nd
total=	100.07	98.43	98.30	97.56	99.42	99.04	97.03	100.08	98.40	98.19	99.81
Mg#	80.3	-	-	55.9	81.0	-	55.8	81.1	-	57.8	81.6
An	-	-	-	-	-	72.6	-	-	75.8	-	-

155 OL133,MV521,R587,1158C,19HR,F-8.2,PTFE,E
156 CPX45,MV521,R587,1158C,19HR,F-8.2,PTFE,E
157 CPX46,MV521,R587,1158C,19HR,F-8.2,PTFE,E
158 GL20R,MV521,R450,1166C,6.5HR,F-8.2,+OL+PL+SPMT+GL,PTFE,E
159 OL18,MV521,R450,1166C,6.5HR,F-8.2,PTFE,E
160 PL8,MV521,R450,1166C,6.5HR,F-8.2,PTFE,E
161 GL353,REVERSAL,MV521,R528,1171C,16HR,F-8.2,+OL+PL+SPMT+GL,PTFE,E
162 OL119,REVERSAL,MV521,R528,1171C,16HR,F-8.2,PTFE,E
163 PL156,REVERSAL,MV521,R528,1171C,16HR,F-8.2,PTFE,E
164 GL55,MV521,R449,1177C,14.5HR,F-8.0,+OL+PL+SPMT+GL,PTFE,E
165 OL23,MV521,R449,1177C,14.5HR,F-8.0,PTFE,E

	166	167	168	169	170	171	172	173	174	175	176
SiO2	40.03	48.44	49.45	45.91	40.04	40.06	0.32	45.65	39.72	45.64	39.77
TiO2	nd	0.17	0.24	3.02	0.14	nd	1.49	3.01	0.16	3.02	0.11
Al2O3	0.32	31.65	31.37	15.02	nd	nd	34.85	14.83	nd	14.74	nd
Fe2O3	nd	nd	nd	2.53	nd	nd	8.72	2.63	nd	2.55	nd
Cr2O3	nd	nd	nd	nd	nd	nd	23.07	0.06	nd	0.04	nd
FeO	16.81	0.86	0.96	8.73	15.78	15.96	17.07	8.68	15.77	9.04	15.75
MnO	0.28	nd	nd	0.08	0.18	0.25	0.14	0.11	0.20	nd	0.27
NiO	0.42	nd	nd	nd	0.40	0.29	nd	nd	0.23	nd	0.47
MgO	41.91	nd	nd	7.15	43.17	43.22	14.43	7.36	43.13	7.74	43.58
CaO	0.73	15.82	15.16	11.90	0.60	0.59	nd	11.68	0.62	11.60	0.53
Na2O	nd	2.40	2.68	2.70	nd	nd	nd	2.78	nd	2.50	nd
K2O	nd	0.20	0.28	1.18	nd	nd	nd	1.18	nd	1.10	nd
V2O3	nd	nd	nd	nd	nd	nd	0.19	nd	nd	nd	nd
total=	100.50	99.54	100.14	98.22	100.31	100.37	100.28	97.97	99.83	97.97	100.48
Mg#	81.6	-	-	59.3	83.0	82.8	60.1	60.2	83.0	60.4	83.1
An	-	77.5	74.5	-	-	-	-	-	-	-	-

166 OL24,MV521,R449,1177C,14.5HR,F-8.0,PTFE,E
167 PL12,MV521,R449,1177C,14.5HR,F-8.0,PTFE,E
168 PL13,MV521,R449,1177C,14.5HR,F-8.0,PTFE,E
169 GL29,MV521,R447,1191C,5HR,F-7.8,+OL+SPMT+GL,PTFE,E
170 OL14,MV521,R447,1191C,5HR,F-7.8,PTFE,E
171 OL15,MV521,R447,1191C,5HR,F-7.8,PTFE,E
172 SPMT6,MV521,R447,1191C,5HR,F-7.8,PTFE,E
173 GL7,MV521,R446,1200C,6.5HR,F-7.6,+OL+SPMT+GL,PTFE,E
174 OL1,MV521,R446,1200C,6.5HR,F-7.6,PTFE,E
175 GL43,MV521,R445,1207C,3HR,F-7.6,+OL+SPMT+GL,PTFE,E
176 OL17,MV521,R445,1207C,3HR,F-7.6,PTFE,E

	177	178	179	180	181	182	183	184	185	186	187
SiO2	45.42	40.32	39.78	45.22	39.77	39.20	45.13	40.16	44.63	39.84	45.51
TiO2	2.99	0.11	0.15	2.87	nd	0.14	2.92	nd	2.89	nd	2.95
Al2O3	14.70	nd	nd	14.46	nd	nd	14.41	0.23	13.93	nd	14.11
Fe2O3	2.68	nd	nd	2.54	nd	nd	2.54	nd	2.65	nd	2.51
Cr2O3	nd	nd	nd	0.11	nd	nd	nd	nd	0.06	nd	0.11
FeO	8.83	15.09	15.15	8.93	14.45	14.92	9.03	13.94	8.93	13.64	9.23
MnO	0.11	0.18	0.24	0.17	0.16	0.17	0.19	0.18	0.19	0.16	0.07
NiO	nd	0.47	0.43	nd	0.53	0.31	nd	0.38	nd	0.42	nd
MgO	7.85	43.82	44.32	8.09	44.24	44.13	8.91	44.34	8.95	44.71	9.68
CaO	11.63	0.58	0.54	11.56	0.56	0.57	11.52	0.53	11.19	0.48	11.21
Na2O	2.47	nd	nd	2.54	nd	nd	2.34	nd	2.40	nd	2.40
K2O	1.10	nd	nd	1.16	nd	nd	1.08	nd	1.11	nd	0.98
total=	97.78	100.57	100.61	97.65	99.71	99.44	98.07	99.76	96.93	99.25	98.76
Mg#	61.3	83.8	83.9	61.8	84.5	84.1	63.7	85.0	64.1	85.4	65.1

177 GL19,MV521,R444,1211C,6HR,F-7.4,+OL+SPMT+GL,PTFE,E
178 OL5,MV521,R444,1211C,6HR,F-7.4,PTFE,E
179 OL6,MV521,R444,1211C,6HR,F-7.4,PTFE,E
180 GL16,MV521,R443,1222C,7HR,F-7.4,+OL+SPMT+GL,SPT,E
181 OL3,MV521,R443,1222C,7HR,F-7.4,SPT,E
182 OL4,MV521,R443,1222C,7HR,F-7.4,SPT,E
183 GL13,MV521,R442,1236C,6HR,F-7.2,+OL+SPMT+GL,SPT,E
184 OL8,MV521,R442,1236C,6HR,F-7.2,SPT,E
185 GL6,MV521,R441,1245C,6HR,F-7.0,+OL+SPMT+GL,SPT,E
186 OL6RR,MV521,R441,1245C,6HR,F-7.0,SPT,E
187 GL19,MV521,R440,1256C,6.5HR,F-7.0,+OL+SPMT+GL,SPT,E

	188	189	190	191	192	193	194	195	196	197	198
SiO2	40.21	45.28	40.32	44.98	40.36	45.13	44.79	49.03	38.54	38.48	38.23
TiO2	nd	2.84	nd	2.76	nd	2.62	2.76	2.67	0.11	nd	nd
Al2O3	nd	14.04	0.16	13.48	nd	13.50	13.51	14.89	nd	nd	nd
Fe2O3	nd	2.47	nd	2.63	nd	2.42	2.30	2.72	nd	nd	nd
Cr2O3	nd	nd	nd	0.05	nd	nd	nd	nd	nd	nd	nd
FeO	12.93	8.83	12.23	9.25	12.50	9.31	9.28	8.57	23.20	24.32	24.36
MnO	0.23	0.16	0.28	0.18	0.27	0.11	0.18	0.19	0.45	0.27	0.43
NiO	0.40	nd	0.31	nd	0.39	nd	nd	nd	0.44	0.41	0.46
MgO	45.83	10.06	46.22	10.50	46.67	10.71	10.98	4.17	36.87	35.56	35.95
CaO	0.42	11.04	0.45	10.75	0.50	10.63	10.59	9.01	0.52	0.62	0.58
Na2O	nd	2.28	nd	2.15	nd	1.93	2.28	4.03	nd	nd	nd
K2O	nd	1.02	nd	0.99	nd	0.93	0.90	1.91	nd	nd	nd
P2O5	nd	nd	nd	nd	nd	0.34	0.79	nd	nd	nd	nd
total=	100.02	98.02	99.97	97.72	100.69	97.63	98.36	97.19	100.13	99.66	100.01
Mg#	86.3	67.0	87.1	66.9	86.9	67.2	67.8	46.4	73.9	72.3	72.5

188 OL8,MV521,R440,1256C,6.5HR,F-7.0,SPT,E
189 GL9,MV521,R439,1266C,7.5HR,F-6.8,+OL+SPMT+GL,PT,E
190 OL5,MV521,R439,1266C,7.5HR,F-6.8,PT,E
191 GL35,MV521,R451,1277C,6.5HR,F-6.6,+OL+GL,PTFE,E
192 OL23,MV521,R451,1277C,6.5HR,F-6.6,PTFE,E
193 GL369,MV521,R497,1288C,18HR,F-6.6,+OL+GL,PTFE,E
194 GL1903,MV521,R4-253,1291C,2HR,F-6.7,-GL,PTFE,W
195 GL5,MV723,R471,1129C,21HR,F-8.6,+OL+CPX+PL+SPMT+GL,SPT,E
196 OL2,MV723,R471,1129C,21HR,F-8.6,SPT,E
197 OL3,MV723,R471,1129C,21HR,F-8.6,SPT,E
198 OL5,MV723,R471,1129C,21HR,F-8.6,SPT,E

	199	200	201	202	203	204	205	206	207	208	209
SiO2	51.14	51.70	51.37	49.98	50.97	50.44	3.68	49.22	39.24	39.60	39.07
TiO2	0.34	0.19	0.20	1.68	1.12	1.23	10.08	2.11	nd	nd	nd
Al2O3	28.49	28.55	29.46	4.28	3.41	3.34	8.77	14.86	nd	nd	nd
Fe2O3	nd	nd	nd	nd	nd	nd	17.12	2.49	nd	nd	nd
Cr2O3	nd	nd	nd	0.44	0.37	0.26	12.25	nd	nd	nd	nd
FeO	1.48	1.32	0.66	7.59	7.02	6.92	36.40	8.78	20.03	19.83	19.96
MnO	nd	nd	nd	0.12	0.14	0.16	nd	0.14	0.32	0.30	0.36
NiO	nd	nd	nd	nd	nd	nd	nd	nd	0.44	0.50	0.64
MgO	0.37	0.20	nd	13.43	14.39	14.36	5.93	5.26	39.33	39.69	40.04
CaO	12.95	12.71	13.03	21.88	22.14	22.42	nd	10.61	0.62	0.63	0.64
Na2O	3.73	3.96	3.65	0.45	nd	nd	nd	3.80	nd	nd	nd
K2O	0.40	0.36	0.25	nd	nd	nd	nd	1.43	nd	nd	nd
V2O3	nd	nd	nd	nd	nd	nd	0.68	nd	nd	nd	nd
total=	98.90	98.99	98.62	99.85	99.56	99.13	94.91	98.70	99.98	100.55	100.71
Mg#	-	-	-	-	-	-	22.5	51.6	77.8	78.1	78.1
An	64.2	62.6	65.4	-	-	-	-	-	-	-	-

199 PL2,MV723,R471,1129C,21HR,F-8.6,SPT,E
200 PL4,MV723,R471,1129C,21HR,F-8.6,SPT,E
201 PL5,MV723,R471,1129C,21HR,F-8.6,SPT,E
202 CPX2,MV723,R471,1129C,21HR,F-8.6,SPT,E
203 CPX4,MV723,R471,1129C,21HR,F-8.6,SPT,E
204 CPX5,MV723,R471,1129C,21HR,F-8.6,SPT,E
205 SPMT1,MV723,R471,1129C,21HR,F-8.6,SPT,E
206 GL41,MV723,R470,1151C,17HR,F-8.4,+OL+CPX+PL+SPMT+GL,SPT,E
207 OL34,MV723,R470,1151C,17HR,F-8.4,SPT,E
208 OL35,MV723,R470,1151C,17HR,F-8.4,SPT,E
209 OL39,MV723,R470,1151C,17HR,F-8.4,SPT,E

	210	211	212	213	214	215	216	217	218	219	220
SiO2	39.16	51.52	51.81	51.25	51.59	51.30	50.87	49.73	0.46	0.21	48.81
TiO2	nd	0.12	nd	0.15	nd	1.13	1.20	1.23	2.69	2.18	1.89
Al2O3	nd	29.97	30.15	30.10	30.14	3.52	3.76	4.89	23.12	22.45	15.04
Fe2O3	nd	nd	nd	nd	nd	nd	nd	nd	17.00	19.44	2.26
Cr2O3	nd	nd	nd	nd	nd	0.61	0.31	1.02	22.43	22.10	nd
FeO	20.03	0.72	0.59	0.81	0.83	6.29	6.95	6.59	22.37	22.46	8.28
MnO	0.34	nd	nd	nd	nd	nd	0.13	nd	nd	0.29	0.13
NiO	0.62	nd	nd	nd	nd	0.14	0.13	nd	nd	nd	nd
MgO	39.72	nd	nd	nd	nd	14.41	14.49	13.86	10.38	9.69	5.71
CaO	0.56	13.74	13.43	13.83	13.42	22.74	22.37	22.05	nd	nd	10.99
Na2O	nd	3.70	3.58	3.50	3.67	0.21	0.21	0.46	nd	nd	3.66
K2O	nd	0.22	0.22	0.22	0.30	nd	nd	nd	nd	nd	1.26
P2O5	nd	nd	nd	nd	nd	nd	nd	nd	nd	nd	0.09
V2O3	nd	nd	nd	nd	nd	nd	nd	nd	0.73	1.09	nd
total=	100.43	99.99	99.78	99.86	99.95	100.35	100.42	99.83	99.18	99.91	98.12
Mg#	77.9	-	-	-	-	-	-	-	45.3	43.5	55.1
An	-	66.4	66.6	67.7	65.7	-	-	-	-	-	-

210 OL40,MV723,R470,1151C,17HR,F-8.4,SPT,E
211 PL37,MV723,R470,1151C,17HR,F-8.4,SPT,E
212 PL38,MV723,R470,1151C,17HR,F-8.4,SPT,E
213 PL39,MV723,R470,1151C,17HR,F-8.4,SPT,E
214 PL42,MV723,R470,1151C,17HR,F-8.4,SPT,E
215 CPX36,MV723,R470,1151C,17HR,F-8.4,SPT,E
216 CPX37,MV723,R470,1151C,17HR,F-8.4,SPT,E
217 CPX38,MV723,R470,1151C,17HR,F-8.4,SPT,E
218 SPMT14,MV723,R470,1151C,17HR,F-8.4,SPT,E
219 SPMT15,MV723,R470,1151C,17HR,F-8.4,SPT,E
220 GL776,MV723,R513,1161C,14HR,F-8.3,+OL+CPX+PL+SPMT+GL,SPT,E

	221	222	223	224	225	226	227	228	229	230	231
SiO2	39.09	48.68	39.30	49.95	48.88	38.91	1.68	48.06	39.11	48.14	39.69
TiO2	nd	1.92	0.12	0.16	1.91	nd	2.76	1.69	nd	1.66	nd
Al2O3	nd	15.03	nd	30.86	15.28	nd	22.44	16.01	0.08	15.80	nd
Fe2O3	nd	2.41	nd	nd	2.33	nd	14.75	2.04	nd	2.23	nd
Cr2O3	nd	nd	nd	nd	0.08	nd	22.02	nd	nd	nd	nd
FeO	18.65	8.38	18.12	0.92	8.26	17.72	23.02	8.16	15.83	8.17	15.70
MnO	0.30	0.20	0.31	nd	0.16	0.28	0.28	0.14	0.25	0.15	0.21
NiO	0.57	nd	0.82	nd	nd	0.64	nd	nd	0.58	nd	0.57
MgO	41.40	5.48	41.43	nd	5.98	41.58	10.63	6.67	42.82	6.65	42.59
CaO	0.67	10.94	0.47	14.40	11.10	0.62	nd	10.67	0.47	10.80	0.51
Na2O	nd	3.51	nd	3.03	3.44	nd	nd	3.52	nd	3.37	nd
K2O	nd	1.29	nd	0.24	1.26	nd	nd	1.08	nd	1.09	nd
P2O5	nd	nd	nd	nd	nd	nd	nd	0.15	nd	nd	nd
V2O3	nd	nd	nd	nd	nd	nd	0.76	nd	nd	nd	nd
total=	100.68	97.84	100.57	99.56	98.68	99.75	98.34	98.19	99.14	98.06	99.27
Mg#	79.8	53.8	80.3	-	56.3	80.7	45.1	59.3	82.8	59.2	82.9
An	-	-	-	71.4	-	-	-	-	-	-	-

221 OL263,MV723,R513,1161C,14HR,F-8.3,SPT,E
222 GL938,MV723,R533,1168C,20HR,F-8.1,+OL+PL+SPMT+GL,PTFE,E
223 OL311,MV723,R533,1168C,20HR,F-8.1,PTFE,E
224 PL300,MV723,R533,1168C,20HR,F-8.1,PTFE,E
225 GL14,MV723,R438,1176C,7HR,F-8.0,+OL+PL+SPMT+GL,SPT,E
226 OL10,MV723,R438,1176C,7HR,F-8.0,SPT,E
227 SPMT1,MV723,R438,1176C,7HR,F-8.0,SPT,E
228 GL2045,MV723,R5-730,1187C,14HR,F-8.0,+OL+SPMT+GL,SPT,W
229 OL902,MV723,R5-730,1187C,14HR,F-8.0,SPT,W
230 GL14,MV723,R436,1197C,8HR,F-7.7,+OL+SPMT+GL,SPT,E
231 OL10,MV723,R436,1197C,8HR,F-7.7,SPT,E

	232	233	234	235	236	237	238	239	240	241	242
SiO2	48.15	47.84	47.90	38.15	47.95	39.23	48.86	40.26	47.27	40.16	39.99
TiO2	1.54	1.68	1.63	nd	1.61	0.02	1.56	nd	1.60	0.02	0.02
Al2O3	15.61	15.80	15.63	nd	15.74	0.09	15.72	nd	15.01	0.09	0.09
Fe2O3	2.15	2.16	2.20	nd	2.27	nd	2.24	nd	2.49	nd	nd
Cr2O3	0.04	nd	0.06	nd	nd	nd	0.09	nd	nd	nd	nd
FeO	7.99	8.13	7.86	19.84	8.11	15.33	8.36	14.93	8.80	13.35	14.06
MnO	0.12	0.20	0.19	0.36	0.16	0.21	0.21	0.22	0.17	0.19	0.19
NiO	nd	nd	nd	0.59	0.05	0.69	nd	0.62	0.07	1.10	0.99
MgO	6.97	6.92	7.28	39.75	6.91	43.51	7.23	43.90	8.20	44.97	44.39
CaO	10.81	10.88	10.67	0.48	10.60	0.50	10.59	0.48	10.55	0.37	0.41
Na2O	3.21	2.89	3.39	nd	3.57	nd	3.23	nd	3.36	nd	nd
K2O	1.12	1.12	1.11	nd	1.08	nd	1.06	nd	1.00	nd	nd
total=	97.71	97.62	97.92	99.17	98.05	99.58	99.15	100.41	98.52	100.25	100.14
Mg#	60.9	60.3	62.3	78.1	60.3	83.5	60.6	84.0	62.4	85.7	84.9

232 GL14,MV723,R422,1205C,2HR,F-7.6,+OL+SPMT+GL,PT,E
233 GL5,MV723,R421,1206C,2HR,F-7.6,+OL+SPMT+GL,PT,E
234 GL7,MV723,R424,1208C,2HR,F-7.5,+OL+SPMT+GL,PT,E
235 OL3,MV723,R424,1208C,2HR,F-7.5,PT,E
236 GLNIC10,MV723,R418,1209C,3HR,F-7.5,+OL+SPMT+GL,PT,W
237 OLNIC7,MV723,R418,1209C,3HR,F-7.5,PT,W
238 GL6,MV723,R437,1211C,6HR,F-7.5,+OL+SPMT+GL,SPT,E
239 OL4,MV723,R437,1211C,6HR,F-7.5,SPT,E
240 GLNIC20,MV723,R414,1243C,2HR,F-7.0,+OL+SPMT+GL,PT,W
241 OLNIC17,MV723,R414,1243C,2HR,F-7.0,PT,W
242 OLNIC19,MV723,R414,1243C,2HR,F-7.0,PT,W

	243	244	245	246	247	248	249	250	251	252	253
SiO2	48.22	40.28	40.03	47.36	39.50	39.25	0.21	0.21	48.44	47.75	40.77
TiO2	1.61	nd	0.11	1.52	0.02	0.02	1.76	1.75	1.40	1.59	nd
Al2O3	15.28	nd	nd	14.99	0.09	0.09	13.29	13.30	14.97	14.60	nd
Fe2O3	2.30	nd	nd	2.30	nd	nd	31.13	32.77	2.23	2.28	nd
Cr2O3	nd	nd	nd	nd	nd	nd	22.92	23.08	0.09	nd	nd
FeO	8.29	12.98	13.64	8.38	12.29	13.30	15.02	13.49	8.23	8.08	12.91
MnO	0.23	0.19	0.20	0.17	0.18	0.17	0.24	0.23	0.22	0.15	0.15
NiO	nd	0.98	0.85	0.08	0.95	0.97	nd	0.67	nd	0.06	0.71
MgO	8.32	45.03	44.94	8.38	45.92	45.05	13.21	13.23	8.79	9.18	45.67
CaO	10.36	0.38	0.45	10.23	0.34	0.37	nd	0.30	9.96	9.99	0.30
Na2O	3.03	nd	nd	3.43	nd	nd	nd	nd	3.27	3.36	nd
K2O	1.07	nd	nd	1.00	nd	nd	nd	0.09	1.04	0.87	nd
V2O3	nd	nd	nd	nd	nd	nd	1.75	nd	nd	nd	nd
total=	98.71	99.84	100.22	97.84	99.29	99.22	99.53	99.12	98.64	97.91	100.51
Mg#	64.1	86.1	85.4	64.1	86.9	85.8	61.1	63.6	65.6	66.9	86.3

243 GL57,MV723,R415,1244C,2HR,F-7.0,+OL+SPMT+GL,PT,E
244 OL4,MV723,R415,1244C,2HR,F-7.0,PT,E
245 OL5,MV723,R415,1244C,2HR,F-7.0,PT,E
246 GLNIC5,MV723,R417,1248C,3HR,F-7.0,+OL+SPMT+GL,PT,W
247 OLNIC2,MV723,R417,1248C,3HR,F-7.0,PT,W
248 OLNIC5,MV723,R417,1248C,3HR,F-7.0,PT,W
249 SPMT1,MV723,R417,1248C,3HR,F-7.0,PT,E
250 SPMTUN,MV723,R417,1248C,3HR,F-7.0,PT,E
251 GL12,MV723,R416,1255C,1.5HR,F-6.9,+OL+SPMT+GL,PT,E
252 GLNIC16,MV723,R413,1258C,5.5HR,F-6.8,+OL+SPMT+GL,PT,W
253 OL1,MV723,R413,1258C,5.5HR,F-6.8,PT,E

	254	255	256	257	258	259	260	261	262	263	264
SiO2	39.56	39.76	48.10	40.16	47.47	48.33	46.39	0.23	47.43	47.28	47.59
TiO2	0.02	0.02	1.50	nd	1.55	1.50	1.55	0.99	1.51	1.56	1.63
Al2O3	0.09	0.09	14.49	nd	14.74	14.54	15.21	21.63	14.77	14.74	14.76
Fe2O3	nd	nd	2.35	nd	2.16	2.23	2.19	10.20	2.08	2.34	2.19
Cr2O3	nd	nd	nd	nd	0.05	0.06	0.06	36.09	0.07	0.07	0.09
FeO	12.88	12.64	8.69	12.40	8.59	8.81	8.75	14.04	8.59	8.67	8.69
MnO	0.16	0.16	0.20	0.18	0.16	0.13	0.16	nd	0.14	0.19	0.19
NiO	0.60	0.59	nd	0.88	0.15	nd	0.07	nd	0.18	0.08	0.08
MgO	45.82	45.84	9.79	46.24	9.81	9.65	9.90	14.18	9.94	9.96	9.94
CaO	0.28	0.33	10.11	0.42	9.75	10.11	9.89	nd	9.80	9.80	9.75
Na2O	nd	nd	2.89	nd	2.96	2.78	3.15	nd	3.10	2.93	2.86
K2O	nd	nd	0.94	nd	0.78	0.93	0.77	nd	0.99	0.70	0.58
P2O5	nd	nd	nd	nd	0.13	nd	0.16	nd	0.20	0.23	0.15
V2O3	nd	nd	nd	nd	nd	nd	nd	0.18	nd	nd	nd
total=	99.41	99.43	99.06	100.28	98.30	99.07	98.25	97.54	98.80	98.55	98.50
Mg#	86.4	86.6	66.8	86.9	67.1	66.1	66.8	64.3	67.3	67.2	67.1

254 OLNIC15,MV723,R413,1258C,5.5HR,F-6.8,PT,W
255 OLNIC16,MV723,R413,1258C,5.5HR,F-6.8,PT,W
256 GL45,MV723,R451,1277C,6.5HR,F-6.6,+OL+SPMT+GL,SPT,E
257 OL28,MV723,R451,1277C,6.5HR,F-6.6,SPT,E
258 GL1234,MV723,R549,1287C,14HR,F-6.6,+SPMT+GL,PTFE,W
259 GL363,MV723,R497,1288C,18HR,F-6.6,+SPMT+GL,SPT,E
260 GL14,MV723,R525,1297C,22HR,F-6.5,+SPMT+GL,SPT,W
261 SPMT25,MV723,R525,1297C,22HR,F-6.5,SPT,E
262 GL1246,MV723,R546,1297C,3HR,F-6.6,+SPMT+GL,PTFE,W
263 GL1205,MV723,R526,1309C,19HR,F-6.2,-GL,SPT,W
264 GL1207,MV723,R527,1321C,16.5HR,F-6.2,-GL,SPT,W

	265	266	267	268	269	270	271	272	273	274	275
SiO2	47.56	40.55	47.40	47.48	45.68	39.65	47.32	45.45	39.21	51.43	46.15
TiO2	1.54	nd	1.52	1.53	3.58	nd	2.86	3.56	nd	0.31	3.36
Al2O3	14.67	nd	14.58	14.65	14.70	nd	7.53	14.10	nd	28.75	14.49
Fe2O3	2.08	nd	2.18	2.06	2.70	nd	nd	2.79	nd	nd	2.70
Cr2O3	0.06	nd	0.06	0.06	nd	nd	0.32	nd	nd	nd	0.06
FeO	8.61	12.15	8.62	8.48	8.83	19.67	7.83	8.76	19.04	1.19	8.42
MnO	0.19	0.24	0.16	0.17	0.29	0.39	0.14	0.25	0.43	nd	0.20
NiO	0.01	0.13	0.07	0.06	nd	0.23	nd	nd	0.26	nd	nd
MgO	9.98	46.58	10.11	10.00	5.53	40.81	12.05	5.63	40.49	0.18	6.14
CaO	9.67	0.40	9.70	9.79	11.30	0.54	21.93	11.14	0.62	13.01	11.71
Na2O	3.09	nd	2.98	3.19	3.89	nd	0.59	3.95	nd	3.91	3.83
K2O	0.75	nd	0.92	0.91	1.11	nd	nd	1.15	nd	0.26	1.02
P2O5	0.09	nd	0.11	0.07	0.81	nd	nd	0.77	nd	nd	0.57
total=	98.30	100.05	98.41	98.45	98.42	101.29	100.57	97.55	100.05	99.04	98.65
Mg#	67.4	87.2	67.6	67.8	52.7	78.7	-	53.4	79.1	-	56.5
An	-	-	-	-	-	-	-	-	-	63.8	-

265 GL1155,MV723F,R547,1277C,14HR,F-6.8,+OL+SPMT+GL,PTFE,W
266 OL105,MV723F,R547,1277C,14HR,F-6.8,PTFE,W
267 GL1230,MV723F,R549,1287C,14HR,F-6.6,+SPMT+GL,PTFE,W
268 GL1244,MV723F,R546,1297C,3HR,F-6.6,-GL,PTFE,W
269 GL996,MV109,R510,1145C,18HR,F-8.5,+OL+CPX+PL+SPMT+GL,PTFE,E
270 OL325,MV109,R510,1145C,18HR,F-8.5,PTFE,E
271 CPX94,MV109,R510,1145C,18HR,F-8.5,PTFE,E
272 GL1089,MV109,R552,1148C,22HR,F-8.4,+OL+CPX+PL+SPMT+GL,PTFE,E
273 OL349,MV109,R552,1148C,22HR,F-8.4,PTFE,E
274 PL323,MV109,R552,1148C,22HR,F-8.4,PTFE,E
275 GL416,MV109,R587,1158C,19HR,F-8.2,+OL+PL+SPMT+GL,PTFE,E

	276	277	278	279	280	281	282	283	284	285	286
SiO2	39.20	50.92	45.73	38.77	49.07	45.68	45.39	39.68	46.04	40.39	45.35
TiO2	0.19	0.25	3.20	0.15	0.32	2.86	2.90	nd	2.78	nd	2.71
Al2O3	nd	29.58	14.76	nd	31.01	15.38	15.53	nd	14.07	nd	13.97
Fe2O3	nd	nd	2.47	nd	nd	2.30	2.36	nd	2.35	nd	2.37
Cr2O3	nd	nd	0.04	nd	nd	nd	nd	nd	nd	nd	0.09
FeO	18.11	1.08	8.52	17.32	1.35	8.32	8.21	15.77	8.89	12.87	8.69
MnO	0.33	nd	0.20	0.18	nd	0.20	0.18	0.24	0.13	0.17	0.19
NiO	0.40	nd	nd	0.34	nd	nd	nd	0.56	nd	0.50	nd
MgO	41.98	nd	6.13	42.23	nd	6.69	6.94	44.19	9.34	46.25	9.76
CaO	0.53	13.77	11.69	0.64	14.85	11.65	11.32	0.50	10.73	0.55	10.73
Na2O	nd	3.16	3.48	nd	2.86	3.43	3.66	nd	2.85	nd	3.04
K2O	nd	0.17	1.01	nd	0.12	0.90	0.90	nd	0.80	nd	0.80
P2O5	nd	nd	0.58	nd	nd	0.54	0.53	nd	0.46	nd	0.34
total=	100.74	98.93	97.81	99.63	99.58	97.95	97.92	100.94	98.44	100.73	98.04
Mg#	80.5	-	56.2	81.3	-	58.9	60.1	83.3	65.2	86.5	66.7
An	-	69.9	-	-	73.6	-	-	-	-	-	-

276 OL138,MV109,R587,1158C,19HR,F-8.2,PTFE,E
277 PL171,MV109,R587,1158C,19HR,F-8.2,PTFE,E
278 GL779,MV109,R513,1161C,14HR,F-8.3,+OL+PL+SPMT+GL,PTFE,E
279 OL264,MV109,R513,1161C,14HR,F-8.3,PTFE,E
280 PL264,MV109,R513,1161C,14HR,F-8.3,PTFE,E
281 GL741,MV109,R515,1176C,16.5HR,F-8.1,+OL+PL+SPMT+GL,PTFE,E
282 GL751,MV109,R516,1186C,12.5HR,F-7.9,+OL+SPMT+GL,PTFE,E
283 OL250,MV109,R516,1186C,12.5HR,F-7.9,PTFE,E
284 GL381,MV109,R524,1252C,20HR,F-7.1,+OL+SPMT+GL,PTFE,E
285 OL124,MV109,R524,1252C,20HR,F-7.1,PTFE,E
286 GL1019,MV109,R523,1265C,17HR,F-6.9,+OL+SPMT+GL,PTFE,E

	287	288	289	290	291	292	293	294	295	296	297
SiO2	39.58	1.11	45.78	45.16	46.73	37.76	47.22	37.85	45.86	38.32	50.63
TiO2	nd	2.09	2.66	2.71	5.57	nd	5.85	0.31	5.39	nd	0.19
Al2O3	nd	26.68	13.90	14.05	12.68	nd	12.22	nd	12.19	nd	29.81
Fe2O3	nd	8.32	2.36	2.23	0.43	nd	0.48	nd	3.43	nd	nd
Cr2O3	nd	28.81	nd	nd	nd	nd	nd	nd	nd	nd	nd
FeO	12.43	16.68	9.15	8.93	9.81	27.38	11.93	26.14	10.07	24.29	0.78
MnO	0.14	0.17	0.20	0.20	0.08	0.33	0.22	0.27	0.22	0.27	nd
NiO	0.30	nd	nd	nd	nd	0.26	nd	0.15	nd	0.17	nd
MgO	45.64	14.52	9.96	10.01	4.54	34.13	4.64	35.15	5.27	36.62	nd
CaO	0.51	nd	10.81	10.35	8.87	0.40	9.90	0.61	10.43	0.52	14.06
Na2O	nd	nd	2.56	2.71	2.85	nd	2.86	nd	2.41	nd	3.09
K2O	nd	nd	0.72	0.65	1.68	nd	1.20	nd	0.96	nd	0.22
P2O5	nd	nd	0.40	0.46	1.40	nd	0.59	nd	nd	nd	nd
V2O3	nd	0.29	nd	nd	nd	nd	nd	nd	nd	nd	nd
total=	98.60	98.67	98.50	97.46	94.64	100.26	97.11	100.48	96.23	100.19	98.78
Mg#	86.7	60.8	66.0	66.6	45.2	69.0	40.9	70.6	48.3	72.9	-
An	-	-	-	-	-	-	-	-	-	-	70.6

287 OL338,MV109,R523,1265C,17HR,F-6.9,PTFE,E
288 SPMT65,MV109,R523,1265C,17HR,F-6.9,PTFE,E
289 GL282,MV109,R522,1277C,18HR,F-6.8,+SPMT+GL,PTFE,E
290 GL1912,MV109,R4-253,1291C,2HR,F-6.7,-GL,PTFE,W
291 GL925,MV106,R574,1113C,19HR,F-13.1,+OL+CPX+PL+IL+GL,PTFE,E
292 OL307,MV106,R574,1113C,19HR,F-13.1,PTFE,E
293 GL1111,MV106,R573,1128C,16HR,F-13.0,+OL+CPX+PL+GL,PTFE,E
294 OL356,MV106,R573,1128C,16HR,F-13.0,PTFE,E
295 GL13R,MV106,R471,1129C,21HR,F-8.6,+OL+CPX+PL+SPMT+GL,PTFE,E
296 OL12,MV106,R471,1129C,21HR,F-8.6,PTFE,E
297 PL12,MV106,R471,1129C,21HR,F-8.6,PTFE,E

	298	299	300	301	302	303	304	305	306	307	308
SiO2	50.27	52.21	46.85	49.04	0.47	46.89	38.31	50.76	49.77	46.05	38.65
TiO2	0.27	0.81	2.69	2.07	15.70	4.80	0.26	0.20	1.84	4.34	0.12
Al2O3	29.79	2.01	6.59	4.46	6.35	12.77	nd	30.65	5.12	12.29	nd
Fe2O3	nd	nd	nd	nd	18.49	0.43	nd	nd	nd	2.87	nd
Cr2O3	nd	0.29	0.12	0.37	13.94	nd	nd	nd	0.67	nd	nd
FeO	1.02	6.75	7.72	7.14	35.76	11.68	23.40	0.83	6.21	9.53	19.37
MnO	nd	0.27	nd	0.24	0.20	0.23	0.21	nd	nd	0.23	0.27
NiO	nd	nd	nd	nd	nd	nd	0.25	nd	nd	nd	0.20
MgO	0.13	15.77	12.62	13.52	6.82	5.72	37.47	nd	13.97	6.24	40.03
CaO	13.85	21.00	22.33	22.14	0.49	11.04	0.56	14.42	21.46	11.23	0.59
Na2O	3.18	nd	nd	nd	nd	2.86	nd	3.11	nd	2.27	nd
K2O	0.21	nd	nd	nd	nd	0.91	nd	0.26	nd	0.79	nd
P2O5	nd	nd	nd	nd	nd	0.77	nd	nd	nd	nd	nd
total=	98.72	99.11	98.92	98.98	98.22	98.10	100.46	100.23	99.04	95.84	99.23
Mg#	-	-	-	-	25.4	46.6	74.1	-	-	53.9	78.6
An	69.8	-	-	-	-	-	-	70.8	-	-	-

298 PL15,MV106,R471,1129C,21HR,F-8.6,PTFE,E
299 CPX14,MV106,R471,1129C,21HR,F-8.6,PTFE,E
300 CPX15,MV106,R471,1129C,21HR,F-8.6,PTFE,E
301 CPX16,MV106,R471,1129C,21HR,F-8.6,PTFE,E
302 SPMT5,MV106,R471,1129C,21HR,F-8.6,PTFE,E
303 GL1074,MV106,R569,1142C,12HR,F-12.8,+OL+CPX+PL+GL,PTFE,E
304 OL346,MV106,R569,1142C,12HR,F-12.8,PTFE,E
305 PL320,MV106,R569,1142C,12HR,F-12.8,PTFE,E
306 CPX97,MV106,R569,1142C,12HR,F-12.8,PTFE,E
307 GL107,MV106,R470,1151C,17HR,F-8.4,+OL+CPX+PL+SPMT+GL,PTFE,E
308 OL75,MV106,R470,1151C,17HR,F-8.4,PTFE,E

	309	310	311	312	313	314	315	316	317	318	319
SiO2	50.16	48.54	46.53	38.84	47.93	46.56	39.51	50.17	49.28	46.78	39.25
TiO2	0.25	1.99	3.97	0.17	2.20	3.90	0.12	0.18	1.61	3.72	nd
Al2O3	30.23	4.42	13.12	0.30	4.65	12.55	nd	29.81	4.69	13.08	nd
Fe2O3	nd	nd	0.40	nd	nd	2.85	nd	nd	nd	2.63	nd
Cr2O3	nd	0.30	nd	nd	0.31	nd	nd	nd	0.65	nd	nd
FeO	0.79	7.04	11.04	21.50	7.17	9.27	18.82	0.79	6.02	9.26	18.37
MnO	nd	0.14	0.13	0.27	0.13	0.19	0.27	nd	nd	0.14	0.44
NiO	nd	nd	nd	0.22	nd	nd	0.38	nd	nd	nd	0.39
MgO	0.14	13.69	6.21	38.43	13.56	6.61	40.31	nd	14.44	6.64	40.64
CaO	14.27	22.19	11.62	0.70	22.56	11.38	0.79	13.95	21.85	11.54	0.48
Na2O	3.02	nd	2.30	nd	nd	2.34	nd	3.23	nd	2.24	nd
K2O	0.17	nd	0.76	nd	nd	0.75	nd	0.21	nd	0.66	nd
P2O5	nd	nd	0.63	nd	nd	0.49	nd	nd	nd	nd	nd
total=	99.03	98.31	96.71	100.43	98.51	96.89	100.20	98.34	98.54	96.69	99.57
Mg#	-	-	50.1	76.1	-	56.0	79.2	-	-	56.1	79.8
An	71.6	-	-	-	-	-	-	69.6	-	-	-

309 PL98,MV106,R470,1151C,17HR,F-8.4,PTFE,E
310 CPX46,MV106,R470,1151C,17HR,F-8.4,PTFE,E
311 GL592R,MV106,R567,1156C,12HR,F-12.5,+OL+CPX+PL+GL,PTFE,E
312 OL199,MV106,R567,1156C,12HR,F-12.5,PTFE,E
313 CPX68,MV106,R567,1156C,12HR,F-12.5,PTFE,E
314 GL414,MV106,R587,1158C,19HR,F-8.2,+OL+CPX+PL+SPMT+GL,PTFE,E
315 OL137,MV106,R587,1158C,19HR,F-8.2,PTFE,E
316 PL170,MV106,R587,1158C,19HR,F-8.2,PTFE,E
317 CPX48,MV106,R587,1158C,19HR,F-8.2,PTFE,E
318 GL14,MV106,R450,1166C,6.5HR,F-8.2,+OL+PL+SPMT+GL,PTFE,E
319 OL13,MV106,R450,1166C,6.5HR,F-8.2,PTFE,E

	320	321	322	323	324	325	326	327	328	329	330
SiO2	38.85	50.31	47.33	39.23	51.14	47.21	40.12	50.36	1.04	47.14	39.39
TiO2	0.14	0.23	3.58	0.17	0.28	3.44	nd	0.18	3.60	3.25	0.12
Al2O3	nd	30.22	13.65	nd	29.90	14.09	nd	30.12	23.22	14.56	nd
Fe2O3	nd	nd	0.36	nd	nd	2.53	nd	nd	10.81	0.34	nd
Cr2O3	nd	nd	0.12	nd	nd	nd	nd	nd	26.82	0.04	nd
FeO	18.41	0.72	10.35	19.14	0.69	9.04	17.05	0.87	21.89	10.09	17.67
MnO	0.20	nd	0.15	0.32	nd	0.17	0.19	nd	nd	0.17	0.18
NiO	0.22	nd	nd	0.26	nd	nd	0.38	nd	nd	nd	0.20
MgO	40.95	nd	6.69	40.76	0.35	7.16	42.40	0.32	11.87	7.22	42.02
CaO	0.56	14.59	11.67	0.56	14.10	11.47	0.44	14.19	nd	11.37	0.47
Na2O	nd	3.01	2.19	nd	3.07	2.26	nd	3.15	nd	2.23	nd
K2O	nd	0.23	0.64	nd	0.18	0.66	nd	0.24	nd	0.63	nd
P2O5	nd	nd	0.55	nd	nd	nd	nd	nd	nd	0.35	nd
V2O3	nd	nd	nd	nd	nd	nd	nd	nd	0.33	nd	nd
total=	99.33	99.31	97.28	100.44	99.71	98.03	100.58	99.43	99.58	97.39	100.05
Mg#	79.9	-	53.5	79.1	-	58.5	81.6	-	49.1	56.1	80.9
An	-	71.8	-	-	71.0	-	-	70.3	-	-	-

320 OL14,MV106,R450,1166C,6.5HR,F-8.2,PTFE,E
321 PL5,MV106,R450,1166C,6.5HR,F-8.2,PTFE,E
322 GL1046,MV106,R565,1171C,11.5HR,F-12.3,+OL+PL+GL,PTFE,E
323 OL342,MV106,R565,1171C,11.5HR,F-12.3,PTFE,E
324 PL315,MV106,R565,1171C,11.5HR,F-12.3,PTFE,E
325 GL49,MV106,R449,1177C,14.5HR,F-8.0,+OL+PL+SPMT+GL,PTFE,E
326 OL22,MV106,R449,1177C,14.5HR,F-8.0,PTFE,E
327 PL7,MV106,R449,1177C,14.5HR,F-8.0,PTFE,E
328 SPMT8,MV106,R449,1177C,14.5HR,F-8.0,PTFE,E
329 GL975,MV106,R563,1185C,15HR,F-12.1,+OL+PL+GL,PTFE,E
330 OL320,MV106,R563,1185C,15HR,F-12.1,PTFE,E

	331	332	333	334	335	336	337	338	339	340	341
SiO2	50.38	47.53	39.23	49.93	0.89	46.48	39.17	47.16	39.85	49.33	46.94
TiO2	0.22	3.27	nd	0.16	3.80	2.70	nd	2.88	nd	0.22	2.82
Al2O3	30.97	14.25	nd	30.94	30.40	15.68	nd	15.34	nd	30.78	15.23
Fe2O3	nd	2.48	nd	nd	10.95	0.33	nd	2.33	nd	nd	2.22
Cr2O3	nd	0.04	nd	nd	18.60	nd	nd	0.08	nd	nd	0.05
FeO	0.68	8.96	16.89	0.92	20.22	10.57	17.89	8.53	15.32	1.10	8.38
MnO	nd	0.14	0.25	nd	0.28	0.20	0.20	0.13	0.16	nd	nd
NiO	nd	nd	0.27	nd	nd	nd	nd	nd	0.52	nd	nd
MgO	nd	7.25	42.26	nd	13.36	7.34	42.48	7.81	43.80	0.51	7.86
CaO	14.37	11.39	0.34	14.66	nd	11.46	0.48	11.24	0.51	15.37	11.27
Na2O	2.93	2.27	nd	2.85	nd	2.12	nd	2.11	nd	2.51	2.34
K2O	0.17	0.58	nd	0.13	nd	0.62	nd	0.56	nd	0.14	0.58
P2O5	nd	nd	nd	nd	nd	0.20	nd	nd	nd	nd	nd
V2O3	nd	nd	nd	nd	0.39	nd	nd	nd	nd	nd	nd
total=	99.72	98.16	99.24	99.59	98.89	97.70	100.22	98.17	100.16	99.96	97.69
Mg#	-	59.1	81.7	-	54.1	55.3	80.9	62.0	83.6	-	62.6
An	72.3	-	-	73.4	-	-	-	-	-	76.5	-

331 PL306,MV106,R563,1185C,15HR,F-12.1,PTFE,E
332 GL24R,MV106,R447,1191C,5HR,F-7.8,+OL+PL+SPMT+GL,PTFE,E
333 OL13,MV106,R447,1191C,5HR,F-7.8,PTFE,E
334 PL4R,MV106,R447,1191C,5HR,F-7.8,PTFE,E
335 SPMT5R,MV106,R447,1191C,5HR,F-7.8,PTFE,E
336 GL958,MV106,R562,1199C,20HR,F-11.9,+OL+PL+GL,PTFE,E
337 OL316,MV106,R562,1199C,20HR,F-11.9,PTFE,E
338 GL16,MV106,R446,1200C,6.5HR,F-7.6,+OL+PL+SPMT+GL,PTFE,E
339 OL9,MV106,R446,1200C,6.5HR,F-7.6,PTFE,E
340 PL3R,MV106,R446,1200C,6.5HR,F-7.6,PTFE,E
341 GL37,MV106,R445,1207C,3HR,F-7.6,+OL+PL+SPMT+GL,PTFE,E

	342	343	344	345	346	347	348	349	350	351	352
SiO2	40.16	40.05	46.98	40.39	39.85	46.28	39.58	46.36	39.94	39.40	46.84
TiO2	0.12	nd	2.78	nd	nd	2.84	nd	2.78	nd	nd	2.74
Al2O3	nd	nd	15.29	nd	nd	15.49	nd	14.90	nd	nd	15.29
Fe2O3	nd	nd	2.39	nd	nd	0.31	nd	2.27	nd	nd	0.30
Cr2O3	nd	nd	nd	nd	nd	nd	nd	nd	nd	nd	0.05
FeO	15.13	14.73	8.50	14.19	14.60	10.11	16.09	8.79	14.06	13.95	9.96
MnO	0.26	0.18	0.12	0.26	0.16	0.14	0.24	0.13	0.16	0.18	0.16
NiO	0.41	0.45	nd	0.46	0.48	nd	0.36	nd	0.61	0.25	nd
MgO	44.15	44.16	8.21	44.73	44.53	8.08	43.84	8.68	44.83	44.89	8.52
CaO	0.52	0.47	11.21	0.40	0.41	11.25	0.43	11.02	0.42	0.49	11.23
Na2O	nd	nd	2.31	nd	nd	2.17	nd	2.13	nd	nd	1.93
K2O	nd	nd	0.53	nd	nd	0.55	nd	0.49	nd	nd	0.52
P2O5	nd	nd	nd	nd	nd	0.29	nd	nd	nd	nd	0.33
total=	100.75	100.04	98.32	100.43	100.03	97.51	100.54	97.55	100.02	99.16	97.87
Mg#	83.9	84.2	63.3	84.9	84.5	58.8	82.9	63.8	85.0	85.2	60.4

342 OL13,MV106,R445,1207C,3HR,F-7.6,PTFE,E
343 OL14,MV106,R445,1207C,3HR,F-7.6,PTFE,E
344 GL22,MV106,R444,1211C,6HR,F-7.4,+OL+SPMT+GL,PTFE,E
345 OL7,MV106,R444,1211C,6HR,F-7.4,PTFE,E
346 OL8,MV106,R444,1211C,6HR,F-7.4,PTFE,E
347 GL599,MV106,R568,1214C,5HR,F-11.8,+OL+GL,PTFE,E
348 OL201,MV106,R568,1214C,5HR,F-11.8,PTFE,E
349 GL15,MV106,R443,1222C,7HR,F-7.4,+OL+SPMT+GL,PTFE,E
350 OL10,MV106,R443,1222C,7HR,F-7.4,PTFE,E
351 OL11,MV106,R443,1222C,7HR,F-7.4,PTFE,E
352 GL580,MV106,R566,1227C,5HR,F-11.6,+OL+GL,PTFE,E

	353	354	355	356	357	358	359	360	361	362	363
SiO2	40.31	46.55	40.30	46.87	39.99	45.98	39.91	46.82	40.28	46.43	47.14
TiO2	nd	2.83	nd	2.70	0.16	2.72	nd	2.66	nd	2.71	2.73
Al2O3	nd	15.03	nd	15.23	nd	14.72	0.16	15.07	nd	14.60	14.82
Fe2O3	nd	2.22	nd	0.27	nd	2.26	nd	0.27	nd	2.13	2.14
Cr2O3	nd	nd	nd	0.07	nd	0.07	nd	0.04	nd	nd	0.15
FeO	15.36	8.47	13.30	9.26	14.20	8.45	13.00	8.84	12.58	8.48	8.08
MnO	nd	0.11	0.14	nd	0.22	0.05	0.12	0.12	0.16	0.09	0.18
NiO	0.31	nd	0.57	nd	0.15	nd	0.50	nd	nd	nd	nd
MgO	44.73	8.93	45.03	9.13	45.69	9.31	45.53	9.74	45.98	9.80	9.88
CaO	0.48	11.05	0.52	11.02	0.44	10.69	0.43	10.98	0.39	10.59	10.76
Na2O	nd	2.10	nd	1.79	nd	1.93	nd	1.74	nd	2.01	2.08
K2O	nd	0.47	nd	0.57	nd	0.43	nd	0.57	nd	0.51	0.52
P2O5	nd	nd	nd	0.41	nd	nd	nd	0.15	nd	nd	nd
total=	101.19	97.76	99.86	97.32	100.85	96.61	99.65	97.00	99.39	97.35	98.48
Mg#	83.8	65.3	85.8	63.7	85.2	66.3	86.2	66.3	86.7	67.3	68.5

353 OL194,MV106,R566,1227C,5HR,F-11.6,PTFE,E
354 GL11,MV106,R442,1236C,6HR,F-7.2,+OL+SPMT+GL,SPT,E
355 OL6,MV106,R442,1236C,6HR,F-7.2,SPT,E
356 GL994,MV106,R564,1240C,4.5HR,F-11.5,+OL+GL,PTFE,E
357 OL323,MV106,R564,1240C,4.5HR,F-11.5,PTFE,E
358 GL8,MV106,R441,1245C,6HR,F-7.0,+OL+SPMT+GL,SPT,E
359 OL8,MV106,R441,1245C,6HR,F-7.0,SPT,E
360 GL302,MV106,R561,1255C,15.5HR,F-11.2,+OL+GL,PTFE,E
361 OL105,MV106,R561,1255C,15.5HR,F-11.2,PTFE,E
362 GL21,MV106,R440,1256C,6.5HR,F-7.0,+SPMT+GL,SPT,E
363 GL13,MV106,R439,1266C,7.5HR,F-6.8,-GL,PT,E

	364	365	366	367	368	369	370	371	372	373	374
SiO2	46.73	45.57	46.22	49.88	49.71	39.04	39.12	38.87	52.47	51.03	50.22
TiO2	2.69	2.67	2.64	2.83	3.12	0.14	nd	nd	0.26	1.26	1.45
Al2O3	14.49	14.62	14.51	15.97	13.89	0.21	0.16	0.21	28.56	3.66	3.83
Fe2O3	0.30	2.10	0.30	0.06	2.76	nd	nd	nd	nd	nd	nd
Cr2O3	nd	nd	0.16	nd	0.06	nd	nd	nd	nd	0.79	0.23
FeO	10.06	8.79	10.87	4.61	8.91	23.44	23.32	23.24	1.27	7.02	8.25
MnO	0.12	0.16	0.18	0.24	0.07	0.40	0.37	0.25	nd	nd	nd
NiO	nd	nd	nd	nd	nd	0.31	0.47	0.40	nd	nd	0.19
MgO	9.82	9.72	9.43	10.16	4.33	36.92	37.28	36.04	nd	14.30	14.57
CaO	10.85	10.51	10.66	11.70	9.04	0.62	0.56	0.78	13.11	21.81	20.75
Na2O	1.77	2.21	1.65	1.22	3.65	nd	nd	nd	3.66	nd	0.25
K2O	0.58	0.51	0.53	0.61	1.74	nd	nd	nd	0.34	nd	nd
P2O5	0.09	0.53	0.17	nd	nd	nd	nd	nd	nd	nd	nd
total=	97.50	97.39	97.32	97.28	97.28	101.08	101.28	99.79	99.67	99.87	99.74
Mg#	63.5	66.3	60.7	79.7	46.4	73.7	74.0	73.4	-	-	-
An	-	-	-	-	-	-	-	-	65.1	-	-

364 GL296,MV106,R560,1270C,5HR,F-11.1,-GL,PTFE,E
365 GL2023,MV106,R5-729,1284C,5HR,F-6.8,-GL,SPT,W
366 GL1033,MV106,R558,1299C,3HR,F-10.9,-GL,PTFE,E
367 GL1039,MV106,R557,1300C,13HR,F-12.5,+ML-GL,PTFE,E,
368 GL90,MV164,R469,1127C,5HR,F-8.7,+OL+CPX+PL+SPMT+GL,PTFE,E
369 OL59,MV164,R469,1127C,5HR,F-8.7,PTFE,E
370 OL60,MV164,R469,1127C,5HR,F-8.7,PTFE,E
371 OL62,MV164,R469,1127C,5HR,F-8.7,PTFE,E
372 PL80,MV164,R469,1127C,5HR,F-8.7,PTFE,E
373 CPX39,MV164,R469,1127C,5HR,F-8.7,PTFE,E
374 CPX40,MV164,R469,1127C,5HR,F-8.7,PTFE,E

	375	376	377	378	379	380	381	382	383	384	385
SiO2	51.64	1.24	49.65	38.87	38.94	38.81	53.23	52.83	52.59	51.54	51.73
TiO2	1.26	6.31	2.86	nd	nd	nd	0.22	0.23	nd	1.09	1.03
Al2O3	2.85	14.44	14.28	nd	nd	nd	28.77	28.08	28.30	2.13	2.00
Fe2O3	nd	16.25	2.64	nd	nd	nd	nd	nd	nd	nd	nd
Cr2O3	0.25	22.07	nd	nd	nd	nd	nd	nd	nd	0.32	0.26
FeO	8.30	28.56	8.66	22.25	22.25	22.07	0.92	0.77	0.94	7.11	7.17
MnO	0.13	0.29	0.19	0.27	0.32	0.30	nd	nd	nd	0.18	nd
NiO	nd	nd	nd	0.49	0.37	0.47	nd	nd	nd	nd	nd
MgO	14.09	7.67	4.87	37.98	38.21	37.83	nd	nd	nd	14.90	15.03
CaO	21.01	nd	9.31	0.51	0.47	0.48	12.26	12.14	12.32	21.92	21.73
Na2O	nd	nd	3.71	nd	nd	nd	4.07	4.21	4.10	nd	nd
K2O	nd	nd	1.66	nd	nd	nd	0.32	0.36	0.34	nd	nd
V2O3	nd	0.54	nd	nd	nd	nd	nd	nd	nd	nd	nd
total=	99.53	97.37	97.83	100.37	100.56	99.96	99.79	98.62	98.59	99.19	98.95
Mg#	-	32.4	50.1	75.3	75.4	75.3	-	-	-	-	-
An	-	-	-	-	-	-	61.3	60.1	61.2	-	-

375 CPX41,MV164,R469,1127C,5HR,F-8.7,PTFE,E
376 SPMT5,MV164,R469,1127C,5HR,F-8.7,PTFE,E
377 GL104,MV164,R468,1140C,19HR,F-8.5,+OL+CPX+PL+SPMT+GL,PTFE,E
378 OL101,MV164,R468,1140C,19HR,F-8.5,PTFE,E
379 OL102,MV164,R468,1140C,19HR,F-8.5,PTFE,E
380 OL103,MV164,R468,1140C,19HR,F-8.5,PTFE,E
381 PL101,MV164,R468,1140C,19HR,F-8.5,PTFE,E
382 PL106,MV164,R468,1140C,19HR,F-8.5,PTFE,E
383 PL108,MV164,R468,1140C,19HR,F-8.5,PTFE,E
384 CPX101,MV164,R468,1140C,19HR,F-8.5,PTFE,E
385 CPX102,MV164,R468,1140C,19HR,F-8.5,PTFE,E

	386	387	388	389	390	391	392	393	394	395	396
SiO2	50.21	51.40	50.68	0.26	0.42	0.47	0.28	49.40	39.00	51.61	49.26
TiO2	1.63	1.07	1.27	5.64	6.13	7.40	2.38	2.38	nd	0.33	2.34
Al2O3	3.84	3.17	2.95	13.73	12.82	10.41	24.67	14.76	nd	29.09	15.06
Fe2O3	nd	nd	nd	18.20	17.84	19.72	11.37	2.36	nd	nd	2.35
Cr2O3	0.53	0.73	0.50	25.09	25.05	22.52	27.19	nd	nd	nd	0.08
FeO	7.55	7.24	7.14	26.16	26.90	28.40	22.87	8.36	19.29	1.16	8.20
MnO	0.18	0.15	nd	0.22	nd	nd	nd	0.17	0.39	nd	0.20
NiO	nd	0.23	nd	nd	nd	nd	nd	nd	0.30	nd	nd
MgO	13.58	15.04	14.61	8.07	8.04	7.45	9.91	5.29	40.57	0.23	5.69
CaO	21.73	21.39	21.47	nd	nd	nd	nd	9.81	0.47	12.90	9.84
Na2O	nd	nd	0.34	nd	nd	nd	nd	3.52	nd	3.79	3.49
K2O	nd	nd	nd	nd	nd	nd	nd	1.42	nd	0.22	1.35
P2O5	nd	nd	nd	nd	nd	nd	nd	0.15	nd	nd	0.11
V2O3	nd	nd	nd	0.52	0.56	0.73	0.44	nd	nd	nd	nd
total=	99.25	100.42	98.96	97.89	97.76	97.10	99.11	97.62	100.02	99.33	97.97
Mg#	-	-	-	35.5	34.8	31.9	43.6	53.0	78.9	-	55.3
An	-	-	-	-	-	-	-	-	-	64.4	-

386 CPX104,MV164,R468,1140C,19HR,F-8.5,PTFE,E
387 CPX105,MV164,R468,1140C,19HR,F-8.5,PTFE,E
388 CPX106,MV164,R468,1140C,19HR,F-8.5,PTFE,E
389 SPMT100,MV164,R468,1140C,19HR,F-8.5,PTFE,E
390 SPMT101,MV164,R468,1140C,19HR,F-8.5,PTFE,E
391 SPMT102,MV164,R468,1140C,19HR,F-8.5,PTFE,E
392 SPMT103,MV164,R468,1140C,19HR,F-8.5,PTFE,E
393 GL703,MV164,R467,1151C,16HR,F-8.4,+OL+CPX+PL+SPMT+GL,PTFE,E
394 OL228,MV164,R467,1151C,16HR,F-8.4,PTFE,E
395 PL242,MV164,R467,1151C,16HR,F-8.4,PTFE,E
396 GL559,MV164,R466,1161C,16HR,F-8.2,+OL+PL+SPMT+GL,PTFE,E

	397	398	399	400	401	402	403	404	405	406	407
SiO2	39.35	51.32	49.35	39.73	48.60	39.13	48.95	39.33	0.97	48.36	39.46
TiO2	0.13	0.22	2.09	nd	2.10	nd	2.07	nd	1.77	2.09	0.12
Al2O3	nd	28.79	15.51	nd	15.60	nd	15.48	nd	26.39	15.38	nd
Fe2O3	nd	nd	2.25	nd	2.34	nd	2.30	nd	10.11	2.35	nd
Cr2O3	nd	nd	nd	nd	nd	nd	nd	nd	27.14	0.08	nd
FeO	18.98	1.23	8.04	16.90	8.26	18.14	8.31	17.51	19.86	8.58	16.88
MnO	0.25	nd	0.08	0.18	0.17	0.34	0.16	0.20	nd	0.11	0.22
NiO	0.45	nd	nd	0.44	nd	0.35	nd	0.54	nd	nd	0.73
MgO	40.93	nd	6.09	42.04	5.84	41.81	6.21	42.44	12.22	6.75	42.88
CaO	0.50	13.26	9.82	0.47	9.72	0.43	9.69	0.43	nd	9.64	0.51
Na2O	nd	3.60	3.39	nd	3.46	nd	3.47	nd	nd	3.14	nd
K2O	nd	0.34	1.25	nd	1.36	nd	1.25	nd	nd	1.20	nd
P2O5	nd	nd	0.14	nd	nd	nd	0.14	nd	nd	0.18	nd
V2O3	nd	nd	nd	nd	nd	nd	nd	nd	0.30	nd	nd
total=	100.59	98.76	98.01	99.76	97.45	100.20	98.03	100.45	98.76	97.86	100.80
Mg#	79.4	-	57.4	81.6	55.8	80.4	57.1	81.2	52.3	58.4	81.9
An	-	65.7	-	-	-	-	-	-	-	-	-

397 OL185R,MV164,R466,1161C,16HR,F-8.2,PTFE,E
398 PL211R,MV164,R466,1161C,16HR,F-8.2,PTFE,E
399 GL533,MV164,R464,1174C,19HR,F-8,+OL+PL+SPMT+GL,PTFE,E
400 OL176,MV164,R464,1174C,19HR,F-8,PTFE,E
401 GL550,MV164,R465,1174C,16HR,F-8.0,+OL+PL+SPMT+GL,PTFE,E
402 OL181,MV164,R465,1174C,16HR,F-8.0,PTFE,E
403 GL529,MV164,R463,1183C,5.5HR,F-7.9,+OL+SPMT+GL,PTFE,E
404 OL174,MV164,R463,1183C,5.5HR,F-7.9,PTFE,E
405 SPMT35,MV164,R463,1183C,5.5HR,F-7.9,PTFE,E
406 GL521,MV164,R462,1196C,5HR,F-7.7,+OL+SPMT+GL,PTFE,E
407 OL171,MV164,R462,1196C,5HR,F-7.7,PTFE,E

	408	409	410	411	412	413	414	415	416	417	418
SiO2	39.81	48.39	39.78	48.16	39.61	48.15	39.32	48.55	39.36	48.25	39.57
TiO2	0.16	1.90	0.11	1.99	nd	1.91	nd	2.02	nd	1.95	nd
Al2O3	nd	14.97	nd	15.07	nd	14.46	nd	14.56	nd	14.54	nd
Fe2O3	nd	2.32	nd	2.34	nd	2.49	nd	2.47	nd	2.41	nd
Cr2O3	nd	0.09	nd	nd	nd	0.05	nd	nd	nd	nd	nd
FeO	16.89	8.58	15.89	8.74	16.11	8.86	15.14	8.73	15.74	8.85	15.11
MnO	0.25	0.16	0.31	0.24	0.22	nd	0.27	0.18	0.24	0.08	0.16
NiO	0.61	nd	0.60	nd	0.45	nd	0.52	nd	0.40	nd	0.62
MgO	42.37	6.91	42.94	7.15	43.25	7.77	43.28	7.50	43.51	7.91	43.68
CaO	0.60	9.52	0.43	9.55	0.37	9.28	0.42	9.52	0.44	9.33	0.44
Na2O	nd	3.11	nd	3.32	nd	3.12	nd	3.24	nd	3.00	nd
K2O	nd	1.16	nd	1.22	nd	1.15	nd	1.19	nd	1.12	nd
P2O5	nd	0.14	nd	0.22	nd	nd	nd	nd	nd	nd	nd
total=	100.69	97.25	100.06	98.00	100.01	97.24	98.95	97.96	99.69	97.44	99.58
Mg#	81.7	58.9	82.8	59.3	82.7	61.0	83.6	60.5	83.1	61.4	83.7

408 OL172,MV164,R462,1196C,5HR,F-7.7,PTFE,E
409 GL608,MV164,R460,1204C,3HR,F-7.6,+OL+SPMT+GL,PTFE,E
410 OL203,MV164,R460,1204C,3HR,F-7.6,PTFE,E
411 GL619,MV164,R461,1208C,3HR,F-7.6,+OL+SPMT+GL,PTFE,E
412 OL204,MV164,R461,1208C,3HR,F-7.6,PTFE,E
413 GL85,MV164,R458,1212C,17HR,F-7.4,+OL+SPMT+GL,PTFE,E
414 OL14,MV164,R458,1212C,17HR,F-7.4,PTFE,E
415 GL73,MV164,R457,1223C,19HR,F-7.3,+OL+SPMT+GL,PTFE,E
416 OL12,MV164,R457,1223C,19HR,F-7.3,PTFE,E
417 GL46,MV164,R455,1233C,24HR,F-7.2,+OL+SPMT+GL,PTFE,E
418 OL7,MV164,R455,1233C,24HR,F-7.2,PTFE,E

	419	420	421	422	423	424	425	426	427	428	429
SiO2	48.19	39.58	48.30	40.14	39.67	48.18	40.21	39.66	48.44	40.07	40.46
TiO2	1.95	nd	1.97	nd	nd	2.01	nd	nd	2.01	nd	nd
Al2O3	14.38	nd	14.35	nd	nd	14.18	nd	nd	13.89	nd	nd
Fe2O3	2.44	nd	2.40	nd	nd	2.43	nd	nd	2.45	nd	nd
Cr2O3	nd	nd	nd	nd	nd	0.23	nd	nd	nd	nd	nd
FeO	8.96	15.09	8.98	14.81	14.73	9.20	14.04	14.39	9.11	13.41	13.33
MnO	0.20	0.26	0.16	0.19	0.22	0.11	0.18	0.16	0.20	0.23	0.20
NiO	nd	0.49	nd	0.58	0.69	nd	0.55	0.43	nd	0.57	0.64
MgO	8.09	43.32	8.49	44.30	43.88	8.80	44.74	44.63	9.64	44.90	45.33
CaO	9.35	0.40	9.11	0.38	0.40	9.01	0.40	0.40	8.90	0.31	0.39
Na2O	3.13	nd	3.05	nd	nd	3.13	nd	nd	2.99	nd	nd
K2O	1.13	nd	1.10	nd	nd	1.09	nd	nd	1.10	nd	nd
total=	97.82	99.14	97.91	100.40	99.59	98.37	100.12	99.67	98.73	99.49	100.35
Mg#	61.7	83.7	62.8	84.2	84.2	63.0	85.0	84.7	65.3	85.6	85.8

419 GL64,MV164,R456,1234C,17HR,F-7.2,+OL+SPMT+GL,PTFE,E
420 OL10,MV164,R456,1234C,17HR,F-7.2,PTFE,E
421 GL25,MV164,R454,1243C,16.5HR,F-7.1,+OL+SPMT+GL,PTFE,E
422 OL3,MV164,R454,1243C,16.5HR,F-7.1,PTFE,E
423 OL4,MV164,R454,1243C,16.5HR,F-7.1,PTFE,E
424 GL13,MV164,R453,1253C,8.5HR,F-7.0,+OL+SPMT+GL,PTFE,E
425 OL1,MV164,R453,1253C,8.5HR,F-7.0,PTFE,E
426 OL2,MV164,R453,1253C,8.5HR,F-7.0,PTFE,E
427 GL44,MV164,R452,1265C,16HR,F-6.8,+OL+SPMT+GL,PTFE,E
428 OL25,MV164,R452,1265C,16HR,F-6.8,PTFE,E
429 OL26,MV164,R452,1265C,16HR,F-6.8,PTFE,E

	430	431	432	433	434	435	436	437	438	439	440
SiO2	48.43	40.66	48.03	45.68	37.62	44.78	37.47	51.87	48.47	46.26	39.03
TiO2	2.09	nd	1.82	5.40	0.30	5.57	0.29	0.44	2.65	4.49	0.17
Al2O3	14.00	nd	13.64	14.39	nd	13.77	nd	29.47	4.67	13.97	nd
Fe2O3	2.55	nd	2.35	0.52	nd	0.51	nd	nd	nd	0.42	nd
Cr2O3	nd	nd	nd	nd	nd	nd	nd	nd	0.18	0.07	nd
FeO	9.31	13.29	9.39	11.89	27.49	12.23	26.11	1.07	7.73	10.99	21.51
MnO	0.16	0.17	0.18	0.20	0.41	0.19	0.39	nd	nd	0.20	0.17
NiO	nd	0.42	nd	nd	0.21	nd	0.30	nd	nd	nd	0.30
MgO	9.93	45.63	10.22	4.06	34.04	4.67	34.05	0.19	13.43	5.16	39.39
CaO	8.82	0.36	8.71	9.88	0.70	10.55	0.75	12.88	22.35	11.05	0.68
Na2O	2.94	nd	2.70	3.50	nd	3.17	nd	3.50	nd	2.98	nd
K2O	1.04	nd	1.00	2.14	nd	1.91	nd	0.59	nd	1.66	nd
P2O5	nd	nd	0.11	0.63	nd	0.60	nd	nd	nd	0.22	nd
total=	99.27	100.53	98.15	98.29	100.77	97.95	99.36	100.01	99.48	97.47	101.25
Mg#	65.5	86.0	66.0	37.8	68.8	40.5	69.9	-	-	45.6	76.5
An	-	-	-	-	-	-	-	64.7	-	-	-

430 GL32,MV164,R451,1277C,6.5HR,F-6.6,+OL+SPMT+GL,PTFE,E
431 OL22,MV164,R451,1277C,6.5HR,F-6.6,PTFE,E
432 GL367,MV164,R497,1288C,18HR,F-6.6,-GL,PTFE,E
433 GL922,MV166,R574,1113C,19HR,F-13.1,+OL+CPX+PL+IL+GL,PTFE,E
434 OL306,MV166,R574,1113C,19HR,F-13.1,PTFE,E
435 GL928,MV166,R573,1128C,16HR,F-13.0,+OL+CPX+PL+GL,PTFE,E
436 OL309,MV166,R573,1128C,16HR,F-13.0,PTFE,E
437 PL298,MV166,R573,1128C,16HR,F-13.0,PTFE,E
438 CPX90,MV166,R573,1128C,16HR,F-13.0,PTFE,E
439 GL506,MV166,R569,1142C,12HR,F-12.8,+OL+CPX+PL+GL,PTFE,E
440 OL168,MV166,R569,1142C,12HR,F-12.8,PTFE,E

	441	442	443	444	445	446	447	448	449	450	451
SiO2	48.13	45.03	38.55	49.72	47.05	46.69	45.02	38.39	49.98	47.73	46.95
TiO2	2.91	4.22	nd	0.21	2.87	2.39	4.26	nd	0.25	2.60	2.51
Al2O3	5.44	14.03	0.17	30.99	6.12	6.41	14.15	0.18	30.85	5.37	7.49
Fe2O3	nd	2.89	nd	nd	nd	nd	2.81	nd	nd	nd	nd
Cr2O3	0.43	nd	nd	nd	0.23	0.39	nd	nd	nd	0.24	0.60
FeO	7.08	9.60	20.35	0.51	7.72	6.95	9.23	20.28	0.71	7.43	6.66
MnO	0.11	0.16	0.27	nd	0.16	0.15	0.16	0.27	nd	0.17	0.12
NiO	0.14	nd	0.50	nd	nd	nd	nd	0.44	nd	nd	nd
MgO	13.22	5.63	39.16	0.12	12.48	13.15	5.56	39.15	0.13	13.09	12.12
CaO	22.17	11.29	0.59	13.84	20.98	21.48	11.01	0.71	13.91	21.33	21.57
Na2O	nd	3.28	nd	3.18	0.67	0.42	3.33	nd	3.22	0.52	0.63
K2O	nd	1.48	nd	0.33	nd	nd	1.57	nd	0.31	nd	nd
P2O5	nd	0.53	nd	nd	nd	nd	0.52	nd	nd	nd	nd
total=	99.63	98.14	99.59	98.90	98.28	98.03	97.62	99.42	99.36	98.48	98.65
Mg#	-	51.1	77.4	-	-	-	51.8	77.5	-	-	-
An	-	-	-	69.2	-	-	-	-	69.2	-	-

441 CPX64,MV166,R569,1142C,12HR,F-12.8,PTFE,E
442 GL2056,MV166,R5-725,1145C,15HR,F-8.6,+OL+CPX+PL+SPMT+GL,PTFE,W
443 OL906,MV166,R5-725,1145C,15HR,F-8.6,PTFE,W
444 PL901,MV166,R5-725,1145C,15HR,F-8.6,PTFE,W
445 CPX906,MV166,R5-725,1145C,15HR,F-8.6,PTFE,W
446 CPX907,MV166,R5-725,1145C,15HR,F-8.6,PTFE,W
447 GL2060,MV166,R5-725,1145C,15HR,F-8.6,+OL+CPX+PL+SPMT+GL,PT,W
448 OL907,MV166,R5-725,1145C,15HR,F-8.6,PT,W
449 PL900,MV166,R5-725,1145C,15HR,F-8.6,PT,W
450 CPX900,MV166,R5-725,1145C,15HR,F-8.6,PT,W
451 CPX901,MV166,R5-725,1145C,15HR,F-8.6,PT,W

	452	453	454	455	456	457	458	459	460	461	462
SiO2	45.90	39.14	38.90	49.44	48.97	45.03	39.21	46.67	46.69	47.58	45.40
TiO2	3.88	0.14	0.18	0.38	1.83	3.87	nd	2.62	2.75	2.72	3.59
Al2O3	14.33	nd	nd	30.95	5.08	14.28	0.15	6.48	6.01	5.28	14.54
Fe2O3	0.42	nd	nd	nd	nd	2.71	nd	nd	nd	nd	2.60
Cr2O3	0.04	nd	nd	nd	0.14	nd	nd	0.29	0.32	0.13	nd
FeO	11.02	22.71	21.47	0.89	7.71	9.09	18.41	7.35	7.20	7.53	8.77
MnO	0.17	0.44	0.17	nd	0.12	0.17	0.25	0.16	0.14	0.13	0.14
NiO	nd	0.33	0.41	nd	nd	nd	0.38	nd	nd	nd	nd
MgO	5.92	38.15	39.53	nd	13.81	6.05	41.24	12.77	12.81	12.88	6.52
CaO	12.12	0.59	0.79	14.80	21.54	11.91	0.65	21.89	22.06	21.41	12.10
Na2O	2.65	nd	nd	3.17	nd	3.07	nd	0.49	0.50	0.55	2.88
K2O	1.36	nd	nd	0.26	nd	1.33	nd	nd	nd	nd	1.23
P2O5	0.33	nd	nd	nd	nd	0.12	nd	nd	nd	nd	0.57
total=	98.14	101.50	101.45	99.89	99.20	97.63	100.29	98.72	98.48	98.21	98.34
Mg#	48.9	75.0	76.6	-	-	54.3	80.0	-	-	-	57.0
An	-	-	-	71.0	-	-	-	-	-	-	-

452 GL586,MV166,R567,1156C,12HR,F-12.5,+OL+CPX+PL+GL,PTFE,E
453 OL196,MV166,R567,1156C,12HR,F-12.5,PTFE,E
454 OL197,MV166,R567,1156C,12HR,F-12.5,PTFE,E
455 PL220,MV166,R567,1156C,12HR,F-12.5,PTFE,E
456 CPX67,MV166,R567,1156C,12HR,F-12.5,PTFE,E
457 GL2052,MV166,R5-726,1157C,12.5HR,F-8.4,+OL+CPX+PL+SPMT+GL,PTFE,W
458 OL904,MV166,R5-726,1157C,12.5HR,F-8.4,PTFE,W
459 CPX908,MV166,R5-726,1157C,12.5HR,F-8.4,PTFE,W
460 CPX909,MV166,R5-726,1157C,12.5HR,F-8.4,PTFE,W
461 CPX910,MV166,R5-726,1157C,12.5HR,F-8.4,PTFE,W
462 GL2048,MV166,R5-728,1167C,12HR,F-8.2,+OL+PL+SPMT+GL,SPT,W

	463	464	465	466	467	468	469	470	471	472	473
SiO2	39.52	45.97	39.20	46.62	48.77	45.37	39.18	46.38	39.67	45.70	39.83
TiO2	nd	3.64	0.11	0.38	0.26	3.52	nd	3.46	0.14	3.53	0.16
Al203	0.14	14.47	nd	31.33	30.58	14.42	nd	14.76	nd	14.34	nd
Fe203	nd	0.39	nd	nd	nd	2.75	nd	0.34	nd	2.80	nd
Cr203	nd	0.06	nd	nd	nd	nd	nd	nd	nd	0.16	nd
FeO	17.46	10.57	19.79	0.96	0.79	8.96	17.47	9.53	17.40	8.77	16.56
MnO	0.24	0.06	0.38	nd	nd	0.18	0.26	0.09	0.19	0.06	0.27
NiO	0.51	nd	0.37	nd	nd	nd	0.47	nd	nd	nd	0.40
MgO	42.38	6.30	40.09	0.39	nd	6.49	41.99	7.09	42.81	6.83	42.64
CaO	0.68	12.64	0.76	16.26	15.12	12.59	0.61	12.28	0.61	12.44	0.61
Na20	nd	2.58	nd	1.86	2.49	2.47	nd	2.46	nd	2.69	nd
K20	nd	1.17	nd	0.27	0.29	1.33	nd	1.08	nd	1.20	nd
P205	nd	0.31	nd	nd	nd	nd	nd	0.19	nd	nd	nd
total=	100.93	98.16	100.70	98.07	98.30	98.08	99.98	97.66	100.82	98.52	100.47
Mg#	81.2	51.5	78.3	-	-	56.4	81.1	57.0	81.4	58.1	82.1
An	-	-	-	81.5	75.7	-	-	-	-	-	-

463 OL903,MV166,R5-728,1167C,12HR,F-8.2,SPT,W
464 GL1052,MV166,R565,1171C,11.5HR,F-12.3,+OL+PL+GL,PTFE,E
465 OL343,MV166,R565,1171C,11.5HR,F-12.3,PTFE,E
466 PL317,MV166,R565,1171C,11.5HR,F-12.3,PTFE,E
467 PL318,MV166,R565,1171C,11.5HR,F-12.3,PTFE,E
468 GL15,MV166,R438,1176C,7HR,F-8.0,+OL+SP+GL,SPT,E
469 OL11,MV166,R438,1176C,7HR,F-8.0,SPT,E
470 GL981,MV166,R563,1185C,15HR,F-12.1,+OL+GL,PTFE,E
471 OL322,MV166,R563,1185C,15HR,F-12.1,PTFE,E
472 GL115,MV166,R434,1185C,12HR,F-7.8,+OL+SPMT+GL,SPT,E
473 OL105,MV166,R434,1185C,12HR,F-7.8,SPT,E

	474	475	476	477	478	479	480	481	482	483	484
SiO2	45.23	39.51	45.98	39.37	45.28	39.99	40.11	45.59	38.83	39.04	38.82
TiO2	3.43	nd	3.36	nd	3.36	nd	nd	3.45	nd	nd	nd
Al203	13.97	nd	14.52	nd	13.93	nd	nd	13.84	0.09	0.11	0.08
Fe203	2.75	nd	0.36	nd	2.81	nd	nd	0.40	nd	nd	nd
Cr203	0.09	nd	nd	nd	nd	nd	nd	0.12	0.06	0.07	0.08
FeO	8.90	15.97	10.40	17.66	9.25	15.09	15.32	11.59	17.74	18.28	17.83
MnO	0.13	0.21	0.06	0.27	0.13	0.18	0.18	0.19	0.21	0.23	0.24
NiO	nd	0.47	nd	0.21	nd	0.57	0.72	nd	0.23	0.24	0.29
MgO	7.38	41.95	7.49	41.99	7.86	44.04	43.80	7.70	42.23	42.28	42.28
CaO	12.23	0.49	11.98	0.58	11.99	0.54	0.62	12.23	0.47	0.52	0.57
Na20	2.84	nd	2.16	nd	2.67	nd	nd	2.40	nd	nd	nd
K20	1.19	nd	0.98	nd	1.16	nd	nd	1.06	nd	nd	nd
P205	nd	nd	0.25	nd	nd	nd	nd	0.26	nd	nd	nd
total=	98.14	98.60	97.54	100.08	98.44	100.41	100.75	98.83	99.86	100.77	100.19
Mg#	59.6	82.4	56.2	80.9	60.2	83.9	83.6	54.2	80.9	80.5	80.9

474 GL12,MV166,R436,1197C,8HR,F-7.7,+OL+SPMT+GL,SPT,E
475 OL8,MV166,R436,1197C,8HR,F-7.7,SPT,E
476 GL960,MV166,R562,1199C,20HR,F-11.9,+OL+GL,PTFE,E
477 OL317,MV166,R562,1199C,20HR,F-11.9,PTFE,E
478 GL12,MV166,R437,1211C,6HR,F-7.5,+OL+SPMT+GL,SPT,E
479 OL7,MV166,R437,1211C,6HR,F-7.5,SPT,E
480 OL8R,MV166,R437,1211C,6HR,F-7.5,SPT,E
481 GL499,MV166,R568,1214C,5HR,F-11.8,+OL+GL,PTFE,E
482 OL504,MV166,R568,1214C,5HR,F-11.8,PTFE,W
483 OL505,MV166,R568,1214C,5HR,F-11.8,PTFE,W
484 OL506,MV166,R568,1214C,5HR,F-11.8,PTFE,W

	485	486	487	488	489	490	491	492	493	494	495
SiO2	45.45	39.70	46.19	40.57	40.34	45.47	39.29	45.80	40.60	45.65	39.72
TiO2	3.34	0.16	3.54	0.13	nd	3.37	0.14	3.30	0.13	3.16	nd
Al203	13.80	nd	13.59	nd	nd	13.98	nd	13.64	nd	13.65	nd
Fe203	2.82	nd	2.84	nd	nd	0.37	nd	2.73	nd	0.34	nd
Cr203	0.04	nd	0.09	nd	nd	0.23	nd	0.05	nd	0.05	nd
FeO	9.19	15.44	8.91	15.75	15.83	10.99	17.00	8.97	13.76	10.45	15.98
MnO	0.18	0.17	0.11	0.19	0.17	0.08	0.21	0.13	0.24	0.15	0.24
NiO	nd	0.49	nd	0.42	0.37	nd	0.24	nd	0.42	nd	0.29
MgO	8.26	44.13	8.50	43.24	43.58	8.08	43.46	8.86	45.02	8.83	44.19
CaO	11.87	0.40	12.17	0.55	0.54	11.95	0.55	11.67	0.64	11.63	0.49
Na20	2.53	nd	2.32	nd	nd	2.17	nd	2.60	nd	2.28	nd
K20	1.13	nd	1.04	nd	nd	1.04	nd	1.16	nd	0.97	nd
P205	nd	nd	nd	nd	nd	0.31	nd	nd	nd	0.07	nd
total=	98.61	100.49	99.30	100.85	100.83	98.04	100.89	98.91	100.81	97.23	100.91
Mg#	61.6	83.6	63.0	83.0	83.1	56.7	82.0	63.8	85.4	60.1	83.1

485 GL3,MV166,R429,1223C,6HR,F-7.3,+OL+SPMT+GL,PTFE,E
486 OL3,MV166,R429,1223C,6HR,F-7.3,PTFE,E
487 GL12,MV166,R428,1226C,8HR,F-7.2,+OL+SPMT+GL,PTFE,E
488 OLX10,MV166,R428,1226C,8HR,F-7.2,PTFE,E
489 OLX9,MV166,R428,1226C,8HR,F-7.2,PTFE,E
490 GL582,MV166,R566,1227C,5HR,F-11.6,+OL+GL,PTFE,E
491 OL195,MV166,R566,1227C,5HR,F-11.6,PTFE,E
492 GL105R,MV166,R433,1232C,6.5HR,F-7.2,+OL+SPMT+GL,PT,E
493 OL101,MV166,R433,1232C,6.5HR,F-7.2,PT,E
494 GL993,MV166,R564,1240C,4.5HR,F-11.5,+OL+GL,PTFE,E
495 OL324,MV166,R564,1240C,4.5HR,F-11.5,PTFE,E

	496	497	498	499	500	501	502	503	504	505	506
SiO2	45.55	40.82	44.53	40.21	46.47	39.99	40.59	44.83	45.88	39.96	44.38
TiO2	3.32	nd	3.35	0.15	3.31	0.14	0.17	3.30	3.17	0.13	3.24
Al2O3	13.15	nd	13.22	nd	13.59	nd	nd	13.44	13.30	nd	13.07
Fe2O3	2.88	nd	2.78	nd	0.32	nd	nd	2.84	0.34	nd	2.54
Cr2O3	0.26	nd	nd	nd	0.04	nd	nd	0.15	0.15	nd	nd
FeO	9.25	13.37	9.23	14.80	9.63	13.88	13.29	9.66	10.45	14.40	9.37
MnO	0.23	0.15	0.15	0.20	0.19	0.28	0.19	nd	0.22	0.12	0.18
NiO	nd	0.75	nd	0.51	nd	nd	nd	nd	nd	0.36	nd
MgO	9.08	45.23	9.16	44.36	9.66	45.08	45.49	9.93	9.91	44.41	10.10
CaO	11.39	0.56	11.60	0.50	11.58	0.61	0.47	11.36	11.44	0.48	11.00
Na2O	2.46	nd	2.60	nd	1.63	nd	nd	2.34	1.86	nd	2.47
K2O	1.11	nd	1.04	nd	0.81	nd	nd	0.95	0.93	nd	1.04
P2O5	nd	nd	0.33	nd	nd	nd	nd	nd	0.11	nd	0.16
total=	98.68	100.88	97.99	100.73	97.23	99.98	100.20	98.80	97.76	99.86	97.55
Mg#	63.6	85.8	63.9	84.2	64.1	85.3	85.9	64.7	62.8	84.6	65.8

496 GL4,MV166,R427,1243C,5HR,F-7.0,+OL+SP+GL,PT,E
497 OLX2,MV166,R427,1243C,5HR,F-7.0,PT,E
498 GL2092,MV166,R426,1250C,5HR,F-7.0,+OL+SPMT+GL,PT,W
499 OL224,MV166,R426,1250C,5HR,F-7.0,PT,E
500 GL299,MV166,R561,1255C,15.5HR,F-11.2,+OL+GL,PTFE,E
501 OL103,MV166,R561,1255C,15.5HR,F-11.2,PTFE,E
502 OL104,MV166,R561,1255C,15.5HR,F-11.2,PTFE,E
503 GL13,MV166,R425,1263C,7.5HR,F-6.8,+OL+SP+GL,PT,E
504 GL294,MV166,R560,1270C,5HR,F-11.1,+OL+GL,PTFE,E
505 OL102,MV166,R560,1270C,5HR,F-11.1,PTFE,E
506 GL2027,MV166,R5-727,1271C,6.5HR,F-6.9,+SPMT+GL,SPT,W

	507	508	509	510	511	512	513	514	515	516	517
SiO2	46.61	46.13	44.21	44.37	43.94	45.81	37.56	50.69	46.21	38.43	38.46
TiO2	3.28	3.21	3.23	3.22	3.29	3.92	0.12	0.26	3.63	0.16	nd
Al2O3	13.35	13.59	13.06	13.03	12.69	13.72	nd	29.41	14.26	nd	nd
Fe2O3	0.30	0.30	2.52	2.54	2.70	3.44	nd	nd	3.04	nd	nd
Cr2O3	0.05	0.08	nd	nd	0.09	0.06	nd	nd	0.02	nd	nd
FeO	9.55	10.23	9.51	9.62	11.09	10.04	23.90	1.02	9.78	23.65	22.66
MnO	0.23	0.17	0.16	0.17	0.15	0.24	0.39	nd	0.23	0.37	0.38
NiO	nd	nd	nd	nd	nd	nd	0.41	nd	nd	0.45	0.36
MgO	10.27	10.52	10.12	10.18	11.29	4.42	35.63	nd	5.18	35.77	36.12
CaO	11.68	11.51	11.03	11.03	9.88	9.90	0.69	13.68	10.56	0.65	0.69
Na2O	1.25	1.55	2.51	2.48	2.60	3.68	nd	3.43	3.42	nd	nd
K2O	0.70	0.83	1.03	1.05	0.44	1.92	nd	0.34	1.61	nd	nd
P2O5	0.06	0.20	0.21	0.24	0.23	0.73	nd	nd	nd	nd	nd
total=	97.33	98.32	97.59	97.93	98.39	97.88	98.70	98.83	97.94	99.48	98.67
Mg#	65.7	64.7	65.5	65.3	64.5	44.0	72.7	-	48.6	72.9	74.0
An	-	-	-	-	-	-	-	67.4	-	-	-

507 GL290,MV166,R559,1284C,13HR,F-10.9,-GL,PTFE,E
508 GL1035,MV166,R558,1299C,3HR,F-10.9,-GL,PTFE,E
509 GL2022,MV166(1),R5-729,1284C,5HR,F-6.8,-GL,SPT,W
510 GL2019,MV166(2),R5-729,1284C,5HR,F-6.8,-GL,SPT,W
511 GL259,MV718,R580,1302C,2HR,F-6.6,-GL,PTFE,E
512 GL392R,MV703,R483,1122C,19.5HR,F-8.7,+OL+CPX+PL+SPMT+GL,PTFE,E
513 OL128,MV703,R483,1122C,19.5HR,F-8.7,PTFE,E
514 PL161,MV703,R483,1122C,19.5HR,F-8.7,PTFE,E
515 GL70,MV703,R482,1135C,6.5HR,F-8.6,+OL+CPX+PL+SPMT+GL,PTFE,E
516 OL45,MV703,R482,1135C,6.5HR,F-8.6,PTFE,E
517 OL46,MV703,R482,1135C,6.5HR,F-8.6,PTFE,E

	518	519	520	521	522	523	524	525	526	527	528
SiO2	48.39	49.99	48.60	47.86	49.10	48.27	48.62	49.54	46.17	38.82	50.46
TiO2	0.32	0.18	0.44	2.53	1.92	2.55	2.11	2.18	3.23	0.19	0.31
Al2O3	30.67	31.64	31.14	6.18	4.82	7.16	5.47	4.67	13.96	0.23	30.02
Fe2O3	nd	nd	nd	nd	nd	nd	nd	nd	2.88	nd	nd
Cr2O3	nd	nd	nd	0.64	0.40	nd	0.55	0.25	nd	nd	nd
FeO	1.29	0.71	1.30	7.35	7.08	7.49	6.63	7.62	9.27	20.11	1.06
MnO	nd	nd	nd	0.12	0.12	nd	nd	nd	0.21	0.38	nd
NiO	nd	nd	nd	nd	nd	nd	nd	nd	nd	0.35	nd
MgO	nd	nd	0.31	12.58	13.45	12.47	13.30	13.47	5.58	38.91	0.38
CaO	14.90	15.01	15.43	21.47	22.55	21.91	22.43	21.82	11.23	0.65	14.00
Na2O	2.40	2.58	2.35	nd	0.26	0.34	0.28	nd	3.13	nd	3.18
K2O	0.31	0.21	0.30	nd	nd	nd	nd	nd	1.43	nd	0.31
total=	98.28	100.32	99.87	98.73	99.70	100.19	99.39	99.55	97.09	99.64	99.72
Mg#	-	-	-	-	-	-	-	-	51.8	77.5	-
An	76.0	75.3	77.0	-	-	-	-	-	-	-	69.6

518 PL59R,MV703,R482,1135C,6.5HR,F-8.6,PTFE,E
519 PL65,MV703,R482,1135C,6.5HR,F-8.6,PTFE,E
520 PL66,MV703,R482,1135C,6.5HR,F-8.6,PTFE,E
521 CPX27,MV703,R482,1135C,6.5HR,F-8.6,PTFE,E
522 CPX28,MV703,R482,1135C,6.5HR,F-8.6,PTFE,E
523 CPX31,MV703,R482,1135C,6.5HR,F-8.6,PTFE,E
524 CPX32,MV703,R482,1135C,6.5HR,F-8.6,PTFE,E
525 CPX34,MV703,R482,1135C,6.5HR,F-8.6,PTFE,E
526 GL33,MV703,R481,1146C,20HR,F-8.4,+OL+CPX+PL+SPMT+GL,PTFE,E
527 OL21,MV703,R481,1146C,20HR,F-8.4,PTFE,E
528 PL38,MV703,R481,1146C,20HR,F-8.4,PTFE,E

	529	530	531	532	533	534	535	536	537	538	539
SiO2	49.22	48.05	46.60	39.26	47.85	46.63	39.81	47.65	46.01	39.34	48.79
TiO2	1.71	2.05	3.06	0.11	0.23	2.84	0.14	0.17	2.75	0.15	0.24
Al2O3	4.95	5.62	14.19	nd	31.57	14.58	nd	32.12	15.10	0.17	30.14
Fe2O3	nd	nd	2.86	nd	nd	2.77	nd	nd	2.43	nd	nd
Cr2O3	0.51	0.65	nd	nd	nd	0.04	nd	nd	nd	nd	nd
FeO	6.87	6.96	9.23	19.20	1.12	9.04	18.08	0.91	9.00	18.17	0.98
MnO	0.13	nd	0.18	0.20	nd	0.21	0.29	nd	0.17	0.29	nd
NiO	0.23	0.18	nd	0.50	nd	nd	0.45	nd	nd	0.51	nd
MgO	13.27	13.14	6.09	40.90	nd	6.24	41.36	nd	6.24	40.74	nd
CaO	21.82	21.52	11.81	0.63	16.39	11.54	0.58	16.19	11.77	0.68	15.10
Na2O	nd	0.53	2.94	nd	2.00	2.92	nd	2.17	2.89	nd	2.55
K2O	nd	nd	1.35	nd	0.22	1.25	nd	0.14	1.14	nd	0.21
P2O5	nd	nd	0.46	nd	nd	0.33	nd	nd	0.27	nd	nd
total=	98.71	98.70	98.77	100.80	99.38	98.39	100.71	99.35	97.77	100.05	98.01
Mg#	-	-	54.0	79.2	-	55.2	80.3	-	55.3	80.0	-
An	-	-	-	-	80.9	-	-	79.8	-	-	75.6

529 CPX15,MV703,R481,1146C,20HR,F-8.4,PTFE,E
530 CPX16,MV703,R481,1146C,20HR,F-8.4,PTFE,E
531 GL148,MV703,R480,1157C,19HR,F-8.2,+OL+CPX+PL+SPMT+GL,PTFE,E
532 OL85,MV703,R480,1157C,19HR,F-8.2,PTFE,E
533 PL122,MV703,R480,1157C,19HR,F-8.2,PTFE,E
534 GL207,MV703,R479,1169C,14HR,F-8.0,+OL+PL+SPMT+GL,PTFE,E
535 OL95,MV703,R479,1169C,14HR,F-8.0,PTFE,E
536 PL141,MV703,R479,1169C,14HR,F-8.0,PTFE,E
537 GL352,REVERSAL,MV703,R528,1171C,16HR,F-8.2,+OL+PL+SPMT+GL,PTFE,E
538 OL120,REVERSAL,MV703,R528,1171C,16HR,F-8.2,PTFE,E
539 PL157,REVERSAL,MV703,R528,1171C,16HR,F-8.2,PTFE,E

	540	541	542	543	544	545	546	547	548	549	550
SiO2	46.11	38.96	46.40	40.38	46.00	39.69	39.36	45.74	39.81	45.72	39.58
TiO2	2.68	nd	2.67	0.11	2.61	nd	nd	2.60	0.12	2.49	nd
Al2O3	15.00	nd	15.40	nd	15.09	nd	nd	14.83	nd	15.02	nd
Fe2O3	2.51	nd	2.51	nd	2.51	nd	nd	2.66	nd	2.43	nd
Cr2O3	0.07	nd	0.09	nd	nd	nd	nd	nd	nd	nd	nd
FeO	9.07	17.16	8.90	16.11	9.00	16.25	16.35	8.95	15.70	9.10	15.26
MnO	0.18	0.33	0.12	0.25	0.24	0.35	0.38	0.18	0.30	0.22	0.30
NiO	nd	0.47	nd	0.58	nd	0.60	0.52	nd	0.58	nd	0.47
MgO	6.57	42.29	7.13	43.25	7.07	42.76	42.37	7.61	43.01	7.94	43.98
CaO	11.37	0.53	11.53	0.61	11.63	0.55	0.61	11.39	0.70	11.24	0.54
Na2O	2.74	nd	2.88	nd	2.49	nd	nd	2.59	nd	2.34	nd
K2O	1.19	nd	1.03	nd	1.15	nd	nd	1.08	nd	1.03	nd
P2O5	0.13	nd	0.25	nd	0.27	nd	nd	0.20	nd	0.16	nd
total=	97.62	99.74	98.91	101.29	98.06	100.20	99.59	97.83	100.22	97.69	100.13
Mg#	56.3	81.5	58.8	82.7	58.3	82.4	82.2	60.2	83.0	60.9	83.7

540 GL206,MV703,R478,1179C,9HR,F-8.0,+OL+PL+SPMT+GL,PTFE,E
541 OL94,MV703,R478,1179C,9HR,F-8.0,PTFE,E
542 GL220,MV703,R477,1189C,18.5HR,F-7.8,+OL+SPMT+GL,PTFE,E
543 OL96,MV703,R477,1189C,18.5HR,F-7.8,PTFE,E
544 GL193,MV703,R476,1198C,19HR,F-7.7,+OL+SPMT+GL,PTFE,E
545 OL90,MV703,R476,1198C,19HR,F-7.7,PTFE,E
546 OL92,MV703,R476,1198C,19HR,F-7.7,PTFE,E
547 GL154,MV703,R473,1211C,2.5HR,F-7.4,+OL+SPMT+GL,PTFE,E
548 OL88,MV703,R473,1211C,2.5HR,F-7.4,PTFE,E
549 GL626,MV703,R496,1223C,19HR,F-7.4,+OL+SPMT+GL,PTFE,E
550 OL208,MV703,R496,1223C,19HR,F-7.4,PTFE,E

	551	552	553	554	555	556	557	558	559	560	561
SiO2	45.81	39.93	46.10	45.85	45.44	46.20	38.56	47.08	46.58	40.03	46.25
TiO2	2.38	0.12	2.47	2.39	2.28	2.73	nd	2.21	2.48	nd	2.37
Al2O3	14.70	nd	14.50	14.34	14.68	15.63	nd	6.31	15.34	0.20	16.19
Fe2O3	2.38	nd	2.33	2.40	2.26	2.49	nd	nd	2.53	nd	2.33
Cr2O3	nd	nd	0.12	nd	nd	nd	nd	0.50	nd	nd	nd
FeO	9.33	15.35	9.25	9.36	9.02	7.93	18.38	7.08	7.87	17.50	7.80
MnO	0.24	0.25	0.17	0.21	0.19	0.22	0.28	0.18	0.15	0.28	0.19
NiO	nd	0.43	nd	nd	nd	nd	0.46	nd	nd	0.49	nd
MgO	8.25	43.16	9.28	9.22	9.17	5.04	40.99	12.39	5.45	41.26	5.57
CaO	11.28	0.41	10.75	11.05	10.85	11.36	0.64	22.86	11.57	0.83	11.51
Na2O	2.36	nd	2.13	2.19	2.24	3.26	nd	nd	3.14	nd	3.13
K2O	1.03	nd	0.98	1.04	0.90	2.54	nd	nd	2.32	nd	2.30
P2O5	0.37	nd	nd	0.11	0.11	0.47	nd	nd	0.46	nd	0.28
total=	98.13	99.65	98.08	98.16	97.14	97.87	99.31	98.61	97.89	100.59	97.92
Mg#	61.2	83.4	64.1	63.7	64.4	53.1	79.9	-	55.2	80.8	56.0

551 GL338,MV703,R529,1238C,18.5HR,F-7.3,+OL+SPMT+GL,PTFE,E
552 OL115,MV703,R529,1238C,18.5HR,F-7.3,PTFE,E
553 GL383,MV703,R524,1252C,20HR,F-7.1,+OL+SPMT+GL,PTFE,E
554 GL274,MV703,R522,1277C,18HR,F-6.8,-GL,PTFE,E
555 GL657,MV703,R521,1287C,16HR,F-6.7,-GL,PTFE,E
556 GL1011R,MV520,R511,1151C,18.5HR,F-8.4,+OL+CPX+PL+SPMT+GL,SPT,E
557 OL335R,MV520,R511,1151C,18.5HR,F-8.4,SPT,E
558 CPX96R,MV520,R511,1151C,18.5HR,F-8.4,SPT,E
559 GL418,MV520,R587,1158C,19HR,F-8.2,+OL+PL+SPMT+GL,PTFE,E
560 OL139,MV520,R587,1158C,19HR,F-8.2,PTFE,E
561 GL724,MV520,R514,1165C,16HR,F-8.2,+OL+SPMT+GL,SPT,E

	562	563	564	565	566	567	568	569	570	571	572
SiO2	39.24	45.85	39.43	45.48	39.11	45.50	40.11	46.15	39.92	45.82	45.71
TiO2	nd	2.36	0.19	2.33	nd	2.30	nd	2.25	nd	2.26	2.27
Al2O3	nd	15.76	nd	15.67	nd	15.10	nd	15.25	nd	15.17	14.80
Fe2O3	nd	2.24	nd	2.34	nd	2.20	nd	2.19	nd	2.28	2.38
Cr2O3	nd	nd	nd	0.07	nd	0.05	nd	0.07	nd	nd	0.09
FeO	16.72	7.77	16.29	7.88	15.78	8.08	13.20	8.09	13.86	8.33	8.41
MnO	0.34	0.22	0.20	0.14	0.28	0.11	0.20	0.27	0.16	0.20	0.15
NiO	0.41	nd	0.47	nd	0.35	nd	0.46	nd	0.52	nd	nd
MgO	42.58	5.96	43.35	6.15	42.99	8.04	45.22	8.19	45.19	8.34	8.23
CaO	0.61	11.31	0.67	11.23	0.66	10.89	0.63	10.91	0.52	10.78	10.86
Na2O	nd	2.97	nd	2.87	nd	2.71	nd	2.56	nd	2.64	2.56
K2O	nd	2.19	nd	2.22	nd	1.99	nd	1.95	nd	1.86	1.90
P2O5	nd	0.38	nd	0.44	nd	0.35	nd	0.29	nd	0.34	0.31
total=	99.90	97.01	100.60	96.82	99.17	97.32	99.82	98.17	100.17	98.02	97.67
Mg#	81.9	57.8	82.6	58.2	82.9	63.9	85.9	64.3	85.3	64.1	63.6

562 OL239,MV520,R514,1165C,16HR,F-8.2,SPT,E
563 GL737,MV520,R515,1176C,16.5HR,F-8.1,+OL+SPMT+GL,SPT,E
564 OL244,MV520,R515,1176C,16.5HR,F-8.1,SPT,E
565 GL743,MV520,R516,1186C,12.5HR,F-7.9,+OL+SPMT+GL,SPT,E
566 OL248,MV520,R516,1186C,12.5HR,F-7.9,SPT,E
567 GL821,MV520,R530,1232C,16HR,F-7.4,+OL+SPMT+GL,PTFE,E
568 OL274,MV520,R530,1232C,16HR,F-7.4,PTFE,E
569 GL811,MV520,R529,1238C,18.5HR,F-7.3,+OL+SPMT+GL,PTFE,E
570 OL272,MV520,R529,1238C,18.5HR,F-7.3,PTFE,E
571 GL1029,MV520,R524,1252C,20HR,F-7.1,+SPMT+GL,SPT,E
572 GL1026,MV520,R523,1265C,17HR,F-6.9,-GL,SPT,E

	573	574	575	576	577	578	579	580	581	582	583
SiO2	46.56	49.10	48.97	38.35	48.00	39.14	53.05	49.19	47.50	39.09	50.51
TiO2	2.30	4.12	4.05	0.20	3.73	0.11	0.39	2.25	3.59	0.22	0.48
Al2O3	14.91	14.39	14.39	nd	14.37	nd	27.91	3.91	14.32	nd	28.15
Fe2O3	2.36	2.64	2.72	nd	2.58	nd	nd	nd	2.67	nd	nd
Cr2O3	0.06	0.07	nd	nd	nd	nd	nd	0.13	nd	nd	nd
FeO	8.47	7.79	8.16	24.26	8.52	21.74	1.25	7.19	8.31	20.58	1.84
MnO	0.14	0.16	0.06	0.36	0.19	0.37	nd	0.12	0.15	0.27	nd
NiO	nd	nd	nd	0.43	nd	0.41	nd	nd	nd	0.42	nd
MgO	8.22	3.43	3.83	36.94	4.79	38.68	nd	13.70	4.86	39.63	0.55
CaO	10.92	7.48	8.38	0.58	9.72	0.65	11.33	21.74	9.99	0.61	12.99
Na2O	2.58	3.23	3.24	nd	3.07	nd	4.06	0.35	2.93	nd	3.52
K2O	1.89	3.59	3.09	nd	2.38	nd	0.86	nd	2.30	nd	0.67
P2O5	0.09	1.05	0.74	nd	0.65	nd	nd	nd	0.53	nd	nd
total=	98.50	97.05	97.63	101.12	98.00	101.10	98.85	98.58	97.15	100.82	98.71
Mg#	63.4	44.0	45.6	73.1	50.1	76.0	-	-	51.0	77.4	-
An	-	-	-	-	-	-	57.5	-	-	-	64.4

573 GL276,MV520,R522,1277C,18HR,F-6.8,-GL,SPT,E
574 GL888,MV178,R519,1108C,21HR,F-9.1,+OL+CPX+PL+SPMT+GL,PTFE,E
575 GL866,MV178,R518,1120C,20HR,F-8.9,+OL+CPX+PL+SPMT+GL,PTFE,E
576 OL291,MV178,R518,1120C,20HR,F-8.9,PTFE,E
577 GL848,MV178,R517,1131C,12HR,F-8.8,+OL+CPX+PL+SPMT+GL,PTFE,E
578 OL285,MV178,R517,1131C,12HR,F-8.8,PTFE,E
579 PL276,MV178,R517,1131C,12HR,F-8.8,PTFE,E
580 CPX81,MV178,R517,1131C,12HR,F-8.8,PTFE,E
581 GL941,MV178,R534,1143C,12.5HR,F-8.5,+OL+PL+SPMT+GL,PTFE,E
582 OL312,MV178,R534,1143C,12.5HR,F-8.5,PTFE,E
583 PL301R,MV178,R534,1143C,12.5HR,F-8.5,PTFE,E

	584	585	586	587	588	589	590	591	592	593	594
SiO2	47.83	39.41	47.05	39.26	47.85	39.36	47.38	39.71	46.70	39.76	47.73
TiO2	3.16	nd	3.13	nd	3.06	nd	3.10	nd	2.95	nd	3.06
Al2O3	15.14	nd	15.08	nd	15.06	nd	14.94	nd	14.06	nd	13.97
Fe2O3	2.40	nd	2.50	nd	2.44	nd	2.44	nd	2.49	nd	2.39
Cr2O3	nd	nd	nd	nd	nd	nd	nd	nd	nd	nd	0.06
FeO	8.25	19.32	8.00	18.15	8.11	17.94	8.65	17.16	9.04	15.00	8.59
MnO	0.18	0.28	0.15	nd	0.15	0.21	0.15	0.25	0.22	0.14	0.17
NiO	nd	0.41	nd	0.45	nd	0.48	nd	0.45	nd	0.54	nd
MgO	5.52	41.41	5.67	41.56	5.93	41.14	6.39	41.94	8.06	44.05	8.02
CaO	9.91	0.55	9.86	0.50	9.58	0.52	9.57	0.36	9.05	0.34	9.35
Na2O	2.98	nd	3.05	nd	2.76	nd	2.99	nd	2.93	nd	2.57
K2O	2.06	nd	2.09	nd	2.02	nd	1.99	nd	1.87	nd	1.81
P2O5	0.60	nd	0.52	nd	0.36	nd	0.34	nd	0.35	nd	0.42
total=	98.03	101.38	97.10	99.92	97.32	99.65	97.94	99.87	97.72	99.83	98.14
Mg#	54.4	79.3	55.8	80.3	56.6	80.3	56.8	81.3	61.4	84.0	62.5

584 GL765,MV178,R512,1155C,24HR,F-8.4,+OL+PL+SPMT+GL,PTFE,E
585 OL258,MV178,R512,1155C,24HR,F-8.4,PTFE,E
586 GL838,MV178,R533,1168C,20HR,F-8.1,+OL+SPMT+GL,PTFE,E
587 OL281,MV178,R533,1168C,20HR,F-8.1,PTFE,E
588 GL834,MV178,R532,1176C,20.5HR,F-8.0,+OL+SPMT+GL,PTFE,E
589 OL279,MV178,R532,1176C,20.5HR,F-8.0,PTFE,E
590 GL830,MV178,R531,1186C,20HR,F-8.0,+OL+SPMT+GL,PTFE,E
591 OL277,MV178,R531,1186C,20HR,F-8.0,PTFE,E
592 GL818,MV178,R530,1232C,16HR,F-7.4,+OL+SPMT+GL,PTFE,E
593 OL273,MV178,R530,1232C,16HR,F-7.4,PTFE,E
594 GL341,MV178,R529,1238C,18.5HR,F-7.3,+OL+SPMT+GL,PTFE,E

	595	596	597	598	599	600	601	602	603	604	605
SiO2	39.44	47.00	47.41	40.29	46.65	47.53	47.56	50.07	38.23	38.57	38.43
TiO2	0.12	2.90	2.97	0.15	2.90	2.92	2.94	3.50	nd	nd	0.13
Al2O3	nd	13.71	13.47	nd	13.59	13.67	13.78	13.86	nd	nd	nd
Fe2O3	nd	2.46	2.54	nd	2.46	2.51	2.58	2.66	nd	nd	nd
Cr2O3	nd	nd	nd	nd	nd	nd	nd	0.02	nd	nd	nd
FeO	15.24	9.05	9.24	13.79	9.22	9.21	9.06	8.52	23.70	23.70	23.55
MnO	0.28	0.05	0.21	0.14	0.18	0.17	0.17	0.12	0.26	0.34	0.31
NiO	0.41	nd	nd	0.58	nd	nd	nd	nd	0.31	0.42	0.47
MgO	43.52	8.69	8.74	44.86	8.91	8.82	9.08	4.26	37.36	37.07	37.20
CaO	0.45	9.00	9.04	0.45	9.00	9.05	9.16	8.43	0.46	0.52	0.45
Na2O	nd	2.41	2.44	nd	2.45	2.33	2.48	3.81	nd	nd	nd
K2O	nd	1.72	1.75	nd	1.69	1.67	1.70	1.94	nd	nd	nd
P2O5	nd	0.32	0.37	nd	0.35	0.32	0.33	nd	nd	nd	nd
total=	99.46	97.31	98.18	100.26	97.40	98.20	98.84	97.19	100.32	100.62	100.54
Mg#	83.6	63.1	62.8	85.3	63.3	63.1	64.1	47.1	73.8	73.6	73.8

595 OL116,MV178,R529,1238C,18.5HR,F-7.3,PTFE,E
596 GL1031,MV178,R524,1252C,20HR,F-7.1,+OL+GL,PTFE,E
597 GL373,MV178,R543,1252C,12.5HR,F-7.1,+OL+GL,PTFE,E
598 OL122,MV178,R543,1252C,12.5HR,F-7.1,PTFE,E
599 GL324,MV178,R540,1264C,19HR,F-7.0,-GL,PTFE,E
600 GL1068R,MV178,R547,1277C,14HR,F-6.8,-GL,PTFE,E
601 GL134,MV178,R525,1297C,22HR,F-6.5,-GL,PTFE,E
602 GL29,MV114,R491,1124C,19HR,F-8.8,+OL+CPX+PL+SPMT+GL,SPT,E
603 OL18,MV114,R491,1124C,19HR,F-8.8,SPT,E
604 OL19,MV114,R491,1124C,19HR,F-8.8,SPT,E
605 OL20,MV114,R491,1124C,19HR,F-8.8,SPT,E

	606	607	608	609	610	611	612	613	614	615	616
SiO2	53.29	51.74	50.80	50.89	50.25	38.45	38.68	53.59	52.36	51.54	50.29
TiO2	0.25	1.22	1.37	2.97	3.29	nd	nd	0.28	0.28	0.28	3.07
Al2O3	27.94	1.94	2.87	5.66	14.00	nd	nd	28.19	28.20	28.64	14.38
Fe2O3	nd	nd	nd	nd	2.60	nd	nd	nd	nd	nd	2.45
Cr2O3	nd	0.25	0.69	0.13	nd	nd	nd	nd	nd	nd	nd
FeO	0.88	7.86	7.05	1.66	8.50	21.89	21.90	0.95	1.10	1.14	8.24
MnO	nd	nd	nd	0.12	0.13	0.23	0.33	nd	nd	nd	0.16
NiO	nd	nd	nd	0.15	nd	0.37	0.37	nd	nd	nd	nd
MgO	nd	14.97	14.70	16.99	4.73	38.52	38.57	nd	nd	nd	4.75
CaO	11.72	20.99	21.45	20.22	9.00	0.57	0.44	11.80	12.25	12.96	8.81
Na2O	4.31	0.26	0.32	0.40	3.60	nd	nd	4.42	4.05	3.74	3.53
K2O	0.41	nd	nd	nd	1.77	nd	nd	0.39	0.36	0.30	1.79
P2O5	nd	nd	nd	nd	nd	nd	nd	nd	nd	nd	0.48
total=	98.80	99.23	99.25	99.19	97.87	100.03	100.29	99.62	98.60	98.60	97.95
Mg#	-	-	-	-	49.8	75.8	75.8	-	-	-	50.7
An	58.6	-	-	-	-	-	-	58.2	61.2	64.5	-

606 PL33,MV114,R491,1124C,19HR,F-8.8,SPT,E
607 CPX11,MV114,R491,1124C,19HR,F-8.8,SPT,E
608 CPX12,MV114,R491,1124C,19HR,F-8.8,SPT,E
609 CPX13,MV114,R491,1124C,19HR,F-8.8,SPT,E
610 GL8,MV114,R490,1137C,19HR,F-8.6,+OL+CPX+PL+SPMT+GL,SPT,E
611 OL5,MV114,R490,1137C,19HR,F-8.6,SPT,E
612 OL7,MV114,R490,1137C,19HR,F-8.6,SPT,E
613 PL6,MV114,R490,1137C,19HR,F-8.6,SPT,E
614 PL7,MV114,R490,1137C,19HR,F-8.6,SPT,E
615 PL8,MV114,R490,1137C,19HR,F-8.6,SPT,E
616 GL437,MV114,R510,1145C,18HR,F-8.5,+OL+PL+SPMT+GL,PTFE,E

	617	618	619	620	621	622	623	624	625	626	627
SiO2	38.89	53.04	49.79	39.23	49.67	38.97	49.64	39.21	39.06	49.83	39.00
TiO2	nd	0.34	2.89	0.14	2.83	nd	2.81	0.15	nd	2.83	nd
Al2O3	nd	27.28	15.08	nd	14.84	nd	14.77	nd	nd	14.61	nd
Fe2O3	nd	nd	2.30	nd	2.42	nd	2.45	nd	nd	2.51	nd
Cr2O3	nd	nd	0.05	nd	nd	nd	nd	nd	nd	nd	nd
FeO	21.79	1.33	8.21	19.08	8.44	19.23	8.45	18.69	18.93	8.57	18.15
MnO	0.32	nd	0.12	0.39	0.20	0.24	0.06	0.20	0.24	0.11	0.20
NiO	0.25	nd	nd	0.24	nd	0.26	nd	0.47	0.52	nd	0.66
MgO	38.77	nd	5.27	41.13	5.40	40.38	5.77	40.99	40.86	6.12	41.02
CaO	0.43	12.00	8.88	0.54	8.81	0.43	8.65	0.38	0.42	8.64	0.43
Na2O	nd	4.18	3.45	nd	3.50	nd	3.35	nd	nd	3.44	nd
K2O	nd	0.45	1.59	nd	1.61	nd	1.61	nd	nd	1.58	nd
P2O5	nd	nd	0.34	nd	nd	nd	nd	nd	nd	nd	nd
total=	100.45	98.62	97.97	100.75	97.72	99.51	97.56	100.09	100.03	98.24	99.46
Mg#	76.0	-	53.4	79.3	53.3	78.9	54.9	79.6	79.4	56.0	80.1
An	-	59.7	-	-	-	-	-	-	-	-	-

617 OL147,MV114,R510,1145C,18HR,F-8.5,PTFE,E
618 PL182,MV114,R510,1145C,18HR,F-8.5,PTFE,E
619 GL767,MV114,R512,1155C,24HR,F-8.4,+OL+PL+SPMT+GL,PTFE,E
620 OL259,MV114,R512,1155C,24HR,F-8.4,PTFE,E
621 GL17,MV114,R450,1166C,6.5HR,F-8.2,+OL+SPMT+GL,SPT,E
622 OL15,MV114,R450,1166C,6.5HR,F-8.2,SPT,E
623 GL2,MV114,R449,1177C,14.5HR,F-8.0,+OL+SPMT+GL,SPT,E
624 OL26,MV114,R449,1177C,14.5HR,F-8.0,SPT,E
625 OL27,MV114,R449,1177C,14.5HR,F-8.0,SPT,E
626 GL23,MV114,R447,1191C,5HR,F-7.8,+OL+SPMT+GL,SPT,E
627 OL10,MV114,R447,1191C,5HR,F-7.8,SPT,E

	628	629	630	631	632	633	634	635	636	637	638
SiO2	1.38	49.46	39.43	39.50	49.52	39.92	39.83	49.23	39.33	40.04	49.05
TiO2	6.09	2.72	nd	nd	2.73	nd	0.12	2.73	0.19	0.11	2.63
Al2O3	16.16	14.64	nd	nd	14.55	0.18	nd	14.32	nd	nd	14.23
Fe2O3	14.03	2.61	nd	nd	2.51	nd	nd	2.65	nd	nd	2.47
Cr2O3	24.83	nd	nd	nd	nd	nd	nd	nd	nd	nd	0.04
FeO	25.76	8.66	18.06	17.65	8.74	17.35	17.06	8.59	16.66	16.75	8.70
MnO	nd	0.18	0.28	0.17	0.16	0.29	0.29	0.14	0.25	0.26	0.14
NiO	nd	nd	0.49	0.54	nd	0.48	0.42	nd	0.60	0.54	nd
MgO	10.17	6.66	41.95	41.83	6.70	41.99	42.77	7.02	42.37	42.94	7.28
CaO	nd	8.63	0.46	0.49	8.55	0.53	0.43	8.52	0.36	0.46	8.43
Na2O	nd	3.52	nd	nd	3.39	nd	nd	3.41	nd	nd	3.37
K2O	nd	1.56	nd	nd	1.53	nd	nd	1.52	nd	nd	1.44
V2O3	0.36	nd	nd	nd	nd	nd	nd	nd	nd	nd	nd
total=	98.78	98.64	100.67	100.18	98.38	100.74	100.92	98.13	99.76	101.10	97.78
Mg#	41.3	57.8	80.5	80.9	57.7	81.2	81.7	59.3	81.9	82.0	59.9

628 SPMT4R,MV114,R447,1191C,5HR,F-7.8,SPT,E
629 GL13,MV114,R446,1200C,6.5HR,F-7.6,+OL+SPMT+GL,SPT,E
630 OL6,MV114,R446,1200C,6.5HR,F-7.6,SPT,E
631 OL7,MV114,R446,1200C,6.5HR,F-7.6,SPT,E
632 GL46,MV114,R445,1207C,3HR,F-7.6,+OL+SPMT+GL,SPT,E
633 OL19,MV114,R445,1207C,3HR,F-7.6,SPT,E
634 OL20,MV114,R445,1207C,3HR,F-7.6,SPT,E
635 GL25,MV114,R444,1211C,6HR,F-7.4,+OL+SPMT+GL,SPT,E
636 OL10,MV114,R444,1211C,6HR,F-7.4,SPT,E
637 OL9,MV114,R444,1211C,6HR,F-7.4,SPT,E
638 GL6,MV114,R443,1222C,7HR,F-7.4,+OL+SPMT+GL,SPT,E

	639	640	641	642	643	644	645	646	647	648	649
SiO2	39.50	48.67	39.97	40.03	48.28	39.26	39.95	48.65	49.49	45.15	44.07
TiO2	nd	2.70	0.11	nd	2.58	nd	0.16	2.62	2.65	5.06	5.11
Al2O3	nd	14.02	nd	nd	13.74	nd	0.34	13.79	13.96	14.28	13.48
Fe2O3	nd	2.56	nd	nd	2.53	nd	nd	2.42	2.47	3.15	3.39
Cr2O3	nd	nd	nd	nd	0.15	nd	nd	nd	0.16	nd	nd
FeO	15.78	9.04	15.03	14.96	8.59	15.04	14.53	8.80	8.50	9.41	10.15
MnO	0.20	0.22	0.20	0.23	0.15	0.18	0.27	0.12	0.18	0.24	0.18
NiO	0.57	nd	0.62	0.61	nd	0.61	0.49	nd	nd	nd	nd
MgO	43.47	7.89	43.58	43.57	8.11	44.16	43.30	8.33	8.57	4.40	4.78
CaO	0.35	8.19	0.44	0.32	8.16	0.34	0.63	8.05	8.20	9.48	10.39
Na2O	nd	3.18	nd	nd	3.06	nd	nd	2.96	3.24	4.92	4.39
K2O	nd	1.42	nd	nd	1.39	nd	nd	1.48	1.46	1.37	1.14
P2O5	nd	nd	nd	nd	nd	nd	nd	nd	nd	1.11	0.82
total=	99.87	97.89	99.95	99.72	96.74	99.59	99.67	97.22	98.88	98.57	97.90
Mg#	83.1	60.9	83.8	83.8	62.7	84.0	84.2	62.8	64.2	45.5	45.6

639 OL13,MV114,R443,1222C,7HR,F-7.4,SPT,E
640 GL5,MV114,R442,1236C,6HR,F-7.2,+OL+SPMT+GL,SPT,E
641 OL1,MV114,R442,1236C,6HR,F-7.2,SPT,E
642 OL2,MV114,R442,1236C,6HR,F-7.2,SPT,E
643 GL2,MV114,R441,1245C,6HR,F-7.0,+OL+GL,SPT,E
644 OL1,MV114,R441,1245C,6HR,F-7.0,SPT,E
645 OL2,MV114,R441,1245C,6HR,F-7.0,SPT,E
646 GL23,MV114,R440,1256C,6.5HR,F-7.0,-GL,SPT,E
647 GL11R,MV114,R439,1266C,7.5HR,F-6.8,-GL,PT,E
648 GL880,MV716,R519,1108C,21HR,F-9.1,+OL+CPX+PL+SPMT+GL,PTFE,E
649 GL857,MV716,R518,1120C,20HR,F-8.9,+OL+CPX+PL+SPMT+GL,PTFE,E

	650	651	652	653	654	655	656	657	658	659	660
SiO2	52.17	46.93	43.80	38.34	44.62	38.91	50.04	43.88	38.95	44.07	39.08
TiO2	0.50	3.28	4.66	0.24	4.22	0.16	0.42	3.97	nd	3.82	nd
Al2O3	29.28	6.53	14.00	nd	14.63	nd	29.89	15.27	nd	14.99	nd
Fe2O3	nd	nd	3.09	nd	3.10	nd	nd	2.92	nd	2.97	nd
Cr2O3	nd	nd	0.06	nd	nd	nd	nd	nd	nd	nd	nd
FeO	1.16	7.59	10.11	21.74	10.14	20.79	1.06	9.91	20.14	9.97	18.95
MnO	nd	0.18	0.15	0.27	0.12	0.33	nd	0.13	0.22	0.14	0.15
NiO	nd	nd	nd	nd	nd	0.25	nd	nd	0.47	nd	0.36
MgO	nd	12.16	5.30	38.43	5.56	39.85	nd	6.06	40.80	6.24	41.95
CaO	12.62	21.67	10.74	0.78	10.45	0.56	13.61	10.50	0.61	10.27	0.47
Na2O	4.50	0.72	4.15	nd	4.00	nd	3.39	3.86	nd	3.69	nd
K2O	0.31	nd	0.91	nd	0.82	nd	0.12	0.69	nd	0.71	nd
P2O5	nd	nd	0.59	nd	0.44	nd	nd	0.50	nd	0.30	nd
total=	100.54	99.06	97.56	99.80	98.10	100.85	98.53	97.69	101.19	97.17	100.96
Mg#	-	-	48.3	75.9	49.4	77.4	-	52.2	78.3	52.7	79.8
An	59.7	-	-	-	-	-	68.4	-	-	-	-

650 PL279,MV716,R518,1120C,20HR,F-8.9,PTFE,E
651 CPX82R,MV716,R518,1120C,20HR,F-8.9,PTFE,E
652 GL851,MV716,R517,1131C,12HR,F-8.8,+OL+PL+SPMT+GL,PTFE,E
653 OL286,MV716,R517,1131C,12HR,F-8.8,PTFE,E
654 GL758,MV716,R511,1151C,18.5HR,F-8.4,+OL+PL+SPMT+GL,PTFE,E
655 OL253,MV716,R511,1151C,18.5HR,F-8.4,PTFE,E
656 PL260,MV716,R511,1151C,18.5HR,F-8.4,PTFE,E
657 GL728,MV716,R514,1165C,16HR,F-8.2,+OL+PL+SPMT+GL,PTFE,E
658 OL242,MV716,R514,1165C,16HR,F-8.2,PTFE,E
659 GL836,MV716,R532,1176C,20.5HR,F-8.0,+OL+SPMT+GL,PTFE,E
660 OL280,MV716,R532,1176C,20.5HR,F-8.0,PTFE,E

	661	662	663	664	665	666	667	668	669	670	671
SiO2	43.88	39.17	44.06	39.45	44.02	39.91	43.47	39.74	44.21	40.55	44.09
TiO2	3.92	0.15	3.63	0.13	3.80	nd	3.60	0.15	3.57	0.11	3.61
Al2O3	15.07	nd	14.38	nd	13.73	nd	13.75	nd	13.45	nd	13.71
Fe2O3	2.82	nd	2.80	nd	2.91	nd	2.94	nd	2.84	nd	2.91
Cr2O3	nd	nd	0.08	nd	nd	nd	0.04	nd	nd	nd	nd
FeO	10.16	18.14	10.58	16.62	10.90	15.70	10.97	14.33	10.89	14.17	10.84
MnO	0.20	0.32	0.15	0.24	0.19	0.19	0.17	0.16	0.17	0.19	0.20
NiO	nd	0.33	nd	0.35	nd	0.61	nd	0.49	nd	0.49	nd
MgO	6.86	41.59	8.38	43.20	9.03	44.72	9.70	44.28	10.42	45.42	10.50
CaO	10.14	0.46	9.61	0.38	9.38	0.31	9.35	0.33	9.25	0.34	9.20
Na2O	3.81	nd	3.08	nd	2.86	nd	2.86	nd	2.98	nd	2.76
K2O	0.64	nd	0.66	nd	0.64	nd	0.65	nd	0.58	nd	0.54
P2O5	0.35	nd	0.41	nd	0.31	nd	0.36	nd	0.21	nd	0.23
total=	97.85	100.16	97.82	100.37	97.77	101.44	97.86	99.48	98.57	101.27	98.59
Mg#	54.6	80.3	58.5	82.2	59.6	83.5	61.2	84.6	63.0	85.1	63.3

661 GL827,MV716,R531,1186C,20HR,F-8.0,+OL+SPMT+GL,PTFE,E
662 OL276,MV716,R531,1186C,20HR,F-8.0,PTFE,E
663 GL807,MV716,R529,1238C,18.5HR,F-7.3,+OL+SPMT+GL,PTFE,E
664 OL271,MV716,R529,1238C,18.5HR,F-7.3,PTFE,E
665 GL379,MV716,R524,1252C,20HR,F-7.1,+OL+SPMT+GL,PTFE,E
666 OL123,MV716,R524,1252C,20HR,F-7.1,PTFE,E
667 GL1024,MV716,R523,1265C,17HR,F-6.9,+OL+GL,PTFE,E
668 OL339,MV716,R523,1265C,17HR,F-6.9,PTFE,E
669 GL1066,MV716,R547,1277C,14HR,F-6.8,+OL+GL,PTFE,E
670 OL345R,MV716,R547,1277C,14HR,F-6.8,PTFE,E
671 GL1071,MV716,R549,1287C,14HR,F-6.6,-GL,PTFE,E

	672	673	674	675	676	677	678	679	680	681	682
SiO2	44.23	43.63	51.48	48.74	44.13	39.15	49.04	44.58	39.07	44.26	39.58
TiO2	3.51	3.62	0.42	2.09	3.53	0.14	2.04	3.26	nd	2.97	nd
Al2O3	13.35	14.25	29.24	5.25	14.30	0.27	5.03	14.40	0.22	14.76	nd
Fe2O3	2.92	3.05	nd	nd	2.83	nd	nd	2.73	nd	2.60	nd
Cr2O3	nd	nd	nd	0.21	nd	nd	0.12	0.06	nd	nd	nd
FeO	10.99	9.54	1.26	7.74	9.28	20.29	7.35	8.93	18.82	9.10	18.32
MnO	nd	0.23	nd	0.14	0.26	0.41	0.14	0.22	0.37	0.24	0.25
NiO	nd	nd	nd	nd	nd	0.21	nd	nd	0.34	nd	0.27
MgO	10.50	5.19	nd	12.30	5.57	38.36	13.20	5.85	40.69	6.15	41.45
CaO	9.22	11.33	12.54	21.92	11.78	0.80	22.49	12.10	0.80	12.07	0.68
Na2O	2.64	3.83	3.87	0.56	3.63	nd	nd	3.45	nd	3.29	nd
K2O	0.58	1.45	0.45	nd	1.36	nd	nd	1.31	nd	1.11	nd
P2O5	0.12	1.23	nd	nd	1.28	nd	nd	1.00	nd	0.95	nd
total=	98.06	97.35	99.26	98.95	97.95	99.63	99.41	97.89	100.31	97.50	100.55
Mg#	63.0	49.2	-	-	51.7	77.1	-	53.9	79.4	54.6	80.1
An	-	-	62.5	-	-	-	-	-	-	-	-

672 GL386,MV716,R525,1297C,22HR,F-6.5,-GL,PTFE,E
673 GL575,MV78,R472,1128C,5.5HR,F-8.7,+OL+CPX+PL+SPMT+GL,PTFE,E
674 PL218,MV78,R472,1128C,5.5HR,F-8.7,PTFE,E
675 CPX66,MV78,R472,1128C,5.5HR,F-8.7,PTFE,E
676 GL423,MV78,R509,1140C,13HR,F-8.6,+OL+CPX+PL+SPMT+GL,SPT,E
677 OL141,MV78,R509,1140C,13HR,F-8.6,SPT,E
678 CPX49,MV78,R509,1140C,13HR,F-8.6,SPT,E
679 GL1010,MV78,R511,1151C,18.5HR,F-8.4,+OL+CPX+PL+SPMT+GL,PTFE,E
680 OL333,MV78,R511,1151C,18.5HR,F-8.4,PTFE,E
681 GL773,MV78,R513,1161C,14HR,F-8.3,+OL+SPMT+GL,PTFE,E
682 OL262,MV78,R513,1161C,14HR,F-8.3,PTFE,E

	683	684	685	686	687	688	689	690	691	692	693
SiO2	44.66	44.64	39.49	43.77	39.36	44.06	39.67	44.25	38.97	43.69	43.75
TiO2	3.10	3.21	0.16	2.97	nd	2.90	0.15	2.97	0.16	3.03	2.81
Al2O3	14.77	14.58	nd	14.31	nd	14.37	nd	14.17	0.28	14.20	14.07
Fe2O3	2.73	2.84	nd	2.74	nd	2.76	nd	2.93	nd	2.88	2.82
Cr2O3	nd	0.13	nd	0.12	nd	0.06	nd	nd	nd	nd	nd
FeO	9.03	9.14	16.69	9.27	16.45	9.41	14.87	9.01	15.50	9.40	9.27
MnO	0.20	0.27	0.22	0.18	0.31	0.26	0.43	0.25	0.37	0.23	0.28
NiO	nd	nd	0.28	nd	0.38	nd	0.33	nd	0.42	nd	nd
MgO	6.60	7.17	42.29	7.12	42.40	7.51	43.54	7.73	43.49	7.93	7.62
CaO	11.88	11.90	0.63	11.56	0.53	11.64	0.55	11.58	0.44	11.61	11.63
Na2O	3.44	3.27	nd	2.93	nd	3.12	nd	3.33	nd	3.27	3.26
K2O	1.11	1.06	nd	1.11	nd	1.15	nd	1.06	nd	1.07	1.12
P2O5	nd	nd	nd	nd	nd	nd	nd	nd	nd	nd	0.89
total=	97.52	98.21	99.76	96.08	99.43	97.24	99.54	97.28	99.63	97.31	97.52
Mg#	56.6	58.3	81.9	57.8	82.1	58.7	83.9	60.5	83.3	60.1	59.4

683 GL2,MV78,R438,1176C,7HR,F-8.0,+OL+SPMT+GL,SPT,E
684 GL113,MV78,R434,1185C,12HR,F-7.8,+OL+SPMT+GL,SPT,E
685 OL104,MV78,R434,1185C,12HR,F-7.8,SPT,E
686 GL18,MV78,R436,1197C,8HR,F-7.7,+OL+SPMT+GL,SPT,E
687 OL14,MV78,R436,1197C,8HR,F-7.7,SPT,E
688 GL11,MV78,R421,1206C,2HR,F-7.6,+OL+SPMT+GL,PT,E
689 OL1,MV78,R421,1206C,2HR,F-7.6,PT,E
690 GL14,MV78,R432,1207C,2HR,F-7.4,+OL+SPMT+GL,PT,E
691 OL9,MV78,R432,1207C,2HR,F-7.4,PT,E
692 GL11,MV78,R424,1208C,2HR,F-7.5,+OL+SPMT+GL,PT,E
693 GL668,MV78,R418,1209C,3HR,F-7.5,+OL+SPMT+GL,PT,E

	694	695	696	697	698	699	700	701	702	703	704
SiO2	39.30	44.40	39.90	43.80	43.96	39.77	43.93	43.77	43.93	46.63	38.50
TiO2	nd	2.97	0.14	2.89	2.88	0.15	2.85	2.93	2.93	3.95	0.14
Al2O3	nd	14.33	0.20	13.87	13.63	nd	13.74	13.73	13.88	14.54	nd
Fe2O3	nd	2.76	nd	2.70	2.74	nd	2.90	2.83	2.56	3.02	nd
Cr2O3	nd	0.06	nd	0.07	0.07	nd	nd	nd	nd	0.04	nd
FeO	14.44	9.33	15.25	9.22	9.22	14.16	9.54	9.52	9.56	8.63	22.14
MnO	0.32	0.24	0.27	0.25	0.24	0.28	0.24	0.23	0.26	0.27	0.42
NiO	0.43	nd	0.51	nd	nd	0.21	nd	nd	nd	nd	nd
MgO	43.87	8.13	43.50	7.72	8.79	44.32	8.88	9.17	9.09	4.80	37.76
CaO	0.66	11.59	0.68	11.46	11.28	0.51	11.17	11.18	11.00	9.85	0.52
Na2O	nd	3.12	nd	2.99	2.97	nd	2.94	3.09	3.14	4.08	nd
K2O	nd	1.08	nd	1.14	1.00	nd	1.11	1.01	0.98	1.90	nd
P2O5	nd	nd	nd	0.88	nd	nd	nd	nd	1.03	nd	nd
total=	99.02	98.01	100.45	96.99	96.78	99.40	97.30	97.46	98.36	97.71	99.48
Mg#	84.4	60.8	83.6	59.9	63.0	84.8	62.4	63.2	62.9	49.8	75.2

694 OL221,MV78,R418,1209C,3HR,F-7.5,PT,E
695 GL4,MV78,R437,1211C,6HR,F-7.5,+OL+GL,SPT,E
696 OL2,MV78,R437,1211C,6HR,F-7.5,SPT,E
697 GL676,MV78,R419,1214C,2HR,F-7.5,+OL+GL,PT,E
698 GL8,MV78,R433,1232C,6.5HR,F-7.2,+OL+GL,SPT,E
699 OL4,MV78,R433,1232C,6.5HR,F-7.2,SPT,E
700 GL52,MV78,R415,1244C,2HR,F-7.0,-GL,PT,E
701 GL21,MV78,R417,1248C,3HR,F-7.0,-GL,PT,E
702 GL2041,MV78,R5-729,1284C,5HR,F-6.8,-GL,SPT,W
703 GL22,MV406,R472,1128C,5.5HR,F-8.6,+OL+CPX+PL+SPMT+GL,PTFE,E
704 OL16,MV406,R472,1128C,5.5HR,F-8.6,PTFE,E

	705	706	707	708	709	710	711	712	713	714	715
SiO2	38.40	52.02	51.59	50.94	49.38	48.28	46.05	46.51	0.28	0.33	46.39
TiO2	nd	0.22	0.36	0.30	1.57	2.34	2.96	2.35	9.07	6.89	3.72
Al2O3	nd	29.42	28.86	29.29	4.90	5.20	8.29	7.19	12.92	20.75	14.48
Fe2O3	nd	nd	nd	nd	nd	nd	nd	nd	20.67	17.47	2.93
Cr2O3	nd	nd	nd	nd	0.53	0.13	0.46	0.57	16.88	17.30	nd
FeO	22.11	0.73	1.17	1.08	6.01	7.79	7.31	6.60	29.55	26.98	8.59
MnO	0.46	nd	nd	nd	nd	0.12	0.11	nd	0.16	0.22	0.24
NiO	0.30	nd	nd	nd	nd	nd	nd	nd	nd	nd	nd
MgO	38.36	nd	nd	0.17	14.02	12.51	11.90	12.77	7.85	9.48	4.84
CaO	0.60	12.64	13.01	13.23	22.35	21.78	22.52	22.90	nd	nd	10.06
Na2O	nd	3.78	3.84	3.45	0.24	0.61	0.28	0.51	nd	nd	3.96
K2O	nd	0.33	0.36	0.43	nd	nd	nd	nd	nd	nd	1.82
V2O3	nd	nd	nd	nd	nd	nd	nd	nd	0.63	0.49	nd
total=	100.23	99.14	99.19	98.89	99.00	98.76	99.88	99.40	98.01	99.91	97.03
Mg#	75.6	-	-	-	-	-	-	-	32.1	38.5	50.1
An	-	63.6	63.8	66.2	-	-	-	-	-	-	-

705 OL17,MV406,R472,1128C,5.5HR,F-8.6,PTFE,E
706 PL18,MV406,R472,1128C,5.5HR,F-8.6,PTFE,E
707 PL19,MV406,R472,1128C,5.5HR,F-8.6,PTFE,E
708 PL20,MV406,R472,1128C,5.5HR,F-8.6,PTFE,E
709 CPX17,MV406,R472,1128C,5.5HR,F-8.6,PTFE,E
710 CPX19,MV406,R472,1128C,5.5HR,F-8.6,PTFE,E
711 CPX20,MV406,R472,1128C,5.5HR,F-8.6,PTFE,E
712 CPX21,MV406,R472,1128C,5.5HR,F-8.6,PTFE,E
713 SPMT4,MV406,R472,1128C,5.5HR,F-8.6,PTFE,E
714 SPMT5,MV406,R472,1128C,5.5HR,F-8.6,PTFE,E
715 GL31,MV406,R471,1129C,21HR,F-8.6,+OL+CPX+PL+SPMT+GL,SPT,E

	716	717	718	719	720	721	722	723	724	725	726
SiO2	38.70	39.08	38.76	38.74	50.20	51.47	51.12	48.69	48.52	50.11	49.54
TiO2	0.11	0.12	nd	nd	0.29	0.34	0.42	1.87	2.21	1.68	1.50
Al2O3	nd	nd	nd	nd	29.68	28.33	28.78	4.84	6.04	4.60	4.51
Cr2O3	nd	nd	nd	nd	nd	nd	nd	0.23	0.41	0.45	0.55
FeO	21.42	21.25	21.00	21.10	1.05	1.31	1.16	6.80	7.34	6.11	6.48
MnO	0.31	0.37	0.41	0.49	nd	nd	nd	nd	0.12	0.12	nd
NiO	0.41	0.35	0.30	0.29	nd	nd	nd	nd	nd	nd	nd
MgO	38.73	38.19	38.47	38.32	nd	0.20	0.28	13.75	12.72	14.14	14.28
CaO	0.42	0.62	0.60	0.48	13.85	12.38	13.09	22.51	21.98	22.88	22.71
Na2O	nd	nd	nd	nd	3.04	3.90	3.62	nd	0.55	nd	0.28
K2O	nd	nd	nd	nd	0.30	0.48	0.35	nd	nd	nd	nd
total=	100.10	99.98	99.54	99.42	98.41	98.41	98.82	98.69	99.89	100.09	99.85
Mg#	76.3	76.2	76.6	76.4	-	-	-	-	-	-	-
An	-	-	-	-	70.3	61.9	65.3	-	-	-	-

716 OL23,MV406,R471,1129C,21HR,F-8.6,SPT,E
717 OL24,MV406,R471,1129C,21HR,F-8.6,SPT,E
718 OL26,MV406,R471,1129C,21HR,F-8.6,SPT,E
719 OL27,MV406,R471,1129C,21HR,F-8.6,SPT,E
720 PL27,MV406,R471,1129C,21HR,F-8.6,SPT,E
721 PL30,MV406,R471,1129C,21HR,F-8.6,SPT,E
722 PL32,MV406,R471,1129C,21HR,F-8.6,SPT,E
723 CPX22,MV406,R471,1129C,21HR,F-8.6,SPT,E
724 CPX25,MV406,R471,1129C,21HR,F-8.6,SPT,E
725 CPX26,MV406,R471,1129C,21HR,F-8.6,SPT,E
726 CPX27,MV406,R471,1129C,21HR,F-8.6,SPT,E

	727	728	729	730	731	732	733	734	735	736	737
SiO2	0.30	46.50	39.25	51.93	48.48	1.00	46.97	38.89	51.93	0.72	46.58
TiO2	10.72	3.57	nd	0.35	1.71	10.57	3.46	nd	0.37	9.64	3.28
Al2O3	10.12	14.47	nd	28.73	4.41	11.73	14.62	nd	28.31	12.10	14.96
Fe2O3	21.48	2.68	nd	nd	nd	19.78	2.70	nd	nd	19.35	2.56
Cr2O3	16.97	0.17	nd	nd	0.40	14.71	nd	nd	nd	16.41	0.02
FeO	29.90	8.63	20.42	1.24	6.41	30.17	8.49	19.50	1.28	28.63	8.43
MnO	0.47	0.21	0.35	nd	nd	0.49	0.23	0.33	nd	0.23	0.21
NiO	nd	nd	0.24	nd	nd	nd	nd	0.22	nd	nd	nd
MgO	7.85	5.00	39.55	0.18	14.33	8.60	5.21	40.24	0.42	8.71	5.55
CaO	0.35	10.29	0.57	13.08	22.33	nd	10.27	0.50	12.64	nd	10.24
Na2O	nd	3.80	nd	3.63	nd	nd	3.65	nd	3.79	nd	3.70
K2O	nd	1.70	nd	0.41	nd	nd	1.69	nd	0.44	nd	1.60
P2O5	nd	0.63	nd	nd	nd	nd	0.58	nd	nd	nd	nd
V2O3	nd	nd	nd	nd	nd	0.89	nd	nd	nd	0.64	nd
total=	98.16	97.65	100.38	99.55	98.07	97.94	97.87	99.68	99.18	96.43	97.13
Mg#	31.9	50.8	77.5	-	-	33.7	52.2	78.6	-	35.2	54.0
An	-	-	-	65.0	-	-	-	-	63.1	-	-

727 SPMT10,MV406,R471,1129C,21HR,F-8.6,SPT,E
728 GL427,MV406,R509,1140C,13HR,F-8.6,+OL+CPX+PL+SPMT+GL,SPT,E
729 OL143,MV406,R509,1140C,13HR,F-8.6,SPT,E
730 PL174,MV406,R509,1140C,13HR,F-8.6,PTFE,E
731 CPX51,MV406,R509,1140C,13HR,F-8.6,SPT,E
732 SPMT29,MV406,R509,1140C,13HR,F-8.6,PTFE,E
733 GL1092,MV406,R552,1148C,22HR,F-8.4,+OL+PL+SPMT+GL,PTFE,E
734 OL350,MV406,R552,1148C,22HR,F-8.4,PTFE,E
735 PL324,MV406,R552,1148C,22HR,F-8.4,PTFE,E
736 SPMT70,MV406,R552,1148C,22HR,F-8.4,PTFE,E
737 GL100,MV406,R470,1151C,17HR,F-8.4,+OL+PL+SPMT+GL,SPT,E

	738	739	740	741	742	743	744	745	746	747	748
SiO2	39.05	39.15	39.07	51.28	50.53	50.27	46.64	39.20	49.69	1.10	46.91
TiO2	0.11	nd	0.15	0.30	0.37	0.32	3.27	0.13	0.35	5.73	3.14
Al2O3	nd	nd	nd	29.41	28.91	29.79	15.47	nd	30.19	21.02	15.53
Fe2O3	nd	nd	nd	nd	nd	nd	2.48	nd	nd	14.78	2.45
Cr2O3	nd	nd	nd	nd	nd	nd	nd	nd	nd	19.26	nd
FeO	18.47	18.69	19.02	0.77	1.25	1.24	8.53	18.47	1.23	24.83	8.42
MnO	0.42	0.40	0.39	nd	nd	nd	0.17	0.33	nd	nd	0.19
NiO	0.48	0.42	0.38	nd	nd	nd	nd	0.27	nd	nd	nd
MgO	40.89	41.09	40.69	nd	nd	0.25	5.62	40.54	nd	10.62	5.68
CaO	0.53	0.53	0.57	13.13	13.73	14.01	10.28	0.57	13.99	nd	10.30
Na2O	nd	nd	nd	3.45	3.23	3.30	3.60	nd	3.03	nd	3.57
K2O	nd	nd	nd	0.30	0.37	0.30	1.54	nd	0.31	nd	1.56
P2O5	nd	nd	nd	nd	nd	nd	0.55	nd	nd	nd	0.53
V2O3	nd	nd	nd	nd	nd	nd	nd	nd	nd	0.48	nd
total=	99.95	100.28	100.27	98.64	98.39	99.48	98.15	99.51	98.79	97.82	98.28
Mg#	79.8	79.7	79.2	-	-	-	54.0	79.6	-	43.3	54.6
An	-	-	-	66.5	68.6	68.9	-	-	70.5	-	-

738 OL66,MV406,R470,1151C,17HR,F-8.4,SPT,E
739 OL67,MV406,R470,1151C,17HR,F-8.4,SPT,E
740 OL68,MV406,R470,1151C,17HR,F-8.4,SPT,E
741 PL86,MV406,R470,1151C,17HR,F-8.4,SPT,E
742 PL87,MV406,R470,1151C,17HR,F-8.4,SPT,E
743 PL88,MV406,R470,1151C,17HR,F-8.4,SPT,E
744 GL769,MV406,R512,1155C,24HR,F-8.4,+OL+PL+SPMT+GL,PTFE,E
745 OL260,MV406,R512,1155C,24HR,F-8.4,PTFE,E
746 PL262,MV406,R512,1155C,24HR,F-8.4,PTFE,E
747 SPMT44,MV406,R512,1155C,24HR,F-8.4,PTFE,E
748 GL781,MV406,R513,1161C,14HR,F-8.3,+OL+PL+SPMT+GL,SPT,E

	749	750	751	752	753	754	755	756	757	758	759
SiO2	39.16	50.89	0.77	46.47	39.41	38.85	46.29	39.62	46.47	38.99	39.43
TiO2	nd	0.15	4.75	3.11	0.15	0.17	3.03	nd	3.12	nd	nd
Al2O3	nd	30.40	24.05	15.49	nd	nd	15.71	nd	15.51	nd	nd
Fe2O3	nd	nd	14.19	2.46	nd	nd	2.42	nd	2.57	nd	nd
Cr2O3	nd	nd	19.94	0.05	nd	nd	0.07	nd	0.05	nd	nd
FeO	18.15	1.03	22.98	8.31	18.51	18.35	7.99	17.58	8.54	17.50	17.71
MnO	0.49	nd	0.25	0.27	0.28	0.39	0.18	0.27	0.21	0.36	0.41
NiO	0.25	nd	nd	nd	0.44	0.31	nd	0.43	nd	0.36	0.39
MgO	41.24	nd	11.26	5.72	41.24	40.78	5.89	42.57	5.93	41.58	41.16
CaO	0.52	13.80	nd	10.25	0.59	0.61	10.13	0.52	10.06	0.47	0.44
Na2O	nd	3.29	nd	3.62	nd	nd	3.70	nd	3.65	nd	nd
K2O	nd	0.22	nd	1.52	nd	nd	1.44	nd	1.49	nd	nd
P2O5	nd	nd	nd	nd	nd	nd	0.44	nd	nd	nd	nd
V2O3	nd	nd	0.31	nd	nd	nd	nd	nd	nd	nd	nd
total=	99.81	99.78	98.50	97.27	100.62	99.46	97.29	100.99	97.60	99.26	99.54
Mg#	80.2	-	46.6	55.1	79.9	79.8	56.8	81.2	55.3	80.9	80.6
An	-	68.9	-	-	-	-	-	-	-	-	-

749 OL265,MV406,R513,1161C,14HR,F-8.3,SPT,E
750 PL265,MV406,R513,1161C,14HR,F-8.3,SPT,E
751 SPMT45,MV406,R513,1161C,14HR,F-8.3,SPT,E
752 GL11,MV406,R450,1166C,6.5HR,F-8.2,+OL+PL+SPMT+GL,PTFE,E
753 OL10,MV406,R450,1166C,6.5HR,F-8.2,PTFE,E
754 OL11,MV406,R450,1166C,6.5HR,F-8.2,PTFE,E
755 GL840,MV406,R533,1168C,20HR,F-8.1,+OL+SPMT+GL,PTFE,E
756 OL282,MV406,R533,1168C,20HR,F-8.1,PTFE,E
757 GL5,MV406,R449,1177C,14.5HR,F-8.0,+OL+SPMT+GL,PTFE,E
758 OL3,MV406,R449,1177C,14.5HR,F-8.0,PTFE,E
759 OL5,MV406,R449,1177C,14.5HR,F-8.0,PTFE,E

	760	761	762	763	764	765	766	767	768	769	770
SiO2	0.92	0.58	46.89	39.68	46.69	39.42	0.28	0.24	46.70	40.12	46.78
TiO2	2.54	5.31	3.11	0.18	3.05	0.15	7.55	5.65	3.01	0.13	2.99
Al2O3	30.80	23.41	15.47	nd	15.23	nd	19.86	21.93	15.10	0.17	14.97
Fe2O3	10.58	15.78	2.61	nd	2.71	nd	18.68	17.43	2.61	nd	2.70
Cr2O3	20.27	18.58	nd	nd	0.07	nd	16.42	20.33	0.08	nd	nd
FeO	20.08	22.71	8.63	16.92	8.68	16.41	23.57	21.00	8.70	16.22	8.50
MnO	0.36	0.35	0.21	0.30	0.21	0.34	0.18	0.52	0.19	0.34	0.23
NiO	nd	nd	nd	0.46	nd	0.40	nd	nd	nd	0.38	nd
MgO	12.63	11.50	6.38	42.50	6.68	42.74	11.72	12.50	6.67	42.66	7.19
CaO	nd	nd	10.15	0.48	9.90	0.45	nd	nd	9.97	0.47	9.82
Na2O	nd	nd	3.68	nd	3.64	nd	nd	nd	3.70	nd	3.52
K2O	nd	nd	1.51	nd	1.48	nd	nd	nd	1.47	nd	1.46
V2O3	0.27	0.45	nd	nd	nd	nd	0.44	0.30	nd	nd	nd
total=	98.45	98.67	98.64	100.52	98.34	99.91	98.70	99.90	98.20	100.49	98.16
Mg#	52.9	47.4	56.9	81.7	57.8	82.3	47.0	51.5	57.7	82.4	60.1

760 SPMT1,MV406,R449,1177C,14.5HR,F-8.0,PTFE,E
761 SPMT2,MV406,R449,1177C,14.5HR,F-8.0,PTFE,E
762 GL36,MV406,R447,1191C,5HR,F-7.8,+OL+SPMT+GL,PTFE,E
763 OL17,MV406,R447,1191C,5HR,F-7.8,PTFE,E
764 GL10,MV406,R446,1200C,6.5HR,F-7.6,+OL+SPMT+GL,PTFE,E
765 OL4,MV406,R446,1200C,6.5HR,F-7.6,PTFE,E
766 SPMT1,MV406,R446,1200C,6.5HR,F-7.6,PTFE,E
767 SPMT2,MV406,R446,1200C,6.5HR,F-7.6,PTFE,E
768 GL40,MV406,R445,1207C,3HR,F-7.6,+OL+SPMT+GL,PTFE,E
769 OL15,MV406,R445,1207C,3HR,F-7.6,PTFE,E
770 GL28,MV406,R444,1211C,6HR,F-7.4,+OL+SPMT+GL,PTFE,E

	771	772	773	774	775	776	777	778	779	780	781
SiO2	39.84	46.16	39.47	39.70	46.23	40.01	0.22	45.30	39.65	46.60	0.26
TiO2	nd	2.93	0.11	nd	2.98	nd	2.02	2.93	nd	2.97	3.55
Al2O3	nd	14.68	nd	nd	14.66	0.22	31.98	14.25	nd	14.52	27.19
Fe2O3	nd	2.60	nd	nd	2.63	nd	12.34	2.67	nd	2.52	13.09
Cr2O3	nd	0.07	nd	nd	0.04	nd	21.61	0.07	nd	nd	22.62
FeO	15.74	8.83	15.35	15.19	8.87	14.49	15.78	8.76	13.87	8.93	17.12
MnO	0.32	0.22	0.32	0.34	0.21	0.31	0.21	0.29	0.31	0.17	nd
NiO	0.39	nd	0.25	0.53	nd	0.57	nd	nd	0.39	nd	nd
MgO	43.45	7.46	43.61	43.43	7.95	43.89	14.85	8.31	44.20	8.88	14.47
CaO	0.57	9.64	0.48	0.35	9.73	0.39	nd	9.25	0.49	9.50	nd
Na2O	nd	3.54	nd	nd	3.41	nd	nd	3.28	nd	3.24	nd
K2O	nd	1.40	nd	nd	1.43	nd	nd	1.35	nd	1.30	nd
V2O3	nd	nd	nd	nd	nd	nd	nd	nd	nd	nd	0.31
total=	100.31	97.53	99.59	99.54	98.14	99.88	99.01	96.46	98.91	98.63	98.61
Mg#	83.1	60.1	83.5	83.6	61.5	84.4	62.6	62.8	85.0	63.9	60.1

771 OL11,MV406,R444,1211C,6HR,F-7.4,PTFE,E
772 GL13,MV406,R443,1222C,7HR,F-7.4,+OL+SPMT+GL,PTFE,E
773 OL1,MV406,R443,1222C,7HR,F-7.4,PTFE,E
774 OL2,MV406,R443,1222C,7HR,F-7.4,PTFE,E
775 GL8,MV406,R442,1236C,6HR,F-7.2,+OL+SPMT+GL,SPT,E
776 OL4,MV406,R442,1236C,6HR,F-7.2,SPT,E
777 SPMT2,MV406,R442,1236C,6HR,F-7.2,SPT,E
778 GL4,MV406,R441,1245C,6HR,F-7.0,+OL+SPMT+GL,SPT,E
779 OL3RR,MV406,R441,1245C,6HR,F-7.0,SPT,E
780 GL17,MV406,R440,1256C,6.5HR,F-7.0,+SPMT+GL,SPT,E
781 SPMT2,MV406,R440,OKB,1256C,6.5HR,F-7.0,SPT,E

	782	783	784	785	786	787	788	789	790	791	792
SiO2	46.84	46.45	46.58	46.31	46.14	45.05	47.97	38.60	50.81	48.17	52.23
TiO2	2.83	2.91	2.98	2.86	2.88	2.54	3.01	nd	1.58	2.74	0.22
Al2O3	14.55	14.47	14.35	14.31	14.51	14.91	13.47	nd	2.24	13.62	28.92
Fe2O3	2.48	2.71	2.46	2.58	2.43	2.27	2.73	nd	nd	2.77	nd
Cr2O3	0.16	nd	0.08	nd	nd	0.09	nd	nd	0.18	nd	nd
FeO	8.47	9.00	8.89	9.26	9.22	9.25	9.52	22.04	8.18	9.61	0.99
MnO	0.22	0.20	0.23	0.24	0.22	0.33	0.27	0.52	0.21	0.28	nd
NiO	nd	nd	nd	nd	nd	nd	nd	0.47	nd	nd	nd
MgO	8.89	8.93	8.77	8.74	8.80	8.73	5.42	38.74	13.62	5.88	nd
CaO	9.49	9.41	9.67	9.40	9.34	11.16	10.51	0.53	21.62	10.67	13.09
Na2O	3.17	3.17	3.15	2.85	3.15	1.27	2.72	nd	0.38	2.47	3.42
K2O	1.33	1.26	1.22	1.19	1.20	1.44	1.34	nd	nd	1.18	0.24
P2O5	nd	nd	0.36	0.35	0.65	0.41	0.48	nd	nd	0.36	nd
total=	98.43	98.51	98.74	98.09	98.54	97.45	97.44	100.90	98.82	97.75	99.11
Mg#	65.2	63.9	63.7	62.7	63.0	62.7	50.4	75.8	-	52.2	-
An	-	-	-	-	-	-	-	-	-	-	66.9

782 GL6,MV406,R439,1266C,7.5HR,F-6.8,+SPMT+GL,PT,E
783 GL29,MV406,R451,1277C,6.5HR,F-6.6,+SPMT+GL,PTFE,E
784 GL272,MV406,R522,1277C,18HR,F-6.8,+SPMT+GL,SPT,E
785 GL365,MV406,R497,1288C,18HR,F-6.6,-GL,SPT,E
786 GL1907,MV406,R4-253,1291C,2HR,F-6.7,-GL,PTFE,W
787 GL250,MV400,R580,1302C,2HR,F-6.6,-GL,PTFE,E
788 GL756,MV501,R511,1151C,18.5HR,F-8.4,+OL+CPX+PL+SPMT+GL,SPT,E
789 OL252,MV501,R511,1151C,18.5HR,F-8.4,SPT,E
790 CPX80,MV501,R511,1151C,18.5HR,F-8.4,SPT,E
791 GL407,MV501,R587,1158C,19HR,F-8.2,+OL+PL+SPMT+GL,PTFE,E
792 PL165,MV501,R587,1158C,19HR,F-8.2,PTFE,E

	793	794	795	796	797	798	799	800	801	802	803
SiO2	48.22	38.60	47.56	39.15	50.93	47.67	39.34	48.01	39.64	47.42	39.48
TiO2	2.69	0.12	2.55	0.22	0.19	2.33	nd	2.36	nd	2.40	nd
Al2O3	14.25	nd	14.59	nd	29.12	14.84	nd	14.32	nd	13.99	nd
Fe2O3	2.54	nd	2.48	nd	nd	2.24	nd	2.49	nd	2.45	nd
Cr2O3	0.05	nd	0.05	nd	nd	nd	nd	nd	nd	nd	nd
FeO	9.23	19.14	9.00	18.26	1.23	8.94	17.36	9.37	16.23	9.39	15.88
MnO	0.25	0.43	0.28	0.33	nd	0.22	0.26	0.30	0.29	0.21	0.32
NiO	nd	0.20	nd	0.46	nd	nd	0.34	nd	0.52	nd	0.61
MgO	6.08	40.09	6.54	41.18	0.21	6.85	42.37	7.45	42.22	7.93	43.17
CaO	10.70	0.64	10.70	0.45	13.53	10.44	0.45	10.30	0.48	10.27	0.40
Na2O	2.72	nd	2.70	nd	3.50	2.62	nd	2.53	nd	2.45	nd
K2O	1.14	nd	1.05	nd	0.23	0.99	nd	1.01	nd	1.01	nd
P2O5	0.37	nd	0.14	nd	nd	0.34	nd	0.25	nd	0.30	nd
total=	98.24	99.22	97.64	100.05	98.94	97.48	100.12	98.39	99.38	97.82	99.86
Mg#	54.0	78.9	56.4	80.1	-	57.7	81.3	58.6	82.3	60.1	82.9
An	-	-	-	-	67.2	-	-	-	-	-	-

793 GL722,MV501,R514,1165C,16HR,F-8.2,+OL+PL+SPMT+GL,SPT,E
794 OL238,MV501,R514,1165C,16HR,F-8.2,SPT,E
795 GL832,MV501,R532,1176C,20.5HR,F-8.0,+OL+PL+SPMT+GL,PTFE,E
796 OL278,MV501,R532,1176C,20.5HR,F-8.0,PTFE,E
797 PL272,MV501,R532,1176C,20.5HR,F-8.0,PTFE,E
798 GL824,MV501,R531,1186C,20HR,F-8.0,+OL+SPMT+GL,PTFE,E
799 OL275,MV501,R531,1186C,20HR,F-8.0,PTFE,E
800 GL320,MV501,R538,1215C,16.5HR,F-7.5,+OL+SPMT+GL,PTFE,E
801 OL111,MV501,R538,1215C,16.5HR,F-7.5,PTFE,E
802 GL322,MV501,R539,1226C,21HR,F-7.4,+OL+SPMT+GL,PTFE,E
803 OL112,MV501,R539,1226C,21HR,F-7.4,PTFE,E

	804	805	806	807	808	809	810	811	812	813	814
SiO2	47.38	47.38	47.93	46.92	37.84	51.52	50.86	47.25	38.61	47.27	38.90
TiO2	2.25	2.34	2.29	4.56	0.15	0.14	1.35	3.96	0.21	3.68	nd
Al2O3	14.09	14.05	14.11	13.28	nd	29.23	1.96	13.20	0.24	13.63	0.22
Fe2O3	2.30	2.41	2.39	3.11	nd	nd	nd	2.87	nd	2.80	nd
Cr2O3	nd	nd	0.14	nd	nd	nd	nd	nd	nd	0.19	nd
FeO	9.44	9.53	9.36	9.73	25.20	1.00	9.25	9.69	23.48	9.67	22.52
MnO	0.25	0.36	0.30	0.20	0.33	nd	0.22	0.20	0.21	0.18	0.25
NiO	nd	nd	nd	nd	0.40	nd	nd	nd	0.29	nd	0.49
MgO	8.49	8.40	8.16	4.50	35.64	nd	13.83	5.13	37.10	5.18	37.81
CaO	10.03	9.86	10.06	9.46	0.62	12.74	21.27	10.05	0.74	9.77	0.55
Na2O	2.39	2.23	2.29	2.75	nd	3.66	nd	3.05	nd	2.62	nd
K2O	0.94	1.05	1.00	1.97	nd	0.45	nd	1.71	nd	1.55	nd
P2O5	0.19	0.19	0.26	1.17	nd	nd	nd	0.95	nd	1.04	nd
total=	97.75	97.80	98.29	97.65	100.18	98.74	98.74	98.06	100.88	97.58	100.74
Mg#	61.6	61.1	60.8	45.2	71.6	-	-	48.5	73.8	48.8	75.0
An	-	-	-	-	-	64.0	-	-	-	-	-

804 GL814,MV501,R530,1232C,16HR,F-7.4,+SPMT+GL,PTFE,E
805 GL380,MV501,R524,1252C,20HR,F-7.1,-GL,SPT,E
806 GL280,MV501,R522,1277C,18HR,F-6.8,-GL,SPT,E
807 GL946,MV167,R535,1118C,20HR,F-8.9,+OL+CPX+PL+SPMT+GL,PTFE,E
808 OL313,MV167,R535,1118C,20HR,F-8.9,PTFE,E
809 PL302,MV167,R535,1118C,20HR,F-8.9,PTFE,E
810 CPX92,MV167,R535,1118C,20HR,F-8.9,PTFE,E
811 GL845,MV167,R517,1131C,12HR,F-8.8,+OL+CPX+PL+SPMT+GL,SPT,E
812 OL284R,MV167,R517,1131C,12HR,F-8.8,SPT,E
813 GL432,MV167,R509,1140C,13HR,F-8.6,+OL+PL+SPMT+GL,SPT,E
814 OL145,MV167,R509,1140C,13HR,F-8.6,SPT,E

	815	816	817	818	819	820	821	822	823	824	825
SiO2	51.74	47.57	39.04	51.07	47.00	38.94	49.66	47.19	39.59	38.90	48.92
TiO2	0.28	3.51	nd	0.17	3.19	0.11	0.21	2.88	nd	nd	0.41
Al2O3	28.89	14.21	0.20	29.93	14.92	nd	30.42	15.50	nd	nd	30.20
Fe2O3	nd	2.78	nd	nd	2.62	nd	nd	2.47	nd	nd	nd
FeO	1.07	9.42	21.22	1.03	9.11	18.60	1.25	8.54	16.91	17.94	1.44
MnO	nd	0.06	0.17	nd	0.13	0.17	nd	0.14	0.20	0.24	nd
NiO	nd	nd	0.40	nd	nd	0.46	nd	nd	0.37	0.41	nd
MgO	nd	5.57	39.40	nd	6.12	40.52	0.28	6.62	41.74	41.76	0.59
CaO	12.94	9.86	0.49	13.56	9.68	0.55	14.33	9.74	0.45	0.46	14.46
Na2O	3.70	2.84	nd	3.44	2.78	nd	2.95	2.73	nd	nd	2.82
K2O	0.45	1.66	nd	0.40	1.34	nd	0.30	1.29	nd	nd	0.26
P2O5	nd	0.82	nd	nd	nd	nd	nd	nd	nd	nd	nd
total=	99.07	98.30	100.92	99.60	96.89	99.35	99.40	97.10	99.26	99.71	99.10
Mg#	-	51.3	76.8	-	54.5	79.5	-	58.0	81.5	80.6	-
An	64.2	-	-	66.9	-	-	71.6	-	-	-	72.8

815 PL180,MV167,R509,1140C,13HR,F-8.6,SPT,E
816 GL1006,MV167,R511,1151C,18.5HR,F-8.4,+OL+PL+SPMT+GL,SPT,E
817 OL330,MV167,R511,1151C,18.5HR,F-8.4,SPT,E
818 PL311,MV167,R511,1151C,18.5HR,F-8.4,SPT,E
819 GL4,MV167,R438,1176C,7HR,F-8.0,+OL+PL+SPMT+GL,SPT,E
820 OL13,MV167,R438,1176C,7HR,F-8.0,SPT,E
821 PL2,MV167,R438,1176C,7HR,F-8.0,SPT,E
822 GL10,MV167,R434,1185C,12HR,F-7.8,+OL+PL+SPMT+GL,SPT,E
823 OL103,MV167,R434,1185C,12HR,F-7.8,SPT,E
824 OL6,MV167,R434,1185C,12HR,F-7.8,SPT,E
825 PL4,MV167,R434,1185C,12HR,F-7.8,SPT,E

	826	827	828	829	830	831	832	833	834	835	836
SiO2	46.81	46.47	46.93	47.07	39.63	46.26	46.81	39.21	47.01	39.99	46.81
TiO2	2.86	2.97	2.93	2.83	nd	2.82	2.71	nd	2.84	0.19	2.86
Al2O3	15.55	15.59	15.40	15.47	0.26	15.33	15.09	nd	15.32	nd	15.12
Fe2O3	2.47	2.51	2.49	2.56	nd	2.51	2.48	nd	2.50	nd	2.49
Cr2O3	nd	nd	nd	nd	nd	0.07	0.07	nd	0.11	nd	nd
FeO	8.84	9.01	9.06	8.49	15.82	8.92	8.81	15.66	9.05	15.90	9.15
MnO	0.23	0.23	0.14	0.13	0.28	nd	0.16	0.21	0.08	0.27	0.13
NiO	nd	nd	nd	nd	0.59	nd	nd	0.65	nd	0.69	nd
MgO	6.71	7.20	7.42	7.45	43.33	7.53	7.48	43.89	7.79	43.43	7.56
CaO	9.57	9.70	9.87	9.63	0.48	9.50	9.54	0.37	9.73	0.42	9.77
Na2O	2.75	2.71	2.69	2.76	nd	2.55	2.65	nd	2.72	nd	2.58
K2O	1.26	1.28	1.21	1.20	nd	1.27	1.25	nd	1.18	nd	1.17
P2O5	nd	nd	nd	nd	nd	nd	0.56	nd	nd	nd	0.63
total=	97.05	97.67	98.14	97.59	100.39	96.76	97.61	99.99	98.33	100.89	98.27
Mg#	57.5	58.8	59.3	61.0	83.0	60.1	60.2	83.3	60.5	83.0	59.6

826 GL16,MV167,R436,1197C,8HR,F-7.7,+OL+SPMT+GL,SPT,E
827 GL19,MV167,R422,1205C,2HR,F-7.6,+OL+SPMT+GL,PT,E
828 GL3,MV167,R421,1206C,2HR,F-7.6,+OL+SPMT+GL,PT,E
829 GL6,MV167,R432,1207C,2HR,F-7.4,+OL+SPMT+GL,PT,E
830 OL11,MV167,R432,1207C,2HR,F-7.4,PT,E
831 GL2,MV167,R424,1208C,2HR,F-7.5,+OL+SPMT+GL,PT,E
832 GL666,MV167,R418,1209C,3HR,F-7.5,+OL+SPMT+GL,PT,E
833 OL220,MV167,R418,1209C,3HR,F-7.5,PT,E
834 GL10,MV167,R437,1211C,6HR,F-7.5,+OL+SPMT+GL,SPT,E
835 OL6,MV167,R437,1211C,6HR,F-7.5,SPT,E
836 GL674,MV167,R419,1214C,2HR,F-7.5,+OL+SPMT+GL,PT,E

	837	838	839	840	841	842	843	844	845	846	847
SiO2	46.62	39.99	39.74	47.02	39.22	46.80	46.66	46.81	46.84	46.45	46.47
TiO2	2.77	nd	nd	2.69	nd	2.70	2.77	2.78	2.67	2.76	2.76
Al2O3	15.34	0.09	0.11	15.29	nd	15.40	15.28	15.32	15.21	15.16	15.23
Fe2O3	2.37	nd	nd	2.40	nd	2.38	2.37	2.32	2.49	2.35	2.34
Cr2O3	0.03	nd	nd	nd	nd	nd	0.05	0.04	0.05	0.04	0.06
FeO	9.18	15.43	15.49	9.07	15.45	8.55	9.10	9.25	8.56	9.22	9.32
MnO	0.17	0.23	0.24	0.15	0.23	0.13	0.16	0.14	0.19	0.17	0.18
NiO	0.06	0.64	0.68	nd	0.59	nd	nd	0.05	nd	0.03	0.04
MgO	8.00	43.60	43.85	7.98	44.30	8.06	8.22	8.39	8.12	8.31	8.26
CaO	9.18	0.38	0.37	9.60	0.45	9.37	9.30	9.25	9.47	9.16	9.22
Na2O	2.86	nd	nd	2.46	nd	2.59	2.77	2.68	2.81	2.62	2.86
K2O	1.04	nd	nd	1.23	nd	1.22	1.26	1.14	1.15	1.00	0.96
P2O5	0.51	nd	nd	0.54	nd	nd	0.52	0.47	nd	0.54	0.61
total=	98.13	100.36	100.48	98.43	100.24	97.20	98.46	98.64	97.56	97.81	98.31
Mg#	60.8	83.4	83.5	61.1	83.6	62.7	61.7	61.8	62.8	61.6	61.2

837 GL1158,MV167,R548,1219C,3.5HR,F-7.5,+OL+SPMT+GL,PTFE,W
838 OL110,MV167,R548,1219C,3.5HR,F-7.5,PTFE,W
839 OL111,MV167,R548,1219C,3.5HR,F-7.5,PTFE,W
840 GL624,MV167,R496,1223C,19HR,F-7.4,+OL+SPMT+GL,SPT,E
841 OL207,MV167,R496,1223C,19HR,F-7.4,SPT,E
842 GL108,MV167,R433,1232C,6.5HR,F-7.2,+SPMT+GL,SPT,E
843 GL1224,MV167,R550,1236C,3HR,F-7.3,+SPMT+GL,PTFE,W
844 GL1221,MV167,R551,1248C,16HR,F-7.2,+SPMT+GL,PTFE,W
845 GL15,MV167,R412,1260C,1HR,F-6.8,+SPMT+GL,PT,E
846 GL1120,MV167,R555,1261C,20HR,F-7.0,+SPMT+GL,PTFE,W
847 GL1165,MV167,R570,1274C,3.5HR,F-6.9,-GL,PTFE,W

	848	849	850	851	852	853	854	855	856	857	858
SiO2	47.17	39.31	39.42	39.35	39.13	46.32	38.78	39.17	39.25	39.53	46.70
TiO2	2.70	nd	nd	nd	nd	2.78	0.09	nd	nd	nd	2.72
Al2O3	15.64	0.08	0.17	0.15	0.13	15.33	0.07	0.15	0.13	0.11	15.26
Fe2O3	2.41	nd	nd	nd	nd	2.40	nd	nd	nd	nd	2.34
Cr2O3	0.02	nd	nd	nd	nd	0.04	0.04	nd	nd	nd	0.04
FeO	8.92	18.14	17.32	15.94	18.29	9.09	17.37	17.18	16.30	15.79	9.17
MnO	0.15	0.27	0.26	0.24	0.27	0.18	0.23	0.23	0.21	0.23	0.17
NiO	0.06	0.18	0.12	0.15	0.16	0.01	0.12	0.14	0.15	0.21	0.01
MgO	7.53	41.67	41.91	43.50	41.70	7.67	42.83	43.00	43.59	44.16	7.93
CaO	9.48	0.35	0.46	0.34	0.42	9.51	0.35	0.41	0.43	0.41	9.37
Na2O	2.83	nd	nd	nd	nd	2.76	0.02	nd	nd	nd	2.76
K2O	1.15	nd	nd	nd	nd	1.00	nd	nd	nd	nd	0.86
P2O5	0.36	nd	nd	nd	nd	0.59	nd	nd	nd	nd	0.59
total=	98.42	100.00	99.66	99.67	100.10	97.68	99.90	100.28	100.06	100.44	97.92
Mg#	60.1	80.4	81.2	82.9	80.3	60.1	81.5	81.7	82.7	83.3	60.7

848 GL1241,MV167F,R544,1205C,2HR,F-7.6,+OL+SPMT+GL,PTFE,W
849 OL142,MV167F,R544,1205C,2HR,F-7.6,PTFE,W
850 OL143,MV167F,R544,1205C,2HR,F-7.6,PTFE,W
851 OL144,MV167F,R544,1205C,2HR,F-7.6,PTFE,W
852 OL146,MV167F,R544,1205C,2HR,F-7.6,PTFE,W
853 GL1213,MV167F,R542,1208C,2.5HR,F-7.6,+OL+SPMT+GL,PTFE,W
854 OL100,MV167F,R542,1208C,2.5HR,F-7.6,PTFE,W
855 OL101R,MV167F,R542,1208C,2.5HR,F-7.6,PTFE,W
856 OL102,MV167F,R542,1208C,2.5HR,F-7.6,PTFE,W
857 OL103,MV167F,R542,1208C,2.5HR,F-7.6,PTFE,W
858 GL1160,MV167F,R548,1219C,3.5HR,F-7.5,+OL+SPMT+GL,PTFE,W

	859	860	861	862	863	864	865	866	867	868	869
SiO2	39.93	46.78	39.22	39.60	46.79	46.49	46.52	55.16	51.19	50.06	54.74
TiO2	nd	2.66	nd	nd	2.63	2.65	2.62	3.99	4.25	1.22	3.32
Al2O3	0.11	15.07	0.09	0.12	15.03	14.82	14.86	12.73	11.59	2.15	12.89
Fe2O3	nd	2.34	nd	nd	2.26	2.29	2.31	0.41	3.17	nd	0.38
Cr2O3	nd	0.04	nd	nd	0.05	0.05	0.05	nd	nd	nd	nd
FeO	17.59	9.24	15.04	15.03	9.29	9.15	9.39	11.06	10.80	15.16	10.60
MnO	0.27	0.16	0.24	0.22	0.16	0.17	0.20	0.20	0.11	0.26	0.18
NiO	0.14	0.05	0.17	0.16	0.07	nd	nd	nd	nd	nd	nd
MgO	42.64	8.68	43.94	43.84	8.97	8.96	8.90	3.32	3.92	12.50	3.71
CaO	0.33	9.35	0.39	0.38	9.33	9.21	9.23	7.04	7.67	17.19	7.45
Na2O	nd	2.63	nd	nd	2.63	2.61	2.73	2.60	2.86	nd	3.08
K2O	nd	1.07	nd	nd	0.89	0.87	0.91	1.46	1.07	nd	1.26
P2O5	nd	0.51	nd	nd	0.50	0.56	0.50	0.64	0.52	nd	0.34
total=	101.01	98.58	99.09	99.35	98.60	97.83	98.22	98.61	97.15	98.54	97.95
Mg#	81.2	62.6	83.9	83.9	63.2	63.6	62.8	34.9	39.3	-	38.4

859 OL112,MV167F,R548,1219C,3.5HR,F-7.5,PTFE,W
860 GL1226,MV167F,R550,1236C,3HR,F-7.3,+OL+SPMT+GL,PTFE,W
861 OL137,MV167F,R550,1236C,3HR,F-7.3,PTFE,W
862 OL139,MV167F,R550,1236C,3HR,F-7.3,PTFE,W
863 GL1220,MV167F,R551,1248C,16HR,F-7.2,+SPMT+GL,PTFE,W
864 GL1117,MV167F,R555,1261C,20HR,F-7.0,-GL,PTFE,W
865 GL1162,MV167F,R570,1274C,3.5HR,F-6.9,-GL,PTFE,W
866 GL930R,MV40B,R575,1099C,17HR,F-13.3,+OL+CPX+PL+IL+GL,PTFE,E
867 GL463,MV40B,R494,1104C,19HR,F-9.1,+OL+CPX+PL+SPMT+GL,PTFE,E
868 CPX58,MV40B,R494,1104C,19HR,F-9.1,PTFE,E
869 GL912,MV40B,R574,1113C,19HR,F-13.1,+OL+CPX+PL+GL,PTFE,E

	870	871	872	873	874	875	876	877	878	879	880
SiO2	37.59	53.07	51.76	51.69	37.57	54.00	49.57	52.07	52.60	37.90	38.16
TiO2	0.15	0.21	0.98	3.86	0.15	0.18	1.77	0.76	3.33	0.15	0.13
Al2O3	nd	28.52	1.26	11.83	nd	27.94	2.53	1.55	12.17	nd	nd
Fe2O3	nd	nd	nd	3.03	nd	nd	nd	nd	2.78	nd	nd
Cr2O3	nd	nd	0.24	nd	nd	nd	nd	0.46	nd	nd	nd
FeO	30.25	0.84	11.23	10.32	28.19	0.75	12.94	9.62	10.00	26.77	26.54
MnO	0.41	nd	0.27	0.12	0.35	nd	0.31	0.20	0.14	0.42	0.41
NiO	0.27	nd	nd	nd	0.54	nd	nd	nd	nd	0.60	0.62
MgO	31.89	nd	16.36	4.10	32.97	nd	13.12	16.36	4.43	34.88	35.05
CaO	0.67	12.28	17.30	7.91	0.52	11.72	18.10	17.88	8.33	0.56	0.43
Na2O	nd	4.43	nd	2.86	nd	4.43	0.30	nd	2.87	nd	nd
K2O	nd	0.23	nd	1.03	nd	0.18	nd	nd	0.87	nd	nd
P2O5	nd	nd	nd	0.36	nd	nd	nd	nd	nd	nd	nd
total=	101.23	99.58	99.40	97.11	100.29	99.20	98.64	98.90	97.52	101.28	101.34
Mg#	65.3	-	-	41.5	67.6	-	-	-	44.1	69.9	70.2
An	-	59.7	-	-	-	58.7	-	-	-	-	-

870 OL303,MV40B,R574,1113C,19HR,F-13.1,PTFE,E
871 PL295,MV40B,R574,1113C,19HR,F-13.1,PTFE,E
872 CPX88,MV40B,R574,1113C,19HR,F-13.1,PTFE,E
873 GL454,MV40B,R493,1115C,17.5HR,F-8.9,+OL+CPX+PL+SPMT+GL,PTFE,E
874 OL155,MV40B,R493,1115C,17.5HR,F-8.9,PTFE,E
875 PL194,MV40B,R493,1115C,17.5HR,F-8.9,PTFE,E
876 CPX55,MV40B,R493,1115C,17.5HR,F-8.9,PTFE,E
877 CPX57,MV40B,R493,1115C,17.5HR,F-8.9,PTFE,E
878 GL12,MV40B,R491,1124C,19HR,F-8.8,+OL+CPX+PL+SPMT+GL,PTFE,E
879 OL11R,MV40B,R491,1124C,19HR,F-8.8,PTFE,E
880 OL8,MV40B,R491,1124C,19HR,F-8.8,PTFE,E

	881	882	883	884	885	886	887	888	889	890	891
SiO2	38.12	53.62	51.95	54.18	53.19	51.13	51.31	52.26	51.20	50.80	52.22
TiO2	0.13	0.22	0.25	0.15	0.14	1.16	0.90	0.80	1.06	1.72	3.11
Al2O3	nd	27.85	29.29	28.09	28.94	2.44	2.30	1.55	2.40	3.89	12.58
Fe2O3	nd	nd	nd	nd	nd	nd	nd	nd	nd	nd	0.37
Cr2O3	nd	nd	nd	nd	nd	0.35	0.86	0.36	0.40	0.27	nd
FeO	26.54	0.95	1.01	0.90	0.90	10.91	8.56	10.63	11.56	11.38	11.29
MnO	0.41	nd	nd	nd	nd	0.30	0.15	0.17	0.25	0.22	0.14
NiO	0.62	nd	nd	nd	nd	nd	nd	nd	nd	nd	nd
MgO	34.77	nd	nd	nd	nd	15.84	15.75	16.87	16.39	13.61	4.14
CaO	0.43	11.95	13.27	12.25	12.50	16.98	19.46	16.94	16.13	17.93	8.32
Na2O	nd	4.65	3.74	4.49	4.05	nd	nd	nd	nd	nd	2.85
K2O	nd	nd	nd	nd	0.13	nd	nd	nd	nd	nd	0.88
P2O5	nd	nd	nd	nd	nd	nd	nd	nd	nd	nd	0.35
total=	101.02	99.24	99.51	100.06	99.85	99.11	99.29	99.58	99.39	99.82	96.25
Mg#	70.0	-	-	-	-	-	-	-	-	-	39.5
An	-	58.7	66.2	60.1	62.5	-	-	-	-	-	-

881 OL8R,MV40B,R491,1124C,19HR,F-8.8,PTFE,E
882 PL10,MV40B,R491,1124C,19HR,F-8.8,PTFE,E
883 PL11,MV40B,R491,1124C,19HR,F-8.8,PTFE,E
884 PL12,MV40B,R491,1124C,19HR,F-8.8,PTFE,E
885 PL16,MV40B,R491,1124C,19HR,F-8.8,PTFE,E
886 CPX10,MV40B,R491,1124C,19HR,F-8.8,PTFE,E
887 CPX5,MV40B,R491,1124C,19HR,F-8.8,PTFE,E
888 CPX6,MV40B,R491,1124C,19HR,F-8.8,PTFE,E
889 CPX7,MV40B,R491,1124C,19HR,F-8.8,PTFE,E
890 CPX9,MV40B,R491,1124C,19HR,F-8.8,PTFE,E
891 GL1098,MV40B,R573,1128C,16HR,F-13.0,+OL+CPX+PL+GL,PTFE,E

	892	893	894	895	896	897	898	899	900	901	902
SiO2	38.07	37.11	37.45	52.55	38.62	54.83	52.45	0.58	52.45	38.19	52.86
TiO2	0.14	0.11	0.12	2.92	nd	0.27	0.87	8.64	2.86	nd	0.27
Al2O3	nd	nd	nd	12.82	nd	26.99	2.26	7.77	13.11	nd	27.95
Fe2O3	nd	nd	nd	2.60	nd	nd	nd	17.24	0.36	nd	nd
Cr2O3	nd	nd	nd	0.04	nd	nd	0.45	24.73	0.09	nd	nd
FeO	27.24	28.06	28.30	9.59	24.06	1.06	10.99	30.67	11.21	25.75	1.02
MnO	0.38	0.39	0.39	0.19	0.34	nd	0.34	0.33	0.06	0.37	nd
NiO	0.46	0.24	0.23	nd	0.38	nd	nd	nd	nd	0.35	nd
MgO	33.73	33.31	33.58	4.83	37.66	nd	17.57	6.31	4.77	35.81	0.22
CaO	0.54	0.54	0.53	8.60	0.48	11.01	13.80	nd	8.95	0.42	12.50
Na2O	nd	nd	nd	2.99	nd	4.68	nd	nd	3.03	nd	3.88
K2O	nd	nd	nd	0.75	nd	0.18	nd	nd	0.78	nd	0.11
P2O5	nd	nd	nd	0.30	nd	nd	nd	nd	0.30	nd	nd
V2O3	nd	nd	nd	nd	nd	nd	nd	0.75	nd	nd	nd
total=	100.56	99.76	100.60	98.18	101.54	99.02	98.73	97.02	97.97	100.89	98.81
Mg#	68.8	67.9	67.9	47.3	73.6	-	-	26.8	43.1	71.3	-
An	-	-	-	-	-	55.9	-	-	-	-	63.6

892 OL353,MV40B,R573,1128C,16HR,F-13.0,PTFE,E
893 OL354,MV40B,R573,1128C,16HR,F-13.0,PTFE,E
894 OL354,MV40B,R573,1128C,16HR,F-13.0,PTFE,E
895 GL901,MV40B,R490,1137C,19HR,F-8.6,+OL+CPX+PL+SPMT+GL,PTFE,E
896 OL300,MV40B,R490,1137C,19HR,F-8.6,PTFE,E
897 PL292,MV40B,R490,1137C,19HR,F-8.6,PTFE,E
898 CPX86,MV40B,R490,1137C,19HR,F-8.6,PTFE,E
899 SPMT48,MV40B,R490,1137C,19HR,F-8.6,PTFE,E
900 GL501,MV40B,R569,1142C,12HR,F-12.8,+OL+PL+GL,PTFE,E
901 OL166,MV40B,R569,1142C,12HR,F-12.8,PTFE,E
902 PL203,MV40B,R569,1142C,12HR,F-12.8,PTFE,E

	903	904	905	906	907	908	909	910	911	912	913
SiO2	51.64	38.39	52.92	51.26	37.67	52.52	51.40	38.74	53.26	51.55	38.97
TiO2	2.70	nd	nd	2.61	nd	0.34	2.37	0.18	0.34	2.26	nd
Al2O3	13.66	nd	28.75	13.60	0.19	27.69	14.27	nd	27.98	14.88	nd
Fe2O3	2.41	nd	nd	0.35	nd	nd	2.39	nd	nd	0.32	nd
FeO	9.41	22.56	0.98	10.62	24.42	1.57	9.38	20.84	1.13	10.37	21.55
MnO	0.16	0.26	nd	0.18	0.34	nd	0.14	0.21	nd	0.19	0.29
NiO	nd	0.47	nd	nd	0.35	nd	nd	0.61	nd	nd	0.51
MgO	5.28	38.36	nd	5.16	36.44	0.29	5.79	39.35	nd	5.83	38.73
CaO	8.74	0.38	12.48	8.84	0.50	12.32	8.84	0.44	11.87	8.94	0.47
Na2O	2.90	nd	4.00	3.13	nd	3.93	2.99	nd	4.59	2.98	nd
K2O	0.67	nd	nd	0.76	nd	0.25	0.67	nd	0.16	0.63	nd
P2O5	0.25	nd	nd	0.13	nd	nd	0.11	nd	nd	0.28	nd
total=	97.82	100.42	99.13	96.64	99.91	98.91	98.35	100.37	99.33	98.23	100.52
Mg#	50.0	75.2	-	46.4	72.7	-	52.4	77.1	-	50.0	76.2
An	-	-	63.3	-	-	62.4	-	-	58.3	-	-

903 GL891,MV40B,R489,1147C,18HR,F-8.5,+OL+PL+SPMT+GL,PTFE,E
904 OL296,MV40B,R489,1147C,18HR,F-8.5,PTFE,E
905 PL287,MV40B,R489,1147C,18HR,F-8.5,PTFE,E
906 GL596,MV40B,R567,1156C,12HR,F-12.5,+OL+PL+GL,PTFE,E
907 OL200,MV40B,R567,1156C,12HR,F-12.5,PTFE,E
908 PL225,MV40B,R567,1156C,12HR,F-12.5,PTFE,E
909 GL708,MV40B,R488,1158C,19HR,F-8.3,+OL+PL+SPMT+GL,PTFE,E
910 OL231,MV40B,R488,1158C,19HR,F-8.3,PTFE,E
911 PL247,MV40B,R488,1158C,19HR,F-8.3,PTFE,E
912 GL1054R,MV40B,R565,1171C,11.5HR,F-12.3,+OL+PL+GL,PTFE,E
913 OL344,MV40B,R565,1171C,11.5HR,F-12.3,PTFE,E

	914	915	916	917	918	919	920	921	922	923	924
SiO2	52.48	52.41	39.63	51.29	39.27	50.91	39.31	50.95	51.25	39.23	51.08
TiO2	2.27	2.29	nd	2.25	nd	2.27	nd	2.19	2.23	nd	2.19
Al2O3	14.33	14.82	nd	14.88	nd	14.28	0.25	13.94	14.84	0.22	14.25
Fe2O3	2.45	2.42	nd	0.33	nd	2.30	nd	2.30	0.34	nd	2.44
Cr2O3	nd	0.05	nd	nd	nd	nd	nd	nd	0.06	nd	nd
FeO	9.07	9.31	19.10	10.54	20.93	8.99	18.12	9.06	10.84	19.93	9.42
MnO	0.22	0.12	0.25	0.20	0.27	0.17	0.21	0.18	0.18	0.17	0.16
NiO	nd	nd	0.80	nd	nd	nd	0.66	nd	nd	nd	nd
MgO	5.91	6.37	41.61	6.22	39.02	6.73	41.01	6.95	6.77	40.32	6.93
CaO	8.94	8.94	0.32	8.66	0.55	8.51	0.48	8.38	8.57	0.49	8.59
Na2O	3.08	2.78	nd	3.13	nd	2.89	nd	2.64	2.92	nd	2.60
K2O	0.57	0.60	nd	0.68	nd	0.61	nd	0.54	0.71	nd	0.56
P2O5	nd	0.23	nd	0.16	nd	0.09	nd	0.14	nd	nd	0.13
total=	99.32	100.34	101.71	98.34	100.04	97.75	100.04	97.27	98.71	100.36	98.35
Mg#	53.7	54.9	79.5	51.3	76.9	57.2	80.1	57.8	52.7	78.3	56.7

914 GL242,MV40B,R487,1171C,17.5HR,F-8.0,+OL+PL+SPMT+GL,PTFE,E
915 GL232,MV40B,R486,1180C,17.5HR,F-7.9,+OL+SPMT+GL,PTFE,E
916 OL98,MV40B,R486,1180C,17.5HR,F-7.9,PTFE,E
917 GL972,MV40B,R563,1185C,15HR,F-12.1,+OL+GL,PTFE,E
918 OL319,MV40B,R563,1185C,15HR,F-12.1,PTFE,E
919 GL798,MV40B,R485,1191C,18.5HR,F-7.8,+OL+SPMT+GL,PTFE,E
920 OL269,MV40B,R485,1191C,18.5HR,F-7.8,PTFE,E
921 GL403,MV40B,R484,1197C,19.5HR,F-7.7,+OL+SPMT+GL,PTFE,E
922 GL956,MV40B,R562,1199C,20HR,F-11.9,+OL+GL,PTFE,E
923 OL315,MV40B,R562,1199C,20HR,F-11.9,PTFE,E
924 GL166,MV40B,R474,1209C,3HR,F-7.5,+SPMT+GL,PTFE,E

	925	926	927	928	929	930	931	932	933	934	935
SiO2	50.88	51.57	50.77	48.62	48.50	0.25	0.53	0.48	38.26	38.27	50.73
TiO2	2.20	2.19	2.12	4.30	4.51	49.04	48.38	48.63	0.17	0.17	0.17
Al2O3	14.16	14.11	13.96	13.92	13.82	0.52	0.61	0.64	nd	nd	30.08
Fe2O3	0.32	2.29	0.33	0.51	3.19	8.15	9.04	9.19	nd	nd	nd
Cr2O3	0.08	nd	nd	nd	nd	0.23	nd	0.33	nd	nd	nd
FeO	10.74	9.06	11.05	12.04	9.04	32.77	32.28	32.67	27.20	26.57	1.12
MnO	0.17	nd	0.14	0.16	0.19	0.36	0.44	0.36	0.44	0.45	nd
NiO	nd	nd	nd	nd	nd	nd	nd	nd	0.24	0.31	nd
MgO	6.98	7.13	7.13	3.45	3.73	6.32	6.40	6.32	33.60	33.81	nd
CaO	8.50	8.50	8.53	8.48	8.23	nd	nd	nd	0.54	0.61	13.97
Na2O	2.97	2.76	2.86	3.51	3.43	nd	nd	nd	nd	nd	3.19
K2O	0.62	0.59	0.61	2.66	2.55	nd	nd	nd	nd	nd	0.44
P2O5	nd	0.07	0.13	0.86	nd	nd	nd	nd	nd	nd	nd
total=	97.62	98.27	97.63	98.51	97.19	97.64	97.68	98.62	100.45	100.19	99.70
Mg#	53.7	58.4	53.5	33.8	42.4	-	-	-	68.8	69.4	-
An	-	-	-	-	-	-	-	-	-	-	68.9

925 GL494,MV40B,R568,1214C,5HR,F-11.8,+OL+GL,PTFE,E
926 GL359,MV40B,R496,1223C,19HR,F-7.4,-GL,PTFE,E
927 GL1061,MV40B,R566,1227C,5HR,F-11.6,-GL,PTFE,E
928 GL933,MV160,R575,1099C,17HR,F-13.3,+OL+CPX+PL+IL+GL,PTFE,E
929 GL7,MV160,R494,1104C,19HR,F-9.0,+OL+CPX+PL+SPMT+IL+GL,PTFE,E
930 IL1,MV160,R494,1104C,19HR,F-9.0,PTFE,E
931 IL2,MV160,R494,1104C,19HR,F-9.0,PTFE,E
932 IL3,MV160,R494,1104C,19HR,F-9.0,PTFE,E
933 OL1,MV160,R494,1104C,19HR,F-9.0,PTFE,E
934 OL4,MV160,R494,1104C,19HR,F-9.0,PTFE,E
935 PL1,MV160,R494,1104C,19HR,F-9.0,PTFE,E

	936	937	938	939	940	941	942	943	944	945	946
SiO2	52.90	49.15	49.34	49.90	0.60	0.49	47.57	0.26	37.47	54.06	1.62
TiO2	0.37	2.19	2.20	2.21	21.24	21.45	5.14	53.51	0.13	0.36	24.78
Al2O3	27.83	3.76	3.90	3.51	3.98	3.77	13.43	0.42	nd	28.22	5.28
Fe2O3	nd	nd	nd	nd	22.31	22.44	0.51	nd	nd	nd	nd
Cr2O3	nd	0.14	nd	nd	1.17	1.15	0.05	1.05	nd	nd	11.79
FeO	1.11	8.81	9.03	8.50	42.13	42.73	11.87	35.05	28.85	0.75	44.03
MnO	nd	0.16	0.16	nd	0.40	0.33	0.14	0.39	0.50	nd	0.28
NiO	nd	nd	nd	nd	nd	nd	nd	nd	0.23	nd	nd
MgO	nd	13.28	12.95	13.10	5.53	5.37	3.87	6.77	32.79	nd	6.35
CaO	11.84	21.74	21.74	21.95	0.50	0.32	9.06	nd	0.60	11.03	0.66
Na2O	4.20	0.29	0.34	nd	nd	nd	2.95	nd	nd	4.54	nd
K2O	0.58	nd	nd	nd	nd	nd	2.22	nd	nd	0.64	nd
P2O5	nd	nd	nd	nd	nd	nd	0.72	nd	nd	nd	nd
total=	98.83	99.52	99.66	99.17	97.86	98.05	97.53	97.45	100.57	99.60	94.79
Mg#	-	-	-	-	19.0	18.3	36.8	-	66.9	-	20.4
An	58.8	-	-	-	-	-	-	-	-	55.1	-

936 PL5,MV160,R494,1104C,19HR,F-9.0,PTFE,E
937 CPX1,MV160,R494,1104C,19HR,F-9.0,PTFE,E
938 CPX2,MV160,R494,1104C,19HR,F-9.0,PTFE,E
939 CPX3,MV160,R494,1104C,19HR,F-9.0,PTFE,E
940 SPMT2,MV160,R494,1104C,19HR,F-9.0,PTFE,E
941 SPMT3,MV160,R494,1104C,19HR,F-9.0,PTFE,E
942 GL914,MV160,R574,1113C,19HR,F-13.1,+OL+CPX+PL+SPMT+IL+GL,PTFE,E
943 IL,MV160,R574,1113C,19HR,F-13.1,PTFE,E
944 OL304,MV160,R574,1113C,19HR,F-13.1,PTFE,E
945 PL296,MV160,R574,1113C,19HR,F-13.1,PTFE,E
946 SPMT,MV160,R574,1113C,19HR,F-13.1,PTFE,E

	947	948	949	950	951	952	953	954	955	956	957
SiO2	1.53	47.71	37.98	38.28	38.05	52.58	52.81	48.80	49.94	50.12	0.50
TiO2	24.90	4.75	0.11	nd	nd	0.32	0.44	2.59	2.28	1.84	19.94
Al2O3	5.42	13.26	nd	nd	nd	28.32	28.22	4.46	4.04	2.98	4.55
Fe2O3	nd	3.32	nd	nd	nd	nd	nd	nd	nd	nd	22.55
Cr2O3	11.95	nd	nd	nd	nd	nd	nd	0.12	0.13	0.14	2.96
FeO	43.97	9.66	25.83	25.89	26.14	0.84	1.39	8.93	9.09	8.20	41.01
MnO	0.21	0.28	0.30	0.32	0.33	nd	nd	nd	0.17	0.17	0.38
NiO	nd	nd	0.53	0.39	0.37	nd	nd	nd	nd	nd	nd
MgO	6.31	4.25	35.22	35.35	34.99	nd	nd	13.11	13.18	14.19	6.11
CaO	0.57	8.87	0.54	0.52	0.48	12.19	12.08	21.15	21.16	21.73	nd
Na2O	nd	3.60	nd	nd	nd	4.15	4.13	0.40	0.38	0.27	nd
K2O	nd	2.12	nd	nd	nd	0.44	0.54	nd	nd	nd	nd
V2O3	nd	nd	nd	nd	nd	nd	nd	nd	nd	nd	0.90
total=	94.86	97.82	100.51	100.75	100.36	98.84	99.61	99.56	100.37	99.64	98.90
Mg#	20.4	43.9	70.8	70.9	70.5	-	-	-	-	-	21.0
An	-	-	-	-	-	60.3	59.8	-	-	-	-

947 SPMT,MV160,R574,1113C,19HR,F-13.1,PTFE,E
948 GL3,MV160,R493,1115C,17.5HR,F-8.9,+OL+CPX+PL+SPMT+GL,PTFE,E
949 OL2,MV160,R493,1115C,17.5HR,F-8.9,PTFE,E
950 OL3,MV160,R493,1115C,17.5HR,F-8.9,PTFE,E
951 OL4,MV160,R493,1115C,17.5HR,F-8.9,PTFE,E
952 PL1,MV160,R493,1115C,17.5HR,F-8.9,PTFE,E
953 PL5,MV160,R493,1115C,17.5HR,F-8.9,PTFE,E
954 CPX1,MV160,R493,1115C,17.5HR,F-8.9,PTFE,E
955 CPX2,MV160,R493,1115C,17.5HR,F-8.9,PTFE,E
956 CPX3,MV160,R493,1115C,17.5HR,F-8.9,PTFE,E
957 SPMT1,MV160,R493,1115C,17.5HR,F-8.9,PTFE,E

	958	959	960	961	962	963	964	965	966	967	968
SiO2	0.72	47.16	38.51	51.51	46.55	38.12	47.26	38.24	51.12	47.13	38.59
TiO2	20.37	4.32	nd	0.41	4.63	nd	3.96	nd	0.23	4.28	0.18
Al2O3	4.42	13.86	0.63	28.60	13.70	nd	14.48	nd	29.32	14.29	nd
Fe2O3	21.23	3.19	nd	nd	0.45	nd	3.09	nd	nd	0.43	nd
Cr2O3	2.78	nd	nd	nd	nd	nd	nd	nd	nd	0.09	nd
FeO	41.70	9.68	24.01	1.35	11.86	26.44	9.77	22.94	0.94	11.71	24.21
MnO	0.28	0.17	0.33	nd	0.18	0.40	0.07	0.27	nd	0.20	0.36
NiO	nd	nd	0.41	nd	nd	nd	nd	0.36	nd	nd	nd
MgO	6.03	4.49	35.82	0.20	4.34	35.26	4.87	36.97	0.17	4.68	36.68
CaO	nd	8.98	0.65	13.09	9.14	0.57	8.92	0.48	13.47	9.07	0.49
Na2O	nd	3.51	nd	3.45	2.84	nd	3.33	nd	3.56	3.22	nd
K2O	nd	1.85	nd	0.36	1.85	nd	1.83	nd	0.32	1.72	nd
P2O5	nd	nd	nd	nd	0.67	nd	nd	nd	nd	0.51	nd
V2O3	0.74	nd	nd	nd	nd	nd	nd	nd	nd	nd	nd
total=	98.27	97.21	100.36	98.97	96.21	100.79	97.58	99.26	99.13	97.33	100.51
Mg#	20.5	45.3	72.7	-	39.5	70.4	47.0	74.2	-	41.6	73.0
An	-	-	-	66.2	-	-	-	-	66.4	-	-

958 SPMT2,MV160,R493,1115C,17.5HR,F-8.9,PTFE,E
959 GL84,MV160,R469,1127C,5HR,F-8.7,+OL+PL+SPMT+GL,PTFE,E
960 OL57,MV160,R469,1127C,5HR,F-8.7,PTFE,E
961 PL78,MV160,R469,1127C,5HR,F-8.7,PTFE,E
962 GL1103,MV160,R573,1128C,16HR,F-13.0,+OL+PL+SPMT?+GL,PTFE,E
963 OL355,MV160,R573,1128C,16HR,F-13.0,PTFE,E
964 GL6,MV160,R468,1140C,19HR,F-8.5,+OL+PL+SPMT+GL,PTFE,E
965 OL7,MV160,R468,1140C,19HR,F-8.5,PTFE,E
966 PL7,MV160,R468,1140C,19HR,F-8.5,PTFE,E
967 GL509,MV160,R569,1142C,12HR,F-12.8,+OL+PL+GL,PTFE,E
968 OL169,MV160,R569,1142C,12HR,F-12.8,PTFE,E

	969	970	971	972	973	974	975	976	977	978	979
SiO2	51.23	46.99	38.90	50.83	47.98	38.21	50.59	46.93	38.88	47.44	38.66
TiO2	0.26	3.73	0.27	0.47	3.84	0.27	0.41	3.49	nd	3.30	nd
Al2O3	29.14	14.91	nd	29.23	15.45	nd	29.95	15.53	nd	16.08	nd
Fe2O3	nd	2.81	nd	nd	0.39	nd	nd	2.85	nd	0.37	nd
Cr2O3	nd	nd	nd	nd	0.04	nd	nd	nd	nd	nd	nd
FeO	0.91	9.52	21.31	1.34	10.70	24.79	0.82	9.59	20.60	10.63	21.66
MnO	nd	0.16	0.25	nd	0.17	0.30	nd	0.08	0.27	0.14	0.21
NiO	nd	nd	0.50	nd	nd	0.46	nd	nd	0.66	nd	0.28
MgO	nd	5.16	38.94	0.23	5.00	36.85	nd	5.37	39.61	5.53	39.11
CaO	13.64	8.66	0.46	13.42	8.73	0.48	13.78	8.88	0.42	8.89	0.41
Na2O	3.40	3.23	nd	3.37	3.17	nd	3.28	3.24	nd	3.17	nd
K2O	0.27	1.63	nd	0.40	1.72	nd	0.39	1.64	nd	1.52	nd
P2O5	nd	0.35	nd	nd	0.30	nd	nd	0.34	nd	0.28	nd
total=	98.85	97.15	100.63	99.29	97.49	101.36	99.22	97.94	100.44	97.35	100.33
Mg#	-	49.1	76.5	-	45.4	72.6	-	49.9	77.4	48.1	76.3
An	67.8	-	-	67.1	-	-	68.3	-	-	-	-

969 PL205,MV160,R569,1142C,12HR,F-12.8,PTFE,E
970 GL701,MV160,R467,1151C,16HR,F-8.4,+OL+PL+SPMT+GL,PTFE,E
971 OL227,MV160,R467,1151C,16HR,F-8.4,PTFE,E
972 PL241,MV160,R467,1151C,16HR,F-8.4,PTFE,E
973 GL589,MV160,R567,1156C,12HR,F-12.5,+OL+PL+GL,PTFE,E
974 OL198,MV160,R567,1156C,12HR,F-12.5,PTFE,E
975 PL221,MV160,R567,1156C,12HR,F-12.5,PTFE,E
976 GL561,MV160,R466,1161C,16HR,F-8.2,+OL+PL+SPMT+GL,PTFE,E
977 OL186,MV160,R466,1161C,16HR,F-8.2,PTFE,E
978 GL1043,MV160,R565,1171C,11.5HR,F-12.3,+OL+PL+GL,PTFE,E
979 OL340,MV160,R565,1171C,11.5HR,F-12.3,PTFE,E

	980	981	982	983	984	985	986	987	988	989	990
SiO2	49.76	46.61	38.69	46.39	39.08	47.63	38.74	45.97	38.88	46.88	38.66
TiO2	0.16	3.15	0.15	3.23	nd	3.21	0.11	3.24	0.17	3.20	0.11
Al2O3	30.90	15.94	0.22	15.50	nd	16.30	nd	15.32	nd	15.81	nd
Fe2O3	nd	2.62	nd	2.58	nd	0.36	nd	2.68	nd	0.38	nd
FeO	0.78	9.06	19.43	9.15	18.67	10.48	19.64	9.34	18.20	11.33	20.49
MnO	nd	0.17	0.23	0.18	0.38	nd	0.22	0.17	0.29	0.17	0.20
NiO	nd	nd	0.75	nd	0.59	nd	0.35	nd	0.68	nd	nd
MgO	nd	6.00	40.45	6.17	41.77	5.87	40.66	6.50	41.79	6.58	39.89
CaO	14.87	8.89	0.56	8.77	0.40	9.06	0.48	8.63	0.45	8.66	0.47
Na2O	2.42	3.23	nd	2.84	nd	3.06	nd	2.82	nd	2.93	nd
K2O	0.25	1.47	nd	1.36	nd	1.45	nd	1.44	nd	1.31	nd
P2O5	nd	0.36	nd	0.40	nd	0.20	nd	0.34	nd	0.09	nd
total=	99.14	97.50	100.48	96.57	100.89	97.62	100.20	96.45	100.46	97.34	99.82
Mg#	-	54.1	78.8	54.6	80.0	50.0	78.7	55.4	80.4	50.9	77.6
An	76.1	-	-	-	-	-	-	-	-	-	-

980 PL314,MV160,R565,1171C,11.5HR,F-12.3,PTFE,E
981 GL548,MV160,R465,1174C,16HR,F-8.0,+OL+PL+SPMT+GL,PTFE,E
982 OL179,MV160,R465,1174C,16HR,F-8.0,PTFE,E
983 GL531,MV160,R463,1183C,5.5HR,F-7.9,+OL+SPMT+GL,PTFE,E
984 OL175,MV160,R463,1183C,5.5HR,F-7.9,PTFE,E
985 GL978,MV160,R563,1185C,15HR,F-12.1,+OL+GL,PTFE,E
986 OL321,MV160,R563,1185C,15HR,F-12.1,PTFE,E
987 GL616,MV160,R462,1196C,5HR,F-7.7,+OL+SPMT+GL,PTFE,E
988 OL206,MV160,R462,1196C,5HR,F-7.7,PTFE,E
989 GL965,MV160,R562,1199C,20HR,F-11.9,+OL+GL,PTFE,E
990 OL318,MV160,R562,1199C,20HR,F-11.9,PTFE,E

	991	992	993	994	995	996	997	998	999	1000	1001
SiO2	46.34	38.60	46.26	39.58	46.65	38.85	38.92	46.17	46.59	46.55	46.14
TiO2	3.05	0.19	3.21	0.15	3.18	nd	nd	3.22	3.08	3.27	3.15
Al2O3	15.54	nd	15.50	nd	15.33	0.10	0.10	15.29	15.28	15.40	15.38
Fe2O3	2.68	nd	2.56	nd	0.38	nd	nd	2.75	0.37	2.68	2.71
Cr2O3	nd	nd	nd	nd	0.18	0.05	0.06	0.09	0.08	nd	nd
FeO	9.50	18.33	9.21	17.15	11.58	20.09	19.68	9.34	11.47	9.22	9.48
MnO	0.19	0.33	0.06	0.24	nd	0.25	0.25	0.15	0.16	0.04	0.04
NiO	nd	0.69	nd	0.72	nd	0.31	0.27	nd	nd	nd	nd
MgO	7.07	41.54	7.12	41.87	6.91	40.71	41.15	7.24	7.50	7.33	7.32
CaO	8.55	0.47	8.66	0.48	8.79	0.42	0.40	8.65	8.59	8.66	8.61
Na2O	3.12	nd	3.00	nd	2.95	nd	nd	2.99	2.81	2.89	2.94
K2O	1.42	nd	1.41	nd	1.43	nd	nd	1.39	1.34	1.37	1.37
P2O5	0.35	nd	0.38	nd	0.33	nd	nd	nd	0.33	nd	nd
total=	97.81	100.15	97.37	100.19	97.71	100.78	100.83	97.28	97.60	97.41	97.14
Mg#	57.0	80.2	57.9	81.3	51.5	78.3	78.8	58.0	53.8	58.6	57.9

991 GL604,MV160,R460,1204C,3HR,F-7.6,+OL+SPMT+GL,PTFE,E
992 OL202,MV160,R460,1204C,3HR,F-7.6,PTFE,E
993 GL620,MV160,R461,1208C,3HR,F-7.6,+OL+SPMT+GL,PTFE,E
994 OL205,MV160,R461,1208C,3HR,F-7.6,PTFE,E
995 GL497,MV160,R568,1214C,5HR,F-11.8,+OL+GL,PTFE,E
996 OL502,MV160,R568,1214C,5HR,F-11.8,PTFE,W
997 OL503,MV160,R568,1214C,5HR,F-11.8,PTFE,W
998 GL71,MV160,R457,1223C,19HR,F-7.3,+SPMT+GL,PTFE,E
999 GL1058,MV160,R566,1227C,5HR,F-11.6,-GL,PTFE,E
1000 GL49,MV160,R455,1233C,24HR,F-7.2,+SPMT+GL,PTFE,E
1001 GL58,MV160,R456,1234C,17HR,F-7.2,+SPMT+GL,PTFE,E

	1002	1003	1004	1005	1006	1007	1008	1009	1010	1011	1012
SiO2	46.84	46.53	47.03	47.40	48.98	0.73	37.07	0.75	47.38	37.89	51.74
TiO2	3.17	3.16	3.35	3.25	4.19	47.30	nd	20.94	4.68	0.25	0.16
Al2O3	15.41	15.18	15.57	15.68	13.30	0.67	nd	3.44	12.94	0.28	28.49
Fe2O3	2.73	2.63	2.82	0.32	3.14	9.95	nd	23.19	3.40	nd	nd
Cr2O3	0.04	0.04	0.09	nd	nd	0.19	nd	0.68	nd	nd	nd
FeO	9.49	9.18	9.76	10.64	9.51	32.22	28.87	43.07	10.14	27.69	0.95
MnO	0.16	0.18	0.19	0.18	0.22	0.26	0.30	0.47	0.22	0.45	nd
MgO	7.18	7.23	7.38	7.53	3.52	6.13	32.85	5.35	4.20	34.03	nd
CaO	8.61	8.70	8.67	8.76	8.04	nd	0.44	nd	8.59	0.64	12.84
Na2O	3.10	2.89	2.77	2.59	2.72	nd	nd	nd	2.66	nd	3.47
K2O	1.36	1.39	1.28	1.29	2.96	nd	nd	nd	2.52	nd	0.59
P2O5	nd	nd	nd	0.09	0.98	nd	nd	nd	0.68	nd	nd
V2O3	nd	nd	nd	nd	nd	nd	nd	0.84	nd	nd	nd
total=	98.09	97.11	98.91	97.73	97.56	97.45	99.53	98.73	97.41	101.23	98.24
Mg#	57.4	58.4	57.4	55.8	39.7	-	67.0	18.1	42.5	68.7	-
An	-	-	-	-	-	-	-	-	-	-	64.8

1002 GL34,MV160,R454,1243C,16.5HR,F-7.1,+SPMT+GL,PTFE,E
1003 GL10,MV160,R453,1253C,8.5HR,F-7.0,-GL,PTFE,E
1004 GL38,MV160,R452,1265C,16HR,F-6.8,-GL,PTFE,E
1005 GL1037,MV160,R558,1299C,3HR,F-10.9,-GL,PTFE,E
1006 GL461,MV514,R494,1104C,19HR,F-9.1,+OL+CPX+PL+SPMT+IL+GL,PTFE,E
1007 IL10,MV514,R494,1104C,19HR,F-9.1,PTFE,E
1008 OL157,MV514,R494,1104C,19HR,F-9.1,PTFE,E
1009 SPMT33,MV514,R494,1104C,19HR,F-9.1,PTFE,E
1010 GL451,MV514,R493,1115C,17.5HR,F-8.9,+OL+PL+SPMT+GL,PTFE,E
1011 OL154,MV514,R493,1115C,17.5HR,F-8.9,PTFE,E
1012 PL193,MV514,R493,1115C,17.5HR,F-8.9,PTFE,E

	1013	1014	1015	1016	1017	1018	1019	1020	1021	1022	1023
SiO2	0.62	46.84	37.63	0.45	46.73	38.46	47.10	50.86	47.75	46.83	38.72
TiO2	20.98	4.39	0.17	18.32	3.78	0.17	3.40	0.24	3.29	2.76	nd
Al2O3	4.40	13.61	0.16	5.54	14.80	nd	15.68	29.86	15.76	16.36	nd
Fe2O3	21.54	3.31	nd	22.38	2.95	nd	2.80	nd	2.85	2.32	nd
Cr2O3	1.22	nd	nd	3.73	nd	nd	0.06	nd	nd	0.04	nd
FeO	43.10	10.19	26.40	39.52	10.32	24.47	10.03	1.10	9.81	9.33	18.57
MnO	0.35	0.20	0.31	0.27	0.21	0.43	0.18	nd	0.23	0.13	0.32
NiO	nd	nd	0.23	nd	nd	0.22	nd	nd	nd	nd	0.44
MgO	5.43	4.37	34.40	5.86	5.01	37.09	5.46	0.32	5.92	6.33	40.89
CaO	nd	8.28	0.53	nd	8.27	0.50	8.36	13.75	8.52	8.90	0.30
Na2O	nd	2.77	nd	nd	2.68	nd	2.87	3.40	2.70	2.47	nd
K2O	nd	2.40	nd	nd	2.03	nd	1.82	0.46	1.71	1.49	nd
P2O5	nd	0.75	nd	nd	0.51	nd	0.52	nd	0.46	0.39	nd
V2O3	1.03	nd	nd	0.90	nd	nd	nd	nd	nd	nd	nd
total=	98.67	97.11	99.83	96.97	97.29	101.34	98.28	99.99	99.00	97.35	99.24
Mg#	18.3	43.3	69.9	20.9	46.4	73.0	49.2	-	51.8	54.7	79.7
An	-	-	-	-	-	-	-	67.2	-	-	-

1013 SPMT31,MV514,R493,1115C,17.5HR,F-8.9,PTFE,E
1014 GL578,MV514,R472,1128C,5.5HR,F-8.7,+OL+PL+SPMT+GL,PTFE,E
1015 OL193,MV514,R472,1128C,5.5HR,F-8.7,PTFE,E
1016 SPMT37,MV514,R472,1128C,5.5HR,F-8.7,PTFE,E
1017 GL894,MV514,R489,1147C,18HR,F-8.5,+OL+PL+SPMT+GL,PTFE,E
1018 OL297,MV514,R489,1147C,18HR,F-8.5,PTFE,E
1019 GL710,MV514,R488,1158C,19HR,F-8.3,+OL+PL+SPMT+GL,PTFE,E
1020 PL248,MV514,R488,1158C,19HR,F-8.3,PTFE,E
1021 GL244,MV514,R487,1171C,17.5HR,F-8.0,+OL+PL+SPMT+GL,PTFE,E
1022 GL356,REVERSAL,MV514,R528,1171C,16HR,F-8.2,+OL+PL+SPMT+GL,PTFE,E
1023 OL118,REVERSAL,MV514,R528,1171C,16HR,F-8.2,PTFE,E

	1024	1025	1026	1027	1028	1029	1030	1031	1032	1033	1034
SiO2	0.23	48.18	50.82	46.70	39.19	47.14	47.58	47.93	46.84	50.07	37.02
TiO2	1.82	2.88	0.26	2.69	nd	2.71	2.83	2.82	2.77	3.98	0.62
Al2O3	43.15	16.71	29.56	16.90	nd	16.46	16.63	16.78	16.62	13.91	0.20
Fe2O3	9.31	2.62	nd	2.43	nd	2.43	2.48	2.56	2.63	3.04	nd
Cr2O3	11.87	nd	nd	nd	nd	0.07	0.04	nd	0.07	nd	nd
FeO	17.29	9.50	1.10	9.27	17.93	9.17	9.45	9.17	9.30	9.07	28.31
MnO	nd	0.19	nd	0.15	0.29	0.08	0.15	0.18	0.16	0.15	0.42
NiO	nd	nd	nd	nd	0.29	nd	nd	nd	nd	nd	0.47
MgO	15.06	6.46	nd	6.70	41.87	6.85	6.94	7.06	7.16	3.50	32.89
CaO	nd	8.69	14.25	8.76	0.38	8.61	8.74	8.75	8.83	7.86	0.64
Na2O	nd	2.76	2.84	2.54	nd	2.38	2.58	2.63	2.70	3.36	nd
K2O	nd	1.62	0.37	1.50	nd	1.51	1.49	1.52	1.41	2.60	nd
P2O5	nd	0.36	nd	0.43	nd	0.28	nd	nd	nd	0.95	nd
V2O3	0.19	nd	nd	nd	nd	nd	nd	nd	nd	nd	nd
total=	98.92	99.97	99.20	98.07	99.95	97.69	98.91	99.40	98.49	98.49	100.57
Mg#	60.8	54.8	-	56.3	80.6	57.1	56.7	57.8	57.8	40.7	67.4
An	-	-	71.9	-	-	-	-	-	-	-	-

1024 SPMT24,REVERSAL,MV514,R528,1171C,16HR,F-8.2,PTFE,E
1025 GL236,MV514,R486,1180C,17.5HR,F-7.9,+OL+PL+SPMT+GL,PTFE,E
1026 PL149,MV514,R486,1180C,17.5HR,F-7.9,PTFE,E
1027 GL800,MV514,R485,1191C,18.5HR,F-7.8,+OL+SPMT+GL,PTFE,E
1028 OL270,MV514,R485,1191C,18.5HR,F-7.8,PTFE,E
1029 GL405,MV514,R484,1197C,19.5HR,F-7.7,+SPMT+GL,PTFE,E
1030 GL35,MV514,R448,1208C,3HR,F-7.6,-GL,PTFE,E
1031 GL18,MV514,R429,1223C,6HR,F-7.3,-GL,PTFE,E
1032 GL17,MV514,R425,1263C,7.5HR,F-6.8,-GL,PT,E
1033 GL654Q,MV74,R520,1099C,15HR,F-9.1,+OL+CPX+PL+SPMT+IL+GL,PTFE,E
1034 OL218,MV74,R520,1099C,15HR,F-9.1,PTFE,E

	1035	1036	1037	1038	1039	1040	1041	1042	1043	1044	1045
SiO2	51.12	50.08	48.88	0.98	49.06	37.37	50.69	48.73	38.52	52.29	48.31
TiO2	0.19	1.86	4.40	46.91	4.28	0.46	nd	4.13	0.11	0.25	3.82
Al2O3	29.06	3.75	13.42	0.82	13.63	0.24	29.43	14.01	0.23	29.00	14.13
Fe2O3	nd	nd	2.93	9.07	2.85	nd	nd	2.77	nd	nd	2.77
Cr2O3	nd	0.17	nd	0.49	0.07	nd	nd	0.06	nd	nd	nd
FeO	0.98	9.74	9.22	31.63	8.90	25.33	0.98	9.25	24.08	1.13	9.18
MnO	nd	nd	0.15	0.30	nd	0.38	nd	0.14	0.35	nd	0.08
NiO	nd	nd	nd	nd	nd	0.43	nd	nd	0.57	nd	nd
MgO	nd	13.65	3.81	6.41	4.16	34.90	nd	4.58	36.20	nd	4.74
CaO	12.84	20.79	8.08	nd	8.77	0.63	13.10	8.62	0.55	12.47	8.55
Na2O	3.78	nd	3.31	nd	3.50	nd	3.69	3.48	nd	3.77	3.19
K2O	0.48	nd	2.26	nd	2.03	nd	0.39	1.88	nd	0.40	1.69
P2O5	nd	nd	0.68	nd	0.68	nd	nd	0.54	nd	nd	0.47
total=	98.45	100.04	97.14	96.61	97.93	99.74	98.28	98.19	100.61	99.31	96.93
Mg#	-	-	42.4	-	45.4	71.1	-	46.9	72.8	-	47.9
An	63.4	-	-	-	-	-	64.7	-	-	63.1	-

1035 PL238,MV74,R520,1099C,15HR,F-9.1,PTFE,E
1036 CPX79R,MV74,R520,1099C,15HR,F-9.1,PTFE,E
1037 GL877R,MV74,R519,1108C,21HR,F-9.1,+OL+CPX+PL+SPMT+IL+GL,PTFE,E
1038 IL60,MV74,R519,1108C,21HR,F-9.1,PTFE,E
1039 GL861R,MV74,R518,1120C,20HR,F-8.9,+OL+PL+SPMT+GL,PTFE,E
1040 OL289R,MV74,R518,1120C,20HR,F-8.9,PTFE,E
1041 PL280,MV74,R518,1120C,20HR,F-8.9,PTFE,E
1042 GL843,MV74,R517,1131C,12HR,F-8.8,+OL+PL+SPMT+GL,PTFE,E
1043 OL283,MV74,R517,1131C,12HR,F-8.8,PTFE,E
1044 PL274,MV74,R517,1131C,12HR,F-8.8,PTFE,E
1045 GL438,MV74,R510,1145C,18HR,F-8.5,+OL+PL+SPMT+GL,SPT,E

	1046	1047	1048	1049	1050	1051	1052	1053	1054	1055	1056
SiO2	52.30	48.57	38.89	51.73	48.18	38.77	51.07	50.32	48.67	48.61	50.61
TiO2	0.27	3.45	0.17	0.53	3.30	0.16	0.18	0.26	2.98	3.02	0.25
Al2O3	28.51	15.09	nd	28.06	15.28	0.15	29.46	29.85	15.89	16.24	29.93
Fe2O3	nd	2.45	nd	nd	2.55	nd	nd	nd	2.19	2.36	nd
Cr2O3	nd	nd	nd	nd	nd	nd	nd	nd	0.04	nd	nd
FeO	1.22	8.60	19.94	1.49	9.02	19.53	0.80	0.94	8.30	8.46	1.02
MnO	nd	0.11	0.37	nd	0.15	0.28	nd	nd	nd	0.09	nd
NiO	nd	nd	0.56	nd	nd	0.78	nd	nd	nd	nd	nd
MgO	0.21	5.25	40.41	0.30	5.61	39.65	nd	nd	5.92	6.14	0.16
CaO	12.68	8.62	0.43	12.28	8.68	0.56	13.11	13.58	8.88	8.82	13.86
Na2O	3.68	3.24	nd	3.74	3.22	nd	3.70	3.56	2.99	3.16	3.40
K2O	0.39	1.63	nd	0.47	1.46	nd	0.37	0.26	1.41	1.41	0.33
P2O5	nd	0.36	nd	nd	nd	nd	nd	nd	0.35	nd	nd
total=	99.26	97.37	100.77	98.60	97.45	99.88	98.69	98.77	97.62	98.31	99.56
Mg#	-	52.1	78.3	-	52.6	78.3	-	-	56.0	56.4	-
An	64.0	-	-	62.6	-	-	64.8	66.8	-	-	67.9

1046 PL181,MV74,R510,1145C,18HR,F-8.5,SPT,E
1047 GL763,MV74,R512,1155C,24HR,F-8.4,+OL+PL+SPMT+GL,PTFE,E
1048 OL256,MV74,R512,1155C,24HR,F-8.4,PTFE,E
1049 PL261,MV74,R512,1155C,24HR,F-8.4,PTFE,E
1050 GL8,MV74,R450,1166C,6.5HR,F-8.2,+OL+PL+SPMT+GL,SPT,E
1051 OL8,MV74,R450,1166C,6.5HR,F-8.2,SPT,E
1052 PL1,MV74,R450,1166C,6.5HR,F-8.2,SPT,E
1053 PL3R,MV74,R450,1166C,6.5HR,F-8.2,SPT,E
1054 GL354,REVERSAL,MV74,R528,1171C,16HR,F-8.2,+SPMT+GL,PTFE,E
1055 GL52,MV74,R449,1177C,14.5HR,F-8.0,+PL+SPMT+GL,SPT,E
1056 PL10,MV74,R449,1177C,14.5HR,F-8.0,SPT,E

	1057	1058	1059	1060	1061	1062	1063	1064	1065	1066	1067
SiO2	49.75	48.61	48.35	48.33	48.15	48.35	48.63	46.74	48.17	0.43	51.93
TiO2	0.22	2.97	2.96	3.00	3.00	3.15	4.37	4.86	5.01	47.31	0.45
Al2O3	30.84	16.22	16.04	16.16	16.10	16.16	12.64	12.60	13.17	0.62	27.90
Fe2O3	nd	2.39	2.49	2.41	2.54	2.38	3.42	3.40	3.28	10.51	nd
Cr2O3	nd	nd	nd	nd	nd	nd	nd	nd	nd	0.34	nd
FeO	0.93	8.49	8.44	8.45	8.41	8.26	10.09	10.18	10.03	30.22	1.35
MnO	nd	0.21	0.16	0.14	nd	0.17	0.22	0.17	0.20	0.37	nd
MgO	0.17	6.03	6.08	6.08	6.09	6.09	3.79	4.05	4.49	6.99	nd
CaO	14.52	8.77	8.87	8.74	8.82	8.76	8.40	8.51	8.44	nd	12.46
Na2O	3.00	3.19	3.16	3.22	3.07	3.17	2.68	2.56	2.71	nd	3.86
K2O	0.20	1.36	1.35	1.34	1.35	1.36	2.47	2.06	2.18	nd	0.55
P2O5	nd	nd	nd	nd	nd	nd	0.94	0.72	nd	nd	nd
total=	99.63	98.24	97.90	97.87	97.53	97.85	97.65	95.85	97.68	96.79	98.50
Mg#	-	55.9	56.2	56.2	56.3	56.8	40.1	41.5	44.4	-	-
An	71.9	-	-	-	-	-	-	-	-	-	62.0

1057 PL9,MV74,R449,1177C,14.5HR,F-8.0,SPT,E
1058 GL20,MV74,R447,1191C,5HR,F-7.8,+SPMT+GL,SPT,E
1059 GL4,MV74,R446,1200C,6.5HR,F-7.6,+SPMT+GL,SPT,E
1060 GL9,MV74,R443,1222C,7HR,F-7.4,+SPMT+GL,SPT,E
1061 GL10,MV74,R441,1245C,6HR,F-7.0,-GL,SPT,E
1062 GL25,MV74,R440,1256C,6.5HR,F-7.0,-GL,SPT,E
1063 GL480,MV72,R495,1105C,19HR,F-9.0,+OL+CPX+PL+SPMT+IL+GL,PTFE,E
1064 GL442R,MV72,R492,1114C,19.5HR,F-8.9,+OL+PL+SPMT+IL+GL,PTFE,E
1065 GL117,MV72,R491,1124C,19HR,F-8.8,+OL+PL+SPMT+IL+GL,PTFE,E
1066 IL1,MV72,R491,1124C,19HR,F-8.8,PTFE,E
1067 PL109,MV72,R491,1124C,19HR,F-8.8,PTFE,E

	1068	1069	1070	1071	1072	1073	1074	1075	1076	1077	1078
SiO2	2.01	46.66	51.68	46.19	38.02	50.48	46.34	38.84	50.76	46.34	39.12
TiO2	19.84	4.95	0.30	4.70	0.14	0.45	4.27	0.15	0.44	4.12	0.29
Al2O3	5.01	13.86	29.39	14.26	nd	29.56	14.92	0.22	28.77	15.00	0.54
Fe2O3	19.24	3.18	nd	3.08	nd	nd	2.98	nd	nd	2.87	nd
Cr2O3	2.19	nd	nd	nd	nd	nd	nd	nd	nd	nd	nd
FeO	43.40	10.04	0.85	10.25	23.37	1.16	10.16	22.36	1.54	9.96	21.20
MnO	0.32	0.21	nd	0.19	0.41	nd	0.19	0.32	nd	0.17	0.25
NiO	nd	nd	nd	nd	0.17	nd	nd	0.29	nd	nd	nd
MgO	5.96	4.80	nd	5.03	36.38	nd	5.57	38.83	0.34	5.79	38.17
CaO	nd	8.23	12.67	8.28	0.57	13.24	8.48	0.49	13.34	8.47	0.61
Na2O	nd	2.49	3.85	2.68	nd	3.61	2.71	nd	3.54	2.37	nd
K2O	nd	2.03	0.46	1.80	nd	0.45	1.65	nd	0.48	1.56	nd
P2O5	nd	0.57	nd	0.68	nd	nd	0.40	nd	nd	0.40	nd
V2O3	1.19	nd	nd	nd	nd	nd	nd	nd	nd	nd	nd
total=	99.16	97.02	99.20	97.14	99.06	98.95	97.67	101.50	99.21	97.05	100.18
Mg#	19.7	46.0	-	46.7	73.5	-	49.4	75.6	-	50.9	76.2
An	-	-	62.8	-	-	65.2	-	-	65.7	-	-

1068 SPMT9,MV72,R491,1124C,19HR,F-8.8,PTFE,E
1069 GL906,MV72,R490,1137C,19HR,F-8.6,+OL+PL+SPMT+GL,PTFE,E
1070 PL294,MV72,R490,1137C,19HR,F-8.6,PTFE,E
1071 GL898,MV72,R489,1147C,18HR,F-8.5,+OL+PL+SPMT+GL,PTFE,E
1072 OL299,MV72,R489,1147C,18HR,F-8.5,PTFE,E
1073 PL291,MV72,R489,1147C,18HR,F-8.5,PTFE,E
1074 GL712,MV72,R488,1158C,19HR,F-8.3,+OL+PL+SPMT+GL,PTFE,E
1075 OL233,MV72,R488,1158C,19HR,F-8.3,PTFE,E
1076 PL250,MV72,R488,1158C,19HR,F-8.3,PTFE,E
1077 GL514,MV72,R487,1171C,17.5HR,F-8.1,+OL+PL+GL,PTFE,E
1078 OL170,MV72,R487,1171C,17.5HR,F-8.1,PTFE,E

	1079	1080	1081	1082	1083	1084	1085	1086	1087	1088	1089
SiO2	49.59	46.50	39.14	47.13	39.60	50.75	46.16	46.38	47.68	47.92	37.39
TiO2	0.23	3.55	nd	3.61	0.26	0.30	3.64	3.58	2.54	3.68	0.19
Al2O3	30.45	15.83	nd	16.30	nd	30.80	15.99	15.92	15.80	13.42	nd
Fe2O3	nd	2.51	nd	2.75	nd	nd	2.63	2.70	2.39	3.06	nd
FeO	1.09	9.67	19.47	9.61	19.45	0.89	9.49	9.45	9.08	9.81	29.05
MnO	nd	0.17	0.19	0.16	0.21	nd	0.19	0.21	0.18	0.27	0.42
NiO	nd	nd	0.27	nd	0.20	nd	nd	nd	nd	nd	0.16
MgO	nd	6.27	40.40	6.51	41.72	nd	6.79	6.97	6.31	3.54	32.72
CaO	14.54	8.73	0.20	8.89	0.29	14.66	8.56	8.61	8.62	7.76	0.64
Na2O	2.88	2.51	nd	2.75	nd	2.60	2.54	2.49	3.21	3.91	nd
K2O	0.26	1.38	nd	1.39	nd	0.27	1.35	1.38	1.51	1.90	nd
P2O5	nd	0.35	nd	0.43	nd	nd	0.40	0.39	0.30	0.70	nd
total=	99.04	97.47	99.67	99.53	101.73	100.27	97.74	98.08	97.62	95.97	100.57
Mg#	-	53.6	78.7	54.7	79.3	-	56.0	56.8	55.3	39.1	66.7
An	72.5	-	-	-	-	74.5	-	-	-	-	-

1079 PL207,MV72,R487,1171C,17.5HR,F-8.1,PTFE,E
1080 GL355,REVERSAL,MV72,R528,1171C,16HR,F-8.2,+OL+GL,PTFE,E
1081 OL117,REVERSAL,MV72,R528,1171C,16HR,F-8.2,PTFE,E
1082 GL230,MV72,R486,1180C,17.5HR,F-7.9,+OL+PL+GL,PTFE,E
1083 OL97,MV72,R486,1180C,17.5HR,F-7.9,PTFE,E
1084 PL148,MV72,R486,1180C,17.5HR,F-7.9,PTFE,E
1085 GL802,MV72,R485,1191C,18.5HR,F-7.8,-GL,PTFE,E
1086 GL172,MV72,R474,1209C,3HR,F-7.5,-GL,PTFE,E
1087 GL253,MV516,R580,1302C,2HR,F-6.6,-GL,PTFE,E
1088 GL471,MV704,R494,1104C,19HR,F-9.1,+OL+CPX+PL+SPMT+GL,PTFE,E
1089 OL162,MV704,R494,1104C,19HR,F-9.1,PTFE,E

	1090	1091	1092	1093	1094	1095	1096	1097	1098	1099	1100
SiO2	51.39	48.36	46.64	37.11	54.02	47.68	47.43	37.87	51.82	49.46	46.82
TiO2	0.15	2.47	4.07	nd	0.15	2.23	3.73	nd	0.35	0.24	3.54
Al2O3	28.75	4.35	12.97	nd	27.03	4.44	14.03	nd	27.78	29.60	14.09
Fe2O3	nd	nd	3.55	nd	nd	nd	3.22	nd	nd	nd	3.20
Cr2O3	nd	nd	nd	nd	nd	nd	0.03	nd	nd	nd	nd
FeO	1.26	9.74	11.07	28.13	0.95	9.95	10.72	26.24	1.57	1.24	10.66
MnO	nd	0.21	0.25	0.48	nd	0.15	0.20	0.39	nd	nd	0.21
NiO	nd	nd	nd	0.24	nd	nd	nd	0.44	nd	nd	nd
MgO	nd	12.21	4.04	33.02	nd	12.92	4.61	34.27	0.18	nd	4.71
CaO	12.78	21.08	9.00	0.65	11.01	21.43	8.71	0.65	12.68	14.66	9.05
Na2O	3.53	nd	3.85	nd	4.93	nd	3.84	nd	3.87	2.90	3.65
K2O	0.35	nd	1.60	nd	0.42	nd	1.14	nd	0.29	0.18	1.21
P2O5	nd	nd	0.51	nd	nd	nd	0.20	nd	nd	nd	nd
total=	98.21	98.42	97.55	99.63	98.51	98.80	97.86	99.86	98.54	98.28	97.14
Mg#	-	-	39.4	67.7	-	-	43.4	69.9	-	-	44.1
An	65.3	-	-	-	53.9	-	-	-	63.3	72.9	-

1090 PL201,MV704,R494,1104C,19HR,F-9.1,PTFE,E
1091 CPX62,MV704,R494,1104C,19HR,F-9.1,PTFE,E
1092 GL473,MV704,R493,1115C,17.5HR,F-8.9,+OL+CPX+PL+SPMT+GL,PTFE,E
1093 OL163,MV704,R493,1115C,17.5HR,F-8.9,PTFE,E
1094 PL202,MV704,R493,1115C,17.5HR,F-8.9,PTFE,E
1095 CPX63,MV704,R493,1115C,17.5HR,F-8.9,PTFE,E
1096 GL1357,MV704,R469,1127C,5HR,F-8.7,+OL+PL+SPMT+GL,PTFE,W
1097 OL51,MV704,R469,1127C,5HR,F-8.7,PTFE,E
1098 PL76,MV704,R469,1127C,5HR,F-8.7,PTFE,E
1099 PL77Y,MV704,R469,1127C,5HR,F-8.7,PTFE,E
1100 GL2,MV704,R468,1140C,19HR,F-8.5,+OL+PL+SPMT+GL,PTFE,E

	1101	1102	1103	1104	1105	1106	1107	1108	1109	1110	1111
SiO2	37.58	51.27	47.08	38.60	51.79	46.76	38.40	48.94	46.90	39.14	49.26
TiO2	nd	0.52	3.01	nd	0.17	3.04	nd	0.29	2.46	nd	0.38
Al2O3	0.16	27.83	14.90	nd	29.04	15.14	nd	30.36	16.35	nd	29.99
Fe2O3	nd	nd	2.90	nd	nd	2.92	nd	nd	2.62	nd	nd
FeO	25.16	1.87	10.42	23.11	1.44	10.17	22.23	1.13	9.76	19.60	1.34
MnO	0.35	nd	0.12	0.32	nd	0.19	0.25	nd	0.16	0.28	nd
NiO	0.49	nd	nd	0.41	nd	nd	0.46	nd	nd	0.46	nd
MgO	35.36	0.34	5.25	37.93	nd	5.43	37.71	nd	6.08	40.58	0.31
CaO	0.55	13.02	8.84	0.50	12.94	8.85	0.50	14.32	9.04	0.47	14.32
Na2O	nd	4.10	3.74	nd	4.01	3.75	nd	3.11	3.53	nd	2.98
K2O	nd	0.29	1.19	nd	0.27	1.16	nd	0.12	0.96	nd	0.12
P2O5	nd	nd	0.24	nd	nd	0.22	nd	nd	0.27	nd	nd
total=	99.65	99.24	97.69	100.87	99.66	97.63	99.55	98.27	98.13	100.53	98.70
Mg#	71.5	-	47.3	74.5	-	48.8	75.1	-	52.6	78.7	-
An	-	62.6	-	-	63.1	-	-	71.3	-	-	72.1

1101 OL3,MV704,R468,1140C,19HR,F-8.5,PTFE,E
1102 PL1,MV704,R468,1140C,19HR,F-8.5,PTFE,E
1103 GL705,MV704,R467,1151C,16HR,F-8.4,+OL+PL+SPMT+GL,PTFE,E
1104 OL229,MV704,R467,1151C,16HR,F-8.4,PTFE,E
1105 PL244,MV704,R467,1151C,16HR,F-8.4,PTFE,E
1106 GL557,MV704,R466,1161C,16HR,F-8.2,+OL+PL+SPMT+GL,PTFE,E
1107 OL184,MV704,R466,1161C,16HR,F-8.2,PTFE,E
1108 PL210,MV704,R466,1161C,16HR,F-8.2,PTFE,E
1109 GL545,MV704,R465,1174C,16HR,F-8.0,+OL+PL+SPMT+GL,PTFE,E
1110 OL178,MV704,R465,1174C,16HR,F-8.0,PTFE,E
1111 PL209,MV704,R465,1174C,16HR,F-8.0,PTFE,E

	1112	1113	1114	1115	1116	1117	1118	1119	1120	1121	1122
SiO2	46.93	39.05	49.48	46.61	46.37	46.77	46.71	46.93	47.38	52.86	49.38
TiO2	2.40	nd	0.15	2.34	2.35	2.43	2.35	4.08	3.85	0.14	1.85
Al2O3	16.81	nd	30.97	16.64	16.38	16.50	16.44	12.99	13.01	28.43	4.79
Fe2O3	2.47	nd	nd	2.55	2.46	2.57	2.61	3.21	3.11	nd	nd
Cr2O3	nd	nd	nd	nd	0.15	nd	nd	nd	nd	nd	nd
FeO	9.46	18.50	1.11	9.69	9.45	9.49	9.50	9.53	9.61	0.72	8.71
MnO	0.18	0.14	nd	0.17	0.13	nd	0.14	0.25	0.23	nd	0.22
NiO	nd	0.54	nd	nd	nd	nd	nd	nd	nd	nd	nd
MgO	6.33	40.43	nd	6.62	6.40	6.55	6.53	3.70	4.06	nd	12.73
CaO	9.17	0.42	14.72	9.14	9.09	9.13	9.14	8.49	8.71	12.14	20.98
Na2O	3.31	nd	2.68	3.31	3.32	3.33	3.22	3.16	3.13	3.98	0.41
K2O	0.93	nd	0.09	0.91	0.93	0.91	0.88	2.19	2.06	0.45	nd
P2O5	0.09	nd	nd	0.23	nd	nd	nd	1.04	0.86	nd	nd
total=	98.08	99.08	99.20	98.21	97.03	97.68	97.52	95.57	96.01	98.72	99.07
Mg#	54.4	79.6	-	54.9	54.7	55.2	55.1	40.9	43.0	-	-
An	-	-	74.8	-	-	-	-	-	-	61.1	-

1112 GL523,MV704,R463,1183C,5.5HR,F-7.9,+OL+PL+SPMT+GL,PTFE,E
1113 OL173,MV704,R463,1183C,5.5HR,F-7.9,PTFE,E
1114 PL208,MV704,R463,1183C,5.5HR,F-7.9,PTFE,E
1115 GL602,MV704,R460,1204C,3HR,F-7.6,-GL,PTFE,E
1116 GL610,MV704,R461,1208C,3HR,F-7.6,-GL,PTFE,E
1117 GL37,MV704,R454,1243C,16.5HR,F-7.1,-GL,PTFE,E
1118 GL4,MV704,R452,1265C,16HR,F-6.8,-GL,PTFE,E
1119 GL489,MV506,R495,1105C,19HR,F-9.0,+OL+CPX+PL+SPMT+GL,PTFE,E
1120 GL447,MV506,R492,1114C,19.5HR,F-8.9,+OL+CPX+PL+SPMT+GL,PTFE,E
1121 PL189,MV506,R492,1114C,19.5HR,F-8.9,PTFE,E
1122 CPX53,MV506,R492,1114C,19.5HR,F-8.9,PTFE,E

	1123	1124	1125	1126	1127	1128	1129	1130	1131	1132	1133
SiO2	48.40	50.84	52.03	47.65	51.29	48.21	38.11	52.65	48.01	38.57	50.33
TiO2	3.62	0.27	0.45	3.11	0.11	3.05	0.17	0.24	2.85	0.19	0.44
Al2O3	13.71	29.44	28.04	14.40	30.51	14.77	0.20	29.24	15.20	nd	28.86
Fe2O3	2.97	nd	nd	2.73	nd	2.56	nd	nd	2.57	nd	nd
FeO	9.66	1.22	1.53	9.39	0.74	9.08	22.97	0.67	9.12	21.47	1.58
MnO	0.21	nd	nd	0.18	nd	0.20	0.32	nd	0.18	0.33	nd
NiO	nd	nd	nd	nd	nd	nd	0.25	nd	nd	0.17	nd
MgO	4.52	0.28	0.39	4.84	nd	5.15	37.79	nd	5.41	38.93	0.49
CaO	9.05	13.60	12.47	8.74	13.60	8.75	0.60	12.25	8.78	0.50	13.36
Na2O	3.25	3.46	4.03	3.21	3.59	3.20	nd	4.30	3.26	nd	3.46
K2O	2.01	0.36	0.48	1.79	0.27	1.76	nd	0.41	1.66	nd	0.41
P2O5	nd	nd	nd	0.69	nd	0.65	nd	nd	0.64	nd	nd
total=	97.40	99.47	99.42	96.73	100.11	97.38	100.41	99.76	97.68	100.16	98.93
Mg#	45.5	-	-	47.9	-	50.3	74.6	-	51.4	76.4	-
An	-	67.0	61.3	-	66.6	-	-	59.7	-	-	66.4

1123 GL115,MV506,R491,1124C,19HR,F-8.8,+OL+PL+GL,PTFE,E
1124 PL107,MV506,R491,1124C,19HR,F-8.8,PTFE,E
1125 PL108,MV506,R491,1124C,19HR,F-8.8,PTFE,E
1126 GL904,MV506,R490,1137C,19HR,F-8.6,+OL+PL+GL,PTFE,E
1127 PL293,MV506,R490,1137C,19HR,F-8.6,PTFE,E
1128 GL896,MV506,R489,1147C,18HR,F-8.5,+OL+PL+GL,PTFE,E
1129 OL298,MV506,R489,1147C,18HR,F-8.5,PTFE,E
1130 PL290,MV506,R489,1147C,18HR,F-8.5,PTFE,E
1131 GL706,MV506,R488,1158C,19HR,F-8.3,+OL+PL+GL,PTFE,E
1132 OL230,MV506,R488,1158C,19HR,F-8.3,PTFE,E
1133 PL245,MV506,R488,1158C,19HR,F-8.3,PTFE,E

	1134	1135	1136	1137	1138	1139	1140	1141	1142	1143	1144
SiO2	53.81	49.05	49.25	51.60	47.95	49.78	48.32	49.35	48.24	48.20	51.81
TiO2	0.28	2.73	2.35	0.12	2.40	0.16	2.41	0.23	2.48	2.41	3.27
Al2O3	28.65	15.70	16.05	30.62	16.70	30.24	17.04	30.53	16.56	17.18	13.00
Fe2O3	nd	2.62	2.40	nd	2.25	nd	2.24	nd	2.38	2.17	2.80
Cr2O3	nd	nd	nd	nd	nd	nd	nd	nd	nd	nd	0.11
FeO	0.76	8.85	8.66	0.79	8.23	0.68	8.08	1.17	8.24	8.10	9.07
MnO	nd	nd	0.21	nd	0.19	nd	0.18	nd	0.12	0.17	0.06
MgO	nd	5.72	6.16	nd	5.94	nd	5.75	nd	5.54	5.79	4.65
CaO	11.35	8.92	8.96	14.39	9.08	14.29	9.19	14.29	9.15	9.06	8.68
Na2O	4.72	3.35	3.12	3.26	3.19	3.22	3.17	3.16	3.28	3.35	2.99
K2O	0.53	1.63	1.38	0.31	1.42	0.29	1.40	0.24	1.36	1.37	1.29
P2O5	nd	0.64	0.52	nd	0.56	nd	0.56	nd	0.48	0.55	nd
total=	100.10	99.21	99.06	101.09	97.91	98.66	98.34	98.97	97.83	98.35	97.73
Mg#	-	53.5	55.9	-	56.3	-	55.9	-	54.5	56.0	47.7
An	55.3	-	-	69.7	-	69.8	-	70.4	-	-	-

1134 PL246,MV506,R488,1158C,19HR,F-8.3,PTFE,E
1135 GL240,MV506,R487,1171C,17.5HR,F-8.0,+OL+PL+GL,PTFE,E
1136 GL238,MV506,R486,1180C,17.5HR,F-7.9,+OL+PL+GL,PTFE,E
1137 PL150,MV506,R486,1180C,17.5HR,F-7.9,PTFE,E
1138 GL805,MV506,R485,1191C,18.5HR,F-7.8,+PL+GL,PTFE,E
1139 PL267,MV506,R485,1191C,18.5HR,F-7.8,PTFE,E
1140 GL792,MV506,R484,1197C,19.5HR,F-7.7,+PL+GL,PTFE,E
1141 PL266,MV506,R484,1197C,19.5HR,F-7.7,PTFE,E
1142 GL170,MV506,R474,1209C,3HR,F-7.5,-GL,PTFE,E
1143 GL2034,MV506,R5-727,1271C,6.5HR,F-6.9,-GL,PTFE,W
1144 GL9,MV122,R469,1127C,5HR,F-8.6,+OL+CPX+PL+SPMT+GL,PTFE,E

	1145	1146	1147	1148	1149	1150	1151	1152	1153	1154	1155
SiO2	38.50	52.86	50.86	51.05	38.42	53.16	51.40	39.12	51.86	50.67	39.04
TiO2	0.18	0.15	1.24	3.14	0.19	0.16	2.76	0.13	nd	2.75	nd
Al2O3	0.21	28.39	3.11	13.48	nd	27.95	14.09	nd	30.04	13.84	nd
Fe2O3	nd	nd	nd	2.67	nd	nd	2.42	nd	nd	2.51	nd
Cr2O3	nd	nd	0.53	nd	nd	nd	0.04	nd	nd	nd	nd
FeO	24.25	0.89	8.83	9.16	23.11	1.07	8.94	21.31	0.86	9.00	20.28
MnO	0.14	nd	0.14	nd	0.16	nd	0.08	0.15	nd	0.15	0.14
NiO	0.69	nd	0.15	nd	0.86	nd	nd	0.87	nd	nd	0.79
MgO	35.39	nd	15.10	4.89	37.24	0.17	5.17	38.61	nd	5.55	39.15
CaO	0.56	12.25	19.09	8.73	0.53	12.40	8.61	0.47	13.23	8.46	0.50
Na2O	nd	4.18	nd	3.04	nd	4.25	2.91	nd	3.49	2.91	nd
K2O	nd	0.32	nd	1.25	nd	0.31	1.13	nd	0.20	1.16	nd
P2O5	nd	nd	nd	nd	nd	nd	0.33	nd	nd	0.36	nd
total=	99.92	99.04	99.05	97.41	100.51	99.47	97.88	100.66	99.68	97.36	99.90
Mg#	72.2	-	-	48.8	74.2	-	50.8	76.4	-	52.4	77.5
An	-	60.7	-	-	-	60.6	-	-	66.9	-	-

1145 OL8,MV122,R469,1127C,5HR,F-8.6,PTFE,E
1146 PL6,MV122,R469,1127C,5HR,F-8.6,PTFE,E
1147 CPX5,MV122,R469,1127C,5HR,F-8.6,PTFE,E
1148 GL4,MV122,R468,1140C,19HR,F-8.5,+OL+PL+SPMT+GL,PTFE,E
1149 OL4,MV122,R468,1140C,19HR,F-8.5,PTFE,E
1150 PL4,MV122,R468,1140C,19HR,F-8.5,PTFE,E
1151 GL566,MV122,R467,1151C,16HR,F-8.4,+OL+PL+SPMT+GL,PTFE,E
1152 OL187,MV122,R467,1151C,16HR,F-8.4,PTFE,E
1153 PL213,MV122,R467,1151C,16HR,F-8.4,PTFE,E
1154 GL554,MV122,R466,1161C,16HR,F-8.2,+OL+SPMT+GL,PTFE,E
1155 OL183,MV122,R466,1161C,16HR,F-8.2,PTFE,E

	1156	1157	1158	1159	1160	1161	1162	1163	1164	1165	1166
SiO2	50.61	50.47	38.95	50.41	50.39	50.98	50.73	51.27	50.68	49.19	0.55
TiO2	2.68	2.80	nd	2.72	2.85	2.75	2.87	2.79	2.71	3.80	47.31
Al2O3	13.71	13.63	0.20	13.66	13.59	13.82	13.65	13.64	13.67	12.98	0.60
Fe2O3	2.46	2.55	nd	2.52	2.58	2.61	2.65	2.66	2.69	3.05	9.85
Cr2O3	nd	nd	nd	nd	nd	nd	nd	0.07	0.04	nd	0.15
FeO	8.58	8.96	19.83	9.06	8.95	9.15	9.00	9.15	9.12	10.11	33.11
MnO	0.06	0.15	nd	nd	0.07	nd	0.13	nd	0.04	0.26	0.35
NiO	nd	nd	0.81	nd	nd	nd	nd	nd	nd	nd	nd
MgO	5.70	5.99	39.63	6.08	5.87	6.22	6.00	5.95	6.05	3.78	5.46
CaO	8.46	8.47	0.46	8.50	8.51	8.41	8.46	8.51	8.47	8.02	nd
Na2O	3.05	3.00	nd	2.87	2.93	3.03	2.92	2.99	2.96	3.14	nd
K2O	1.23	1.16	nd	1.13	1.15	1.13	1.15	1.11	1.12	1.79	nd
P2O5	0.31	0.22	nd	0.23	0.35	0.27	nd	nd	nd	0.62	nd
total=	96.85	97.40	99.88	97.18	97.24	98.37	97.56	98.14	97.55	96.74	97.38
Mg#	54.2	54.4	78.1	54.5	53.9	54.8	54.3	53.7	54.2	40.0	-

1156 GL537,MV122,R464,1174C,19HR,F-8,+OL+SPMT+GL,PTFE,E
1157 GL552,MV122,R465,1174C,16HR,F-8.0,+OL+SPMT+GL,PTFE,E
1158 OL182,MV122,R465,1174C,16HR,F-8.0,PTFE,E
1159 GL527,MV122,R463,1183C,5.5HR,F-7.9,+SPMT+GL,PTFE,E
1160 GL618,MV122,R462,1196C,5HR,F-7.7,+SPMT+GL,PTFE,E
1161 GL178,MV122,R475,1203C,2.5HR,F-7.6,+SPMT+GL,PTFE,E
1162 GL52,MV122,R455,1233C,24HR,F-7.2,-GL,PTFE,E
1163 GL31,MV122,R454,1243C,16.5HR,F-7.1,-GL,PTFE,E
1164 GL7,MV122,R452,1265C,16HR,F-6.8,-GL,PTFE,E
1165 GL467,MV702,R494,1104C,19HR,F-9.1,+OL+CPX+PL+SPMT+IL+GL,PTFE,E
1166 IL12,MV702,R494,1104C,19HR,F-9.1,PTFE,E

	1167	1168	1169	1170	1171	1172	1173	1174	1175	1176	1177
SiO2	47.28	46.89	37.86	50.15	1.45	47.26	49.13	50.68	47.24	37.39	51.29
TiO2	4.85	4.63	nd	0.31	18.73	4.05	nd	0.45	3.94	0.13	0.20
Al2O3	12.37	12.77	0.29	29.27	5.06	14.52	31.32	29.39	14.11	nd	29.35
Fe2O3	3.53	3.45	nd	nd	20.44	3.13	nd	nd	3.18	nd	nd
Cr2O3	0.15	nd	nd	nd	2.58	nd	nd	nd	nd	nd	nd
FeO	10.93	10.49	26.88	1.14	42.28	10.48	0.81	1.63	10.48	24.01	0.83
MnO	0.13	0.21	0.26	nd	0.21	0.17	nd	nd	0.15	0.33	nd
NiO	nd	nd	0.32	nd	nd	nd	nd	nd	nd	0.55	nd
MgO	4.21	4.36	34.07	nd	5.21	4.69	nd	0.29	5.05	35.67	nd
CaO	8.77	8.34	0.58	13.65	nd	8.42	15.01	13.26	8.30	0.45	12.95
Na2O	2.92	2.93	nd	3.34	nd	3.34	2.46	3.67	3.39	nd	3.75
K2O	1.52	1.41	nd	0.27	nd	1.37	0.23	0.26	1.32	nd	0.22
P2O5	0.54	0.48	nd	nd	nd	0.35	nd	nd	0.32	nd	nd
V2O3	nd	nd	nd	nd	1.21	nd	nd	nd	nd	nd	nd
total=	97.20	95.96	100.26	98.13	97.17	97.78	98.96	99.63	97.48	98.53	98.59
Mg#	40.7	42.6	69.3	-	18.0	44.4	-	-	46.2	72.6	-
An	-	-	-	68.2	-	-	76.1	65.6	-	-	64.8

1167 GL475,MV702,R493,1115C,17.5HR,F-8.9,+OL+PL+SPMT+GL,PTFE,E
1168 GL389,MV702,R483,1122C,19.5HR,F-8.7,+OL+PL+SPMT+GL,PTFE,E
1169 OL127,MV702,R483,1122C,19.5HR,F-8.7,PTFE,E
1170 PL160,MV702,R483,1122C,19.5HR,F-8.7,PTFE,E
1171 SPMT27,MV702,R483,1122C,19.5HR,F-8.7,PTFE,E
1172 GL718,MV702,R482,1135C,6.5HR,F-8.6,+OL+PL+SPMT+GL,PTFE,E
1173 PL253,MV702,R482,1135C,6.5HR,F-8.6,PTFE,E
1174 PL254,MV702,R482,1135C,6.5HR,F-8.6,PTFE,E
1175 GL714,MV702,R481,1146C,20HR,F-8.4,+OL+PL+SPMT+GL,PTFE,E
1176 OL234,MV702,R481,1146C,20HR,F-8.4,PTFE,E
1177 PL251,MV702,R481,1146C,20HR,F-8.4,PTFE,E

	1178	1179	1180	1181	1182	1183	1184	1185	1186	1187	1188
SiO2	47.71	38.29	50.26	51.82	48.20	47.92	39.28	49.93	48.17	50.39	48.56
TiO2	3.62	0.11	0.14	0.40	3.27	3.10	0.12	0.27	3.08	0.13	3.02
Al2O3	14.41	nd	29.39	28.34	15.44	15.85	nd	31.64	16.20	31.24	16.74
Fe2O3	2.98	nd	nd	nd	2.81	2.55	nd	nd	2.45	nd	2.39
Cr2O3	0.05	nd	nd	nd	nd	nd	nd	nd	nd	nd	0.12
FeO	9.98	22.89	1.08	1.32	9.65	9.51	19.56	1.09	8.94	0.95	8.75
MnO	0.16	0.36	nd	nd	0.19	0.22	0.27	nd	0.11	nd	0.07
NiO	nd	0.46	nd	nd	nd	nd	0.87	nd	nd	nd	nd
MgO	5.08	37.13	nd	nd	5.62	6.07	40.68	nd	6.17	nd	5.95
CaO	8.26	0.56	13.92	12.96	8.42	8.48	0.40	15.25	8.75	14.79	8.64
Na2O	3.03	nd	3.27	3.76	3.10	3.23	nd	2.93	3.00	3.17	3.27
K2O	1.20	nd	0.24	0.30	1.10	1.02	nd	0.14	0.92	0.15	0.95
P2O5	0.28	nd	nd	nd	0.34	0.30	nd	nd	0.24	nd	0.20
total=	96.76	99.80	98.30	98.90	98.14	98.25	101.18	101.25	98.03	100.82	98.66
Mg#	47.6	74.3	-	-	50.9	53.2	78.8	-	55.2	-	54.8
An	-	-	69.2	64.4	-	-	-	73.6	-	71.4	-

1178 GL152,MV702,R480,1157C,19HR,F-8.2,+OL+PL+SPMT+GL,PTFE,E
1179 OL87,MV702,R480,1157C,19HR,F-8.2,PTFE,E
1180 PL124,MV702,R480,1157C,19HR,F-8.2,PTFE,E
1181 PL125,MV702,R480,1157C,19HR,F-8.2,PTFE,E
1182 GL211,MV702,R479,1169C,14HR,F-8.0,+OL+PL+SPMT+GL,PTFE,E
1183 GL198,MV702,R478,1179C,9HR,F-8.0,+OL+PL+SPMT+GL,PTFE,E
1184 OL93,MV702,R478,1179C,9HR,F-8.0,PTFE,E
1185 PL140,MV702,R478,1179C,9HR,F-8.0,PTFE,E
1186 GL218,MV702,R477,1189C,18.5HR,F-7.8,+PL+GL,PTFE,E
1187 PL143,MV702,R477,1189C,18.5HR,F-7.8,PTFE,E
1188 GL186,MV702,R476,1198C,19HR,F-7.7,+PL+GL,PTFE,E

	1189	1190	1191	1192	1193	1194	1195	1196	1197	1198	1199
SiO2	48.77	50.35	48.06	49.33	47.60	48.72	47.84	49.00	48.02	48.63	47.32
TiO2	0.25	0.16	2.82	0.38	2.75	0.26	2.59	0.17	2.57	0.13	2.45
Al2O3	31.25	30.87	16.91	29.06	17.54	31.65	18.38	31.00	18.44	32.28	18.71
Fe2O3	nd	nd	2.42	nd	2.30	nd	2.06	nd	2.01	nd	2.04
FeO	1.07	0.93	8.65	1.74	8.54	1.07	8.15	0.96	7.81	0.84	7.95
MnO	nd	nd	0.13	nd	0.15	nd	nd	nd	0.06	nd	nd
MgO	nd	nd	5.65	0.39	5.70	nd	5.26	nd	5.16	nd	4.87
CaO	15.34	14.51	9.07	14.56	9.20	15.67	9.31	15.32	9.56	15.70	9.71
Na2O	2.20	2.91	3.11	2.74	3.14	2.49	3.29	2.55	3.16	2.28	2.96
K2O	0.24	0.18	0.89	0.14	0.99	0.17	0.92	0.09	0.97	0.08	0.84
P2O5	nd	nd	0.26	nd	0.21	nd	nd	nd	nd	nd	0.24
total=	99.12	99.91	97.97	98.34	98.12	100.03	97.80	99.09	97.76	99.94	97.09
Mg#	-	-	53.8	-	54.3	-	53.5	-	54.1	-	52.2
An	78.2	72.6	-	74.0	-	76.9	-	76.4	-	78.8	-

1189 PL133,MV702,R476,1198C,19HR,F-7.7,PTFE,E
1190 PL134,MV702,R476,1198C,19HR,F-7.7,PTFE,E
1191 GL164,MV702,R474,1209C,3HR,F-7.5,+PL+GL,PTFE,E
1192 PL128,MV702,R474,1209C,3HR,F-7.5,PTFE,E
1193 GL622,MV702,R496,1223C,19HR,F-7.4,+PL+GL,PTFE,E
1194 PL226,MV702,R496,1223C,19HR,F-7.4,PTFE,E
1195 GL816,MV702,R530,1232C,16HR,F-7.4,+PL+GL,PTFE,E
1196 PL271,MV702,R530,1232C,16HR,F-7.4,PTFE,E
1197 GL809,MV702,R529,1238C,18.5HR,F-7.3,+PL+GL,PTFE,E
1198 PL269,MV702,R529,1238C,18.5HR,F-7.3,PTFE,E
1199 GL334,MV702,R543,1252C,12.5HR,F-7.1,+PL+GL,PTFE,E

	1200	1201	1202	1203	1204	1205	1206	1207	1208	1209	1210
SiO2	48.40	47.85	47.96	51.47	0.27	36.46	54.00	50.58	50.87	0.34	50.05
TiO2	0.11	2.53	2.61	3.71	47.55	0.37	0.43	1.21	1.32	20.45	4.22
Al2O3	31.02	18.57	19.17	12.32	0.49	nd	27.46	2.72	2.17	3.03	12.05
Fe2O3	nd	2.01	1.95	3.06	10.40	nd	nd	nd	nd	22.67	3.27
Cr2O3	nd	0.05	nd	nd	0.55	nd	nd	0.21	0.26	3.18	nd
FeO	0.93	7.87	7.69	10.50	33.14	31.96	1.41	10.82	10.64	43.49	10.43
MnO	nd	0.13	0.12	0.21	0.21	0.35	nd	0.22	0.21	0.28	0.16
NiO	nd	nd	nd	nd	nd	0.38	nd	nd	nd	nd	nd
MgO	nd	4.83	5.07	3.39	5.46	30.15	nd	13.91	14.40	4.61	3.75
CaO	15.47	9.76	9.53	7.53	nd	0.59	10.90	19.19	19.17	nd	7.87
Na2O	2.07	3.00	3.38	3.02	nd	nd	4.78	nd	nd	nd	3.03
K2O	nd	0.86	0.84	1.60	nd	nd	0.44	nd	nd	nd	1.36
P2O5	nd	nd	0.12	1.09	nd	nd	nd	nd	nd	nd	0.93
V2O3	nd	nd	nd	nd	nd	nd	nd	nd	nd	1.06	nd
total=	98.00	97.46	98.44	97.90	98.07	100.26	99.42	98.86	99.04	99.11	97.12
Mg#	-	52.2	54.0	36.5	-	62.7	-	-	-	15.9	39.1
An	80.5	-	-	-	-	-	54.3	-	-	-	-

1200 PL154R,MV702,R543,1252C,12.5HR,F-7.1,PTFE,E
1201 GL335,MV702,R540,1264C,19HR,F-7.0,-GL,PTFE,E
1202 GL2037,MV702,R5-729,1284C,5HR,F-6.8,-GL,SPT,W
1203 GL627R,MV39B,R501,1092C,19.5HR,F-9.3,+OL+CPX+PL+SPMT+IL+GL,SPT,E
1204 IL50,MV39B,R501,1092C,19.5HR,F-9.3,SPT,E
1205 OL209,MV39B,R501,1092C,19.5HR,F-9.3,SPT,E
1206 PL228,MV39B,R501,1092C,19.5HR,F-9.3,SPT,E
1207 CPX69,MV39B,R501,1092C,19.5HR,F-9.3,SPT,E
1208 CPX70,MV39B,R501,1092C,19.5HR,F-9.3,SPT,E
1209 SPMT38,MV39B,R501,1092C,19.5HR,F-9.3,SPT,E
1210 GL648,MV39B,R520,1099C,15HR,F-9.1,+OL+CPX+PL+SPMT+IL+GL,PTFE,E

	1211	1212	1213	1214	1215	1216	1217	1218	1219	1220	1221
SiO2	0.37	36.90	53.07	50.75	50.03	37.38	49.94	37.56	53.26	49.87	37.86
TiO2	46.28	0.26	0.28	1.23	4.20	0.21	3.94	0.14	0.36	3.89	0.14
Al2O3	0.38	nd	27.99	2.04	12.39	nd	12.72	nd	27.39	12.87	nd
Fe2O3	11.44	nd	nd	nd	2.98	nd	2.99	nd	nd	3.17	nd
Cr2O3	0.67	nd	nd	0.20	nd	nd	0.04	nd	nd	0.03	nd
FeO	31.65	30.47	0.87	10.42	10.12	27.86	10.47	27.25	1.50	10.17	26.81
MnO	0.26	0.38	nd	0.22	0.17	0.32	0.12	0.31	nd	0.22	0.52
NiO	nd	0.46	nd	0.13	nd	0.59	nd	0.65	nd	nd	0.61
MgO	5.69	31.57	nd	14.45	4.14	34.04	4.43	34.71	nd	4.59	34.86
CaO	nd	0.48	11.44	19.75	8.09	0.45	8.17	0.46	11.58	8.12	0.50
Na2O	nd	nd	4.58	nd	3.27	nd	3.09	nd	4.09	3.33	nd
K2O	nd	nd	0.23	nd	1.27	nd	1.21	nd	0.33	1.13	nd
P2O5	nd	nd	nd	nd	0.75	nd	0.80	nd	nd	nd	nd
total=	96.74	100.52	98.46	99.19	97.41	100.85	97.92	101.08	98.51	97.39	101.30
Mg#	-	64.9	-	-	42.2	68.5	43.0	69.4	-	44.6	69.9
An	-	-	57.2	-	-	-	-	-	59.8	-	-

1211 IL55,MV39B,R520,1099C,15HR,F-9.1,PTFE,E
1212 OL216,MV39B,R520,1099C,15HR,F-9.1,PTFE,E
1213 PL236,MV39B,R520,1099C,15HR,F-9.1,PTFE,E
1214 CPX77,MV39B,R520,1099C,15HR,F-9.1,PTFE,E
1215 GL885,MV39B,R519,1108C,21HR,F-9.1,+OL+CPX+PL+SPMT+GL,SPT,E
1216 OL295,MV39B,R519,1108C,21HR,F-9.1,SPT,E
1217 GL869,MV39B,R518,1120C,20HR,F-8.9,+OL+PL+SPMT+GL,SPT,E
1218 OL292,MV39B,R518,1120C,20HR,F-8.9,SPT,E
1219 PL283,MV39B,R518,1120C,20HR,F-8.9,SPT,E
1220 GL26,MV39B,R471,1129C,21HR,F-8.6,+OL+PL+SPMT+GL,SPT,E
1221 OL18,MV39B,R471,1129C,21HR,F-8.6,SPT,E

	1222	1223	1224	1225	1226	1227	1228	1229	1230	1231	1232
SiO2	38.16	37.33	54.35	54.52	53.40	1.78	50.12	38.64	53.42	50.12	37.81
TiO2	0.15	0.15	0.18	0.30	0.31	15.09	3.52	0.14	0.22	3.40	nd
Al2O3	nd	nd	26.92	27.06	27.22	6.31	13.59	0.17	27.89	14.48	nd
Fe2O3	nd	nd	nd	nd	nd	18.00	2.81	nd	nd	2.72	nd
Cr2O3	nd	nd	nd	nd	nd	11.53	nd	nd	nd	nd	nd
FeO	26.08	25.72	0.96	1.14	1.20	38.14	10.29	24.08	1.21	9.94	23.30
MnO	0.37	0.32	nd	nd	nd	0.42	0.15	0.25	nd	0.16	0.26
NiO	0.74	0.70	nd	nd	nd	nd	nd	0.68	nd	nd	0.77
MgO	34.39	34.73	nd	nd	0.25	5.72	5.04	35.60	nd	5.24	37.28
CaO	0.29	0.44	10.87	10.94	11.96	0.49	7.99	0.47	11.80	8.17	0.42
Na2O	nd	nd	4.76	4.80	4.33	nd	3.25	nd	4.47	3.19	nd
K2O	nd	nd	0.33	0.23	0.29	nd	1.04	nd	0.20	0.99	nd
P2O5	nd	nd	nd	nd	nd	nd	0.65	nd	nd	0.44	nd
total=	100.18	99.39	98.37	98.99	98.96	97.48	98.45	100.03	99.21	98.85	99.84
Mg#	70.2	70.6	-	-	-	21.1	46.6	72.5	-	48.4	74.0
An	-	-	54.7	55.0	59.4	-	-	-	58.6	-	-

1222 OL21,MV39B,R471,1129C,21HR,F-8.6,SPT,E
1223 OL22,MV39B,R471,1129C,21HR,F-8.6,SPT,E
1224 PL24,MV39B,R471,1129C,21HR,F-8.6,SPT,E
1225 PL25,MV39B,R471,1129C,21HR,F-8.6,SPT,E
1226 PL26,MV39B,R471,1129C,21HR,F-8.6,SPT,E
1227 SPMT8,MV39B,R471,1129C,21HR,F-8.6,SPT,E
1228 GL425,MV39B,R509,1140C,13HR,F-8.6,+OL+PL+SPMT+GL,SPT,E
1229 OL142,MV39B,R509,1140C,13HR,F-8.6,SPT,E
1230 PL176,MV39B,R509,1140C,13HR,F-8.6,SPT,E
1231 GL1008,MV39B,R511,1151C,18.5HR,F-8.4,+OL+PL+SPMT+GL,SPT,E
1232 OL332,MV39B,R511,1151C,18.5HR,F-8.4,SPT,E

	1233	1234	1235	1236	1237	1238	1239	1240	1241	1242	1243
SiO2	53.45	49.30	38.79	49.78	39.42	38.98	49.55	49.50	49.75	49.09	49.76
TiO2	nd	3.17	0.18	3.23	nd	nd	3.15	3.12	3.17	3.13	3.20
Al2O3	29.20	14.60	nd	14.63	nd	nd	14.46	14.38	14.39	14.46	14.56
Fe2O3	nd	2.59	nd	2.69	nd	nd	2.74	2.76	2.74	2.91	2.87
Cr2O3	nd	nd	nd	0.07	nd	nd	0.08	0.06	0.04	0.02	0.02
FeO	0.70	9.94	21.22	9.53	20.73	21.25	9.60	9.80	9.26	10.03	10.07
MnO	nd	0.18	0.28	0.15	0.28	0.27	0.18	0.14	0.17	0.17	0.18
NiO	nd	nd	0.91	nd	1.08	0.80	nd	nd	0.05	0.05	0.01
MgO	nd	5.62	38.26	5.88	39.11	39.47	6.20	6.11	6.33	6.29	6.33
CaO	12.07	8.26	0.48	8.29	0.37	0.30	8.04	8.04	7.97	7.90	7.98
Na2O	4.48	2.97	nd	3.46	nd	nd	3.13	3.41	3.38	3.31	3.29
K2O	0.24	0.95	nd	0.94	nd	nd	0.87	0.89	0.90	0.89	0.88
P2O5	nd	0.46	nd	nd	nd	nd	nd	nd	nd	nd	nd
total=	100.14	98.04	100.12	98.65	100.99	101.07	98.00	98.21	98.15	98.25	99.15
Mg#	-	50.2	76.3	52.4	77.1	76.8	53.5	52.6	54.9	52.8	52.8
An	59.0	-	-	-	-	-	-	-	-	-	-

1233 PL312,MV39B,R511,1151C,18.5HR,F-8.4,SPT,E
1234 GL783,MV39B,R513,1161C,14HR,F-8.3,+OL+SPMT+GL,SPT,E
1235 OL266,MV39B,R513,1161C,14HR,F-8.3,SPT,E
1236 GL4,MV39B,R438,1176C,7HR,F-8.0,+OL+SPMT+GL,SPT,E
1237 OL3R,MV39B,R438,1176C,7HR,F-8.0,SPT,E
1238 OL4R,MV39B,R438,1176C,7HR,F-8.0,SPT,E
1239 GL112R,MV39B,R434,1185C,12HR,F-7.8,+SPMT+GL,SPT,E
1240 GL2,MV39B,R436,1197C,8HR,F-7.7,+SPMT+GL,SPT,E
1241 GL17,MV39B,R430,1206C,5HR,F-7.5,-GL,PT,W
1242 GL44,MV39B,R430,1206C,5HR,F-7.5,-GL,PTFE,W
1243 GL58,MV39B,R431,1209C,24HR,F-7.5,-GL,PTFE,W

	1244	1245	1246	1247	1248	1249	1250	1251	1252	1253	1254
SiO2	49.80	56.53	49.60	48.52	49.27	53.23	0.87	37.53	50.21	53.06	37.79
TiO2	3.17	3.81	3.14	3.42	2.92	3.64	46.52	0.17	1.13	3.52	0.17
Al2O3	13.97	15.40	14.47	13.99	14.55	12.50	0.73	nd	2.01	12.79	nd
Fe2O3	2.57	0.06	2.75	3.09	2.84	2.67	9.89	nd	nd	2.54	nd
Cr2O3	0.06	nd	nd	nd	nd	nd	0.83	nd	0.16	nd	nd
FeO	8.75	0.17	9.71	10.51	9.69	8.82	32.29	30.04	12.13	8.82	27.35
MnO	0.23	0.15	0.19	0.16	0.26	0.15	0.49	0.45	0.32	0.17	0.44
NiO	0.02	nd	nd	nd	nd	nd	nd	0.59	nd	nd	0.97
MgO	6.28	7.17	6.01	6.52	6.12	3.22	5.66	31.78	14.07	3.50	33.95
CaO	8.00	9.27	8.05	8.32	8.12	6.67	nd	0.54	18.10	7.29	0.43
Na2O	3.31	2.99	3.16	2.77	3.39	2.30	nd	nd	nd	3.04	nd
K2O	0.88	1.11	0.92	0.78	0.87	1.91	nd	nd	nd	1.70	nd
P2O5	nd	nd	nd	nd	nd	0.76	nd	nd	nd	0.67	nd
total=	97.04	96.66	98.00	98.08	98.03	95.87	97.28	101.10	98.13	97.10	101.10
Mg#	56.1	98.7	52.4	52.5	53.0	39.4	-	65.3	-	41.4	68.9

1244 GL82,MV39B,R431,1209C,24HR,F-7.5,-GL,PT,W
1245 GL83SMALLBEAD,MV39B,R431,1209C,24HR,F-7.5,-GL,PT,W
1246 GL8,MV39B,R437,1211C,6HR,F-7.5,-GL,SPT,E
1247 GL55,MV39B,R415,1244C,2HR,F-7.0,-GL,PT,E
1248 GL7,MV39B,R416,1255C,1.5HR,F-6.9,-GL,PT,E
1249 GL645,MV121A,R520,1099C,15HR,F-9.1,+OL+CPX+PL+SPMT+IL+GL,PTFE,E
1250 IL54,MV121A,R520,1099C,15HR,F-9.1,PTFE,E
1251 OL215,MV121A,R520,1099C,15HR,F-9.1,PTFE,E
1252 CPX75,MV121A,R520,1099C,15HR,F-9.1,PTFE,E
1253 GL875I,MV121A,R519,1108C,21HR,F-9.1,+OL+CPX+PL+SPMT+GL,PTFE,E
1254 OL293,MV121A,R519,1108C,21HR,F-9.1,PTFE,E

	1255	1256	1257	1258	1259	1260	1261	1262	1263	1264	1265
SiO2	56.57	52.66	37.90	52.99	38.12	54.35	53.07	39.02	54.51	52.38	38.31
TiO2	0.39	3.20	nd	3.22	nd	0.30	2.83	nd	0.25	2.71	0.13
Al2O3	25.50	13.42	nd	13.85	nd	27.58	14.86	nd	27.76	14.31	nd
Fe2O3	nd	2.46	nd	2.52	nd	nd	2.29	nd	nd	2.28	nd
Cr2O3	nd	nd	nd	0.07	nd	nd	nd	nd	nd	nd	nd
FeO	1.71	8.67	26.15	8.79	25.30	1.24	8.50	22.41	1.33	8.49	21.73
MnO	nd	0.13	0.31	0.18	0.45	nd	0.12	0.24	nd	0.07	0.22
NiO	nd	nd	0.88	nd	0.69	nd	nd	1.16	nd	nd	0.91
MgO	0.22	3.96	34.70	4.22	36.00	nd	4.75	37.85	0.27	5.04	38.81
CaO	9.41	7.37	0.36	7.43	0.43	11.28	7.44	0.37	11.43	7.47	0.35
Na2O	5.68	3.34	nd	2.85	nd	4.43	3.18	nd	4.12	3.34	nd
K2O	0.51	1.58	nd	1.56	nd	0.36	1.38	nd	0.33	1.41	nd
P2O5	nd	0.58	nd	0.60	nd	nd	0.34	nd	nd	0.37	nd
total=	99.99	97.37	100.30	98.28	100.99	99.54	98.76	101.05	100.00	97.87	100.46
Mg#	-	44.9	70.3	46.1	71.7	-	49.9	75.1	-	51.4	76.1
An	46.4	-	-	-	-	57.2	-	-	59.3	-	-

1255 PL284,MV121A,R519,1108C,21HR,F-9.1,PTFE,E
1256 GL854,MV121A,R518,1120C,20HR,F-8.9,+OL+PL+SPMT+GL,PTFE,E
1257 OL287,MV121A,R518,1120C,20HR,F-8.9,PTFE,E
1258 GL570,MV121A,R472,1128C,5.5HR,F-8.7,+OL+PL+SPMT+GL,PTFE,E
1259 OL189,MV121A,R472,1128C,5.5HR,F-8.7,PTFE,E
1260 PL216,MV121A,R472,1128C,5.5HR,F-8.7,PTFE,E
1261 GL998,MV121A,R510,1145C,18HR,F-8.5,+OL+PL+SPMT+GL,PTFE,E
1262 OL327,MV121A,R510,1145C,18HR,F-8.5,PTFE,E
1263 PL308,MV121A,R510,1145C,18HR,F-8.5,PTFE,E
1264 GL760,MV121A,R512,1155C,24HR,F-8.4,+OL+SPMT+GL,PTFE,E
1265 OL255,MV121A,R512,1155C,24HR,F-8.4,PTFE,E

	1266	1267	1268	1269	1270	1271	1272	1273	1274	1275	1276
SiO2	51.95	51.84	52.70	52.38	52.19	51.49	52.63	47.44	49.58	0.38	36.60
TiO2	2.57	2.70	2.74	2.76	2.74	2.64	2.74	3.51	3.89	46.96	0.23
Al2O3	14.34	14.19	14.42	14.44	14.22	14.13	14.59	15.72	13.54	0.58	nd
Fe2O3	2.32	2.33	2.42	2.48	2.48	2.60	2.62	2.54	3.14	10.76	nd
Cr2O3	nd	nd	nd	nd	0.04	nd	nd	0.04	nd	0.15	nd
FeO	8.65	8.73	8.66	8.52	8.81	8.95	8.60	9.09	9.62	32.27	29.71
MnO	0.15	0.22	0.22	nd	0.14	0.14	0.14	0.19	0.22	0.28	0.49
NiO	nd	nd	nd	nd	nd	nd	nd	nd	nd	nd	0.22
MgO	5.25	5.33	5.26	5.26	5.30	5.35	5.32	5.49	3.32	5.68	31.73
CaO	7.36	7.29	7.32	7.29	7.45	7.41	7.25	9.14	7.95	nd	0.46
Na2O	3.03	3.21	3.40	3.38	3.25	3.13	3.43	2.67	3.35	nd	nd
K2O	1.37	1.35	1.38	1.34	1.33	1.36	1.40	1.51	2.21	nd	nd
P2O5	0.40	0.38	0.35	0.38	nd	0.37	nd	0.36	1.17	nd	nd
total=	97.39	97.57	98.87	98.23	97.95	97.57	98.72	97.70	97.99	97.06	99.44
Mg#	52.0	52.1	52.0	52.4	51.7	51.6	52.4	51.8	38.1	-	65.6

1266 GL787R,MV121A,R514,1165C,16HR,F-8.2,+OL+SPMT+GL,PTFE,E
1267 GL732,MV121A,R515,1176C,16.5HR,F-8.1,+SPMT+GL,PTFE,E
1268 GL745,MV121A,R516,1186C,12.5HR,F-7.9,+SPMT+GL,PTFE,E
1269 GL180,MV121A,R475,1203C,2.5HR,F-7.6,+SPMT+GL,PTFE,E
1270 GL40,MV121A,R448,1208C,3HR,F-7.6,-GL,PTFE,E
1271 GL694,MV121A,R427,1243C,5HR,F-7.1,-GL,PT,E
1272 GL15,MV121A,R425,1263C,7.5HR,F-6.8,-GL,PT,E
1273 GL247,MV71A,R580,1302C,2HR,F-6.6,-GL,PTFE,E
1274 GL652,MV52,R520,1099C,15HR,F-9.1,+OL+CPX+PL+SPMT+IL+GL,PTFE,E
1275 IL56,MV52,R520,1099C,15HR,F-9.1,PTFE,E
1276 OL217,MV52,R520,1099C,15HR,F-9.1,PTFE,E

	1277	1278	1279	1280	1281	1282	1283	1284	1285	1286	1287
SiO2	50.58	0.87	46.80	0.85	37.36	54.37	0.85	46.83	37.88	52.98	46.61
TiO2	1.51	20.99	4.84	47.38	0.18	0.36	21.17	4.96	0.16	0.27	4.78
Al2O3	2.39	3.50	12.20	0.93	nd	26.90	3.76	12.84	nd	27.85	13.48
Fe2O3	nd	21.63	3.43	8.61	nd	nd	20.67	3.39	nd	nd	3.41
Cr2O3	nd	0.41	nd	0.38	nd	nd	0.97	0.05	nd	nd	nd
FeO	10.06	43.99	10.82	32.43	28.07	1.34	43.62	10.81	27.16	0.74	10.79
MnO	0.20	0.47	0.22	0.16	0.29	nd	0.31	0.16	0.34	nd	0.19
NiO	nd	nd	nd	nd	0.43	nd	nd	nd	0.56	nd	nd
MgO	13.62	4.51	4.16	6.19	32.73	0.21	5.10	4.65	34.62	nd	4.80
CaO	20.85	nd	8.82	nd	0.52	10.94	nd	8.93	0.49	11.48	8.90
Na2O	nd	nd	3.26	nd	nd	4.56	nd	3.21	nd	4.63	3.06
K2O	nd	nd	1.68	nd	nd	0.61	nd	1.50	nd	0.41	1.47
P2O5	nd	nd	0.65	nd	nd	nd	nd	0.68	nd	nd	0.57
V2O3	nd	0.53	nd	nd	nd	nd	0.96	nd	nd	nd	nd
total=	99.21	96.90	96.88	96.93	99.58	99.29	97.41	98.01	101.21	98.36	98.06
Mg#	-	15.4	40.7	-	67.5	-	17.2	43.4	69.4	-	44.2
An	-	-	-	-	-	54.9	-	-	-	56.4	-

1277 CPX78,MV52,R520,1099C,15HR,F-9.1,PTFE,E
1278 SPMT43,MV52,R520,1099C,15HR,F-9.1,PTFE,E
1279 GL879,MV52,R519,1108C,21HR,F-9.1,+OL+CPX+PL+SPMT+IL+GL,PTFE,E
1280 IL61,MV52,R519,1108C,21HR,F-9.1,PTFE,E
1281 OL294,MV52,R519,1108C,21HR,F-9.1,PTFE,E
1282 PL285,MV52,R519,1108C,21HR,F-9.1,PTFE,E
1283 SPMT47,MV52,R519,1108C,21HR,F-9.1,PTFE,E
1284 GL864,MV52,R518,1120C,20HR,F-8.9,+OL+PL+SPMT+GL,PTFE,E
1285 OL290,MV52,R518,1120C,20HR,F-8.9,PTFE,E
1286 PL281,MV52,R518,1120C,20HR,F-8.9,PTFE,E
1287 GL572,MV52,R472,1128C,5.5HR,F-8.7,+OL+PL+SPMT+GL,PTFE,E

	1288	1289	1290	1291	1292	1293	1294	1295	1296	1297	1298
SiO2	38.17	46.76	38.67	53.17	46.73	38.50	53.31	46.46	38.33	53.13	46.85
TiO2	0.16	4.26	0.16	0.18	3.93	0.15	0.27	3.72	0.13	nd	3.61
Al2O3	nd	14.22	nd	29.06	14.63	nd	28.34	15.13	nd	28.12	15.64
Fe2O3	nd	3.11	nd	nd	2.93	nd	nd	2.83	nd	nd	2.67
Cr2O3	nd	nd	nd	nd	nd	nd	nd	nd	nd	nd	0.05
FeO	26.16	10.65	23.97	0.77	10.54	22.56	0.95	10.12	21.32	0.89	9.88
MnO	0.38	0.22	0.26	nd	0.16	0.31	nd	0.11	0.12	nd	0.13
NiO	0.45	nd	0.55	nd	nd	0.41	nd	nd	0.90	nd	nd
MgO	35.73	5.04	37.23	nd	5.53	38.63	nd	5.80	38.84	nd	5.92
CaO	0.56	8.82	0.47	12.24	8.73	0.53	11.38	8.81	0.41	11.50	8.99
Na2O	nd	2.90	nd	4.23	3.04	nd	4.65	3.06	nd	4.57	3.13
K2O	nd	1.31	nd	0.34	1.26	nd	0.44	1.14	nd	0.44	1.05
P2O5	nd	0.51	nd	nd	0.45	nd	nd	0.50	nd	nd	0.35
total=	101.61	97.80	101.31	99.99	97.93	101.09	99.34	97.68	100.05	98.65	98.27
Mg#	70.9	45.8	73.5	-	48.3	75.3	-	50.5	76.5	-	51.6
An	-	-	-	60.3	-	-	56.0	-	-	56.7	-

1288 OL190,MV52,R472,1128C,5.5HR,F-8.7,PTFE,E
1289 GL1000,MV52,R510,1145C,18HR,F-8.5,+OL+PL+SPMT+GL,PTFE,E
1290 OL328,MV52,R510,1145C,18HR,F-8.5,PTFE,E
1291 PL309,MV52,R510,1145C,18HR,F-8.5,PTFE,E
1292 GL771,MV52,R512,1155C,24HR,F-8.4,+OL+PL+SPMT+GL,PTFE,E
1293 OL261,MV52,R512,1155C,24HR,F-8.4,PTFE,E
1294 PL263,MV52,R512,1155C,24HR,F-8.4,PTFE,E
1295 GL726,MV52,R514,1165C,16HR,F-8.2,+OL+PL+SPMT+GL,PTFE,E
1296 OL241,MV52,R514,1165C,16HR,F-8.2,PTFE,E
1297 PL258,MV52,R514,1165C,16HR,F-8.2,PTFE,E
1298 GL735,MV52,R515,1176C,16.5HR,F-8.1,+SPMT+GL,PTFE,E

	1299	1300	1301	1302	1303	1304	1305	1306	1307	1308	1309
SiO2	46.70	46.83	46.93	47.47	46.58	48.17	0.28	36.78	53.97	51.49	0.99
TiO2	3.55	3.59	3.66	3.90	3.69	3.94	47.14	0.18	0.34	1.17	20.72
Al2O3	15.65	16.01	15.61	15.36	15.68	11.62	0.49	nd	27.27	1.59	2.87
Fe2O3	2.71	2.87	2.85	3.21	2.73	3.43	11.61	nd	nd	nd	22.03
Cr2O3	0.21	nd	0.04	nd	nd	nd	0.15	nd	nd	nd	0.66
FeO	9.70	9.82	9.93	10.22	9.71	11.54	32.52	32.64	1.36	10.34	44.66
MnO	0.15	nd	0.19	0.16	0.15	0.18	0.57	0.44	nd	0.22	0.31
NiO	nd	nd	nd	nd	nd	nd	nd	0.47	nd	nd	nd
MgO	5.90	5.88	5.83	6.02	5.91	3.68	5.40	29.46	0.19	14.61	4.10
CaO	9.02	8.95	8.97	9.08	8.85	8.26	nd	0.56	11.16	19.87	nd
Na2O	3.04	3.19	3.23	3.02	3.23	2.98	nd	nd	4.49	nd	nd
K2O	1.11	1.13	1.08	1.06	1.08	1.50	nd	nd	0.31	nd	nd
P2O5	0.46	0.53	nd	nd	0.32	1.55	nd	nd	nd	nd	nd
V2O3	nd	nd	nd	nd	nd	nd	nd	nd	nd	nd	0.76
total=	98.20	98.80	98.32	99.50	97.93	96.85	98.16	100.53	99.09	99.29	97.10
Mg#	52.0	51.6	51.1	51.2	52.0	36.2	-	61.7	-	-	14.1
An	-	-	-	-	-	-	-	-	56.8	-	-

1299 GL747,MV52,R516,1186C,12.5HR,F-7.9,+SPMT+GL,PTFE,E
1300 GL176,MV52,R475,1203C,2.5HR,F-7.6,+SPMT+GL,PTFE,E
1301 GL46,MV52,R448,1208C,3HR,F-7.6,-GL,PTFE,E
1302 GL2,MV52,R427,1243C,5HR,F-7.0,-GL,PT,E
1303 GL2030,MV52,R5-727,1271C,6.5HR,F-6.9,-GL,PTFE,W
1304 GL640,MV39A,R501,1092C,19.5HR,F-9.3,+OL+CPX+PL+SPMT+IL+GL,PTFE,E
1305 IL53,MV39A,R501,1092C,19.5HR,F-9.3,PTFE,E
1306 OL213,MV39A,R501,1092C,19.5HR,F-9.3,PTFE,E
1307 PL234,MV39A,R501,1092C,19.5HR,F-9.3,PTFE,E
1308 CPX74,MV39A,R501,1092C,19.5HR,F-9.3,PTFE,E
1309 SPMT42,MV39A,R501,1092C,19.5HR,F-9.3,PTFE,E

	1310	1311	1312	1313	1314	1315	1316	1317	1318	1319	1320
SiO2	46.90	46.13	37.10	54.46	47.01	37.50	54.45	47.21	37.81	37.93	54.82
TiO2	4.65	4.70	0.18	0.18	4.53	0.31	0.45	4.32	0.20	nd	nd
Al2O3	11.23	12.09	nd	27.65	12.24	nd	26.71	13.35	nd	nd	28.05
Fe2O3	3.76	3.62	nd	nd	3.67	nd	nd	3.37	nd	nd	nd
Cr2O3	nd	0.05	nd	nd	nd	nd	nd	0.04	nd	nd	nd
FeO	11.62	11.86	28.63	0.90	11.59	27.48	1.69	11.63	25.83	26.10	0.91
MnO	0.21	0.22	0.32	nd	0.19	0.31	nd	0.21	0.35	0.29	nd
NiO	nd	nd	0.64	nd	nd	0.67	nd	nd	0.65	0.63	nd
MgO	4.12	4.57	33.41	nd	4.55	32.90	nd	5.12	34.46	34.38	nd
CaO	8.85	8.47	0.39	11.02	8.51	0.76	10.69	8.27	0.54	0.51	11.10
Na2O	2.81	2.88	nd	4.56	2.96	nd	4.82	3.09	nd	nd	5.00
K2O	1.24	1.03	nd	0.29	1.02	nd	0.36	0.91	nd	nd	0.31
P2O5	1.19	0.80	nd	nd	0.95	nd	nd	nd	nd	nd	nd
total=	96.58	96.42	100.67	99.06	97.22	99.93	99.17	97.52	99.84	99.84	100.19
Mg#	38.7	40.7	67.5	-	41.2	68.1	-	44.0	70.4	70.1	-
An	-	-	-	56.2	-	-	53.9	-	-	-	54.1

1310 GL482,MV39A,R495,1105C,19HR,F-9.0,+OL+CPX+PL+SPMT+GL,PTFE,E
1311 GL445,MV39A,R492,1114C,19.5HR,F-8.9,+OL+PL+SPMT+GL,PTFE,E
1312 OL150,MV39A,R492,1114C,19.5HR,F-8.9,PTFE,E
1313 PL188,MV39A,R492,1114C,19.5HR,F-8.9,PTFE,E
1314 GL394,MV39A,R483,1122C,19.5HR,F-8.7,+OL+PL+SPMT+GL,PTFE,E
1315 OL129,MV39A,R483,1122C,19.5HR,F-8.7,PTFE,E
1316 PL162,MV39A,R483,1122C,19.5HR,F-8.7,PTFE,E
1317 GL57A,MV39A,R482,1135C,6.5HR,F-8.6,+OL+PL+SPMT+GL,PTFE,E
1318 OL24,MV39A,R482,1135C,6.5HR,F-8.6,PTFE,E
1319 OL25,MV39A,R482,1135C,6.5HR,F-8.6,PTFE,E
1320 PL45,MV39A,R482,1135C,6.5HR,F-8.6,PTFE,E

	1321	1322	1323	1324	1325	1326	1327	1328	1329	1330	1331
SiO2	52.72	52.92	46.90	37.47	37.40	37.81	37.84	37.89	38.46	53.95	54.24
TiO2	0.12	0.26	4.04	0.29	0.19	0.26	0.12	0.25	0.12	0.26	0.23
Al2O3	28.77	28.62	13.59	nd	nd	nd	nd	nd	nd	28.62	28.73
Fe2O3	nd	nd	3.28	nd	nd	nd	nd	nd	nd	nd	nd
Cr2O3	nd	nd	0.01	nd	nd	nd	nd	nd	nd	nd	nd
FeO	1.11	1.12	11.20	24.77	25.00	24.66	25.20	24.71	25.25	1.05	1.01
MnO	nd	nd	0.18	0.29	0.35	0.32	0.34	0.27	0.32	nd	nd
NiO	nd	nd	nd	0.79	0.83	0.85	0.72	0.85	0.92	nd	nd
MgO	nd	nd	5.28	35.40	35.19	35.85	35.98	35.77	34.88	nd	nd
CaO	12.50	12.06	8.25	0.41	0.40	0.44	0.48	0.40	0.42	11.31	11.42
Na2O	4.26	4.27	3.20	nd	nd	nd	nd	nd	nd	4.67	4.42
K2O	0.22	0.20	0.87	nd	nd	nd	nd	nd	nd	0.24	0.27
total=	99.70	99.45	96.80	99.42	99.36	100.19	100.68	100.14	100.37	100.10	100.32
Mg#	-	-	45.7	71.8	71.5	72.2	71.8	72.1	71.1	-	-
An	61.1	60.2	-	-	-	-	-	-	-	56.4	57.9

1321 PL46,MV39A,R482,1135C,6.5HR,F-8.6,PTFE,E
1322 PL47,MV39A,R482,1135C,6.5HR,F-8.6,PTFE,E
1323 GL62,MV39A,R481,1146C,20HR,F-8.4,+OL+PL+SPMT+GL,PTFE,E
1324 OL26,MV39A,R481,1146C,20HR,F-8.4,PTFE,E
1325 OL27,MV39A,R481,1146C,20HR,F-8.4,PTFE,E
1326 OL29,MV39A,R481,1146C,20HR,F-8.4,PTFE,E
1327 OL30,MV39A,R481,1146C,20HR,F-8.4,PTFE,E
1328 OL32,MV39A,R481,1146C,20HR,F-8.4,PTFE,E
1329 OL37,MV39A,R481,1146C,20HR,F-8.4,PTFE,E
1330 PL56,MV39A,R481,1146C,20HR,F-8.4,PTFE,E
1331 PL57,MV39A,R481,1146C,20HR,F-8.4,PTFE,E

	1332	1333	1334	1335	1336	1337	1338	1339	1340	1341	1342
SiO2	54.78	47.45	38.66	38.38	38.84	38.10	54.85	54.94	54.53	52.49	52.59
TiO2	nd	3.82	nd	nd	0.11	0.17	nd	0.18	0.11	0.23	0.14
Al2O3	28.21	14.28	nd	nd	nd	nd	28.38	27.94	28.47	29.35	29.16
Fe2O3	nd	3.19	nd	nd	nd	nd	nd	nd	nd	nd	nd
FeO	0.97	10.82	23.53	23.56	23.72	23.37	0.96	1.00	0.87	1.17	1.09
MnO	nd	0.14	0.26	0.23	0.20	0.25	nd	nd	nd	nd	nd
NiO	nd	nd	0.65	0.76	0.74	0.83	nd	nd	nd	nd	nd
MgO	nd	5.67	37.33	37.30	37.11	36.97	nd	nd	nd	nd	nd
CaO	10.91	8.42	0.34	0.39	0.36	0.44	11.67	11.11	11.86	13.08	12.92
Na2O	4.86	3.36	nd	nd	nd	nd	4.80	4.68	4.66	3.92	3.97
K2O	0.28	0.84	nd	nd	nd	nd	0.20	0.27	0.21	0.18	0.24
total=	100.01	97.99	100.77	100.62	101.08	100.13	100.86	100.12	100.71	100.42	100.11
Mg#	-	48.3	73.9	73.8	73.6	73.8	-	-	-	-	-
An	54.4	-	-	-	-	-	56.7	55.8	57.7	64.2	63.4

1332 PL58,MV39A,R481,1146C,20HR,F-8.4,PTFE,E
1333 GL22,MV39A,R480,1157C,19HR,F-8.2,+OL+PL+SPMT+GL,PTFE,E
1334 OL12,MV39A,R480,1157C,19HR,F-8.2,PTFE,E
1335 OL14,MV39A,R480,1157C,19HR,F-8.2,PTFE,E
1336 OL15,MV39A,R480,1157C,19HR,F-8.2,PTFE,E
1337 OL16,MV39A,R480,1157C,19HR,F-8.2,PTFE,E
1338 PL17,MV39A,R480,1157C,19HR,F-8.2,PTFE,E
1339 PL19,MV39A,R480,1157C,19HR,F-8.2,PTFE,E
1340 PL20,MV39A,R480,1157C,19HR,F-8.2,PTFE,E
1341 PL21,MV39A,R480,1157C,19HR,F-8.2,PTFE,E
1342 PL22,MV39A,R480,1157C,19HR,F-8.2,PTFE,E

	1343	1344	1345	1346	1347	1348	1349	1350	1351	1352	1353
SiO2	53.26	52.54	53.43	52.29	47.44	38.16	38.59	47.62	52.18	53.53	52.89
TiO2	0.17	0.16	0.15	0.19	3.84	nd	nd	3.42	0.34	0.17	0.14
Al2O3	28.69	29.31	29.18	28.55	14.56	0.11	0.14	14.84	28.51	28.40	28.81
Fe2O3	nd	nd	nd	nd	3.04	nd	nd	3.00	nd	nd	nd
Cr2O3	nd	nd	nd	nd	0.02	nd	nd	0.03	nd	nd	nd
FeO	1.00	1.08	0.79	1.16	10.70	22.43	22.52	10.32	1.38	0.98	0.68
MnO	nd	nd	nd	nd	0.20	0.33	0.31	0.19	nd	nd	nd
NiO	nd	nd	nd	nd	0.05	0.98	0.94	nd	nd	nd	nd
MgO	nd	nd	nd	nd	5.90	37.51	37.36	5.55	nd	nd	nd
CaO	12.39	12.87	12.44	12.66	8.19	0.37	0.36	8.63	12.88	12.35	12.45
Na2O	4.53	4.24	4.34	4.05	3.41	nd	nd	3.16	3.80	4.43	4.19
K2O	0.28	0.08	0.16	0.16	0.71	nd	nd	0.79	0.13	0.16	0.19
P2O5	nd	nd	nd	nd	0.44	nd	nd	0.74	nd	nd	nd
total=	100.32	100.28	100.49	99.06	98.50	99.89	100.22	98.29	99.22	100.02	99.35
Mg#	-	-	-	-	49.6	74.9	74.7	48.9	-	-	-
An	59.2	62.4	60.7	62.7	-	-	-	-	64.7	60.1	61.5

1343 PL23,MV39A,R480,1157C,19HR,F-8.2,PTFE,E
1344 PL24,MV39A,R480,1157C,19HR,F-8.2,PTFE,E
1345 PL25,MV39A,R480,1157C,19HR,F-8.2,PTFE,E
1346 PL28,MV39A,R480,1157C,19HR,F-8.2,PTFE,E
1347 GL1172,MV39A,R571,1160C,12.5HR,F-8.2,+OL+PL+SPMT+GL,PTFE,W
1348 OL151,MV39A,R571,1160C,12.5HR,F-8.2,PTFE,W
1349 OL152,MV39A,R571,1160C,12.5HR,F-8.2,PTFE,W
1350 GL138,MV39A,R479,1169C,14HR,F-8.0,+PL+SPMT+GL,PTFE,E
1351 PL111,MV39A,R479,1169C,14HR,F-8.0,PTFE,E
1352 PL112,MV39A,R479,1169C,14HR,F-8.0,PTFE,E
1353 PL114,MV39A,R479,1169C,14HR,F-8.0,PTFE,E

	1354	1355	1356	1357	1358	1359	1360	1361	1362	1363	1364
SiO2	47.13	47.59	47.62	48.31	47.34	47.07	46.82	37.81	38.05	38.44	47.41
TiO2	3.56	3.51	3.61	3.44	3.61	3.51	4.20	nd	nd	nd	3.77
Al2O3	15.01	15.08	15.15	15.22	15.28	14.75	13.95	0.08	0.12	0.12	14.51
Fe2O3	3.03	2.88	2.91	2.89	2.92	3.05	3.37	nd	nd	nd	3.03
Cr2O3	0.01	nd	0.02	nd	0.04	nd	0.02	nd	nd	nd	0.03
FeO	10.49	10.48	10.42	10.21	10.37	10.45	11.17	24.82	24.66	24.00	10.81
MnO	0.18	0.11	0.20	0.22	0.21	0.11	0.25	0.40	0.39	0.40	0.22
NiO	0.05	nd	0.05	nd	0.03	nd	0.02	0.15	0.17	0.22	0.02
MgO	5.77	5.37	5.81	5.68	5.83	5.44	5.62	35.97	36.21	36.77	6.06
CaO	8.36	8.64	8.28	8.62	8.33	8.64	8.38	0.42	0.41	0.39	8.36
Na2O	3.34	3.20	3.29	3.21	3.36	3.11	3.33	nd	nd	nd	3.30
K2O	0.82	0.79	0.65	0.82	0.75	0.76	0.72	nd	nd	nd	0.66
P2O5	0.72	0.71	0.36	0.54	0.50	0.55	0.64	nd	nd	nd	0.53
total=	98.47	98.36	98.37	99.16	98.57	97.44	98.49	99.65	100.01	100.34	98.71
Mg#	49.5	47.7	49.8	49.8	50.1	48.1	47.3	72.1	72.4	73.2	50.0

1354 GL1128,MV39A,R556,1171C,3HR,F-8.0,+PL+SPMT+GL,PTFE,W
1355 GL200,MV39A,R478,1179C,9HR,F-8.0,+SPMT+GL,PTFE,E
1356 GL1151,MV39A,R554,1182C,18.5HR,F-7.9,+SPMT+GL,PTFE,W
1357 GL226,MV39A,R477,1189C,18.5HR,F-7.8,-GL,PTFE,E
1358 GL1202,MV39A,R476,1198C,19HR,F-7.7,-GL,PTFE,W
1359 GL168,MV39A,R474,1209C,3HR,F-7.5,-GL,PTFE,E
1360 GL1187,MV39AF,R577,1148C,13HR,F-8.3,+OL+PL+SPMT+GL,PTFE,W
1361 OL116,MV39AF,R577,1148C,13HR,F-8.3,PTFE,W
1362 OL117,MV39AF,R577,1148C,13HR,F-8.3,PTFE,W
1363 OL118,MV39AF,R577,1148C,13HR,F-8.3,PTFE,W
1364 GL1170,MV39AF,R571,1160C,12.5HR,F-8.2,+OL+PL+GL,PTFE,W

	1365	1366	1367	1368	1369	1370	1371	1372	1373	1374	1375
SiO2	38.10	47.14	47.53	47.89	47.71	36.46	50.21	50.09	47.63	37.97	49.05
TiO2	nd	3.61	3.52	3.66	3.88	0.13	0.31	1.74	3.23	0.17	1.92
Al2O3	0.09	14.90	15.26	15.32	12.48	0.26	30.82	3.20	12.34	0.42	3.65
Fe2O3	nd	3.02	2.83	2.71	0.55	nd	nd	nd	3.47	nd	nd
Cr2O3	nd	nd	0.02	0.02	nd	nd	nd	0.53	nd	nd	0.25
FeO	22.63	10.48	10.22	9.85	14.72	33.73	1.05	10.37	11.72	27.53	10.63
MnO	0.34	0.22	0.21	0.22	0.24	0.55	nd	0.18	nd	0.51	0.27
NiO	0.24	0.01	0.02	0.01	nd	nd	nd	nd	nd	0.49	nd
MgO	37.71	5.90	5.76	5.80	3.96	28.45	nd	12.82	4.54	32.71	12.72
CaO	0.35	8.45	8.42	8.51	9.66	0.76	14.93	20.11	9.68	0.90	19.84
Na2O	nd	3.28	3.22	3.27	2.81	nd	3.03	nd	2.42	nd	nd
K2O	nd	0.78	0.60	0.57	1.50	nd	0.23	nd	1.28	nd	nd
P2O5	nd	0.60	0.40	0.56	0.66	nd	nd	nd	0.53	nd	nd
total=	99.46	98.39	98.01	98.39	98.17	100.34	100.58	99.04	96.84	100.70	98.33
Mg#	74.8	50.1	50.1	51.2	32.4	60.1	-	-	40.8	67.9	-
An	-	-	-	-	-	-	72.2	-	-	-	-

1365 OL147,MV39AF,R571,1160C,12.5HR,F-8.2,PTFE,W
1366 GL1130,MV39AF,R556,1171C,3HR,F-8.0,+PL+GL,PTFE,W
1367 GL1153,MV39AF,R554,1182C,18.5HR,F-7.9,-GL,PTFE,W
1368 GL1145,MV39AF,R553,1193C,17HR,F-7.8,-GL,PTFE,W
1369 GL918,MV402,R574,1113C,19HR,F-13.1,+OL+CPX+PL+GL,PTFE,E
1370 OL305,MV402,R574,1113C,19HR,F-13.1,PTFE,E
1371 PL297,MV402,R574,1113C,19HR,F-13.1,PTFE,E
1372 CPX89,MV402,R574,1113C,19HR,F-13.1,PTFE,E
1373 GL397R,MV402,R483,1122C,19.5HR,F-8.7,+OL+CPX+PL+SPMT+GL,PTFE,E
1374 OL130,MV402,R483,1122C,19.5HR,F-8.7,PTFE,E
1375 CPX44,MV402,R483,1122C,19.5HR,F-8.7,PTFE,E

	1376	1377	1378	1379	1380	1381	1382	1383	1384	1385	1386
SiO2	0.43	48.44	36.55	52.94	49.61	47.76	37.80	52.03	49.67	53.02	49.47
TiO2	13.54	3.49	0.15	0.36	1.89	3.07	0.17	nd	0.14	nd	nd
Al2O3	5.44	12.49	nd	28.03	3.80	12.74	nd	29.06	31.19	28.57	30.36
Fe2O3	26.48	0.46	nd	nd	nd	3.19	nd	nd	nd	nd	nd
Cr2O3	8.18	0.06	nd	nd	0.19	0.05	nd	nd	nd	nd	nd
FeO	37.26	13.51	30.64	1.26	9.70	11.18	25.37	1.09	0.99	1.07	1.05
MnO	0.33	0.16	0.50	nd	0.17	0.20	0.37	nd	nd	nd	nd
NiO	nd	nd	0.37	nd	nd	nd	0.67	nd	nd	nd	nd
MgO	4.41	4.38	30.98	0.20	13.41	4.94	34.88	nd	nd	nd	nd
CaO	nd	10.02	0.74	12.60	20.70	10.31	0.67	13.00	14.39	12.47	14.89
Na2O	nd	2.69	nd	4.43	nd	2.72	nd	3.86	2.93	4.14	2.83
K2O	nd	1.25	nd	0.37	nd	1.16	nd	0.29	0.17	0.31	0.20
P2O5	nd	0.37	nd	nd	nd	nd	nd	nd	nd	nd	nd
V2O3	0.86	nd	nd	nd	nd	nd	nd	nd	nd	nd	nd
total=	96.93	97.32	99.93	100.19	99.47	97.32	99.93	99.33	99.48	99.58	98.80
Mg#	17.4	36.6	64.3	-	-	44.1	71.0	-	-	-	-
An	-	-	-	59.8	-	-	-	63.9	72.3	61.3	73.5

1376 SPMT28,MV402,R483,1122C,19.5HR,F-8.7,PTFE,E
1377 GL1096,MV402,R573,1128C,16HR,F-13.0,+OL+CPX+PL+GL,PTFE,E
1378 OL352,MV402,R573,1128C,16HR,F-13.0,PTFE,E
1379 PL325,MV402,R573,1128C,16HR,F-13.0,PTFE,E
1380 CPX102,MV402,R573,1128C,16HR,F-13.0,PTFE,E
1381 GL37,MV402,R482,1135C,6.5HR,F-8.6,+OL+CPX+PL+SPMT+GL,PTFE,E
1382 OL22,MV402,R482,1135C,6.5HR,F-8.6,PTFE,E
1383 PL39,MV402,R482,1135C,6.5HR,F-8.6,PTFE,E
1384 PL40,MV402,R482,1135C,6.5HR,F-8.6,PTFE,E
1385 PL43,MV402,R482,1135C,6.5HR,F-8.6,PTFE,E
1386 PL44,MV402,R482,1135C,6.5HR,F-8.6,PTFE,E

	1387	1388	1389	1390	1391	1392	1393	1394	1395	1396	1397
SiO2	50.18	48.89	49.50	49.15	48.01	52.63	48.92	48.60	38.64	52.87	53.40
TiO2	1.17	2.02	1.78	1.85	2.99	0.26	2.14	2.84	0.15	0.18	0.14
Al2O3	3.64	4.47	3.70	4.53	12.90	28.17	4.09	13.35	nd	29.62	28.99
Fe2O3	nd	nd	nd	nd	0.43	nd	nd	2.99	nd	nd	nd
Cr2O3	0.47	0.34	0.41	0.39	0.05	nd	0.28	0.03	nd	nd	nd
FeO	7.38	8.71	8.25	8.39	13.27	1.04	9.47	10.57	22.94	0.97	0.88
MnO	nd	0.15	0.14	0.24	0.13	nd	0.27	0.09	0.35	nd	nd
NiO	nd	nd	nd	nd	nd	nd	nd	nd	0.71	nd	nd
MgO	14.19	13.42	13.43	13.05	4.94	nd	13.10	5.47	35.46	nd	0.15
CaO	21.50	21.04	21.48	21.20	10.62	12.76	20.53	10.59	0.64	13.06	12.64
Na2O	nd	0.38	0.23	nd	2.58	3.68	nd	2.65	nd	3.86	3.92
K2O	nd	nd	nd	nd	1.11	0.35	nd	1.03	nd	0.29	0.32
P2O5	nd	nd	nd	nd	0.58	nd	nd	nd	nd	nd	nd
total=	98.53	99.42	98.92	98.80	97.61	98.89	98.80	98.21	98.89	100.85	100.44
Mg#	-	-	-	-	39.9	-	-	48.0	73.4	-	-
An	-	-	-	-	-	64.3	-	-	-	64.1	62.8

1387 CPX18,MV402,R482,1135C,6.5HR,F-8.6,PTFE,E
1388 CPX19,MV402,R482,1135C,6.5HR,F-8.6,PTFE,E
1389 CPX21,MV402,R482,1135C,6.5HR,F-8.6,PTFE,E
1390 CPX23,MV402,R482,1135C,6.5HR,F-8.6,PTFE,E
1391 GL512,MV402,R569,1142C,12HR,F-12.8,+OL+CPX+PL+GL,PTFE,E
1392 PL206,MV402,R569,1142C,12HR,F-12.8,PTFE,E
1393 CPX65,MV402,R569,1142C,12HR,F-12.8,PTFE,E
1394 GL74,MV402,R481,1146C,20HR,F-8.4,+OL+CPX+PL+SPMT+GL,PTFE,E
1395 OL47,MV402,R481,1146C,20HR,F-8.4,PTFE,E
1396 PL68,MV402,R481,1146C,20HR,F-8.4,PTFE,E
1397 PL70,MV402,R481,1146C,20HR,F-8.4,PTFE,E

	1398	1399	1400	1401	1402	1403	1404	1405	1406	1407	1408
SiO2	51.49	49.53	50.04	50.64	50.03	48.08	51.30	48.38	49.72	51.07	48.34
TiO2	0.18	1.55	1.29	0.98	1.55	2.61	0.27	2.68	0.19	0.26	2.51
Al2O3	29.86	4.88	5.22	4.34	4.12	13.68	28.89	13.27	29.84	30.18	13.74
Fe2O3	nd	nd	nd	nd	nd	0.40	nd	2.95	nd	nd	2.90
Cr2O3	nd	0.76	0.80	0.65	0.13	nd	nd	nd	nd	nd	0.12
FeO	1.21	7.10	7.91	7.04	9.21	11.76	0.88	10.06	1.28	0.90	9.74
MnO	nd	0.14	nd	0.15	0.18	0.16	nd	0.16	nd	nd	0.18
NiO	nd	nd	0.14	nd	nd	nd	nd	nd	nd	nd	nd
MgO	nd	14.00	13.19	14.72	13.10	5.37	0.30	5.58	0.17	nd	5.49
CaO	13.61	21.87	19.98	20.28	20.10	10.90	13.26	11.03	15.05	14.20	11.09
Na2O	3.21	nd	0.43	nd	0.25	2.52	3.70	2.70	2.84	3.27	2.87
K2O	0.28	nd	nd	nd	nd	1.04	0.26	1.02	0.24	0.25	0.99
P2O5	nd	nd	nd	nd	nd	0.19	nd	0.43	nd	nd	0.47
total=	99.84	99.83	99.00	98.80	98.67	96.71	98.86	98.26	99.33	100.13	98.44
Mg#	-	-	-	-	-	44.9	-	49.7	-	-	50.1
An	68.9	-	-	-	-	-	65.4	-	73.5	69.6	-

1398 PL71,MV402,R481,1146C,20HR,F-8.4,PTFE,E
1399 CPX35,MV402,R481,1146C,20HR,F-8.4,PTFE,E
1400 CPX36,MV402,R481,1146C,20HR,F-8.4,PTFE,E
1401 CPX37,MV402,R481,1146C,20HR,F-8.4,PTFE,E
1402 CPX38,MV402,R481,1146C,20HR,F-8.4,PTFE,E
1403 GL593,MV402,R567,1156C,12HR,F-12.5,+OL+PL+GL,PTFE,E
1404 PL223,MV402,R567,1156C,12HR,F-12.5,PTFE,E
1405 GL145,MV402,R480,1157C,19HR,F-8.2,+PL+SPMT+GL,PTFE,E
1406 PL119,MV402,R480,1157C,19HR,F-8.2,PTFE,E
1407 PL121,MV402,R480,1157C,19HR,F-8.2,PTFE,E
1408 GL214,MV402,R479,1169C,14HR,F-8.0,+PL+SPMT+GL,PTFE,E

	1409	1410	1411	1412	1413	1414	1415	1416	1417	1418	1419
SiO2	48.63	51.29	49.62	50.53	48.92	50.25	49.01	50.60	0.49	48.91	49.55
TiO2	2.61	nd	2.64	0.29	2.40	0.21	2.62	0.27	5.52	2.42	0.27
Al2O3	14.09	29.82	14.66	28.97	15.04	29.99	14.85	29.69	18.27	15.57	30.35
Fe2O3	0.39	nd	2.66	nd	0.37	nd	2.68	nd	18.20	2.55	nd
Cr2O3	0.04	nd	0.04	nd	0.08	nd	nd	nd	20.35	0.09	nd
FeO	11.53	1.04	9.62	1.53	10.93	0.85	9.35	1.26	26.38	9.16	1.58
MnO	0.21	nd	0.15	nd	0.20	nd	0.17	nd	0.26	0.14	nd
MgO	5.34	0.19	5.25	0.25	5.31	0.22	5.23	nd	8.65	5.04	nd
CaO	11.04	14.31	11.29	14.28	11.13	14.40	11.29	14.64	nd	11.22	15.06
Na2O	2.66	3.24	2.65	3.32	2.93	2.91	2.63	2.87	nd	2.77	2.55
K2O	1.02	0.26	1.00	0.22	0.93	0.22	0.98	0.23	nd	0.89	0.22
P2O5	0.34	nd	0.43	nd	0.26	nd	0.40	nd	nd	0.38	nd
V2O3	nd	nd	nd	nd	nd	nd	nd	nd	0.53	nd	nd
total=	97.90	100.15	100.01	99.39	98.50	99.05	99.21	99.56	98.65	99.14	99.58
Mg#	45.2	-	49.3	-	46.4	-	49.9	-	36.9	49.5	-
An	-	69.9	-	69.5	-	72.3	-	72.8	-	-	75.5

1409 GL1050,MV402,R565,1171C,11.5HR,F-12.3,+PL+GL,PTFE,E
1410 PL316,MV402,R565,1171C,11.5HR,F-12.3,PTFE,E
1411 GL196,MV402,R478,1179C,9HR,F-8.0,+PL+SPMT+GL,PTFE,E
1412 PL138,MV402,R478,1179C,9HR,F-8.0,PTFE,E
1413 GL970,MV402,R563,1185C,15HR,F-12.1,+PL+GL,PTFE,E
1414 PL305,MV402,R563,1185C,15HR,F-12.1,PTFE,E
1415 GL222,MV402,R477,1189C,18.5HR,F-7.8,+PL+SPMT+GL,PTFE,E
1416 PL145,MV402,R477,1189C,18.5HR,F-7.8,PTFE,E
1417 SPMT10,MV402,R477,1189C,18.5HR,F-7.8,PTFE,E
1418 GL190,MV402,R476,1198C,19HR,F-7.7,+PL+SPMT+GL,PTFE,E
1419 PL136,MV402,R476,1198C,19HR,F-7.7,PTFE,E

	1420	1421	1422	1423	1424	1425	1426	1427	1428	1429	1430
SiO2	50.53	48.74	50.10	48.25	48.54	48.74	49.21	50.71	0.40	37.32	52.62
TiO2	0.15	2.51	0.24	2.41	2.32	2.31	2.19	3.58	47.87	0.15	0.45
Al2O3	30.01	15.31	30.79	15.83	15.84	15.97	16.08	13.40	0.54	nd	27.98
Fe2O3	nd	0.34	nd	2.69	0.35	2.45	0.34	2.90	10.26	nd	nd
Cr2O3	nd	0.09	nd	nd	0.06	0.06	0.07	nd	nd	nd	nd
FeO	1.48	9.79	0.66	8.96	10.95	8.81	10.52	9.27	33.33	30.97	1.38
MnO	nd	0.21	nd	0.15	0.06	0.07	0.20	0.09	0.40	0.54	nd
NiO	nd	nd	nd	nd	nd	nd	nd	nd	nd	0.42	nd
MgO	0.27	4.98	nd	4.68	4.72	4.58	4.87	3.15	5.49	31.05	nd
CaO	14.25	11.30	14.87	11.48	11.44	11.49	11.48	7.28	nd	0.52	11.76
Na2O	3.07	2.55	2.79	2.60	2.74	2.73	2.76	3.01	nd	nd	4.20
K2O	0.23	0.99	0.18	0.96	0.83	0.86	0.96	2.81	nd	nd	0.56
P2O5	nd	nd	nd	0.35	0.41	0.29	0.12	1.05	nd	nd	nd
total=	99.99	96.81	99.63	98.36	98.26	98.36	98.80	97.25	98.29	100.97	98.95
Mg#	-	47.6	-	48.2	43.4	48.1	45.2	37.7	-	64.1	-
An	71.0	-	73.9	-	-	-	-	-	-	-	58.7

1420 PL137,MV402,R476,1198C,19HR,F-7.7,PTFE,E
1421 GL963,MV402,R562,1199C,20HR,F-11.9,+PL+GL,PTFE,E
1422 PL304,MV402,R562,1199C,20HR,F-11.9,PTFE,E
1423 GL156,MV402,R473,1211C,2.5HR,F-7.4,+PL+SPMT+GL,PTFE,E
1424 GL491,MV402,R568,1214C,5HR,F-11.8,-GL,PTFE,E
1425 GL361,MV402,R496,1223C,19HR,F-7.4,-GL,PTFE,E
1426 GL1064R,MV402,R566,1227C,5HR,F-11.6,-GL,PTFE,E
1427 GL633R,MV13,R501,1092C,19.5HR,F-9.3,+OL+CPX+PL+SPMT+IL+GL,PTFE,E
1428 IL51,MV13,R501,1092C,19.5HR,F-9.3,PTFE,E
1429 OL211,MV13,R501,1092C,19.5HR,F-9.3,PTFE,E
1430 PL231R,MV13,R501,1092C,19.5HR,F-9.3,PTFE,E

	1431	1432	1433	1434	1435	1436	1437	1438	1439	1440	1441
SiO2	51.06	49.26	0.53	49.06	37.05	53.21	0.29	48.58	37.97	0.40	47.63
TiO2	1.39	1.77	21.06	4.03	0.13	0.26	21.74	4.16	0.27	21.28	4.28
Al2O3	2.17	3.34	3.10	12.88	0.32	27.79	3.58	13.46	0.34	4.26	14.14
Fe2O3	nd	nd	23.12	3.07	nd	nd	22.25	3.14	nd	21.74	3.24
Cr2O3	nd	nd	0.33	nd	nd	nd	0.26	nd	nd	0.52	nd
FeO	11.25	9.60	43.45	9.65	28.54	0.95	43.70	9.95	27.80	42.94	10.36
MnO	0.34	0.21	0.39	0.17	0.37	nd	0.42	0.18	0.42	0.35	0.23
NiO	0.16	nd	nd	nd	0.45	nd	nd	nd	0.60	nd	nd
MgO	12.77	13.14	4.70	3.51	31.84	nd	4.89	3.90	31.93	5.22	4.21
CaO	19.83	20.69	nd	7.43	0.59	11.68	nd	7.40	0.61	nd	7.47
Na2O	nd	nd	nd	3.10	nd	4.54	nd	3.07	nd	nd	3.22
K2O	nd	nd	nd	2.35	nd	0.60	nd	2.15	nd	nd	1.91
P2O5	nd	nd	nd	0.83	nd	nd	nd	0.75	nd	nd	nd
V2O3	nd	nd	0.63	nd	nd	nd	0.74	nd	nd	0.64	nd
total=	98.97	98.01	97.31	96.08	99.29	99.03	97.87	96.74	99.94	97.35	96.69
Mg#	-	-	16.2	39.3	66.5	-	16.6	41.1	67.2	17.8	42.0
An	-	-	-	-	-	56.7	-	-	-	-	-

1431 CPX71,MV13,R501,1092C,19.5HR,F-9.3,PTFE,E
1432 CPX72,MV13,R501,1092C,19.5HR,F-9.3,PTFE,E
1433 SPMT40,MV13,R501,1092C,19.5HR,F-9.3,PTFE,E
1434 GL469,MV13,R494,1104C,19HR,F-9.1,+OL+PL+SPMT+GL,PTFE,E
1435 OL161,MV13,R494,1104C,19HR,F-9.1,PTFE,E
1436 PL200,MV13,R494,1104C,19HR,F-9.1,PTFE,E
1437 SPMT34,MV13,R494,1104C,19HR,F-9.1,PTFE,E
1438 GL457,MV13,R493,1115C,17.5HR,F-8.9,+OL+PL+SPMT+GL,PTFE,E
1439 OL156,MV13,R493,1115C,17.5HR,F-8.9,PTFE,E
1440 SPMT32,MV13,R493,1115C,17.5HR,F-8.9,PTFE,E
1441 GL77R,MV13,R469,1127C,5HR,F-8.7,+OL+PL+SPMT+GL,PTFE,E

	1442	1443	1444	1445	1446	1447	1448	1449	1450	1451	1452
SiO2	37.45	38.08	52.98	0.55	47.58	38.02	37.60	0.76	47.05	37.72	53.31
TiO2	0.17	0.18	0.39	20.22	4.24	nd	nd	19.88	4.08	nd	0.31
Al2O3	0.23	0.36	27.75	5.25	14.93	0.09	0.14	5.58	14.88	nd	28.25
Fe2O3	nd	nd	nd	23.48	3.32	nd	nd	24.40	3.16	nd	nd
Cr2O3	nd	nd	nd	0.77	0.01	nd	nd	0.85	nd	nd	nd
FeO	26.64	26.37	1.61	41.36	10.54	25.74	25.94	39.30	10.30	25.48	0.87
MnO	0.43	0.24	nd	0.25	0.22	0.37	0.42	0.31	0.22	0.31	nd
NiO	0.89	0.95	nd	nd	0.03	0.93	0.88	1.00	nd	1.06	nd
MgO	34.33	33.71	0.20	5.76	4.68	34.67	34.35	5.91	4.64	34.95	nd
CaO	0.49	0.48	12.04	0.33	7.23	0.45	0.48	0.43	7.53	0.32	11.96
Na2O	nd	nd	4.02	nd	3.47	nd	nd	0.02	3.37	nd	4.44
K2O	nd	nd	0.52	nd	1.68	nd	nd	0.29	1.80	nd	0.40
P2O5	nd	nd	nd	nd	0.47	nd	nd	nd	nd	nd	nd
total=	100.63	100.37	99.51	97.97	98.40	100.27	99.81	98.73	97.03	99.84	99.54
Mg#	69.7	69.5	-	19.9	44.2	70.6	70.2	21.1	44.5	71.0	-
An	-	-	60.4	-	-	-	-	-	-	-	58.4

1442 OL48,MV13,R469,1127C,5HR,F-8.7,PTFE,E
1443 OL50R0Q,MV13,R469,1127C,5HR,F-8.7,PTFE,E
1444 PL74,MV13,R469,1127C,5HR,F-8.7,PTFE,E
1445 SPMT3,MV13,R469,1127C,5HR,F-8.7,PTFE,E
1446 GL1196,MV13,R583,1135C,13HR,F-8.5,+OL+PL+SPMT+GL,PTFE,W
1447 OL160,MV13,R583,1135C,13HR,F-8.5,PTFE,W
1448 OL161,MV13,R583,1135C,13HR,F-8.5,PTFE,W
1449 SPMT101C,MV13,R583,1135C,13HR,F-8.5,PTFE,W
1450 GL8,MV13,R468,1140C,19HR,F-8.5,+OL+PL+SPMT+GL,PTFE,E
1451 OL8,MV13,R468,1140C,19HR,F-8.5,PTFE,E
1452 PL8,MV13,R468,1140C,19HR,F-8.5,PTFE,E

	1453	1454	1455	1456	1457	1458	1459	1460	1461	1462	1463
SiO2	52.04	47.79	37.86	37.87	47.21	50.90	47.33	47.26	47.20	47.45	46.60
TiO2	0.44	3.96	nd	nd	3.86	0.38	3.78	3.64	3.77	3.74	3.64
Al2O3	28.30	15.61	nd	0.09	15.56	29.05	15.83	15.74	15.79	15.79	15.49
Fe2O3	nd	3.18	nd	nd	2.90	nd	3.02	2.95	3.13	2.86	3.02
Cr2O3	nd	0.02	nd	nd	nd	nd	nd	nd	nd	nd	nd
FeO	1.27	10.37	24.16	24.40	10.06	1.48	10.31	10.13	10.35	9.58	10.16
MnO	nd	0.20	0.35	0.35	0.09	nd	0.17	0.22	0.18	0.20	0.08
NiO	nd	0.06	1.29	1.10	nd	nd	0.06	nd	0.09	nd	nd
MgO	nd	5.06	35.82	35.53	4.94	nd	5.20	5.00	5.17	5.06	4.90
CaO	12.10	7.30	0.41	0.41	7.53	12.87	7.35	7.66	7.40	7.51	7.59
Na2O	4.26	3.53	nd	nd	3.36	3.86	3.44	3.19	3.46	3.23	3.16
K2O	0.41	1.55	nd	nd	1.68	0.34	1.54	1.65	1.57	1.62	1.64
P2O5	nd	0.38	nd	nd	0.47	nd	0.48	0.44	0.50	0.48	0.48
total=	98.82	99.01	99.89	99.75	97.66	98.88	98.51	97.88	98.61	97.52	96.76
Mg#	-	46.5	72.5	72.2	46.7	-	47.3	46.8	47.1	48.5	46.2
An	59.6	-	-	-	-	63.5	-	-	-	-	-

1453 PL9,MV13,R468,1140C,19HR,F-8.5,PTFE,E
1454 GL1184,MV13,R577,1148C,13HR,F-8.3,+OL+PL+SPMT+GL,PTFE,W
1455 OL120,MV13,R577,1148C,13HR,F-8.3,PTFE,W
1456 OL122,MV13,R577,1148C,13HR,F-8.3,PTFE,W
1457 GL568,MV13,R467,1151C,16HR,F-8.4,+OL+PL+SPMT+GL,PTFE,E
1458 PL215,MV13,R467,1151C,16HR,F-8.4,PTFE,E
1459 GL1108,MV13,R571,1160C,12.5HR,F-8.2,+PL+SPMT+GL,PTFE,W
1460 GL563,MV13,R466,1161C,16HR,F-8.2,+SPMT+GL,PTFE,E
1461 GL1126,MV13,R556,1171C,3HR,F-8.0,+SPMT+GL,PTFE,W
1462 GL541,MV13,R464,1174C,19HR,F-8,+SPMT+GL,PTFE,E
1463 GL543,MV13,R465,1174C,16HR,F-8.0,+SPMT+GL,PTFE,E

	1464	1465	1466	1467	1468	1469	1470	1471	1472	1473	1474
SiO2	47.67	47.87	47.08	47.28	47.07	47.49	47.20	47.35	37.68	53.19	0.15
TiO2	3.87	3.89	3.81	3.85	3.78	3.86	3.80	4.34	nd	0.29	19.16
Al2O3	15.90	15.96	15.55	15.53	15.59	15.92	15.62	14.81	nd	27.92	6.17
Fe2O3	3.03	2.95	3.26	3.20	3.13	3.06	3.10	3.41	nd	nd	26.45
Cr2O3	0.02	0.02	nd	nd	nd	0.03	nd	0.02	nd	nd	0.69
FeO	10.31	10.20	10.22	10.18	10.11	10.12	10.06	10.81	27.16	1.05	38.41
MnO	0.19	0.19	0.17	0.14	0.18	0.20	0.14	0.23	0.43	nd	0.30
NiO	0.06	0.05	nd	nd	nd	0.06	nd	0.01	0.08	nd	0.05
MgO	5.17	5.20	5.01	4.85	4.85	5.13	5.03	4.66	34.35	nd	6.27
CaO	7.39	7.44	7.59	7.61	7.52	7.36	7.66	7.16	0.44	11.98	0.31
Na2O	3.39	3.41	3.32	3.28	3.31	3.47	3.44	3.48	nd	4.35	0.03
K2O	1.44	1.45	1.62	1.57	1.63	1.34	1.59	1.67	nd	0.49	0.23
P2O5	0.54	0.42	nd	nd	nd	0.29	nd	0.49	nd	nd	nd
total=	98.98	99.05	97.63	97.49	97.17	98.33	97.64	98.44	100.14	99.27	98.22
Mg#	47.2	47.6	46.6	45.9	46.1	47.5	47.1	43.4	69.3	-	22.5
An	-	-	-	-	-	-	-	-	-	58.6	-

1464 GL1147,MV13,R554,1182C,18.5HR,F-7.9,+SPMT+GL,PTFE,W
1465 GL1141,MV13,R553,1193C,17HR,F-7.8,+SPMT+GL,PTFE,W
1466 GL83,MV13,R458,1212C,17HR,F-7.4,+SPMT+GL,PTFE,E
1467 GL75,MV13,R457,1223C,19HR,F-7.3,-GL,PTFE,E
1468 GL67,MV13,R456,1234C,17HR,F-7.2,-GL,PTFE,E
1469 GL1199,MV13,R454,1243C,16.5HR,F-7.1,-GL,PTFE,W
1470 GL19,MV13,R453,1253C,8.5HR,F-7.0,-GL,PTFE,E
1471 GL1193,MV13F,R583,1135C,13HR,F-8.5,+OL+PL+SPMT+GL,PTFE,W
1472 OL156,MV13F,R583,1135C,13HR,F-8.5,PTFE,W
1473 PL151,MV13F,R583,1135C,13HR,F-8.5,PTFE,E
1474 SPMT100C,MV13F,R583,1135C,13HR,F-8.5,PTFE,W

	1475	1476	1477	1478	1479	1480	1481	1482	1483	1484	1485
SiO2	0.46	0.22	47.52	38.01	38.03	47.50	47.24	47.25	47.38	50.16	0.97
TiO2	18.93	19.42	4.09	nd	nd	3.86	3.80	3.79	3.87	3.75	46.56
Al2O3	6.45	5.80	15.47	0.12	0.11	15.89	15.74	15.87	15.85	12.81	0.81
Fe2O3	25.39	25.63	3.28	nd	nd	3.03	3.11	3.11	3.04	3.11	9.70
Cr2O3	0.63	0.43	0.01	nd	nd	0.02	nd	nd	0.01	0.11	0.26
FeO	40.40	40.39	10.59	24.55	23.93	10.36	10.31	10.33	10.38	10.28	33.35
MnO	0.31	0.22	0.22	0.38	0.35	0.19	0.19	0.17	0.19	0.28	0.35
NiO	nd	nd	0.03	0.06	0.06	0.01	0.01	0.06	0.01	nd	nd
MgO	6.24	6.18	5.10	36.50	37.09	5.32	5.34	5.31	5.30	3.20	5.23
CaO	nd	nd	7.24	0.36	0.44	7.49	7.30	7.37	7.35	7.67	nd
Na2O	nd	nd	3.57	nd	nd	3.54	3.42	3.44	3.55	3.35	nd
K2O	nd	nd	1.57	nd	nd	1.42	1.58	1.76	1.49	1.86	nd
P2O5	nd	nd	0.34	nd	nd	0.36	0.52	0.43	0.38	1.03	nd
V2O3	0.79	0.67	nd	nd	nd	nd	nd	nd	nd	nd	nd
total=	99.60	98.96	99.03	99.98	100.01	98.99	98.56	98.89	98.80	97.61	97.23
Mg#	21.6	21.4	46.2	72.6	73.4	47.8	48.0	47.8	47.6	35.7	-

1475 SPMT20,MV13F,R583,1135C,13HR,F-8.5,PTFE,E
1476 SPMT21R,MV13F,R583,1135C,13HR,F-8.5,PTFE,E
1477 GL1181,MV13F,R577,1148C,13HR,F-8.3,+OL+PL+SPMT+GL,PTFE,W
1478 OL123,MV13F,R577,1148C,13HR,F-8.3,PTFE,W
1479 OL124,MV13F,R577,1148C,13HR,F-8.3,PTFE,W
1480 GL1175,MV13F,R571,1160C,12.5HR,F-8.2,-GL,PTFE,W
1481 GL1123,MV13F,R556,1171C,3HR,F-8.0,-GL,PTFE,W
1482 GL1239,MV13F,R544,1205C,2HR,F-7.6,-GL,PTFE,W
1483 GL1210,MV13F,R542,1208C,2.5HR,F-7.6,-GL,PTFE,W
1484 GL636,MV40A,R501,1092C,19.5HR,F-9.3,+OL+CPX+PL+SPMT+IL+GL,PTFE,E
1485 IL52,MV40A,R501,1092C,19.5HR,F-9.3,PTFE,E

	1486	1487	1488	1489	1490	1491	1492	1493	1494	1495	1496
SiO2	36.43	53.15	51.01	0.37	48.82	49.16	36.96	53.26	55.76	48.82	37.71
TiO2	0.13	0.26	0.90	21.61	4.01	3.95	0.13	0.27	0.14	3.81	nd
Al2O3	nd	27.96	1.48	2.88	12.18	12.68	nd	27.47	26.09	13.05	nd
Fe2O3	nd	nd	nd	22.63	3.31	3.29	nd	nd	nd	3.26	nd
Cr2O3	nd	nd	nd	0.81	0.07	nd	nd	nd	nd	nd	nd
FeO	31.22	1.38	12.16	44.23	10.61	10.74	29.59	1.02	0.79	10.48	28.42
MnO	0.50	nd	0.23	0.34	0.19	0.24	0.38	nd	nd	0.05	0.41
NiO	0.60	nd	nd	nd	nd	nd	0.60	nd	nd	nd	0.71
MgO	30.96	nd	14.07	4.57	4.03	4.08	32.04	nd	nd	4.35	33.28
CaO	0.56	11.51	18.53	nd	7.58	7.53	0.47	11.39	9.49	7.24	0.44
Na2O	nd	4.63	nd	nd	2.96	3.40	nd	4.44	5.37	3.32	nd
K2O	nd	0.40	nd	nd	1.62	1.51	nd	0.31	0.51	1.47	nd
P2O5	nd	nd	nd	nd	0.89	0.95	nd	nd	nd	0.87	nd
V2O3	nd	nd	nd	0.71	nd	nd	nd	nd	nd	nd	nd
total=	100.40	99.29	98.38	98.15	96.27	97.53	100.17	98.16	98.15	96.72	100.97
Mg#	63.9	-	-	15.6	40.4	40.4	65.9	-	-	42.5	67.6
An	-	56.5	-	-	-	-	-	57.5	47.9	-	-

1486 OL212,MV40A,R501,1092C,19.5HR,F-9.3,PTFE,E
1487 PL233,MV40A,R501,1092C,19.5HR,F-9.3,PTFE,E
1488 CPX73,MV40A,R501,1092C,19.5HR,F-9.3,PTFE,E
1489 SPMT41,MV40A,R501,1092C,19.5HR,F-9.3,PTFE,E
1490 GL486,MV40A,R495,1105C,19HR,F-9.0,+OL+PL+SPMT+GL,PTFE,E
1491 GL449R,MV40A,R492,1114C,19.5HR,F-8.9,+OL+PL+SPMT+GL,PTFE,E
1492 OL152R,MV40A,R492,1114C,19.5HR,F-8.9,PTFE,E
1493 PL191R,MV40A,R492,1114C,19.5HR,F-8.9,PTFE,E
1494 PL192R,MV40A,R492,1114C,19.5HR,F-8.9,PTFE,E
1495 GL398R,MV40A,R483,1122C,19.5HR,F-8.7,+OL+PL+SPMT+GL,PTFE,E
1496 OL131,MV40A,R483,1122C,19.5HR,F-8.7,PTFE,E

	1497	1498	1499	1500	1501	1502	1503	1504	1505	1506	1507
SiO2	53.22	48.46	37.05	52.51	53.84	48.69	37.59	52.25	49.43	52.14	53.45
TiO2	0.18	3.46	0.18	0.45	0.43	3.24	nd	0.16	3.06	nd	0.22
Al2O3	27.66	13.95	nd	27.66	27.77	14.58	nd	29.20	14.98	29.19	27.83
Fe2O3	nd	2.98	nd	nd	nd	2.84	nd	nd	2.79	nd	nd
FeO	0.88	10.45	26.79	1.87	1.62	9.95	24.17	0.94	9.66	0.80	1.03
MnO	nd	nd	0.35	nd	nd	0.17	0.31	nd	0.15	nd	nd
NiO	nd	nd	0.82	nd	nd	nd	0.77	nd	nd	nd	nd
MgO	nd	4.55	34.41	0.26	0.22	4.74	35.75	nd	4.90	nd	0.15
CaO	11.48	7.49	0.47	11.84	11.57	7.25	0.45	12.11	7.60	12.85	11.74
Na2O	4.62	3.17	nd	4.13	4.66	3.41	nd	4.24	3.31	4.22	4.52
K2O	0.28	1.40	nd	0.35	0.40	1.26	nd	0.23	1.25	0.18	0.24
P2O5	nd	0.62	nd	nd	nd	0.23	nd	nd	0.63	nd	nd
total=	98.32	96.53	100.07	99.07	100.51	96.36	99.04	99.13	97.76	99.38	99.18
Mg#	-	43.7	69.6	-	-	45.9	72.5	-	47.5	-	-
An	56.9	-	-	60.0	56.5	-	-	60.4	-	62.1	58.1

1497 PL164,MV40A,R483,1122C,19.5HR,F-8.7,PTFE,E
1498 GL720,MV40A,R482,1135C,6.5HR,F-8.6,+OL+PL+SPMT+GL,PTFE,E
1499 OL237,MV40A,R482,1135C,6.5HR,F-8.6,PTFE,E
1500 PL255R,MV40A,R482,1135C,6.5HR,F-8.6,PTFE,E
1501 PL256,MV40A,R482,1135C,6.5HR,F-8.6,PTFE,E
1502 GL716,MV40A,R481,1146C,20HR,F-8.4,+OL+PL+SPMT+GL,PTFE,E
1503 OL235,MV40A,R481,1146C,20HR,F-8.4,PTFE,E
1504 PL252,MV40A,R481,1146C,20HR,F-8.4,PTFE,E
1505 GL142RR,MV40A,R480,1157C,19HR,F-8.2,+PL+SPMT+GL,PTFE,E
1506 PL116,MV40A,R480,1157C,19HR,F-8.2,PTFE,E
1507 PL117,MV40A,R480,1157C,19HR,F-8.2,PTFE,E

	1508	1509	1510	1511	1512	1513	1514	1515	1516	1517	1518
SiO2	53.45	49.85	52.59	49.98	52.11	50.80	52.73	50.04	51.59	51.25	53.90
TiO2	0.13	2.86	nd	2.91	0.38	2.91	0.15	2.71	0.25	0.25	0.13
Al2O3	28.48	15.58	28.21	16.11	28.27	16.50	29.64	17.14	30.15	29.29	29.14
Fe2O3	nd	2.71	nd	2.53	nd	2.50	nd	2.36	nd	nd	nd
Cr2O3	nd	nd	nd	0.06	nd	nd	nd	nd	nd	nd	nd
FeO	0.78	9.26	0.95	9.21	1.73	8.67	0.74	8.40	0.94	1.54	0.94
MnO	nd	0.08	nd	0.20	nd	0.19	nd	0.12	nd	nd	nd
MgO	nd	4.53	nd	4.64	0.30	4.34	nd	4.35	nd	nd	nd
CaO	11.89	7.74	11.99	7.94	12.75	8.04	12.83	8.13	13.82	13.07	11.99
Na2O	4.48	3.48	4.50	3.57	3.74	3.68	3.94	3.67	3.37	3.66	4.52
K2O	0.29	1.15	0.18	1.14	0.36	1.16	0.20	1.14	0.17	0.23	0.22
P2O5	nd	0.70	nd	0.61	nd	0.40	nd	0.53	nd	nd	nd
total=	99.50	97.94	98.42	98.90	99.64	99.19	100.23	98.59	100.29	99.29	100.84
Mg#	-	46.6	-	47.3	-	47.2	-	48.0	-	-	-
An	58.4	-	58.9	-	63.9	-	63.5	-	68.7	65.5	58.7

1508 PL118,MV40A,R480,1157C,19HR,F-8.2,PTFE,E
1509 GL209,MV40A,R479,1169C,14HR,F-8.0,+PL+SPMT+GL,PTFE,E
1510 PL142,MV40A,R479,1169C,14HR,F-8.0,PTFE,E
1511 GL228,MV40A,R478,1179C,9HR,F-8.0,+PL+GL,PTFE,E
1512 PL147,MV40A,R478,1179C,9HR,F-8.0,PTFE,E
1513 GL224,MV40A,R477,1189C,18.5HR,F-7.8,+PL+GL,PTFE,E
1514 PL146R,MV40A,R477,1189C,18.5HR,F-7.8,PTFE,E
1515 GL183,MV40A,R476,1198C,19HR,F-7.7,+PL+GL,PTFE,E
1516 PL129,MV40A,R476,1198C,19HR,F-7.7,PTFE,E
1517 PL130,MV40A,R476,1198C,19HR,F-7.7,PTFE,E
1518 PL131,MV40A,R476,1198C,19HR,F-7.7,PTFE,E

	1519	1520	1521	1522	1523	1524	1525	1526	1527	1528	1529
SiO2	50.95	49.63	49.29	50.39	35.65	55.70	51.34	1.28	49.73	0.51	50.10
TiO2	0.12	2.62	3.14	2.73	0.43	0.36	1.20	22.23	2.48	17.56	2.62
Al2O3	30.16	17.16	16.55	12.96	0.30	25.48	2.73	2.75	12.78	3.44	13.65
Fe2O3	nd	2.48	2.67	3.26	nd	nd	nd	18.60	3.26	30.76	2.96
Cr2O3	nd	0.17	0.07	0.03	nd	nd	0.12	0.14	nd	0.21	nd
FeO	0.95	8.29	8.89	9.95	37.10	1.66	12.51	47.83	9.79	42.22	10.28
MnO	nd	0.19	0.13	0.20	0.55	nd	0.30	0.34	nd	0.36	0.24
NiO	nd	nd	nd	nd	0.29	nd	nd	nd	nd	nd	nd
MgO	nd	3.95	3.76	2.58	25.29	nd	12.94	3.04	3.23	3.78	3.26
CaO	13.60	8.48	5.83	6.83	0.63	9.28	18.70	nd	6.94	nd	6.75
Na2O	3.28	3.44	3.69	3.00	nd	5.52	nd	nd	3.07	nd	3.45
K2O	0.14	1.07	2.94	3.07	nd	0.95	nd	nd	2.63	nd	2.59
P2O5	nd	0.46	0.40	2.07	nd	nd	nd	nd	2.12	nd	1.74
V2O3	nd	nd	nd	nd	nd	nd	nd	0.33	nd	0.30	nd
total=	99.20	97.94	97.36	97.07	100.24	98.95	99.84	96.54	96.03	99.14	97.64
Mg#	-	45.9	43.0	31.6	54.9	-	-	10.2	37.0	13.8	36.1
An	69.0	-	-	-	-	45.5	-	-	-	-	-

1519 PL132,MV40A,R476,1198C,19HR,F-7.7,PTFE,E
1520 GL158,MV40A,R473,1211C,2.5HR,F-7.4,-GL,PTFE,E
1521 GL262,MV165,R580,1302C,2HR,F-6.6,-GL,PTFE,E
1522 GL951,MV51,R537,1074C,16HR,F-9.4,+OL+CPX+PL+SPMT+AP+GL,PTFE,E
1523 OL314,MV51,R537,1074C,16HR,F-9.4,PTFE,E
1524 PL303,MV51,R537,1074C,16HR,F-9.4,PTFE,E
1525 CPX93,MV51,R537,1074C,16HR,F-9.4,PTFE,E
1526 SPMT60,MV51,R537,1074C,16HR,F-9.4,PTFE,E
1527 GL327,MV51,R541,1086C,16HR,F-9.1,+OL+PL+SP+GL,PTFE,E
1528 SPMT23,MV51,R541,1086C,16HR,F-9.1,PTFE,E
1529 GL631,MV51,R501,1092C,19.5HR,F-9.3,+OL+PL+SPMT+GL,PTFE,E

	1530	1531	1532	1533	1534	1535	1536	1537	1538	1539	1540
SiO2	36.19	54.47	53.68	0.42	49.38	48.71	36.55	0.88	49.45	56.07	54.15
TiO2	0.12	0.38	0.43	18.31	2.67	2.70	nd	16.70	2.74	0.18	0.20
Al2O3	nd	26.12	27.23	4.15	13.86	14.26	nd	4.98	14.73	26.69	27.75
Fe2O3	nd	nd	nd	28.68	3.15	3.11	nd	28.09	3.07	nd	nd
Cr2O3	nd	nd	nd	0.22	nd	nd	nd	0.35	0.03	nd	nd
FeO	33.63	1.99	1.67	42.37	10.76	10.89	31.48	40.87	11.02	1.13	1.08
MnO	0.59	nd	nd	0.45	0.07	0.26	0.48	0.35	0.16	nd	nd
NiO	0.43	nd	nd	nd	nd	nd	0.61	nd	nd	nd	nd
MgO	29.31	nd	nd	4.05	3.40	3.82	30.31	4.17	3.74	nd	nd
CaO	0.53	9.94	10.61	nd	6.65	6.63	0.46	nd	6.74	9.91	10.91
Na2O	nd	5.19	4.69	nd	3.39	3.55	nd	nd	3.58	5.29	4.63
K2O	nd	0.79	0.74	nd	2.24	2.14	nd	nd	2.14	0.57	0.51
P2O5	nd	nd	nd	nd	1.72	1.51	nd	nd	nd	nd	nd
V2O3	nd	nd	nd	0.33	nd	nd	nd	0.39	nd	nd	nd
total=	100.80	98.88	99.05	98.98	97.29	97.58	99.89	96.78	97.40	99.84	99.23
Mg#	60.8	-	-	14.6	36.0	38.5	63.2	15.4	37.7	-	-
An	-	49.0	53.1	-	-	-	-	-	-	49.2	54.8

1530 OL210,MV51,R501,1092C,19.5HR,F-9.3,PTFE,E
1531 PL229,MV51,R501,1092C,19.5HR,F-9.3,PTFE,E
1532 PL230,MV51,R501,1092C,19.5HR,F-9.3,PTFE,E
1533 SPMT39,MV51,R501,1092C,19.5HR,F-9.3,PTFE,E
1534 GL484,MV51,R495,1105C,19HR,F-9.0,+OL+PL+SPMT+GL,PTFE,E
1535 GL440,MV51,R492,1114C,19.5HR,F-8.9,+OL+PL+SPMT+GL,PTFE,E
1536 OL148,MV51,R492,1114C,19.5HR,F-8.9,PTFE,E
1537 SPMT30,MV51,R492,1114C,19.5HR,F-8.9,PTFE,E
1538 GL119,MV51,R491,1124C,19HR,F-8.8,+PL+SPMT+GL,PTFE,E
1539 PL100,MV51,R491,1124C,19HR,F-8.8,PTFE,E
1540 PL101,MV51,R491,1124C,19HR,F-8.8,PTFE,E

	1541	1542	1543	1544	1545	1546	1547	1548
SiO2	54.07	54.34	0.68	48.84	48.88	49.05	49.55	49.32
TiO2	0.26	nd	16.38	2.68	2.57	2.51	2.62	2.69
Al2O3	28.12	28.12	5.73	15.26	15.02	14.79	14.99	15.07
Fe2O3	nd	nd	28.95	3.03	3.00	3.03	3.06	3.21
Cr2O3	nd	nd	1.18	nd	0.06	nd	nd	nd
FeO	1.20	1.04	40.12	10.91	10.96	10.68	10.66	10.65
MnO	nd	nd	0.32	0.20	0.21	0.16	0.25	0.17
MgO	nd	nd	4.77	3.46	3.56	3.44	3.48	3.37
CaO	11.43	11.33	nd	6.80	6.80	6.87	6.74	6.92
Na2O	4.83	5.09	nd	3.60	3.67	3.67	3.60	3.51
K2O	0.50	0.44	nd	2.01	2.04	2.06	2.04	2.09
P2O5	nd	nd	nd	1.30	1.27	1.24	1.32	1.28
V2O3	nd	nd	0.44	nd	nd	nd	nd	nd
total=	100.41	100.36	98.57	98.09	98.04	97.50	98.31	98.28
Mg#	-	-	17.5	36.1	36.7	36.5	36.8	36.1
An	55.0	53.8	-	-	-	-	-	-

1541 PL103,MV51,R491,1124C,19HR,F-8.8,PTFE,E
1542 PL104,MV51,R491,1124C,19HR,F-8.8,PTFE,E
1543 SPMT8,MV51,R491,1124C,19HR,F-8.8,PTFE,E
1544 GL908,MV51,R490,1137C,19HR,F-8.6,+SPMT+GL,PTFE,E
1545 GL519R,MV51,R489,1147C,18HR,F-8.5,+SPMT+GL,PTFE,E
1546 GL517,MV51,R488,1158C,19HR,F-8.3,-GL,PTFE,E
1547 GL516,MV51,R487,1171C,17.5HR,F-8.1,-GL,PTFE,E
1548 GL234,MV51,R486,1180C,17.5HR,F-7.9,-GL,PTFE,E

APPENDIX 5

Representative analyses of phases in the natural rocks

Electron microprobe analyses of the natural minerals are presented below. Samples are listed in order of decreasing whole-rock Mg#. The four ultramafic inclusions in the study are presented at the end of the appendix.

Titles are formatted to give some details of the individual points analysed.The following phase abbreviations have been used :

OL - olivine
CPX - high-Ca clinopyroxene
OPX - low-Ca pyroxene
PL - plagioclase
SP - spinel
MT - titanomagnetite
IL - ilmenite
BI - biotite
AP - apatite
AF - alkali feldspar
NE - nepheline
AC - analcime

Titles are presented in the order :
phase
rock identifier
phenocryst(P) or nodule phase(PN) or groundmass phase(GR)
core(C) or interior(I) or rim(R) zone
phenocryst or nodule assemblage(only with the first analysis of each rock)
analysis by EDS(E) or WDS(W) techniques.

The cation ratios beneath the analyses are:
Mg# - $100*Mg/(Mg+Fe^{2+})$ for olivines,pyroxenes and spinels
An - 100*Ca/(Ca+Na+K) for plagioclases
Al ratio - AlVI/AlIV ratio for clinopyroxenes(after Fe has been recast on the basis of stoichiometry)

Fe203 contents of spinels,magnetites and ilmenites have been calculated on the basis of stoichiometry. Pyroxene Mg# 's have been calculated from analyses recast on the basis of stoichiometry.

	1	2	3	4	5	6	7	8	9	10	11
SiO2	39.51	39.48	39.17	38.49	37.41	38.61	39.17	37.65	39.28	38.83	37.72
TiO2	nd	0.13	nd	nd	nd	nd	nd	nd	nd	nd	0.11
FeO	16.44	18.40	18.08	20.77	26.31	19.57	16.50	25.02	20.46	21.15	29.15
MnO	0.14	0.29	0.25	0.24	0.48	0.26	0.20	0.44	0.27	0.23	0.56
NiO	nd	nd	nd	nd	0.08	0.12	nd	0.08	nd	0.21	nd
MgO	43.26	41.92	42.69	40.45	35.69	41.21	43.66	36.52	40.53	39.70	33.43
CaO	0.26	0.17	0.19	0.20	0.32	0.20	0.23	0.28	0.19	0.14	0.38
total=	99.61	100.39	100.38	100.15	100.29	99.97	99.76	99.99	100.73	100.26	101.35
Mg#	82.4	80.2	80.8	77.6	70.7	79.0	82.5	72.2	77.9	77.0	67.1

1 OL15,AS2,P,I,+OL+CPX+PL+SP,E
2 OL27,AS2,P,C,E
3 OL404,AS2,P,C,W
4 OL405,AS2,P,C,W
5 OL406,AS2,P,R,W
6 OL407,AS2,P,C,W
7 OL408,AS2,P,C,W
8 OL409,AS2,P,C,W
9 OL41,AS2,P,I,E
10 OL42,AS2,P,C,E
11 OL44,AS2,GR,C,E

	12	13	14	15	16	17	18	19	20	21	22
SiO2	52.56	49.78	49.61	48.99	50.10	49.24	54.17	50.47	52.05	50.27	53.29
TiO2	0.16	0.07	0.06	0.06	0.06	0.06	0.06	0.20	0.13	0.16	nd
Al2O3	28.88	31.21	31.33	31.65	30.88	31.60	28.00	31.08	29.47	30.89	29.10
FeO	0.77	0.49	0.56	0.70	0.49	0.59	0.54	0.66	0.67	0.77	0.45
MgO	nd	0.03	0.04	0.04	0.03	0.05	0.13	nd	nd	nd	nd
CaO	12.15	14.46	14.64	14.76	14.02	14.90	10.71	14.48	12.35	13.99	11.94
Na2O	4.41	3.26	3.29	3.09	3.59	3.03	5.25	3.33	4.29	3.46	4.56
K2O	0.25	0.16	0.18	0.13	0.20	0.16	0.44	0.12	0.32	0.14	0.30
total=	99.18	99.46	99.71	99.42	99.37	99.63	99.30	100.34	99.28	99.68	99.64
An	59.5	70.4	70.4	72.0	67.6	72.4	51.7	70.1	60.3	68.5	58.1

12 PL10,AS2,P,R,E
13 PL1006,AS2,P,C,W
14 PL1007,AS2,P,I,W
15 PL1008,AS2,P,R,W
16 PL1009,AS2,P,C,W
17 PL1010,AS2,P,I,W
18 PL1014,AS2,P,C,W
19 PL11,AS2,P,C,E
20 PL12,AS2,P,R,E
21 PL13,AS2,GR,C,E
22 PL6,AS2,P,C,E

	23	24	25	26	27	28	29	30	31	32	33
SiO2	50.20	50.59	50.46	48.98	48.33	48.38	48.64	47.99	48.86	47.99	48.92
TiO2	0.13	0.26	nd	1.92	2.32	1.18	1.29	1.95	1.28	1.30	1.16
Al2O3	30.98	30.56	30.98	4.36	4.79	8.29	6.45	5.17	6.75	7.98	7.27
Cr2O3	nd	nd	nd	0.23	0.02	0.30	0.12	0.29	0.16	0.32	0.35
FeO	0.50	0.54	0.52	7.67	8.12	6.40	6.30	7.36	6.01	6.11	6.13
MnO	nd	nd	nd	0.15	0.18	0.14	0.15	0.17	0.13	0.14	0.14
MgO	nd	nd	nd	13.35	13.11	14.29	14.58	13.28	14.49	14.13	14.50
CaO	14.42	13.94	14.22	21.90	21.98	19.68	21.00	21.95	21.24	20.41	20.03
Na2O	3.18	3.58	3.51	0.53	0.49	0.66	0.38	0.50	0.38	0.56	0.57
K2O	0.20	0.19	0.21	nd	nd	nd	nd	nd	nd	nd	nd
total=	99.61	99.66	99.90	99.09	99.34	99.32	98.91	98.66	99.30	98.94	99.07
Mg#	-	-	-	80.3	79.9	83.5	85.2	83.0	84.8	84.9	83.1
An	70.6	67.5	68.3	-	-	-	-	-	-	-	-
Al ratio	-	-	-	0.2	0.1	0.7	0.5	0.2	0.5	0.6	0.7

23 PL7,AS2,P,I,E
24 PL8,AS2,P,C,E
25 PL9,AS2,P,I,E
26 CPX1013,AS2,P,C,W
27 CPX1014,AS2,P,R,W
28 CPX1015,AS2,P,C,W
29 CPX1016,AS2,P,I,W
30 CPX1017,AS2,P,R,W
31 CPX1018,AS2,P,C,W
32 CPX1019,AS2,P,C,W
33 CPX1020,AS2,P,C,W

	34	35	36	37	38	39	40	41	42	43	44
SiO2	49.19	48.27	47.64	47.99	48.78	50.12	47.88	48.17	48.49	49.01	47.42
TiO2	2.27	1.33	1.32	1.22	1.05	1.19	2.32	1.24	2.07	1.17	2.42
Al2O3	4.29	8.29	8.28	8.13	7.81	4.58	4.86	8.76	4.86	7.32	5.92
Cr2O3	nd	0.23	0.35	0.24	0.34	0.17	0.03	0.23	0.26	0.48	0.23
FeO	7.80	6.04	6.37	6.18	6.14	6.31	7.93	6.57	8.02	6.13	8.26
MnO	0.19	0.12	0.15	0.15	0.17	0.20	0.16	0.13	0.22	0.12	nd
MgO	13.35	14.09	14.07	14.35	14.71	15.19	13.21	14.31	13.06	14.71	12.60
CaO	22.04	20.58	20.34	20.49	20.07	21.62	22.00	19.50	22.29	20.65	22.14
Na2O	0.54	0.56	0.56	0.58	0.54	0.42	0.51	0.35	0.25	0.37	0.21
total=	99.67	99.51	99.08	99.33	99.61	99.80	98.90	99.26	99.52	99.96	99.20
Mg#	79.5	84.2	85.5	87.0	84.9	86.9	82.2	79.8	77.8	83.6	76.0
Al ratio	0.1	0.6	0.5	0.5	0.6	0.3	0.1	0.8	0.2	0.6	0.2

34 CPX1021,AS2,P,R,W
35 CPX1022,AS2,P,C,W
36 CPX1023,AS2,P,C,W
37 CPX1024,AS2,P,C,W
38 CPX1025,AS2,P,C,W
39 CPX1026,AS2,P,I,W
40 CPX1027,AS2,P,R,W
41 CPX16,AS2,P,C,E
42 CPX17,AS2,P,R,E
43 CPX32,AS2,P,C,E
44 CPX51,AS2,P,R,E

	45	46	47	48	49	50	51	52	53	54	55
SiO2	50.19	0.10	0.14	0.08	0.08	0.06	0.08	0.11	nd	0.37	0.17
TiO2	2.05	0.77	0.97	1.29	1.00	1.66	0.77	0.81	0.90	0.70	1.32
Al2O3	3.56	56.72	56.08	54.41	55.34	52.93	56.04	55.81	56.09	60.95	53.21
Fe2O3	nd	9.21	8.38	10.11	9.99	9.31	9.89	9.92	9.39	3.30	7.52
Cr2O3	nd	1.56	1.57	1.55	1.48	2.54	1.52	1.50	1.55	2.08	3.88
FeO	7.65	14.68	15.59	16.63	15.86	18.72	14.86	14.91	14.99	15.57	18.38
MnO	0.27	0.19	0.20	0.22	0.21	0.25	0.16	0.17	0.22	0.16	0.18
MgO	13.59	17.73	17.01	16.43	16.89	15.06	17.51	17.47	17.33	17.86	15.11
CaO	22.14	nd	nd	nd	nd	nd	nd	nd	nd	nd	nd
Na2O	0.24	nd	nd	nd	nd	nd	nd	nd	nd	nd	nd
total=	99.69	100.96	99.94	100.72	100.85	100.53	100.83	100.70	100.47	100.99	99.77
Mg#	76.0	68.3	66.0	63.8	65.5	58.9	67.7	67.6	67.3	67.2	59.4
Al ratio	0.3	-	-	-	-	-	-	-	-	-	-

45 CPX54,AS2,GR,C,E
46 SP1001,AS2,P,C,W
47 SP1002,AS2,P,R,W
48 SP1003,AS2,P,C,W
49 SP1004,AS2,P,C,W
50 SP1005,AS2,P,C,W
51 SP1006,AS2,P,C,W
52 SP1007,AS2,P,C,W
53 SP11,AS2,P,C,E
54 SP25,AS2,P,C,E
55 SP26,AS2,P,C,E

	56	57	58	59	60	61	62	63	64	65	66
SiO2	0.15	0.14	0.34	0.08	0.13	0.11	39.11	40.01	40.12	39.86	39.38
TiO2	0.75	23.65	25.65	25.71	51.73	52.65	nd	nd	nd	nd	nd
Al2O3	57.30	2.01	1.47	1.81	0.13	0.13	nd	nd	nd	nd	nd
Fe2O3	6.13	15.11	14.16	14.49	3.60	2.86	nd	nd	nd	nd	nd
Cr2O3	2.67	2.77	0.22	0.25	0.07	0.08	nd	nd	nd	nd	nd
FeO	16.90	50.66	52.76	52.27	37.70	38.70	19.30	14.00	13.91	13.62	13.90
MnO	0.13	1.50	1.45	1.82	0.73	0.71	0.34	0.19	0.22	0.14	0.22
NiO	nd	nd	nd	nd	nd	nd	0.32	0.23	0.42	0.36	0.36
MgO	16.31	0.12	0.13	0.13	4.62	4.52	40.72	45.30	45.40	45.34	46.42
CaO	nd	nd	nd	nd	nd	nd	0.18	0.14	0.20	0.22	0.23
total=	100.34	95.96	96.18	96.56	98.71	99.76	99.97	99.87	100.27	99.54	100.51
Mg#	63.2	-	-	-	-	-	79.0	85.2	85.3	85.6	85.6

56 SP30,AS2,P,C,E
57 MT1000,AS2,GR,C,W
58 MT1009,AS2,GR,C,W
59 MT1010,AS2,GR,C,W
60 IL1008,AS2,GR,C,W
61 IL1008R,AS2,GR,C,W
62 OL0 1,MV403,P,R,+OL+CPX+SP,E
63 OL0YM,MV403,P,C,E
64 OL11,MV403,P,I,E
65 OL13,MV403,P,C,E
66 OL14,MV403,P,C,E

	67	68	69	70	71	72	73	74	75	76	77
SiO2	39.89	39.51	39.96	39.66	38.76	40.59	39.57	40.11	40.19	40.66	38.87
TiO2	nd	nd	nd	nd	nd	nd	nd	0.02	0.02	nd	0.05
Al2O3	nd	nd	nd	nd	nd	nd	nd	0.08	0.07	nd	0.06
Cr2O3	nd	nd	nd	nd	nd	nd	nd	0.08	0.06	nd	0.06
FeO	14.09	13.65	14.13	14.48	17.02	15.97	13.90	14.06	13.97	15.54	20.89
MnO	0.15	0.22	0.12	0.20	0.28	0.22	0.31	0.15	0.14	0.15	0.31
NiO	0.29	0.43	0.25	0.37	0.43	0.39	0.22	0.36	0.34	0.26	0.33
MgO	44.82	46.36	44.74	45.19	43.20	43.43	45.83	45.78	45.56	43.31	40.18
CaO	0.26	0.24	0.22	0.21	0.18	0.23	0.22	0.21	0.22	0.31	0.22
total=	99.50	100.41	99.42	100.11	99.87	100.83	100.05	100.85	100.57	100.23	100.97
Mg#	85.0	85.8	84.9	84.8	81.9	82.9	85.5	85.3	85.3	83.2	77.4

67 OL14QSUW,MV403,P,C,E
68 OL15,MV403,P,I,E
69 OL15QSUW,MV403,P,C,E
70 OL16,MV403,P,R,E
71 OL17,MV403,P,R,E
72 OL17QSUW,MV403,P,R,E
73 OL18,MV403,P,I,E
74 OL18,MV403,P,C,W
75 OL19,MV403,P,I,W
76 OL19QSUW,MV403,P,I,E
77 OL20,MV403,P,R,W

	78	79	80	81	82	83	84	85	86	87	88
SiO2	40.07	40.55	39.62	37.36	39.65	37.15	39.56	39.70	39.26	40.08	39.21
TiO2	0.02	nd	0.03	nd	0.02	nd	0.01	0.02	0.03	nd	nd
Al2O3	0.07	nd	0.05	nd	0.07	nd	0.05	0.08	0.05	nd	nd
Cr2O3	0.04	nd	0.08	nd	0.06	nd	0.04	0.08	0.08	nd	nd
FeO	14.26	15.00	16.79	29.01	13.96	29.61	15.76	15.75	18.45	13.43	19.87
MnO	0.14	0.26	0.20	0.46	0.16	0.50	0.16	0.18	0.25	0.15	0.35
NiO	0.31	0.19	0.30	0.22	0.36	0.22	0.37	0.21	0.25	0.50	0.15
MgO	45.84	43.83	43.86	33.03	45.58	31.77	44.13	44.77	42.24	46.24	41.18
CaO	0.22	0.28	0.20	0.27	0.18	0.32	0.18	0.23	0.22	0.27	0.14
total=	100.97	100.11	101.13	100.35	100.04	99.57	100.26	101.02	100.83	100.67	100.90
Mg#	85.1	83.9	82.3	67.0	85.3	65.7	83.3	83.5	80.3	86.0	78.7

78 OL21,MV403,P,C,W
79 OL21QSUW,MV403,P,C,E
80 OL22,MV403,P,R,W
81 OL22QSUW,MV403,GR,C,E
82 OL23,MV403,P,C,W
83 OL23QSUW,MV403,GR,C,E
84 OL24,MV403,P,R,W
85 OL25,MV403,P,C,W
86 OL26,MV403,P,R,W
87 OL36,MV403,P,C,E
88 OL37,MV403,P,C,E

	89	90	91	92	93	94	95	96	97	98	99
SiO2	39.68	39.54	39.61	51.97	51.08	45.96	51.14	48.52	48.73	51.55	45.21
TiO2	nd	nd	nd	0.17	0.11	3.36	0.84	1.82	1.59	0.93	2.33
Al2O3	nd	nd	nd	30.27	30.23	10.07	3.01	6.31	5.98	2.48	8.73
Cr2O3	nd	nd	nd	nd	nd	0.68	0.59	1.16	0.93	0.57	0.09
FeO	14.63	18.00	13.57	0.83	0.79	5.99	6.84	6.93	6.97	7.10	9.09
MnO	0.17	0.32	0.12	nd	nd	nd	nd	0.18	0.20	0.24	0.18
NiO	0.20	nd	0.39	nd	nd	nd	nd	nd	nd	nd	nd
MgO	45.85	42.55	45.58	nd	nd	14.04	16.09	14.18	14.08	15.61	12.12
CaO	0.26	0.17	0.24	13.45	14.03	19.37	20.62	21.62	21.47	21.05	20.16
Na2O	nd	nd	nd	4.52	3.29	nd	nd	nd	nd	nd	0.69
K2O	nd	nd	nd	0.26	0.18	nd	nd	nd	nd	nd	nd
total=	100.79	100.58	99.51	101.47	99.71	99.47	99.13	100.72	99.95	99.53	98.60
Mg#	84.8	80.8	85.7	-	-	80.7	80.8	79.5	78.4	79.7	80.2
An	-	-	-	61.3	69.5	-	-	-	-	-	-
Al ratio	-	-	-	-	-	0.5	0.3	0.3	0.4	0.3	0.3

89 OL38,MV403,P,C,E
90 OL39,MV403,P,C,E
91 OL9,MV403,P,C,E
92 PL6QSUWQ,MV403,GR,C,E
93 PL8QSUWQ,MV403,GR,C,E
94 CPX27QSUW,MV403,P,C,E
95 CPX28QSUW,MV403,GR,C,E
96 CPX29QSUW,MV403,GR,C,E
97 CPX30QSUW,MV403,P,C,E
98 CPX31QSUW,MV403,P,C,E
99 CPX333,MV403,P,C,W

	100	101	102	103	104	105	106	107	108	109	110
SiO2	46.48	50.55	50.92	51.21	49.92	49.97	50.14	49.17	52.10	47.18	0.18
TiO2	2.66	1.29	0.35	0.36	1.34	1.08	1.99	1.56	0.93	2.71	1.56
Al2O3	6.46	2.89	2.95	1.40	3.05	3.70	3.30	5.39	2.93	5.73	34.73
Fe2O3	nd	nd	nd	nd	nd	nd	nd	nd	nd	nd	6.68
Cr2O3	0.21	0.49	0.07	0.05	0.50	0.16	0.21	1.12	0.53	0.52	25.14
FeO	8.83	7.36	11.10	14.67	7.80	8.38	8.73	6.59	7.31	8.53	16.90
MnO	0.17	0.18	0.37	0.57	0.16	0.19	0.15	nd	0.20	0.22	0.32
NiO	nd	nd	nd	nd	nd	nd	nd	nd	nd	nd	0.22
MgO	12.86	14.86	12.57	11.05	14.97	15.54	13.89	14.62	16.31	13.21	14.10
CaO	21.02	21.41	20.35	19.60	21.16	19.56	21.32	21.42	19.99	20.88	0.02
Na2O	0.37	0.37	0.81	0.66	0.39	0.36	nd	nd	nd	nd	nd
total=	99.06	99.40	99.49	99.57	99.29	98.94	99.73	99.87	100.30	98.98	99.85
Mg#	78.6	82.1	72.3	60.0	83.9	81.9	73.9	79.8	79.9	73.9	59.8
Al ratio	0.2	0.1	0.5	0.5	-	0.2	0.2	0.3	0.5	0.2	-

100 CPX334,MV403,P,C,W
101 CPX335,MV403,P,R,W
102 CPX336,MV403,P,C,W
103 CPX337,MV403,P,C,W
104 CPX338,MV403,P,R,W
105 CPX339,MV403,P,I,W
106 CPX36QSUW,MV403,GR,C,E
107 CPX37QSUW,MV403,P,C,E
108 CPX38QSUW,MV403,P,C,E
109 CPX39QSUW,MV403,GR,C,E
110 SP10,MV403,P,C,W

	111	112	113	114	115	116	117	118	119	120	121
SiO2	0.37	0.31	nd	nd	0.21	0.27	0.43	0.25	0.12	nd	0.13
TiO2	0.94	0.60	1.51	1.63	0.77	1.26	2.30	0.89	1.01	1.11	1.40
Al2O3	39.38	41.41	35.61	38.53	36.29	39.89	21.61	46.89	45.25	46.38	48.94
Fe2O3	5.38	5.89	6.15	5.04	8.61	6.80	11.28	4.03	5.09	4.19	3.73
Cr2O3	23.86	20.36	26.10	24.28	23.22	20.37	32.43	17.29	17.71	18.03	13.47
FeO	15.56	17.46	17.00	16.92	18.25	19.71	22.87	13.67	13.52	13.75	15.38
MnO	0.19	0.30	0.37	0.20	0.23	0.26	0.46	0.22	0.18	0.23	0.20
NiO	nd	nd	nd	nd	nd	nd	nd	nd	0.36	nd	0.25
MgO	15.86	14.31	14.33	14.98	13.37	13.32	9.80	17.58	17.16	17.45	16.57
CaO	nd	nd	nd	nd	nd	nd	nd	nd	0.01	nd	nd
total=	101.54	100.64	101.07	101.58	100.95	101.88	101.18	100.82	100.41	101.14	100.07
Mg#	64.5	59.4	60.0	61.2	56.6	54.6	43.3	69.6	69.3	69.3	65.8

111 SP10QSUW,MV403,P,C,E
112 SP11QSUW,MV403,P,C,E
113 SP12QSUW,MV403,P,C,E
114 SP13QSUW,MV403,P,C,E
115 SP15QSUW,MV403,P,C,E
116 SP16QSUW,MV403,P,C,E
117 SP18QSUW,MV403,P,C,E
118 SP6SUWJW,MV403,P,C,E
119 SP7,MV403,P,C,W
120 SP7QSUWQ,MV403,P,C,E
121 SP8,MV403,P,C,W

	122	123	124	125	126	127	128	129	130	131	132
SiO2	0.24	0.09	0.43	0.31	50.24	51.55	56.80	nd	nd	36.57	37.34
TiO2	1.20	1.10	24.30	50.14	nd	nd	nd	nd	nd	6.98	5.42
Al2O3	44.25	52.65	1.89	nd	31.07	30.51	27.26	nd	nd	13.94	13.98
Fe2O3	2.19	4.59	18.35	6.98	nd	nd	nd	nd	nd	nd	nd
Cr2O3	21.31	10.12	0.38	0.12	nd	nd	nd	nd	nd	nd	nd
FeO	15.02	13.94	50.19	37.30	0.40	0.54	0.32	0.28	0.36	17.65	13.75
MnO	0.27	0.18	2.01	0.56	nd	nd	nd	0.04	0.04	0.13	0.07
NiO	nd	0.22	nd	nd	nd	nd	nd	nd	nd	nd	nd
MgO	16.65	17.85	1.19	4.26	nd	nd	nd	0.18	0.21	12.00	15.59
CaO	nd	nd	0.12	nd	14.13	12.11	9.07	53.82	53.37	nd	nd
Na2O	nd	nd	nd	nd	3.27	3.78	6.04	nd	nd	0.70	0.68
K2O	nd	nd	nd	nd	0.08	0.73	0.49	nd	nd	9.11	9.21
P2O5	nd	nd	nd	nd	nd	nd	nd	41.04	40.96	nd	nd
BaO	nd	nd	nd	nd	nd	nd	0.35	nd	nd	nd	nd
total=	101.13	100.74	98.86	99.67	99.19	99.22	100.33	95.36	94.94	97.08	96.04
F	-	-	-	-	-	-	-	2.98	2.52	0.45	0.57
Cl	-	-	-	-	-	-	-	0.24	0.23	-	-
Mg#	66.4	69.5	-	-	-	-	-	-	-	-	-
An	-	-	-	-	70.1	61.1	44.1	-	-	-	-

122 SP8QSUWQ,MV403,P,C,E
123 SP9,MV403,P,C,W
124 MT7QSUWQ,MV403,GR,C,E
125 IL4QSUWQ,MV403,GR,C,E
126 PL2,ES2058,GR,C,+OL+CPX+SP,E
127 PL3,ES2058,GR,C,E
128 PL4,ES2058,GR,C,E
129 AP2,ES2058,GR,C,W
130 AP3,ES2058,GR,C,W
131 BI1,ES2058,GR,C,W
132 BI3,ES2058,GR,C,W

	133	134	135	136	137	138	139	140	141	142	143
SiO2	36.34	40.36	39.26	39.87	39.88	39.53	37.02	38.50	39.42	39.06	49.97
TiO2	8.27	nd	nd	nd	nd	nd	nd	nd	nd	nd	0.11
Al2O3	14.11	nd	nd	nd	nd	nd	nd	nd	nd	nd	30.92
FeO	16.44	12.69	18.07	15.61	12.85	17.30	29.48	20.47	15.61	17.30	0.47
MnO	0.13	0.11	0.31	0.24	0.14	0.22	0.54	0.27	0.23	0.24	nd
NiO	nd	0.31	nd	0.23	0.31	0.21	0.11	0.15	0.27	0.24	nd
MgO	12.12	46.13	42.66	44.28	46.90	43.25	32.91	40.47	44.05	42.92	0.06
CaO	0.01	nd	0.26	0.28	0.09	0.25	0.38	0.33	0.35	0.27	14.32
Na2O	0.80	nd	nd	nd	nd	nd	nd	nd	nd	nd	3.32
K2O	8.96	nd	nd	nd	nd	nd	nd	nd	nd	nd	0.17
total=	97.18	99.60	100.56	100.51	100.17	100.76	100.44	100.19	99.93	100.03	99.34
F	0.42	-	-	-	-	-	-	-	-	-	-
Mg#	-	86.6	80.8	83.5	86.7	81.7	66.6	77.9	83.4	81.6	-
An	-	-	-	-	-	-	-	-	-	-	69.8

133 BI4,ES2058,GR,C,W
134 OL18,ES2058,P,C,E
135 OL20,ES2058,P,I,E
136 OL21,ES2058,P,C,E
137 OL440,ES2058,P,C,W
138 OL441,ES2058,P,I,W
139 OL442,ES2058,P,R,W
140 OL443,ES2058,P,C,W
141 OL444,ES2058,P,C,W
142 OL445,ES2058,P,C,W
143 PL1000,ES2058,GR,C,W

	144	145	146	147	148	149	150	151	152	153	154
SiO2	50.80	55.17	50.05	50.73	50.40	51.68	52.27	51.77	50.17	51.32	50.04
TiO2	0.09	0.11	0.11	0.10	0.09	0.11	0.12	0.13	0.19	0.18	1.15
Al2O3	30.99	27.94	31.17	30.82	30.57	30.61	29.91	30.09	31.21	30.56	4.45
Cr2O3	nd	nd	nd	nd	nd	nd	nd	nd	nd	nd	0.42
FeO	0.29	0.33	0.51	0.32	0.39	0.43	0.49	0.52	0.71	0.48	6.31
MnO	nd	nd	nd	nd	nd	nd	nd	nd	nd	nd	0.10
MgO	0.02	0.04	0.05	0.03	0.03	0.04	0.05	0.05	nd	nd	14.97
CaO	13.95	10.04	14.27	13.43	13.47	13.52	12.54	12.77	14.13	13.02	21.64
Na2O	3.40	5.47	3.32	3.65	3.69	3.68	4.32	4.13	3.53	4.02	0.41
K2O	0.13	0.28	0.14	0.19	0.13	0.13	0.15	0.21	nd	0.09	nd
total=	99.67	99.38	99.62	99.27	98.77	100.20	99.85	99.67	99.94	99.67	99.49
Mg#	-	-	-	-	-	-	-	-	-	-	85.7
An	68.9	49.5	69.8	66.3	66.3	66.5	61.1	62.3	68.9	63.8	-
Al ratio	-	-	-	-	-	-	-	-	-	-	0.3

144 PL1001,ES2058,GR,R,W
145 PL1002,ES2058,GR,C,W
146 PL1003,ES2058,GR,C,W
147 PL1004,ES2058,GR,C,W
148 PL1005,ES2058,GR,C,W
149 PL1007,ES2058,GR,C,W
150 PL1008,ES2058,GR,C,W
151 PL1009,ES2058,GR,C,W
152 PL5,ES2058,GR,C,E
153 PL6,ES2058,GR,C,E
154 CPX1001,ES2058,P,C,W

	155	156	157	158	159	160	161	162	163	164	165
SiO2	47.80	49.81	46.48	50.79	47.21	46.51	50.79	50.25	50.53	51.18	45.63
TiO2	1.72	1.53	3.39	0.82	2.23	2.91	0.95	1.02	1.12	0.89	3.54
Al2O3	6.98	4.68	6.57	4.35	6.99	6.36	4.90	4.93	4.30	4.39	6.99
Cr2O3	0.67	0.18	0.01	0.62	0.48	0.01	0.25	0.67	0.42	0.37	0.01
FeO	6.58	6.34	8.12	5.59	6.80	8.12	6.14	5.73	5.82	5.77	8.32
MnO	0.11	0.10	0.11	0.11	0.11	0.12	0.11	0.08	0.12	0.11	0.12
MgO	13.46	14.21	12.00	15.62	12.81	12.22	15.35	15.09	15.12	15.29	11.81
CaO	21.76	22.44	22.39	21.07	22.53	22.54	20.71	21.52	21.63	21.06	22.28
Na2O	0.47	0.41	0.63	0.50	0.49	0.57	0.53	0.48	0.38	0.50	0.59
total=	99.55	99.70	99.70	99.47	99.65	99.36	99.73	99.77	99.44	99.56	99.29
Mg#	84.1	83.9	79.5	86.9	83.9	81.9	84.2	86.4	84.7	83.6	79.9
Al ratio	0.4	0.3	0.1	0.5	0.3	0.1	0.6	0.4	0.4	0.7	0.1

155 CPX1002,ES2058,P,I,W
156 CPX1003,ES2058,P,I,W
157 CPX1004,ES2058,P,R,W
158 CPX1005,ES2058,P,C,W
159 CPX1006,ES2058,P,I,W
160 CPX1007,ES2058,P,R,W
161 CPX1008,ES2058,P,C,W
162 CPX1009,ES2058,P,C,W
163 CPX1010,ES2058,P,C,W
164 CPX1011,ES2058,P,C,W
165 CPX1012,ES2058,GR,C,W

	166	167	168	169	170	171	172	173	174	175	176
SiO2	46.90	50.35	47.08	47.74	0.19	0.23	0.16	0.31	0.37	0.16	0.33
TiO2	2.96	0.80	1.94	2.84	2.56	3.29	2.51	3.80	3.19	4.04	1.72
Al2O3	5.81	3.95	6.80	5.54	29.17	29.84	27.11	21.19	20.72	20.18	28.77
Fe2O3	nd	nd	nd	nd	11.45	7.92	13.61	17.10	18.01	18.32	7.35
Cr2O3	0.17	0.95	0.46	nd	23.26	23.61	24.05	21.83	22.48	21.25	29.98
FeO	8.30	5.21	6.93	8.00	23.76	25.66	23.72	30.14	30.01	30.66	22.15
MnO	0.24	0.11	0.18	0.14	0.26	nd	0.18	0.32	0.33	nd	nd
MgO	12.57	16.04	13.17	12.55	9.95	9.29	9.87	5.64	5.39	5.33	10.93
CaO	22.25	20.72	22.03	22.62	nd	nd	nd	nd	nd	nd	nd
Na2O	0.49	0.31	0.37	0.46	nd	nd	nd	nd	nd	nd	nd
total=	99.69	98.44	98.96	99.89	100.60	99.84	101.21	100.33	100.50	99.94	101.23
Mg#	80.8	87.1	84.1	78.8	42.7	39.2	42.6	25.0	24.2	23.7	46.8
Al ratio	0.1	0.4	0.3	0.1	-	-	-	-	-	-	-

166 CPX24,ES2058,P,R,E
167 CPX25,ES2058,P,C,E
168 CPX28,ES2058,P,I,E
169 CPX29,ES2058,P,R,E
170 SP10,ES2058,P,C,E
171 SP11,ES2058,P,C,E
172 SP12,ES2058,P,C,E
173 SP13,ES2058,P,C,E
174 SP14,ES2058,P,C,E
175 SP15,ES2058,P,C,E
176 SP9,ES2058,P,C,E

	177	178	179	180	181	182	183	184	185	186	187
SiO2	0.17	0.23	0.25	0.21	49.18	46.27	45.10	45.12	49.82	46.89	47.70
TiO2	20.28	16.80	52.06	53.05	1.39	2.33	3.39	2.88	1.27	1.68	1.77
Al2O3	3.07	7.97	0.28	nd	5.10	8.15	8.27	8.33	4.41	8.65	7.26
Fe2O3	26.51	22.34	3.41	2.06	nd	nd	nd	nd	nd	nd	nd
Cr2O3	nd	7.32	nd	nd	0.47	nd	0.03	0.02	0.45	0.11	0.05
FeO	47.10	39.50	40.91	40.79	5.60	7.02	7.02	7.16	5.54	6.76	7.58
MnO	0.74	0.32	0.90	0.84	0.09	0.14	0.12	0.11	0.11	0.12	0.16
MgO	1.75	5.65	2.97	3.54	14.67	12.46	11.71	11.78	14.96	13.02	11.82
CaO	nd	nd	nd	nd	22.28	22.21	23.32	23.21	22.26	21.33	22.48
Na2O	nd	nd	nd	nd	0.56	0.96	0.50	0.49	0.51	0.70	0.79
total=	99.62	100.13	100.78	100.49	99.34	99.54	99.46	99.10	99.33	99.26	99.61
Mg#	-	20.3	-	-	90.7	91.1	84.6	86.0	89.7	86.3	81.0
Al ratio	-	-	-	-	0.2	0.3	0.2	0.2	0.2	0.5	0.4

177 MT12,ES2058,GR,C,E
178 SPMT13,ES2058,P,C,E
179 IL3,ES2058,GR,C,E
180 IL4,ES2058,GR,C,E
181 CPX1028,MV93,P,I,+OL+CPX+SP,W
182 CPX1029,MV93,P,C,W
183 CPX1030,MV93,P,R,W
184 CPX1031,MV93,P,C,W
185 CPX1032,MV93,P,I,W
186 CPX1034,MV93,P,C,W
187 CPX1035,MV93,P,C,W

	188	189	190	191	192	193	194	195	196	197	198
SiO2	45.67	43.17	48.75	48.48	43.81	48.44	46.44	42.96	49.52	48.42	44.28
TiO2	2.78	3.96	1.05	1.63	3.88	1.62	2.62	4.00	1.06	1.39	3.95
Al2O3	7.37	10.50	7.42	6.08	9.48	6.16	6.36	9.66	7.03	8.71	9.14
Cr2O3	0.43	nd	0.24	0.37	0.04	0.13	nd	0.01	0.59	0.49	nd
FeO	6.45	8.11	6.12	5.87	7.12	6.11	7.24	7.16	5.32	6.30	7.64
MnO	0.10	0.16	0.12	0.11	0.12	0.09	0.13	0.13	nd	0.21	nd
MgO	12.64	9.93	14.48	14.08	11.25	13.57	12.41	10.94	14.38	13.65	11.64
CaO	23.28	22.90	20.85	22.21	23.24	22.67	23.15	23.30	21.76	21.31	23.14
Na2O	0.41	0.65	0.59	0.62	0.51	0.58	0.47	0.52	0.23	0.44	0.29
total=	99.13	99.38	99.62	99.45	99.45	99.37	98.82	98.68	99.89	100.92	100.08
Mg#	89.1	78.1	87.0	89.6	84.9	87.8	85.3	86.4	82.8	82.2	81.3
Al ratio	0.1	0.3	0.6	0.3	0.2	0.3	0.1	0.1	0.7	0.6	0.2

188 CPX1036,MV93,P,I,W
189 CPX1037,MV93,P,R,W
190 CPX1038,MV93,P,C,W
191 CPX1039,MV93,P,I,W
192 CPX1040,MV93,P,R,W
193 CPX1041,MV93,P,C,W
194 CPX1042,MV93,GR,C,W
195 CPX1043,MV93,GR,C,W
196 CPX3,MV93,P,C,E
197 CPX4,MV93,P,I,E
198 CPX5,MV93,P,R,E

	199	200	201	202	203	204	205	206	207	208	209
SiO2	47.16	45.06	48.02	0.30	0.19	0.25	0.11	0.23	0.28	0.33	nd
TiO2	2.22	3.64	1.30	1.09	1.92	2.36	1.71	1.91	11.20	2.72	1.91
Al2O3	8.56	8.15	8.49	38.41	30.80	30.06	33.49	30.74	15.69	33.36	35.55
Fe2O3	nd	nd	nd	6.06	9.86	11.31	9.13	9.72	16.67	9.99	8.98
Cr2O3	nd	nd	0.40	22.90	22.92	23.24	22.85	23.39	15.24	20.08	22.72
FeO	7.01	7.07	6.94	15.05	23.53	20.08	17.85	20.67	37.64	22.19	17.38
MnO	0.16	nd	nd	0.40	0.64	0.52	0.46	0.51	0.42	nd	0.17
MgO	12.48	12.15	13.26	15.62	9.37	12.06	13.20	11.16	4.77	11.77	14.43
CaO	21.50	23.44	21.82	nd	nd	nd	nd	nd	nd	nd	nd
Na2O	0.86	0.39	0.77	nd	nd	nd	nd	nd	nd	nd	nd
total=	99.95	99.90	101.00	99.83	99.23	99.88	98.80	98.33	101.91	100.44	101.14
Mg#	83.3	85.5	87.3	64.9	41.5	51.7	56.9	49.0	18.4	48.6	59.7
Al ratio	0.5	0.1	0.5	-	-	-	-	-	-	-	-

199 CPX6,MV93,P,C,E
200 CPX8,MV93,P,R,E
201 CPX9,MV93,P,C,E
202 SP1011,MV93,P,C,W
203 SP1012,MV93,P,C,W
204 SP1013,MV93,P,C,W
205 SP1014,MV93,P,C,W
206 SP1015,MV93,P,C,W
207 SP3,MV93,P,C,E
208 SP4,MV93,P,C,E
209 SP5,MV93,P,C,E

	210	211	212	213	214	215	216	217	218	219	220
SiO2	0.23	0.21	40.07	39.67	40.12	39.42	40.13	39.41	39.82	38.54	39.41
TiO2	1.53	22.77	nd	0.01	nd	0.02	0.01	0.02	0.01	0.03	0.01
Al2O3	38.74	8.72	nd	0.07	0.07	0.07	0.04	0.07	0.07	0.07	0.05
Fe2O3	6.83	11.13	nd	nd	nd	nd	nd	nd	nd	nd	nd
Cr2O3	21.20	2.34	nd	0.04	0.04	0.05	0.03	0.04	0.04	0.02	0.02
FeO	17.15	47.68	15.33	14.29	13.94	16.67	15.13	17.76	15.64	21.47	16.17
MnO	nd	0.54	0.40	0.18	0.18	0.23	0.19	0.26	0.19	0.36	0.20
NiO	nd	nd	0.28	0.31	0.33	0.25	0.27	0.18	0.27	0.18	0.19
MgO	14.89	2.99	43.88	45.50	45.66	43.33	44.72	42.68	44.59	39.91	44.18
CaO	nd	0.12	0.40	0.21	0.20	0.30	0.24	0.34	0.26	0.30	0.17
total=	100.57	96.50	100.36	100.28	100.54	100.34	100.76	100.76	100.89	100.88	100.40
Mg#	60.7	10.1	83.6	85.0	85.4	82.2	84.0	81.1	83.6	76.8	83.0

210 SP6,MV93,P,C,E
211 SPMT6,MV93,P?,C,E
212 OL1,MV521,P,I,+OL+CPX+SP,E
213 OL1,MV521,P,C,W
214 OL10,MV521,P,C,W
215 OL11,MV521,P,R,W
216 OL12,MV521,P,C,W
217 OL13,MV521,P,R,W
218 OL14,MV521,P,C,W
219 OL15,MV521,P,R,W
220 OL16,MV521,P,C,W

	221	222	223	224	225	226	227	228	229	230	231
SiO2	39.81	39.55	38.85	39.93	37.85	39.91	39.04	40.00	39.26	39.30	38.70
TiO2	0.02	nd	0.02	nd	nd	nd	nd	nd	nd	nd	nd
Al2O3	0.06	nd	0.07	nd	nd	nd	nd	0.07	nd	nd	nd
Cr2O3	0.05	nd	0.03	nd	nd	nd	nd	0.05	nd	nd	nd
FeO	15.36	16.09	19.85	13.70	23.43	15.25	18.84	13.96	16.84	15.16	21.76
MnO	0.19	0.25	0.30	0.23	0.46	0.26	0.33	0.17	nd	0.17	0.29
NiO	0.24	0.24	0.15	0.24	0.17	0.23	nd	0.32	0.18	0.41	nd
MgO	44.56	43.59	40.93	46.24	37.44	44.64	42.13	45.65	43.55	44.90	39.43
CaO	0.26	0.25	0.29	0.19	0.44	0.26	0.18	0.21	0.35	0.26	0.33
total=	100.55	99.97	100.49	100.53	99.79	100.55	100.52	100.43	100.18	100.20	100.51
Mg#	83.8	82.8	78.6	85.7	74.0	83.9	79.9	85.4	82.2	84.1	76.4

221 OL17,MV521,P,R,W
222 OL2,MV521,P,C,E
223 OL2,MV521,P,R,W
224 OL26,MV521,P,C,E
225 OL27,MV521,P,R,E
226 OL28,MV521,P,I,E
227 OL29,MV521,P,C,E
228 OL3,MV521,P,I,W
229 OL30,MV521,P,R,E
230 OL31,MV521,P,C,E
231 OL32,MV521,P,R,E

	232	233	234	235	236	237	238	239	240	241	242
SiO2	39.91	39.73	38.36	39.72	37.73	40.22	39.86	39.31	39.38	49.75	48.63
TiO2	nd	nd	nd	nd	nd	nd	nd	0.01	nd	0.16	0.12
Al2O3	nd	nd	nd	0.07	nd	0.08	0.07	0.07	0.06	30.80	31.65
Cr2O3	nd	nd	nd	0.04	nd	0.04	0.04	0.02	0.05	nd	nd
FeO	15.14	14.51	24.07	13.05	23.15	13.25	15.24	18.57	15.46	0.86	0.71
MnO	0.23	0.29	0.43	0.15	0.45	0.18	0.18	0.28	0.19	nd	nd
NiO	0.22	0.29	0.17	0.28	nd	0.31	0.34	0.21	0.27	nd	nd
MgO	44.75	44.87	37.49	45.92	38.20	46.17	44.67	42.14	44.32	nd	nd
CaO	0.24	0.22	0.42	0.23	0.41	0.27	0.18	0.30	0.18	14.47	14.90
Na2O	nd	nd	nd	nd	nd	nd	nd	nd	nd	3.80	3.05
K2O	nd	nd	nd	nd	nd	nd	nd	nd	nd	0.27	0.20
total=	100.49	99.91	100.94	99.46	99.94	100.52	100.58	100.91	99.91	100.11	99.26
Mg#	84.0	84.6	73.5	86.2	74.6	86.1	83.9	80.2	83.6	-	-
An	-	-	-	-	-	-	-	-	-	66.8	72.1

232 OL33,MV521,P,I,E
233 OL34,MV521,P,C,E
234 OL4,MV521,GR,C,E
235 OL4,MV521,P,C,W
236 OL5,MV521,GR,C,E
237 OL6,MV521,P,I,W
238 OL7,MV521,P,C,W
239 OL8,MV521,P,R,W
240 OL9,MV521,P,I,W
241 PL1,MV521,GR,C,E
242 PL2,MV521,GR,C,E

	243	244	245	246	247	248	249	250	251	252	253
SiO2	45.86	43.32	45.19	45.71	45.94	45.65	44.74	44.58	45.23	46.94	46.39
TiO2	2.20	4.14	3.57	2.70	2.52	3.35	3.81	3.34	3.02	2.02	2.26
Al2O3	8.19	8.79	7.57	7.85	7.75	7.61	8.04	9.28	8.67	7.06	7.51
Cr2O3	1.08	nd	0.11	0.30	0.18	nd	nd	0.07	0.18	0.59	0.61
FeO	6.28	8.47	8.07	6.65	6.80	7.86	8.15	7.43	7.15	6.19	6.31
MnO	nd	0.12	0.16	0.08	0.09	0.11	0.14	0.07	0.08	0.09	0.08
NiO	0.16	nd	nd	0.02	0.01	0.01	0.01	0.02	0.01	0.02	nd
MgO	13.14	10.65	11.47	12.47	12.47	11.73	11.15	11.60	12.05	13.04	12.80
CaO	22.34	22.51	23.01	22.65	22.63	22.62	22.76	22.45	22.24	22.73	22.77
Na2O	nd	0.51	0.51	0.45	0.44	0.49	0.58	0.53	0.49	0.48	0.48
total=	99.25	98.51	99.66	98.88	98.83	99.43	99.38	99.37	99.12	99.16	99.21
Mg#	83.5	78.4	81.0	85.9	85.3	79.7	79.7	82.7	82.8	87.7	87.7
Al ratio	0.3	0.1	0.1	0.2	0.2	0.2	0.1	0.2	0.3	0.2	0.2

243 CPX1,MV521,P,I,E
244 CPX1,MV521,P,R,W
245 CPX10,MV521,GR,C,E
246 CPX10,MV521,P,I,W
247 CPX11,MV521,P,R,W
248 CPX12,MV521,P,R,W
249 CPX13,MV521,P,R,W
250 CPX14,MV521,P,R,W
251 CPX15,MV521,P,I,W
252 CPX16,MV521,P,I,W
253 CPX17,MV521,P,C,W

	254	255	256	257	258	259	260	261	262	263	264
SiO2	49.35	48.58	44.74	46.80	44.46	44.37	43.74	45.77	47.48	45.47	50.13
TiO2	1.37	1.53	3.55	2.35	3.23	3.55	4.24	2.90	1.64	2.97	1.19
Al2O3	5.73	6.15	9.07	7.72	8.87	9.42	8.86	8.00	7.32	8.17	4.92
Cr2O3	0.47	0.70	0.11	0.85	0.26	0.12	0.03	0.31	1.00	0.31	0.79
FeO	5.22	5.70	7.60	5.88	7.08	7.23	8.05	6.88	5.55	6.83	5.13
MnO	0.07	0.08	nd	0.08	0.09	0.09	0.12	nd	nd	nd	0.16
NiO	0.02	0.01	nd	0.03	0.03	nd	0.02	0.03	nd	nd	nd
MgO	14.49	13.93	11.59	13.12	11.88	11.64	11.02	12.31	13.90	12.22	14.95
CaO	22.11	21.92	22.32	22.37	22.84	22.77	22.66	22.42	22.07	23.04	22.08
Na2O	0.53	0.54	0.46	0.54	0.46	0.52	0.55	0.45	0.83	0.43	0.64
total=	99.36	99.14	99.44	99.74	99.20	99.71	99.29	99.07	99.79	99.44	99.99
Mg#	87.9	86.2	79.6	87.3	86.2	84.4	80.5	82.8	94.8	85.3	90.0
Al ratio	0.4	0.4	0.2	0.3	0.2	0.2	0.1	0.2	0.3	0.2	0.3

254 CPX18,MV521,P,C,W
255 CPX19,MV521,P,C,W
256 CPX2,MV521,P,R,W
257 CPX20,MV521,P,I,W
258 CPX21,MV521,P,I,W
259 CPX22,MV521,P,R,W
260 CPX23,MV521,P,R,W
261 CPX3,MV521,P,I,W
262 CPX4,MV521,P,I,E
263 CPX4,MV521,P,I,W
264 CPX5,MV521,P,C,E

	265	266	267	268	269	270	271	272	273	274	275
SiO2	46.18	47.53	48.12	47.20	0.12	0.34	0.16	0.28	0.30	0.21	0.20
TiO2	2.51	1.86	2.12	2.11	1.96	1.82	1.28	1.26	1.40	1.97	1.20
Al2O3	7.62	5.96	6.36	6.33	33.43	40.53	38.59	34.34	37.70	33.09	38.80
Fe2O3	nd	nd	nd	nd	11.15	4.36	6.51	8.78	8.08	10.84	8.66
Cr2O3	0.28	0.28	0.21	0.17	22.15	20.60	21.06	23.41	21.30	22.56	20.90
FeO	6.64	6.50	6.57	6.59	17.13	16.98	16.39	17.09	16.23	17.26	15.41
MnO	0.07	0.09	0.08	0.08	0.30	0.20	0.20	nd	nd	0.30	nd
NiO	0.01	nd	nd	0.02	0.26	nd	nd	nd	nd	0.22	nd
MgO	12.80	13.36	13.88	13.21	14.11	15.24	14.68	14.06	15.30	14.09	15.90
CaO	23.03	22.78	21.82	22.92	0.02	nd	nd	nd	nd	0.01	nd
Na2O	0.47	0.41	0.39	0.41	nd	nd	nd	nd	nd	nd	nd
total=	99.61	98.77	99.55	99.04	100.63	100.07	98.87	99.22	100.31	100.55	101.07
Mg#	88.7	87.1	83.6	87.3	59.5	61.5	61.5	59.5	62.7	59.3	64.8
Al ratio	0.2	0.2	0.3	0.2	-	-	-	-	-	-	-

265 CPX5,MV521,P,I,W
266 CPX6,MV521,P,C,W
267 CPX7,MV521,P,C,W
268 CPX8,MV521,P,I,W
269 SP1,MV521,P,C,W
270 SP11,MV521,P,C,E
271 SP12,MV521,P,C,E
272 SP14,MV521,P,C,E
273 SP2,MV521,P,C,E
274 SP2,MV521,P,C,W
275 SP3,MV521,P,C,E

	276	277	278	279	280	281	282	283	284	285	286
SiO2	0.12	0.23	0.40	0.24	0.24	0.13	0.21	0.27	0.33	0.26	nd
TiO2	2.02	2.27	1.20	2.49	2.40	1.43	2.35	2.35	1.63	4.58	2.07
Al2O3	31.34	33.06	39.40	29.27	29.94	40.13	28.54	29.65	32.23	24.62	31.14
Fe2O3	12.91	11.63	7.49	11.94	11.86	6.87	13.00	13.02	9.65	16.78	11.88
Cr2O3	22.01	19.62	20.40	21.79	21.95	20.06	21.67	21.49	22.61	18.94	22.57
FeO	17.66	19.84	16.26	20.50	21.76	14.77	21.66	20.90	18.77	23.73	19.02
MnO	0.33	nd	nd	0.40	nd	0.22	nd	0.17	nd	0.30	nd
NiO	0.19	nd	nd	nd	nd	0.24	nd	nd	nd	nd	nd
MgO	13.48	12.68	15.50	11.47	11.19	15.98	10.81	11.62	12.73	10.48	12.71
CaO	0.01	nd	nd	nd	nd	0.02	nd	nd	nd	nd	nd
total=	100.07	99.33	100.65	98.10	99.34	99.85	98.24	99.47	97.95	99.69	99.39
Mg#	57.6	53.3	62.9	49.9	47.8	65.9	47.1	49.8	54.7	44.0	54.4

276 SP3,MV521,P,C,W
277 SP4,MV521,P,C,E
278 SP4,MV521,P,C,E
279 SP5,MV521,P,C,E
280 SP6,MV521,P,C,E
281 SP6,MV521,P,C,W
282 SP7,MV521,P,C,E
283 SP7,MV521,P,C,E
284 SP8,MV521,P,C,E
285 SP8,MV521,P,C,E
286 SP9,MV521,P,C,E

	287	288	289	290	291	292	293	294	295	296	297
SiO2	0.33	0.24	0.20	0.39	0.63	37.61	35.80	37.29	36.26	36.91	37.87
TiO2	1.88	7.88	19.73	24.70	25.30	nd	nd	nd	nd	nd	nd
Al2O3	31.22	17.99	6.73	4.95	4.52	nd	nd	nd	nd	nd	nd
Fe2O3	11.52	29.45	25.01	12.49	11.09	nd	nd	nd	nd	nd	nd
Cr2O3	22.46	4.52	nd	nd	0.12	nd	nd	nd	nd	nd	nd
FeO	17.66	32.31	40.71	52.08	51.94	28.01	35.56	28.09	32.96	31.99	25.39
MnO	0.14	0.52	0.50	1.13	1.41	0.39	0.64	0.50	0.55	0.54	0.43
NiO	nd	nd	nd	nd	nd	0.15	nd	0.18	0.18	0.19	0.14
MgO	13.56	5.31	5.68	0.52	0.90	34.29	28.12	34.24	30.20	31.14	36.19
CaO	nd	0.40	0.48	0.24	0.21	0.44	0.43	0.44	0.41	0.42	0.44
total=	98.77	98.62	99.04	96.50	96.12	100.89	100.55	100.74	100.56	101.19	100.46
Mg#	57.8	22.7	-	-	-	68.6	58.5	68.5	62.0	63.4	71.8

287 SP9,MV521,P,C,E
288 SPUN10,MV521,P,C,E
289 MT1,MV521,GR?,C,E
290 MT3,MV521,GR,C,E
291 MT4,MV521,GR,C,E
292 OL13,MV723,P,I,+OL+SP,E
293 OL14,MV723,P,R,E
294 OL15,MV723,P,C,E
295 OL16,MV723,GR,C,E
296 OL17,MV723,GR,C,E
297 OL307,MV723,P,C,W

	298	299	300	301	302	303	304	305	306	307	308
SiO2	38.26	36.87	37.55	36.70	37.52	52.33	51.64	51.20	50.09	52.18	0.22
TiO2	nd	nd	nd	nd	nd	nd	0.11	1.18	2.20	0.95	2.36
Al2O3	nd	nd	nd	nd	nd	30.01	29.76	3.45	3.87	2.70	17.62
Fe2O3	nd	nd	nd	nd	nd	nd	nd	nd	nd	nd	22.57
Cr2O3	nd	nd	nd	nd	nd	nd	nd	0.20	nd	0.54	22.84
FeO	24.23	27.56	28.86	34.05	28.08	0.57	0.49	6.71	8.45	6.37	29.24
MnO	0.38	0.46	0.51	0.65	0.44	nd	nd	0.19	nd	nd	0.34
NiO	0.16	0.16	0.13	0.11	0.12	nd	nd	nd	nd	nd	nd
MgO	37.11	34.46	33.38	29.19	34.31	nd	nd	14.85	13.29	15.50	4.80
CaO	0.33	0.41	0.44	0.40	0.38	12.86	12.99	22.51	22.41	22.07	nd
Na2O	nd	nd	nd	nd	nd	4.14	4.04	0.21	0.34	nd	nd
K2O	nd	nd	nd	nd	nd	0.26	0.21	nd	nd	nd	nd
total=	100.47	99.92	100.87	101.10	100.85	100.17	99.24	100.50	100.65	100.31	99.99
Mg#	73.2	69.0	67.3	60.4	68.5	-	-	82.0	75.0	81.3	22.6
An	-	-	-	-	-	62.2	63.2	-	-	-	-
Al ratio	-	-	-	-	-	-	-	0.3	0.2	0.4	-

298 OL308,MV723,P,C,W
299 OL309,MV723,P,C,W
300 OL310,MV723,P,I,W
301 OL311,MV723,P,R,W
302 OL313,MV723,P,C,W
303 PL2,MV723,GR,C,E
304 PL3,MV723,GR,C,E
305 CPX19,MV723,GR,C,E
306 CPX20,MV723,GR,R,E
307 CPX21,MV723,GR,C,E
308 SP1,MV723,P,C,E

	309	310	311	312	313	314	315	316	317	318	319
SiO2	0.16	0.16	0.30	0.18	0.34	0.42	0.07	0.31	0.37	0.05	0.03
TiO2	1.03	1.89	2.11	1.11	6.71	23.17	26.34	26.43	26.68	53.98	53.68
Al2O3	26.56	23.23	19.90	23.14	12.15	1.09	1.92	2.50	2.26	nd	0.11
Fe2O3	14.82	14.70	22.14	16.11	21.39	22.21	16.64	15.92	15.59	0.79	1.36
Cr2O3	25.13	26.80	20.84	25.55	20.95	nd	0.12	0.21	0.31	0.04	nd
FeO	26.06	27.47	27.93	26.28	33.75	51.41	51.42	51.32	51.82	41.56	41.97
MnO	0.32	0.25	0.32	0.23	0.32	0.86	0.59	0.50	0.89	0.65	0.70
MgO	7.36	6.57	5.66	6.48	3.87	0.65	2.48	3.07	2.66	3.58	3.16
CaO	nd	nd	nd	nd	nd	nd	nd	nd	0.12	nd	nd
total=	101.44	101.07	99.20	99.08	99.48	99.81	99.58	100.26	100.70	100.65	101.01
Mg#	33.5	29.9	26.5	30.5	17.0	-	-	-	-	-	-

309 SP2,MV723,P,C,E
310 SP4,MV723,P,C,E
311 SP6,MV723,P,C,E
312 SP7,MV723,P,C,E
313 SP8,MV723,P,C,E
314 MT10,MV723,GR,C,E
315 MT300,MV723,GR,C,W
316 MT8,MV723,GR,C,E
317 MT9,MV723,GR,C,E
318 IL300,MV723,GR,C,W
319 IL301,MV723,GR,C,W

	320	321	322	323	324	325	326	327	328	329	330
SiO2	39.13	39.08	38.56	38.70	38.55	39.29	39.30	38.40	38.16	39.14	39.61
TiO2	nd	nd	nd	0.18	nd	nd	nd	nd	nd	nd	nd
FeO	21.09	19.41	21.31	22.06	21.88	15.81	16.40	21.38	21.88	15.75	14.89
MnO	0.37	0.27	0.22	0.43	0.31	0.22	0.26	0.27	0.42	0.23	0.20
NiO	0.29	0.26	0.21	nd	0.24	0.28	0.24	0.24	nd	0.27	0.21
MgO	39.86	41.18	39.02	39.06	38.47	43.84	43.40	39.90	38.76	43.47	44.74
CaO	0.09	0.32	0.40	0.53	0.40	0.24	0.22	0.09	0.46	0.24	0.25
total=	100.83	100.52	99.72	100.96	99.85	99.68	99.82	100.28	99.68	99.10	99.90
Mg#	77.1	79.1	76.5	75.9	75.8	83.2	82.5	76.9	75.9	83.1	84.3

320 OL1,MV109,P,C,+OL+CPX+SP+MT,E
321 OL10,MV109,P,I,E
322 OL11,MV109,P,R,E
323 OL12,MV109,GR,C,E
324 OL3,MV109,P,R,E,G,E
325 OL4,MV109,P,C,E
326 OL428,MV109,P,C,W
327 OL429,MV109,P,C,W
328 OL430,MV109,P,R,W
329 OL431,MV109,P,C,W
330 OL432,MV109,P,C,W

	331	332	333	334	335	336	337	338	339	340	341
SiO2	39.15	39.38	39.45	38.04	37.89	49.16	47.62	43.29	45.95	49.33	48.65
TiO2	nd	nd	nd	nd	nd	0.16	2.38	3.87	2.70	2.07	2.40
Al2O3	nd	nd	nd	nd	nd	31.65	5.46	10.44	8.42	4.53	4.73
Cr2O3	nd	nd	nd	nd	nd	nd	0.30	0.31	0.92	0.01	0.01
FeO	17.62	19.45	16.30	26.15	27.16	0.75	7.01	7.59	6.39	7.51	7.56
MnO	0.20	0.32	0.31	0.26	0.45	nd	0.15	nd	nd	0.16	0.13
NiO	0.21	nd	0.40	nd	0.22	nd	nd	nd	nd	nd	nd
MgO	42.61	41.20	43.60	36.35	35.25	nd	13.88	11.42	12.59	13.37	13.32
CaO	nd	0.27	0.16	0.25	0.14	14.93	22.60	22.51	22.57	22.47	22.30
Na2O	nd	nd	nd	nd	nd	2.88	nd	0.35	nd	0.44	0.46
K2O	nd	nd	nd	nd	nd	0.17	nd	nd	nd	nd	nd
total=	99.79	100.62	100.22	101.05	101.11	99.70	99.40	99.78	99.54	99.89	99.56
Mg#	81.2	79.1	82.7	71.2	69.8	-	82.5	82.1	78.8	79.8	80.5
An	-	-	-	-	-	73.4	-	-	-	-	-
Al ratio	-	-	-	-	-	-	0.1	0.2	0.3	0.2	0.1

331 OL433,MV109,P,C,W
332 OL5,MV109,P,I,E
333 OL6,MV109,P,C,E
334 OL7,MV109,P,I,E
335 OL8,MV109,P,C,E
336 PL1,MV109,GR,C,E
337 CPX1,MV109,P,C,E
338 CPX2,MV109,P,C,E
339 CPX3,MV109,P,C,E
340 CPX387,MV109,P,C,W
341 CPX388,MV109,P,C,W

	342	343	344	345	346	347	348	349	350	351	352
SiO2	49.01	45.05	45.80	47.13	44.24	44.01	0.24	nd	nd	0.22	0.35
TiO2	2.00	3.55	3.24	2.52	4.14	3.93	1.01	2.00	0.43	2.03	17.21
Al2O3	4.78	8.47	7.78	5.94	8.93	9.31	50.15	43.54	54.05	21.78	7.03
Fe2O3	nd	nd	nd	nd	nd	nd	10.21	16.62	7.27	15.31	28.20
Cr2O3	0.40	0.47	0.38	0.22	0.20	0.58	6.38	4.67	7.81	28.91	3.06
FeO	6.33	6.78	6.88	7.29	8.19	7.23	18.25	22.23	14.00	22.35	38.41
MnO	0.12	0.11	0.13	0.26	nd	0.20	nd	0.27	0.15	0.35	0.52
MgO	14.00	11.88	12.51	13.43	11.36	11.74	15.20	12.04	17.77	9.75	6.70
CaO	22.50	22.60	22.90	22.50	22.30	22.69	nd	nd	nd	nd	nd
Na2O	0.45	0.44	0.49	nd	0.24	0.42	nd	nd	nd	nd	nd
total=	99.59	99.35	100.11	99.29	99.60	100.11	101.44	101.37	101.48	100.70	101.48
Mg#	85.0	81.6	86.0	81.1	75.2	83.9	59.7	49.1	69.3	43.7	-
Al ratio	0.2	0.2	0.1	0.1	0.2	0.1	-	-	-	-	-

342 CPX389,MV109,P,C,W
343 CPX390,MV109,P,C,W
344 CPX391,MV109,P,C,W
345 CPX4,MV109,P,C,E
346 CPX6,MV109,GR,C,E
347 CPX7,MV109,GR,C,E
348 SP1,MV109,P,C,E
349 SP2,MV109,P,C,E
350 SP3,MV109,P,C,E
351 SP4,MV109,P,C,E
352 MTSP1,MV109,P,C,E

	353	354	355	356	357	358	359	360	361	362	363
SiO2	0.33	38.10	40.58	39.09	39.80	40.28	40.60	40.24	39.20	40.32	39.97
TiO2	16.51	nd	nd	nd	nd	nd	nd	nd	nd	nd	nd
Al2O3	7.22	nd	nd	nd	nd	nd	nd	nd	nd	nd	nd
Fe2O3	28.80	nd	nd	nd	nd	nd	nd	nd	nd	nd	nd
Cr2O3	3.90	nd	nd	nd	nd	nd	nd	nd	nd	nd	nd
FeO	37.32	24.32	13.18	19.23	18.30	15.01	15.04	16.22	20.53	14.41	17.25
MnO	0.41	0.39	0.25	0.30	0.25	0.17	0.25	0.27	0.27	0.13	0.35
NiO	nd	0.17	0.31	0.26	0.22	0.23	0.24	nd	0.14	0.29	0.23
MgO	7.09	36.49	45.06	40.86	40.94	43.33	43.65	42.99	38.46	43.72	42.24
CaO	nd	0.22	0.20	0.40	0.23	0.24	0.27	0.35	0.45	0.27	0.27
total=	101.58	99.69	99.58	100.14	99.74	99.26	100.05	100.07	99.05	99.14	100.31
Mg#	-	72.8	85.9	79.1	79.9	83.7	83.8	82.5	77.0	84.4	81.4

353 MTSP3,MV109,P,C,E
354 OL19,MV106,GR,C,+OL+CPX+SP,E
355 OL33,MV106,P,C,E
356 OL34,MV106,P,R,E
357 OL37,MV106,P,C,E
358 OL38,MV106,P,C,E
359 OL39,MV106,P,C,E
360 OL40,MV106,P,C,E
361 OL41,MV106,P,R,E
362 OL43,MV106,P,C,E
363 OL44,MV106,P,C,E

	364	365	366	367	368	369	370	371	372	373	374
SiO2	40.58	39.94	39.90	40.10	40.07	39.95	39.87	39.80	39.84	39.65	50.83
Al2O3	nd	nd	nd	nd	nd	nd	nd	nd	nd	nd	30.78
FeO	14.38	15.27	16.10	13.52	14.80	14.35	15.43	14.37	14.12	14.26	0.60
MnO	0.38	0.21	0.38	0.22	0.19	0.20	0.24	0.25	0.24	0.22	nd
NiO	0.20	0.25	0.26	0.24	0.25	0.22	0.16	0.20	0.23	0.23	nd
MgO	43.29	43.16	42.25	45.58	44.82	45.00	44.23	44.84	44.72	44.81	nd
CaO	0.30	0.22	0.41	0.28	nd	0.12	0.31	0.27	0.29	0.30	13.96
Na2O	nd	nd	nd	nd	nd	nd	nd	nd	nd	nd	3.20
K2O	nd	nd	nd	nd	nd	nd	nd	nd	nd	nd	0.29
total=	99.13	99.05	99.30	99.94	100.13	99.84	100.24	99.73	99.44	99.47	99.66
Mg#	84.3	83.4	82.4	85.7	84.4	84.8	83.6	84.8	84.9	84.8	-
An	-	-	-	-	-	-	-	-	-	-	69.5

364 OL45,MV106,P,C,E
365 OL46,MV106,P,C,E
366 OL47,MV106,P,C,E
367 OL300,MV106,P,C,W
368 OL301,MV106,P,C,W
369 OL302,MV106,P,I,W
370 OL303,MV106,P,R,W
371 OL304,MV106,P,C,W
372 OL305,MV106,P,C,W
373 OL306,MV106,P,C,W
374 PL19,MV106,GR,C,E

	375	376	377	378	379	380	381	382	383	384	385
SiO2	51.12	50.71	45.20	48.19	48.83	48.00	43.37	49.77	50.54	47.03	50.69
TiO2	nd	0.18	4.09	2.63	2.17	2.89	5.01	1.51	1.55	2.12	1.25
Al2O3	30.59	30.47	7.47	5.50	4.55	4.24	8.08	4.97	4.65	7.31	4.72
Cr2O3	nd	nd	nd	nd	0.19	nd	nd	0.48	0.48	1.07	0.71
FeO	0.70	0.62	8.30	7.95	6.97	8.71	9.80	6.07	6.09	5.73	5.23
MnO	nd	nd	0.21	0.19	0.26	0.19	0.17	0.22	nd	nd	0.13
MgO	nd	nd	11.38	12.75	13.43	12.35	9.88	15.27	15.46	13.23	15.41
CaO	13.67	14.18	22.37	22.33	22.36	22.18	21.95	21.71	21.53	22.80	22.34
Na2O	3.64	2.82	nd	nd	nd	nd	nd	nd	nd	nd	nd
K2O	0.33	0.41	nd	nd	nd	nd	nd	nd	nd	nd	nd
total=	100.05	99.39	99.02	99.54	98.76	98.56	98.26	100.00	100.30	99.29	100.48
Mg#	-	-	71.0	74.1	77.4	71.6	64.2	82.9	81.9	81.5	84.0
An	66.2	71.7	-	-	-	-	-	-	-	-	-
Al ratio	-	-	0.2	0.3	0.3	0.1	0.1	0.3	0.4	0.3	0.4

375 PL20,MV106,GR,C,E
376 PL23,MV106,GR,C,E
377 CPX21,MV106,GR,C,E
378 CPX25,MV106,GR,C,E
379 CPX26,MV106,GR,C,E
380 CPX29,MV106,GR,C,E
381 CPX31,MV106,GR,C,E
382 CPX39,MV106,P,C,E
383 CPX40,MV106,P,C,E
384 CPX41,MV106,P,C,E
385 CPX42,MV106,P,C,E

	386	387	388	389	390	391	392	393	394	395	396
SiO2	50.73	47.64	47.21	48.55	47.49	41.80	46.63	0.35	0.30	0.33	0.41
TiO2	1.09	2.18	2.98	1.87	2.34	4.77	2.18	3.42	2.84	1.20	1.58
Al2O3	4.73	5.45	5.43	5.26	5.55	10.30	7.90	33.05	32.97	38.72	38.56
Fe2O3	nd	nd	nd	nd	nd	nd	nd	10.24	13.16	9.55	9.22
Cr2O3	0.54	0.04	0.01	0.22	0.02	nd	0.28	20.42	18.86	18.82	17.53
FeO	5.45	7.19	7.86	6.28	7.45	8.54	6.99	18.60	18.25	16.51	19.83
MnO	nd	0.12	0.15	0.08	nd	0.13	nd	nd	nd	0.23	nd
MgO	15.43	13.56	12.64	14.28	13.38	10.68	13.25	14.55	14.39	14.97	13.24
CaO	22.33	22.28	22.18	22.54	21.97	22.08	21.38	nd	nd	nd	nd
Na2O	nd	0.39	0.48	0.37	0.43	0.55	0.58	nd	nd	nd	nd
total=	100.30	98.85	98.94	99.45	98.63	98.85	99.19	100.63	100.77	100.33	100.37
Mg#	83.5	84.9	79.5	87.6	82.9	81.7	85.4	58.2	58.4	61.8	54.3
Al ratio	0.5	0.1	0.1	0.2	0.2	0.1	0.3	-	-	-	-

386 CPX43,MV106,P,C,E
387 CPX300,MV106,P,C,W
388 CPX301,MV106,P,R,W
389 CPX302,MV106,P,C,W
390 CPX303,MV106,P,C,W
391 CPX304,MV106,P,C,W
392 CPX305,MV106,P,C,W
393 SP11,MV106,P,C,E
394 SP12,MV106,P,C,E
395 SP13,MV106,P,C,E
396 SP14,MV106,P,C,E

	397	398	399	400	401	402	403	404	405	406	407
SiO2	0.31	0.05	0.09	0.04	nd	0.05	0.07	0.08	0.99	40.25	39.87
TiO2	1.60	28.02	27.76	27.40	27.60	27.88	27.42	27.90	49.74	0.02	0.02
Al2O3	38.80	4.43	3.92	4.24	3.75	3.94	3.65	3.51	0.44	0.07	0.07
Fe2O3	9.38	10.13	10.17	11.70	11.43	11.25	11.67	11.26	1.62	nd	nd
Cr2O3	18.32	0.03	0.02	0.05	0.03	0.03	0.03	0.03	0.02	0.07	0.08
FeO	16.47	50.70	52.82	50.26	51.95	51.42	51.21	52.23	41.69	15.19	16.14
MnO	nd	0.56	0.93	0.61	0.95	0.66	0.68	0.76	0.89	0.20	0.19
NiO	nd	nd	nd	nd	nd	nd	nd	nd	nd	0.30	0.27
MgO	15.36	3.89	2.09	3.80	2.54	3.38	3.04	2.76	1.86	44.54	43.75
CaO	nd	nd	nd	nd	nd	nd	nd	nd	nd	0.18	0.24
total=	100.24	97.81	97.80	98.10	98.25	98.61	97.77	98.53	97.25	100.82	100.63
Mg#	62.4	-	-	-	-	-	-	-	-	83.9	82.8

397 SP17,MV106,P,C,E
398 MT221,MV106,GR,C,W
399 MT222,MV106,GR,C,W
400 MT225,MV106,GR,C,W
401 MT226,MV106,GR,R,W
402 MT228,MV106,GR,C,W
403 MT302,MV106,GR,C,W
404 MT306,MV106,GR,C,W
405 IL302,MV106,GR,C,W,
406 OL13,MV164,P,C,+OL+SP,W
407 OL14,MV164,P,I,W

	408	409	410	411	412	413	414	415	416	417	418
SiO2	38.33	33.59	39.41	39.40	39.51	37.67	39.52	39.58	37.90	39.79	38.04
TiO2	0.04	nd	0.02	0.13	0.05	nd	0.01	nd	0.06	nd	nd
Al2O3	0.05	nd	0.04	nd	0.05	nd	0.03	nd	0.05	nd	nd
Cr2O3	0.05	nd	0.09	nd	0.07	nd	0.05	nd	0.05	nd	nd
FeO	24.56	49.63	17.22	19.13	17.98	30.26	17.46	15.94	27.44	14.89	27.82
MnO	0.34	1.05	0.24	0.29	0.23	0.50	0.23	0.19	0.40	0.23	0.39
NiO	0.16	nd	0.24	0.19	0.22	nd	0.27	0.17	0.13	0.30	0.18
MgO	37.41	15.63	43.25	41.31	42.57	32.96	42.84	44.76	35.24	44.58	34.80
CaO	0.31	0.86	0.29	0.24	0.28	0.35	0.19	0.27	0.34	0.26	0.36
total=	101.25	100.76	100.80	100.69	100.96	101.74	100.60	100.91	101.61	100.05	101.59
Mg#	73.1	36.0	81.7	79.4	80.8	66.0	81.4	83.3	69.6	84.2	69.0

408 OL15,MV164,P,R,W
409 OL16,MV164,P,R,E
410 OL16,MV164,P,I,W
411 OL17,MV164,P,C,E
412 OL17,MV164,P,I,W
413 OL18,MV164,P,R,E
414 OL18,MV164,P,C,W
415 OL19,MV164,P,C,E
416 OL19,MV164,P,R,W
417 OL21,MV164,P,C,E
418 OL22,MV164,P,R,E

	419	420	421	422	423	424	425	426	427	428	429
SiO2	39.68	39.08	39.54	39.23	38.61	40.30	39.59	39.89	39.31	39.34	38.69
FeO	17.55	17.37	15.48	15.53	23.91	15.18	15.37	17.18	17.04	19.93	22.85
MnO	0.38	0.31	nd	0.26	0.38	0.11	0.25	0.19	0.32	0.28	0.36
NiO	0.41	0.48	0.39	0.37	0.17	0.34	0.29	0.18	0.36	0.36	nd
MgO	42.15	42.58	44.86	44.55	38.07	44.74	44.86	43.02	43.17	41.33	39.33
CaO	0.31	0.27	0.27	0.23	0.33	0.17	0.29	0.28	0.25	0.27	0.28
total=	100.48	100.09	100.54	100.17	101.47	100.84	100.65	100.74	100.45	101.51	101.51
Mg#	81.1	81.4	83.8	83.6	73.9	84.0	83.9	81.7	81.9	78.7	75.4

419 OL23,MV164,P,C,E
420 OL23,MV164,P,R,E
421 OL25,MV164,P,I,E
422 OL26,MV164,P,C,E
423 OL26,MV164,P,R,E
424 OL27,MV164,P,C,E
425 OL28,MV164,P,C,E
426 OL29,MV164,P,C,E
427 OL30,MV164,P,I,E
428 OL31,MV164,P,R,E
429 OL32,MV164,P,R,E

	430	431	432	433	434	435	436	437	438	439	440
SiO2	38.35	52.27	52.47	50.81	49.65	0.25	nd	nd	0.14	0.21	0.26
TiO2	nd	0.14	nd	1.58	2.22	2.10	2.16	1.86	1.99	1.90	2.08
Al2O3	nd	29.97	29.69	1.86	3.64	25.65	28.74	27.85	28.79	27.20	27.32
Fe2O3	nd	nd	nd	nd	nd	10.27	9.13	10.11	8.88	9.76	9.50
Cr2O3	nd	nd	nd	0.14	nd	29.13	26.95	28.20	28.09	28.45	28.24
FeO	24.55	0.59	0.56	10.81	9.94	22.12	20.95	18.75	18.77	19.73	20.86
MnO	0.37	nd	nd	0.31	0.19	0.18	nd	0.34	0.37	0.34	0.41
NiO	nd	nd	nd	nd	nd	nd	nd	0.16	0.19	0.15	nd
MgO	36.58	nd	nd	13.00	12.91	10.40	11.24	12.12	12.41	11.61	11.20
CaO	0.41	12.85	13.08	21.19	21.46	nd	nd	nd	0.02	0.01	nd
Na2O	nd	4.33	4.44	nd	nd	nd	nd	nd	nd	nd	nd
K2O	nd	0.31	0.31	nd	nd	nd	nd	nd	nd	nd	nd
total=	100.26	100.46	100.55	99.70	100.01	100.10	99.17	99.39	99.65	99.36	99.87
Mg#	72.6	-	-	68.2	69.8	45.6	48.9	53.5	54.1	51.2	48.9
An	-	61.0	60.9	-	-	-	-	-	-	-	-
Al ratio	-	-	-	-	0.2	-	-	-	-	-	-

430 OLXX,MV164,GR,C,E
431 PLX,MV164,GR,C,E
432 PLXX,MV164,GR,C,E
433 CPXJJ,MV164,GR,C,E
434 CPXKK,MV164,GR,C,E
435 SP1,MV164,P,C,E
436 SP1,MV164,P,C,E
437 SP10,MV164,P,C,W
438 SP11,MV164,P,C,W
439 SP12,MV164,P,C,W
440 SP2,MV164,P,C,E

	441	442	443	444	445	446	447	448	449	450	451
SiO2	0.23	0.44	0.27	0.29	0.27	0.23	38.09	38.54	39.75	38.67	38.81
TiO2	3.33	1.85	1.93	2.04	26.46	50.65	nd	0.03	0.04	0.03	0.05
Al2O3	24.17	27.28	28.44	28.60	1.89	nd	nd	0.09	0.07	0.09	0.08
Fe2O3	11.24	8.98	9.15	9.94	13.98	4.11	nd	nd	nd	nd	nd
Cr2O3	27.83	28.58	26.52	26.77	0.16	nd	nd	0.02	0.01	0.02	0.01
FeO	23.44	20.21	22.18	20.29	55.17	42.47	21.37	21.57	16.56	21.57	21.73
MnO	nd	nd	0.25	nd	0.75	0.69	0.27	0.21	0.18	0.21	0.22
NiO	nd	nd	nd	nd	nd	nd	nd	nd	0.20	nd	0.09
MgO	10.29	11.75	10.31	11.98	nd	1.49	40.34	39.54	43.64	40.77	40.36
CaO	nd	nd	nd	nd	nd	nd	0.20	0.24	0.22	0.24	0.23
Na2O	nd	nd	nd	nd	nd	nd	nd	0.01	nd	0.01	nd
total=	100.53	99.09	99.05	99.91	98.68	99.64	100.27	100.25	100.67	101.61	101.58
Mg#	43.9	50.9	45.3	51.3	-	-	77.1	76.6	82.4	77.1	76.8

441 SPKK,MV164,P,C,E
442 SPWW,MV164,P,C,E
443 SPWWWIII,MV164,P,C,E
444 SPZZ,MV164,P,C,E
445 MTX,MV164,GR,C,E
446 ILX,MV164,GR,C,E
447 OL1,MV166,P,C,+OL+CPX+SP,E
448 OL1,MV166,P,C,W
449 OL1,MV166,P,C,W
450 OL1,MV166,P,C,W
451 OL10,MV166,P,C,W

	452	453	454	455	456	457	458	459	460	461	462
SiO2	37.02	36.42	36.29	36.92	37.36	38.24	39.16	36.55	39.41	37.26	38.38
TiO2	nd	0.24	nd	nd	nd	nd	0.04	0.05	nd	nd	nd
Al2O3	nd	nd	nd	nd	nd	nd	0.08	0.05	nd	nd	nd
Cr2O3	nd	nd	nd	nd	nd	nd	0.01	nd	nd	nd	nd
FeO	31.84	35.18	34.00	29.06	28.72	21.76	21.01	32.95	17.90	27.68	22.63
MnO	0.51	0.71	0.67	0.44	0.46	0.25	0.26	0.54	0.29	0.53	0.29
NiO	nd	nd	nd	nd	nd	0.18	0.17	0.03	0.21	nd	nd
MgO	31.03	28.11	29.31	33.87	33.42	39.43	40.32	30.32	42.38	33.85	38.63
CaO	0.48	0.29	0.37	0.39	0.33	0.21	0.26	0.33	0.15	0.29	0.20
Na2O	nd	nd	nd	nd	nd	nd	nd	0.03	nd	nd	nd
total=	100.88	100.95	100.64	100.68	100.29	100.07	101.31	100.85	100.34	99.61	100.13
Mg#	63.5	58.7	60.6	67.5	67.5	76.4	77.4	62.1	80.8	68.5	75.3

452 OL10QSUW,MV166,P,C,E
453 OL12QSUW,MV166,GR,C,E
454 OL13QSUW,MV166,GR,C,E
455 OL19,MV166,P,C,E
456 OL1QSUWQ,MV166,P,I,E
457 OL2,MV166,P,C,E
458 OL2,MV166,P,I,W
459 OL2,MV166,P,R,W
460 OL21,MV166,P,C,E
461 OL23,MV166,P,R,E
462 OL24,MV166,P,C,E

	463	464	465	466	467	468	469	470	471	472	473
SiO2	38.28	38.52	38.12	37.32	39.77	39.67	39.94	39.31	38.55	37.66	36.47
TiO2	nd	nd	0.02	nd	nd	nd	nd	nd	nd	nd	0.07
Al2O3	nd	nd	0.04	nd	nd	nd	nd	nd	nd	nd	0.05
FeO	22.96	25.71	24.40	28.31	16.21	16.68	13.65	19.61	24.10	24.41	33.87
MnO	0.24	0.35	0.30	0.46	0.24	0.20	0.15	0.17	0.23	0.37	0.61
NiO	0.19	nd	0.07	nd	0.24	nd	0.42	nd	0.19	nd	0.06
MgO	38.51	35.82	37.50	34.08	44.01	43.79	46.31	41.58	36.38	38.05	29.39
CaO	0.28	0.20	0.24	0.33	0.20	0.15	0.15	0.21	0.27	0.24	0.38
Na2O	nd	nd	0.02	nd	nd	nd	nd	nd	nd	nd	0.02
total=	100.46	100.60	100.71	100.50	100.67	100.49	100.62	100.88	99.72	100.73	100.92
Mg#	74.9	71.3	73.3	68.2	82.9	82.4	85.8	79.1	72.9	73.5	60.7

463 OL26,MV166,P,C,E
464 OL2QSUWQ,MV166,P,C,E
465 OL3,MV166,P,C,W
466 OL30,MV166,P,R,E
467 OL31,MV166,P,C,E
468 OL32,MV166,P,C,E
469 OL34,MV166,P,C,E
470 OL35,MV166,P,C,E
471 OL3QSUWQ,MV166,P,I,E
472 OL4,MV166,P,C,E
473 OL4,MV166,P,R,W

	474	475	476	477	478	479	480	481	482	483	484
SiO2	38.88	37.06	38.45	36.77	36.85	38.96	38.20	37.94	39.24	37.07	39.19
TiO2	nd	nd	0.02	nd	0.06	nd	0.04	nd	0.02	0.07	0.06
Al2O3	nd	nd	0.08	nd	0.05	nd	0.07	nd	0.09	0.05	0.08
Cr2O3	nd	nd	nd	nd	nd	nd	0.01	nd	0.01	0.01	nd
FeO	23.40	31.12	22.24	31.51	32.56	24.81	25.45	23.37	20.59	31.68	19.67
MnO	0.30	0.57	0.24	0.64	0.54	0.20	0.29	0.34	0.23	0.47	0.22
NiO	nd	nd	0.14	nd	0.06	nd	nd	nd	0.22	0.05	0.09
MgO	38.06	32.18	39.21	31.40	30.91	36.12	37.02	38.67	40.36	31.67	41.53
CaO	0.22	0.34	0.23	0.33	0.36	0.27	0.19	0.12	0.22	0.44	0.23
Na2O	nd	nd	0.02	nd	0.01	nd	0.02	nd	nd	0.02	nd
total=	100.86	101.27	100.63	100.65	101.40	100.36	101.29	100.44	100.98	101.53	101.07
Mg#	74.4	64.8	75.9	64.0	62.9	72.2	72.2	74.7	77.7	64.1	79.0

474 OL4QSUWQ,MV166,P,C,E
475 OL5,MV166,P,R,E
476 OL5,MV166,P,C,W
477 OL6,MV166,P,R,E
478 OL6,MV166,P,R,W
479 OL6QUXUI,MV166,P,I,E
480 OL7,MV166,P,C,W
481 OL8,MV166,P,C,E
482 OL8,MV166,P,C,W
483 OL8,MV166,P,R,W
484 OL9,MV166,P,C,W

	485	486	487	488	489	490	491	492	493	494	495
SiO2	38.73	49.84	49.98	50.46	48.17	46.95	46.86	46.35	49.57	49.49	47.64
TiO2	nd	0.14	0.17	0.17	2.75	1.91	2.04	2.04	1.14	1.14	2.64
Al2O3	nd	31.67	31.21	31.52	4.80	8.61	8.81	8.94	6.15	6.13	5.30
Cr2O3	nd	nd	nd	nd	0.17	0.22	0.26	0.26	0.14	0.14	nd
FeO	22.38	0.52	0.40	0.36	7.56	8.00	8.14	7.86	6.40	6.40	7.85
MnO	0.14	nd	nd	nd	nd	0.15	nd	nd	0.11	0.11	nd
NiO	nd	nd	nd	nd	nd	nd	nd	nd	0.04	0.04	nd
MgO	38.20	nd	nd	nd	13.39	13.27	12.99	13.26	15.76	15.25	13.32
CaO	0.24	14.71	14.45	14.04	22.36	20.33	20.56	20.46	19.91	19.91	22.48
Na2O	nd	3.93	2.96	3.12	nd	nd	nd	nd	0.58	0.58	nd
K2O	nd	0.13	0.13	0.07	nd	nd	nd	nd	nd	nd	nd
total=	99.69	100.94	99.30	99.74	99.20	99.44	99.66	99.17	99.80	99.19	99.23
Mg#	75.3	-	-	-	75.9	74.7	74.0	76.1	87.9	85.3	77.7
An	-	66.9	72.4	71.0	-	-	-	-	-	-	-
Al ratio	-	-	-	-	0.1	0.5	0.5	0.5	0.4	0.5	0.1

485 OL9QSUWQ,MV166,P,C,E
486 PL2QSUWQ,MV166,GR,C,E
487 PL3QSUWQ,MV166,GR,C,E
488 PL5QSUWQ,MV166,GR,C,E
489 CPX01,MV166,P,R,E
490 CPX04,MV166,P,I,E
491 CPX05,MV166,P,C,E
492 CPX08,MV166,P,I,E
493 CPX1,MV166,P,C,W
494 CPX1,MV166,P,C,W
495 CPX10QSUW,MV166,P,R,E

	496	497	498	499	500	501	502	503	504	505	506
SiO2	47.37	48.26	46.81	48.34	48.89	46.91	45.98	47.02	47.08	47.64	49.87
TiO2	1.84	2.71	1.97	2.51	1.39	1.68	2.74	2.95	2.95	3.08	1.02
Al2O3	8.52	4.87	8.02	4.50	5.79	8.90	9.39	5.24	5.25	5.57	5.92
Cr2O3	0.30	0.21	0.28	nd	0.30	0.17	nd	0.06	0.06	0.24	0.16
FeO	7.37	7.26	8.23	7.54	6.87	7.77	8.48	7.94	7.94	8.01	6.51
MnO	nd	0.17	nd	nd	nd	nd	0.11	nd	nd	nd	0.15
NiO	nd	nd	nd	nd	nd	0.13	nd	0.01	0.01	nd	nd
MgO	13.57	13.39	13.49	13.60	14.72	13.38	12.76	12.82	13.25	12.96	15.57
CaO	20.69	22.61	20.32	22.90	21.37	20.54	19.90	22.31	22.32	22.37	19.53
Na2O	nd	nd	nd	nd	nd	nd	nd	0.42	0.42	nd	nd
total=	99.66	99.48	99.12	99.39	99.33	99.48	99.36	98.77	99.28	99.87	98.73
Mg#	76.6	77.0	75.8	78.9	81.1	76.5	72.8	80.6	83.2	74.3	81.0
Al ratio	0.6	0.1	0.4	0.1	0.4	0.6	0.5	-	-	0.1	0.7

496 CPX11QSUW,MV166,P,C,E
497 CPX12QSUW,MV166,P,R,E
498 CPX15QSUW,MV166,P,C,E
499 CPX16QSUW,MV166,P,R,E
500 CPX17QS,MV166,P,C,E
501 CPX19QSUW,MV166,P,C,E
502 CPX1QSUWQ,MV166,P,C,E
503 CPX2,MV166,P,R,W
504 CPX2,MV166,P,R,W
505 CPX20QSUW,MV166,P,R,E
506 CPX22QSUW,MV166,P,C,E

	507	508	509	510	511	512	513	514	515	516	517
SiO2	49.42	49.00	47.96	46.65	46.71	48.45	49.05	49.11	49.25	46.82	46.75
TiO2	2.20	2.40	2.78	1.87	1.87	2.64	2.26	2.26	2.57	2.17	2.17
Al2O3	3.95	3.90	5.40	8.77	8.78	5.16	3.79	3.80	4.58	7.95	7.94
Cr2O3	nd	nd	0.12	0.21	0.21	0.15	0.02	0.02	0.11	0.12	0.12
FeO	7.71	8.07	7.78	8.00	8.00	7.58	8.13	8.13	7.65	9.57	9.57
MnO	nd	nd	0.17	0.12	0.12	nd	0.14	0.14	nd	0.15	0.15
NiO	nd	nd	nd	nd	nd	nd	0.01	0.01	nd	0.02	0.02
MgO	13.52	13.36	13.02	12.92	13.35	13.41	13.18	13.63	13.06	13.66	13.22
CaO	22.63	22.63	22.60	20.09	20.09	22.67	22.24	22.24	22.74	18.62	18.61
Na2O	nd	nd	nd	0.66	0.66	nd	0.49	0.49	nd	0.68	0.68
total=	99.43	99.36	99.83	99.29	99.79	100.06	99.31	99.83	99.96	99.76	99.23
Mg#	75.8	75.0	75.5	80.7	83.2	76.4	78.9	81.4	75.3	79.2	76.8
Al ratio	0.2	0.1	0.2	0.5	0.4	0.2	0.1	-	0.2	0.3	0.4

507 CPX24QSUW,MV166,GR,C,E
508 CPX25QSUW,MV166,GR,C,E
509 CPX2QSUWQ,MV166,P,R,E
510 CPX3,MV166,P,C,W
511 CPX3,MV166,P,C,W
512 CPX3QSUWQ,MV166,P,C,E
513 CPX4,MV166,P,R,W
514 CPX4,MV166,P,R,W
515 CPX4QSUWQ,MV166,P,R,E
516 CPX5,MV166,P,C,W
517 CPX5,MV166,P,C,W

	518	519	520	521	522	523	524	525	526	527	528
SiO2	49.53	49.46	49.73	49.48	46.49	46.43	47.15	nd	nd	0.09	nd
TiO2	1.96	1.96	0.80	1.28	2.20	2.20	1.94	1.77	1.77	1.01	0.90
Al2O3	3.24	3.23	5.38	6.50	7.19	7.18	9.22	50.86	51.27	56.83	57.19
Fe2O3	nd	nd	nd	nd	nd	nd	nd	12.80	13.11	9.30	9.01
Cr2O3	nd	nd	0.35	0.27	0.31	0.31	0.14	1.48	0.36	0.24	0.29
FeO	8.13	8.13	6.19	6.55	7.58	7.58	7.30	20.78	19.43	16.36	16.32
MnO	0.15	0.15	0.12	nd	0.11	0.11	0.17	nd	nd	0.11	nd
NiO	0.01	0.01	0.03	nd	0.01	0.01	nd	nd	nd	0.18	nd
MgO	13.37	12.93	16.18	15.09	13.17	12.74	13.36	13.86	14.56	16.66	16.71
CaO	22.30	22.30	18.66	20.33	21.93	21.92	20.85	nd	nd	0.03	nd
Na2O	0.49	0.49	0.58	nd	0.45	0.45	0.60	nd	nd	nd	nd
total=	99.18	98.66	98.02	99.50	99.44	98.93	100.73	101.55	100.50	100.81	100.42
Mg#	79.5	77.1	86.2	80.4	86.1	83.5	83.7	54.3	57.2	64.5	64.6
Al ratio	-	0.1	0.6	0.6	0.2	0.2	0.5	-	-	-	-

518 CPX6,MV166,P,R,W
519 CPX6,MV166,P,R,W
520 CPX7,MV166,P,C,W
521 CPX7QSUWQ,MV166,P,C,E
522 CPX8,MV166,P,R,W
523 CPX8,MV166,P,R,W
524 CPX9QSUWQ,MV166,P,C,E
525 SP1,MV166,P,C,E
526 SP1,MV166,P,C,E
527 SP1,MV166,P,C,W
528 SP10,MV166,P,C,E

	529	530	531	532	533	534	535	536	537	538	539
SiO2	nd	nd	0.23	nd	0.84	nd	0.12	0.12	0.09	0.83	0.19
TiO2	1.17	1.09	0.93	1.27	2.52	1.85	1.17	1.17	1.10	2.98	9.45
Al2O3	57.19	56.93	56.95	56.68	26.80	51.20	51.33	51.25	56.60	28.99	10.73
Fe2O3	7.52	8.89	8.79	6.92	23.27	12.41	11.31	10.78	8.73	16.06	31.28
Cr2O3	0.31	0.27	0.30	0.41	9.15	0.34	2.50	2.50	0.31	13.56	6.51
FeO	20.42	16.26	16.35	22.48	31.57	20.06	20.96	21.44	17.57	30.93	38.12
MnO	0.20	0.16	nd	0.20	0.31	0.13	0.19	0.19	0.13	0.26	0.31
NiO	nd	nd	nd	nd	nd	nd	0.14	0.14	0.14	nd	nd
MgO	14.20	16.71	16.89	12.82	4.68	14.00	13.20	12.77	15.87	5.73	2.09
CaO	nd	nd	nd	nd	nd	nd	0.01	0.01	0.02	nd	nd
total=	101.01	100.31	100.44	100.78	99.14	99.99	100.93	100.37	100.56	99.34	98.68
Mg#	55.3	64.7	64.8	50.4	20.9	55.4	52.9	51.5	61.7	24.8	8.9

529 SP11,MV166,P,R,E
530 SP12,MV166,P,C,E
531 SP13,MV166,P,C,E
532 SP13,MV166,P,R,E
533 SP2,MV166,P,C,E
534 SP2,MV166,P,C,E
535 SP2,MV166,P,C,W
536 SP2,MV166,P,C,W
537 SP2,MV166,P,I,W
538 SP2QSUWQ,MV166,P,C,E
539 SP3,MV166,P,C,E

	540	541	542	543	544	545	546	547	548	549	550
SiO2	0.36	0.11	0.11	0.05	0.42	0.35	nd	nd	0.06	nd	0.26
TiO2	1.34	0.97	0.97	1.21	0.92	2.76	1.58	2.23	1.12	0.96	2.43
Al2O3	53.94	57.49	57.61	57.14	54.01	19.29	53.31	49.98	58.17	53.26	32.04
Fe2O3	7.83	8.76	9.42	6.87	9.36	22.10	10.87	13.93	5.61	9.76	18.12
Cr2O3	0.51	0.21	0.21	0.35	1.70	19.48	0.36	0.43	0.43	2.27	11.35
FeO	24.44	16.61	16.01	21.76	21.21	31.02	21.33	20.21	22.76	21.05	30.43
MnO	nd	0.12	0.12	0.18	0.21	0.39	0.30	0.14	0.19	0.14	0.28
NiO	nd	0.15	0.15	0.12	nd	nd	nd	0.11	0.08	nd	nd
MgO	11.56	16.64	17.19	13.27	13.64	4.00	13.37	14.14	12.73	13.20	5.82
CaO	nd	0.02	0.02	0.08	nd	nd	nd	0.03	0.12	nd	nd
total=	99.98	101.08	101.81	101.03	101.47	99.39	101.12	101.20	101.27	100.64	100.73
Mg#	45.7	64.1	65.7	52.1	53.4	18.7	52.8	55.5	49.9	52.8	25.4

540 SP3,MV166,P,C,E
541 SP3,MV166,P,C,W
542 SP3,MV166,P,C,W
543 SP3,MV166,P,R,W
544 SP3QSUWQ,MV166,P,C,E
545 SP4,MV166,P,C,E
546 SP4,MV166,P,I,E
547 SP4,MV166,P,C,W
548 SP4,MV166,P,R,W
549 SP4QSUWQ,MV166,P,C,E
550 SP5,MV166,P,C,E

	551	552	553	554	555	556	557	558	559	560	561
SiO2	0.23	0.11	0.30	0.29	0.20	0.05	nd	0.07	0.07	0.11	0.22
TiO2	1.82	2.21	3.02	2.50	1.98	1.79	2.22	1.80	1.80	2.12	1.62
Al2O3	51.06	50.32	18.95	19.64	52.15	52.88	49.46	51.34	51.43	49.20	46.43
Fe2O3	12.80	13.30	21.68	21.65	10.27	10.04	13.39	13.30	13.90	14.31	15.48
Cr2O3	0.25	0.43	19.67	19.72	0.40	0.51	0.39	0.30	0.30	nd	2.40
FeO	19.20	20.84	31.45	31.28	22.13	23.54	20.23	19.40	18.86	22.84	24.50
MnO	0.22	0.12	0.40	0.34	0.21	0.17	nd	0.13	0.13	0.18	0.24
NiO	nd	0.09	nd	nd	nd	0.09	nd	0.11	0.11	0.13	nd
MgO	14.73	13.92	3.76	3.63	13.05	12.09	13.93	14.62	15.11	12.35	10.95
CaO	nd	0.02	nd	nd	nd	0.01	nd	0.01	0.01	0.02	nd
total=	100.31	101.36	99.23	99.05	100.39	101.17	99.62	101.08	101.72	101.26	101.84
Mg#	57.8	54.3	17.6	17.1	51.2	47.8	55.1	57.3	58.8	49.1	44.3

551 SP5,MV166,P,C,E
552 SP5,MV166,P,C,W
553 SP5QSWQJ,MV166,P,C,E
554 SP6,MV166,P,C,E
555 SP6,MV166,P,R,E
556 SP6,MV166,P,R,W
557 SP7,MV166,P,C,E
558 SP7,MV166,P,C,W
559 SP7,MV166,P,C,W
560 SP7,MV166,P,I,W
561 SP8,MV166,P,C,E

	562	563	564	565	566	567	568	569	570	571	572
SiO2	nd	0.07	0.25	0.06	nd	nd	0.23	0.37	0.23	0.32	0.25
TiO2	2.03	1.63	4.47	1.43	1.86	20.32	21.86	16.36	9.98	17.04	16.45
Al2O3	51.21	52.97	33.48	51.53	50.77	2.08	5.00	3.57	10.38	3.17	3.37
Fe2O3	11.36	8.60	23.23	10.95	13.45	26.91	20.16	32.04	27.53	32.89	33.26
Cr2O3	0.45	2.34	2.24	1.84	0.31	0.40	1.53	0.55	10.04	0.29	0.42
FeO	22.12	19.41	30.26	21.42	18.32	46.66	47.17	44.32	37.14	44.47	44.48
MnO	0.13	0.17	0.32	0.18	0.20	0.54	0.53	0.48	0.51	0.56	0.44
NiO	nd	0.13	nd	0.16	0.21	nd	nd	nd	nd	nd	nd
MgO	12.80	14.40	7.38	12.92	14.92	1.74	3.07	1.51	2.97	1.86	1.57
CaO	nd	0.02	nd	0.03	nd	nd	nd	nd	nd	0.18	nd
total=	100.10	99.74	101.63	100.52	100.04	98.65	99.55	99.20	98.78	100.78	100.24
Mg#	50.8	56.9	30.3	51.8	59.2	-	-	-	12.5	-	-

562 SP8,MV166,P,R,E
563 SP8,MV166,P,C,W
564 SP9,MV166,P,C,E
565 SP9,MV166,P,C,W
566 SPMO,MV166,P,C,E
567 MT,MV166,GR,C,E
568 MTQ2,MV166,GR?,C,E
569 MT1QSUWQ,MV166,GR?,C,E
570 SPMT2QSUWQ,MV166,P,C,E
571 MT4QSUWQ,MV166,GR,C,E
572 MT5QSUWQ,MV166,GR,C,E

	573	574	575	576	577	578	579	580	581	582	583
SiO2	0.28	0.24	0.26	38.70	39.11	38.25	39.81	39.05	49.59	48.41	52.28
TiO2	51.89	52.19	52.27	nd	nd	nd	nd	nd	0.04	0.06	0.08
Al2O3	nd	nd	nd	0.07	0.07	0.08	0.08	0.07	31.75	32.34	29.87
Fe2O3	3.41	3.01	2.91	nd	nd	nd	nd	nd	nd	nd	nd
Cr2O3	nd	0.13	nd	nd	nd	nd	nd	nd	nd	nd	nd
FeO	39.61	40.14	40.40	20.05	19.59	23.59	14.92	18.05	0.34	0.33	0.33
MnO	0.75	0.67	0.51	0.28	0.27	0.39	0.20	0.24	nd	nd	nd
NiO	nd	nd	nd	0.22	0.21	0.17	0.25	0.26	nd	nd	nd
MgO	3.72	3.59	3.59	40.82	41.59	37.93	45.00	42.11	0.05	0.05	0.06
CaO	nd	nd	nd	0.25	0.30	0.30	0.27	0.33	14.99	15.72	12.54
Na2O	nd	nd	nd	nd	nd	nd	nd	nd	2.91	2.54	4.15
K2O	nd	nd	nd	nd	nd	nd	nd	nd	0.17	0.15	0.32
total=	99.66	99.97	99.94	100.39	101.14	100.71	100.53	100.11	99.84	99.60	99.63
Mg#	-	-	-	78.4	79.1	74.1	84.3	80.6	-	-	-
An	-	-	-	-	-	-	-	-	73.3	76.7	61.4

573 IL1QSUWQ,MV166,GR,C,E
574 IL2QSUWQ,MV166,GR,C,E
575 IL3QSUWQ,MV166,GR,C,E
576 OL121,AS1,P,C,+OL+CPX+PL+SP+MT,W
577 OL122,AS1,P,I,W
578 OL123,AS1,P,R,W
579 OL124,AS1,P,C,W
580 OL125,AS1,P,R,W
581 PL100,AS1,P,C,W
582 PL101,AS1,P,C,W
583 PL102,AS1,P,I,W

	584	585	586	587	588	589	590	591	592	593	594
SiO2	53.64	53.92	54.96	51.95	54.61	54.47	53.38	52.16	50.23	55.40	51.60
TiO2	0.09	0.05	0.04	0.11	0.15	0.14	0.16	0.11	0.08	0.03	0.06
Al2O3	29.32	28.66	28.02	29.91	28.13	28.30	29.03	29.81	30.73	27.30	29.78
FeO	0.30	0.30	0.31	0.57	0.54	0.51	0.61	0.70	0.59	0.29	0.55
MgO	0.06	0.06	0.05	0.08	0.08	0.08	0.09	0.14	nd	0.06	0.09
CaO	11.72	11.17	10.30	12.72	10.79	10.83	11.63	12.73	13.98	9.82	12.99
Na2O	4.72	4.87	5.25	4.01	4.90	5.05	4.62	4.07	3.38	5.41	3.81
K2O	0.38	0.41	0.61	0.39	0.60	0.63	0.56	0.38	0.35	0.57	0.36
total=	100.23	99.44	99.54	99.74	99.80	100.01	100.08	100.10	99.34	98.88	99.24
An	56.6	54.6	50.2	62.2	53.0	52.3	56.3	62.0	68.2	48.4	63.9

584 PL103,AS1,P,I,W
585 PL104,AS1,P,I,W
586 PL105,AS1,P,I,W
587 PL106,AS1,P,R,W
588 PL108,AS1,P,R,W
589 PL109,AS1,P,R,W
590 PL110,AS1,GR?,C,W
591 PL111,AS1,GR?,C,W
592 PL41,AS1,P,I,W
593 PL44,AS1,P,C,W
594 PL46,AS1,P,R,W

	595	596	597	598	599	600	601	602	603	604	605
SiO2	51.91	47.73	48.07	50.12	47.62	46.94	54.33	52.49	54.30	55.80	55.02
TiO2	0.11	0.06	0.04	0.06	0.03	0.04	0.06	0.11	0.16	0.07	0.07
Al2O3	29.59	32.35	32.38	30.81	32.93	32.76	28.75	29.32	27.92	26.85	27.63
FeO	0.63	0.48	0.47	0.52	0.35	0.32	0.30	0.52	0.62	0.25	0.35
MgO	0.11	0.08	0.08	0.08	0.06	0.04	0.06	0.07	0.07	0.02	0.04
CaO	12.75	15.91	15.55	14.17	16.40	16.60	11.31	12.22	10.82	9.35	10.04
Na2O	3.85	2.34	2.35	3.14	2.09	2.08	4.67	4.18	4.96	5.63	5.34
K2O	0.44	0.18	0.17	0.29	0.16	0.11	0.46	0.50	0.64	0.71	0.57
total=	99.39	99.13	99.11	99.19	99.64	98.89	99.94	99.41	99.49	98.68	99.06
An	63.0	78.1	77.7	70.2	80.5	81.0	55.7	60.0	52.6	45.9	49.3

595 PL47,AS1,P,R,W
596 PL48,AS1,P,C,W
597 PL49,AS1,P,I,W
598 PL51,AS1,P,R,W
599 PL52,AS1,P,C,W
600 PL53,AS1,P,I,W
601 PL54R,AS1,P,R,W
602 PL57,AS1,P,I,W
603 PL58,AS1,P,R,W
604 PL59,AS1,P,C,W
605 PL62,AS1,P,I,W

	606	607	608	609	610	611	612	613	614	615	616
SiO2	52.49	49.73	53.22	54.71	55.18	48.66	52.04	52.87	54.75	54.06	52.16
TiO2	0.11	0.11	0.07	0.09	0.09	0.11	0.11	0.16	0.16	nd	0.14
Al2O3	29.27	31.72	29.00	27.91	27.24	31.34	29.40	28.93	27.51	28.01	29.14
FeO	0.51	0.30	0.31	0.33	0.34	0.56	0.53	0.54	0.59	0.54	0.63
MgO	0.08	0.04	0.05	0.05	0.06	0.09	nd	0.09	0.11	0.08	0.08
CaO	12.44	14.87	11.71	10.56	9.89	15.22	12.64	11.93	10.39	10.94	12.35
Na2O	4.24	2.93	4.53	5.05	5.36	2.67	4.15	4.46	5.11	4.85	4.10
K2O	0.45	0.17	0.39	0.55	0.74	0.22	0.35	0.49	0.79	0.63	0.45
total=	99.59	99.87	99.28	99.25	98.90	98.87	99.22	99.47	99.41	99.11	99.05
An	60.2	73.0	57.5	51.9	48.3	74.9	61.5	58.0	50.5	53.5	60.8

606 PL63,AS1,P,R,W
607 PL64,AS1,P,C,W
608 PL65,AS1,P,I,W
609 PL66,AS1,P,I,W
610 PL67,AS1,P,I,W
611 PL69,AS1,P,C,W
612 PL70,AS1,P,I,W
613 PL71,AS1,P,R,W
614 PL73,AS1,P,C,W
615 PL74,AS1,P,I,W
616 PL75,AS1,P,R,W

	617	618	619	620	621	622	623	624	625	626	627
SiO2	54.62	47.90	47.65	48.33	47.23	50.17	47.34	49.06	46.97	48.71	47.03
TiO2	0.19	0.04	0.06	0.05	0.04	1.60	2.23	1.57	2.14	2.03	1.81
Al2O3	27.56	33.21	32.97	32.37	33.17	3.36	5.99	3.68	6.30	3.73	7.17
Cr2O3	nd	nd	nd	nd	nd	0.14	0.01	nd	0.04	0.02	0.18
FeO	0.57	0.36	0.34	0.34	0.33	8.46	8.16	8.24	8.05	8.48	6.86
MnO	nd	nd	nd	nd	nd	0.24	0.14	0.18	0.13	0.18	0.11
MgO	nd	0.04	0.04	0.05	0.07	14.07	13.04	13.71	12.88	12.91	13.33
CaO	10.39	16.10	16.23	15.43	16.31	21.73	21.27	21.69	21.52	22.20	21.73
Na2O	5.14	2.28	2.21	2.54	2.04	0.34	0.57	0.48	0.58	0.46	0.48
K2O	0.74	0.12	0.11	0.17	0.09	nd	nd	nd	nd	nd	nd
total=	99.21	100.05	99.61	99.28	99.28	100.11	98.75	98.61	98.61	98.72	98.70
Mg#	-	-	-	-	-	78.9	81.3	81.8	82.9	78.5	85.8
An	50.5	79.0	79.7	76.3	81.1	-	-	-	-	-	-
Al ratio	-	-	-	-	-	0.1	0.2	0.1	0.2	-	0.3

617 PL76,AS1,P,R,W
618 PL96,AS1,P,C,W
619 PL97,AS1,P,C,W
620 PL98,AS1,P,C,W
621 PL99,AS1,P,C,W
622 CPX200,AS1,P,C,E
623 CPX214,AS1,P,C,W
624 CPX215,AS1,P,C,W
625 CPX219,AS1,P,C,W
626 CPX222,AS1,P,R,W
627 CPX223,AS1,P,C,W

	628	629	630	631	632	633	634	635	636	637	638
SiO2	47.59	47.62	48.29	47.89	47.66	48.03	49.50	49.53	48.29	47.21	0.04
TiO2	1.25	1.34	2.18	1.32	1.97	2.14	1.04	0.94	2.17	1.43	2.08
Al2O3	7.38	7.00	3.88	6.71	5.29	3.80	2.75	2.49	3.73	7.50	44.68
Fe2O3	nd	nd	nd	nd	nd	nd	nd	nd	nd	nd	9.79
Cr2O3	0.74	0.62	0.02	0.90	nd	0.04	nd	nd	nd	0.60	10.97
FeO	5.51	5.68	8.44	5.19	8.48	8.61	11.61	11.65	8.50	5.68	17.99
MnO	0.09	0.09	0.21	0.09	0.18	0.16	0.41	0.44	0.19	0.09	0.27
MgO	14.03	13.99	12.99	14.34	13.03	13.05	11.37	11.42	13.00	13.87	14.95
CaO	21.98	21.96	22.06	21.47	21.66	22.18	21.51	21.69	22.18	21.74	nd
Na2O	0.38	0.45	0.49	0.47	0.56	0.49	0.49	0.48	0.48	0.45	nd
total=	98.95	98.75	98.56	98.38	98.83	98.50	98.68	98.64	98.54	98.57	100.77
Mg#	89.3	89.6	80.0	89.1	82.3	81.6	67.8	68.7	80.3	89.2	59.7
Al ratio	0.4	0.4	-	0.4	0.1	-0.1	0.2	0.1	-	0.4	-

628 CPX226,AS1,P,C,W
629 CPX227,AS1,P,I,W
630 CPX228,AS1,P,R,W
631 CPX229,AS1,P,C,W
632 CPX231,AS1,P,C,W
633 CPX233,AS1,P,R,W
634 CPX238,AS1,P,C,W
635 CPX239,AS1,P,I,W
636 CPX240,AS1,P,R,W
637 CPX241,AS1,P,C,W
638 SP104,AS1,P,C,W

	639	640	641	642	643	644	645	646	647	648	649
SiO2	0.11	nd	0.12	0.11	0.12	0.11	0.13	0.01	nd	0.01	0.07
TiO2	1.64	1.28	1.17	0.99	1.29	1.28	1.31	1.91	2.00	12.25	2.19
Al2O3	32.61	29.56	39.89	43.47	41.53	38.96	41.20	32.66	28.81	10.80	27.27
Fe2O3	6.91	8.76	10.50	9.92	7.49	8.85	7.38	9.92	10.61	18.78	10.71
Cr2O3	27.91	28.54	17.03	13.72	18.37	19.98	18.40	21.34	25.15	17.24	26.62
FeO	15.40	18.44	15.53	14.69	14.45	14.89	14.49	24.22	24.32	35.39	24.85
MnO	0.42	0.46	0.33	0.30	0.34	0.37	0.30	0.40	0.62	0.69	0.57
MgO	14.96	12.15	15.38	16.06	16.34	15.81	16.23	9.20	8.76	5.71	8.58
total=	99.96	99.19	99.95	99.26	99.93	100.25	99.44	99.66	100.27	100.87	100.86
Mg#	63.4	54.0	63.8	66.1	66.8	65.4	66.6	40.4	39.1	22.3	38.1

639 SP105,AS1,P,C,W
640 SP106,AS1,P,C,W
641 SP107,AS1,P,C,W
642 SP108,AS1,P,C,W
643 SP109,AS1,P,C,W
644 SP110,AS1,P,C,W
645 SP111,AS1,P,C,W
646 SP112,AS1,P,C,W
647 SP113,AS1,P,C,W
648 SP115,AS1,P,I,W
649 SP116,AS1,P,C,W

	650	651	652	653	654	655	656	657	658	659	660
SiO2	nd	nd	nd	0.02	0.11	0.07	0.14	0.07	0.05	0.09	0.05
TiO2	0.66	1.96	1.83	19.31	15.07	16.46	16.35	24.66	24.77	19.20	10.20
Al2O3	56.18	33.94	37.19	5.07	8.67	7.27	7.31	3.53	3.47	6.20	4.41
Fe2O3	7.87	13.04	13.25	19.38	32.53	31.32	31.32	18.69	18.71	27.27	45.01
Cr2O3	4.21	19.36	15.01	8.48	0.07	0.06	0.07	0.24	0.09	nd	0.05
FeO	11.89	19.70	18.32	41.43	36.57	37.86	37.79	46.68	46.47	40.05	35.97
MnO	0.11	0.32	0.29	0.67	0.31	0.30	0.28	0.50	0.52	0.45	0.47
MgO	19.25	12.59	13.43	5.03	6.32	6.09	6.14	4.68	4.81	6.10	3.03
total=	100.17	100.91	99.32	99.39	99.65	99.43	99.40	99.05	98.89	99.36	99.19
Mg#	74.3	53.2	56.6	17.8	-	-	-	-	-	-	-

650 SP117,AS1,P,C,W
651 SP118,AS1,P,C,W
652 SP119,AS1,P,C,W
653 SPMT206,AS1,P,I,W
654 MT200,AS1,P,C,W
655 MT201,AS1,P,C,W
656 MT202,AS1,P,C,W
657 MT203,AS1,P,C,W
658 MT204,AS1,P,C,W
659 MT205,AS1,P,C,W
660 MT208,AS1,P,C,W

	661	662	663	664	665	666	667	668	669	670	671
SiO2	0.05	0.02	0.13	0.03	0.06	39.03	38.72	39.11	38.36	38.43	37.57
TiO2	24.98	25.20	26.38	51.84	51.60	nd	nd	nd	nd	nd	nd
Al2O3	3.52	3.49	2.70	0.36	0.33	0.09	0.11	0.08	nd	0.09	0.09
Fe2O3	19.09	18.07	13.11	5.85	6.29	nd	nd	nd	nd	nd	nd
Cr2O3	0.14	0.11	0.19	nd	0.01	nd	nd	nd	nd	nd	nd
FeO	47.83	47.48	51.85	35.57	35.25	19.69	19.90	19.05	22.83	22.81	28.66
MnO	0.66	0.61	1.09	0.58	0.56	0.28	0.25	0.27	0.38	0.32	0.55
NiO	nd	nd	nd	nd	nd	0.21	0.16	0.16	0.19	0.09	0.08
MgO	4.31	4.44	1.51	5.89	5.98	41.42	41.19	41.59	38.66	38.73	34.13
CaO	nd	nd	nd	nd	nd	0.23	0.25	0.26	0.29	0.27	0.35
total=	100.58	99.42	96.96	100.12	100.08	100.95	100.58	100.52	100.71	100.74	101.43
Mg#	-	-	-	-	-	78.9	78.7	79.6	75.1	75.2	68.0

661 MT209,AS1,P,C,W
662 MT210,AS1,P,C,W
663 MT211,AS1,GR,C,W
664 IL100,AS1,P?,C,W
665 IL101,AS1,P?,C,W
666 OL107,36017,P,C,+OL+CPX+PL+SP+MT,W
667 OL108,36017,P,I,W
668 OL109,36017,P,I,W
669 OL110,36017,P,R,W
670 OL111,36017,P,C,W
671 OL112,36017,P,R,W

	672	673	674	675	676	677	678	679	680	681	682
SiO2	38.90	39.35	39.72	39.54	37.71	39.05	39.06	38.63	47.04	47.38	50.33
TiO2	nd	nd	nd	nd	nd	nd	nd	nd	0.06	0.09	0.12
Al2O3	0.09	0.08	0.07	0.06	0.07	0.06	0.07	0.07	32.75	32.71	30.57
FeO	21.71	17.92	17.91	17.69	29.18	20.99	19.23	20.91	0.41	0.40	0.50
MnO	0.29	0.23	0.23	0.21	0.55	0.27	0.25	0.27	nd	nd	nd
NiO	0.12	0.20	0.20	0.24	0.17	0.16	0.16	0.17	nd	nd	nd
MgO	39.81	43.09	43.15	43.05	33.87	40.32	41.54	40.44	0.10	0.09	0.10
CaO	0.26	0.23	0.26	0.24	0.42	0.33	0.26	0.25	16.82	16.54	14.38
Na2O	nd	nd	nd	nd	nd	nd	nd	nd	1.82	1.95	3.14
K2O	nd	nd	nd	nd	nd	nd	nd	nd	0.11	0.13	0.26
total=	101.18	101.10	101.54	101.03	101.97	101.18	100.57	100.74	99.11	99.29	99.40
Mg#	76.6	81.1	81.1	81.3	67.4	77.4	79.4	77.5	-	-	-
An	-	-	-	-	-	-	-	-	83.1	81.8	70.6

672 OL113,36017,P,C,W
673 OL114,36017,P,C,W
674 OL115,36017,P,I,W
675 OL116,36017,P,I,W
676 OL117,36017,P,R,W
677 OL118,36017,P,C,W
678 OL119,36017,P,C,W
679 OL120,36017,P,C,W
680 PL201,36017,P,C,W
681 PL202,36017,P,C,W
682 PL204,36017,P,I,W

	683	684	685	686	687	688	689	690	691	692	693
SiO2	51.48	51.64	54.16	55.22	56.23	55.55	51.66	56.27	52.98	55.56	56.03
TiO2	0.13	0.12	0.29	0.07	0.07	0.07	0.12	0.05	0.09	0.08	0.05
Al2O3	29.76	29.66	27.41	27.48	26.74	27.18	29.89	26.71	29.17	27.18	27.03
FeO	0.47	0.54	0.79	0.32	0.24	0.31	0.64	0.31	0.46	0.32	0.28
MgO	0.11	0.11	0.14	0.05	0.04	0.07	0.09	0.03	0.08	0.05	0.05
CaO	13.24	13.05	10.74	9.63	8.94	9.63	13.04	9.33	11.96	9.67	9.25
Na2O	3.70	3.74	4.84	5.52	5.80	5.54	3.88	5.83	4.23	5.61	5.84
K2O	0.33	0.39	0.71	0.74	0.72	0.72	0.40	0.76	0.46	0.74	0.65
total=	99.22	99.25	99.08	99.03	98.78	99.07	99.72	99.29	99.43	99.21	99.18
An	65.1	64.3	52.8	47.0	44.1	46.9	63.5	44.9	59.3	46.7	44.9

683 PL205,36017,P,I,W
684 PL206,36017,P,I,W
685 PL207,36017,P,I,W
686 PL78,36017,P,C,W
687 PL79,36017,P,I,W
688 PL80,36017,P,R,W
689 PL81,36017,P,R,W
690 PL82,36017,P,C,W
691 PL83,36017,P,R,W
692 PL84,36017,P,I,W
693 PL86,36017,P,I,W

	694	695	696	697	698	699	700	701	702	703	704
SiO2	55.87	57.24	47.18	47.42	54.32	49.96	47.51	47.26	46.36	47.88	49.16
TiO2	0.07	0.19	0.06	0.06	0.16	0.09	0.09	1.67	2.09	1.21	1.81
Al2O3	26.96	25.80	32.86	32.77	28.11	31.50	32.71	7.35	6.99	6.39	3.10
Cr2O3	nd	nd	nd	nd	nd	nd	nd	0.23	0.02	0.77	0.02
FeO	0.27	0.46	0.50	0.52	0.54	0.46	0.62	6.33	8.00	5.23	8.21
MnO	nd	nd	nd	nd	nd	nd	nd	0.11	0.14	0.07	0.18
MgO	0.05	0.08	0.09	0.07	0.07	nd	0.09	13.63	12.84	14.42	13.48
CaO	9.33	8.01	16.41	16.26	10.89	14.56	16.25	21.50	21.44	21.84	21.97
Na2O	5.71	5.98	1.98	2.11	4.82	3.14	2.20	0.47	0.57	0.43	0.46
K2O	0.69	1.13	0.13	0.14	0.62	0.21	0.18	nd	nd	nd	nd
total=	98.95	98.89	99.21	99.35	99.53	99.92	99.65	98.55	98.45	98.24	98.39
Mg#	-	-	-	-	-	-	-	86.2	84.6	90.8	80.2
An	45.5	39.7	81.4	80.3	53.5	71.1	79.5	-	-	-	-
Al ratio	-	-	-	-	-	-	-	0.4	0.2	0.3	-

694 PL87,36017,P,I,W
695 PL90,36017,P,R,W
696 PL91,36017,P,C,W
697 PL92,36017,P,I,W
698 PL93,36017,P,R,W
699 PL94,36017,P,C,W
700 PL95,36017,P,R,W
701 CPX243,36017,P,C,W
702 CPX247,36017,P,C,W
703 CPX248,36017,P,I,W
704 CPX249,36017,P,R,W

	705	706	707	708	709	710	711	712	713	714	715
SiO2	46.47	47.05	46.98	46.19	46.16	43.47	47.79	43.46	0.12	0.11	0.12
TiO2	1.85	2.16	1.39	1.72	1.64	2.15	2.26	2.11	1.32	1.81	1.25
Al2O3	7.33	5.94	7.33	8.35	8.36	14.18	18.91	17.26	34.57	32.88	28.12
Fe2O3	nd	nd	nd	nd	nd	nd	nd	nd	9.86	13.12	9.86
Cr2O3	0.18	0.02	0.98	0.81	0.69	nd	nd	nd	22.84	19.73	28.27
FeO	7.71	8.43	5.44	5.88	5.84	11.93	6.33	9.35	15.58	18.24	21.61
MnO	0.12	0.15	0.04	0.09	0.07	0.20	0.12	nd	0.29	0.36	0.51
MgO	12.93	13.00	13.95	13.41	13.32	4.66	4.13	5.40	14.80	13.08	10.11
CaO	21.23	21.09	21.76	21.74	21.98	4.90	4.43	4.85	nd	nd	nd
Na2O	0.58	0.57	0.43	0.46	0.44	1.28	5.13	3.95	nd	nd	nd
K2O	nd	nd	nd	nd	nd	5.66	1.03	0.88	nd	nd	nd
P2O5	nd	nd	nd	nd	nd	0.91	0.34	0.50	nd	nd	nd
total=	98.40	98.41	98.30	98.65	98.50	89.34	90.47	87.76	99.38	99.33	99.85
Mg#	84.7	81.6	90.4	89.5	89.9	41.0	53.8	50.7	62.9	56.1	45.5
Al ratio	0.3	0.2	0.3	0.3	0.3	-1.4	-1.5	-1.5	-	-	-

705 CPX251,36017,P,C,W
706 CPX252,36017,P,C,W
707 CPX254,36017,P,I,W
708 CPX255,36017,P,I,W
709 CPX256,36017,P,R,W
710 QUENCH,36017,W,DEFOCUSSED BEAM
711 QUENCH,36017,W,DEFOCUSSED BEAM
712 QUENCH,36017,W,DEFOCUSSED BEAM
713 SP120,36017,P,C,W
714 SP121,36017,P,C,W
715 SP122,36017,P,C,W

	716	717	718	719	720	721	722	723	724	725	726
SiO2	0.14	nd	0.12	0.18	38.49	38.02	38.14	37.85	38.12	38.12	38.00
TiO2	1.26	3.20	24.78	26.06	nd	nd	nd	nd	nd	nd	nd
Al2O3	39.80	34.50	3.45	2.95	nd	nd	nd	nd	nd	nd	nd
Fe2O3	10.22	13.21	18.90	13.83	nd	nd	nd	nd	nd	nd	nd
Cr2O3	16.89	15.78	0.23	0.26	nd	nd	nd	nd	nd	nd	nd
FeO	14.93	18.63	46.39	50.64	23.05	23.49	21.92	22.53	21.72	24.46	24.42
MnO	0.28	0.34	0.66	0.79	0.32	0.37	0.25	0.35	0.27	0.33	0.42
NiO	nd	nd	nd	nd	nd	0.09	0.15	0.13	0.20	0.09	0.09
MgO	15.72	13.74	4.96	2.40	38.71	38.04	39.83	38.71	39.57	37.57	37.27
CaO	nd	nd	nd	nd	0.15	0.22	0.15	0.26	0.09	0.18	0.27
total=	99.24	99.40	99.49	97.11	100.72	100.23	100.44	99.83	99.97	100.75	100.47
Mg#	65.2	56.8	-	-	75.0	74.3	76.4	75.4	76.5	73.2	73.1

716 SP123,36017,P,C,W
717 SP124,36017,P,C,W
718 MT212,36017,P,C,W
719 MT213,36017,P,R,W
720 OL4,MV718,P,C,+OL+CPX+SP+MT,E
721 OL416,MV718,P,C,W
722 OL417,MV718,P,C,W
723 OL418,MV718,P,C,W
724 OL419,MV718,P,C,W
725 OL420,MV718,P,C,W
726 OL421,MV718,P,R,W

	727	728	729	730	731	732	733	734	735	736	737
SiO2	38.28	48.40	42.85	42.68	46.82	48.32	44.09	48.86	47.58	47.75	51.34
TiO2	nd	2.27	4.78	4.82	3.03	2.46	4.01	2.19	3.51	3.42	0.56
Al2O3	nd	5.85	10.18	9.82	6.55	5.18	9.03	5.19	6.38	5.57	2.58
Cr2O3	nd	0.11	nd	0.03	0.06	0.02	0.12	0.23	nd	nd	0.40
FeO	24.89	7.74	8.29	8.43	8.06	7.46	8.05	7.34	7.44	7.41	10.12
MnO	0.25	0.15	0.11	0.13	0.09	0.13	0.12	0.14	nd	nd	0.30
MgO	37.46	13.81	10.79	10.88	12.71	13.45	11.43	13.85	12.63	12.96	12.93
CaO	0.20	22.14	22.41	22.42	21.91	22.03	22.39	21.37	22.04	22.52	22.37
Na2O	nd	0.57	0.49	0.52	0.45	0.53	0.43	0.67	0.96	0.72	0.50
total=	101.08	101.04	99.90	99.73	99.68	99.58	99.67	99.84	100.54	100.35	101.10
Mg#	72.8	85.6	78.7	80.5	79.6	82.2	79.8	82.9	82.3	82.5	75.3
Al ratio	-	0.1	0.2	0.1	0.2	0.1	0.2	0.2	0.1	0.1	0.1

727 OL6,MV718,P,C,E
728 CPX2,MV718,P,I,E
729 CPX3,MV718,P,R,E
730 CPX382,MV718,P,C,W
731 CPX383,MV718,P,C,W
732 CPX384,MV718,P,R,W
733 CPX385,MV718,P,C,W
734 CPX386,MV718,P,C,W
735 CPX4,MV718,GR,C,E
736 CPX5,MV718,GR,C,E
737 CPX6,MV718,P,C,E

	738	739	740	741	742	743	744	745	746	747	748
SiO2	43.62	0.18	nd	nd	nd	0.25	0.30	0.14	0.12	0.13	nd
TiO2	4.25	1.24	1.22	0.78	0.79	16.33	21.03	18.40	18.07	15.53	52.99
Al2O3	8.91	47.53	50.09	50.93	50.02	8.89	3.13	2.82	2.47	7.70	0.08
Fe2O3	nd	14.69	12.09	13.60	13.43	29.90	22.92	27.88	28.41	30.94	3.78
Cr2O3	0.29	3.42	3.45	1.91	1.78	0.35	4.37	1.71	0.91	0.35	0.15
FeO	8.40	22.10	20.20	20.67	20.39	40.89	44.47	44.30	46.85	40.19	35.99
MnO	0.22	0.19	0.28	0.34	0.08	0.31	0.50	0.55	0.65	0.32	0.58
MgO	11.83	12.39	13.51	13.07	12.95	4.85	4.57	2.19	0.13	4.06	6.21
CaO	22.49	nd	nd	nd	nd	nd	nd	nd	nd	nd	nd
Na2O	0.49	nd	nd	nd	nd	nd	nd	nd	nd	nd	nd
total=	100.50	101.74	100.84	101.30	99.44	101.77	101.29	97.99	97.61	99.22	99.78
Mg#	85.5	50.0	54.4	53.0	53.1	-	-	-	-	-	-

738 CPX7,MV718,P,R,E
739 SP1,MV718,P,C,E
740 SP2,MV718,P,C,E
741 SP3,MV718,P,C,E
742 SP305,MV718,P,C,W
743 MT1,MV718,P,C,E
744 MT3,MV718,P,C,E
745 MT345,MV718,P,C,W
746 MT346,MV718,P,C,W
747 MT347,MV718,P,C,W
748 IL328,MV718,P(MT),C,W

	749	750	751	752	753	754	755	756	757	758	759
SiO2	nd	37.87	37.60	38.88	38.53	38.63	37.94	38.16	37.95	38.76	37.82
TiO2	51.81	nd	0.04	0.02	0.03	nd	nd	nd	nd	nd	nd
Al2O3	0.08	nd	0.06	0.08	0.07	nd	nd	nd	nd	nd	nd
Fe2O3	5.00	nd	nd	nd	nd	nd	nd	nd	nd	nd	nd
Cr2O3	0.07	nd	0.02	0.01	0.01	nd	nd	nd	nd	nd	nd
FeO	36.89	24.09	23.65	20.68	22.20	23.41	25.56	22.79	24.75	20.79	29.29
MnO	0.55	0.32	0.37	0.29	0.26	0.28	0.32	0.41	0.42	0.28	0.46
NiO	nd	0.15	0.12	0.15	0.19	0.21	nd	nd	nd	0.21	0.14
MgO	5.13	36.99	38.53	40.88	39.73	38.06	36.61	39.03	36.62	40.82	33.49
CaO	nd	0.53	0.40	0.28	0.32	0.47	0.48	0.40	0.47	0.24	0.60
total=	99.53	99.95	100.79	101.27	101.34	101.06	100.91	100.79	100.21	101.10	101.80
Mg#	-	73.2	74.4	77.9	76.1	74.3	71.9	75.3	72.5	77.8	67.1

749 IL329,MV718,P(MT),C,W
750 OL1,MV703,P,C,+OL+CPX+SP,E
751 OL1,MV703,P,C,W
752 OL10,MV703,P,C,W
753 OL11,MV703,P,C,W
754 OL13,MV703,P,C,E
755 OL14,MV703,P,R,E
756 OL15,MV703,P,C,E
757 OL16,MV703,P,R,E
758 OL17,MV703,P,C,E
759 OL18,MV703,P,R,E

	760	761	762	763	764	765	766	767	768	769	770
SiO2	39.22	37.98	38.00	37.60	39.51	37.80	37.04	37.28	38.04	37.61	37.41
TiO2	nd	nd	0.03	nd	nd	nd	0.13	0.22	nd	0.08	nd
Al2O3	nd	nd	0.06	nd	nd	nd	nd	nd	nd	0.06	nd
Cr2O3	nd	nd	nd	nd	nd	nd	nd	nd	nd	0.01	nd
FeO	20.51	24.53	23.04	26.30	17.28	24.37	30.67	27.94	25.85	25.71	24.41
MnO	0.35	0.38	0.31	0.60	0.22	0.42	0.54	0.51	0.44	0.40	0.37
NiO	0.33	nd	0.11	0.18	0.25	nd	nd	nd	nd	0.09	nd
MgO	40.65	37.06	39.02	35.94	42.86	36.92	32.14	34.34	36.28	36.69	36.90
CaO	0.24	0.55	0.34	0.46	0.29	0.56	0.50	0.57	0.60	0.56	0.56
total=	101.30	100.50	100.91	101.08	100.41	100.07	101.02	100.86	101.21	101.21	99.65
Mg#	77.9	72.9	75.1	70.9	81.6	73.0	65.1	68.7	71.4	71.8	72.9

760 OL19,MV703,P,C,E
761 OL2,MV703,P,C,E
762 OL2,MV703,P,I,W
763 OL20,MV703,P,R,E
764 OL21,MV703,P,C,E
765 OL22,MV703,P,R,E
766 OL23,MV703,GR,C,E
767 OL24,MV703,GR,C,E
768 OL3,MV703,P,C,E
769 OL3,MV703,P,R,W
770 OL4,MV703,P,C,E

	771	772	773	774	775	776	777	778	779	780	781
SiO2	37.89	38.19	37.73	37.95	36.93	39.18	38.30	39.31	38.23	52.18	49.47
TiO2	0.04	nd	0.04	nd	0.03	0.02	nd	0.02	0.04	0.11	0.18
Al2O3	0.05	nd	0.07	nd	0.08	0.07	nd	0.06	0.07	28.98	31.23
Cr2O3	0.03	nd	0.01	nd	0.01	0.01	nd	0.01	0.02	nd	nd
FeO	18.27	27.85	19.16	25.57	23.14	18.64	23.79	18.91	23.58	0.68	0.66
MnO	0.24	0.48	0.26	0.45	0.34	0.23	0.36	0.24	0.33	nd	nd
NiO	0.17	nd	0.15	nd	0.14	0.20	nd	0.18	0.11	nd	nd
MgO	42.41	34.71	41.74	36.05	38.35	42.12	37.45	41.96	38.61	nd	nd
CaO	0.27	0.61	0.28	0.49	0.43	0.34	0.57	0.21	0.41	12.49	14.82
Na2O	nd	nd	nd	nd	nd	nd	nd	nd	nd	4.23	2.41
K2O	nd	nd	nd	nd	nd	nd	nd	nd	nd	0.33	0.22
total=	99.37	101.84	99.44	100.51	99.45	100.81	100.47	100.90	101.40	99.00	98.99
Mg#	80.5	69.0	79.5	71.5	74.7	80.1	73.7	79.8	74.5	-	-
An	-	-	-	-	-	-	-	-	-	60.8	76.2

771 OL4,MV703,P,C,W
772 OL5,MV703,P,C,E
773 OL5,MV703,P,I,W
774 OL6,MV703,P,C,E
775 OL6,MV703,P,R,W
776 OL7,MV703,P,C,W
777 OL8,MV703,P,R,E
778 OL8,MV703,P,C,W
779 OL9,MV703,P,I,W
780 PL1,MV703,GR,C,E
781 PL3,MV703,GR,C,E

	782	783	784	785	786	787	788	789	790	791	792
SiO2	52.32	46.32	47.95	52.95	48.54	46.25	48.36	48.54	49.24	51.75	49.92
TiO2	0.61	2.58	2.40	0.28	1.72	3.77	1.80	1.87	1.74	0.91	1.05
Al2O3	1.14	6.82	4.72	0.82	5.81	6.03	5.72	4.78	4.54	2.40	4.12
Cr2O3	0.41	0.67	nd	0.70	0.26	0.01	0.26	0.48	0.44	0.83	0.38
FeO	6.08	7.40	7.55	5.78	6.66	9.12	6.80	6.88	6.86	6.32	6.34
MnO	0.21	0.19	nd	0.17	0.15	0.17	0.12	nd	nd	nd	0.15
NiO	nd	nd	nd	nd	0.01	nd	nd	nd	0.03	nd	nd
MgO	15.96	12.47	13.38	17.09	13.90	11.45	13.47	13.68	13.69	15.55	14.88
CaO	21.81	22.26	22.18	20.95	22.12	21.82	22.32	22.48	22.56	22.01	21.44
Na2O	nd	nd	nd	nd	0.33	0.61	0.32	0.39	0.39	nd	nd
K2O	nd	nd	nd	nd	nd	0.01	nd	nd	nd	nd	nd
total=	98.54	98.71	98.18	98.74	99.50	99.24	99.17	99.10	99.49	99.77	98.28
Mg#	82.4	76.6	76.7	84.0	83.8	73.7	82.1	83.7	82.1	81.4	80.7
Al ratio	0.1	0.2	0.2	0.1	0.3	0.1	0.3	0.1	0.2	0.2	0.5

782 CPX1,MV703,P,C,E
783 CPX12,MV703,P,R,E
784 CPX14,MV703,GR,C,E
785 CPX2,MV703,P,C,E
786 CPX24,MV703,P,C,W
787 CPX25,MV703,P,R,W
788 CPX26,MV703,P,C,W
789 CPX27,MV703,P,I,W
790 CPX29,MV703,P,I,W
791 CPX3,MV703,P,C,E
792 CPX8,MV703,P,C,E

	793	794	795	796	797	798	799	800	801	802	803
SiO2	49.68	0.18	nd	0.38	0.33	0.36	nd	65.15	37.00	37.03	38.35
TiO2	1.29	1.44	1.37	27.62	27.49	50.59	51.31	nd	6.06	6.99	0.52
Al2O3	4.46	28.01	29.50	2.92	2.88	nd	0.29	19.97	13.80	13.59	13.83
Fe2O3	nd	19.15	18.45	10.76	11.47	3.32	3.15	nd	nd	nd	nd
Cr2O3	0.36	17.37	17.79	0.15	nd	nd	nd	nd	nd	nd	nd
FeO	6.56	22.58	22.58	54.74	53.78	41.77	42.10	nd	17.01	17.83	16.07
MnO	nd	0.33	0.15	0.95	1.04	0.84	1.12	nd	0.13	0.19	0.15
NiO	nd	0.13	nd	nd	nd	nd	nd	nd	nd	nd	nd
MgO	15.02	9.28	9.67	1.04	1.45	1.85	1.63	nd	13.23	12.01	17.07
CaO	21.19	nd	nd	nd	nd	nd	nd	0.77	nd	nd	nd
Na2O	nd	nd	nd	nd	nd	nd	nd	4.65	0.83	0.51	0.22
K2O	nd	nd	nd	nd	nd	nd	nd	9.09	9.06	9.09	9.77
BaO	nd	nd	nd	nd	nd	nd	nd	1.13	nd	nd	nd
total=	98.56	98.47	99.51	98.56	98.44	98.73	99.60	100.76	97.12	97.24	95.98
Mg#	80.3	42.3	43.3	-	-	-	-	-	-	-	-
Al ratio	0.4	-	-	-	-	-	-	-	-	-	-

793 CPX9,MV703,P,C,E
794 SP1,MV703,P,C,W
795 SP3,MV703,P,C,E
796 MT1,MV703,GR,C,E
797 MT2,MV703,GR,C,E
798 IL1,MV703,GR,C,E
799 IL2,MV703,GR,C,E
800 AF1,MV520,GR,C,+OL+CPX+PL+MT,E
801 BI1,MV520,GR,C,E
802 BI2,MV520,GR,C,E
803 BI3,MV520,GR,C,E

	804	805	806	807	808	809	810	811	812	813	814
SiO2	37.86	38.10	37.92	37.31	37.36	36.44	35.53	38.21	38.31	38.20	38.22
Al2O3	nd	0.08	0.06	0.08	nd	0.08	nd	0.07	0.08	0.08	0.09
FeO	27.53	24.19	26.24	26.09	28.02	31.88	35.79	23.70	24.07	23.26	23.75
MnO	0.62	0.47	0.50	0.56	0.55	0.66	0.86	0.45	0.52	0.45	0.49
NiO	nd	0.09	0.12	0.09	0.08	0.08	0.09	nd	0.12	0.08	nd
MgO	34.36	36.94	35.35	35.00	33.85	30.31	27.15	37.19	36.63	37.69	37.17
CaO	0.50	0.50	0.47	0.49	0.46	0.54	0.55	0.46	0.45	0.41	0.49
total=	100.87	100.37	100.66	99.62	100.32	99.99	99.97	100.08	100.18	100.17	100.21
Mg#	69.0	73.1	70.6	70.5	68.3	62.9	57.5	73.7	73.1	74.3	73.6

804 OL11,MV520,P,C,E
805 OL162,MV520,P,C,W
806 OL163,MV520,P,I,W
807 OL164,MV520,P,I,W
808 OL165,MV520,P,I,W
809 OL166,MV520,P,R,W
810 OL167,MV520,P,R,W
811 OL168,MV520,P,C,W
812 OL169,MV520,P,R,W
813 OL170,MV520,P,C,W
814 OL171,MV520,P,R,W

	815	816	817	818	819	820	821	822	823	824	825
SiO2	35.68	35.49	38.36	38.76	47.70	47.99	47.73	51.30	45.91	48.73	49.50
TiO2	nd	nd	nd	nd	2.40	2.48	2.09	1.12	3.69	2.40	1.71
Al2O3	nd	nd	nd	nd	6.60	6.58	6.52	2.39	8.47	4.51	4.17
Cr2O3	nd	nd	nd	nd	0.18	0.14	0.28	nd	0.20	nd	nd
FeO	39.25	40.88	23.23	23.73	7.99	7.49	7.17	9.86	8.10	9.96	8.15
MnO	0.82	0.89	0.41	0.42	nd	nd	nd	0.23	0.12	0.24	0.16
NiO	0.17	nd	nd	nd	nd	nd	nd	nd	nd	nd	nd
MgO	25.07	23.91	38.28	38.39	12.27	12.63	13.21	12.03	11.20	10.86	12.30
CaO	0.59	0.53	0.43	0.54	22.80	22.66	22.61	22.82	22.85	22.56	23.13
Na2O	nd	nd	nd	nd	0.41	0.33	0.27	0.61	0.34	0.60	0.51
total=	101.58	101.70	100.71	101.84	100.35	100.30	99.88	100.36	100.88	99.86	99.63
Mg#	53.2	51.0	74.6	74.2	77.9	77.5	81.9	71.3	73.3	67.9	76.7
Al ratio	-	-	-	-	0.3	0.3	0.3	0.3	0.3	0.3	0.3

815 OL5,MV520,P,R,E
816 OL8,MV520,P,R,E
817 OLHG1,MV520,P,C,E
818 OLHG10,MV520,P,R,E
819 CPX10,MV520,P,I,E
820 CPX11,MV520,P,I,E
821 CPX12,MV520,P,I,E
822 CPX13,MV520,P,R,E
823 CPX14,MV520,P,I,E
824 CPX15,MV520,GR,C,E
825 CPX16,MV520,GR,C,E

	826	827	828	829	830	831	832	833	834	835	836
SiO2	47.48	48.15	50.56	47.65	44.43	45.79	43.50	46.78	43.66	47.24	43.29
TiO2	2.34	2.38	0.67	2.80	3.14	2.43	3.91	2.05	3.39	2.17	3.55
Al2O3	7.06	5.81	1.83	6.62	10.05	9.05	9.43	7.40	9.59	6.43	10.56
Cr2O3	0.14	0.13	0.20	nd	0.08	0.04	0.03	0.07	0.08	0.11	0.06
FeO	8.04	7.91	14.52	7.66	7.51	7.53	8.03	7.63	8.01	7.38	8.23
MnO	0.11	nd	0.33	nd	0.12	0.16	0.13	0.13	0.14	0.11	0.12
MgO	11.91	12.18	8.97	12.28	11.37	12.00	10.91	12.15	11.01	12.50	10.49
CaO	22.01	22.79	22.85	23.00	22.23	21.59	22.43	21.70	22.15	22.49	21.68
Na2O	0.29	0.54	0.68	0.47	0.63	0.77	0.57	0.72	0.58	0.54	0.66
total=	99.38	99.89	100.61	100.48	99.56	99.36	98.94	98.63	98.61	98.97	98.64
Mg#	72.6	77.5	56.5	78.6	83.0	83.7	81.0	81.7	81.6	82.5	77.9
Al ratio	0.5	0.3	0.1	0.2	0.3	0.4	0.2	0.4	0.2	0.3	0.3

826 CPX17R,MV520,P,C,E
827 CPX18,MV520,P,R,E
828 CPX8,MV520,P,R,E
829 CPX9,MV520,P,R,E
830 CPXDARK100,MV520,P,C,W
831 CPXLIGHT101,MV520,P,C,W
832 CPXDARK102,MV520,P,C,W
833 CPXLIGHT103,MV520,P,C,W
834 CPXDARK104,MV520,P,C,W
835 CPXLIGHT105,MV520,P,C,W
836 CPXDARK106,MV520,P,I,W

	837	838	839	840	841	842	843	844	845	846	847
SiO2	47.56	44.84	47.70	43.32	47.08	44.25	46.04	45.02	47.56	45.12	47.86
TiO2	2.06	3.04	2.18	3.72	2.18	3.56	2.89	3.12	2.44	3.10	2.40
Al2O3	6.96	9.16	6.57	10.66	7.48	9.52	7.86	8.81	6.28	9.00	6.00
Cr2O3	0.07	0.22	0.19	0.14	0.12	0.13	0.20	0.13	0.07	0.07	0.01
FeO	7.60	7.53	7.04	7.94	7.39	7.73	7.48	7.87	7.85	8.16	7.91
MnO	0.14	0.11	0.12	0.12	0.14	0.13	0.13	0.12	0.14	0.13	0.16
MgO	12.59	11.40	12.82	10.74	12.59	11.11	12.00	11.35	12.34	11.03	12.27
CaO	21.76	22.37	22.32	21.84	21.56	22.56	22.30	22.36	22.12	21.87	22.07
Na2O	0.66	0.52	0.54	0.64	0.60	0.55	0.53	0.58	0.53	0.68	0.61
total=	99.40	99.19	99.48	99.12	99.14	99.54	99.43	99.36	99.33	99.16	99.29
Mg#	81.2	80.7	82.3	79.5	81.0	80.7	80.7	80.3	78.2	77.3	77.8
Al ratio	0.4	0.3	0.3	0.3	0.4	0.2	0.3	0.3	0.3	0.3	0.3

837 CPXLIGHT107,MV520,P,I,W
838 CPXDARK108,MV520,P,I,W
839 CPXLIGHT109,MV520,P,I,W
840 CPXDARK110,MV520,P,I,W
841 CPXLIGHT111,MV520,P,I,W
842 CPXDARK112,MV520,P,I,W
843 CPXLIGHT113,MV520,P,I,W
844 CPXDARK114,MV520,P,I,W
845 CPXLIGHT115,MV520,P,I,W
846 CPXDARK116,MV520,P,R,W
847 CPXLIGHT117,MV520,P,R,W

	848	849	850	851	852	853	854	855	856	857	858
SiO2	47.13	48.50	51.16	44.26	46.14	45.16	47.81	48.89	46.70	44.54	44.13
TiO2	2.64	2.20	1.16	3.10	2.42	3.06	2.32	2.01	2.50	3.42	3.74
Al2O3	6.45	5.43	2.39	9.02	7.47	8.05	5.74	5.03	7.10	9.04	9.55
Cr2O3	0.02	0.03	nd	0.16	nd	0.11	0.03	0.02	0.03	0.14	nd
FeO	8.07	7.79	9.56	7.59	7.49	7.82	7.82	7.91	7.92	7.77	8.00
MnO	0.17	0.17	0.21	0.12	0.15	0.14	0.15	0.16	0.12	0.13	0.14
MgO	11.32	12.11	12.18	11.45	12.21	11.55	12.54	12.13	11.87	11.37	10.87
CaO	22.56	22.71	22.30	22.53	22.42	22.27	22.19	22.64	22.16	22.53	22.17
Na2O	0.71	0.64	0.78	0.57	0.52	0.55	0.55	0.65	0.63	0.54	0.59
total=	99.07	99.58	99.74	98.80	98.82	98.71	99.15	99.44	99.03	99.48	99.19
Mg#	76.5	77.8	72.8	84.7	83.5	80.6	79.5	77.0	79.4	81.6	78.0
Al ratio	0.3	0.3	0.3	0.2	0.2	0.2	0.2	0.3	0.3	0.2	0.3

848 CPXDARK118,MV520,P,R,W
849 CPXLIGHT119,MV520,P,R,W
850 CPX120,MV520,P,R,W
851 CPX121,MV520,P,I,W
852 CPX122,MV520,P,I,W
853 CPX123,MV520,P,C,W
854 CPX125,MV520,P,I,W
855 CPX126,MV520,P,R,W
856 CPX127,MV520,P,C,W
857 CPX128,MV520,P,I,W
858 CPX129,MV520,P,I,W

	859	860	861	862	863	864	865	866	867	868	869
SiO2	46.83	47.76	43.70	44.79	42.17	43.18	46.14	44.88	47.04	44.69	46.91
TiO2	2.95	2.16	3.45	3.27	4.50	3.97	2.78	3.73	2.28	3.20	2.27
Al2O3	6.96	6.08	10.26	8.63	11.33	10.25	8.41	8.11	6.64	8.88	7.02
Cr2O3	nd	0.15	0.15	0.08	0.07	0.15	0.19	nd	nd	0.16	0.05
FeO	8.31	6.97	7.48	7.35	8.45	8.01	6.82	8.07	7.30	7.58	7.65
MnO	0.18	0.16	0.12	0.14	0.14	0.16	0.13	0.18	0.12	0.12	0.13
MgO	11.13	13.00	11.10	11.57	10.10	10.70	11.78	10.85	12.63	11.62	12.56
CaO	22.46	22.44	22.48	22.61	21.92	22.12	22.28	22.26	22.45	22.49	22.07
Na2O	0.76	0.49	0.58	0.58	0.69	0.64	0.63	0.67	0.51	0.52	0.59
total=	99.58	99.21	99.32	99.02	99.37	99.18	99.16	98.75	98.97	99.26	99.25
Mg#	75.8	83.1	83.3	83.5	78.1	80.4	80.5	76.7	83.2	82.9	82.9
Al ratio	0.3	0.2	0.3	0.2	0.2	0.2	0.4	0.2	0.2	0.2	0.3

859 CPX130,MV520,P,R,W
860 CPX131,MV520,P,C,W
861 CPX132,MV520,P,I,W
862 CPX133,MV520,P,I,W
863 CPX134,MV520,P,I,W
864 CPX135,MV520,P,I,W
865 CPX136,MV520,P,I,W
866 CPX137,MV520,P,R,W
867 CPX138,MV520,P,I,W
868 CPX139,MV520,P,I,W
869 CPX140,MV520,P,C,W

	870	871	872	873	874	875	876	877	878	879	880
SiO2	47.40	42.17	45.95	45.01	44.57	47.41	47.00	48.00	47.04	47.05	0.33
TiO2	2.36	4.40	2.54	3.28	3.17	2.70	2.90	2.30	2.63	2.14	19.88
Al2O3	6.58	11.19	8.44	9.88	10.13	6.39	6.97	6.75	6.98	7.39	1.91
Fe2O3	nd	nd	nd	nd	nd	nd	nd	nd	nd	nd	26.51
Cr2O3	0.07	0.07	nd	nd	0.27	0.18	0.22	0.17	0.32	0.22	0.14
FeO	7.64	8.31	7.38	8.01	8.06	7.61	7.92	7.53	7.50	7.60	47.80
MnO	0.14	0.13	0.14	0.16	0.15	0.15	nd	0.20	nd	nd	0.68
MgO	12.44	10.08	12.00	11.20	11.23	12.59	12.00	12.67	12.50	12.55	0.78
CaO	22.28	22.06	22.34	22.47	22.53	23.11	23.30	22.41	22.96	22.47	nd
Na2O	0.55	0.71	0.69	0.54	0.74	0.43	0.54	0.32	0.39	0.43	nd
total=	99.46	99.12	99.48	100.55	100.85	100.57	100.85	100.35	100.32	99.85	98.03
Mg#	80.4	79.2	84.6	78.8	84.5	82.0	80.8	77.7	81.3	81.6	-
Al ratio	0.3	0.2	0.3	0.3	0.2	0.1	0.2	0.3	0.2	0.3	-

870 CPX141,MV520,P,I,W
871 CPX142,MV520,P,I,W
872 CPXDARKOL30,MV520,P,R,W
873 CPXHG1,MV520,P,C,E
874 CPXHG2,MV520,P,C,E
875 CPXHG3,MV520,P,R,E
876 CPXHG4,MV520,P,R,E
877 CPXHG5,MV520,P,C,E
878 CPXHG6,MV520,P,C,E
879 CPXHG7,MV520,P,C,E
880 MT2,MV520,GR,C,E

	881	882	883	884	885	886	887	888	889	890	891
SiO2	0.32	0.27	0.35	0.40	0.36	0.28	39.13	39.23	39.66	39.61	38.26
TiO2	18.97	17.77	17.68	18.08	51.19	49.83	nd	nd	nd	nd	nd
Al2O3	1.95	7.10	6.99	8.55	nd	0.19	nd	nd	nd	nd	nd
Fe2O3	28.28	24.29	23.83	23.21	3.26	4.95	nd	nd	nd	nd	nd
Cr2O3	0.26	2.71	3.15	1.73	nd	nd	nd	nd	nd	nd	nd
FeO	46.78	43.60	43.06	39.66	41.59	39.81	18.08	15.88	15.29	14.63	21.69
MnO	0.97	0.56	0.41	0.43	1.04	1.08	0.26	0.18	0.16	0.15	0.45
NiO	nd	nd	nd	nd	nd	nd	0.15	0.20	0.22	0.20	0.09
MgO	0.65	3.17	3.53	5.48	2.14	2.38	42.43	44.19	44.65	45.16	39.15
CaO	0.14	nd	nd	0.70	nd	nd	0.23	0.22	0.17	0.22	0.36
total=	98.32	99.47	99.00	98.24	99.58	98.52	100.28	99.90	100.15	99.97	100.00
Mg#	-	-	-	-	-	-	80.7	83.2	83.9	84.6	76.3

881 MT3,MV520,GR,C,E
882 MTSP4,MV520,P,C,E
883 MTSP5,MV520,P,C,E
884 MTSP6,MV520,P,C,E
885 IL1,MV520,GR,C,E
886 IL2,MV520,GR,C,E
887 OL434,MV178,P,C,+OL+CPX+SP,W
888 OL435,MV178,P,C,W
889 OL436,MV178,P,C,W
890 OL437,MV178,P,C,W
891 OL438,MV178,P,R,W

	892	893	894	895	896	897	898	899	900	901	902
SiO2	39.00	40.00	39.32	39.82	40.29	45.26	45.16	54.94	46.68	44.19	47.25
TiO2	nd	nd	nd	nd	nd	nd	nd	0.35	2.66	3.73	2.08
Al2O3	nd	nd	nd	nd	nd	35.08	35.51	27.64	7.03	8.82	6.18
Cr2O3	nd	nd	nd	nd	nd	nd	nd	nd	0.73	0.37	0.34
FeO	19.54	14.72	20.82	16.01	14.39	0.14	0.27	0.88	7.32	7.91	6.78
MnO	0.16	0.19	0.50	0.20	0.16	nd	nd	nd	nd	0.12	0.07
NiO	0.23	0.17	0.14	0.21	0.21	nd	nd	nd	nd	nd	nd
MgO	41.55	44.90	40.18	44.66	45.29	nd	nd	nd	13.07	12.04	13.50
CaO	0.17	0.21	0.32	0.13	0.26	18.52	18.98	10.46	22.00	21.42	21.62
Na2O	nd	nd	nd	nd	nd	1.23	1.00	5.17	0.39	0.58	0.53
K2O	nd	nd	nd	nd	nd	0.12	nd	0.44	nd	nd	nd
total=	100.65	100.19	101.28	101.03	100.60	100.35	100.92	99.88	99.88	99.18	98.35
Mg#	79.1	84.5	77.5	83.3	84.9	-	-	-	82.6	82.7	85.5
An	-	-	-	-	-	88.7	91.3	51.4	-	-	-
Al ratio	-	-	-	-	-	-	-	-	0.2	0.2	0.2

892 OL439,MV178,P,C,W
893 OL5,MV178,P,C,E
894 OL6,MV178,P,R,E
895 OL7,MV178,P,C,E
896 OL9,MV178,P,C,E
897 PL2,MV178,P?,C,E
898 PL3,MV178,P?,C,E
899 PL4,MV178,P?,R,E
900 CPX10,MV178,P,C,E
901 CPX306,MV178,P,C,W
902 CPX307,MV178,P,R,W

	903	904	905	906	907	908	909	910	911	912	913
SiO2	nd	nd	nd	0.50	0.23	0.20	38.20	37.94	37.44	38.20	38.23
TiO2	0.13	0.15	0.24	21.53	16.50	21.20	nd	nd	nd	nd	nd
Al2O3	60.03	59.26	59.88	1.41	3.70	2.16	nd	nd	nd	nd	nd
Fe2O3	1.75	2.99	1.37	21.52	30.10	28.18	nd	nd	nd	nd	nd
Cr2O3	8.62	8.44	8.55	0.58	6.21	0.21	nd	nd	nd	nd	nd
FeO	9.24	8.53	9.45	49.04	37.50	42.12	23.85	25.73	28.89	24.58	23.68
MnO	nd	nd	nd	1.24	0.51	0.75	0.31	0.29	0.50	0.38	0.33
NiO	nd	nd	nd	nd	nd	nd	0.21	0.24	0.17	0.20	0.13
MgO	21.41	21.79	21.23	0.32	6.22	5.43	38.25	36.48	33.72	37.13	37.33
CaO	nd	nd	nd	nd	0.16	0.27	0.22	0.41	0.35	0.34	0.30
total=	101.18	101.16	100.72	96.14	101.13	100.52	101.04	101.09	101.07	100.83	100.00
Mg#	80.5	82.0	80.0	-	22.8	-	74.1	71.6	67.5	72.9	73.7

903 SP7,MV178,P,C,E
904 SP8,MV178,P,I,E
905 SP9,MV178,P,R,E
906 MT308,MV178,GR,C,W
907 SPMT8,MV178,P,R,E
908 MT9,MV178,GR,C,E
909 OL1,MV114,P,C,+OL+CPX+SP,E
910 OL10,MV114,P,R,E
911 OL17,MV114,GR,C,E
912 OL334,MV114,P,C,W
913 OL335,MV114,P,C,W

	914	915	916	917	918	919	920	921	922	923	924
SiO2	37.99	37.75	38.18	38.83	38.30	38.57	53.42	56.89	52.33	52.38	52.59
TiO2	nd	nd	nd	nd	nd	nd	0.19	0.24	0.20	nd	0.13
Al2O3	nd	nd	nd	nd	nd	nd	28.55	25.71	29.73	29.66	29.47
FeO	23.92	25.86	24.65	20.72	23.69	24.32	0.59	0.60	0.53	0.62	0.53
MnO	0.35	0.36	0.36	0.29	0.35	0.32	nd	nd	nd	nd	nd
NiO	0.17	0.17	0.15	0.24	0.18	nd	nd	nd	nd	nd	nd
MgO	37.40	36.03	36.96	40.24	37.43	37.05	nd	nd	nd	nd	nd
CaO	0.28	0.41	0.37	0.22	0.26	0.39	11.50	8.43	12.33	12.58	12.78
Na2O	nd	nd	nd	nd	nd	nd	4.71	6.12	3.81	3.81	3.98
K2O	nd	nd	nd	nd	nd	nd	0.37	0.84	0.39	0.36	0.33
total=	100.11	100.58	100.67	100.54	100.21	100.65	99.33	98.83	99.32	99.41	99.81
Mg#	73.6	71.3	72.8	77.6	73.8	73.1	-	-	-	-	-
An	-	-	-	-	-	-	56.2	41.1	62.6	63.2	62.7

914 OL336,MV114,P,I,W
915 OL337,MV114,P,R,W
916 OL338,MV114,P,C,W
917 OL339,MV114,P,C,W
918 OL340,MV114,P,C,W
919 OL7,MV114,P,I,E
920 PL32,MV114,GR,C,E
921 PL33,MV114,GR,C,E
922 PL34,MV114,GR,C,E
923 PL36,MV114,GR,C,E
924 PL37,MV114,GR,R,E

	925	926	927	928	929	930	931	932	933	934	935
SiO2	55.96	48.73	50.46	49.49	49.89	49.00	49.05	50.93	50.04	50.29	50.48
TiO2	0.24	2.51	1.51	1.73	1.44	1.84	2.47	1.49	1.60	1.67	1.24
Al2O3	26.57	3.75	2.58	3.78	2.99	2.71	4.36	2.04	3.36	3.19	1.53
Cr2O3	nd	0.15	0.65	0.59	0.99	nd	0.42	nd	0.61	0.65	nd
FeO	0.67	8.69	7.14	7.27	6.82	13.08	7.44	9.21	7.35	7.32	11.77
MnO	nd	0.25	0.12	0.12	0.21	0.19	0.16	0.20	0.12	0.14	0.29
NiO	nd	nd	nd	nd	nd	nd	nd	nd	0.16	0.17	nd
MgO	nd	13.77	15.42	14.39	15.03	11.44	13.85	15.25	14.35	15.00	13.15
CaO	9.41	20.93	21.09	21.45	21.66	20.52	22.29	20.17	21.62	21.67	20.39
Na2O	5.15	nd	nd	nd	nd	nd	nd	nd	nd	nd	nd
K2O	0.69	nd	nd	nd	nd	nd	nd	nd	nd	nd	nd
total=	98.69	98.78	98.97	98.82	99.03	98.78	100.04	99.29	99.21	100.10	98.85
Mg#	-	73.8	79.5	77.9	81.2	60.9	76.8	75.1	77.7	79.6	66.8
An	48.1	-	-	-	-	-	-	-	-	-	-
Al ratio	-	0.1	-	0.2	-	0.1	0.1	-	0.2	-	-

925 PL39,MV114,GR,R,E
926 CPX21,MV114,GR,C,E
927 CPX22,MV114,GR,C,E
928 CPX23,MV114,P,C,E
929 CPX24,MV114,P,I,E
930 CPX25,MV114,P,R,E
931 CPX26,MV114,P,I,E
932 CPX27,MV114,P,R,E
933 CPX28,MV114,P,C,E
934 CPX29,MV114,P,I,E
935 CPX30,MV114,P,R,E

	936	937	938	939	940	941	942	943	944	945	946
SiO2	49.89	50.57	48.56	49.51	50.16	50.11	49.87	49.88	nd	0.26	0.18
TiO2	1.69	0.97	2.44	1.95	1.55	1.43	1.75	1.47	22.92	10.64	12.99
Al2O3	3.35	2.66	3.51	3.59	3.13	2.92	3.15	2.70	6.06	11.03	9.10
Fe2O3	nd	nd	nd	nd	nd	nd	nd	nd	15.10	17.14	17.78
Cr2O3	0.55	0.08	0.03	0.33	0.64	0.61	0.33	nd	4.55	20.81	18.00
FeO	7.37	8.67	10.93	7.29	7.10	7.11	8.14	13.38	44.66	32.74	34.78
MnO	0.12	0.24	0.22	0.14	0.13	0.14	0.20	0.22	0.36	0.25	0.20
MgO	14.63	14.39	12.61	14.41	14.98	15.00	14.64	11.66	5.28	6.78	6.58
CaO	21.77	21.04	20.77	21.53	21.50	21.20	21.53	20.81	nd	nd	nd
Na2O	nd	0.40	0.46	0.39	0.37	0.39	nd	nd	nd	nd	nd
total=	99.37	99.02	99.53	99.14	99.56	98.91	99.61	100.12	98.93	99.65	99.61
Mg#	78.6	79.4	71.8	81.7	83.5	83.3	78.1	61.0	17.4	27.0	25.2
Al ratio	0.1	0.1	-	0.1	-	-	-	0.2	-	-	-

936 CPX31,MV114,P,C,E
937 CPX315,MV114,P,C,W
938 CPX316,MV114,P,R,W
939 CPX317,MV114,P,I,W
940 CPX318,MV114,P,C,W
941 CPX319,MV114,P,C,W
942 CPX33,MV114,P,I,E
943 CPX34,MV114,P,R,E
944 SPMT005,MV114,P,C,E
945 SP1,MV114,P,C,E
946 SP2,MV114,P,C,E

	947	948	949	950	951	952	953	954	955	956	957
SiO2	0.30	0.36	0.27	0.32	nd	0.48	0.52	0.40	0.08	0.07	0.04
TiO2	3.02	10.49	11.25	11.25	22.92	26.00	26.32	25.46	50.26	49.41	50.31
Al2O3	19.34	10.16	9.20	9.78	6.05	0.54	0.34	0.61	0.05	0.07	0.03
Fe2O3	15.98	17.10	16.87	16.09	15.06	14.98	14.74	15.71	3.44	5.71	4.79
Cr2O3	27.78	20.29	20.99	20.96	4.68	0.02	0.01	0.03	nd	0.01	0.02
FeO	25.47	33.23	33.61	34.29	44.69	52.22	52.07	51.58	43.70	42.46	43.21
MnO	nd	nd	nd	0.32	0.35	2.48	3.06	2.31	0.67	0.64	0.66
MgO	8.21	6.14	6.32	5.85	5.29	0.17	0.16	0.19	0.51	0.79	0.79
total=	100.10	97.77	98.51	98.86	99.04	96.89	97.22	96.29	98.71	99.16	99.85
Mg#	36.5	24.8	25.1	23.3	17.4	-	-	-	-	-	-

947 SP3,MV114,P,C,E
948 SP4,MV114,P,C,E
949 SP6,MV114,P,C,E
950 SP7,MV114,P,C,E
951 SPMT2,MV114,P,C,E
952 MT320,MV114,GR,C,W
953 MT322,MV114,GR,C,W
954 MT323,MV114,GR,C,W
955 IL308R,MV114,GR,C,W
956 IL309,MV114,GR,C,W
957 IL310,MV114,GR,C,W

	958	959	960	961	962	963	964	965	966	967	968
SiO2	0.02	0.28	37.90	38.18	37.63	37.65	37.55	37.78	37.70	37.63	47.02
TiO2	50.87	48.57	nd	nd	nd	nd	nd	nd	nd	nd	nd
Al2O3	0.03	nd	nd	nd	nd	nd	nd	nd	nd	nd	32.37
Fe2O3	3.61	7.06	nd	nd	nd	nd	nd	nd	nd	nd	nd
FeO	43.11	41.95	25.89	25.79	25.98	25.11	26.32	26.75	25.22	26.10	0.44
MnO	0.64	0.66	0.40	0.56	0.40	0.44	0.47	0.49	0.38	0.46	nd
NiO	nd	nd	0.16	nd	0.06	0.11	0.08	0.09	nd	0.09	nd
MgO	1.13	0.78	36.61	36.33	36.28	36.72	35.84	35.75	36.78	36.10	nd
CaO	nd	nd	0.24	0.29	0.25	0.25	0.35	0.34	0.21	0.36	1.25
Na2O	nd	nd	nd	nd	nd	nd	nd	nd	nd	nd	15.03
K2O	nd	nd	nd	nd	nd	nd	nd	nd	nd	nd	3.65
total=	99.41	99.30	101.20	101.15	100.60	100.28	100.61	101.20	100.29	100.74	99.76
Mg#	-	-	71.6	71.5	71.3	72.3	70.8	70.4	72.2	71.1	-

958 IL311,MV114,GR,C,W
959 IL6,MV114,GR,C,E
960 OL2,MV716,P,C,+OL+CPX+SP+MT,E
961 OL3,MV716,P,I,E
962 OL410,MV716,P,C,W
963 OL411,MV716,P,C,W
964 OL412,MV716,P,R,W
965 OL413,MV716,P,C,W
966 OL414,MV716,P,C,W
967 OL415,MV716,P,C,W
968 NE1,MV716,P?,C,E,PL/NE composite

	969	970	971	972	973	974	975	976	977	978	979
SiO2	46.49	47.02	53.51	54.12	54.12	52.87	46.46	48.36	52.37	46.97	47.75
TiO2	0.03	nd	nd	0.13	nd	0.45	3.70	1.90	0.27	2.09	2.77
Al2O3	33.30	32.37	28.77	28.64	27.75	1.70	6.55	5.31	1.34	7.11	5.11
Cr2O3	nd	nd	nd	nd	nd	nd	0.13	0.03	0.01	nd	0.01
FeO	0.40	0.44	0.46	0.28	0.95	10.21	7.57	7.75	9.67	7.94	7.25
MnO	nd	nd	nd	nd	nd	0.33	nd	0.15	0.33	0.15	0.16
MgO	0.02	nd	nd	nd	nd	13.73	12.35	13.92	14.17	12.28	12.90
CaO	1.26	1.25	11.42	10.94	10.71	20.74	22.60	21.51	20.68	21.69	22.37
Na2O	15.55	15.03	4.76	4.86	5.05	0.51	0.31	0.55	0.69	0.64	0.73
K2O	3.45	3.65	0.35	0.31	0.37	nd	nd	nd	nd	nd	nd
V2O3	nd	nd	nd	nd	0.48	nd	nd	nd	nd	nd	nd
total=	100.50	99.76	99.27	99.28	99.43	100.54	99.67	99.48	99.53	98.87	99.05
Mg#	8.2	-	-	-	-	71.2	77.3	84.7	76.9	80.7	84.0
An	-	-	55.8	54.4	52.8	-	-	-	-	-	-
Al ratio	-	-	-	-	-	1.0	0.1	0.2	0.3	0.3	0.1

969 NE2,MV716,P?,C,W,PL/NE composite
970 NE3,MV716,P?,C,E,PL/NE composite
971 PL1,MV716,P?,C,E,PL/NE composite
972 PL327,MV716,P?,C,W,PL/NE composite
973 PL2,MV716,P?,R,E,PL/NE composite
974 CPX1,MV716,P,C,E
975 CPX2,MV716,P,R,E
976 CPX340,MV716,P,C,W
977 CPX341,MV716,P,C,W
978 CPX342,MV716,P,C,W
979 CPX343,MV716,P,R,W

	980	981	982	983	984	985	986	987	988	989	990
SiO2	0.74	0.26	0.39	0.23	0.44	0.27	0.71	0.20	nd	0.41	45.17
TiO2	0.79	10.82	21.03	21.48	20.02	20.74	18.09	53.68	53.24	52.88	3.87
Al2O3	51.53	12.80	4.03	3.47	2.95	4.00	4.50	nd	0.09	0.18	7.07
Fe2O3	11.93	29.60	25.52	24.97	27.28	23.68	26.86	4.76	3.96	3.96	nd
Cr2O3	0.47	5.14	0.22	0.42	0.54	0.19	0.30	nd	0.02	nd	0.14
FeO	23.57	36.77	45.21	45.55	44.25	46.23	45.64	35.99	35.75	37.43	8.42
MnO	0.20	0.41	0.51	0.50	0.69	0.60	0.60	0.54	0.55	0.71	0.20
MgO	11.96	4.30	4.18	3.93	3.77	2.62	1.75	6.72	6.49	5.55	11.94
CaO	nd	nd	nd	nd	nd	nd	0.20	nd	nd	nd	22.98
total=	101.19	100.10	101.09	100.55	99.94	98.33	98.65	101.89	100.10	101.12	99.79
Mg#	47.5	17.2	-	-	-	-	-	-	-	-	76.4
Al ratio	-	-	-	-	-	-	-	-	-	-	0.1

980 SP1,MV716,P,C,E
981 SPMT2,MV716,P,C,E
982 MT1,MV716,P,C,E
983 MT2,MV716,P,C,E
984 MT3,MV716,P,C,E
985 MT326,MV716,P,C,W
986 MT4,MV716,GR,C,E
987 IL1R,MV716,P(MT),C,E
988 IL314,MV716,P(MT),C,W
989 IL4,MV716,GR,C,E
990 CPX10,MV78,P,R,+OL+CPX+SP,E

	991	992	993	994	995	996	997	998	999	1000	1001
SiO2	47.94	43.46	48.77	53.94	45.01	49.09	49.89	49.13	49.17	44.76	44.27
TiO2	2.51	4.50	2.08	0.20	3.68	2.12	1.77	2.00	1.95	3.64	3.98
Al2O3	5.62	8.98	4.89	0.12	8.04	4.60	3.94	4.96	4.11	7.69	8.46
Cr2O3	nd	nd	0.13	nd	0.19	0.02	0.13	nd	0.08	0.09	0.22
FeO	7.80	9.52	7.20	8.34	7.64	6.90	6.45	7.37	6.74	7.91	7.76
MnO	0.19	0.27	0.22	0.26	0.11	0.12	0.12	0.17	0.11	0.12	0.12
MgO	12.06	11.19	13.66	13.75	11.54	13.29	13.92	12.79	13.67	11.70	11.33
CaO	23.64	22.12	23.11	23.45	22.86	23.21	23.12	22.60	23.18	23.25	22.76
Na2O	nd	nd	nd	0.48	0.58	0.45	0.51	0.71	0.46	0.53	0.60
total=	99.76	100.04	100.06	100.54	99.65	99.80	99.85	99.73	99.47	99.69	99.50
Mg#	73.9	72.8	80.2	76.2	82.1	82.6	85.1	81.0	85.2	85.4	82.6
Al ratio	0.3	0.1	0.2	1.9	0.1	0.2	0.1	0.3	0.1	0.1	0.1

991 CPX12,MV78,GR,C,E
992 CPX13,MV78,GR,C,E
993 CPX3,MV78,P,C,E
994 CPX367,MV78,P?,C,W
995 CPX368,MV78,P,C,W
996 CPX369,MV78,P,I,W
997 CPX370,MV78,P,I,W
998 CPX371,MV78,P,R,W
999 CPX372,MV78,P,C,W
1000 CPX373,MV78,P,C,W
1001 CPX374,MV78,P,C,W

	1002	1003	1004	1005	1006	1007	1008	1009	1010	1011	1012
SiO2	49.67	48.95	45.03	49.67	48.98	45.95	47.77	49.17	0.11	0.14	0.13
TiO2	1.81	2.08	3.41	1.98	1.91	3.04	2.46	1.95	8.28	7.96	6.11
Al2O3	4.26	5.20	8.37	4.19	4.93	7.76	5.69	4.60	10.37	11.89	11.74
Fe2O3	nd	nd	nd	nd	nd	nd	nd	nd	26.60	23.76	25.54
Cr2O3	0.13	0.06	nd	0.17	nd	nd	0.13	0.15	13.61	15.24	17.01
FeO	6.58	7.49	7.96	7.02	7.20	7.86	7.87	6.96	34.62	33.99	32.68
MnO	0.12	0.17	0.13	nd	nd	0.12	nd	nd	0.76	0.76	0.76
MgO	13.93	12.76	11.76	14.04	12.64	12.10	12.48	13.99	3.07	3.46	3.17
CaO	23.15	22.74	23.07	23.69	23.15	22.99	23.22	23.25	nd	nd	nd
Na2O	0.44	0.71	nd	nd	0.57	nd	nd	nd	nd	nd	nd
total=	100.09	100.16	99.73	100.76	99.38	99.82	99.62	100.07	97.42	97.20	97.14
Mg#	85.0	81.8	77.0	81.2	80.5	76.7	75.2	81.1	13.6	15.4	14.7
Al ratio	0.1	0.2	0.2	0.1	0.3	0.2	0.2	0.2	-	-	-

1002 CPX375,MV78,P,C,W
1003 CPX376,MV78,P,C,W
1004 CPX4,MV78,P,R,E
1005 CPX5,MV78,P,C,E
1006 CPX6,MV78,P,R,E
1007 CPX7,MV78,P,C,E
1008 CPX8,MV78,P,R,E
1009 CPX9,MV78,P,C,E
1010 SPMT331,MV78,P,C,W
1011 SPMT333,MV78,P,C,W
1012 SPMT334,MV78,P,C,W

	1013	1014	1015	1016	1017	1018	1019	1020	1021	1022	1023
SiO2	0.13	0.16	40.61	39.70	39.95	40.43	40.22	39.47	40.27	39.58	38.72
TiO2	21.71	48.39	nd	nd	nd	nd	nd	0.02	nd	0.01	0.04
Al2O3	1.80	0.16	nd	nd	nd	nd	nd	0.05	nd	0.06	0.06
Fe2O3	22.91	7.79	nd	nd	nd	nd	nd	nd	nd	nd	nd
Cr2O3	0.06	0.04	nd	nd	nd	nd	nd	0.04	nd	0.04	0.03
FeO	47.20	37.39	14.98	17.75	16.45	15.09	15.27	15.22	15.45	15.53	18.67
MnO	0.79	4.70	0.21	0.21	0.23	0.27	0.31	0.19	0.20	0.21	0.26
NiO	nd	nd	0.28	0.27	0.42	0.35	0.20	0.25	0.22	0.24	0.17
MgO	1.66	0.87	43.30	41.30	42.13	43.05	43.72	44.31	43.72	44.04	41.49
CaO	nd	nd	0.23	0.29	0.28	0.37	0.26	0.26	0.29	0.28	0.34
total=	96.26	99.50	99.61	99.52	99.46	99.56	99.98	99.81	100.15	99.99	99.78
Mg#	-	-	83.7	80.6	82.0	83.6	83.6	83.8	83.5	83.5	79.8

1013 MT336,MV78,GR,C,W
1014 IL320,MV78,P,C,W
1015 OL14,MV406,P,C,+OL+CPX+SP+MT,E
1016 OL15,MV406,P,R,E
1017 OL16,MV406,P,C,E
1018 OL18,MV406,P,C,E
1019 OL20,MV406,P,C,E
1020 OL20,MV406,P,C,W
1021 OL21,MV406,P,C,E
1022 OL21,MV406,P,I,W
1023 OL22,MV406,P,R,W

	1024	1025	1026	1027	1028	1029	1030	1031	1032	1033	1034
SiO2	39.63	38.54	39.99	40.07	40.38	40.22	39.09	38.32	51.00	50.37	51.65
TiO2	0.02	nd	0.03	nd	0.02	nd	0.14	nd	nd	0.13	0.20
Al2O3	0.07	nd	0.07	nd	0.08	nd	nd	nd	30.59	30.94	29.32
Cr2O3	0.02	nd	0.04	nd	0.12	nd	nd	nd	nd	nd	nd
FeO	15.31	23.94	15.74	14.87	15.45	15.79	21.50	23.98	0.80	0.78	0.62
MnO	0.21	0.48	0.22	0.26	0.19	0.22	0.31	0.38	nd	nd	nd
NiO	0.27	nd	0.21	0.32	0.26	0.17	nd	0.28	nd	nd	nd
MgO	44.14	37.05	43.99	43.82	44.57	43.06	39.51	38.13	nd	nd	nd
CaO	0.28	0.45	0.31	0.32	0.26	0.26	0.26	0.34	13.82	14.18	12.91
Na2O	nd	nd	nd	nd	nd	nd	nd	nd	3.24	3.16	3.64
K2O	nd	nd	nd	nd	nd	nd	nd	nd	0.31	0.24	0.29
total=	99.95	100.46	100.60	99.66	101.33	99.72	100.81	101.43	99.76	99.80	98.63
Mg#	83.7	73.4	83.3	84.0	83.7	82.9	76.6	73.9	-	-	-
An	-	-	-	-	-	-	-	-	68.9	70.3	65.1

1024 OL23,MV406,P,C,W
1025 OL24,MV406,P,R,E
1026 OL24,MV406,P,I,W
1027 OL25,MV406,P,C,E
1028 OL25,MV406,P,I,W
1029 OL26,MV406,P,C,E
1030 OL6,MV406,GR,C,E
1031 OL7,MV406,GR,C,E
1032 PL10,MV406,GR,C,E
1033 PL11,MV406,GR,C,E
1034 PL8,MV406,GR,C,E

	1035	1036	1037	1038	1039	1040	1041	1042	1043	1044	1045
SiO2	45.46	47.76	45.70	43.98	44.26	46.05	50.31	43.64	47.29	46.31	47.63
TiO2	3.16	2.43	3.19	3.65	3.56	2.54	1.49	3.80	2.36	2.71	2.32
Al2O3	8.36	5.70	8.17	8.80	9.28	7.48	4.42	9.20	7.22	7.56	5.54
Cr2O3	0.63	0.13	0.35	0.27	0.61	0.56	0.40	0.02	0.53	0.53	nd
FeO	6.98	7.36	7.77	7.16	7.04	6.76	6.11	8.08	6.55	6.59	7.31
MnO	nd	0.12	nd	0.09	0.13	0.09	nd	nd	0.19	0.14	nd
NiO	nd	nd	nd	nd	nd	0.02	nd	0.02	nd	nd	0.01
MgO	12.11	13.45	12.22	11.96	11.57	12.66	14.69	11.38	12.98	12.88	13.50
CaO	22.77	22.23	22.08	22.64	22.62	22.23	22.55	22.21	23.00	22.54	22.46
Na2O	nd	nd	nd	0.47	nd	0.49	nd	0.47	nd	nd	0.34
total=	99.47	99.18	99.48	99.02	99.07	98.88	99.97	98.82	100.12	99.26	99.11
Mg#	77.0	78.1	74.5	86.7	76.3	85.2	81.1	81.3	79.7	79.7	83.9
Al ratio	0.3	0.2	0.3	0.1	0.3	0.2	0.4	0.2	0.3	0.3	0.1

1035 CPX1,MV406,P,C,E
1036 CPX10,MV406,P,C,E
1037 CPX10,MV406,GR,C,E
1038 CPX10,MV406,P,C,W
1039 CPX11,MV406,P,C,E
1040 CPX11,MV406,P,I,W
1041 CPX12,MV406,P,C,E
1042 CPX12,MV406,P,I,W
1043 CPX13,MV406,P,C,E
1044 CPX14,MV406,P,C,E
1045 CPX14,MV406,P,C,W

	1046	1047	1048	1049	1050	1051	1052	1053	1054	1055	1056
SiO2	44.47	48.29	45.75	49.47	48.39	48.80	49.55	45.82	49.54	48.69	47.51
TiO2	3.33	2.08	2.39	1.76	1.93	2.13	1.70	4.06	1.73	2.16	2.28
Al2O3	8.44	5.85	7.33	4.61	5.00	5.37	4.26	7.70	4.82	5.59	7.26
Cr2O3	0.36	0.51	0.61	0.26	0.26	nd	0.46	nd	0.53	0.13	0.56
FeO	7.45	6.37	6.70	6.70	6.60	7.22	6.50	8.44	5.79	7.35	6.46
MnO	0.09	nd	0.09	0.15	0.13	0.16	nd	0.21	nd	nd	0.14
NiO	0.03	nd	0.01	nd	nd	nd	nd	nd	nd	nd	nd
MgO	12.01	13.55	12.76	14.22	13.94	13.55	14.47	11.20	13.99	13.52	13.03
CaO	22.73	22.92	22.63	22.51	22.98	22.86	22.74	22.58	22.95	22.30	22.61
Na2O	0.43	nd	0.44	nd	nd	nd	nd	nd	nd	nd	nd
total=	99.34	99.57	98.71	99.68	99.23	100.09	99.68	100.01	99.35	99.74	99.85
Mg#	85.8	79.8	88.4	79.8	82.7	78.4	81.5	70.3	81.2	76.6	78.2
Al ratio	0.1	0.3	0.2	0.3	0.2	0.3	0.2	0.2	0.4	0.3	0.4

1046 CPX15,MV406,P,I,W
1047 CPX16,MV406,P,C,E
1048 CPX16,MV406,P,I,W
1049 CPX17,MV406,P,C,E
1050 CPX18,MV406,P,C,E
1051 CPX20,MV406,P,C,E
1052 CPX21,MV406,P,C,E
1053 CPX4,MV406,P,R,E
1054 CPX5,MV406,P,C,E
1055 CPX6,MV406,P,C,E
1056 CPX7,MV406,P,C,E

	1057	1058	1059	1060	1061	1062	1063	1064	1065	1066	1067
SiO2	48.00	44.12	49.23	45.26	0.33	0.27	0.20	0.21	0.15	0.23	0.18
TiO2	2.05	4.28	1.75	3.81	1.57	1.62	1.79	3.39	1.60	1.59	1.49
Al2O3	5.60	8.24	4.60	7.63	35.56	36.32	36.60	26.61	36.89	36.09	36.18
Fe2O3	nd	nd	nd	nd	9.87	9.69	9.15	15.89	9.19	9.17	9.95
Cr2O3	0.47	nd	0.46	nd	21.99	19.56	20.65	19.94	21.18	21.54	21.20
FeO	6.21	8.65	6.06	8.38	16.38	16.26	16.96	20.64	16.73	17.16	15.60
MnO	nd	nd	0.17	0.25	0.25	0.25	0.26	0.32	0.25	nd	0.28
NiO	0.16	nd	nd	nd	nd	0.20	0.19	0.21	0.23	nd	nd
MgO	13.91	11.61	14.13	11.75	15.08	14.61	14.55	11.62	14.66	14.58	15.27
CaO	22.99	21.63	22.79	22.15	nd	0.01	0.02	0.04	0.03	nd	nd
total=	99.39	98.53	99.19	99.23	101.03	98.79	100.37	98.87	100.91	100.36	100.15
Mg#	83.7	71.6	81.1	72.4	62.1	61.6	60.5	50.1	61.0	60.2	63.6
Al ratio	0.2	0.2	0.3	0.2	-	-	-	-	-	-	-

1057 CPX8,MV406,P,C,E
1058 CPX8,MV406,GR,C,E
1059 CPX9,MV406,P,C,E
1060 CPX9,MV406,GR,C,E
1061 SP1,MV406,P,C,E
1062 SP13,MV406,P,C,W
1063 SP14,MV406,P,C,W
1064 SP15,MV406,P,C,W
1065 SP16,MV406,P,C,W
1066 SP2,MV406,P,C,E
1067 SP5,MV406,P,C,E

	1068	1069	1070	1071	1072	1073	1074	1075	1076	1077	1078
SiO2	0.23	0.23	0.25	nd	0.07	0.25	0.07	0.08	0.11	0.13	49.50
TiO2	1.81	3.11	2.42	1.61	26.20	24.18	22.79	18.23	26.76	26.55	0.15
Al2O3	33.46	27.69	31.75	36.81	5.45	5.74	5.90	8.36	3.66	2.77	30.87
Fe2O3	11.56	14.69	11.46	9.11	8.05	9.57	14.13	15.56	11.85	11.67	nd
Cr2O3	21.42	21.83	21.40	21.73	3.39	4.78	5.07	9.89	0.74	0.06	nd
FeO	19.43	19.87	19.01	15.99	49.25	48.34	47.31	42.82	51.28	51.67	0.68
MnO	0.30	0.25	0.31	nd	1.12	1.61	0.72	0.75	0.78	3.10	nd
MgO	12.89	12.60	13.06	15.27	3.35	2.65	3.38	3.91	2.57	0.27	nd
CaO	nd	nd	nd	nd	nd	nd	nd	nd	nd	nd	14.43
Na2O	nd	nd	nd	nd	nd	nd	nd	nd	nd	nd	3.04
K2O	nd	nd	nd	nd	nd	nd	nd	nd	nd	nd	0.29
total=	101.10	100.27	99.66	100.52	96.88	97.12	99.37	99.60	97.75	96.22	98.96
Mg#	54.2	53.1	55.0	63.0	-	-	-	14.0	-	-	-
An	-	-	-	-	-	-	-	-	-	-	71.2

1068 SP6,MV406,P,C,E
1069 SP7,MV406,P,C,E
1070 SP8,MV406,P,C,E
1071 SP9,MV406,P,C,E
1072 MTSP210,MV406,P,C,W
1073 MTSP211,MV406,P,C,W
1074 MTSP216,MV406,P,C,W
1075 SPMT217,MV406,P,R,W
1076 MT218,MV406,P,R,W
1077 MT219,MV406,GR,C,W
1078 PL10,MV400,GR,C,+OL+CPX+SP,E

	1079	1080	1081	1082	1083	1084	1085	1086	1087	1088	1089
SiO2	50.39	48.00	45.97	42.73	49.64	43.39	45.97	46.04	47.08	41.03	47.81
TiO2	0.17	2.12	2.70	4.13	1.33	3.87	2.17	2.21	2.40	5.13	2.26
Al2O3	30.92	5.60	8.43	9.72	5.09	8.74	8.06	8.24	6.47	11.58	5.78
Cr2O3	nd	0.17	0.34	0.25	0.51	0.11	0.75	0.77	0.25	nd	nd
FeO	0.68	7.12	6.61	7.50	5.73	8.19	5.65	5.86	7.56	8.25	7.64
MnO	nd	0.13	0.12	0.11	0.14	0.16	0.11	nd	nd	nd	0.14
MgO	nd	13.87	13.00	11.20	15.35	11.38	13.02	12.99	13.19	10.57	13.58
CaO	14.62	22.17	22.56	22.49	21.29	22.51	22.40	22.38	22.43	22.80	22.64
Na2O	3.04	0.30	0.38	0.43	0.41	0.53	0.44	0.42	nd	nd	nd
K2O	0.32	nd	nd	nd	nd	nd	nd	nd	nd	nd	nd
total=	100.14	99.48	100.11	98.56	99.49	98.88	98.57	98.91	99.38	99.36	99.85
Mg#	-	84.2	87.1	83.6	87.6	84.8	89.0	87.6	79.1	77.0	80.5
An	71.3	-	-	-	-	-	-	-	-	-	-
Al ratio	-	0.2	0.2	0.1	0.3	0.1	0.3	0.3	0.2	0.2	0.2

1079 PL9,MV400,GR,C,E
1080 CPX25,MV400,P,C,W
1081 CPX26,MV400,P,C,W
1082 CPX27,MV400,P,C,W
1083 CPX28,MV400,P,C,W
1084 CPX29,MV400,P,R,W
1085 CPX30,MV400,P,C,W
1086 CPX30R,MV400,P,C,W
1087 CPX32,MV400,P,C,E
1088 CPX33,MV400,P,R,E
1089 CPX34,MV400,P,C,E

	1090	1091	1092	1093	1094	1095	1096	1097	1098	1099	1100
SiO2	45.31	50.47	44.55	48.03	42.40	0.20	0.15	0.18	0.15	0.12	0.20
TiO2	3.21	1.18	3.78	2.59	3.94	1.10	0.99	0.94	1.54	5.14	7.61
Al2O3	7.93	4.75	8.18	5.22	9.51	41.87	41.73	42.32	32.87	24.60	18.56
Fe2O3	nd	nd	nd	nd	nd	8.04	8.47	7.49	9.99	15.36	18.09
Cr2O3	0.13	0.65	0.14	nd	nd	17.83	18.04	18.54	24.60	19.04	17.42
FeO	7.98	5.57	9.08	7.72	9.42	14.61	13.92	13.65	16.08	25.81	29.99
MnO	nd	0.13	nd	0.12	nd	0.29	0.27	0.32	0.38	0.55	0.54
NiO	nd	nd	0.16	nd	nd	nd	nd	nd	nd	nd	nd
MgO	11.67	15.65	10.77	13.13	11.63	16.33	16.66	16.89	14.56	9.21	7.34
CaO	22.98	21.46	22.46	22.53	21.31	nd	nd	nd	nd	nd	nd
Na2O	nd	0.32	0.44	0.23	0.40	nd	nd	nd	nd	nd	nd
total=	99.21	100.18	99.56	99.57	98.61	100.27	100.23	100.33	100.17	99.83	99.75
Mg#	75.3	86.3	74.7	78.8	82.6	66.6	68.1	68.8	61.7	38.9	30.4
Al ratio	0.2	0.4	0.2	0.1	0.1	-	-	-	-	-	-

1090 CPX35,MV400,P,R,E
1091 CPX36,MV400,P,C,E
1092 CPX37,MV400,P,R,E
1093 CPX39,MV400,GR,C,E
1094 CPX40,MV400,GR,C,E
1095 SP1,MV400,P,C,W
1096 SP2,MV400,P,C,W
1097 SP3,MV400,P,C,W
1098 SP4,MV400,P,C,W
1099 SP5,MV400,P,C,W
1100 SP6,MV400,P,C,W

	1101	1102	1103	1104	1105	1106	1107	1108	1109	1110	1111
SiO2	51.94	53.75	53.69	52.25	46.85	44.35	46.69	46.35	49.91	48.13	0.42
TiO2	0.14	0.08	0.09	nd	2.10	2.97	2.22	2.10	1.23	2.24	27.52
Al2O3	30.01	28.38	28.42	29.33	7.21	8.74	6.71	7.11	3.65	5.66	1.97
Fe2O3	nd	nd	nd	nd	nd	nd	nd	nd	nd	nd	10.77
Cr2O3	nd	nd	nd	nd	0.64	0.07	0.36	0.18	0.27	0.33	0.18
FeO	0.86	0.67	0.66	0.76	7.13	8.71	7.54	8.00	7.17	8.58	52.46
MnO	nd	nd	nd	nd	0.11	0.15	nd	0.13	0.16	nd	4.30
MgO	nd	0.03	0.03	0.04	13.03	11.62	12.86	12.58	14.82	13.36	nd
CaO	13.17	11.30	11.06	12.31	21.60	21.68	22.21	21.66	21.44	21.70	nd
Na2O	3.98	4.94	5.09	4.26	0.50	0.50	0.43	0.48	0.33	nd	nd
K2O	0.20	0.32	0.34	0.28	nd	nd	nd	nd	nd	nd	nd
total=	100.30	99.47	99.38	99.23	99.17	98.79	99.02	98.59	98.98	100.00	97.62
Mg#	-	-	-	-	83.5	81.4	83.7	82.4	83.5	75.0	-
An	63.9	54.8	53.5	60.5	-	-	-	-	-	-	-
Al ratio	-	-	-	-	0.3	0.2	0.2	0.2	0.2	0.2	-

1101 PL11R,MV501,GR,C,+OL+CPX+PL,E
1102 PL310,MV501,P,C,W
1103 PL311R,MV501,P,C,W
1104 PL312,MV501,P,R,W
1105 CPX320,MV501,P,C,W
1106 CPX321,MV501,P,R,W
1107 CPX322,MV501,P,C,W
1108 CPX324,MV501,P,C,W
1109 CPX325,MV501,P,C,W
1110 CPX41,MV501,GR,C,E
1111 MT16,MV501,GR,C,E

	1112	1113	1114	1115	1116	1117	1118	1119	1120	1121	1122
SiO2	0.36	0.08	nd	37.88	38.12	53.64	53.65	53.49	57.13	52.80	54.75
TiO2	24.79	50.77	50.86	nd	nd	0.07	0.09	0.07	0.02	0.07	0.06
Al2O3	2.02	0.11	0.14	0.06	0.05	28.28	28.45	28.59	26.51	28.81	27.32
Fe2O3	15.96	2.92	4.33	nd	nd	nd	nd	nd	nd	nd	nd
Cr2O3	0.12	0.02	0.05	nd	nd	nd	nd	nd	nd	nd	nd
FeO	49.68	40.82	39.69	26.12	26.12	0.50	0.51	0.43	0.34	0.45	0.42
MnO	4.00	4.23	3.49	0.32	0.31	nd	nd	nd	nd	nd	nd
NiO	nd	nd	nd	0.15	0.16	nd	nd	nd	nd	nd	nd
MgO	0.21	0.36	1.41	35.88	36.20	0.16	0.16	0.16	0.12	0.12	0.14
CaO	nd	nd	nd	0.28	0.29	11.64	11.68	11.86	9.36	12.19	10.88
Na2O	nd	nd	nd	nd	nd	4.69	4.57	4.60	5.82	4.21	5.08
K2O	nd	nd	nd	nd	nd	0.23	0.24	0.25	0.38	0.27	0.34
total=	97.14	99.31	99.97	100.69	101.25	99.21	99.35	99.45	99.68	98.92	98.99
Mg#	-	-	-	71.0	71.2	-	-	-	-	-	-
An	-	-	-	-	-	57.1	57.7	57.9	46.0	60.6	53.1

1112 MT324,MV501,GR,C,W
1113 IL312,MV501,GR,C,W
1114 IL313R,MV501,GR,C,W
1115 OL101,MV40B,GR,C,+PL,W
1116 OL102,MV40B,GR,C,W
1117 PL21,MV40B,P,C,W
1118 PL22,MV40B,P,I,W
1119 PL24,MV40B,P,C,W
1120 PL25,MV40B,P,I,W
1121 PL27,MV40B,P,C,W
1122 PL28,MV40B,P,I,W

	1123	1124	1125	1126	1127	1128	1129	1130	1131	1132	1133
SiO2	57.96	56.03	55.65	52.43	58.85	53.81	52.73	53.78	56.32	51.20	50.78
TiO2	0.07	0.05	0.06	0.08	0.05	0.08	0.07	nd	nd	1.14	1.24
Al2O3	25.27	26.59	27.02	28.91	24.62	28.28	28.79	28.48	26.26	2.00	2.36
Cr2O3	nd	nd	nd	nd	nd	nd	nd	nd	nd	0.14	0.30
FeO	0.61	0.40	0.32	0.42	0.68	0.67	0.51	0.50	0.75	12.27	10.68
MnO	nd	nd	nd	nd	nd	nd	nd	nd	nd	0.30	0.26
MgO	0.08	0.11	0.09	0.12	0.07	0.18	0.18	0.18	0.14	16.45	15.75
CaO	8.24	9.89	10.05	12.32	7.41	11.88	12.42	11.84	9.87	15.41	17.53
Na2O	6.50	5.41	5.30	4.33	6.87	4.56	4.38	4.58	5.59	0.24	0.27
K2O	0.56	0.45	0.35	0.26	0.69	0.26	0.28	0.23	0.42	nd	nd
total=	99.29	98.93	98.84	98.87	99.24	99.72	99.36	99.59	99.35	99.15	99.17
Mg#	-	-	-	-	-	-	-	-	-	71.4	74.1
An	39.9	48.9	50.1	60.2	35.9	58.1	60.1	58.0	48.2	-	-
Al ratio	-	-	-	-	-	-	-	-	-	0.1	0.1

1123 PL29,MV40B,P,R,W
1124 PL30,MV40B,P,C,W
1125 PL31,MV40B,P,C,W
1126 PL32,MV40B,P,C,W
1127 PL34,MV40B,P,R,W
1128 PL35,MV40B,GR,C,W
1129 PL36,MV40B,GR,C,W
1130 PL37,MV40B,GR,C,W
1131 PL39,MV40B,GR,R,W
1132 CPX200,MV40B,GR,C,W
1133 CPX201,MV40B,GR,C,W

	1134	1135	1136	1137	1138	1139	1140	1141	1142	1143	1144
SiO2	0.07	0.08	0.04	0.01	0.01	37.06	38.30	40.02	39.84	39.95	39.88
TiO2	24.38	47.75	47.63	49.35	48.52	nd	0.04	0.01	nd	0.01	nd
Al2O3	1.50	0.22	0.25	0.12	0.20	nd	0.06	0.08	0.07	0.06	0.05
Fe2O3	18.36	8.54	8.41	5.43	6.89	nd	nd	nd	nd	nd	nd
Cr2O3	0.06	0.01	nd	nd	0.02	nd	0.02	0.03	0.03	0.02	0.03
FeO	51.55	40.92	40.64	41.59	41.22	29.64	22.43	15.69	15.55	15.00	14.95
MnO	1.64	0.38	0.39	0.48	0.37	0.46	0.17	0.11	0.11	nd	0.12
NiO	nd	nd	nd	nd	nd	nd	0.02	0.13	nd	0.12	nd
MgO	0.05	0.81	0.97	1.21	1.10	32.80	39.50	44.74	44.86	45.12	45.00
CaO	0.05	0.22	0.09	0.12	0.07	0.38	0.17	0.30	0.24	0.28	0.24
Na2O	nd	0.02	0.02	nd	nd	nd	nd	nd	nd	nd	nd
total=	97.66	98.95	98.44	98.31	98.40	100.34	100.71	101.11	100.70	100.56	100.27
Mg#	-	-	-	-	-	66.4	75.8	83.6	83.7	84.3	84.3

1134 MT104,MV40B,GR,C,W
1135 IL100,MV40B,GR,C,W
1136 IL101,MV40B,GR,C,W
1137 IL102,MV40B,GR,C,W
1138 IL105,MV40B,GR,C,W
1139 OL1,MV160,GR,C,+OL+CPX+PL+SP+MT,E
1140 OL12,MV160,P,C,W
1141 OL15,MV160,P,C,W
1142 OL16,MV160,P,I,W
1143 OL18,MV160,P,C,W
1144 OL19,MV160,P,R,W

	1145	1146	1147	1148	1149	1150	1151	1152	1153	1154	1155
SiO2	37.66	38.32	36.72	39.70	40.43	38.99	39.14	40.16	40.68	50.27	52.25
TiO2	nd	0.05	0.06	nd	nd	nd	nd	nd	nd	0.18	0.16
Al2O3	nd	0.06	0.08	nd	nd	nd	nd	nd	nd	30.05	29.44
Cr2O3	nd	nd	0.09	nd	nd	nd	nd	nd	nd	nd	nd
FeO	27.98	23.24	29.52	15.51	15.61	22.68	22.02	16.06	14.85	0.88	0.47
MnO	0.41	0.17	0.35	0.18	0.25	0.26	0.35	0.20	0.18	nd	nd
NiO	nd	nd	0.05	0.20	0.15	nd	nd	nd	0.31	nd	nd
MgO	34.73	39.01	33.33	43.56	43.50	37.81	37.79	43.11	44.17	0.25	nd
CaO	0.22	0.20	0.34	0.23	0.23	0.27	0.23	0.27	0.31	13.67	12.79
Na2O	nd	nd	nd	nd	nd	nd	nd	nd	nd	3.39	4.12
K2O	nd	nd	nd	nd	nd	nd	nd	nd	nd	0.35	0.40
total=	101.00	101.05	100.54	99.38	100.17	100.01	99.53	99.80	100.50	99.04	99.63
Mg#	68.9	74.9	66.8	83.3	83.2	74.8	75.4	82.7	84.1	-	-
An	-	-	-	-	-	-	-	-	-	67.6	61.7

1145 OL2,MV160,GR,C,E
1146 OL20,MV160,P,C,W
1147 OL21,MV160,P,I,W
1148 OL27,MV160,P,C,E
1149 OL28,MV160,P,R,E
1150 OL29,MV160,P,C,E
1151 OL30,MV160,P,C,E
1152 OL31,MV160,P,C,E
1153 OL32,MV160,P,C,E
1154 PL1,MV160,GR,C,E
1155 PL10,MV160,P,C,E

	1156	1157	1158	1159	1160	1161	1162	1163	1164	1165	1166
SiO2	53.14	52.59	54.01	54.93	52.60	52.84	50.37	51.81	53.16	54.17	51.30
TiO2	nd	0.11	nd	0.21	0.14	nd	nd	0.08	0.08	0.09	0.09
Al2O3	29.64	29.56	28.16	27.67	29.58	29.58	30.39	29.62	28.98	28.09	29.65
FeO	0.53	0.56	0.69	0.60	0.66	0.42	0.84	0.41	0.35	0.36	0.49
MgO	nd	nd	nd	nd	nd	nd	nd	nd	0.06	0.06	0.08
CaO	12.86	12.71	11.30	10.54	12.37	12.63	13.68	12.59	11.61	10.48	12.83
Na2O	3.64	4.11	4.97	5.10	4.60	4.30	3.60	4.08	4.53	4.82	3.96
K2O	0.32	0.37	0.69	0.62	0.32	0.40	0.25	0.40	0.51	0.62	0.38
total=	100.13	100.01	99.82	99.67	100.27	100.17	99.13	98.99	99.28	98.69	98.78
An	64.9	61.7	53.5	51.4	58.7	60.5	66.8	61.6	56.9	52.6	62.7

1156 PL11,MV160,P,R,E
1157 PL12,MV160,P,R,E
1158 PL13,MV160,P,C,E
1159 PL14,MV160,P,C,E
1160 PL15,MV160,P,C,E
1161 PL16,MV160,P,C,E
1162 PL2,MV160,GR,C,E
1163 PL313,MV160,P,C,W
1164 PL314,MV160,P,C,W
1165 PL315,MV160,P,I,W
1166 PL316,MV160,P,R,W

	1167	1168	1169	1170	1171	1172	1173	1174	1175	1176	1177
SiO2	54.38	51.62	50.33	51.16	51.38	51.36	51.58	50.80	50.51	50.59	50.18
TiO2	0.07	nd	0.12	0.11	0.07	0.06	0.08	0.08	0.12	0.15	0.78
Al2O3	27.68	29.94	30.73	30.10	30.26	29.84	30.08	30.02	30.34	29.76	4.62
Cr2O3	nd	nd	nd	nd	nd	nd	nd	nd	nd	nd	0.44
FeO	0.54	0.46	0.70	0.46	0.44	0.38	0.39	0.55	0.64	0.87	5.64
NiO	nd	nd	nd	nd	nd	nd	nd	nd	nd	nd	0.03
MgO	0.17	0.08	0.09	0.09	0.11	0.07	0.09	0.12	0.11	nd	16.60
CaO	10.34	12.73	13.98	13.10	13.08	12.85	12.93	13.40	13.47	13.58	19.53
Na2O	5.16	3.81	3.31	3.72	3.79	3.85	3.95	3.57	3.50	3.95	0.48
K2O	0.55	0.38	0.25	0.34	0.38	0.37	0.37	0.36	0.32	0.32	nd
total=	98.89	99.02	99.51	99.08	99.51	98.78	99.47	98.90	99.01	99.22	98.30
Mg#	-	-	-	-	-	-	-	-	-	-	88.5
An	50.9	63.4	69.0	64.7	64.1	63.4	63.0	66.0	66.7	64.3	-
Al ratio	-	-	-	-	-	-	-	-	-	-	0.4

1167 PL317,MV160,P,C,W
1168 PL318,MV160,P,C,W
1169 PL319,MV160,P,R,W
1170 PL320,MV160,P,I,W
1171 PL321,MV160,P,C,W
1172 PL322,MV160,P,I,W
1173 PL323R,MV160,P,I,W
1174 PL324,MV160,P,I,W
1175 PL325,MV160,P,R,W
1176 PL4,MV160,GR,C,E
1177 CPX18,MV160,P,C,W

	1178	1179	1180	1181	1182	1183	1184	1185	1186	1187	1188
SiO2	48.07	47.55	48.43	52.06	49.33	48.66	49.44	50.42	46.87	51.31	51.10
TiO2	2.30	1.38	2.29	0.70	2.04	1.41	1.13	1.01	2.11	0.82	1.35
Al2O3	3.91	8.14	3.92	4.27	3.34	8.17	6.48	5.98	9.13	4.33	1.90
Cr2O3	0.01	0.07	0.03	0.69	0.13	0.24	0.36	0.55	nd	0.54	nd
FeO	8.78	6.57	8.75	5.47	8.36	6.70	6.30	5.85	8.48	5.52	9.82
MnO	0.17	0.11	0.15	nd	0.12	nd	nd	0.14	0.14	nd	0.24
NiO	0.01	nd	nd	nd	nd	nd	nd	nd	nd	nd	nd
MgO	13.49	14.26	13.27	17.87	13.84	14.19	15.72	15.84	13.35	17.14	13.92
CaO	21.37	19.90	21.85	18.84	22.03	20.29	19.44	20.11	19.16	19.73	21.53
Na2O	0.39	0.54	0.38	nd	nd	nd	nd	0.54	0.53	nd	nd
K2O	0.01	nd	nd	nd	nd	nd	nd	nd	nd	nd	nd
total=	98.51	98.52	99.07	99.90	99.19	99.66	98.87	100.44	99.77	99.39	99.86
Mg#	79.7	84.7	78.7	85.3	76.0	79.1	81.6	86.1	77.3	84.7	71.9
Al ratio	-	0.6	-	0.7	-	0.7	0.7	0.6	0.5	0.6	-

1178 CPX19,MV160,P,R,W
1179 CPX20,MV160,P,C,W
1180 CPX21,MV160,P,R,W
1181 CPX22,MV160,P,C,E
1182 CPX23,MV160,P,R,E
1183 CPX25,MV160,P,C,E
1184 CPX26,MV160,P,C,E
1185 CPX27,MV160,P,C,E
1186 CPX28,MV160,P,C,E
1187 CPX29,MV160,P,C,E
1188 CPX3,MV160,GR,C,E

	1189	1190	1191	1192	1193	1194	1195	1196	1197	1198	1199
SiO2	50.08	51.98	0.20	0.19	0.33	0.34	0.35	38.07	37.83	39.28	37.73
TiO2	1.55	1.00	1.65	24.43	26.56	25.58	50.84	nd	nd	nd	0.02
Al2O3	4.62	3.01	24.16	3.96	1.97	2.65	nd	nd	nd	nd	0.09
Fe2O3	nd	nd	14.34	18.30	14.17	16.20	3.62	nd	nd	nd	nd
Cr2O3	0.15	nd	25.22	1.06	0.39	0.88	0.12	nd	nd	nd	0.03
FeO	10.64	10.29	24.65	48.57	51.62	50.14	40.43	27.34	26.77	20.73	17.05
MnO	0.29	0.23	0.37	0.51	0.65	0.45	0.74	0.47	0.48	0.28	0.22
NiO	nd	nd	0.06	nd	nd	nd	nd	nd	nd	nd	0.12
MgO	13.68	12.83	7.70	3.83	2.22	3.14	2.78	33.67	34.53	39.16	44.19
CaO	19.18	20.65	0.03	nd	0.21	0.15	nd	0.37	0.40	0.19	0.21
Na2O	nd	0.90	nd	nd	nd	nd	nd	nd	nd	nd	nd
total=	100.19	100.89	98.38	100.85	98.12	99.53	98.88	99.92	100.01	99.64	99.66
Mg#	69.6	71.0	35.8	-	-	-	-	68.7	69.7	77.1	82.2
Al ratio	0.5	0.7	-	-	-	-	-	-	-	-	-

1189 CPX30,MV160,P,C,E
1190 CPX4,MV160,GR,C,E
1191 SP2,MV160,P,C,W
1192 MT1,MV160,P,C,E
1193 MT1,MV160,GR,C,E
1194 MT2,MV160,P,R,E
1195 IL1,MV160,GR,C,E
1196 OL24QSUW,MV514,GR,C,+OL+CPX+PL+SP,E
1197 OL25QSUW,MV514,GR,C,E
1198 OL26QSUW,MV514,P,I,E
1199 OL27,MV514,P,I,W

	1200	1201	1202	1203	1204	1205	1206	1207	1208	1209	1210
SiO2	36.97	38.58	37.69	38.24	38.38	39.91	38.13	38.66	51.02	50.34	50.05
TiO2	0.04	0.01	0.05	0.05	nd	nd	0.17	nd	0.21	0.12	0.09
Al2O3	0.07	0.07	0.07	0.07	nd	nd	nd	nd	30.13	30.44	30.95
Cr2O3	0.01	0.03	0.01	0.02	nd	nd	nd	nd	nd	nd	nd
FeO	26.01	19.46	22.88	20.65	21.84	18.23	25.29	18.48	0.71	0.65	0.60
MnO	0.34	0.22	0.28	0.24	0.28	0.27	0.39	0.32	nd	nd	nd
NiO	0.13	0.14	0.09	0.17	nd	nd	nd	0.20	nd	nd	nd
MgO	36.89	42.10	39.24	41.19	39.60	41.14	35.72	41.34	nd	0.20	0.12
CaO	0.37	0.20	0.24	0.20	0.26	0.28	0.25	0.24	13.94	13.50	14.36
Na2O	nd	nd	nd	nd	nd	nd	nd	nd	4.25	3.60	3.27
K2O	nd	nd	nd	nd	nd	nd	nd	nd	0.30	0.27	0.24
total=	100.83	100.81	100.55	100.83	100.36	99.83	99.95	99.24	100.56	99.12	99.68
Mg#	71.7	79.4	75.3	78.0	76.4	80.1	71.6	79.9	-	-	-
An	-	-	-	-	-	-	-	-	63.4	66.4	69.8

1200 OL28,MV514,P,R,W
1201 OL29,MV514,P,C,W
1202 OL30,MV514,P,R,W
1203 OL31,MV514,P,C,W
1204 OL40,MV514,P,I,E
1205 OL6,MV514,P,C,E
1206 OL7,MV514,P,R,E
1207 OL8,MV514,P,C,E
1208 PL10QSUW,MV514,GR,C,E
1209 PL302,MV514,P,C,W
1210 PL303,MV514,P,C,W

	1211	1212	1213	1214	1215	1216	1217	1218	1219	1220	1221
SiO2	50.22	50.29	49.90	52.04	49.89	51.99	48.43	49.83	51.46	50.86	50.78
TiO2	0.09	0.18	0.12	0.14	0.11	nd	2.24	1.56	0.50	0.57	0.64
Al2O3	30.85	30.43	30.92	29.30	30.63	30.10	4.14	4.19	5.31	5.60	5.80
Cr2O3	nd	nd	nd	nd	nd	nd	0.14	0.31	0.22	0.23	0.34
FeO	0.57	0.87	0.72	0.71	0.65	0.77	8.16	7.61	5.42	5.35	5.28
MnO	nd	nd	nd	nd	nd	nd	0.15	0.12	0.18	nd	0.16
MgO	nd	0.13	0.09	0.07	0.09	nd	13.34	14.62	16.97	16.47	17.01
CaO	13.92	13.56	14.06	12.36	14.27	13.64	22.29	21.77	19.80	19.54	19.18
Na2O	3.29	3.60	3.34	4.26	3.31	3.90	nd	nd	nd	nd	nd
K2O	0.28	0.29	0.25	0.30	0.26	0.26	nd	nd	nd	nd	nd
total=	99.22	99.35	99.40	99.18	99.21	100.66	98.89	100.01	99.86	98.62	99.19
Mg#	-	-	-	-	-	-	76.2	79.0	84.8	84.6	85.2
An	68.9	66.4	68.9	60.5	69.4	64.9	-	-	-	-	-
Al ratio	-	-	-	-	-	-	0.1	0.2	0.9	1.0	0.8

1211 PL304,MV514,P,C,W
1212 PL306,MV514,GR,C,W
1213 PL307,MV514,GR,C,W
1214 PL308,MV514,GR,C,W
1215 PL309,MV514,GR,C,W
1216 PL9QSUWQ,MV514,GR,C,E
1217 CPX012,MV514,P,R,E
1218 CPX013,MV514,P,R,E
1219 CPX014,MV514,P,I,E
1220 CPX015,MV514,P,I,E
1221 CPX016,MV514,P,C,E

	1222	1223	1224	1225	1226	1227	1228	1229	1230	1231	1232
SiO2	51.11	51.05	49.68	48.74	48.97	44.18	46.87	46.78	51.38	51.72	51.13
TiO2	0.66	0.62	0.81	1.36	1.98	4.60	3.04	3.43	0.59	0.67	0.64
Al2O3	5.82	5.87	6.35	5.52	3.91	7.43	5.66	5.41	5.52	5.07	5.73
Cr2O3	0.22	0.33	0.43	0.59	nd	nd	nd	nd	0.26	0.24	0.19
FeO	5.49	5.64	5.87	7.24	8.02	9.67	9.32	9.17	5.98	5.95	5.60
MnO	0.13	nd	0.13	nd	0.13	nd	nd	0.27	0.12	nd	0.09
NiO	0.13	nd	nd	nd	nd	nd	nd	nd	nd	0.13	0.01
MgO	16.99	16.33	14.93	14.46	13.56	11.02	12.13	11.80	17.36	17.46	16.95
CaO	19.29	19.46	20.07	20.88	22.06	21.84	22.20	22.26	18.25	18.11	18.69
Na2O	nd	nd	nd	nd	nd	0.57	nd	nd	nd	nd	0.55
total=	99.84	99.30	98.27	98.79	98.63	99.31	99.22	99.12	99.46	99.35	99.58
Mg#	84.7	83.8	81.9	78.7	75.7	74.6	71.3	69.6	83.8	83.9	86.0
Al ratio	0.8	1.0	0.9	0.4	0.2	-	0.1	0.1	0.9	1.0	0.8

1222 CPX017,MV514,P,C,E
1223 CPX019,MV514,P,I,E
1224 CPX020,MV514,P,I,E
1225 CPX021,MV514,P,R,E
1226 CPX022,MV514,P,R,E
1227 CPX33QSUW,MV514,GR,C,E
1228 CPX34QSUW,MV514,GR,C,E
1229 CPX35QSUW,MV514,GR,C,E
1230 CPX4,MV514,P,C,E
1231 CPX5,MV514,P,R,E
1232 CPX7,MV514,P,C,W

	1233	1234	1235	1236	1237	1238	1239	1240	1241	1242	1243
SiO2	47.68	nd	nd	nd	0.34	0.36	0.18	0.36	35.89	37.32	36.71
TiO2	2.19	1.00	0.98	0.85	3.04	1.37	0.79	28.26	nd	nd	nd
Al2O3	4.34	57.36	57.76	57.61	41.55	44.21	58.29	2.12	nd	nd	nd
Fe2O3	nd	9.30	8.32	9.49	12.95	9.91	8.52	9.06	nd	nd	nd
Cr2O3	0.02	nd	nd	0.02	8.56	12.36	nd	0.26	nd	nd	nd
FeO	8.50	16.21	16.96	16.01	21.47	20.36	17.18	54.79	36.05	30.02	33.30
MnO	0.12	0.25	0.14	0.12	0.27	0.18	0.11	1.29	0.59	0.38	0.55
NiO	0.05	nd	nd	0.14	nd	nd	nd	nd	0.14	nd	nd
MgO	13.10	16.80	16.33	16.90	13.29	13.60	16.53	0.47	28.00	33.39	30.54
CaO	21.68	nd	nd	0.01	nd	nd	nd	0.35	0.35	0.24	0.27
Na2O	0.44	nd	nd	nd	nd	nd	nd	nd	nd	nd	nd
total=	98.12	100.92	100.49	101.15	101.47	102.35	101.60	96.96	101.02	101.35	101.37
Mg#	80.5	64.9	63.2	65.3	52.5	54.3	63.2	-	58.1	66.5	62.0

1233 CPX8,MV514,P,R,W
1234 SP12,MV514,P,C,E
1235 SP14,MV514,P,C,E
1236 SP2,MV514,P,R,W
1237 SP21QSUW,MV514,P,C,E
1238 SP22QSUW,MV514,P,C,E
1239 SP25QSUW,MV514,P,R,E
1240 MT9QSUWQ,MV514,GR,C,E
1241 OL12,MV74,P,R,+OL+CPX+PL+MT+IL,E
1242 OL13,MV74,P,C,E
1243 OL14,MV74,P,R,E

	1244	1245	1246	1247	1248	1249	1250	1251	1252	1253	1254
SiO2	37.40	37.90	38.24	36.61	36.78	38.33	38.07	36.40	37.81	37.23	37.99
FeO	27.49	26.35	23.92	34.42	31.04	23.12	22.80	32.69	24.63	27.98	24.01
MnO	0.41	0.33	0.32	0.47	0.45	0.23	0.27	0.48	0.30	0.38	0.27
NiO	nd	nd	nd	nd	0.06	0.06	0.07	0.13	0.06	0.09	0.06
MgO	35.36	36.01	38.75	29.75	32.22	39.07	39.00	30.69	37.25	34.79	37.67
CaO	0.25	0.28	0.19	0.37	0.31	0.25	0.24	0.38	0.22	0.30	0.21
total=	100.91	100.87	101.42	101.62	100.86	101.06	100.45	100.77	100.27	100.77	100.21
Mg#	69.6	70.9	74.3	60.6	64.9	75.1	75.3	62.6	72.9	68.9	73.7

1244 OL15,MV74,P,C,E
1245 OL16,MV74,P,C,E
1246 OL17,MV74,P,C,E
1247 OL3,MV74,P,R,E
1248 OL348,MV74,P,C,W
1249 OL349,MV74,P,C,W
1250 OL350,MV74,P,I,W
1251 OL351,MV74,P,R,W
1252 OL352,MV74,P,C,W
1253 OL353,MV74,P,C,W
1254 OL354,MV74,P,I,W

	1255	1256	1257	1258	1259	1260	1261	1262	1263	1264	1265
SiO2	36.71	36.81	36.76	52.18	54.03	51.69	53.43	52.72	55.11	54.90	54.96
TiO2	nd	nd	nd	0.16	0.12	0.20	0.16	0.18	0.14	0.15	0.15
Al2O3	nd	nd	nd	29.09	28.48	29.16	29.07	29.34	27.30	28.02	27.47
FeO	31.97	30.18	32.10	0.74	0.38	0.71	0.78	0.69	0.27	0.44	0.37
MnO	0.45	0.47	0.49	nd	nd	nd	nd	nd	nd	nd	nd
NiO	0.08	nd	nd	nd	nd	nd	nd	nd	nd	nd	nd
MgO	31.88	33.53	31.30	nd	nd	nd	nd	nd	nd	nd	nd
CaO	0.35	0.31	0.36	12.65	11.41	12.43	11.81	12.29	9.82	10.49	10.05
Na2O	nd	nd	nd	3.79	4.57	4.18	4.31	4.21	5.55	4.71	4.85
K2O	nd	nd	nd	0.45	0.54	0.44	0.39	0.51	0.83	0.78	0.78
total=	101.44	101.30	101.01	99.06	99.53	98.81	99.95	99.94	99.02	99.49	98.63
Mg#	64.0	66.4	63.5	-	-	-	-	-	-	-	-
An	-	-	-	63.1	56.1	60.6	58.8	59.9	47.1	52.6	50.9

1255 OL355,MV74,P,C,W
1256 OL5,MV74,P,C,E
1257 OL6,MV74,P,R,E
1258 PL1,MV74,P,R,E
1259 PL10,MV74,P,C,E
1260 PL10,MV74,P,R,E
1261 PL11,MV74,GR,C,E
1262 PL12,MV74,GR,C,E
1263 PL3,MV74,P,I,E
1264 PL4,MV74,P,C,E
1265 PL4,MV74,P,I,E

	1266	1267	1268	1269	1270	1271	1272	1273	1274	1275	1276
SiO2	54.08	53.16	54.71	55.26	55.74	54.57	52.04	51.43	49.99	48.80	48.64
TiO2	0.24	0.14	0.12	nd	nd	0.20	0.12	0.47	1.65	1.25	1.18
Al2O3	27.83	29.47	27.27	27.51	28.02	28.10	29.81	4.27	2.78	6.98	6.90
Cr2O3	nd	nd	nd	nd	nd	nd	nd	1.01	0.25	0.54	0.58
FeO	0.44	0.36	0.53	0.50	0.47	0.37	0.65	5.54	8.53	6.62	6.69
MnO	nd	nd	nd	nd	nd	nd	nd	0.13	nd	0.12	0.12
MgO	nd	nd	nd	nd	nd	nd	nd	18.30	14.80	14.57	14.61
CaO	11.01	12.09	10.36	10.02	10.58	10.71	13.08	17.99	20.80	19.83	19.80
Na2O	4.65	4.31	5.00	5.17	5.28	4.74	3.93	nd	nd	nd	nd
K2O	0.66	0.57	0.66	0.71	0.69	0.72	0.36	nd	nd	nd	nd
total=	98.91	100.10	98.65	99.17	100.78	99.41	99.99	99.14	98.80	98.71	98.52
Mg#	-	-	-	-	-	-	-	85.5	76.2	79.7	79.6
An	54.5	58.8	51.3	49.6	50.5	53.2	63.4	-	-	-	-
Al ratio	-	-	-	-	-	-	-	0.6	0.1	0.7	0.7

1266 PL5,MV74,P,C,E
1267 PL6,MV74,P,C,E
1268 PL6,MV74,P,C,E
1269 PL7,MV74,P,C,E
1270 PL7,MV74,P,R,E
1271 PL8,MV74,P,C,E
1272 PL9,MV74,P,R,E
1273 CPX1,MV74,P,C,E
1274 CPX10,MV74,P,R,E
1275 CPX12,MV74,P,I,E
1276 CPX13,MV74,P,I,E

	1277	1278	1279	1280	1281	1282	1283	1284	1285	1286	1287
SiO2	48.84	52.02	47.32	48.84	49.50	49.20	49.16	51.91	50.67	50.80	47.69
TiO2	1.12	0.45	1.79	2.34	1.90	1.94	1.87	0.61	1.62	0.70	1.43
Al2O3	7.07	3.85	7.59	3.78	3.14	3.59	3.89	3.70	2.19	4.46	7.49
Cr2O3	0.53	0.79	0.34	0.35	0.36	0.34	0.67	0.76	0.21	0.40	0.47
FeO	6.94	5.59	8.80	8.97	8.75	9.09	8.40	5.20	8.89	6.62	6.87
MnO	0.25	nd	0.19	0.22	0.17	0.14	0.18	nd	0.18	nd	0.14
MgO	14.80	17.85	13.47	13.42	14.03	13.96	14.62	17.52	13.75	17.22	14.65
CaO	19.88	18.60	19.19	20.97	21.04	20.59	20.31	18.69	21.52	18.17	19.49
Na2O	nd	nd	nd	nd	nd	nd	nd	nd	nd	nd	0.60
total=	99.43	99.15	98.69	98.89	98.89	98.85	99.10	98.39	99.03	98.37	98.83
Mg#	79.2	85.1	73.2	72.7	74.1	73.2	76.1	85.7	73.4	82.3	85.8
Al ratio	0.6	0.8	0.5	0.1	0.1	0.1	0.1	0.9	0.1	0.7	0.4

1277 CPX16,MV74,P,C,E
1278 CPX2,MV74,P,C,E
1279 CPX20,MV74,P,R,E
1280 CPX23,MV74,P,R,E
1281 CPX24,MV74,P,R,E
1282 CPX25,MV74,P,R,E
1283 CPX26,MV74,P,R,E
1284 CPX29,MV74,P,C,E
1285 CPX3,MV74,P,R,E
1286 CPX30,MV74,P,I,E
1287 CPX309,MV74,P,C,W

	1288	1289	1290	1291	1292	1293	1294	1295	1296	1297	1298
SiO2	51.06	46.96	48.80	47.89	46.24	49.74	49.64	51.08	50.64	50.52	49.40
TiO2	1.32	1.95	2.21	1.37	2.30	1.07	1.70	1.54	1.68	1.61	2.15
Al2O3	2.31	7.33	3.63	7.39	8.16	4.75	2.72	2.59	2.71	2.45	3.45
Cr2O3	nd	0.25	0.19	0.47	0.06	nd	0.20	0.18	nd	0.13	nd
FeO	7.68	8.57	8.70	6.77	9.01	7.20	8.47	8.44	8.69	9.73	8.51
MnO	0.26	0.16	0.13	0.11	0.12	0.74	0.14	0.27	0.24	0.15	0.16
MgO	14.85	13.94	13.85	14.60	13.30	13.22	14.10	14.07	13.85	13.56	13.80
CaO	21.76	18.60	20.88	19.59	18.75	22.17	21.58	21.54	21.58	21.10	21.46
Na2O	nd	0.70	0.40	0.61	0.71	nd	nd	nd	nd	nd	nd
total=	99.24	98.46	98.79	98.80	98.65	98.89	98.55	99.71	99.39	99.25	98.93
Mg#	77.6	81.0	78.1	85.4	79.2	76.6	75.9	74.8	74.0	71.3	74.3
Al ratio	0.1	0.4	-	0.5	0.4	0.6	-	0.2	0.2	0.2	0.1

1288 CPX31,MV74,P,C,E
1289 CPX310,MV74,P,I,W
1290 CPX311,MV74,P,R,W
1291 CPX312,MV74,P,C,W
1292 CPX313,MV74,P,C,W
1293 CPX32,MV74,P,C,E
1294 CPX33,MV74,P,R,E
1295 CPX4,MV74,P,R,E
1296 CPX41,MV74,GR,C,E
1297 CPX42,MV74,GR,C,E
1298 CPX5,MV74,P,C,E

	1299	1300	1301	1302	1303	1304	1305	1306	1307	1308	1309
SiO2	49.02	50.63	0.20	0.11	0.06	0.09	0.21	0.30	0.13	0.02	0.02
TiO2	2.04	1.37	24.03	20.35	23.12	24.78	50.55	50.64	51.88	53.36	52.03
Al2O3	3.29	1.99	2.35	2.90	7.16	1.55	nd	nd	0.18	0.11	0.14
Fe2O3	nd	nd	17.05	24.40	15.87	17.32	6.07	6.09	3.44	2.48	3.59
Cr2O3	0.28	nd	1.77	1.22	0.70	0.32	nd	nd	0.07	0.05	0.06
FeO	8.89	10.56	48.30	45.72	47.81	51.60	39.97	39.73	40.21	40.46	41.04
MnO	0.14	0.34	1.71	0.56	0.47	1.91	0.53	0.53	0.55	0.48	0.51
MgO	13.93	13.80	1.98	2.34	3.34	0.16	2.92	3.16	3.39	3.96	2.95
CaO	21.19	20.69	0.23	nd	nd	nd	nd	nd	nd	nd	nd
total=	98.78	99.38	97.62	97.60	98.53	97.73	100.25	100.45	99.85	100.92	100.34
Mg#	74.9	70.4	-	-	-	-	-	-	-	-	-

1299 CPX6,MV74,P,R,E
1300 CPX7,MV74,P,R,E
1301 MT1,MV74,P,C,E
1302 MT310,MV74,P,C,W
1303 MT311,MV74,P,C,W
1304 MT317,MV74,GR,C,W
1305 IL1,MV74,GR,C,E
1306 IL2,MV74,GR,C,E
1307 IL307,MV74,GR,C,W
1308 IL312,MV74,P,C,W
1309 IL313,MV74,GR,C,W

	1310	1311	1312	1313	1314	1315	1316	1317	1318	1319	1320
SiO2	0.02	0.07	53.33	52.51	52.53	53.06	53.44	52.31	53.04	52.03	51.93
TiO2	52.12	51.33	nd	0.11	0.13	nd	nd	0.17	0.13	nd	0.18
Al2O3	0.13	0.11	28.83	29.80	29.79	29.57	29.11	29.70	29.12	29.76	29.81
Fe2O3	3.73	4.21	nd	nd	nd	nd	nd	nd	nd	nd	nd
Cr2O3	0.03	0.02	nd	nd	nd	nd	nd	nd	nd	nd	nd
FeO	40.80	40.93	0.48	0.62	0.68	0.51	0.41	0.73	0.53	0.65	0.78
MnO	0.47	0.53	nd	nd	nd	nd	nd	nd	nd	nd	nd
MgO	3.15	2.68	nd	nd	nd	nd	nd	nd	nd	nd	nd
CaO	nd	nd	11.35	12.48	12.33	12.10	11.63	12.79	11.98	12.75	12.60
Na2O	nd	nd	4.68	3.54	4.33	4.76	4.55	4.03	4.28	3.51	4.04
K2O	nd	nd	0.54	0.29	0.28	0.38	0.53	0.32	0.45	0.37	0.25
total=	100.45	99.88	99.21	99.35	100.07	100.38	99.67	100.05	99.53	99.07	99.59
An	-	-	55.5	64.9	60.1	57.2	56.7	62.5	59.1	65.2	62.4

1310 IL314,MV74,GR,C,W
1311 IL318,MV74,GR,C,W
1312 PL20,MV72,P,C,+OL+CPX+PL,E
1313 PL22,MV72,P,R,E
1314 PL23,MV72,P,C,E
1315 PL24,MV72,P,R,E
1316 PL26,MV72,P,I,E
1317 PL27,MV72,P,R,E
1318 PL28,MV72,P,C,E
1319 PL29,MV72,P,R,E
1320 PL30,MV72,GR,C,E

	1321	1322	1323	1324	1325	1326	1327	1328	1329	1330	1331
SiO2	52.52	48.57	49.83	50.07	49.04	49.73	49.68	49.24	50.51	0.55	nd
TiO2	nd	1.63	2.07	1.90	2.03	1.86	1.81	2.07	1.71	23.34	51.76
Al2O3	29.48	4.24	3.59	3.08	3.21	3.40	3.04	3.44	2.75	2.00	0.12
Fe2O3	nd	nd	nd	nd	nd	nd	nd	nd	nd	17.91	4.35
Cr2O3	nd	nd	nd	nd	0.26	0.03	0.04	0.03	0.02	0.03	nd
FeO	0.74	10.00	8.66	9.24	8.99	9.11	9.22	8.79	9.27	50.62	40.60
MnO	nd	0.21	0.27	0.15	0.16	0.18	0.18	0.14	0.17	1.72	0.64
MgO	nd	13.66	13.54	13.81	13.75	13.79	13.52	13.59	13.71	0.23	2.97
CaO	12.72	21.17	21.86	21.74	21.79	21.60	21.68	21.72	21.72	nd	nd
Na2O	4.47	nd	nd	nd	nd	0.36	0.40	0.39	0.39	nd	nd
K2O	0.32	nd	nd	nd	nd	nd	nd	nd	nd	nd	nd
total=	100.25	99.48	99.82	99.99	99.23	100.06	99.57	99.41	100.25	96.40	100.44
Mg#	-	75.6	73.6	73.3	75.7	77.7	77.2	78.2	76.1	-	-
An	60.0	-	-	-	-	-	-	-	-	-	-
Al ratio	-	0.1	0.2	0.1	-0.1	-	-	-	-	-	-

1321 PL31,MV72,GR,C,E
1322 CPX17,MV72,P,C,E
1323 CPX18,MV72,P,R,E
1324 CPX19,MV72,GR,C,E
1325 CPX20,MV72,GR,C,E
1326 CPX363,MV72,P,C,W
1327 CPX364,MV72,P,R,W
1328 CPX365,MV72,P,C,W
1329 CPX366,MV72,P,C,W
1330 MT329,MV72,GR,C,W
1331 IL317,MV72,GR,C,W

	1332	1333	1334	1335	1336	1337	1338	1339	1340	1341	1342
SiO2	nd	0.23	40.23	40.00	38.82	37.77	38.60	39.01	38.81	38.76	36.96
TiO2	52.24	51.23	nd	0.14	nd	nd	nd	nd	nd	nd	nd
Al2O3	0.07	0.35	nd	nd	nd	nd	nd	nd	nd	nd	nd
Fe2O3	2.66	5.26	nd	nd	nd	nd	nd	nd	nd	nd	nd
Cr2O3	nd	nd	nd	nd	0.03	nd	nd	nd	nd	nd	nd
FeO	41.65	39.36	17.26	15.49	21.32	28.73	18.21	18.58	18.48	20.64	31.42
MnO	0.79	0.73	0.13	0.12	0.34	0.53	0.19	0.26	0.21	0.28	0.66
NiO	nd	nd	nd	0.17	nd	nd	0.19	0.18	0.19	0.14	nd
MgO	2.54	3.50	42.66	43.48	39.84	33.76	42.38	42.25	42.21	40.53	31.51
CaO	nd	nd	0.19	0.17	0.24	0.32	0.18	0.20	0.18	0.23	0.38
total=	99.95	100.66	100.47	99.57	100.59	101.11	99.75	100.48	100.08	100.58	100.93
Mg#	-	-	81.5	83.3	76.9	67.7	80.6	80.2	80.3	77.8	64.1

1332 IL318,MV72,GR,C,W
1333 IL4,MV72,GR,C,E
1334 OL03,MV516,P,C,+OL+CPX+SP,E
1335 OL1,MV516,P,C,E
1336 OL1001R,MV516,P,C,W
1337 OL2,MV516,P,R,E
1338 OL356,MV516,P,C,W
1339 OL357,MV516,P,C,W
1340 OL358,MV516,P,C,W
1341 OL359,MV516,P,I,W
1342 OL360,MV516,P,R,W

	1343	1344	1345	1346	1347	1348	1349	1350	1351	1352	1353
SiO2	39.00	39.21	39.12	39.08	40.29	40.10	39.32	55.04	51.76	54.41	55.28
TiO2	nd	nd	nd	nd	nd	nd	nd	0.27	nd	0.12	0.22
Al2O3	nd	nd	nd	nd	nd	nd	nd	27.91	29.65	28.04	27.52
FeO	18.64	18.15	15.24	22.76	18.38	16.53	17.94	0.70	0.49	0.61	0.77
MnO	0.20	0.20	0.18	0.25	0.17	0.22	0.27	nd	nd	nd	nd
NiO	0.18	0.21	0.27	nd	nd	0.17	nd	nd	nd	nd	nd
MgO	42.29	42.62	44.32	38.17	41.72	43.08	41.91	nd	nd	0.05	nd
CaO	0.16	0.19	0.24	0.25	0.23	0.19	0.17	11.02	13.21	10.68	10.39
Na2O	nd	nd	nd	nd	nd	nd	nd	4.97	3.76	5.24	5.26
K2O	nd	nd	nd	nd	nd	nd	nd	0.38	0.31	0.34	0.33
total=	100.47	100.58	99.37	100.51	100.79	100.29	99.61	100.29	99.18	99.49	99.77
Mg#	80.2	80.7	83.8	74.9	80.2	82.3	80.6	-	-	-	-
An	-	-	-	-	-	-	-	53.8	64.8	51.9	51.2

1343 OL361,MV516,P,C,W
1344 OL362,MV516,P,C,W
1345 OL363,MV516,P,C,W
1346 OL4,MV516,P,I,E
1347 OL5,MV516,P,C,E
1348 OL6,MV516,P,C,E
1349 OL7,MV516,P,C,E
1350 PL02,MV516,GR,C,E
1351 PL1,MV516,GR,C,E
1352 PL10001,MV516,GR,C,W
1353 PL3,MV516,GR,C,E

	1354	1355	1356	1357	1358	1359	1360	1361	1362	1363	1364
SiO2	53.79	51.75	45.61	47.76	48.81	48.74	50.21	51.66	52.19	53.61	49.01
TiO2	0.12	1.28	4.17	3.26	1.06	2.45	2.03	1.13	1.18	0.37	2.45
Al2O3	28.99	1.96	6.88	5.05	6.59	4.78	3.56	2.27	1.93	0.18	4.12
Cr2O3	nd	0.22	nd	nd	0.53	nd	nd	nd	nd	nd	0.22
FeO	0.72	9.06	9.96	9.09	5.98	8.96	8.40	9.80	8.69	9.42	9.05
MnO	nd	0.15	0.17	0.20	0.11	0.18	0.19	0.35	0.22	0.23	0.15
MgO	nd	13.74	10.98	12.16	15.07	12.96	13.62	13.56	14.15	14.01	12.86
CaO	11.81	21.38	21.59	21.70	20.89	21.55	21.53	21.37	21.58	22.04	21.66
Na2O	4.52	0.29	0.68	0.66	0.50	0.48	0.52	0.48	0.45	0.38	0.21
K2O	0.15	nd	nd	nd	nd	nd	nd	nd	nd	nd	nd
total=	100.10	99.83	100.04	99.88	99.54	100.10	100.06	100.62	100.39	100.24	99.73
Mg#	-	73.0	71.7	74.8	89.2	75.8	76.6	73.6	75.3	73.0	71.8
An	58.6	-	-	-	-	-	-	-	-	-	-
Al ratio	-	0.3	0.1	0.1	0.4	0.2	0.2	0.2	0.3	1.3	0.2

1354 PL4,MV516,GR,C,E
1355 CPX1,MV516,P?,C,E
1356 CPX1044,MV516,GR,C,W
1357 CPX1045,MV516,GR,C,W
1358 CPX1046,MV516,P,C,W
1359 CPX1047,MV516,P,I,W
1360 CPX1048,MV516,P,R,W
1361 CPX1049,MV516,P?,I,W
1362 CPX1050,MV516,P?,I,W
1363 CPX1051,MV516,P?,C,W
1364 CPX3,MV516,P?,C,E

	1365	1366	1367	1368	1369	1370	1371	1372	1373	1374	1375
SiO2	54.03	53.48	48.45	50.24	0.39	0.16	0.17	0.20	0.38	0.22	0.23
TiO2	0.62	0.73	2.96	2.10	1.92	0.86	1.01	0.87	0.86	1.03	3.22
Al2O3	0.92	0.43	4.68	2.96	28.94	50.24	46.40	47.55	48.72	53.17	33.60
Fe2O3	nd	nd	nd	nd	9.57	7.84	8.96	7.40	6.00	7.49	13.81
Cr2O3	0.24	nd	nd	nd	25.07	8.25	10.44	10.93	11.08	5.71	13.89
FeO	9.03	9.18	9.27	10.02	24.76	17.05	19.96	17.77	17.10	17.46	25.33
MnO	0.22	0.18	0.17	0.25	0.15	0.24	0.32	0.29	0.28	0.13	0.33
MgO	13.48	13.87	12.00	13.25	8.99	15.41	13.24	14.58	15.34	15.89	9.61
CaO	21.80	21.97	21.66	21.08	nd	nd	nd	nd	nd	nd	nd
Na2O	0.31	0.30	0.43	0.36	nd	nd	nd	nd	nd	nd	nd
total=	100.65	100.14	99.62	100.26	99.79	100.05	100.50	99.59	99.76	101.10	100.02
Mg#	72.7	72.9	69.8	71.5	39.3	61.7	54.2	59.4	61.5	61.9	40.3
Al ratio	9.8	1.1	0.2	0.1	-	-	-	-	-	-	-

1365 CPX4,MV516,GR,C,E
1366 CPX5,MV516,P?,C,E
1367 CPX8,MV516,GR,C,E
1368 CPX9,MV516,GR,C,E
1369 SP01,MV516,P,C,E
1370 SP1023,MV516,P,C,W
1371 SP1027,MV516,P,C,W
1372 SP1028,MV516,P,C,W
1373 SP1029,MV516,P,C,W
1374 SP2,MV516,P,C,E
1375 SP3,MV516,P,C,E

	1376	1377	1378	1379	1380	1381	1382	1383	1384	1385	1386
SiO2	0.25	nd	0.20	0.15	0.27	0.44	0.08	53.21	38.53	37.33	38.16
TiO2	1.13	0.79	11.74	24.65	25.21	49.37	50.88	nd	nd	nd	nd
Al2O3	46.73	50.30	1.60	1.85	2.16	0.23	0.04	24.30	nd	nd	nd
Fe2O3	8.02	8.21	42.91	18.30	16.64	5.43	4.42	nd	nd	nd	nd
Cr2O3	9.85	8.54	0.26	0.21	0.88	nd	0.09	nd	nd	nd	nd
FeO	21.76	16.51	40.32	50.80	51.25	41.43	40.21	nd	26.38	30.94	27.12
MnO	0.21	nd	0.55	0.91	0.83	1.12	0.99	nd	0.32	0.62	0.38
MgO	12.26	15.76	0.71	1.46	1.86	1.32	2.60	nd	35.24	31.01	34.80
CaO	nd	nd	nd	nd	nd	nd	nd	1.06	0.28	0.46	0.28
Na2O	nd	nd	nd	nd	nd	nd	nd	10.86	nd	nd	nd
K2O	nd	nd	nd	nd	nd	nd	nd	0.43	nd	nd	nd
total=	100.21	100.11	98.29	98.33	99.10	99.34	99.31	89.86	100.75	100.36	100.74
Mg#	50.1	63.0	-	-	-	-	-	-	70.4	64.1	69.6

1376 SP4,MV516,P,C,E
1377 SP5,MV516,P,C,E
1378 MT1024,MV516,GR,C,W
1379 MT1030,MV516,GR,C,W
1380 MT1031,MV516,GR,C,W
1381 IL1,MV516,GR,C,E
1382 IL1025,MV516,GR,C,W
1383 AC1,MV516,GR,C,E
1384 OL10,MV704,P,C,+OL+PL+MT,E
1385 OL11,MV704,P,R,E
1386 OL12,MV704,P,C,E

	1387	1388	1389	1390	1391	1392	1393	1394	1395	1396	1397
SiO2	38.07	37.90	38.19	37.53	37.12	36.83	37.87	38.14	38.02	37.40	37.45
TiO2	nd	nd	0.14	nd	nd	nd	nd	nd	nd	nd	nd
FeO	26.99	27.09	27.61	28.22	31.37	28.70	26.69	27.31	27.42	28.60	28.85
MnO	0.37	0.35	0.35	0.38	0.43	0.40	0.41	0.24	0.32	0.40	0.33
NiO	nd	nd	nd	nd	nd	0.15	nd	nd	0.17	nd	nd
MgO	34.39	34.52	33.97	33.73	31.68	33.25	34.68	35.16	34.24	33.90	32.92
CaO	0.36	0.35	0.36	0.42	0.41	0.37	0.26	0.35	0.42	0.40	0.29
total=	100.18	100.21	100.62	100.28	101.01	99.70	99.91	101.20	100.59	100.70	99.84
Mg#	69.4	69.4	68.7	68.1	64.3	67.4	69.8	69.6	69.0	67.9	67.0

1387 OL13,MV704,P,C,E
1388 OL14,MV704,P,C,E
1389 OL15,MV704,P,C,E
1390 OL16,MV704,P,C,E
1391 OL17,MV704,P,C,E
1392 OL17,MV704,GR,C,E
1393 OL18,MV704,P,C,E
1394 OL18,MV704,GR,C,E
1395 OL19,MV704,P,C,E
1396 OL2,MV704,GR,C,E
1397 OL20,MV704,P,C,E

	1398	1399	1400	1401	1402	1403	1404	1405	1406	1407	1408
SiO2	37.59	37.80	37.39	37.55	37.33	37.76	37.02	37.38	38.26	51.99	51.71
TiO2	nd	nd	nd	nd	nd	nd	nd	nd	0.11	nd	0.13
Al2O3	nd	nd	nd	nd	nd	nd	nd	nd	nd	30.47	30.25
FeO	27.27	27.40	26.96	26.40	27.03	26.35	29.89	27.03	26.67	0.50	0.54
MnO	0.51	0.50	0.41	0.37	0.38	0.38	0.50	0.41	0.32	nd	nd
NiO	nd	nd	0.09	0.07	0.06	0.05	0.04	0.05	nd	nd	nd
MgO	34.38	34.50	35.27	35.80	35.08	35.92	33.15	35.45	34.89	nd	nd
CaO	0.40	0.50	0.44	0.38	0.39	0.34	0.40	0.41	0.37	13.32	13.64
Na2O	nd	nd	nd	nd	nd	nd	nd	nd	nd	3.92	3.94
K2O	nd	nd	nd	nd	nd	nd	nd	nd	nd	0.17	0.28
total=	100.15	100.70	100.56	100.57	100.27	100.80	101.00	100.73	100.62	100.37	100.49
Mg#	69.2	69.2	70.0	70.7	69.8	70.8	66.4	70.0	70.0	-	-
An	-	-	-	-	-	-	-	-	-	64.6	64.6

1398 OL21,MV704,P,C,E
1399 OL3,MV704,GR,C,E
1400 OL341,MV704,P,C,W
1401 OL343,MV704,P,I,W
1402 OL344,MV704,P,R,W
1403 OL345,MV704,P,C,W
1404 OL346,MV704,P,C,W
1405 OL347,MV704,P,C,W
1406 OL9,MV704,P,C,E
1407 PL1,MV704,P,C,E
1408 PL10,MV704,P,C,E

	1409	1410	1411	1412	1413	1414	1415	1416	1417	1418	1419
SiO2	51.34	51.53	51.21	50.64	50.80	50.35	51.28	50.94	51.11	53.91	50.45
TiO2	0.09	0.15	0.06	nd	0.08	nd	0.08	nd	0.08	nd	nd
Al2O3	30.80	30.69	30.80	31.22	30.85	30.96	30.82	30.45	30.46	28.65	30.44
FeO	0.39	0.42	0.35	0.62	0.39	0.54	0.41	0.35	0.72	0.41	0.78
MgO	0.11	nd	0.14	nd	0.12	nd	0.11	nd	0.22	nd	nd
CaO	13.29	14.16	13.09	14.60	13.08	14.65	13.24	14.00	13.06	12.06	14.49
Na2O	3.89	3.28	3.96	3.12	3.89	3.61	4.00	3.96	3.89	4.17	3.33
K2O	0.24	0.17	0.24	0.16	0.21	0.22	0.25	0.22	0.24	0.36	0.22
total=	100.15	100.40	99.85	100.36	99.42	100.33	100.19	99.92	99.78	99.56	99.71
An	64.5	69.8	63.7	71.4	64.2	68.3	63.7	65.3	64.1	60.2	69.7

1409 PL10,MV704,P,C,W
1410 PL11,MV704,P,C,E
1411 PL11,MV704,P,C,W
1412 PL12,MV704,P,R,E
1413 PL12,MV704,P,C,W
1414 PL13,MV704,P,C,E
1415 PL13,MV704,P,C,W
1416 PL14,MV704,P,C,E
1417 PL14,MV704,P,C,W
1418 PL15,MV704,P,R,E
1419 PL15,MV704,GR,C,E

	1420	1421	1422	1423	1424	1425	1426	1427	1428	1429	1430
SiO2	51.56	52.28	51.66	50.58	52.29	52.00	51.87	52.43	50.45	50.02	51.53
TiO2	0.15	0.16	nd	nd	0.11	nd	0.14	nd	nd	nd	0.13
Al2O3	30.13	29.02	30.33	30.27	29.47	30.30	30.28	29.77	31.33	31.04	30.38
FeO	0.59	0.95	0.62	0.70	0.61	0.46	0.48	0.27	0.44	0.57	0.35
CaO	13.33	12.53	13.80	13.78	12.88	13.56	13.13	13.31	14.45	14.88	14.08
Na2O	3.74	4.08	3.68	3.44	3.87	3.63	4.05	3.57	3.04	2.99	3.73
K2O	0.22	0.36	0.17	0.14	0.25	0.17	0.23	0.25	0.25	0.20	0.19
total=	99.72	99.38	100.26	98.91	99.48	100.12	100.18	99.60	99.96	99.70	100.39
An	65.5	61.6	66.8	68.3	63.8	66.7	63.3	66.3	71.4	72.5	66.9

1420 PL16,MV704,P,C,E
1421 PL16,MV704,GR,C,E
1422 PL17,MV704,P,R,E
1423 PL17,MV704,GR,C,E
1424 PL18,MV704,P,C,E
1425 PL2,MV704,P,C,E
1426 PL20,MV704,P,C,E
1427 PL21,MV704,P,C,E
1428 PL22,MV704,P,R,E
1429 PL24,MV704,P,C,E
1430 PL25,MV704,P,C,E

	1431	1432	1433	1434	1435	1436	1437	1438	1439	1440	1441
SiO2	52.69	51.59	52.71	52.20	49.95	51.26	47.19	46.33	48.20	46.96	47.10
TiO2	nd	nd	nd	0.11	0.12	0.07	2.95	3.20	2.50	3.19	2.80
Al2O3	29.97	29.78	30.14	29.48	30.89	31.09	4.60	5.25	4.10	5.38	4.50
FeO	0.42	0.46	0.28	0.47	0.80	0.37	10.50	11.17	10.40	10.38	10.50
MnO	nd	nd	nd	nd	nd	nd	0.25	0.18	0.20	nd	0.20
MgO	nd	nd	nd	nd	nd	0.15	12.19	12.02	12.20	12.30	12.40
CaO	13.36	13.38	13.42	13.45	14.67	13.21	21.26	20.73	21.10	21.62	21.20
Na2O	3.72	3.81	3.52	4.08	2.97	3.84	nd	nd	nd	nd	nd
K2O	0.25	0.21	0.22	0.20	0.17	0.24	nd	nd	nd	nd	nd
total=	100.41	99.23	100.29	99.99	99.57	100.23	98.94	98.88	98.70	99.83	98.70
Mg#	-	-	-	-	-	-	68.8	67.9	67.6	70.0	70.2
An	65.5	65.2	66.9	63.8	72.5	64.6	-	-	-	-	-
Al ratio	-	-	-	-	-	-	-	-	0.2	0.1	-

1431 PL5,MV704,P,C,E
1432 PL6,MV704,P,C,E
1433 PL7,MV704,P,C,E
1434 PL8,MV704,P,C,E
1435 PL9,MV704,P,R,E
1436 PL9,MV704,P,C,W
1437 CPX20,MV704,GR,C,E
1438 CPX21,MV704,GR,C,E
1439 CPX6,MV704,GR,C,E
1440 CPX6,MV704,GR,C,E
1441 CPX7,MV704,GR,C,E

	1442	1443	1444	1445	1446	1447	1448	1449	1450	1451	1452
SiO2	0.40	0.22	0.19	0.34	0.56	0.05	0.20	0.08	0.08	0.36	62.50
TiO2	27.10	25.85	26.16	26.30	24.27	26.85	26.10	23.19	50.66	50.12	nd
Al2O3	1.40	1.87	1.62	1.77	2.19	1.25	1.40	3.60	0.08	0.15	22.68
Fe2O3	12.84	16.27	15.65	15.47	17.24	15.23	16.84	20.19	3.86	3.67	nd
Cr2O3	0.20	0.20	0.19	0.14	0.42	0.03	0.30	0.21	0.02	0.02	nd
FeO	54.65	51.69	52.99	52.80	51.56	53.33	51.85	47.38	41.82	42.62	0.57
MnO	1.10	0.76	0.67	0.56	0.67	0.70	0.70	0.44	1.04	0.87	nd
MgO	0.30	1.76	1.10	1.69	1.26	1.19	2.00	3.25	1.56	1.12	nd
CaO	0.20	0.12	0.11	nd	nd	nd	nd	nd	nd	nd	3.78
Na2O	nd	nd	nd	nd	nd	nd	nd	nd	nd	nd	6.67
K2O	nd	nd	nd	nd	nd	nd	nd	nd	nd	nd	3.25
BaO	nd	nd	nd	nd	nd	nd	nd	nd	nd	nd	1.12
total=	98.19	98.74	98.68	99.07	98.17	98.63	99.39	98.34	99.12	98.93	100.57

1442 MT1,MV704,P,C,E
1443 MT11,MV704,GR,C,E
1444 MT12,MV704,GR,C,E
1445 MT13,MV704,GR,C,E
1446 MT15,MV704,P,C,E
1447 MT2,MV704,GR,C,W
1448 MT3,MV704,P,C,E
1449 MT3,MV704,GR,C,W
1450 IL20,MV704,GR,C,W
1451 IL21,MV704,GR,C,W
1452 AF2,MV506,GR,C,+OL+CPX+PL,E

	1453	1454	1455	1456	1457	1458	1459	1460	1461	1462	1463
SiO2	51.22	51.41	53.77	50.86	52.31	51.75	52.27	50.85	53.77	51.96	50.89
TiO2	0.09	0.07	0.12	0.06	0.06	0.06	0.07	0.06	0.18	0.16	nd
Al2O3	30.03	30.22	28.80	30.53	29.66	29.85	29.59	30.51	29.59	30.01	31.53
FeO	0.44	0.44	0.44	0.48	0.41	0.46	0.54	0.54	0.66	0.61	0.55
MgO	nd	0.08	0.08	0.09	0.06	0.06	0.08	nd	nd	nd	nd
CaO	13.18	13.67	11.85	13.96	12.77	12.94	12.99	13.95	11.62	13.14	14.35
Na2O	3.67	3.73	4.61	3.40	4.05	3.92	3.95	3.49	4.54	4.25	3.00
K2O	0.30	0.27	0.33	0.22	0.26	0.28	0.26	0.22	0.24	0.24	0.18
total=	98.93	99.89	100.00	99.60	99.58	99.32	99.75	99.62	100.60	100.37	100.50
An	65.3	65.9	57.6	68.5	62.6	63.5	63.5	68.0	57.7	62.2	71.8

1453 PL333,MV506,P,C,W
1454 PL333R,MV506,P,C,W
1455 PL334,MV506,P,R,W
1456 PL335,MV506,P,C,W
1457 PL336,MV506,P,C,W
1458 PL337,MV506,P,C,W
1459 PL338,MV506,P,C,W
1460 PL339,MV506,P,C,W
1461 PL6,MV506,GR,C,E
1462 PL7,MV506,P,C,E
1463 PL8,MV506,P,R,E

	1464	1465	1466	1467	1468	1469	1470	1471	1472	1473	1474
SiO2	52.25	50.43	49.64	50.20	51.02	47.99	49.09	48.47	47.00	50.24	48.51
TiO2	nd	1.87	1.88	1.31	1.43	1.78	1.33	2.23	2.23	1.10	1.52
Al2O3	30.30	3.23	3.39	4.32	2.24	5.98	5.63	4.68	6.81	5.34	6.26
Cr2O3	nd	nd	nd	nd	nd	0.13	0.25	0.02	0.06	0.38	0.28
FeO	0.42	9.60	8.90	7.82	10.50	8.11	7.11	8.92	8.18	6.25	6.80
MnO	nd	0.25	nd	0.13	0.19	0.15	0.15	0.18	0.12	0.15	0.13
NiO	nd	nd	nd	0.14	nd	nd	nd	nd	nd	nd	nd
MgO	nd	12.78	13.24	14.11	12.33	13.10	14.01	12.66	12.53	14.69	13.63
CaO	13.45	22.54	22.89	22.11	22.52	22.23	21.17	21.94	21.92	21.28	21.68
Na2O	4.07	nd	nd	nd	nd	nd	0.48	0.54	0.54	0.61	0.51
K2O	0.25	nd	nd	nd	nd	nd	nd	nd	nd	nd	nd
total=	100.74	100.70	99.94	100.14	100.23	99.47	99.22	99.64	99.39	100.04	99.32
Mg#	-	70.4	74.4	77.1	67.7	76.9	82.2	77.4	81.2	84.9	83.5
An	63.7	-	-	-	-	-	-	-	-	-	-
Al ratio	-	0.2	0.1	0.4	0.2	0.3	0.4	0.1	0.2	0.5	0.4

1464 PL9,MV506,P,C,E
1465 CPX14,MV506,GR,C,E
1466 CPX15,MV506,GR,C,E
1467 CPX16,MV506,P,C,E
1468 CPX17,MV506,P,R,E
1469 CPX18,MV506,P,C,E
1470 CPX356,MV506,P,C,W
1471 CPX357,MV506,P,R,W
1472 CPX358,MV506,P,C,W
1473 CPX359,MV506,P,C,W
1474 CPX360,MV506,P,C,W

	1475	1476	1477	1478	1479	1480	1481	1482	1483	1484	1485
SiO2	50.87	49.32	0.34	59.24	53.46	52.36	53.79	53.60	52.38	53.62	54.09
TiO2	0.91	2.03	54.04	0.16	0.13	nd	nd	0.13	nd	nd	0.20
Al2O3	4.17	4.07	0.29	25.18	29.17	29.65	28.64	29.04	29.59	29.02	28.76
Cr2O3	0.31	0.05	nd	nd	nd	nd	nd	nd	nd	nd	nd
FeO	6.18	8.49	41.03	0.17	0.55	0.56	0.52	0.57	0.61	0.50	0.78
MnO	0.15	0.19	1.28	nd	nd	nd	nd	nd	nd	nd	nd
MgO	15.34	12.98	2.47	nd	nd	nd	nd	nd	nd	nd	nd
CaO	21.13	22.20	nd	7.21	12.14	12.41	11.52	11.83	12.88	11.84	11.57
Na2O	0.57	0.47	nd	7.01	4.48	4.34	4.64	4.71	4.04	3.97	4.42
K2O	nd	nd	nd	0.76	0.29	0.28	0.30	0.30	0.24	0.34	0.31
total=	99.63	99.80	99.45	99.73	100.22	99.60	99.41	100.18	99.74	99.29	100.13
Mg#	86.0	77.2	-	-	-	-	-	-	-	-	-
An	-	-	-	34.7	59.0	60.3	56.8	57.1	62.9	60.9	58.0
Al ratio	0.4	0.1	-	-	-	-	-	-	-	-	-

1475 CPX361,MV506,P,C,W
1476 CPX362,MV506,P,R,W
1477 IL3,MV506,GR,C,E
1478 PL1,MV122,P,C,+OL+CPX+PL,E
1479 PL11,MV122,P,C,E
1480 PL13,MV122,P,R,E
1481 PL14,MV122,P,C,E
1482 PL15,MV122,P,R,E
1483 PL16,MV122,P,R,E
1484 PL17,MV122,P,R,E
1485 PL18,MV122,GR,C,E

	1486	1487	1488	1489	1490	1491	1492	1493	1494	1495	1496
SiO2	55.93	53.49	53.66	54.83	53.50	60.90	49.64	50.09	48.31	50.06	51.47
TiO2	nd	nd	nd	0.15	nd	0.16	1.40	1.07	1.83	1.56	1.31
Al2O3	26.44	28.70	28.61	27.88	28.33	24.28	4.14	2.71	5.20	2.99	1.69
Cr2O3	nd	nd	nd	nd	nd	nd	0.34	nd	0.50	0.27	0.24
FeO	0.63	0.82	0.63	0.61	0.78	0.25	9.46	11.43	8.87	10.42	10.90
MnO	nd	nd	nd	nd	nd	nd	0.21	0.40	0.16	0.18	0.30
NiO	nd	nd	nd	nd	nd	nd	nd	nd	nd	nd	0.17
MgO	nd	nd	nd	nd	nd	nd	14.77	13.62	14.72	14.23	15.30
CaO	9.54	11.92	11.34	10.89	11.72	6.29	19.09	19.72	19.90	20.31	19.06
Na2O	5.73	4.71	4.18	5.32	4.59	7.42	nd	nd	nd	nd	nd
K2O	0.62	0.36	0.34	0.33	0.26	0.90	nd	nd	nd	nd	nd
total=	98.89	100.00	98.76	100.01	99.18	100.20	99.05	99.04	99.49	100.02	100.44
Mg#	-	-	-	-	-	-	73.6	69.0	77.7	72.3	72.1
An	46.2	57.1	58.7	52.1	57.6	30.3	-	-	-	-	-
Al ratio	-	-	-	-	-	-	0.4	0.2	0.2	0.1	-0.1

1486 PL2,MV122,P,I,E
1487 PL3,MV122,P,R,E
1488 PL4,MV122,P,C,E
1489 PL5,MV122,P,I,E
1490 PL6,MV122,P,R,E
1491 PL8,MV122,P,C,E
1492 CPX1,MV122,P,C,E
1493 CPX12,MV122,P,C,E
1494 CPX13,MV122,P,I,E
1495 CPX15,MV122,GR,C,E
1496 CPX16,MV122,GR,C,E

	1497	1498	1499	1500	1501	1502	1503	1504	1505	1506	1507
SiO2	49.52	49.68	50.58	50.63	49.23	49.73	50.13	51.85	49.35	50.77	49.64
TiO2	1.34	1.23	1.00	1.38	1.82	1.49	1.28	1.26	1.56	1.17	1.30
Al2O3	4.10	4.49	3.82	2.02	4.58	4.46	4.38	1.87	5.33	3.70	4.88
Cr2O3	0.27	0.47	0.61	0.13	0.17	0.46	0.47	0.26	0.25	0.29	0.60
FeO	9.74	8.98	8.45	10.73	8.63	8.35	8.22	10.54	8.23	9.53	7.63
MnO	0.18	nd	0.17	0.21	0.18	0.14	0.19	0.16	0.15	0.19	0.14
MgO	15.18	14.62	16.93	14.73	14.35	14.89	15.42	15.00	14.89	15.39	15.54
CaO	19.01	20.04	17.61	19.23	20.33	19.72	19.29	19.78	19.13	18.49	19.35
Na2O	nd	nd	0.42	0.33	0.50	0.48	0.46	nd	0.59	0.48	0.50
total=	99.34	99.51	99.59	99.39	99.79	99.72	99.84	100.72	99.48	100.01	99.58
Mg#	75.4	74.8	82.2	74.2	80.0	80.0	80.7	71.7	80.4	76.9	83.2
Al ratio	0.2	0.4	0.2	-0.1	0.2	0.3	0.3	0.1	0.4	0.3	0.3

1497 CPX2,MV122,P,I,E
1498 CPX3,MV122,P,R,E
1499 CPX345,MV122,P,R,W
1500 CPX346,MV122,P,R,W
1501 CPX347,MV122,P,C,W
1502 CPX348,MV122,P,I,W
1503 CPX349,MV122,P,I,W
1504 CPX35,MV122,P,R,E
1505 CPX350,MV122,P,C,W
1506 CPX351,MV122,P,C,W
1507 CPX352,MV122,P,C,W

	1508	1509	1510	1511	1512	1513	1514	1515	1516	1517	1518
SiO2	49.81	49.08	46.44	47.18	48.82	51.34	51.37	51.29	48.72	47.58	46.47
TiO2	1.44	1.76	2.60	2.37	1.70	1.01	0.99	0.96	1.70	2.05	2.76
Al2O3	4.16	5.13	7.69	6.93	5.85	2.87	3.23	3.20	5.55	6.33	8.02
Cr2O3	0.34	0.84	0.25	nd	0.87	0.70	0.46	0.43	0.94	0.62	0.31
FeO	9.06	6.76	8.39	9.53	7.16	6.66	7.27	7.16	7.42	7.78	8.55
MnO	0.19	0.13	0.13	nd	0.21	nd	0.17	0.25	0.13	nd	0.14
NiO	nd	nd	nd	nd	0.19	nd	nd	nd	nd	nd	nd
MgO	15.17	14.58	13.52	13.82	15.27	16.04	17.02	17.01	15.12	14.11	13.45
CaO	19.14	20.80	19.63	19.95	20.16	20.54	19.73	19.66	20.23	20.86	20.38
Na2O	0.53	0.48	0.59	nd	nd	nd	nd	nd	nd	nd	nd
total=	99.84	99.56	99.24	99.78	100.23	99.16	100.24	99.96	99.81	99.33	100.08
Mg#	80.3	83.1	80.7	74.7	80.8	81.1	82.3	82.5	79.9	78.6	75.4
Al ratio	0.2	0.3	0.3	0.3	0.3	0.3	0.2	0.2	0.3	0.3	0.3

1508 CPX353,MV122,P,C,W
1509 CPX354,MV122,P,C,W
1510 CPX355,MV122,P,I,W
1511 CPX36,MV122,P,I,E
1512 CPX37,MV122,P,I,E
1513 CPX39,MV122,P,C,E
1514 CPX4,MV122,P,C,E
1515 CPX40,MV122,P,C,E
1516 CPX41,MV122,P,C,E
1517 CPX42,MV122,P,I,E
1518 CPX43,MV122,P,I,E

	1519	1520	1521	1522	1523	1524	1525	1526	1527	1528	1529
SiO2	47.61	51.43	48.52	46.19	49.98	0.23	nd	0.22	nd	0.09	50.02
TiO2	2.26	1.18	1.79	2.85	1.62	16.34	48.66	47.68	49.11	49.29	0.11
Al2O3	6.51	1.75	5.75	7.82	3.07	1.83	nd	nd	0.06	0.11	30.52
Fe2O3	nd	nd	nd	nd	nd	31.98	9.24	10.28	8.24	7.81	nd
Cr2O3	nd	0.14	0.83	nd	0.15	0.96	0.29	nd	0.11	0.11	nd
FeO	9.65	11.32	7.18	8.98	10.35	45.60	38.29	38.06	39.63	39.26	0.71
MnO	0.23	0.27	0.16	0.24	0.25	0.39	0.54	0.51	0.36	0.39	nd
MgO	13.96	14.76	14.94	13.07	14.88	0.04	2.76	2.56	2.34	2.68	nd
CaO	19.88	19.36	20.36	20.06	19.03	nd	nd	nd	nd	nd	14.06
Na2O	nd	nd	nd	0.58	nd	nd	nd	nd	nd	nd	3.67
total=	100.10	100.21	99.53	99.79	99.33	97.37	99.78	99.31	99.85	99.74	99.09
Mg#	74.8	70.2	79.8	79.9	72.5	-	-	-	-	-	-
An	-	-	-	-	-	-	-	-	-	-	67.9
Al ratio	0.3	-	0.3	0.2	0.1	-	-	-	-	-	-

1519 CPX44,MV122,P,I,E
1520 CPX45,MV122,P,R,E
1521 CPX5,MV122,P,I,E
1522 CPX7,MV122,P,I,E
1523 CPX8,MV122,P,R,E
1524 MT328,MV122,GR,C,W
1525 IL1,MV122,GR,C,E
1526 IL2,MV122,GR,C,E
1527 IL315,MV122,GR,C,W
1528 IL316,MV122,GR,C,W
1529 PL17,MV702,P,R,+PL,E

	1530	1531	1532	1533	1534	1535	1536	1537	1538	1539	1540
SiO2	51.15	49.28	51.16	51.36	51.16	51.44	51.21	51.12	51.20	49.57	50.47
TiO2	0.16	nd	0.06	0.06	0.05	0.06	0.07	0.06	0.07	0.03	0.04
Al2O3	29.94	31.39	29.82	29.86	29.79	29.90	29.81	29.87	29.92	30.94	30.60
FeO	0.48	0.62	0.56	0.47	0.52	0.56	0.56	0.50	0.53	0.54	0.54
MgO	nd	nd	0.13	0.15	0.16	0.15	0.14	0.14	0.13	0.13	0.14
CaO	13.76	15.19	12.95	13.25	13.19	13.40	13.37	13.37	13.46	14.68	14.00
Na2O	3.64	2.51	3.68	3.76	3.68	3.81	3.71	3.76	3.64	3.02	3.49
K2O	0.13	0.12	0.19	0.20	0.22	0.21	0.23	0.22	0.23	0.16	0.18
total=	99.26	99.11	98.55	99.11	98.77	99.53	99.10	99.04	99.18	99.07	99.46
An	67.1	76.4	65.3	65.3	65.6	65.2	65.7	65.4	66.2	72.2	68.2

1530 PL4,MV702,P,C,E
1531 PL7,MV702,P,C,E
1532 PL1,MV702,P,C,W
1533 PL10,MV702,P,C,W
1534 PL11,MV702,P,C,W
1535 PL12,MV702,P,I,W
1536 PL13,MV702,P,I,W
1537 PL14,MV702,P,R,W
1538 PL15,MV702,P,R,W
1539 PL16,MV702,P,C,W
1540 PL17,MV702,P,I,W

	1541	1542	1543	1544	1545	1546	1547	1548	1549	1550	1551
SiO2	49.22	52.13	50.81	63.11	50.78	48.91	50.94	48.26	50.61	50.64	56.30
TiO2	0.04	0.13	0.05	0.16	0.06	0.06	0.06	0.05	0.04	0.06	0.12
Al2O3	31.28	29.10	29.90	21.79	30.45	31.38	30.12	31.66	29.88	30.15	26.45
FeO	0.57	0.61	0.56	0.40	0.57	0.59	0.53	0.52	0.50	0.51	0.53
MgO	0.15	0.14	0.13	0.05	0.11	nd	0.13	0.12	0.14	0.14	0.09
CaO	14.95	12.64	13.51	3.56	14.08	15.21	13.52	15.35	13.61	13.64	9.28
Na2O	2.80	4.14	3.62	7.75	3.38	2.80	3.76	2.66	3.70	3.61	5.72
K2O	0.15	0.30	0.24	2.44	0.20	0.17	0.24	0.14	0.20	0.19	0.61
total=	99.16	99.19	98.82	99.26	99.63	99.12	99.30	98.76	98.68	98.94	99.10
An	74.0	61.7	66.4	17.4	68.9	74.3	65.6	75.5	66.2	66.9	45.6

1541 PL18,MV702,P,I,W
1542 PL19,MV702,P,R,W
1543 PL2,MV702,P,I,W
1544 PL20,MV702,P,R,W
1545 PL3,MV702,P,R,W
1546 PL4,MV702,P,C,W
1547 PL5,MV702,P,I,W
1548 PL6,MV702,P,R,W
1549 PL7,MV702,P,C,W
1550 PL8,MV702,P,I,W
1551 PL9,MV702,P,R,W

	1552	1553	1554	1555	1556	1557	1558	1559	1560	1561	1562
SiO2	47.51	0.09	0.12	0.04	0.11	0.05	0.36	35.65	36.67	54.89	56.43
TiO2	2.58	30.06	30.29	53.36	52.09	52.22	50.85	0.02	0.08	0.13	0.09
Al2O3	4.17	1.51	1.82	0.15	0.13	0.12	nd	0.06	0.05	28.01	26.98
Fe2O3	nd	7.05	5.96	1.46	1.16	1.92	3.55	nd	nd	nd	nd
Cr2O3	nd	0.23	0.07	nd	nd	nd	nd	nd	0.04	nd	nd
FeO	10.09	56.16	55.79	43.38	43.40	43.51	42.43	37.94	32.81	0.65	0.56
MnO	0.15	2.29	2.39	0.63	0.83	0.84	0.74	0.53	0.44	nd	nd
MgO	12.59	0.08	0.31	2.25	1.53	1.49	1.67	26.51	30.70	0.09	0.08
CaO	20.98	nd	nd	nd	nd	nd	nd	0.34	0.27	10.73	9.69
Na2O	nd	nd	nd	nd	nd	nd	nd	0.02	0.01	5.28	5.95
K2O	nd	nd	nd	nd	nd	nd	nd	nd	nd	0.45	0.56
total=	98.07	97.47	96.75	101.27	99.25	100.15	99.60	101.07	101.07	100.23	100.34
Mg#	69.9	-	-	-	-	-	-	55.5	62.5	-	-
An	-	-	-	-	-	-	-	-	-	51.5	45.9
Al ratio	0.1	-	-	-	-	-	-	-	-	-	-

1552 CPX15,MV702,GR,C,E
1553 MT208,MV702,GR,C,W
1554 MT209,MV702,GR,C,W
1555 IL210,MV702,GR,C,W
1556 IL211,MV702,GR,C,W
1557 IL212,MV702,GR,C,W
1558 IL3,MV702,GR,C,E
1559 OL126,MV39B,GR,C,+PL+MT+IL,W
1560 OL127,MV39B,GR,C,W
1561 PL130,MV39B,P,C,W
1562 PL131,MV39B,P,I,W

	1563	1564	1565	1566	1567	1568	1569	1570	1571	1572	1573
SiO2	55.43	53.87	57.99	53.80	55.87	54.17	54.28	54.89	53.16	55.75	55.08
TiO2	nd	0.13	nd	0.12	0.15	0.13	0.14	nd	0.11	0.13	0.15
Al2O3	27.16	28.58	25.79	28.86	27.15	28.48	28.79	27.55	28.45	27.14	27.94
FeO	0.78	0.50	0.59	0.48	0.52	0.49	0.49	0.40	0.53	0.61	0.84
MgO	0.17	0.14	0.07	0.11	0.11	0.12	0.08	0.09	nd	0.08	0.09
CaO	10.30	11.50	7.95	11.91	9.85	11.50	11.46	10.19	11.43	9.74	10.84
Na2O	5.64	4.81	6.71	4.64	5.54	4.82	4.87	5.46	4.72	5.73	5.12
K2O	0.50	0.38	1.00	0.36	0.51	0.37	0.37	0.46	0.36	0.52	0.42
total=	99.98	99.91	100.10	100.28	99.70	100.08	100.48	99.04	98.76	99.70	100.48
An	48.8	55.7	37.4	57.4	48.1	55.7	55.3	49.4	56.0	47.0	52.6

1563 PL132,MV39B,P,R,W
1564 PL133,MV39B,GR,C,W
1565 PL134,MV39B,GR,R,W
1566 PL135,MV39B,GR,C,W
1567 PL136,MV39B,GR,I,W
1568 PL138,MV39B,GR,C,W
1569 PL139,MV39B,GR,C,W
1570 PL140,MV39B,P,C,W
1571 PL141,MV39B,P,I,W
1572 PL142,MV39B,P,R,W
1573 PL144,MV39B,GR,C,W

	1574	1575	1576	1577	1578	1579	1580	1581	1582	1583	1584
SiO2	53.84	49.72	50.68	0.13	0.08	0.07	0.07	0.04	0.01	0.01	nd
TiO2	0.13	1.78	1.45	15.61	21.93	22.68	22.80	23.00	52.01	51.04	51.83
Al2O3	28.85	2.70	2.18	4.24	1.35	1.49	1.45	1.36	0.19	0.20	0.15
Fe2O3	nd	nd	nd	19.09	22.87	22.28	22.53	22.14	4.91	5.75	5.04
Cr2O3	nd	0.17	0.12	14.20	0.84	0.69	0.17	0.16	0.13	0.24	0.15
FeO	0.69	10.92	10.84	40.76	47.86	47.62	48.00	48.22	40.41	40.07	40.22
MnO	nd	0.26	0.26	0.52	1.52	1.37	1.58	1.42	0.48	0.40	0.45
MgO	0.09	14.07	14.30	3.02	1.05	1.88	1.58	1.57	3.30	3.05	3.33
CaO	11.55	19.00	19.38	nd	nd	nd	nd	nd	nd	nd	nd
Na2O	4.84	0.38	0.37	nd	nd	nd	nd	nd	nd	nd	nd
K2O	0.37	nd	nd	nd	nd	nd	nd	nd	nd	nd	nd
total=	100.36	99.00	99.58	97.57	97.50	98.08	98.18	97.91	101.44	100.76	101.17
Mg#	-	72.3	72.6	-	-	-	-	-	-	-	-
An	55.7	-	-	-	-	-	-	-	-	-	-

1574 PL145,MV39B,GR,C,W
1575 CPX272,MV39B,GR,C,W
1576 CPX273,MV39B,GR,C,W
1577 MTSP203,MV39B,P,C,W
1578 MT200,MV39B,P,R,W
1579 MT201,MV39B,P,R,W
1580 MT202,MV39B,GR,C,W
1581 MT204,MV39B,GR,C,W
1582 IL200,MV39B,P,I,W
1583 IL201,MV39B,P,C,W
1584 IL202,MV39B,P,R,W

	1585	1586	1587	1588	1589	1590	1591	1592	1593	1594	1595
SiO2	0.15	0.02	0.03	0.04	38.46	36.37	38.18	35.72	36.66	36.19	36.39
TiO2	50.54	51.83	50.50	51.22	nd	0.02	nd	0.04	nd	0.04	nd
Al2O3	0.17	0.14	0.15	0.14	nd	0.05	nd	0.05	nd	0.05	nd
Fe2O3	5.05	4.92	5.35	5.02	nd	nd	nd	nd	nd	nd	nd
Cr2O3	0.07	0.09	0.08	0.02	nd	0.03	nd	0.02	nd	0.01	nd
FeO	41.03	41.38	40.45	40.38	27.36	28.68	28.76	31.08	33.41	30.17	36.13
MnO	0.46	0.45	0.45	0.48	0.45	0.33	0.43	0.43	0.52	0.43	0.61
NiO	nd	nd	nd	nd	0.29	0.17	nd	0.12	nd	0.15	nd
MgO	2.32	2.69	2.55	2.94	34.11	34.81	33.11	32.81	29.53	33.63	27.99
CaO	nd	nd	nd	nd	nd	0.19	0.20	0.19	0.23	0.20	0.29
total=	99.79	101.52	99.56	100.24	100.67	100.65	100.68	100.46	100.35	100.87	101.41
Mg#	-	-	-	-	69.0	68.4	67.2	65.3	61.2	66.5	58.0

1585 IL203,MV39B,GR,C,W
1586 IL204,MV39B,GR,C,W
1587 IL205,MV39B,GR,C,W
1588 IL206,MV39B,GR,C,W
1589 OL1,MV121A,P,C,+OL+CPX+OPX+PL+MT+IL,E
1590 OL1,MV121A,P,C,W
1591 OL2,MV121A,P,C,E
1592 OL2,MV121A,P,R,W
1593 OL3,MV121A,GR,C,E
1594 OL3,MV121A,P,C,W
1595 OL4,MV121A,GR,C,E

	1596	1597	1598	1599	1600	1601	1602	1603	1604	1605	1606
SiO2	37.62	36.61	53.68	53.49	53.34	54.33	56.73	54.72	53.47	53.96	55.93
TiO2	nd	nd	0.19	0.12	nd	0.19	nd	0.18	0.21	nd	0.12
Al2O3	0.04	nd	28.56	28.45	28.55	27.98	26.45	27.58	27.98	28.46	27.26
Cr2O3	0.01	nd	nd	nd	nd	nd	nd	nd	nd	nd	nd
FeO	21.75	34.03	0.57	0.59	0.76	0.75	0.48	0.83	0.77	0.84	0.51
MnO	0.25	0.70	nd	nd	nd	nd	nd	nd	nd	nd	nd
NiO	0.20	nd	nd	nd	nd	nd	nd	nd	nd	nd	nd
MgO	39.88	29.33	nd	nd	nd	nd	nd	nd	nd	nd	nd
CaO	0.25	0.28	11.84	11.74	11.74	11.15	9.48	10.66	11.59	11.44	10.34
Na2O	nd	nd	4.99	5.15	4.79	5.10	5.47	5.14	4.83	4.96	5.41
K2O	nd	nd	0.30	0.41	0.38	0.45	0.48	0.54	0.39	0.39	0.41
total=	100.00	100.95	100.13	99.95	99.56	99.95	99.09	99.65	99.24	100.05	99.98
Mg#	76.6	60.6	-	-	-	-	-	-	-	-	-
An	-	-	55.8	54.5	56.3	53.3	47.5	51.7	55.7	54.8	50.1

1596 OL4,MV121A,P,C,W
1597 OL5,MV121A,GR,C,E
1598 PL1,MV121A,P,C,E
1599 PL2,MV121A,P,C,E
1600 PL3,MV121A,P,R,E
1601 PL4,MV121A,P,R,E
1602 PL5,MV121A,P,C,E
1603 PL5,MV121A,GR,C,E
1604 PL6,MV121A,P,R,E
1605 PL6,MV121A,GR,C,E
1606 PL7,MV121A,P,C,E

	1607	1608	1609	1610	1611	1612	1613	1614	1615	1616	1617
SiO2	53.13	55.46	53.58	53.02	53.81	51.26	50.69	54.05	51.92	54.41	49.50
TiO2	0.37	0.28	0.65	0.38	0.35	0.98	1.20	0.42	0.33	0.32	0.67
Al2O3	3.16	1.77	3.11	3.15	2.08	3.15	3.76	2.07	3.21	2.11	2.20
Cr2O3	0.31	0.44	0.28	0.32	0.38	nd	nd	0.27	0.24	0.42	nd
FeO	14.49	11.41	12.68	14.46	12.18	12.12	11.41	13.53	14.68	12.22	18.46
MnO	0.32	0.20	0.26	0.32	0.26	0.30	0.24	0.22	0.26	0.30	0.50
NiO	0.22	nd	nd	0.22	nd	nd	nd	nd	0.08	nd	nd
MgO	26.29	28.91	28.33	26.27	28.95	14.55	14.25	27.19	26.62	28.64	10.25
CaO	1.62	2.28	2.00	1.62	2.25	18.21	18.57	1.96	1.79	2.26	17.06
Na2O	nd	nd	nd	nd	nd	nd	nd	nd	0.08	nd	0.40
total=	99.91	100.75	100.89	99.76	100.26	100.57	100.12	99.71	99.21	100.68	99.04
Mg#	76.5	81.9	81.7	76.6	83.9	68.1	69.0	78.2	79.9	82.1	51.4
Al ratio	-	-	-	-	-	0.5	0.5	-	-	-	0.4

1607 OPX,MV121A,P,C,E
1608 OPX1,MV121A,P,C,E
1609 OPX10,MV121A,P,C,E
1610 OPX11,MV121A,P,R,E
1611 OPX2,MV121A,P,C,E
1612 CPX2,MV121A,P,C,E
1613 CPX3,MV121A,P,C,E
1614 OPX3,MV121A,P,R,E
1615 OPX3,MV121A,P,C,W
1616 OPX4,MV121A,P,C,E
1617 CPX4,MV121A,P,R,W

	1618	1619	1620	1621	1622	1623	1624	1625	1626	1627	1628
SiO2	54.52	49.58	53.84	52.67	48.68	53.20	52.17	48.25	54.46	49.84	49.65
TiO2	0.33	1.29	0.53	0.41	1.51	0.35	0.57	1.75	0.28	1.21	0.55
Al2O3	2.38	4.06	2.18	2.43	4.40	2.75	2.41	4.49	1.57	3.81	1.95
Cr2O3	0.12	nd	0.25	0.17	0.12	0.22	0.29	0.26	0.19	0.21	nd
FeO	12.82	10.97	13.96	14.87	10.96	13.42	13.18	10.42	13.74	10.94	19.29
MnO	0.14	0.20	0.14	0.23	0.17	0.29	0.22	0.19	0.20	0.21	0.55
NiO	nd	nd	0.18	nd	0.02	nd	0.08	0.01	nd	0.03	nd
MgO	28.01	14.63	27.07	26.71	14.24	27.14	27.60	14.09	27.52	14.33	9.04
CaO	2.11	18.16	2.03	2.13	17.95	1.73	2.33	18.87	1.78	17.61	18.12
Na2O	nd	0.53	nd	0.08	0.56	nd	0.12	0.46	nd	0.53	nd
K2O	nd	nd	nd	nd	nd	nd	0.07	nd	nd	nd	nd
total=	100.43	99.42	100.18	99.70	98.61	99.10	99.04	98.79	99.74	98.72	99.15
Mg#	79.7	75.5	77.9	79.3	75.1	78.8	83.6	76.7	78.1	72.1	45.5
Al ratio	-	0.2	-	-	0.2	-	-	0.1	-	0.4	0.7

1618 OPX5,MV121A,P,C,E
1619 CPX5,MV121A,P,C,W
1620 OPX6,MV121A,P,R,E
1621 OPX6,MV121A,P,R,W
1622 CPX6,MV121A,P,R,W
1623 OPX7,MV121A,P,C,E
1624 OPX8,MV121A,P,R,W
1625 CPX8,MV121A,P,R,W
1626 OPX9,MV121A,P,R,E
1627 CPX9,MV121A,P,C,W
1628 CPXM02,MV121A,P,C,E

	1629	1630	1631	1632	1633	1634	1635	1636	1637	1638	1639
SiO2	49.82	50.25	49.37	54.45	54.03	53.89	54.04	53.92	53.19	53.82	54.24
TiO2	0.53	0.46	0.64	0.35	0.34	0.44	0.38	0.39	0.49	0.38	0.41
Al2O3	1.89	1.78	1.97	1.91	1.97	2.43	2.28	2.60	3.24	2.32	2.13
Cr2O3	nd	nd	nd	0.33	0.33	0.35	0.37	0.38	0.42	0.34	0.39
FeO	19.14	19.06	19.10	12.86	11.62	11.47	11.52	11.79	12.12	11.70	11.94
MnO	0.51	0.46	0.52	0.21	0.19	0.21	0.19	0.23	0.21	0.20	0.20
MgO	9.96	9.95	9.35	28.31	29.08	28.62	28.79	28.39	27.94	28.99	28.53
CaO	17.37	18.14	18.12	1.93	2.02	2.31	2.20	2.20	2.35	2.30	2.15
Na2O	nd	nd	nd	0.07	0.07	0.07	0.08	0.07	0.07	0.07	0.07
total=	99.22	100.10	99.07	100.42	99.65	99.79	99.85	99.97	100.03	100.12	100.06
Mg#	48.1	48.2	46.6	80.8	83.9	83.2	83.3	82.3	82.3	84.4	82.1
Al ratio	0.6	0.5	0.4	-	-	-	-	-	-	-	-

1629 CPXM03,MV121A,P,C,E
1630 CPXM04,MV121A,P,C,E
1631 CPXM05,MV121A,P,R,E
1632 OPX200,MV121A,P,R,W
1633 OPX201,MV121A,P,R,W
1634 OPX202,MV121A,P,I,W
1635 OPX203,MV121A,P,I,W
1636 OPX204,MV121A,P,C,W
1637 OPX205,MV121A,P,C,W
1638 OPX206,MV121A,P,I,W
1639 OPX208,MV121A,P,R,W

	1640	1641	1642	1643	1644	1645	1646	1647	1648	1649	1650
SiO2	53.72	0.27	0.16	0.10	0.18	0.11	0.34	0.19	0.15	nd	0.46
TiO2	0.38	21.51	20.06	21.80	21.50	20.16	19.87	48.51	50.16	49.50	48.36
Al2O3	2.03	2.55	2.31	2.18	1.90	2.02	2.60	0.34	0.26	0.28	0.32
Fe2O3	nd	21.99	26.45	21.70	23.84	26.45	26.18	9.57	7.35	8.96	8.33
Cr2O3	0.35	0.60	0.55	1.04	0.52	0.83	0.94	nd	0.12	0.13	0.07
FeO	13.31	47.33	45.97	46.64	47.26	46.99	45.78	36.74	37.78	37.12	37.61
MnO	0.21	0.90	0.55	1.02	0.52	0.56	0.45	0.45	0.44	0.47	0.50
MgO	27.87	1.72	2.09	2.00	2.03	1.50	2.45	3.73	3.96	3.88	3.32
CaO	2.02	nd	nd	nd	nd	nd	nd	nd	nd	nd	nd
Na2O	0.07	nd	nd	nd	nd	nd	nd	nd	nd	nd	nd
total=	99.96	96.87	98.14	96.48	97.75	98.62	98.61	99.53	100.22	100.34	98.97
Mg#	80.8	-	-	-	-	-	-	-	-	-	-

1640 OPX209,MV121A,P,R,W
1641 MT1016,MV121A,P,R,W
1642 MT1017,MV121A,P,R,W
1643 MT1018,MV121A,P,C,W
1644 MT1020R,MV121A,GR,C,W
1645 MT1021R,MV121A,P,R,W
1646 MT1022R,MV121A,P,R,W
1647 IL1,MV121A,P,C,E
1648 IL1016,MV121A,P,C,W
1649 IL1017,MV121A,P,C,W
1650 IL1019,MV121A,GR?,C,W

	1651	1652	1653	1654	1655	1656	1657	1658	1659	1660	1661
SiO2	0.43	0.04	0.03	0.26	nd	0.24	nd	52.92	51.91	52.39	55.19
TiO2	48.42	49.04	49.14	48.59	48.48	48.07	48.60	0.08	0.08	0.09	0.07
Al2O3	0.31	0.24	0.23	nd	0.39	0.48	0.39	29.27	29.89	29.97	27.69
Fe2O3	8.60	10.15	9.06	9.19	9.90	10.87	11.32	nd	nd	nd	nd
Cr2O3	0.06	0.20	0.18	nd	nd	nd	nd	nd	nd	nd	nd
FeO	37.44	36.72	36.83	37.38	36.87	36.35	35.76	0.43	0.44	0.53	0.37
MnO	0.44	0.49	0.51	0.45	0.32	0.40	0.43	nd	nd	nd	nd
MgO	3.46	3.89	3.86	3.46	3.59	3.79	4.21	0.09	0.09	0.08	0.07
CaO	nd	nd	nd	nd	nd	nd	nd	12.12	13.12	12.68	9.96
Na2O	nd	nd	nd	nd	nd	nd	nd	4.26	3.87	4.13	5.40
K2O	nd	nd	nd	nd	nd	nd	nd	0.51	0.41	0.31	0.76
total=	99.16	100.77	99.84	99.33	99.55	100.20	100.71	99.68	99.81	100.18	99.51
An	-	-	-	-	-	-	-	59.3	63.7	61.8	48.3

1651 IL1019R,MV121A,GR?,C,W
1652 IL1021,MV121A,P,C,W
1653 IL1022R,MV121A,P,C,W
1654 IL2,MV121A,P,C,E
1655 IL3,MV121A,P,C,E
1656 IL5,MV121A,P,C,E
1657 IL6,MV121A,P,C,E
1658 PL112,MV71A,P,C,+OL+CPX+PL+MT,W
1659 PL113,MV71A,P,I,W
1660 PL114,MV71A,P,R,W
1661 PL115,MV71A,P,C,W

	1662	1663	1664	1665	1666	1667	1668	1669	1670	1671	1672
SiO2	54.86	53.78	54.35	53.38	54.83	53.46	54.39	55.21	51.72	50.99	51.65
TiO2	0.07	0.08	nd	0.08	0.07	nd	0.15	0.07	0.08	0.08	0.13
Al2O3	27.70	28.34	28.13	29.15	28.25	28.84	28.59	27.96	29.84	30.46	29.43
FeO	0.37	0.42	0.38	0.34	0.40	0.47	0.73	0.40	0.40	0.45	0.66
MgO	0.07	0.07	0.07	0.07	0.06	0.07	0.06	0.07	0.08	0.08	0.04
CaO	10.29	11.21	10.77	11.51	10.62	11.63	11.26	10.59	12.92	13.59	12.67
Na2O	5.34	4.80	4.90	4.49	4.93	4.55	4.81	5.11	3.86	3.54	4.24
K2O	0.71	0.68	0.71	0.60	0.70	0.57	0.49	0.80	0.35	0.36	0.27
total=	99.41	99.38	99.31	99.62	99.86	99.59	100.48	100.21	99.25	99.55	99.09
An	49.5	54.1	52.6	56.6	52.1	56.6	54.8	50.9	63.6	66.5	61.3

1662 PL116,MV71A,P,I,W
1663 PL118,MV71A,P,C,W
1664 PL119,MV71A,P,I,W
1665 PL121,MV71A,P,C,W
1666 PL122,MV71A,P,C,W
1667 PL123,MV71A,P,I,W
1668 PL124,MV71A,P,R,W
1669 PL125,MV71A,P,C,W
1670 PL126,MV71A,P,C,W
1671 PL127,MV71A,P,R,W
1672 PL128,MV71A,GR,C,W

	1673	1674	1675	1676	1677	1678	1679	1680	1681	1682	1683
SiO2	53.62	50.79	51.24	49.99	47.17	46.73	47.24	48.06	47.40	48.54	47.62
TiO2	0.16	0.73	0.71	1.80	1.97	1.84	1.74	1.85	1.95	1.87	2.39
Al2O3	28.24	4.65	4.59	3.02	7.30	8.20	7.86	7.38	7.64	7.15	5.50
Cr2O3	nd	0.97	0.92	0.02	0.16	0.22	0.15	0.19	0.23	0.21	0.16
FeO	0.71	5.19	5.08	9.12	8.70	7.99	7.73	7.88	7.88	8.67	9.24
MnO	nd	0.12	0.12	0.21	0.18	0.19	0.16	0.14	0.16	0.18	0.20
MgO	0.06	16.40	16.52	13.65	13.91	13.64	13.82	13.84	13.74	13.76	12.76
CaO	10.97	19.82	19.91	21.32	18.84	19.43	19.34	19.87	20.04	19.14	21.05
Na2O	4.99	0.57	0.58	0.38	0.63	0.61	0.64	0.65	0.64	0.64	0.48
K2O	0.41	nd	nd	nd	nd	nd	nd	nd	nd	nd	nd
total=	99.16	99.24	99.67	99.51	98.86	98.85	98.68	99.86	99.68	100.16	99.40
Mg#	-	88.0	87.7	75.8	80.1	82.1	81.7	80.8	82.7	76.5	76.6
An	53.5	-	-	-	-	-	-	-	-	-	-
Al ratio	-	0.5	0.6	0.1	0.4	0.4	0.5	0.4	0.4	0.5	0.2

1673 PL129,MV71A,GR,C,W
1674 CPX258,MV71A,P,C,W
1675 CPX259,MV71A,P,I,W
1676 CPX260,MV71A,P,R,W
1677 CPX261,MV71A,P,C,W
1678 CPX262,MV71A,P,I,W
1679 CPX264,MV71A,P,R,W
1680 CPX265,MV71A,P,C,W
1681 CPX266,MV71A,P,R,W
1682 CPX267,MV71A,P,C,W
1683 CPX268,MV71A,P,R,W

	1684	1685	1686	1687	1688	1689	1690	1691	1692	1693	1694
SiO2	49.56	47.23	0.34	0.03	0.06	38.68	39.12	37.69	39.44	37.66	37.30
TiO2	1.85	3.08	26.85	52.68	53.17	0.11	0.03	nd	nd	nd	nd
Al2O3	2.95	4.72	2.43	0.14	0.13	nd	0.07	nd	nd	nd	nd
Fe2O3	nd	nd	9.90	2.58	1.30	nd	nd	nd	nd	nd	nd
Cr2O3	0.03	0.02	0.30	nd	nd	nd	0.03	nd	nd	nd	nd
FeO	9.20	9.66	53.79	40.67	41.97	20.84	19.84	29.52	19.80	30.16	30.99
MnO	0.22	0.24	1.41	0.60	0.75	0.21	0.21	0.41	0.21	0.52	0.44
NiO	nd	nd	nd	nd	nd	0.20	0.28	nd	0.37	nd	0.17
MgO	13.54	12.20	0.11	3.44	2.89	39.27	41.68	32.43	40.76	32.22	31.90
CaO	21.54	21.17	nd	nd	nd	0.15	0.24	0.27	0.23	0.15	0.24
Na2O	0.42	0.58	nd	nd	nd	nd	nd	nd	nd	nd	nd
total=	99.31	98.90	95.13	100.14	100.27	99.46	101.50	100.32	100.81	100.71	101.04
Mg#	77.4	74.5	-	-	-	77.1	78.9	66.2	78.6	65.6	64.7

1684 CPX269,MV71A,P,R,W
1685 CPX271,MV71A,GR,C,W
1686 MT205,MV71A,P,C,W
1687 IL208,MV71A,GR,C,W
1688 IL209,MV71A,GR,C,W
1689 OL22,MV52,P,C,+OL+CPX+PL+MT,E
1690 OL22,MV52,P,C,W
1691 OL23,MV52,P,R,E
1692 OL24,MV52,P,C,E
1693 OL25,MV52,P,C,E
1694 OL26,MV52,P,C,E

	1695	1696	1697	1698	1699	1700	1701	1702	1703	1704	1705
SiO2	36.76	37.97	38.86	38.76	36.40	38.62	35.82	37.46	38.84	38.63	38.57
TiO2	nd	nd	0.04	0.03	nd	0.14	nd	nd	0.12	nd	nd
Al2O3	nd	nd	0.08	0.06	nd	nd	nd	nd	nd	nd	nd
Cr2O3	nd	nd	0.04	0.02	nd	nd	nd	nd	nd	nd	nd
FeO	34.29	29.40	21.01	22.28	35.83	22.07	39.99	28.93	23.49	18.99	19.49
MnO	0.59	0.45	0.23	0.22	0.57	0.27	0.69	0.32	0.26	0.19	0.20
NiO	nd	nd	0.27	0.22	nd	0.17	nd	nd	0.22	0.24	0.24
MgO	28.65	33.21	40.66	39.41	27.81	38.21	24.56	33.68	37.49	41.49	41.26
CaO	0.33	0.25	0.23	0.21	0.33	0.19	0.35	0.33	0.23	0.23	0.22
total=	100.62	101.28	101.42	101.21	100.94	99.67	101.41	100.72	100.65	99.77	99.98
Mg#	59.8	66.8	77.5	75.9	58.0	75.5	52.3	67.5	74.0	79.6	79.0

1695 OL28,MV52,P,R,E
1696 OL29,MV52,P,C,E
1697 OL29,MV52,P,C,W
1698 OL30,MV52,P,C,W
1699 OL31,MV52,P,R,E
1700 OL32,MV52,P,C,E
1701 OL33,MV52,P,R,E
1702 OL35,MV52,P,C,E
1703 OL36,MV52,P,C,E
1704 OL364,MV52,P,C,W
1705 OL365,MV52,P,I,W

	1706	1707	1708	1709	1710	1711	1712	1713	1714	1715	1716
SiO2	35.73	38.40	37.79	36.21	38.33	38.23	36.64	35.39	51.76	52.61	52.13
TiO2	nd	nd	nd	nd	0.11	nd	nd	nd	0.15	0.11	0.12
Al2O3	nd	nd	nd	nd	nd	nd	nd	nd	29.95	29.00	29.19
Cr2O3	nd	nd	nd	nd	nd	nd	nd	nd	0.01	0.02	0.03
FeO	34.02	19.79	23.80	30.99	27.29	21.14	30.78	42.19	0.68	0.46	0.53
MnO	0.55	0.20	0.28	0.45	0.33	0.22	0.41	0.90	nd	nd	nd
NiO	0.06	0.23	0.13	0.05	nd	0.24	0.09	0.18	0.02	nd	nd
MgO	29.20	41.19	37.75	32.26	34.08	40.01	32.52	22.82	nd	nd	0.11
CaO	0.36	0.17	0.20	0.20	0.18	0.22	0.26	0.40	12.83	12.04	12.34
Na2O	nd	nd	nd	nd	nd	nd	nd	nd	3.96	4.44	4.28
K2O	nd	nd	nd	nd	nd	nd	nd	nd	0.30	0.35	0.34
total=	99.92	99.98	99.95	100.16	100.32	100.06	100.70	101.88	99.66	99.03	99.07
Mg#	60.5	78.8	73.9	65.0	69.0	77.1	65.3	49.1	-	-	-
An	-	-	-	-	-	-	-	-	63.0	58.8	60.2

1706 OL366,MV52,P,R,W
1707 OL367,MV52,P,C,W
1708 OL368,MV52,P,C,W
1709 OL369,MV52,P,C,W
1710 OL37,MV52,P,C,E
1711 OL370,MV52,P,C,W
1712 OL371,MV52,P,C,W
1713 OL4,MV52,GR,C,E
1714 PL1,MV52,P,R,W
1715 PL10,MV52,P,R,W
1716 PL11,MV52,P,R,W

	1717	1718	1719	1720	1721	1722	1723	1724	1725	1726	1727
SiO2	52.36	52.77	54.16	52.55	52.79	52.87	64.54	54.96	52.11	52.94	53.59
TiO2	nd	nd	nd	nd	0.12	nd	0.40	0.11	nd	0.11	nd
Al2O3	29.42	29.06	28.00	29.65	29.24	29.53	21.07	28.41	29.54	28.81	28.68
Cr2O3	0.03	nd	nd	nd	0.01	nd	nd	nd	nd	nd	nd
FeO	0.53	0.58	0.53	0.42	0.67	0.48	0.47	0.45	0.71	0.54	0.39
MnO	nd	nd	nd	nd	0.15	nd	nd	nd	nd	nd	nd
NiO	nd	nd	nd	nd	0.04	nd	nd	nd	nd	nd	nd
MgO	nd	nd	nd	nd	0.13	nd	nd	nd	nd	nd	nd
CaO	12.25	12.28	11.16	12.75	12.25	12.80	2.47	11.11	13.13	12.23	11.91
Na2O	4.29	4.52	4.79	4.53	4.29	3.36	7.53	5.11	4.26	4.80	4.52
K2O	0.29	0.33	0.41	0.30	0.28	0.30	4.06	0.49	0.24	nd	0.25
total=	99.17	99.54	99.05	100.20	99.97	99.34	100.54	100.64	99.99	99.43	99.34
An	60.2	58.9	54.9	59.8	60.2	66.5	11.8	53.1	62.2	58.5	58.4

1717 PL2,MV52,P,R,W
1718 PL26,MV52,P,C,E
1719 PL27,MV52,P,C,E
1720 PL29,MV52,P,C,E
1721 PL3,MV52,P,I,W
1722 PL30,MV52,P,I,E
1723 PL31,MV52,P,R,E
1724 PL32,MV52,P,C,E
1725 PL33,MV52,P,R,E
1726 PL34A,MV52,P,C,E
1727 PL35,MV52,P,C,E

	1728	1729	1730	1731	1732	1733	1734	1735	1736	1737	1738
SiO2	52.96	52.86	52.27	52.72	52.76	53.19	52.67	54.90	52.60	54.40	52.69
TiO2	0.11	0.16	0.14	nd	0.12	0.12	0.08	0.18	0.11	nd	0.11
Al2O3	29.16	29.37	29.44	29.65	29.18	29.35	29.42	27.69	29.29	27.38	29.30
Cr2O3	nd	nd	nd	nd	0.05	0.08	0.01	nd	0.01	nd	0.02
FeO	0.53	0.55	0.51	0.57	0.47	0.44	0.48	0.81	0.49	0.71	0.52
MnO	nd	nd	nd	nd	0.02	0.03	nd	nd	nd	nd	nd
MgO	nd	nd	nd	nd	nd	nd	nd	nd	nd	nd	0.11
CaO	12.19	12.49	12.49	12.83	12.24	12.04	12.06	10.64	12.11	10.95	12.11
Na2O	4.55	4.29	4.21	4.44	4.39	4.53	4.42	5.02	4.45	4.87	4.49
K2O	0.30	0.29	0.33	0.31	0.29	0.31	0.29	0.42	0.30	0.47	0.30
total=	99.80	100.01	99.39	100.52	99.52	100.09	99.43	99.66	99.36	98.78	99.65
An	58.7	60.6	60.9	60.4	59.6	58.4	59.1	52.6	59.0	53.9	58.8

1728 PL36,MV52,P,C,E
1729 PL37,MV52,P,R,E
1730 PL38,MV52,P,C,E
1731 PL39,MV52,P,C,E
1732 PL4,MV52,P,I,W
1733 PL5,MV52,P,I,W
1734 PL6,MV52,P,C,W
1735 PL7,MV52,GR,C,E
1736 PL7,MV52,P,I,W
1737 PL8,MV52,GR,C,E
1738 PL8,MV52,P,I,W

	1739	1740	1741	1742	1743	1744	1745	1746	1747	1748	1749
SiO2	52.32	50.65	48.43	50.22	50.17	50.71	50.70	50.07	49.72	49.17	48.93
TiO2	0.12	1.42	2.20	1.75	1.66	1.64	1.83	1.56	1.73	1.28	1.26
Al2O3	29.27	2.26	3.55	2.81	2.69	2.22	2.66	2.53	2.80	6.70	6.67
Cr2O3	0.02	nd	nd	0.01	0.04	nd	nd	0.08	0.02	0.21	0.22
FeO	0.46	10.06	10.46	9.78	9.63	9.91	9.89	9.64	9.96	8.50	8.83
MnO	nd	0.19	0.19	0.18	0.18	nd	0.27	0.19	0.18	0.12	0.14
NiO	nd	0.01	nd	0.01	nd	nd	nd	nd	0.01	nd	0.01
MgO	0.09	14.23	13.19	13.82	13.99	13.86	14.28	14.12	13.93	15.94	15.72
CaO	12.39	20.78	20.74	21.30	21.35	20.69	21.32	21.15	21.29	17.50	17.48
Na2O	4.33	0.41	0.47	0.41	0.41	nd	nd	0.41	0.41	0.63	0.59
K2O	0.32	nd	nd	nd	nd	nd	nd	nd	nd	nd	nd
total=	99.32	100.01	99.23	100.29	100.12	99.03	100.95	99.75	100.05	100.05	99.85
Mg#	-	76.6	76.0	76.4	77.8	71.4	73.4	78.4	78.5	82.4	81.5
An	60.1	-	-	-	-	-	-	-	-	-	-
Al ratio	-	-0.1	-0.1	-0.1	-0.1	0.2	-	-0.1	-0.1	0.5	0.4

1739 PL9,MV52,P,I,W
1740 CPX1,MV52,P,R,W
1741 CPX10,MV52,P,I,W
1742 CPX11,MV52,P,R,W
1743 CPX12,MV52,P,R,W
1744 CPX14,MV52,GR,C,E
1745 CPX15,MV52,GR,C,E
1746 CPX2,MV52,P,R,W
1747 CPX3,MV52,P,I,W
1748 CPX4,MV52,P,I,W
1749 CPX5,MV52,P,C,W

	1750	1751	1752	1753	1754	1755	1756	1757	1758	1759	1760
SiO2	49.34	47.87	48.68	0.08	0.36	0.31	0.26	35.73	36.87	36.82	36.65
TiO2	1.28	2.60	1.42	19.19	17.08	18.26	50.62	nd	0.12	nd	nd
Al2O3	6.61	5.25	7.20	8.72	0.83	8.90	0.38	nd	nd	nd	nd
Fe2O3	nd	nd	nd	21.71	32.79	22.62	6.11	nd	nd	nd	nd
Cr2O3	0.15	0.18	0.16	2.97	0.38	2.89	nd	nd	nd	nd	nd
FeO	8.37	9.76	9.44	36.48	45.25	39.37	39.89	40.24	34.38	30.08	30.86
MnO	0.15	0.20	0.18	0.27	1.13	0.24	0.60	0.69	0.48	0.44	0.44
NiO	0.01	nd	nd	0.24	nd	nd	nd	nd	nd	0.08	nd
MgO	15.84	13.77	14.23	8.43	0.28	6.61	2.99	24.93	29.50	32.95	32.52
CaO	17.61	20.04	17.63	0.01	0.16	nd	nd	0.28	0.18	0.27	0.27
Na2O	0.63	0.45	0.66	nd	nd	nd	nd	nd	nd	nd	nd
total=	99.99	100.12	99.60	98.10	98.26	99.20	100.85	101.87	101.53	100.64	100.74
Mg#	81.8	77.6	75.4	-	-	-	-	52.5	60.5	66.1	65.3
Al ratio	0.5	0.1	0.6	-	-	-	-	-	-	-	-

1750 CPX6,MV52,P,C,W
1751 CPX7,MV52,P,R,W
1752 CPX8,MV52,P,C,W
1753 MTSP1,MV52,P,C,W
1754 MT10,MV52,GR,C,E
1755 MTSP12,MV52,P,C,E
1756 IL1,MV52,GR,C,E
1757 OL10,MV39A,GR,C,+OL+CPX+PL+MT+IL,E
1758 OL12,MV39A,GR,C,E
1759 OL372,MV39A,P,C,W
1760 OL373,MV39A,P,I,W

	1761	1762	1763	1764	1765	1766	1767	1768	1769	1770	1771
SiO2	36.03	36.14	37.16	38.17	38.31	37.50	37.87	37.48	35.14	38.93	36.39
FeO	32.95	33.05	27.30	19.56	20.16	30.59	30.16	28.96	40.84	20.90	33.58
MnO	0.55	0.53	0.35	0.25	0.25	0.51	0.43	0.40	0.63	0.21	0.46
NiO	nd	nd	0.13	0.26	0.23	nd	nd	nd	nd	0.15	0.15
MgO	30.41	30.56	35.32	40.86	40.22	32.25	32.50	33.56	22.76	39.20	29.74
CaO	0.33	0.28	0.20	0.26	0.28	0.19	0.21	0.22	0.30	0.38	0.37
total=	100.27	100.56	100.46	99.36	99.45	101.04	101.17	100.62	99.67	99.77	100.69
Mg#	62.2	62.2	69.7	78.8	78.0	65.3	65.8	67.4	49.8	77.0	61.2

1761 OL374,MV39A,P,R,W
1762 OL375,MV39A,P,C,W
1763 OL376,MV39A,P,C,W
1764 OL377,MV39A,P,C,W
1765 OL378,MV39A,P,I,W
1766 OL38,MV39A,P,C,E
1767 OL39,MV39A,P,I,E
1768 OL40,MV39A,P,C,E
1769 OL42,MV39A,P,R,E
1770 OL43,MV39A,P,C,E
1771 OL44,MV39A,P,R,E

	1772	1773	1774	1775	1776	1777	1778	1779	1780	1781	1782
SiO2	52.35	53.91	53.15	54.26	55.96	53.07	55.19	56.27	54.85	55.31	55.04
TiO2	0.12	0.17	0.17	0.09	0.09	0.13	0.15	nd	0.12	0.17	0.17
Al2O3	29.35	28.20	28.95	28.19	26.85	28.82	27.01	26.80	27.35	27.48	27.64
Cr2O3	nd	nd	nd	nd	0.01	nd	nd	nd	nd	nd	nd
FeO	0.48	0.84	0.75	0.47	0.87	0.53	0.64	0.58	0.63	0.51	0.68
NiO	nd	nd	nd	nd	0.04	nd	nd	nd	nd	nd	nd
MgO	0.09	nd	nd	0.11	0.42	nd	nd	nd	nd	nd	nd
CaO	12.25	11.34	12.04	10.83	9.48	12.21	10.10	9.48	10.53	10.74	10.54
Na2O	4.19	5.12	4.31	4.94	5.90	4.54	5.66	5.35	5.29	5.32	5.42
K2O	0.28	0.38	0.38	0.32	0.59	0.16	0.51	0.58	0.39	0.37	0.49
total=	99.11	99.96	99.75	99.21	100.21	99.46	99.26	99.06	99.16	99.90	99.98
An	60.7	53.9	59.3	53.7	45.4	59.2	48.2	47.8	51.2	51.6	50.4

1772 PL1,MV39A,P,R,W
1773 PL13,MV39A,GR,C,E
1774 PL14,MV39A,GR,C,E
1775 PL2,MV39A,P,C,W
1776 PL4,MV39A,P,C,W
1777 PL40,MV39A,P,C,E
1778 PL41,MV39A,P,C,E
1779 PL43,MV39A,P,C,E
1780 PL44,MV39A,P,R,E
1781 PL45,MV39A,P,C,E
1782 PL46,MV39A,P,R,E

	1783	1784	1785	1786	1787	1788	1789	1790	1791	1792	1793
SiO2	58.83	56.86	49.84	49.07	50.30	52.21	51.03	49.64	50.69	48.79	51.15
TiO2	0.12	0.11	1.21	1.58	1.47	1.21	1.10	1.49	1.48	1.76	1.29
Al2O3	26.46	26.06	4.93	5.77	2.98	1.32	1.30	5.62	2.40	6.42	1.81
Cr2O3	nd	nd	0.18	0.31	nd	nd	nd	0.33	nd	0.18	nd
FeO	0.54	0.66	9.57	9.27	10.19	10.37	11.13	9.12	10.92	9.30	11.40
MnO	0.01	nd	0.16	0.29	0.25	0.26	0.39	0.14	0.27	0.22	0.26
NiO	0.01	nd	0.04	nd	nd	nd	nd	nd	nd	nd	nd
MgO	0.07	0.09	15.78	15.17	14.26	14.55	14.16	15.32	13.88	14.79	13.90
CaO	7.57	9.06	17.66	18.11	19.67	19.78	19.62	17.99	19.92	18.17	19.63
Na2O	5.86	6.11	0.61	nd	nd	nd	nd	nd	nd	0.58	nd
K2O	0.58	0.65	nd	nd	nd	nd	nd	nd	nd	nd	nd
total=	100.05	99.60	99.98	99.57	99.12	99.70	98.73	99.65	99.56	100.21	99.44
Mg#	-	-	80.3	74.5	71.4	71.4	69.4	75.0	69.4	78.1	68.5
An	40.1	43.4	-	-	-	-	-	-	-	-	-
Al ratio	-	-	0.3	0.5	0.3	0.3	-	0.6	0.2	0.4	0.2

1783 PL5,MV39A,P,I,W
1784 PL6,MV39A,P,R,W
1785 CPX1,MV39A,P,C,W
1786 CPX10,MV39A,P,C,E
1787 CPX12,MV39A,P,C,E
1788 CPX12,MV39A,GR,C,E
1789 CPX13,MV39A,P,R,E
1790 CPX14,MV39A,P,C,E
1791 CPX15,MV39A,GR,C,E
1792 CPX16,MV39A,P,C,E
1793 CPX16,MV39A,GR,C,E

	1794	1795	1796	1797	1798	1799	1800	1801	1802	1803	1804
SiO2	50.85	51.67	48.47	48.07	48.01	49.48	50.21	0.31	nd	0.12	0.12
TiO2	1.58	1.00	1.69	1.72	1.85	1.30	1.63	24.31	23.29	23.12	23.36
Al2O3	2.56	1.33	6.24	6.45	6.52	5.28	2.61	1.34	1.48	1.45	1.46
Fe2O3	nd	nd	nd	nd	nd	nd	nd	21.49	22.67	22.35	21.68
Cr2O3	0.13	nd	0.25	0.14	0.13	0.29	nd	nd	nd	0.21	0.18
FeO	9.42	11.30	9.55	9.50	9.51	9.48	9.66	49.56	48.70	48.73	48.94
MnO	0.27	0.24	0.17	0.12	0.15	0.17	0.21	0.89	0.83	0.67	0.65
NiO	nd	nd	0.01	0.05	0.03	0.05	0.03	nd	nd	nd	nd
MgO	14.81	14.67	14.41	14.50	14.46	15.46	14.38	2.51	1.92	2.04	2.00
CaO	20.62	19.35	18.07	18.03	18.04	17.41	20.06	0.11	0.13	nd	nd
Na2O	nd	nd	0.69	0.65	0.65	0.58	0.39	nd	nd	nd	nd
total=	100.24	99.56	99.55	99.23	99.35	99.50	99.18	100.52	99.02	98.69	98.39
Mg#	74.3	69.8	78.0	78.9	78.7	78.5	75.9	-	-	-	-
Al ratio	0.1	0.1	0.4	0.4	0.3	0.4	-	-	-	-	-

1794 CPX17,MV39A,P,R,E
1795 CPX19,MV39A,GR,C,E
1796 CPX2,MV39A,P,R,W
1797 CPX3,MV39A,P,C,W
1798 CPX4,MV39A,P,R,W
1799 CPX5,MV39A,P,C,W
1800 CPX6,MV39A,P,R,W
1801 MT1,MV39A,GR,C,E
1802 MT10,MV39A,GR,C,E
1803 MT338,MV39A,GR,C,W
1804 MT338R,MV39A,GR,C,W

	1805	1806	1807	1808	1809	1810	1811	1812	1813	1814	1815
SiO2	0.13	0.14	nd	nd	0.38	0.30	0.21	nd	nd	0.03	0.11
TiO2	22.10	22.11	24.18	23.88	22.66	49.10	49.60	49.72	51.04	51.73	48.93
Al2O3	3.17	2.95	1.74	1.08	1.66	0.35	0.42	0.14	0.13	0.09	0.20
Fe2O3	22.99	22.20	20.78	22.08	23.12	7.07	8.01	7.05	5.99	4.12	9.03
Cr2O3	0.26	0.26	0.26	nd	0.19	nd	nd	0.02	0.03	0.03	nd
FeO	44.45	45.50	49.09	48.81	49.25	38.81	38.46	38.43	39.33	39.06	34.81
MnO	0.37	0.37	0.49	0.85	0.64	0.49	0.62	0.48	0.52	0.53	0.32
MgO	4.45	3.60	2.58	2.23	1.92	2.92	3.14	3.25	3.39	3.90	5.05
CaO	nd	nd	nd	nd	nd	nd	0.13	nd	nd	nd	nd
total=	97.92	97.13	99.12	98.93	99.82	99.04	100.59	99.09	100.43	99.49	98.45

1805 MT340,MV39A,P,C,W
1806 MT341,MV39A,P,C,W
1807 MT343,MV39A,GR,C,W
1808 MT8,MV39A,GR,C,E
1809 MT9,MV39A,GR,C,E
1810 IL2,MV39A,GR,C,E
1811 IL3,MV39A,GR,C,E
1812 IL322,MV39A,GR,C,W
1813 IL322R,MV39A,GR,C,W
1814 IL324,MV39A,GR,C,W
1815 IL325,MV39A,P,C,W

	1816	1817	1818	1819	1820	1821	1822	1823	1824	1825	1826
SiO2	nd	nd	51.41	50.57	52.84	50.26	50.56	50.42	49.69	52.70	52.80
TiO2	50.99	50.32	0.17	0.15	0.16	nd	0.13	nd	nd	0.20	0.13
Al2O3	0.15	0.19	29.94	31.05	29.23	31.42	30.63	31.17	31.18	29.21	29.25
Fe2O3	5.86	6.73	nd	nd	nd	nd	nd	nd	nd	nd	nd
Cr2O3	0.02	0.02	nd	nd	nd	nd	nd	nd	nd	nd	nd
FeO	39.21	38.73	1.06	0.61	0.59	0.65	0.94	0.52	1.69	0.90	0.88
MnO	0.50	0.51	nd	nd	nd	nd	nd	nd	nd	nd	nd
MgO	3.44	3.37	nd	nd	nd	nd	nd	nd	nd	nd	nd
CaO	nd	nd	13.54	14.31	12.80	14.68	14.36	14.99	14.69	12.45	12.70
Na2O	nd	nd	3.65	3.66	4.41	2.88	3.22	2.99	3.24	4.28	4.42
K2O	nd	nd	0.19	0.13	0.28	0.15	0.11	0.13	0.12	0.30	0.30
total=	100.17	99.87	99.96	100.48	100.31	100.04	99.95	100.22	100.61	100.04	100.48
An	-	-	66.5	67.9	60.6	73.1	70.7	72.9	71.0	60.6	60.3

1816 IL326,MV39A,GR,C,W
1817 IL327,MV39A,P?,C,W
1818 PL1,MV402,GR,C,+OL+CPX+PL+SP,E
1819 PL17,MV402,P,C,E
1820 PL18,MV402,P,R,E
1821 PL19,MV402,P,C,E
1822 PL20,MV402,P,C,E
1823 PL21,MV402,P,C,E
1824 PL22,MV402,P,C,E
1825 PL3,MV402,GR,C,E
1826 PL4,MV402,GR,C,E

	1827	1828	1829	1830	1831	1832	1833	1834	1835	1836	1837
SiO2	47.77	47.45	46.93	51.35	50.06	48.73	50.57	49.99	48.69	49.42	50.19
TiO2	2.16	2.26	2.87	0.90	1.17	1.30	1.12	0.89	1.19	1.21	1.00
Al2O3	5.58	5.86	4.81	3.59	4.34	4.83	3.03	4.53	6.16	5.58	3.82
Cr2O3	0.46	0.34	0.16	0.46	0.78	0.70	0.43	0.68	0.70	1.02	0.50
FeO	8.28	8.21	12.33	6.66	6.79	6.54	6.72	6.36	6.37	6.36	6.42
MnO	nd	nd	0.22	0.18	0.20	0.13	0.13	0.15	0.13	nd	0.14
NiO	nd	0.14	nd	0.15	nd	nd	nd	nd	nd	nd	nd
MgO	12.82	13.32	10.66	15.40	14.34	14.24	15.01	15.31	14.41	14.40	15.28
CaO	21.59	22.04	21.00	21.60	22.46	22.10	21.92	20.78	21.00	21.85	21.18
Na2O	nd	nd	nd	nd	nd	0.36	0.32	0.42	0.49	nd	0.36
total=	98.66	99.62	98.98	100.29	100.14	98.93	99.25	99.11	99.14	99.84	98.89
Mg#	73.4	78.1	60.6	80.5	80.0	86.6	84.2	85.7	85.7	80.1	85.2
Al ratio	0.3	0.2	0.1	0.4	0.3	0.2	0.1	0.4	0.4	0.4	0.3

1827 CPX1,MV402,P,C,E
1828 CPX2,MV402,P,C,E
1829 CPX3,MV402,P,R,E
1830 CPX31,MV402,P,C,E
1831 CPX32,MV402,P,C,E
1832 CPX326,MV402,P,C,W
1833 CPX327,MV402,P,R,W
1834 CPX328,MV402,P,C,W
1835 CPX329,MV402,P,C,W
1836 CPX33,MV402,P,C,E
1837 CPX330,MV402,P,C,W

	1838	1839	1840	1841	1842	1843	1844	1845	1846	1847	1848
SiO2	48.22	50.52	48.81	49.59	49.67	50.74	48.55	46.00	50.07	46.83	0.05
TiO2	1.32	1.48	1.28	1.27	1.10	1.18	2.16	2.93	1.61	2.83	5.14
Al2O3	5.39	2.66	6.18	4.75	4.82	2.66	4.52	7.17	3.09	6.18	18.80
Fe2O3	nd	nd	nd	nd	nd	nd	nd	nd	nd	nd	19.67
Cr2O3	0.74	0.06	1.11	0.83	0.77	0.14	0.14	0.54	0.23	0.27	20.42
FeO	6.34	9.10	6.36	6.67	6.64	7.97	9.67	9.07	9.62	9.18	24.62
MnO	0.12	0.16	nd	nd	nd	0.21	0.21	nd	0.22	0.26	0.45
MgO	14.03	14.02	14.16	14.52	14.43	14.09	12.92	12.43	14.00	12.64	9.00
CaO	22.09	21.19	21.34	21.89	21.93	21.81	21.71	21.06	20.55	21.56	nd
Na2O	0.37	0.34	nd	nd	nd	nd	nd	nd	nd	nd	nd
total=	98.62	99.53	99.24	99.52	99.36	98.80	99.88	99.20	99.39	99.75	98.15
Mg#	87.1	76.1	79.9	79.9	79.7	75.9	72.0	72.3	72.2	73.5	39.5
Al ratio	0.2	0.1	0.5	0.4	0.4	0.3	0.1	0.2	0.2	0.2	-

1838 CPX331,MV402,P,C,W
1839 CPX332,MV402,P,R,W
1840 CPX34,MV402,P,C,E
1841 CPX35,MV402,P,C,E
1842 CPX36,MV402,P,C,E
1843 CPX4,MV402,GR,C,E
1844 CPX5,MV402,P,R,E
1845 CPX6,MV402,GR,C,E
1846 CPX8,MV402,GR,C,E
1847 CPX9,MV402,GR,C,E
1848 SP300,MV402,P,C,W

	1849	1850	1851	1852	1853	1854	1855	1856	1857	1858	1859
SiO2	0.09	0.09	0.07	0.07	0.13	0.21	0.44	0.26	0.37	37.30	37.27
TiO2	2.00	13.19	1.42	1.82	1.53	2.64	15.91	13.92	14.22	nd	nd
Al2O3	27.65	6.95	29.15	29.92	27.79	25.68	4.77	6.26	6.93	nd	nd
Fe2O3	11.89	21.69	13.58	9.03	12.85	14.10	23.05	23.16	23.01	nd	nd
Cr2O3	25.14	15.57	23.23	27.20	25.25	24.13	9.24	12.35	10.78	nd	nd
FeO	20.27	35.92	19.73	17.91	19.42	21.12	42.12	37.42	39.22	32.64	32.05
MnO	0.38	0.51	0.39	0.36	0.39	0.45	0.37	0.28	0.43	0.51	0.55
MgO	11.15	5.34	11.35	13.00	11.53	10.95	2.67	4.57	3.72	30.38	30.30
CaO	nd	nd	nd	nd	nd	nd	0.40	0.37	0.39	0.36	0.31
total=	98.57	99.26	98.92	99.31	98.89	99.28	98.97	98.59	99.07	101.19	100.48
Mg#	49.5	20.9	50.6	56.4	51.4	48.0	-	-	-	62.4	62.8

1849 SP302,MV402,P,C,W
1850 SPMT303,MV402,P,C,W
1851 SP304,MV402,P,C,W
1852 SP305,MV402,P,C,W
1853 SP306,MV402,P,C,W
1854 SP307,MV402,P,C,W
1855 MTSP2,MV402,GR,C,E
1856 MTSP3,MV402,GR,C,E
1857 MTSP4,MV402,GR,C,E
1858 OL12,MV13,P,C,+OL+PL+MT+IL,E
1859 OL2,MV13,P,I,E

	1860	1861	1862	1863	1864	1865	1866	1867	1868	1869	1870
SiO2	37.12	36.45	36.18	36.19	36.22	36.15	36.53	36.89	37.24	37.18	37.24
TiO2	nd	nd	nd	nd	nd	nd	nd	nd	nd	nd	0.13
FeO	26.32	30.38	31.95	31.86	31.68	32.00	32.06	32.58	33.76	32.60	32.63
MnO	0.32	0.50	0.49	0.52	0.48	0.51	0.53	0.51	0.55	0.48	0.56
NiO	0.08	0.06	0.03	0.06	0.06	0.02	0.02	nd	nd	0.15	nd
MgO	35.73	32.28	30.94	30.89	31.37	31.21	31.10	30.02	29.27	30.03	29.83
CaO	0.19	0.26	0.41	0.43	0.33	0.41	0.39	0.39	0.41	0.34	0.40
total=	99.76	99.93	100.00	99.95	100.14	100.30	100.63	100.39	101.23	100.78	100.79
Mg#	70.8	65.4	63.3	63.3	63.8	63.5	63.4	62.2	60.7	62.1	62.0

1860 OL379,MV13,P,C,W
1861 OL380,MV13,P,I,W
1862 OL381,MV13,P,R,W
1863 OL382,MV13,P,C,W
1864 OL383,MV13,P,I,W
1865 OL384,MV13,P,C,W
1866 OL385,MV13,P,I,W
1867 OL4,MV13,P,C,E
1868 OL5,MV13,P,R,E
1869 OL6,MV13,P,C,E
1870 OL7,MV13,P,R,E

	1871	1872	1873	1874	1875	1876	1877	1878	1879	1880	1881
SiO2	36.91	37.17	37.09	55.64	52.92	54.08	54.18	55.17	53.09	55.30	56.57
TiO2	nd	nd	0.14	nd	nd	0.15	0.14	0.11	nd	0.20	0.12
Al2O3	nd	nd	nd	27.82	28.35	28.90	28.40	27.44	28.92	27.57	26.86
FeO	32.35	32.54	34.20	0.45	1.89	0.75	0.51	0.65	0.82	0.84	0.43
MnO	0.51	0.55	0.62	nd	nd	nd	nd	nd	nd	nd	nd
MgO	30.22	29.89	28.71	nd	0.58	nd	nd	nd	nd	nd	nd
CaO	0.29	0.38	0.50	10.52	11.49	12.15	11.16	10.52	12.06	10.39	9.78
Na2O	nd	nd	nd	5.28	4.61	4.36	4.35	5.12	4.39	5.20	6.03
K2O	nd	nd	nd	0.53	0.48	0.41	0.42	0.59	0.42	0.60	0.60
total=	100.28	100.53	101.26	100.24	100.32	100.80	99.16	99.60	99.70	100.10	100.39
Mg#	62.5	62.1	59.9	-	-	-	-	-	-	-	-
An	-	-	-	50.8	56.3	59.2	57.1	51.3	58.8	50.6	45.7

1871 OL8,MV13,P,C,E
1872 OL9,MV13,P,R,E
1873 OL9A,MV13,P,I,E
1874 PL1,MV13,P,C,E
1875 PL2,MV13,P,R,E
1876 PL4,MV13,P,R,E
1877 PL5,MV13,P,C,E
1878 PL5,MV13,GR,C,E
1879 PL6,MV13,P,R,E
1880 PL6,MV13,GR,C,E
1881 PL7,MV13,P,C,E

	1882	1883	1884	1885	1886	1887	1888	1889	1890	1891	1892
SiO2	53.57	54.24	49.19	48.78	48.60	0.12	0.09	0.12	0.31	0.20	0.02
TiO2	0.16	nd	2.11	2.24	2.31	24.79	18.82	26.18	24.45	25.30	49.92
Al2O3	28.71	28.88	3.26	3.48	3.42	2.55	4.63	2.58	2.41	2.46	0.25
Fe2O3	nd	nd	nd	nd	nd	18.05	26.55	14.52	17.96	17.46	6.20
Cr2O3	nd	nd	nd	nd	nd	0.08	1.08	0.09	0.17	0.14	nd
FeO	0.70	0.45	11.94	11.38	11.25	50.43	42.54	51.20	50.31	50.69	40.44
MnO	nd	nd	0.22	0.25	0.32	0.49	0.34	0.77	0.56	0.52	0.58
MgO	nd	nd	11.82	12.52	12.71	2.19	3.87	2.12	1.97	2.48	2.18
CaO	11.61	11.88	20.39	20.49	20.65	nd	nd	nd	0.14	nd	nd
Na2O	4.57	4.81	nd	nd	nd	nd	nd	nd	nd	nd	nd
K2O	0.48	0.44	nd	nd	nd	nd	nd	nd	nd	nd	nd
total=	99.80	100.70	98.93	99.14	99.26	98.70	97.92	97.58	98.28	99.25	99.59
Mg#	-	-	63.8	66.2	67.8	-	-	-	-	-	-
An	56.8	56.3	-	-	-	-	-	-	-	-	-
Al ratio	-	-	0.2	0.1	-	-	-	-	-	-	-

1882 PL8,MV13,P,R,E
1883 PL9,MV13,P,C,E
1884 CPX11,MV13,GR,C,E
1885 CPX12,MV13,GR,C,E
1886 CPX13,MV13,GR,C,E
1887 MT348,MV13,GR,C,W
1888 MT350,MV13,P,C,W
1889 MT352,MV13,P,C,W
1890 MT7,MV13,GR,C,E
1891 MT9,MV13,GR,C,E
1892 IL330,MV13,GR,C,W

	1893	1894	1895	1896	1897	1898	1899	1900	1901	1902	1903
SiO2	0.03	0.02	0.19	35.30	35.66	35.02	36.87	35.36	35.91	35.70	35.10
TiO2	50.25	50.84	49.55	nd	nd	nd	0.40	nd	nd	nd	nd
Al2O3	0.21	0.20	0.58	nd	nd	nd	0.39	nd	nd	nd	nd
Fe2O3	6.07	5.59	7.35	nd	nd	nd	nd	nd	nd	nd	nd
Cr2O3	nd	nd	0.12	nd	nd	nd	nd	nd	nd	nd	nd
FeO	40.80	38.92	39.14	39.40	38.92	39.93	40.04	41.91	39.54	39.10	39.00
MnO	0.55	0.54	0.50	0.70	0.71	0.71	0.69	0.77	0.53	0.60	0.70
MgO	2.17	3.52	2.88	25.40	25.81	25.41	22.62	23.41	25.13	25.40	25.50
CaO	nd	nd	nd	0.40	0.23	0.25	0.36	0.28	0.28	0.50	0.20
total=	100.08	99.63	100.31	101.20	101.33	101.32	101.37	101.73	101.39	101.30	100.50
Mg#	-	-	-	53.5	54.2	53.1	50.2	49.9	53.1	53.7	53.8

1893 IL331,MV13,GR,C,W
1894 IL332,MV13,P,C,W
1895 IL6A,MV13,GR,C,E
1896 OL1,MV40A,P,R,+OL+CPX+PL+MT+IL,E
1897 OL10,MV40A,P,C,E
1898 OL11,MV40A,P,R,E
1899 OL13,MV40A,GR,C,E
1900 OL14,MV40A,GR,C,E
1901 OL2,MV40A,P,R,E
1902 OL2,MV40A,P,R,E
1903 OL3,MV40A,P,I,E

	1904	1905	1906	1907	1908	1909	1910	1911	1912	1913	1914
SiO2	35.61	35.47	35.87	35.65	35.57	35.44	35.40	35.90	35.40	36.39	36.84
FeO	38.79	38.87	35.31	38.34	38.54	38.96	39.00	36.54	39.00	36.77	35.89
MnO	0.75	0.63	0.55	0.68	0.65	0.67	0.70	0.54	0.60	0.61	0.61
NiO	0.12	0.03	0.06	nd	0.03	0.03	nd	nd	nd	0.15	nd
MgO	25.50	25.76	28.21	25.76	25.59	25.26	25.90	27.87	25.90	27.30	27.90
CaO	0.34	0.27	0.22	0.25	0.28	0.27	0.30	0.26	0.20	0.20	0.32
total=	101.11	101.03	100.22	100.68	100.66	100.63	101.30	101.11	101.10	101.42	101.56
Mg#	54.0	54.2	58.7	54.5	54.2	53.6	54.2	57.6	54.2	57.0	58.1

1904 OL322,MV40A,P,C,W
1905 OL323,MV40A,P,C,W
1906 OL324,MV40A,P,I,W
1907 OL325,MV40A,P,I,W
1908 OL326,MV40A,P,I,W
1909 OL327,MV40A,P,R,W
1910 OL4,MV40A,P,I,E
1911 OL5,MV40A,P,C,E
1912 OL5,MV40A,P,C,E
1913 OL6,MV40A,P,C,E
1914 OL7,MV40A,P,C,E

	1915	1916	1917	1918	1919	1920	1921	1922	1923	1924	1925
SiO2	35.56	35.76	53.15	57.12	57.36	54.75	53.16	52.99	55.37	53.01	53.95
TiO2	0.13	nd	nd	nd	nd	nd	0.11	0.21	0.15	0.13	0.20
Al2O3	nd	nd	29.02	26.29	25.85	27.72	28.73	29.16	28.07	28.96	28.38
FeO	39.21	36.86	0.54	0.42	1.03	0.49	0.58	0.59	0.95	0.37	0.97
MnO	0.67	0.58	nd	nd	nd	nd	nd	nd	nd	nd	nd
MgO	25.43	27.39	nd	nd	0.64	nd	nd	nd	nd	0.22	nd
CaO	0.30	0.25	12.19	9.22	8.63	10.94	11.60	11.72	11.00	11.99	10.99
Na2O	nd	nd	4.27	5.85	6.23	4.74	4.60	4.34	4.85	5.00	5.33
K2O	nd	nd	0.25	0.50	0.56	0.34	0.29	0.29	0.46	0.20	0.39
total=	101.30	100.84	99.42	99.40	100.30	98.98	99.07	99.30	100.85	99.88	100.21
Mg#	53.6	57.0	-	-	-	-	-	-	-	-	-
An	-	-	60.3	45.2	42.0	54.9	57.2	58.8	54.1	56.4	52.1

1915 OL7,MV40A,P,C,E
1916 OL9,MV40A,P,C,E
1917 PL1,MV40A,P,C,E
1918 PL10,MV40A,P,C,E
1919 PL11,MV40A,P,C,E
1920 PL12,MV40A,P,C,E
1921 PL13,MV40A,P,C,E
1922 PL14,MV40A,P,R,E
1923 PL14,MV40A,GR,C,E
1924 PL15,MV40A,P,I,E
1925 PL15,MV40A,GR,C,E

	1926	1927	1928	1929	1930	1931	1932	1933	1934	1935	1936
SiO2	55.91	53.51	53.70	52.88	52.68	53.04	54.01	53.45	56.99	56.63	50.05
TiO2	0.26	0.16	0.13	nd	nd	nd	nd	0.17	nd	0.19	1.01
Al2O3	27.38	28.81	28.09	29.01	28.65	28.75	28.36	28.62	27.21	26.37	2.92
FeO	0.93	0.44	1.17	0.55	0.59	0.55	0.60	0.74	0.52	0.57	15.03
MnO	nd	nd	nd	nd	nd	nd	nd	nd	nd	nd	0.50
MgO	nd	nd	nd	nd	nd	nd	nd	nd	nd	nd	13.61
CaO	10.19	11.75	11.45	11.89	11.96	12.15	11.36	11.43	9.51	8.98	15.97
Na2O	5.74	4.49	4.41	4.40	4.67	4.45	4.53	5.03	5.67	5.89	nd
K2O	0.49	0.28	0.45	0.32	0.21	0.26	0.28	0.35	0.47	0.72	nd
total=	100.90	99.44	99.40	99.05	98.76	99.20	99.14	99.79	100.37	99.35	99.09
Mg#	-	-	-	-	-	-	-	-	-	-	61.7
An	48.2	58.1	57.3	58.8	57.9	59.2	57.1	54.6	46.8	43.8	-
Al ratio	-	-	-	-	-	-	-	-	-	-	0.5

1926 PL16,MV40A,GR,C,E
1927 PL19,MV40A,P,C,E
1928 PL2,MV40A,P,R,E
1929 PL21,MV40A,P,I,E
1930 PL3,MV40A,P,C,E
1931 PL5,MV40A,P,C,E
1932 PL6,MV40A,P,C,E
1933 PL7,MV40A,P,R,E
1934 PL8,MV40A,P,C,E
1935 PL9,MV40A,P,R,E
1936 CPX1,MV40A,P,C,E

	1937	1938	1939	1940	1941	1942	1943	1944	1945	1946	1947
SiO2	50.54	48.30	49.52	48.00	51.85	51.30	51.02	51.46	47.80	50.37	49.80
TiO2	0.76	1.71	1.47	1.90	0.99	0.20	0.26	0.49	1.80	0.95	0.80
Al2O3	2.10	6.42	5.26	6.30	1.26	0.16	0.15	0.13	6.60	3.45	2.20
Cr2O3	0.21	0.33	0.22	0.20	nd	nd	nd	nd	0.30	nd	0.20
FeO	15.83	8.90	9.48	9.20	13.00	27.51	30.32	29.10	9.30	12.24	16.00
MnO	0.45	0.19	0.13	nd	0.35	0.86	0.78	0.86	nd	0.26	0.50
MgO	12.18	14.32	15.00	14.10	14.06	17.10	15.16	15.75	14.10	13.66	11.80
CaO	18.08	18.30	18.14	18.20	18.27	2.49	2.85	3.03	18.40	18.59	18.10
Na2O	nd	nd	nd	0.60	nd	nd	nd	nd	nd	0.62	nd
total=	100.15	98.47	99.22	98.50	99.78	99.62	100.54	100.82	98.30	100.14	99.40
Mg#	57.9	74.1	73.8	76.1	65.8	53.0	47.6	49.1	73.0	71.3	57.5
Al ratio	0.3	0.6	0.5	0.4	0.2	-	-	-	0.5	0.3	0.2

1937 CPX10,MV40A,P,C,E
1938 CPX11,MV40A,P,C,E
1939 CPX12,MV40A,P,C,E
1940 CPX13,MV40A,P,R,E
1941 CPX14,MV40A,GR,C,E
1942 OPX16,MV40A,GR,C,E
1943 OPX17,MV40A,GR,C,E
1944 OPX18,MV40A,GR,C,E
1945 CPX23,MV40A,P,R,E
1946 CPX3,MV40A,P,C,E
1947 CPX3,MV40A,P,I,E

	1948	1949	1950	1951	1952	1953	1954	1955	1956	1957	1958
SiO2	50.26	50.10	48.08	48.07	49.98	49.34	50.00	48.40	49.42	50.30	49.19
TiO2	0.78	0.77	1.87	1.77	1.06	1.52	0.80	1.63	1.47	0.80	1.82
Al2O3	2.33	2.32	6.52	6.35	3.38	5.80	2.30	6.13	5.31	2.20	5.57
Cr2O3	nd	nd	0.18	0.21	nd	0.37	nd	0.30	0.17	nd	0.19
FeO	15.73	15.94	9.14	9.52	11.56	8.86	15.20	8.87	10.12	15.60	10.26
MnO	0.37	0.40	0.14	0.15	0.30	nd	0.30	0.19	0.13	0.40	nd
NiO	0.01	nd	0.01	0.02	nd	nd	0.30	nd	nd	nd	nd
MgO	11.75	11.98	14.41	14.18	13.77	14.85	11.70	14.97	14.36	11.80	13.77
CaO	17.85	17.63	18.24	17.94	18.70	18.53	17.90	18.08	18.61	17.90	18.85
Na2O	0.47	0.45	0.67	0.65	nd	0.75	nd	nd	nd	nd	nd
total=	99.55	99.59	99.26	98.86	98.75	100.02	98.50	98.57	99.59	99.00	99.65
Mg#	59.2	60.1	78.9	76.8	68.0	79.8	57.8	75.0	71.7	57.4	70.5
Al ratio	0.3	0.2	0.4	0.4	0.5	0.4	0.6	0.5	0.5	0.6	0.5

1948 CPX31,MV40A,P,C,W
1949 CPX32,MV40A,P,R,W
1950 CPX33,MV40A,P,C,W
1951 CPX34,MV40A,P,R,W
1952 CPX4,MV40A,P,R,E
1953 CPX5,MV40A,P,C,E
1954 CPX6,MV40A,P,C,E
1955 CPX6,MV40A,P,R,E
1956 CPX7,MV40A,P,C,E
1957 CPX8,MV40A,P,I,E
1958 CPX9,MV40A,P,R,E

	1959	1960	1961	1962	1963	1964	1965	1966	1967	1968	1969
SiO2	0.50	0.29	0.32	0.36	0.49	0.37	0.31	0.30	0.40	0.21	0.19
TiO2	19.60	19.82	18.61	18.36	19.84	19.20	20.98	18.40	49.50	49.95	47.93
Al2O3	1.70	2.45	2.17	2.71	4.49	4.11	2.98	2.50	0.20	0.35	0.22
Fe2O3	26.58	28.01	29.31	30.23	26.57	26.72	25.07	29.64	7.93	7.48	9.06
Cr2O3	0.90	nd	0.28	0.42	0.16	1.74	0.48	0.89	0.30	nd	nd
FeO	47.69	46.30	46.74	46.45	46.28	44.91	46.08	45.43	38.07	38.50	38.01
MnO	0.90	0.51	0.83	0.36	0.40	0.47	0.41	0.50	0.50	0.60	0.64
MgO	0.80	2.16	0.72	1.56	3.01	3.24	3.13	1.90	3.60	3.40	2.62
CaO	nd	nd	0.17	nd	nd	nd	nd	nd	nd	nd	nd
total=	98.67	99.54	99.15	100.45	101.24	100.76	99.44	99.56	100.50	100.49	98.67

1959 MT1,MV40A,P,R,E
1960 MT3,MV40A,P,C,E
1961 MT4,MV40A,P,R,E
1962 MT6,MV40A,P,C,E
1963 MT7,MV40A,P,C,E
1964 MT8,MV40A,P,C,E
1965 MT9,MV40A,P,C,E
1966 MTIL2,MV40A,P,C,E
1967 IL1,MV40A,P,R,E
1968 IL11,MV40A,P,C,E
1969 IL15,MV40A,GR,C,E

	1970	1971	1972	1973	1974	1975	1976	1977	1978	1979	1980
SiO2	0.30	0.20	0.35	0.18	0.20	nd	0.30	0.30	0.20	0.23	nd
TiO2	49.09	49.60	48.77	49.07	49.40	51.09	49.60	49.30	49.84	49.47	49.70
Al2O3	nd	0.20	nd	nd	0.20	nd	0.20	0.20	0.22	0.24	0.40
Fe2O3	9.01	7.96	9.06	9.49	8.18	7.45	7.90	8.57	7.56	8.27	8.35
Cr2O3	nd	nd	nd	nd	0.20	nd	nd	0.20	nd	nd	nd
FeO	37.56	37.74	37.90	37.06	37.84	38.24	38.29	37.59	38.26	38.41	37.59
MnO	0.64	0.50	0.47	0.45	0.40	0.39	0.60	0.50	0.46	0.53	0.50
MgO	3.53	3.70	3.31	3.83	3.60	4.10	3.40	3.70	3.55	3.26	3.70
total=	100.13	99.90	99.86	100.08	100.02	101.27	100.29	100.36	100.09	100.41	100.24

1970 IL2,MV40A,P,C,E
1971 IL2,MV40A,P,I,E
1972 IL3,MV40A,P,R,E
1973 IL4,MV40A,P,C,E
1974 IL4,MV40A,P,C,E
1975 IL5,MV40A,P,C,E
1976 IL5,MV40A,P,C,E
1977 IL6,MV40A,P,I,E
1978 IL6,MV40A,P,R,E
1979 IL7,MV40A,P,C,E
1980 IL7,MV40A,P,I,E

	1981	1982	1983	1984	1985	1986	1987	1988	1989	1990	1991
SiO2	nd	0.30	39.08	36.72	36.27	36.13	36.35	35.27	36.78	36.90	35.32
TiO2	49.81	49.80	nd	nd	nd	nd	nd	nd	nd	nd	nd
Al2O3	0.39	nd	nd	nd	nd	nd	nd	nd	nd	nd	nd
Fe2O3	8.12	6.81	nd	nd	nd	nd	nd	nd	nd	nd	nd
FeO	38.00	38.57	19.41	32.68	34.11	35.10	34.59	39.60	33.32	32.11	39.14
MnO	0.46	0.50	0.29	0.68	0.74	0.75	0.73	0.96	0.67	0.68	0.82
NiO	nd	nd	0.35	0.05	0.05	0.05	0.02	0.04	0.02	0.04	nd
MgO	3.55	3.40	41.72	30.49	29.42	28.31	29.01	24.40	30.13	31.09	24.68
CaO	nd	nd	0.21	0.30	0.34	0.42	0.45	0.48	0.36	0.33	0.41
total=	100.33	99.38	101.06	100.92	100.93	100.76	101.15	100.75	101.28	101.15	100.37
Mg#	-	-	79.3	62.4	60.6	59.0	59.9	52.3	61.7	63.3	52.9

1981 IL8,MV40A,P,C,E
1982 IL8,MV40A,P,R,E
1983 OL23,MV165,P,I,+OL+SP,E
1984 OL314,MV165,P,C,W
1985 OL315,MV165,P,C,W
1986 OL316,MV165,P,C,W
1987 OL317,MV165,P,C,W
1988 OL318,MV165,P,C,W
1989 OL319,MV165,P,C,W
1990 OL320,MV165,P,C,W
1991 OL321,MV165,P,R,W

	1992	1993	1994	1995	1996	1997	1998	1999	2000	2001	2002
SiO2	51.38	50.05	48.83	47.48	0.38	nd	0.27	0.23	0.30	0.15	64.92
TiO2	0.20	nd	2.01	3.37	1.38	4.25	2.95	16.80	16.98	51.64	nd
Al2O3	29.74	31.28	5.95	6.05	23.00	24.36	21.47	7.98	2.56	nd	20.31
Fe2O3	nd	nd	nd	nd	14.56	14.19	17.72	22.53	32.77	3.96	nd
Cr2O3	nd	nd	0.28	0.13	26.87	21.11	22.08	7.19	0.14	nd	nd
FeO	0.53	0.46	6.65	8.31	28.81	28.61	29.86	39.47	44.82	40.66	0.53
MnO	nd	nd	0.14	nd	0.24	nd	0.34	0.38	0.76	0.92	nd
MgO	nd	nd	13.50	12.17	5.50	7.05	5.21	5.65	1.28	2.82	nd
CaO	12.73	14.43	22.60	22.30	nd	nd	nd	nd	nd	nd	1.80
Na2O	4.28	3.19	nd	0.49	nd	nd	nd	nd	nd	nd	6.72
K2O	0.12	0.08	nd	nd	nd	nd	nd	nd	nd	nd	5.09
total=	98.98	99.49	99.96	100.30	100.74	99.57	99.90	100.23	99.61	100.15	99.37
Mg#	-	-	78.3	74.9	25.4	30.5	23.7	20.3	-	-	-
An	61.7	71.1	-	-	-	-	-	-	-	-	-
Al ratio	-	-	0.4	0.2	-	-	-	-	-	-	-

1992 PL7,MV165,GR,C,E
1993 PL8,MV165,GR,C,E
1994 CPX30,MV165,GR,C,E
1995 CPX31,MV165,GR,R,E
1996 SP16,MV165,P,C,E
1997 SP17,MV165,P,C,E
1998 SP18,MV165,P,C,E
1999 SPMT13,MV165,P,C,E
2000 MT14,MV165,GR,C,E
2001 IL5,MV165,GR,C,E
2002 AF1,MV51,GR,C,+PL+MT,E

	2003	2004	2005	2006	2007	2008	2009	2010	2011	2012	2013
SiO2	35.04	34.93	34.92	35.17	34.61	34.18	55.29	55.04	55.06	56.01	51.15
TiO2	nd	nd	nd	nd	nd	nd	0.20	0.18	0.15	0.21	1.30
Al2O3	nd	nd	nd	nd	nd	nd	27.40	27.91	28.27	27.12	2.21
Cr2O3	nd	nd	nd	nd	nd	nd	nd	nd	nd	nd	0.13
FeO	40.10	40.89	41.52	38.59	42.57	43.80	0.68	0.68	0.57	0.98	12.44
MnO	0.78	0.85	0.83	0.72	0.85	0.98	nd	nd	nd	nd	0.29
MgO	24.07	23.71	23.25	25.56	22.18	20.57	nd	nd	nd	nd	12.90
CaO	0.35	0.36	0.37	0.31	0.44	0.40	10.50	10.56	11.08	9.91	20.57
Na2O	nd	nd	nd	nd	nd	nd	5.01	5.81	5.07	5.60	nd
K2O	nd	nd	nd	nd	nd	nd	0.53	0.52	0.52	0.58	nd
total=	100.34	100.74	100.89	100.35	100.65	99.93	99.61	100.70	100.72	100.41	100.99
Mg#	51.7	50.8	50.0	54.1	48.1	45.6	-	-	-	-	64.9
An	-	-	-	-	-	-	52.0	48.7	53.1	47.8	-
Al ratio	-	-	-	-	-	-	-	-	-	-	0.2

2003 OL328,MV51,GR,C,W
2004 OL329,MV51,GR,I,W
2005 OL330,MV51,GR,R,W
2006 OL331,MV51,GR,C,W
2007 OL332,MV51,GR,C,W
2008 OL333,MV51,GR,I,W
2009 PL1,MV51,GR,C,E
2010 PL3,MV51,P,C,E
2011 PL4,MV51,P,C,E
2012 PL5,MV51,P,R,E
2013 CPX1,MV51,GR,C,E

	2014	2015	2016	2017	2018	2019	2020	2021	2022	2023	2024
SiO2	49.31	0.44	0.53	0.31	0.34	0.35	0.25	0.53	0.42	0.38	38.21
TiO2	1.31	24.60	23.96	22.93	19.26	18.51	24.50	23.53	20.88	44.57	nd
Al2O3	2.26	1.62	1.35	1.45	1.70	1.86	1.77	1.32	1.96	0.39	nd
Fe2O3	nd	20.21	20.02	22.02	29.09	30.35	21.29	21.14	25.00	16.95	nd
FeO	11.60	51.10	51.64	49.25	47.23	46.39	50.40	50.71	48.98	35.70	22.85
MnO	0.28	0.64	1.13	0.81	0.78	0.54	0.73	1.22	1.02	0.83	0.27
NiO	nd	nd	nd	nd	nd	nd	nd	nd	nd	nd	0.13
MgO	12.24	2.12	0.86	1.48	0.72	1.21	2.44	1.17	0.54	2.24	39.00
CaO	21.72	nd	nd	0.16	0.34	nd	nd	nd	0.16	nd	0.11
total=	98.72	100.73	99.49	98.41	99.46	99.21	101.38	99.62	98.96	101.06	100.57
Mg#	68.1	-	-	-	-	-	-	-	-	-	75.3

2014 CPX2,MV51,GR,C,E
2015 MT01,MV51,P,C,E
2016 MT2,MV51,P,C,E
2017 MT3,MV51,P,R,E
2018 MT4,MV51,GR,C,E
2019 MT5,MV51,GR,C,E
2020 MT7,MV51,P,C,E
2021 MT8,MV51,P,C,E
2022 MT9,MV51,P,R,E
2023 IL2,MV51,P(MT),C,E
2024 OL393,F1,PN,C,+OL+CPX+SP,W

	2025	2026	2027	2028	2029	2030	2031	2032	2033	2034	2035
SiO2	38.14	38.05	37.92	37.91	38.02	50.74	50.46	46.41	50.28	51.09	50.28
TiO2	nd	nd	nd	nd	nd	0.60	0.67	2.77	0.94	0.67	0.80
Al2O3	nd	nd	nd	nd	nd	5.78	5.95	8.31	6.41	5.81	6.47
Cr2O3	nd	nd	nd	nd	nd	0.45	0.69	0.26	0.50	0.69	0.45
FeO	24.49	23.68	23.44	22.25	23.35	7.84	6.67	5.72	7.97	6.63	6.24
MnO	0.28	0.26	0.27	0.30	0.29	0.29	0.12	nd	0.11	0.11	0.13
NiO	0.14	0.12	0.14	0.14	0.13	nd	nd	nd	nd	nd	nd
MgO	37.53	38.02	38.21	38.62	38.10	16.49	14.04	13.01	15.79	14.79	14.39
CaO	0.11	0.09	nd	0.27	nd	17.30	20.36	22.76	18.02	19.36	20.37
Na2O	nd	nd	nd	nd	nd	0.50	0.68	0.47	0.48	0.70	0.75
total=	100.69	100.22	99.98	99.49	99.89	99.99	99.64	99.71	100.50	99.85	99.88
Mg#	73.2	74.1	74.4	75.6	74.4	80.7	79.2	87.0	79.2	79.9	82.4
Al ratio	-	-	-	-	-	0.8	0.9	0.3	0.7	1.0	0.8

2025 OL394,F1,PN,C,W
2026 OL395,F1,PN,C,W
2027 OL396,F1,PN,C,W
2028 OL397R,F1,PN,R,W
2029 OL398,F1,PN,C,W
2030 CPX19,F1,PN,C,E
2031 CPX20,F1,PN,C,E
2032 CPX21,F1,PN,R,E
2033 CPX23,F1,PN,C,E
2034 CPX24,F1,PN,C,E
2035 CPX377,F1,PN,C,W

	2036	2037	2038	2039	2040	2041	2042	2043	2044	2045	2046
SiO2	50.75	49.49	50.36	51.03	0.88	nd	0.38	nd	1.29	nd	nd
TiO2	0.60	1.42	0.71	0.64	2.88	1.68	12.16	1.88	12.31	2.21	15.89
Al2O3	5.73	6.68	6.61	5.35	42.28	48.80	13.66	49.32	13.05	49.85	11.08
Fe2O3	nd	nd	nd	nd	14.20	12.87	27.36	12.46	25.74	11.88	26.49
Cr2O3	0.63	0.43	0.55	0.64	4.81	4.62	6.11	4.52	5.34	3.49	3.65
FeO	6.01	6.35	6.74	7.74	20.73	18.70	33.60	19.42	33.93	19.27	36.32
MnO	0.14	0.14	0.13	0.17	0.16	0.13	0.41	0.17	0.35	0.16	0.30
MgO	14.70	14.12	14.83	16.76	13.94	14.90	7.62	14.75	7.99	14.96	7.52
CaO	20.36	20.53	19.87	16.64	nd	nd	nd	nd	nd	nd	nd
Na2O	0.82	0.92	0.83	0.68	nd	nd	nd	nd	nd	nd	nd
total=	99.74	100.08	100.63	99.65	99.88	101.70	101.30	102.52	100.00	101.82	101.25
Mg#	84.0	84.6	84.1	80.8	54.5	58.7	28.8	57.5	29.6	58.0	27.0
Al ratio	0.8	0.6	0.7	0.8	-	-	-	-	-	-	-

2036 CPX378,F1,PN,C,W
2037 CPX379,F1,PN,R,W
2038 CPX380,F1,PN,C,W
2039 CPX381,F1,PN,C,W
2040 SP12,F1,PN,C,E
2041 SP13,F1,PN,C,E
2042 SPMT14Y,F1,PN,R,E
2043 SP15,F1,PN,C,E
2044 SPMT16,F1,PN,R,E
2045 SP17,F1,PN,C,E
2046 SPMT18,F1,PN,I,E

	2047	2048	2049	2050	2051	2052	2053	2054	2055	2056	2057
SiO2	0.24	53.59	40.79	40.67	40.69	41.00	52.01	52.15	51.68	51.73	50.96
TiO2	15.95	nd	nd	nd	nd	nd	0.58	0.71	0.55	0.61	0.59
Al2O3	9.91	22.79	0.01	nd	0.03	0.02	6.61	6.47	6.74	6.11	6.58
Fe2O3	25.86	nd	nd	nd	nd	nd	nd	nd	nd	nd	nd
Cr2O3	3.48	nd	nd	nd	nd	nd	0.64	0.78	0.72	0.61	0.63
FeO	37.66	0.11	9.94	9.70	9.96	9.98	3.20	3.02	2.94	3.20	2.98
MnO	0.32	nd	0.16	0.12	0.12	0.14	0.20	nd	nd	nd	nd
NiO	nd	nd	0.40	0.37	0.38	0.38	nd	nd	nd	nd	nd
MgO	6.47	nd	48.97	48.71	48.88	48.70	15.48	15.17	15.00	15.62	15.43
CaO	nd	nd	0.04	0.08	0.04	0.04	20.10	20.32	20.63	20.12	20.11
Na2O	nd	12.95	nd	nd	nd	nd	1.33	1.15	1.18	1.36	1.38
K2O	nd	0.07	nd	nd	nd	nd	nd	nd	nd	nd	nd
total=	99.89	89.51	100.31	99.65	100.10	100.26	100.15	99.77	99.44	99.36	98.66
Mg#	23.4	-	89.8	90.0	89.7	89.7	90.2	90.0	90.1	91.8	93.9
Al ratio	-	-	-	-	-	-	1.3	1.5	1.4	1.2	1.1

2047 SPMT19,F1,PN,R,E
2048 AC3,F1,GR,C,E,IN BASANITE
2049 OL103,F2,PN,C,+OL+CPX+OPX+SP,W
2050 OL104,F2,PN,R,W
2051 OL105,F2,PN,C,W
2052 OL106,F2,PN,C,W
2053 CPX3,F2,PN,C,E
2054 CPX4,F2,PN,C,E
2055 CPX7,F2,PN,C,E
2056 CPX8,F2,PN,C,E
2057 CPX207,F2,PN,C,W

	2058	2059	2060	2061	2062	2063	2064	2065	2066	2067	2068
SiO2	51.48	51.04	54.59	54.53	54.72	54.81	nd	0.05	0.05	0.03	nd
TiO2	0.56	0.57	0.12	0.12	nd	0.13	0.11	0.14	0.25	0.12	0.15
Al2O3	6.48	6.67	4.47	4.65	4.44	4.32	58.49	58.06	58.09	58.02	58.32
Fe2O3	nd	nd	nd	nd	nd	nd	1.52	1.91	1.30	2.16	1.31
Cr2O3	0.60	0.65	0.33	0.35	0.32	0.30	9.59	9.37	9.52	9.34	9.50
FeO	3.01	2.98	6.26	6.28	6.31	6.36	9.61	9.09	8.73	8.93	9.37
MnO	0.09	0.14	0.13	0.13	0.13	0.09	nd	0.18	0.14	0.16	nd
MgO	15.53	15.06	32.63	32.58	32.97	32.82	20.77	20.93	21.16	21.02	20.80
CaO	20.28	20.30	0.71	0.82	0.64	0.72	nd	nd	nd	nd	nd
Na2O	1.44	1.45	nd	0.09	nd	0.09	nd	0.01	0.02	0.01	nd
total=	99.47	98.86	99.24	99.55	99.53	99.64	100.09	99.74	99.26	99.79	99.45
Mg#	94.4	93.6	90.4	91.1	91.1	91.1	79.4	80.4	81.2	80.8	79.8
Al ratio	1.1	1.1	-	-	-	-	-	-	-	-	-

2058 CPX208,F2,PN,I,W
2059 CPX210,F2,PN,C,W
2060 OPX203,F2,PN,I,W
2061 OPX204,F2,PN,R,W
2062 OPX205,F2,PN,C,W
2063 OPX206,F2,PN,I,W
2064 SP1,F2,PN,C,E
2065 SP101,F2,PN,I,W
2066 SP102,F2,PN,R,W
2067 SP103,F2,PN,C,W
2068 SP2,F2,PN,C,E

	2069	2070	2071	2072	2073	2074	2075	2076	2077	2078	2079
SiO2	nd	nd	40.16	40.38	40.32	40.75	40.76	40.68	38.83	39.65	38.61
TiO2	0.16	nd	nd	nd	nd	nd	nd	nd	nd	nd	nd
Al2O3	57.87	57.81	nd	nd	nd	nd	nd	nd	nd	nd	nd
Fe2O3	2.11	1.81	nd	nd	nd	nd	nd	nd	nd	nd	nd
Cr2O3	9.19	9.65	nd	nd	nd	nd	nd	nd	nd	nd	nd
FeO	9.04	8.82	14.23	12.64	12.51	12.16	11.15	11.15	20.10	19.57	22.42
MnO	nd	nd	0.31	0.26	0.19	0.22	0.16	0.16	0.41	0.35	0.59
NiO	nd	nd	0.18	0.22	0.36	0.40	0.49	0.49	0.21	nd	nd
MgO	20.94	20.92	44.69	45.98	46.38	46.84	48.23	47.61	40.31	41.05	38.82
CaO	nd	nd	0.14	0.26	nd	0.18	nd	nd	0.29	0.25	0.36
total=	99.31	99.01	99.71	99.74	99.76	100.55	100.79	100.09	100.15	100.87	100.80
Mg#	80.5	80.9	84.8	86.6	86.9	87.3	88.5	88.4	78.1	78.9	75.5

2069 SP3R,F2,PN,C,E
2070 SP4R,F2,PN,C,E
2071 OL29,F3,PN,C,+OL+CPX+OPX+SP,E
2072 OL30,F3,PN,C,E
2073 OL31,F3,PN,C,E
2074 OL32,F3,PN,R,E
2075 OL33,F3,PN,C,E
2076 OL33R,F3,PN,C,E
2077 OL34,F3,PN,R,E
2078 OL35,F3,PN,R,E
2079 OL37,F3,PN,R,E

	2080	2081	2082	2083	2084	2085	2086	2087	2088	2089	2090
SiO2	51.61	54.79	51.83	55.12	51.95	54.68	52.47	51.79	51.96	46.22	51.77
TiO2	0.48	0.20	0.52	0.14	0.45	0.14	0.47	0.52	0.43	3.33	0.50
Al2O3	4.12	4.84	5.94	4.69	5.72	4.72	6.59	6.60	6.98	7.01	6.66
Cr2O3	0.88	0.31	0.75	0.31	0.69	0.36	0.76	0.88	0.97	nd	0.71
FeO	3.70	7.60	3.95	6.89	3.09	6.31	3.01	3.30	3.26	7.38	3.16
MnO	nd	0.23	nd	0.12	nd	0.13	0.11	0.11	nd	0.11	0.11
NiO	nd	nd	nd	0.17	nd	nd	nd	nd	nd	nd	0.15
MgO	15.61	31.71	15.86	31.95	15.64	32.32	15.26	15.33	14.94	12.25	15.28
CaO	22.60	0.89	19.92	0.81	20.39	0.73	20.46	20.14	20.11	22.77	20.05
Na2O	0.39	nd	0.71	nd	1.15	nd	1.22	1.13	1.25	0.51	1.06
total=	99.39	100.57	99.48	100.20	99.08	99.39	100.35	99.80	99.90	99.58	99.45
Mg#	88.7	88.1	87.7	89.2	90.0	90.1	90.0	89.2	89.1	82.0	89.6
Al ratio	0.7	-	1.3	-	1.4	-	1.5	1.3	1.5	0.1	1.4

2080 CPX33,F3,PN,C,E
2081 OPX35,F3,PN,C,E
2082 CPX36,F3,PN,C,E
2083 OPX37,F3,PN,C,E
2084 CPX38,F3,PN,C,E
2085 OPX39,F3,PN,C,E
2086 CPX40,F3,PN,C,E
2087 CPX42,F3,PN,I,E
2088 CPX44,F3,PN,I,E
2089 CPX45,F3,PN,R,E
2090 CPX46,F3,PN,I,E

	2091	2092	2093	2094	2095	2096	2097	2098	2099	2100	2101
SiO2	nd	nd	38.73	37.70	37.42	37.49	37.70	37.65	37.58	37.62	37.83
TiO2	0.12	0.12	nd	nd	nd	nd	nd	nd	nd	nd	nd
Al2O3	54.82	56.77	nd	0.03	0.02	0.03	0.03	nd	0.02	0.01	nd
Fe2O3	4.51	2.85	nd	nd	nd	nd	nd	nd	nd	nd	nd
Cr2O3	10.07	9.22	nd	nd	nd	nd	nd	nd	nd	nd	nd
FeO	12.02	11.53	23.32	22.96	22.91	22.89	22.97	23.07	23.00	22.95	22.69
MnO	nd	nd	0.27	0.32	0.31	0.32	0.30	0.31	0.29	0.29	0.25
NiO	nd	nd	nd	0.15	0.18	0.15	0.13	0.14	0.14	0.14	0.17
MgO	18.86	19.26	37.85	39.49	39.33	39.31	38.86	39.23	39.14	39.32	38.75
CaO	nd	nd	0.32	0.15	0.13	0.12	0.15	0.18	0.16	0.17	0.13
total=	100.40	99.75	100.49	100.80	100.30	100.31	100.14	100.58	100.33	100.50	99.82
Mg#	73.7	74.9	74.3	75.4	75.4	75.4	75.1	75.2	75.2	75.3	75.3

2091 SP28,F3,PN,C,E
2092 SP29,F3,PN,C,E
2093 OL10,F4,PN,R,+OL+CPX+SP+IL,E
2094 OL12,F4,PN,C,W
2095 OL13,F4,PN,C,W
2096 OL14,F4,PN,C,W
2097 OL15,F4,PN,C,W
2098 OL16,F4,PN,C,W
2099 OL17,F4,PN,C,W
2100 OL18,F4,PN,C,W
2101 OL386,F4,PN,C,W

	2102	2103	2104	2105	2106	2107	2108	2109	2110	2111	2112
SiO2	37.96	37.75	38.22	38.06	38.02	38.11	38.68	38.47	38.71	38.50	38.54
FeO	22.77	22.98	22.83	22.89	22.93	22.96	23.21	23.15	22.91	23.26	23.34
MnO	0.31	0.36	0.27	0.26	0.24	0.24	0.34	0.29	0.20	0.19	0.31
NiO	0.16	nd	0.15	0.14	0.12	0.16	nd	0.20	0.22	0.20	nd
MgO	38.82	38.16	38.78	38.62	38.76	38.79	38.50	38.41	38.54	38.43	38.32
CaO	0.09	0.30	0.18	0.08	0.08	0.11	0.09	0.26	0.15	nd	0.13
total=	100.11	99.55	100.43	100.05	100.15	100.37	100.82	100.78	100.73	100.58	100.64
Mg#	75.2	74.7	75.2	75.0	75.1	75.1	74.7	74.7	75.0	74.6	74.5

2102 OL387,F4,PN,I,W
2103 OL388,F4,PN,R,W
2104 OL389,F4,PN,C,W
2105 OL390,F4,PN,C,W
2106 OL391,F4,PN,C,W
2107 OL392,F4,PN,C,W
2108 OL5,F4,PN,C,E
2109 OL7,F4,PN,R,E
2110 OL7,F4,PN,C,E
2111 OL8,F4,PN,C,E
2112 OL9,F4,PN,I,E

	2113	2114	2115	2116	2117	2118	2119	2120	2121	2122	2123
SiO2	49.86	48.09	46.49	50.18	49.32	49.56	49.60	49.29	49.49	49.67	49.50
TiO2	1.09	1.66	3.24	0.91	1.04	1.03	1.07	1.04	1.04	0.99	1.01
Al2O3	6.16	7.71	6.72	4.97	6.62	6.54	4.76	6.54	6.46	6.39	6.70
Cr2O3	0.66	0.40	0.21	1.12	0.50	0.50	1.31	0.51	0.49	0.46	0.44
FeO	5.05	7.00	6.20	5.13	5.11	5.12	5.46	5.07	5.34	5.07	5.18
MnO	nd	nd	0.23	nd	nd	nd	nd	0.13	0.14	0.14	0.12
MgO	15.11	13.88	12.68	15.71	15.46	15.29	13.93	15.00	15.47	15.35	15.14
CaO	20.68	19.59	23.12	20.14	20.27	20.30	22.50	20.45	20.06	20.34	20.28
Na2O	0.30	0.79	0.38	0.58	0.74	0.75	0.31	0.73	0.73	0.74	0.73
total=	98.91	99.12	99.27	98.74	99.06	99.09	98.94	98.76	99.22	99.15	99.10
Mg#	84.2	81.8	84.1	86.6	90.3	88.8	82.7	88.7	89.3	89.3	88.2
Al ratio	0.7	0.6	0.1	0.5	0.5	0.6	0.4	0.6	0.5	0.6	0.6

2113 CPX10,F4,PN,C,E
2114 CPX11,F4,PN,I,E
2115 CPX12,F4,PN,R,E
2116 CPX13,F4,PN,I,E
2117 CPX13,F4,PN,C,W
2118 CPX14,F4,PN,C,W
2119 CPX15,F4,PN,R,E
2120 CPX15,F4,PN,C,W
2121 CPX16,F4,PN,C,W
2122 CPX18,F4,PN,C,W
2123 CPX19,F4,PN,C,W

	2124	2125	2126	2127	2128	2129	2130	2131	2132	2133	2134
SiO2	49.45	49.78	49.33	49.09	49.01	50.05	49.58	49.89	0.16	nd	nd
TiO2	1.07	0.92	1.01	1.13	1.37	0.93	1.06	1.17	0.78	0.64	0.94
Al2O3	6.65	5.85	6.27	6.99	6.66	5.90	6.70	7.01	54.54	56.76	49.65
Fe2O3	nd	nd	nd	nd	nd	nd	nd	nd	9.59	6.99	12.96
Cr2O3	0.46	1.10	0.84	0.39	0.44	1.16	0.47	0.48	1.98	3.17	2.93
FeO	5.34	4.77	5.17	5.46	6.23	4.93	5.37	5.57	18.59	16.54	19.91
MnO	0.12	0.13	0.12	0.14	0.16	nd	0.12	nd	0.14	0.23	0.17
MgO	15.65	15.43	15.13	14.70	13.85	15.45	15.22	14.86	15.00	16.28	13.36
CaO	19.65	20.41	20.08	20.28	20.79	20.21	20.50	20.68	nd	nd	nd
Na2O	0.76	0.81	0.84	0.83	0.88	0.34	nd	0.53	nd	nd	nd
total=	99.15	99.20	98.79	99.01	99.39	98.97	99.02	100.19	100.78	100.61	99.92
Mg#	89.2	90.7	89.4	88.1	85.2	84.8	83.5	83.4	59.0	63.7	54.5
Al ratio	0.6	0.5	0.5	0.6	0.5	0.7	0.7	0.7	-	-	-

2124 CPX20,F4,PN,C,W
2125 CPX21,F4,PN,C,W
2126 CPX22,F4,PN,C,W
2127 CPX23,F4,PN,C,W
2128 CPX24,F4,PN,C,W
2129 CPX9,F4,PN,C,E
2130 CPX1,F4,PN,C,E
2131 CPX7,F4,PN,C,E
2132 SP10,F4,PN,C,E
2133 SP5,F4,PN,C,E
2134 SP8,F4,PN,C,E

	2135	2136	2137	2138	2139	2140	2141	2142	2143	2144	2145
SiO2	0.73	0.18	0.17	0.14	0.22	nd	0.02	0.01	nd	0.02	0.01
TiO2	0.91	20.20	20.70	52.92	52.00	53.74	53.77	53.89	53.93	53.76	53.65
Al2O3	49.76	8.96	8.95	0.27	0.35	0.26	0.28	0.24	0.28	0.26	0.26
Fe2O3	11.62	19.55	19.25	5.41	6.22	3.65	3.10	3.23	3.13	3.37	3.66
Cr2O3	3.00	3.35	2.62	0.34	0.58	0.58	0.56	0.56	0.58	0.58	0.57
FeO	20.57	40.09	41.02	32.45	32.09	33.66	33.91	34.02	33.92	33.83	33.66
MnO	0.12	0.34	0.25	0.36	0.42	0.38	0.38	0.40	0.38	0.40	0.39
MgO	13.69	7.24	7.05	8.38	8.14	8.01	7.90	7.88	7.96	7.93	7.97
CaO	nd	0.09	nd	nd	nd	nd	nd	nd	nd	nd	nd
total=	100.40	100.00	100.01	100.27	100.02	100.28	99.92	100.23	100.18	100.15	100.17
Mg#	54.3	-	-	-	-	-	-	-	-	-	-

2135 SP9,F4,PN,C,E
2136 MTSP1,F4,PN,R,E
2137 MTSP2,F4,PN,R,E
2138 IL1,F4,PN,C,E
2139 IL1,F4,PN,C,E
2140 IL12,F4,PN,C,W
2141 IL13,F4,PN,C,W
2142 IL14,F4,PN,C,W
2143 IL15,F4,PN,C,W
2144 IL16,F4,PN,C,W
2145 IL17,F4,PN,C,W

	2146	2147	2148	2149	2150	2151	2152
SiO2	nd	nd	0.33	0.23	nd	0.35	0.30
TiO2	53.76	52.57	51.52	51.50	51.57	51.40	51.37
Al2O3	0.24	0.41	0.47	0.22	nd	0.26	0.26
Fe2O3	2.95	5.09	6.57	6.32	6.91	7.20	6.40
Cr2O3	0.57	0.42	0.55	0.61	0.59	0.57	0.53
FeO	33.97	33.10	31.72	31.77	31.37	30.95	32.15
MnO	0.38	0.41	0.44	0.39	0.42	0.37	0.34
MgO	7.85	7.72	8.17	8.09	8.18	8.59	7.89
total=	99.72	99.72	99.77	99.13	99.04	99.69	99.24

2146 IL18,F4,PN,C,W
2147 IL2,F4,PN,C,E
2148 IL3,F4,PN,C,E
2149 IL4,F4,PN,C,E
2150 IL6,F4,PN,C,E
2151 IL8,F4,PN,C,E
2152 IL9,F4,PN,C,E

IT DIDN'T LOOK LIKE A BISCUIT BOX DID IT? I'VE ALWAYS FELT THAT IT MIGHT.

Noël Coward.